Filip M. Vanhoenacker
Paul M. Parizel
Jan L. Gielen *Editors*

Imaging of Soft Tissue Tumors

Fourth Edition

Springer

Imaging of Soft Tissue Tumors

Filip M. Vanhoenacker • Paul M. Parizel
Jan L. Gielen
Editors

Imaging of Soft Tissue Tumors

Fourth Edition

Springer

Editors
Filip M. Vanhoenacker
Dept. of Radiology
University of Antwerp
Edegem
Belgium

Jan L. Gielen
Dept. of Radiology
University of Antwerp
Edegem
Belgium

Paul M. Parizel
Dept. of Radiology
University of Antwerp
Edegem
Belgium

ISBN 978-3-319-46677-4 ISBN 978-3-319-46679-8 (eBook)
DOI 10.1007/978-3-319-46679-8

Library of Congress Control Number: 2017931580

© Springer International Publishing AG 2017
This work is subject to copyright. All rights are reserved by the Publisher, whether the whole or part of the material is concerned, specifically the rights of translation, reprinting, reuse of illustrations, recitation, broadcasting, reproduction on microfilms or in any other physical way, and transmission or information storage and retrieval, electronic adaptation, computer software, or by similar or dissimilar methodology now known or hereafter developed.
The use of general descriptive names, registered names, trademarks, service marks, etc. in this publication does not imply, even in the absence of a specific statement, that such names are exempt from the relevant protective laws and regulations and therefore free for general use.
The publisher, the authors and the editors are safe to assume that the advice and information in this book are believed to be true and accurate at the date of publication. Neither the publisher nor the authors or the editors give a warranty, express or implied, with respect to the material contained herein or for any errors or omissions that may have been made.

Printed on acid-free paper

This Springer imprint is published by Springer Nature
The registered company is Springer International Publishing AG
The registered company address is: Gewerbestrasse 11, 6330 Cham, Switzerland

Preface to the Fourth Edition

In memoriam Prof. Dr. Arthur M. De Schepper
30 November 1937–04 October 2013

I can vividly remember my first meeting with Professor Arthur De Schepper in Antwerp back in 1988. Being a young resident in radiology educated at the Catholic University of Leuven, I registered for an educational course on ultrasound, organized by Professor De Schepper and his team at Antwerp University Hospital (UZA). In those days, each Flemish university had its own program for (post)graduate radiological education, which was open to all radiologists and trainees. I was immediately impressed by the outstanding educational quality of this meeting and particularly by the open-mindedness of Professor De Schepper, a spirit that he was able to transmit to his whole team of the "Antwerp school of radiology." I will never forget that he was so easily accessible and that you could talk to him in a very friendly and relaxed atmosphere following the scientific part of the meeting. From that day on, I became a huge fan of the Antwerp school of radiology, and I faithfully attended every single meeting (better known as the "Radiologisch Uur van het UZA") that was organized in Antwerp.

Later on, after I graduated as a radiologist and I started working at the General Hospital Sint-Maarten Duffel-Mechelen, Professor De Schepper asked me to become a consultant radiologist at Antwerp University Hospital. It was my great privilege to work with him on several projects, such as coediting a book *Medical Imaging of the Spleen* (Springer-Verlag, 2000) and the previous editions of this book *Imaging of Soft Tissue Tumors*, which became his main interest of his very successful scientific career. We developed a close friendship that I will cherish forever.

Arthur De Schepper grew up in Boom, a small industry city south of Antwerp. He completed his medical training at the Catholic University of Leuven and graduated in 1963 as MD. He started his residency of radiology at Stuivenberg General Hospital, under the tutorship of Professor Charles Dochez, who would become a lifelong friend. His main interest in the early stage of his career focused on angiography. He refined his angiography training in the department of Doctor C. Hernandez, at the Hôtel-Dieu Hospital in Paris. After his return to Antwerp, he became chair of radiology at the Stuivenberg General Hospital in 1973. Five years later, he was appointed coordinating chairman of the public assistance hospitals of the city of Antwerp. His special interest in angiography and scientific output in this domain culminated in the successful public defense of his Ph.D. thesis on the ovarian vein syndrome (1976).

In 1978, he was appointed as assistant professor of radiology at the University of Antwerp, and he would become the teacher and mentor of several generations of medical students. At the inauguration of Antwerp University Hospital in 1980, he became chairman of the Department of Radiology. Building from scratch a new imaging department, selecting capable and dedicated collaborators, and developing a structure for teaching residents and students were the challenges he faced. These were exhilarating times, as everything was new and exciting. Arthur De Schepper's success in creating a productive and special ambiance in the Department of Radiology was the result of an intense dedication, true feelings of friendship for his collaborators regardless of their degree or function, critical discussion, and intellectual honesty. He had an uncanny ability to attract students and collaborators of great talent and commitment, and he was able to convey to them his energy and enthusiasm.

Between 1980 and his retirement in 2003, Arthur De Schepper trained more than 80 radiologists. Together with his staff, nurses, technologists, and other collaborators of the department, they constituted his extended family.

His energy and vision resulted in a prolific scientific output. He has authored, or coauthored, more than 350 scientific papers, referenced in PubMed.

In 1986, Antwerp University Hospital was the first academic teaching hospital in Flanders to install a superconducting MRI unit. From then on, Arthur De Schepper developed a keen interest in imaging of bone and soft tissue tumors. He created the "Belgian Soft Tissue Neoplasm Registry" (BSTNR), which provided second opinions to radiologists and other medical specialists from all over the country. His expertise and the BSTNR database led to the publication in 1997 of the first edition of his book *Imaging of Soft Tumors*, which became a huge success. A second edition was published in 2001 followed by a third one in 2006. The book was also translated into Chinese, which reflects the worldwide impact of his work.

After his retirement as chairman of the department in 2003, he remained very active as an expert, and because of his expertise and knowledge, Professor Hans Bloem invited him to become a consultant professor of radiology at Leiden University Medical Center, in the Netherlands. He went on working with unrelenting energy and enthusiasm keeping his body young and his mind alert.

His groundbreaking work on soft tissue tumors made him a world-leading authority on this topic. He was invited to present guest lectures at the European Congress of Radiology (ECR), European Society of Skeletal Radiology (ESSR), Radiological Society of North America (RSNA), and many other major international meetings.

In 2006, Professor De Schepper was awarded Honorary Membership of European Society of Skeletal Radiology (ESSR) for his outstanding contribution to musculoskeletal radiology.

While his medical, scientific, and educational achievements were widely known and appreciated, Arthur De Schepper had human and humane qualities only his family and close friends were allowed to fully appreciate. He was the loving husband of Anya Augustynen, the proud father of 12 children, and the "Papie" of 21 grandchildren. His love for them all, the little things of life, the birds in his garden, and his walks in the woods and wanderings through the mysterious little alleys of Antwerp, it all crystallized into hundreds of poems.

In November 2011, Professor De Schepper suddenly found himself at the other side of the divide, when vague abdominal complaints proved to be symptoms of metastatic colon cancer. With admirable courage, he accepted the diagnosis and its consequences. He never tried to dissimulate the seriousness of his condition and at the same time went on working and helping his colleagues as much as physically possible. On 11 September 2013, at a symposium to celebrate the tenth anniversary of his retirement, he gave his last lecture at the University of Antwerp, an overview of his long career and a lucid summary of what had been and what was to come. Less than 4 weeks later, he left us with a last poem:

to whom it may concern
bury me cautiously
with a bunch of lavender
and pen and paper
one never knows
my soul might write
the timeless poem
I never could alive
forget pomp and circumstance
sprinkle humour in my grave
and a piece of the rainbow
one never knows
my eye might see
a spray of colours
I never could alive
don't bury me loud
put grains of silence in my grave
and an ivory music box
one never knows
there is no heavenly music
but sounds I will hear
I hardly could alive
leave home your funeral wreaths
your elegies and lament
as for an honourable man
put cuddles and caresses in my grave

one never knows
our love survives
(*Kindly translated by Prof. Dr. Jan L.M. Bosmans in English*)

Professor Arthur De Schepper will be remembered as a greatly admired and internationally respected radiologist, with an almost superhuman dedication to his work.

We are grateful for the support, warmth, and friendship, which Arthur De Schepper bestowed upon us throughout his long and illustrious career. He will live in our hearts and minds as a leader in radiology, but even more so as our friend, "our" professor.

Finally, we would like to express our special thanks to the family of Professor De Schepper and Springer-Verlag for giving us the opportunity to edit the fourth edition of this book, which is coedited with Professor Jan Gielen and Professor Paul M. Parizel, who is the chair of the Department of Radiology at Antwerp University Hospital.

On behalf of my coeditors, Professor Jan Gielen and Professor Paul M. Parizel, we would like to dedicate this fourth edition to the memory of Professor Arthur De Schepper.

Antwerp, Belgium Filip M. Vanhoenacker

References

1. Parizel PM, Bosmans JLM. http://www.auntminnieeurope.com/index.aspx?sec=ser&sub=def&pag=dis&ItemID=608826
2. Parizel PM, Bosmans JLM (2013). In memoriam Prof. Dr. Emeritus Arthur M. De Schepper. JBR–BTR. 96:329–330

Preface of the Third Edition

The Belgian Soft Tissue Neoplasm Registry (BSTNR) is a multiinstitutional database project involving the cooperation of nearly all magnetic resonance imaging (MRI) centers in Belgium. This initiative, which was started in 2001, had two main goals. First, the BSTNR provided a second opinion report (within 48 h) as a professional courtesy toward all cooperating radiologists. Second, the BSTNR served as a scientific data bank of soft tissue tumors, which are rare lesions in daily radiological practice. All cooperating radiologists had access to the data of the register for use in clinical scientific studies. The scientific value of the BSTNR increased with the installation of a peer-review group of pathologists, all of whom shared a large amount of experience in soft tissue tumor pathology. They reviewed the pathological findings of all malignant tumors, all exceptional tumors, and all tumors in which there was a discordance between MRI and histopathological findings. They guarantee that the pathological standard remains "gold."

Until now we have included more than 1500 histologically proven soft tissue tumors. This exceptional material constitutes the foundation of this third edition. We are grateful to all the coinvestigators of the BSTNR for their long-term contribution. We asked all coauthors to update their chapters with pertinent new data and images. We also asked them to respect the new World Health Organization classification of soft tissue tumors, which changed considerably in 2002, taking into account the usefulness of the classification for the radiologist. This implies that tumors have moved from one chapter to another according to their tissue of origin and their malignancy grade, e.g., the formerly named malignant fibrous histiocytoma, the synovial cell sarcoma, the hemangiopericytoma, and the solitary fibrous tumor. We also asked our coauthors to include at the end of their chapters a shortlist of striking features and a concise message to take home. The content of many chapters has changed substantially, e.g., the chapter on tumors of connective tissue, on pseudotumors, on biopsy of soft tissue tumors, and on posttreatment follow-up. The chapter on imaging strategy is tuned according to evolution of the MR technique and sequences. In the chapter on MRI, we omit the general principles of the method and focus on the sequences that are currently used in the study of soft tissue tumors. The index at the end of the book is better organized

and more comprehensive. Finally we have added two new chapters, one on pathology and a second on molecular biology and genetics. We asked both authors to focus on those features that are most important to radiologists, who will be the main readers of this book. We are grateful to Springer-Verlag for giving us the opportunity to produce a third edition of a book on a radiological subject, which is a rather exceptional event.

Antwerp, Belgium
March 2005

Arthur M. De Schepper

Preface of the Second Edition

At the time of writing, our group has had more than 10 years' experience in the imaging of soft tissue tumors. We are now,–more than ever,– convinced that a multidisciplinary dialogue between orthopedic surgeons, oncologists, pathologists and radiologists is imperative for the medical management of these lesions. The common goals of all specialists dealing with soft tissue tumors should be: early detection, minimally invasive staging and grading procedures, specific diagnosis (or suitably ordered differential diagnosis), guided percutaneous biopsies, and the most suitable therapy. This approach will guarantee the patient the optimal chances of survival with the best possible quality of life. To help us achieve these goals, we have established a Commission for Bone and Soft Tissue Tumors at the University Hospital in Antwerp, which convenes every 2 weeks. This multidisciplinary group formulates opinions and recommendations on diagnosis, prognosis, treatment and follow-up, and is highly valued by referring physicians. In addition, we are organizing a Belgian Registry of Soft Tissue Tumors with the cooperation of all Belgian centers in which MRI equipment is available and intend to invite students and investigators from all over the world to share our scientific interest in this fascinating field of medical imaging.

The main objective of this second edition of "Imaging of Soft Tissue Tumors" is to provide radiologists with an updated and easy-to-read reference work. This second edition includes new literature references and illustrations. Older illustrations have been replaced with higher quality images, generated by newer equipment and/or MRI pulse sequences. New tables organizing information into summaries have been included and the subject index has been updated. Most importantly, the text contains newer insights (for instance about fibrohistiocytic tumors), and reflects our own experience of increasing understanding of soft tissue tumors and their imaging. The chapter about magnetic resonance imaging has been shortened, and now focuses mainly on principles, pulse sequences and applications that are directly related to the examination of soft tissues and soft tissue tumors. We have included new chapters on "Soft Tissue Tumors in Pediatric Patients" and "Soft Tissue Lymphoma", and also a chapter on the controversial subject of (percutaneous) biopsy.

The readers and the reviewers of our book will judge whether we have succeeded in our objectives.

Finally, we would like to thank our editor and Mrs. Mennecke-Bühler at Springer-Verlag for sharing in the challenge of editing a second edition of this book on a rare pathology.

Antwerp, Belgium
July 2001

Arthur M. De Schepper

Preface of the First Edition

Although the soft tissues constitute a large part of the human body, soft tissue tumors are rare, accounting for less than 1 % of all neoplasms. The annual incidence of benign soft tissue tumors in a hospital population is 300 per 100,000. Moreover, benign lesions outnumber their malignant counterparts by about 100–1. The clinical and biochemical findings of soft tissue tumors are frequently nonspecific. The first sign is usually a soft tissue swelling or a palpable mass with or without pain or tenderness. Laboratory results are frequently normal or show minimal nonspecific changes.

Until a few decades ago, detection of soft tissue tumors usually did not take place until late in the course of disease. This resulted from their low incidence and nonspecific clinical findings and from the poor sensitivity of conventional radiography, which was the only imaging technique available. Soft tissue tumors and soft tissue disorders in general were practically unknown to radiologists until the introduction of ultrasound and computed tomography (CT). Unfortunately, these methods suffered from inherent drawbacks, such as the poor specificity of ultrasound and the poor contrast resolution of CT.

Many of these problems were solved by the introduction of magnetic resonance imaging (MRI). Thanks to its high contrast tissue resolution and its multiplanar imaging capability, new horizons were opened for imaging soft tissues. Today, a correct assessment of disorders of bones, joints, or soft tissues is unimaginable without MRI.

In view of recent developments in surgery, radiation therapy, systemic chemotherapy, and regional perfusion techniques, the imaging of soft tissue tumors is gaining in importance. Correct diagnosis includes the detection, characterization, and staging of the lesions. The inadequate diagnosis and therapy of soft tissue sarcomas frequently results in tumor recurrence, necessitating major therapeutic “aggression.” MRI is the optimal imaging technique for avoiding inadequate assessment.

Despite the interest of many groups of radiologists in the subject and despite the considerable number of overview articles that have been published in the radiologic literature, soft tissue tumors receive only minimal attention in modern state-of-the-art books on musculoskeletal imaging. Nevertheless, since all radiologists involved in the fascinating field of MRI are now confronted with tumoral pathology of soft tissues, there is a need for an illustrated radiologic guide on the subject.

From the beginning of our experience using MRI, back in 1985, we have been interested in soft tissue tumors. Our initial findings were discussed at an international congress in 1992. Conflicting findings in the literature concerning the sensitivity and specificity of MRI, which were mainly caused by the limited number of patients in published series, prompted us to start a multicenter European study. At the European Congress of Radiology 1993 in Vienna, 29 co-investigators from all over Europe agreed to participate (see the list 'Investigators of Multicentric European Study on Magnetic Resonance Imaging of Soft Tissue Tumors'). More than 1000 cases were collected, which constitute the basis of the radiologic work we prepared.

It was not our intention to write the 'all you ever wanted to know' book on soft tissue tumors. This objective has already been achieved for the pathology of soft tissue tumors by Enzinger and Weiss. Although their famous textbook contains a brief discussion of modern medical imaging, you will find it rarely on the office desk of radiologists. This present book is intended to serve as a reference guide for practising radiologists and clinicians seeking the optimal imaging approach for their patients with a soft tissue tumor.

The book is divided into four sections. In the first section we discuss the different imaging modalities and their respective contribution to the diagnosis of soft tissue tumors. As MRI is generally accepted to be the method of choice, there is a detailed theoretical description of this technique combined with a short discussion of imaging sequences. We also included a chapter on scintigraphy of soft tissue tumors, in which the current literature on the subject is summarized because scintigraphy was hardly used in our own patient material.

The second part deals with staging and characterization of soft tissue tumors and is concluded by a chapter on general imaging strategy. Tumor-specific imaging strategy is, where needed, added at the end of the tumor-specific chapters, which are collected in Part III. These chapters include a short description of epidemiology, clinical and pathological presentation, and a detailed discussion of imaging findings. For this Part, we used the classification of E.B.Chung (Current classification of soft tissue tumors. In: Fletcher CD, McKee PH (eds) *Pathobiology of soft tissue tumors*, 1st edn. Churchill Livingstone, Edinburgh, 1990, pp 43–81), which is an updated version of the most comprehensive system of classification, that of the World Health Organization. Because the illustrations originate from different institutions using different MR systems and pulse sequences, the figure legends only mention the plane of imaging (sagittal, axial, coronal), the kind of sequence (SE, TSE, GRE, …), and the weighting (T1, T2).

The fourth part consists of only one chapter dealing with post-treatment imaging findings.

I would like to thank my co-editors Dr. Paul Parizel, Dr. Frank Ramon, Dr. Luc De Beuckeleer, and Dr. Jan Vandevenne, and all the coauthors for the tremendous job they have done. From this work I learned that writing a good book requires a sabbatical leave, which good fortune I did not have.

As previously mentioned, it has been possible to include many of the illustrations shown in the book only because of the cooperation of the 29 European investigators, to whom I owe my gratitude. We gratefully acknowledge the

support of Prof. Eric Van Marck, pathologist at our institution, for reviewing the manuscript, and of Ingrid Van der Heyden (secretary) for her aid in preparing so many chapters. Finally, I wish to express my gratitude to Springer-Verlag and to Dr. Ute Heilmann for sharing the challenge of preparing this book with us.

Antwerp, Belgium
June 1996

Arthur M. De Schepper

Contents

Part I Diagnostic Modalities

1 Ultrasound and Color Doppler Ultrasound of Soft Tissue Tumors and Tumorlike Lesions 3
Jan Gielen, Filip Vanhoenacker, Ruth Ceulemans, Marnix Van Holsbeeck, Henk-Jan Van der Woude, Koenraad L. Verstraete, and Johan L. Bloem

2 Radiography and Computed Tomography 41
R. Botchu, S.L. James, and A.M. Davies

3 PET and PET-CT in Soft Tissue Sarcoma 59
S. Ceyssens and S. Stroobants

4 Magnetic Resonance Imaging: Basic Concepts 71
Peter Brys

5 Magnetic Resonance Imaging: Advanced Imaging Techniques 85
Koenraad L. Verstraete, J.C. Dutoit, J.L. Drapé, and Johan L. Bloem

6 Pathology, Genetics, and Molecular Biology of Soft Tissue Tumors 115
Vasiliki Siozopoulou and Patrick Pauwels

7 Biopsy of Soft Tissue Tumors 131
J. Gielen

Part II Staging, Grading and Tissue Specific Diagnosis

8 Staging 145
K. Wörtler

9 Grading and Tissue-Specific Diagnosis 161
Filip M. Vanhoenacker and Arthur M. De Schepper

10 Diagnostic Algorithm of Soft Tissue Tumors 181
Eline De Smet, Pieter Van Dyck, Jan L. Gielen, and Filip M. Vanhoenacker

Part III Imaging of Soft Tissue Tumors

11 WHO Classification of Soft Tissue Tumors 187
Joan C. Vilanova

12 Adipocytic Tumors 197
Philip Robinson and Filip M. Vanhoenacker

13 Fibroblastic/Myofibroblastic Tumors 243
Jan E. Vandevenne and Arthur M. De Schepper

14 So-Called Fibrohistiocytic Tumours 311
A. Shah, R. Botchu, A.M. Davies, and S.L. James

15 Tumors of Smooth and Skeletal Muscle and Pericytic Tumors 339
Miraude E.A.P.M. Adriaensen, Robert M. Kwee, and Filip M. Vanhoenacker

16 Vascular Tumors 363
Mariem Ben Haj Amor, Caroline Degrugillier-Chopinet, Alexandre Bridoux, François Pontana, Luc Ceugnart, and Anne Cotten

17 Nerve Sheath Tumors 393
Nicolas De Vos, Filip M. Vanhoenacker, Koenraad L. Verstraete, and Paul M. Parizel

18 Tumors of Uncertain Differentiation. 425
Simon David Sprengel, Marc-André Weber, Hendrik R. Degryse, and Filip M. Vanhoenacker

19 Undifferentiated/Unclassified Sarcoma 483
A. Shah, R. Botchu, A.M. Davies, and S.L. James

Part IV Imaging of Other Soft Tissue Masses

20 Synovial Lesions 495
V. Vasilevska Nikodinovska and Filip M. Vanhoenacker

21 Pseudotumoral Lesions. 523
Filip M. Vanhoenacker, Meriem Mechri Rekik, and Rodrigo Salgado

22 Soft Tissue Lymphoma 577
Jan L. Gielen, Filip M. Vanhoenacker, and Peter Bracke

23 Soft Tissue Metastases 593
Hend Riahi, Mohamed Fethi Ladeb, Mouna Chelli Bouaziz, and Meriem Mechri

24 Miscellaneous. 603
Filip M. Vanhoenacker, Astrid Van Hoyweghen, Hendrik R. Degryse, and Annemiek Snoeckx

Part V Soft Tissue Tumors in Pediatric Patients

25 Imaging of Soft Tissue Tumors in the Pediatric Patient 623
Lennart Jans and Koenraad L. Verstraete

Part VI Imaging After Treatment

26 Follow-Up Imaging of Soft Tissue Tumors 635
Johan L. Bloem and Carla S.P. Van Rijswijk

Index 653

Part I

Diagnostic Modalities

1 Ultrasound and Color Doppler Ultrasound of Soft Tissue Tumors and Tumorlike Lesions

Jan Gielen, Filip Vanhoenacker, Ruth Ceulemans, Marnix Van Holsbeeck, Henk-Jan Van der Woude, Koenraad L. Verstraete, and Johan L. Bloem

Contents

1.1 **Introduction** 4

1.2 **General Principles** 4
1.2.1 Color Doppler US 4
1.2.2 Role of US and CDUS in Soft Tissue Lesions 4
1.2.3 US and CDUS Characteristics of Tumor and Tumorlike Lesions 5

1.3 **Superficial Soft Tissue Tumors and Tumorlike Lesions** 11

1.4 **US Findings in Specific Soft Tissue Tumors and Tumorlike Lesions of the Extremities** 11
1.4.1 Articular and Synovial Sheath Masses 11
1.4.2 Peripheral Neurogenic Tumors 14
1.4.3 Pericytic (Perivascular) Tumors 20
1.4.4 Vascular Tumors 21
1.4.5 Lipoma 24
1.4.6 Ganglion Cyst 27
1.4.7 Superficial Soft Tissue Tumors and Tumorlike Lesions 28
1.4.8 Soft Tissue Mineralization Disorders 34
1.4.9 Synovial Sarcoma 35

Conclusion 36

References 36

J. Gielen, MD, PhD (✉)
Department of Radiology, Antwerp University Hospital (UZA), Antwerp, Belgium

Faculty of Medicine, University of Antwerp, Wilrijkstraat 10, 2650, Edegem, Antwerp, Belgium
e-mail: jan.gielen@uza.be

F. Vanhoenacker, MD, PhD
Department of Radiology, Antwerp University Hospital (UZA), AZ-Sint Maarten Duffel-Mechelen, Faculty of Medicine and Health Sciences, Ghent University, Antwerp, Belgium

Faculty of Medicine and Health Sciences, Ghent University, Ghent, Belgium

R. Ceulemans, MD
Henry Ford Hospital, 20509 Northville Place dr Unit 2019, Northville, MI, USA

M. Van Holsbeeck, MD
Radiology, Wayne State University School of Medicine, 540 E Canfield St, Detroit, MI 48201, USA

Henry Ford Health System, 2799 West Grand Boulevard, Detroit, MI, USA

H.-J. Van der Woude, MD, PhD
Department of Radiology, Onze Lieve Vrouwe Gasthuis (OLVG), Oosterpark, Postbus 95500, 1090 HM Amsterdam, The Netherlands

K.L. Verstraete, MD, PhD
Faculty of Medicine and Health Sciences, Ghent University, Ghent, Belgium

J.L. Bloem, MD, PhD
Department of Radiology, Leiden University Medical Center (LUMC), Leiden, The Netherlands

Faculty of Medicine, Leiden University, Gebouw 1. Postbus 9600, 2300 RC Leiden, The Netherlands

© Springer International Publishing AG 2017
F.M. Vanhoenacker et al. (eds.), *Imaging of Soft Tissue Tumors*, DOI 10.1007/978-3-319-46679-8_1

1.1 Introduction

This chapter will illustrate how ultrasound (US) and color Doppler US (CDUS) vascular imaging are currently used in imaging of soft tissue tumors and the skin and will also focus on the advantages and drawbacks of this modality.

US being a readily available, noninvasive, and relatively inexpensive imaging modality plays a significant part in the diagnostic work-up of soft tissue masses and of superficial lesions. In daily practice, US is a powerful tool to differentiate many superficial benign tumors (neurogenic tumors, superficial lipoma) and tumorlike lesions (cysts, ganglia, scar, synovial chondromatosis, lipoma arborescens, etc.) from real tumors. It may help in differentiating a localized mass from diffuse edema and solid from cystic lesions [100]. US is able to identify the lesion size, volume, and configuration to determine its internal characteristics and, in selected cases, to monitor response to chemotherapy. However US cannot detect lesions that are confined to the epidermis or that measure less than 0.1 mm in depth [138]. US supplemented by CDUS interpretation plays an important role in the recognition of potentially malignant lesions. Real-time and dynamic interpretation of the lesion is an important advantage of clinical ultrasound and is mandatory for correct interpretation. Diagnosis solely based on evaluation of hard copies is therefore not recommended.

1.2 General Principles

1.2.1 Color Doppler US

As previously mentioned, CDUS and dynamic interpretation are absolute prerequisites of each US examination improving diagnostic US specificity. In superficially located lesions, sensitivity of CDUS is significantly improved by avoiding skin contact and compression. CDUS is a noninvasive method of detecting blood flow and assessing flow direction simultaneously. The anatomic flow information is superimposed on all or part of the grayscale image. Backscattered signals in CDUS are displayed in color as a function of the motion of the erythrocytes toward or away from the transducer. Lower flow velocities are characterized by higher saturation of colors. The color-coded information is distinct from that yielded by spectral duplex Doppler imaging, which is useful when more detailed information about flow velocity or spectral analysis, of a kind that may aid in tissue characterization, is important [112]. As such, color flow US and spectral Doppler are complementary techniques. The ability of color Doppler US to provide a global view of flow in real time minimizes the chance of missing flow in an unexpected area and facilitates comparison of flow in different anatomic locations. To avoid diagnostic error, however, color flow mapping, which is solely a qualitative method, should be supported by spectral analysis [12, 96, 142]. The use of CDUS as an obligatory additional tool of describing the biologic activity, structure, extension, and blood supply of soft tissue tumors.

1.2.2 Role of US and CDUS in Soft Tissue Lesions

Specificity of US characterization of benign cases (tumors and tumorlike lesions) is higher compared to malignant cases. Thus the appearance of the most common, benign soft tissue tumors on US which have been reported will be emphasized in this chapter. Owing to the nonspecific US characteristics of most soft tissue tumors, the particular roles of US and CDUS are to confirm the presence of a suspected lesion. By differentiating certainly benign from indeterminate (potentially malignant) lesions with US and CDUS, further diagnostic and therapeutic work-up may be guided in the majority of cases.

After an initial US examination, the role of other imaging modalities can be determined. MRI should be reserved for cases in which US fails to establish a specific diagnosis or fails to demonstrate the margins of a soft tissue mass accurately. Nevertheless, additional value of MRI in small and superficial epidermal or dermal lesions remains limited.

Advantages of US over MRI are the lack of partial volume averaging effects, the availability and low cost of the technique, and the short examination time. Moreover, motion artifacts, which may occur in noncooperative patients and children, are of less relevance when US is used but may prevent appropriate CDUS imaging. A limitation of US is evaluation of the extension of a soft tissue tumor, in particular to adjacent bony structures.

The use of US-guided fine-needle aspiration biopsy (FNAB) or core needle biopsy (CNB) will be discussed in Chap. 7. US-guided FNAB or CNB is generally less time consuming and less expensive than those using computerized tomography (CT) or MRI, with easier patient access [110].

1.2.3 US and CDUS Characteristics of Tumor and Tumorlike Lesions

In case of a peripheral, small- to moderate-sized soft tissue mass, high-resolution (15–18 MHz) US can document the size and extent, intra- or extra-articular localization, location superficial or deep to the investing fascia, and relationship to surrounding anatomic structures. This holds true for the skin and hypodermis, neck, all peripheral joints, and especially for the wrist, hand, and fingers [8, 14, 39, 117, 118]. Despite new developments with extended field of view (panoramic US), US has no role, however, in the staging of large, primary soft tissue sarcomas and bone tumors with soft tissue extension. In this setting MRI is the modality of choice.

For the purpose of grading, US-guided biopsy can provide samples for histological and immunohistochemical diagnosis (Chap. 7) [40, 141]. This applies to soft tissue tumors, as well as to bone tumors with marked extra-osseous tumor extension.

Malignant soft tissue tumors are rare; the majority of presenting soft tissue swellings are benign in character [5], 96 % in the series of Hung et al. of lesions superficial to the investing fascia [117]. Even if this benign character is already clinically suspected, US can be used to reassure the patient and the referring physician that this is indeed the case and thereby can obviate the need for further (imaging) work-up. If malignancy is suspected, on the other hand, US can be used to guide an 18–10-gauge (automated gun, Tru-cut, or Spirotome ®) core needle biopsy (CNB) [49]. Since tissue sampling can be guided by US to avoid areas of hemorrhage and tumor necrosis, a high-yield solid component is possible [56, 58, 134, 141]. The constant real-time visualization of the needle tip position that is available on US considerably may increase safety and shorten the procedure time, as opposed to CT and MRI [25].

The advantages of US over CT and MRI are its low cost and availability at short notice: a US examination can often be performed the same day or within a few days of the outpatient's initial visit. One specific advantage over CT is the lack of radiation exposure.

The drawbacks of US are its rather poor specificity in defining the tumor's histological nature of deep-seated lesions. Two studies addressed the accuracy of US in the characterization of soft tissue tumors including deep-seated tumors: a sensitivity of 40–42 % and specificity of 64–86 % for lipoma and sensitivity of 63 % and specificity of 86 % for nerve sheath tumor were calculated [25, 139]. Except for lipoma most benign tumors, sarcoma, lymphoma, nerve tumors, and benign and malignant skin lesions all present as hypoechoic, solid soft tissue masses; angiogenesis is documented in most tumors (Fig. 1.1); hence particularly problematic for specific US diagnosis are the absence of CDUS signal in some superficial vascular malformations and nerve sheath tumors and the poor conspicuity of the entering and exiting nerves in small subcutaneous nerve sheath tumors [25, 39, 47, 56, 117, 130]. US with CDUS is ideally performed with a variable frequency probe in which the upper range of the frequencies (15–18 mHz) are used for the evaluation of the skin layers (epidermis-dermis) and the frequencies lower than 13 mHz are used for the deeper tissues. High and ultrahigh resolution (15 mHz and 20 mHz and higher, respectively) has a definite better diagnostic accuracy for evaluation of lesions superficial to the investing fascia and at

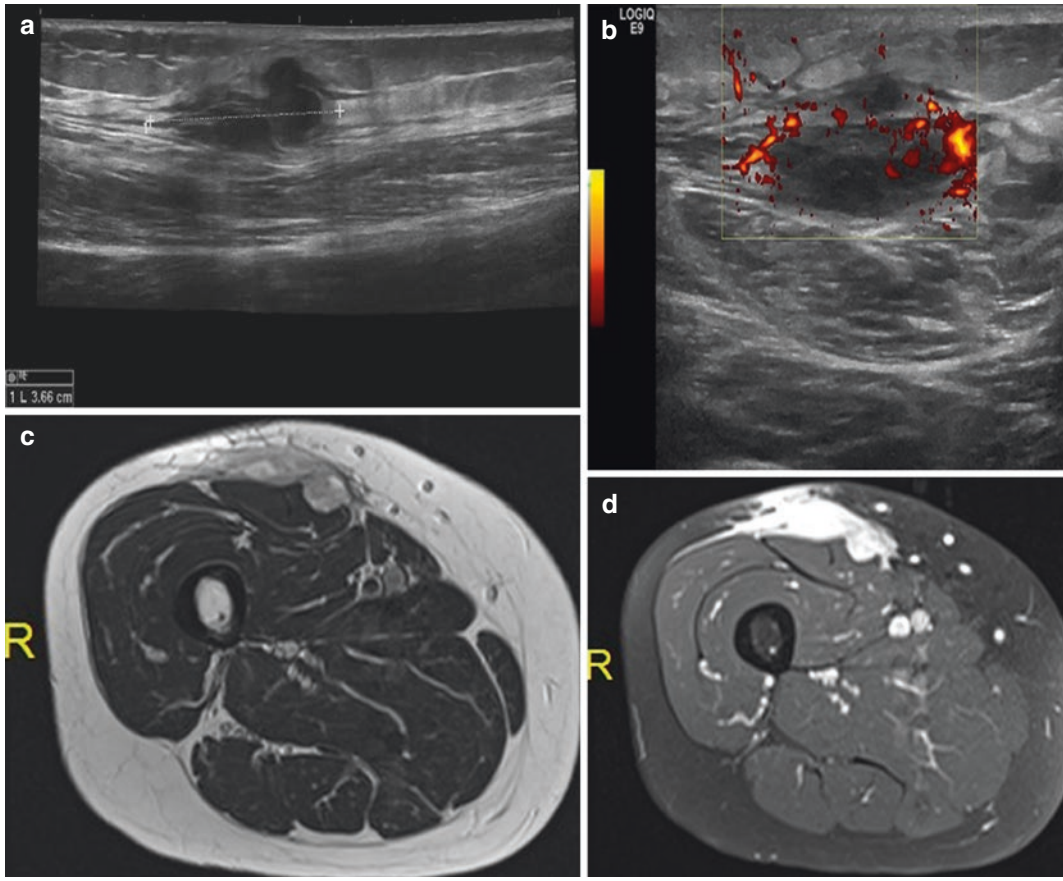

Fig. 1.1 Myxofibrosarcoma in a 65-year-old female patient with painless firm mass at the right thigh. Demonstration of tumoral mass with nonspecific US characteristics for which further MRI examination and subsequent biopsy is mandatory. (**a**) Sagittal EVOFS US image demonstrating a nonhomogeneous hypoechogenic polynodular lesion centered and with a broad base at the superficial fascia of the rectus femoris, protruding into the subcutaneous tissue, maximal longitudinal diameter 3 cm (longest oblique diameter 5 cm). Indistinct borders with infiltrative aspect of the subcutaneous tissue. (**b**) Sagittal CDUS image demonstrating marked nonhomogeneous angiogenesis with areas of absent vessels. (**c**) Axial TSE T2-WI, nonhomogeneous intermediate to low SI lesion with polynodular morphology and stranding at the subcutaneous tissue. (**d**) Axial TSE T1-WI with FS after IV gadolinium administration. Marked nonhomogeneous enhancement of the lesion and the perilesional stranding. Enhancement of the superficial fascia of the rectus femoris muscle and the vastus lateralis muscle, focal invasion at the level of the rectus femoris muscle (*arrow*) confirmed after resection

the skin [1, 138]. Addition of US to clinical examination improved correctness of the diagnosis to 97 % as calculated by Wortsman in a retrospective study in 4338 US examinations [138]. Overall diagnostic accuracy of US was 77 % in tumor and tumorlike lesions superficial to the investing fascia, with a high diagnostic accuracy in differentiating benign from malignant lesions (sensitivity and specificity of 94.1 % and 99.7 %, respectively) as calculated by Hung et al. in a retrospective study on 247 lesions [117]. US overall sensitivity was 99 %, specificity was 100 %, and statistical diagnostic certainty was 99 %. Highest specificity and sensitivity were described for lipoma (95.2 and 94.3 %, respectively), vascular malformation (73 and 97.7 %, respectively), epidermoid cyst (80 and 95 %, respectively), and nerve sheath tumor (68.8 and 95.2 %, respectively). These four tumor types comprised nearly three-quarters (73 %) of all lesions. A small minority of lesions, 4 %, at the subcutaneous tissue were malignant including metastasis (4/11),

lymphoma (3/11), malignant fibrous histiocytoma (1/11), Merkel cell carcinoma (1/11), and dermatofibrosarcoma protuberans (2/11). Previously the relatively low accuracy of US was attributed to the variable appearance of a given soft tissue tumor on US, e.g., cystic hygroma, skeletal muscle hemangioma, lipoma, and melanoma [15, 39, 80]. This is in contradistinction with Hung et al. who concluded that reduced observer awareness of specific tumor and tumorlike entities resulted in underdiagnosis rather than the poor specificity of US findings [117]. Indeed, increasing experience with US combined with relevant clinical information led to improvement of lesion characterization on the basis of their imaging characteristics and to recognize indeterminate lesions needing further diagnostic work-up (Figs. 1.2, 1.3 and 1.4).

US with CDUS criteria that suggest malignancy are nonhomogeneous echotexture and architectural distortion due to infiltration of adjacent structures with angiogenesis with variable caliber of tumor vessels (Fig. 1.1). Benign tumors are more often homogeneous and regularly delineated and cause displacement rather than invasion of adjacent structures [56, 87]. However, there is considerable overlap between these two groups. Benign tumors such as skeletal muscle vascular malformation (formerly known as hemangioma), neurofibroma, and schwannoma can present with features of poor delineation and nonhomogeneous echotexture, while sarcomas on the other hand often demonstrate sharply defined margins due to pseudo-capsule formation [28]. If these sarcomas are small in size at the time of detection, the tumor necrosis that would result in nonhomogeneity on US may not yet have occurred. Some lesions are, however, also characterized by their specific location, e.g., subungual glomus tumor and branchial cyst [45], adding to the specificity of the diagnosis. CDUS and spectral Doppler analysis of soft tissue tumors is of limited value when differentiating benign from malignant tumors. If a multitubular-organized vascular pattern is present, the tumor is more likely to be benign. Flow characteristics are not specific enough to be applicable in clinical practice [54]. Resistive indices cannot be used to distinguish benign from malignant musculoskeletal soft tissue masses [71].

Experience with the potential value of strain and shear wave elastography in soft tissue tumors is still preliminary [86]. The mean strain ratios in strain elastography of malignant tumors were significantly higher than the mean strain ratios of benign tumors. There was no significant

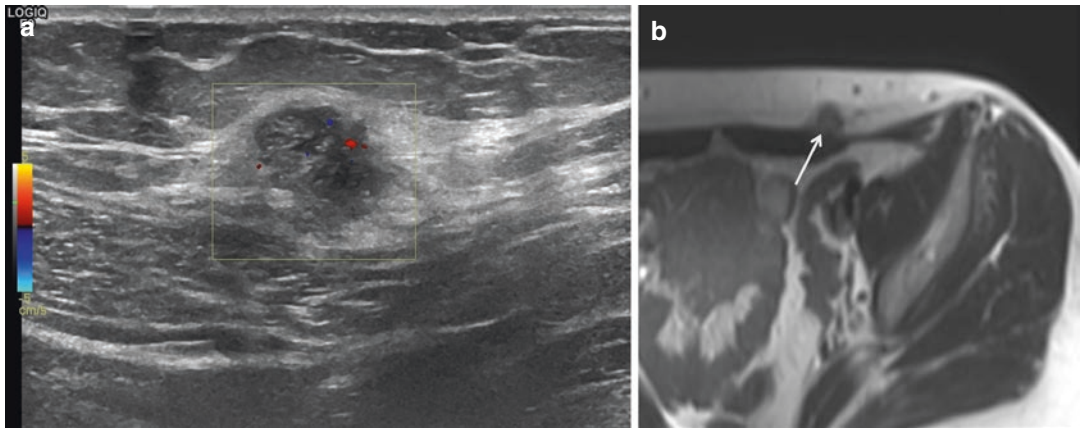

Fig. 1.2 Endometrioma at the abdominal wall in 40-year-old female patient with cyclic painful small mass at the left iliac fossa and previous history of laparoscopic surgery. (**a**) US examination demonstrating nonhomogeneous hypoechogenic small mass lesion demonstrating small vessels, irregular margins with infiltrative aspect in the subcutaneous tissue and at the rectus abdominis fascia. (**b**) MRI axial haste T2-WI with nonhomogeneous low to intermediate SI mass superficially located. Note also infiltration of the superficial muscle fascia of the rectus abdominis muscle

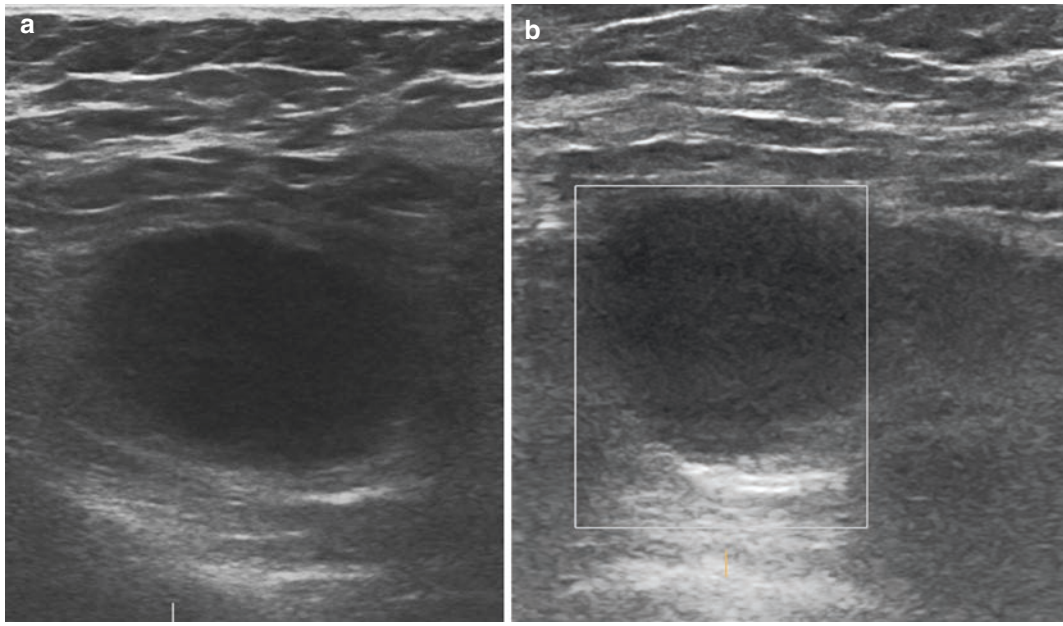

Fig. 1.3 Myxoma at the left gluteus maximus muscle in a 60-year-old female patient presenting with painless mass lesion. (**a**) US examination reveals homogeneous asonant round to oval mass lesion with sharp margins and acoustic retro-enhancement. Maximal diameter 3.5 cm. (**b**) The lesion is avascular on CDUS examination

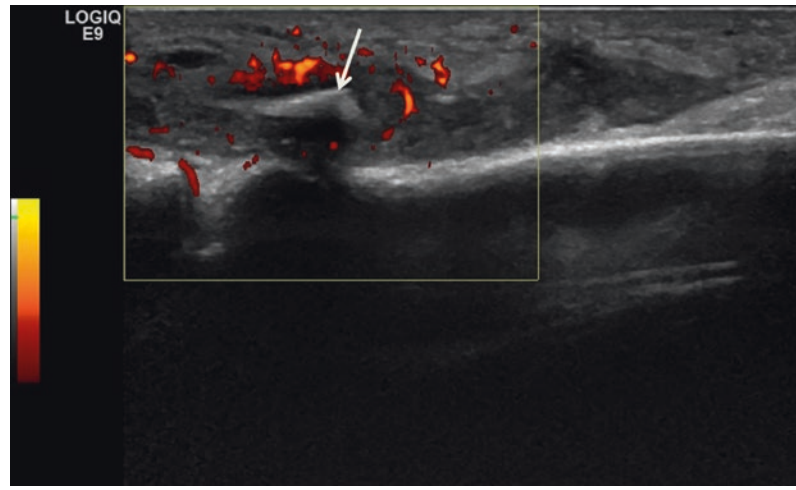

Fig. 1.4 Wood fragment at the subcutaneous tissue of the dorsum of the right foot surrounded with cellulitis area. US demonstrates reflective triangular wood fragment (*arrow*) surrounded with hyporeflective hypervascular tissue

difference for strain histograms and visual scoring. Strain ratios may be used as an additional tool in soft tissue tumor evaluation, possibly minimizing the number of biopsies [108]. Quantitatively and qualitatively, there is no statistically significant association between shear wave velocity and malignancy. Currently, there is no clear additional role compared to B-mode imaging [98].

The best practical approach is to use ultrasound as a tool for selection of those lesions that are confidently diagnosed as benign. To prevent delay in diagnosis, all indetermined lesions should be submitted to further diagnostic work-up by MRI and imaging-guided CNB in that order [16]. Ultrasonographically definite benign lesions are homogeneous cystic lesions with strong posterior enhancement and sharp margins that do not show

any vascular signal with CDUS (at highest sensitivity presets). Careful US examination combined with clinical correlation may suggest a specific diagnosis in the case of an epidermal inclusion cyst (Fig. 1.5), lipoma (Figs. 1.21 and 1.22), or, in the presence of a phlebolith, a skeletal muscle vascular malformation [87, 113]. Also in patients with an initial diagnosis of trauma with Morel-Lavallée, hematoma, or muscle tear, it is evident that an accurate history report is important. A hematoma does not arise spontaneously, except in patients with a coagulation disorder or treated with anticoagulation medication. Hematoma does not keep on growing and has the history of a direct or contusional trauma, mostly severe enough.

The trade-off for high-frequency, linear, musculoskeletal transducers is their limited depth of penetration and the small, static scan field. This is a disadvantage if the soft tissue swelling is large, localized deep in the flexor compartment of the calf, the proximal thigh, buttocks, or trunk or in case of obese patients. Extended field of view sonography (EFOVS) overcomes the disadvantage of a limited, standard field of view [131]. By generating a panoramic EFOVS image, size and anatomical spatial relationships of a soft tissue mass are better evaluated (Fig. 1.1a). EFOVS improves also communication of imaging findings to the referring clinician and contributes to increased reproducibility, which is important for follow-up of lesions [6, 26, 84, 132]. If EFOVS is unavailable, US is not the preferred imaging modality due to its lack of overview and penetration, and MRI should be used as examination of choice [5]. These characteristics of high-frequency transducer characteristics turn into benefits, however, when it comes to diagnosing very small lesions superficially located, lesions as is the case in the wrist, hand, and foot, and lesions of the skin and of peripheral neural origin.

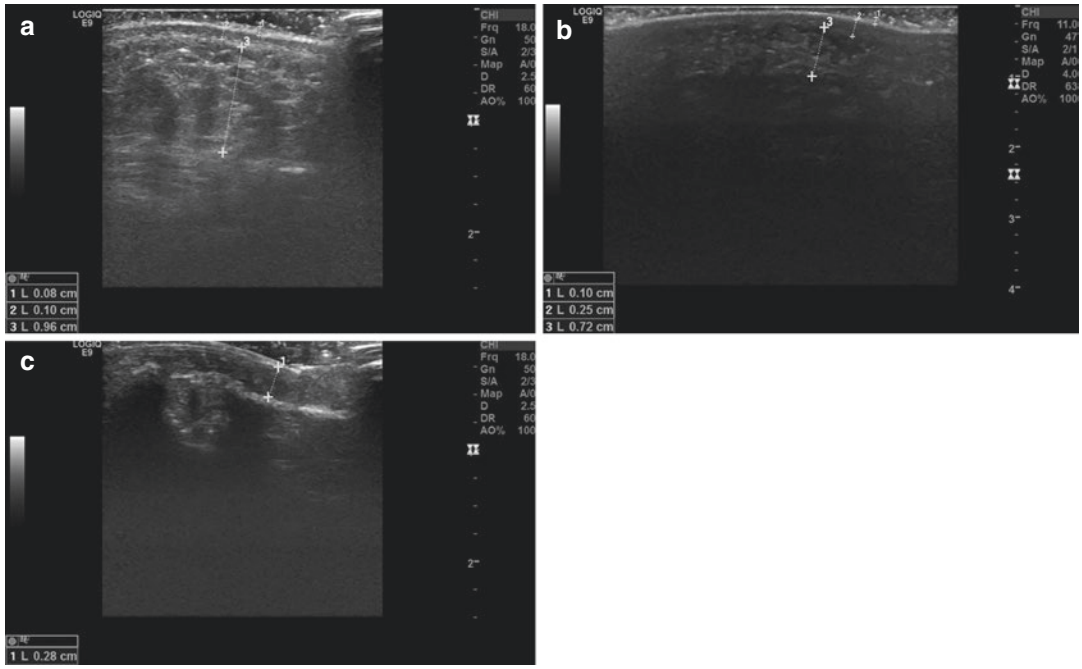

Fig. 1.5 US of the normal skin plantar area (**a**), heel (**b**), and nail bed first toe (**c**), high resolution with differentiation of the epidermis and dermis, for comparison 8–18 mHz 2-cm-wide linear probe and 6–15 mHz 5-cm-wide linear probe (GE healthcare Logic E9 with resp. ML 6–15 and L8-18i). (**a**) Plantar skin area at 18 mHz. Thin hyperreflective epidermis layer (1) with reflective dermal layer (2) and hyporeflective subcutaneous fat layer (3). (**b**) Heel area at 11 mHz. Thin hyperreflective epidermis layer (1) with reflective dermal layer (2) and hyporeflective subcutaneous fat layer (3). (**c**) Nail toe 1. At the nail bed, hypoechoic nail bed and matrix area (*arrows*) is covered with reflective nail superficially and reflective corticalis of the distal phalanx

The scanning plane can be easily adjusted to the complex local anatomy of the hand, wrist, and foot as was discussed [42, 64, 138].

Other applications of US in soft tissue tumor imaging are US-guided interventional procedures, staging and grading of dermatologic lesions. Diagnostic procedures and therapeutic interventions that are guided by US are gaining in popularity in the musculoskeletal imaging, following the already more established use of this technique in mammography and the abdominal-genitourinary field.

Percutaneous interventions range from ganglion aspiration (18–22 gauge), fine-needle aspiration biopsy (FNAB) in suspected carcinoma metastasis, local recurrence of a soft tissue sarcoma, core needle biopsy (CNB) of extra- and intra-articular solid soft tissue masses, and preoperative needle wire localization of nonpalpable solid soft tissue and vascular tumors to aspiration and culture sampling of a fluid collection, percutaneous catheter drainage of subperiosteal abscess, and muscle biopsy in neuromuscular disease [14, 15, 20, 22, 25, 85, 101, 109, 141]. The procedures can be performed after US selection of the approach (site, depth, and needle angulation) and subsequent skin marking, or better, under real-time US guidance [25, 141].

In screening for nonpalpable subcutaneous metastases of melanoma and cancers of the lung, breast, colorectum, stomach, or ovary and for melanoma recurrences, 7.5 MHz linear array transducers can dynamically screen a wide area of the body [1, 38], but this procedure will probably be replaced by FDG-PET scan as a whole-body staging procedure with an overall sensitivity and specificity of 89 and 96 % [102, 114]. CT is obsolete as it underestimates the number of lesions [101].

Ultrahigh resolution US (20–30 MHz) is being used in imaging of nodular and infiltrative epidermal and dermal lesions. The width of the field of view is 1.2 cm, and the depth of penetration only 1–2 cm.

US using frequencies of 15 MHz or more can clearly define the skin layer morphology including changes in the epidermal thickness [124]. Although epidermal lesions are visible, accurate clinical assessment of their depth of extension is not possible without ultrahigh-frequency (>=20 mHz) US. Ultrahigh-frequency US is a sensitive tool in lesion detection and delineation of the deep margin of skin lesions. In the majority of lesions, however, it cannot differentiate malignant from benign lesions and will not obviate further need for biopsy [39]. Even with these ultrahigh-frequency transducers, the normal epidermis cannot be visualized. Exceptions are the sole of the foot and the hypothenar area. Hypodermis can be visualized as a hyperechoic layer.

In the detection of local recurrences of soft tissue sarcoma, MRI and US appear to be equally sensitive. US, however, is the most cost-effective method in the detection of early local recurrences of soft tissue sarcomas and should therefore be used for initial routine follow-up and guided biopsies [4]. The presence of a non-elongated, hypoechoic mass is highly suspicious for local recurrence [23]. However, US may be inconclusive in the early postoperative period (3–6 months postoperatively), as inhomogeneous, hypoechoic masses may also represent hematoma, abscess, or granulation tissue (Fig. 1.4). US follow-up with comparison to a baseline study on MRI, both performed 4–6 weeks after surgery, can help to differentiate such cases. US-guided FNAB and/or CNB represents a possible alternative. MRI diagnosis of a soft tissue tumor recurrence in the immediate postoperative period or after irradiation can be extremely difficult due to the diffuse high signal intensity background in (fast) spin-echo T2-weighted images or post-contrast (fat-suppressed) spin-echo T1-weighted sequences. If the tumor recurs in poorly vascularized postoperative scar tissue, intravenous gadolinium administration may have little effect in terms of tumor enhancement and thereby increased conspicuousness [23, 67]. If scar tissue and recurrence cannot be differentiated, US-guided or CT-guided percutaneous biopsy should be considered [11, 23]. Under those circumstances the exam has prime prognostic and therapeutic value [141].

Obtaining an MR time slot may be a practical problem in most institutions if the imaging-guided biopsy has to be performed on short

notice. In a US- or CT-guided procedure, this problem does not exist. In addition, the technical staff is limited to US operator.

1.3 Superficial Soft Tissue Tumors and Tumorlike Lesions

Superficial soft tissue lesions are a distinct group of lesions in which US with CDUS has a more specific role improving the accuracy of the clinical diagnosis. Superficial soft tissue tumors can be classified into two categories: epidermal-dermal (or cutaneous) lesions and subcutaneous fat layer (or subcutaneous) lesions (Fig. 1.5a–c) (US of the normal skin and nail). The normal hyporeflective subcutaneous fat layer narrows with increasing external compression by the probe. Thickness of the dermis is variable, thin at the forearm and thick, as a result of high collagen content, in the lumbar region [138]. The subcutaneous fat layer is composed of hyposonant fat lobules interspersed with reflective fibrous septa (Fig. 1.5a–c). Cutaneous lesions include tumors originating from the skin appendages such as sweat glands, sebaceous glands, and hair follicles. Subcutaneous tumors include most mesenchymal tumors, but mesenchymal tumors can also occur in the dermal layer [8, 138].

Both cutaneous and subcutaneous tumors are mainly located in the subcutaneous fat layer rather than the dermis because the dermal layer is relatively strong and elastic compared with the subcutaneous fat layer. Benign cutaneous tumors include eccrine spiradenoma, chondroid syringoma, pilomatricoma, dermatofibroma, stump neuroma, schwannoma, and neurofibroma. Other benign tumors that may be located in the subcutaneous fat include vascular malformation, vascular leiomyoma, neurofibroma, schwannoma, lipoma, glomus tumor, and stump neuroma. Malignant cutaneous tumors include melanoma, metastasis, and lymphoma. Other malignant tumors that may be located in the subcutaneous fat are synovial sarcoma, lymphoma, and metastasis. Tumorlike lesions at the subcutaneous area consist of ganglion cysts, Langerhans histiocytosis, nodular fasciitis, rheumatoid nodule, fat necrosis, abscess, tumoral calcinosis, and epidermal inclusion cyst [51]. High-frequency US technique has been a valuable addition to the diagnosis. It allows a real-time view of the skin with discrimination of structures that measure ≥0.1 mm and provide highly useful information on the blood flow in the skin and its surroundings [138] (Table 1.1).

1.4 US Findings in Specific Soft Tissue Tumors and Tumorlike Lesions of the Extremities

1.4.1 Articular and Synovial Sheath Masses

1.4.1.1 Synovial Osteochondromatosis or Synovial Chondromatosis

The condition known as synovial osteochondromatosis or synovial chondromatosis is a metaplastic transformation of synovial cells into cartilage. These cartilaginous nodules often calcify and/or ossify as nodules of equal size. US is the imaging modality of choice when the disease is suggested by clinical examination or radiographs [24]. Both exclusively cartilaginous and calcified nodules can be identified by US (Figs. 1.6 and 1.7). Due to its dynamic scanning ability, US can, in joints that are in the range of US, also differentiate freely moving bodies from nodules embedded in the synovium. Nodules may form an acoustic shadow front if calcified [91, 97, 106]. Synovial osteochondromatosis or chondromatosis usually presents as a monoarticular disease. Rarely bursae and tendon sheaths undergo synovial metaplasia.

1.4.1.2 Tenosynovial Giant Cell Tumor (Pigmented Villonodular Synovitis (PVNS))

Pigmented villonodular synovitis (PVNS), also known as giant cell tumor when it affects the tendon sheath, is a benign inflammatory disorder resulting in diffuse or localized synovial hypertrophy.

Table 1.1 Most frequent mass lesions with frequency and relative frequency at the skin and subcutaneous tissue in the series of Wortsman [138]

Group	Frequency (%)	Specific diagnosis	Relative frequency (%)
Benign nonvascular tumors	46	Lymph node (enlarged)	31
		Lipoma	28
		Epidermoid cyst	23
		Pilomatricoma	6
Articular and periarticular lesions	17.5	Synovial ganglion cyst	60
		Bursitis	21
		Synovitis	19
Inflammatory and infectious lesions	15.5	Fat necrosis	51
		Fluid collections	19
		Fistulae	8
		Warts	8
		Hidradenitis suppurativa	6
Benign vascular tumors	9.2	Hemangioma (hamartoma)	65
		Vascular malformation	34
Nail lesions	5.5	Psoriasis	68
		Glomus tumor	12
		Granuloma	9
		Subungual exostosis	4
Exogenous skin components	3.5	Cosmetic cutaneous fillers	56
		Foreign bodies (glass, wood, thorns)	44
Malignant tumor	1.7	Basal cell carcinoma	55
		Squamous cell carcinoma	24
		Cutaneous metastasis	8
Vascular non-tumoral lesions	1.1	Mondor disease (sclerosing thrombophlebitis of subcutaneous vessels)	35
		Nonsclerosing vascular thrombosis	25
		Anatomic variants	40

In articular PVNS, US depicts hypoechoic synovial proliferation of variable thickness, affecting the entire synovial cavity or only a limited portion (Figs. 1.8 and 1.9). Lobulated soft tissue nodules may project from the synovium into a hypoechoic or anechoic joint effusion, as a result of debris or hemorrhage. Loculations of joint fluid may be created by the synovial infolding [70].

Rheumatoid arthritis, seronegative inflammatory arthritis, hemophilic arthropathy, and gout arthritis should be considered in the differential diagnosis of diffuse synovial hypertrophy on US [70].

PVNS of the tendon sheath is called giant cell tumor and is a common tumor at the hand.

US depicts it as a well-defined, occasionally slightly nonhomogeneous or lobular, hypoechoic, solid soft tissue mass, abutting or eccentrically enveloping the tendon [4, 11, 60, 72] (Fig. 1.10).

1.4.1.3 Amyloidosis

β_2-Amyloid arthropathy occurs in patients undergoing long-standing hemodialysis (more than 5 years) with the cuprophane membranes and in patients with multiple myeloma. The cuprophane membranes' related condition is prone to extinction as these membranes are no longer used. Amyloid arthropathy may involve every joint in a systemic way. Articular deposits are characterized by thickening of the

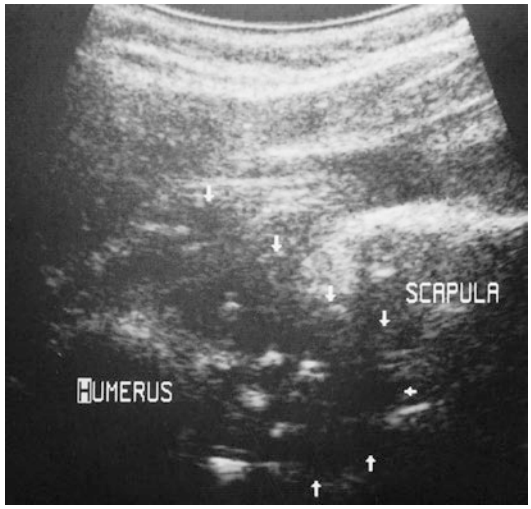

Fig. 1.6 Synovial osteochondromatosis of the left shoulder joint in a 20-year-old woman. Transverse US image of the posterior, caudal aspect of the left shoulder (5 MHz curvilinear transducer). Marked distention of axillary recess (outlined by *small arrows*), filled with synovial proliferation. Embedded are multiple, equal-sized cartilaginous bodies. Synovial proliferation was also noted in the infraspinatus recess and biceps tendon sheath (not shown). The biceps tendon sheath contained multiple, partially calcified, metaplastic nodules. The patient was treated by synovectomy

synovium, and subchondral articular intraosseous amyloid deposits are demonstrated with increasing number and diameter over time and described as growing bone cysts [50]. The US parameters of shoulder amyloid arthropathy are enlargement of the rotator cuff tendons (supraspinatus tendon larger than 8 mm in thickness, its normal range being 4–8 mm), focal intratendinous areas of increased echogenicity, distention of the glenohumeral joint space, the synovial tendon sheath of the long head of the biceps and the subacromial-subdeltoid bursa, irregularity of the humeral head, and abnormal fluid collections around the joint [46] (Figs. 1.10 and 1.11).

The capsular and articular or bursal synovial amyloid deposits have a slightly heterogeneous hypoechoic echotexture.

The US findings of a maximal rotator cuff thickness greater than 8 mm or the presence of hypoechoic pads between the muscle layers of the rotator cuff has a 72–79 % sensitivity and 97–100 % specificity for amyloidosis, in the setting of long-standing hemodialysis [19, 46, 72, 89].

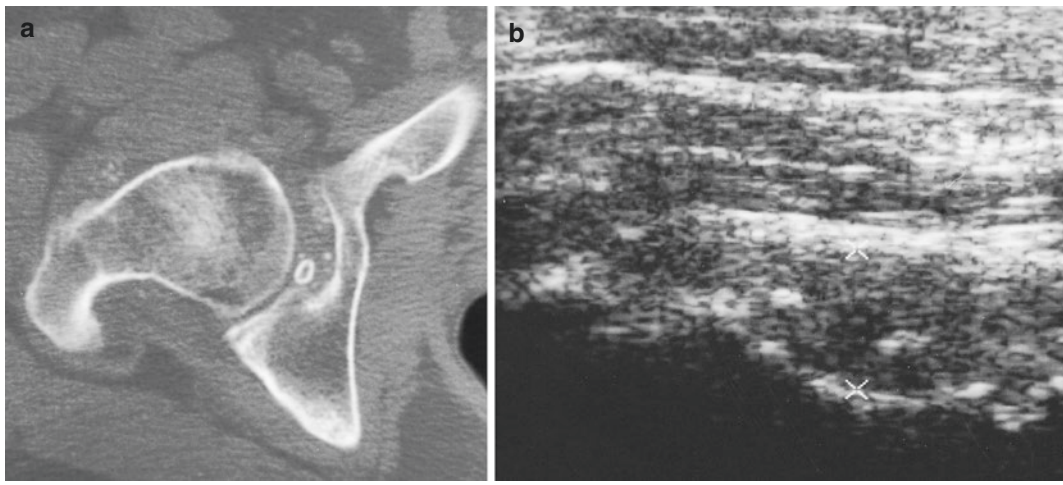

Fig. 1.7 (**a**, **b**) Synovial osteochondromatosis of right hip joint in a 40-year-old white man with a 2 year history of right hip pain. (**a**) Axial CT scan section at tip of greater trochanter; bone window setting. (**b**) Longitudinal, anterior US image. One, larger, peripherally calcified nodule and numerous small, faintly calcified nodules can be identified, predominantly in the medial and anterior joint space (**a**) Marked distention of the anterior hip joint space (**b**) (between calipers). Intra-articular synovial proliferation; two embedded metaplastic nodules. The most proximal, calcified nodule demonstrates posterior acoustic shadowing

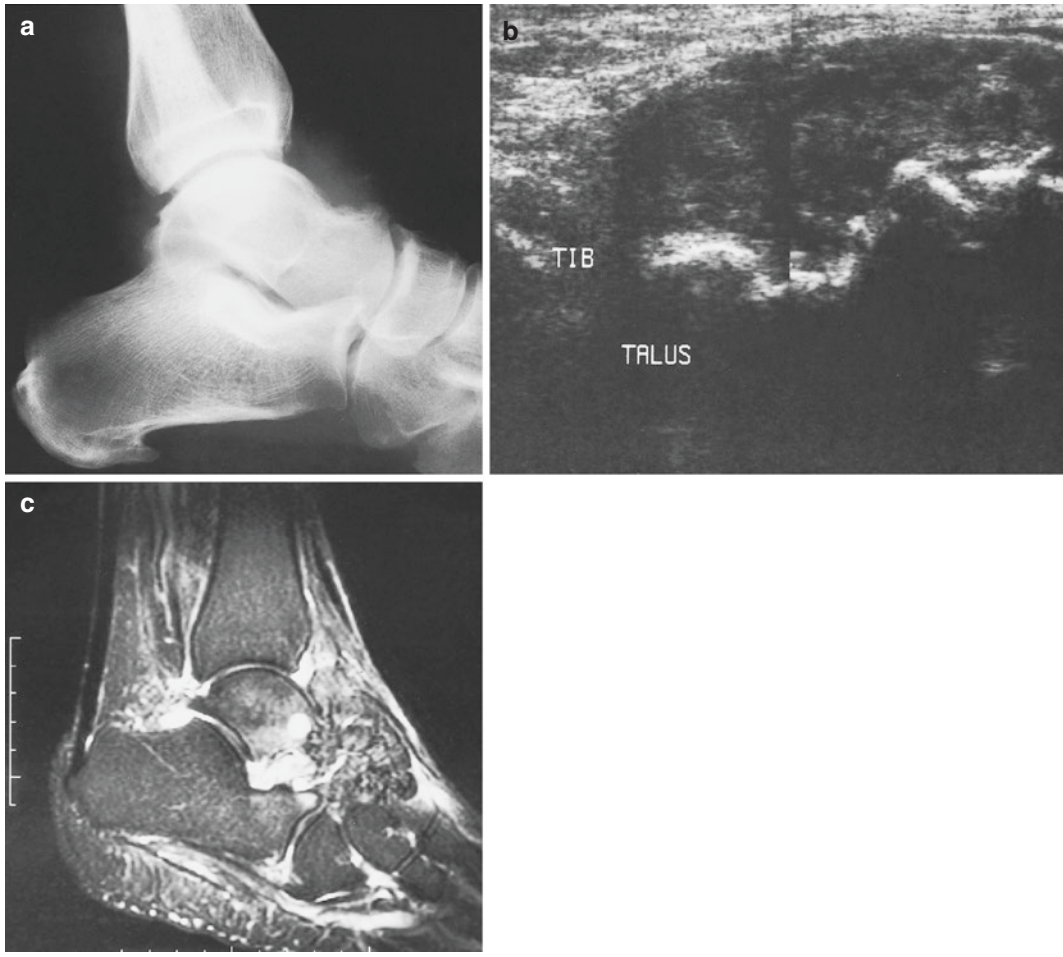

Fig. 1.8 (**a**, **b**) Pigmented villonodular synovitis (PVNS) involving the left talocalcaneonavicular joint in a 47-year-old man. (**a**) Lateral radiograph. (**b**) Longitudinal US image of dorsum of hind foot. (**c**) Sagittal gradient-echo T2-weighted MR image. Radiograph shows dense soft tissue mass along the dorsal aspect of talus and navicular which contains a single calcification. (**a**) Well-defined, inhomogeneous, but predominantly hypoechoic solid soft tissue mass. Minute anechoic foci and small hyperechoic areas are also present. (**b**) Note secondary pressure erosion of the talar neck. The low signal intensity hemosiderin-laden soft tissue mass involves the talonavicular and communicating anterior and middle subtalar joint (**c**)

1.4.2 Peripheral Neurogenic Tumors

Large peripheral nerves of the extremities, such as the sciatic, popliteal, ulnar, and median nerves, can be routinely identified by high- and ultrahigh-resolution real-time US [16, 36, 52, 60, 80]. In a high-frequency US examination, also smaller superficial peripheral normal nerves can be identified as a hyperechoic, fascicular soft tissue structure in its course between muscle bellies and at the subcutaneous tissue (sural nerve) [22]. The configuration is concentric or oval in transverse section and tubular on longitudinal view. The nerve roots of the brachial plexus are homogeneous hyporeflective, whereas the peripheral nerves show on ultrahigh-frequency transducers an alternating pattern of hypo- and hyperechogenicity. The parallel-oriented, but discontinuous, linear, hypoechoic areas represent coalescing bundles of neuronal fascicles, embedded in a hyperechoic background of connective tissue, called

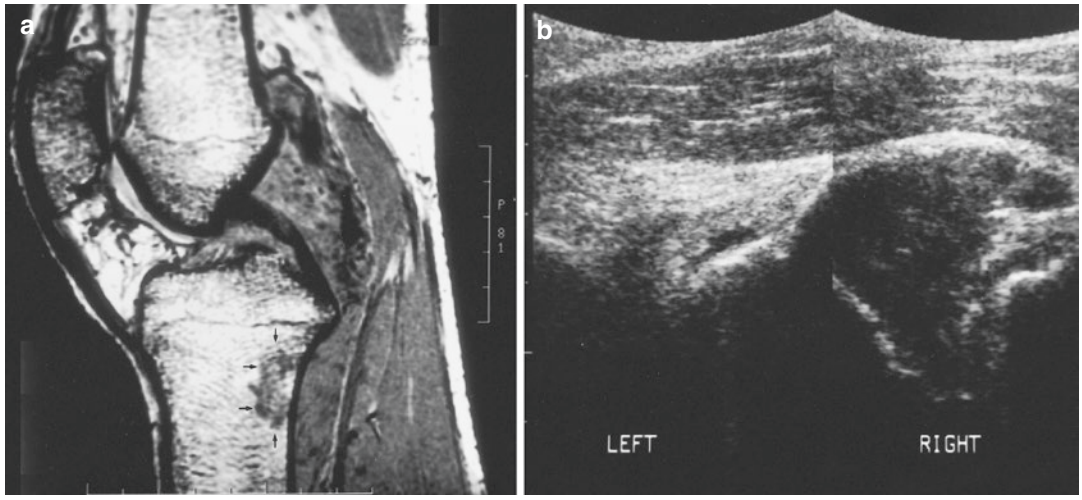

Fig. 1.9 (**a**, **b**) Bifocal pigmented villonodular synovitis of the right knee. (**a**) Sagittal gradient-echo MR image. (**b**) Longitudinal US image; split screen comparison view of dorsal femorotibial joint space. Marked distention of posterior femorotibial joint space, filled with soft tissue mass of intermediate signal intensity. (**a**) Multiple foci of low signal intensity are present both in the deep and superficial dorsal aspect of the mass. Intraosseous tumor extension in the dorsolateral aspect of the tibial proximal metaphysis (**a**, *arrows*) is noted as well. The symptomatic right side (**b**) shows a slightly inhomogeneous, predominantly hypoechoic synovial soft tissue mass, enveloping the posterior cruciate ligament insertion. The mass displaces the posterior capsule. A second tumor focus was localized in the medial aspect of the suprapatellar pouch and was biopsied

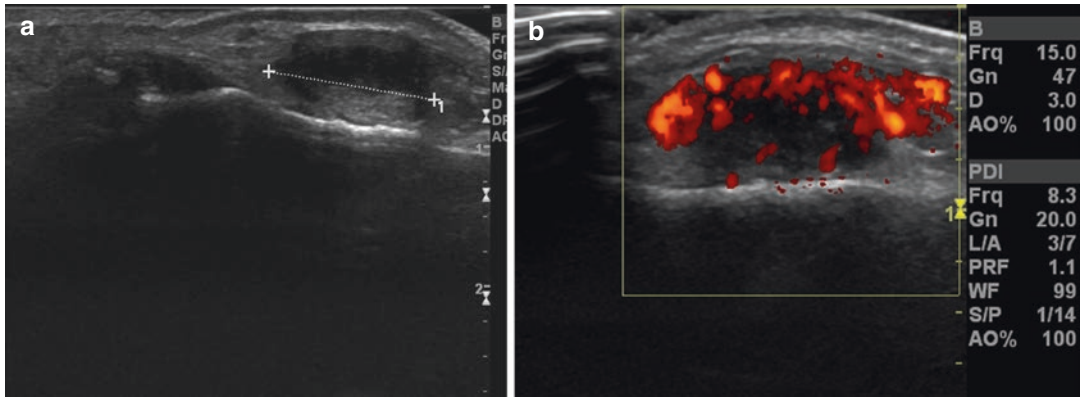

Fig. 1.10 Giant cell tumor of tendon sheath at the lateral volar aspect of the proximal phalanx of the middle finger in a 44-year-old male patient. (**a**) Longitudinal US view demonstrating oval mass lesion at the subcutaneous tissue, lateral adjacent to the flexor tendons, superficial part is hyporeflective, deeper part is more reflective. (**b**) Longitudinal CDUS demonstrating marked vascular signal at the superficial hyporeflective part

endo-, peri-, and epineurium. US underestimates the number of neuronal fascicles, when compared with histological sections. Presumed explanations are the undulating neural course and its resultant obliquity and lateral deformation. With the use of lower US frequencies, the hypoechoic areas within the nerve become less defined and less numerous as a result of degradation in image resolution [80].

The nerve remains immobile in comparison to its surrounding musculotendinous structures during (passive or active) dynamic examination. This is best visualized on longitudinal view. A slight nerve translation on longitudinal view is depicted at the

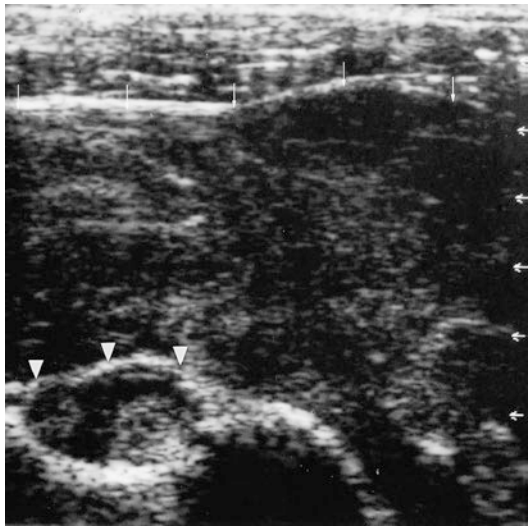

Fig. 1.11 Symmetrical amyloid shoulder arthropathy in multiple myeloma patient. Transverse US image of the anterior aspect of the shoulder. Marked distention of the subacromial-subdeltoid bursa (*arrows*) and the synovial tendon sheath of the long head of the biceps, causing anterior displacement of the transverse ligament (*arrowheads*). Mixed predominantly hypoechoic and faintly hyperechoic synovial amyloid deposits

level of the forearm nerves while the head is bended to the contralateral side. Normal nerves are flattened out by transducer compression in transverse view.

Of key importance in the diagnosis of a peripheral neurogenic tumor is the recognition of the location along the peripheral nerve course.

1.4.2.1 Peripheral Nerve Sheath Tumors

Tumors of peripheral nerves are rare, usually benign, and subcutaneous in location. US reports have documented schwannoma, neurofibroma, and neural fibrolipoma (formerly called fibrolipohamartoma) [9, 11, 21, 29, 59, 62, 64, 77, 78] (Fig. 1.12). In the series of Hung et al., nerve sheath tumors were the third most frequent diagnosis superficial to the investing fascia (16/247) with a US diagnostic sensitivity and specificity of 68.8 and 95.2 %, respectively [1]. With the exception of intraneural ganglion and neural fibrolipoma, all these nerve-related tumors and tumorlike lesions were hypoechoic masses [16, 21, 29, 35, 59, 60, 62, 77, 78]. A plexiform neurofibroma was reported as an almost echo-free mass with poor back wall enhancement [105] (Fig. 1.13). The majority of reported schwannomas and two neurofibromas, both of them in von Recklinghausen's disease, showed posterior acoustic enhancement [16, 21, 62] (Fig. 1.14). A tarsal malignant peripheral nerve sheath tumor (MPNST), arising at the site of multiple, postsurgical in situ recurrences of an initial schwannoma, showed poor delineation, homogeneous hypoechogenicity, and some dorsal acoustic enhancement.

Schwannomas and neurofibromas may show poorly defined contours [59, 64]. Some schwannomas and neurofibromas show intratumoral nonhomogeneity [94] (Fig. 1.14). The majority of reported schwannomas are well defined, the majority of neurofibromas poorly defined.

1.4.2.2 Nerve-Related Tumorlike Lesions

Intraneural ganglion is a cystic, glue-like mass containing fluid and lined with collagen within the epineurium that may cause pain and motor dysfunction due to compression [77, 78]. These are nonneoplastic cysts caused by the accumulation of thick mucinous fluid through a connecting branch with a neighboring joint with growth within the epineurium of peripheral nerves [123]. Histological examination shows nerve fibers dispersed within the mucinous substance of the cyst.

Intraneural ganglia are well known at periarticular sites. Most frequently the peroneal nerve is involved, with drop foot at presentation. US shows a spindle-shaped anechoic soft tissue structure within or abutting the nerve course [77, 78].

These ganglia are common along the course of the suprascapular nerve in the shoulder [57, 120, 126, 127]. They invariably cause infraspinatus weakness and in some cases supraspinatus weakness as well.

Other locations are the tibial nerve, ulnar nerve, sural nerve, and sciatic nerve [99]. US-guided aspiration and injection of corticosteroid of intraneural ganglia is recently described as an alternative to surgical decompression that is the standard of care [83]. In the last 4000 shoulder US studies we conducted,

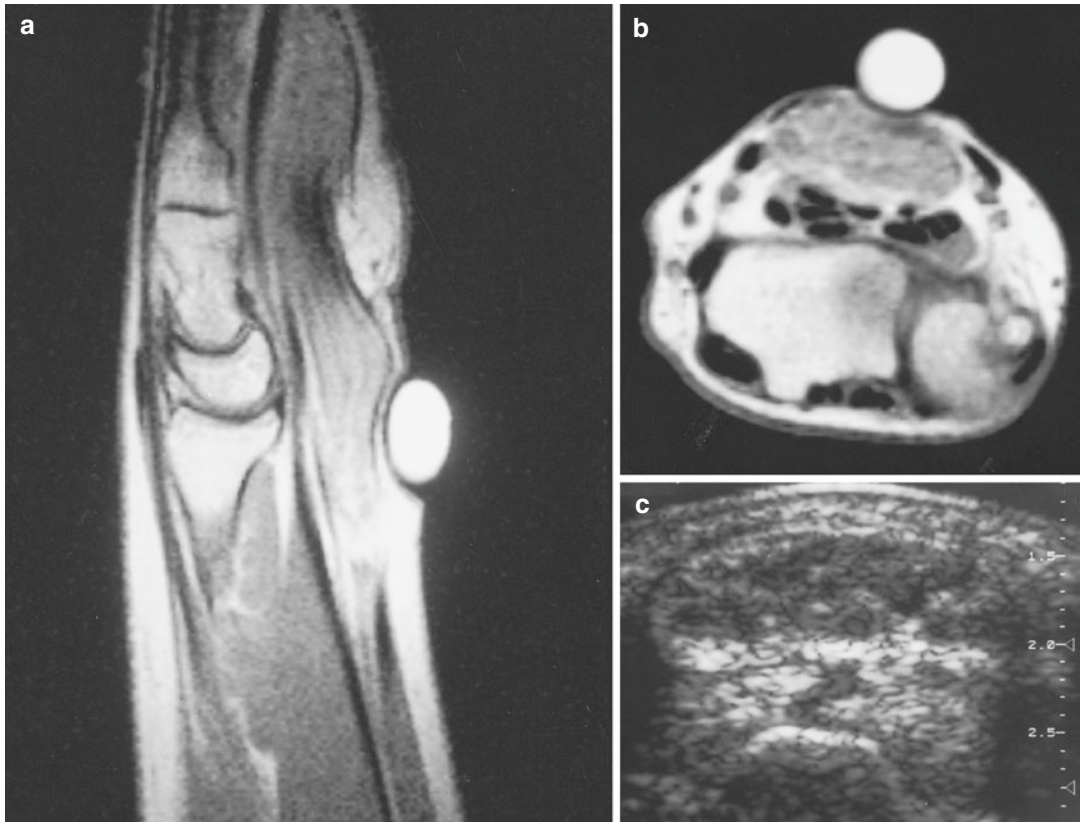

Fig. 1.12 (**a**–**c**) Long-standing fibrolipohamartoma of median nerve (MN) in a 54-year-old woman. (**a**) Sagittal spin-echo T1-weighted MR image of the wrist. (**b**) Axial SE T1-weighted MR image proximal to the carpal tunnel. (**c**) Transverse US image of carpal tunnel. Enlargement of the median nerve in the distal forearm (**b**), carpal tunnel (**c**), and metacarpus. (**a**) The enlarged median nerve contains dot-like thickened neuronal fascicles and some fatty tissue, especially in its deep aspect (**b** and **c**). The thickened bundles of neuronal fascicles are of intermediate signal intensity in (**a** and **b**) and hypoechoic in (**c**)

we recognized this entity in five cases. Two of them were cured by repetitive aspiration under US guidance.

In a reported tuberculoid leprosy of the external popliteal nerve [35], the well-defined hypoechoic mass proved surgically to be a caseous pouch. Within it, the thickened sheath of the enlarged lateral popliteal nerve could be identified as two parallel linear hyperreflectivities on longitudinal view.

Traumatic neuromas occur in postsurgical, postamputation, or posttraumatic patients [11, 16, 64]. Traumatic friction or irritation of a nondisrupted nerve trunk as well as partial or complete transection of the nerve may induce this failed repair mechanism [119]. A traumatic neuroma usually presents as an ill-defined, hypoechoic mass. These neuromas in traumatic complete neurotmesis or amputation are located at the proximal end of the cutted nerve and are called end-neuroma (Fig. 1.15). Sidebulb neuromas are typically formed in incomplete nerve lesion or axonotmesis.

Morton's neuroma is no real neuroma but represents focal perineural fibrosis involving a plantar digital nerve [82, 103, 104]. It occurs in between the metatarsal heads and is quite common. Most commonly affected is the digital nerve of the third web space, followed in decreasing order of frequency by web spaces two, one, and four. Neuroma can be solitary or can simultaneously involve multiple web spaces. Bilateral

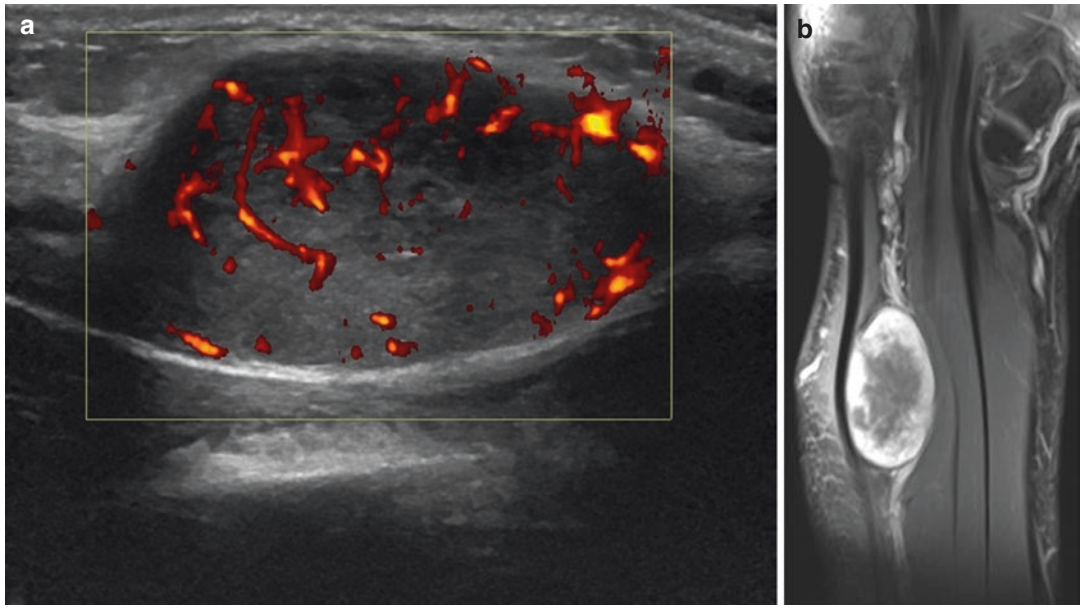

Fig. 1.13 Schwannoma (ancient) of the right median nerve at the forearm in a 45-year-old male patient. Painless firm mass lesion at the flexor side of the forearm. (**a**) Longitudinal US with CDUS demonstrates an oval mass lesion with nonhomogeneous hyporeflective aspect and sharp margins along the course of the median nerve. The median nerve is clearly demonstrated entering and leaving the lesion. Maximal diameter of the lesion is 4 cm. CDUS shows multiple intralesional vascularization with nonhomogeneous distribution. (**b**) Coronal SE T1-WI MRI after IV gadolinium administration reveals nonhomogeneous enhancement of the lesion

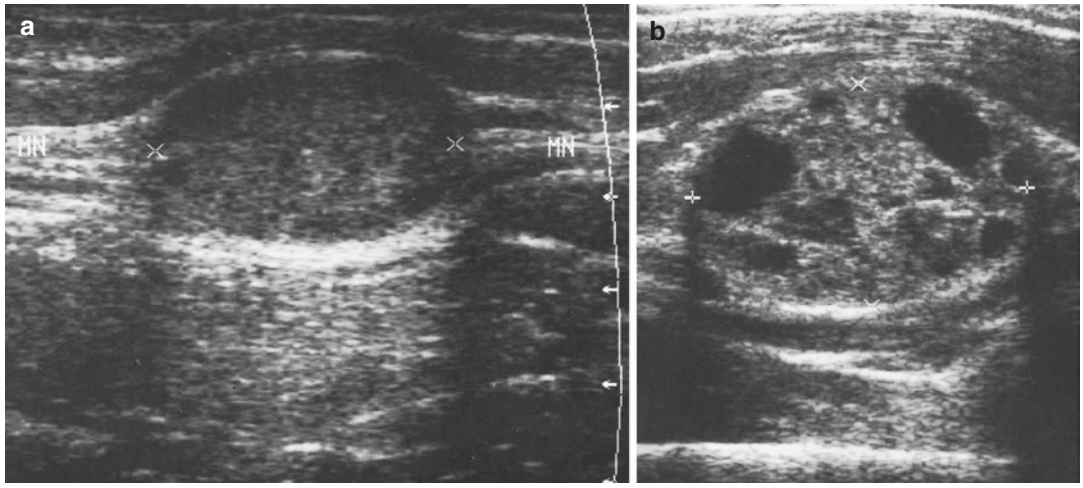

Fig. 1.14 (**a**, **b**) Schwannoma of median nerve in forearm. (**a**) Longitudinal linear 5 MHz US image. (**b**) Longitudinal linear 7.5 MHz US image. The median nerve (MN) courses in and out of the well-defined hypoechoic nerve sheath tumor (**a**) The internal echotexture of the tumor drastically changes when the 7.5 MHz transducer is applied (**b**)

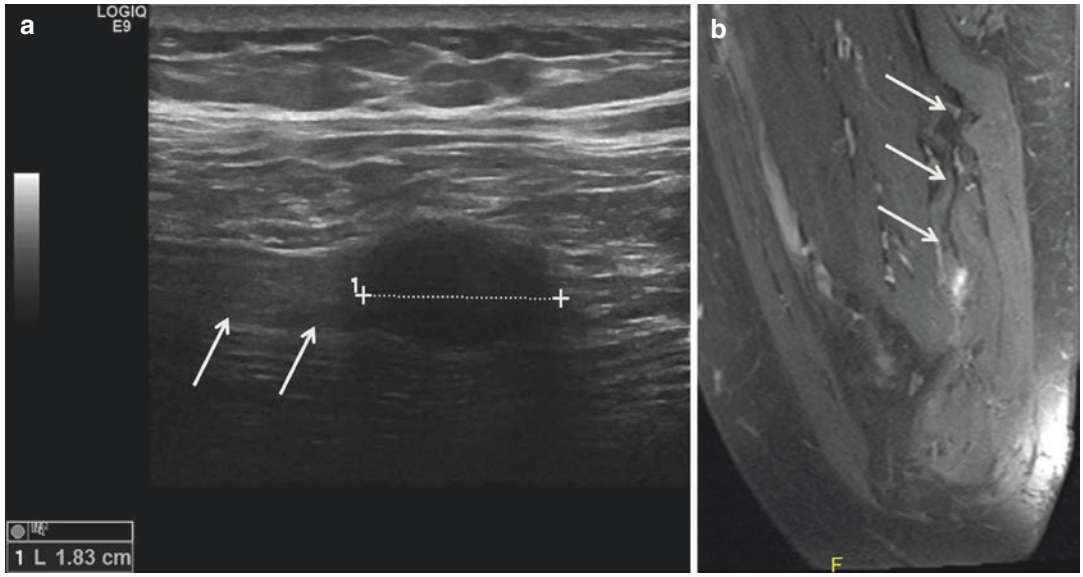

Fig. 1.15 Amputation neuroma at the distal stump of the left sciatic nerve in a 35-year-old male patient, amputation above the knee related to trauma. (**a**) Sagittal US image at the posterior aspect of the thigh demonstrates a hypoechoic oval mass at the end of the sciatic nerve (*arrows*). (**b**) Sagittal TSE T1-WI FS image after intravenous gadolinium contrast administration, partially enhancing mass at the end of the tortuous sciatic nerve (*arrows*)

lesions may also occur. The neuroma is at least 5 mm in size in the majority of cases (95%). If greater than 20 mm in length, the interdigital mass is suspicious for an abnormality other than neuroma, such as a ganglion cyst, a synovial cyst, or a giant cell tumor (GCT) from an adjacent tendon sheath [63].

Middle-aged women are most commonly affected, and they typically complain of pain and numbness in the forefoot, elicited by ambulation and mediolateral compression of the forefoot, when narrow-toed shoes are worn. The normal plantar nerve is only sonographically detectable with high-resolution US. In the presence of a neuroma, US can identify on longitudinal views the plantar digital nerve coursing into the pseudotumoral mass. The abnormal, possibly edematous, nerve is linear, 2–3 mm thick, and hypoechoic; its demonstration in continuity with the interdigital mass improves diagnostic confidence. Morton's neuroma is a predominantly well-defined but occasionally poorly defined soft tissue structure. Majority are hypoechoic masses, and minority demonstrate a mixed echopattern or anechogenicity (Fig. 1.16). They present poorly or not vascularized on power color Doppler. A plantar transducer approach is preferred with imaging in both the longitudinal and transverse plane. The correct transverse section should visualize the hypoechoic rim of cartilage covering the corresponding metatarsal heads.

Extreme flexion of the toes in the direction opposite the transducer or the Mulder maneuver (mediolateral compression of the forefoot and manual digital plantar displacement of the soft tissues in the examined web space with the transducer applied to the sole of the foot) help in rendering the neuroma more superficial and allow it to be better appreciated [63, 82].

In case of major callus at the foot sole, longitudinal dorsal interdigital view may demonstrate the neuroma. In this approach plantar active pressure between the metatarsal heads to decrease the distance between the lesion and the probe is needed.

Before surgical resection confirmation of diagnosis and/or minimal invasive US-guided intervention or treatment with local anesthetics, corticosteroid injection, cryoneurolysis, or even alcoholization is used [5, 46, 129, 140].

1.4.3 Pericytic (Perivascular) Tumors

1.4.3.1 Glomus Tumor

Glomus tumors (GTs) are small but extremely painful skin tumors of mesenchymal origin. Glomus tumors originate from the neuromyoarterial glomus bodies and have a homogeneous, markedly hypoechoic, or even sonolucent echotexture (Fig. 1.17). Predilection site is the fingertip, although the tumor may occur everywhere. In the distal finger, the subungual space is more affected than the pulpar soft tissues [4].

Average lesion size is 6 mm, and lesions as small as 2 mm can be detected.

Therefore, US investigation with at least a linear array 10 MHz transducer is recommended. Although exquisitely tender to palpation, most lesions are not palpable as such.

Glomus tumor may have a flattened configuration when subungually localized and in that case may present as a less conspicuous, thickened hypoechoic subungual space. The normal subungual space is only 1–2 mm thick. If localized lateral to the nail bed or in the palmar digital soft tissues, it assumes an ellipsoid or concentric shape [37, 41]. These lesions show marked (power) Doppler vascular signal that equals vascular signal of the normal nail bed (Fig. 1.18). Differential diagnosis of a thickened hypoechoic subungual space should include angioma and mucoid cyst. Epidermoid inclusion cysts can also present as small, concentric, hypoechoic solid soft tissue mass underlying the nail matrix but show no marked Doppler activity [4, 43].

Glomus tumors located outside the hand region are rare, and the diagnosis is often difficult due to their low incidence. These skin lesions have diameters between 0.5 and 2 cm, and similar US and CDUS characteristics compared to the subungual lesions are described.

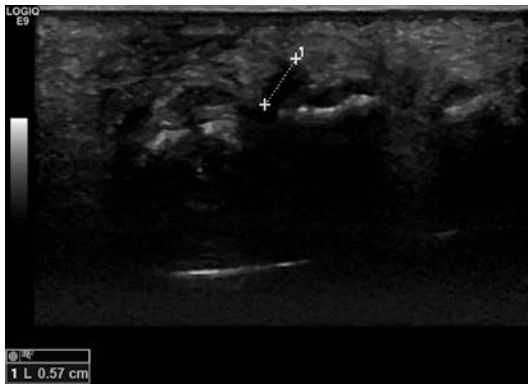

Fig. 1.16 Morton's neuroma located at the second (*left image*) and third (*right image*) web space of the left foot in a 60-year-old female patient. US examination with plantar approach and transverse imaging plane during lateral compression of the metatarsal heads demonstrating a small hyposonant lesions. While compressing the metatarsal heads, the lesion jumps to the plantar aspect of the foot, diameter 7 mm (*right image*) and 6 mm (*left image*)

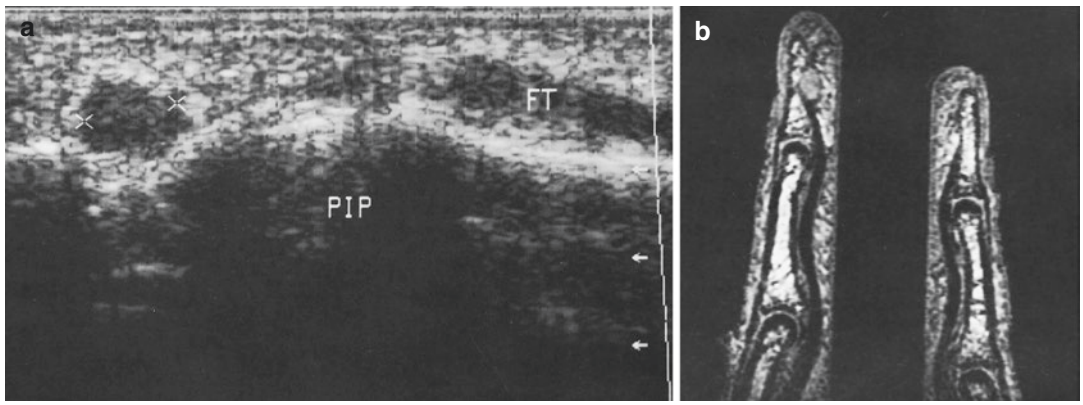

Fig. 1.17 (**a**, **b**) Glomus tumor of the distal phalanx of digit 3. (**a**) Longitudinal US image. (**b**) Sagittal gradient-echo MR image. US identifies the 5 mm hypoechoic nodule (**a**, between calipers) along the palmar aspect of the tuft (FT). MRI depicts intermediate signal intensity tumor (**b**) causing pressure erosion of the underlying cortex

Glomus tumor should be kept in mind in the differential diagnosis of all very painful subcutaneous lesions especially for those with purple reflection on the skin surface and major intralesional CDUS signal [81, 128].

1.4.3.2 Angioleiomyoma (Vascular Leiomyoma or Angiomyoma)

Angioleiomyoma is a less common benign tumor originating from the smooth muscle of arterial or venous walls. All lesions are well defined, solid, and hypoechoic with a moderate degree of organized vascularity on CDUS [26, 51].

1.4.4 Vascular Tumors

Vascular tumors consist of a heterogeneous group of soft tissue lesions. Because different classification systems are used in clinical practice, the terminology of these lesions is often confusing. For further in-depth discussion, we refer to Chap. 16 of this book. This section will be restricted to features which are relevant to the ultrasound operator.

Subcutaneous vascular malformations In the series of Hung et al., vascular malformations were the second most frequent diagnosis superficial to the investing fascia (30/247) with a US diagnostic sensitivity and specificity of 80 and 95.4 %, respectively [1]. Subcutaneous hemangiomas usually present as hypoechoic soft tissue masses. Fornage has, however, reported two hyperechoic angiomas [41] (Figs. 1.19 and 1.20).

Hemangioma of skeletal muscle and subcutaneous tissue Hemangiomas are relatively common congenital vascular hamartomas and represent less than 1 % of all vascular malformations. Patients are usually children, teenagers, or young adults, presenting with either a palpable, painful soft tissue mass or ill-defined muscular pain. The predilection site of skeletal muscle hemangiomas is the lower extremity [90]. The added value of US over characteristic clinical presentation in subcutaneous hemangiomas is limited.

A US examination readily detects the intramuscular soft tissue mass which is well defined in the majority of cases but may have an ominous ill-defined and irregular margin. There is no specific echo pattern; the majority of the reported muscle vascular malformations appear as homogeneous hyperechoic masses. However, both homogeneous hypoechoic lesions and mixed masses (Fig. 1.12) have been reported.

US should not be the modality of choice to identify subtle intralesional phleboliths but can readily appreciate them if they are large enough [32, 53] (Fig. 1.21). They are specific but, however, are only present in 25 % of cases.

Pressure erosion of underlying cortical bone can be visualized. One reported skeletal muscle high-flow vascular malformation (arteriovenous hemangioma) exhibited increased color flow and

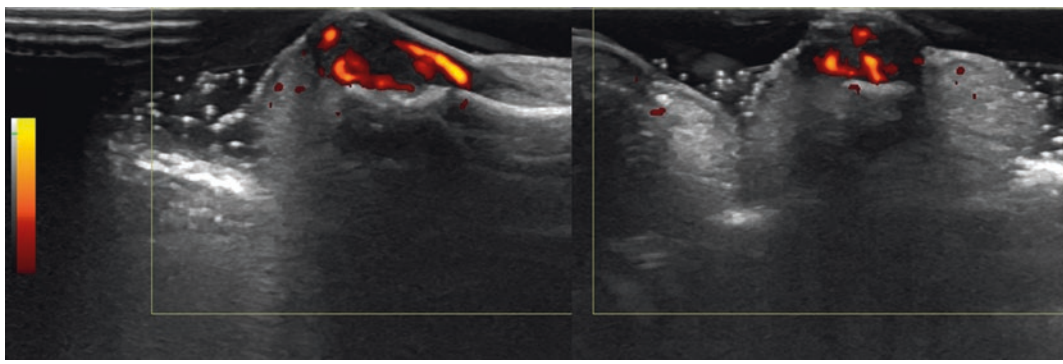

Fig. 1.18 Subungual glomus tumor at the left annular finger in a 50-year-old female patient. US (*right longitudinal and left transverse views*) demonstrates small mass lesion with marked CDUS activity. Thickening of the distal subungual tissue with maximal diameter 1.3 cm, elevation of the nail and erosion of the distal phalanx

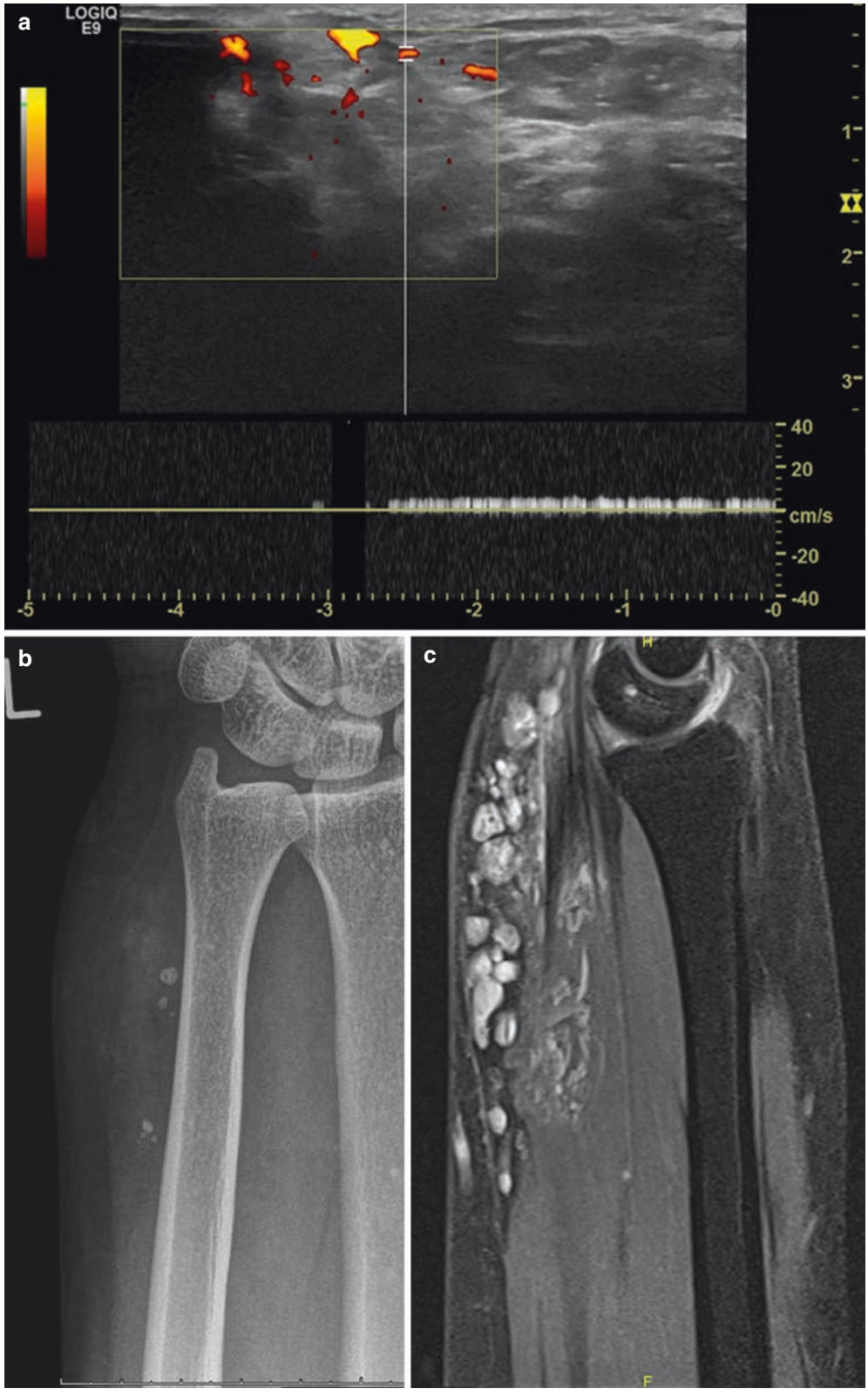
a
LOGIQ
E9
1
2
3
40
20
cm/s
-20
-40
-5
-4
-3
-2
-1
-0
b
c

low resistance arterial Doppler signal [53]. Venous, cavernous, capillary, and mixed hemangioma usually do not show any color or duplex Doppler signal due to the slow blood flow within the lesion.

Preliminary experience with sonographically guided percutaneous injection of 1 % polidocanol for sclerosis of peripheral vascular lesions show that it is simple, effective, and safe. This technique is especially effective in cases of soft tissue venous malformation and lymphangioma [68].

Lymphangioma(cystichygroma) Lymphangiomas (cystic hygromas) are developmental benign tumors that are rare and result from a regional block in lymphatic drainage. Predilection site is the neck, although they can occur everywhere. Fifty percent of them are present at birth, and the majority are discovered by 2 years of age. Usually they are slow-growing, painless soft tissue masses; in other instances, rapid growth may occur due to intralesional hemorrhage or infection. These tumors are usually isolated findings but can also be part of a syndrome.

Cystic hygroma is one of the three histological subtypes of lymphangioma, capillary or simple lymphangioma and cavernous lymphangioma being the other two. The three subtypes will often coexist within the same lesion. Cystic hygroma has a variable appearance on US [76, 115]. It may present as a multiloculated, predominantly anechoic mass with through transmission and internal linear septations, which can vary in thickness (Fig. 1.22). Cystic hygroma may also contain solid components arising from the cyst wall or septa, which pathologically correspond to

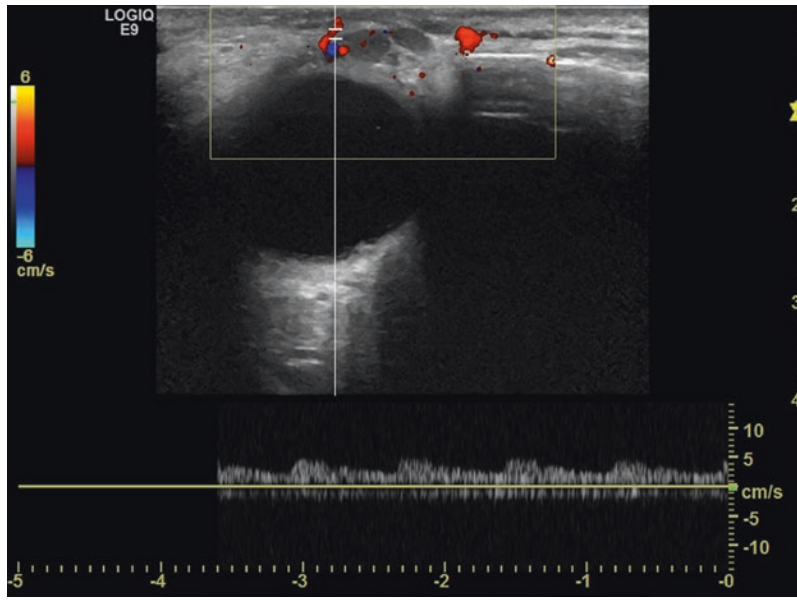

Fig. 1.20 Low flow vascular malformation located at the left superior eyelid in a 50-year-old male patient. CDUS demonstrating serpiginous vascular structures with Doppler activity with venous flow

Fig. 1.19 A 47-year-old female patient with vascular malformation presenting as a long-standing painless mass at the left distal forearm, volar-ulnar aspect. Discoloration of the skin was present. (**a**) CDUS demonstrating multiple tubular structures with serpiginous distribution at the subcutaneous tissue and with extension into the muscular compartment, indistinct borders with infiltrative aspect. Venous Doppler activity in the lesion. (**b**) Radiograph, PA view of the left wrist, demonstrating multiple phleboliths. (**c**) Coronal T1-WI with FS after intravenous administration of gadolinium. Marked enhancement within a multitubular vascular malformation

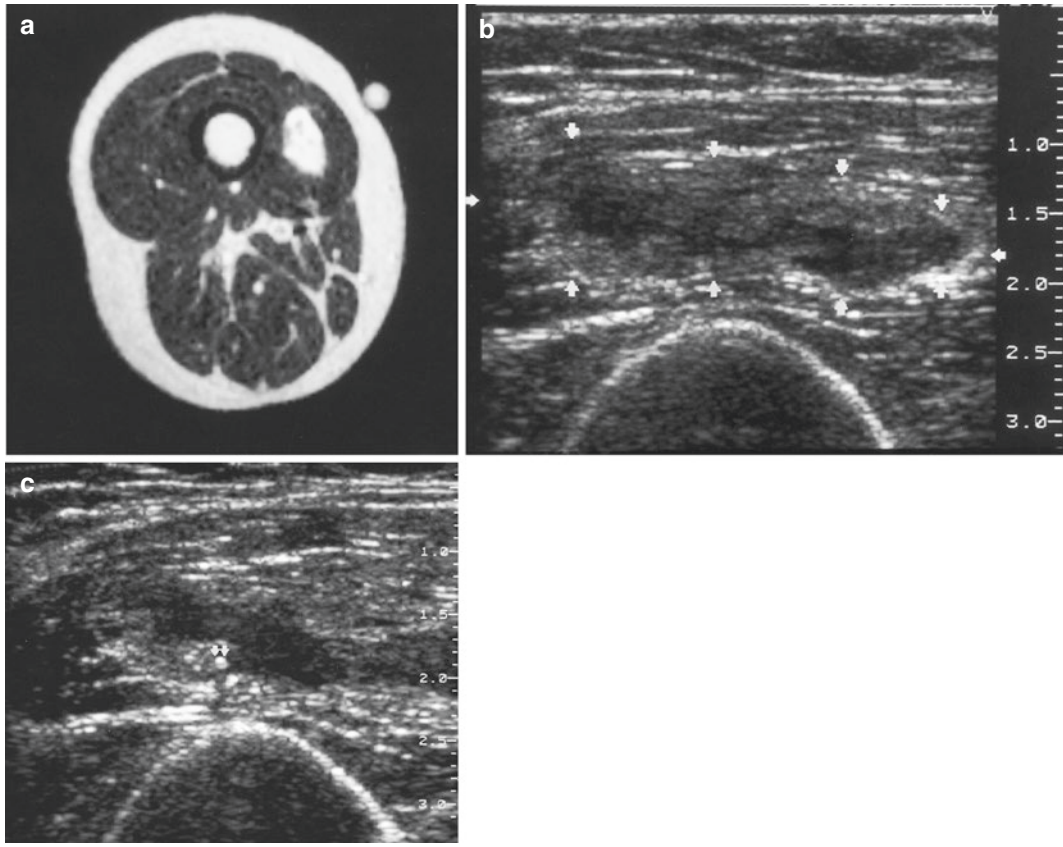

Fig. 1.21 (**a**–**c**) Skeletal muscle hemangioma of vastus medialis muscle in young woman, who complained of swelling and vague pain. (**a**) Axial fast spin-echo T2-weighted MR image. (**b**, **c**) Transverse US images. Well-defined, inhomogeneous, high signal intensity soft tissue structure in the medial vastus. (**a**) A small amount of intratumoral fatty tissue was visualized on coronal spin-echo T1-weighted image (not shown). Intramuscular, inhomogeneous, mixed hypo- and hyperechoic, partially ill-defined soft tissue mass (*arrows*). (**b**) The presence of a single phlebolith (*arrow*) within the mass confirms the diagnosis (**c**)

abnormal lymphatic channels that are too small to be resolved. Less commonly, a complex, hypoechoic mass with a few internal small cystic areas is visualized [76]. Occasionally, an organizing or calcified thrombus will be present in the mass. Larger lesions tend to be poorly defined. The cysts form along tissue planes and render complete resection difficult.

1.4.5 Lipoma

In the series of Hung et al., lipomas were the most frequent diagnosis superficial to the investing fascia (105/247) with a US diagnostic sensitivity and specificity of 73 and 97.7 %, respectively [1]. Lipomas have an elongated shape and are usually oriented parallel to the skin surface [10, 44, 47, 55]. The echo pattern varies according to the number of internal interfaces between fat and connective elements [44]. In a series of 35 superficial lipomas studied by US, 29 % were homogeneously hypoechoic, 29 % were homogeneously hyperechoic (Fig. 1.23), 22 % were isoechoic (Fig. 1.24), and 20 % showed a mixed pattern (Fig. 1.25). The mixed pattern consisted either of intratumoral linear hyperechoic strands parallel to the skin surface or focal areas of hyperechogenicity.

Sixty-six percent of superficial lipomas were well marginated, the remainder poorly defined [44, 47]. Occasionally a distinct echogenic capsule can

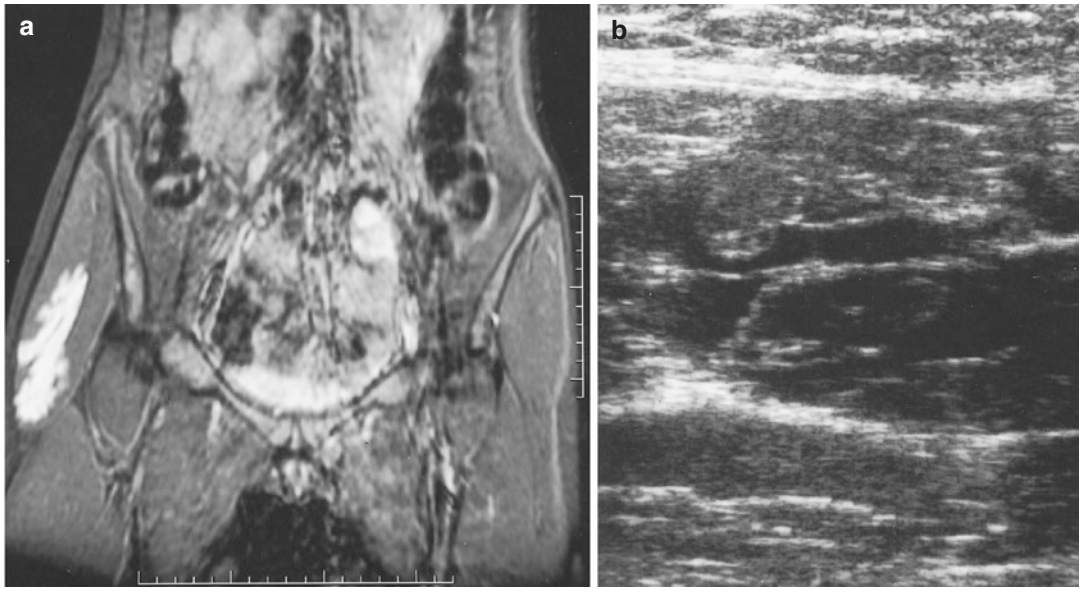

Fig. 1.22 (**a**, **b**) Lymphangioma of right gluteus maximus. The patient complained of swelling of right buttock/thigh when seated. (**a**) Coronal gradient-echo MR image. (**b**) Longitudinal US image. Intramuscular, tubular, hyperintense soft tissue structure. (**a**) Septated, cystic, anechoic soft tissue mass (**b**)

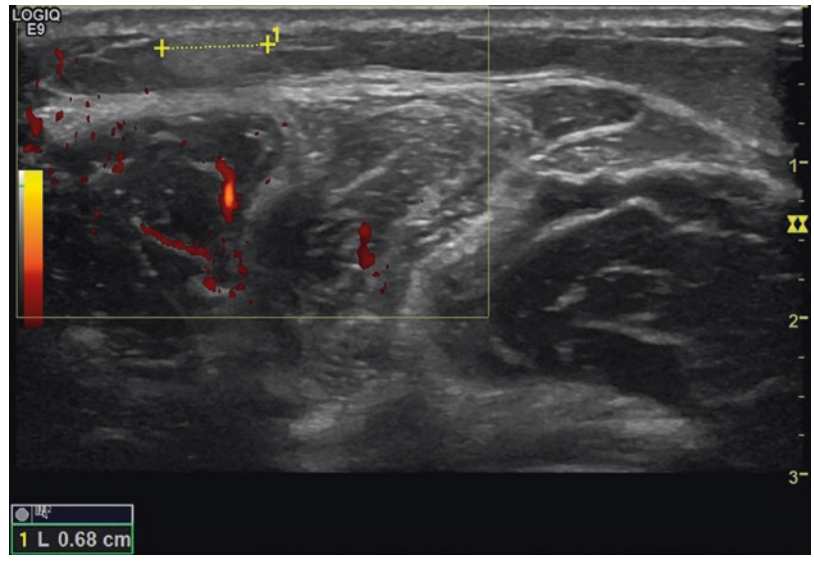

Fig. 1.23 Small, 7 mm, homogeneous reflective lipoma at the subcutaneous tissue of the left elbow in a 51-year-old male. Avascular oval lesion with changing shape during external compression and avascular on CDUS

be identified. Transverse diameter and shape of subcutaneous lipomas is variable with external compression; they are invariably avascular on power Doppler. Intramuscular lipoma has a high postsurgical recurrence rate, which results from incomplete resection due to lipomatous infiltration between muscle fibers which is not fully appreciated by US. An elongated iso- or hyperechoic mass should suggest a lipoma, whereas a hypoechoic mass is associated with a broader differential diagnosis, including malignant tumor. Malignant masses, however, rarely have an elongated or flattened shape [44]. Superficially located lesions that are easily compressible, avascular, and with iso- or

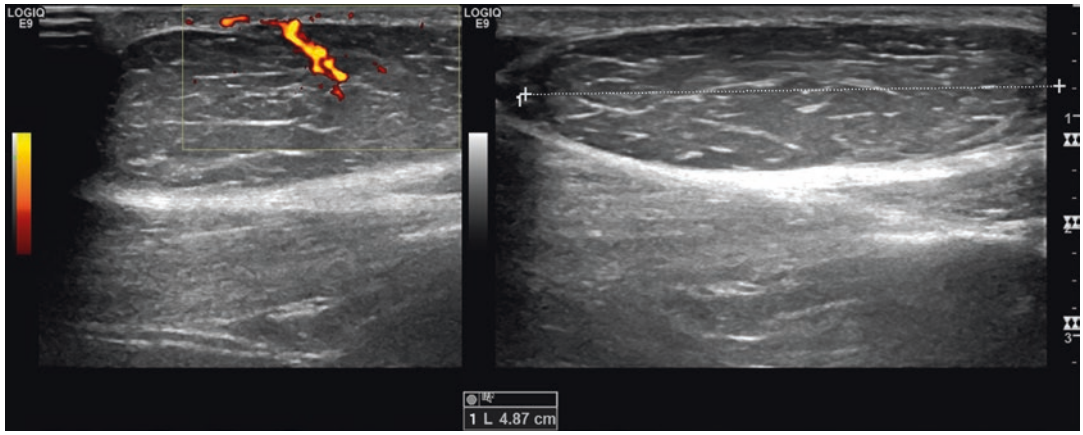

Fig. 1.24 Oval homogeneous isoreflective lipoma, maximal diameter 4.9 cm, at the dorsal aspect of the right shoulder in a 69-year-old female patient. Centrally avascular structure is detected along a septal reflective structure

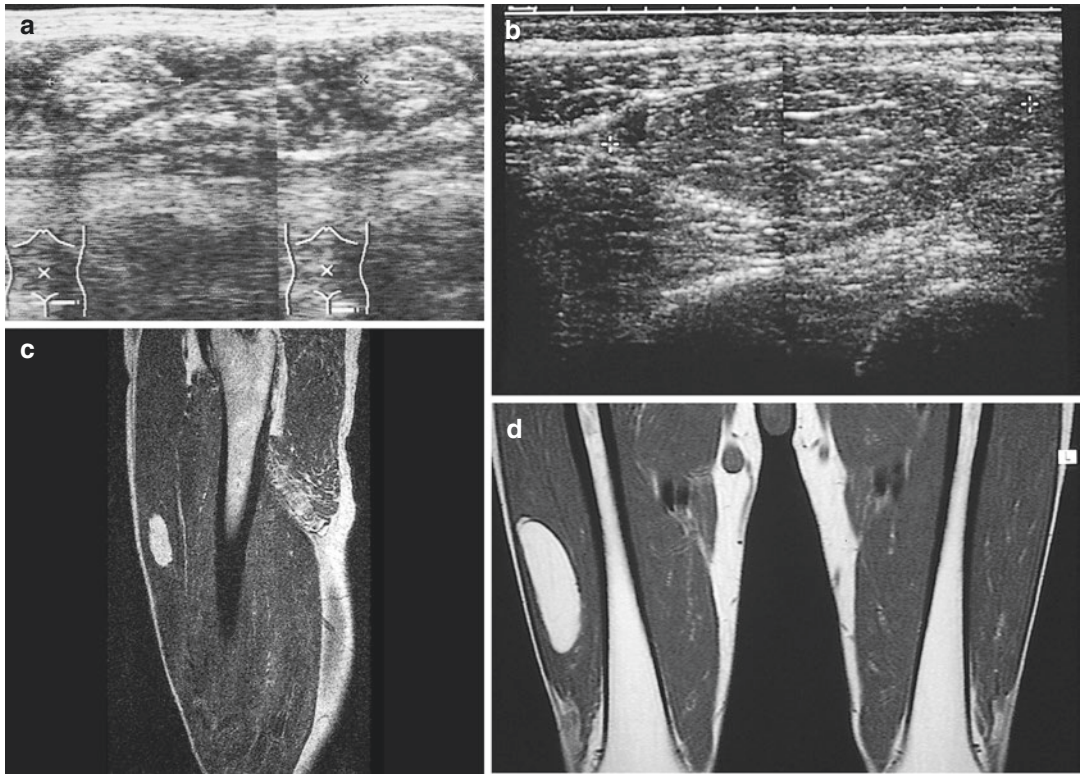

Fig 1.25 (**a**–**d**) Two cases of intramuscular lipoma of the thigh in a 57-year-old man (**a**, **b**) and in a 66-year-old man (**c**, **d**). (**a**) US of the thigh. (**b**) Sagittal spin-echo T1-weighted MR image. (**c**) US of the thigh. (**d**) Coronal spin-echo T1-weighted MR image. Two examples of intramuscular lipoma showing a characteristic elongated shape and orientation parallel to the skin but with nonspecific reflectivity. One lesion is hyperreflective (**a**), while the other is hypo- to isoreflective (**c**) compared with muscle. On MRI both lesions show the same signal intensity compared with fat on all pulse sequences (**b**, **d**)

hyperreflective US texture compared to normal subcutaneous tissue are confidently characterized as lipomas on US examination. Diagnosis on basis of hard copies alone is erroneous and may lead to underscoring of US as a diagnostic tool. This is demonstrated in a retrospective study by Inampudi et al. with sensitivities of only 40 to 52 % and accuracies from 49 to 64 % to differentiate lipomas from non-lipomas [66]. Major differential at the subcutaneous compartment is synovial sarcoma that, if bleeding components are present, may be compressed but is nonhomogeneous and hypervascular on power Doppler.

Also in lipomatous tumors, location is an important diagnostic criterium. Deep-seated lesions always need further diagnostic work-up by MRI.

1.4.6 Ganglion Cyst

A ganglion is a well-defined, anechoic soft tissue structure with posterior acoustic enhancement which arises from a joint or is closely related to a tendon [13, 14, 53, 95]. It may be loculated and contain internal septations. Anechogenicity, posterior acoustic enhancement, and sharp delineation cannot always be demonstrated in a small cyst [30]. Uncomplicated ganglion cysts show no vascularity on CDUS (Fig. 1.26). The ganglion cyst wall is composed of compressed collagen fibers with flattened cells without evidence of an epithelial or synovial lining. The wall is usually thin and regular. In recurrent or long-standing lesions, a thicker wall and intraluminal echoes, thought to be caused by some degree of organization of the cystic fluid or particulate cholesterol crystals, can be visualized [120, 132].

In a minority of wrist ganglion cysts (27–30 %), the communicating stalk with the joint of origin may go undetected [18, 30]. No communicating duct has been documented so far in digital ganglion cysts [13, 107]. US is equally sensitive as MRI in the detection of occult dorsal wrist ganglion cysts, but it offers a slight advantage in differentiating between a small, compressible joint effusion and a small ganglion cyst which does not collapse under compression [18]. A frequent location is the dorsal and volar aspect of the wrist [64, 87], the finger, and the peroneal compartment [14, 18]. Dorsal wrist ganglion cysts predominantly arise from the scapholunate joint, with average size ranging between 3 mm and 3,5 cm. Volar ganglia usually extend superficially between the

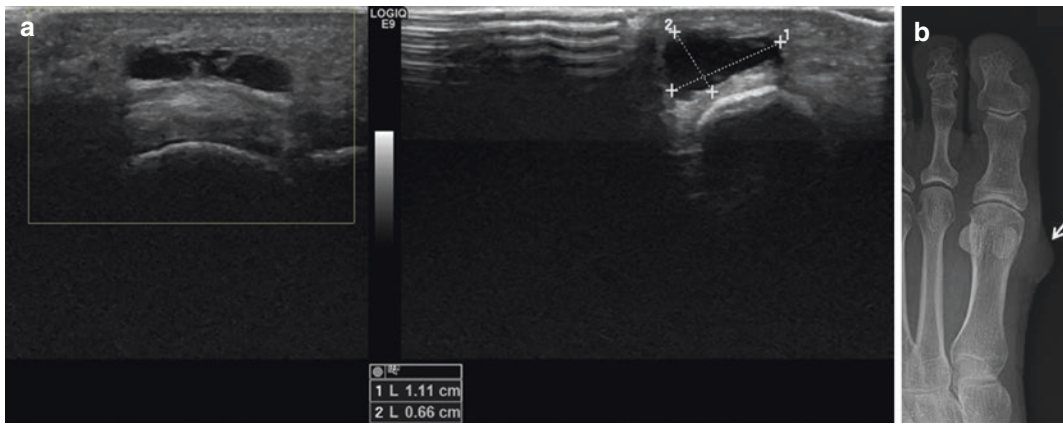

Fig. 1.26 Ganglion cyst connected to the first metatarsophalangeal joint of the left foot in a 60-year-old female patient. (**a**) US (*longitudinal and transverse view*) at the medial aspect of the first metatarsal demonstrates homogeneous and (*left image*) elongated mass with the absence of vascular structures on CDUS and with a stalk to the MTP 1 joint (not demonstrated on this image). (**b**) CR demonstrating focal nonspecific thickening of the soft tissue medially over the first metatarsal head (*arrow*)

radial artery and flexor carpi radialis tendon and may arise from the radioscaphoid, scapholunate, scaphotrapezoid, or second carpometacarpal joint, in that order of decreasing frequency [7].

Aspiration followed by a short immobilization period is one method of conservative treatment [14, 30, 107].

1.4.7 Superficial Soft Tissue Tumors and Tumorlike Lesions

1.4.7.1 Epidermoid Cyst

Epidermoid (inclusion) cysts (formerly sebaceous cysts) are common cutaneous lesions at the scalp, face, trunk, neck, and back. They are formed by proliferation of squamous epithelium in a confined space at the dermis. They are similar to cholesteatomas. The etiology is traumatic/surgical implantation, occlusion of pilosebaceous unit, congenital rests of cells, and HPV infections with palmoplantar location of epidermoid cysts [61, 135]. In the series of Hung et al., epidermoid cysts were the second most frequent diagnosis superficial to the investing fascia (30/247) with a US diagnostic sensitivity and specificity of 68.8 and 95.2 %, respectively [117]. Ultrasonographically, epidermoid cysts are superficially located next to the skin, hypoechoic, and relatively well circumscribed soft tissue masses similar to ganglion cyst. Larger lesions may contain small intralesional hyperreflectivities, presumably representing keratin clusters [64] (Fig. 1.27). Doppler is not demonstrating vascular signal. In case of rupture, a local inflam-

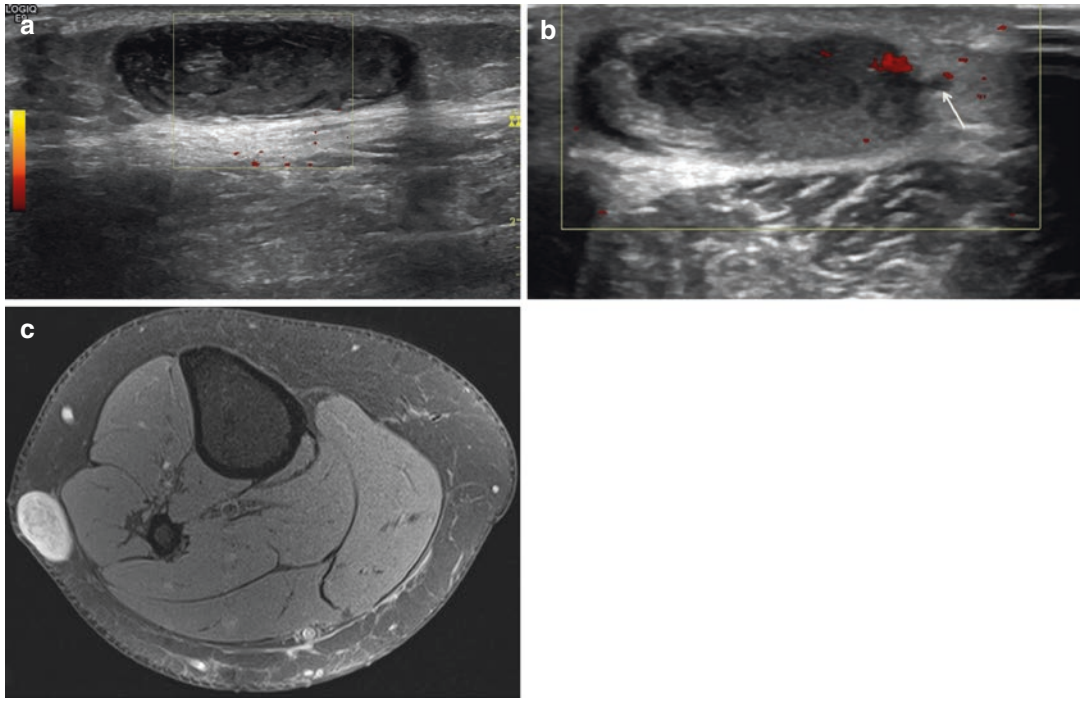

Fig. 1.27 Epidermal inclusion cyst at the posterior lateral aspect of the right knee of a 44-year-old female patient complaining of a firm mass since 4 years. Pathology demonstrated disrupted epidermoid cyst with local perilesional inflammation. (**a**) Avascular nonhomogeneous hypoechogenic oval mass lesion at the subcutaneous tissue. Sharp margins and without vascular signal on CDUS. Maximal diameter 3 cm. (**b**) Ultrasound examination performed 2 years later after minor pain development at the mass lesion demonstrates the oval mass lesion with minor CDUS signal at the margin and concentric area of increased reflectivity. Focal disruption of the margin of the lesion (*arrow*). The lesion was subsequently resected. (**c**) MRI T1-WI with FS. This MRI examination is performed 2 months after the first US examination and reveals nonhomogeneous intermediate SI oval mass lesion on T2-WI (not shown) with nonhomogeneous low SI on T1-WI and intermediate SI on T1-WI with FS related to the high protein content of the lesion. No enhancement after IV gadolinium administration was detected (not shown)

matory response to the necrotic debris may give rise to Doppler signal at the wall and surroundings of the lesions mimicking abscess or cellulitis.

1.4.7.2 Pilomatricoma

Pilomatricoma (formerly pilomatrixoma or calcifying epithelioma of Malherbe) arises from the bulb of normal hair follicles and is a relatively common (1500–2000) usually solitary slow-growing firm mass at the superficial subcutaneous tissue. The overlying skin has a bluish to red discoloration. The lesion is more frequent in female patients (3/2) with a bimodal peak during the first and sixth decades of life. It is characteristically located at the neck and head and less frequent at the upper extremities, trunk, and lower extremities. It might be associated with sarcoidosis, Steinert disease, Gardner, Rubinstein, Turner, myotonic muscular dystrophy syndrome, and skull dysostosis. Excision is usually recommended, as a foreign body reaction due to calcification of the lesion may occur and cause a vigorous inflammatory response with risk of scarring. The characteristics of US features are a well-defined solid ovoid mass at the junction of the dermis and subcutaneous fat with focal thinning of the dermis. The lesions appear as a target with centrally small calcifications and hyperreflective areas with moderate intrinsic vascularity surrounded with a peripheral hypoechoic connective tissue rim [24, 47, 62, 65] (Figs. 1.28 and 1.29). The diameter ranges from 0.5 up to 5 cm. Heterogeneous echotexture combined with calcification pattern with scattered dots and hypoechoic rim was specific with P value of <0.001 [32].

1.4.7.3 Basal Cell Carcinoma

Most lesions are nodular or morpheaform with a hypoechogenic, solid tumor with irregular borders, multiple hyperechogenic dots inside the tumor, and vessels inside and at the periphery of the tumor [136, 137].

1.4.7.4 Fibroblastic/Myofibroblastic Tumors

Benign Lesions

Dermatofibroma (Fibrous Histiocytoma)

Dermatofibroma (fibrous histiocytoma) is a common dermal skin lesion characterized by an increased number of fibrocytes, presence of inflammatory cells (macrophages and lymphocytes), and hyperplasia of adjacent structures [17]. Dermatofibromas are readily recognized by dermatologists in most cases. However, dermatofibroma has many clinical variants, including aneurysmal, palisading, sclerotic, keloidal, and atrophic, making clinical diagnosis difficult. It is suggested that in clinically doubtful cases, US examination can provide clinicians with valuable

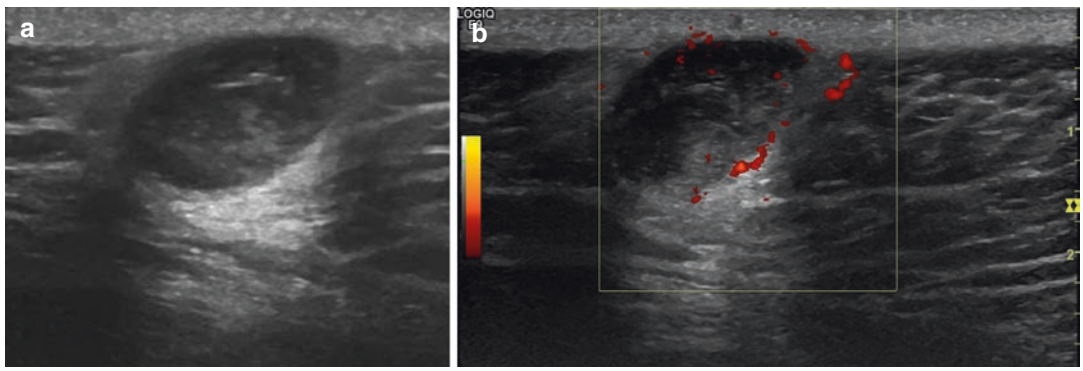

Fig. 1.28 Pilomatricoma in a 74-year-old female patient. Painless firm mass at the right lower leg. (**a**) US examination reveals nonhomogeneous oval mass lesion superficially at the subcutaneous tissue abutting the dermis, acoustic retro-enhancement, hyperreflective internal structure (hair). (**b**) CDUS examination reveals minor intralesional vascular signal

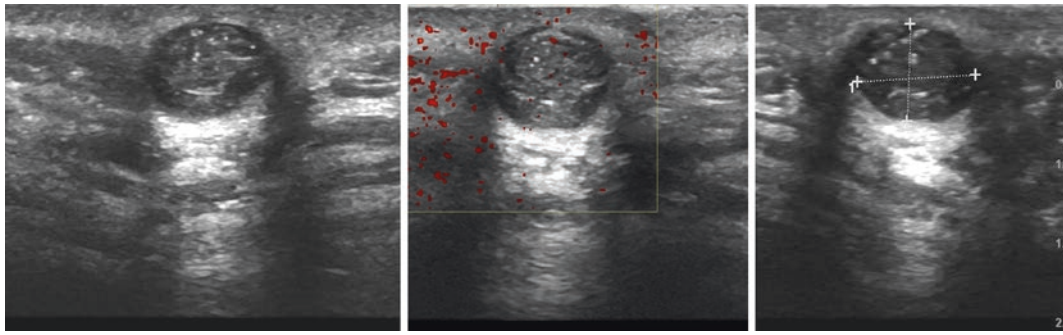

Fig. 1.29 Pilomatricoma in a 53-year-old male patient at the occipital neck area. Small superficial nodular mass thinning the dermal layer, maximal diameter 7.5 mm in size, nonhomogeneous hyporeflective rim with intralesional reflective dots, global retroacoustic enhancement. Minor intralesional vascular signal on CDUS

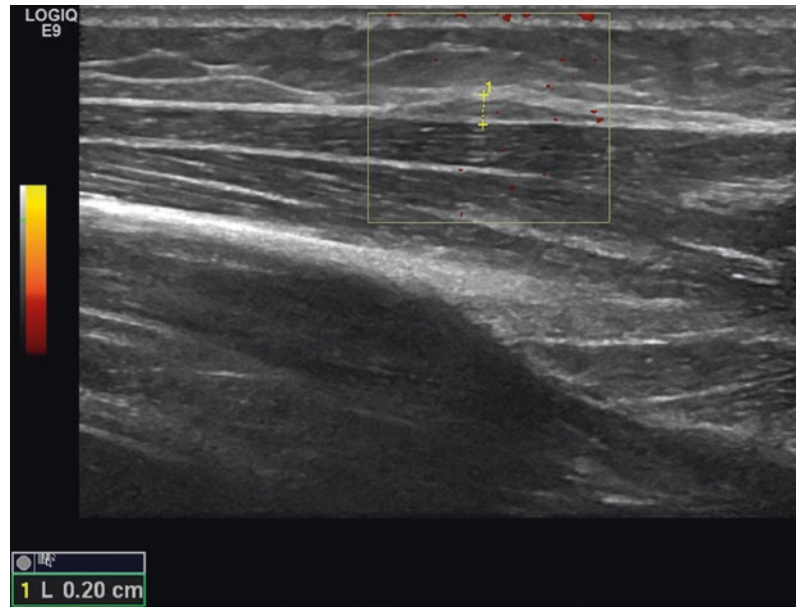

Fig. 1.30 Nodular fasciitis at the right lower arm in a 33-year-old female patient. Focal fusiform thickening of the superficial fascia at the extensor area with maximal diameter 12 mm and thickness of 2 mm, no intralesional vascular structures are detected with CDUS

diagnostic information [138]. Dermatofibromas appear on US as an ill-defined or oval-shaped hypoechogenic tumor in the dermis and/or upper hypodermis, usually with distortion of the local hair follicles [136].

Nodular Fasciitis

Superficial-type nodular fasciitis is a rapidly growing mass, often located in the deep subcutaneous fat, has an oval-lobulated shape, and is rather poorly defined. They are most often near to or with a broad base connected with the muscle fascia. The US appearance is hypoechoic with echogenic foci or peripheral hyperechoic nodules and quite often does not show internal vascular flow (Figs. 1.30 and 1.31). If a superficial soft tissue mass has the above features, superficial-type nodular fasciitis should be included in the differential diagnosis [74, 79].

Elastofibroma

Elastofibroma is prevalent in females, its onset occurs around 60 years of age, and is most frequently localized in the deep subscapular region (93 %), bilateral in 54 % of cases. In 7 % it was found in an atypical isolated suprascapular region, in 7 % it was synchronous to that in the subscapular region. Four ultrasound patterns were described by Battaglia et al.: Type I (54 %) inhomogeneous fasciculated or lamellated

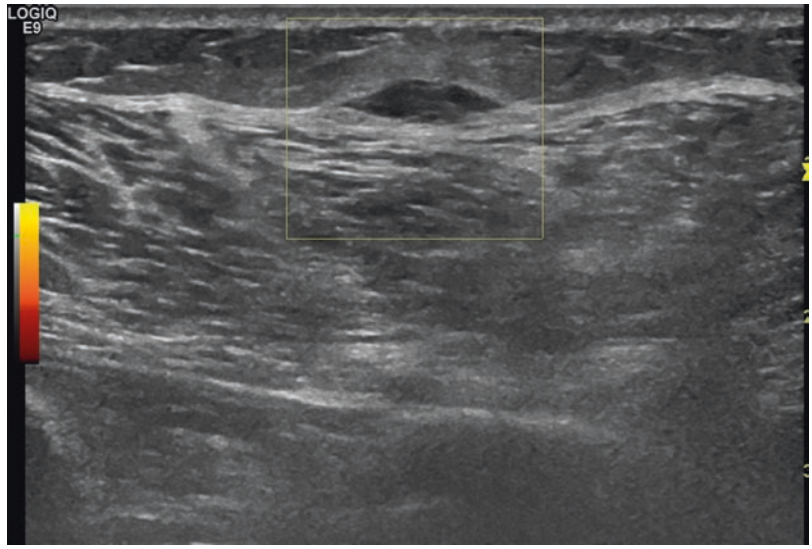

Fig. 1.31 Nodular fasciitis in a 54-year-old female patient. Firm painless thickening at the left lower leg. CDUS demonstrates small (11 mm diameter), avascular hypoechogenic fusiform thickening of the superficial muscle fascia of the anterior lateral muscle compartment of the left lower leg

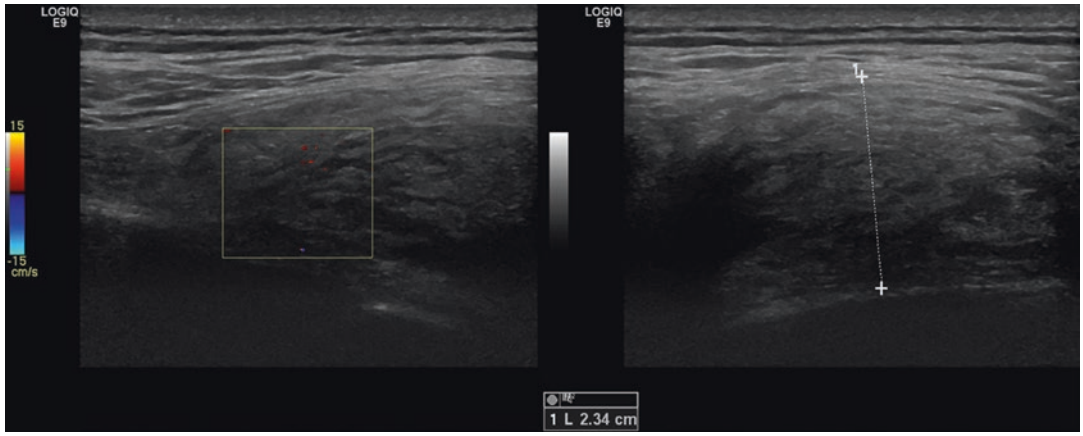

Fig. 1.32 Elastofibroma in a 61-year-old male patient. Typical location at the medial margin of the right scapula with oval mass lesion adjacent to the thoracic wall. Minor intralesional vascular structures. Layered so-called "lasagna" aspect consisting of alternating hypoechogenic and reflective layers. Compression with the probe produces no change in shape of the lesion

(Fig. 1.32), Type II (22%) inhomogeneous nonspecific, Type III (15%) hyperechogenic, and Type IV (9%) hypoechogenic [7]. Demonstration of Type I lesion, or bilateral demonstration of Type II and/or Type III with specific location, results in a specific diagnosis of elastofibroma.

Intermediate and Malignant Lesions

Dermatofibrosarcoma Protuberans

Dermatofibrosarcoma abuts with a wide base against the skin. Rarely the lesion is located intermuscularly [80]. The shape is round or ovoid, dimensions range from 2 to 11 cm. Margin of the lesions are focally lobulated but well defined and may appear as irregular with pseudopodia-like protrusion(s). Hypo- and hyperreflective lesions or areas in lesions are described with frequently posterior enhancement. Color Doppler US shows consistently moderate blood flow patterns with either profuse blood flow or with only flow at the peripheral portions of the tumor. Pathologically, samples corresponding to hypoechoic DP were composed primarily of tumor cells, and samples

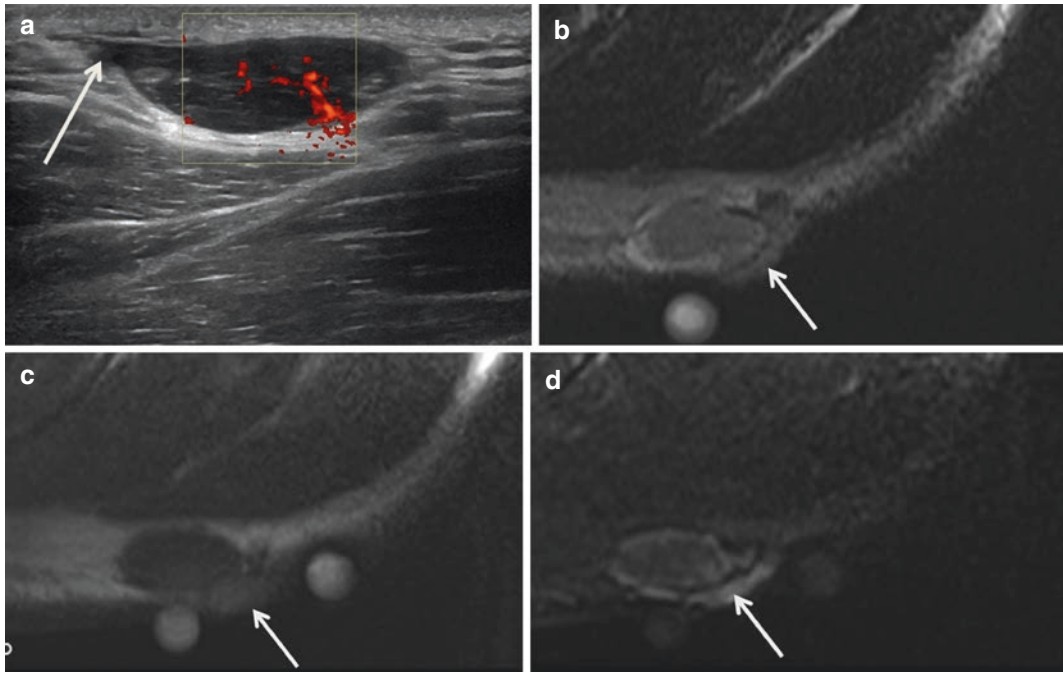

Fig. 1.33 Dermatofibrosarcoma at the back left shoulder of a 44-year-old male patient. (**a**) US demonstration of nonhomogeneous oval mass lesion, 2.6 cm diameter, with irregular margins superficially located at the subcutaneous tissue, broad contact with the epidermis-dermis, fingerlike extension to the skin (*arrow*). Intralesional vascular structures on CDUS. (**b**) MRI axial T2-WI, target aspect of the lesion with peripheral higher and centrally lower SI compared to subcutaneous fat. Lateral-superficial fingerlike extension component with isointense SI compared to subcutaneous fat (*arrow*). (**c**) MRI axial T1-WI demonstrates overall low SI of the deep part of the lesion, slight hyperintense aspect of the lateral superficial component of the lesion (*arrow*). (**d**) MRI axial T1-WI with FS after gadolinium contrast administration, nonhomogeneous enhancement at the periphery of the deep part of the lesion, homogeneous enhancement of the lateral superficial component of the lesion (*arrow*)

corresponding to mixed echogenic DP were composed of tumor cells and fibrous tissues. If a US examination reveals a round or oval mass in the subcutaneous tissue that is abutting against the skin with a broad skin base and has a focal lobulated margin with hypoechogenicity or an irregular margin with mixed echogenicity, a diagnosis of DP should be considered [80, 116] (Fig. 1.33).

1.4.7.5 Rare Sweat Gland and Duct Tumors with Nonspecific US Appearance

These rare small lesions are typically located at the dermis or superficial layers of the subcutaneous fat layer.

Chondroid Syringoma

These are harmless mixed sweat duct tumors located at the dermis or subcutaneous fat in adolescents and adults with African or Asian origin. The lesion is slow growing and typical diameter is 1–3 mm, rarely masses up to 3.5 cm are described in literature. Most of the lesions are found in clusters on the eyelids but they may also arise in the armpits, umbilicus, chest, and vulva, rarely in other locations. Ultrasound is nonspecific and may show several bright foci suggestive of microcalcifications without solid or cystic mass [2]; solid hyperechoic and vascular mass with scarlike central structure or solid hypoechoic well-defined subcutaneous was found [111, 133].

Eccrine Spiradenoma

Eccrine spiradenoma is a rare benign usually small (<1 cm) dermal typically solitary tumor of the sweat gland located at the dermis or superficial subcutaneous tissue. Ultrasound demonstrates a mass with sharp margins with or without lobulations and with or without cystic components but with clear increased intralesional vascularity and vessels connecting the lesion to the deep dermis [69].

Eccrine Acrospiroma

Eccrine acrospiromas (or hidradenoma) are rare lesions that mainly involve the trunk, lower limbs, and head. Although benign, these tumors can recur locally after inadequate resection, and malignant transformation is recognized. Eccrine acrospiroma presents as a cystic mass on US with mural nodules and increased intralesional vascularity. The mural nodules might show calcifications [87, 92].

1.4.7.6 Rheumatoid Nodule

Approximately 20–25 % of patients with rheumatoid arthritis have rheumatoid nodules. Their etiology is unknown and although nodules, they usually constitute a therapeutic challenge. These nodules most commonly involve the soft tissues of the upper extremity, particularly adjacent to the olecranon [34, 93, 122]. The nodules were more homogeneous hypoechogenic with vascular signal on CDUS (Fig. 1.34). Some showed a central sharply demarcated hypoechoic area, possibly corresponding to necrosis inside the rheumatoid nodules.

1.4.7.7 Fat Necrosis

Traumatic fat necrosis is well known in the female breast. It is also described at other areas and in male patients. It has to be taken into account in the differential diagnosis of subcutaneous mass lesions. On US, the appearance of fat necrosis varies from a solid hypoechoic mass with posterior acoustic shadowing to complex intracystic masses that evolve over time. These features depict the histological evolution of fat necrosis and reflect the degree of fibrosis. Cystic anechoic lesions with acoustic enhancement or shadowing may appear complex with mural nodules or internal echogenic bands (Fig. 1.35). The masses may have circumscribed or ill-defined margins [73, 125]. The mass may also present as an isoechoic mass [27]. A mass with echogenic internal bands that shift in orientation with changes in patient position has been described as a specific ultrasound indicator of fat necrosis. It is thought that these bands represent the interface between the lipid and the serous-hemorrhagic components of fat necrosis [121].

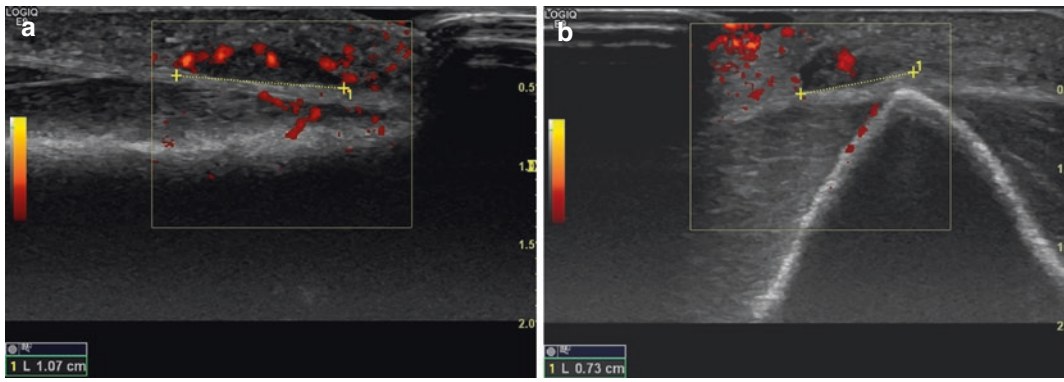

Fig. 1.34 A 50-year-old female patient with active rheumatoid arthritis at the fingers and hands and RA nodule at the left elbow, olecranon. Demonstration of a hypoechogenic oval mass lesion with marked angiogenesis on CDUS, located adjacent to the superficial fascia of the extensor compartment, at the location of an adventitious olecranon bursa, dimensions 10 × 0.7 cm. (**a**) Longitudinal US view. (**b**) Axial US view

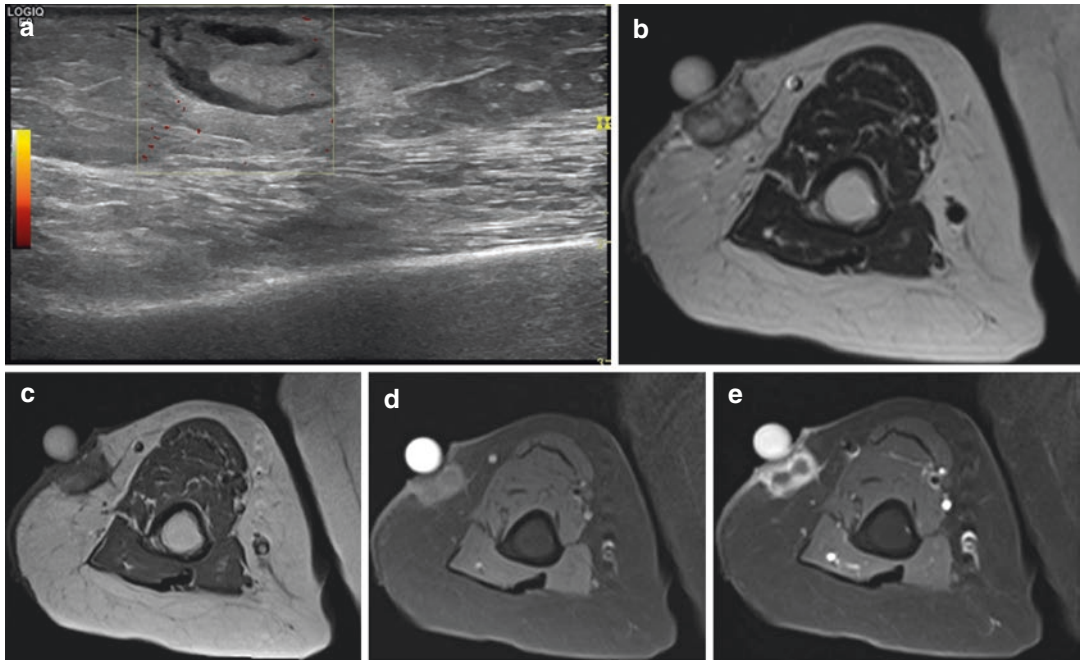

Fig. 1.35 An 80-year-old female patient, presenting with a painless mass at the lateral aspect of the right upper arm, with an area of fat necrosis ("steatonecrosis") at the subcutaneous tissue. US and MRI show characteristics of fatty tissue. (**a**) Oval area superficial at the subcutaneous tissue with distortion of the subcutaneous fat surrounded with hyporeflective margin, diameter 2 cm, avascular on CDUS. (**b**) Axial TSE T2-WI. Nonhomogeneous lesion with thin hypointense margin, and nonhomogeneous central area intermediate to low SI. (**c**) Axial TSE T1-WI. Similar imaging appearance compared to the T2-WI. (**d**) Axial TSE T1-WI FS. Partial suppression of the central area in keeping the fatty content. (**e**) Axial TSE T1-WI FS after intravenous gadolinium contrast administration. Peripheral enhancement of the lesion

1.4.8 Soft Tissue Mineralization Disorders

Physiological biomineralization is a complex multifactorial metabolic process, which in normal conditions is restricted to the extracellular matrix of specific body structures, namely, the bones, teeth, hypertrophic growth plate cartilage, and calcified articular cartilage [33, 75]. The intracellular and extracellular mechanisms, underlying physiological biomineralization, rely on a balanced interplay between mineralization inhibitors and propagators. In physiological circumstances, calcium and inorganic phosphate (Pi) concentrations exceed their solubility in most human tissues; this does not result in mineralization of soft tissues, suggesting that these tissues possess regulatory mechanisms preventing mineral deposition. Mineralizing tissues have regulatory systems that can modulate these mechanisms to enable calcification [75]. When these regulatory systems are inadequate, ectopic mineralization, i.e., inappropriate biomineralization in soft tissues, occurs and causes a spectrum of ectopic calcification disorders. Ectopic mineralization disorders are conventionally classified based on the mechanism through which the mineralization takes place, i.e., metastatic or dystrophic calcification or ectopic ossification:

1. Metastatic calcification, due to hyperphosphatemia and/or hypercalcemia
2. Dystrophic calcification, which occurs in diseased (metabolically impaired or dead) tissue under normal calcium and phosphate homeostasis
3. Ectopic or heterotopic ossification, leading to true bone formation [33, 48]

Ectopic calcifications (metastatic of dystrophic) are typically composed of calcium phosphate salts,

including hydroxyapatite, but can also consist of calcium oxalates and octacalcium phosphate as seen in kidney stones.

1.4.8.1 Dystrophic Calcification

In the absence of a systemic mineral imbalance, ectopic calcification is typically termed dystrophic calcification. Often, these sites show evidence of tissue alteration and/or necrosis. Dystrophic mineralization is commonly observed in soft tissues as a result of injury, disease, and aging. Although most soft tissues can undergo calcification, the skin, kidney, tendons, and cardiovascular tissues appear particularly prone to developing this pathology [3] (Fig. 1.36). Major location is tendon calcifications at the rotator cuff or gluteus medius and minimus tendons.

1.4.8.2 Tumoral Calcinosis

Tumoral calcinosis is an extremely rare benign condition that is characterized by deposits of calcium hydroxyapatite crystals in periarticular soft tissues. Ectopic mineralization – inappropriate biomineralization in soft tissues – is a frequent finding in physiological aging processes and several common disorders, which can be associated with significant morbidity and mortality. Further, pathologic mineralization is seen in several rare genetic disorders, which often present life-threatening phenotypes. These disorders are classified based on the mechanisms through which the mineralization occurs: metastatic or dystrophic calcification or ectopic ossification. Underlying mechanisms have been extensively studied, which resulted in several hypotheses regarding the etiology of mineralization in the extracellular matrix of soft tissue. These hypotheses include intracellular and extracellular mechanisms, such as the formation of matrix vesicles, aberrant osteogenic and chondrogenic signaling, apoptosis, and oxidative stress. Though coherence between the different findings is not always clear, current insights have led to improvement of the diagnosis and management of ectopic mineralization patients, thus translating pathogenetic knowledge (variome) to the phenotype (phenome). Tumoral calcinosis is mainly located around large joints such as the hips, shoulders, and elbows; it may also involve the small joints of the hand and wrist. There are multiple types of tumoral calcinosis with divergent clinical characteristics, but the exact cause is still unknown. Wide resection appears to lead to a good clinical outcome and a low incidence of local relapse [31].

1.4.9 Synovial Sarcoma

Synovial sarcoma is a misnomer. This lesion has no relation with the joint or synovium. It is a rare

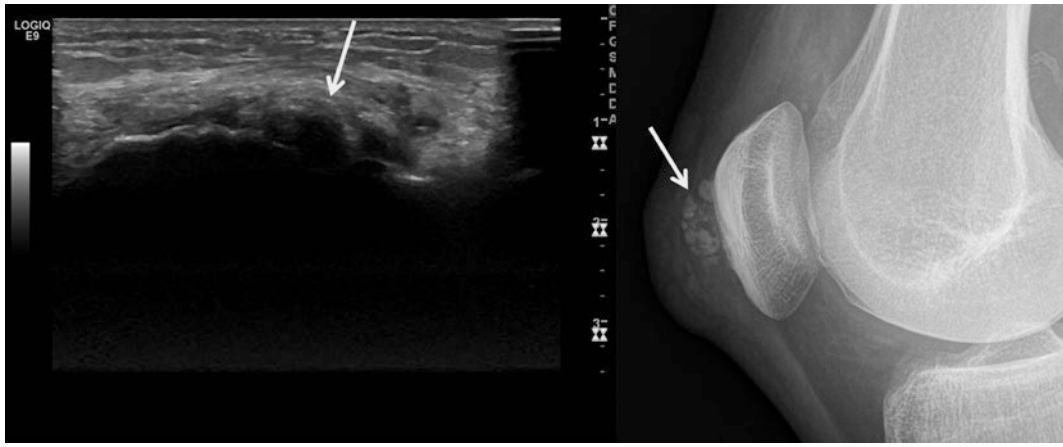

Fig. 1.36 Chronic gout in a 60-year-old male with calcium deposition in multiple articular and soft tissue tophi. (**a**) US (*longitudinal view*) at the prepatellar area with hyperreflective lobulated mass with massive acoustic shadowing (*arrow*). (**b**) Conventional radiograph (*lateral view*) with cluster of calcifications in the prepatellar soft tissue (*arrow*)

malignant mesenchymal tumor of unknown differentiation. Bleeding components are often present. The US appearance of this tumor is nonspecific and may be easily confused with benign cystic lesions such as acute bursitis or organizing hematoma [88]. The other imaging features of this lesion will be discussed in Chap. 18.

Conclusion

US is an important imaging technique in the initial assessment of a soft tissue swelling. In the majority of cases, it will establish that the swelling is benign (e.g., in ganglions, meniscal cysts, or tenosynovitis) or is a neurinoma, lipoma, or elastofibroma and obviate unnecessary further imaging work-up.

In soft tissue tumors in the wrist, hand, fingers, skin, and subcutaneous fat and in peripheral nerve tumors, US imaging is superior to MRI because of its small field of view and excellent anatomical depiction. The drawback of US is its nonspecificity in the setting of a hypoechoic solid soft tissue mass.

In institutions without a biopsy-dedicated CT or MR imaging suite, US is the most accessible and least time-consuming modality for imaging-guided aspiration and biopsy.

Key Points

1. US is an important imaging technique in the initial assessment of a soft tissue swelling.
2. In the majority of cases, US will establish that the soft tissue swelling is benign (cystic) and obviate unnecessary further imaging work-up.
3. The drawback of US is its nonspecificity in the setting of a hypoechoic solid soft tissue mass.
4. US is the most readily available and least time-consuming modality for imaging-guided aspiration and biopsy for superficially located lesions.

References

1. Alexander AA, Nazarian LN, Feld RI (1997) Superficial soft tissue masses suggestive of recurrent malignancy: sonographic localization and biopsy. Am J Roentgenol 169:1449–1451
2. AlSharif S, Tremblay F, Omeroglu A, Altinel G, Sun S, Mesurolle B (2014) Infiltrating syringomatous adenoma of the nipple: sonographic and mammographic features with pathologic correlation. J Clin Ultrasound 42(7):427–429
3. Anderson HC, Morris DC (1993) Mineralization. In: Mundy GR Martin TJ (ed) Physiology and pharmacology of bone. Springer, New York, pp 267–298
4. Arya S, Nagarkatti DG, Dudhat SB, Nadkarni KS, Joshi MS, Shinde SR (2000) Soft tissue sarcomas: ultrasonographic evaluation of local recurrences. Clin Radiol 55(3):193–197
5. Ata AM, Onat ŞŞ, Özçakar L (2016) Ultrasound-guided diagnosis and treatment of Morton's Neuroma. Pain Phys 19(2):E355–E358
6. Barberie JE, Wong AD, Cooperberg PL, Caron BW (1998) Extended field of view sonography in musculoskeletal disorders. Am J Roentgenol 171:751–757
7. Battaglia M, Vanel D, Pollastri P, Balladelli A, Alberghini M, Staals EL, Monti C, Galletti S (2006) Imaging patterns in elastofibroma dorsi. Eur J Radiol 72(1):16–21
8. Beaman FD, Kransdorf MJ, Andrews TR, Murphey MD, Arcara LK, Keeling JH (2007) Superficial soft-tissue masses: analysis, diagnosis, and differential considerations. Radio Graphics 27:509–523
9. Beggs I (1997) Pictorial review: imaging of peripheral nerve tumors. Clin Radiol 52:8–17
10. Behan M, Kazam E (1978) The echographic characteristics of fatty tissues and tumors. Radiology 129:143
11. Belli P, Constantini M, Mirk P, Maresca G, Priolo F, Marano P (2000) Role of color Doppler sonography in the assessment of musculoskeletal masses. J Ultrasound Med 19:823–830
12. Bernardino ME, Jing BS, Thomas JL, Lindell MM, Zornoza J (1981) The extremity soft-tissue lesion: a comparative study of ultrasound, computed tomography and xerography. Radiology 139:53–59
13. Bianchi S, Abdelwahab IF, Zwass A, Calogera R, Banderali A, Brovero P, Votano P (1993) Sonographic findings in examination of digital ganglia: retrospective study. Clin Radiol 48:45–47
14. Bianchi S, Abdelwahab IF, Zwass A, Giacomello P (1994) Ultrasonographic evaluation of wrist ganglia. Skeletal Radiol 23:201–203
15. Braunstein EM, Silver TM, Martel W, Jaffe M (1981) Ultrasonographic diagnosis of extremity masses. Skeletal Radiol 6:157–163
16. Brouns F, Stas M, De Wever I (2003) Delay in diagnosis of soft tissue sarcomas. Eur J Surg Oncol 29(5):440–445

17. Calonje E, Mentzel T, Fletcher CD (1994) Cellular benign fibrous histiocytoma. Clinicopathologic analysis of 74 cases of a distinctive variant of cutaneous fibrous histiocytoma with frequent recurrence. Am J Surg Pathol 18:668–676
18. Cardinal E, Buckwalter KA, Braunstein EM, Mih AD (1994) Occult dorsal carpal ganglion: comparison of US and MR imaging. Radiology 193:259–262
19. Cardinal E, Buckwalter KA, Braunstein EM, Raymond-Tremblay D, Benson MD (1996) Amyloidosis of the shoulder in patients on chronic hemodialysis: sonographic findings. Am J Roentgenol 166:153–156
20. Cardinal E, Chem RK, Beauregard CG (1998) Ultrasound-guided interventional procedures in the musculoskeletal system. Radiol Clin North Am 36:597–604
21. Chinn DH, Filly RA, Callen PW (1982) Unusual ultrasonographic appearance of a solid schwannoma. J Clin Ultrasound 10:243–245
22. Chiou HJ, Chou YH, Chiou SY, Liu JB, Chang CY (2003) Peripheral nerve lesions: role of high-resolution US. Radiographics 23(6):e15
23. Choi H, Varma DGK, Fornage BD, Kim EE, Johnston DA (1991) Soft tissue sarcoma: MR imaging vs sonography for detection of local recurrence after surgery. Am J Roentgenol 157:353–358
24. Choo HJ, Lee SJ, Lee YH, Lee JH, Oh M, Kim MH, Lee EJ, Song JW, Kim SJ, Kim DW (2010) Pilomatricomas: the diagnostic value of ultrasound. Skeletal Radiol 39:243–250
25. Christensen RA, Van Sonnenberg E, Casola G, Wittich GR (1988) Interventional ultrasound in the musculoskeletal system. Radiol Clin North Am 26:145–156
26. Cigna E, Maruccia M, Malzone G, Malpassini F, Soda G, Drudi FM (2012) A large vascular leiomyoma of the leg. J Ultrasound 15:121–123
27. Crystal P, Bukhanov K (2005) Sonographic findings of palpable isoechoic breast fat necrosis: look for skin integrity. J Ultrasound Med 24:105–107
28. Daly BD, Cheung H, Gaines PA, Bradley MJ, Metreweli C (1992) Imaging of alveolar soft part sarcoma. Clin Radiol 46:253–256
29. De Clercq H, De Man R, Van Herck G, Tanghe W, Lateur L (1993) Case report 814: fibrolipoma of the median nerve. Skeletal Radiol 22:610–613
30. De Flaviis L, Nessi R, Del Bo P, Calori G, Balconi G (1987) High-resolution ultrasonography of wrist ganglia. J Clin Ultrasound 15:17–22
31. Del Bravo V, Liuzza F, Perisano C, Chalidis B, Marzetti E, Colelli P, Maccauro G (2012) Gluteal tumoral calcinosis. Hip Int 22(6):585–591
32. Derchi LE, Balconi G, De Flaviis L, Oliva A, Rosso F (1989) Sonographic appearances of hemangiomas of skeletal muscle. J Ultrasound Med 8:263–267
33. De Vilder EY, Vanakker OM (2015) From variome to phenome: pathogenesis, diagnosis and management of ectopic mineralization disorders. World J Clin Cases WJCC 3(7):556–574
34. Ergun T, Inanc N, Tuney D, Kotiloglu EK, Seckin D, Tetik C, Direskeneli H (2008) Skin manifestations of rheumatoid arthritis: a study of 215 Turkish patients. Int J Dermatol 47(9):894–902
35. Fornage BD (1987) Tuberculoid leprosy. J Ultrasound Med 6:105–107
36. Fornage BD (1988) Peripheral nerves of the extremities: imaging with US. Radiology 167:179–182
37. Fornage BD (1988) Glomus tumors in the fingers: diagnosis with US. Radiology 167:183–185
38. Fornage BD, Lorigan J (1989) Sonographic detection and fine-needle aspiration biopsy of nonpalpable recurrent or metastatic melanoma in subcutaneous tissues. J Ultrasound Med 8:421–424
39. Fornage BD, McGavran MH, Duvic M, Waldron CA (1993) Imaging of the skin with 20MHz-US. Radiology 189:69–76
40. Fornage BD, Richli WR, Chuapetcharasopon C (1991) Calcaneal bone cyst: sonographic findings and ultrasound-guided aspiration biopsy. J Clin Ultrasound 19:360–362
41. Fornage BD, Rifkin MD (1988) Ultrasound examination of the hand and foot. Radiol Clin North Am 26:114–129
42. Fornage BD, Schernberg FL, Rifkin MD (1985) Ultrasound examination of the hand. Radiology 155:785–788
43. Fornage BD, Schernberg FL, Rifkin MD, Touche DH (1984) Sonographic diagnosis of glomus tumor of the finger. J Ultrasound Med 3:523–524
44. Fornage BD, Tassin GB (1991) Sonographic appearances of superficial soft tissue lipomas. J Clin Ultrasound 19:215–220
45. Friedman AP, Haller JO, Goodman JD, Nagar H (1983) Sonographic evaluation of non-inflammatory neck masses in children. Radiology 147:693–697
46. Friedman T, Richman D, Adler R (2012) Sonographically guided cryoneurolysis: preliminary experience and clinical outcomes. J Ultrasound Med 31(12):2025–2034
47. Garioni E, Danesino GM, Madonia L (2008) Pilomatricoma: sonographic features. J Ultrasound 11:76–78
48. Giachelli CM (1999) Ectopic calcification: gathering hard facts about soft tissue mineralization. Am J Patol 154(3):671–675
49. Gielen JL, De Schepper AM, Blom R, Van Dyck P, Bosmans JML, Creytens D, Veryser J, Somville J, Parizel PM (2012) Experience with a frontal core biopsy device in soft tissue and bone lesions. Skeletal Radiol 41(4):447–458
50. Gielen JL, van Holsbeeck MT, Hauglustaine D, Verresen L, Verbeken E, Baert AL, Meeus L, Vandevoorde P, Michielsen P, Coral A (1990) Growing bone cysts in long-term hemodialysis. Skeletal Radiol 19(1):43–49

51. Gomez-Dermit V, Gallardo E, Landeras R, Echevarría F, García Barredo R (2006) Subcutaneous angioleiomyomas: gray-scale and color Doppler appearances. J Clin Ultrasound 34:50–54
52. Graif M, Seton A, Nerubai J, Horoszowski H, Itzchak Y (1991) Sciatic nerve: sonographic evaluation and anatomic-pathologic considerations. Radiology 181:405–408
53. Greenspan A, Mc Gahan JP, Vogelsang P, Szabo RM (1992) Imaging strategies in the evaluation of soft-tissue hemangiomas of the extremities: correlation of the findings of plain radiography, angiography, CT, MRI and ultrasonography in 12 histologically proven cases. Skeletal Radiol 21:11–18
54. Griffith JF, Chan DP, Kumta SM, Chow LT, Ahuja AT (2004) Does Doppler analysis of musculoskeletal soft-tissue tumours help predict tumour malignancy? Clin Radiol 59(4):369–375
55. Gritzmann N, Schratter M, Traxler M, Helmer M (1988) Ultrasonography and computed tomography in deep cervical lipomas and lipomatosis of the neck. J Ultrasound Med 7:451–456
56. Harcke HT, Grissom LE, Finkelstein MS (1988) Evaluation of the musculoskeletal system with ultrasonography. Am J Roentgenol 150:1253–1261
57. Hashimoto BE, Kramer DJ, Wiitala L (1999) Applications of musculoskeletal sonography. J Clin Ultrasound 27:293–318
58. Heckmatt JZ, Dubowitz V (1985) Diagnostic advantage of needle muscle biopsy and ultrasound imaging in the detection of focal pathology in a girl with limb girdle dystrophy. Muscle Nerve 8:705–709
59. Hoddick WK, Callen PW, Filly RA, Mahony BS, Edwards MB (1984) Ultrasound evaluation of benign sciatic nerve sheath tumors. J Ultrasound Med 3:505–507
60. Hoglund M, Muren C, Engkvist O (1997) Ultrasound characteristics of five common soft-tissue tumours in the hand and forearm. Acta Radiol 38:348–354
61. Hong SH, Chung HW, Choi JY, Koh YH, Choi JA, Kang HS (2006) MRI findings of subcutaneous epidermal cysts: emphasis on the presence of rupture. AJR Am J Roentgenol 186(4):961–966
62. Hughes DG, Wilson DJ (1986) Ultrasound appearances of peripheral nerve tumors. Br J Radiol 59:1041–1043
63. Hughes J, Lam A, Rogers M (1999) Use of ultrasonography in the diagnosis of childhood pilomatrixoma. Pediatr Dermatol 16(5):341–344
64. Hung EHY, Griffith JF, Ng AW, Lee RKL, Lau DTY, Leung JCS (2014) Ultrasound of musculoskeletal soft-tissue tumors superficial to the investing fascia. Am J Roentgenol 202:W532–W540. doi:10.2214/AJR.13.11457
65. Hwang JY, Lee SW, Lee SM (2005) The common ultrasonographic features of pilomatricoma. J Ultrasound Med 24:1397–1402
66. Inampudi P, Jacobson JA, Fessell DP, Carlos RC, Patel SV, Delaney-Sathy LO, van Holsbeeck MT (2004) Soft-tissue lipomas: accuracy of sonography in diagnosis with pathologic correlation. Radiology 233(3):763–767
67. Jacobson JA (1999) Musculoskeletal sonography and MR imaging. A role for both imaging methods. Radiol Clin North Am 37:713–735
68. Jain R, Bandhu S, Sawhney S, Mittal R (2002) Sonographically guided percutaneous sclerosis using 1% polidocanol in the treatment of vascular malformations. J Clin Ultrasound 30(7):416–423
69. Jin W, Kim GY, Lew BL, Yang DM, Kim HC, Ryu JK, Park JS, Ryu KN (2008) Sonographic findings of an eccrine spiradenoma: case report and literature review. J Ultrasound Med 27(5):813–818. Review
70. Kaufman RA, Towbin RB, Babcock DS, Crawford AH (1982) Arthrosonography in the diagnosis of pigmented villonodular synovitis. Am J Roentgenol 139:396–398
71. Kaushik S, Miller TT, Nazarian LN, Foster WC (2003) Spectral Doppler sonography of musculoskeletal soft tissue masses. J Ultrasound Med 22(12):1333–1336
72. Kay J, Benson CB, Lester S, Corson JM, Pinkus GS, Lazarus JM, Owen WF (1992) Utility of high-resolution ultrasound for the diagnosis of dialysis-related amyloidosis. Arthritis Rheum 35: 926–931
73. Kerridge WD, Kryvenko ON, Thompson A, Shah BA (2015) Fat necrosis of the breast: a pictorial review of the mammographic, ultrasound, CT, and MRI findings with histopathologic correlation. Radiol Res Practice 2015:613139
74. Khuu A, Yablon CM, Jacobson JA, Inyang A, Lucas DR, Biermann JS (2014) Nodular fasciitis: characteristic imaging features on sonography and magnetic resonance imaging. J Ultrasound Med 33(4):565–573
75. Kirsch T (2012) Biomineralization – an active or passive process? Connect Tissue Res 53(6):438–445
76. Kraus R, Bokyung KH, Babcock DS, Oestreich AE (1986) Sonography of neck masses in children. Am J Roentgenol 146:609–613
77. Lang CJG, Neubauer U, Quaiyumi S, Fahlbusch R (1994) Intraneural ganglion of the sciatic nerve: detection by ultrasound [letter]. J Neurol Neurosurg Psychiatry 57:870–871
78. Lee DY, Hwang SC, Jeong ST, Nam DC, Park JS, Lee JH, Na JB, Kim DH (2015) The value of diagnostic ultrasonography in the assessment of a glomus tumor of the subcutaneous layer of the forearm mimicking a hemangioma: a case report. J Med Case Reports 9:191
79. Lee KJ, Jin W, Kim GY, Rhee SJ, Park SY, Park JS, Ryu KN (2015) Sonographic features of superficial-type nodular fasciitis in the musculoskeletal system. J Ultrasound Med 34(8):1465–1471
80. Lee RKL, Griffith JF, Ng AWN, Mac-Moune Lai F (2013) Ultrasound appearances of dermatofibrosarcoma protuberans. J Med Ultrasound 21:21e28

81. Leijten FS, Arts WF, Puylaert JBC (1992) Ultrasound diagnosis of an intraneural ganglion cyst of the peroneal nerve. J Neurosurg 76:538–540
82. Levey DS, Park YH, Sartoris DJ (1995) Radiologic review: imaging of pedal soft tissue neoplasms. J Foot Ankle Surg 34:413–415
83. Liang T, Panu A, Crowther S, Low G, Lambert R (2013) Ultrasound-guided aspiration and injection of an intraneural ganglion cyst of the common peroneal nerve. HSS J 9(3):270–274
84. Lin EC, Middleton WD, Teefey SA (1999) Extended field of view sonography in musculoskeletal imaging. J Ultrasound Med 18:147–152
85. Liu JC, Chiou HJ, Chen WM, Chou YH, Chen TH, Chen W, Yen CC, Chiu SY, Chang CY (2004) Sonographically guided core needle biopsy of soft tissue neoplasms. J Clin Ultrasound 32(6):294–298
86. Magarelli N, Carducci C, Bucalo C, Filograna L, Rapisarda S, De Waure C, Dell'Atti C, Maccauro G, Leone A, Bonomo L (2014) Sonoelastography for qualitative and quantitative evaluation of superficial soft tissue lesions: a feasibility study. Eur Radiol 24(3):566–573
87. Maldjian C, Adam R, Bonakdarpour A, Robinson TM, Shienbaum AJ (1999) MRI appearance of clear cell hidradenoma. Skeletal Radiol 28:104–106
88. Marzano L, Failoni S, Gallazzi M, Garbagna P (2004) The role of diagnostic imaging in synovial sarcoma. Our experience. Radiol Med (Torino) 107(5–6):533–540
89. McMahon LP, Radford J, Dawborn JK (1991) Shoulder ultrasound in dialysis related amyloidosis. Clin Nephrol 35:227–232
90. Morris SJ, Adams H (1995) Case report: paedriatic intramuscular haemangiomata – don't overlook the phlebolith ! Br J Radiol 68:208–211
91. Moss GD, Dishuk W (1984) Ultrasound diagnosis of osteochondromatosis of the popliteal fossa. J Clin Ultrasound 12:232–233
92. Mullaney PJ, Becker E, Graham B, Ghazarian D, Riddell RH, Salonen DC (2007) Benign hidradenoma: magnetic resonance and ultrasound features of two cases. Skeletal Radiol 36(12):1185–1190
93. Nalbant S, Corominas H, Hsu B, Chen LX, Schumacher HR, Kitumnuaypong T (2003) Ultrasonography for assessment of subcutaneous nodules. J Rheumatol 30:1191–1195
94. Obayashi T, Itoh K, Nakano A (1987) Ultrasonic diagnosis of schwannoma. Neurology 37:1817
95. Ogino T, Minami A, Fukuda K, Sakuma T, Kato H (1988) The dorsal occult ganglion of the wrist and ultrasonography. J Hand Surg 13-B:181–183
96. Orr NM, Taylor KJ (1990) Doppler detection of tumtor vascularity. In: Tailor KJ, Strandness DE (eds) Duplex Doppler ultrasound. Churchill Livingstone, New York, pp 149–163
97. Pai VR, van Holsbeeck M (1995) Synovial osteochondromatosis of the hip: role of ultrasonography. J Clin Ultrasound 23:199–203
98. Pass B, Jafari M, Rowbotham E, Hensor EM, Gupta H, Robinson P (2016) Do quantitative and qualitative shear wave elastography have a role in evaluating musculoskeletal soft tissue masses? Eur Radiol. [Epub ahead of print] doi:10.1007/s00330-016-4427-y
99. Patel P, Schucany WG (2012) A rare case of intraneural ganglion cyst involving the tibial nerve. Proc Baylor Uni Med Center 25(2):132–135
100. Pathria MN, Zlatkin M, Sartoris DJ, Scheible W, Resnick D (1988) Ultrasonography of popliteal fossa and lower extremities. Radiol Clin North Am 26:77–85
101. Patten RM, Shuman WP, Teefey S (1989) Subcutaneous metastases from malignant melanoma: prevalence and findings on CT. Am J Roentgenol 152:1009–1012
102. Pawaskar AS, Basu S (2015) Role of 2-Fluoro-2-deoxyglucose PET/computed tomography in carcinoma of unknown primary. PET Clin 10(3):297–310
103. Quinn TJ, Jacobson JA, Craig JG, van Holsbeeck MT (2000) Sonography of Morton's neuroma. Am J Roentgenol 174:1723–1728
104. Redd RA, Peters VJ, Emery SF, Branch HM, Rifkin MD (1989) Morton neuroma: sonographic evaluation. Radiology 171:415–417
105. Reuter KL, Raptopoulos V, De Girolami U, Akins CM (1982) Ultrasonography of plexiform neurofibroma in the politeal fossa. J Ultrasound Med 1:209–211
106. Richardson ML, Selby B, Montana MA, Mack LA (1988) Ultrasonography of the knee. Radiol Clin North Am 26:63–75
107. Richman JA, Gelberman RH, Engber WD, Salamon PB, Bean DJ (1987) Ganglions of the wrist and digits: results of treatment by aspiration and cyst wall puncture. J Hand Surg 12A:1041–1043
108. Riishede I, Ewertsen C, Carlsen J, Petersen MM, Jensen F, Nielsen MB (2015) Strain elastography for prediction of malignancy in soft tissue tumours—preliminary results. Ultraschall Med 36(4):369–374
109. Rowley VA, Cooperberg PL (1987) Ultrasound guided biopsy in interventional ultrasound. Clin Diagn Ultrasound 21:59–76
110. Rubens DJ, Fultz PJ, Gottlieb RH, Rubin SJ (1997) Effective ultrasonographically guided intervention for diagnosis of musculoskeletal lesions. J Ultrasound Med 16:831–842
111. Ryu JK, Jin W, Kim GY, Lee JH (2007) Sonographic and magnetic resonance imaging findings of a chondroid syringoma of the heel: case report and literature review. J Ultrasound Med 26(10):1435–1439
112. Scoutt LM, Zawin ML, Taylor KJ (1990) Doppler US. II clinical applications. Radiol 174:309–319
113. Sherman NH, Rosenberg HK, Heyman S, Templeton J (1985) Ultrasound evaluation of neck masses in children. J Ultrasound Med 4:127–134
114. Shen G, Zhang W, Jia Z, Li J, Wang Q, Deng H (2014) Meta-analysis of diagnostic value of 18F-FDG PET or PET/CT for detecting lymph node and

distant metastases in patients with nasopharyngeal carcinoma. Br J Radiol 87(1044)
115. Sheth S, Nussbaum AR, Hutchins GM, Sanders RC (1987) Cystic hygromas in children: sonographic-pathologic correlation. Radiology 1987:821–824
116. Shin YR, Kim JY, Sung MS, Jung JH (2008) Sonographic findings of dermatofibrosarcoma protuberans with pathologic correlation. J Ultrasound Med 27(2):269–274
117. Silvestri E, Bertolotto RP, Neumaier CE, Derchi LE (1994) Case Report: US detection of tendinous metastasis from malignant melanoma. Clin Radiol 49:288–289
118. Silvestri E, Martinoli C, Derchi LE, Bertolotto M, Chiaramondia M, Rosenberg I (1995) Echotexture of peripheral nerves: correlation between US and histologic findings and criteria to differentiate tendons. Radiology 197:291–296
119. Singson RD, Feldman F, Slipman CW, Gonzalea E, Rosenberg ZS, Kiernan H (1987) Postamputation neuromas and other symptomatic stump abnormalities: detection with CT. Radiology 162:743–745
120. Skirving AP, Kozak TKW, Davis SJ (1994) Infraspinatus paralysis due to spinoglenoid notch ganglion. J Bone Joint Surg 76B:588–591
121. Soo MS, Kornguth PJ, Hertzberg BS (1998) Fat necrosis in the breast: sonographic features. Radiology 206:261–269
122. Spicer PJ, Broussard G, Beaman F (2016) Isolated rheumatoid nodule of the achilles. Ultrasound Q 32(2):187–190
123. Spinner RJ, Harish S, Amrami KK (2014) An historical perspective on ulnar intraneural ganglion cysts and their joint origins. Hand New York, NY 9(3):395–398
124. Stefanidou D, D'Adamo P, Ronfani L, Montico M, Morgutti M, Gasparini P (2009) Detection of epidermal thickening in GJB2 carriers with epidermal US. Radiology 251:280–286
125. Taboada JL, Stephens TW, Krishnamurthy S, Brandt KR, Whitman GJ (2009) The many faces of fat necrosis in the breast. Am J Roentgenol 192(3):815–825
126. Takagishi K, Maeda K, Ikeda T, Itoman M, Yamamoto M (1991) Ganglion causing paralysis of the suprascapular nerve. Acta Orthop Scand 62:391–393
127. Takagishi K, Saitoh A, Tonegawa M, Ikeda T, Itoman M (1994) Isolated paralysis of the infraspinatus muscle. J Bone Joint Surg 76B:584–587
128. Temiz G, Şirinoğlu H, Demirel H, Yeşiloğlu N, Sarıcı M, Filinte GT (2015) Extradigital glomus tumor revisited: painful subcutaneous nodules located in various parts of the body. Indian J Dermatol 61(1):118
129. Veryser J, Gielen J, Declercq L, De Maeseneer M (2013) How we do it: interdigital US guided alcohol injection of Morton's Neuroma. Single Operator Technique with Web Space Compression Conference Paper. Radiological Society of North America 2013 Scientific Assembly and Annual Meeting
130. Vincent LM (1988) Ultrasound of soft tissue abnormalities of the extremities. Radiol Clin North Am 26:140–143
131. Weng L, Tirumalai AP, Lowery CM, Nock LF, Gustafson DE, Von Behren PL, Kim JH (1997) Extended-field-of-view imaging technology. Radiology 203:877–880
132. White EA, Filly RA (1980) Cholesterol crystals as the source of both diffuse and layered echoes in a cystic ovarian tumor. J Clin Ultrasound 8:241–243
133. Whittle C, Mackinnon J, Cabrera R, Silva C, Pires Y, González R (2013) Finger chondroid syringoma as a hypoechoic subcutaneous nodule in ultrasound. Ultrasound Q 29(3):211–213
134. Wilson DJ (1989) Ultrasonic imaging of soft tissues. Clin Radiol 40:341–342
135. Wook Jin MD, Kyung Nam Ryu MD, Gou Young Kim MD, Hyun Cheol Kim MD, Jae Hoon Lee MD, Ji Seon P (2008) Sonographic findings of ruptured epidermal inclusion cysts in superficial soft tissue emphasis on shapes, pericystic changes, and pericystic vascularity MD. J Ultrasound Med 27:171–176
136. Wortsman X, Bouer M (2013) Common benign nonvascular skin tumors. In: Wortsman X, Jemec GBE (eds) Dermatologic ultrasound with clinical and histologic correlations, 1st edn. Springer, New York, pp 119–175
137. Wortsman X, Vergara P, Castro A, Saavedra D, Bobadilla F, Sazunic I, Zemelman V, Wortsman J (2015) Ultrasound as predictor of histologic subtypes linked to recurrence in basal cell carcinoma of the skin. J Eur Acad Dermatol Venereol 29:702–707
138. Wortsman X, Wortsman J (2010) Clinical usefulness of variable-frequency ultrasound in localized lesions of the skin. J Am Acad Dermatol 62(2):247–256
139. Wu S, Liu G, Tu R (2012) Value of ultrasonography in neurilemmoma diagnosis: the role of round shape morphology. Med Ultrason 14:192–196
140. Yablon CM (2013) Ultrasound-guided interventions of the foot and ankle. Semin Musculoskelet Radiol 17(1):60–68
141. Zornoza J, Bernardino ME, Ordonez NG, Thomas JL, Cohen MA (1982) Percutaneous needle biopsy of soft tissue tumors guided by ultrasound and computed tomography. Skeletal Radiol 9:33–36
142. Zwiebel WJ (1990) Color duplex imaging and Doppler spectrum analysis: principles capabilities, and limitations. Semin Ultrasound CT MRI 1:84–96

Radiography and Computed Tomography

2

R. Botchu, S.L. James, and A.M. Davies

Contents

2.1 **Introduction** 41

2.2 **Plain Radiography** 42
2.2.1 Location 42
2.2.2 Size 42
2.2.3 Rate of Growth 42
2.2.4 Shape and Margins 43
2.2.5 Radiodensity 43
2.2.6 Bone Involvement 45

2.3 **Angiography** 47

2.4 **Computed Tomography** 48
2.4.1 CT Features 49
2.4.2 CT Compared with MRI 51

References 56

R. Botchu (✉) • S.L. James • A.M. Davies
Royal Orthopaedic Hospital NHS Foundation Trust, Birmingham, UK
e-mail: drrajeshb@gmail.com

2.1 Introduction

The imaging evaluation of a patient with a suspected soft tissue tumor requires a methodical approach that recognizes the benefits and limitations of the numerous imaging techniques that are available today [4, 14, 25]. Consideration must be given to the financial costs and invasiveness of each technique balanced against the diagnostic reward. The temptation to routinely employ every technique in all patients should be resisted. Similarly, no examination should be reported in isolation without knowledge of relevant clinical details and results of prior investigations. Where possible, the prior investigations should be available for review, as the appreciation of the significance of a new observation may well depend upon a retrospective review of the previous studies [24].

In this chapter we discuss the role of plain radiography, angiography, and computed tomography (CT) in the management of a patient with a soft tissue mass, from detection and diagnosis through to the ultimate aim of medical management, a cure. It is beyond the scope of this book to discuss in detail the technology behind each technique. The reader is referred to subsequent chapters for an in-depth discussion of each type of soft tissue tumor.

© Springer International Publishing AG 2017

F.M. Vanhoenacker et al. (eds.), *Imaging of Soft Tissue Tumors*, DOI 10.1007/978-3-319-46679-8_2

2.2 Plain Radiography

Despite the undoubted technological advances in imaging over the past three decades, the evaluation of a suspected soft tissue mass is complimented with the plain radiograph [2]. It is cheap, universally available, and easy to obtain. The importance of this single piece of advice cannot be overemphasized. It is stated in virtually every textbook on the subject, but is all too frequently overlooked in current day-to-day practice. Indeed it denigrates its value to call it "plain" radiography. In most cases, two views at right angles are mandatory to delineate soft tissue planes and the integrity of adjacent cortical bone.

The lack of contrast resolution is a well-recognized limitation of plain radiography, but the value of the examination should not be underestimated. It may not identify the precise diagnosis in any but a minority of cases, but can still provide valuable information, e.g., the presence of calcification and bone involvement. Too often the humble radiograph is denigrated as noncontributory because it has failed to identify features that might be termed "positive." The absence of said features, however, can be just as significant. The absence, for example, of any bony abnormality immediately indicates that the primary pathology is of soft tissue origin, with a large differential diagnosis. Myositis ossificans, as a more specific example, can be effectively excluded from the differential diagnosis of a mass if there is no radiographic evidence of calcification, in all but the earliest of cases. The radiographic features that should be assessed in each case are discussed below [39].

2.2.1 Location

The identification of the location of a tumor is primarily clinical and will dictate which area is initially imaged. While almost all true soft tissue tumors can occur anywhere in the musculoskeletal system, some have a predilection for certain areas, which will be highlighted in later chapters. Many nonneoplastic processes presenting with a soft tissue mass arise at characteristic locations, for example, gouty tophi in the hands and feet and synovial cysts in the popliteal fossa [27]. Multiple soft tissue masses should suggest neurofibromatosis, lipoma, and occasionally metastatic deposits and Kaposi sarcoma [30, 39]. The vast majority of soft tissue sarcomas, if given the opportunity to metastasize, will do so first to the lungs. It is for this reason that a chest radiograph is a mandatory early investigation in all cases of suspected soft tissue malignancy.

2.2.2 Size

Although the size of a soft tissue mass can have a bearing on subsequent management, the actual size is of limited diagnostic value [30]. Malignant lesions tend to be larger than benign ones [33], but this is rarely helpful in individual cases. Soft tissue masses, irrespective of their tissue of origin, arising in small anatomical areas such as the hands and feet, typically are found relatively early. They therefore tend to be smaller than those arising in large anatomical areas such as the buttocks. It can be anticipated that tumors will be larger at presentation in those countries where access to medical facilities remains poorly developed.

2.2.3 Rate of Growth

Alterations in the size of a soft tissue tumor can be crudely estimated clinically and by comparing serial radiographs. Procrastination in advocating follow-up with serial radiographs should only be employed when the clinical and imaging features indicate a benign lesion with a considerable degree of certainty. Failure to promptly diagnose and treat a soft tissue sarcoma can only prejudice the outcome for the patient. Absent or slow growth is typical of a benign neoplasm, whereas malignant tumors frequently show a rapid rate of growth. It should be noted, however, that hemorrhage and infection will also produce rapidly enlarging soft tissue masses.

2.2.4 Shape and Margins

As with the size of a soft tissue tumor, the shape reveals little diagnostic information [39]. Malignant lesions are more commonly irregularly shaped, distorting and obscuring tissue planes. Benign lesions will tend to displace but not obliterate normal tissue planes. Once again, infective lesions can mimic malignancy, as they are also frequently poorly defined due to fluid infiltration of the adjacent soft tissues. The definition of the margins of a lesion depends on a number of factors. These include the anatomical location relative to normal fat planes and bones and the radiodensity of the constituents of the tumor relative to normal muscle.

2.2.5 Radiodensity

The muscle compartments of the extremities can be visualized radiographically as separated by low-density fat planes. The majority of soft tissue tumors are of a density similar to that of muscle and are, therefore, only revealed by virtue of mass effect. This includes displacement or disruption of the adjacent fat planes (Fig. 2.1), distortion of the skin contour, and involvement of bone.

In a minority of cases, part or all of the tumor may exhibit a radiodensity sufficiently different to that of water for the tumor to be visualized directly. Only fat and gas will give a radiodensity less than that of muscle. Lipomas, the commonest of all the soft tissue tumors, produce a low radiodensity between that of muscle and air. For this reason lipomas are well demarcated from the surrounding soft tissues and can be diagnosed with moderate confidence [21] (Fig. 2.2). It should be noted that low-grade liposarcomas may contain variable amounts of lipomatous tissue, which also appears relatively radiolucent on radiography (Fig. 2.3). Air in the soft tissues is said to be specific to infection [30]. While infection is certainly the commonest cause, it may also be seen in necrotic fungating tumors, albeit with secondary infection (Fig. 2.4), as well as being a normal feature following open biopsy or other surgical procedures. Air in the soft tissues of the thoracic wall and neck always suggests the possibility of surgical emphysema.

Fig. 2.1 Myxofibrosarcoma arising in the adductors of the upper thigh in a 75-year-old man. Plain radiograph. The tumor is only visible by virtue of its mass effect on tissue planes

Increased radiodensity may be seen in the tissues due to hemosiderin, calcification, or ossification. Hemosiderin deposition typically occurs in synovial tissues exposed to repeated hemorrhage, such as (tenosynovial) giant cell tumor, pigmented villonodular synovitis (see Chap. 15), and hemophilic arthropathy. Radiographs can distinguish between calcification and ossification and the differing patterns [54]. Mineralization in the soft tissues is a feature of a large spectrum of disorders including congenital, metabolic, endocrine, traumatic, and parasitic infections [38]. Primary soft tissue tumors are one of the less

Fig. 2.2 Lipoma arising on the radial aspect of the elbow. Plain radiograph. The tumor is sharply marginated with the uniform low density of fat

common causes of calcification that the general radiologist can expect to see in his or her routine practice. Close attention to the clinical details and location will exclude many of the nonneoplastic causes. For example, soft tissue calcifications in the hands and feet are rarely associated with neoplasia, and many of the multifocal lesions will be either due to a collagen vascular disorder or the residuum of a parasitic infection. Again, the clinical details and country of origin of the patient should be pointers to the correct diagnosis. Occasionally certain normal variants, including companion shadows and the fascia lata, may simulate soft tissue calcification or periosteal new bone formation and should not be mistaken for a neoplastic process [23].

Analysis of the pattern of calcification within a soft tissue tumor can indicate the tissue type. Circular foci with a lucent center representing a phlebolith, when identified outside the pelvis, is diagnostic of a hemangioma (Fig. 2.5). Phleboliths are not usually apparent until adolescence, so that conditions such as Maffucci syndrome (Fig. 2.6) in the child may not be radiographically distinguishable from multiple enchondromatosis (Ollier disease).

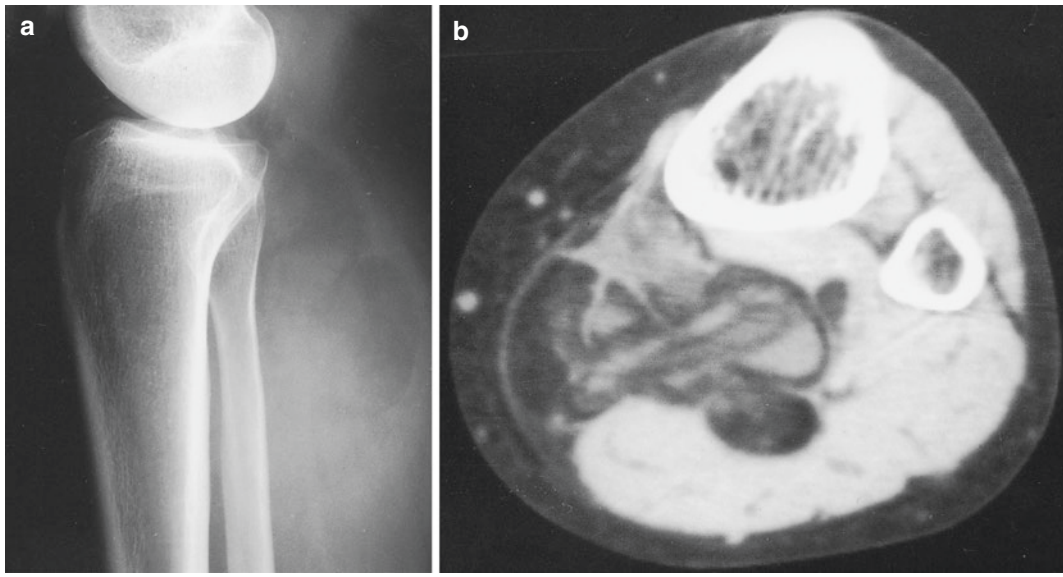

Fig. 2.3 Low-grade liposarcoma arising behind the knee joint in a 55-year-old woman. (**a**) Plain radiograph. (**b**) Computed tomography (CT). Fat density areas are visible on the radiograph (**a**) with mixed fat and soft tissue attenuation on CT (**b**)

Fig. 2.4 Necrotic, fungating clear cell sarcoma in a 62-year-old woman. Plain radiograph. The loculi of gas within the tumor indicate secondary infection

Fig. 2.5 Extensive hemangioma of the forearm in an adolescent male. Plain radiograph. Note the presence of multiple phleboliths

Chondroid tissue reveals ring-and-arc calcification. While this does not distinguish between benign or malignant cartilage formation, the majority of soft tissue masses with this feature, in the vicinity of a joint, will arise from synovial chondromatosis (Fig. 2.7) [37] and in the hands and feet will be soft tissue chondromas. Calcification or ossification in the infrapatellar (Hoffa) fat pad is typical of a para-articular chondroma (Fig. 2.8) [17].

Osteoid mineralization may occur as "cloud-like" densities or mature trabecular bone. The latter suggests a slow-growing lesion such as a lipoma, low-grade liposarcoma, or hemangioma [30]. Poorly defined, amorphous calcification is found in up to 30 % of synovial sarcomas (Fig. 2.9) [6, 18, 31] and approximately 50 % of extraskeletal osteosarcomas (Fig. 2.10). This is an extremely useful distinguishing feature from the tumor-mimicking myositis ossificans, which exhibits marginal calcification (Fig. 2.11) [13, 34]. Another traumatic condition that presents with a peripherally mineralized mass and plate-like configuration of calcification along the course of muscle, almost exclusively in the calf, many years after a major injury, is calcific myonecrosis (Fig. 2.12) [9, 22].

2.2.6 Bone Involvement

It may be difficult to differentiate a primary soft tissue tumor with osseous involvement from a bone tumor with soft tissue extension [29]. As a rule, the site of the more extensive abnormality, be it bone or soft tissue, represents the primary focus [39]. Only a minority of soft tissue tumors involve bone. The degree of bone involvement

Fig. 2.6 Maffucci syndrome in a 32-year-old man. Plain radiograph. Multiple enchondromas and soft tissue hemangiomas indicated by the phleboliths

Fig. 2.7 Soft tissue mass in a 62-year-old man. Plain radiograph. Characteristic chondroid calcifications arising from the posterior aspect of the knee joint due to synovial chondromatosis

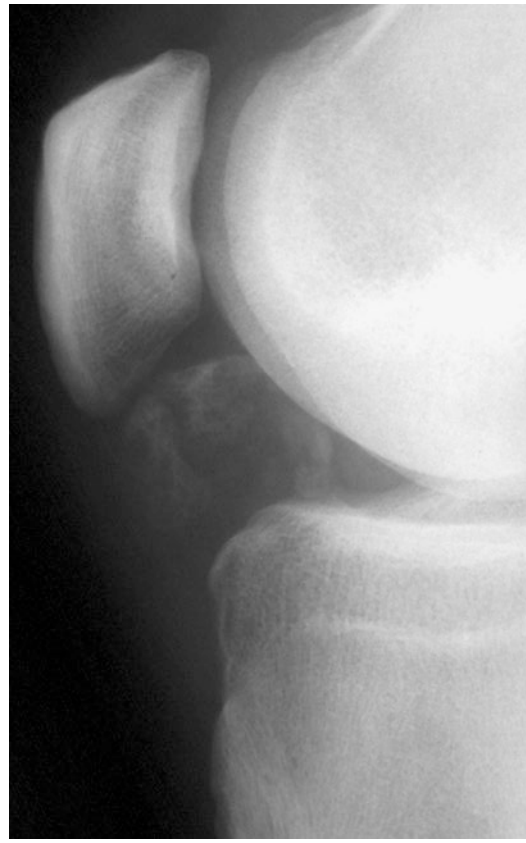

Fig. 2.8 Para-articular chondroma in a 44-year-old man. Plain radiograph. Minor ossification arising in the Hoffa fat pad

may vary from cortical hyperostosis, as seen in a parosteal lipoma (Fig. 2.13), through the pressure erosion seen in slow-growing masses (Fig. 2.14), to direct invasion, as seen in aggressive lesions (Fig. 2.15). The presence of ill-defined cortical destruction is strongly indicative of malignancy, although it may also occur with paraosseous infections. The converse does not apply in that well-defined pressure erosion may occur with both benign and malignant soft tissue tumors (Fig. 2.11). Aggressive fibromatosis (extra-abdominal desmoid tumor) is a benign, but locally invasive condition, which can cause irregular adjacent bone erosion in one-third of cases (Fig. 2.16).

Cortical destruction with an outer, saucer-like configuration, "saucerization," occurs in Ewing's sarcoma and bony metastatic disease and should not be mistaken for secondary bone invasion from a large soft tissue sarcoma [26].

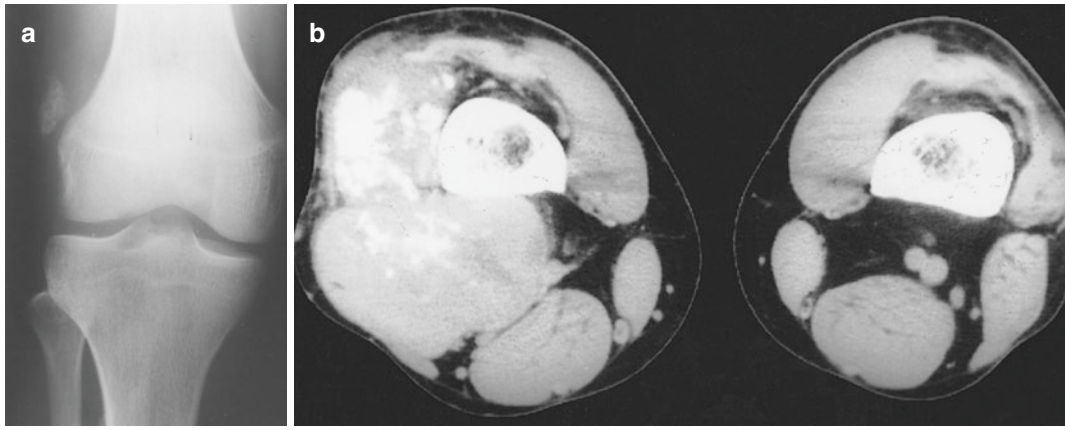

Fig. 2.9 Synovial sarcoma arising in the vastus lateralis in a 66-year-old man. (**a**) Plain radiograph. (**b**) CT. Both imaging techniques demonstrate amorphous calcification

Fig. 2.10 Extraskeletal osteosarcoma in a 50-year-old man. Plain radiograph. Densely mineralized lesion arising in the adductors

Fig. 2.11 Myositis ossificans of the forearm in a 38-year-old woman. Plain radiograph. Soft tissue mass lying on the surface of the proximal radius showing typical peripheral mineralization

2.3 Angiography

Prior to the introduction of cross-sectional imaging, angiography was the most useful imaging technique for the demonstration of soft tissue sarcomas [49, 55, 56]. For many years it was considered an important adjunct to conventional radiography in patient management [19, 28].

Angiography can delineate the full extent of feeding and draining vessels of vascular malformations, but has been largely superseded by CT angiography or magnetic resonance (MR) angiography. Preoperative angiography may continue to be employed in planning surgery in difficult cases or as a prelude to embolotherapy [52, 57].

Angiography can differentiate between the two histological types of hemangioma, capillary

Fig. 2.12 Calcific myonecrosis in an 87-year-old woman. Plain radiograph. Soft tissue mass with peripheral mineralization causing pressure erosion on the adjacent tibia

Fig. 2.13 Parosteal lipoma arising on the surface of the tibia in a 67-year-old woman. Plain radiograph. Lobulated fat density mass with typical periosteal new bone formation

and cavernous. MR angiography can be a useful adjunct to MRI in selected cases. This includes the differentiation of a soft tissue tumor from an aneurysm.

Isolated limb perfusion chemotherapy for melanoma has been shown to be effective in management of advanced melanoma of the extremity.

2.4 Computed Tomography

The introduction of CT proved a revolution in the detection and preoperative management of soft tissue tumors [16, 19, 28, 41, 43, 46].

Although there are some concerns regarding the potential for increasing the radiation dose, thin-section scanning allows for different types of postprocessing, such a multiplanar reconstructions, volume rendering, and surface-shaded display (Fig. 2.17). PET-CT (positron emission tomography-computed tomography) is one of the gold standards of metabolic imaging. This provides functional as well as anatomical information of the lesion, which can be useful in staging of sarcomas. This technique is a useful adjunct in planning biopsies from metabolically active component of the tumor and in monitoring of treatment of soft tissue sarcomas [2, 11]. This will be covered in Chap. 3.

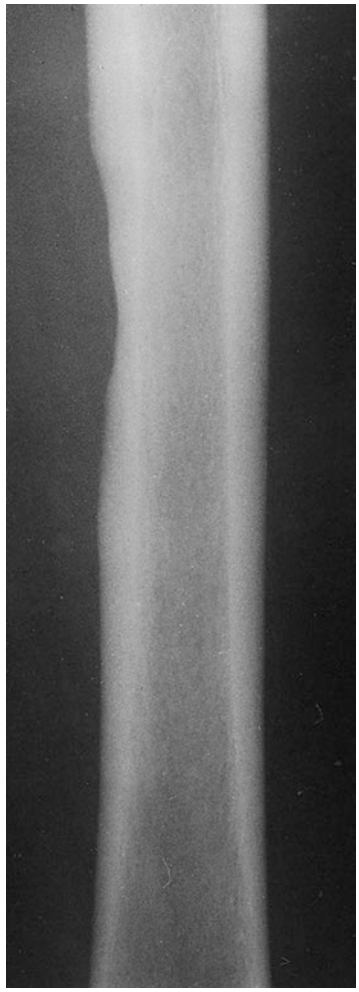

Fig. 2.14 Myxofibrosarcoma of the upper leg in a 65-year-old man. Plain radiograph. Soft tissue mass causing pressure erosion on the medial cortex of the femoral diaphysis

Fig. 2.15 Undifferentiated spindle cell sarcoma of the calf in a 78-year-old woman who refused medical treatment for 2 years. Plain radiograph. The tumor has destroyed the proximal fibula, with extensive invasion of the tibial metaphysis

2.4.1 CT Features

The CT features that should be assessed in each case are similar to those described above for evaluating the conventional radiograph. This reflects the fact that both are radiographic techniques relying on the attenuation of an X-ray source. The principal advantages of CT over the radiograph are the improved soft tissue resolution and the axial, in contrast to longitudinal, imaging plane. The first feature to assess is the attenuation value of the mass. Fat will show the lowest attenuation of any tissue, and a benign lipoma can be diagnosed on CT by the uniformly low attenuation (−70 to −130 HU; Fig. 2.18) [15, 21]. It is not possible to reliably differentiate on CT a simple lipoma from an atypical lipomatous tumor (well-differentiated liposarcoma). In the peripheries this is rarely a management problem, as the treatment of the two conditions is the same. A few fibromuscular septa of soft tissue density traversing the lipoma are acceptable (Fig. 2.19). A tumor comprising a combination of fat and solid component is suggestive of a low-grade liposarcoma (Fig. 2.3b) [8]. Only air will show an attenuation less than that of fat (Fig. 2.19).

Fluid-filled structures, seromas, old hematomas, and synovial cysts have an attenuation value less than that of muscle and more than

Fig. 2.16 Aggressive fibromatosis in a 37-year-old woman. Plain radiograph. There is erosion of the proximal tibia

that of fat (Fig. 2.20) [42, 44, 48]. Such fluid collections are usually homogeneous and well-defined. Abscesses typically have an attenuation value slightly higher than that of simple fluid (Fig. 2.19) [36, 53].

The majority of soft tissue sarcomas have an attenuation value slightly less than that of normal muscle (Fig. 2.21). The highest attenuation found in the soft tissues on CT is that of calcification and ossification, approximating to that of cortical bone. CT exquisitely demonstrates calcification more clearly than conventional radiography (Figs. 2.9) and can easily distinguish between calcification and ossification (Figs. 2.9) [54]. A peripheral ring of calcification is a characteristic CT feature of myositis ossificans (Fig. 2.22) [3, 23]. The differential diagnosis should include the rare soft tissue aneurysmal bone cyst, which also shows peripheral calcification [50].

Tumor margins can easily be defined on CT in most cases provided there is sufficient mass effect or attenuation difference. As might be expected, slow-growing lesions tend to be better defined than aggressive lesions. The margin is an indicator of the rate of growth rather than whether it is benign or malignant. As on conventional radiographs, infective lesions will tend to be poorly defined due to fluid infiltration in the surrounding soft tissues (Fig. 2.19) [36, 53]. The conspicuity of tumor margins and the relationship to adjacent vessels can be improved following enhancement with iodinated contrast medium (Fig. 2.21) [51]. Contrast medium is helpful in those cases where there is doubt as to whether a mass is solid or cystic. Very occasionally a soft tissue tumor will be isodense with muscle on a precontrast CT scan and only be revealed on a postcontrast examination [27]. In this situation, the presence of mass effect will usually be sufficient to alert the wary observer. Contrast enhancement will also give an indication of the vascularity of a tumor, which can be of value in selected cases (Fig. 2.23). CT angiography is an alternative and also an adjunct to MR angiography which provides an accurate description of tumor vascularity and the relationship of a soft tissue tumor and adjacent vessels (Fig 2.24). This is a crucial component of preoperative planning which contributes to successful surgery [28].

CT gives an excellent demonstration of the relationship of a soft tissue tumor to the adjacent bones. It is more accurate than conventional radiography, but less so than MRI, revealing medullary bone involvement. It can be useful in assessing the relationship of a tumor to bone in anatomically complex areas such as the spine and pelvis.

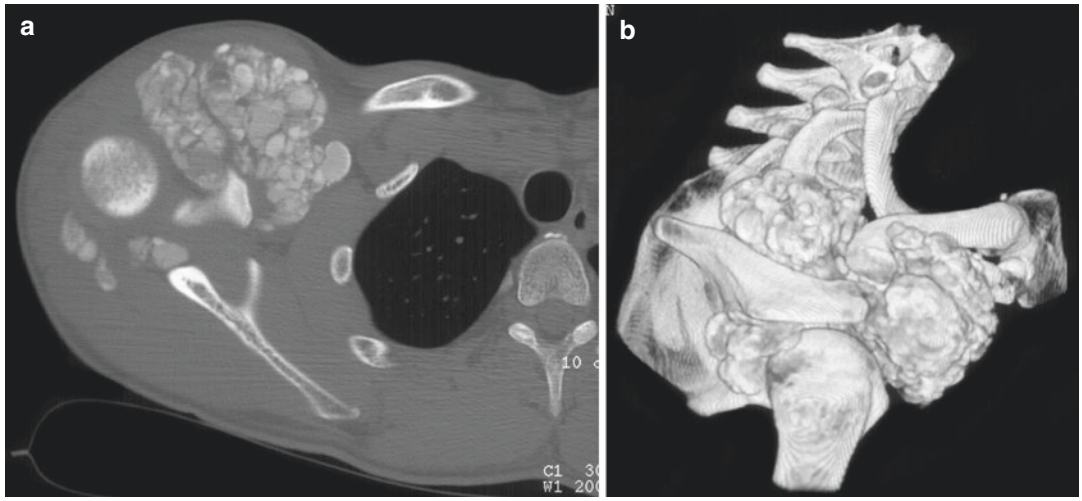

Fig. 2.17 Tumoral calcinosis associated with chronic renal failure. (**a**) Computed tomography. (**b**) Surface-rendered 3D reconstruction. Soft tissue masses with amorphous calcification. The distribution is readily appreciated on the reconstruction (**b**)

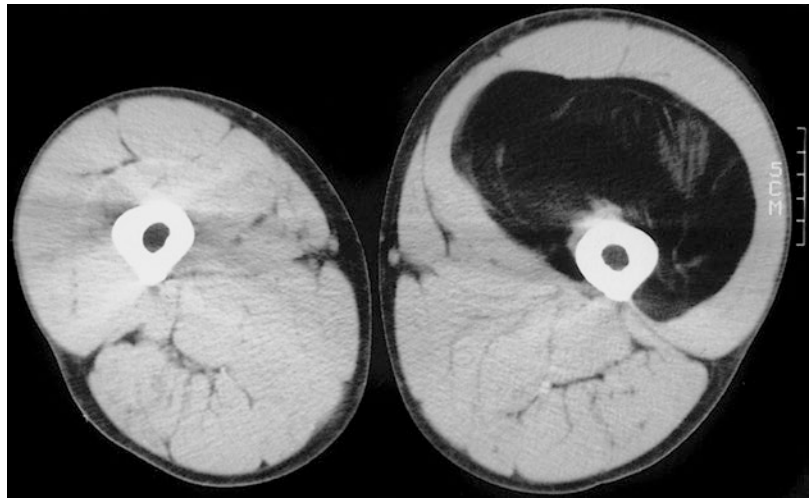

Fig. 2.18 Benign lipoma in the left anterior thigh of a 26-year-old man. Using computed tomography, a few fibromuscular septa can be identified traversing the lipoma

2.4.2 CT Compared with MRI

Studies have suggested that CT tends to overestimate the extent of a soft tissue sarcoma [10, 32], presumably due to local lymphatic obstruction. This is not a problem for management, as curative surgery will require excision of the whole compartment, edema and all. It would be a matter of more concern if CT were to underestimate the true tumor extent, as this would prejudice attempts at curative surgery.

With limb-salvage surgery, the aim in most patients, there is always a risk of local recurrence, particularly in patients with a high-grade sarcoma. The risk is increased considerably if the excision is found to be marginal or even intralesional. MRI is the preferred technique to detect early recurrences, but both techniques are of comparable accuracy if

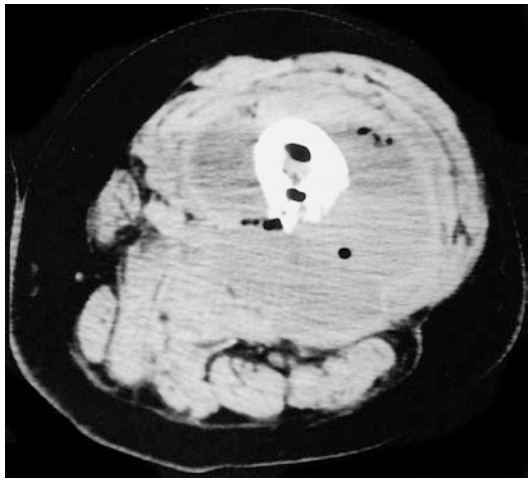

Fig. 2.19 Gas-forming clostridial osteomyelitis of the femur in a 59-year-old man. Computed tomography. Loculi of gas are present within the bone and surrounding abscess

Fig. 2.20 Chronic hematoma in the thigh of a 28-year-old man at the site of nonunion of an old femoral fracture. Computed tomography. The overlapping fracture ends are seen as two separate bony structures. The attenuation of the hematoma measures 20 HU surrounded by a higher attenuation pseudocapsule

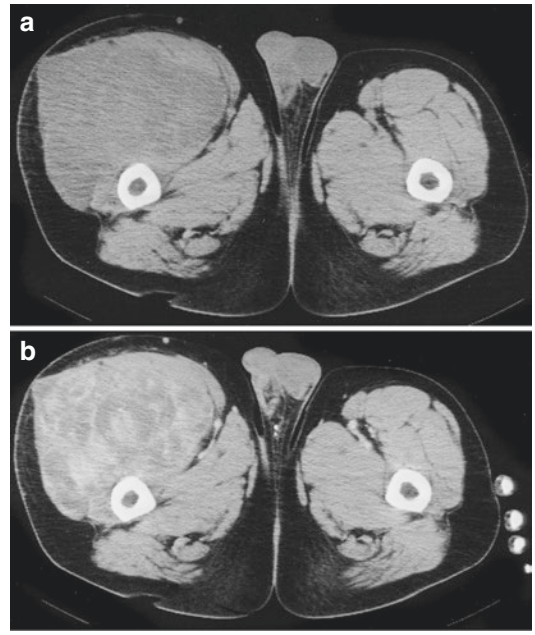

Fig. 2.21 Liposarcoma of the thigh in a 68-year-old man. (**a**) Computed tomography (CT) scan. (**b**) After intravenous contrast medium. Mass arising in the right vastus intermedius muscle slightly hypodense to muscle on unenhanced CT (**a**) and irregularly enhancing after contrast administration (**b**)

the recurrence is greater than 15 cm3 in volume [40]. CT is unable to reliably differentiate residual tumor from hematoma and granulation tissue following excisional biopsy [20].

Twenty years ago it was being claimed that MRI would supersede CT as the primary imaging technique in the evaluation of soft tissue tumors [5, 7]. In the developed world, this prediction has been fulfilled, but where access to MRI remains limited or contraindicated, CT will continue to provide an adequate alternative for the majority of patients with a soft tissue mass. Indeed, one study comparing CT and MRI in the local staging of primary malignant musculoskeletal neoplasms yields the conclusion that both techniques are equally accurate in the local staging of bone and soft tissue neoplasms (Figs. 2.25 and 2.26) [35]. In fairness, this study has been the subject of some controversy since its publication, as critics argue that many of the MR examinations were obtained on older machines, without the use of an intravenous gadolinium chelate [47]. In developing countries, which do not have access to MR, CT angiography remains an integral part of preoperative planning of certain soft tissue sarcomas [1].

Fig. 2.22 Myositis ossificans of the proximal thigh in a 12-year-old girl. (**a**) Computed tomography (CT). (**b**) CT 6 weeks later. Mass with early peripheral calcification in the left iliopsoas muscle (**a**) and the signs of maturation 6 weeks later (**b**)

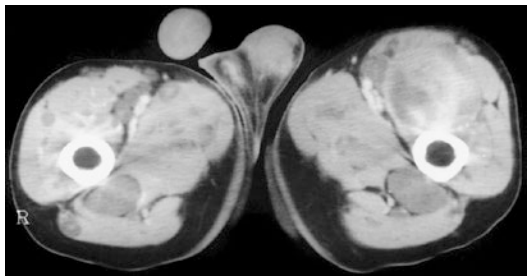

Fig. 2.23 Neurofibromatosis in the proximal thighs of a 23-year-old man. Computed tomography (CT) after iodinated contrast injection. Enhancement of the neurofibrosarcoma in the left anterior thigh. The numerous remaining neurofibromata, particularly involving the sciatic nerves, show no significant enhancement

CT remains preeminent in the investigation of chest metastases, revealing nodules several millimeters in diameter that are not visible on a chest radiograph. A CT examination of the chest should be performed as part of the initial preoperative staging of patients with a soft tissue sarcoma. MDCT, by eliminating respiratory motion and minimizing partial volume errors, results in a high rate of detection of smaller nodules. Routine follow-up of patients with serial chest CT examinations is of doubtful value, particularly in view of the considerable radiation dose involved. CT of the chest is indicated if a follow-up chest radiograph suggests early metastatic disease. Metastatic spread to regional lymph nodes is uncommon in soft tissue sarcomas and is usually present only in the later stages of the disease. CT identifies abnormally enlarged nodes but cannot reliably distinguish reactive change from metastatic involvement.

The risk of venous thromboembolism is significantly increased in patients with tumors including soft tissue sarcomas. The incidence ranges from 0.4 to 25 %. Shantakumar and colleagues had reported an incidence of 3 % of pulmonary embolism in a cohort of 3480 older patients with soft tissue sarcoma [45]. Majority of the thromboembolism occurs within the first three months, and the incidence is significantly increased in patients undergoing chemotherapy.

Computed tomography pulmonary angiography (CTPA) can diagnose pulmonary embolism with a sensitivity of 74 % and specificity of 89 % [42]. Clinically unsuspected pulmonary embolism is frequently diagnosed in patients undergoing routine CT for staging or as a part of monitoring. The incidence of unsuspected pulmonary embolism ranges from 1 to 5 %. However, a normal renal function, measured by the estimated glomerular filtration rate (eGFR), is required for contrast-enhanced examinations. One needs to be aware of the risk of contrast-induced acute kidney

Fig. 2.24 Arteriovenous malformation (AVM). (**a**) Axial CT, postcontrast.(**b**) coronal reconstruction of CT angiogram. (**c**) 3D reconstruction. AVM in the first web space (Image courtesy F.M. Vanhoenacker)

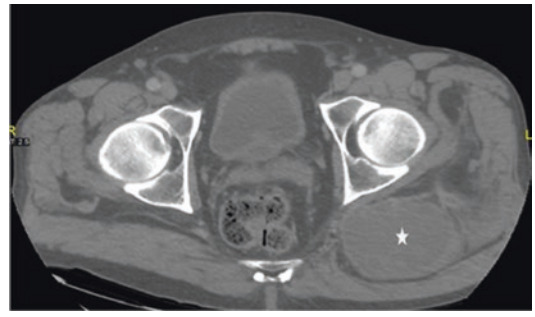

Fig. 2.25 Undifferentiated spindle cell sarcoma in a 45-year-old man. Computed tomography (CT) with intravenous contrast medium shows the tumor arising in the left buttocks (*)

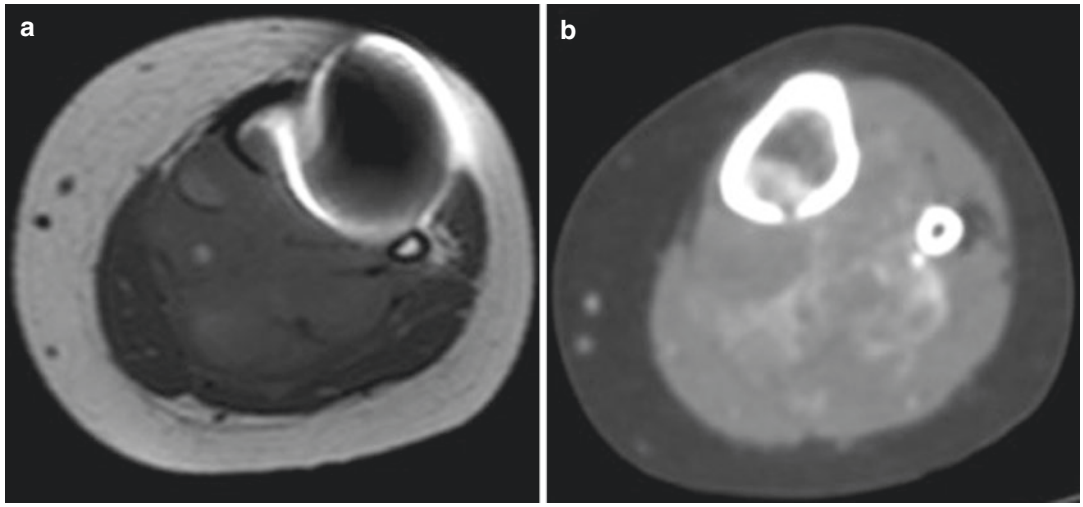

Fig. 2.26 High-grade undifferentiated pleomorphic sarcoma in a 40-year-old man. (**a**) Axial T1-weighted, fast spin-echo image. (**b**) Computed tomography (CT) with intravenous contrast medium. The tumor is partially obscured due to bloom artifact from metal on MR. CT shows the true extent of the tumor

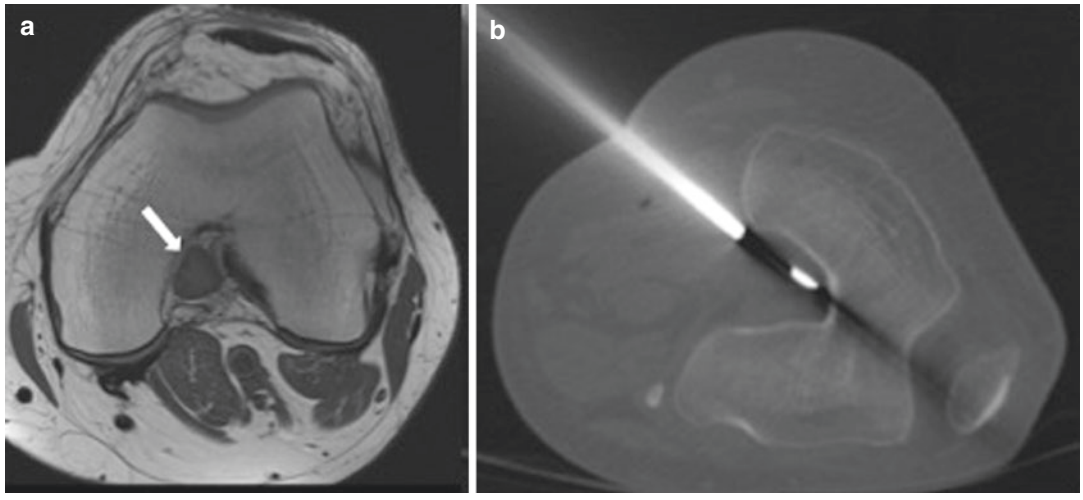

Fig. 2.27 Soft tissue mass in a 45-year-old man. (**a**) Axial proton density image. (**b**) Computed tomography (CT). MR shows the soft tissue synovial mass (*arrow*), which was biopsied under CT guidance

injury that can be associated with iodinated contrast, which is commonly used while performing CT [12].

CT can be used to facilitate biopsy of soft tissue tumors, particularly utilizing CT fluoroscopy [57]. It is usually reserved for those cases in which tumors are either small (i.e., impalpable) or situated in a relatively inaccessible location (for instance, in the intercondylar notch of the knee) (Fig. 2.27).

Key Points

1. Evaluation of a suspected soft tissue mass should always commence with plain radiography. Valuable information may be derived from the presence of calcifications or ossifications, internal fatty components, and air and bone involvement.
2. Angiography has been largely replaced by MRI for soft tissue tumor characterization. It may still be used to preclude embolotherapy or in the case of isolated limb perfusion with chemotherapy.
3. CT has been superseded by MRI for soft tissue tumor characterization, but it remains valuable for guiding biopsy and for the detection of distant tumor spread in the lungs. PET-CT is one of the gold standards of metabolic imaging and a useful adjunct in management of soft tissue sarcomas.

References

1. Adigun IA, Rahman GA, Ogundipe KO (2010) Soft tissue sarcoma of the thigh: need for angiography in the developing countries. Ann Afr Med 9(1):39–43
2. Aga P, Singh R, Parihar A, Parashari U (2011) Imaging spectrum in soft tissue sarcomas. Indian J Surg Oncol 2(4):271–279
3. Amendola MA, Glazer GM, Agha FP, Francis IR, Weatherhouse L, Martel W (1983) Myositis ossificans circumscripta: computed tomographic diagnosis. Radiology 149:775–779
4. Angervall L, Kindblom LG, Rydholm A, Stener B (1986) The diagnosis and prognosis of soft tissue tumors. Semin Diagn Pathol 3:40–258
5. Bland K, McCoy DM, Kinard RE, Copeland EM (1987) Application of magnetic resonance imaging and computed tomography as an adjunct to the surgical management of soft tissue tumors. Ann Surg 205:473–480
6. Cadman NL, Soule EH, Kelly PJ (1965) Synovial sarcoma: analysis of 134 tumors. Cancer 18:613–627
7. Chang AE, Matory YL, Dwyer AJ, Hill SC, Girton ME, Steinberg SM, Knop RH, Frank YA, Hyams D, Doppman YL (1987) Magnetic resonance imaging versus computed tomography in the evaluation of soft tissue tumors of the extremities. Ann Surg 205:340–348
8. deSantos LA, Ginaldi S, Wallace S (1981) Computed tomography in liposarcoma. Cancer 47:46–54
9. Dhillon M, Davies AM, Benham J, Evans N, Mangham DC, Grimer RJ (2004) Calcific myonecrosis: a report of ten new cases. Eur Radiol 14:1974–1979
10. Egund N, Ekeland L, Sako M, Persson B (1981) CT of soft tissue tumors. AJR Am J Roentgenol 137: 725–729
11. Etchebehere EC, Hobbs BP, Milton DR, Malawi O, Patel S, Benjamin RS, Macapinlac HA (2015) Assessing the role of 18F-FDG PET and 18F-FDG PET/CT in the diagnosis of soft tissue musculoskeletal malignancies: a systematic review and meta-analysis. Eur J Nucl Med Mol Imaging 43(5):860–870, Dec 3. [Epub ahead of print]
12. Goldfarb S, McCullough PA, McDermott J, Gay SB (2009) Contrast-induced acute kidney injury: specialty-specific protocols for interventional radiology, diagnostic computed tomography radiology, and interventional cardiology. Mayo Clin Proc 84(2):170–179
13. Goldman AB (1976) Myositis ossificans circumscripta: a benign lesion with a malignant differential diagnosis. AJR Am J Roentgenol 126:32–40
14. Greenfield GB, Arrington JA (1995) Imaging of bone tumors. Lippincott, Philadelphia
15. Halldorsdottir A, Ekelund L, Rydholm A (1982) CT diagnosis of lipomatous tumors of the soft tissues. Arch Orthop Trauma Surg 100:211–216
16. Heiken JP, Lee JKT, Smathers RL, Totty WG, Murphy WA (1984) CT of benign soft tissue masses of the extremities. AJR Am J Roentgenol 142:575–580
17. Helpert C, Davies AM, Evans N, Grimer RJ (2004) Differential diagnosis of tumors and tumor-like lesions of the infrapatellar (Hoffa's) fat pad. Eur Radiol 14:2337–2346
18. Horowitz AL, Resnick D, Watson RC (1973) The roentgen features of synovial sarcoma. Clin Radiol 24:481–484
19. Hudson TM, Hass G, Enneking WF (1975) Angiography in the management of musculoskeletal tumors. Surg Gynecol Obstet 141:11–21
20. Hudson TM, Schakel M, Springfield DS (1985) Limitations of computed tomography following excisional biopsy of soft tissue sarcomas. Skeletal Radiol 13:49–54
21. Hunter JC, Johnston WH, Genant HK (1979) Computed tomography evaluation of fatty tumors of the somatic soft tissues: clinical utility and radiology-pathologic correlation. Skeletal Radiol 4:79–91
22. Karkhanis S, Botchu R, James S, Evans N (2013) Bilateral calcific myonecrosis associated with epilepsy. Clin Radiol 68(6):e349–e352
23. Keats TE (1992) Atlas of normal variants that may simulate disease, 5th edn. Mosby Year Book, St. Louis
24. Kransdorf MJ, Meis JM, Jelinek JS (1991) Myositis ossificans: MR appearance with radiologic-pathologic correlation. AJR Am J Roentgenol 157:1243–1248
25. Kransdorf MJ, Jelinek JS, Moser RP Jr (1993) Imaging soft tissue tumors. Radiol Clin North Am 31:359–372
26. Kricun ME (1983) Radiographic evaluation of solitary bone lesions. Orthop Clin North Am 14:39–64

27. Lec KR, Cox GC, Neff JR, Arnett GR, Murphy MD (1987) Cystic masses of the knee; arthrographic and CT evaluation. AJR Am J Roentgenol 148:329–334
28. Levine E, Lec KR, Neff JR, Maklad NF, Robinson RG, Preston DF (1979) Comparison of computed tomography and other imaging modalities in the evaluation of musculoskeletal tumors. Radiology 131:431–437
29. Li Y, Zheng Y, Lin J, Cai A, Zhou X, Wei X, Cheng Y, Liu G (2013) Evaluation of the relationship between extremity soft tissue sarcomas and adjacent major vessels using contrast-enhanced multidetector CT and three-dimensional volume-rendered CT angiography: a preliminary study. Acta Radiol 54(8):966–972
30. Madewell JE, Moser RP Jr (1995) Radiologic evaluation of soft tissue tumors. In: Enzinger FM, Weiss SW (eds) Soft tissue tumors, 3rd edn. Mosby, St Louis, pp 39–88
31. Murray JA (1977) Synovial sarcoma. Orthop Clin North Am 8:963–972
32. Neifield JP, Walsh JW, Lawrence W (1983) Computed tomography in the management of soft tissue tumors (abstract). Radiology 147:911
33. Nessi R, Gattoni F, Mazzoni R, de Coopmans Y, Veronesi U (1981) Xeroradiography of soft tissue tumors. Fortschr Rontgenstr 134:669–673
34. Norman A, Dorfman HD (1970) Juxtacortical circumscribed myositis ossificans: evolution and radiographic features. Radiology 96:301–306
35. Panicek DM, Gatsonis CG, Rosenthal DI et al (1997) CT and MRI in the local staging of primary malignant musculoskeletal neoplasms: report of the Radiology Diagnostic Oncology Group. Radiology 202:237–246
36. Patel RB, Barton P, Salimi Z, Molitor J (1983) Computed tomography of complicated psoas abscess with intraabscess contrast medium injection. J Comput Assist Tomogr 7:911–913
37. Pope TL, Keats TE, de Lange EE, Fechner RE, Harvey YW (1987) Idiopathic synovial chondromatosis in two unusual sites: inferior radioulnar joint and ischial bursa. Skeletal Radiol 16:205–208
38. Reeder MM (1993) Gamuts in bones, joints and spine radiology. Springer, Berlin/Heidelberg/New York, pp 365–373
39. Resnick D (1995) Diagnosis of bone and joint disorders, 3rd edn. Saunders, Philadelphia, pp 4491–4500
40. Resther G, Mutscher W (1990) Detection of local recurrent disease in musculoskeletal tumors: magnetic resonance imaging versus computed tomography. Skeletal Radiol 19:85–90
41. Rydberg J, Liang Y, Teague SD (2004) Fundamentals of multichannel CT. Semin Musculoskelet Radiol 8:137–146
42. Safriel Y, Zinn H (2002) CT pulmonary angiography in the detection of pulmonary emboli: a meta-analysis of sensitivities and specificities. Clin Imaging 26(2):101–105
43. Sartoris DJ, Danzig L, Gilula LA, Greenway G, Resnick D (1985) Synovial cysts of the hip joint and iliopsoas bursitis: a spectrum of imaging abnormalities. Skeletal Radiol 14:85–94
44. Schwimmer M, Edelstein G, Heiken JP, Gilula LA (1983) Synovial cysts of the knee: CT evaluation. Radiology 154:175–177
45. Shantakumar S, Connelly-Frost A, Kobayashi MG, Allis R, Li L (2015) Older soft tissue sarcoma patients experience increased rates of venous thromboembolic events: a retrospective cohort study of SEER-Medicare data. Clin Sarcoma Res 5:18
46. Soye I, Levine E, DeSmet AA, Neff YR (1982) Computed tomography in the preoperative evaluation of masses arising in or near the joints of the extremities. Radiology 143:727–732
47. Steinbach LS (1998) CT and MRI in the local staging of primary malignant musculoskeletal neoplasms: comments. Sarcoma 2:57–58
48. Steinbach LS, Schneider R, Goldman AB (1985) Bursae and abscess cavities communicating with the hip: diagnosis using arthrography and CT. Radiology 156:303–307
49. Viamonte MM, Roen S, LePage J (1973) Nonspecificity of abnormal vascularity in the radiographic diagnosis of malignant neoplasms. Radiology 106:59–69
50. Wang XL, Gielen JL, Salgado R, Delrue F, De Schepper AMA (2004) Soft tissue aneurysmal bone cyst: case report. Skeletal Radiol 33:477–480
51. Weekes RG, McLeod RA, Reiman HM, Pritchard DJ (1985) CT of soft tissue neoplasms. AJR Am J Roentgenol 144:355–360
52. Widlow DM, Murray RR, White RI, Osterman FA Jr, Schrieber ER, Satre RW, Mitchell SE, Kaufman SL, Williams GM, Weiland AJ (1988) Congenital arteriovenous malformations: tailored embolotherapy. Radiology 169:511–516
53. Wolverson MK, Jaggannadharao B, Sundaram M, Heiberg E, Grider R (1981) Computed tomography in the diagnosis of gluteal abscess and other peripelvic collections. J Comput Assist Tomogr 5:34–38
54. Wybier M, Laredo JD (2004) Place et limites de la radiographie et du scanner dans le diagnostic des tumeurs et pseudotumeurs des parties molles. In: Laredo JD, Tomeno B, Malghem J, Drape JL, Wybier M, Railhac JJ (eds) Conduite á tenir devant une image osseuse ou des parties molles d'allure tumorale. Sauramps Medical, Montpelier, pp 285–295
55. Yaghmai I (1979) Angiography of bone and soft tissue lesions. Springer, Berling/Heidelberg/New York, pp 365–366
56. Yakes WF, Pevsner R, Reed M, Donohue HJ, Ghaed W (1986) Serial embolization of an extremity arteriovenous malformation with alcohol via direct percutaneous puncture. AJR Am J Roentgenol 146: 1038–1040
57. Zornoza J, Bernardino ME, Ordonez NG, Cohen MA, Thomas YL (1982) Percutaneous needle biopsy of soft tissues guided by ultrasound and computed tomography. Skeletal Radiol 9:33–36

PET and PET-CT in Soft Tissue Sarcoma

3

S. Ceyssens and S. Stroobants

Contents

3.1 **Introduction** 59
3.2 **Characterization and Grading** 60
3.3 **Evaluation of Disease Extent** 62
3.4 **Response Evaluation** 64
3.5 **Detection of Recurrence** 66
Conclusion 66
References 67

3.1 Introduction

Sarcomas are a group of various malignancies originating in the bone (primary bone sarcoma) or soft tissue (STS), including fibrous connective tissue, fat, muscle, vascular tissue, neural tissue, and visceral tissue.

Although surgical resection is the cornerstone of curative treatment, it is still under debate how extensive that surgical excision should be, whether it should be preceded or followed by chemotherapy and/or irradiation and whether or not an elective lymphadenectomy should be done [23, 24].

Beside tumor size and location, tumor grade is up till now considered the most important prognostic variable [39], all of them having major implications on further management. Consequently, the approach to a patient with a mass suspicious of a sarcoma usually starts with a biopsy in order to obtain tissue for diagnosis. In many situations core-needle biopsies are accepted as an appropriate alternative to open biopsy in the evaluation of a musculoskeletal mass. However, a biopsy may underestimate true tumor grade, due to the often large and heterogeneous nature of STS [11]. Hence, it is comprehensible that there is a growing interest in using imaging modalities to guide biopsies toward the biologically most active zone. Together with pathology, imaging modalities are the basis for accurate staging, evaluating locoregional extent of the primary lesion, and screening for occult metastases.

S. Ceyssens (✉) • S. Stroobants
Department of Nuclear Medicine, Antwerp University Hospital, Edegem, Belgium
e-mail: Sarah.Ceyssens@uza.be

© Springer International Publishing AG 2017

F.M. Vanhoenacker et al. (eds.), *Imaging of Soft Tissue Tumors*, DOI 10.1007/978-3-319-46679-8_3

3.2 Characterization and Grading

Correct differentiation between a benign and malignant soft tissue lesion and a sarcoma versus other malignancies is essential to define further therapeutic strategy.

Conventional radiography still remains the first line imaging modality in the diagnostic work up of sarcoma in general. Although its value in the evaluation of STS is rather limited due to its poor resolution compared with cross-sectional modalities, it can be used for the assessment of calcifications in the tumoral mass, which can aid the classification of the lesion (see Chap. 2). As a result of its high contrast resolution, *magnetic resonance imaging* (MRI) is at present the main imaging modality to establish the local extent of the lesion, especially in the extremities, pelvis, and trunk (see Chap. 9). Although some benign soft tissue masses (like lipomas, hemangiomas, myositis ossificans) have a typical appearance on MRI and can be correctly diagnosed as benign lesions, discriminating benign from malignant masses for those lesions whose appearance is nonspecific might not be so straightforward (see Chap. 10) [8, 30]. In these cases a biopsy is still warranted (see Chap. 7).

Computed tomography (CT) offers a better spatial resolution but an inferior soft tissue contrast resolution compared to MRI and may be used for initial staging when MRI is contraindicated or in case of diagnostic doubt (see Chap. 2).

Several studies have already investigated the role of 2-fluoro-2-deoxy-D-glucose, [^{18}F] FDG, *positron emission tomography* (PET) in the characterization and grading of soft tissue masses. ^{18}F-FDG PET can be used to determine tumor metabolism in lesions by measuring the standard uptake value (SUV). In a study of Ioannidis et al. [27], ^{18}F-FDG PET was found to be very successful in discriminating benign from malignant soft tissue lesions. ^{18}F-FDG uptake correlated with the histological grade of the tumor, with a significant higher uptake in intermediate-/high-grade tumors compared to low-grade tumors, although there was some overlap. Almost all intermediate-/high-grade tumors were correctly diagnosed on the basis of visual analysis, with a sensitivity and specificity of 92 % and 73 %, respectively, almost all of these lesions having a SUV higher than 2.0 (sensitivity and specificity 87 and 79 % for SUV >2.0 and 70 and 87 % for SUV > 3.0). False-negative results were seen in low-grade sarcomas, while false-positive findings were seen in inflammatory lesions or lesions with high cellularity (e.g., giant cell tumor).

Taking into account other parameters such as the uptake pattern (a more heterogeneous pattern in high-grade lesions versus homogeneous in low-grade sarcoma) [34, 37], the difference in reaching peak activity concentration (where high-grade malignant lesions tend to show a steady increase in ^{18}F-FDG uptake with a peak activity at approximately 4 h, benign lesions usually show peak within 30 min followed by a washout) [21, 32] and SUV-based parameters such as SUV_{peak} and SUV_{peak}/SUV_{liver} [20] can help to distinguish intermediate-/high-grade lesions from low-grade/benign lesions. However, ^{18}F-FDG PET may not always offer adequate discrimination between low-grade tumors and benign lesions.

Folpe found a strong correlation between SUV and pathological grade, as well as between SUV and cellularity, mitotic activity, MIB labeling index, and p53 overexpression, all of these factors known to have prognostic value [22].

Pretreatment SUV was also shown to correlate with the final outcome, with a high SUV being associated with a significant shorter disease-free survival (DFS) ($p < 0.001$) and overall survival (OS) ($p < 0.003$) [14]. In a study of Baum and colleagues, 41 patients with rhabdomyosarcoma underwent ^{18}F-FDG PET or PET-CT. ^{18}F-FDG PET seemed to be predictive of the outcome: patients with a highly metabolic active primary tumor with a ratio of SUV_{max} to SUV_{liver} above 4.6 showed a significantly shorter overall survival (5-year survival of 56 % compared to 100 % in the low metabolic active primary tumor group) [2] (see also Fig. 3.1).

After correction for standard clinical prognostic factors such as histology, grade, age, and sex, SUV was found to be an independent predictor of survival and disease progression [14]. Also the heterogeneity in tissue uptake of ^{18}F-FDG was

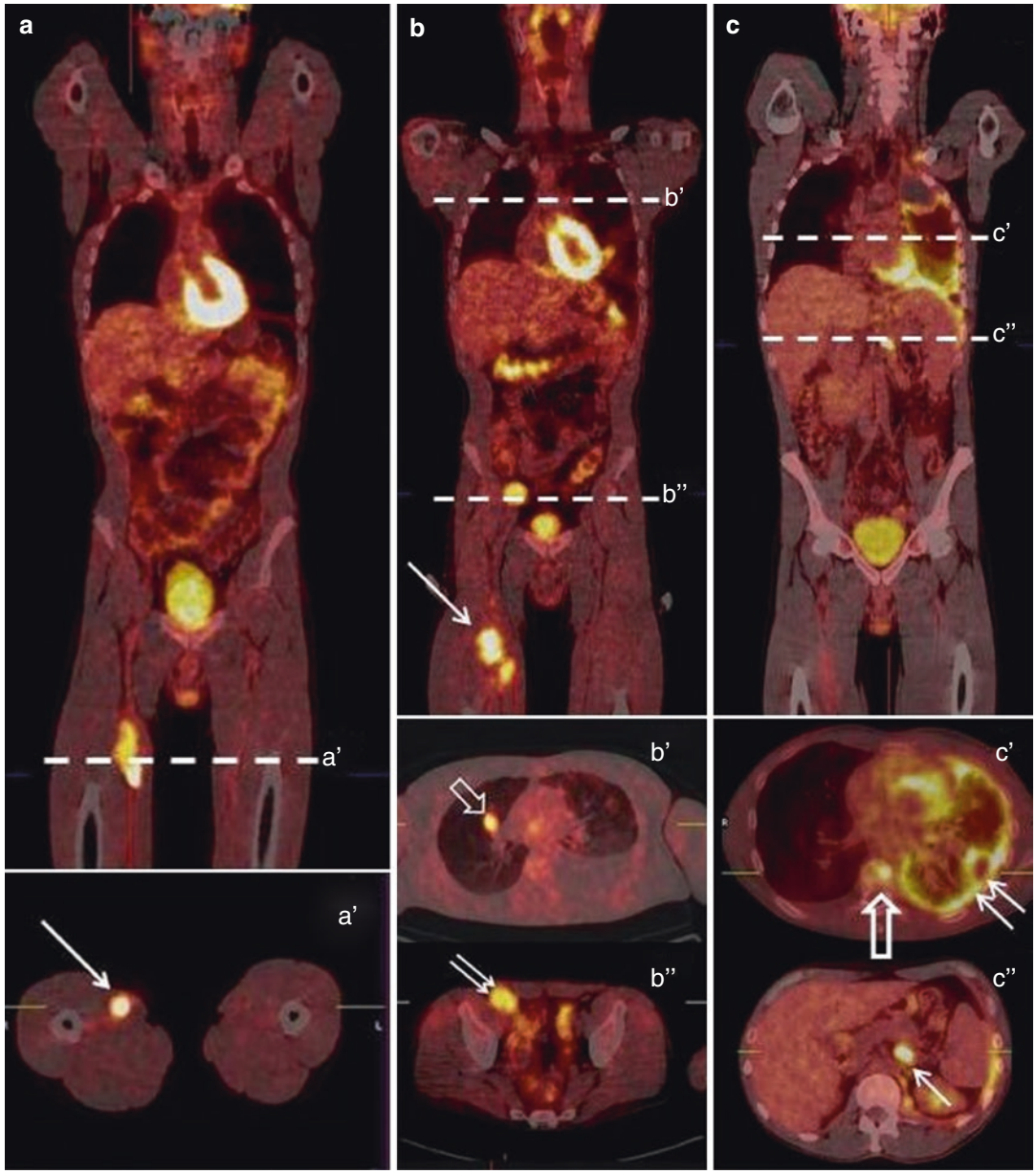

Fig. 3.1 ^{18}F-FDG PET is predictive of the outcome: patients with a highly metabolic active primary tumor show a significantly shorter overall survival. A 39-year-old patient with a high-grade malignant schwannoma in the right thigh (*arrow,* **a**+**a'**). SUVmax on the baseline ^{18}F-FDG PET scan was 9.75. Within 6 months after resection of the primary lesion, ^{18}F-FDG PET showed local recurrence (*arrow*, **b**), as well as metastases in the right lung (*open arrow*, **b'**) and in soft tissue (*double arrow,***b''**)). Follow-up ^{18}F-FDG PET showed progressive disease with the development of pleural (double arrow, **c'**), bone (*open arrow*, **c'**), and lymph node metastases (*arrow*, **c''**)

found to be a strong predictor of the final outcome [15].

Since STS tend to be large and heterogeneous, there is a risk of sampling error when taking a biopsy. In the previous studies, diagnostic discrepancies in malignancy grade were found in about 10 % of cases when determined by fine-needle aspiration (FNA) and core-needle biopsy

(CNB) compared with final histologic diagnosis on the resection specimen [11]. ^{18}F-FDG accumulates in the cells in proportion to the rate of glucose metabolism, giving information on biological activity of the tumoral parts, and subsequent the identification of intratumoral heterogeneity, reflected as areas of high and low SUV (see also Fig. 3.2). In a study of Rakheja, a close correlation was not only found between SUV_{max} and mitotic count but also with the presence of tumor necrosis [44]. By identifying the most metabolically active portion of a tumor mass, nuclear medicine techniques can guide biopsy to a site most likely to contain tumor tissue of the highest grade present.

In conclusion, the main role of the current imaging modalities is to recognize patients with typically benign disease, in whom further invasive staging can be omitted, and select those patients with a suspected malignancy, who should be referred for biopsy. Following appropriate imaging assessment, biopsy of the mass completes the staging process. Since STS tend to be large and heterogeneous, there is a risk of sampling error; imaging can help to guide the biopsy toward the most aggressive zone.

3.3 Evaluation of Disease Extent

As a result of its clear, detailed images of soft tissues, MRI represents an ideal imaging modality to evaluate the anatomical compartments being affected by a primary tumor originating in the mesenchymal tissues of muscles, fat, blood vessels, nerves, tendons, and synovial tissues and its relation to adjacent structures.

Approximately 20 % of all patients with a sarcoma will have metastatic disease at initial diagnosis, 75–80 % of the metastases arising intrathoracic [42, 46]. Völker et al. evaluated the impact of ^{18}F-FDG PET for initial staging and therapy planning in 46 pediatric patients [57], demonstrating that ^{18}F-FDG PET is a valuable tool for initial staging and additionally having a significant impact on therapy planning. In this study, ^{18}F-FDG PET was clearly superior to conventional imaging modalities (CIMs) – including ultrasound, computed tomography (CT), magnetic resonance imaging (MRI) and bone scintigraphy – in the detection of lymph node involvement (sensitivity, 95 % for PET versus 25 % for CIMs, respectively) and bone lesions (sensitivity, 90 % versus 57 %, respectively). These findings are in accordance with other studies showing a higher sensitivity and specificity for ^{18}F-FDG PET-CT in detecting malignant lesions than CIMs when excluding lung metastases (83 %, 98 % and 78 %, 97 %, respectively) [33].

With regard to the detection of lymph node metastases, the power of ^{18}F-FDG PET exists in its ability to show tumoral involvement in normal-sized nodes and to exclude disease in reactively enlarged nodes [13]. In view of the fact that lymphatic spread is presumed rare in the natural course of STS, ^{18}F-FDG PET is currently considered useful only in tumor types with a higher incidence of lymphatic spread (angiosarcoma, epithelioid sarcoma, and rhabdomyosarcoma). However, it is possible that with the growing use of ^{18}F-FDG PET-CT, the prevalence of detectable lymph node metastases may increase [53].

In these same studies as mentioned above, ^{18}F-FDG PET-CT had a higher specificity than CIMs in lung lesions (96 % compared to 87 %) but a lower sensitivity (80 % compared to 93 %), most likely due to a combination of factors such as lung lesions with a size below the limits of resolution of ^{18}F-FDG PET (i.e., 4–5 mm), partial volume effects, and breathing motion [42, 46]. High-resolution CT remains the most sensitive imaging modality to detect lung metastases, although it was shown to be only cost-effective in patients with high-grade T2 lesions or T2 extremity lesions [41]. The higher specificity of ^{18}F-FDG PET-CT emphasizes the complementary roles of these imaging modalities in the assessment of lung lesions [57].

Regarding the detection of bone lesions, whole ^{18}F-FDG PET and bone scanning seem superior to conventional CIMs, although one should take into account the type of the primary lesion. Most of these studies are done in patients with bone sarcoma, showing a comparable or a clearly superior sensitivity of ^{18}F-FDG PET and bone scanning compared to CIMs in patients

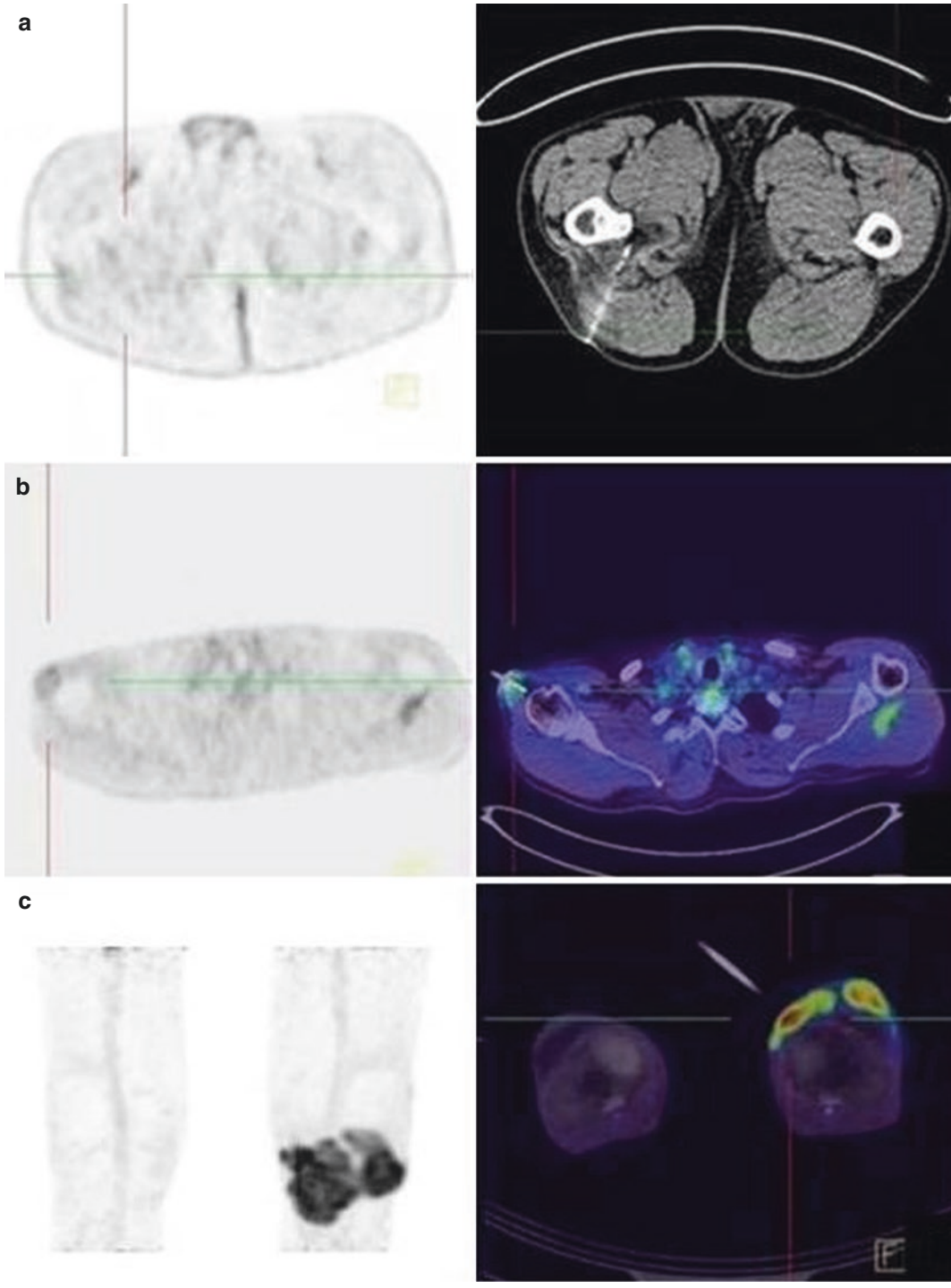

Fig. 3.2 ^{18}F-FDG accumulates in the cells in proportion to the rate of glucose metabolism, giving information on biological activity of the tumoral parts, and subsequent the identification of intratumoral heterogeneity, reflected as areas of high and low SUV. By identifying the most metabolically active portion of a tumor mass, nuclear medicine techniques can guide a biopsy to a site most likely to contain tumor tissue of the highest grade present. From our own database: a biopsy of a lesion under ^{18}F-FDG PET guidance. A lipoma, showing no ^{18}F-FDG uptake (**a**). A low-grade myxofibrosarcoma of the right shoulder showing only a discrete and homogenous ^{18}F-FDG uptake (**b**). A high-grade myxofibrosarcoma of the left knee with an intense and heterogeneous ^{18}F-FDG uptake (**c**)

with osteosarcoma and Ewing sarcoma, respectively [33, 57]. However, since tumor spread to bones is rare in STS, the use of bone scintigraphy seems only to be encouraged in symptomatic patients [28].

Liver metastases may be the first sign of dissemination in primary intra-abdominal STS and are usually visualized on the abdominal CT performed to evaluate the primary mass. To the best of our knowledge, no specific literature is available on the accuracy of PET for the detection of liver metastases in sarcoma. Several groups reported on the value of ^{18}F-FDG PET, ^{18}F-FDG PET-CT, and/or subsequent MRI for PET-MRI fusion for the detection of liver metastases in different kinds of tumors [3, 9, 12, 45]. All of them found a high sensitivity and accuracy for ^{18}F-FDG PET, ^{18}F-FDG PET-CT, as well as combined with subsequent MRI for PET-MRI fusion.

Although clinical experience with ^{18}F-FDG PET/MRI is limited, first results seem promising. The main advantages of this one stop shop approach lies in combining the strength of the T staging equal to that of an MR alone, complemented by the N and M staging from the PET component [38].

In summary, the main power of ^{18}F-FDG PET and ^{18}F-FDG PET-CT lies in the ability to screen the entire patient for distant metastases without significantly increasing the radiation burden. The key role of ^{18}F-FDG PET-CT lies largely in detecting metastases at unexpected sites, outside the standard field of view of CT and MRI, and in the exclusion of disease in equivocal results on conventional imaging. Although further studies are required, preliminary clinical experiences with ^{18}F-FDG PET-MRI seem promising.

3.4 Response Evaluation

The purpose of therapy monitoring is to provide an early and still accurate differentiation between responders and nonresponders with the ultimate goal of adapting therapy to the information provided. In this way, responders can continue treatment, whereas therapy can be adapted in those patients in whom there is a lack of response.

Response to treatment in solid tumors is usually defined as a significant decrease in tumor dimensions by anatomic imaging techniques. In version 1.0 of the Response Evaluation Criteria in Solid Tumors (RECIST), partial response was defined as a decrease of at least 30 % in the sum of diameters of the target lesions, with the baseline sum of diameters as reference. However, these criteria are not always capable of distinguishing responders from nonresponders to neoadjuvant therapy [5, 18, 26, 50].

There are weaknesses in the evaluation of tumor response by volume changes, especially in STS. Firstly, precise measurement of tumor dimensions can be challenging in ill-defined lesions like bone, bowel and peritoneal lesions. Secondly, chemotherapy can induce profound tissue changes like necrosis and fibrosis [35]. As a result of this, a reduction in viable tumor cell fraction is not always associated with a reduction in volume. Moreover, volume changes are rather late events and therefore changes measured by computer tomography are often not significant when performed earlier than two to three months after the start of treatment. In this way, patients can be unnecessarily exposed to ineffective, toxic, or expensive treatments during a prolonged period. It can even reduce the chance of a curative resection by postponing surgery in the neoadjuvant setting. Finally, the goal of new anti-vascular and cytostatic agents is rather a stabilization of tumor growth than tumor shrinkage. Therefore, no major volume changes are to be expected. Recently the RECIST criteria have been revised (version 1.1) [16] to overcome these limitations, but clinical validation of these newer approaches is still required.

Several studies have shown promising results for ^{18}F-FDG PET in treatment monitoring. In various tumors, such as breast cancer, lymphoma, esophageal, stomach, colorectal, head and neck and non-small-cell lung cancers, a good correlation between an early and significant decline in metabolic activity and response to therapy was found, as well as a good correlation between the early decrease in ^{18}F-FDG uptake and patient outcome [36]. Since ^{18}F-FDG PET can differentiate between viable cells and necrotic or fibrotic

inactive tissue, one can tell apart responders and nonresponders early after the start of treatment [4, 49].

Evilevitch et al. evaluated whether changes in ^{18}F-FDG uptake and size measured by a combined PET-CT scan before and after neoadjuvant chemotherapy in high-grade soft tissue sarcoma could accurately assess histopathologic response defined as ≥95 % pathologic necrosis on the resected tumor. Quantitative ^{18}F-FDG PET outperforms the size-based criteria to distinguish responders from nonresponders to neoadjuvant therapy. Using a 60 % decrease in ^{18}F-FDG uptake resulted in a sensitivity of 100 % and specificity of 71 % for PET, whereas for RECIST a sensitivity of 25 % and specificity of 100 % was seen [18].

Schuetze and coworkers measured ^{18}F-FDG uptake before and after neoadjuvant chemotherapy in 46 patients with high-grade localized sarcomas. They found a significant correlation between the change in the maximum standardized uptake value (SUV_{max}) and the amount of residual viable tumor in the resected specimens. ^{18}F-FDG was found to be a valuable tool to predict outcome, in this way that a SUV_{max} higher than 6 at baseline and less than 40 % decrease in ^{18}F-FDG uptake were associated with a high risk for systemic disease recurrence, whereas patients with a ≥40 % decline in SUV_{max} after chemotherapy were at a significantly lower risk for recurrent disease and death after complete resection and adjuvant radiotherapy [47] (see also Fig. 3.1). A study of Fendler likewise reported PET response, determined by changes in peak SUV (SUV_{peak}) from baseline to follow up in accordance with modified PET Response Criteria in Solid Tumors (PERCIST 1.0), to be an independent predictor of progression-free survival as well as for local and distant progression in STS patients after 2–4 cycles of chemotherapy in combination with regional hyperthermia [19].

Clinical trials in gastrointestinal stromal tumors (GISTs) show a significant improvement in relapse-free survival and overall survival in high-risk patients treated with the molecular-targeted therapy imatinib as adjuvant treatment for 3 years [29], as well as a significant increase in progression-free survival and overall survival compared in locally advanced inoperable and metastatic patients compared to historical controls [10, 55].

Although tumor response occurs within a few days after start of treatment in responders, objective tumor shrinkage is minimal and usually occurs only after several weeks or months. Moreover, since tumor tissue can be replaced by necrotic or fibrotic tissue, a reduction in the viable tumor cell fraction is not always reflected by a volume reduction. Metabolic imaging with ^{18}F-FDG PET has proven to be highly sensitive in detecting early tumor response to Glivec treatment and precedes tumor shrinkage by several weeks to months. A complete normalization of all hypermetabolic foci is seen within 1 week of treatment and is predictive for favorable outcome [52, 54]. Since RECIST underestimates the effect of imatinib on metastatic GIST, especially at the early stage of treatment, and is a poor predictor of clinical benefit, CT criteria were reevaluated. Given that a cystic-like appearance with "near"-fluid attenuation and loss of contrast enhancement is the typical appearance of responding lesion on CT, the use of Hounsfield unit (HU) measurements is proposed as an alternative response marker [1]. Using the CHOI criteria, where response is defined as a decrease in tumor size of more than 10 % or a decrease in tumor density of more than 15 %, the prognostic value of these new CT response criteria is comparable to the one obtained with ^{18}F-FDG PET [6].

Once GISTs have responded to therapy, treatment should be continued ad infinitum, since interruption of treatment usually gives rise to a relatively rapid tumor progression. Thus, monitoring of tumor response should be done in the early phases of treatment, whereas follow-up should be continued throughout the treatment, due to a persistent risk of secondary progression over time [17].

In conclusion, ^{18}F-FDG PET seems promising in treatment monitoring. A good correlation was found between an early and significant decline in metabolic activity and response to therapy in different types of sarcoma. Furthermore, ^{18}F-FDG uptake is an independent predictor for overall and disease-free survival.

3.5 Detection of Recurrence

Although recurrences predominantly develop within 2 years of resection of the primary tumor, late recurrences (>5 years after treatment) are not uncommon [31, 40]. Main predictors for local recurrence are positive surgical margins, whereas grade, size, and tumor-node-metastasis (TNM) stage predict the development of metastatic disease and overall survival [51]. Early detection and treatment of local recurrence is desirable if surgical control is to be achieved, even if this does not necessarily influence the final outcome of the patient.

As a result of its high-contrast resolution, MRI is currently the technique of choice for the evaluation of suspected local recurrence in the extremities. However, radiotherapy- and chemotherapy-induced changes such as soft tissue trabeculation, increased fatty marrow, focal marrow abnormalities, and hemorrhage can complicate the evaluation of the affected region. On the other hand, the use of an organized systematic approach and certain algorithms can reduce the challenge [25, 56].

Although detection of local recurrence of STS is still a rather controversial indication for ^{18}F-FDG PET-CT, preliminary results for the use of PET-CT for this purpose in bone sarcomas [43, 48], as well as STS, seem promising [7]. However, further studies are necessary.

Conclusion

Since no imaging technique can surpass pathology in the purpose of determining exact histology and grading of the primary tumor, the main role of the current imaging modalities is to recognize patients with typically benign lesions, in whom no further invasive staging is warranted, and to select those patients who should be referred for biopsy. In view of the fact that sarcomas can be large and heterogeneous, nuclear medicine techniques can guide a biopsy to a site most likely to contain tumor tissue of the highest grade present.

In most cases, conventional radiography, MRI, and CT still remain the first-line imaging modalities in the diagnostic workup of sarcoma. Due to its limited spatial resolution and its weak anatomical detail, ^{18}F-FDG PET as a standalone technique is of no use in the evaluation of the local extent of the tumor. However, we have entered a new era of hybrid imaging machines, uniting the anatomical information of the CT and/or MR and the metabolic information of the PET, improving diagnostic accuracy, providing surgery and radiation therapy planning, and by merging all necessary information in one single procedure guiding biopsies even better. Still, studies are required to evaluate the impact of combining these imaging techniques on the overall diagnostic performance in sarcoma.

The key role of ^{18}F-FDG PET-CT is mainly an additional role, situated in the detection of metastases at unexpected sites, outside the standard field of view of CT and MRI, and in the exclusion of disease in equivocal results on conventional imaging. Hence, high resolution CT still remains the modality of choice to detect lung metastases. Additionally, liver metastases are usually visualized on the abdominal CT performed to evaluate the primary mass and can be detected as the first sign of dissemination in primary intra-abdominal STS. With regard to detection of bone metastases, ^{18}F-FDG PET is clearly superior in case of Ewing sarcoma compared to conventional imaging. However, in case of an osteosarcoma, the sensitivity of the former technique is similar to that of bone scanning.

Apart from staging the amount of ^{18}F-FDG uptake as measured by PET is an independent predictor for overall and disease-free survival.

Key Points

1. By identifying the most metabolically active portion of a tumor mass, ^{18}F-FDG PET-CT can guide a biopsy toward the most aggressive zone.
2. The strength of ^{18}F-FDG PET-CT in staging and restaging of a sarcoma patient lies in its ability to detect

metastases outside the standard field of view of CT and MRI and in the exclusion of disease in equivocal results on conventional imaging.

3. In treatment monitoring, there is a good correlation between an early and significant decline in metabolic activity and response to therapy in different types of sarcoma. Additionally, ^{18}F-FDG uptake is an independent predictor for overall and disease-free survival.
4. Although further studies are necessary, the use of ^{18}F-FDG PET-CT seems promising in the detection of local recurrence of STS.

References

1. Antoch G, Kanja J, Bauer S, Kuehl H, Renzing-Koehler K, Schuette J, Bockisch A, Debatin JF, Freudenberg LS (2004) Comparison of PET, CT, and dual-modality PET/CT imaging for monitoring of imatinib (STI571) therapy in patients with gastrointestinal stromal tumors. J Nucl Med 45:357–365
2. Baum SH, Frühwald M, Rahbar K, Wessling J, Schober O, Weckesser M (2011) Contribution of PET/CT to prediction of outcome in children and young adults with rhabdomyosarcoma. J Nucl Med 52(10):1535–1540
3. Beiderwellen K, Geraldo L, Ruhlmann V, Heusch P, Gomez B, Nensa F, Umutlu L, Lauenstein TC (2015) Accuracy of [18F] FDG PET/MRI for the detection of liver metastases. PLoS One 10(9), e0137285
4. Canellos GP (1988) Residual mass in lymphoma may not be residual disease. J Clin Oncol 6:931–933
5. Ceresoli GL, Chiti A, Zucali PA et al (2007) Assessment of tumor response in malignant pleural mesothelioma. Cancer Treat Rev 33:533–541
6. Choi H, Charnsangavej C, Faria SC, Macapinlac HA, Burgess MA, Patel SR, Chen LL, Podoloff DA, Benjamin RS (2007) Correlation of computed tomography and positron emission tomography in patients with metastatic gastrointestinal stromal tumor treated at a single institution with imatinib mesylate: proposal of new computed tomography response criteria. J Clin Oncol 25:1753–1759
7. Dancheva Z, Bochev P, Chaushev B, Yordanova T, Klisarova A (2016) Dual-time point 18FDG-PET/CT imaging may be useful in assessing local recurrent disease in high grade bone and soft tissue sarcoma. Nucl Med Rev Cent East Eur 19(1):22–27
8. De Schepper AM, De Beuckeleer L, Vandevenne J, Somville J (2000) Magnetic resonance imaging of soft tissue tumors. Eur Radiol 10:213–223
9. Delbeke D, Martin WH, Sandler MP, Chapman WC, Wright JK Jr, Pinson CW (1998) Evaluation of benign vs malignant hepatic lesions with positron emission tomography. Arch Surg 133:510–515
10. Demetri GD, von Mehren M, Blanke CD et al (2002) Efficacy and safety of imatinib mesylate in advanced gastrointestinal stromal tumors. N Engl J Med 347:472–480
11. Domanski HA, Akerman M, Carlén B et al (2005) Core-needle biopsy performed by the cytopathologist: a technique to complement fine-needle aspiration of soft tissue and bone lesions. Cancer 105(4):229–239
12. Donati OF, Hany TF, Reiner CS, von Schulthess GK, Marincek B, Seifert B, Weishaupt D (2010) Value of retrospective fusion of PET and MR images in detection of hepatic metastases: comparison with 18F-FDG PET/CT and Gd-EOB-DTPA-enhanced MRI. J Nucl Med 51(5):692–699
13. Dwamena BA, Sonnad SS, Angobaldo JO, Wahl RL (1999) Metastases from non-small cell lung cancer: mediastinal staging in the 1990s--meta-analytic comparison of PET and CT. Radiology 213:530–536
14. Eary JF, O'Sullivan F, Powitan Y, Chandhury KR, Vernon C, Bruckner JD, Conrad EU (2002) Sarcoma tumor FDG uptake measured by PET and patient outcome: a retrospective analysis. Eur J Nucl Med Mol Imaging 29:1149–1154
15. Eary JF, O'Sullivan F, O'Sullivan J, Conrad EU (2008) Spatial heterogeneity in sarcoma 18F-FDG uptake as a predictor of patient outcome. J Nucl Med 49:1973–1979
16. Eisenhauer EA, Therasse P, Bogaerts J, Schwartz LH, Sargent D, Ford R, Dancey J, Arbuck S, Gwyther S, Mooney M, Rubinstein L, Shankar L, Dodd L, Kaplan R, Lacombe D, Verweij J (2009) New response evaluation criteria in solid tumours: revised RECIST guideline (version 1.1). Eur J Cancer 45:228–247
17. ESMO/European Sarcoma Network Working Group (2014) Gastrointestinal stromal tumours: ESMO Clinical Practice Guidelines for diagnosis, treatment and follow-up. Ann Oncol 25(3):iii21–iii26
18. Evilevitch V, Weber WA, Tap WD et al (2008) Reduction of glucose metabolic activity is more accurate than change in size at predicting histopathologic response to neoadjuvant therapy in high-grade soft-tissue sarcomas. Clin Cancer Res 14:715–720
19. Fendler WP, Lehmann M, Todica A, Herrmann K, Knösel T, Angele MK, Dürr HR, Rauch J, Bartenstein P, Cyran CC, Hacker M, Lindner LH (2015) PET response criteria in solid tumors predicts progression-free survival and time to local or distant progression after chemotherapy with regional hyperthermia for soft-tissue sarcoma. J Nucl Med 56(4):530–537
20. Fendler WP, Chalkidis RP, Ilhan H, Knösel T, Herrmann K, Issels RD, Bartenstein P, Cyran CC, Lindner LH, Hacker M (2015) Evaluation of several

FDG PET parameters for prediction of soft tissue tumour grade at primary diagnosis and recurrence. Eur Radiol 25(8):2214–2221
21. Ferner RE, Lucas JD, O'Doherty MJ, Hughes RA, Smith MA, Cronin BF, Bingham J (2000) Evaluation of (18) fluorodeoxyglucose positron emission tomography ((18) FDG PET) in the detection of malignant peripheral nerve sheath tumours arising from within plexiform neurofibromas in neurofibromatosis 1. J Neurol Neurosurg Psychiatry 68:353–357
22. Folpe AL, Lyles RH, Sprouse JT (2000) (F-18) fluorodeoxyglucose positron emission tomography as a predictor of pathologic grade and other prognostic variables in bone and soft tissue sarcoma. Clin Cancer Res 6:1279–1287, Conrad EU 3rd, Eary JF
23. Fong Y, Coit DG, Woodruff JM, Brennan MF (1993) Lymph node metastasis from soft tissue sarcoma in adults. Analysis of data from a prospective database of 1772 sarcoma patients. Ann Surg 217:72–217
24. Gaakeer HA, Albus-Lutter CE, Gortzak E, Zoetmulder FA (1988) Regional lymph node metastases in patients with soft tissue sarcomas of the extremities, what are the therapeutic consequences? Eur J Surg Oncol 14:151–156
25. Garner HW, Kransdorf MJ, Bancroft LW, Peterson JJ, Berquist TH, Murphey MD (2009) Benign and malignant soft-tissue tumors: posttreatment MR imaging. Radiographics 29:119–134
26. Goffin J, Baral S, Tu D, Nomikos D, Seymour L (2005) Objective responses in patients with malignant melanoma or renal cell cancer in early clinical studies do not predict regulatory approval. Clin Cancer Res 11:5928–5934
27. Ioannidis JP, Lau J (2003) 18F-FDG PET for the diagnosis and grading of soft-tissue sarcoma: a meta-analysis. J Nucl Med 44:717–724
28. Jager PL, Hoekstra HJ, Leeuw J, van Der Graaf WT, de Vries EG, Piers D (2000) Routine bone scintigraphy in primary staging of soft tissue sarcoma; Is it worthwhile? Cancer 89:1726–1731
29. Joensuu H, Eriksson M, Sundby Hall K, Hartmann JT, Pink D, Schütte J, Ramadori G, Hohenberger P, Duyster J, Al-Batran SE, Schlemmer M, Bauer S, Wardelmann E, Sarlomo-Rikala M, Nilsson B, Sihto H, Monge OR, Bono P, Kallio R, Vehtari A, Leinonen M, Alvegård T, Reichardt P (2012) One vs three years of adjuvant imatinib for operable gastrointestinal stromal tumor: a randomized trial. JAMA 307(12):1265–1272
30. Kransdorf MJ, Murphey MD (2000) Radiologic evaluation of soft-tissue masses: a current perspective. AJR Am J Roentgenol 175:575–587
31. Lewis JJ, Leung D, Casper ES, Woodruff J, Hajdu SI, Brennan MF (1999) Multifactorial analysis of long-term follow-up (more than 5 years) of primary extremity sarcoma. Arch Surg 134:190–194
32. Lodge MA, Lucas JD, Marsden PK, Cronin BF, O'Doherty MJ, Smith MA (1999) A PET study of 18FDG uptake in soft tissue masses. Eur J Nucl Med 26:22–30
33. London K, Stege C, Cross S, Onikul E, Graf N, Kaspers G, Dalla-Pozza L, Howman-Giles R (2012) 18F-FDG PET/CT compared to conventional imaging modalities in pediatric primary bone tumors. Pediatr Radiol 42(4):418–430
34. Lucas JD, O'Doherty MJ, Cronin BF, Marsden PK, Lodge MA, McKee PH, Smith MA (1999) Prospective evaluation of soft tissue masses and sarcomas using fluorodeoxyglucose positron emission tomography. Br J Surg 86:550–556
35. Lucas DR, Kshirsagar MP, Biermann JS, Hamre MR, Thomas DG, Schuetze SM, Baker LH (2008) Histologic alterations from neoadjuvant chemotherapy in high-grade extremity soft tissue sarcoma: clinicopathological correlation. Oncologist 13(4): 451–458
36. Malik E, Juweid MD, Bruce D, Cheson MD (2006) Positron-emission tomography and assessment of cancer therapy. N Engl J Med 354:496–507
37. Mayerhoefer ME, Breitenseher M, Amann G, Dominkus M (2008) Are signal intensity and homogeneity useful parameters for distinguishing between benign and malignant soft tissue masses on MR images?: objective evaluation by means of texture analysis. Magn Reson Imaging 26:91316–91322
38. Partovi S, Kohan AA, Zipp L, Faulhaber P, Kosmas C, Ros PR, Robbin MR (2014) Hybrid PET/MR imaging in two sarcoma patients - clinical benefits and implications for future trials. Int J Clin Exp Med 7(3):640–648
39. Pisters PW, Leung DH, Woodruff J, Shi W, Brennan MF (1996) Analysis of prognostic factors in 1041 patients with localized soft tissue sarcomas of the extremities. J Clin Oncol 14:1679–1689
40. Pisters PW, Pollock RE, Lewis VO, Yasko AW, Cormier JN, Respondek PM, Feig BW, Hunt KK, Lin PP, Zagars G, Wei C, Ballo MT (2007) Long-term results of prospective trial of surgery alone with selective use of radiation for patients with T1 extremity and trunk soft tissue sarcomas. Ann Surg 246: 675–681
41. Porter GA, Cantor SB, Ahmad SA, Lenert JT, Ballo MT, Hunt KK, Feig BW, Patel SR, Benjamin RS, Pollock RE, Pisters PW (2002) Cost-effectiveness of staging computed tomography of the chest in patients with T2 soft tissue sarcomas. Cancer 94:197–204
42. Quartuccio N, Treglia G, Salsano M, Mattoli MV, Muoio B, Piccardo A, Lopci E, Cistaro A (2013) The role of Fluorine-18-Fluorodeoxyglucose positron emission tomography in staging and restaging of patients with osteosarcoma. Radiol Oncol 47(2):97–102
43. Quartuccio N, Fox J, Kuk D, Wexler LH, Baldari S, Cistaro A, Schöder H (2015) Pediatric bone sarcoma: diagnostic performance of 18F-FDG PET/CT versus conventional imaging for initial staging and follow-up. AJR Am J Roentgenol 204(1):153–160
44. Rakheja R, Makis W, Skamene S, Nahal A, Brimo F, Azoulay L, Assayag J, Turcotte R, Hickeson M (2012) Correlating metabolic activity on 18F-FDG

PET/CT with histopathologic characteristics of osseous and soft-tissue sarcomas: a retrospective review of 136 patients. AJR Am J Roentgenol 198(6): 1409–1416
45. Reiner CS, Stolzmann P, Husmann L, Burger IA, Hüllner MW, Schaefer NG, Schneider PM, von Schulthess GK, Veit-Haibach P (2014) Protocol requirements and diagnostic value of PET/MR imaging for liver metastasis detection. Eur J Nucl Med Mol Imaging 41(4):649–658
46. Roberge D, Vakilian S, Alabed YZ, Turcotte RE, Freeman CR, Hickeson M (2012) FDG PET/CT in initial staging of adult soft-tissue sarcoma. Sarcoma 2012:960194
47. Schuetze SM, Rubin BP, Vernon C et al (2005) Use of positron emission tomography in localized extremity soft tissue sarcoma treated with neoadjuvant chemotherapy. Cancer 103:339–348
48. Sharma P, Khangembam BC, Suman KC, Singh H, Rastogi S, Khan SA, Bakhshi S, Thulkar S, Bal C, Malhotra A, Kumar R (2013) Diagnostic accuracy of 18F-FDG PET/CT for detecting recurrence in patients with primary skeletal Ewing sarcoma. Eur J Nucl Med Mol Imaging 40(7):1036–1043
49. Spaepen K, Stroobants S, Dupont P et al (2001) Prognostic value of positron emission tomography (PET) with fluorine-18 fluorodeoxyglucose ([18F] FDG) after first line chemotherapy in non-Hodgkin's lymphoma: is [18F] FDG-PET a valid alternative to conventional diagnostic methods? J Clin Oncol 19:414–419
50. Stacchiotti S, Collini P, Messina A, Morosi C, Barisella M, Bertulli R, Piovesan C, Dileo P, Torri V, Gronchi A, Casali PG (2009) High-grade soft-tissue sarcomas: tumor response assessment--pilot study to assess the correlation between radiologic and pathologic response by using RECIST and choi criteria. Radiology 251(2):447–456
51. Stefanovski PD, Bidoli E, De Paoli A et al (2002) Prognostic factors in soft tissue sarcomas: a study of 395 patients. Eur J Surg Oncol 28:153–164
52. Stroobants S, Goeminne J, Seegers M, Dimitrijevic S, Dupont P, Nuyts J, Martens M, van den Borne B, Cole P, Sciot R, Dumez H, Silberman S, Mortelmans L, van Oosterom A (2003) 18FDG-Positron emission tomography for the early prediction of response in advanced soft tissue sarcoma treated with imatinib mesylate (Glivec). Eur J Cancer 39:2012–2020
53. Ulaner GA, Magnan H, Healey JH, Weber WA, Meyers PA (2014) Is methylene diphosphonate bone scan necessary for initial staging of Ewing sarcoma if 18F-FDG PET/CT is performed? Am J Roentgenol 202(4):859–867
54. Van den Abbeele AD, Badawi RD (2002) Use of positron emission tomography in oncology and its potential role to assess response to imatinib mesylate therapy in gastrointestinal stromal tumors (GISTs). Eur J Cancer 38:S60–S65
55. van Oosterom AT, Judson I, Verweij J, Stroobants S, Donato Di Paola E, Dimitrijevic S, Martens M, Webb A, Sciot R, Van Glabbeke M, Silberman S, Nielsen OS (2001) European Organisation for Research and Treatment of Cancer Soft Tissue and Bone Sarcoma Group. Safety and efficacy of imatinib (STI571) in metastatic gastrointestinal stromal tumours: a phase I study. Lancet 358:1421–1423
56. Vanel D, Shapeero LG, Tardivon A, Western A, Guinebretiere JM (1998) Dynamic contrast-enhanced MRI with subtraction of aggressive soft tissue tumors after resection. Skeletal Radiol 27:505–510
57. Völker T, Denecke T, Steffen I, Misch D, Schönberger S, Plotkin M, Ruf J, Furth C, Stöver B, Hautzel H, Henze G, Amthauer H (2007) Positron emission tomography for staging of pediatric sarcoma patients: results of a prospective multicenter trial. J Clin Oncol 25:5435–5441

Magnetic Resonance Imaging: Basic Concepts

4

Peter Brys

Contents

4.1 **Introduction** 71

4.2 **Imaging Planes** 72

4.3 **Unenhanced MRI** 72
4.3.1 T1-Weighted Imaging (T1-WI) 73
4.3.2 Fat-Suppressed T1-Weighted Imaging (FS T1-WI) 76
4.3.3 Fluid-Sensitive Sequences 77
4.3.4 T2* Gradient Echo Imaging 78

4.4 **Contrast-Enhanced MRI** 79
4.4.1 Contrast-Enhanced T1-Weighted Imaging 79
4.4.2 Fat-Suppressed Contrast-Enhanced T1-Weighted Imaging 79
4.4.3 Subtraction Images 81
4.4.4 Static Versus Dynamic Enhanced MRI 81

References 82

P. Brys
Department of Radiology, University Hospitals Leuven, Herestraat 49, B-3000 Leuven, Belgium
e-mail: peter.brys@uzleuven.be

4.1 Introduction

Due to its unequaled soft tissue contrast and multiplanar imaging capability, MRI is the modality of choice to image soft tissue tumors. This chapter is dedicated to basic unenhanced and static enhanced MRI. Advanced MRI and posttreatment imaging are discussed in other chapters. Distinction will be made between imaging for local staging and tissue characterization purpose, as well as between what is essential, what should be avoided, and what are useful additional techniques.

MR imaging should be of the highest possible quality to provide all necessary information needed for adequate local staging as well as grading of a soft tissue tumor.

Local Staging Accurate staging needs precise localization of a tumor within its anatomical compartment and relative to important surrounding landmarks and determination whether a mass is confined to its compartment or whether it is invading or encasing surrounding structures [2]. Imaging should always precede biopsy, as blood and edema that follow a biopsy can be difficult to differentiate from tumor or the peritumoral reactive zone, with or without Gd administration. An appropriate decision whether or not to perform limb-salvaging surgery based on a post-biopsy MR examination may be impossible.

© Springer International Publishing AG 2017
F.M. Vanhoenacker et al. (eds.), *Imaging of Soft Tissue Tumors*, DOI 10.1007/978-3-319-46679-8_4

Tissue Characteristics Although tissue characteristics derived from MRI alone are often insufficient to predict a specific pathological diagnosis, a well-performed MRI helps to narrow down the differential diagnosis, facilitating the clinical management. MRI is essential for the decision whether or not to perform a biopsy and planning of the optimal, most informative biopsy site. Lesions in which the observer is highly confident of a benign diagnosis at MR may not require histologic biopsy [25].

4.2 Imaging Planes

The strategy in designing the optimal MR examination depends on the location of a lesion, the desired coverage of the region to be examined, the available hardware (field strength, coils), the time constraints, and the local preferences. The MR examination should be supervised, tailored to the individual patient. Careful assessment of the region of clinical concern should precede any imaging to ensure its complete coverage with the most appropriate coil and to avoid waste of time due to repositioning of the patient after the first imaging sequence.

Demarcation of subtle, doubtful, or diffuse lesions with a lipid marker prior to imaging may be helpful. Care should be taken not to compress the mass by this marker. Images should be of sufficiently high spatial resolution to demonstrate relevant morphologic features and anatomic detail. The use of a large field-of-view results in loss of spatial resolution. It is usually not necessary to examine the contralateral side for comparison when an extremity is being evaluated. A wider field-of-view may be used for initial detection or when multiple lesions are suspected, followed by a smaller field-of-view targeted to the lesion.

Imaging usually starts with a sequence in the most appropriate longitudinal plane. Anteriorly or posteriorly located lesions are best imaged in a sagittal plane, medial or lateral localizations in a coronal plane. Care should be taken to respect the anatomical orthogonal planes since with excessive rotation of a limb, inappropriate positioning of longitudinal scan planes results in images which are difficult to interpret and probably useless for surgical planning. Since this sequence should depict the lesion, together with eventually surrounding edema, with the highest conspicuity and over its entire cephalocaudal extent, fat-suppressed fast spin-echo T2-weighted or STIR imaging with a large field-of-view is recommended.

This first sequence in the longitudinal plane is usually followed by imaging in the axial plane. Since most anatomical compartments of the extremities are oriented longitudinally, accurate assessment of localization and extent of a tumor requires imaging in the axial plane, in which the majority of sequences should be obtained. Not only the tumor but also the peritumoral edema at its proximal and distal poles should be covered by these axial sequences. As a rule, the most proximal and distal slices should show no pathology. Usually T1- and T2-weighted acquisitions are obtained in the axial plane at exactly the same location, thus allowing an image-by-image comparison. Contrast-enhanced images have to be acquired at least in the axial and the most useful longitudinal plane and at the same positions as the precontrast images.

The choice of an additional imaging plane depends on the location of the lesion and the clinical questions to be answered. Inclusion of the nearest joint, or another key anatomic landmark, serving as a reference in at least one of the longitudinal imaging planes is essential for surgical planning since especially deeply situated masses can be hard to localize based on clinical examination alone. Oblique planes may also be useful. Typical examples are oblique sagittal images for optimal depiction of a lesion's relation to the scapula or the iliac wing.

4.3 Unenhanced MRI

For detection, local staging, and characterization of a mass, the use of conventional spin-echo sequences is recommended. It is the most reproducible technique, the one with which we are most familiar for tumor evaluation, and the most often referenced in tumor imaging literature [19].

4.3.1 T1-Weighted Imaging (T1-WI)

Local Staging In delineation of a soft tissue tumor, distinction must be made between tumor-to-muscle and tumor-to-fat contrast. On T1-WI, with exception of fat-containing tumors, soft tissue tumors are generally more or less isointense to muscle, resulting in low tumor-to-muscle but high tumor-to-fat contrast (Figs. 4.1b, 4.2a, 4.3a, and 4.4a). As a conse-

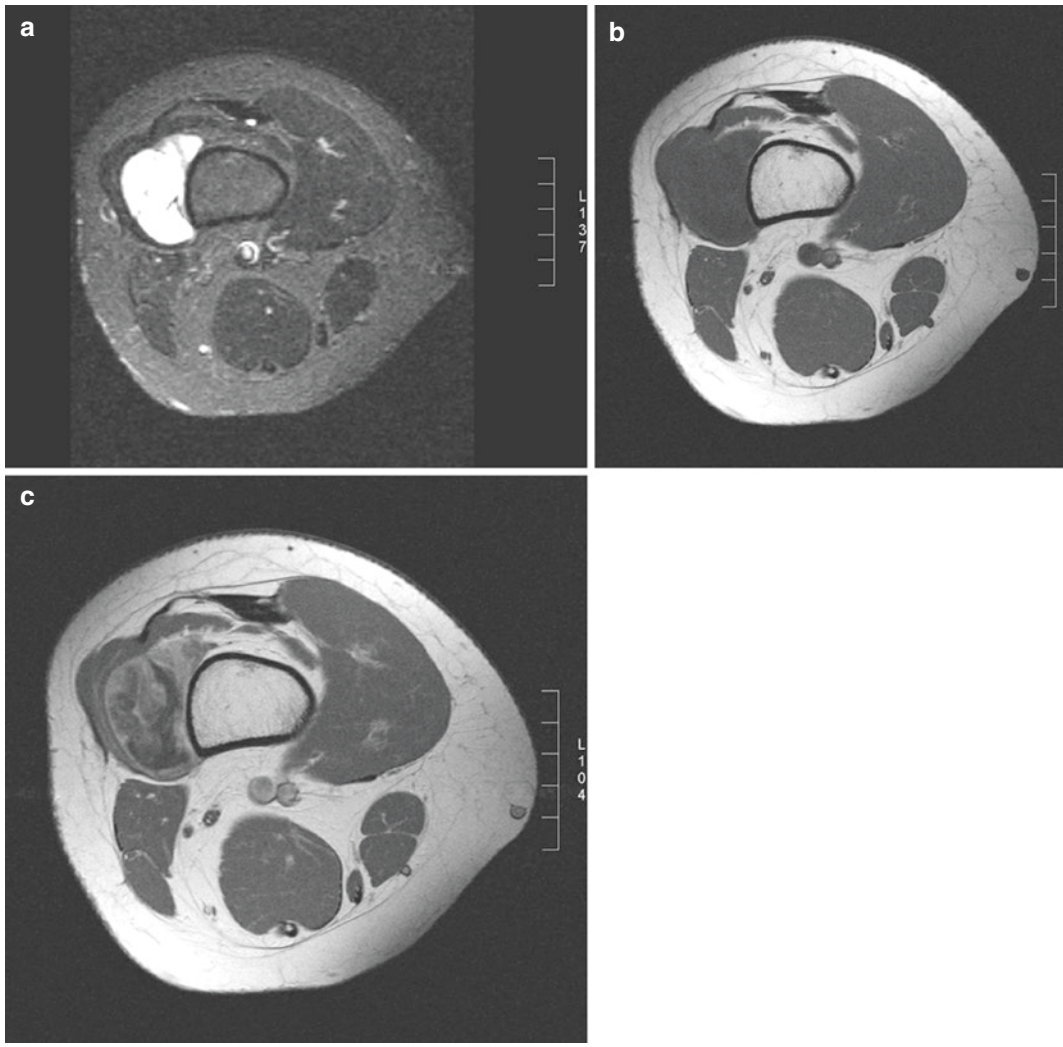

Fig. 4.1 (**a–c**) Myxoid liposarcoma in the distal thigh. (**a**) Axial STIR sequence. A sharply margined mass lesion with homogeneous high signal intensity is interposed between the vastus lateralis muscle and the distal femur. (**b**) Axial unenhanced T1-weighted image. A very low tumor-to-muscle contrast is shown with the lesion's signal intensity slightly lower than muscle. In combination with the high signal intensity on STIR sequence, this lesion could be mistaken for a cyst based on unenhanced sequences alone. Also note the very high tumor-to-fat contrast, typical for unenhanced T1-weighted images. (**c**) Axial Gd-enhanced T1-weighted image. The lesion shows a definite and heterogeneous enhancement, inconsistent with a cystic origin of the lesion. Although there is a decreased tumor-to-fat contrast, delineation of the tumor from the adjacent fat still is perfectly possible. In addition, due to a clear increase in tumor-to-muscle contrast, this sequence is very suitable for surgical planning. Beside the adequate delineation of the tumor, this enhanced T1-weighted sequence improves the evaluation of the internal structure of the tumor. It helps to differentiate viable tumor from a cyst, with a totally different surgical approach, and helps to select an appropriate biopsy site. Because it mainly consists of less well-vascularized and myxoid or necrotic tissue, a biopsy in de posterior part of the lesion should be avoided

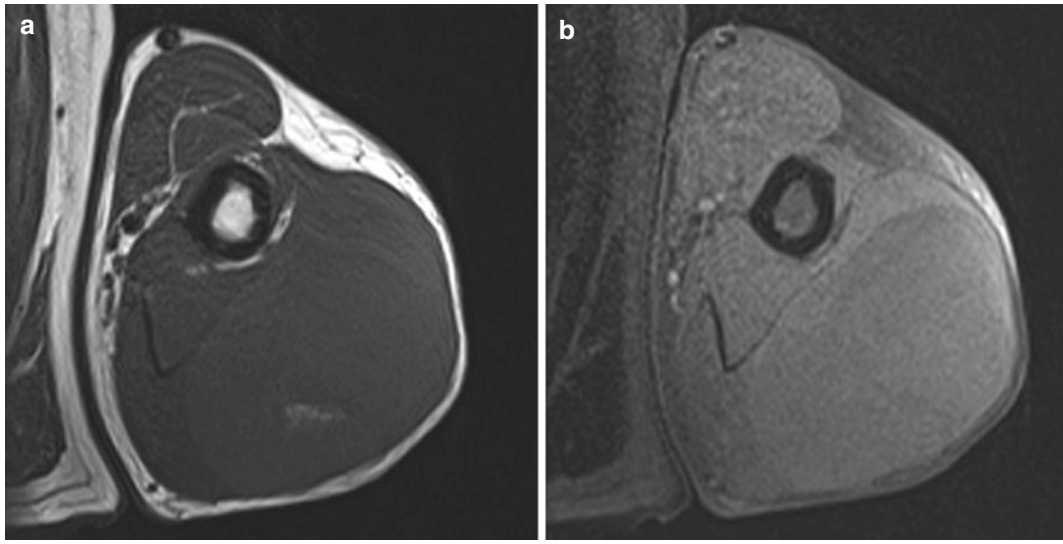

Fig. 4.2 (**a**, **b**) Myxoid round cell liposarcoma in the upper arm. (**a**) Axial unenhanced SE T1-weighted image. Large tumor in the lateral head of the triceps muscle, isointense to muscle, resulting in poor tumor-to-muscle but high tumor-to-fat contrast. In the posterior half of the lesion, a small hyperintense area is visible, consistent with fat or another short-T1 tissue. (**b**) Axial unenhanced fat-suppressed SE T1-weighted image. Fat suppression clearly decreases the signal intensity of the small area, consistent with fatty tissue, raising the suspicion of a possible liposarcoma

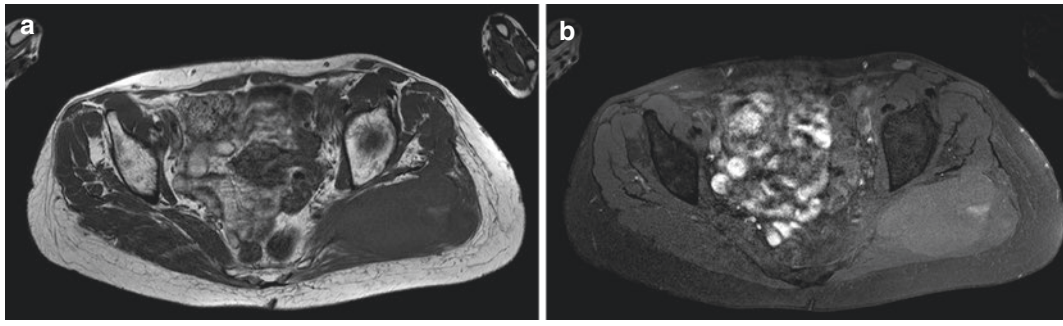

Fig. 4.3 (**a**, **b**) B-cell non-Hodgkin lymphoma of the left buttock. (**a**) Axial unenhanced SE T1-weighted image. Large mass in the left gluteus maximus muscle, slightly hyperintense to muscle. Due to high muscle-to-fat contrast, a fat plane is clearly visible anterior to the mass. In the lateral part, a small hyperintense area is visible, consistent with fat or another short-T1 tissue. (**b**) Axial unenhanced fat-suppressed SE T1-weighted image. Due to the rescaling effect, the subtle hyperintensity of the mass compared with the surrounding muscle is magnified, hence becoming more obvious. Fat suppression doesn't decrease the signal intensity of the small lateral area, and rescaling even increases its signal intensity. Hence, it is unlikely that we are dealing with a liposarcoma. Notice fat suppression results in obscuring of anatomical fat planes

quence T1-WI is essential in the identification of anatomical structures and delineation of a tumor from intermuscular fat planes (Figs. 4.1b and 4.3a), fat surrounding neurovascular structures, subcutaneous fat, and fatty bone marrow. Since identification of anatomical fat planes is essential for surgical planning, nonfat-suppressed T1-WI in the axial plane is mandatory.

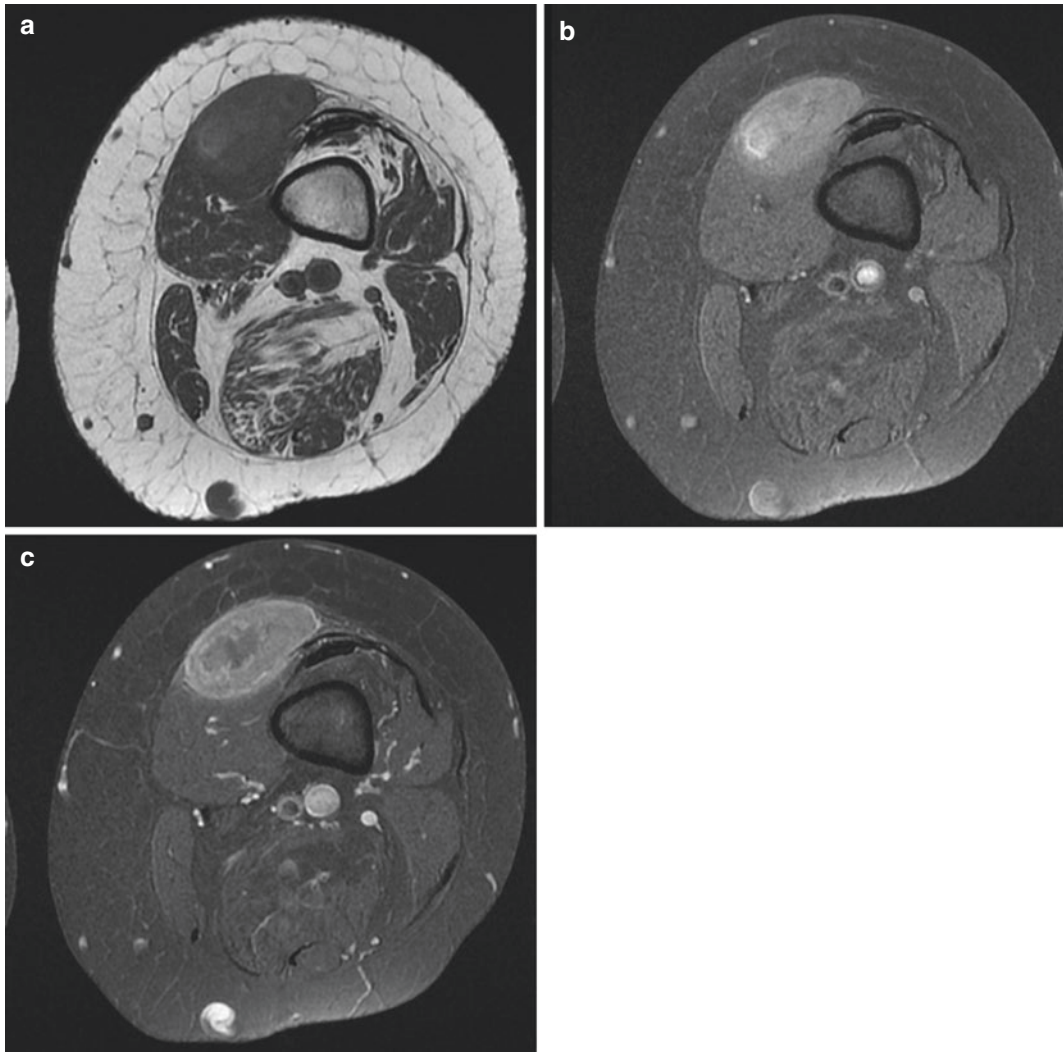

Fig. 4.4 (**a**–**c**) Malignant peripheral nerve sheath tumor in the distal vastus medialis muscle of the thigh. (**a**) Axial unenhanced SE T1-weighted image. The signal intensity of the mass is heterogeneous, grossly isointense to muscle with some slightly hyperintense areas. (**b**) Axial unenhanced fat-suppressed SE T1-weighted image. Fat suppression results in magnification of the signal heterogeneity, increasing the conspicuity of a small hyperintense area in the medial half of the lesion. (**c**) Axial Gd-enhanced fat-suppressed SE T1-weighted image. After Gd administration two rims of enhancement are visible, one surrounding the lesion and another surrounding a hypointense area in the medial half of the lesion. Since Gd-enhanced blood vessels now are the most hyperintense structures, rescaling occurs resulting in downscaling of the slightly hyperintense area in the medial half of the lesion. Due to the same rescaling, assessment of Gd uptake in the lateral half and posterior part of the lesion is difficult. Most likely the uptake is slight. This would be even more difficult if precontrast fat-suppressed images weren't available and assessment was based on comparison of **a** with **c**. In this case subtraction images, subtracting sequence **b** from **c**, and/or nonfat-suppressed Gd-enhanced T1-WI would have been of great value

Because of the low tumor-to-muscle contrast, T1-WI in another than the axial plane usually is not useful. For fatty tumors, with excellent tumor-to-muscle contrast, additional T1-WI in a longitudinal plane might be helpful for local staging.

Tissue Characteristics Tissue characterization is based on several imaging parameters, some of them related to the signal intensity on T1-WI [4]. Unenhanced T1-WI also is essential as a baseline for contrast-enhanced studies.

4.3.2 Fat-Suppressed T1-Weighted Imaging (FS T1-WI)

Extra information can be derived from the addition of a fat-suppression technique to a T1-weighted sequence. Chemical shift-based, also known as frequency selective, fat suppression should be used in these cases.

Local Staging Suppression of the high signal intensity of fat results in loss of tumor-to-fat contrast, obscuring fat planes, which is a major disadvantage in planning of surgery (Figs. 4.2b and 4.3b). For this reason FS T1-WI should never be performed without its non-FS equivalent.

Tissue Characteristics The added value of FS T1-WI for tissue characterization is threefold : a more efficient use of the dynamic range for display of tissue contrast, differentiation between fat and other short-T1 tissues, and a baseline for comparison with FS contrast-enhanced T1-WI.

Suppression of the high signal intensity of fat induces a rescaling, a redistribution of gray levels, leading to a more efficient use of the dynamic range for display of tissue contrast [12]. Minor differences in signal intensity between tissues on non-FS T1-WI get magnified, and signal inhomogeneity, an important parameter in characterization, is better evaluated [10] (Figs. 4.3a, b and 4.4a, b)

A signal hyperintense to muscle is considered to be hyperintense on T1-WI. Hyperintense substances on T1-WI include fat, methemoglobin, melanin, and proteinaceous fluid [30]. Chemical shift-based FS selectively decreases the signal intensity of fat, while other hyperintense tissues remain hyperintense [18, 22] (Figs. 4.2, 4.3, and 4.5b). FS T1-WI is useful if a lesion shows high

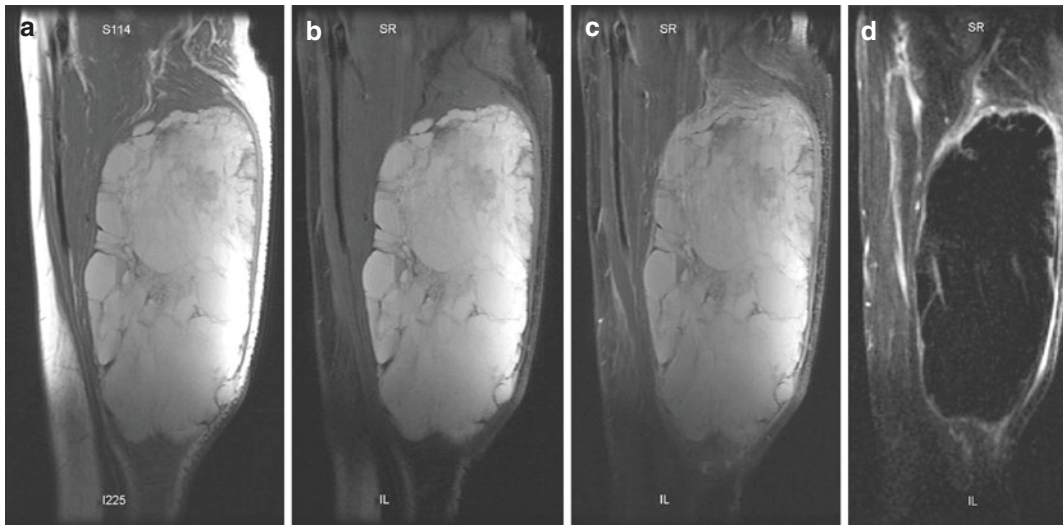

Fig. 4.5 (**a**–**d**) Necrotic, hemorrhagic high-grade pleiomorphic sarcoma of the posterior thigh compartment. (**a**) Sagittal unenhanced T1-weighted image. The large mass lesion is showing an inhomogeneous high signal intensity, possibly of lipomatous origin. (**b**) Sagittal fat-suppressed-unenhanced T1-weighted image. Persistence of the high signal intensity despite fat suppression is inconsistent with the hypothesis of a fatty tumor and in favor of the presence of methemoglobin in a large hematoma or hemorrhagic tumor. (**c**) Sagittal fat-suppressed Gd-enhanced T1-weighted image. Differentiation between hematoma and hemorrhagic tumor needs administration of gadolinium (Gd) contrast. Unfortunately, because of the presence of intralesional methemoglobin, the conspicuity of Gd enhancement doesn't benefit from the fat-suppression technique. Based on this sequence, it is virtually impossible to differentiate enhancement from methemoglobin. (**d**) Sagittal subtraction image (**b** subtracted from **c**). Subtraction of pre- from post-Gd fat-suppressed T1-weighted images permits to isolate the areas of Gd enhancement, showing a thin rim enhancement and only some small foci of mural enhancement in the upper posterior part of the lesion

signal intensity on the T1-WI [24, 30], e.g., to differentiate fatty tissue from a recent hematoma. It is important to perform the sequence with frequency-selective FS. Inversion-recovery FS is nonspecific and can cause loss of signal of not only fat but also of other short-T1 substances [30].

As explained in the contrast-enhanced section, it is essential to ensure that a precontrast fat-suppressed sequence is available for comparison if the postcontrast image is intended to be a fat-saturated T1-WI [12]. When time constraints are an issue, performing FS T1-WI frequently is not useful when the lesion is isointense or hypointense to muscle on T1-WI.

4.3.3 Fluid-Sensitive Sequences

Local Staging Fluid-sensitive sequences are important for the detection of a tumor and the differentiation of a hyperintense tumor and its surrounding edema from the hypointense surrounding muscles (Fig. 4.6b). The reactive edema around a tumor often contains satellite tumor micronodules and is considered as an integral part of the lesion and therefore is removed en bloc with the tumor [14, 17, 21, 23]. The conspicuity of this peritumoral edema should be as high as possible. The conspicuity with a classic double-echo T2-weighted sequence is acceptable. Its main disadvantage remains the relatively long acquisition times [19], which can be overcome by the use of a FSE T2-weighted sequence. However, since fat appears bright on FSE sequences [2, 13], with subsequent decrease of conspicuity of tumors or edema juxtaposed to fat [19], FSE T2-weighted sequences without fat suppression should not be used in tumor imaging (Fig. 4.6a). For maximal conspicuity of a tumor and its surrounding edema against the background of muscle and fat, a fat-suppressed fluid-sensitive sequence should be used. Usually a chemical shift-based fat-suppression technique is chosen. Its

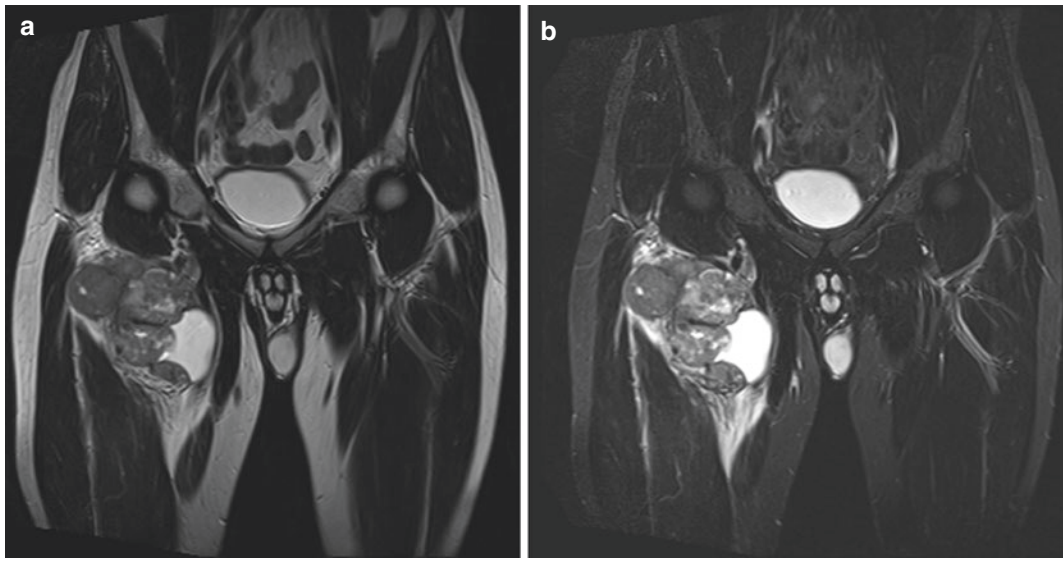

Fig. 4.6 (**a**, **b**) Synovial sarcoma of the proximal thigh. (**a**) Coronal FSE T2-weighted image. A mass consisting of several intermediate to hypointense nodulus and a strongly hyperintense medial area is shown. No clear perilesional edema is visible, although this assessment is difficult due to the artificially high signal intensity of fat, typical for this FSE T2-weighted sequence. (**b**) Coronal STIR sequence. Signal intensity of the mass is comparable with the previous sequence. However, due to the decreased signal intensity of fat by this inversion recovery type of fat suppression, resulting in a high fluid-to-fat contrast, a reactive zone of perilesional edema at the distal pole of the lesion becomes unequivocally visible. This case illustrates the ineffectiveness of FSE T2-WI for local staging purpose

acquisition time is shorter with a higher signal-to-noise ratio compared to STIR imaging [8]. A disadvantage is its susceptibility to magnetic field inhomogeneities. STIR provides more uniform fat suppression but results in longer scan times or lower signal-to-noise ratio [3].

Tissue Characteristics Spin-echo T2-WI is essential for tumor characterization [4]. Since fat appears artificially bright on FSE sequences, FSE T2-WI without fat suppression should not be used in tumor characterization [2, 13]. It is important to realize that the signal intensity of a mass can appear quite different on a FS T2-WI, as compared with the corresponding non-FS T2-WI because of the rescaling effect. FS sequences alone cannot be used to reliably describe the signal characteristics of a mass [30].

As with T1-WI chemical shift-based FS T2-WI can be used to confirm the presence of fat in a lesion. In addition it also increases the conspicuity of non-lipomatous components in lipomatous tumors, the latter helping in distinguishing lipoma from well-differentiated liposarcoma [9].

Since its fat suppression is nonspecific, STIR imaging should not be used for tissue characterization. Nonfatty tissues can be suppressed along with fat, and fatty tissues may not be fully suppressed. Knowledge of this pitfall is necessary for correct image interpretation [1].

4.3.4 T2* Gradient Echo Imaging

Tissue Characteristics In some selected applications, a T2*-weighted gradient echo sequence can be very useful. In the absence of gas or calcifications on radiographs and computed tomography, a marked signal loss on GRE sequences is almost pathognomonic for hemosiderin

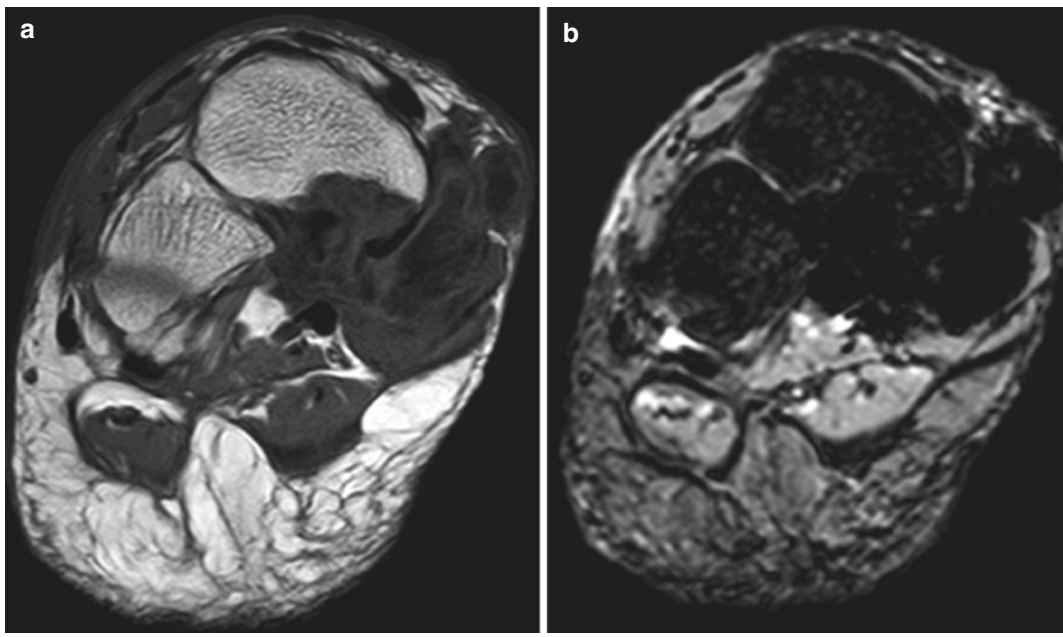

Fig. 4.7 (**a**, **b**) Giant cell tumor of tendon sheath of the foot. (**a**) Axial unenhanced SE T1-weighted image. Unsharply demarcated mass along the tibialis posterior insertion, deep to the abductor hallucis muscle, causing an erosion at the medioplantar side of the navicular bone. The lesion shows a heterogeneous signal intensity with strongly hypointense areas, consistent with possible collagen content, calcifications, or hemosiderin. (**b**) Axial T2*-weighted gradient echo image. On this gradient echo sequence, the whole lesion shows a profound signal loss, the so-called blooming effect, highly suggestive of the presence of hemosiderin, consistent with giant cell tumor of tendon sheath (extra-articular type of PVNS)

(Fig. 4.7) [11]. When present in sufficient quantities, hemosiderin can appear more prominent, the so-called blooming, and therefore useful in the diagnosis of hemangiomas, PVNS, and mature hematomas [16].

4.4 Contrast-Enhanced MRI

Routine IV Gd administration is not a requirement and unnecessary when the result wouldn't influence patient care. Characterization and delineation of, e.g., lipomas and some subtypes of vascular malformations are easily performed on unenhanced sequences. However, contrast administration is certainly helpful in staging, characterization, and clinical management of most of the soft tissue tumors. Generally contrast is administered in a nondynamic fashion: after contrast injection a relatively longer acquisition of a high spatial resolution is obtained.

Local Staging Enhanced T1-WI improves the delineation of a tumor (Figs. 4.1b, c and 4.5), helping to highlight tissue planes to aid in assessing the degree of invasion into surrounding structures [15].

Tissue Characteristics Enhanced T1-WI improves the evaluation of the internal structure of a tumor (Figs. 4.1b, c and 4.5). It demonstrates the relative vascularity of a tumor and helps to differentiate well-perfused, viable tumor from tumor necrosis, intratumoral hemorrhage from hematoma, cysts from solid tumors (Fig. 4.1), and cystic parts from myxoid parts. Contrast-enhanced MR is essential for the decision whether or not to perform a biopsy and planning of the biopsy site. Since every additional procedure increases the risk of inadvertent tumor cell contamination, the selection of the biopsy site should be well considered. A biopsy containing well-vascularized viable tumor will be of greater value than a nondiagnostic specimen with hemorrhage, edema, or necrotic tissue. If only static enhanced MRI is used, the area showing the most intense enhancement should be selected as biopsy site [26] (Fig. 4.1c).

4.4.1 Contrast-Enhanced T1-Weighted Imaging

Local Staging On T1-WI tumor-to-muscle contrast usually increases markedly after contrast administration (Fig. 4.1b, c). Although there is no improvement of this tumor-to-muscle contrast when compared with fluid-sensitive sequences [6, 28], the static enhanced T1-weighted sequence without fat suppression is very useful. As an "almost-all-in-one sequence," it has the anatomical detail, fat planes inclusive, typical of T1-WI, a tumor-to-muscle contrast equal to that of fluid-sensitive sequences, and it provides useful information on tumor content due to the Gd administration (Fig. 4.1c). Most surgeons use these images for planning their interventions. A disadvantage of enhanced T1-WI is a decreased tumor-to-fat contrast (Fig. 4.8).

Tissue Characteristics As already mentioned, this sequence provides useful information on tumor content.

4.4.2 Fat-Suppressed Contrast-Enhanced T1-Weighted Imaging

Chemical shift-based fat suppression may be applied on contrast-enhanced T1-WI. STIR sequences should not be used since not only fat but also enhancing tissue will be shown with a reduced signal intensity [1].

Local Staging Enhanced T1-WI decreases or even obscures the tumor-to-fat contrast. Applying fat suppression to postcontrast T1-WI restores the optimal tumor-to-fat contrast (Fig. 4.8). Since FS Gd-enhanced T1-WI shows areas of contrast enhancement with a greater conspicuity compared with T1-WI without fat suppression, subsequently resulting in images which are easier to interpret, the use of this sequence became very popular. However, since fat suppression results in obscured fat planes, which is a major disadvantage in planning of surgery, this sequence should never be acquired without its non-FS equivalent.

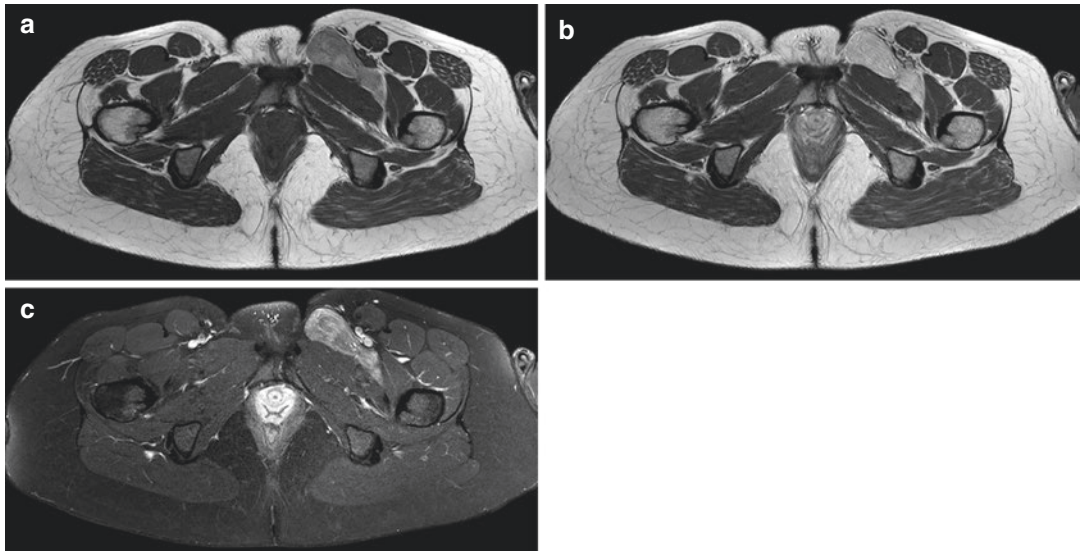

Fig. 4.8 (**a**–**c**) Hibernoma of the left groin. (**a**) Axial unenhanced SE T1-weighted image. Mass between the femoral neurovascular bundle and the pectineus muscle, hyperintense to muscle, and hypointense to fat, resulting in an excellent tumor-to-fat contrast. (**b**) Axial Gd-enhanced SE T1-weighted image. The strong Gd uptake by the lesion causes a complete loss of tumor-to-fat contrast. (**c**) Axial fat-suppressed Gd-enhanced SE T1-weighted image. Due to suppression of the high signal intensity of fat, the excellent tumor-to-fat contrast is restored, allowing the exclusion of infiltration of the mass into the surrounding fat

For local staging purpose, it is only recommended when tumor abuts or infiltrates adjacent fat.

Tissue Characteristics The assessment of Gd uptake usually occurs by comparison of non-FS precontrast T1-WI with postcontrast T1-WI. With these images detection of Gd uptake can be difficult when differences are subtle in case of minor Gd uptake, or when on precontrast images the lesion already shows hyperintense areas (Fig. 4.5).

Conspicuity of Gd uptake increases with the use of FS T1-WI. Suppression of the high signal intensity of fat induces a rescaling, magnifying minor differences in signal intensity between tissues due to subtle Gd uptake. This rescaling effect is responsible for an apparently obvious Gd enhancement of tissue that only shows minimal enhancement on non-FS T1-WI [10, 12].

When on precontrast images, the lesion shows hyperintense areas, the assessment of Gd uptake will only benefit from fat suppression when hyperintensity is due to fat, resulting in suppression of the hypersignal with subsequently increased conspicuity of enhancement along or within these fatty areas. When the precontrast hyperintensity is of nonfatty origin, fat suppression doesn't decrease the signal, enhancement conspicuity might not increase, and areas that are slightly hyperintense might be rescaled moderately to strongly hyperintense.

One should be aware of the risk of misinterpretation when Gd uptake is evaluated by comparison of FS-enhanced T1-WI with non-FS precontrast T1-WI since a high signal intensity of a lesion on FS-enhanced T1-WI can be the consequence of two variables that have been changed [12]. The change of one variable by applying fat suppression to precontrast T1-WI causes a rescaling effect, leading to an increased signal intensity of tissues, especially those which are hyperintense to muscle on non-FS images. Differences in signal intensity between T1-WI and FS T1-WI are the result of fat suppression and rescaling (Figs. 4.2, 4.3, and 4.4).

IV administration of Gd changes another variable. Differences in signal intensity between pre- and postcontrast T1-WI, or between pre- and

postcontrast FS T1-WI, are the result of Gd uptake in vascularized tissues (Figs. 4.1, 4.4, and 4.8). The change of two variables simultaneously by comparison of precontrast T1-WI with postcontrast FS T1-WI might hamper interpretation since differences in signal intensity can be the result of fat suppression, rescaling, or Gd uptake. The rescaling effect might be responsible for apparently obvious Gd enhancement of tissue that only shows minimal enhancement on non-FS T1-WI [10, 12], or even apparently slight or moderate enhancement of tissue which is non-enhancing on non-FS T1-WI (Fig. 4.4).

Gd administration might cause a downscaling effect on FS T1-WI. Hyperintense areas may lose signal intensity when they are not or only minimally enhancing due to rescaling induced by strongly Gd-enhancing tissue (Fig. 4.4). In these cases interpretation might be more difficult. Availability of non-FS pre- and postcontrast T1-WI, or the use of subtraction images, might facilitate interpretation.

As a consequence, reliable interpretation of FS Gd-enhanced T1-WI is only possible if also unenhanced FS T1-WI and enhanced non-FS T1-WI are obtained, resulting in longer examination times. However, the use of FS-enhanced T1-WI certainly is not a routine requirement [12].

4.4.3 Subtraction Images

With subtraction imaging, an unenhanced T1-WI sequence is digitally subtracted from the identical Gd-enhanced sequence by means of a postprocessing tool. The exact similarity in all imaging parameters between both sequences to be subtracted is required. Any gray scale value other than signal void on subtraction images is consistent with Gd enhancement. To obtain useful subtraction images, the patient should not change position during the examination, and IV access should be acquired before the start of the examination.

Tissue Characteristics Subtraction images are especially useful in lesions showing hyperintense signal on precontrast T1-WI due to nonfatty content (methemoglobin, melanin, or proteinaceous fluid). Determination of the presence or absence of enhancement in these lesions might be critical, and visual assessment of enhancement is difficult or even impossible [5]. The subtraction technique can adequately determine Gd enhancement on a background of hyperintense signal, which is extremely important in differentiation between a subacute hematoma and a hemorrhagic tumor (Fig. 4.5). When time constraints are a matter, enhancement conspicuity can also be obtained by the use of image subtraction.

4.4.4 Static Versus Dynamic Enhanced MRI

Static Gd-enhanced MRI is performed in the equilibrium state when the Gd concentration in the interstitium equals that of plasma. Dynamic Gd-enhanced MRI provides physiologic information, such as tissue perfusion and vascularization, capillary permeability, and the volume of the interstitial space, which is not available on static Gd-enhanced MRI (see Chap. 5) [27, 29].

Local Staging Reliable differentiation between tumor and peritumoral edema cannot be made by means of T2-WI nor by static enhanced T1-WI. Dynamic enhanced MR studies can contribute to the differentiation of tumor from edema, because edema shows a much more gradual increase in signal intensity than the tumor tissue.

Tissue Characteristics Static enhanced MRI has a limited value in the characterization of soft tissue tumors and the differentiation of benign from malignant lesions. Dynamic enhanced studies improve differentiation between highly vascularized, less well-vascularized, and necrotic tumor areas, which further narrows down the differential diagnosis, helps to increase the suspicion of malignant lesions [25], and is important in the selection of the highest vascularized, highest-grade part of the tumor for the biopsy site [20, 26].

Since dynamic enhanced sequences are obtained with lower spatial resolution, these should be followed by a delayed static enhanced study, which produces higher spatial resolution [7].

Key Points

1. MR imaging should always precede biopsy since tumor staging based on a post-biopsy MR examination may be impossible.
2. Adequate evaluation of tumor extent requires multiplanar imaging, but the axial plane is probably the most important. Meticulous description of the extent of peritumoral edema is mandatory.
3. FSE T2-weighted sequences without fat suppression are far less appropriate for depiction of local tumor extent than fat-suppressed T2-WI.
4. When contrast-enhanced MR is performed, pre- and postcontrast T1-WI without fat suppression is mandatory. Pre- and postcontrast fat-suppressed T1-WI is optional.

   The use of fat-suppressed-enhanced T1-WI is only recommended when tumor abuts or infiltrates adjacent fat. Gd-enhancement conspicuity can also be obtained from subtraction images.
5. Don't use fat-suppressed T1-WI without their nonfat-suppressed equivalent since they obscure surgically important fat planes and because of the risk of misinterpretation of Gd enhancement.
6. Since its fat suppression is nonspecific, STIR imaging should not be used for tissue characterization.

References

1. Amini B, Jessop AC, Ganeshan DM, Tseng WW, Madewell JE (2015) Contemporary imaging of soft tissue sarcomas. J Surg Oncol 111:496–503
2. Constable RT, Anderson AW, Zhong J, Gore JC (1992) Factors influencing contrast in fast spin-echo MR imaging. Magn Reson Imaging 10:497–511
3. Delfaut EM, Beltran J, Johnson G, Rousseau J, Marchandise X, Cotton A (1999) Fat suppression in MR imaging: techniques and pitfalls. Radiographics 19:373–382
4. De Schepper AM (2006) Grading and characterization of soft tissue tumors. In: De Schepper AM, Vanhoenacker F, Gielen J, Parizel PM (eds) Imaging of soft tissue tumors, 3rd edn. Springer, Berlin/Heidelberg/New York, pp 139–162
5. Eid M, Abougabal A (2014) Subtraction images: a really helpful tool in non-vascular MRI. Egypt J Radiol Nucl Med 45:909–919
6. Erlemann R, Reiser MF, Peters PE, Vasallo P, Nommensen B, Kusnierz-Glaz CR, Ritter J, Roessner A (1989) Musculoskeletal neoplasms: static and dynamic Gd-DTPA-enhanced MR imaging. Radiology 171:767–773
7. Fayad LM, Jacobs MA, Wang X, Carrino JA, Bluemke DA (2012) Musculoskeletal tumors: how to use anatomic, functional, and metabolic MR techniques. Radiology 265(2):340–356
8. Fleckenstein JL, Archer BT, Barker BA, Vaughan JT, Parkey RW, Peshock RM (1991) Fast short-tau inversion-recovery MR imaging. Radiology 179:499–504
9. Galant J, Marti-Bonmati L, Saez F, Soler R, Alcala-Santaella R, Navarro M (2003) The value of fat-suppressed T2 or STIR sequences in distinguishing lipoma from well-differentiated liposarcoma. Eur Radiol 13:337–343
10. Gielen J, De Schepper A, Parizel P, Wang X, Vanhoenacker F (2003) Additional value of magnetic resonance with spin echo T1-weighted imaging with suppression in characterization of soft tissue tumors. J Comput Assist Tomogr 27(3):434–441
11. Hardy PA, Kucharczyk W, Henkelman RM (1990) Cause of signal loss in MR images of old hemorrhagic lesions. Radiology 174:549–555
12. Helms CA (1999) The use of fat suppression in gadolinium-enhanced MR imaging of the musculoskeletal system : a potential source of error. AJR Am J Roentgenol 173:234–236
13. Henkelman RM, Hardy PA, Bishop JE, Poon CS, Piewes DB (1992) Why is fat bright in RARE and fast spin-echo imaging. J Magn Reson Imaging 2:533–540
14. Kaya M, Wada T, Nagoya S, Sasaki M, Matsumura T, Yamaguchi T, Hasegawa T, Yamashita T (2008) MRI and histological evaluation of the infiltrative growth pattern of myxofibrosarcoma. Skeletal Radiol 37:1085–1090
15. Kransdorf MJ, Murphey MD (2000) Radiologic evaluation of soft-tissue masses: a current perspective. AJR Am J Roentgenol 175:575–587
16. Mallinson PI, Chou H, Forster BB, Munk PL (2014) Radiology of soft tissue tumors. Surg Oncol Clin N Am 29:911–936
17. McDonald DJ (1994) Limb-salvage surgery for treatment of sarcomas of the extremities. AJR Am J Roentgenol 163:509–513
18. Mirowitz SA, Apicella P, Reinus WR, Hammerman AM (1994) MR imaging of bone marrow lesions: relative conspicuousness on T1-weighted, fat-suppressed T2-weighted, and STIR-images. AJR Am J Roentgenol 162:215–221
19. Rubin DA, Kneeland JB (1994) MR imaging of the musculoskeletal system: technical considerations for enhancing image quality and diagnostic yield. AJR Am J Roentgenol 163:1155–1163

20. Shapeero LG, Vanel D, Verstraete KL, Bloem JL (2002) Fast magnetic resonance imaging with contrast for soft tissue sarcoma viability. Clin Orthop Relat Res 397:212–227
21. Shuman WP, Patten RM, Baron RI, Liddell RM, Conrad EU, Richardson ML (1991) Comparison of STIR and spin-echo MR imaging at 1.5 T in 45 suspected extremity tumors: lesion conspicuity and extent. Radiology 179:247–252
22. Soulie D, Boyer B, Lescop J, Pujol A, Le Friant G, Cordoliani YS (1995) Liposarcome myxoide. Aspects en IRM. J Radiol 1:29–36
23. Stark D, Bradley W (1992) Magnetic resonance imaging, 2nd edn. Mosby Year Book, St.Louis
24. Taïeb S, Penel N, Vanseymortier L, Ceugnart L (2009) Soft tissue sarcomas or intramuscular haematomas ? Eur J Radiol 72:44–49
25. van Rijswijk CS, Geirnaerdt MJ, Hogendoorn PC, Taminiau AH, van Coevorden F, Zwinderman AH, Pope TL, Bloem JL (2004) Soft tissue tumors: value of static and dynamic Gadopentetate dimeglumine-enhanced MR imaging in prediction of malignancy. Radiology 233:493–502
26. Verstraete KL, Lang P (2000) Bone and soft tissue tumors: the role of contrast agents for MR imaging. Eur J Radiol 34:229–246
27. Verstraete KL, De Deene Y, Roels H, Dierick A, Uyttendaele D, Kunnen M (1994) Benign and malignant musculoskeletal lesions: dynamic contrast-enhanced MR imaging – parametric 'first-pass' images depict tissue vascularization and perfusion. Radiology 192:835–843
28. Verstraete KL, Vanzieleghem B, De Deene Y, Palmans H, De Greef D, Kristoffersen DT, Uyttendaele D, Roels H, Hamers J, Kunnen M (1995) Static, dynamic and first-pass MR imaging of musculoskeletal lesions using gadodiamide injection. Acta Radiol 36(1):27–36
29. Verstraete KL, Van der Woude HJ, Hogendoorn PC, De Deene Y, Kunnen M, Bloem JL (1996) Dynamic contrast-enhanced MR imaging of musculoskeletal tumors: basic principles and clinical applications. J Magn Reson Imaging 6(2):311–321
30. Wu JS, Hochman MG (2009) Soft-tissue tumors and tumorlike lesions: a systematic imaging approach. Radiology 253(2):297–316

Magnetic Resonance Imaging: Advanced Imaging Techniques

5

Koenraad L. Verstraete, J.C. Dutoit, J.L. Drapé, and Johan L. Bloem

Contents

5.1 **Dynamic Contrast-Enhanced MRI** 85
5.1.1 Basic Principles 85
5.1.2 Imaging Techniques 87
5.1.3 Evaluation and Postprocessing Techniques 88
5.1.4 Clinical Applications 101

5.2 **Diffusion MRI** 106
5.2.1 Imaging Technique 106
5.2.2 Clinical Applications 108

5.3 **Proton Nuclear MR Spectroscopy** 109

Conclusions 109

References 110

K.L. Verstraete (✉) • J.C. Dutoit
Department of Radiology and Nuclear Medicine and Faculty of Medicine and Health Sciences, Ghent University, De Pintelaan, 185, 9000 Gent, Belgium
e-mail: Koenraad.Verstraete@UGent.be

J.L. Drapé
Service de Radiologie B, Hôpital Cochin, Université Paris Descartes, Sorbonne Paris Centre, 27 rue du Faubourg-Saint-Jacques, Paris, France

J.L. Bloem
Department of Radiology, Leiden University Medical Center (LUMC), Gebouw 1. Postbus 9600 2300 RC, Leiden, The Netherlands

5.1 Dynamic Contrast-Enhanced MRI

5.1.1 Basic Principles

In patients with tumors and tumorlike lesions of the musculoskeletal system, MRI is performed with (fast-) spin-echo sequences, before and after administration of a water-soluble chelate of gadolinium, at a dose of 0.1 mmol/kg and a concentration of 0.5 M. As these sequences last for minutes, tissues are imaged in a quasi-equilibrium state of the water-soluble contrast agent between the blood and interstitial space [1–5]. Therefore, this type of imaging is referred to as "static MRI," in which spatial resolution is emphasized over temporal resolution, in order to define anatomy.

This is in contrast to "dynamic MRI," where imaging is performed during and immediately after bolus injection, to study a dynamic physiological phenomenon, i.e., the initial distribution of the contrast agent in the capillaries and into the interstitial space of the tissues. This type of physiological imaging requires attention to a sufficiently high temporal resolution and serial imaging. According to the Nyquist theorem limit, in physiological imaging, the process of interest must be sampled at twice the frequency of the dynamic event being measured [3]. After bolus injection (0.2 ml/kg) at an injection rate of 5 ml/s, the first pass of a contrast agent through a tissue generally lasts for about 7–15 s [2]. An imaging frequency of at least one image or image series per 3.5–7 s is thus mandatory.

© Springer International Publishing AG 2017

F.M. Vanhoenacker et al. (eds.), *Imaging of Soft Tissue Tumors*, DOI 10.1007/978-3-319-46679-8_5

The extracellular distribution of fluid MR contrast agents is among blood plasma and the interstitial spaces. When such a contrast agent is administered intravenously by a rapid bolus injection, it is first diluted in the blood of the peripheral vein and the right heart, before it passes through the lungs and the left heart into the peripheral circulation (Fig. 5.1a). During the first pass of the contrast agent through the capillaries, a net unidirectional, fast diffusion occurs into the tissue, due to the high concentration gradient between the intravascular and the interstitial space: in normal tissues, approximately 50 % of the circulating contrast agent diffuses from the blood into the extravascular compartment during the first pass [1, 4–7]. This first-pass diffusion is essentially different from that during the second pass and later: at this initial moment, there is no contrast agent in the interstitial space, and the agent has its highest possible plasma

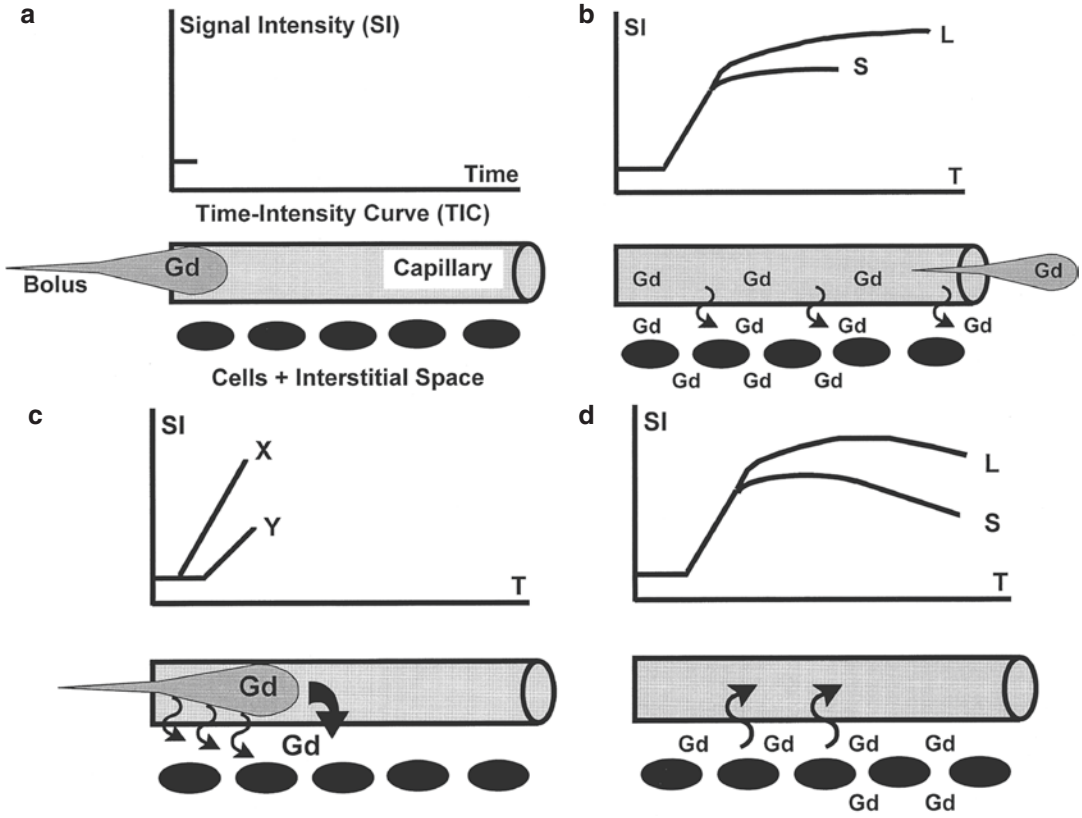

Fig. 5.1 (**a**–**d**) Factors determining early tissue enhancement. The *lower parts* of **a**–**d** show what occurs at the level of the capillary and the interstitial space after intravenous bolus injection; the *upper parts* graphically display the changes in signal intensity (SI) in a time-intensity curve. (**a**) The time interval between the intravenous bolus injection and arrival of the bolus in the capillary is determined by the injection rate, the heart rate, cardiac output, the localization of the lesion in the body, and the local capillary resistance (tissue perfusion). (**b**) The enhancement rate during the first pass of the contrast agent is determined by number of vessels (tissue vascularization), local capillary resistance (tissue perfusion), and capillary permeability. Tissues with high vascularization, perfusion, and capillary permeability (*X*) will enhance earlier and faster than tissues with a lower number of vessels, higher capillary resistance, and lower capillary permeability (*Y*). (**c**) After the first pass of the bolus, the SI increases further until the concentration of the gadolinium (*Gd*) contrast medium in the blood and the interstitial space of the tissue are equal. In tissues with a small (*S*) interstitial space, this equilibrium is reached earlier than in tissues with a larger (*L*) interstitial space. (**d**) As the arterial concentration of the contrast medium decreases, the SI drops, while the Gd is progressively washed out from the interstitial space. This process occurs faster in tissues with a small (*S*) interstitial space than in tissues with a large (*L*) interstitial space

concentration, because it is diluted in only a very small part of the total plasma volume, namely, that volume that enters into the right side of the heart at the same time as the bolus, i.e., approximately 300 ml for a person weighing 75 kg at an injection rate of 5 ml/s (Fig. 5.1b). After the first pass, the diffusion rate immediately drops, because the concentration of the recirculating contrast medium has decreased owing to further dilution in the blood and partial accumulation in the interstitial space throughout the body (Fig. 5.1c). The length of the time interval between the end of the first pass and the equilibrium state, with equal concentrations of contrast medium in plasma and interstitial space, depends on the size of the interstitial space (Fig. 5.1c). This time interval may vary from less than 20 s in lesions with a small interstitial space to more than 3–5 min in tissues with a larger interstitial space [4, 5, 8]. After this equilibrium phase, the contrast medium is progressively washed out from the interstitial space as the arterial concentration decreases (Fig. 5.1d). Only in highly vascular lesions with a small interstitial space does early washout occur within the first minutes after bolus injection [8]. The aim of dynamic contrast-enhanced MRI is to detect and depict differences in early intravascular and interstitial distribution, as this process is influenced by pathological changes in tissues [2, 4, 5, 9–14].

5.1.2 Imaging Techniques

To study the early enhancement characteristics of a lesion with DCE-MRI, several factors have to be taken into account: type of sequence, selection and orientation of the imaging plane, number of slices, temporal resolution of the dynamic sequence, and spatial resolution of the images.

5.1.2.1 Sequence Parameters

As a rule, dynamic contrast-enhanced imaging has to be performed within the first 3 min after contrast injection: in this period of early intravascular and interstitial distribution, and large concentration gradients between these two compartments, important physiological information on tissue vascularization, perfusion, capillary permeability, and interstitial composition can be obtained. Due to the short distribution half-life of all water-soluble contrast agents and extravascular leakage of about 50 % of the contrast agent during the first pass, most of this information is not available after a few recirculations, when capillary and interstitial space concentrations reach equilibrium [1, 4–7].

In ideal circumstances, a multi-slice sequence, covering the whole lesion, with a moderate spatial resolution and high temporal resolution, should be used (e.g., 192 × 192 matrix; 2 mm in-plane resolution for each image in one multi-slice series with eight parallel slices, repeated every 1.6 s lasting for 2–3 min). Alternatively, a single-slice sequence through the most representative part of the lesion can be performed. Imaging with a high temporal resolution (e.g., for multi-slice DCE-MRI: one series of images per 3 s or less; for single-slice DCE-MRI one image per 3 s or less) is preferable in order to obtain at least three or four images or series of images during the first pass, but this is at the cost of spatial resolution and number of slices.

For single-slice DCE-MRI, fast or ultrafast MRI sequences using gradient echos such as turbo FLASH (Siemens; Erlangen, Germany), turbo field echo (TFE; Philips, Best, The Netherlands), inversion recovery (IR) prepared fast GRASS, and fast (multiplanar) spoiled GRASS [F(M)SPGR; General Electric, Milwaukee, USA] permit study of the earliest contrast enhancement kinetics with a sufficiently high temporal and satisfactory spatial resolution by rapid acquisition in the order of 1–3 s per image [34–36]. These so-called snapshot-imaging techniques are based on a gradient-echo sequence with a very short repetition and echo time (less than 10 ms). The present generation of MR units permit multi-slice snapshot dynamic studies with a temporal resolution of less than 3 s per image series and a matrix of at least 128 × 128 [2, 14, 31–33, 37, 38]. Frequently used multi-slice MRI sequences are TWIST (Siemens; Erlangen, Germany), 4D-THRIVE (Philips, Best, The Netherlands), and 3D-TRICKS [General Electric, Milwaukee, USA]

In dynamic MRI, the use of more than one average per acquisition should be avoided, as this decreases temporal resolution. Imaging with two (or more) averages per acquisition instead of one would lead to a loss of important temporal physiological information, which is now available on two (or more) images, obtained in the same time interval. Although fat saturation might be useful, e.g., by use of a selective-preparation radiofrequency pulse, in practice this is not done, as fat is adequately suppressed by most postprocessing techniques, e.g., in subtraction and first-pass images.

5.1.2.2 Selection of the Imaging Plane

The main disadvantage of the single-slice snapshot dynamic technique is that after bolus injection only one dynamic examination can be performed in the same patient (the examination cannot be repeated before all contrast is excreted from the body, i.e., at least 12 h) and that images for analysis are usually obtained at only one level [2, 41]. It is presumed that this section represents the contrast enhancement behavior of the entire lesion. Nevertheless, significant variations in enhancement have been described in different regions within musculoskeletal lesions [25]. Due to this nonuniform contrast enhancement, the single-slice technique is subject to sampling error. To minimize this inevitable sampling error, the different components of the lesion should be thoroughly evaluated on the precontrast T1- and T2-weighted images, to find an imaging plane which includes most components of the lesion. This preselection may provide a representative imaging plane in small and uniformly enhancing lesions. Nevertheless, the nonuniform contrast enhancement must be considered an important motivation for the use of multi-slice techniques that permit sampling the entire lesion [25, 41]. Inclusion of an artery in the imaging plane is useful to evaluate differences in time of onset of enhancement in various parts of the lesion, compared with the time of arrival of the bolus. Muscle tissue should be used as reference tissue for comparison with the lesion.

5.1.2.3 Imaging Procedure

In practice, one test snapshot image (single-slice DCE-MRI) or series of images (multi-slice DCE-MRI) should be obtained after preselection of a representative imaging plane. If the lesion and the regional artery are displayed well on this test image(s), the dynamic snapshot sequence can be started simultaneously with the bolus injection. During all acquisitions of the dynamic study, the transmitter and receiver gains should be held constant. Overall, the dynamic study should last for at least 3 min after bolus injection. The whole procedure lengthens the MR examination for about 5–10 min [2, 40]. To obtain high concentrations of contrast medium during the first pass, the bolus injection should be performed at an injection rate of 3–5 ml/s in the *right* antecubital vein, which is easily accessible and nearer to the heart than the left one: this causes less dilution of the bolus. To empty the contrast medium completely from the infusion line, the bolus should be followed immediately by a saline flush of about 20 ml at the same injection rate. At this rapid injection rates, no serious side effects have been observed [2, 14, 33, 38, 42]. As reproducibility is dependent on the injection rate and on the patient's cardiovascular status, use of a power injector is preferable whenever repeat examinations are considered; e.g., for monitoring the effect of chemotherapy, a dynamic study should be performed before biopsy, during chemotherapy, and just before surgery [2, 14, 38, 43–45].

5.1.3 Evaluation and Postprocessing Techniques

After performing a dynamic study, a large number of images (up to 180) have to be evaluated qualitatively and/or quantitatively. Evaluation of a series of images obtained with dynamic contrast-enhanced MRI can be performed in different ways. Each technique has its own advantages and disadvantages.

5.1.3.1 Native Review Method

A simple, fast, but subjective, qualitative method is the "native review method," in which an

observer examines contrast enhancement sequentially on all images of the dynamic sequence. This can be done by viewing all images in "cine mode" on a console or simply by printing all images on a film and reviewing them one by one on a viewing box (Fig. 5.2). With this method, detection of small areas of enhancement or of areas with discrete enhancement may be difficult. Moreover, delineation of enhancing areas from fat and hemorrhage may be very difficult (Fig. 5.3). Therefore, it is preferable that the physiological information behind the dynamic MR images is extracted by postprocessing.

5.1.3.2 Subtraction Method

A readily available qualitative method is the "subtraction method," in which the first image of the single-slice DCE sequence or the first series of images of the multi-slice DCE-MRI sequence (i.e., before contrast injection) are subtracted from all subsequent images of the dynamic study [9, 30, 37] (Fig. 5.2). In this way, all (especially discrete, early, and small) enhancing areas are easily detected, and high signals from fat and hemorrhage are nullified (Figs. 5.3 and 5.4). Subtraction images are evaluated in cine mode on a console. Using this method, it is easy to evaluate the time interval between the onset of arterial and tumoral enhancement and to detect the most "active" parts in tumors, e.g., in order to indicate the best site for biopsy or to determine the degree of response to preoperative chemotherapy qualitatively [9, 30, 37] (Fig. 5.3). However, late-enhancing tissues such as fat and connective tissue may be hardly recognizable on early subtraction images (Fig. 5.3).

5.1.3.3 Region-of-Interest Method

Another operator-dependent and more time-consuming but quantitative method is the region-of-interest (ROI) method [13, 19–21, 33]. In this method, signal intensities (SI) in one or more circular or freely determined ROIs are measured and plotted against time in a time-intensity curve (TIC; Figs. 5.4, 5.5, 5.6, and 5.7). Most often, ROIs encircling the whole lesion and the quickest-enhancing area are evaluated [13, 19–21, 33] (Fig. 5.8). An ROI positioned in a feeding artery (to see arterial input) and in a muscle (as reference tissue) should always be used to compare with the lesion. The area enhancing fastest can often be delineated easily after review of the native or subtraction images or from other postprocessing methods. Several types of TICs have been described [8, 31]. These TICs provide a graphic display of the early pharmacokinetics

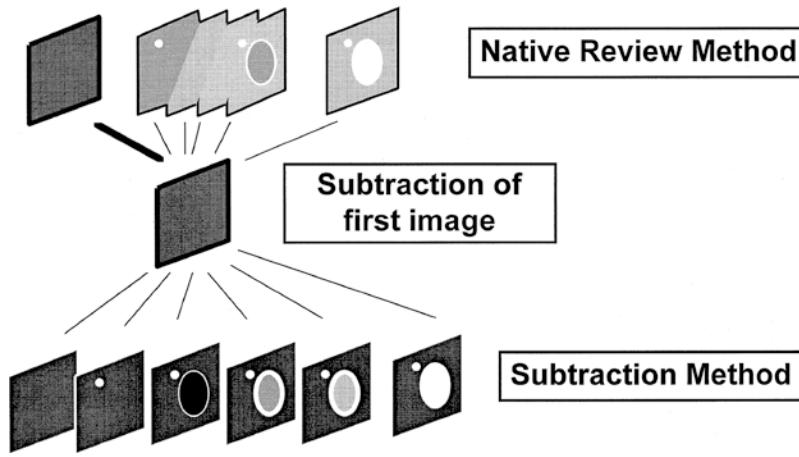

Fig. 5.2 Evaluation and postprocessing of a dynamic study with the "native review" and the "subtraction" method. In the native review method (*top*), the observer examines contrast enhancement sequentially on all images of the dynamic sequence. In the subtraction method (*bottom*), contrast enhancement is easily detected, as the first image (i.e., before bolus injection) is subtracted from all subsequent images of the dynamic study. In this way, only enhancing areas will be displayed on subtraction

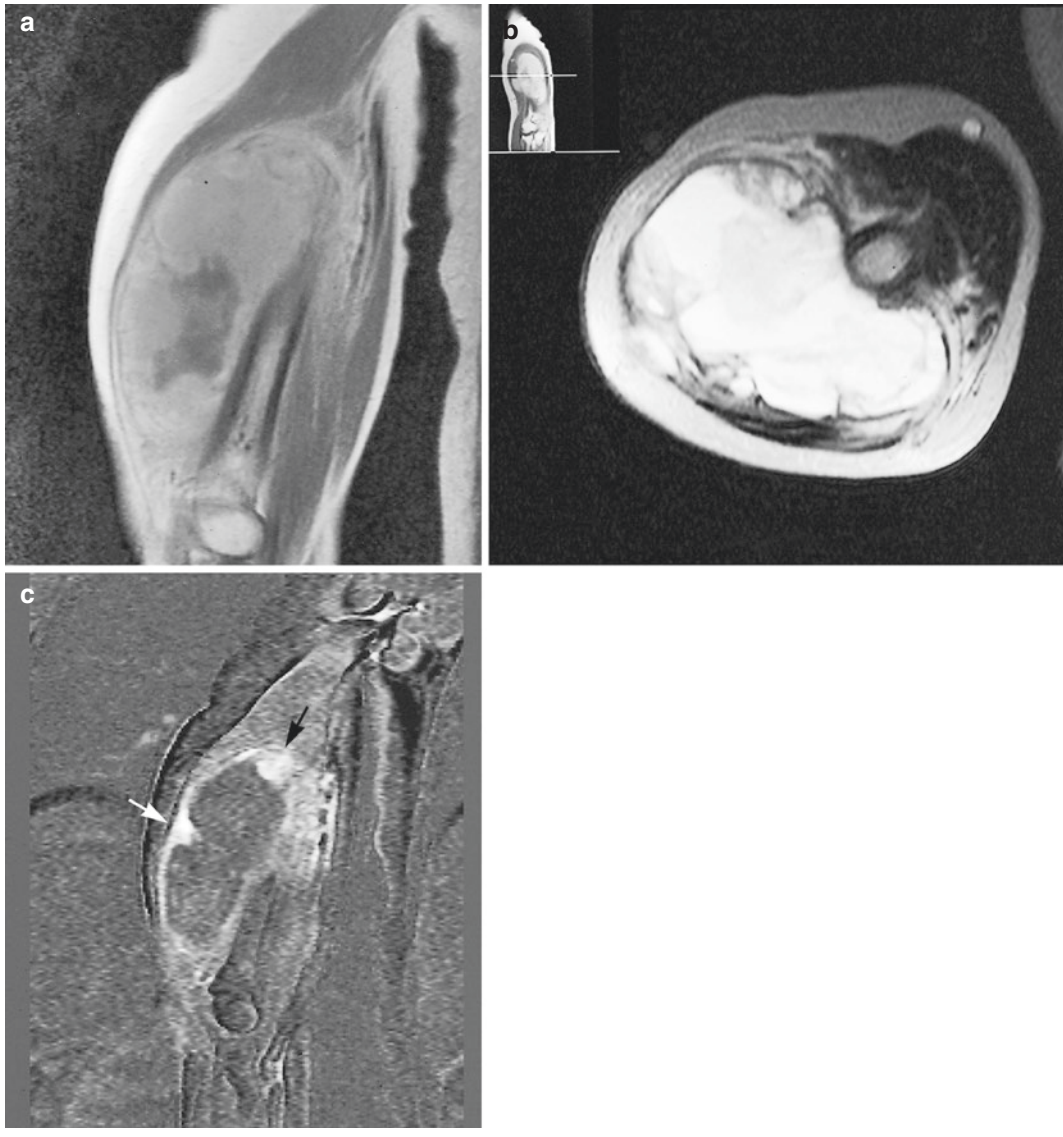

Fig. 5.3 (**a**–**c**) Indication of biopsy site on subtraction images. A 50-year-old woman with large soft tissue mass of the upper arm. Histological diagnosis of myxofibrosarcoma. (**a**) The coronal contrast-enhanced, spin-echo T1-weighted image (TR 600 ms, TE 20 ms) shows a soft tissue mass, predominantly of high signal intensity. There is an area of low signal intensity in the central part. (**b**) On the axial turbo spin-echo T2-weighted image (TR 3,873 ms, TE 150 ms), the mass has an inhomogeneous appearance and consists of areas of high and very high signal intensity. (**c**) Fast gradient-echo, dynamic contrast-enhanced subtraction image (turbo field echo; 0.5 T; TR 15 ms, TE 6.8 ms, TI 741 ms, flip angle 30°) reveals that only the periphery of the tumor shows (early) enhancement, whereas the central part lacks enhancement due to recent hemorrhage and necrosis. The solid areas at the periphery (*arrows*) should be attacked selectively to obtain a representative biopsy after enhancement of the popliteal artery (*arrowhead*), shows intense enhancement of an area (*arrow*) that proved to be recurrent tumor after resection. Onset of tumoral enhancement was already visible on the subtraction image, obtained 3 s after arrival of the bolus in the artery. Notice the improved delineation of the lesion due to the nullified surrounding fat. (**e**) Corresponding time-intensity curves of artery (*1*), muscle (*2*), and recurrent tumor (*3*). The slope of the curve representing tumor parallels the arterial curve, indicating very high vascularization, perfusion, and capillary permeability. The early plateau phase is indicative of a small interstitial space in the tumor

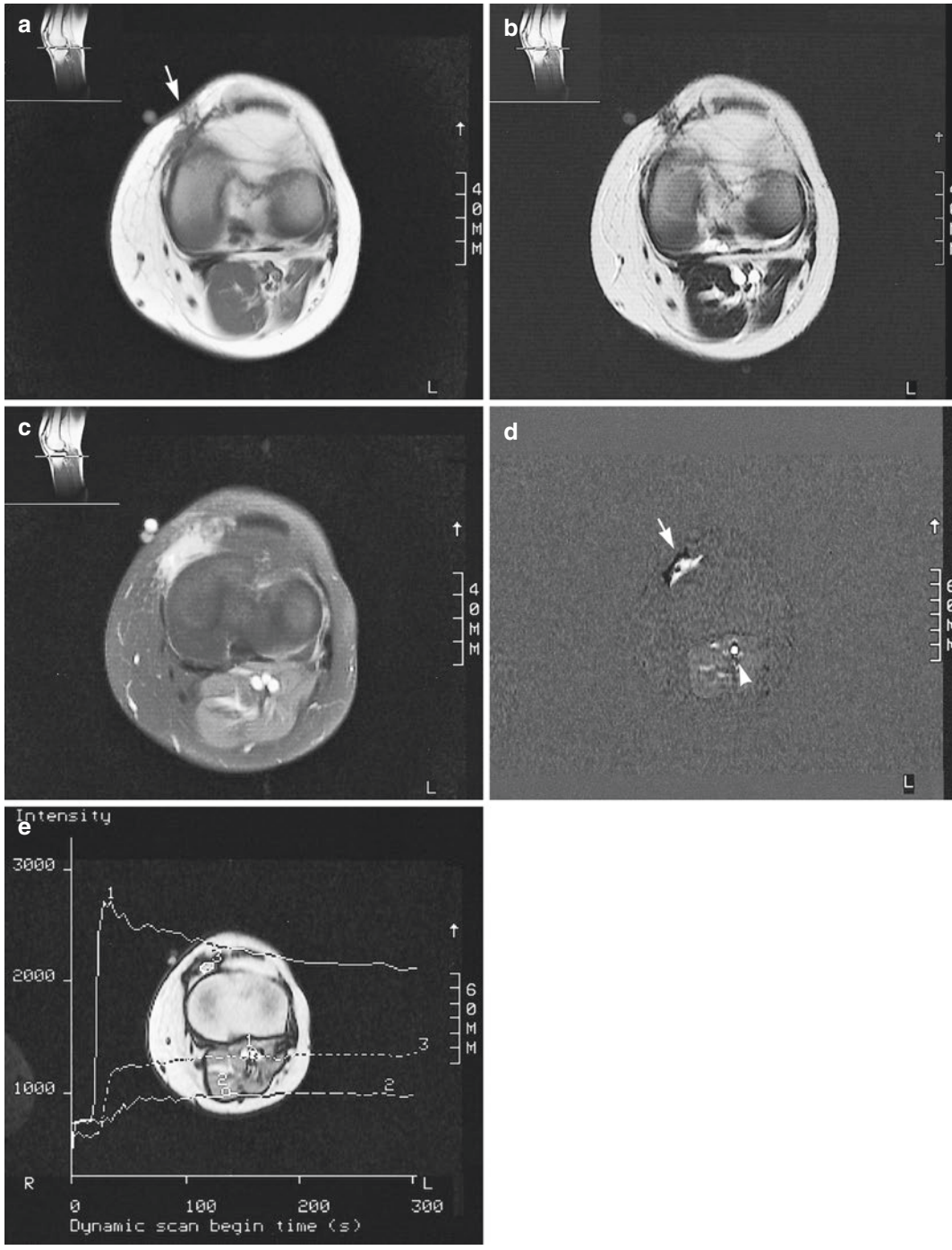

Fig. 5.4 (**a**–**e**) Detection of recurrent tumor. A 40-year-old woman with recurrence of a previously surgically treated synovial sarcoma around the knee. (**a**) Axial spin-echo T1-weighted image (TR 600 ms, TE 20 ms) at the level of the patella reveals a subcutaneous area of low signal intensity (*arrow*) abutting the femoral cortical bone. Differentiation of recurrent tumor tissue from granulation tissue is not possible. (**b**) Axial turbo spin-echo T2-weighted image (TR 4,587 ms, TE 150 ms) at the same level shows low signal intensity, which makes the possibility of local recurrence less likely. (**c**) Static contrast-enhanced, spin-echo T1-weighted image with fat-selective presaturation shows inhomogeneous enhancement of this area. It is not possible to discriminate between postoperative changes and recurrent tumor. (**d**) Subtracted, dynamic contrast-enhanced, gradient-echo image (turbo field echo; 0.5 T; TR 15 ms, TE 6.8 ms, TI 741 ms, flip angle 30°) at the same level, obtained 11 s

of the contrast agent during and immediately after the first pass (Figs. 5.1, 5.5, and 5.8). From these curves, quantitative information can be obtained: time of onset of enhancement (T_{start}), slope (enhancement rate during the first pass, FP), maximum enhancement (E_{max}), time to peak or maximum enhancement, and eventually negative slope (i.e., washout rate; Figs. 5.5 and 5.8). The time of onset of enhancement in a lesion (T_{start}) can be measured relative to arterial enhancement. The difference in time between local arterial enhancement and tissue enhancement is mainly determined by tissue perfusion and thus indirectly by the local capillary

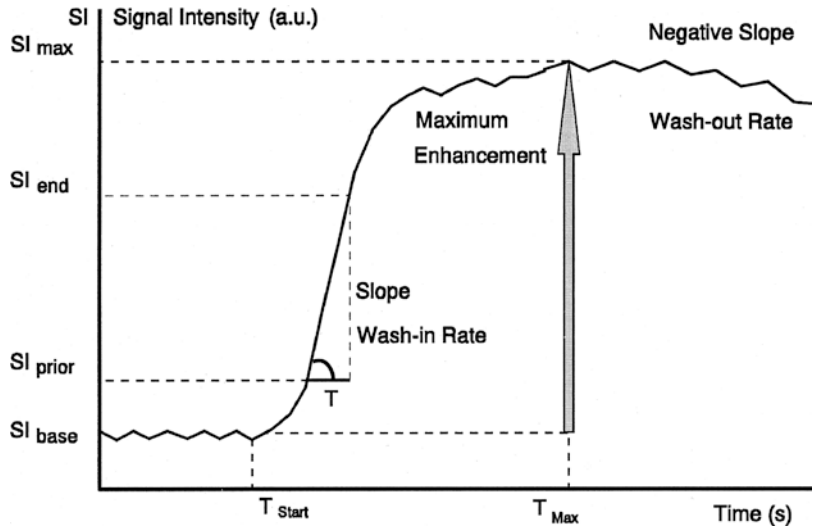

Fig. 5.5 Time-intensity curve (TIC). In a TIC, the temporal change of the signal intensity in a region of interest (ROI; or pixel) is plotted against time. At T_{start}, when the bolus enters the ROI, the signal intensity rises above the baseline signal intensity (SI_{base}). The steepest slope represents the highest enhancement rate during the first pass (wash-in rate) and is mainly determined by tissue vascularization, perfusion, and capillary permeability. At T_{max}, the time of maximum enhancement, capillary and interstitial concentrations reach equilibrium. The time period between the end of the first pass and the maximum enhancement is mainly determined by the volume of the interstitial space. The washout rate can be calculated from the negative slope of the curve. (*a.u.* arbitrary units, *T* time interval between SI_{end} and SI_{prior})

Fig. 5.6 (**a**–**h**) Fig. 5.6 g, h. Differentiation of capillary (high-flow) from cavernous (slow-flow) hemangioma with dynamic MRI. (**a**) On the T2-weighted spin-echo image of the right lower leg in a 10-year-old girl, the hemangioma is visible as a high signal intensity mass against the fibula (*arrow*). (**b**) The T2-weighted image of the left thigh in a 14-year-old boy shows a soft tissue lesion with a high signal intensity, corresponding to a large hemangioma (*arrows*). The spin-echo images do not allow differentiation of highly and slowly perfused hemangiomas. (**c**, **d**) On the TIC, the capillary hemangioma (**c**) has a high first-pass enhancement, indicating high perfusion, whereas the cavernous hemangioma (**d**) has a slow perfusion. (**e**) On the first-pass image (turbo FLASH; 1.5 T; TR 9 ms, TE 4 ms, TI 200 ms, flip angle 8°), the capillary hemangioma (*arrow*) appears as bright as the major arteries (*arrowheads*) due to high perfusion. (**f**) The cavernous hemangioma appears dark on the first-pass image due to slow perfusion (*arrowheads*). (**g**) A photomicrograph of the capillary hemangioma shows numerous capillaries in the highly perfused hemangioma (factor VIII stain, specific for endothelial cells). (**h**) A photomicrograph of the cavernous hemangioma shows numerous red blood cells in the large lumina of the cavernous vessels, indicative of slow perfusion (H&E)

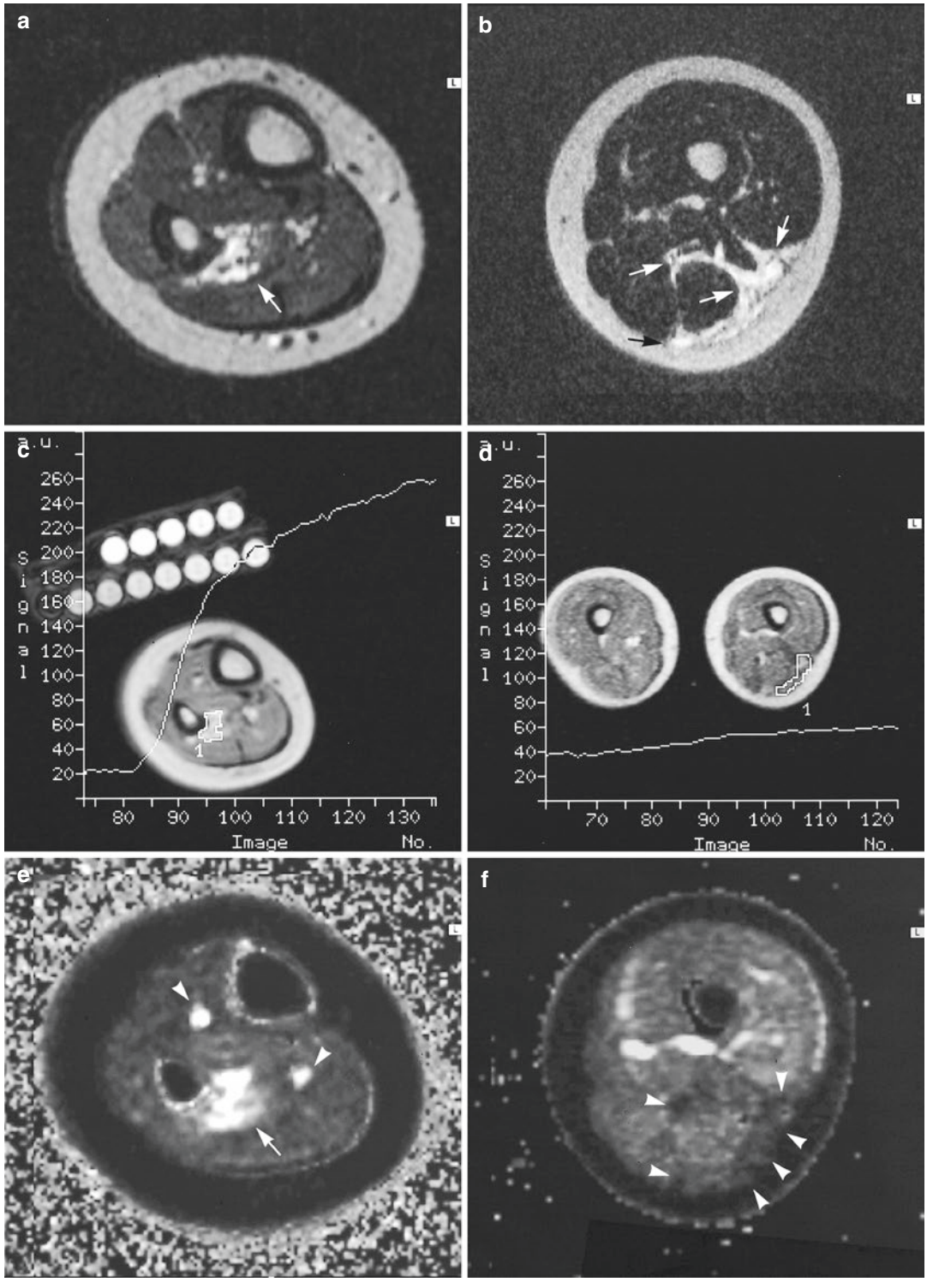
a
b
c
a.u.
260
240
220
200
180
160
140
120
100
80
60
40
20
Signal
80 90 100 110 120 130
Image No.
1
d
a.u.
280
240
220
200
180
160
140
120
100
80
60
40
20
Signal
70 80 90 100 110 120
Image No.
1
e
f

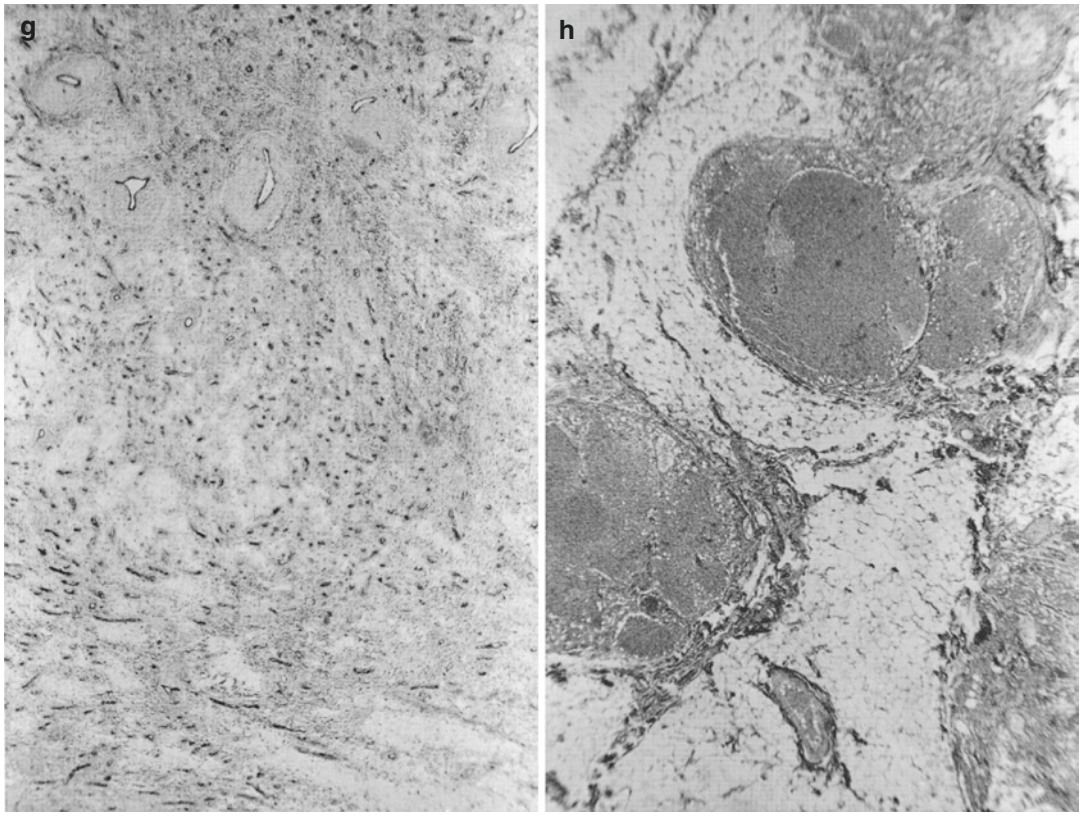

Fig. 5.6 (Continued)

resistance [33, 46]. The slope represents the maximum enhancement rate during the first pass and is mainly determined by tissue vascularization (i.e., number of vessels) and perfusion [2, 8]. However, capillary permeability may also play an important role [47]. During the first pass, approximately 50 % of the contrast agent (or even more in pathological tissues) enters the interstitial space [1, 4–7]. After the first pass, the concentration gradient and diffusion rate of the contrast agent drop immediately. The change in signal intensity is now mainly determined by the capillary permeability and the composition of the interstitial space (Fig. 5.1c). In tissues with a small interstitial space, a rapid equilibrium and even a washout of contrast will occur, whereas in tissues with a larger interstitial space, a further wash-in will still be going on (Fig. 5.1d) [8].

The main advantage of the ROI method is that quantitative data are available and that the early

Fig. 5.7 (**a**–**f**) Tissue characterization with dynamic MRI. T2-weighted image (**a**, **c**, **e**) and TIC (**b**, **d**, **f**) in a 23-year-old woman with chronic osteomyelitis and a soft tissue abscess in the left thigh (**a**, **b**), in a 23-year-old woman with posttraumatic myonecrosis of the left deltoid muscle (**c**, **d**), and in a 77-year-old man with a myxofibrosarcoma of the left quadriceps muscle (**e**, **f**). Dynamic MRI does not allow differentiation of benign and malignant lesions, as some highly vascularized and perfused benign lesions [such as granulation tissue at the periphery of an abscess (**b**) or of posttraumatic myonecrosis (**d**)] have slope values in the same range as malignant tumors, such as undifferentiated pleomorphic sarcoma (formerly known as malignant fibrous histiocytoma) (**f**). All three lesions show an early and fast enhancement at the periphery, where the most "active" part of the lesion is located

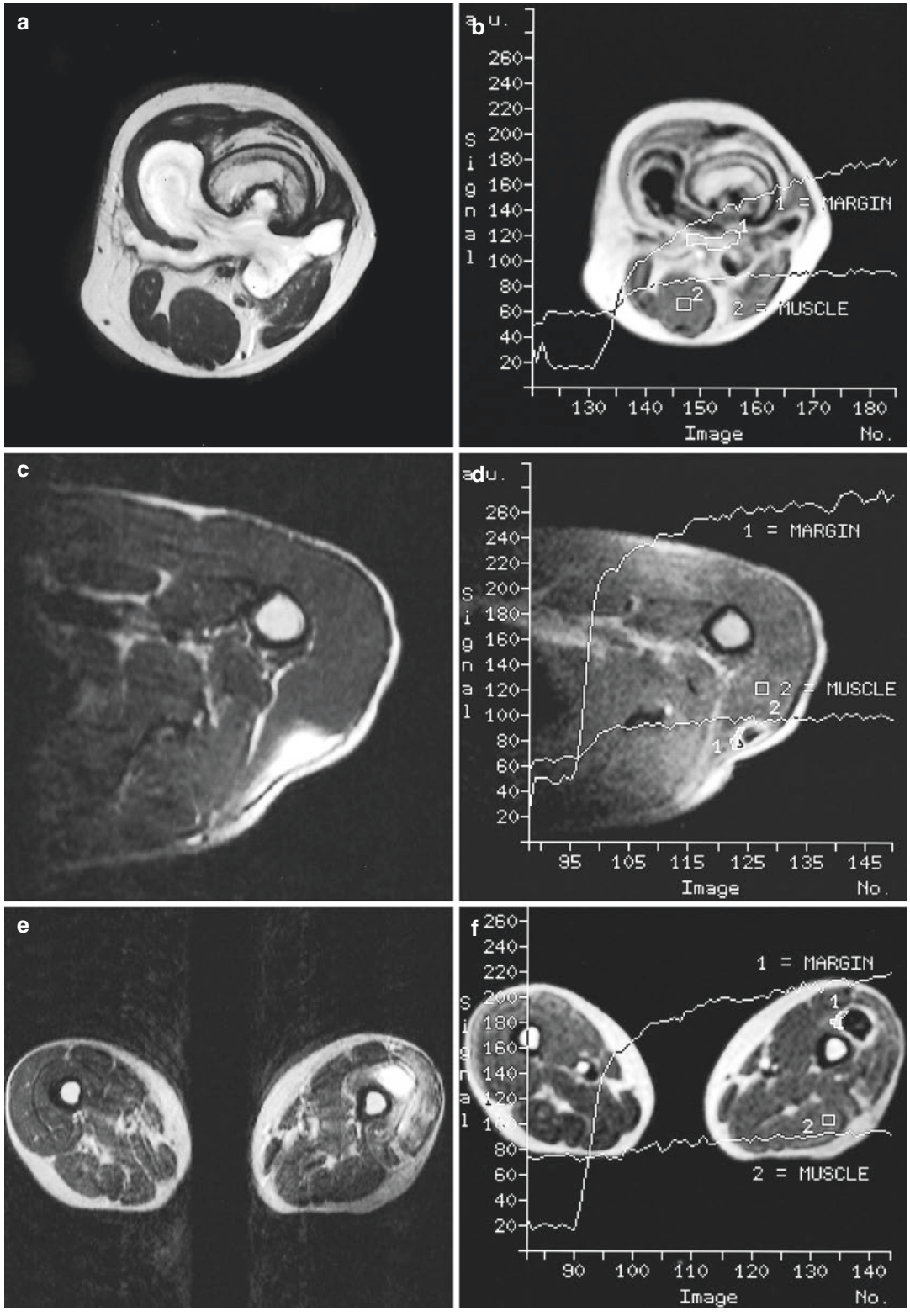
a
b
a.u.
Signal
1 = MARGIN
2 = MUSCLE
Image No.
c
d
e
f

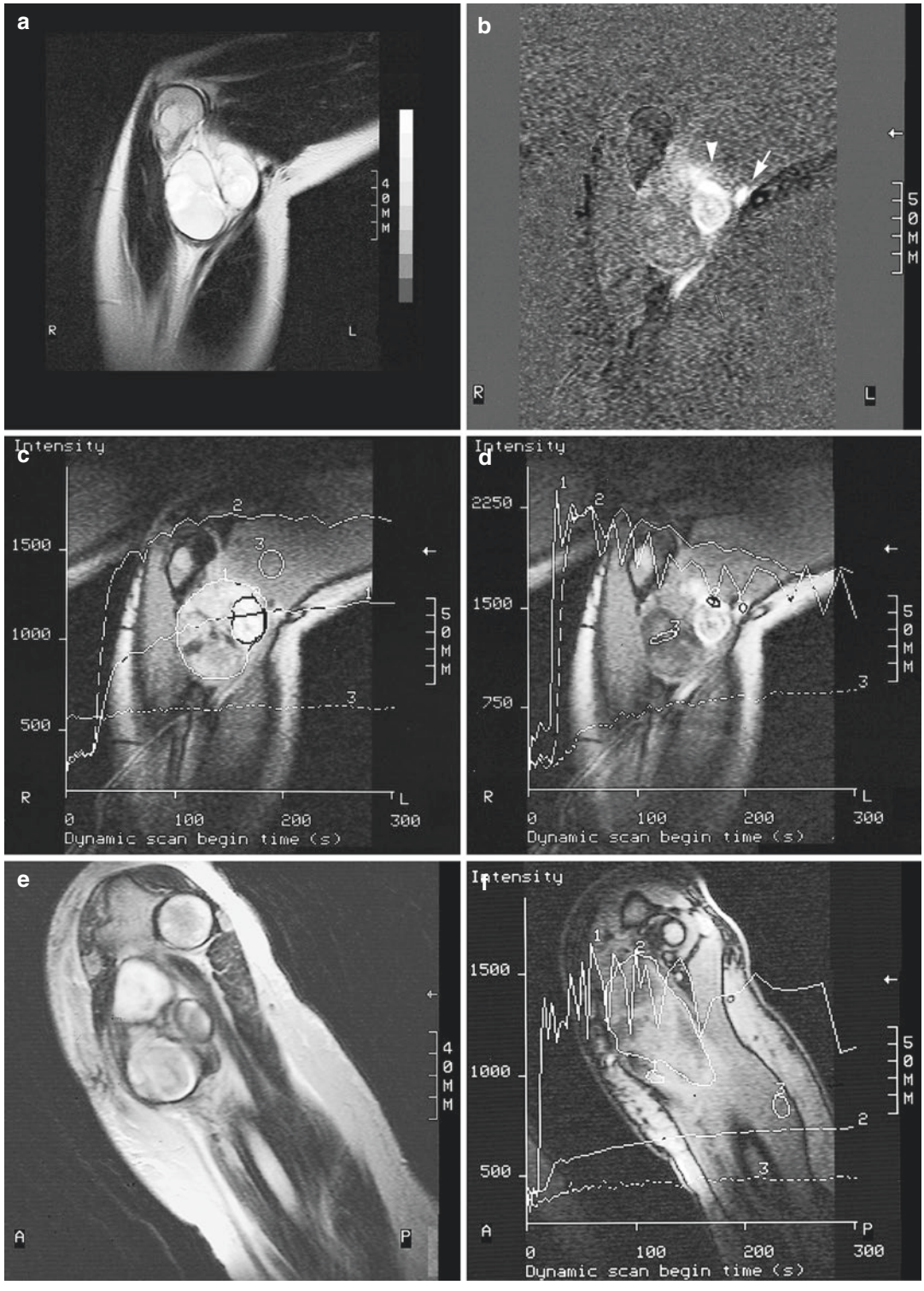
a
R
L
40MM
b
R
L
50MM
c
Intensity
1500
1000
500
R
L
0
100
200
300
Dynamic scan begin time (s)
50MM
d
Intensity
2250
1500
750
R
L
0
100
200
300
Dynamic scan begin time (s)
50MM
e
A
P
40MM
f
Intensity
1500
1000
500
A
P
0
100
200
300
Dynamic scan begin time (s)
50MM

pharmacokinetics of the contrast agent in the lesion are visually displayed in a TIC (Figs. 5.1, 5.5, 5.6, 5.7, and 5.8). The ROI method has, however, some disadvantages: it is operator dependent, and only the selected regions are studied. Moreover, it is a time-consuming procedure, especially when several areas have to be investigated (Fig. 5.8). To overcome the main disadvantages of the ROI method, several groups of investigators have tried to develop fast, operator-independent postprocessing techniques that evaluate the physiological information on a pixel-by-pixel basis [2, 14, 16, 31, 48].

5.1.3.4 First-Pass Images

Another, rapid, largely operator-independent postprocessing technique that creates "first-pass images" focuses on the maximum enhancement rate during the first pass of the contrast agent, by calculating the first-pass slope value on a pixel-by-pixel basis, according to the equation (Fig. 5.9) [2, 14, 32, 33]:

$$\text{steepest slope} = \frac{\left(SI_{end} - SI_{prior}\right)}{\left(SI_{baseline} \times t\right)\left(\text{Eq.1}\right)} \times 100\left(\%/s\right)$$

In this equation, $SI_{baseline}$ represents the mean signal intensity in a pixel before arrival of the bolus; t is the time interval between the acquisition of two consecutive images with the largest change in signal intensity in a pixel (i.e., from SI_{prior} to SI_{end}) and corresponds to the temporal resolution of the dynamic sequence. By displaying the steepest slope value of all pixels with a grayscale value identical to the fastest enhancement rate, this method simultaneously provides quantitative and qualitative information in a new parametric image, the first-pass image (Figs. 5.6 and 5.10). In this way, the operator-dependent selection of different ROIs with the subsequent time-consuming calculation of the slope value from the TIC can be avoided. It was shown by radiological–pathological and angiographic correlation that these images depict tissue (micro) vascularization and perfusion very well [2]. However, a visual display of the early pharmacokinetics of the contrast agent, as observed on a TIC, obtained with the ROI method, is not available with this method (Fig. 5.6).

A variant of this postprocessing method, "spatial mapping of instantaneous enhancement rates," applies an exponential-fitting algorithm

Fig. 5.8 (**a**–**f**) Monitoring chemotherapy with dynamic MRI. A 51-year-old man with inflammatory myxofibrosarcoma of the soft tissues in the cubital fossa before (**a**–**d**) and after (**e**, **f**) isolated perfusion with tumor necrosis factor-alpha. Histological response was good. (**a**) Sagittal turbo spin-echo T2-weighted image (TR 3,873 ms, TE 150 ms) before treatment shows a lobulated mass with a predominantly high signal intensity. (**b**) Fast, dynamic gradient-echo, gadolinium–diethyltriamine pentaacetic acid (DTPA)-enhanced subtraction image (turbo field echo; 0.5 T; TR 15 ms, TE 6.8 ms, TI 741 ms, flip angle 30°) acquired 3 s after arrival of the bolus of contrast medium in the artery (*arrow*). Early peripheral enhancement of the tumor is clearly shown (*arrowhead*). (**c**) TIC of the whole tumor (*1*), a fast-enhancing nodule within the tumor (*2*), and the brachial muscle (*3*). (**d**) TIC of the brachial artery (*1*), a peripheral, very fast, and early-enhancing tumor nodule, with early washout (*2*), and a central, more slowly enhancing area within the tumor (*3*). Note that the curve of the peripheral tumor nodule (*2*) parallels the arterial curve (*1*), indicating a very high vascularization, perfusion, and capillary permeability. (**e**) After therapy, there is an inhomogeneous residual mass with high signal intensity areas on the turbo spin-echo T2-weighted images. The degree of response to chemotherapy cannot be assessed on spin-echo images. (**f**) The dynamic contrast-enhanced gradient-echo images show delayed onset of enhancement of the tumor relative to the artery and to the first examination. No focal areas of early enhancement consistent with viable tumor can be seen. The corresponding TICs now show gradual enhancement of the whole tumor (*2*) relative to the artery (*1*), with absence of an early plateau phase or early washout, indicating decreased vascularization, perfusion, and capillary permeability. Histological response to chemotherapy was good

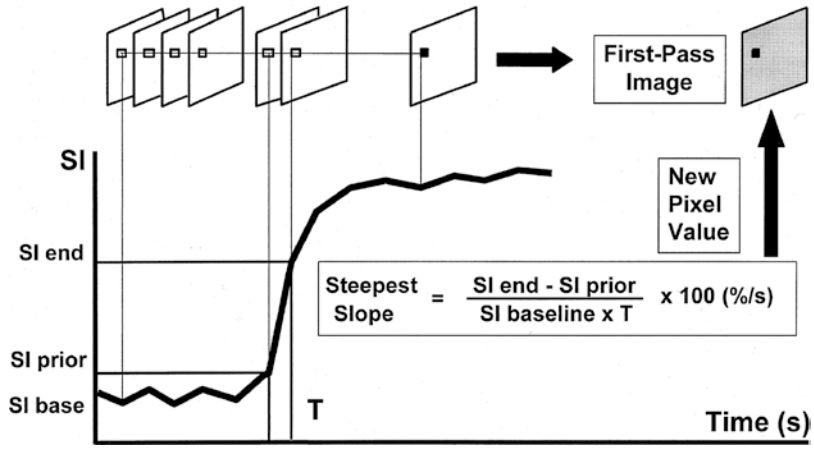

Fig. 5.9 First-pass images: postprocessing procedure. For each pixel of the dynamic image, the steepest slope of the TIC is calculated. This value represents the highest enhancement rate during the first pass. Subsequently, a single new image with the same matrix can be composed. The value of each pixel in this image is equal to the spatially corresponding first-pass slope value. This parametric image is therefore called the first-pass image [64, 65, 67]

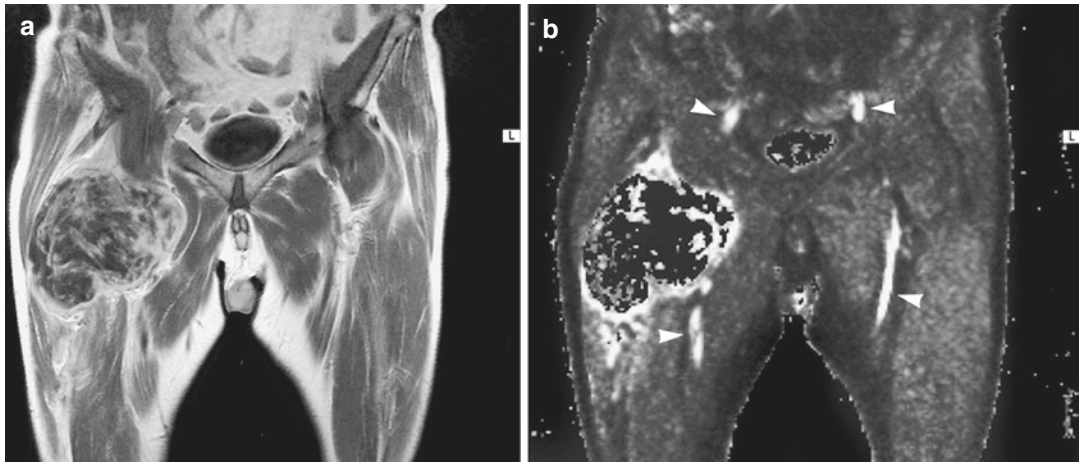

Fig. 5.10 (**a**, **b**) Monitoring chemotherapy with first-pass images. (**a**) The coronal contrast-enhanced T1-weighted image shows inhomogeneous enhancement in a large myxofibrosarcoma after two cycles of chemotherapy. The degree of response cannot be assessed on the spin-echo images. (**b**) The first-pass image (turbo FLASH; 1.5 T; TR 9 ms, TE 4 ms, T1 200 ms, flip angle 8°) shows high first-pass enhancement rates in the arteries (*arrowheads*) and at the periphery of the tumor. Histologically, these fast-enhancing areas corresponded to residual viable tumor

on a pixel-by-pixel basis to allow derivation of the initial slope of the TIC, in order to create parametric "slope images" [49]. Nowadays, many software packages create other parametric images in gray or color scale, displaying on a pixel-by-pixel base the physiologic information available from the TIC, such as the initial and delayed rate of contrast agent accumulation, the maximum enhancement, and the initial area under the contrast agent concentration–time curve (IAUC), which integrates the concentration of contrast agent observed in the tissue of interest over time [48, 72]. When normalized to surrounding normal tissue, IAUC has been demonstrated to parallel parameters of vessel permeability obtained using more complex mathematical modeling. One disadvantage of using IAUC is that the parameter represents a conglomerate

of physiologic processes, including blood flow, blood volume, endothelial permeability, and the volume of the extravascular–extracellular space (EES). As a result, modeled parameters have the capacity to provide more physiologically meaningful information.

5.1.3.5 Pharmacokinetic Modeling Techniques

Quantitative approaches have the ability to produce measurements that reflect the physiologic and anatomic structure of the tumor microvasculature, blood flow, blood volume, endothelial permeability, and the volume of the extravascular–extracellular space. This is of great value for improving the characterization of tumors before treatment and for detecting the effects of new therapies on tumor vascular function. Quantitative approaches also offer the potential for development of more precise and reproducible measures, independent of scanner acquisition and tissue type. Such measures might then be used to guide treatment in individual patients or as surrogate markers of therapeutic efficacy in multicenter drug trials.

Quantitative assessment of the dynamic contrast enhancement can be performed with modeling techniques, which are usually based on a two-compartmental pharmacokinetic model with plasma space and extravascular–extracellular space (EES) [70–74]. After performing a baseline T1 mapping and acquisition of the DCE MR perfusion images, signal intensity data are converted to gadolinium concentration. Then the vascular input function is determined and the pharmacokinetic modeling can be done. With pharmacokinetic modeling of DCE MR perfusion data, several metrics are commonly derived: the transfer constant (k^{trans}), the fractional volume of the extravascular–extracellular space (v_e), the rate constant (k^{ep}, where $k^{ep} = k^{trans}/v_e$), and the fractional volume of the plasma space (vp) [72, 73].

The most frequently used metric in DCE MR perfusion is k^{trans}, which describes the transendothelial transport of low-molecular-weight contrast media in tissues: blood perfusion, transport of contrast agent across vessel walls (depending on capillary permeability), and diffusion of contrast medium in the interstitial space. It can have different interpretations depending on blood flow and permeability. When there is very high permeability (e.g., in synovial sarcoma), the flux of gadolinium-based contrast agent is limited only by flow, and thus k^{trans} mainly reflects blood flow. In situations in which there is very low permeability (e.g., in fibrotic scar tissue and muscle), the gadolinium-based contrast agent cannot leak easily into the extravascular–extracellular space, and thus k^{trans} mainly reflects permeability [74]. However, in many tissues and tumors, both blood flow and capillary permeability determine the value of k^{trans}.

After transport across the vessel wall, the contrast medium also begins to diffuse into tissue compartments further removed from the vasculature, including areas of necrosis and fibrosis. Over a period typically lasting several minutes to hours, the contrast agent diffuses back into the vasculature (described by the rate constant kep) from which it is excreted by the kidneys. When capillary permeability is very high and the EES is small (e.g., in high-grade malignant soft tissue tumors with high cell density and small interstitial space), the return of contrast medium is typically quick, resulting in fast washout, even within the first 2 min. Contrast medium elimination from very slow exchange tissues, such as fibrosis or necrosis, occurs slowly, explaining the persistent delayed enhancement characteristic of some tumors [72].

5.1.3.6 Practical Guidelines

In practice, review of the native images, or preferentially of subtracted images, in cine mode, quickly provides information on the vascularization and perfusion of the lesion (e.g., to help characterize a lesion, to indicate the best site for biopsy, or to detect residual nests of viable tumor; Figs. 5.3, 5.4, 5.11, 5.12, and 5.13). TICs can be obtained by delineating the whole lesion, the fastest-enhancing area, a feeding artery, and a reference tissue (e.g., muscle; Figs. 5.4, 5.6, 5.7, and 5.13). These curves provide graphic information on perfusion, the wash-in rate, and eventually the washout rate. They can be used to calculate the steepest slope and to monitor chemotherapy. First-pass images and other pixel-by-pixel post-processing techniques such as subtraction can be

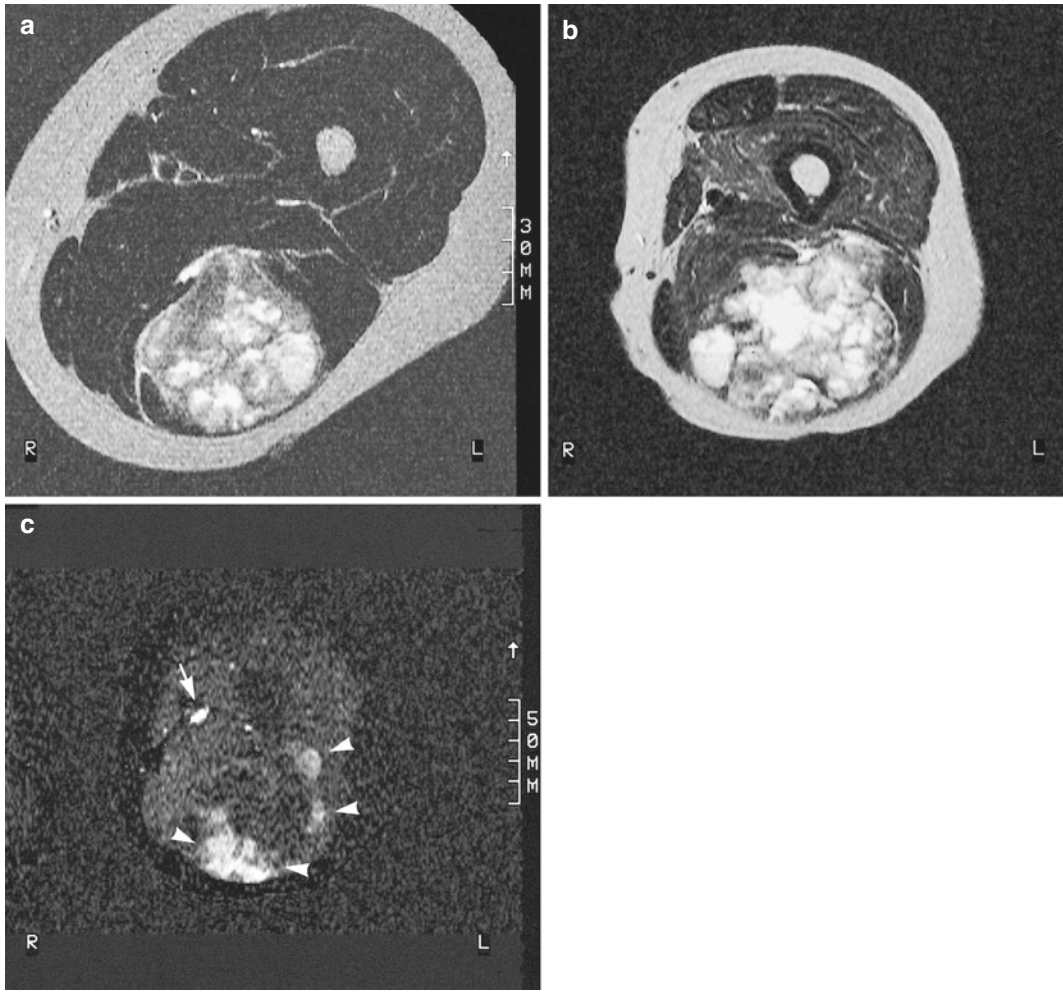

Fig. 5.11 (**a**–**c**) Monitoring chemotherapy with dynamic MRI. A 23-year-old woman with soft tissue metastasis of an osteosarcoma in the thigh before (**a**) and after (**b**, **c**) treatment with isolated limb perfusion with tumor necrosis factor-alpha. Histological response to chemotherapy was poor. (**a**) Axial turbo spin-echo T2-weighted image (TR 4,598 ms, TE 150 ms) shows inhomogeneous mass with areas of intermediate and high signal intensity. (**b**) Axial turbo spin-echo T2-weighted image (TR 4,590 ms, TE 150 ms) after therapy displays a large heterogeneous mass, mainly composed of high signal intensity areas with fluid levels compatible with hemorrhage and/or necrosis. However, the degree of response cannot be assessed on the spin-echo images. (**c**) Early dynamic gadolinium-enhanced, gradient-echo subtraction image (turbo field echo; 0.5 T; TR 15 ms, TE 6.8 ms, TI 741 ms, flip angle 30°) shows rapidly progressive enhancing areas (*arrowheads*) at the periphery of the mass, starting within 3 s after arterial enhancement (*arrow*). These early-enhancing foci corresponded to areas of highly cellular, residual viable tumor. The central part of the tumor lacked enhancement, corresponding to necrosis

performed to evaluate all physiological information in one or only a few images (Figs. 5.4, 5.6, 5.10, 5.11, 5.12, and 5.13).

After pharmacokinetic modeling, measuring the concentration–time data may be performed for an ROI, for a VOI (ROIs from several slices covering the whole tumor), or for each voxel in the image (requiring good SNR). The ROI or VOI approach can make model fitting more robust, at the expense of lost detail in heterogeneous tumors. Analysis will usually be performed on data from the whole tumor or from a representative subset of the tumor volume. Global tumor parameters may be a fit of the average signal from an ROI/VOI or ideally a median or mean of the result of all fitted voxels [75].

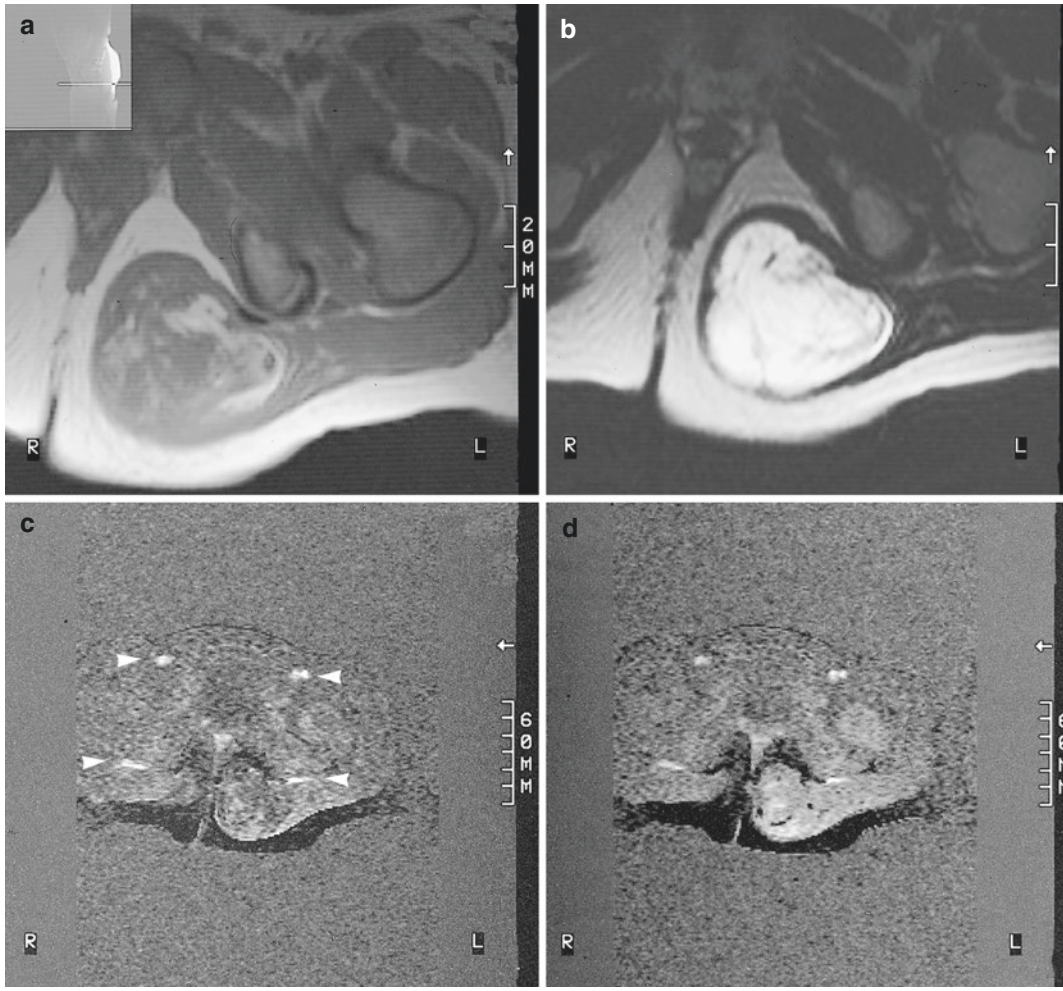

Fig. 5.12 (**a**–**d**) Tissue characterization with dynamic MRI. A 5-year-old boy with painful swelling of the buttocks. (**a**) The axial spin-echo T1-weighted image shows a poorly defined mass in the left gluteus maximus muscle. The tumor is heterogeneous, with both ill-defined areas of intermediate signal intensity and areas of high signal intensity corresponding to fat. (**b**) On the turbo spin-echo T2-weighted image, the mass is well defined and predominantly of very high signal intensity, with some serpentine areas of intermediate signal intensity corresponding to fatty tissue. (**c**) Early dynamic, gadolinium-enhanced gradient-echo subtraction image (turbo field echo; 0.5 T; TR 15 ms, TE 6.8 ms, TI 741 ms, flip angle 30°), acquired 3 s after enhancement of the arteries (*arrowheads*), shows no enhancement in the tumor. (**d**) Late dynamic, gadolinium-enhanced gradient-echo subtraction image, acquired 112 s after arterial enhancement, shows only discrete enhancement in the tumor. The late and low enhancement makes the diagnosis of a high-grade soft tissue sarcoma (e.g., liposarcoma or rhabdomyosarcoma) less likely. Biopsy and subsequent tumor resection in this patient revealed a (benign) lipoblastoma

5.1.4 Clinical Applications

Dynamic contrast-enhanced MRI has been used as an additional imaging technique in various clinical applications, such as differentiation of benign from malignant lesions, tissue characterization by narrowing down the differential diagnosis, identification of areas of viable tumor before biopsy, differentiation of tumor from perineoplastic edema (which enhances later and less than tumor), early detection of avascular necrosis and inflammatory sacroiliitis, and evaluation of rheumatoid arthritis and carpal tunnel syndrome [2, 11, 12, 14, 15, 18, 19, 23, 24, 25, 26, 27, 28, 33, 40, 49]. In all these applications, this technique provides global information on tissue vascularization, perfusion,

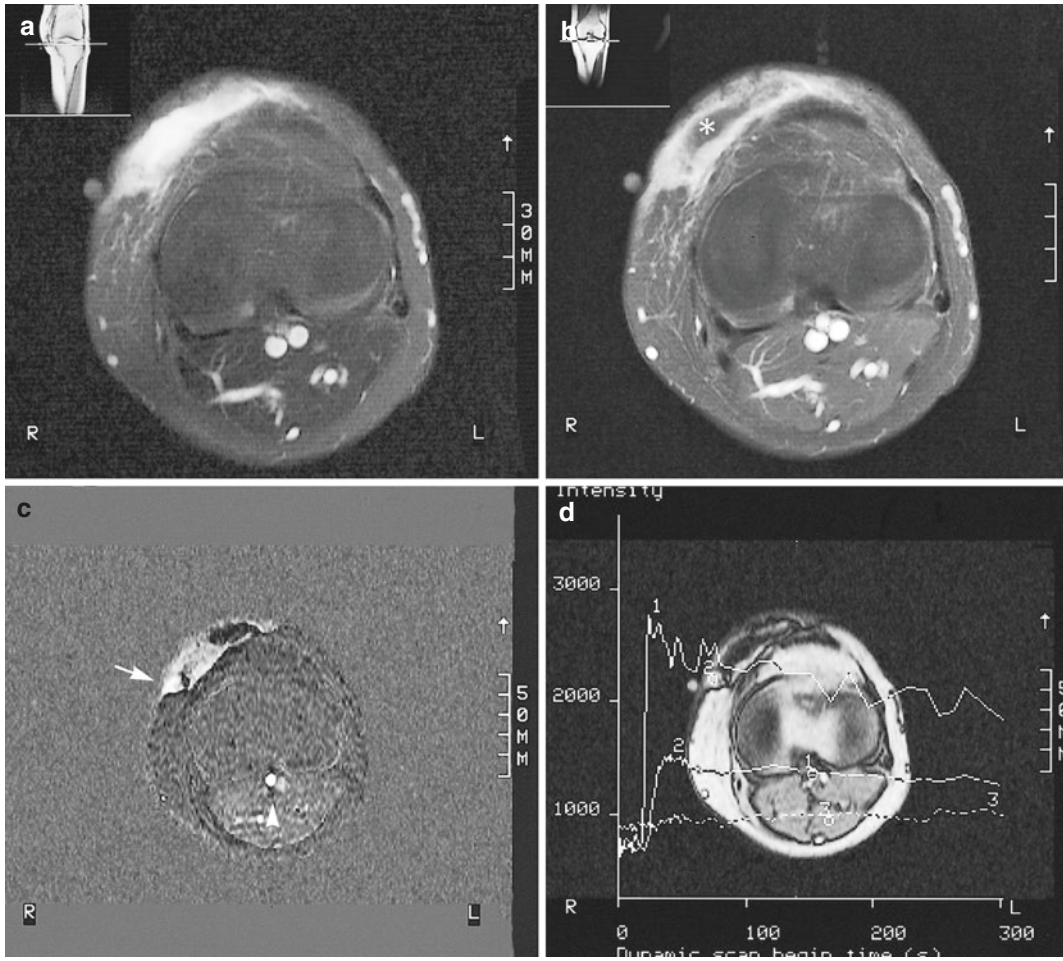

Fig. 5.13 (**a**–**d**) Detection of residual tumor with dynamic MRI. A 58-year-old woman referred for an MRI examination after marginal resection of what was originally thought to be a lipoma but proved to be a myxofibrosarcoma. (**a**) Axial fat-saturated, turbo spin-echo T2-weighted image (1,901 ms/100 ms) at the level of the scar, which is marked with a vitamin A pearl. There is a nonspecific area of high signal intensity within the subcutaneous tissue; differentiation of residual tumor tissue and granulation tissue is not possible. (**b**) Static T1-weighted, contrast-enhanced image with fat-selective presaturation displays nonspecific enhancement of the scar region: differentiation of residual tumor tissue and granulation tissue is not possible. The nonenhancing area (*asterisk*) represents a postoperative fluid collection (seroma). (**c**) Subtracted dynamic contrast-enhanced gradient-echo image (turbo field echo; 0.5 T; TR 15 ms, TE 6.8 ms, TI 741 ms, flip angle 30°) at the same level, obtained 30 s after bolus injection. There is a small, nodular area of very high signal intensity (*arrow*) abutting the seroma cavity. Enhancement started 6 s after arrival of the bolus in the artery (*arrowhead*). The early and intense enhancements are more suggestive of residual tumor tissue than postoperative granulation tissue. (**d**) The TIC of this small nodular area (*2*) parallels the arterial curve, (*1*) and an early plateau phase is seen, followed by a gradual washout. Histology of the biopsy revealed residual myxofibrosarcoma

capillary permeability, and composition of the interstitial space. The most important applications in the musculoskeletal system, however, are identification of viable areas in a tumor before biopsy, monitoring of chemotherapy, and detection of residual or recurrent tumor tissue after therapy [9, 10, 16, 17, 20–22, 29, 30, 48, 50].

5.1.4.1 Monitoring Chemotherapy

The most important application of dynamic MRI in the musculoskeletal system is evaluation of response to preoperative chemotherapy in bone tumors and soft tissue tumors, because plain radiography, CT, and static MRI are not reliable means of solving this problem [51]. The aim of

monitoring is to predict the percentage of tumor necrosis in order to differentiate responders from nonresponders. Moreover, response to initial chemotherapy is one of the most reliable predictors of outcome [52–56]. Assessment of the effect of preoperative chemotherapy is important, because a poor response may affect the feasibility of future conservative surgery and change the postoperative (adjuvant) chemotherapy [54, 56, 57]. In contrast, a good responsive tumor that was considered inoperable at the time of first presentation can conceivably become operable [58]. Optimal follow-up of patients with malignant soft tissue tumors requires three DCE-MRI studies, i.e., before biopsy, during chemotherapy, and, at the end of chemotherapy, immediately before surgery [39].

Many studies have assessed the value of dynamic MRI in monitoring the response to preoperative chemotherapy in osteosarcoma, Ewing sarcoma, rhabdomyosarcoma, and synovial sarcoma [2, 9, 10, 14, 16, 17, 20, 21, 38, 41, 50, 59, 60]. The promising results, with accuracy levels to distinguish responders from nonresponders of 85.7–100 %, can largely be explained by the possibility of dynamic MRI to depict tissue vascularization. Other successful methods, such as angiography, color Doppler flow imaging, and blood-pool scintigraphy with technetium-99 m diphosphonate (99mTc-labeled MDP), are also based on the demonstration of a significant decrease in tumor vascularization and perfusion in responders [46, 61–64].

In dynamic MRI, the ROI method allows creation of TICs from regions encircling the whole tumor [2, 14, 20, 21]. An increase in slope value during follow-up indicates poor response, whereas a decrease in type of curve and slope not always indicates good response, because small nests of residual tumor tissue may be missed. To detect these areas, smaller areas of interest should be investigated, e.g., by MR mapping [10, 41]. This is very time-consuming, and therefore computerized, pixel-by-pixel postprocessing techniques are preferable.

The most easy, qualitative postprocessing method to evaluate dynamic contrast-enhanced images is subtraction MR [9, 38] (Figs. 5.6, 5.8, and 5.11). Subtraction images display areas with remaining viable tumor cells as high signal intensity nodules and allow a good differentiation between viable tumor and inflammation (Figs. 5.8 and 5.11).

In first-pass images, all structures are displayed with a gray or color scale equal to the highest enhancement rate (i.e., during the first pass; Figs. 5.9 and 5.10) [2, 32]. In this way, quantitative evaluation of the effect of chemotherapy is possible by measuring the first-pass enhancement rate of the whole tumor (i.e., the mean value of all pixels in the tumor) in consecutive examinations during preoperative chemotherapy. Direct visual inspection (qualitative evaluation) of these images, and also of the parametric color images derived from the pharmacokinetic modeling (displaying k^{trans}, v_e, k^{ep}, and vp), allows easy detection of highly vascular and/or highly perfused viable tumor tissue. This is useful for the qualitative assessment of tumor response (Fig. 5.10). Whenever areas with a bright appearance are detected, poor response, with more than 10 % of tumor tissue remaining vital, should be suspected. In such cases, the first-pass image was useful to guide a new biopsy or to focus the attention of the pathologist on those areas in the resected specimen, in which tumor cells might have survived chemotherapy [2] (Figs. 5.10 and 5.11). However, with this and other postprocessing techniques, young granulation tissue replacing tumor necrosis may mimic vital tumor areas, especially in the early phase of chemotherapy and in the first months after radiation therapy. In a second and third follow-up DCE-MRI study, 3 and 6 months later, tumor tissue will still be highly vascular, whereas all parameters will be lower in reactive tissue.

5.1.4.2 Tissue Characterization: Differentiation of Benign from Malignant Lesions

Attempts have been made to use the slope of a TIC as a differential diagnostic criterion to differentiate benign (low-slope) from malignant (high-slope) lesions (Table 5.1; Figs. 5.5 and 5.7) [2, 14, 19–21, 33, 50]. In these studies, evaluation of the malignant potential of musculoskeletal lesions with the slope of TICs was possible with levels of sensitivity and specificity ranging from 72 % to

Table 5.1 Slope values of soft tissue tumors

Slope value	3–40 %/s	40–96 %/s	>100 %/s
Benign lesions	Lipoma	Myositis	
	Lipoblastoma	Capillary (high-flow) hemangioma	
	Elastofibroma	Abscess	
	Organizing old hematoma	Granulation tissue	
	Ganglion	Myositis ossificans	
	Dermoid		
	Fat necrosis		
	Cavernous hemangioma (slow flow)		
	Angiolipoma		
	Synovial chondromatosis		
	Pigmented villonodular synovitis		
	Neurofibroma		
	Rheumatoid nodule		
	Calcifying tendinitis		
	Schwannoma		
Malignant lesions		Epithelioid sarcoma	
		Lymphoma	
		Liposarcoma	
		Fibrosarcoma	
			Undifferentiated pleomorphic sarcoma
			Synovial sarcoma

The slope values were obtained using a single-slice turbo FLASH sequence on a 1.5-T magnet, with the following parameters: TR 9 ms; TE 4 ms; TI 200 ms; flip angle 8°; matrix 128×128; one average per acquisition; slice thickness 6–10 mm; acquisition time 1.41 s/image; linear view order

83 % and 77 % to 89 %, respectively. Although there was a highly statistically significant difference in slope values of benign and malignant lesions, there was some overlap: some highly vascularized or perfused benign lesions, such as aneurysmal bone cyst, eosinophilic granuloma, giant cell tumor, osteoid osteoma, acute osteomyelitis, myositis ossificans, and occasionally aggressive fibromatosis, fibrous dysplasia, neurinoma, and neurofibroma, had slope values in the same range as malignant tumors (Figs. 5.6 and 5.7; Table 5.1). The highest slope values were found in synovial sarcoma and fibrosarcoma. On the other hand, low-slope values seemed to have a high predictive value in favor of a benign lesion (Fig. 5.12, Table 5.1). Due to this overlap between benign and malignant lesions, TICs and slope values should only be used in conjunction with conventional spin-echo images and other radiological, anatomical, and clinical data to narrow down the differential diagnostic possibilities, by providing physiological information on the vascularization and perfusion of the lesion, rather than to predict the benignity or malignancy of a lesion. A study evaluating the value of static and dynamic gadopentetate dimeglumine-enhanced MRI in prediction of malignancy showed that contrast-enhanced MRI parameters that favored malignancy were liquefaction, early dynamic enhancement (within 6 s after arterial enhancement), peripheral or inhomogeneous dynamic enhancement, and rapid initial dynamic enhancement followed by a plateau or washout phase [40]. The slope of the TIC, the time of onset of enhancement (relative to the onset of enhancement in a local artery), and the type of curve are not helpful to differentiate benign from

malignant lesions, although curves with a high slope, early equilibrium phase, and early washout seem to occur more frequently in undifferentiated pleomorphic sarcoma (formerly known as malignant fibrous histiocytoma) and synovial sarcoma [8, 37] (Fig. 5.13).

Dynamic contrast-enhanced MRI has been used successfully to differentiate capillary and arteriovenous (high-flow) hemangiomas from cavernous (slow-flow) hemangiomas [2, 31, 33] (Fig. 5.6).

5.1.4.3 Identification of Viable Tumor Tissue

Identification of viable areas in a tumor is important for biopsy, as, on histopathological examination, well-vascularized viable tumor will be of greater value for determining the tumor type and grade than a biopsy specimen containing a mixture of poorly vascularized tumor tissue, edema, or necrotic material. Dynamic contrast-enhanced MRI may provide useful information for guiding the biopsy needle toward representative areas, as areas with well-vascularized viable tumor tissue will be depicted considerably better than on contrast-enhanced spin-echo images [33] (Fig. 5.3). During the first pass of the contrast agent in the tumor, the most highly vascular areas will appear brighter than other tumor components and peritumoral edema, due to a faster enhancement (Figs. 5.3, 5.4, 5.8, and 5.13) [49].

5.1.4.4 Detection of Residual or Recurrent Tumor

After resection of a musculoskeletal tumor, regular follow-up studies are mandatory. Whenever a mass is detected with high signal intensity on fat-saturated or STIR T2 images, dynamic contrast-enhanced MRI is indicated, as differentiation between inflammatory changes, seromas, and residual or recurrent tumor tissue is not possible with static MRI [30, 65–69]. According to Vanel et al., no enhancement occurs in seromas; slow increase observed with dynamic contrast-enhanced MRI indicates pseudomass (= reactive tissue and inflammation, usually visible as high signal intensity area, without real mass), whereas early, fast, and high increase of signal intensity indicates recurrence [29, 30] (Figs. 5.4, 5.13, and 5.14). Two exceptions are recurrence of PVNS and fibromatosis, which may present as al low signal intensity mass (Fig. 5.14).

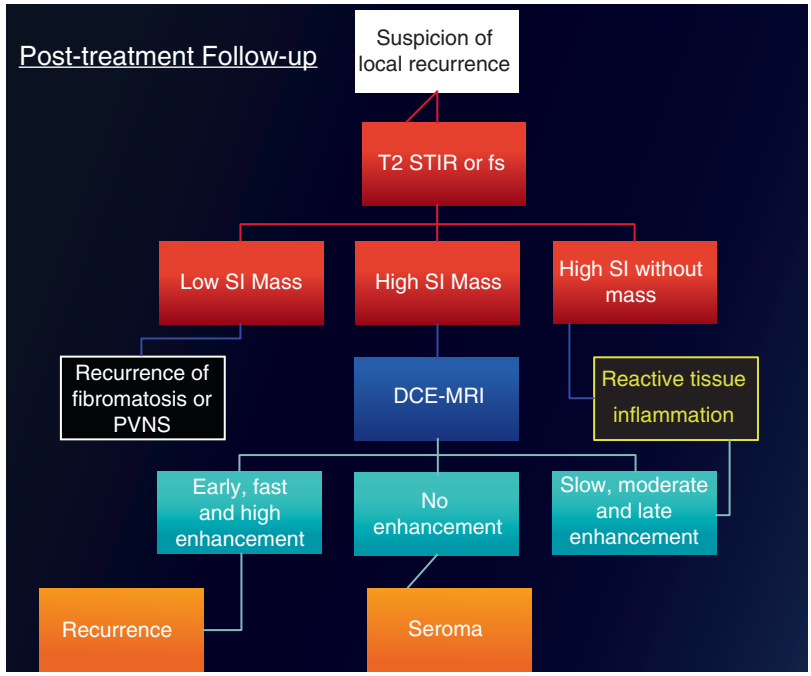

Fig. 5.14 Flow chart for follow-up of soft tissue tumors after therapy (see text 5.1.4.4)

5.2 Diffusion MRI

5.2.1 Imaging Technique

Diffusion MRI provides quantitative and qualitative assessments of tissue cellularity and cell membrane integrity. It is widely used for tumor detection, characterization, and monitoring during treatment. Diffusion MRI supplies functional information that complements the structural evaluation [76]. Diffusion MRI measures the random movements of water molecules in the body (Brownian motion). Water molecule motion is assessed in vivo in the extracellular, intracellular, and transcellular compartments, as well as in the intravascular compartment (microcirculation–perfusion) [77]. Blood flow in the intravascular compartment leads to water-molecule diffusion over longer distances, compared to the extracellular and intracellular compartments. The contribution of intravascular water-molecule diffusion to the diffusion image varies across tissues; it can be significant in highly vascularized tumors. Restriction of water-molecule diffusion within biological tissues correlates negatively with tissue cellularity and membrane integrity [78]. Restriction is greater in highly cellular tissues that have intact cell membranes and a small extracellular compartment.

Tumors differ regarding their cellular characteristics, and the differences can serve to differentiate tumor types. Cellularity is greater in malignant tumors, in which restriction of water-molecule diffusion tends to be greater, compared to benign tumors [76, 79].

5.2.1.1 Qualitative Diffusion MRI

Diffusion MRI is performed using a conventional T2-weighted sequence with diffusion gradients to filter the signal from highly mobile water molecules and to improve the detection of diffusion and mobility. Available diffusion sequences include spin-echo diffusion-weighted imaging (DWI), echoplanar imaging (EPI), and steady-state free precession (SSFP) imaging [77]. EPI has a short acquisition time and is consequently the most widely used sequence, with a single-shot or multi-shot technique. To improve interpretation accuracy, at least two different *b*-values are generally used (0 and 600 or 1000 s/mm^2). The *b*-value reflects the diffusion force and diffusion weighting of the image, just as the echo time (TE) reflects T2 weighting of T2 images [11, 76]. Cystic tumors exhibit greater signal attenuation on high *b*-value images, reflecting the smaller degree of water-molecule motion restriction, whereas solid masses and cellular tumors continue to generate a high-intensity signal.

5.2.1.2 Quantitative Diffusion MRI

Diffusion MRI with multiple *b*-values provides a quantitative analysis via the apparent diffusion coefficient (ADC). ADC is an exponential function of the tumor signal on the images acquired with different *b*-values. The ADC is computed for each pixel of the image, and a map of the ADC values is created. Tissues can be differentiated by using ROIs on the ADC map. Highly cellular sites with restricted diffusion have lower ADC values compared to sites characterized by lower cell densities. Sites with low ADC values generate higher signal intensity on diffusion images. However, the ADC depends not only on water-molecule diffusion in the extracellular tumor compartment but also on the degree of tumor perfusion [79]. The perfusion fraction (microcirculation) in malignant soft tissue tumors tends to be greater and to make a larger contribution to ADC elevation than in benign soft tissue tumors. Thus, perfusion can produce a larger ADC increase in malignant tumors, leading to overlap between ADC values of malignant and benign tumors [76]. Diffusion images corrected for perfusion (perfusion-insensitive ADC value, PIADC) limit the impact of this effect [79]. Conventional ADC values are measured with *b*-values of 0 and 600 s/mm^2. Water molecules that move freely and diffuse over long distances (e.g., in the intravascular compartment) show signal attenuation at low *b*-values (50–100 s/mm^2). In contrast, water molecules that move slowly or diffuse over short distances exhibit more gradual signal attenuation with increasing *b*-values (1000 s/mm^2).

High-grade tumors with high cellularity and small interstitial spaces tend to produce lower ADC values [16]. Benign non-myxoid tumors have a higher mean ADC value compared to malignant lesions ($1.31 \pm 0.46\ 0.46 \times 10^{-3}$ mm^2/s versus $0.94 \pm 0.25 \times 10^{-3}$ mm^2/s, $P < 0.001$) (NEW Fig. 5.15.) [80]. In combination with standard structural MRI parameters, the ADC value improves tumor characterization [81]. ADC measurements may be difficult in heterogeneous large soft tissue sarcomas. ROI measurements of ADC should avoid necrosis, hemorrhage, calcification, and mucoid components. Minimum ADC may be more discriminant than mean ADC to differentiate benign form malignant tumors.

Diffusion MRI can also be used to monitor tumors during chemotherapy. Tumor necrosis results in loss of cell membrane integrity and in expansion of the extracellular compartment, leading to greater water-molecule diffusion with an increase in the ADC value [76].

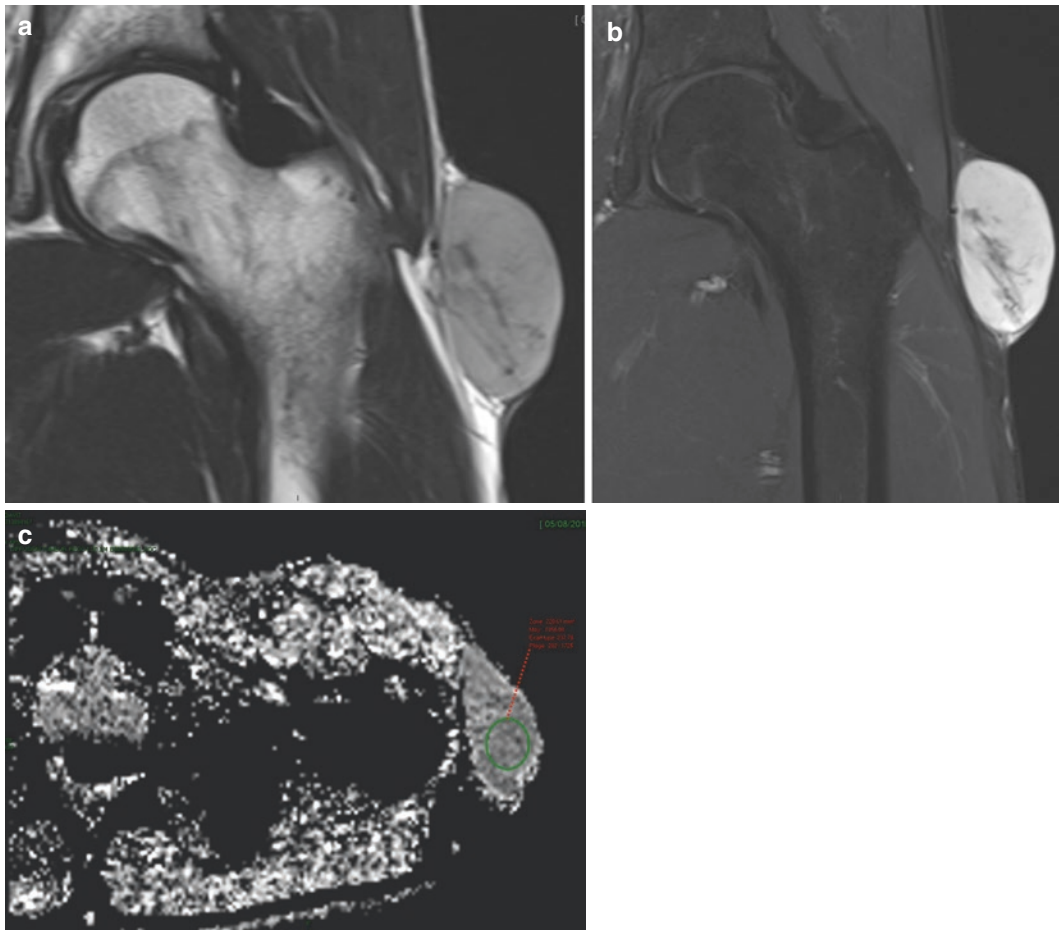

Fig. 5.15 (**a**–**c**) Dermatofibrosarcoma protuberans of the left thigh. (**a**) Coronal fast spin-echo T2 MR image shows oval subcutaneous soft tissue mass. (**b**) Coronal fat-saturated T1 MR image after intravenous injection of gadolinium contrast medium shows intense enhancement of the tumor. (**c**) ADC map of the hip regions shows highly cellular tissue with restricted diffusion. The mean ADC measured in the ROI (1.06×10^{-3} mm^2/s) is suggestive for a malignant tumor

5.2.2 Clinical Applications

5.2.2.1 Abscesses, Hematomas, and Necrotic Tumors

Necrotic tumors and abscesses may have similar appearances on conventional MRI. A definite diagnosis of abscess modifies the management strategy, as drainage is in order. Abscesses may have a rich blood supply in the active wall, with perfusion slopes similar to those seen in malignant tumors [40]. Abscesses contain inflammatory cells, a protein matrix, cellular debris, and bacteria within highly viscous pus, limiting water-molecule mobility. Therefore, the abscess cavity is characterized by a low ADC value and a high signal on high b-value diffusion MR images. In the necrotic part of necrotized tumors, diffusion tends to be greater than in abscesses, because the composition of tumor necrosis allows more random movements of water molecules than viscous necrosis in an abscess. In the highly cellular solid part of aggressive malignancies, water motion is restricted and the ADC value will be low [76].

Differentiating a hematoma from a hemorrhagic malignant tumor may be challenging [76]. Diffusion MRI can differentiate a growing chronic hematoma from a malignant tumor. The mean ADC value is significantly higher in hematomas than in soft tissue malignancies ($1.55 \pm 0.121 \times 10^{-3}$ mm^2/s versus $0.92 \pm 0.139 \times 10^{-3}$ mm^2/s, $P < 0.01$). Acute and subacute hematomas produce characteristic MRI features with methemoglobin, and the ADC map shows restricted diffusion in the center of the lesion. Contrast enhancement is rare in benign hematomas but may be present in the periphery of the hematoma, as a mild and regular enhancement.

5.2.2.2 Myxoid Tumors

Myxoid tissue is found in myxoma, myxoid liposarcoma, and myxofibrosarcoma [39]. The high mucin and low collagen contents of these water-rich lesions, which allow more random movements of water molecules, result in higher ADC values in malignant and nonmalignant myxoid soft tissue tumors than in nonmyxoid tumors ($2.08 \pm 0.51 \times 10^{-3}$ mm^2/s versus $1.13 \pm 0.40 \times 10^{-3}$ mm^2/s, $P < 0.001$) [76, 79] (NEW Fig. 5.16). However, there is not so much difference of the myxoid component in malignant and nonmalignant myxoid soft tissue tumors,

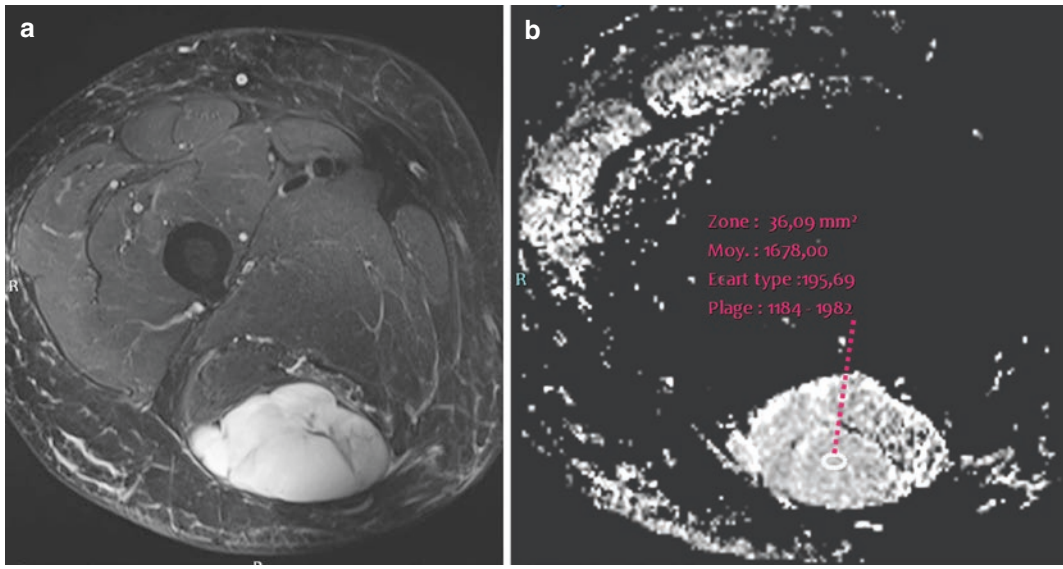

Fig. 5.16 (**a**, **b**) Myxofibrosarcoma of the right thigh. (**a**) Axial fat-saturated T2 MR image shows a very high signal intensity of the mucoid component of this malignant tumor. (**b**) ADC map of the right thigh regions shows water-rich lesion with mean ADC of 1.67×10^{-3} mm^2/s, suggestive for myxoid tissue with high mucin and low collagen contents, which allows more random movements of water molecules resulting in higher ADC value

resulting in considerable overlap between the ADC values of benign and malignant myxoid tumors.

5.2.2.3 Monitoring the Treatment Response

Diffusion MRI can also be used to estimate residual tumor activity after treatment and to detect recurrences at an early stage when curative treatment is still possible. Differentiating treatment-related tissue changes from residual or recurrent tumor tissue is a common problem, given the lack of specificity of the signal abnormalities by standard MRI (low signal on T1 images and high signal on T2 images). Diffusion shows larger increases in diffusion in foci of treatment-related tumor necrosis than in viable tumor remnants or recurrences. Solid tumors are characterized by high cellularity and intact cell membranes, contrasting with the lower cellularity and membrane damage seen in treatment-altered tissues [82]. Further studies are necessary to determine the optimum shortest delay necessary to detect a response to chemotherapy.

5.3 Proton Nuclear MR Spectroscopy

Proton NMR spectroscopy is not routinely performed for the evaluation of soft tissue tumors but can be used to characterize the molecules present in malignant musculoskeletal tumors [83, 84]. The lesions are characterized based on their metabolic constituents, such as choline, a phospholipid found in the cell membrane. An increased proportion of choline indicates accelerated cell membrane turnover, which is an indirect marker for malignancy [83, 84]. Proton NMR spectroscopy has been used in bone and soft tissue tumors, breast cancer, prostate cancer, and cervical cancer. The results differentiate malignant from benign musculoskeletal tumors [83, 84]. Proton NMR spectroscopy results can be translated into pixel intensity maps based on the relative signal from the metabolite (water, choline, creatine, and lipids), using multi-voxel and single-voxel techniques. Multi-voxel proton NMR spectroscopy has been proved feasible for characterizing musculoskeletal tumors [84]. The ROIs must be painstakingly positioned at sites of early marked enhancement that do not contain bony structures, necrotic or hemorrhagic foci, calcifications, fat, or muscle. For tumors exhibiting weak and slow enhancement or no enhancement after 5 min, the voxel is positioned at sites of delayed enhancement. The choline peak serves to differentiate benign and malignant tumors. A choline peak is in favor of a malignant lesion but can be found in metabolically active benign lesions and in abscesses [83, 85]. A lipid peak is usually visible in abscess walls, solid components of malignant masses, and treated tumors, where it reflects cell membrane turnover. Care should be taken to avoid peak contamination by neighboring structures, as well as excessive noise.

Conclusions

Dynamic MRI is a promising method of physiological imaging which provides clinically useful information, by depicting tissue vascularization and perfusion, capillary permeability, and composition of the interstitial space. The most important applications in the musculoskeletal system are an indication of the biopsy site, tissue characterization, monitoring of preoperative chemotherapy, and detection of residual or recurrent tumor tissue.

Key Points

1. Dynamic contrast-enhanced imaging can be performed in less than 5 min and provides information on tissue vascularization, perfusion, and capillary permeability during the first pass of the contrast medium and on the interstitial space after the first pass.
2. Diffusion MR provides information on tissue cellularity and water motion.
3. Proton NMR spectroscopy detects water, choline, creatine, and lipids.

4. Advanced MR imaging techniques can be helpful for identification of necrosis, abscess, hematoma, and myxoid tissue.
5. Advanced MR imaging techniques can be helpful to narrow the differential diagnosis and differentiate benign from malignant lesions, to monitor chemotherapy, to indicate the best site for biopsy, to detect tumor recurrence, and to differentiate recurrence from reactive tissue.
6. Interpretation of a dynamic contrast-enhanced imaging study can be done using regions of interest (e.g., whole tumor, fastest-enhancing area, muscle, and artery) and time-intensity curves or with more advanced pixel-by-pixel postprocessing and pharmacokinetic modeling techniques.
7. Interpretation of diffusion MRI can be done qualitatively by evaluating signal intensity on low and high b-value images or quantitatively by calculating the apparent diffusion coefficient and using regions-of-interest on ADC maps.

References

1. Brasch RC (1992) New directions in the development of MR imaging contrast-media. Radiology 183:1–11
2. Verstraete KL, Dedeene Y, Roels H, Dierick A, Uyttendaele D, Kunnen M (1994) Benign and malignant musculoskeletal lesions – dynamic contrast-enhanced MR-imaging – parametric first-pass images depict tissue vascularization and perfusion. Radiology 192:835–843
3. Wolf GL (1991) Contrast agents in spine and body MRI: introduction. In: Hasso AN, Stark DD (ed) American Roentgen Ray Society – categorical course syllabus: spine and body magnetic resonance imaging. Reston, Congres of ARRS in Boston, 1991. Reston, VA, USA pp 111–115
4. Dean PB, Kormano M (1977) Intravenous bolus of 125I-labeled meglumine diatrizoate. Early extravascular distribution. Acta Radiol Diagn (Stockh) 18:293–304
5. Kormano M, Dean PB (1976) Extravascular contrast material: the major component of contrast enhancement. Radiology 121:379–382
6. Tong CY, Prato FS, Wisenberg G et al (1993) Measurement of the extraction efficiency and distribution volume for Gd-DT-PA in normal and diseased canine myocardium. Magn Reson Med 30:337–346
7. Tong CY, Prato FS, Wisenberg G et al (1993) Techniques for the measurement of the local myocardial extraction efficiency for inert diffusible contrast agents such as gadopentetate dimeglumine. Magn Reson Med 30:332–336
8. Verstraete KL et al (1992) Dynamic contrast enhanced MRI of musculoskeletal neoplasms: different types and slopes of TICs (abstract). Proceedings of Society of Magnetic Resonance in Medicine. Berkely, p 2609
9. Debaere T, Vanel D, Shapeero LG, Charpentier A, Terrier P, Dipaola M (1992) Osteosarcoma after chemotherapy – evaluation with contrast material enhanced subtraction MR imaging. Radiology 185:587–592
10. Hanna SL, Parham DM, Fairclough DL, Meyer WH, Le AH, Fletcher BD (1992) Assessment of osteosarcoma response to preoperative chemotherapy using dynamic flash gadolinium-DTPA-enhanced magnetic-resonance mapping. Invest Radiol 27:367–373
11. Konig H, Sieper J, Wolf KJ (1990) Rheumatoid arthritis – evaluation of hypervascular and fibrous pannus with dynamic MR imaging enhanced with Gd-DTPA. Radiology 176:473–477
12. Konig H, Sieper J, Wolf KJ (1990) Dynamic MRI for the differentiation of inflammatory joint lesions. Rofo Fortschr Geb Rontgenstr Neuen Bildgeb Verfahr 153:1–5
13. Ross JS, Delamarter R, Hueftle MG et al (1989) Gadolinium-DTPA-enhanced MRI of the postoperative lumbar spine: time course and mechanism of enhancement. AJR Am J Roentgenol 152:825–834
14. Verstraete KL, Dierick A, De Deene Y et al (1994) First-pass images of musculoskeletal lesions: a new and useful diagnostic application of dynamic contrast-enhanced MRI. Magn Reson Imaging 12:687–702
15. Bollow M, Braun J, Hamm B et al (1995) Early sacroiliitis in patients with spondyloarthropathy – evaluation with dynamic gadolinium-enhanced MR-imaging. Radiology 194:529–536
16. Bonnerot V, Charpentier A, Frouin F, Kalifa C, Vanel D, Dipaola R (1992) Factor-analysis of dynamic magnetic-resonance-imaging in predicting the response of osteosarcoma to chemotherapy. Invest Radiol 27:847–855
17. Charpentier E et al (1990) Factor analysis processing of dynamic MRI: new method to assess osteosarcoma preoperative chemotherapy response (abstract). Radiology 177(Suppl):221
18. Cova M, Kang YS, Tsukamoto H et al (1991) Bone-marrow perfusion evaluated with gadolinium-enhanced dynamic fast MR imaging in a dog-model. Radiology 179:535–539
19. Erlemann R, Reiser MF, Peters PE et al (1989) Musculoskeletal neoplasms – static and dynamic Gd-DTPA enhanced MR imaging. Radiology 171: 767–773
20. Erlemann R, Sciuk J, Bosse A et al (1990) Response of osteosarcoma and Ewing sarcoma to preoperative chemotherapy – assessment with dynamic and static

MR imaging and skeletal scintigraphy. Radiology 175:791–796
21. Fletcher BD, Hanna SL, Fairclough DL, Gronemeyer SA (1992) Pediatric musculoskeletal tumors – use of dynamic contrast-enhanced MR imaging to monitor response to chemotherapy. Radiology 184:243–248
22. Hanna SL, Fletcher BD, Fairclough DL, Le A (1990) Use of dynamic Gd-DTPA enhanced MRI in musculoskeletal malignancies (abstract). Proceedings of Society of Magnetic Resonance Imaging, p 9
23. Lang P, Stevens M, Vahlensieck M (1991) Rheumatoid arthritis of the hand and wrist: evaluation of soft-tissue inflammation and quantification of inflammatory activity using unenhanced and dynamic Gd-DTPA enhanced MRI (abstract). Proceedings of Society of Magnetic Resonance in Medicine p 66
24. Mirowitz SA, Totty WG, Lee JKT (1990) Evaluation of musculoskeletal masses with dynamic Gd-DTPA enhanced rapid-acquisition spin-echo imaging (abstract). Radiology 177(Suppl):221
25. Mirowitz SA, Totty WG, Lee JKT (1992) Characterization of musculoskeletal masses using dynamic Gd-DTPA enhanced spin-echo MRI. J Comput Assist Tomogr 16:120–125
26. Reiser MF, Bongartz GP, Erlemann R et al (1989) Gadolinium-DTPA in rheumatoid-arthritis and related diseases – first results with dynamic magnetic-resonance imaging. Skeletal Radiol 18:591–597
27. Sugimoto H, Miyaji N, Ohsawa T (1994) Carpal-tunnel syndrome – evaluation of median nerve circulation with dynamic contrast-enhanced MR-imaging. Radiology 190:459–466
28. Tsukamoto H, Kang YS, Jones LC et al (1992) Evaluation of marrow perfusion in the femoral-head by dynamic magnetic-resonance-imaging – effect of venous occlusion in a dog-model. Invest Radiol 27:275–281
29. Vanel D et al (1993) Dynamic contrast-enhanced subtraction MRI in follow-up of aggressive soft-tissue tumors: a prospective study of 74 patients (abstract). Radiology 189(Suppl):205
30. Vanel D, Shapeero LG, Debaere T et al (1994) MR-imaging in the follow-up of malignant and aggressive soft-tissue tumors – results of 511 examinations. Radiology 190:263–268
31. Verstraete K (1994) Dynamic contrast-enhanced MRI of tumor and tumor-like lesions of the musculoskeletal system, pp 63–185. Thesis, University of Gent, Gent, Belgium
32. Verstraete KL, Dierick A, De Deene Y et al (1993) First-pass images of musculoskeletal lesions: a new and useful diagnostic application of dynamic contrast-enhanced MRI. Proc. Soc. Magn. Reson. Med. 2, New York 869
33. Verstraete KL, Vanzieleghem B, De Deene Y et al (1995) Static, dynamic and first-pass MRI of musculoskeletal lesions using gadodiamide injection. Acta Radiol 36:27–36
34. Chien D, Edelman RR (1991) Ultrafast imaging using gradient echos. Magn Reson Q 7:31–56
35. Haase A, Matthaei D, Bartkowski R, Duhmke E, Leibfritz D (1989) Inversion recovery snapshot FLASH MR imaging. J Comput Assist Tomogr 13:1036–1040
36. Haase A (1990) Snapshot FLASH MRI – applications to T1, T2, and chemical-shift imaging. Magn Reson Med 13:77–89
37. Van der Woude H et al (1995) Double slice dynamic contrast-enhanced subtraction MR images in 60 patients with musculoskeletal tumors or tumor-like lesions (abstract). Eur Radiol (Suppl 5):181
38. Van der Woude HJ, Bloem JL, Verstraete KL, Taminiau AH, Nooy MA, Hogendoorn PC (1995) Osteosarcoma and Ewing's sarcoma after neoadjuvant chemotherapy: value of dynamic MR imaging in detecting viable tumor before surgery. AJR Am J Roentgenol 165:593–8
39. Verstraete KL, Lang P (2000) Bone and soft tissue tumors: the role of contrast agents for MRI. Eur J Radiol 34:229–246
40. van Rijswijk CS, Geirnaerdt MJ, Hogendoorn PC et al (2004) Soft-tissue tumors: value of static and dynamic gadopentetate dimeglumine-enhanced MRI in prediction of malignancy. Radiology 233:493–502
41. Shapeero LG, Henry-Amar M, Vanel D (1992) Response of osteosarcoma and Ewing sarcoma to preoperative chemotherapy: assessment with dynamic and static MRI and skeletal scintigraphy. Invest Radiol 27:989–991
42. Kashanian FK, Goldstein HA, Blumetti RF, Holyoak WL, Hugo FP, Dolker M (1990) Rapid bolus injection of gadopentetate dimeglumine: absence of side effects in normal volunteers. AJNR Am J Neuroradiol 11:853–856
43. Chambers TP, Baron RL, Lush RM, Dodd GD, Miller WJ, Confer SR (1993) Hepatic CT enhancement – a method to demonstrate reproducibility. Radiology 188:627–631
44. Chambers TP, Baron RL, Lush RM (1994) Hepatic CT enhancement. 1. Alterations in the volume of contrast material within the same patients. Radiology 193:513–517
45. Chambers TP, Baron RL, Lush RM (1994) Hepatic CT enhancement. 2. Alterations in contrast material volume and rate of injection within the same patients. Radiology 193:518–522
46. Vanderwoude HJ, Bloem JL, Schipper J et al (1994) Changes in tumor perfusion induced by chemotherapy in bone sarcomas – color Doppler flow imaging compared with contrast-enhanced MR-imaging and 3-phase bone-scintigraphy. Radiology 191:421–431
47. Vaupel P, Kallinowski F, Okunieff P (1989) Blood-flow, oxygen and nutrient supply, and metabolic microenvironment of human-tumors – a review. Cancer Res 49:6449–6465
48. Reddick WE, Langston JW, Meyer WH et al (1994) Discrete signal-processing of dynamic contrast-enhanced MR-imaging – statistical validation and preliminary clinical-application. J Magn Reson Imaging 4:397–404

49. Lang P, Honda G, Roberts T et al (1995) Musculoskeletal neoplasm: perineoplastic edema versus tumor on dynamic post-contrast MR images with spatial mapping of instantaneous enhancement rates. Radiology 197:831–839
50. Erlemann R (1993) Dynamic gadolinium-enhanced MR imaging to monitor tumor response to chemotherapy. Radiology 186:904
51. Lawrence JA, Babyn PS, Chan HSL, Thorner PS, Pron GE, Krajbich IJ (1993) Extremity osteosarcoma in childhood – prognostic value of radiologic imaging. Radiology 189:43–47
52. Glasser DB, Lane JM, Huvos AG, Marcove RC, Rosen G (1992) Survival, prognosis, and therapeutic response in osteogenic-sarcoma – the Memorial Hospital Experience. Cancer 69:698–708
53. Hudson M, Jaffe MR, Jaffe N et al (1990) Pediatric osteosarcoma – therapeutic strategies, results, and prognostic factors derived from a 10-year experience. J Clin Oncol 8:1988–1997
54. Meyers PA, Heller G, Healey J et al (1992) Chemotherapy for nonmetastatic osteogenic-sarcoma – the Memorial Sloan-Kettering experience. J Clin Oncol 10:5–15
55. Oberlin O, Patte C, Demeocq F et al (1985) The response to initial chemotherapy as a prognostic factor in localized Ewing sarcoma. Eur J Cancer Clin Oncol 21:463–467
56. Rosen G, Caparros B, Huvos AG et al (1982) Preoperative chemotherapy for osteogenic-sarcoma – selection of postoperative adjuvant chemotherapy based on the response of the primary tumor to preoperative chemotherapy. Cancer 49:1221–1230
57. Winkler K, Beron G, Delling G et al (1988) Neoadjuvant chemotherapy of osteo-sarcoma – results of a randomized cooperative trial (Coss-82) with salvage chemotherapy based on histological tumor response. J Clin Oncol 6:329–337
58. Raymond AK, Chawla SP, Carrasco CH et al (1987) Osteosarcoma chemotherapy effect – a prognostic factor. Semin Diagn Pathol 4:212–236
59. Erlemann R, Sciuk J, Wuisman P et al (1992) Dynamic MR tomography in diagnosis of inflammatory and tumorous space-occupying growths of the musculoskeletal system. Rofo Fortschr Geb Rontgenstr Neuen Bildgeb Verfahr 156:353–359
60. Fletcher B, Hanna S (1989) Musculoskeletal neoplasms: dynamic Gd-DTPA-enhanced MRI (letter). Radiology 177:287–288
61. Carrasco CH, Charnsangavej C, Raymond AK et al (1989) Osteosarcoma – angiographic assessment of response to preoperative chemotherapy. Radiology 170:839–842
62. Chuang VP, Benjamin R, Jaffe N et al (1982) Radiographic and angiographic changes in osteosarcoma after intraarterial chemotherapy. AJR Am J Roentgenol 139:1065–1069
63. Knop J, Delling G, Heise U, Winkler K (1990) Scintigraphic evaluation of tumor-regression during preoperative chemotherapy of osteosarcoma – correlation of Tc-99m-methylene diphosphonate parametric imaging with surgical histopathology. Skeletal Radiol 19:165–172
64. Kumpan W, Lechner G, Wittich GR et al (1986) The angiographic response of osteosarcoma following pre-operative chemotherapy. Skeletal Radiol 15:96–102
65. Biondetti PR, Ehman RL (1992) Soft-tissue sarcomas: use of textural patterns in skeletal muscle as a diagnostic feature in postoperative MRI. Radiology 183:845–848
66. Bloem JL, Reiser MF, Vanel D (1990) Magnetic resonance contrast agents in the evaluation of the musculoskeletal system. Magn Reson Q 6:136–163
67. Maas R (1992) Radiological-diagnosis of recurrent soft-tissue sarcoma. Radiologe 32:597–605
68. Reuther G, Mutschler W (1990) Detection of local recurrent disease in musculoskeletal tumors – magnetic-resonance-imaging versus computed-tomography. Skeletal Radiol 19:85–90
69. Vanel D, Lacombe MJ, Couanet D, Kalifa C, Spielmann M, Genin J (1987) Musculoskeletal tumors – follow-up with MR imaging after treatment with surgery and radiation-therapy. Radiology 164:243–245
70. Padhani AR (2002) Dynamic contrast-enhanced MRI in clinical oncology: current status and future directions. J Magn Reson Imaging 16:407–422
71. Essig M, Shiroishi M, Nguyen T et al (2013) Perfusion MRI: the five most frequently asked technical questions. AJR Am J Roentgenol 200(1):24–34
72. Paldino MJ, Barboriak DP (2009) Fundamentals of quantitative dynamic contrast-enhanced MR imaging. Magn Reson Imaging Clin N Am 17:277–289
73. Tofts PS, Brix G, Buckley DL et al (1999) Estimating kinetic parameters from dynamic contrast-enhanced T(1)-weighted MRI of a diffusable tracer: standardized quantities and symbols. J Magn Reson Imaging 10:223–232
74. Miller JC, Pien HH, Sahani D, Sorensen AG, Thrall JH (2005) Imaging angiogenesis: applications and potential for drug development. J Natl Cancer Inst 97:172–187
75. Leach MO, Morgan B, Tofts PS et al (2012) Imaging vascular function for early stage clinical trials using dynamic contrast-enhanced magnetic resonance imaging. Eur Radiol 22:1465–1478
76. Costa FM, Ferreira EC, Vianna EM (2011) Diffusion-weighted magnetic resonance imaging for the evaluation of musculoskeletal tumors. Magn Reson Imaging Clin N Am 19(1):159–180
77. Baur A, Reiser MF (2000) Diffusion-weighted imaging of the musculoskeletal system in humans. Skeletal Radiol 29(10):555–562
78. Lang P, Wendland MF, Saeed M et al (1998) Osteogenic sarcoma: noninvasive in vivo assessment of tumor necrosis with diffusion weighted MR imaging. Radiology 206(1):227–235
79. Van Rijswijk CS, Kunz P, Hogendoorn PC et al (2002) Diffusion weighted MRI in the characterization of

soft-tissue tumors. J Magn Reson Imaging 15(3):302–307
80. Nagata S, Nishimura H, Uchida M et al (2008) Diffusion-weighted imaging of soft tissue tumors: usefulness of the apparent diffusion coefficient for differential diagnosis. Radiat Med 26: 287–295
81. Maeda M, Matsumine A, Kato H et al (2007) Soft-tissue tumors evaluated by line-scan diffusion-weighted imaging: influence of myxoid matrix on the apparent diffusion coefficient. J Magn Reson Imaging 25:119–204
82. Bley TA, Wieben O, Uhl M, Diffusion-weighted MR (2009) imaging in musculoskeletal radiology: applications in trauma, tumors, and inflammation. Magn Reson Imaging Clin N Am 17(2):263–275
83. Fayad LM, Barker PB, Jacobs MA et al (2007) Characterization of musculoskeletal lesions on 3-T proton MR spectroscopy. AJR Am J Roentgenol 188(6):1513–1520
84. Fayad LM, Bluemke DA, McCarthy EF, Weber KL et al (2006) Musculoskeletal tumors: use of proton MR spectroscopic imaging for characterization. J Magn Reson Imaging 23(1):23–28
85. Doganay S, Altinok T, Alkan A et al (2011) The role of MRS in the differentiation of benign and malignant soft tissue and bone tumors. Eur J Radiol 20(2):219–225

Pathology, Genetics, and Molecular Biology of Soft Tissue Tumors

6

Vasiliki Siozopoulou and Patrick Pauwels

Contents

6.1 **Introduction** 115

6.2 **Tissue Sampling** 116
6.2.1 Adequate Tissue Sampling 116
6.2.2 Treatment of the Fresh Material 116
6.2.3 Fixation and Its Role to Diagnosis 118

6.3 **Role of Frozen Section in Soft Tissue Pathology** 118

6.4 **Tumor Bank** 118

6.5 **Role of Light Microscopy in the Diagnosis of Soft Tissue Tumors** 119
6.5.1 Histology 119
6.5.2 Immunohistochemistry 120

6.6 **Role of Genetics and Molecular Studies in the Diagnoses of Soft Tissue Tumors** 122
6.6.1 Genetic Alterations in Soft Tissue Tumors 122
6.6.2 Molecular Techniques in Clinical Practice 124
6.6.3 Role of Molecular Biology in Soft Tissue Tumors 124

6.7 **World Health Organization (WHO) Classification of Tumors 2013** 126

6.8 **Pathology Grading and Staging** 126
6.8.1 Common Used Grading Classifications 127
6.8.2 Staging 127

References 128

V. Siozopoulou (✉) • P. Pauwels
University Hospital of Antwerp (UZA), Edegem, Belgium

Center for Oncological Research (CORE), University of Antwerp, Edegem, Belgium
e-mail: vasiliki.siozopoulou@uza.be; patrick.pauwels@uza.be

6.1 Introduction

Soft tissue tumors are rare entities which results in difficulties defining the right criteria for a correct diagnosis. Although they comprise <1 % of all adult malignancies and 12 % of pediatric cancers, there exists more than 100 benign and malignant subtypes [1, 2], which makes those tumors diagnostically challenging and difficult. The role of the pathologist is to differentiate malignant from benign tumors and pseudotumors. There are also entities such as solitary fibrous tumor, whose prognosis is from pathologic point of view unpredictable. If possible, subclassification of the lesion will add to a more specific and correct diagnosis, and of course in cases of malignancy, histologic grade is very important as it has been shown to be one of the best predictors of outcome, including both metastatic risk and disease-free survival, in adult soft tissue sarcomas [3–10].

Immunohistochemistry came to support and enhance the role of the histomorphology. Over the years this has led to a better understanding of the tumor's nature by indentifying and specifying the cell lineage of the particular lesions which resulted in further classification of the tumors. Nevertheless, no immunohistochemical staining is specific to a single lesion or cell type; therefore, the need for new diagnostic strategies became necessary.

In recent years the advances in cytogenetic and molecular pathology have not only helped

© Springer International Publishing AG 2017

F.M. Vanhoenacker et al. (eds.), *Imaging of Soft Tissue Tumors*, DOI 10.1007/978-3-319-46679-8_6

us understand the underlying biology of these neoplasms but have also proven to be powerful diagnostic and predictive markers.

It has to be emphasized that the final diagnosis is made based not only on pathologic data as clinical and radiological information are equally important. Especially in cases of biopsy, radiology provides to the pathologist very important information about location, size, consistency, growth pattern, presence or absence of necrosis, etc. A typical example is myxoid liposarcomas that almost never occur primarily in the retroperitoneum. Without knowledge of clinical and imaging data, the pathologist could make a wrong diagnosis. Decision about diagnosis and treatment options requires therefore a multidisciplinary approach.

6.2 Tissue Sampling

6.2.1 Adequate Tissue Sampling

A pathologist quote "tissue is the issue" emphasizes the importance of adequate tissue sampling for a correct diagnosis. Adequate tissue means first of all representative tumor material. Many tumors are inhomogeneous, containing low- and high-grade areas, which means that material from different areas of the tumor is needed for the correct diagnosis and also for the correct grading of the tumor. Biopsy material containing exclusively low-grade areas may create diagnostic confusion as whether the tumor is benign or malignant. These can lead to erroneous treatment choices. Necrosis is also a predominant feature of many malignant soft tissue lesions; the presence of necrotic components in the biopsy specimen could – in addition to tumor morphology – indicate malignancy. On the other hand, if the biopsy sample consists solely of necrosis, the tissue is inappropriate for further assessment, as it does not allow evaluation of the cellular components. In cases of tumors treated with chemo- and/or radiotherapy, the presence and percentage of necrosis indicate response to the particular therapy. Therefore, the presence of necrosis in the sample could in many cases be of diagnostic and prognostic value. Adequate tissue means also enough amount of tumor material in order to perform special techniques, such as immunohistochemistry and molecular testing, for further (sub) classification of the lesion. This underscores the need for appropriate cooperation between pathologists and radiologists for choosing the tumor areas that are best suited for sampling.

Of the techniques used for this purpose, the gold standard was open (incision) biopsy (IB). Given its high cost and complications, the need for other techniques has emerged. Nowadays, fine-needle aspiration (FNA) and core biopsy (CB) are both increasingly used for diagnostic purposes mostly for superficial masses. As it is apparent, IB provides to the pathologist the best material in terms of adequacy [11–13]. CB provides also very good material for diagnosis, but in comparison to IB, tissue samples are more often nondiagnostic. FNA has also been used for the diagnosis of soft tissue tumors. Despite the fact that from clinical and radiological point of view, it may be a preferable technique, it is not very useful for pathologic diagnosis. First of all, it does not provide insights into the architecture and the growth pattern of the tumor cells, which for soft tissue tumors is a very helpful and important diagnostic tool. Furthermore, given that most soft tissue tumors are solid masses, the amount of tumor cells extracted with this procedure can be very limited. If the tumor contains necrotic areas that are less firm due to loss of cell adhesion and presence of exudative material, it is likely that the sample will contain solely necrotic and inflammatory cells. For all of the abovementioned reasons, decision on the biopsy technique in each individual case should be discussed in the multidisciplinary team.

6.2.2 Treatment of the Fresh Material

Fresh tissue samples must be delivered to the pathology laboratory frozen and placed in a transport media to keep the cells alive or, in other way, deliver them as soon as possible to prevent autolysis of the cells.

Whenever material arrives in a pathology laboratory, it is treated appropriately according to the needs of each particular case. It can range from a tiny biopsy to a large specimen.

Biopsies are usually immediately fixated and proceeded for histologic examination. If the material is sufficient enough, tissue could be frozen for the tumor bank. In case of excisional biopsies, the material has first to be macroscopically examined before proceeding to fixation.

There are seven major components in processing a gross specimen:

1. Reliable and rapid transfer of the specimen from surgery to pathology
2. Accurate identification of all specimens
3. Accurate description of original specimens
4. Accurate description of additional specimens received from the same patient
5. Recording normal and abnormal features of the specimen including markers (e.g., sutures) which orientate the specimens
6. Special studies requested and/or needed
7. The location from which specific sections of tissue are taken for histologic evaluation [14]

When received, the specimen has first to be oriented following the instructions of the surgeon (and the radiologist). The surface of the specimen is often covered with special ink that is preserved after fixation in order to mark the margins of the specimen. Different color inks can be used to identify different areas if needed. When sections are made and processed, the ink will mark the actual margin on the slide. This provides more accurate estimation of the excision margins. Both the specimen itself and the tumor have to be measured. Another very important step of macroscopy is recognizing and describing the composition of the lesion. Tumors may show solid, myxoid, cystic, or necrotic areas that have to be macroscopically recognized and sampled for further microscopic evaluation. Those areas contain very important information regarding tumor type and grade. Whether the tumor is well demarcated or has infiltrative borders is an important diagnostic parameter. For instance, schwannomas are always very well demarcated and circumscribed, showing sometimes also a fine fibrous capsule on the surface (Fig. 6.1). Thus, if a neurogenic tumor shows infiltrative growth pattern, it is unlikely to be a schwannoma. On the other hand, a desmoid tumor shows a characteristic infiltrative growth pattern into the surrounding tissue (Fig. 6.2), making the complete excision of this otherwise benign tumor very difficult.

In most centers fresh frozen material will be stored apart for the Tumor Bank. Subsequently the remaining material will be fixated, embedded in paraffin blocks which will be used for further microscopic, immunohistochemic, and molecular evaluation of the tissue.

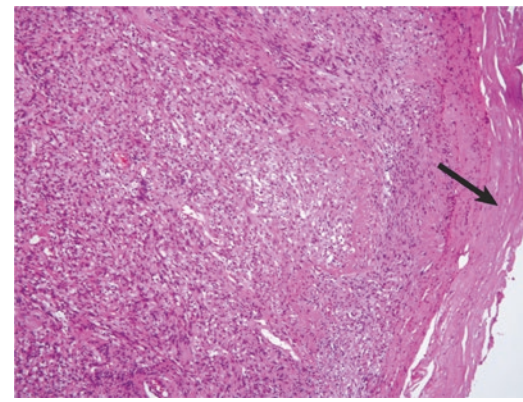

Fig. 6.1 HE, 100×. Schwannomas are well-demarcated lesions surrounded by a fine fibrous capsule (*arrow*)

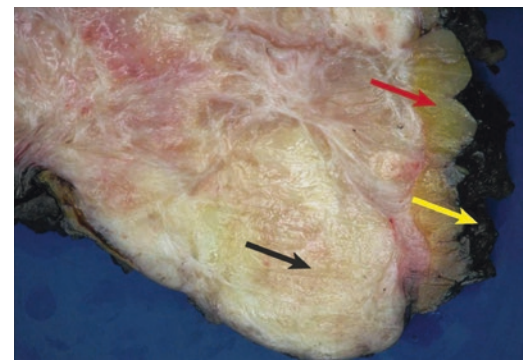

Fig. 6.2 Macroscopic image of desmoid tumor (*black arrow*) infiltrating the surrounding adipose tissue (red arrow). The margins are demarcated with black ink (*yellow* arrow) (Color figure online)

6.2.3 Fixation and Its Role to Diagnosis

Adequate fixation of the material plays a crucial role in pathology in order to allow preservation of the cells. Different fixatives have been used such as aldehydes, mercurials, alcohols, oxidizing agents, and picrates. Formaldehyde does not harm the proteins significantly, so that antigenicity is not lost. Therefore, formaldehyde is a good fixative for immunohistochemical techniques. In pathology the most widely used are 10 % and 4 % formaldehyde solutions. The latest has the ability to penetrate the tissue at a rate of 2–4 mm in 24 h [15]. Biopsies and small specimens will be fixated immediately, while bigger specimens have to be cut into thinner slides of maximum 10 mm thickness in order for the fixative to penetrate the tissue. Fixation has to start soon (<30 min) after surgical removal of the tissue, and overfixation (>24–48 h) has to be avoided [16], since this can influence the immunoreactivity of tissue antigens [17]. Also delayed fixation is proven to influence the number of observable mitotic figures in tissues [18, 19].

Once the tissue is fixated, it will be embedded in paraffin and stored in blocks, where the tissue can remain for prolonged periods.

6.3 Role of Frozen Section in Soft Tissue Pathology

Frozen section is one of the most difficult and demanding procedures. It requires well-trained workforce and is costly. The pathologist has to be experienced in the evaluation of soft tissue pathology and to have a close cooperation with the surgeon and the radiologist. Based on a material which has not undergone fixation and without the ability of any ancillary investigation, the pathologist should provide a very specific answer in a limited period of time. The surgeon has therefore first to decide if a frozen section will anyway influence the surgical procedure. If not, the procedure is not indicated [20].

The aim of a frozen section is to evaluate whether the biopsy specimen is representative of the lesion and sufficient enough for further permanent examination. An experienced pathologist can also determine the nature of the lesion, particularly to differentiate between benignity and malignancy. However, specific diagnosis and grading of the lesion depend on permanent sections, and ancillary investigation may also be required for final diagnosis.

Gross specimens submitted for frozen section are examined to evaluate the resection margins in order to intraoperatively determine the level of excision or amputation.

Whenever a metastatic spread of the tumor is suspected radiologically, then a frozen section during surgery could determine whether the lesion is metastatic or not. As expected this requires knowledge of clinical and radiological data, emphasizing once more the need for the collaboration of the different specialties of the multidisciplinary team.

6.4 Tumor Bank

Nowadays, the role of targeted therapy is gaining more and more importance, and individualized therapy is one of the perspectives of cancer research. The aim is to restrict the use of drugs to those patients whose tumor expresses the target, thereby minimizing cost and morbidity. Until today macroscopy, light microscopy, and special techniques in pathology are used to categorize the tumor and determine the stage. Scientists look forward to recognize specific biomarkers for each individual patient that will predict the metastatic risk of his/her disease.

The primary objective of Tumor Bank is to collect high-quality biospecimens and associated clinical data to promote scientific cancer research.

The material that is used for this purpose is fresh tissue that is not needed anymore for pathological examination, as pathology must not be compromised. The tissue is frozen in liquid nitrogen and stored in low temperature. It is very

important that the tissue will be proceeded for fixation immediately after removal from the human body, because ischemia can cause degradation of biomarkers. Nevertheless it remains controversial if a prolonged time of cold ischemia after a long warm ischemia is of scientific importance [21]. Studies have indicated that the RNA does not change rapidly after tissues are removed from the body [22–24] and that degradation of RNA happens more extensively at the time of warm ischemia when the vascular supply to the organs is compromised.

When received, the tissue will be frozen in liquid nitrogen and stored in low temperature. Optimal storage temperature is of paramount importance for a high-quality tissue. It is shown that protein activity may persist at low temperatures, even below −80 C [25–31]. Therefore, storage at temperatures at which water particles are still mobile and proteins are still active will result in degradation of the biospecimen [32].

6.5 Role of Light Microscopy in the Diagnosis of Soft Tissue Tumors

6.5.1 Histology

Histology means examination of the tissue on a thin slide stained with hematoxylin and eosin (HE) and remains the gold standard for diagnosis. Histology provides information about the morphology and the architecture of the lesion. Soft tissue tumors in most cases infiltrate diffusely, which is quite consistent for those tumors, in contrast to epithelioid neoplasms, where the cells usually form aggregates. There are of course exceptions to the rules, for instance, a biphasic synovial sarcoma contains also an epithelioid component that is composed of cell groups. On the other hand, an epithelioid neoplasm may also grow diffusely. Some tumors have a very characteristic architecture; examples are solitary fibrous tumor that shows a distinctive "patternless pattern," schwannoma with also the distinctive Antoni A and Antoni B tissue, representing compact areas alternating with loosely arranged foci of spindle cells (Fig. 6.3) and alveolar rhabdomyosarcoma with discrete nests with discohesive cells. As expected there are atypical forms of these tumors making their diagnosis more difficult and challenging. Of utmost importance is that lymphomas can also infiltrate diffusely; however, lymphomas have other morphological characteristics and a different clinico-radiological presentation.

Cell type can be also recognized on histology. In general soft tissue tumors are composed of cells that are elongated or spindled and have eosinophilic cytoplasm and indistinctive cell borders (Fig. 6.4). The nucleus differs from case to case with the more aggressive and malignant

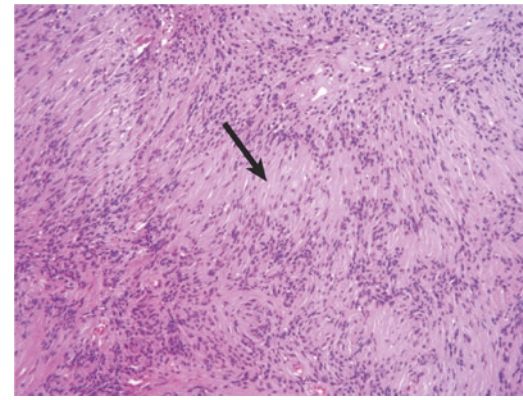

Fig. 6.3 HE, 200×. Nuclear palisading around fibrillary process (Verocay bodies, *arrow*) in cellular area of a schwannoma

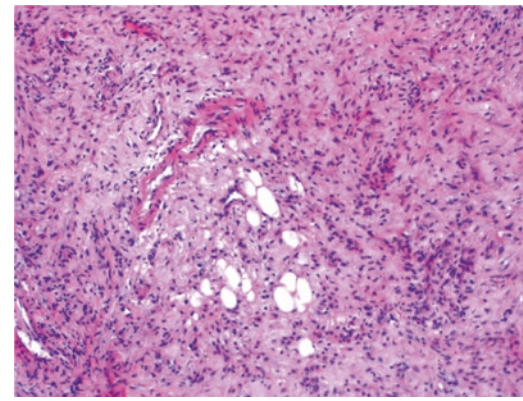

Fig. 6.4 HE, 100×. DDLPS composed mainly of spindle cells without prominent pleomorphism. Centrally scant lipomatous component

tumors that demonstrate more pleomorphism with enlarged nuclei, abnormal nuclear membrane, and sometimes an evident (macro)nucleolus. Multinucleation may indicate an aggressive cell type, but one has to bear in mind that giant cells are also multinucleated and that some benign tumor cells can also merged into giant forms. Desmoid tumors exhibit at the edge of the lesion multinucleated cells with strong eosinophilic cytoplasm, which is nothing more than degeneration of entrapped muscle cells when the tumor infiltrates between striated muscle (Fig. 6.5).

Not all soft tissue tumors are composed of spindle cells. Some neoplasms have an epithelioid morphology, such as epithelioid sarcoma, making the diagnosis more complicated.

It is evident that beyond the morphology of the tumor and the cellular composition, there are also other elements that can lead to the diagnosis. Many neoplasms show a vascular pattern that in many cases is diagnostic for this neoplasm. Thus, a "chicken wire" vascular pattern is described in myxoid lipomas and liposarcomas and a hemangiopericytoma-like pattern in solitary fibrous tumor, while schwannomas show hyalinization of the vascular wall.

Histology serves not only in tissue-specific diagnosis but plays also an important role in grading the tumor by recognizing and counting, for instance, the mitotic activity of the cells as well as identifying necrotic areas (Fig. 6.6). On histology one can also estimate the resection margins of a specimen.

Special histochemical techniques can be used to reveal material in the cell itself as well as in the tumor background (e.g., mucin). In alveolar soft part sarcoma (Fig. 6.7), the cells contain rod-shaped intracytoplasmic crystals that can be easily demonstrated with PAS staining (Fig. 6.8), which is pathognomonic of the lesion.

6.5.2 Immunohistochemistry

As it is already mentioned, morphology is the gold standard of diagnosis. For many years the diagnosis is made solely on basis of the mor-

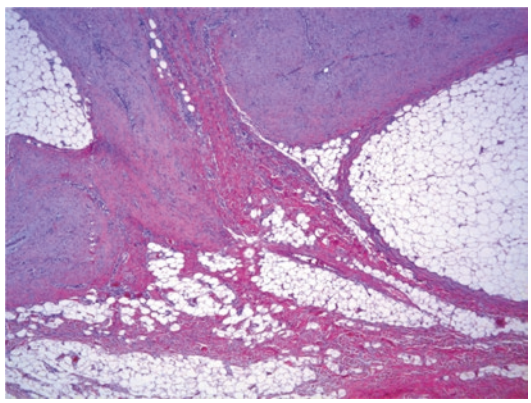

Fig. 6.5 HE, 40×. Desmoid tumor with characteristic infiltrating growth pattern in the surrounding fibro-adipose tissue

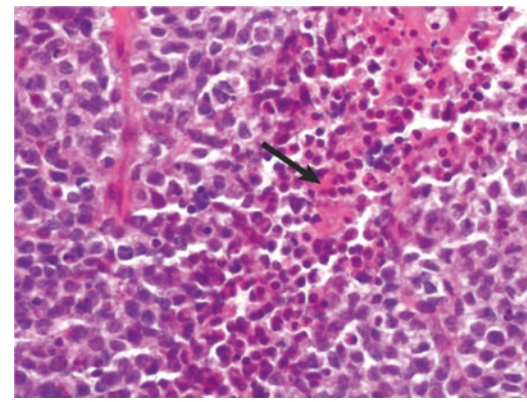

Fig. 6.6 HE, 400×. A case of a small blue round cell tumor (in this case alveolar rhabdomyosarcoma) with a central area of necrosis (*arrow*)

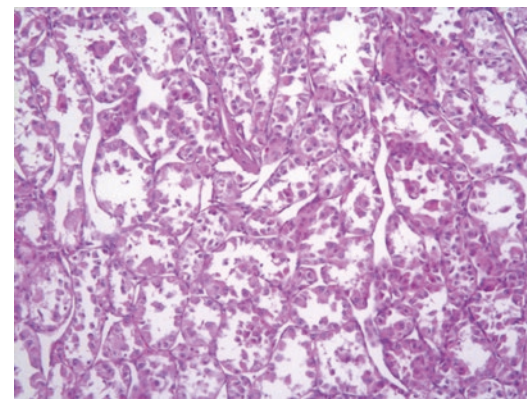

Fig. 6.7 HE, 200×. Alveolar growth pattern in a case of alveolar soft part sarcoma

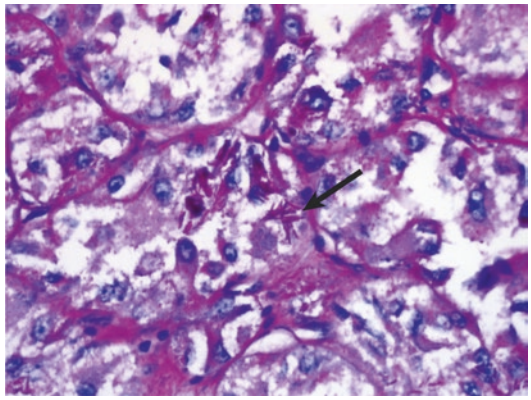

Fig. 6.8 PAS, 400×. Alveolar soft part sarcoma with rod-shaped intracytoplasmic crystals (arrow)

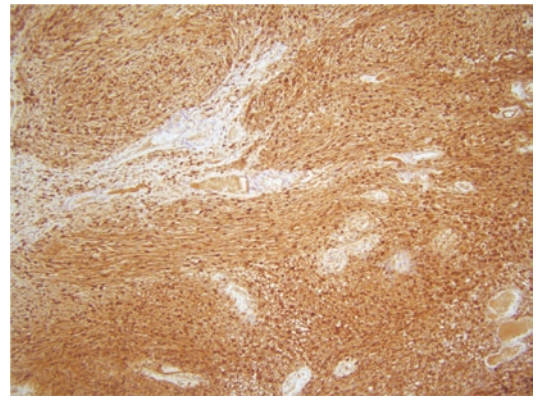

Fig. 6.9 S100 (DAB), 100×. Strong and diffuse, nuclear, and cytoplasmic staining in all tumoral cells, characteristic of a schwannoma

phology. It is apparent that many of the subtypes that exist nowadays would not be recognized if there was no possibility of further examination. Immunohistochemistry uses antibodies that are specific to epitopes located on the cells of interest. The antibodies are not specific for malignancy with some exceptions that will be discussed further. That means antibodies indicate the type of cell differentiation in nonmalignant cells but also in tumor cells arising from this type, which will also stain for the same antibody. For instance, endothelial cells stain for CD31; thus, angiosarcomas will stain for the same marker. Combining morphology and immunohistochemistry may allow a more precise diagnosis. However, many tumors present nonspecific positive staining for markers of another differentiation lineage, and unfortunately most antibodies are not specific to one differentiation line. A typical example is S100, an antibody that is widely used in everyday practice. In soft tissue pathology, S100 is known for its strong and diffuse positivity in schwannomas (Fig. 6.9). It stains in neural crest-derived tissue (such as Schwann cells, melanocytes, glial cells), in adipocytes, chondrocytes, dendritic cells, Langerhans cells, macrophages, and myoepithelial and melanocytic cells. This makes things complicated because an undifferentiated tumor with S100 positivity comprises a wide differential diagnosis. Furthermore, tumor cells can lose the antibody expression that reveals the differentiation line, making sometimes the diagnosis impossible or one of exclusion. Less than half of the malignant peripheral nerve sheath tumors (MPNSTs) stain positive for S100, and the staining is usually focal. Diffuse staining for S100 is rarely compatible with conventional MPNSTs and should raise the possibility of other tumors [2].

It is thus of paramount importance to have immunohistochemical markers that are specific and sensitive for the different lines of cell differentiation or for the different tumor types. Nowadays, new antibodies have been added in the armamentarium of a soft tissue pathologist. Some of the most important ones are anti-MDM2 and CDK4. Atypical lipomatous tumor/well-differentiated liposarcoma (ALT/WDLPS) and dedifferentiated liposarcoma (DDLPS) display amplification of MDM2 and CDK4 genes that are located in chromosome 12q13-15. By immunohistochemistry, overexpression of MDM2 and CDK4 is indicated by nuclear staining for the corresponding antibodies (Fig. 6.10). This positivity is very sensitive for ALT/WDLPS and DDLPS and shows a strong correlation with the gene amplification status [33]. Still, as the majority of antibodies are used in pathology, they are not specific to these entities. It has been shown that intimal sarcomas of pul-

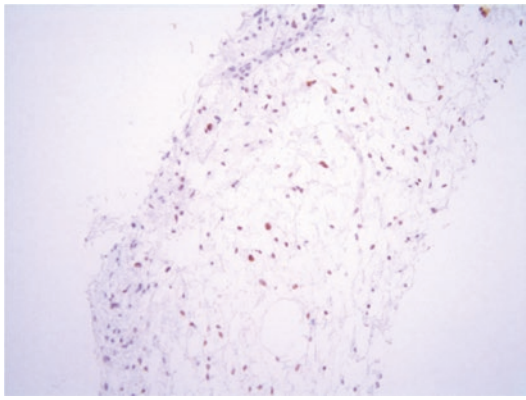

Fig. 6.10 MDM2 (DAB), 200×. Core needle biopsy with nuclear immunoreactivity of the cells for MDM2. Case of a WDLPS

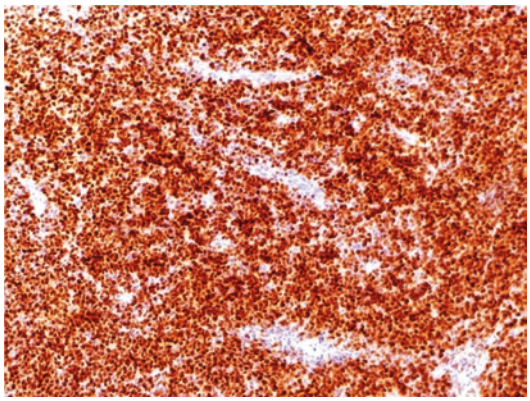

Fig. 6.11 Myogenin (DAB), 200×. Nuclear staining in almost every tumor cell in a case of alveolar rhabdomyosarcoma

monary artery show consistent genetic alteration (gains and amplifications in the 12q13-14 region) and overexpression of the MDM2 gene [34]. Very recently it has been demonstrated that almost half of the MPNSTs exhibit loss of histone H3K27 trimethylation (H3K27me3) which can be highlighted immunohistochemically by loss of nuclear staining for the corresponding antibody. H3K27me3 loss although not very sensitive is a highly specific marker for malignant peripheral nerve sheath tumor, and immunohistochemistry may be useful in differential diagnosis from other high-grade spindle cell sarcomas [35].

There are many novel antibodies with very promising results in defining diagnosis, but one has to be aware of their limitations, as most of them are not entirely specific to one entity or differentiation line.

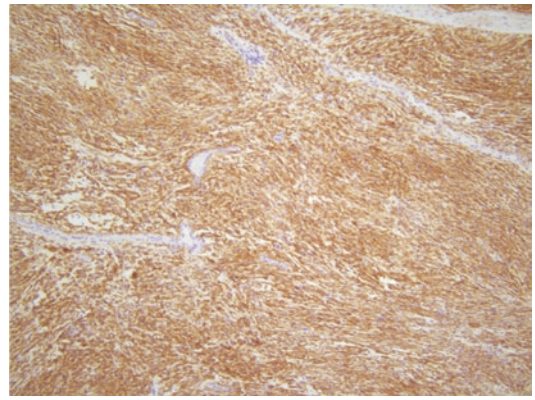

Fig. 6.12 DOG1 (DAB), 100×. This staining is very specific for GISTs

Jason Hornick et al. separated the novel antibodies into three categories: (1) lineage-restricted transcription factors, (2) protein correlates of molecular alterations, and (3) diagnostic markers identified by gene expression profiling [36], emphasizing on a close correlation of the immunohistochemical profile to the cytogenetic and molecular events in the tumors (Table 6.1) (Figs. 6.9, 6.10, 6.11 and 6.12).

6.6 Role of Genetics and Molecular Studies in the Diagnoses of Soft Tissue Tumors

6.6.1 Genetic Alterations in Soft Tissue Tumors

Over the last few decades, remarkable advances are made in the understanding of molecular biology of the tumors. This paved the way for improving our diagnostic effectiveness, by defining the underlying genes and the corresponding pathways involved in tumorigenesis. Already in the previous WHO edition of 2002, 11 % of all benign and malignant tumors presented with a karyotypic abnormality, whereas an additional 19 % was also described in the corresponding molecular findings [37].

Table 6.1 Immunohistochemical antibodies and most common expression in soft tissue

Immuunohistochemical marker	Soft tissue type
Myogenin, MyoD1	Skeletal muscle differentiation
ERG	Endothelial cells
Brachyury	Chordoma
β-catenin	Desmoid tumor
INI1(loss of expression)	Epithelioid sarcoma
STAT6	Solitary fibrous tumor
DOG1	GIST
ALK	Inflammatory myofibroblastic tumor
MDM2/CDK4	ALT/WDLPS/DDLPS
MUC4	Low-grade fibromyxoid sarcoma
GLUT1	Congenital vascular malformation

Many soft tissue tumors harbor a recurrent chromosomal translocation caused by rearrangement of part of genes between nonhomologous chromosomes. This event lead to development of fusion genes which in turn encodes altered proteins that are oncogenic. The most extensively studied translocations relate to Ewing sarcoma. The majority of these sarcomas demonstrate rearrangement between chromosomes 11 and 22, namely, a t(11;22)(q24;q12) [38] or a t(11;22)(q22;q12) [39] rearrangement that results in EWSR1-FLI1 or EWSR1-ERG fusion gene, respectively. The EWSR1 gene located in the q12 domain of chromosome 22 can rarely present translocations with different partner genes located at different chromosomes resulting in a number of other fusion proteins which are also described in Ewing sarcoma [40]. In addition, EWSR1 gene translocations are involved in a variety of non-Ewing sarcomas. For instance, myxoid liposarcoma can show a t(12;22)(q13;q12) reciprocal translocation resulting in a EWSR1-CHOP fusion protein [41].

Another molecular event that is observed in sarcomas is gene amplification. The most illustrative examples are atypical lipomatous tumor/well-differentiated liposarcoma (ALT/WDLPS) and dedifferentiated liposarcoma (DDLPS). These entities are characterized by amplified sequences in the region q14-15 of chromosome 12 where are located the murine double minute (MDM2) and the cyclin-dependent kinase 4 (CDK4) genes. Co-amplification of those genes represents the hallmark for ALT/WDLPS and DDLPS [42], although recently it has also been described in other entities as well, such as intimal sarcoma to name one [43].

A gene mutation is a permanent alteration in the DNA sequence that makes up a gene. It can affect a single base pair or larger segments of the DNA band. Gastrointestinal stromal tumor (GIST) is a mesenchymal neoplasm that is believed to arise from or is differentiated toward interstitial cell of Cajal. It is proven that these neoplasms can harbor a somatic oncogenetically activating mutation. The vast majority demonstrate KIT (which is a proto-oncogene receptor tyrosine kinase) mutations on exon 11. This can be an insertion, a deletion, or a missense mutation. After this initial discovery, three other less frequent hot spots came into light, regarding exons 9, 13, and 17 [44]. PDGFRA gene encodes platelet-derived growth factor receptor A. A small percentage of GIST that does not show KIT mutations can demonstrate a PDGFRA mutation. The exons involved in this case are 12, 14, and 18 with the last being the most common one [44]. Both KIT and PDGFRA are driver mutations and are presumed to be the initiating oncogenic event. These mutations are mutually exclusive, namely, when one happens, the other is not present. The overall mutation frequency for KIT and PDGFA is 86 % with 14 % being wild type. Nowadays it is known that many of those wild-type GISTs contain another mutation, with most extensively described the BRAF V600E mutation [44].

From a genetical point of view, sarcomas are divided in two groups. First is the group with a simple karyotype that presents one main genetic alteration. As previously described, this alteration can be either a somatic mutation, or a gene amplification, or a recurrent translocation, or even an intergene deletion. Second are those presenting with more complex karyotypes [37,

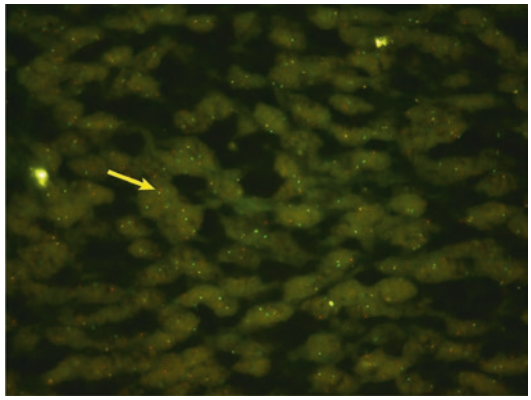

Fig. 6.13 FISH by synovial sarcoma. SYT break-apart probe, showing splitting of red and green signals (By Dr. Karen Zwaenepoel, biomedical scientist, department of pathology, University Hospital of Antwerp) (Color figure online)

45–48]. This last group represents almost two-thirds of soft tissue sarcomas and shows aberrant chromosomal events but no recurrent reciprocal translocations. Most demonstrate mutations involving p53 gene and retinoblastoma gene [45, 46, 48].

6.6.2 Molecular Techniques in Clinical Practice

Three main technical approaches are nowadays used in clinical practice regarding soft tissue tumors. Those are conventional cytogenetic analysis, fluorescence in situ hybridization (FISH) and Reverse Transcription Polymerase Chain Reaction (RT-PCR) [37, 45].

Conventional cytogenetic analysis or simply karyotyping aims to detect numerical and/or large structural chromosome abnormalities in metaphase cells. Both primary and secondary changes can be identified. This study is limited to fresh, not fixated, sterile tumor tissue and demands special culture for the tumor cells to grow.

FISH detects the presence, absence, relative positioning, and/or the copy number of specific DNA segments by fluorescence microscopy. It can be performed on either fresh or formalin-fixed and paraffin-embedded (FFPE) tissue. In contrast to the karyotyping, this method requires the knowledge of the specific target examined. FISH testing uses dual-color/fusion or dual-color/break-apart probes to detect specific rearrangements, involving a variety of translocation events (Fig. 6.13). There are also the locus-specific probes coupled with a control probe usually pointing the centromere of the chromosome and aim to identify gene amplifications or losses.

RT-PCR uses specific primers to copy or amplify a small section of a DNA or RNA sequence. It is quick and simple and can be performed on either snap-frozen or FFPE material. Its role in soft tissue pathology is to identify chimeric or fusion genes as well as oncogenic mutations.

Next-generation sequencing (NGS) takes nowadays more and more part in molecular biology of human tissue. It is a high-throughput DNA sequencing technique that aims to investigate simultaneously in the same specimen a large number of mutation genes that are proven to cause tumorigenesis. It can be performed on FFPE tissue which makes this technique even more applicable. The advantage of this technique is that different genetic aberrations can be tested simultaneously. This technique requires high-quality DNA/RNA.

6.6.3 Role of Molecular Biology in Soft Tissue Tumors

6.6.3.1 Diagnosis

The ultimate goal of the pathologist is to give the lesion a name. This happens through three main steps. The first step consists of seeing and recognizing. That means for an experienced pathologist to recognize immediately the morphology that is unique for the lesion and allows him (or her) to classify it as such. Secondly, when the morphology is not typical enough and creates diagnostic doubts to the pathologist, the use of immunohistochemistry is mandatory. In any case a confident diagnosis is made by correlating

pathological findings with the clinical and radiological image.

Yet for a relative large amount of entities, the diagnosis remains very difficult, as they present with similar morphological and immunohistochemical characteristics. For instance, most soft tissue neoplasms present with a spindle cell morphology. A monophasic synovial sarcoma is thus a spindle cell neoplasm with no striking pleomorphism and with no specific immunohistochemical profile. It can be positive for CD99 which is also expressed in a large variety of other tumors. The expression of EMA and cytokeratin can be very limited or even absent in cases of monophasic synovial sarcoma. Given the right clinical and radiological information, one can suspect the diagnosis. The identification of the molecular event that happens in these tumor is often necessary for establishing the definitive diagnosis: in this case a t(X;18) rearrangement results in a SS18-SSX fusion gene that is highly specific and sensitive for synovial sarcomas.

Moreover, molecular analysis can help to differentiate between benign and not benign entities. For instance, a spindle cell/pleomorphic lipoma can sometimes be confused with an ALT/WDLPS or rarely with DDLPS when the lipomatous component is very scant. Co-amplification of the MDM2 and CDK4 genes is observed only in ALT/WDLPS and DDLPS, and in this way, a pleomorphic lipoma can be excluded.

Low-grade fibromyxoid sarcoma is a morphological indolent entity consisting of slender, spindle cells with alternating hypocellular areas, resembling perineurioma. More interestingly these tumors can express EMA, as do perineuriomas. In the past low-grade fibromyxoid sarcomas were often misdiagnosed as perineuriomas or other benign fibrous or neural proliferations. We now know that those are malignant tumors that eventually can metastasize even after decade(s). RT-PCR or FISH for detection of FUS-CREB3L2 fusion can be useful to distinguish those entities [45].

6.6.3.2 Prognosis

In addition the knowledge of the genetic profile of a tumor can be of prognostic value. Alveolar rhabdomyosarcoma (ARMS) is an aggressive malignant neoplasm of the childhood. There are two main fusion proteins described in ARMS, both involving FOXO1 on chromosome 13, either with PAX3 on chromosome 2 or with PAX7 on chromosome 1. The presence of a PAX3-FOXO1 fusion was associated with a worse prognosis compared to the PAX7-FOXO1 fusion [37, 45, 47, 49, 50]. Moreover, ARMS without a PAX3- or PAX7-FOXO1 fusion had a more favorable outcome, similar to embryonal rhabdomyosarcomas when given therapy designed for intermediate-risk rhabdomyosarcomas [37, 51, 52].

In Ewing sarcomas type 1 EWS-FLI1 fusion, which is the most common fusion type, is a positive predictor of overall survival compared to other fusion types [45, 46, 53].

6.6.3.3 Treatment

Treatment of soft tissue tumors is a difficult task that requires a multidisciplinary approach with surgeons, radiologists, oncologists, and pathologists. The gold standard of treatment is surgery for the excision of the lesion. Yet, in many cases of high-grade or unrespectable tumors, a combination with chemotherapy and/or radiotherapy must be considered. Advances in the understanding of molecular mechanisms of soft tissue tumors can lead in the implementation of targeted therapy.

Imatinib mesylate, was originally developed to target BCR-ABL kinase in chronic myelogenous leukemia. Imatinib can also inhibit a small number of related kinases, such as KIT, PDGFRA, and PDGFB. The identification of KIT and PDGFA mutations in the majority of GISTs makes these tumors a good candidate for this therapy [44].

In addition, dermatofibrosarcoma protuberans (DFSPs) show a t(17;22)(q22;q13) translocation. This generates a COL1A1-PDGFB fusion gene

Table 6.2 Current genetics in soft tissue tumors

Soft tissue tumor	Most common genetic alteration	Gene(s) involved
Atypical lipomatous tumor/well-differentiated liposarcoma Dedifferentiated liposarcoma	Amplified sequencing in the 12q14-15 region	Amplification of MDM2 and CDK4 genes
Myxoid liposarcoma	t(12;16)(q13;p11)	FUS-DDIT3 fusion
Nodular fasciitis	t(17;22)(p13;q13)	MYH9-USP6 fusion
Desmoid-type fibromatosis	Sporadic lesions: mutations in the gene encoding β-catenin (CTNNB1) Gardner-type [a]FAP: mutations of the APC gene	
Dermatofibrosarcoma protuberans	t(17;22)(q22;q13)	COL1A1-PDGFB fusion
Inflammatory myofibroblastic tumor	2p23 rearrangements with different partners	ALK gene
Low-grade fibromyxoid sarcoma	t(7;16)(q33;p11)	FUS-CREB3L2 fusion
Infantile fibrosarcoma	t(12;15)(p13;q25)	ETV6-NTRK3 fusion
Alveolar rhabdomyosarcoma	t(2;13)(q35;q14) t(1;13)(p36;q14)	PAX3-FOXO1A fusion PAX7-FOXO1A fusion
Epithelioid hemangioendothelioma	t(1;3)(p36;q25)	WWTR1-CAMTA1 fusion
Gastrointestinal stromal tumor	Mutations in the KIT and PDGFRA genes	
Neurofibroma Malignant peripheral nerve sheath tumor	In patients with NF1: involving the 17q11.2 region	Germline alterations of the NF1 gene
Angiomatoid fibrous histiocytoma	t(2;22)(q33;q12)	EWSR1-CREB1 fusion
Myoepithelioma	t(6;22)(p21;q12) t(1;22)(q23;q12)	EWSR1-POU5F1 fusion EWSR1-PBX1 fusion
Synovial sarcoma	t(X;18)(p11;q11)	SS18-SSX(1,2 or 4)
Alveolar soft part sarcoma	t(X;17)(p11;q25)	TFE3-ASPL fusion
Clear cell sarcoma of soft tissue	t(12;22)(q13;q12)	EWSR1-ATF1 fusion
Extraskeletal myxoid chondrosarcoma	t(9;22)(q22;q12)	EWSR1-NR4A3 fusion
Desmoplastic small round cell tumor	t(11;22)(p13;q12)	EWSR1-WT1 fusion
Intimal sarcoma	Amplified sequencing in the 12q12-15 region	Amplification of MDM2 and CDK4 genes
Ewing sarcoma/primitive neuroectodermal tumor (PNET)	t(11;22)(q24;q12) t(21;22)(q22;q12)	EWSR1-FLI1 fusion EWSR1-ERG fusion

[a]Familial adenomatous polyposis

which results in the constitutional upregulation of PDGFB expression. DFSPs have hence been treated with imatinib with promising results [54] (Table 6.2).

6.7 World Health Organization (WHO) Classification of Tumors 2013

The WHO provides a classification of soft tissue tumors essentially based on the line of differentiation of each neoplasm. The advances in cytogenetic and molecular genetics have led to better understanding of some entities which in turn resulted in modifications in the new WHO book of 2013 [2]. This new classification and its implication for the radiologist will be further discussed in Chap. 11 of this book.

6.8 Pathology Grading and Staging

One of the most important objectives of pathology in addition to tissue diagnosis or characterization is to determine the tumors aggressiveness, namely, its metastatic potential, as well as to provide information about the most effective treatment for the patient. It is shown that grade and stage are better predictors of outcome than histologic type.

6.8.1 Common Used Grading Classifications

There are two main grading systems, provided by the National Cancer Institute (NCI) [55] and the Fédèration Nationale des Centres de Lutte Contre le Cancer (FNCLCC) [56]. NCI is based on histologic type, location, and necrosis, while FNCLCC is based on histologic type/differentiation, necrosis, and mitotic activity. Both are three-grade system, where grade 1 represents the most and grade 3 the least favorable edge of the scale. In a comparative study, the FNCLCC system showed slightly increased ability to predict distant metastasis development and tumor mortality [57]. The weakness of this system is the definition of differentiation, since some tumors have no normal tissue counterpart, e.g., epithelioid sarcoma [58]. Mitotic activity is counted in ten consecutive high-power fields (HPF) in a hot spot area. Hypocellular areas as well as areas with necrosis and ulceration should be avoided [3] as the number of mitosis in those last ones can be misleadingly increased. Fixation status as previously mentioned can also affect the number of mitoses. Necrosis should be evaluated macroscopically and microscopically. One has to bear in mind that previous chemotherapy or radiation therapy can influence grading by reducing the amount of mitoses and increasing necrosis.

Grading should not be applied to tumors of intermediate malignancy. Furthermore, there are some rare sarcomas, such as epithelioid sarcoma, clear cell sarcoma, and alveolar soft part sarcoma, that are very difficult to grade. It seems that for those types, the histologic classification plays a more important role than grade in prognosis. The same applies to pediatric sarcomas, namely, rhabdomyosarcomas and Ewing/PNET tumors [3, 58]. Especially for rhabdomyosarcomas, subclassification provides also prognostic information, as botryoid and spindle cell/sclerosing show better clinical outcome than alveolar rhabdomyosarcoma.

The application of grade on core needle biopsies has been an issue of controversy over the years. With the universal use of core needle biopsy, pathologists are more and more asked to apply a grading system on a restricted amount of material. Although studies have shown that Tru-cut biopsy is sensitive and sensitive in subtyping and grading soft tissue sarcomas [59], this of course depends on how representative is the tissue sample. Given that the same tumor can show different degrees of differentiation ranging from low to high grade, it is obvious that only high-grade tumors can be successfully graded. A seemingly histologically low-grade tumor can radiologically show high-grade features. Moreover, some tumors may show high mitotic rate indicating malignancy but are otherwise benign in nature (e.g., nodular fasciitis) and therefore excluded from grading. Like previously mentioned, the final report depends largely on correlation with the clinical and imaging data, and multidisciplinary approach is therefore recommended in this regard (Table 6.3).

6.8.2 Staging

The staging system that is widely used is the TNM classification. The letter "T" refers to the characteristics of the tumor, "N" stands for the lymph nodes status, and "M" stands for the pres-

Table 6.3 FNCLCC grading system: definition of parameters

Tumor differentiation
Score 1: Sarcomas closely resembling normal adult mesenchymal tissue (e.g., well-differentiated liposarcoma)
Score 2: Sarcomas for which histologic typing is certain (e.g., myxoid liposarcoma)
Score 3: Embryonal and undifferentiated sarcomas, sarcomas of doubtful type, synovial sarcomas, osteosarcomas, PNET
Mitotic count
Score 1: 0–9 mitoses per 10 HPF[a]
Score 2: 10–19 mitoses per 10 HPF
Score 3: ≥20 mitoses per 10 HPF
Tumor necrosis
Score 0: No necrosis
Score 1: <50 % tumor necrosis
Score 2: ≥50 % tumor necrosis
Histologic grade
Grade 1: Total score 2, 3
Grade 2: Total score 4, 5
Grade 3: Total score 6, 7, 8

[a]*HPF* high-power field

ence or absence of metastasis. The "T" category includes the size and the depth of the lesion. The cutoff for size is the 5 cm maximum diameter of the lesion. Tumors that are 5 cm or less are classified as T1, while tumors more than 5 cm are classified as T2. T1 and T2 are subdivided into T1a and T2a for superficial located tumors and into T1b and T2b for deep-seated tumors. The anatomical margin between superficial and deep tumors is the superficial fascia.

One can use also the prefixes "m," "r," and "y." "m" is applied for multiple tumors of the same type, "r" for recurrent, and "y" for tumors that have previously been treated.

Key Points

1. It is important for the pathologist to describe all parameters contributing to the correct diagnosis, such as macroscopical (e.g., size) and microscopical features (e.g., mitotic activity, necrosis if present) of the tumor and ancillary techniques (immunohistochemistry, molecular testing).
2. Depending on the quality and the amount of the material, the histologic type, subtype, and grade (in case of malignancy) should be mentioned in the report.
3. A multidisciplinary cooperation is needed for obtaining correct tissue samples, grading, and characterization of soft tissue tumors.
4. In small biopsy specimens in which the material is not representative or insufficient, the pathologist has to make clear that no final diagnosis can be achieved and ask for more tissue. This may avoid diagnostic errors that may be harmful for the treatment of the patient.
5. The resection margins have to be described in large specimens. If not possible, this has to be discussed with the other members of the multidisciplinary team.

References

1. Siegel RL, Miller KD, Jemal A (2016) Cancer statistics, 2016. CA Cancer J Clin 66:7
2. Fletcher CDM, Bridge JA, Hogendoorn PCW, Mertens F (2013) WHO classification tumours of soft tissue and bone. IARC Press, Lyon
3. Coindre JM (2006) Grading of soft tissue sarcomas: review and update. Arch Pathol Lab Med 30(10):1448–1453
4. Coindre JM, Terrier P, Guillou L, Le Doussal V, Collin F, Ranchère D, Sastre X, Vilain MO, Bonichon F, N'Guyen Bui B (2001) Predictive value of grade for metastasis development in the main histologic types of adult soft tissue sarcomas: a study of 1240 patients from the French Federation of Cancer Centers Sarcoma Group. Cancer 91(10):1914–1926
5. Gaynor JJ, Tan CC, Casper ES, Collin CF, Friedrich C, Shiu M, Hajdu SI, Brennan MF (1992) Refinement of clinicopathologic staging for localized soft tissue sarcoma of the extremity: a study of 423 adults. J Clin Oncol 10(8):1317–1329
6. Heise HW, Myers MH, Russell WO, Suit HD, Enzinger FM, Edmonson JH, Cohen J, Martin RG, Miller WT, Hajdu SI (1986) Recurrence-free survival time for surgically treated soft tissue sarcoma patients: multivariate analysis of five prognostic factors. Cancer 57(1):172–177
7. Markhede G, Angervall L, Stener B (1982) A multivariate analysis of the prognosis after surgical treatment of malignant soft-tissue tumors. Cancer 49(8):1721–1733
8. Pisters PW, Leung DH, Woodruff J, Shi W, Brennan MF (1996) Analysis of prognostic factors in 1,041 patients with localized soft tissue sarcomas of the extremities. J Clin Oncol 14(5):1679–1689
9. Saddegh MK, Lindholm J, Lundberg A, Nilsonne U, Kreicbergs A (1992) Staging of soft-tissue sarcomas: prognostic analysis of clinical and pathological features. J Bone Joint Surg Br 74(4):495–500
10. Zagars GK, Ballo MT, Pisters PW, Pollock RE, Patel SR, Benjamin RS, Evans HL (2003) Prognostic factors for patients with localized soft-tissue sarcoma treated with conservation surgery and radiation therapy: an analysis of 1225 patients. Cancer 97(10):2530–2543
11. Aboulafia AJ (2008) Biopsy. In: Schwartz HS (ed) Orthopaedic knowledge update: musculoskeletal tumors 2. AAOS, Rosemont, pp 3–11
12. Kasraeian S, Allison DC, Ahlmann ER, Fedenko AN, Menendez LR (2010) A comparison of fine-needle aspiration, core biopsy, and surgical biopsy in the diagnosis of extremity soft tissue masses. Clin Orthop Relat Res 468(11):2992–3002
13. Rougraff BT, Aboulafia A, Biermann JS, Healey J (2009) Biopsy of soft tissue masses: evidence-based medicine for the Musculoskeletal Tumor Society. Clin Orthop Relat Res 467:2783–2791

14. Bell WC, Young ES, Billings PE, Grizzle WE (2008) The efficient operation of the surgical pathology gross room. Biotech Histochem 83(2):71–82
15. Start RD, Layton CM, Cross SS, Smith JH (1992) Reassessment of the rate of fixative diffusion. J Clin Pathol 45(12):1120–1121
16. Werner M, Chott A, Fabiano A, Battifora H (2000) Effect of formalin tissue fixation and processing on immunohistochemistry. Am J Surg Pathol 24(7):1016–1019
17. Pelstring RJ, Allred DC, Esther RJ, Lampkin SR, Banks PM (1991) Differential antigen preservation during tissue autolysis. Hum Pathol 22:237–241
18. Cross SS, Start RD, Smith JHF (1990) Does delay in fixation affect the number of mitotic figures in processed tissue? J Clin Pathol 43:597–599
19. Start RD, Flynn MS, Cross SS, Rogers K, Smith JHF (1991) Is the grading of breast carcinoma affected by delay in fixation? Virchows Arch (Pathol Anat) 419:475–477
20. Nakazawa J, Rosen P, Lowe N, Lattes R (1968) Frozen section diagnosis experience in 3000 cases. Am J Clin Pathol 49:41–51
21. Bell WC, Sexton KC, Grizzle WE (2009) How to efficiently obtain human tissues to support specific biomedical research projects. Cancer Epidemiol Biomarkers Prev 18(6):1676–1679
22. Huang J, Qi R, Quackenbush J, Dauway E, Lazaridis E, Yeatman T (2001) Effects of ischemia on gene expression. J Surg Res 99:222–227
23. Jewell SD, Srinivasan M, McCart LM, Williams N, Grizzle WH, LiVolsi V, MacLennan G, Sedmak DD (2002) Analysis of the molecular quality of human tissues: an experience from the Cooperative Human Tissue Network. Am J Clin Pathol 118:733–741
24. Spruessel A, Steimann G, Jung M, Lee SA, Carr T, Fentz AK, Spangenberg J, Zornig C, Juhl HH, David KA (2004) Tissue ischemia time affects gene and protein expression patterns within minutes following surgical tumor excision. Biotechniques 36:1030–1037
25. Bauminger E, Cohen S, Nowik I, Ofer S, Yariv J (1983) Dynamics of heme iron in crystals of metmyoglobin and deoxymyoglobin. Proc Natl Acad Sci 80:736–740
26. Doster W, Cusack S, Petry W (1989) Dynamical transition of myoglobin revealed by inelastic neutron scattering. Nature 337:754–756
27. Hartmann H, Parak F, Steigemann W, Petsko G, Ponzi DR, Frauenfelder H (1982) Conformational substates in a protein: structure and dynamics of metmyoglobin at 80 K. Proc Natl Acad Sci 79:4967–4971
28. Loncharich RJ, Brooks BR (1990) Temperature dependence of dynamics of hydrated myoglobin: comparison of force field calculations with neutron scattering data. J Mol Biol 215:439–455
29. More N, Daniel RM, Petach HH (1995) The effect of low temperatures on enzyme activity. Biochem J 305:17–20
30. Rasmussen BF, Stock AM, Ringe D, Petsko GA (1992) Crystalline ribonuclease a loses function below the dynamical transition at 220 K. Nature 357:423–424
31. Tilton RF Jr, Dewan JC, Petsko GA (1992) Effects of temperature on protein structure and dynamics: X-ray crystallographic studies of the protein ribonuclease-A at nine different temperatures from 98 to 320 K. Biochemistry 31:2469–2481
32. Hubel A, Spindler R, Skubitz AP (2014) Storage of human biospecimens: selection of the optimal storage temperature. Biopreserv Biobank 12(3):165–175
33. Binh MB, Sastre-Garau X, Guillou L, de Pinieux G, Terrier P, Lagacé R, Aurias A, Hostein I, Coindre JM (2005) MDM2 and CDK4 immunostainings are useful adjuncts in diagnosing well-differentiated and dedifferentiated liposarcoma subtypes: a comparative analysis of 559 soft tissue neoplasms with genetic data. Am J Surg Pathol 29(10):1340–1347
34. Bode-Lesniewska B, Zhao J, Speel EJ, Biraima AM, Turina M, Komminoth P, Heitz PU (2001) Gains of 12q13-14 and overexpression of mdm2 are frequent findings in intimal sarcomas of the pulmonary artery. Virchows Arch 438(1):57–65
35. Schaefer IM, Fletcher CD, Hornick JL (2016) Loss of H3K27 trimethylation distinguishes malignant peripheral nerve sheath tumors from histologic mimics. Mod Pathol 29:4–13
36. Hornick JL (2014) Novel uses of immunohistochemistry in the diagnosis and classification of soft tissue tumors. Mod Pathol 27:47–63
37. Bridge JA (2014) The role of cytogenetics and molecular diagnostics in the diagnosis of soft-tissue tumors. Mod Pathol 27(Suppl 1):S80–S97
38. Turc-Carel C, Aurias A, Mugneret F, Lizard S, Sidaner I, Volk C, Thiery JP, Olschwang S, Philip I, Berger MP et al (1988) Chromosomes in Ewing's sarcoma. I. An evaluation of 85 cases of remarkable consistency of t(11;22)(q24;q12). Cancer Genet Cytogenet 32(2):229–238
39. Sorensen PH, Lessnick SL, Lopez-Terrada D, Liu XF, Triche TJ, Denny CT (1994) A second Ewing's sarcoma translocation, t(21;22), fuses the EWS gene to another ETS-family transcription factor, ERG. Nat Genet 6(2):146–151
40. Sankar S, Lessnick SL (2011) Promiscuous partnerships in Ewing's sarcoma. Cancer Genet 204(7):351–365
41. Panagopoulos I, Höglund M, Mertens F, Mandahl N, Mitelman F, Aman P (1996) Fusion of the EWS and CHOP genes in myxoid liposarcoma. Oncogene 12(3):489–494
42. Coindre JM, Pédeutour F, Aurias A (2010) Well-differentiated and dedifferentiated liposarcomas. Virchows Arch 456(2):167–179
43. Zhang H, Macdonald WD, Erickson-Johnson M, Wang X, Jenkins RB, Oliveira AM (2007) Cytogenetic and molecular cytogenetic findings of intimal sarcoma. Cancer Genet Cytogenet 179(2):146–149

44. Rubin BP, Heinrich MC (2015) Genotyping and immunohistochemistry of gastrointestinal stromal tumors: an update. Semin Diagn Pathol 32(5):392–399
45. Antonescu CR (2006) The role of genetic testing in soft tissue sarcoma. Histopathology 48:13–21
46. Helman LJ, Meltzer P (2003) Mechanisms of sarcoma development. Nat Rev Cancer 3(9):685–694
47. Norberg SM, Movva S (2015) Role of genetic and molecular profiling in sarcomas. Curr Treat Options Oncol 16(5):24
48. Quesada J, Amato R (2012) The molecular biology of soft-tissue sarcomas and current trends in therapy. Sarcoma 2012:849456
49. Davis RJ, D'Cruz CM, Lovell MA, Biegel JA, Barr FG (1994) Fusion of PAX7 to FKHR by the variant t(1;13)(p36;q14) translocation in alveolar rhabdomyosarcoma. Cancer Res 54:2869–2872
50. Sorensen PH, Lynch JC, Qualman SJ, Tirabosco R, Lim JF, Maurer HM, Bridge JA, Crist WM, Triche TJ, Barr FG (2002) PAX3-FKHR and PAX7-FKHR gene fusions are prognostic indicators in alveolar rhabdomyosarcoma: a report from the children's oncology group. J Clin Oncol 20:2672–2679
51. Parham DM, Ellison DA (2006) Rhabdomyosarcomas in adults and children: an update. Arch Pathol Lab Med 130:1454–1465
52. Raney RB, Anderson JR, Barr FG, Donaldson SS, Pappo AS, Qualman SJ, Wiener ES, Maurer HM, Crist WM (2001) Rhabdomyosarcoma and undifferentiated sarcoma in the first two decades of life: a selective review of intergroup rhabdomyosarcoma study group experience and rationale for Intergroup Rhabdomyosarcoma Study V. J Pediatr Hematol Oncol 23:215–220
53. de Alava E, Kawai A, Healey JH, Fligman I, Meyers PA, Huvos AG, Gerald WL, Jhanwar SC, Argani P, Antonescu CR, Pardo-Mindan FJ, Ginsberg J, Womer R, Lawlor ER, Wunder J, Andrulis I, Sorensen PH, Barr FG, Ladanyi M (1998) EWS-FLI1 fusion transcript structure is an independent determinant of prognosis in Ewing's sarcoma. J Clin Oncol 16(4):1248–1255
54. Rutkowski P, Wozniak A, Switaj T (2011) Advances in molecular characterization and targeted therapy in dermatofibrosarcoma protuberans. Sarcoma 2011:959132
55. Costa J, Wesley RA, Glatstein E, Rosenberg SA (1984) The grading of soft tissue sarcomas: results of a clinicopathological correlation in a series of 163 cases. Cancer 53:530–541
56. Trojani M, Contesso G, Coindre JM, Rouesse J, Bui NB, de Mascarel A, Goussot JF, David M, Bonichon F, Lagarde C (1984) Soft tissue sarcomas of adults: study of pathological prognostic variables and definition of histopathological grading system. Int J Cancer 33:37–42
57. Guillou L, Coindre JM, Bonichon F, Nguyen BB, Terrier P, Collin F, Vilain MO, Mandard AM, Le Doussal V, Leroux A, Jacquemier J, Duplay H, Sastre-Garau X, Costa J (1997) Comparative study of the National Cancer Institute and French Federation of Cancer Centers Sarcoma Group grading systems in a population of 410 adult patients with soft tissue sarcoma. J Clin Oncol 15(1):350–362
58. Deyrup AT, Weiss SW (2006) Grading of soft tissue sarcomas: the challenge of providing precise information in an imprecise world. Histopathology 48(1):42–50
59. Hoeber I, Spillane AJ, Fisher C, Thomas JM (2001) Accuracy of biopsy techniques for limb and limb girdle soft tissue tumors. Ann Surg Oncol 8(1):80–87

Biopsy of Soft Tissue Tumors

7

J. Gielen

Contents

7.1 **Introduction** 131
7.2 **Intra- Versus Extra-Compartmental Spread** 131
7.3 **General Rules for Biopsy Safety** 133
7.4 **Diagnostic Accuracy** 133
7.5 **Immunohistochemistry** 138
7.6 **Technique and Choice of Needle** 138
Conclusion 139
References 140

7.1 Introduction

Staging of soft tissue tumors frequently includes a biopsy that is mostly performed percutaneously using imaging guidance (ultrasound, (PET)–computed tomography, or (PET)–magnetic resonance imaging). A biopsy is necessary when the orthopedic surgeon and the radiologist believe they might be dealing with a progressive process, requiring intervention [27]. Any lesion that cannot be unequivocally characterized by MRI as benign should be considered indeterminate and requires biopsy. Otherwise, unexpected manipulation of a soft tissue sarcoma can influence its biological behavior and prognosis [33]. Moreover, biopsy of soft tissue tumors with large needles involves a risk of seeding malignant cells along the needle track. Because biopsy is considered part of the surgical therapy, en bloc resection of a malignant tumor with needle track is mostly needed [25]. For this reason, centralized referral should preferably be done from the time a sarcoma is suspected, and it is recommended to perform the biopsy in the same hospital where the patient is treated.

7.2 Intra- Versus Extra-Compartmental Spread

Determination of whether the location and/or extension of a tumor is intracompartmental or extracompartmental is an important element in

J. Gielen, MD, PhD
University Hospital of Antwerp, Department of Radiology and Sports Medicine, University of Antwerp, Faculty of Medicine,
Wilrijkstraat 10, 2650 Edegem, Belgium
e-mail: jan.gielen@uza.be

© Springer International Publishing AG 2017

F.M. Vanhoenacker et al. (eds.), *Imaging of Soft Tissue Tumors*, DOI 10.1007/978-3-319-46679-8_7

staging. Extracompartmental spread and inadvertent tumor spread can be due to a poorly planned biopsy [1]. If uninvolved anatomic compartments are crossed to obtain the biopsy specimen, the result may be a more radical resection or even amputation. Therefore, knowledge of compartmental anatomy and discussion of the needle tract with the surgeon that will remove the lesion are mandatory for planning and performance of a percutaneous needle biopsy [3, 6]. For treatment of the different compartments of the upper and lower extremities, the reader is referred to the excellent article of Anderson et al. [3], whose cross-sectional diagrams of the different compartments are reprinted here (Fig. 7.1, 7.2, 7.3, 7.4, and 7.5).

Generally, the skin and subcutaneous fat, bone, para-osseous spaces, and joint spaces are regarded as a compartment. For the upper extremity, the periclavicular region, axilla, antecubital

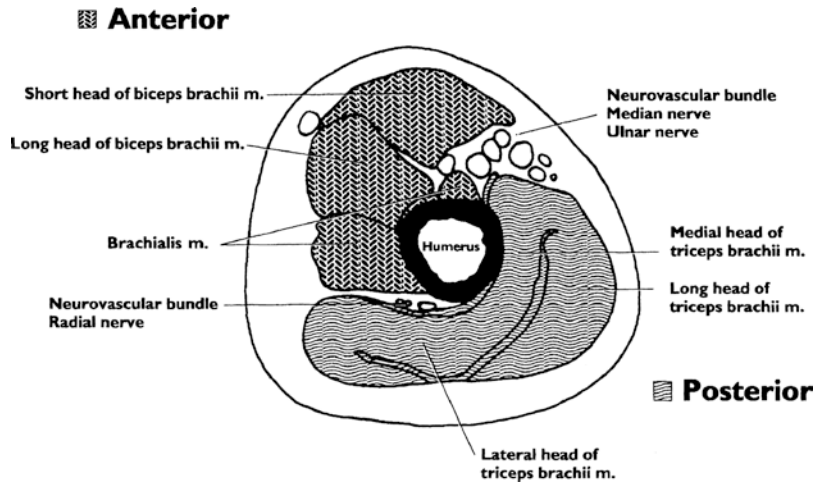

Fig. 7.1 Cross section of the mid-upper arm shows contents of anterior and posterior compartments (Reprinted from Anderson et al. [3] with permission)

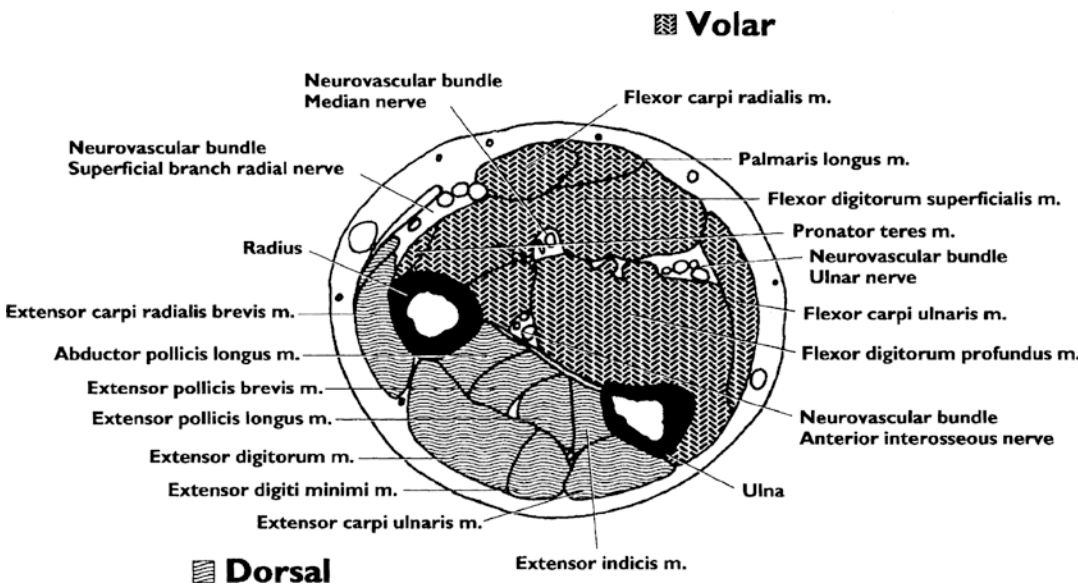

Fig. 7.2 Cross section of the mid-forearm shows contents of volar and dorsal compartments (Reprinted from Anderson et al. [3] with permission)

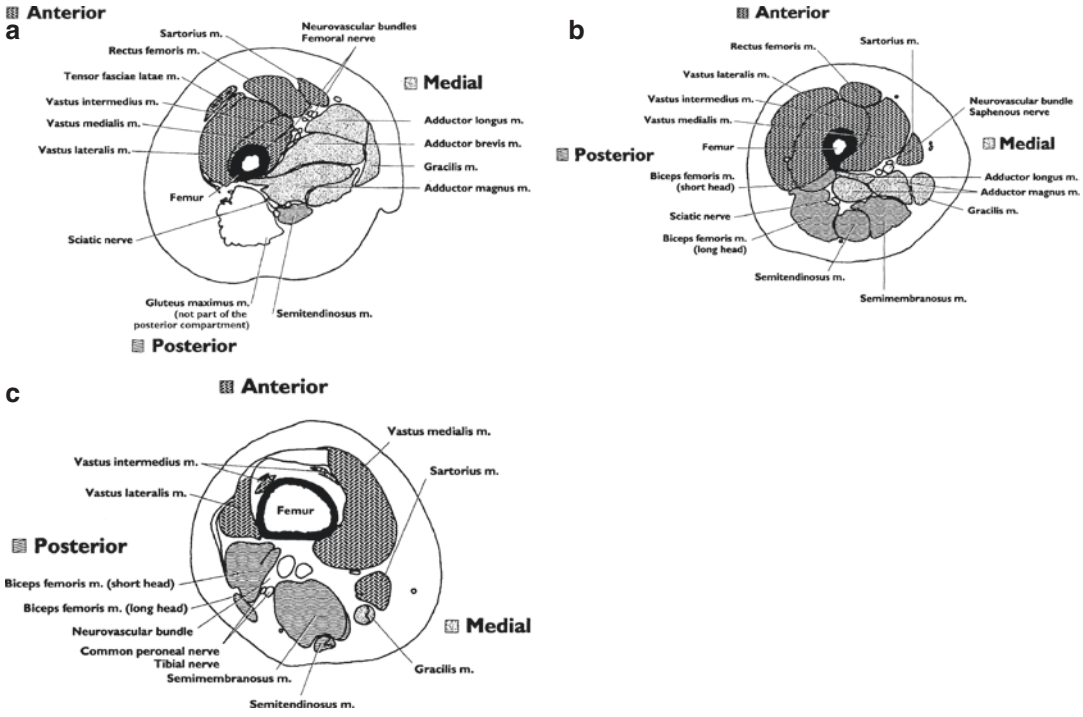

Fig. 7.3 (**a**–**c**) Cross section of the thigh shows contents and relative positions of anterior, medial, and posterior compartments at these levels. (**a**) Proximal thigh, (**b**) mid-thigh, **c** distal thigh (Reprinted from Anderson et al. [3] with permission)

fossa, wrist, and dorsum of the hand and for the lower extremity the groin, popliteal fossa, ankle, and dorsum of the foot are considered extracompartmental.

7.3 General Rules for Biopsy Safety

A CT scan with intravenous iodine contrast injection or MRI is performed to localize the lesion precisely and to plan and guide the biopsy [11]. Ultrasound with Doppler and sonoelastography may be used in superficial lesions [7]. The entry point and the pathway are determined, avoiding nerve, vascular, articular, and visceral structures (Fig 7.6).

General principles for safe percutaneous biopsy include:

1. The shortest path between the skin and the lesion should be chosen.
2. The needle should not traverse an uninvolved compartment.
3. Joint and neurovascular bundles should be avoided.
4. The anticipated needle path should be discussed with the surgeon who will be performing the definitive surgery (Fig.7.7).

7.4 Diagnostic Accuracy

Percutaneous musculoskeletal biopsy (PMSB) can be performed by fine-needle aspiration biopsy (FNAB), core needle biopsy (CNB), or open (incisional) biopsy. Excisional biopsy should be used only for small lesions (<3 cm) or when the radiologist is convinced that the lesion is benign [7, 10, 20].

It is now generally accepted that in nonhomogeneous lesions, biopsy should be planned to include vital tumor tissue that is characterized by angiogenesis on Doppler ultrasound, contrast

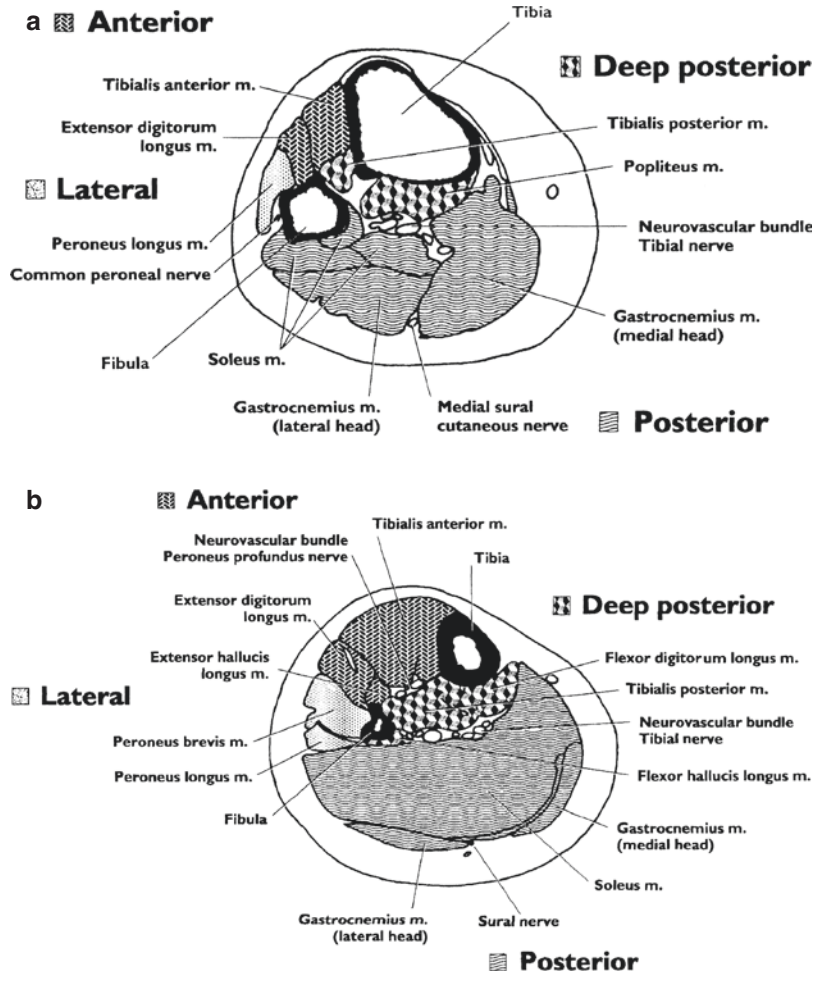

Fig. 7.4 (**a**, **b**) Lower leg. Cross section of the (**a**) proximal calf and (**b**) mid-calf shows contents of anterior, deep posterior, posterior, and lateral compartments (Reprinted from Anderson et al. [3] with permission)

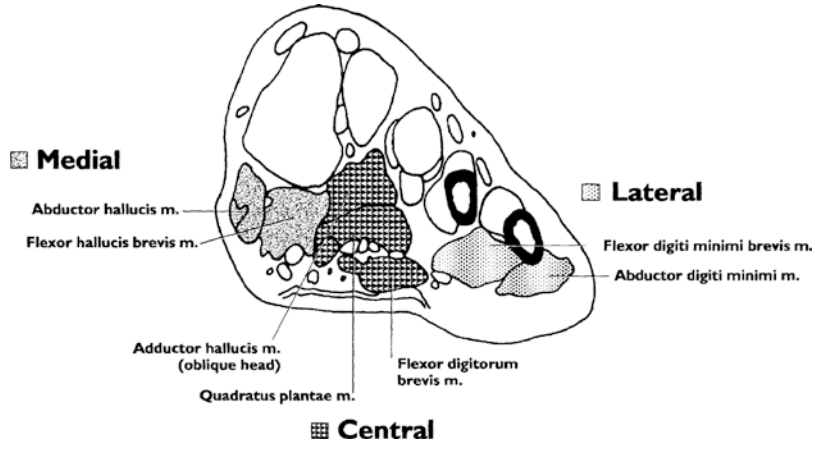

Fig. 7.5 Cross section of the foot shows contents of medial, central, and lateral compartments (Reprinted from Anderson et al. [3] with permission)

Fig. 7.6 Percutaneous core needle biopsy, with CT guidance, of a deeply seated mass lesion with intralesional calcification. Histologic examination revealed a myositis ossificans. Control examination after conservative therapy showed more typical, zonal calcification of the lesion

enhancement on CT, or MRI and/or nuclear activity on PET imaging. To improve accuracy two or multiple samples might be taken at different locations including morphologic different lesion characteristics.

Open surgical biopsy is advocated by Huvos [19], who claims that only an adequate amount of removed tissue will allow for a maximal diagnostic benefit.

Kilpatrick et al. [23] used fine-needle aspiration biopsy (FNAB) and obtained a histogenetically specific diagnosis in 93 % of cases of pediatric bone and soft tissue tumors, all of which were correctly recognized as either benign or malignant. In adults FNAB is recommended for diagnosis of tumors in the head and neck region [30] and whenever direct incisional biopsy is contraindicated [10, 13]. Gonzalez [13, 14] reported a specificity of FNAB of more than 90 %, the method being most effective when performed by an experienced pathologist. Concordance between FNAB histopathological and cytologic grading in musculoskeletal sarcomas treated by FNAB was studied by Jones et al. Although a statistically significant correlation between cytologically assigned grade and final histopathological grade is found, statistical analysis revealed only a moderate correlation between the two with an overall r value of approximately 0.57. Cytological analysis tended to undergrade in comparison to final histopathological grading. FNAB was moderately successful at predicting histopathological grading. Only analysis of nuclear atypia showed good correlation with final surgical grade [21].

Skrzynski et al. [31] performed a prospective study on the value of closed core needle biopsy (CNB) in 62 patients with soft tissue tumors or bone tumors with soft tissue extension. The diagnostic accuracy was 84 % or 96 %, respectively, for groups of patients who underwent open biopsy performed by the same surgeon. Disadvantages include a nondiagnostic biopsy, indeterminate biopsy, and potential errors in histological grade. The hospital charges for a closed core biopsy were $1106 compared with $7234 for an open biopsy! Comparable results are reported by Hodge [16] with a diagnostic accuracy of 76.9 %.

Bennert [4] evaluated the diagnostic yield of FNAB relative to that of CNB in 117 patients with soft tissue lesions (STL). FNAB was unsatisfactory in 44 patients, 22 of whom were correctly diagnosed with CNB. The author's conclusion was that FNAB gave a yield identical to that of CNB and that unsatisfactory FNAB should prompt further evaluation by CNB.

Hau et al. [15] studied the accuracy of CT-guided FNAB relative to CNB in a large number of patients ($N=359$) with musculoskeletal lesions. They found an overall accuracy of 71 %, i.e., 63 % for FNAB ($N=101$) and 74 % for CNB ($N=258$). Biopsies of 81 pelvic lesions had a higher rate of diagnostic accuracy (81 %) compared to non-pelvic sites (68 %). The lowest accuracy (61 % and 50 %, respectively) was noted in lesions of the spine and infectious diseases [15].

The best results were reported by Dupuy et al. [9], who performed 176 CNB and 45 FNAB of musculoskeletal neoplasms under CT guidance. They obtained an accuracy of 93 % for CNB and 80 % for FNAB. Complication rate was less than 1 %.

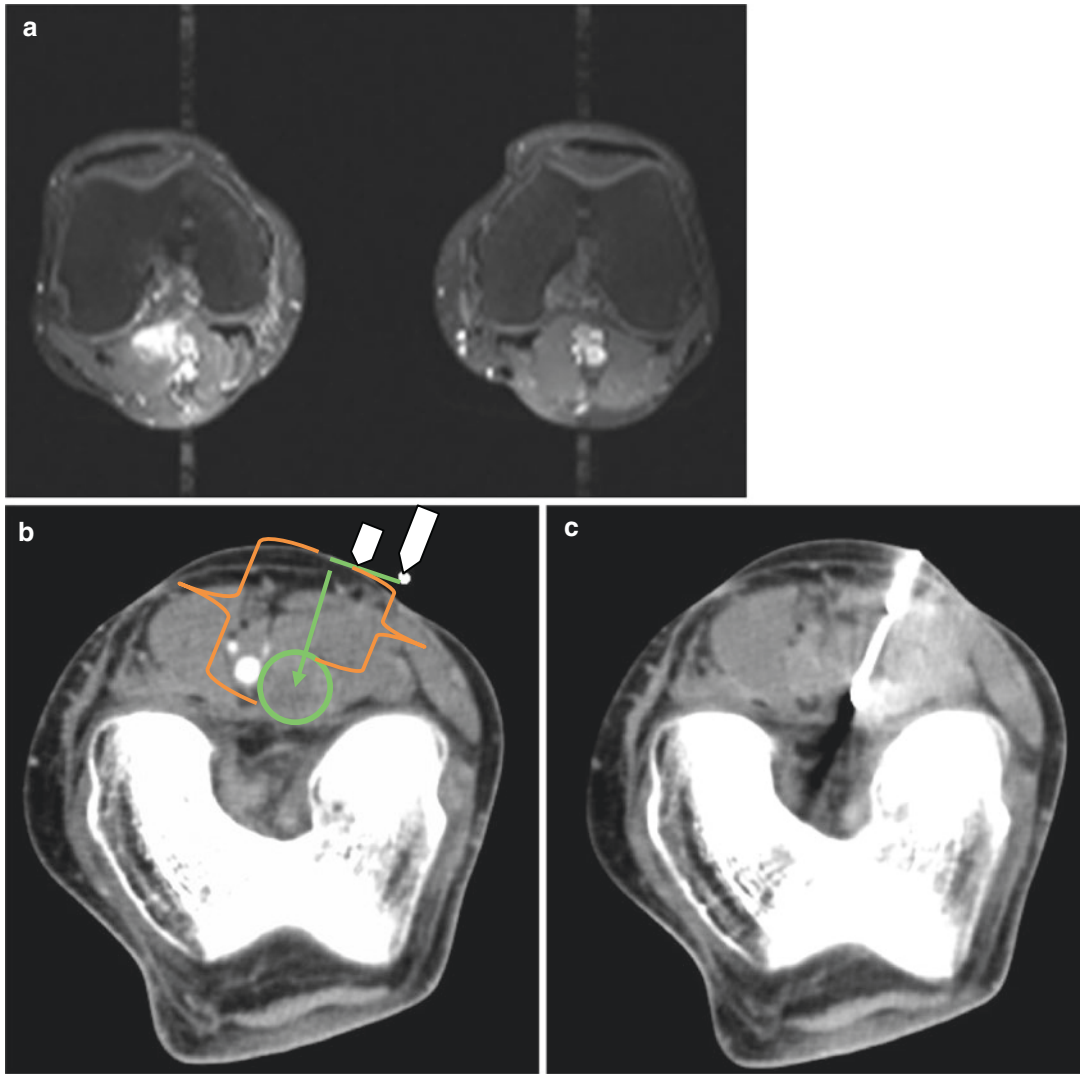

Fig. 7.7 (**a**–**c**) Small, pigmented villonodular synovitis (PVNS) in a young female patient at the right popliteal space. (**a**) MRI of both knees in supine position, axial spin-echo T1-weighted image with fat suppression (FS) and after intravenous gadolinium-DTPA administration. A small, markedly enhancing mass lesion at the left popliteal space adjacent to the popliteal neurovascular structures is seen (*white arrow*). (**b**) Computed tomography of the left knee, axial plane in prone position with soft tissue window and level settings and after intravenous administration of iodinated contrast material. The nonenhancing, hypointense mass lesion is seen at the lateral aspect of the enhancing popliteal neurovascular bundle (*circle*). Entry point in relation to an external radiopaque marker is measured (*arrowheads*); biopsy pathway (*arrow*) and skin-to-lesion interval and skin to deepest margin of the lesion (*braces*) are determined. (**c**) Computed tomography of the left knee after insertion of biopsy needle, comparable axial plane, verification of needle position before cut

In a recent prospective study on categorizing (malignant–benign) and grading of 18 soft tissue tumors by Kaur et al. by biopsy with FNAB and CNB, FNAB had a categorizing specificity of 90.9 % and CNB a specificity of 100 %. Cytologic grade was concordant with CNB in 81.1 %. They conclude that FNAB and CNB alleviate the need for an open biopsy in diagnosing and grading of musculoskeletal neoplasms [22]. Strauss et al. in a prospective study on 530 patients CNB could differentiate soft tissue sarcomas from benign soft tissue tumors with an accuracy of 97.6 %.

High-grade lesions were differentiated from low-grade sarcomas with an accuracy of 86.3 % [32].

Ray-Coquard et al. evaluated CNB in 110 STS patients. They found lower sensitivity in low-grade sarcomas (85 %) compared to high-grade sarcomas (100 %). Histological grading on CNB seems hardly feasible, except for grade III tumors [28]. Didolkar et al. concluded that CNB in malignant MSK lesions had a higher diagnostic yield of 94 % compared to benign lesions with a diagnostic yield of 58 % [8]. This is in contradistinction with a study performed in our institution in which the accuracy of PMSB (bone and soft tissue lesions) was higher in benign lesions (90.2 %) compared to 86 % for malignant lesions. This study performed in our institution in 2012 compared surgical open biopsy, CT-guided CNB, and PET–CT-guided CNB in 149 musculoskeletal lesions (36 soft tissue lesions (STL) and 113 bone lesions (BL)). In PET–CT-guided biopsy, the biopsy was performed during the PET examination at the area in the tumor of most intense radiolabeling with PET–CT-fused images to prove the needle localization (Fig. 7.8). Characterization and grading accuracy was, respectively, 80.5 %/90.2 % for surgical biopsy, 88.2 %/95.6 % for CT-guided biopsy, and 92.5 %/95 % for PET–CT-guided biopsy. For

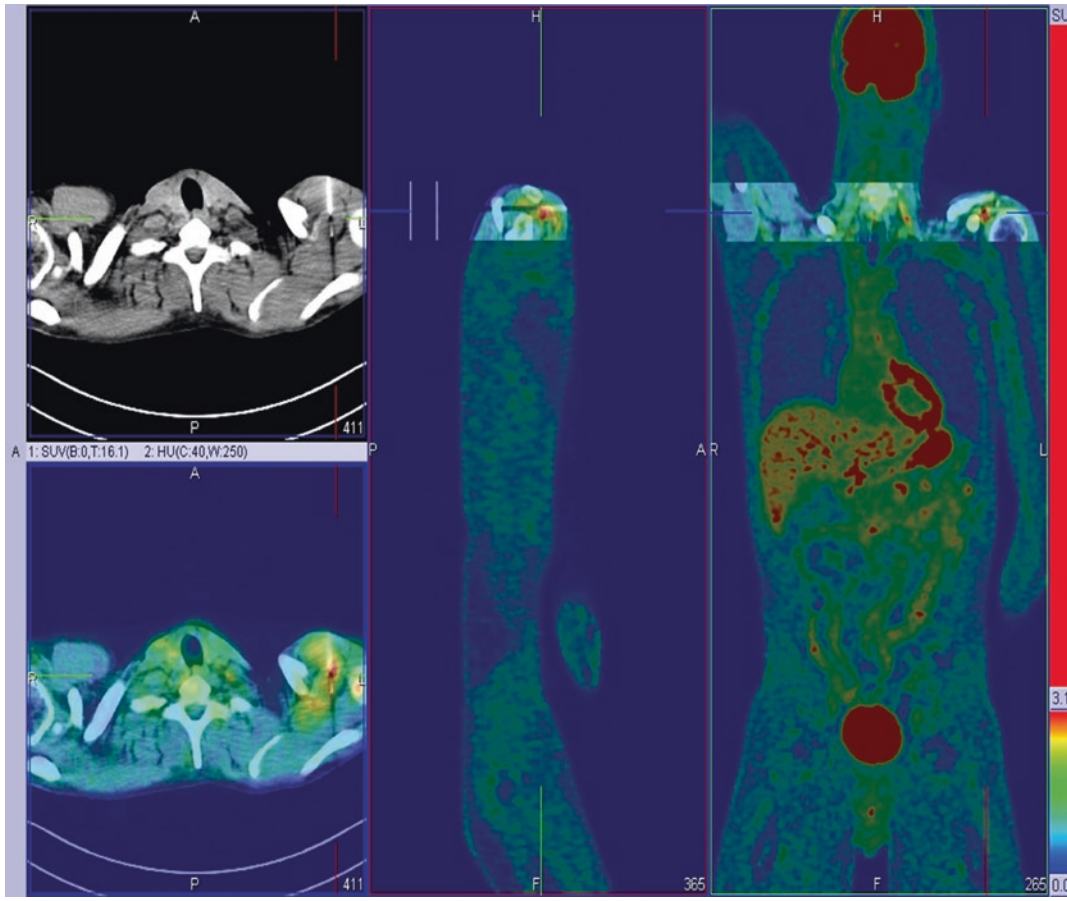

Fig. 7.8 A 40-three-year-old male patient with mass at the left shoulder. Subacromiosubdeltoid mass was detected on ultrasound and subsequent MRI examination. PET–CT-guided biopsy is performed with Spirotome needle (10G) with pathway anteriorly in the axial and sagittal plane. The sample location was defined at the area of most intense radiolabeling (red area on PET). Axial, sagittal, and coronal PET–CT-fused images are made with the needle in position to prove the sample location at the area of most intense radiolabeling (AMIR). Pathology on biopsy and resection specimen revealed synovial cell sarcoma

STL the characterization efficacy was 80 % for surgical biopsy, 77.8 % for CT-guided biopsy, and 88.2 % for PET–CT-guided biopsy. In our institution (Belgium), the cost of surgical biopsy ranges from €262 to 380, CT-guided biopsy €159 to 296, and PET–CT-guided biopsy €530 to 667. We concluded that PET–CT-guided biopsy was not cost effective but that PET information, if available, should be used to determine the biopsy location in the specific area of most intense radiolabeling. Surgical biopsy should only be performed in case of inconclusive CT guided [12].

In case of impalpable soft tissue tumors, a needle containing a hookwire with an overbent hook that springs open when protruded beyond the needle top and anchors the wire in the lesion is positioned under ultrasound guidance and will facilitate excisional biopsy [29].

These authors demonstrate that diagnostic accuracy of PMSB is not only dependent on the used sampling technique but also of the location and the ultimate histological diagnosis of the lesion [22].

7.5 Immunohistochemistry

Considerable progress has been made in the clinical and biological understanding of soft tissue sarcomas. This has led to the launch of a new revised and extended WHO classification of soft tissue tumors in 2013, which integrates morphological data with the explosion of tumor-specific (cyto-) genetics and molecular genetic information over the past 20 years [18]. Worldwide consensus has grown how to predict biological/clinical behavior based on a specific grading system and which specific types of tumors seem not to obey these rules. Immunohistochemical characterization plays a key role in the diagnostic work-up of STS. The determination line is not only crucial in order to ensure proper classification but also to provide predictive information. The new classification includes categorization of biological behavior which allows for two distinct types of intermediate malignancy, identified, respectively, as "locally aggressive" and "rarely metastasizing." The uncertain line of differentiation in so-called angiomatoid MFH and extraskeletal myxoid chondrosarcoma has resulted in their reclassification into the chapter of tumors of uncertain differentiation. The recent identification of tumor-specific drug targets by immunohistochemistry has had impact on specimen requirements and handling as well as laboratory standards [17]. Thus, these new insights influence sampling technique promoting thick (≤14G) CNB samples at multiple sites in nonhomogeneous lesions. Tissue sample fixation is also adapted to permit immunohistochemical characterization. Acetic acid solutions are avoided because mitotic figures are hardly visible after treatment with 70 % acetic acid. Thus, formerly used technique with alcohol–formalin–acetic acid (AFA) fixation is abandoned [5]. Actually a buffered 4 % dilution of formalin (NF4) is recommended for tissue samples (CNB), and an alcoholic solution (Saccomano or CytoLyt) is used for cell samples if CNB tissue sampling is not possible (FNAB) [24, 34].

7.6 Technique and Choice of Needle

In STS not only cytology but also matrix, architectural structure, and immunohistochemistry add to the pathologic diagnostic clue.

FNAB essentially obtains cells without revealing its tissue architecture or matrix. It is able to study cyto-nuclear disturbances but not tumor differentiation and matrix components. The pathologist is often only able to differentiate malignant from benign lesions [2, 26]. Good results are obtained in tumors at the soft tissues in patients with known adenocarcinoma or myeloma and lymphoma or if the magnetic resonance imaging characteristics are suggestive for lymphoma [5].

CNB is able to provide tissue in which matrix is disclosed and the architectural structure may be preserved. It is evident that 10-gauge needles produce better results than 14- or 20-gauge needles are. Side-loading (Trucut) and end-loading (Spirotome) biopsy systems are available in multiple thicknesses and lengths. Spirotome allows direct imaging control of needle tip during the sample procedure with a sample length up to a

maximum of 2 cm. The needle choice depends on the experience of the radiologist and the risk related to the specific location of the lesion. Open incisional or excisional biopsy also provides information of the reactive processes around the lesion. These latter techniques (CNB and open) show best diagnostic accuracy in cases of primary soft tissue tumors.

Moreover nonhomogeneity of tumors also may influence CNB technique. Highest graded zones in a tumor predict outcome; lowest graded zones are best differentiated, may produce matrix, and help to characterize lesions. As a consequence location of the biopsy in the lesion itself depends on its imaging characteristics. In homogeneous lesions the trajectory is only determined according to its compartmental anatomy. Best results in nonhomogeneous lesions are gained if also lesion's inner architecture is taken into account, if possible a single long trajectory which encompasses evolving segments with imaging characteristics of high grade, i.e., cellular parts avoiding necrotic parts and more differentiated matrix (calcified)-producing parts. Two or more slightly angled trajectories that involve the same anatomic compartments may be necessary.

Because of these reasons, consensus grows to centralize tissue sampling to dedicated centers and to prefer CNB over FNAB.

Conclusion

Although the choice of biopsy type largely depends on the particular clinical setting and the experience of the clinician, radiologist, orthopedic or oncologic surgeon, and pathologist, CNB is recommended as the first-choice procedure for obtaining representative specimens of soft tissue tumors for histologic and immunohistochemical examination because of its high diagnostic accuracy and low complication rate. It allows one-surgery or neoadjuvant chemotherapy planning when combined with appropriate imaging. Except for FNAB, it is less time consuming, less painful, and cheaper than other procedures. It can be performed under (PET)–CT or ultrasound guidance, CT being preferred for deep-seated lesions or those that are difficult to reach. There are only few reports of MR guidance. The entry point and the pathway are determined in cross talk with the managing surgeon, avoiding nerve, vascular, and visceral structures. Two or more slightly angled trajectories that involve the same anatomic compartments may be necessary in radiologically nonhomogeneous lesions. Tissue sample fixation is adapted to permit immunohistochemical characterization. Open biopsy is mandatory if CNB is inadequate.

Key Points

1. MRI examination with local tumor staging should be performed before the biopsy procedure.
2. Any lesion that cannot be unequivocally characterized by MRI as benign should be considered indeterminate and requires biopsy.
3. The shortest safe path between the skin and the lesion should be chosen, and the anticipated needle path should be discussed with the surgeon who will perform the definitive surgery.
4. The needle tracts that traverse an uninvolved compartment should be avoided.
5. Compared to FNAB, CNB is able to provide tissue in which matrix is disclosed, and the architectural structure may be preserved.
6. Soft tissue tumors often are spatially heterogeneous with respect to tumor grade and characterization features, and tumor necrosis may be widespread. Tissue samples of enhancing areas, angiogenesis with Doppler activity, and/or highest scintigraphic activity are preferred. Thus, two or more biopsy samples may be necessary.
7. Tissue sample fixation should permit immunohistochemical characterization. A buffered 4 % dilution of formalin (NF4) is recommended for tissue samples (CNB), and an alcoholic solution (CytoLyt) is used for cell samples (FNAB).

References

1. Aboulafia AJ (1999) Biopsy. Instr Course Lect 48:587–590
2. Amin MS, Luqman M, Jamal S, Mamoon N, Anwar M (2003) Fine needle aspiration biopsy of soft tissue tumours. J Coll Physicians Surg Pak 13(11):625–628
3. Anderson MW, Temple HT, Dussault RG, Kaplan PA (1999) Compartmental anatomy: relevance to staging and biopsy of musculoskeletal tumors. AJR 173:1663–1671
4. Bennert KW, Abdul Karim FW (1994) Fine needle aspiration cytology vs. needle core biopsy of soft tissue tumors. A comparison. Acta Cytol 38(3):381–384
5. Bettio D, Rizzi N, Colombo P, Bianchi P, Gaetani P (2004) Unusual cytogenetic findings in a synovial sarcoma arising in the paranasal sinuses. Cancer Genet Cytogenet 155(1):79–81
6. Bickels J, Jelinek JS, Shmookler BM, Neff RS, Malawer MM (1999) Biopsy of musculoskeletal tumors. Current concepts. Clin Orthop (368):212–219
7. Bradley M (2015) The role of sonoelastography in planning percutaneous biopsy of soft tissue tumours. Ultrasound 23(4):212–215
8. Didolkar MM, Anderson ME, Hochman MG, Rissmiller JG, Goldsmith JD, Gebhardt MG, Wu JS (2013) Image guided core needle biopsy of musculoskeletal lesions: Are nondiagnostic results clinically useful? Clin Orthop Relat Res 471(11):3601–3609
9. Dupuy DE, Rosenberg AE, Punyaratabandhu T, Tan MH, Mankin HJ (1998) Accuracy of CT-guided needle biopsy of musculoskeletal neoplasms. Am J Roentgenol 171(3):759–762
10. Frassica FJ, McCarthy EF, Bluemke DA (2000) Soft-tissue masses: when and how to biopsy. Instr Course Lect 49:437–442
11. Gangi A, Guth S, Dietemann J-L, Roy C (2001) Interventional Musculoskeletal Procedures Radiographics 21: E1-e1 (online only)
12. Gielen JLMA, De Schepper AM, Ceyssens S, Creytens DH, Somville J,Van Dyck P, Pauwels P, Peeters M, Parizel PM (2013) Comparison of efficacy of surgical-, CT- and PET-CT-guided biopsy in musculoskeletal lesions. Insights Imaging, 4, supplement 1, Conference Abstract ECR B-0732
13. Gonzalez Campora R (2000) Fine needle aspiration cytology of soft tissue tumors. Acta Cytol 44(3): 337–343
14. Gonzalez Campora R, Munoz Arias G, Otal Salaverri C et al (1992) Fine needle aspiration cytology of primary soft tissue tumors. Morphologic analysis of the most frequent types. Acta Cytol 36(6):905–917
15. Hau MA, Kim JI, Kattapuram S, Hornicek FJ, Rosenberg AE, Gebhardt MC, Mankin HJ (2002) Accuracy of CT-guided biopsies in 359 patients with musculoskeletal lesions. Skeletal Radiol 31:349–353
16. Hodge JC (1999) Percutaneous biopsy of the musculoskeletal system : a review of 77 cases. Can Assoc Radiol J 50(2):121–125
17. Hogendoorn PCW, Collin F, Daugaard S, Dei Tos PA, Fisher C, Schneider U, Sciot R, pathology and biology subcommittee of the EORTC Soft Tissue and Bone Sarcoma Group (2004) Changing concepts in the pathological basis of soft tissue and bone sarcoma treatment. Eur J Cancer 40(11):1644–1654
18. http://www.iarc.fr/en/publications/pdfs-online/patgen/bb5/bb5-classifsofttissue.pdf
19. Huvos AG (1995) The importance of the open surgical biopsy in the diagnosis and treatment of bone and soft-tissue tumors. Hematol Oncol Clin North Am 9(3):541–544
20. Iwamoto Y (1999) Diagnosis and treatment of soft tissue tumors. J Orthop Sci 4(1):54–65
21. Jones C, Liu K, Hirschowigz S, Klipfel N, Layfield LJ (2002) Concordance of histopahtologic and cytologic grading in musculoskeletal sarcomas: can grades obtained from analysis by the fine-needle aspirates serve as the basis for therapeutic decisions? Cancer 96(2):83–91
22. Kaur L, Handa U, Kundu R, Garg SK, Mohan H (2016) Role of fine-needle aspiration cytology and core needle biopsy in diagnosing musculoskeletal neoplasms. J Cytol 33(1):7–12
23. Kilpatrick SE, Ward WG, Chauvenet AR, Pettenati MJ (1998) The role of fine-needle aspiration biopsy in the initial diagnosis of pediatric bone and soft tissue tumors: an institutional experience. Mod Pathol 11(10):923–928
24. Kurtycz DF, Logrono R, Leopando M, Slattery A, Inhorn SL (1997) Immunocytochemistry controls using cell culture. Diagn Cytopathol 17(1):74–79
25. Laredo JD (1999) Percutaneous biopsy of primary soft tissue tumors. Semin Musculoskelet Radiol 3:139–144
26. Nagira K, Yamamoto T, Akisue T, Marui T, Hitora T, Nakatani T, Kurosaka M, Ohbayashi C (2002) Reliability of fine-needle aspiration biopsy in the initial diagnosis of soft-tissue lesions. Diagn Cytopathol 27(6):354–361
27. Peabody TD, Simon MA (1996) Making the diagnosis:keys to a succesful biopsy in children with bone and soft-tissue tumors. Orthop Clin North Am 27(3):453–459
28. Ray-Coquard I, Ranchere-Vince D, Thiesse P, Ghesquieres H, Biron P, Sunyach MP, Rivoire M, Lancry L, Meeus P, Sebban C, Blay JY (2006) Evaluation of core needle biopsy as a substitute to open biopsy in the diagnosis of soft-tissue masses. Eur J Cancer 39(14):2021–2025
29. Rutten MJ, Schreurs BW, van Kampen A, Schreuder HW (1997) Excisional biopsy of impalpable soft tissue tumors. Us-guided preoperative localization in 12 cases. Acta Orthop Scand 68(4):384–386
30. Skoog L, Pereira ST, Tani E (1999) Fine-needle aspiration cytology and immunocytochemistry of soft-tissue tumors and osteo/chondrosarcomas of the head and neck. Diagn Cytopathol 20(3):131–136
31. Skrzynski MC, Biermann JS, Montag A, Simon MA (1996) Diagnostic accuracy and charge-savings of

outpatient core needle biopsy compared with open biopsy of musculoskeletal tumors. J Bone Joint Surg Am 78(5):644–649
32. Strauss DC, Qureshi YA, Hayes AJ, Thway K, Fisher C, Thomas JM (2010) The role of core needle biopsy in the diagnosis of suspected soft tissue tumours. J Surg Oncol 102(5):523–529
33. Van Geel AN, Van Unnik JA, Keus RB (1995) Consensus soft tissue tumors. Dutch Workgroup Soft-Tissue Tumors. Ned Tijdschr Geneeskd 139(6):833–837
34. Werner M, Chott A, Fabiano A, Battifora H (2000) Effect of formalin tissue fixation and processing on immunohistochemistry. Am J Surg Pathol 24(7):1016–1019

Part II

Staging, Grading and Tissue Specific Diagnosis

Staging

8

K. Wörtler

Contents

8.1 **Staging Rationale** 145

8.2 **Staging Systems for Soft Tissue Sarcoma** 145
8.2.1 AJCC/UICC Staging System 145
8.2.2 MSTS/Enneking Staging System 146
8.2.3 Tumor Size 147
8.2.4 Tumor Depth 147
8.2.5 Intra- or Extracompartmental Tumor Growth 149
8.2.6 Lymph Node Metastasis 149
8.2.7 Distant Metastasis 149
8.2.8 Histologic Grade 150

8.3 **Local Staging** 150
8.3.1 Neurovascular Encasement 151
8.3.2 Bone Involvement 151
8.3.3 Joint Invasion 152
8.3.4 Local Staging After Inadequate Resection 154

8.4 **Surveillance and Repeat Staging** 154

References 158

8.1 Staging Rationale

Patients with soft tissue sarcomas should generally be evaluated and managed by a multidisciplinary team with expertise and experience in sarcoma prior to the initiation of therapy [22, 37]. Staging provides information necessary for evaluating prognosis, determining the best treatment approach, and defining groups for inclusion in clinical trials [22]. In addition to *oncologic staging* according to commonly used staging systems, *local staging* of tumor extent with MR imaging has become increasingly important. Whereas the diagnosis of an extremity soft tissue sarcoma usually implied amputation or other mutilating surgical procedures in the past, the standard surgical treatment is nowadays wide resection, if indicated, in combination with adjuvant or neoadjuvant radiation therapy or chemotherapy [22, 37, 41]. Recent advances in surgical and radio-oncological techniques have facilitated limb-sparing local treatment with an equivalent or even better prognosis than radical resection or amputation [12, 38, 41].

8.2 Staging Systems for Soft Tissue Sarcoma

8.2.1 AJCC/UICC Staging System

The staging system of the American Joint Committee on Cancer (AJCC) adopted by the

K. Wörtler
Department of Radiology, Technische Universität München, Ismaninger Str. 22, D-81675 Munich, Germany
e-mail: klaus.woertler@tum.de

© Springer International Publishing AG 2017
F.M. Vanhoenacker et al. (eds.), *Imaging of Soft Tissue Tumors*, DOI 10.1007/978-3-319-46679-8_8

Union Internationale Contre le Cancer (UICC) is widely used for *oncologic staging* of soft tissue sarcoma in Europe (Table 8.1).It represents a TNM system which has been expanded by adding the *grade of histologic tumor differentiation* (G) as a key determinant of prognosis with a view to local recurrence, development of distant metastasis, and disease-specific survival [6, 11, 22, 31, 34, 37, 41, 42].

The T stage is determined by maximum tumor diameter (T1/T2) and location relative to the muscle fascia (a/b). N and M stages describe the absence or presence of regional lymph node and distant metastasis, respectively. For grading (G), the former four-grade system has been replaced by a three-grade system as proposed by the French Federation of Cancer Centers (Fédération Nationale des Centres de Lutte Contre le Cancer (FNCLCC)) [7, 11, 22, 41].

The AJCC/UICC stage is predictive of overall survival. The general prognosis is better with well-differentiated tumors, smaller and superficial tumors, and in the absence of nodal involvement and distant metastasis. The presence of distant metastasis at any site indicates stage IV disease regardless of histologic tumor grade. The 5-year survival rates of extremity soft tissue sarcomas are 80–90 % at stage I and II, 56 % at stage III, and less than 20 % at stage IV [17, 22, 34, 41].

Table 8.1 AJCC/UICC staging system for soft tissue sarcoma [11]

Stage	T	N	M	G
IA	T1a T1b	N0 N0	M0 M0	G1, GX G1, GX
IB	T2a T2b	N0 N0	M0 M0	G1, GX G1, GX
IIA	T1a T1b	N0 N0	M0 M0	G2, G3 G2, G3
IIB	T2a T2b	N0 No	M0 M0	G2 G2
III	T2a, T2b Any T	N0 N1	M0 M0	G3 Any G
IV	Any T	Any N	M1	Any G

T primary tumor, *TX* primary tumor cannot be assessed, *T1* tumor ≤ 5 cm in greatest dimension, *T1a* superficial tumor, *T1b* deep tumor, *T2* tumor > 5 cm in greatest dimension, *T2a* superficial tumor, *T2b* deep tumor, *N* regional lymph nodes, *NX* regional lymph nodes cannot be assessed, *N0* no regional lymph node metastasis, *N1* regional lymph node metastasis, *M* distant metastasis, *M0* no distant metastasis, *M1* distant metastasis, *G* Histologic Grade (FNCLCC system preferred), *GX* grade cannot be assessed, *G1* well differentiated, *G2* moderately differentiated, *G3* poorly differentiated

Table 8.2 MSTS/Enneking staging system for musculoskeletal tumors [14]

Stage	G	T	M
IA	G1	T1	M0
IB	G1	T2	M0
IIA	G2	T1	M0
IIB	G2	T1	M0
III	G1 or G2	T1 or T2	M1

G histologic grade, *G1* low grade, *G2* high grade, *T* tumor, *T1* intracompartmental, *T2* extracompartmental, *M* distant metastasis, *M0* no distant metastasis, *M1* distant metastasis

8.2.2 MSTS/Enneking Staging System

The staging system of the Musculoskeletal Tumor Society (MSTS) developed by Enneking (Table 8.2) is applicable to both *soft tissue and bone sarcomas* and has a more surgical orientation [14, 31, 41, 42]. It has been designed before advanced imaging techniques and adjuvant therapy were routinely used.

Like the AJCC/UICC system, it includes the *grading* (G) of the tumor but only distinguishes between low-grade and high-grade lesions. This two-tiered grading was favored, because it could better be related to surgical procedures (wide vs. radical excision) [41]. Regional lymph node metastasis is *disregarded* in this system. The size of the tumor is only an indirect variable, because the T stage is determined by grouping the lesions as either *intracompartmental* (T1) or *extracompartmental* (T2) rather than by absolute size [14, 41, 42,]. This makes the MSTS system best applicable to sarcomas located in the extremities [41].

8.2.3 Tumor Size

Tumor size has an influence on the prognosis of soft tissue sarcomas, mainly because it is more difficult to eradicate larger tumors surgically. The designation of 5 cm used as a cutoff value between T1 and T2 lesions in the AJCC/UICC staging system is however more or less arbitrary [22, 41]. To measure the true dimensions of a soft tissue sarcoma on MR imaging might be difficult, if the mass is surrounded by an indistinct *pseudocapsule*. The pseudocapsule is a peripheral zone of reactive tissue that can develop due to compression, hyperemia, and chronic inflammation of soft tissue adjacent to the sarcoma and might contain tumoral digitations and satellites [5, 6, 41]. On MR images, it is seen as a zone of peritumoral "edema" [5]. The true tumor diameter (with *exclusion* of the pseudocapsule) can be best measured on T2-weighted or contrast-enhanced MR images without fat suppression (Fig. 8.1).

If measurements of resected specimens at pathologic examination are used as standard of reference, tumor size is often "overestimated" on preoperative MR images, especially for large masses. Possible explanations for this effect are changes in tumor shape and suspension of perfusion after resection, rupture of cystic tumor components, fragmentation, and shrinkage due to tissue fixation on pathologic preparation [4, 10, 20, 28].

8.2.4 Tumor Depth

Tumor depth is defined in the AJCC/UICC staging system on the basis of tumor location relative to the muscle (deep) fascia (Fig. 8.2). *Superficial tumors* are located subcutaneously and entirely

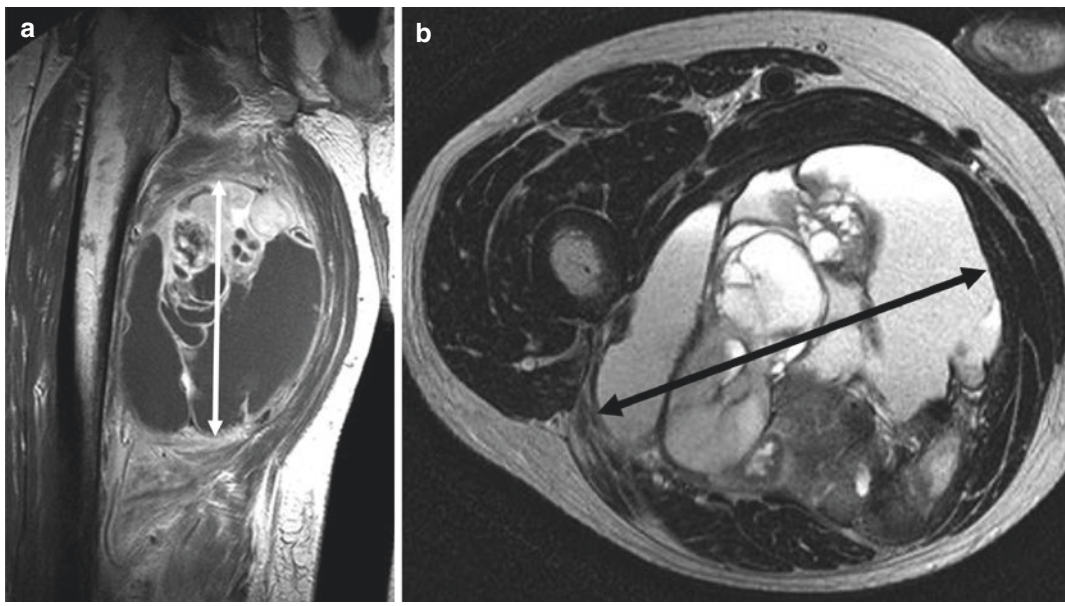

Fig. 8.1 (**a**, **b**) T stage according to AJCC/UICC and MSTS. (**a**) Coronal contrast-enhanced T1-weighted SE and (**b**) axial T2-weighted TSE images of a patient with a pleomorphic sarcoma show a large tumor in the posterior compartment of the thigh. Tumor diameter is measured with exclusion of the pseudocapsule as demonstrated. According to AJCC/UICC, the tumor would be classified as T2b (>5 cm, deep tumor). If the MSTS system is used, the tumor represents a T1 lesion, because it is confirmed to one anatomic compartment (intracompartmental), albeit the compartmental boundaries are bulged by the mass effect

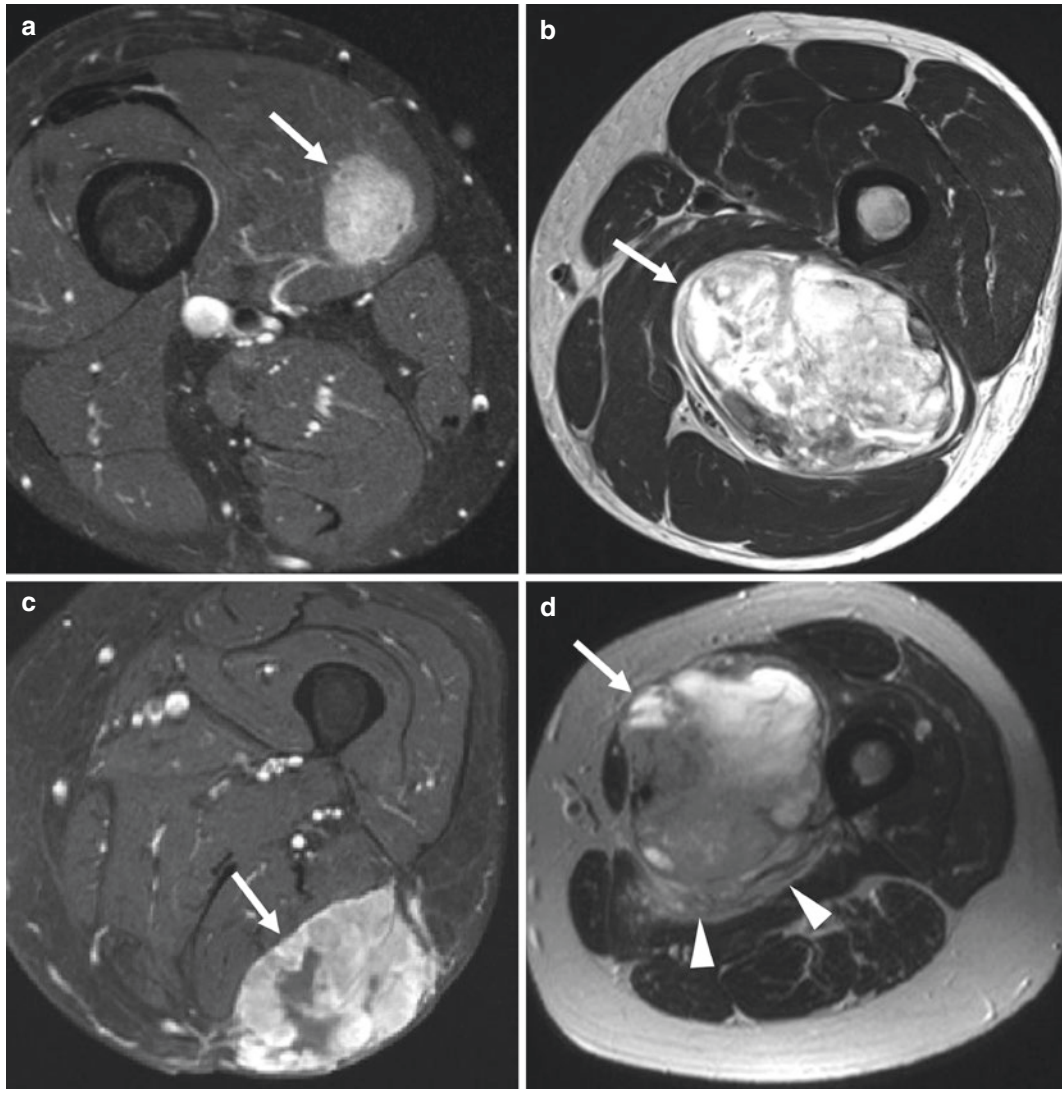

Fig. 8.2 (**a–d**) T stage according to AJCC/UICC and MSTS. (**a**) Axial contrast-enhanced T1-weighted TSE image with fat suppression shows intramuscular leiomyosarcoma (*arrow*) in the anterior compartment of the thigh. AJCC/UICC: T1b, MSTS: T1. (**b**) Axial T2-weighted TSE image demonstrates pleomorphic sarcoma (*arrow*) in the posterior compartment of the thigh. AJCC/UICC: T2b, MSTS: T1. (**c**) Axial contrast-enhanced T1-weighted TSE image with fat suppression shows pleomorphic sarcoma (*arrow*) in the subcutaneous tissue involving to the muscle fascia and deep compartment. AJCC/UICC: T2b, MSTS: T2 (**d**) Axial T2-weighted TSE image reveals pleomorphic sarcoma (*arrow*) in the anterior compartment of the thigh. The reactive zone extends to the lateral compartment (*arrowheads*). AJCC/UICC: T2b, MSTS: T2

superficial to the muscle fascia without invading it. *Deep tumors* lie either entirely beneath the muscle fascia, above the fascia and invading it, or both above and beneath the fascia [42]. On MR imaging, it is particularly difficult to differentiate close contact without fascial invasion and true invasion in tumors with subcutaneous location. Tumor depth might therefore be overestimated rather than underestimated on radiologic assessment [20].

Mediastinal, retroperitoneal, and pelvic soft tissue sarcomas are generally classified as deep tumors [6, 11, 41, 42].

8.2.5 Intra- or Extracompartmental Tumor Growth

An *anatomic compartment* is defined as an anatomical structure or space bounded by natural barriers, such as cortical bone, fascia and fascial septa, articular cartilage, joint capsule, tendons, tendon sheaths, and ligaments [2, 6]. With a view to tumor spread, the *five basic compartments* are the skin and subcutaneous tissue, the muscle compartments, the paraosseous space, the bone, and the joints. Anatomic regions that lack such firm barriers are regarded as *extracompartmental spaces*. These include the head and neck, paraspinal tissues, periclavicular tissue, axilla, antecubital fossa, wrist, dorsum of the hand, groin, popliteal fossa, ankle, and dorsum of the foot [2, 42].

Intracompartmental tumors are confined to a single anatomic compartment, although they might distort the boundaries of their compartment of origin. Within a muscular compartment, intracompartmental lesions might involve more than one muscle. In contrast, *extracompartmental tumors* have secondarily spread past the barriers of the original compartment or primarily involve more than one anatomic compartment. It is important to note that a soft tissue sarcoma is also considered extracompartmental, if its reactive zone (peritumoral "edema") extends beyond the compartmental barriers (Figs. 8.1 and 8.2). Furthermore, all tumors that arise within or secondarily involve one of the extracompartmental spaces mentioned above are defined as extracompartmental. Finally, extracompartmental spread might also result from hemorrhage or due to an operative procedure, such as an unplanned resection or a technically poor biopsy [2, 6, 14, 41, 42].

8.2.6 Lymph Node Metastasis

With an overall prevalence of 1–3 %, regional lymph node metastasis is relatively rare in patients with soft tissue sarcomas, although higher rates of up to 10 % were reported in some series, probably due to a higher proportion of specific histological subtypes. Spread to regional lymph nodes is most commonly seen in *rhabdomyosarcoma, angiosarcoma, clear cell sarcoma, epithelioid sarcoma*, and *synovial sarcoma*. In these entities, prevalences of up to 40 % have been observed. In the absence of distant metastasis, the affection of regional lymph nodes represents a strong prognostic factor [16, 21, 34, 35].

Fig. 8.3 Lymph node metastasis of synovial sarcoma. Axial contrast-enhanced CT image of the pelvis obtained for initial staging depicts enlarged external iliac lymph nodes on the right. Biopsy verified lymph node metastasis (*arrows*) of known biphasic synovial sarcoma. The primary tumor was located above the right knee

Dependent on the location of the original tumor, CT should be used to assess the cervical, axillary, mediastinal, retroperitoneal, and/or inguinal lymph nodes on initial staging, especially in sarcoma subtypes with a high likelihood of lymphogenic spread (Fig. 8.3). So far PET, PET/CT, and PET/MRI are not recommended for routine work-up of patients with soft tissue sarcomas [37]. Due to the strong heterogeneity of this group of tumors, FDG uptake in lymph node metastasis is virtually unpredictable and thus might lead to false-negative assessments. False-positive findings can be caused by unspecific glucose uptake in reactive axillary, retroperitoneal, or inguinal lymph nodes which are commonly seen with larger tumors of the extremities.

8.2.7 Distant Metastasis

The presence of distant metastasis represents the strongest predictor of poor outcome in soft tissue sarcomas [22, 32, 36]. Distant metastasis occurs

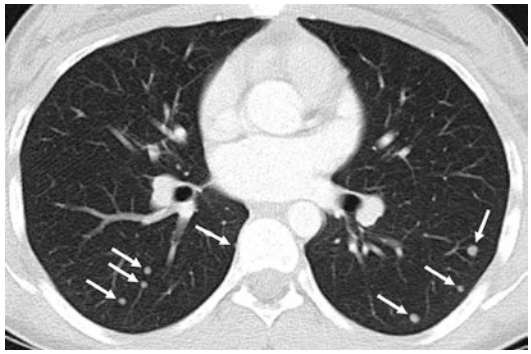

Fig. 8.4 Lung metastasis of alveolar soft part sarcoma. Axial CT image of the chest (lung window setting) obtained for initial staging shows bilateral pulmonary nodules (*arrows*). The primary tumor was located in the thigh

in up to 25 % of patients with the most common sites being the *lung* (75–80 %) followed by the *bones* (10 %) [39]. CT of the chest should routinely be performed in initial staging of all soft tissue sarcomas (Fig. 8.4). Synchronous lung metastasis in the absence of extrapulmonary disease is usually treated by chemotherapy and, if possible, consequent surgical resection of all residual lesions. The standard treatment for metachronous resectable lung metastasis is surgery, if there is no evidence of extrapulmonary disease and complete excision of all lesions is feasible [37]. In specific sarcoma subtypes with a known tendency to metastasize to bone, such as *myxoid liposarcoma*, whole-body MRI may be recommended to assess the entire skeletal system.

8.2.8 Histologic Grade

Histologic grading of soft tissue sarcomas according to the FNCLCC system is based on *tumor differentiation*, *mitosis count*, and *tumor necrosis* (Table 8.3) [7, 19]. The histologic grade has a higher prognostic weight than tumor size and depth [22]. It should be kept in mind that grading is *not* practicable in post-chemotherapy or post-radiotherapy specimens. It is therefore mandatory to obtain a sufficient amount of representative material for pathologic analysis prior to therapy.

Table 8.3 FNCLCC Grading System for Adult Soft Tissue Sarcomas [7] FNCLCC = Fédération Nationale des Centres de Lutte Contre le Cancer

Parameter	Criterion
Tumor differentiation	
Score 1	Sarcomas closely resembling normal adult mesenchymal tissue
Score 2	Sarcomas for which histological typing is certain
Score 3	Embryonal sarcomas, undifferentiated sarcomas, and sarcomas of doubtful tumor type
Mitosis count	
Score 1	0–9 per 10 HPF
Score 2	10–19 per 10 HPF
Score 3	>20 per 10 HPF
Tumor necrosis	
Score 0	No necrosis
Score 1	≤50 % tumor necrosis
Score 2	>50 % tumor necrosis
Histologic grade	
Grade 1	Total score 2, 3
Grade 2	Total score 4, 5
Grade 3	Total score 6, 7, 8

HPF high-power fields

8.3 Local Staging

Local staging of soft tissue sarcoma is of major importance for surgical treatment with a view to preservation of function and, at the same time, sufficient radicality. Resections with microscopically positive margins have been shown to increase the risk for local recurrence and consecutively for the development of distant metastases and for tumor-associated mortality [6, 12, 20, 22, 32, 36, 38]. Preoperatively, the surgeon needs detailed information on *local tumor extent* and in particular on the presence or absence of *neurovascular encasement*, *bone involvement*, and *joint invasion. MR imaging* represents the most informative imaging technique in this regard. It is imperative to complete the imaging evaluation of locoregional tumor extent *prior to biopsy*. Principally, any soft tissue mass, which is examined by MR imaging, should be examined in a way that allows to answer all relevant questions for a potential wide surgical resection.

8.3.1 Neurovascular Encasement

Encasement of major vessels and nerves is seen in 4–10 % of soft tissue sarcomas but might be more common in specific anatomic locations, such as the popliteal fossa, or with specific tumor subtypes [20, 28–30]. A close anatomic relationship between the mass and the neurovascular bundle is frequently observed in patients with soft tissue sarcomas. *Abutment* or *displacement* of vessels and nerves is however more frequent than *true encasement* [6, 20]. Evaluation of the neurovascular structures on MR imaging is of central importance for surgical treatment planning. Whereas in case of vascular encasement, the limb can often be spared by resecting the involved vessels together with the sarcoma and replacing the artery with a graft, encasement of a major nerve, especially the sciatic nerve, almost inevitably leads to amputation. On the other hand, if the tumor only abuts the nerve with or without *adherence*, a small but tumor-free margin can be created by perineural resection. In this procedure, the epineurium is longitudinally incised opposite to the tumor, dissected from the nerve, and finally removed en bloc with the tumor [6, 20].

On *MR imaging*, the location of a musculoskeletal sarcoma relative to major neurovascular structures can be best assessed on *transverse sections with T2 contrast* and a high spatial resolution (Fig. 8.5). It is however still controversial whether these pulse sequences should be obtained without or with fat suppression. The main advantage of using T2-weighted pulse sequences without fat suppression is the superior visibility of nerves, nerve fascicles, and perineurium, which appear hypointense against the surrounding fat. This contrast is lost if fat suppression is applied, and therefore, the neural structures become less discernible.

In a series of 174 soft tissue sarcomas, MR imaging showed a *sensitivity* of 82 %, a *specificity* of 92–96 %, and a high *interrater agreement* in the assessment of neurovascular encasement. Encasement of arteries, veins, and nerves was diagnosed, if the contact between the tumor and the vascular or neural circumference *exceeded 180°* on axial T2-weighted TSE images without fat suppression [20]. In order to avoid false-positive assessments, which might preclude patients from limb-sparing surgery, neurovascular encasement should only be diagnosed if the abovementioned criterion is fulfilled or if direct invasion of a vascular/neural structure by tumor tissue is seen (Fig. 8.5).

MR angiography can be applied to demonstrate the anatomic relation between large arterial vessels and musculoskeletal tumors [15]. Arterial adherence or encasement can be diagnosed, if this results in a *stenosis* of the involved vessel, but can neither be diagnosed nor excluded, if this is not the case. MR angiography can therefore not replace morphologic imaging but should, if at all, only be used as an adjunct to routine sequences.

8.3.2 Bone Involvement

Secondary *involvement of neighboring bones* by cortical destruction and invasion of bone marrow occurs in approximately 9 % of soft tissue sarcomas but might even be more common in some subtypes such as synovial sarcoma [20, 30, 42]. For the surgeon, it is important to know whether the tumor only *abuts* the bone surface or truly *invades* the bone. With mere contact, it is usually sufficient to remove the periosteum together with the sarcoma to obtain an adequate surgical margin. If the adjacent skeletal element is invaded, composite resection of bone and soft tissue might be performed to achieve a wide surgical margin [6, 24].

MR imaging is highly accurate in the diagnosis of osseous invasion by soft tissue sarcomas. In different series, *sensitivities* and *specificities* between 90 % and 100 % could be determined [13, 20, 28]. The presence of signal alterations of cortical and medullary bone at the contact zone with the tumor is indicative of invasion [13, 20]. The true extent of bone marrow involvement can be best defined on T1-weighted SE/TSE images, where it is visualized as an area of complete *bone marrow replacement* (Fig. 8.6). Close contact without signal alterations, on the other hand, should not be considered indicative of bone

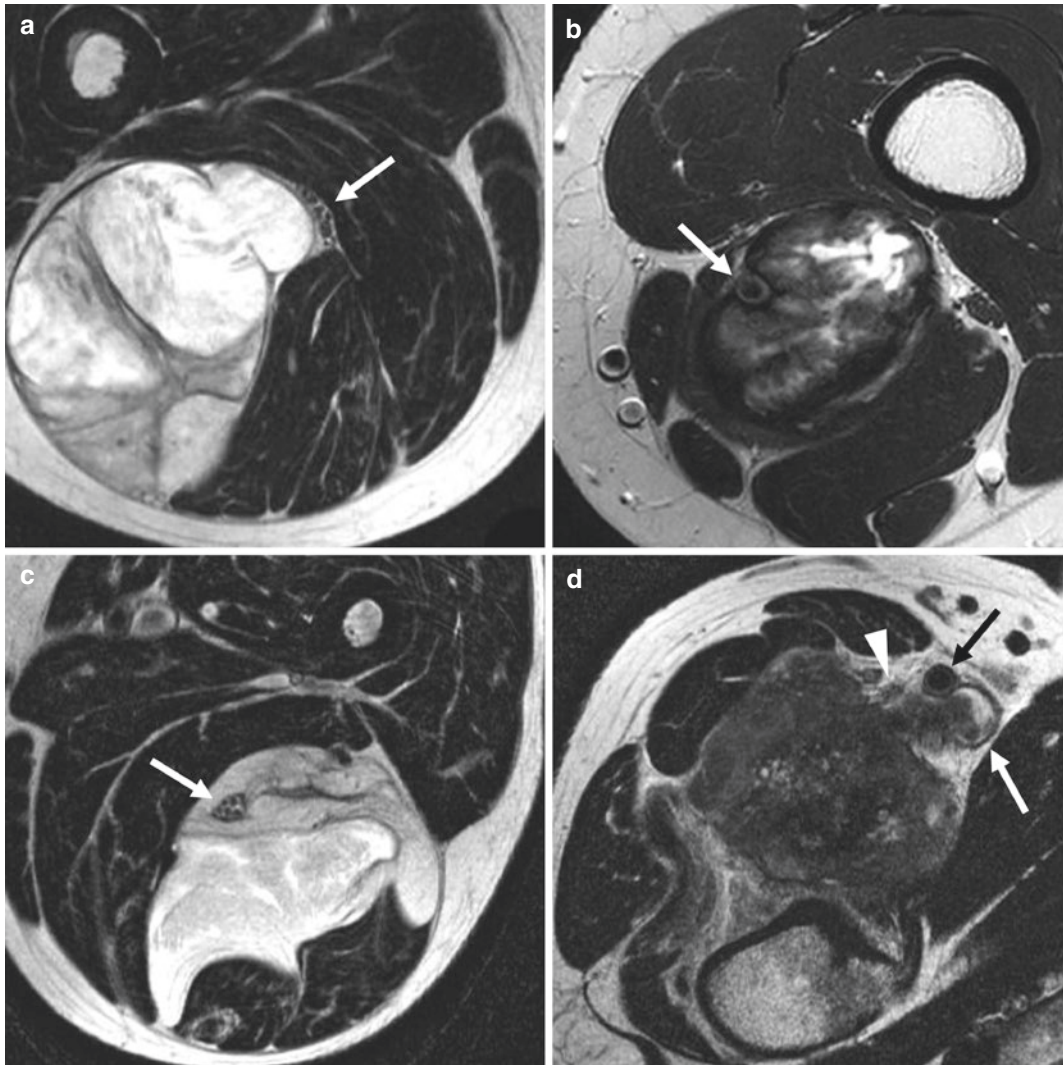

Fig. 8.5 (**a–d**) Neurovascular encasement. (**a**) Axial T2-weighted TSE image shows myxoid liposarcoma abutting the sciatic nerve (*arrow*). The tumor contacts less than 180° of the neural circumference. Intraoperatively, the nerve could be dissected from the tumor. (**b**) Axial T2-weighted TSE image demonstrates fibromyxoid sarcoma contacting more than 180° of the circumference of the femoral artery (*arrow*). The arterial segment had to be resected en bloc with the tumor and be replaced by a graft. (**c**) Axial T2-weighted TSE image shows well-differentiated liposarcoma (ALT) completely encasing the sciatic nerve (*arrow*). (**d**) Axial T2-weighted TSE image demonstrates pleomorphic sarcoma directly invading the femoral vein (*white arrow*). The femoral artery (*black arrow*) and nerve (*arrowhead*) are separated from the tumor by a thin plane of fatty tissue. The tumor could be resected together with the vein

invasion. The *length* of the contact zone between the soft tissue mass and the bone surface appears not to be statistically significant with regard to bone involvement [13]. It should however be determined in both longitudinal and transverse dimensions for surgical planning.

8.3.3 Joint Invasion

Invasion of a nearby joint by a primarily extra-articular soft tissue sarcoma is rare [20, 28]. A tumor is only considered *intra-articular* if it has *crossed the synovial membrane*. Consequently,

Fig. 8.6 (**a–c**) Bone involvement. (**a**) Sagittal T1-weighted and (**b**, **c**) sagittal and axial fat-suppressed T2-weighted TSE images show clear cell sarcoma involving the subcutaneous tissue, extensor mechanism and Hoffa's fat pat of the knee. Invasion of patellar marrow is visualized as an area of bone marrow replacement on T1-weighted image (*arrow*). Cortical destruction is best seen on axial image (*arrowheads*)

an adequate surgical margin can only be achieved by performing an extra-articular resection with en bloc removal of the joint or, if this is not possible, by amputation.

The diagnostic criteria for diagnosing articular invasion on MR imaging have rarely been defined. It should only be assumed if tumorous tissue is directly visualized *within the borders of*

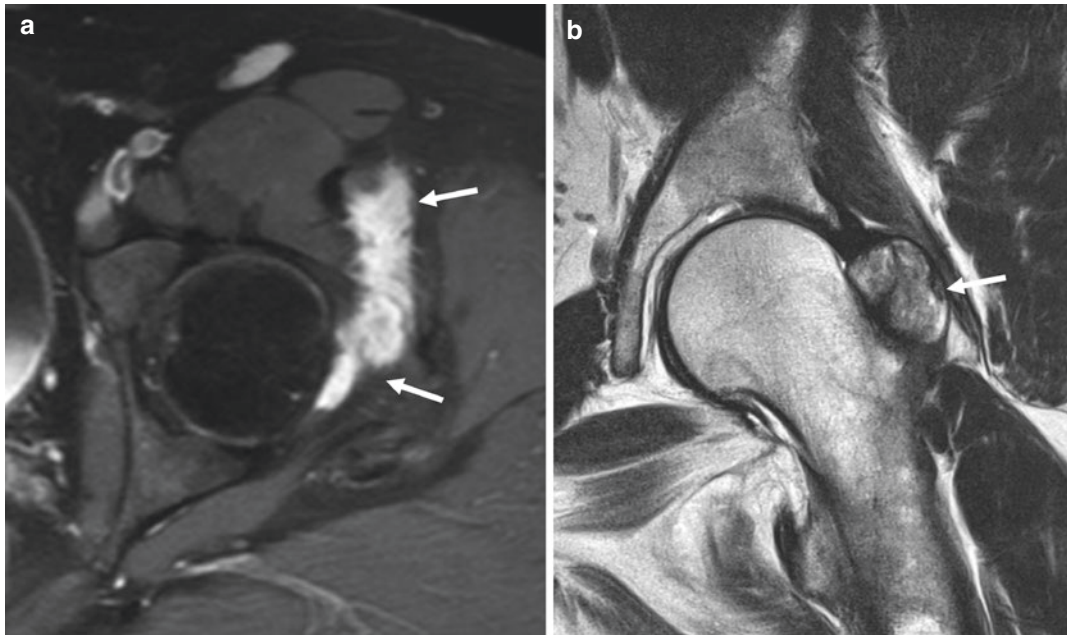

Fig. 8.7 (**a**, **b**) Joint invasion. (**a**) Axial contrast-enhanced T1-weighted TSE image with fat suppression and (**b**) coronal T2-weighted TSE image show fibromyxoid sarcoma (*arrows*) invading the hip joint. On coronal image, true intra-articular spread is seen

the synovial membrane (Fig. 8.7). Contact of tumor tissue to the joint capsule or joint effusion is *not* indicative of articular invasion [20].

8.3.4 Local Staging After Inadequate Resection

Inadequate resection represents a common problem in patients with soft tissue sarcomas [8, 26, 33]. Most unplanned procedures are performed by surgeons who erroneously expect to find a *lipoma*, *ganglion*, *hematoma,* or *lymph node*, in particular if the soft tissue mass is relatively small, located subcutaneously or close to a joint, or has occurred in a young patient [18, 26, 33]. Although adequate local tumor control can usually be accomplished by wide reexcision, these patients have a worse prognosis owing to an increased rate of distant metastasis [33].

The fact that preoperative imaging has not been performed in many of these cases makes the evaluation by MR imaging following inadequate resection even more difficult, because information on exact tumor size, location, and morphology is lacking. In a series of 111 cases, MR imaging had a *sensitivity* of only 64 % and a *specificity* of 93 % in the assessment of residual tumor in this situation. Whereas larger and/or nodular tumor remnants could confidently be diagnosed, *false-negative results* were commonly obtained in small (<1 cm) or microscopic residual lesions or in cases with prominent postoperative changes, which might have obscured tumor tissue left behind [8]. For planning of a reexcision, MR imaging remains nevertheless useful to evaluate the extent of the primary surgical procedure, to diagnose or exclude involvement of the deep fascia and deep compartments, to assess the size of major residual tumor, and to depict postoperative hematomas and seromas (Fig. 8.8).

8.4 Surveillance and Repeat Staging

So far there are no evidence-based guidelines for follow-up examinations in patients with surgically treated soft tissue sarcomas. The European Society for Medical Oncology (ESMO) and the European

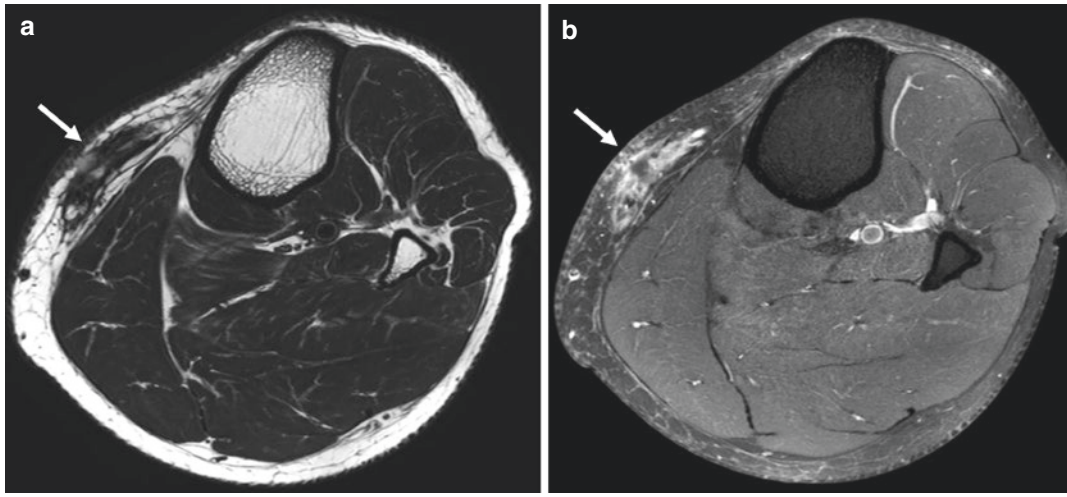

Fig. 8.8 (**a**, **b**) Inadequate resection of pleomorphic sarcoma. (**a**) Axial T2-weighted and (**b**) fat-suppressed contrast-enhanced T1-weighted TSE images show an area of inhomogeneous signal intensity and contrast enhancement in the subcutaneous tissue of the lower leg without nodular components. Although small tumor remnants cannot be excluded, the images are valuable for planning reexcision, because involvement of the deep fascia and muscular compartments is not evident

Society of Musculoskeletal Radiology (ESSR) recommend the following *practical approach*. Patients with surgically treated *intermediate or high-grade sarcomas* should be examined by MR imaging of the original tumor site and chest CT every 3–4 months in the first 2–3 years, then twice a year up to the 5th year, and once a year up to the 10th year. Patients with *low-grade sarcomas* may be followed for local recurrence every 4–6 months and with (facultative) chest CT at longer intervals in the first 3–5 years, then annually up to the 10th year [27, 37].

In surgically treated soft tissue sarcomas, local relapse occurs in 10–20 % after wide resection and in 70–90 % after local resections with histologically positive margins [8, 12, 23]. *MR imaging* represents the modality of choice for the diagnosis of recurrent tumors (Figs. 8.9 and 8.10). Repeat staging follows the same basic principles as evaluation of the original lesion.

For assessment of the surgical bed on MR imaging, information on previous radiation therapy, reconstructive surgery, and histopathology of the original tumor is mandatory [40]. A comparison of follow-up with pretreatment images is very helpful, because the MR morphology of a recurrent lesion frequently *mirrors* that of the original tumor [40].

Tumor recurrence is typically characterized by the presence of a *discrete nodular mass* with prolonged T1 and T2 relaxation times rather than by more diffuse signal alterations or ill-defined contrast uptake. The evaluation of the former surgical field can be hindered by postoperative granulation tissue, hematomas, seromas, and radiation-induced changes of soft tissues and bone. All of these can lead to increased T2-weighted signal intensity and contrast enhancement on MR images and thus, on the one hand, might be misdiagnosed as tumor recurrence and, on the other hand, might obscure recurrent masses. Local relapse of *myxoid sarcomas* can erroneously be diagnosed as seroma, in particular if the radiologist is not aware of the MR morphology of the original lesion and its inherent high signal intensity on T2-weighted images (Fig. 8.9). Mature scar tissue typically reveals low signal intensity on images of all pulse sequences and thus can usually be distinguished from tumor tissue. *Intravenous gadolinium contrast application* facilitates the differentiation of seromas, hematomas, and abscesses from recurrent tumor, but static contrast-enhanced sequences might not allow a distinction from granulation tissue and edema-like soft tissue

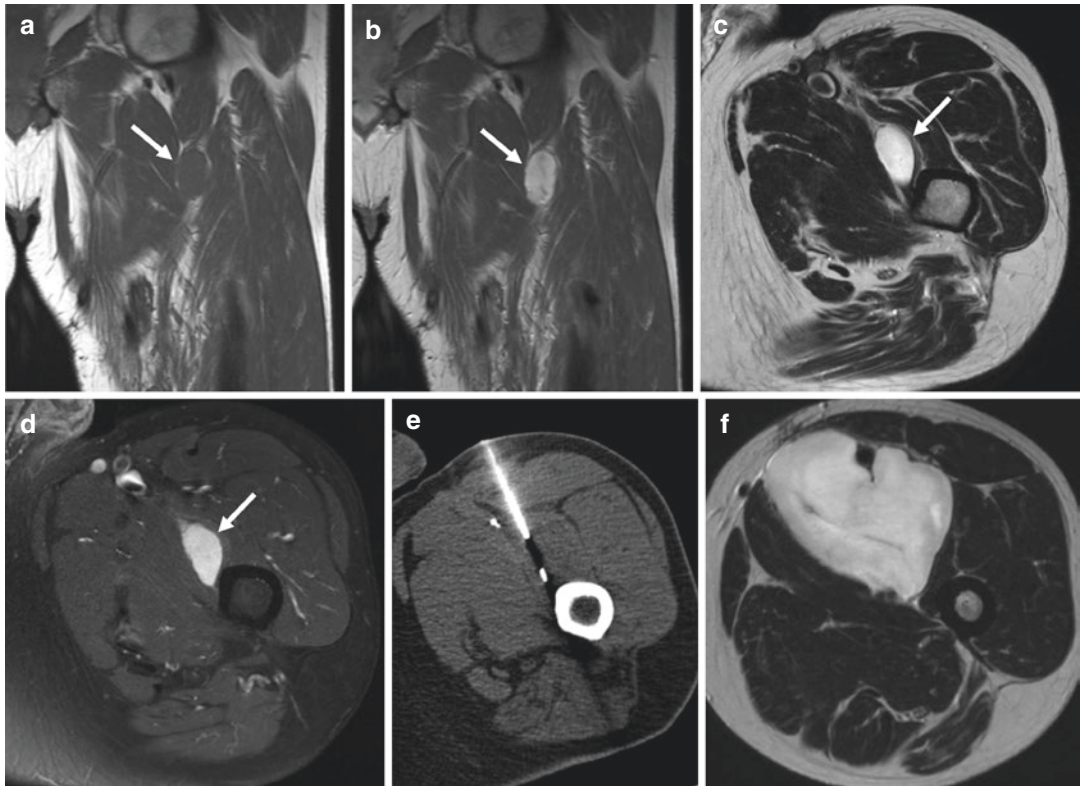

Fig. 8.9 (**a–f**) Local recurrence of myxofibrosarcoma (grade 1) 3 years after surgical resection. (**a**) Coronal T1-weighted, (**b**) corresponding contrast-enhanced T1-weighted, (**c**) axial T2-weighted and (**d**) fat-suppressed contrast-enhanced T1-weighted TSE images show tumor recurrence (*arrow*) in the anterior compartment of the thigh. (**e**) CT image was used for guidance of core needle biopsy to verify diagnosis. (**f**) Transverse T2-weighted TSE image of original tumor shows more distally located mass with encasement of femoral artery. Note similarity of T2-signal of original and recurrent tumor

changes [25]. *Image subtraction* (Fig. 8.10) might improve detection of recurrent tumors and increase lesion conspicuity rather than post-contrast images with fat suppression [1]. If added to a standard protocol, *diffusion-weighted pulse sequences* have been shown to increase the specificity of MR imaging in distinguishing recurrent soft tissue sarcoma from postsurgical scarring [3, 9]. *Ultrasound* can also represent a useful adjunct in unclear cases and might also be applied to guide biopsy in order to verify or rule out local relapse.

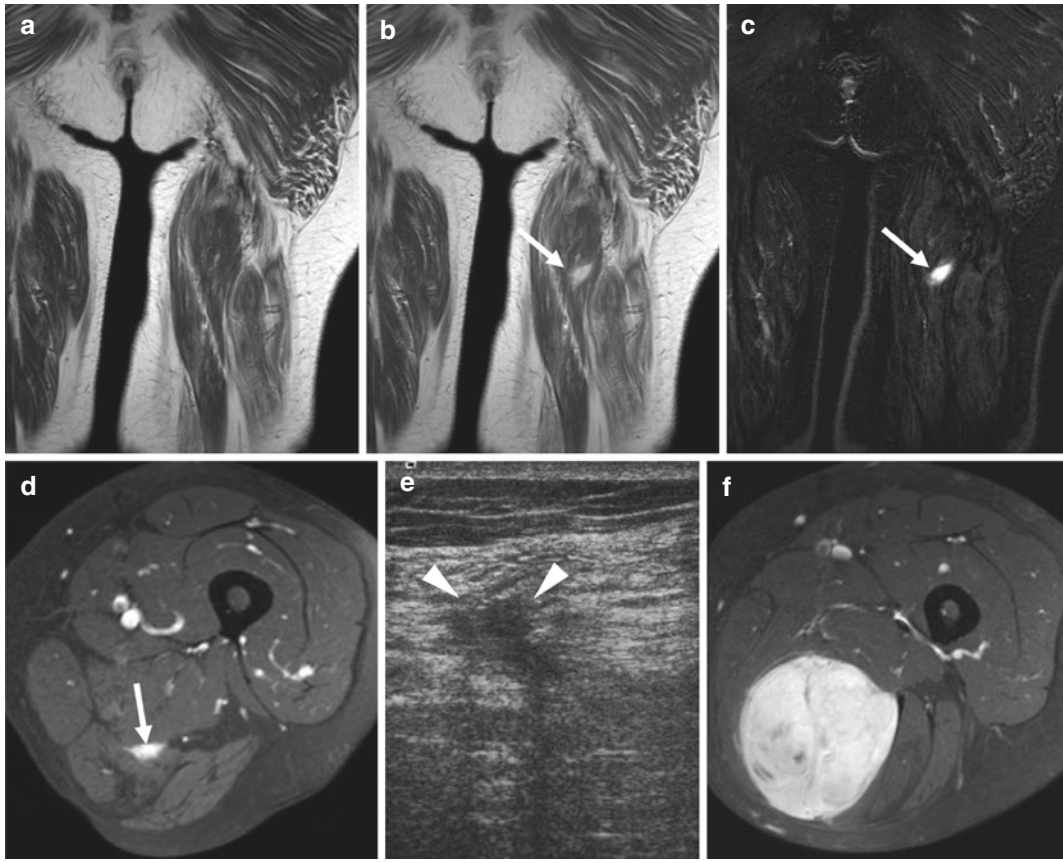

Fig. 8.10 (**a–f**) Local recurrence of pleomorphic sarcoma 4 years after surgical resection. (**a**) Coronal T1-weighted TSE, (**b**, **c**) corresponding contrast-enhanced T1-weighted and subtraction image, and (**d**) transverse fat-suppressed contrast-enhanced T1-weighted TSE image show contrast-enhancing nodular lesion (*arrows*) in the region of the former surgical bed. (**e**) The lesion was also visible on US (*arrowheads*), and relapse could be verified by US-guided core needle biopsy. (**f**) Transverse fat-suppressed contrast-enhanced T1-weighted TSE shows location and MR morphology of the original sarcoma

Key Points

1. The AJCC/UICC system is widely used for oncologic staging of soft tissue sarcoma. It includes tumor size, depth, nodal involvement, distant metastasis, and histologic grade and is predictive of overall survival.
2. As the lung represents the most common site of distant metastasis, CT of the chest should routinely be performed in initial staging of soft tissue sarcomas.
3. Local staging is of central importance for surgical treatment planning. In addition to assessment of tumor size and anatomic location, information on neurovascular encasement, bone involvement, and joint invasion is required. For local staging, MR imaging should always be performed prior to biopsy.
4. Anatomic relation to major nerves and vessels is the most important determinant for limb-sparing resection of soft tissue sarcomas. Neurovascular encasement should only be diagnosed, if the contact between tumor and neural/vascular circumference exceeds 180°.

5. Local recurrence occurs in 10–20 % of soft tissue sarcomas treated by wide resection and in 70–90 % after resections with positive surgical margins. On follow-up, the assessment of the surgical bed with MR imaging might be difficult, and thus, detailed information on previous treatment, histopathology of the original tumor, familiarity with preoperative imaging studies, and, last but not least, much experience is required. Most recurrent lesions present as a discrete nodular mass that often mirrors the MR morphology of the original sarcoma.

References

1. Ahlawan S, Morris C, Fayad LM (2016) Three-dimensional volumetric MRI with isotropic resolution: improved speed of acquisition, spatial resolution and assessment of lesion conspicuity in patients with recurrent soft tissue sarcoma. Skeletal Radiol 45:645–652
2. Anderson MW, Temple T, Dussalut RG, Kaplan PA (1999) Compartmental anatomy: relevance to staging and biopsy of musculoskeletal tumors. AJR Am J Roentgenol 173:1663–1671
3. Baur A, Huber A, Arbogast S et al (2001) Diffusion-weighted imaging of tumor recurrencies and post-therapeutical soft-tissue changes in humans. Eur Radiol 11:828–833
4. Bell RS, O'Sullivan B, Liu FF (1989) The surgical margin in soft-tissue sarcoma. J Bone Joint Surg Am 71:370–375
5. Beltran J, Simon DC, Katz W, Weis LD (1987) Increased MR signal intensity in skeletal muscle adjacent to malignant tumors: pathologic correlation and clinical relevance. Radiology 162:251–255
6. Campanacci M (1999) Bone and soft tissue tumors, 2nd edn. Springer, Padua/Wien/New York/Heidelberg
7. Coindre JM, Trojani M, Contesso G (1986) Reproducibility of a histopathologic grading system for adult soft tissue sarcoma. Cancer 58:306–309
8. Davies AM, Mehr A, Parsonage S, Evans N, Grimer RJ, Pynsent PB (2004) MR imaging in the assessment of residual tumour following inadequate primary excision of soft tissue sarcomas. Eur Radiol 14:506–513
9. Del Grande F, Subhawong T, Weber K et al (2014) Detection of soft-tissue sarcoma recurrence: added value of functional MR imaging techniques at 3.0 T. Radiology 271:499–511
10. Docquier PL, Paul L, Cartiaux O et al (2010) Formalin fixation could interfere with the clinical assessment of the tumor-free margin in tumor surgery: magnetic resonance imaging-based study. Oncology 78: 115–124
11. Edge S, Byrd DR, Compton CC et al (2010) AJCC cancer staging manual, 7th edn. Springer, New York
12. Eilber FC, Rosen G, Nelson SD, Selch M, Dorey F, Eckardt J, Eilber FR (2003) High-grade extremity sift tissue sarcomas: factors predictive of local recurrence and its effect on morbidity and mortality. Ann Surg 237:218–226
13. Elias DA, White LM, Simpson DJ, Kandel RA, Tomlinson G, Bell RS, Wunder JS (2003) Osseous invasion by soft-tissue sarcoma: assessment with MR imaging. Radiology 229:145–152
14. Enneking WF, Spanier SS, Goodman MA (1980) A system for the surgical staging of musculoskeletal sarcoma. Clin Orthop 153:106–120
15. Feydy A, Anract P, Tomeno B, Chevrot A, Drapé JL (2006) Assessment of vascular invasion by musculoskeletal tumors of the limbs: use of contrast-enhanced MR angiography. Radiology 238:611–621
16. Fong Y, Coit DG, Woodruff JM et al (1993) Lymph node metastasis from soft tissue sarcoma in adults. Analysis of data from a prospective database of 1772 patients. Ann Surg 217:72–77
17. Gaynor JJ, Tan CC, Casper ES, Collin CF, Friedrich C, Shiu M, Hajdu SI, Brennan MF (1992) Refinement of clinicopathologic staging for localized soft tissue sarcoma of the extremity: a study of 423 adults. J Clin Oncol 10:1317–1329
18. Giuliano AE, Eilber FR (1985) The rationale for planned reoperation after unplanned total excision of soft-tissue sarcomas. J Clin Oncol 3:1344–1348
19. Guillou L, Coindre JM, Bonichon F et al (1997) Comparative study of the National Cancer Institute and French Federation of Cancer Centers Sarcoma Group grading systems in a population of 410 adult patients with soft tissue sarcoma. J Clin Oncol 15: 350–362
20. Holzapfel K, Regler J, Baum T et al (2015) Local staging of soft-tissue sarcoma: emphasis on assessment of neurovascular invasion – value of MR imaging in 174 confirmed cases. Radiology 275:501–509
21. Johannesmeyer D, Smith V, Cole DJ, Esnaola NF, Camp R (2013) The impact of lymph node disease in extremity soft-tissue sarcomas: a population-based analysis. Am J Surg 206:289–295
22. Kneisl JS, Coleman MM, Chandrajit PR (2014) Outcomes in the management of adult soft tissue sarcomas. J Surg Oncol 110:527–538
23. Lewis JJ, Leung D, Heslin M, Woodruff JM, Brennan MF (1997) Association of local recurrence with subsequent survival in extremity soft tissue sarcoma. J Clin Oncol 15:646–652
24. Lin PP, Pino ED, Normand AN et al (2007) Periosteal margin in soft-tissue sarcoma. Cancer 109:598–60225
25. May DA, Good RB, Smith DK, Parsons TW (1997) MR imaging of musculoskeletal tumors and tumor

mimickers with intravenous gadolinium: experience with 242 patients. Skeletal Radiol 26:2–15
26. Mori T, Aoyagi T, Tajima T et al (2015) Unplanned resection of a soft tissue sarcoma: clinical characteristics and impact on oncological and functional outcome. J Orthop Sci 20:373–379
27. Noebauer-Huhmann IM, Weber MA, Lalam RK et al (2015) Soft tissue tumors in adults: ESSR-approved guidelines for diagnostic imaging. Semin Musculoskelet Radiol 19:475–482
28. Panicek DM, Gatsonis C, Rosenthal DI et al (1997) CT and MR imaging in the local staging of primary malignant musculoskeletal neoplasms: report of the Radiology Diagnostic Oncology Group. Radiology 202:237–246
29. Panicek DM, Go SD, Healey JH, Leung DH, Brennan MF, Lewis JJ (1997) Soft-tissue sarcoma involving bone or neurovascular structures: MR imaging prognostic factors. Radiology 205:871–875
30. Panicek DM, Hilton S, Schwartz LH (1997) Assessment of neurovascular involvement by malignant musculoskeletal tumors. Sarcoma 1:61–63
31. Peabody TD, Gibbs CP, Simon MA (1998) Evaluation and staging of musculoskeletal neoplasms. J Bone Joint Surg A86:1207
32. Pisters PWT, Leung DHY, Woodruff J, Shi W, Brennan MF (1996) Analysis of prognostic factors in 1,041 patients with localized soft tissue sarcomas of the extremities. J Clin Oncol 14:1679–1689
33. Rehders A, Stoecklein NH, Poremba C, Alexander A, Knoefel WT, Peiper M (2009) Reexcision of soft tissue sarcoma: sufficient local control but increased rate of metastasis. World J Surg 33:2599–2605
34. Rubin P, Hansen JT (2012) TNM staging atlas with oncoanatomy, 2nd edn. Lippincott Williams & Wilikins, Philadelphia
35. Sherman KL, Kinnier CV, Farina DA et al (2014) Examination of national lymph node evaluation practices for adult extremity soft tissue sarcoma. J Surg Oncol 110:682–688
36. Stojadinovic A, Leung DH, Allen P, Lewis JJ, Jaques DP, Brennan MF (2002) Primary adult soft tissue sarcoma: time-dependent influence of prognostic variables. J Clin Oncol 20:4344–4352
37. The ESMO/European Sarcoma Network Working Group (2014) Soft tissue and visceral sarcomas: ESMO clinical practice guidelines for diagnosis, treatment and follow-up. Ann Oncol 25(S3):102–112
38. Trovik CS, Bauer HC, Alvergard TA (2000) Surgical margins, local recurrence and metastasis in soft tissue sarcomas: 559 surgically-treated patients from the Scandinavian Sarcoma Group Register. Eur J Cancer 36:710–716
39. Vincenzi B, Frezza AM, Schiavon G et al (2013) Bone metastases in soft tissue sarcoma: a survey of natural history, prognostic value and treatment options. Clin Sarcoma 3:6
40. Warren Garner H, Kransdorf MJ, Bancroft LW et al (2009) Benign and malignant soft-tissue tumors: post-treatment MR imaging. Radiographics 29:119–134
41. Weiss SW, Goldblum JR (2001) Enzinger and Weiss's soft tissue tumors, 4th edn. Mosby, St. Lois/London/Philadelphia/Sydney/Tokyo
42. Woertler K (2014) Musculoskeletal tumors. In: Waldt S, Woertler K (eds) Measurements and classifications in musculoskeletal radiology. Thieme, Stuttgart/New York

Grading and Tissue-Specific Diagnosis

9

Filip M. Vanhoenacker and Arthur M. De Schepper†

Contents

9.1 **Introduction** 161

9.2 **Grading** 162
9.2.1 Individual Parameters 162
9.2.2 Combined Parameters 164

9.3 **Tissue-Specific Diagnosis** 165
9.3.1 Nonimaging Parameters 165
9.3.2 Imaging Parameters 166

References 178

9.1 Introduction

Characterization consists of both grading and tissue-specific diagnosis.

While *tissue-specific diagnosis* implies pathological typing, *grading* implies a differentiation between benign and malignant tumors and definition of malignancy grade. Although pathology will always remain the gold standard in the diagnosis of soft tissue tumors, prediction of a specific histologic diagnosis remains one of the ultimate goals of each imaging technique, as decisions regarding biopsy and treatment could be simplified if a specific diagnosis or a limited differential diagnosis could be provided on the basis of imaging [20].

Sundaram stressed the importance of "naming" soft tissue masses based on MR imaging criteria, working on the premise that one's inability to "name" or provide a succinct differential diagnosis requires the lesion to be considered "indeterminate" and biopsied. The approach to such indeterminate lesions is that they are sarcomas until histopathologically proven otherwise [30, 41]. Soft tissue masses that do not demonstrate distinguishing features on MR imaging should be considered indeterminate and will require biopsy [21, 31, 39].

Benign soft tissue tumors (STT) outnumber their malignant counterparts by about 100–1. Otherwise most cutaneous and subcutaneous masses are very small and are often excised without imaging studies. As a consequence 60 % of

†Author was deceased at the time of publication.

F.M. Vanhoenacker, MD, PhD (✉) •
A.M. De Schepper†
Department of Radiology, AZ Sint-Maarten, Duffel-Mechelen, Rooienberg, 25, B-2570 Duffel, Belgium

Faculty of Medicine and Health Sciences, Antwerp University and University Ghent, Wilrijkstraat,10, B-2650 Edegem, Belgium
e-mail: filip.vanhoenacker@telenet.be

© Springer International Publishing AG 2017

F.M. Vanhoenacker et al. (eds.), *Imaging of Soft Tissue Tumors*, DOI 10.1007/978-3-319-46679-8_9

the soft tissue tumors in adults who are referred for evaluation by medical imaging are benign, this proportion increasing to 75 % in the pediatric age group. The major role of grading consists merely in recognizing benign soft tissue tumors which will be excluded from further invasive diagnostic and therapeutic procedures.

The significance and the predictive value of the various histologic parameters vary in different types of sarcoma. Because of morphologic variations in different portions of the tumor, the grade is determined on the basis of the least differentiated area and its extent [13, 40].

9.2 Grading

The World Health Organization (WHO) recognizes four categories of soft tissue tumors (STT): benign, intermediate (locally aggressive), intermediate (rarely metastasizing), and malignant [10]. Well-known histological grading parameters are cellularity, cellular pleomorphism, mitotic rate, matrix, and the presence of necrosis. Tumor necrosis, tumor size, and most importantly mitotic count are significantly correlated with the duration of survival or the time to distant metastases [22, 33] Most of these parameters influence signal intensity on MRI. Nevertheless, there is still much controversy regarding the value of conventional MRI in the differentiation of benign and malignant soft tissue tumors [1, 7].

A variety of imaging-grading parameters have been described in the literature and are listed in Table 9.1. We will comment first on the value of each individual parameter followed by a summary on the strength of a combination of multiple grading parameters.

9.2.1 Individual Parameters

Examples of commonly used individual parameters for predicting malignancy are *intensity* and *homogeneity of the MR signal* with different pulse sequences. Signal characteristics of both benign and malignant tumors overlap frequently.

Table 9.1 Soft tissue tumor (STT) grading parameters

Origin (subcutaneous, fascial, intramuscular, mixed)
Location
Distribution
Intracompartmental
Extracompartmental
Size
Shape
Margins
Relationship with superficial fasciae
Neurovascular bundle displacement/encasement
Bone involvement
Signal intensity on different pulse sequences
Signal homogeneity
Changing pattern of homogeneity
Low-signal-intensity septations
Peritumoral edema
Hemorrhage
Contrast enhancement
Static studies (type, intensity)
Dynamic studies (ratio, slope)
Diffusion-weighted MRI

High signal intensity (SI) on T2-WI and inhomogeneity on T1-WI are sensitive but unfortunately nonspecific parameters. Although most malignant lesions are inhomogeneous, smaller lesions tend to be more homogeneous, irrespective whether they are benign or malignant [39]. Concerning signal intensity, high-grade malignant soft tissue tumors may present with low to intermediate signal intensity on T2-WI as a consequence of hypercellularity, increased nucleocytoplasmic index, and an altered ratio between cellular and interstitial components both resulting in a decreased amount of intra- and extracellular water [1, 3, 26]. In this regard, lymphomas and nondifferentiated (high-grade) sarcomas may present with low SI on T2-weighted images and have to be differentiated from tumors showing recurrent intralesional bleeding and hemosiderin loading causing shortening of the T2-relaxation time and consequently lower SI on T2-WI.

Clear cell sarcomas may present with increased SI on T1-weighted images, depending on their content on melanin which shortens the T1-relaxation time [2].

Changing homogeneity (from homogeneous on T1-WI to heterogeneous on T2-WI) and the presence of a lobular morphology with intervening low-signal intratumoral septations were reported by Hermann, respectively, with a sensitivity of 72 and 80 %, respectively, and a specificity of 87 and 91 %, respectively, in predicting malignancy [14].

Galant et al. described a grading system of subcutaneous soft tissue tumors by means of their *relationship with the superficial fascia* on MRI. Obtuse angles between superficial fascia and a subcutaneous mass crossing the fascia indicate a probability of malignancy six to seven times that for lesions that do not cross the fascia or have contact with acute angles. Exceptions are vascular and neurogenic tumors, which can cross the fascia through preexisting anatomical channels and fibromatosis [11].

Location has a limited value in differentiating benign and malignant soft tissue tumors. In contradistinction to malignant tumors, benign ones frequently have a preferential location (see also 9.3 Tissue-Specific Diagnosis). Typical examples are elastofibroma dorsi which has a predilection for the subscapular region, PVNS for the joints, nodular fasciitis for the forearm, desmoids for the deltoid and gluteal region, glomus tumors for the subungual soft tissues while soft tissue tumors of the hand and wrist are benign in more than 90 % of the cases, and intraarticular tumoral lesions being almost always benign. Generally, soft tissue sarcomas have a predilection for the thigh and in particular synovial cell sarcomas for the foot. Although the *size* and *shape* of the lesion at detection seem unlikely to contribute to tumor grading, Tung combined the data from three investigations and postulated that a diameter of less than 3 cm is a reasonable indicator that a lesion is benign, as this threshold is associated with a positive predictive value of 88 %. Conversely, a diameter of 5 cm predicts malignancy with a sensitivity of 74 %, specificity of 59 %, and an accuracy of 66 % [6, 32].

Although benign tumors tend to be well delineated and, conversely, malignant tumors have rather ill-defined margins, several studies have concluded that the *margin* (well defined versus infiltrating) of a soft tissue mass on MRI is of no statistical relevance in predicting of malignancy. Moreover, Bongartz reported that aggressive sarcomas may have a pseudocapsule, while benign lesions such as desmoid tumors may invade neighboring tissues [3, 34, 39].

Peritumoral edema, shown on T2-weighted images as an ill-defined area of high signal intensity, can indicate infiltrative tumor [5] but may be seen in reparative inflammation as well [13].

Involvement of adjacent bone, *extracompartmental distribution*, and *encasement of the neurovascular bundle* are relatively uncommon findings that are insensitive signs of malignancy. They are also seen in aggressive benign soft tissue lesions including desmoids, hemangiomas, and pigmented villonodular synovitis.

The parameter *growth rate* is related to the aggressiveness of a soft tissue tumor and not to its malignancy grade [5].

Intratumoral hemorrhage is a rare finding, which can be observed in both benign and malignant lesions, and is difficult to differentiate from nontumoral soft tissue hematoma. Hemorrhage is of high signal on T1-weighted images, coupled with low or high signal on T2-weighted images, provided the tissue was not isointense to fat on all sequences. A low-signal hemosiderin rim is indicative as evidence of prior hemorrhage [20].

Malignant tumors show increased vascularity and have large extracellular spaces and usually reveal greater enhancement and an increased rate of enhancement on dynamic contrast-enhanced imaging [23], although there is a significant overlap in *degree and pattern of enhancement* and malignancy grade [19, 37, 39].

In a multivariate analysis of 140 soft tissue tumors, Van Rijswijk et al. revealed that combined nonenhanced static and dynamic contrast-enhanced MR imaging parameters were significantly superior to nonenhanced MR imaging parameters alone and to nonenhanced MR imaging parameters combined with static contrast-enhanced MR imaging parameters in prediction of malignancy. The most discriminat-

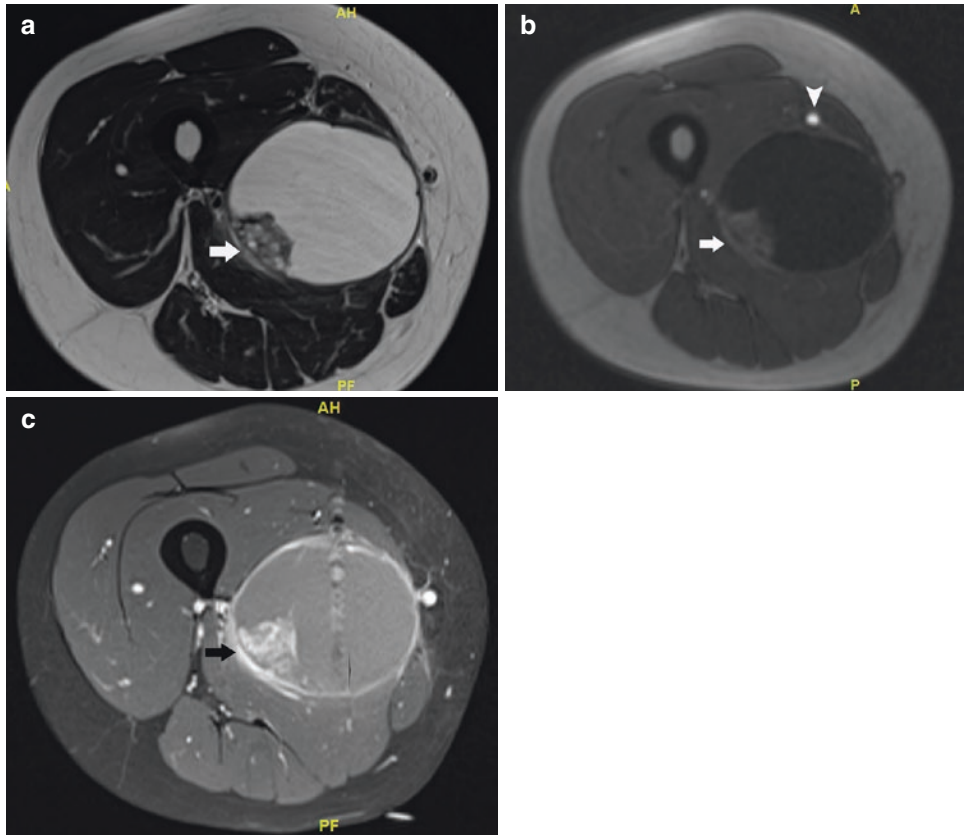

Fig. 9.1 (**a**–**c**). High grade pleiomorphic sarcoma of the right adductor compartment in a 54-year-old female: (**a**) Axial T2-weighted MR image showing a large inhomogeneous intramuscular lesion with myxoid and solid (*white arrow*) components; (**b**) Axial dynamic MR sequence after intravenous bolus injection of gadolinium contrast showing very rapid enhancement of the solid part of the lesion (*white arrow*) following arterial enhancement (*white arrowhead*); (**c**) Delayed fatsuppressed T1-weighted MR image shows inhomogeneous enhancement with peripheral enhancing nodule (*black arrow*). The large size of the lesion, inhomogeneity of the lesion and the rapid and inhomogeneous enhancement are in favor of a malignant lesion

ing parameters were presence of liquefaction, start of dynamic enhancement (time interval between start of arterial and tumor enhancement), and lesion size (diameter) (Fig. 9.1).

Additional diffusion-weighted imaging (DWI) has proven to be useful in the differential diagnosis of malignant versus benign STT [5, 15, 18, 24]. True diffusion coefficients of malignant STT are significantly lower than those of benign masses, whereas ADC values between both groups are not significantly different.

The value of dynamic contrast-enhanced MRI and DWI in the differentiation of benign versus malignant STT is further discussed in Chap. 5.

PET-CT and PET-MRI may be useful to target active metabolic areas within a STT [4, 9].

9.2.2 Combined Parameters

Although most investigators failed to establish reliable criteria for distinguishing benign from malignant lesions, a combination of individual parameters yields higher sensitivity and specificity [1, 5, 6, 25, 27].

Our research group performed multivariate statistical analysis to determine the accuracy of ten parameters, individually and in combination,

for predicting malignancy. When the following signs were observed together, malignancy was predicted with a sensitivity of 81 % and a specificity of 81 %: absence of low signal intensity on T2-weighted images, signal inhomogeneity on T1-weighted images, and mean diameter of the lesion greater than 33 mm (Fig. 9.2). Malignancy was predicted with the highest sensitivity when a lesion had high signal intensity on T2-weighted images, was larger than 33 mm in diameter, and had an inhomogeneous signal intensity on T1-weighted images. Signs that had the greatest specificity for malignancy included the presence of tumor necrosis, bone or neurovascular involvement, and a mean diameter of more than 66 mm. Of the malignant lesions, 80 % had irregular or partially irregular margins, while a similar percentage of benign masses had well-defined or partially irregular margins. The majority of both benign and malignant lesions showed moderate or strong enhancement, no predominant enhancement pattern emerged for either type of mass. In contrast to the study of Berquist et al. [1], margin, signal homogeneity on T2-weighted images, signal intensity on T1-weighted images, shape, and enhancement pattern were statistically nondiscriminatory [27].

Our group also prospectively assessed the value of MRI in grading soft tissue tumors in a series of 548 untreated patients originating from a multi-institutional database, 123 with malignant and 425 with benign tumors. The thresholds to differentiate between malignant and benign STT are interpreted in a nonquantitative way using grading parameters described in literature. We obtained a sensitivity of 93 %, a specificity of 82 %, a negative predictive value of 98 %, and a positive predictive value of 60 % in diagnosing malignancy [12].

More recently, we showed that a second opinion report by a center with large expertise in STT may improve the overall accuracy of grading and characterization from 83 % up to 92 % [35].

MR parameters that suggest malignancy of a soft tissue mass are summarized in Table 9.2.

Table 9.2 Most useful MR parameters that suggest malignancy of a soft tissue lesion

Large size (more than 3 cm)
Ill-defined margins
Inhomogeneity on all pulse sequences
Intralesional hemorrhage or necrosis
Marked and peripheral enhancement pattern (with papillary projections) on static contrast examination
Rapid enhancement with steep slope on dynamic contrast examination
Extracompartmental extension
Invasion of adjacent bones and neurovascular bundles

9.3 Tissue-Specific Diagnosis

Benign soft tissue lesions often have a characteristic imaging appearance obviating the need of further histological confirmation. Unfortunately, a tissue-specific diagnosis (characterization) cannot be obtained in all STT, particularly not in malignant STT.

A combination of nonimaging parameters and imaging parameters on different imaging modalities may however be helpful in noninvasive characterization of STT.

9.3.1 Nonimaging Parameters

Relative Prevalence, Location, and Patient's Age

The overall annual clinical incidence of STT is relatively rare, accounting for 250 per 100,000 for benign STT as compared with 3 per 100,000 for malignant ones. Although some individual entities are rare and therefore difficult to remember for the radiologist, fortunately 70 % of benign and 80 % of malignant tumors can be classified in, respectively, six and seven "diagnostic categories," which are summarized in Table 9.3 [16, 17].

Table 9.3 Major diagnostic groups of soft tissue tumors

70 % benign	80 % malignant
Lipoma and variants	Myxofibrosarcoma
Fibrous histiocytoma	Liposarcoma
Nodular fasciitis	Leiomyosarcoma
Hemangioma	Malignant peripheral nerve sheath tumor
Fibromatosis	Synovial sarcoma
Neurofibroma-schwannoma	Fibrosarcoma
	Sarcoma NOS (not otherwise specified)

In addition, location of the lesion and the age/gender of the patient are very useful nonimaging parameters that may help to suggest a tissue-specific diagnosis on imaging. The usefulness of these nonimaging parameters, including relative prevalence, age at presentation, sex distribution, and zonal distribution, has been well documented by Kransdorf in a large referral population of benign and malignant STT [16, 17].

This study is subject to inherent selection bias (e.g., malignant looking STT are more referred for second opinion than benign ones; small superficial lesions are excised or sampled without imaging). Despite the limitations of the study, the tables from Kransdorf's paper are highly useful in the evaluation of soft tissue tumor pathology (Tables 9.4 and 9.5) [16, 17].

Preferential location of STT is summarized in Table 9.6 and further discussed in the each chapter of part III of this book.

Multiplicity/Bilateral Lesions
Multiplicity is another nonimaging parameter that may help to narrow down the differential diagnosis.

If multiple or bilateral soft tissue lesions are encountered, one should think of neurogenic tumors (see Chap. 17), soft tissue metastases (see Chap. 23), xanthomatosis of tendons (Fig. 9.3), multiple desmoid tumors (see Chap. 13), elastofibroma dorsi (Fig. 9.4) [36], etc. (see Table 9.7).

Concomitant Diseases
Recognition of a soft tissue tumor and a concomitant disease may lead to a highly specific diagnosis on imaging (see Table 9.8).

9.3.2 Imaging Parameters

Plain Films
Certain STT contain intralesional calcifications or ossifications, which may increase specificity in diagnosis [25].

Anaerobic soft tissue infection or abscess may contain air bubbles (see Chap. 2 for further discussion).

Computed Tomography
Computed tomography (CT) is currently surpassed by MRI for evaluation of soft tissue tumors, because of its relatively low contrast resolution and because of radiation constraints. The technique may – however – be useful for demonstration of subtle intralesional calcifications/ossifications or in case of contraindications for MRI (see Chap. 2).

Ultrasound
Ultrasound is often used for detection and characterization of superficially located benign periarticular cysts (see Chap. 1). Further imaging is rarely needed in these scenarios. However, myxoid tumors should not be misinterpreted as true cystic lesions. Ultrasound is not recommended for tissue-specific diagnosis of solid, large, and deeply located lesions.

Table 9.4 Distribution of common benign soft tissue tumors by anatomic location and age

Age (years)	Hand and wrist	%	Upper extremity	%	Axilla and shoulder	%	Foot and ankle	%	Lower extremity	%	Hip, groin, and buttocks	%	Head and neck	%	Trunk	%	Retroperitoneum	%
0–5	Hemangioma	15	Fibrous hamartoma of infancy	16	Fibrous hamartoma of infancy	29	Granuloma annulare	30	Granuloma annulare	23	Fibrous hamartoma of infancy	20	Nodular fasciitis	20	Hemangioma	18	Lipoblastoma	37
6–15	Fibrous histiocytoma	14	Fibrous histiocytoma	23	Fibrous histiocytoma	34	Fibromatosis	23	Hemangioma	22	Nodular fasciitis	27	Nodular fasciitis	33	Nodular fasciitis	28	Lymphangioma	37
16–25	GCTTS	20	Nodular fasciitis	35	Fibrous histiocytoma	36	Fibromatosis	22	Fibrous histiocytoma	24	Neurofibroma	16	Nodular fasciitis	21	Nodular fasciitis	24	Fibromatosis	20
26–45	Fibrous histiocytoma	18	Nodular fasciitis	38	Lipoma	28	Fibromatosis	21	Fibrous histiocytoma	25	Lipoma	17	Lipoma	29	Lipoma	19	Schwannoma	23
46–65	GCTTS	23	Nodular fasciitis	20	Lipoma	58	Fibromatosis	25	Lipoma	23	Lipoma	35	Lipoma	46	Lipoma	44	Schwannoma	19
66 and over	GCTTS	21	Lipoma	22	Lipoma	58	Fibromatosis	14	Lipoma	26	Lipoma	21	Lipoma	50	Lipoma	42	Schwannoma	26

From Kransdorf [28] with permission
GCTTS giant cell tumor of tendon sheath

Table 9.5 Distribution of common malignant soft tissue tumors by anatomic location and age

Age (years)	Hand and wrist	%	Upper extremity	%	Axilla and shoulder	%	Foot and ankle	%	Lower extremity	%	Hip, groin, and buttocks	%	Trunk	%	Retroperitoneum	%
0–5	Fibrosarcoma	45	Fibrosarcoma	29	Fibrosarcoma	56	Fibrosarcoma	45	Fibrosarcoma	45	Fibrosarcoma	32	Fibrosarcoma	26	Fibrosarcoma	20
6–15	Epithelioid sarcoma	21	Angiomatoid MFH	33	Angiomatoid MFH	21	Synovial sarcoma	21	Synovial sarcoma	22	Angiomatoid MFH	21	Rhabdomyosarcoma	15	Rhabdomyosarcoma	31
16–25	Epithelioid sarcoma	29	Synovial sarcoma	23	Synovial sarcoma	18	Synovial sarcoma	30	Synovial sarcoma	22	Synovial sarcoma	18	MFH	23	Malignant schwannoma	20
26–45	MFH	18	MFH	28	DFSP	33	Synovial sarcoma	26	Liposarcoma	28	Liposarcoma	18	DFSP	30	Leiomyosarcoma	32
46–65	MFH	19	MFH	46	MFH	35	MFH	25	MFH	43	Liposarcoma	24	MFH	31	Liposarcoma	33
66 and over	MFH	35	MFH	60	MFH	50	Kaposi's sarcoma	37	MFH	55	MFH	46	MFH	44	Liposarcoma	39

From Kransdorf [27with permission
DFSP dermatofibrosarcoma protuberans, *MFH* malignant fibrous histiocytoma (myxofibrosarcoma)

Table 9.6 Preferential location of soft tissue tumors

Location		Tumor
Neck		Cystic hygroma – lymphangioma (infants)
		Capillary hemangioma (infants)
		Myofibroma (children)
		Infantile desmoid fibromatosis (children)
	Dorsal neck	Nuchal fibroma
	Sternocleidomastoid muscle	Fibromatosis colli (children)
	Carotid bifurcation	Glomus tumor
Trunk	Axilla	Cystic hygroma – lymphangioma
	Subscapular	Elastofibroma
	Spinoglenoid notch	Ganglion cyst
	Paraspinal gutter	Neurogenic tumor
Abdomen	Rectus abdominis muscle	Abdominal desmoid
	Costal gutter – paraspinal gutter	Neurogenic tumor
	Psoas muscle, parapsoatic	Plexiform neurofibroma
Pelvis	Presacral	Plexiform neurofibroma
	Buttock, lateral aspect	Desmoid
		Injection granuloma
	Coccyx	Extraspinal ependymoma
Upper limb	Deltoid, subcutaneous	Desmoid
		Injection granuloma
	Forearm, volar aspect	Nodular fasciitis
	Medial epitrochlear lymph node	Cat scratch disease
	Wrist	Ganglion cyst
	Wrist, volar aspect	Fibrolipohamartoma of median nerve
	Hand	Gouty tophi
	Hand, volar aspect	Palmar fibromatosis
		Fibrolipohamartoma of median nerve
	Hypothenar	Hypothenar hammer syndrome
	Finger	Macrodystrophia lipomatosa
	Finger, volar aspect	Giant cell tumor of tendon sheath
	Finger, dorsal aspect	Digital fibroma (children)
	Finger, tip	Epidermoid cyst
		Glomus tumor
Lower limb	Flexor aspect, along major nerves	Schwannoma
	Thigh	Fibrohamartoma of infancy (infants)
		Alveolar soft part sarcoma (adults)
		Sarcoma (liposarcoma) (older men)
	Knee	Synovial hemangioma
		Pigmented villonodular synovitis (young, middle-aged men)
		Lipoma arborescens (older men)
	Knee, popliteal fossa	Pigmented villonodular synovitis
		Baker's cyst

(continued)

Table 9.6 (continued)

Location		Tumor
		Synovial cyst
		Ganglion cyst
		Meniscal cyst
		Nerve sheath tumor
		Aneurysm of popliteal artery
	Knee, tibiofibular joint	Ganglion cyst
	Ankle	Ganglion cyst
	Foot, extensor aspect	Ganglion cyst
	Sole	Synoviosarcoma (young adults)
		Plantar fibromatosis
	Heel	Clear cell sarcoma
	Metatarsals	Morton's neuroma (women)
	Toes	Giant cell tumor of tendon sheath
Upper and lower limb		Fibrous histiocytoma
		Myxofibrosarcoma
		Myositis ossificans
	Extensor aspect	Leiomyoma (young adults)
Joints, periarticular		Synovial hemangioma
		Amyloidosis
		Lipoma arborescens
		Pigmented villonodular synovitis
		Synoviosarcoma
Tendons	(Achilles tendon, bilateral)	Xanthoma
		Giant cell tumor of tendon sheath
Course of major nerves		Nerve sheath tumors
Cutis, subcutis		Desmoid
		Neurofibroma
		Nodular fasciitis
		Dermatofibrosarcoma protuberans
		Granular cell tumor

Any lesion with increased (color) Doppler flow should be regarded as a potential malignancy and should be referred for MRI [21]. Further evaluation with MRI is then needed.

A clear history of trauma is required to make the reliable diagnosis of an intramuscular hematoma. Meticulous correlation with clinical findings is always required in order not to overlook potential malignancy. Careful clinical and imaging follow-up is needed.

Magnetic Resonance Imaging

Like previously mentioned for grading, MRI is also the most useful imaging technique for suggesting a tissue-specific diagnosis if the following MR parameters are combined: morphology, signal intensities on T1- and T2-weighted images (WIs), fat suppression (FS), homogeneity, and pattern and degree of contrast enhancement on (dynamic) contrast-enhanced MRI [23, 28, 38, 39].

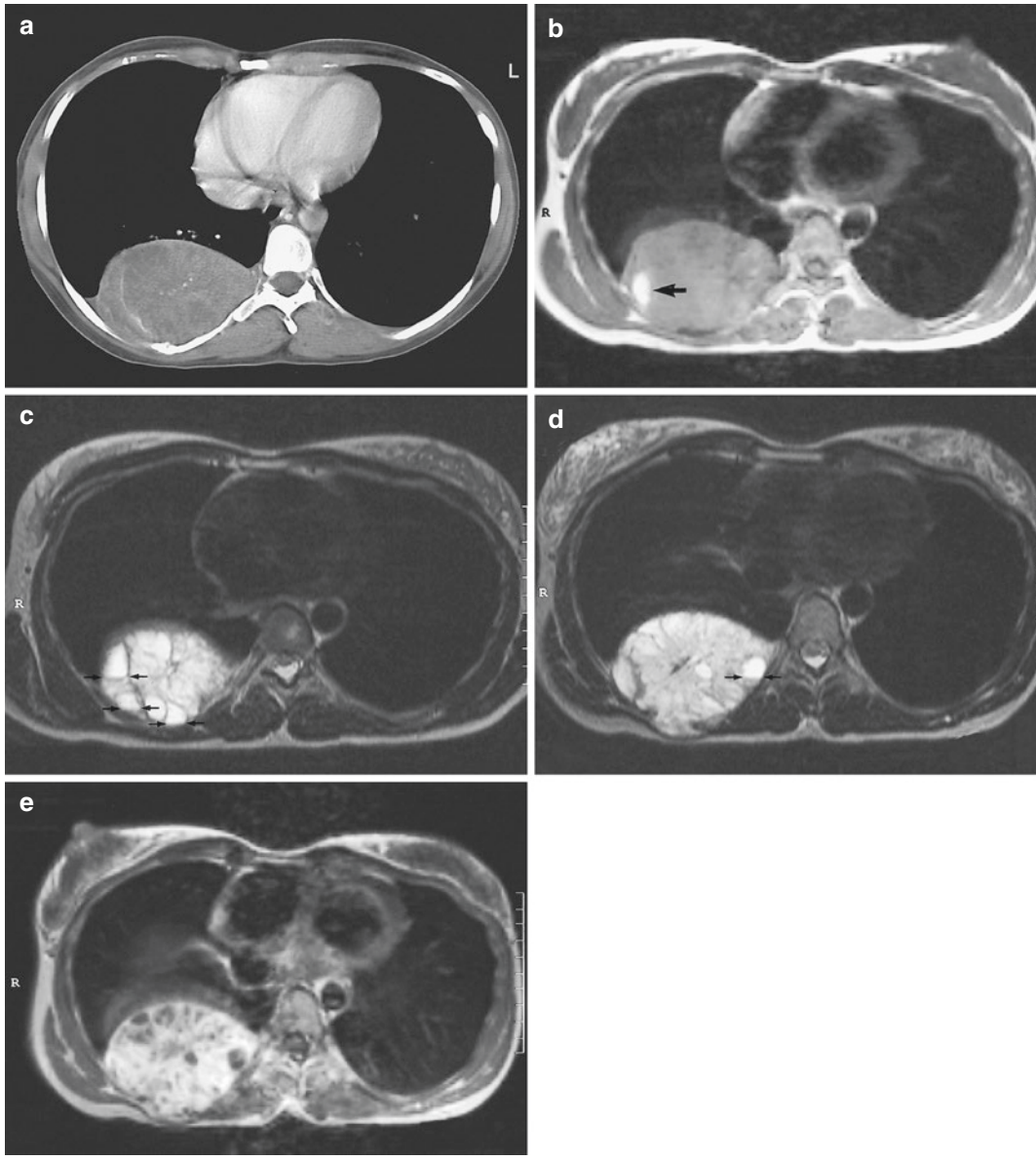

Fig. 9.2 (**a**–**e**). Malignant peripheral nerve sheath tumor of the chest wall in a 29-year-old woman: (**a**) CT scan of the chest after I-contrast injection; (**b**) axial SE T1-weighted MR image; (**c**,**d**) axial SE T2-weighted MR image; (**e**) axial SE T2-weighted MR image after Gd-contrast injection. On CT scan of the chest, there is a large, rounded, and sharply demarcated mass located in the costovertebral gutter, with the presence of intralesional calcifications and spoke-wheel-like enhancement after contrast injection (**a**). On T1-WI the lesion is inhomogeneous and of intermediate SI. There is a small area of high SI laterally within the mass (*arrow*) (**b**). On T2-WI there is again a spoke-wheel appearance of the lesion; there are multiple fluid-fluid levels and rounded high SI areas (*small arrows*) on a background of intermediate to high SI (**c**,**d**). On T1-WI after contrast injection, there is marked enhancement without enhancement of the rounded high SI areas on T2-WI (compare (**d**) with (**e**)). Large size (50×80×80 mm), extracompartmental extension and bone involvement, inhomogeneous distribution of SI, and the presence of amorphous calcifications within the lesion are parameters, predicting malignancy. Sharp margins and the presence of intralesional hemorrhage are nondiscriminatory parameters. Localization is in favor of a neurogenic tumor. Histologic diagnosis after resection confirmed the diagnosis of a malignant nerve sheath tumor (right 8th intercostal nerve)

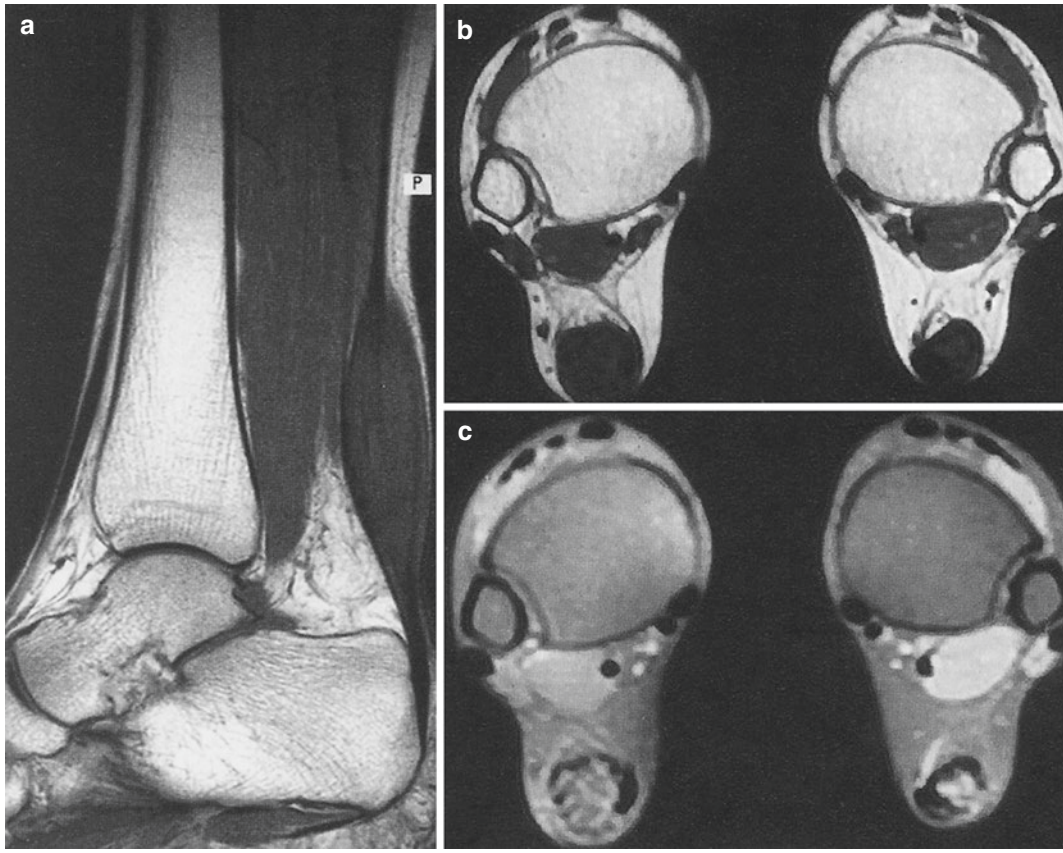

Fig. 9.3 (**a**–**c**). Xanthoma of both Achilles tendons in a patient with familial hypercholesterolemia. The lesions are fusiform on sagittal images (only one side shown) (**a**) and have a speckled appearance on axial SE-T1-WI (**b**), and the signal of intratendinous xanthomatous areas is not reduced on fat-suppressed T1-WI (**c**)

Table 9.7 Lesion that may be multiple or bilateral

Venous malformation
Lipoma 5–8 %
Lipoma of tendon sheath (50 %)
Desmoid
Neurofibroma
Myxoma
Metastasis
Dermatofibrosarcoma protuberans
Kaposi's sarcoma
Xanthoma
Injection granuloma

Morphology is particularly helpful in prediction of tissue-specific diagnosis (Table 9.9). Typical morphological signs are lasagna sign in elastofibroma dorsi (Fig. 9.4 and Chap. 21, Fig. 21.43), broccoli sign in lipoma arborescens (see Chap. 12, Fig. 12.28 and Chap. 20, Fig. 20.21), target sign in neurofibroma (Fig. 9.5 and Chap. 17), fluid-fluid sign in hemangioma/lymphangioma (Table 9.10) (Fig. 9.6 and Chap. 16), and other STT in which hemorrhage occurred.

Based on the analysis of signal intensity (SI) on T1-WI and T2-WI, four major characteristic groups of STT can be distinguished (Table 9.11). The use of FS techniques may be helpful to differentiate between lipomatous and nonlipomatous components.

- *Group I*: Lesions which are of high SI on T1-WI similar to subcutaneous fat, intermediate on TSE T2-WI, and suppressed equally to fat on FS images may indicate the presence of fat (see examples in Chap. 12).

Table 9.8 Concomitant diseases

Concomitant osseous involvement	Pigmented villonodular synovitis
	Lymphoma
	Desmoid
	Angiomatosis
	Parosteal lipoma
	Myofibromatosis (children)
	Juvenile hyaline fibromatosis (children)
Maffucci's disease	Cavernous hemangioma(s)
Fibrous dysplasia (Mazabraud)	Myxoma(s)
Neurofibromatosis	Schwannoma(s)
	Neurofibroma(s)
Gardner's syndrome	Fibromatosis
Dupuytren's disease (flexion contractures)	Palmar fibromatosis
Macrodystrophia lipomatosa of the digits	Fibrolipohamartoma of the median nerve
Familial hypercholesterolemia	Xanthoma
Normolipidemia + lymphoma or granuloma	Cutaneous xanthoma
Multiple myeloma	Amyloidosis
Turner's syndrome	Lymphangioma
Diabetes + degenerative joint disease + trauma	Lipoma arborescens

Table 9.9 Morphology

Fusiform (ovoid)	Neurofibroma
	Lipoma
Dumbbell	Neurofibroma
	Desmoid
Moniliform	Neurofibroma
	Synovial – ganglion cyst
Round	Cyst
	Schwannoma
Serpiginous	Hemangioma
Soap bubbles – cauliflower	Lipoma arborescens
Nodular	Fibromatosis (plantaris, palmaris)
Branching (bilateral)	Plexiform neurofibroma
Finger-like	

- *Group II*: Intermediate to high SI on T1-WI compared to normal muscle and a high SI on T2-WI may correspond to subacute blood, slow-flowing blood in slow-flow vascular malformations, high protein content in lymphangiomas (see Chap. 16), and melanin in melanoma and clear cell sarcomas (see Chap. 18). In contradistinction to fat-containing lesions, there is absence of signal drop.
- *Group III*: A combination of low SI on T1-WI and high SI on T2-WI is seen in cystic lesions (Fig. 9.7 and Chap. 20) and myxoid-containing tumors such as myxoma (see Chap. 18) and other sarcoma containing myxoid components such as myxoid liposarcoma (see Chap. 12) [29]. Myxoid-containing lesions show a moderate decrease in SI after FS when compared with non-FS T1-WI.
- *Group IV*: Low SI on T1-WI and T2-WI can be caused by fibrous tissue in desmoids and other fibromatoses, hemosiderin in old hematomas, and pigmented villonodular synovitis (PVNS) (Fig. 9.8 and Chap. 14). Hypercellularity in high-grade malignancies and lymphomas (see Chap. 22) may also cause a relatively low SI, especially on T2-WI. The presence of blooming on gradient-echo sequences indicating susceptibility artifacts due to hemosiderin is particularly helpful to distinguish PVNS from other lesions with a low T1 and T2 signals. Certain lesion may demonstrate an intratumoral signal void (Table 9.12).

The abovementioned MRI characteristics for some specific tumors are further described in the respective chapters.

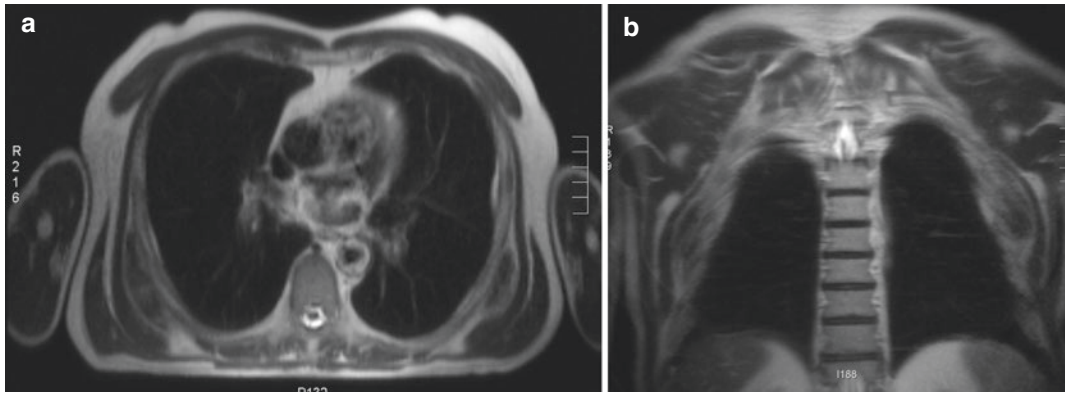

Fig. 9.4 (**a**, **b**) Bilateral elastofibroma dorsi. (**a**) Axial TSE T2-weighted MR image; (**b**) coronal TSE T2-weighted MR image. Elastofibroma dorsi has a typical multilayered morphology, consisting of alternating bands of low signal with intermingled fatty components, resembling lasagna. The lesions are often bilateral and are typically located in the periscapular region between the thoracic wall muscles and the ribs

Table 9.10 Fluid-fluid levels

Hemangioma
Cystic lymphangioma
Synoviosarcoma
Myxoma
Hematoma
Myositis
Metastasis

A second opinion report by a center with large expertise in STT may improve the overall accuracy of grading and also tissue-specific diagnosis [35].

The role of advanced MR techniques such as diffusion-weighted imaging, diffusion tensor imaging, and MR spectroscopy for tissue-specific diagnosis is still debated [8] (see also Chap. 5).

Other Diagnostics Techniques

The role of cytogenetics and molecular genetics in tissue-specific diagnosis of STT is discussed in Chap. 6.

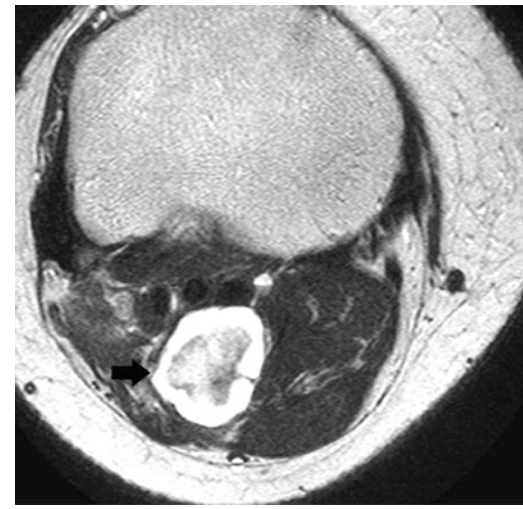

Fig. 9.5 Target sign in neurofibroma of the tibial nerve. Axial TSE T2-weighted MR image showing a lesion located on the course of the tibial nerve. The lesion has a target-like appearance (*black arrow*), consisting of a hypointense center and a hyperintense periphery (see also Chap. 17 for further explanation of this sign)

Table 9.11 Major diagnostic groups of STT according to their signal intensities on T1- and T2-weighted images

Group I	
High signal intensity on T1-weighted images, intermediate signal intensity on T2-weighted images	Lipoma
	Liposarcoma
	Lipoblastoma
	Hibernoma
	Elastofibroma
	Fibrolipohamartoma
	Metastasis of melanoma (melanin)
	Clear cell sarcoma (melanin)
Group II	
High signal intensity on T1-weighted images, high signal intensity on T2-weighted images	Hemangioma
	Lymphangioma
	Subacute hematoma
	Small arteriovenous malformation
Group III	
Low signal intensity on T1-weighted images, high signal intensity on T2-weighted images	Cyst
	Myxoma
	Myxoid liposarcoma
	Most sarcoma
Group IV	
Low to intermediate signal intensity on T1-weighted images, low to intermediate signal intensity on T2-weighted images	Desmoid and other fibromatoses
	Pigmented villonodular synovitis
	Morton's neuroma
	Fibrolipohamartoma
	Giant cell tumor of tendon sheath
	Acute hematoma (few days)
	Old hematoma
	Xanthoma
	High-flow arteriovenous malformation
	Mineralized mass
	Scar tissue
	Amyloidosis
	Granuloma annulare
	Lymphoma
	High-grade malignancies

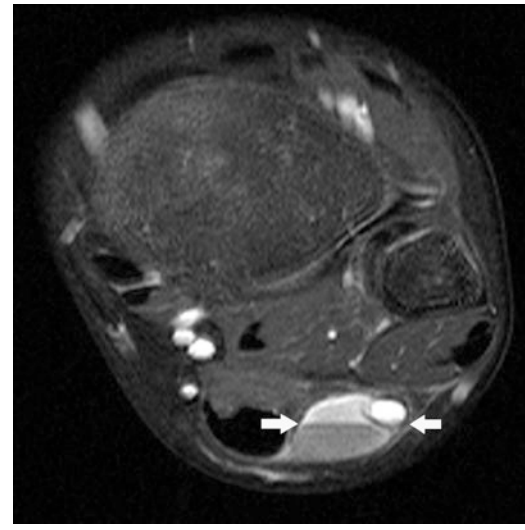

Fig. 9.6 Fluid-fluid level (*white arrows*) in a hemangioma located on the course of the sural nerve on an axial FS TSE T2-weighted MR image (see also Chap. 16)

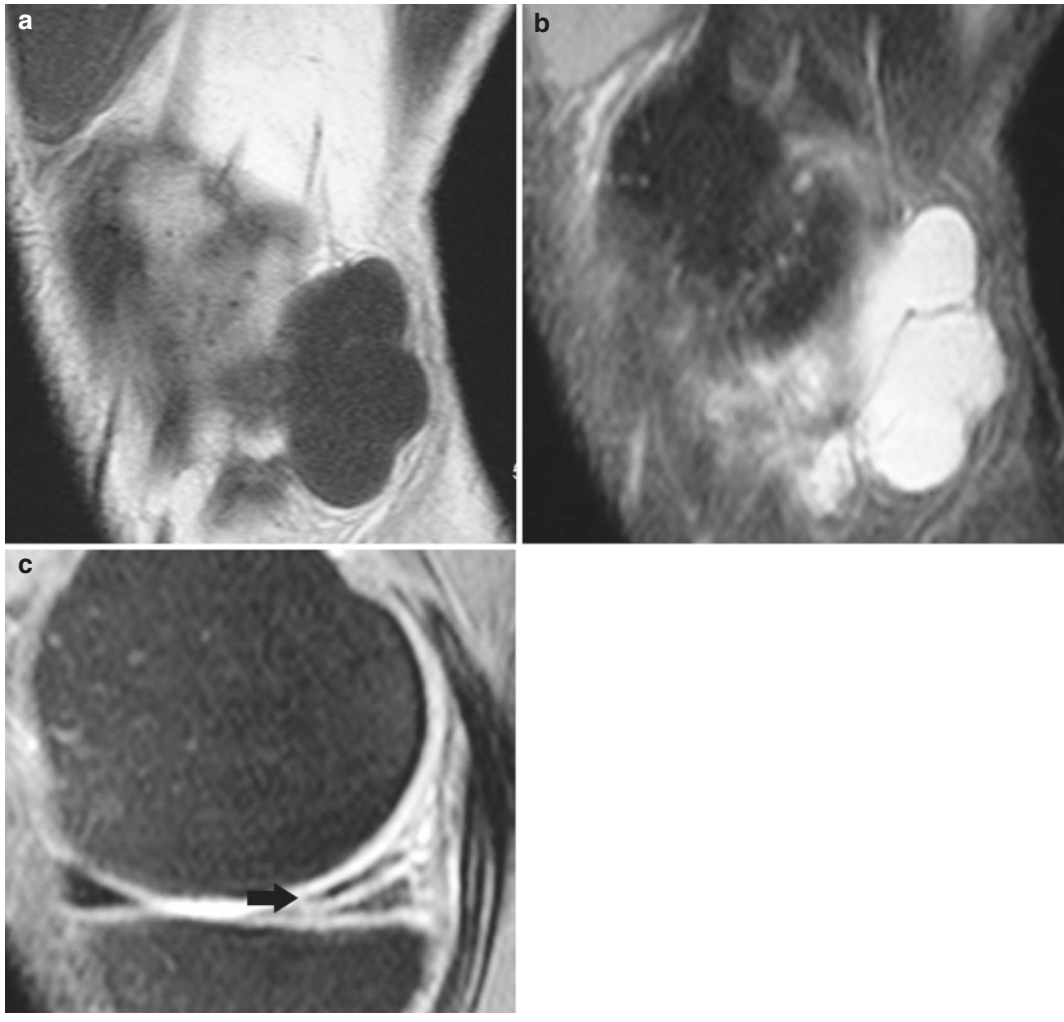

Fig. 9.7 Meniscal cyst: (**a**) sagittal T1-weighted MR image; (**b**) sagittal FS T2-weighted MR image of the knee; (**c**) sagittal FS T2-weighted MR image of the knee at the level of the medial meniscus. The lesion isointense to muscle on T1-WI (**a**) and of high SI on FS T2-WI (**b**). Adjacent to the cystic lesion, there is a transverse medial meniscus tear (*black arrow*) communicating with the cystic lesion

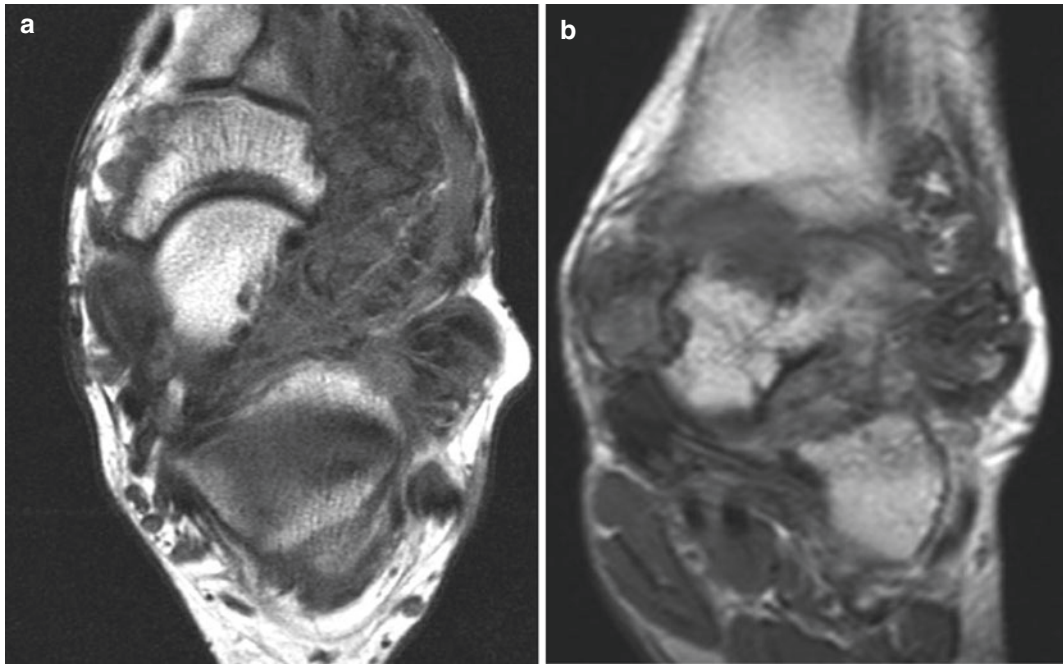

Fig. 9.8 Pigmented villonodular synovitis (PVNS): (**a**) axial T1-weighted MR image; **b**) coronal T2-weighted MR image of the left ankle. There is a large intra-articular lesion, causing erosions of the margins of the talocrural joint. The lesions contain large foci of low signal, in keeping with old blood components (hemosiderin)

Table 9.12 Intratumoral signal void

Flow	Hemangioma (capillary)
	Arteriovenous malformation
Calcification	Hemangioma (phlebolith)
	Lipoma (well-differentiated and dedifferentiated)
	Desmoid
	Cartilaginous tumors
	Osteosarcoma of soft tissue
	Synoviosarcoma (poorly defined, amorphous)
	Chordoma
	Alveolar soft part sarcoma
	Myositis ossificans (marginal-zonal)
High content of collagen	Desmoid

Key Points

1. Most soft tissue tumors are benign (60–75 %). The major role of grading consists in recognizing benign soft tissue tumors, which will be excluded from further invasive diagnostic and therapeutic procedures.
2. Accuracy of individual (MR imaging) parameters is low.
3. Best results are obtained by combining individual grading parameters. Besides age and location, morphology, signal intensities on different pulse sequences, the presence of signal voids, the presence of fluid-fluid levels, multiplicity, and

knowledge of associated diseases are major tissue-specific parameters. Here also, combination of different parameters increases imaging performance.

4. Four groups of soft tissue tumors are defined, according to their signal intensities on T1- and T2-weighted MR images. High SI on T1-weighted and low SI on T2-weighted images have the best predictive value concerning tissue-specific diagnosis.
5. Multi-institutional approach of soft tissue tumors guarantees best diagnostic and therapeutic results. A second opinion report by a center with large experience in diagnosis and treatment of STT will enhance diagnostic accuracy.

Acknowledgment The current revision of this chapter is gratefully dedicated to the memory of Professor Arthur De Schepper (November 30, 1937–October 4, 2013).

References

1. Berquist TH, Ehman RL, King BF, Hodgman CG, Ilstrup DM (1990) Value of MR imaging in differentiating benign from malignant soft-tissue masses: study of 95 lesions. AJR Am J Roentgenol 155:1251–1255. doi:10.2214/ajr.155.6.2122675
2. De Beuckeleer LH, De Schepper AM, Vandevenne JE, Bloem JL, Davies AM, Oudkerk M, Hauben E, Van Marck E, Somville J, Vanel D, Steinbach LS, Guinebretière JM, Hogendoorn PC, Mooi WJ, Verstraete K, Zaloudek C, Jones H (2000) MR imaging of clear cell sarcoma (malignant melanoma of the soft parts): a multicenter correlative MRI-pathology study of 21 cases and literature review. Skeletal Radiol 29:187–195
3. Bongartz G, Vestring T, Peters PE (1992) Magnetic resonance tomography of soft tissue tumors. Radiologe 32:584–590
4. Buchbender C, Heusner TA, Lauenstein TC, Bockisch A, Antoch G (2012) Oncologic PET/MRI, part 2: bone tumors, soft-tissue tumors, melanoma, and lymphoma. J Nucl Med 53:1244–1252. doi:10.2967/jnumed.112.109306
5. Chen C-K, Wu H-T, Chiou H-J, Wei C-J, Yen C-H, Chang C-Y, Chen W-M (2009) Differentiating benign and malignant soft tissue masses by magnetic resonance imaging: role of tissue component analysis. J Chin Med Assoc 72:194–201. doi:10.1016/S1726-4901(09)70053-X
6. Chung WJ, Chung HW, Shin MJ, Lee SH, Lee MH, Lee JS, Kim M-J, Lee WK (2012) MRI to differentiate benign from malignant soft-tissue tumours of the extremities: a simplified systematic imaging approach using depth, size and heterogeneity of signal intensity. Br J Radiol 85:e831–e836. doi:10.1259/bjr/27487871
7. Crim JR, Seeger LL, Yao L, Chandnani V, Eckardt JJ (1992) Diagnosis of soft-tissue masses with MR imaging: can benign masses be differentiated from malignant ones? Radiology 185:581–586. doi:10.1148/radiology.185.2.1410377
8. Fayad LM, Jacobs MA, Wang X, Carrino JA, Bluemke DA (2012) Musculoskeletal tumors: how to use anatomic, functional, and metabolic MR techniques. Radiology 265:340–356. doi:10.1148/radiol.12111740
9. Fisher SM, Joodi R, Madhuranthakam AJ, Öz OK, Sharma R, Chhabra A (2016) Current utilities of imaging in grading musculoskeletal soft tissue sarcomas. Eur J Radiol 85:1336–1344. doi:10.1016/j.ejrad.2016.05.003
10. Fletcher CDM, Bridge JA, Hogendoorn PCW, Mertens F (eds) (2013) WHO classification of tumours of soft tissue and bone. IARC Press, Lyon
11. Galant J, Martí-Bonmatí L, Soler R, Saez F, Lafuente J, Bonmatí C, Gonzalez I (1998) Grading of subcutaneous soft tissue tumors by means of their relationship with the superficial fascia on MR imaging. Skeletal Radiol 27:657–663
12. Gielen JLMA, De Schepper AM, Vanhoenacker F, Parizel PM, Wang XL, Sciot R, Weyler J (2004) Accuracy of MRI in characterization of soft tissue tumors and tumor-like lesions. A prospective study in 548 patients. Eur Radiol 14:2320–2330. doi:10.1007/s00330-004-2431-0
13. Hanna SL, Fletcher BD (1995) MR imaging of malignant soft-tissue tumors. Magn Reson Imaging Clin N Am 3:629–650
14. Hermann G, Abdelwahab IF, Miller TT, Klein MJ, Lewis MM (1992) Tumour and tumour-like conditions of the soft tissue: magnetic resonance imaging features differentiating benign from malignant masses. Br J Radiol 65:14–20. doi:10.1259/0007-1285-65-769-14
15. Jeon JY, Chung HW, Lee MH, Lee SH, Shin MJ (2016) Usefulness of diffusion-weighted MR imaging for differentiating between benign and malignant superficial soft tissue tumours and tumour-like lesions. Br J Radiol 89:20150929. doi:10.1259/bjr.20150929
16. Kransdorf MJ (1995) Benign soft-tissue tumors in a large referral population: distribution of specific diagnoses by age, sex, and location. AJR Am J Roentgenol 164:395–402. doi:10.2214/ajr.164.2.7839977
17. Kransdorf MJ (1995) Malignant soft-tissue tumors in a large referral population: distribution of diagnoses by age, sex, and location. AJR Am J Roentgenol 164:129–134. doi:10.2214/ajr.164.1.7998525

18. Lee S-Y, Jee W-H, Jung J-Y, Park MY, Kim S-K, Jung C-K, Chung Y-G (2016) Differentiation of malignant from benign soft tissue tumours: use of additive qualitative and quantitative diffusion-weighted MR imaging to standard MR imaging at 3.0 T. Eur Radiol 26:743–754. doi:10.1007/s00330-015-3878-x
19. Mirowitz SA, Totty WG, Lee JK (1992) Characterization of musculoskeletal masses using dynamic Gd-DTPA enhanced spin-echo MRI. J Comput Assist Tomogr 16:120–125
20. Moulton JS, Blebea JS, Dunco DM, Braley SE, Bisset GS, Emery KH (1995) MR imaging of soft-tissue masses: diagnostic efficacy and value of distinguishing between benign and malignant lesions. AJR Am J Roentgenol 164:1191–1199. doi:10.2214/ajr.164.5.7717231
21. Noebauer-Huhmann IM, Weber M-A, Lalam RK, Trattnig S, Bohndorf K, Vanhoenacker F, Tagliafico A, Van Rijswijk C, Vilanova JC, Afonso PD, Breitenseher M, Beggs I, Robinson P, De Jonge MC, Krestan C, Bloem JL (2015) Soft tissue tumors in adults: ESSR-approved guidelines for diagnostic imaging. Semin Musculoskelet Radiol 19:475–482. doi:10.1055/s-0035-1569251
22. Oliveira AM, Nascimento AG (2001) Grading in soft tissue tumors: principles and problems. Skeletal Radiol 30:543–559. doi:10.1007/s002560100408
23. van Rijswijk CSP, Geirnaerdt MJA, Hogendoorn PCW, Taminiau AHM, van Coevorden F, Zwinderman AH, Pope TL, Bloem JL (2004) Soft-tissue tumors: value of static and dynamic gadopentetate dimeglumine-enhanced MR imaging in prediction of malignancy. Radiology 233:493–502. doi:10.1148/radiol.2332031110
24. van Rijswijk CSP, Kunz P, Hogendoorn PCW, Taminiau AHM, Doornbos J, Bloem JL (2002) Diffusion-weighted MRI in the characterization of soft-tissue tumors. J Magn Reson Imaging 15:302–307
25. De Schepper AM, Bloem JL (2007) Soft tissue tumors: grading, staging, and tissue-specific diagnosis. Top Magn Reson Imaging 18:431–444. doi:10.1097/rmr.0b013e3181652220
26. De Schepper AM, Ramon FA, Degryse HR (1992) Magnetic resonance imaging of soft tissue tumors. J Belge Radiol 75:286–296
27. De Schepper AM, Ramon FA, Degryse HR (1992) Statistical analysis of MRI parameters predicting malignancy in 141 soft tissue masses. RöFo Fortschritte auf dem Gebiete der Röntgenstrahlen und der Nukl 156:587–591. doi:10.1055/s-2008-1032948
28. Sen J, Agarwal S, Singh S, Sen R, Goel S (2010) Benign vs malignant soft tissue neoplasms: limitations of magnetic resonance imaging. Indian J Cancer 47:280–286. doi:10.4103/0019-509X.64725
29. Sundaram M (1999) MR imaging of soft tissue tumors: an overview. Semin Musculoskelet Radiol 3:15–20. doi:10.1055/s-2008-1080048
30. Sundaram M, McLeod RA (1990) MR imaging of tumor and tumorlike lesions of bone and soft tissue. AJR Am J Roentgenol 155:817–824. doi:10.2214/ajr.155.4.2119115
31. Sundaram M, Sharafuddin MJ (1995) MR imaging of benign soft-tissue masses. Magn Reson Imaging Clin N Am 3:609–627
32. Tung GA, Davis LM (1993) The role of magnetic resonance imaging in the evaluation of the soft tissue mass. Crit Rev Diagn Imaging 34:239–308
33. van Unnik JA, Coindre JM, Contesso C, Albus-Lutter CE, Schiodt T, Sylvester R, Thomas D, Bramwell V, Mouridsen HT (1993) Grading of soft tissue sarcomas: experience of the EORTC Soft Tissue and Bone Sarcoma Group. Eur J Cancer 29A:2089–2093
34. Vandevenne JE, De Schepper AM, De Beuckeleer L, Van Marck E, Aparisi F, Bloem JL, Erkorkmaz Z, Brijs S (1997) New concepts in understanding evolution of desmoid tumors: MR imaging of 30 lesions. Eur Radiol 7:1013–1019. doi:10.1007/s003300050243
35. Vanhoenacker FM, Van Looveren K, Trap K, Desimpelaere J, Wouters K, Van Dyck P, Parizel PM, De Schepper AM (2012) Grading and characterization of soft tissue tumors on magnetic resonance imaging: the value of an expert second opinion report. Insights Imaging 3:131–138. doi:10.1007/s13244-012-0151-6
36. Vanhoenacker FM, Verstraete KL (2015) Soft tissue tumors about the shoulder. Semin Musculoskelet Radiol 19:284–299. doi:10.1055/s-0035-1549322
37. Verstraete KL, De Deene Y, Roels H, Dierick A, Uyttendaele D, Kunnen M (1994) Benign and malignant musculoskeletal lesions: dynamic contrast-enhanced MR imaging--parametric "first-pass" images depict tissue vascularization and perfusion. Radiology 192:835–843. doi:10.1148/radiology.192.3.8058957
38. Walker EA, Fenton ME, Salesky JS, Murphey MD (2011) Magnetic resonance imaging of benign soft tissue neoplasms in adults. Radiol Clin North Am 49:1197–217. doi:10.1016/j.rcl.2011.07.007, vi
39. Walker EA, Salesky JS, Fenton ME, Murphey MD (2011) Magnetic resonance imaging of malignant soft tissue neoplasms in the adult. Radiol Clin North Am 49:1219–34. doi:10.1016/j.rcl.2011.07.006, vi
40. Wetzel LH, Levine E (1990) Soft-tissue tumors of the foot: value of MR imaging for specific diagnosis. AJR Am J Roentgenol 155:1025–1030. doi:10.2214/ajr.155.5.2120930
41. Woertler K (2005) Soft tissue masses in the foot and ankle: characteristics on MR imaging. Semin Musculoskelet Radiol 9:227–242. doi:10.1055/s-2005-921942

Diagnostic Algorithm of Soft Tissue Tumors

10

Eline De Smet, Pieter Van Dyck, Jan L. Gielen, and Filip M. Vanhoenacker

Content

Reference 183

The initial work-up of a (suspected) soft tissue tumor (STT) comprises a thorough history and clinical examination, as certain findings (e.g., age of the patient, location and size of the lesion, history of trauma, etc.) may point the physician toward a presumptive diagnosis. As explained in Chaps. 9 and 10 plays clinical information a pivotal role in the initial work-up of a STT lesion. We also refer to the guidelines for diagnostic imaging of STTs approved by the European Society of Skeletal Radiology (ESSR) [1].

Figure 10.1 provides a diagnostic algorithm for initial imaging diagnosis of a STT. The proposed imaging pathway may provide a rough guide to diagnosis of soft tissue tumor in most clinical scenarios.

It must be emphasized – however – that this summary is by no way exhaustive or exclusive. The diversity and rarity of soft tissue tumors demand for a tailored approach of each lesion, dependent of tumor characteristics.

E. De Smet • P. Van Dyck (✉) • J.L. Gielen
Department of Radiology and Faculty of Medicine, University of Antwerp, Antwerp University Hospital (UZA), Wilrijkstraat, 10, 2650 Edegem, Belgium
e-mail: pieter.vandyck@uza.be

F.M. Vanhoenacker
Department of Radiology and Faculty of Medicine, University of Antwerp, Antwerp University Hospital (UZA), Wilrijkstraat, 10, 2650 Edegem, Belgium

Department of Radiology, AZ Sint-Maarten Duffel-Mechelen, Rooienberg, 25, B-2570 Duffel, Belgium

Faculty of Medicine and Health Sciences, Ghent University, Ghent, Belgium

© Springer International Publishing AG 2017
F.M. Vanhoenacker et al. (eds.), *Imaging of Soft Tissue Tumors*, DOI 10.1007/978-3-319-46679-8_10

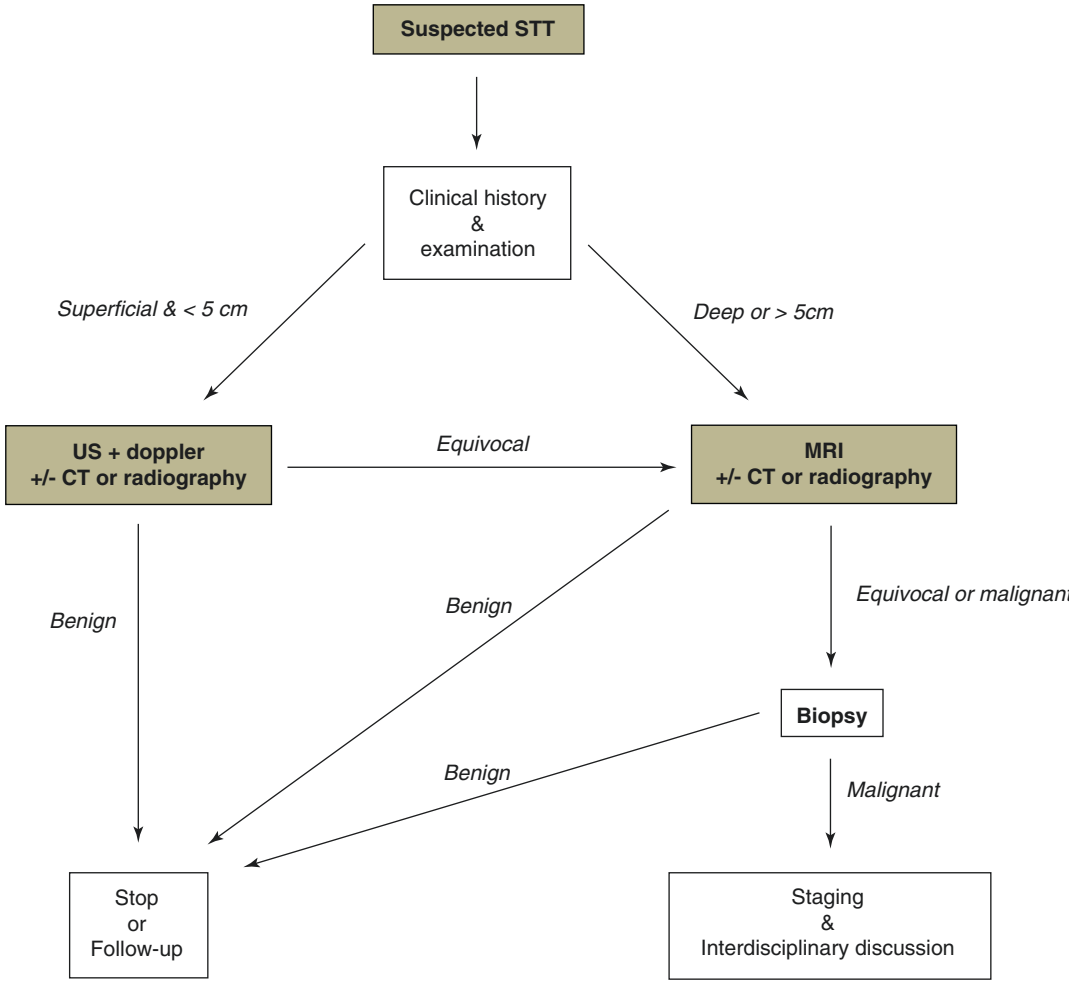

Fig. 10.1 Diagnostic algorithm for initial imaging diagnosis of a STT

Key Points

1. Clinical information is of utmost importance in the diagnosis of STTs.
2. Initial imaging evaluation of a patient presenting with a superficial STT starts with Doppler ultrasound. Plain films (or CT) may provide complementary information by showing soft tissue calcification and bone involvement.
3. If the lesion has no definite benign characteristics on these imaging modalities, MRI has to be performed for further evaluation of the lesion.
4. For evaluation of deeply located or large soft tissue lesions, MRI is preferred as initial imaging modality. Also in this scenario, plain films (or CT) may provide complementary information.
5. If the mass suggests malignancy on MR images, biopsy is mandatory.
6. MRI is the best method for local staging of a STT.
7. Close cooperation between radiologists and pathologists increases diagnostic accuracy.

Reference

1. Noebauer-Huhmann I, Weber M-A, Lalam R et al (2015) Soft tissue tumors in adults: ESSR-approved guidelines for diagnostic imaging. Semin Musculoskelet Radiol 19:478–486

Part III

Imaging of Soft Tissue Tumors

WHO Classification of Soft Tissue Tumors

11

Joan C. Vilanova

Contents

11.1 **Introduction** 187
11.2 **Adipocytic Tumors** 188
11.3 **Fibroblastic/Myofibroblastic Tumors** 189
11.4 **So-Called Fibrohistiocytic Tumors** 190
11.5 **Smooth Muscle Tumors** 190
11.6 **Pericytic (Perivascular) Tumors** 191
11.7 **Skeletal Muscle Tumors** 191
11.8 **Vascular Tumors** 192
11.9 **Chondro-Osseous Tumors** 192
11.10 **Gastrointestinal Stromal Tumors** 193
11.11 **Peripheral Nerve Sheath Tumors** 193
11.12 **Tumors of Uncertain Differentiation** 193
11.13 **Undifferentiated/Unclassified Sarcoma** 195
References 195

J.C. Vilanova, MD, PhD
Department of Radiology, Clínica Girona. Institute Catalan of Health – IDI. University of Girona, Girona, Spain
e-mail: kvilanova@comg.cat

11.1 Introduction

Soft tissue tumors (STT) represent a complex group of lesions that may show a broad range of differentiation. The WHO (World Health Organization) classification was established and up-to-dated in 2013 for the purpose of uniformity [1]. The WHO system helps to unify the lexicon for the performance of clinical trials and to serve as a guide for the multidisciplinary working group of specialists such as radiologists, pathologists, and orthopedic oncologists, to improve the patient's management and outcome. The nomenclature has been adapted by the American Joint Cancer Commission (AJCC) for sarcoma staging and by the College of American Pathologists Cancer protocols for soft tissue sarcomas. The 2013 classification is the 4th edition and replaces the previous edition in 2002 [2]. The major modifications from the previous edition are the addition of three new chapters: gastrointestinal stromal tumors (GIST), nerve sheath tumors, and undifferentiated/unclassified sarcomas.

The WHO classification incorporates detailed clinical, histological, and genetic data. There are also imaging features in the new edition of soft tissue tumor classification.

The classification of soft tissue tumors of the WHO includes the following groups: (1) adipocytic tumors, (2) fibroblastic/myofibroblastic tumors, (3) so-called fibrohistiocytic tumors, (4) smooth muscle tumors, (5) pericytic (perivascular) tumors, (6) skeletal muscle tumors, (7) vas-

© Springer International Publishing AG 2017

F.M. Vanhoenacker et al. (eds.), *Imaging of Soft Tissue Tumors*, DOI 10.1007/978-3-319-46679-8_11

Table 11.1 Changes and update relevant for radiologists in the 2013 WHO classification of tumors of the soft tissue

Tumor category	Major changes
Adipocytic	Mixed-type liposarcoma removed
Fibroblastic	DFSP and giant cell fibroblastoma included for the first time
Myofibroblastic	"Hemangiopericytoma" removed as a synonym for SFT
	Recognition of nodular fasciitis and variants as true neoplasms
So-called fibrohistiocytic	"Malignant fibrous histiocytoma" removed
Smooth muscle	Angioleiomyoma reclassified as pericytic tumor
Pericytic	Angioleiomyoma reclassified as a pericytic tumor
	Myofibroma now classified as pericytic tumor
Skeletal muscle	Spindle cell/sclerosing rhabdomyosarcoma classified together and separated from others subtypes
Vascular	Pseudomyogenic (epithelioid sarcoma-like)
	Hemangioendothelioma added as a new entity
Gastrointestinal stromal	GIST included in the volume on STT for the first time
Nerve sheath	Peripheral nerve sheath tumors included volume on STT for the first time
	New hybrid benign nerve sheath tumors included (schwannoma/perineurioma)
Tumors of uncertain differentiation	New tumors: acral fibromyxoma, hemosiderotic fibrolipomatous tumor differentiation
	Phosphaturic mesenchymal tumor
	Atypical fibroxanthoma now included
	PNET removed as synonym for Ewing's sarcoma
Undifferentiated/other category	Includes tumors that cannot be classified into any unclassified sarcoma

Abbreviations: *WHO* World Health Organization, *DFSP* dermatofibrosarcoma protuberans, *SFT* solitary fibrous tumor, *GIST* gastrointestinal stromal tumor, *STT* soft tissue tumor, *PNET* primitive neuroectodermal tumor

cular tumors, (8) gastrointestinal stromal tumors, (9) nerve sheath tumors, (10) chondro-osseous tumors, (11) tumors of uncertain differentiation, and (12) undifferentiated/unclassified sarcomas.

Generally, the WHO classification divides each group in four categories according to biological behavior: benign, intermediate (locally aggressive), intermediate (rarely metastasizing), and malignant.

The new classification has incorporated more detailed cytogenetic and molecular data in accordance with the rapidly increasing knowledge of genetics of tumors.

This chapter reviews the main features of the classification with the major changes within the different categories of soft tissue tumors. Table 11.1 summarizes all relevant changes of the 2013 WHO classification of STT.

11.2 Adipocytic Tumors

Due to the high incidence of lipomas, angiolipomas, and liposarcomas, adipocytic tumors represent the largest single group of mesenchymal tumors. The WHO classification persists to consider atypical lipoma (atypical lipomatous tumor) and well-differentiated liposarcoma as essentially synonymous (Table 11.2) and considered locally aggressive with no potential for metastasis [1]. The terms "mixed-type liposarcoma" and myxolipoma have been deleted.

In children diffuse lipoblastoma is now the preferred term for lipoblastomatosis.

The definition of dedifferentiated liposarcoma has been slightly modified and is currently subdivided into four groups (see Table 11.1). Chondroid lipoma may resemble myxoid liposarcoma. Unlike myxoid liposar-

Table 11.2 Group 1 – Adipocytic tumors

Benign
Lipoma
Lipomatosis
Lipomatosis of the nerve
Lipoblastoma
Angiolipoma
Myolipoma of the soft tissue
Chondroid lipoma
Spindle cell lipoma/pleomorphic lipoma
Hibernoma
Intermediate (locally aggressive)
Atypical lipomatous tumor/well-differentiated liposarcoma
Malignant
Dedifferentiated liposarcoma
Myxoid liposarcoma
Pleomorphic liposarcoma
Liposarcoma, not otherwise specified

coma chondroid lipoma usually shows calcifications, which are best demonstrated by radiographs, CT, or US [3].

11.3 Fibroblastic/Myofibroblastic Tumors

Fibroblastic/myofibroblastic tumors represent a very large group of mesenchymal tumors, many of which contain fibroblastic as well as myofibroblastic elements (Table 11.3). The current WHO classification recognizes that nodular fasciitis, proliferative fasciitis, and proliferative myositis (Fig. 11.1) are neoplastic [4], whereas previously they were believed to be reactive lesions.

Other changes were the inclusion of the closely related giant cell fibroblastoma and dermatofibrosarcoma protuberans (DFSP), formerly included in volume on skin lesions. DFSP is categorized as a rarely metastasizing (intermediate) tumor, although it should be noted that metastatic potential is gained only when a component of a fibrosarcomatous change is present [5]. Giant cell fibroblastoma is classified in the

Table 11.3 Group 2 – Fibroblastic/myofibroblastic tumors

Benign
Nodular fasciitis (proliferative fasciitis/proliferative myositis)
Myositis ossificans
Elastofibroma
Fibromatosis colli
Fibrous hamartoma of infancy
Juvenile hyaline fibromatosis
Inclusion body fibromatosis
Fibroma of the tendon sheath
Desmoplastic fibroblastoma
Mammary-type myofibroblastoma
Calcifying fibrous tumor
Angiofibroma
Angiomyofibroblastoma
Gardner fibroma
Calcifying fibrous tumor
Intermediate (locally aggressive)
Superficial fibromatosis (plantar/palmar)
Desmoid-type fibromatosis
Lipofibromatosis
Giant cell fibroblastoma
Intermediate (rarely metastasizing)
Dermatofibrosarcoma protuberans
Solitary fibrous tumor
Inflammatory myofibroblastic tumor
Myofibroblastic sarcoma/atypical myxoinflammatory fibroblastic tumor
Infantile fibrosarcoma
Malignant
Adult fibrosarcoma
Myxofibrosarcoma
Low-grade fibromyxoid sarcoma
Sclerosing epithelioid fibrosarcoma

locally aggressive (intermediate) category because it recurs in approximately 50 % of cases, but does not metastasize [6]. Hemangiopericytoma has been removed from the classification of "extrapleural solitary fibrous tumor" because it is well established that this outdated term included tumors that represented cellular examples of SFT [5]. Lipomatous hemangiopericytoma and giant cell angiofibroma have also been included as SFT. The term

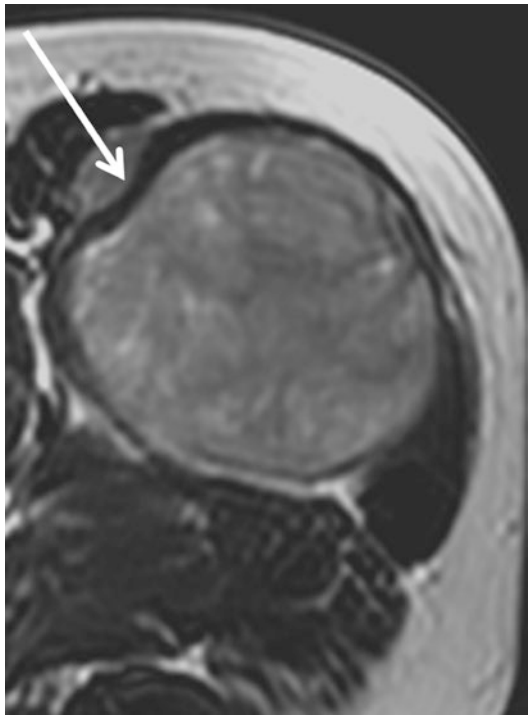

Fig. 11.1 Proliferative myositis of the thigh. Axial T2-WI image shows a well-defined mass (*arrow*) within the adductor muscle with inhomogeneous mild high signal intensity with areas of low signal within the lesion due to the fibrous content

"atypical myxoinflammatory fibroblastic tumor" was introduced for as synonym for "myxoinflammatory fibroblastic sarcoma." This new term better reflects the extremely low potential for metastasis for this tumor type.

11.4 So-Called Fibrohistiocytic Tumors

As the concept of fibrohistiocytic differentiation has been a matter of debate [7], malignant fibrous histiocytoma (MFH) has been finally deleted from the current WHO classification. MFH and its subtypes have been reclassified in the new separate group of unclassified/undifferentiated sarcomas (group 12). Thus, group 3 now does not include malignant tumors (Table 11.4). It includes the common tenosynovial giant cell tumors, the uncommon giant cell tumor

Table 11.4 Group 3 – The so-called fibrohistiocytic tumors

Benign
Tenosynovial giant cell tumor
Localized type
Diffuse type
Malignant
Deep benign fibrous histiocytoma
Intermediate (rarely metastasizing)
Plexiform fibrohistiocytic tumor
Giant cell tumor of the soft tissue

Fig. 11.2 Giant cell tumor of the soft tissue with Paget's disease. Axial T2-WI image shows an intermediate signal nodular lesion in the pretibial subcutaneous space (*thin arrow*). Note the cortical thickening due to Paget's disease (*thick arrow*)

(Fig. 11.2) of soft tissues, and the plexiform fibrohistiocytic tumor.

11.5 Smooth Muscle Tumors

Smooth muscle tumors arising at non-cutaneous, non-uterine locations have been the focus of a considerable conceptual shift in the past but there were no major changes in this category (Table 11.5). The only change is that

Table 11.5 Group 4 – Smooth muscle tumors

Benign
Leiomyoma of the deep soft tissue
Malignant
Leiomyosarcoma (excluding the skin)

angioleiomyoma (vascular leiomyoma) was reallocated to the category of pericytic (perivascular) tumors (group 5). There are no changes on the deep leiomyosarcoma, although some tumors classified as undifferentiated pleomorphic sarcoma closely resemble a subset of leiomyosarcoma, which may suggest the existence of "dedifferentiated leiomyosarcoma."

11.6 Pericytic (Perivascular) Tumors

The lesions in the pericytic/perivascular category were first included in the 2002 edition. At the same time, hemangiopericytoma was removed from this group and listed as synonym for solitary fibrous tumor (group 2). Although rare, the most common tumor analyzed on imaging in this group is glomus tumor [8], composed of cells resembling the modified smooth muscle cells of the normal glomus body. It has been acknowledged that myofibroma/myofibromatosis represent morphological features along the spectrum of myopericytic neoplasms (Table 11.6) instead of fibroblastic/myofibroblastic tumors (group 2), which were included in the past. Angioleiomyoma (vascular leiomyoma) which typically presents as a painful lesion in the distal extremities of middle-aged adults has now been included in this group [9, 10].

Table 11.6 Group 5 – Pericytic (perivascular) tumors

Benign
Glomus tumors (and variants)
Glomangiomatosis
Malignant glomus tumor
Myopericytoma
Myofibroma
Myofibromatosis
Angioleiomyoma

Table 11.7 Group 6 – Skeletal muscle tumors

Benign
Rhabdomyoma
Adult type
Fetal type
Genital type
Malignant
Embryonal rhabdomyosarcoma
Alveolar rhabdomyosarcoma
Pleomorphic rhabdomyosarcoma
Spindle cell/sclerosing rhabdomyosarcoma

11.7 Skeletal Muscle Tumors

Two entities have been added: rhabdomyoma and rhabdomyosarcoma (Table 11.7).

Rhabdomyoma is subdivided into cardiac and extracardiac types and pathologically as adult, fetal (immature skeletal muscle fibers), and genital (female or male genital tract). Extracardiac adult rhabdomyoma (Fig. 11.3) is rarely reported on imaging [11]. Spindle cell/sclerosing rhabdomyosarcoma is recognized as a separate tumor different from embryonal rhabdomyosarcoma.

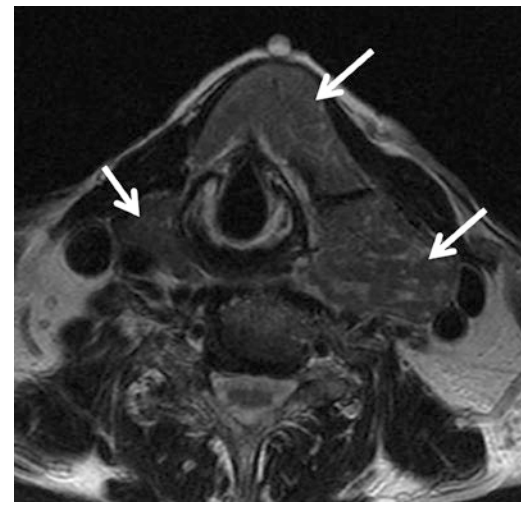

Fig. 11.3 Rhabdomyoma of the neck. Axial T2-WI image shows a large well-circumscribed lesion of intermediate signal intensity within the parapharyngeal space extending anteriorly bilaterally in the subfascial planes of the muscles and showing a lobulated appearance (*arrows*)

The prognosis of spindle cell rhabdomyosarcoma in adults is worse than in children, and recent insights into genetics of this tumor suggest that there may be underlying genetic differences between pediatric and adult cases [12].

11.8 Vascular Tumors

Benign vascular tumors are very common and most frequently occur in the skin. It is often difficult to determine whether they represent malformations, true neoplasms, or reactive processes [13]. Hemangiomas are classified histologically as synovial, venous, arteriovenous, mixed malformations, and intramuscular (Table 11.8). "Pseudomyogenic (epithelioid sarcoma-like) hemangioendothelioma" [14] has been added as a rarely metastasizing neoplasm. This tumor commonly arises in young adult males, often presents as multiple discontiguous nodules in different tissue planes of a limb (Fig. 11.4), and may involve the skin as well as deep soft tissues and the bone. This tumor tends to be highly FDG-avid, and therefore PET-CT is useful for the detection of deep lesions.

There are no changes on the classification of angiosarcoma and epithelioid hemangioendothelioma (EHE) although new genetic data has shown that multifocal EHE most likely arises as a result of metastatic disease rather than representing synchronous primary tumors as previously thought.

Immunohistochemical analysis can differentiate postradiation vascular proliferation from angiosarcoma [15].

11.9 Chondro-Osseous Tumors

There are no changes on the chondro-osseous soft tissue tumors (Table 11.9). Myositis ossificans was regarded as a (myo)fibroblastic lesion in the 2002 version, and extraskeletal myxoid chondrosarcoma (EMC) was also classified in the tumors of uncertain differentiation, since it shows little evidence of cartilaginous differentiation [2], despite the name. A synonym for EMC is chordoid sarcoma.

Table 11.8 Group 7 – Vascular tumors

Benign
Hemangioma
Synovial
Venous
Arteriovenous hemangioma/malformation
Epithelioid hemangioma
Angiomatosis
Lymphangioma
Intermediate (locally aggressive)
Kaposiform hemangioendothelioma
Intermediate (rarely metastasizing)
Retiform hemangioendothelioma
Papillary intralymphatic angioendothelioma
Composite hemangioendothelioma
Pseudomyogenic (epithelioid sarcoma-like) hemangioendothelioma
Kaposi sarcoma
Malignant
Epithelioid hemangioendothelioma
Angiosarcoma of the soft tissue

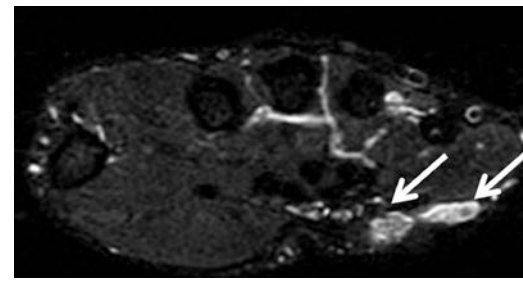

Fig. 11.4 Pseudomyogenic (epithelioid sarcoma-like) hemangioendothelioma of the hand. Axial STIR MR image of the hand shows two nodular high signal intensity lesions at the subcutaneous tissue of the hypothenar region (*arrows*)

Table 11.9 Group 8 – Chondro-osseous tumors

Benign
Soft tissue chondroma
Malignant
Mesenchymal chondrosarcoma
Extraskeletal osteosarcoma

Mesenchymal chondrosarcoma of soft tissues occurs less frequently than the EMC, but nearly half of the mesenchymal chondrosarcomas are extraskeletal in location [16].

Extraskeletal osteosarcoma, soft tissue osteosarcoma, shows similar histologic features of bone osteosarcoma without systematic genetic differences [1].

11.10 Gastrointestinal Stromal Tumors

This group has been added, gastrointestinal stromal tumor (GIST), which is the most common primary mesenchymal tumor in the gastrointestinal tract. Histologically GIST are classified as benign, uncertain malignant potential, and malignant. Prognostic factors are tumor size, mitotic activity, and anatomical site [17]. Almost 50% arise in the stomach, 30% in the small intestine, and the rest for the colon, rectum, and esophagus and primary disseminated with unspecified site of origin. Isolated cases have been reported in the appendix. As GIST present with abdominal symptoms and are detected by ultrasound or CT scans of the abdomen (Fig. 11.5), these lesions are not referred to as musculoskeletal tumors as such.

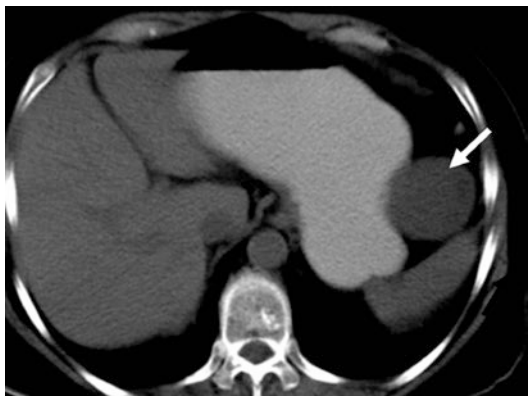

Fig. 11.5 Gastrointestinal stromal tumor (GIST) of the stomach. Non-contrast-enhanced CT shows a bulky exophytic gastric mass with well-circumscribed outer contours (*arrow*). No calcifications are present

11.11 Peripheral Nerve Sheath Tumors

Nerve sheath tumors were previously included in the 2007 WHO classification of tumors of the central nervous system. Although imaging reviews on soft tissue tumors already regarded nerve sheath tumors previously as typical soft tissue tumors [18], nerve sheath tumors have been included for the first time in the WHO classification of soft tissue tumors since 2013 (Table 11.10). Hybrid nerve sheath tumors, such as schwannoma/perineurioma [19] and neurofibroma/schwannoma, have been included in the group of peripheral nerve sheath tumors. The latter might be related to NF-2, NF-1, or schwannomatosis [20].

11.12 Tumors of Uncertain Differentiation

Tumors with unknown clear line of cell differentiation are included in this group. It includes a long list of tumors (Table 11.11). New entities have been

Table 11.10 Group 10 – Peripheral nerve sheath tumors

Benign
Schwannoma (including variants)
Melanotic schwannoma
Neurofibroma (including variants)
Perineurioma
Malignant intermediate perineurioma
Granular cell tumor
Dermal nerve sheath myxoma
Solitary circumscribed neuroma
Ectopic meningioma
Nasal glial heterotopia
Benign triton tumor
Hybrid nerve sheath tumors
Malignant
Malignant peripheral nerve sheath tumor
Epithelioid malignant peripheral nerve sheath tumor
Malignant triton tumor
Malignant granular cell tumor
Ectomesenchymoma

Table 11.11 Group 11 – Tumors of uncertain differentiation

Benign
Acral/digital fibromyxoma
Intramuscular – juxtaarticular myxoma
Deep ("aggressive") angiomyxoma
Pleomorphic hyalinizing angiectatic tumor
Ectopic hamartomatous thymoma
Intermediate (locally aggressive)
Hemosiderotic fibrolipomatous tumor
Intermediate (rarely metastasizing)
Atypical fibroxanthoma
Angiomatoid fibrous histiocytoma
Ossifying fibromyxoid tumor
Mixed tumor
Myoepithelioma/carcinoma
Phosphaturic mesenchymal tumor
Malignant
Synovial sarcoma
Epithelioid sarcoma
Alveolar soft part sarcoma
Clear cell sarcoma of the soft tissue
Extraskeletal myxoid chondrosarcoma
Malignant mesenchymoma
Desmoplastic small round cell tumor
Extraskeletal Ewing sarcoma
Extrarenal rhabdoid tumor
Neoplasms with perivascular epithelioid cell differentiation (PEComa)
Intimal sarcoma

included: acral fibromyxoma (digital fibromyxoma), hemosiderotic fibrolipomatous tumor, phosphaturic mesenchymal tumor, and atypical fibroxanthoma. Among the group of malignant lesions, primitive neuroectodermal tumor (PNET) has been dropped as a synonym for Ewing's sarcoma in order to minimize confusion with similarity named lesions in the CNS and female genital tract.

Extraskeletal myxoid chondrosarcoma is included in this category as there is no convincing evidence of cartilaginous differentiation.

Deep ("aggressive") angiomyxoma is an uncommon slowly growing neoplasm with a predilection for pelvic and perineal regions [21] and tendency to local recurrence and characteristic features on MR (Fig. 11.6).

Ossifying fibromyxoid tumor of the soft tissue is a well-circumscribed lobulated hard tumor covered by a thick fibrous pseudocapsule (Fig. 11.7).

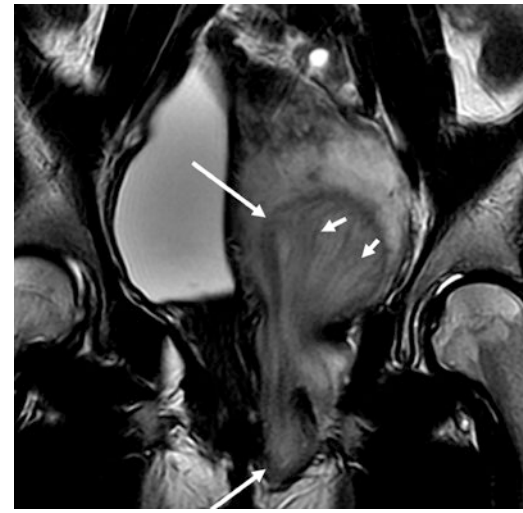

Fig. 11.6 Aggressive angiomyxoma of the pelvis. Coronal T2-WI shows an hyperintense mass (*long arrows*) extending through the left ischiorectal fossa with a layered appearance (*short arrows*)

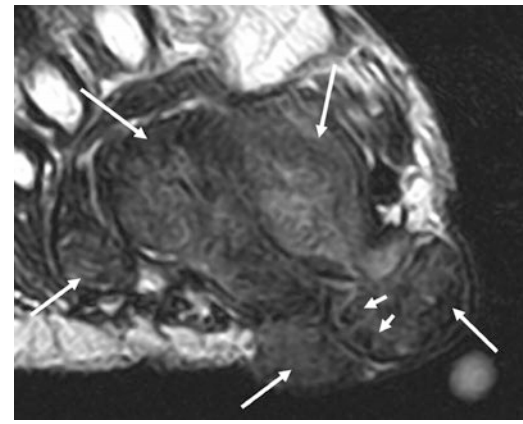

Fig. 11.7 Ossifying fibromyxoid tumor of the foot. Axial T2-WI shows a large mass (*long arrows*) of low signal intensity extending within the subcutaneous tissue. The low signal intensity can be attributed to calcification (*short arrows*)

It was surprising that the term "synovial sarcoma" remained unchanged in the current updated classification. As the lesion is not derived from true synovial cells and may involve virtually any body part (Fig. 11.8) [21, 22], the term "synovial sarcoma" is indeed a misnomer. Therefore, future revisions of the WHO classification on STT should consider to abandon the confusing term "synovial sarcoma."

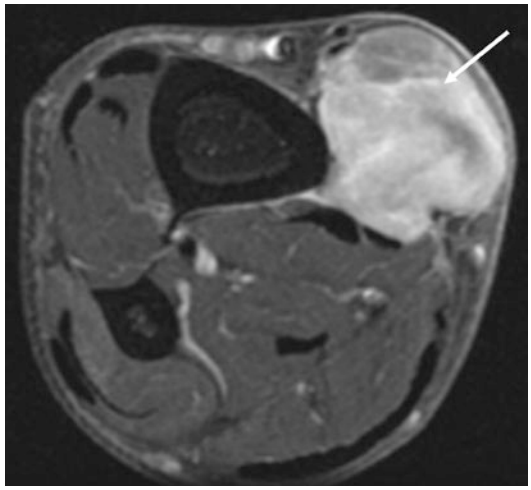

Fig. 11.8 The so-called synovial sarcoma of the lower leg. Axial fat-suppressed T1-WI after contrast shows homogeneously enhancing lesion in the subcutaneous tissue extending through the muscular fascia to deep compartment (*arrow*). As no nearby synovial tissue can be related to the mass in this location, the term "synovial" is a misnomer for this lesion which is derived from undifferentiated mesenchymal stem cell

11.13 Undifferentiated/ Unclassified Sarcoma

This new category of tumors, introduced for the first time in the 2013 classification, recognizes the fact that a small, but significant, subset of sarcomas cannot be classified into any presently defined categories [23]. This group of tumors was previously included in the fibrohistiocytic group (group 3), namely, "malignant fibrous histiocytoma." This group of tumors might have spindle cell, pleomorphic, round cell, or epithelioid morphology (Table 11.12). A subset of radiation-associated sarcomas falls into this category. These lesions show no definable line of differentiation using currently available technologies. Dedifferentiated types of specific sarcomas are not included in this category. Undifferentiated/unclassified sarcoma accounts for up to 20 % of all sarcomas and about a quarter of these are radiation-associated tumors [24]. It is likely that this group of lesions will be subject to future reclassification along with ongoing progress in molecular genetics.

Table 11.12 Group 12 – Undifferentiated/unclassified sarcoma

Undifferentiated spindle cell sarcoma
Undifferentiated pleomorphic sarcoma
Undifferentiated round cell sarcoma
Undifferentiated epithelioid sarcoma
Undifferentiated sarcoma, not otherwise specified

Key Points

1. The WHO classification of soft tissue tumors has been up-to-dated in 2013 for the purpose of uniformity.
2. The new WHO classification has included three new groups of tumors: gastrointestinal stromal tumors (GIST), nerve sheath tumors, and undifferentiated/unclassified sarcomas.
3. Each group of tumors is divided in four categories regarding the biological potential: benign, intermediate (locally aggressive), intermediate (rarely metastasizing), and malignant.
4. Radiologist should know the WHO classification to serve as a guide to work in a multidisciplinary committee with clinicians, surgeons, and pathologists.
5. Imaging (especially MRI) plays a pivotal role in the work-up of soft tissue tumors.

References

1. Fletcher CDM, Bridge JA, Hogendoorn PCW, Mertens F (eds) (2013) WHO classification of tumours of soft tissue and bone. IARC Press, Lyon
2. Fletcher CDM, Unni KK, Mertens F (eds) (2002) WHO classification of tumours. Pathology and genetics of tumours of soft tissue and bone. IARC Press, Lyon
3. Green AR, Cannon SR, Flanagan AM (2004) Chondroid lipoma: correlation of imaging findings and histopathology of an unusual benign lesion. Skeletal Radiol 33(11):670–673
4. Erickson-Johnson MR, Chou MM, Evers BR, Roth CW, Seys AR, Jin L et al (2011) Nodular fasciitis: a novel model of transient neoplasia induced by MYH9-USP6 gene fusion. Lab Invest J Tech Methods Pathol 91(10):1427–1433
5. Doyle LA (2014) Sarcoma classification: an update based on the 2013 world health organization classification of tumors of soft tissue and bone. Cancer 120(12):1763–1774

6. Fletcher CDM (2014) The evolving classification of soft tissue tumours – an update based on the new 2013 WHO classification. Histopathology 64(1):2–11
7. Rosenberg AE (2003) Malignant fibrous histiocytoma: past, present, and future. Skeletal Radiol 32(11):613–618
8. Vilanova JC, Barcelo J, Smirniotopoulos JG, Perez-Andres R, Villalon M, Miro J et al (2004) Hemangioma from head to toe: MR imaging with pathologic correlation. Radiographics 24(2):367–385
9. Vanhoenacker FM, Camerlinck M, Somville J (2009) Imaging findings of a subcutaneous angioleiomyoma. JBR-BTR Organe Société R Belge Radiol SRBR Orgaan Van K Belg Ver Voor Radiol KBVR 92(2):80–82
10. Yoo HJ, Choi J-A, Chung J-H, Oh JH, Lee G-K, Choi J-Y et al (2009) Angioleiomyoma in soft tissue of extremities: MRI findings. AJR Am J Roentgenol 192(6):W291–W294
11. Liang GS, Loevner LA, Kumar P (2000) Laryngeal rhabdomyoma involving the paraglottic space. AJR Am J Roentgenol 174(5):1285–1287
12. Szuhai K, de Jong D, Leung WY, Fletcher CDM, Hogendoorn PCW (2014) Transactivating mutation of the MYOD1 gene is a frequent event in adult spindle cell rhabdomyosarcoma. J Pathol 232(3):300–307
13. Tekes A, Koshy J, Kalayci TO, Puttgen K, Cohen B, Redett R et al (2014) S.E. Mitchell Vascular Anomalies Flow Chart (SEMVAFC): a visual pathway combining clinical and imaging findings for classification of soft-tissue vascular anomalies. Clin Radiol 69(5):443–457
14. Hornick JL, Fletcher CDM (2011) Pseudomyogenic hemangioendothelioma: a distinctive, often multicentric tumor with indolent behavior. Am J Surg Pathol 35(2):190–201
15. Guo T, Zhang L, Chang N-E, Singer S, Maki RG, Antonescu CR (2011) Consistent MYC and FLT4 gene amplification in radiation-induced angiosarcoma but not in other radiation-associated atypical vascular lesions. Genes Chromosomes Cancer 50(1):25–33
16. Torigoe T, Yazawa Y, Takagi T, Terakado A, Kurosawa H (2007) Extraskeletal osteosarcoma in Japan: multi-institutional study of 20 patients from the Japanese Musculoskeletal Oncology Group. J Orthop Sci Off J Jpn Orthop Assoc 12(5):424–429
17. Dow N, Giblen G, Sobin LH, Miettinen M (2006) Gastrointestinal stromal tumors: differential diagnosis. Semin Diagn Pathol 23(2):111–119
18. Vilanova JC, Woertler K, Narvaez JA, Barcelo J, Martinez SJ, Villalon M et al (2007) Soft-tissue tumors update: MR imaging features according to the WHO classification. Eur Radiol 17(1): 125–138
19. Hornick JL, Bundock EA, Fletcher CDM (2009) Hybrid schwannoma/perineurioma: clinicopathologic analysis of 42 distinctive benign nerve sheath tumors. Am J Surg Pathol 33(10):1554–1561
20. Feany MB, Anthony DC, Fletcher CD (1998) Nerve sheath tumours with hybrid features of neurofibroma and schwannoma: a conceptual challenge. Histopathology 32(5):405–410
21. Stewart ST, McCarthy SM (2004) Case 77: aggressive angiomyxoma. Radiology 233(3):697–700
22. Thway K, Fisher C (2014) Synovial sarcoma: defining features and diagnostic evolution. Ann Diagn Pathol 18(6):369–380
23. Fletcher CDM (2008) Undifferentiated sarcomas: what to do? And does it matter? A surgical pathology perspective. Ultrastruct Pathol 32(2):31–36
24. Reichardt P (2014) Soft tissue sarcomas, a look into the future: different treatments for different subtypes. Future Oncol Lond Engl 10(8 Suppl):s19–s27

Adipocytic Tumors

12

Philip Robinson and Filip M. Vanhoenacker

Contents

12.1 **Introduction** 197

12.2 **Benign Adipocytic Tumors** 198
12.2.1 Lipoma 198
12.2.2 Lipomatosis 203
12.2.3 Lipomatosis of Nerve 208
12.2.4 Lipoblastoma 210
12.2.5 Angiolipoma 211
12.2.6 Myolipoma of Soft Tissue 212
12.2.7 Chondroid Lipoma 213
12.2.8 Spindle Cell Lipoma and Pleomorphic Lipoma 215
12.2.9 Hibernoma 217
12.2.10 Other Variants of Lipoma 220

12.3 **Intermediate (Locally Aggressive) Adipocytic Tumors** 225
12.3.1 Well-Differentiated Liposarcoma 225

12.4 **Malignant Adipocytic Tumors** 230
12.4.1 Dedifferentiated Liposarcoma 232
12.4.2 Myxoid Liposarcoma 232
12.4.3 Pleomorphic Liposarcomas 237
12.4.4 Liposarcoma, Not Otherwise Specified 237

12.5 **Differential Diagnosis of Lipomatous Tumors** 237
12.5.1 Other Lesions Containing Fat or Mimicking Its Presence 237

Conclusions 238

References 238

P. Robinson (✉)
Department of Radiology, Leeds Teaching Hospitals, Chapel Allerton Hospital, Chapeltown Road, Leeds, UK

Leeds Musculoskeletal Biomedical Research Unit, University of Leeds, Leeds, UK
e-mail: philip.robinson10@nhs.net

F.M. Vanhoenacker
University Hospital Antwerp, Department of Radiology, Wilrijkstraat, 10, B-2650 Edegem, Belgium

General Hospital Sint-Maarten Duffel-Mechelen, Rooienberg 25, B-2570 Duffel, Belgium

Faculty of Medicine and Health Sciences, University of Ghent, Ghent, Belgium

12.1 Introduction

Histologically adipose tissue is classified into two main types: white fat (lipocytes), widely distributed through the body, and brown fat, which is more common in rodents and hibernating animals. Brown fat is considered an immature form of white fat and is chiefly found in the interscapular region, neck, mediastinum, axilla, and retroperitoneum [31, 36].

Adipocytic tumors are common mesenchymal lesions that can be benign, locally aggressive, or malignant. There is a wide range of histological subtypes, the lipoma being the most frequent of

© Springer International Publishing AG 2017

F.M. Vanhoenacker et al. (eds.), *Imaging of Soft Tissue Tumors*, DOI 10.1007/978-3-319-46679-8_12

them. Some tumors, including lipoma and some types of liposarcoma, will display typical features, which allow a specific diagnosis to be made [44, 45]. In recent years there have been marked advances in cytogenetic and molecular analysis of tumors with many of the benign and malignant adipocytic variants associated with specific genetic abnormalities (also see Chap. 6). In the following discussion, only the subdivisions of adipocytic tumors that arise in the soft tissues of the trunk and extremities are considered.

The role of magnetic resonance imaging (MRI) for the study and evaluation of these common tumors is emphasized throughout this chapter. The superiority of this technique stems from its exquisite sensitivity in displaying minor differences in tissue composition and its ability to specifically characterize normal fat signal. Many investigators have reported MRI to be diagnostically valuable in distinguishing fat-containing tumors from other tumors, because of its ability for detecting fatty components [39, 48]. On plain radiographs, adipocytic tumors are often not apparent or can occasionally be detected as a mass of increased density or of fatty opacity. On ultrasound scans, these tumors can show different patterns of echogenicity: they are mostly isoechoic or hyperechoic, although a hypoechoic pattern may be also encountered [1]. Using computed tomography (CT), diagnosis of an adipocytic tumor can be straightforward when typical low attenuation values are found (−65 to−120 HU). On MRI the signal intensity (SI) of fatty tumors tends to be equal to that of subcutaneous fat on all pulse sequences, including those obtained with fat suppression: short-tau inversion recovery (STIR) or chemical shift pulse sequences [48, 75] (Fig. 12.1).

12.2 Benign Adipocytic Tumors

The benign adipocytic tumors represent a very common and varied group, and according to the most recent World Health Organization's Committee for the Classification of Soft Tissue Tumors (2013), nine distinct entities are distinguished [26]: lipoma, lipomatosis, lipomatosis of nerve, lipoblastoma, angiolipoma, myolipoma of soft tissue, chondroid lipoma, spindle cell/pleomorphic lipoma, and hibernoma. However, this classification does not distinguish true neoplasms, hamartomatous processes, or simple overgrowth of fat, mainly because the differentiation is devoid of any clinical consequences. Myolipoma of soft tissue, extrarenal angiomyolipoma, and extra-adrenal myelolipoma are rare predominantly intra-abdominal lipoma variants, which are not discussed in this chapter, which focuses on truncal and extremity masses.

12.2.1 Lipoma

Microscopically a lipoma is usually a well-circumscribed and encapsulated mass composed of mature fat (adipocytes) differing very little from the surrounding fat. Although lipomas are well vascularized, this feature may not be readily apparent owing to vascular compression caused by the distended adipocytes.

Lipoma is the most common mesenchymal tumor, and in a review of 18,677 benign soft tissue tumors, lipoma and lipoma variants were the most common group, representing 16 % of all lesions [44]. Lipomas generally affect patients in the fifth to seventh decade of life, more frequently in obese people but with no definite sex predilection [21, 44].

Lipomas can be superficially or deeply located (subcutaneous or deep lipomas); they occur most commonly in the subcutaneous tissue and more rarely in the deep soft tissue. Subcutaneous lipomas are most frequently found in the upper back and neck, shoulder, abdomen, and proximal portions of the extremities, while the less common deep lipomas tend to be larger and less circumscribed than the superficial ones; please see Sect. 12.2.1.1 later [31, 48, 49].

Symptoms depend on the location and size of the tumors. A lipoma typically appears as a slowly growing, painless mass, but rapidly growing lipomas have been reported. Pain is rare but may occur as a consequence of neurovascular compression depending on the location and relationship to adjacent structures. Subsequent

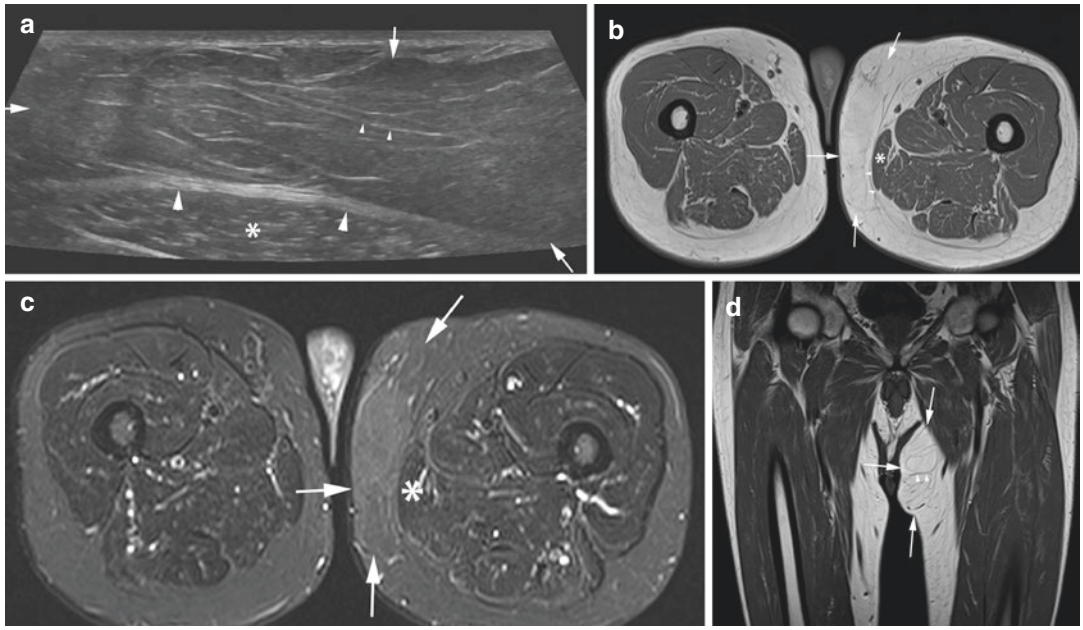

Fig. 12.1 (**a**–**d**) Subcutaneous lipoma in the left thigh overlying gracilis (*). (**a**) Ultrasound. (**b**) Axial SE T1-weighted MR image. (**c**) Axial fat-suppressed T2-weighted MR image. (**d**) Coronal SE T1-weighted MR image. There is a left thigh medial mass within the subcutaneous tissue (large *arrows*), isoechoic on ultrasound (**a**) and with SI similar to adjacent subcutaneous fat on all pulse sequences (**b**–**d**). There are multiple thin septa (small *arrowheads*) within the mass, echogenic on ultrasound (**a**) and low SI on T1-weighted images (**b** and **d**)

symptoms such as carpal or tarsal tunnel syndrome and chronic lower extremity deep vein thrombosis due to femoral vein compression have been reported.

Superficial lipoma manifests usually as a small mass, less than 5 cm, rarely exceeding 10 cm [49]. Subcutaneous lipomas are easily diagnosed at clinical examination, without the need for radiographic evaluation. The radiograph may occasionally demonstrate a radiolucent soft tissue mass and rarely osseous deformity by mass effect.

The most frequent sonographic appearance of lipoma is that of an elliptical, compressible, homogenous, and well-defined mass parallel to the skin surface. They are intrinsic multiple echogenic lines (Figs. 12.1 and 12.2) which relate to fibrovascular septi which can often show linear blood flow on Doppler interrogation [50]. The echogenicity can vary but is usually hyperechoic compared to adjacent fat; however, the homogenous nature is the most important reassuring feature [1, 50].

On CT and MR images, lipomas also present as homogeneous, well-circumscribed, and encapsulated masses of fatty nature, without diffuse enhancement after intravenous contrast administration. The differentiation between the superficial lipoma and the surrounding fat may be difficult due to their similarity on density and SI (Fig. 12.1). Regular, thin septations can be seen both on CT and MR images [47, 75]. The septa appear as soft tissue density strands on CT scans and as low-intensity strands on T1-weighted MR images, which may become hyperintense on T2-weighted MR images (due to the blood vessels within). The width of these septa can be unmeasurable, with a slight enhancement after intravenous contrast administration, which is more clearly demonstrated on fat-suppressed T1-weighted MR images [38].

Lipomas composed of tissue other than adipose tissue may differ from the classic sonographic, CT, or MR imaging appearance (see Variants of Lipoma). Non-tumor changes such as calcification, mechanical edema in superficial

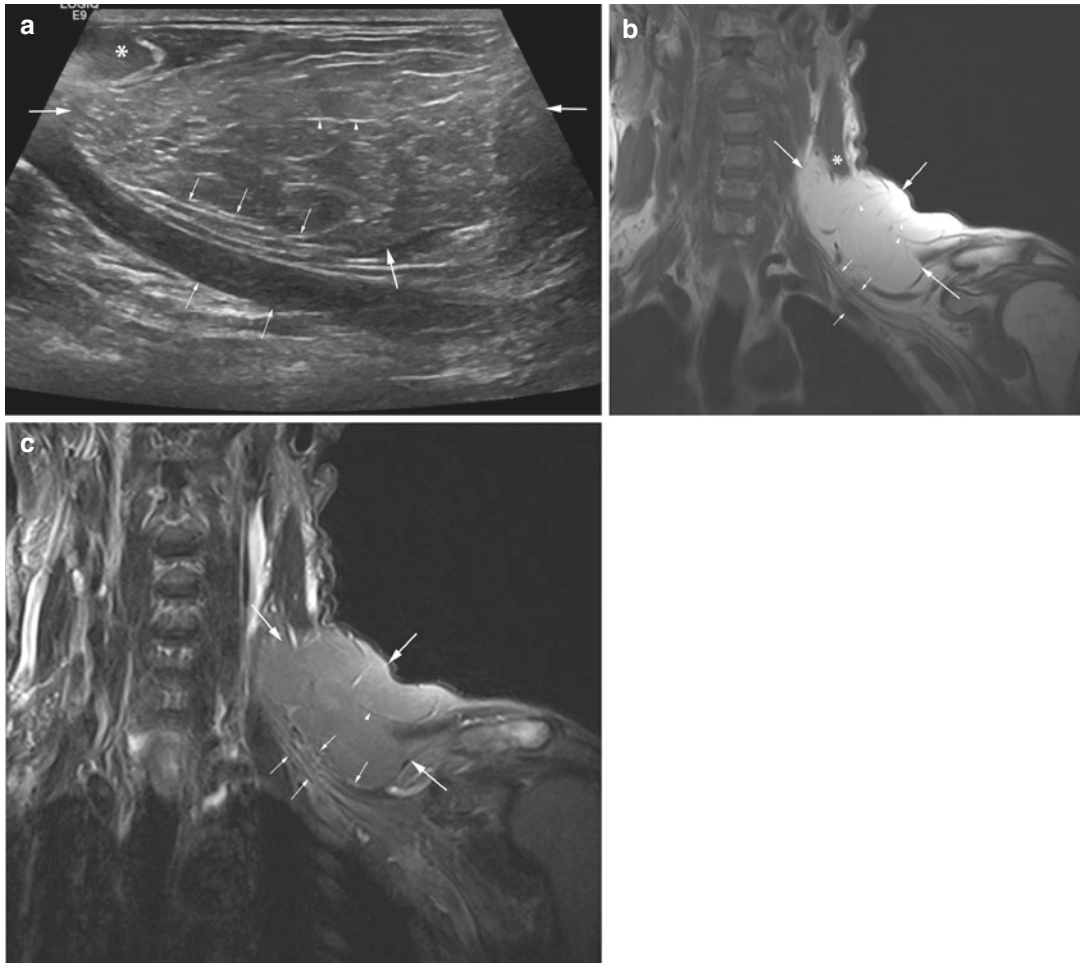

Fig. 12.2 (**a**–**c**) Lipoma of the left neck and supraclavicular region with left arm symptoms. (**a**) Ultrasound. (**b**) Coronal SE T1-weighted and (**c**) fat-suppressed T2-weighted MR images. The lipoma is intramuscular and subcutaneous. Ultrasound examination shows a homogenous, hyperechoic mass (*large arrows*) (**a**). On MRI the mass is homogeneous and SI is equal to that of subcutaneous fat on different pulse sequences (**b**–**c**). All images show sternocleidomastoid muscle (*), thin septi (*arrowheads*), and mass effect by the lipoma on the brachial plexus and subclavian vessels (*small arrows*)

lipomas, or intrinsic fat necrosis should be considered rather than always assuming sarcomatous change (Figs.12.3, 12.4, and 12.5) [71].

12.2.1.1 Intramuscular and Intermuscular Lipoma

On gross inspection of intramuscular and intermuscular lipomas, fat has replaced the muscle tissue. Microscopically mature lipocytes infiltrate the muscle fibers, which may show some degree of atrophy. Widespread invasion of one or more muscles may occur. Intramuscular lipoma has also been referred to as "infiltrating lipoma" due to its frequently infiltrative aspect on histological examination. Intramuscular lipoma is more frequent than the intermuscular variant, and it can affect both the muscular and intermuscular tissues [5, 47].

Intramuscular lipoma affects all age groups, mostly occurring in patients over 40 years of age, and, although rare, it has also been reported in children [35, 49]. Most authors have described a male predominance. These lesions tend to involve most commonly the large muscles of the

Fig. 12.3 (**a**–**c**) Subcutaneous lipoma of the neck. (**a**) Ultrasound. (**b**) Sagittal SE T1-weighted MR image. (**c**) Sagittal STIR image. The distal aspect of the mass (*) is homogenous on ultrasound and fat SI on MRI. The proximal mass (*arrowheads*) is heterogeneous on ultrasound (**a**) and edematous on MRI but with no nodular mass (**b**–**c**). Histology confirmed lipoma, MDM2 negative, and proximal fat necrosis

extremities, especially of the thigh, trunk, shoulder, and upper arm [31, 49].

The clinical picture is one of a painless, slow-growing lesion, but occasionally the symptoms may be very different from those of the common subcutaneous variety, and intramuscular lipoma may present as a rapidly growing mass with nerve entrapment (Figs.12.2 and 12.6). The size of the lipoma varies from a small mass of less than 3 cm to more than 20 cm in diameter [31, 49, 57]. The imaging findings in these heterotopic lipomas are basically the same as in other lipomas [57]. Although most of the intramuscular lipomas are well-defined lesions on CT or MR images, they also may show infiltrative margins if they extend between the muscle fibers, corresponding to the infiltrative type of intramuscular lipoma (Figs.12.6 and 12.7) [35, 47, 57]. On CT and on MR images, some intramuscular lipomas are septate, inhomogeneous masses, with tissue

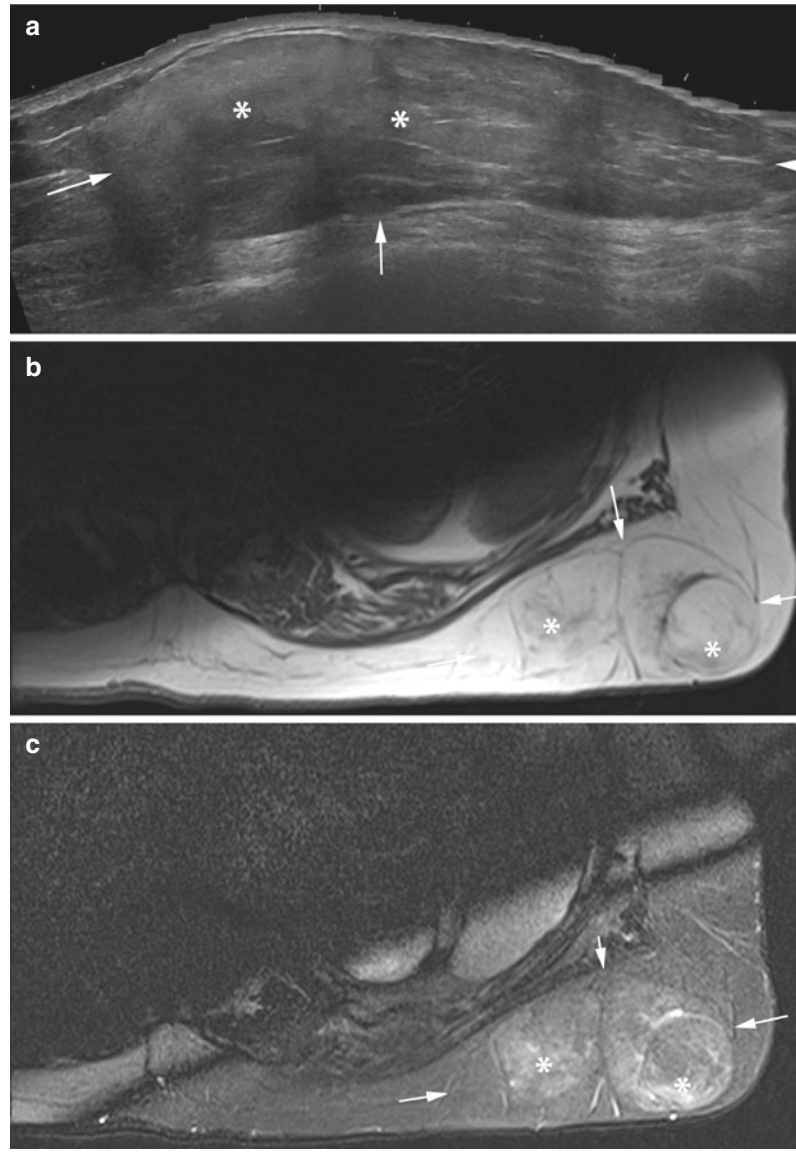

Fig. 12.4 (**a**–**c**) Subcutaneous lipoma of the back. (**a**) Ultrasound. (**b**) Axial SE T1-weighted MR image. (**c**) Axial fat-suppressed SE T2-weighted MR image. The majority of the mass (*arrows*) is homogenous on ultrasound and fat SI on MRI. The superficial aspects of the mass (*) are slightly heterogeneous on ultrasound (**a**) and edematous on MRI but with no nodular mass (**b**–**c**). Histology confirmed lipoma, MDM2 negative, and congested edematous fat superficially

attenuation and interspersed regions of decreased signal on T1- and T2-weighted images, which probably represent either muscle or fibrous tissue within the mass [57] (Fig. 12.8). Matsumoto et al. have reported the MR findings of 17 cases of intramuscular lipoma, 12 being homogeneous and the remaining 5 inhomogeneous with intermingled muscle fibers that were isointense with normal muscle on both T1- and T2-weighted images [57]. On ultrasound the masses usually appear homogenous, but the muscle fibers can cause reverberation artifact obscuring intrinsic detail unless the probe position is altered (Fig.12.8c).

Although the absence of contrast enhancement and unilobularity are useful signs in the differential diagnosis of intramuscular lipoma from well-differentiated liposarcoma/atypical lipomatous tumor (Table 12.1), these signs are not 100 % reliable [68]. This makes the differential diagnosis with well-differentiated liposarcoma difficult radiologically, and this may also extend to histological examination [57]. Additional cytogenetic analysis is often the crucial test for confirming or

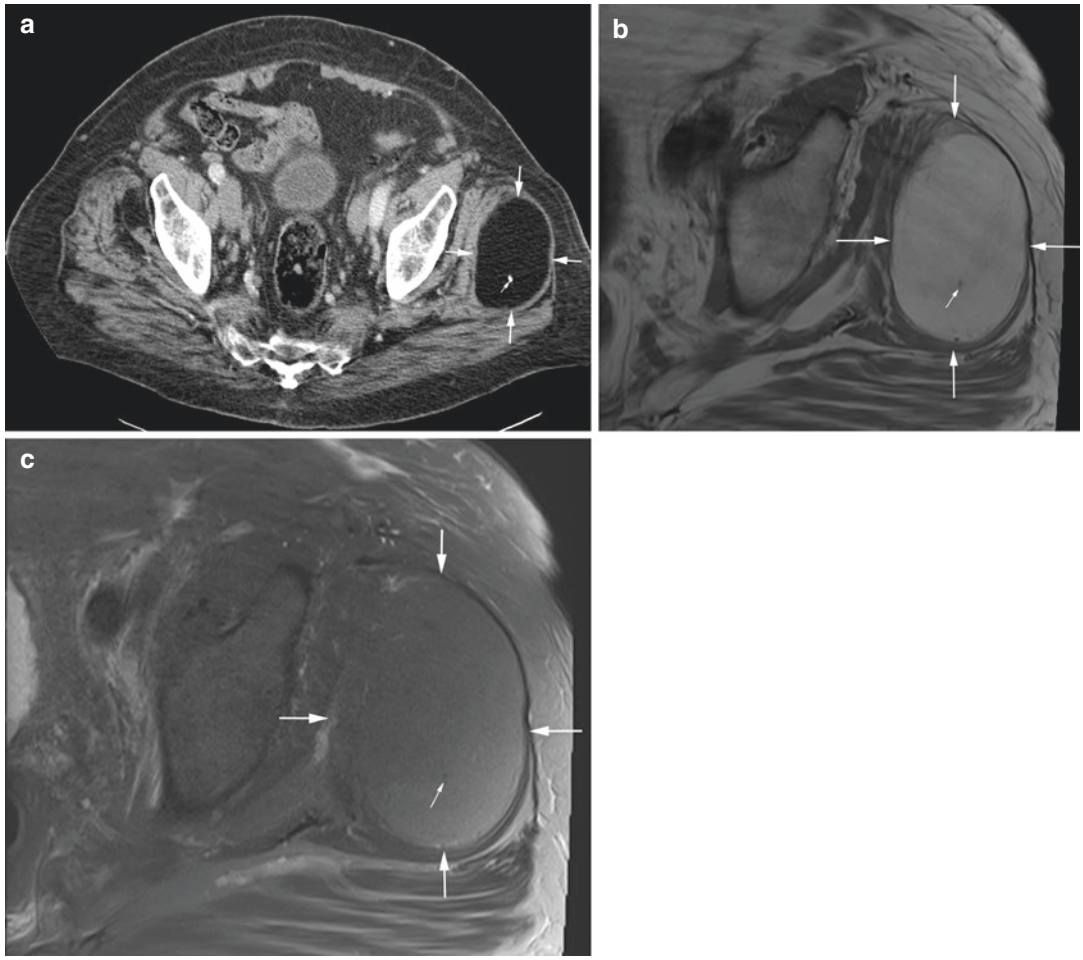

Fig. 12.5 (**a**–**c**) Intramuscular lipoma of the left gluteus medius thigh. (**a**) CT scan. (**b**) Axial SE-T1-weighted MR image. (**c**) Axial TSE T2-weighted fat-suppressed MR image. Large mass in gluteus medius muscle (*arrows*) of the left thigh with low attenuation values on CT (**a**). The signal intensity on different MR sequences equals that of fat (**b**, **c**). Note the presence of small focus of higher-density calcification on CT (**a**) and lower SI (**b**, **c**) on MRI (*small arrow*)

excluding sarcomatous change [63]. Please see Sect. 12.3.1 later.

12.2.1.2 Multiple Lipomas

Some patients, especially males, may have multiple lipomas, which are grossly and microscopically similar to other lipomas. They occur predominantly in the back, shoulder, and upper arms, sometimes in a symmetrical distribution [31]. A familiar disorder exists, referred to as "familial multiple lipoma" which shows this typical clinical presentation. Associated hyperlipidemia and hypercholesterolemia have been described in some cases [31, 49, 72].

12.2.2 Lipomatosis

Lipomatosis, also known as diffuse lipomatosis, represents a diffuse overgrowth of mature adipose tissue histologically similar to simple lipoma. The fatty tissue extensively infiltrates the adjacent structures and contiguous muscles, leading to deformities and limb asymmetry. The distinction between infiltrating lipoma and lipomatosis can be arbitrary at times, and some authors use the two terms interchangeably [48]. However, lipomatosis implies a more extensive process with diffuse involvement of the subcutaneous and muscular tissue, while

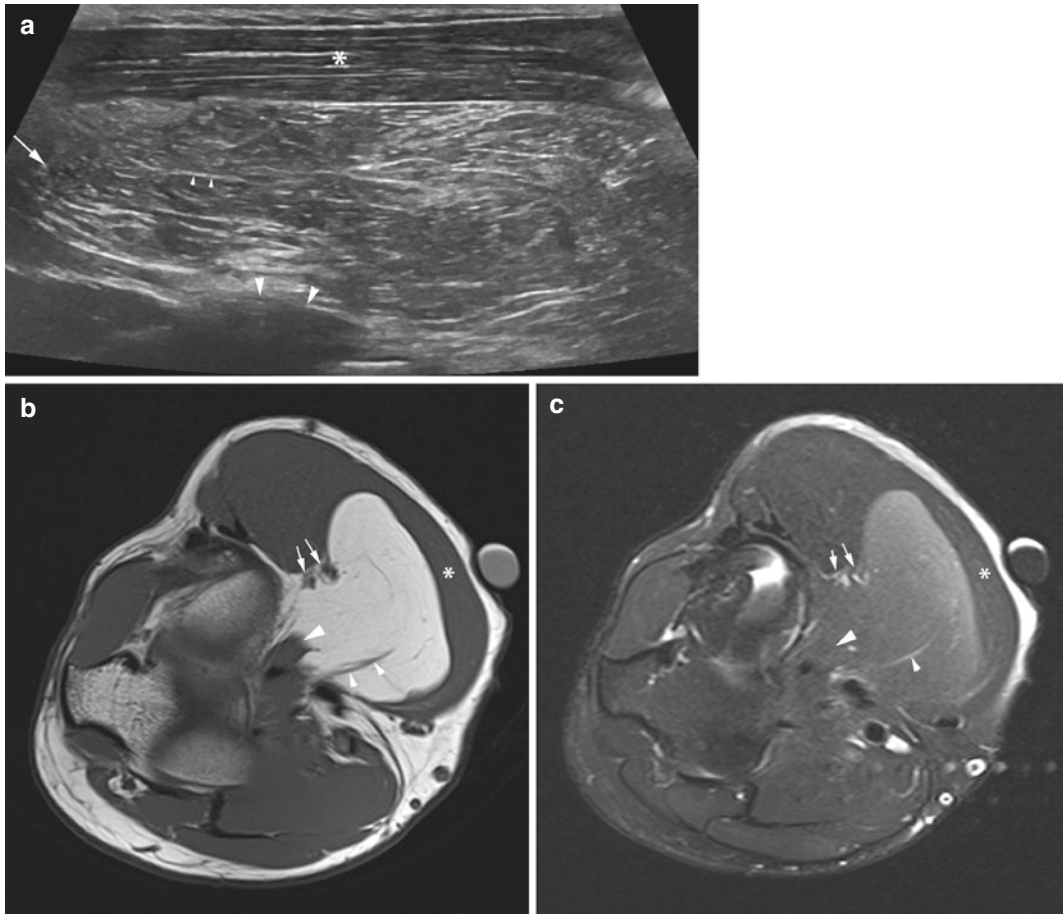

Fig. 12.6 (**a**–**c**) Intramuscular lipoma of the right arm. (**a**) Ultrasound. (**b**) Axial SE T1-weighted MR image. (**c**) Axial fat-suppressed SE T2-weighted MR image. On ultrasound the mass is homogenous and hyperechoic (**a**), and the signal intensity on different MR sequences equals that of fat (**b**, **c**). The radial neurovascular bundle, (*large arrows*) septi (*small arrowheads*), and relationship to brachioradialis (*) are shown with both techniques, but MRI gives a better overview and better definition of the whole mass especially the deeper aspect (*large arrowhead*)

the intramuscular lipoma is always confined to a muscle or intermuscular tissue space.

Diffuse lipomatosis is an extremely rare condition that affects most commonly large portions of the trunk or an extremity. Most cases occur during the first 2 years of life, but they also have been reported in adolescents and adults [31, 49]. Lipomatosis may also be associated with osseous hypertrophy and macrodactyly, but unlike neural fibrolipoma/macrodystrophia lipomatosa, nerves are not involved, and the condition is not confined to the extremities.

The radiological findings in lipomatosis include the presence of fatty tissue diffusely distributed within and between the involved muscles (Fig. 12.9). "Infiltrating congenital lipomatosis of the face" is a related entity present at birth or in infancy, consisting of an unencapsulated, infiltrating fatty mass characteristically involving the face [19, 67]. MR images depict an infiltrating fatty mass, and distortion of the facial bones and displacement of the airway by the lesion have been reported.

12.2.2.1 Multiple Symmetrical Lipomatosis

This rare condition, predominantly affecting middle-aged men, is also known as Madelung disease or Launois-Bensaude syndrome. A familial occurrence

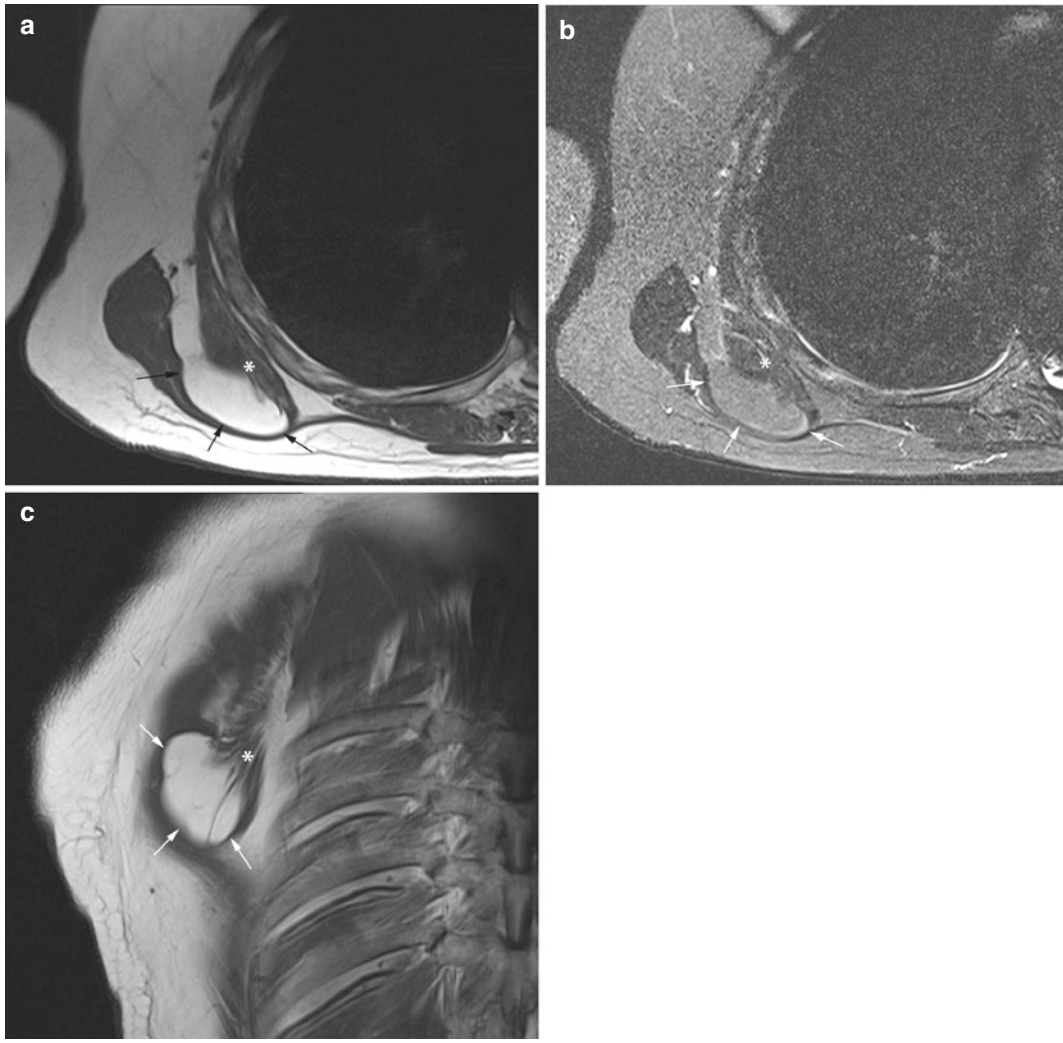

Fig. 12.7 (**a**–**c**) Intramuscular lipoma of left serratus anterior. (**a**) Axial SE T1-weighted MR image. (**b**) Axial fat-suppressed SE T2-weighted MR image. (**c**) Coronal SE T1-weighted MR image. The mass (*arrows*) is homogenous with a signal intensity on all sequences equal to fat (**a**–**c**). The deeper aspect is more ill-defined due to interdigitation with the muscle fibers (*) but still benign in appearance

has been described. The exact cause is unknown, although a hyperplastic mechanism has been considered [21, 55]. Symmetrical lipomatosis is usually associated with excessive alcohol intake, liver disease, diabetes, hyperlipidemia, hyperuricemia, malignant tumors of the upper airway, and neuropathy. Occurrence is usually sporadic, but some investigators believe an underlying hereditary factor may be present in the form of a mitochondrial dysfunction that disturbs the lipid metabolism.

Patients with symmetrical lipomatosis present with massive symmetrical deposition of mature fat in the neck, but also the cheeks, breast, upper arm, axilla, chest, abdominal wall, and groin may be involved [31, 49]. The fatty accumulation progresses frequently over many years and is painless. These fatty masses are unencapsulated, so they are poorly circumscribed with involvement of the subcutaneous fat and deep tissues, mostly posterior relative to the trapezius and sternocleidomastoid muscles, in

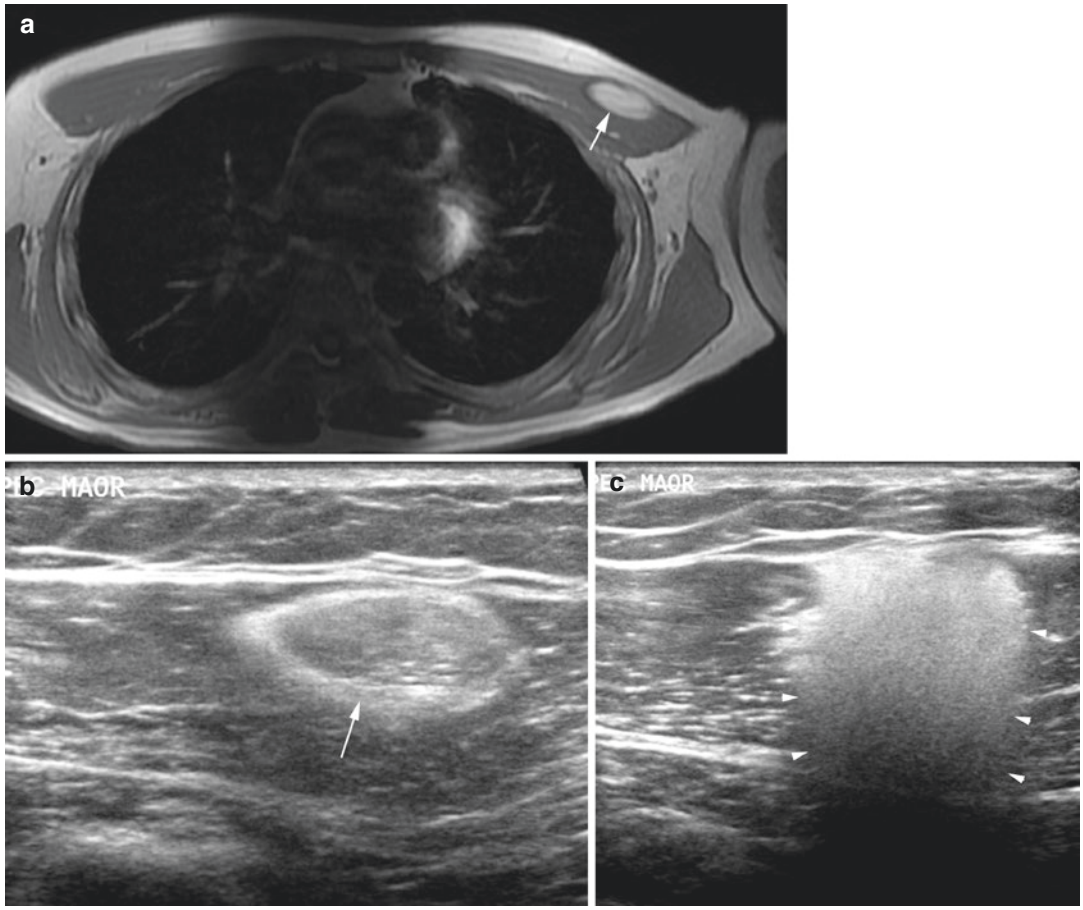

Fig. 12.8 (**a**–**c**) Intramuscular lipoma of left pectoralis major. (**a**) Axial SE T1-weighted MR image. (**b**, **c**) Ultrasound images. On MRI (**a**) and ultrasound (**b**) the mass is homogenous (*arrow*). Careful ultrasound technique is required as angulation can result in reverberation artifact (*arrowheads*) (**c**) due to the multiple muscle fibers within the lipoma

Table 12.1 Differential diagnostic criteria between lipoma and liposarcoma

	Lipoma	Intramuscular lipoma	Liposarcoma
Age	Adult (mean 52 years)	Adult	Adult (mean 65 years)
Location	Superficially located (subcutaneous fat)	Muscle	Muscles/fascias
	Back, shoulder, neck, arm, thigh, abdomen	Thigh, shoulder, arm	Muscle/fascia
			Thigh, retroperitoneum
Size	<5 cm (80 %)	Frequently >5 cm	Exceptionally <5 cm
	<10 cm (95 %)		
Margins	Well defined	Infiltrating or well defined	Usually well defined
Shape	Uninodular	Uninodular (>85 %)	Multinodular (>90 %)
Septa or nodules	Absent or <2 mm	Intermingled muscle fibers	Thick (>2 mm)
	Hypo on FS T2-WI	Isointense to muscle	Hyper on FS T2-WI
	No or weak enhancement	Enhancement rare	Strong enhancement

Modified from Ghadimi et al. [30]

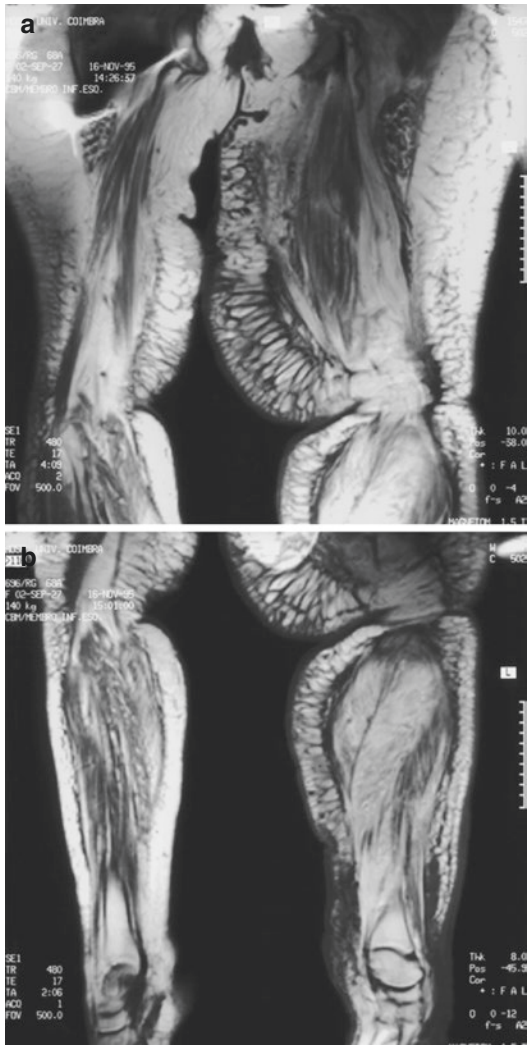

Fig. 12.9 (**a**, **b**) Diffuse lipomatosis of the thighs and legs in a 66-year-old woman. (**a**) Coronal SE T1-weighted MR image of the thighs. (**b**) Coronal SE T1-weighted MR image of the legs. Fat is diffusely distributed within and between the muscles of both thighs (**a**) and legs (**b**) and the subcutaneous fat. Although there is an asymmetry of the size of the limbs, the MR appearances are similar in both sides

the supraclavicular fossa, or between the paraspinal muscles. However, deep fat accumulation may be independent of involvement of adjacent subcutaneous fat, which can be atrophic. This suggests a local formation of fatty masses, rather than penetration of adipocytic tissue by subcutaneous fat. This preferential involvement of compartments distinguishes this disease from

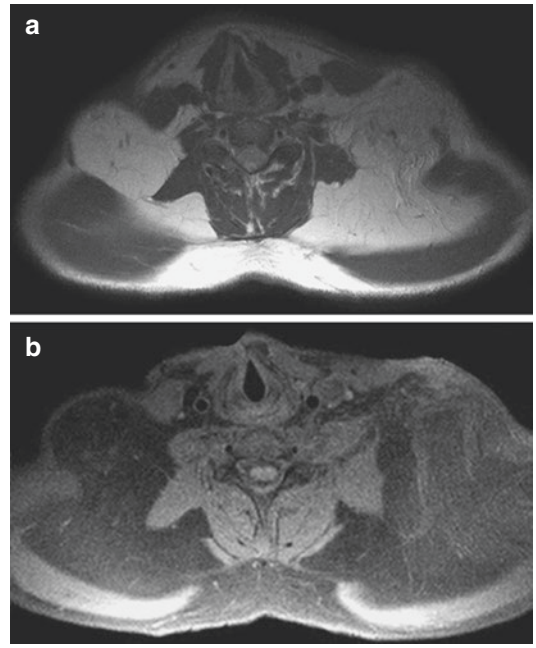

Fig. 12.10 (**a**, **b**) Madelung disease in a 53-year-old man with a history of alcohol abuse. (**a**) Axial SE T1-weighted MR image of the neck. (**b**) Axial FS SE T1-weighted MR image of the neck. Symmetric fatty deposits under trapezius and sternocleidomastoid muscles and anteriorly in the neck

obesity. When symmetrical lipomatosis involves the deep soft tissues of the neck and mediastinum, it may cause dysphagia, hoarseness, severe respiratory insufficiency by extrinsic compression of the trachea, and signs of vascular compression (superior vena cava syndrome) [22, 31, 49, 56].

On CT and MR images, symmetric accumulation of fatty, unencapsulated, deep, or superficial masses have been reported (Figs. 12.10 and 12.11), with calcifications rarely being observed [22, 56]. Surgical debulking is the treatment of choice, but recurrence is common.

12.2.2.2 Adiposis Dolorosa (Dercum Disease)

This condition must be differentiated from symmetrical lipomatosis. It consists of diffuse or nodular painful, multiple subcutaneous fatty deposits (Fig.12.12). Adiposis dolorosa predominates in postmenopausal women and affects predominantly the regions of the pelvic girdle and the thigh. The patients complain of

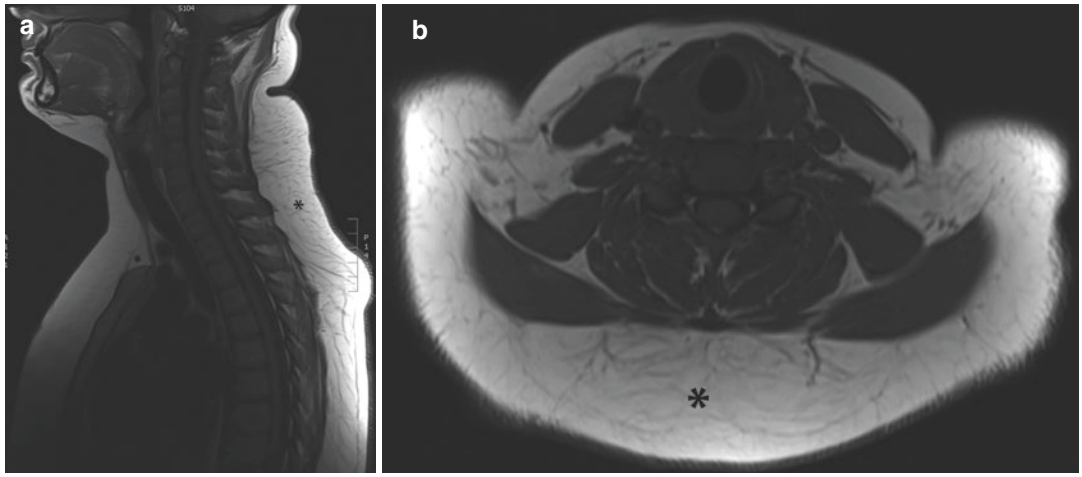

Fig. 12.11 (**a**, **b**) Madelung disease. (**a**) Sagittal SE T1-weighted MR image. (**b**) Axial SE T1-weighted MR image of the neck. Diffuse fatty deposition (*) throughout the subcutaneous tissues in the neck

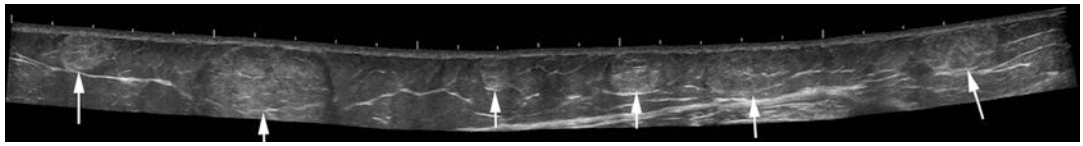

Fig. 12.12 Adiposis dolorosa in a 34-year-old man with bilateral diffuse lipomata. Extended field-of-view longitudinal ultrasound of the right thigh shows multiple lipomas (*arrows*) throughout the subcutaneous tissues

marked asthenia, depression, and psychogenic disturbances. The inheritance is autosomal dominant with variable penetrance [27].

12.2.2.3 Shoulder Girdle Lipomatosis

This syndrome was first described by Enzi et al., involving the scapulohumeral girdle, with fatty infiltration of muscles in six female adult patients [22]. This is a subtype of lipomatosis with different clinical, pathological, and radiological findings. It presents unilateral gradual enlargement and deformity of the shoulder and proximal part of the arm, with shoulder girdle muscle weakness, and motor and sensory neuropathy in the involved limb [22, 59]. Enzi et al. have also noted respiratory symptoms due to compression of the upper airway or infiltration of the laryngeal wall by fatty tissue [22]. MR imaging demonstrates diffuse accumulation of fat, within or between the involved muscles, with high SI identical to normal subcutaneous fat, on T1- and T2-weighted images, without cellular or edematous areas [59].

Bannayan-Zonana syndrome is a rare hamartomatous disorder, which affects men in 68 % of cases. Inheritance is autosomal dominant with variable expression. This syndrome is characterized by the presence of moderate macrocephaly, multiple hemangiomas, and subcutaneous and visceral lipomas (in up to 76 % of cases) [27].

12.2.3 Lipomatosis of Nerve

Lipomatosis of nerve has also been designated in the past as fibrolipomatous hamartoma, fibrofatty overgrowth, lipomatous hamartoma, lipofibroma, neurolipoma, intraneural lipoma, fatty infiltration of the nerve, and neural fibrolipoma. In 2013 the WHO continued with the designation of lipomatosis of nerve [26, 61]. The common term "neural fibrolipoma" is, however, still frequently used because it reflects the nature of this entity. It is a very rare tumor, characterized by a proliferation of fatty and fibrous components that surrounds

the thickened nerve bundles and infiltrates both the epineurium and the perineurium. No vascular abnormalities are associated with the lesion [31, 49]. The cause is unknown, but some consider this condition as a congenital lesion, since it is occasionally present at birth, whereas others believe a relationship exists with a history of prior trauma. This tumor affects predominantly children or young adults, although a late presentation at the age of 75 years has been reported recently [23, 55]. According to Enzinger et al., males are affected more frequently than females, although a similar incidence has also been noted [31, 44, 49].

Lipomatosis of nerve occurs chiefly in the volar aspects of the hands, wrist, and forearm and usually involves the median nerve, although occasional involvement of other nerves such as the cubital, radial, ulnar, tibial, superficial peroneal, and sciatic has also been reported [17, 55, 66]. This entity is less common in the lower extremities. A soft tissue mass is frequently present several years before onset of symptoms. Lipomatosis of nerve usually gives rise to pain, paresthesia, or decreased sensation or muscle strength, in the area innervated by the affected nerves. According to some authors, in 27–66 % of patients with lipomatosis of nerve, there is associated bone overgrowth and macrodactyly of either the fingers or the toes, a condition described as macrodystrophia lipomatosa [31, 49]. Macrodactyly has also been noted in association with neurofibromatosis and vascular lesions or as idiopathic conditions. On plain radiographs, lipomatosis of nerve may manifest by a soft tissue mass or will only be suspected by indirect signs such as the presence of macrodactyly, usually affecting the second and third digits of the hand or foot [12, 48, 78]. There is a soft tissue and osseous hypertrophy, including long, broad, and splayed phalanges (Fig. 12.13). Calcifications on plain radiographs due to metaplastic bone formation have been noted [55].

CT and MRI can be used to identify the neural origin of the tumor due to the presence of tortuous tubular structures, corresponding to enlarged nerve bundles within a predominantly fatty mass (Fig. 12.14). These structures, clearly depicted on MR images, show low SI on both T1- and T2-weighted images according to their fibrous content [12, 17, 23, 55, 66]. The tumor has the tendency to spread along the branches of the nerve, with a significant variation in the distribution of fat along the nerves and their innervated muscle [17]. The lesion consists of serpiginous low-intensity nerve fibers interspersed by fatty tissue [55]. The contrast between the low-signal nerve fascicles and surrounding high-signal fat results in a "cable-like" appearance of the tumor when visualized on axial planes on T1-weighted MR images and a "spaghettilike" appearance on coronal planes [23, 55]. The MR imaging findings of lipomatosis of nerve are very characteristic allowing a confident diagnosis and obviating the need for biopsy [55]. Lipomatosis of nerve must be differentiated from a nerve sheath lipoma. MRI allows differentiation between these two entities, since lipoma manifests as a focal mass separated from the nerve bundles. Resection

Fig. 12.13 Macrodystrophia lipomatosa. Posteroanterior radiograph. Osseous and soft tissue enlargement, affecting the second digit

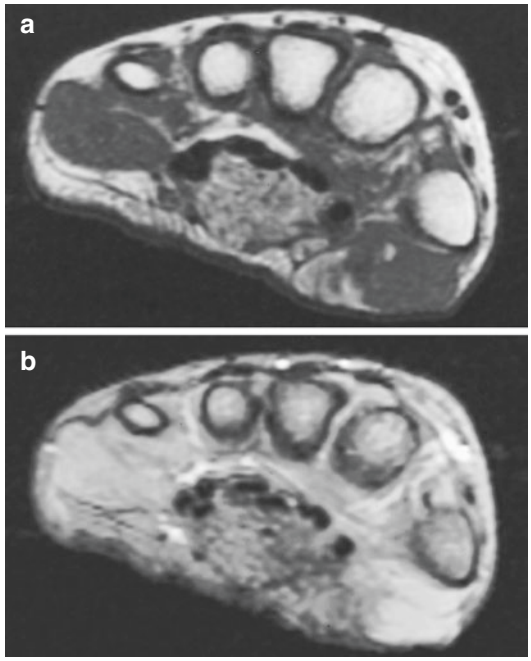

Fig. 12.14 (**a**, **b**) Lipomatosis of nerve of the median nerve at the level of the carpal tunnel in a 40-year-old man. (**a**) Axial SE T1-weighted MR image. (**b**) Axial gradient echo T2*-weighted MR image. These MR images show a heterogeneous mass within the carpal tunnel. There is a mixed SI of fatty components, fibrous components, and neural fascicles (**a**, **b**). The signal intensity and localization are highly characteristic of a neurofibrolipoma of the median nerve

of involved neural elements causes considerable sensory and motor deficits, but the symptoms can be relieved by carpal tunnel release [12].

12.2.4 Lipoblastoma

Lipoblastoma is a well-encapsulated lesion, confined to the subcutis, and is composed of lobules of fat with septations, lipocytes, and lipoblasts (immature fat cells) and poorly differentiated mesenchymal cells in a myxoid stroma with lipoblasts in different stages of development [31, 49]. Cytogenetic analysis has shown it be associated with excess or structural rearrangements of chromosome 8 within the tumor cells [63]. If it infiltrates the subcutis and adjacent muscles and extends across anatomical planes, it was previously referred to as lipoblastomatosis, but now diffuse lipoblastoma is the preferred term. Lipoblastoma is approximately twice as common as diffuse lipoblastoma, which is generally more deeply located [31, 49].

Eighty-eight percent of lipoblastomas occur in patients below 3 years of age, 55 % of the cases in patients below 1 year of age, and in some instances they are present at birth. The occurrence of lipoblastoma in patients older than 8 years of age is rare, although it has been documented in some patients of 10–18 years of age and affects boys more often than girls [15, 31]. This entity most commonly occurs in the extremities, but lipoblastoma may be apparent in other locations such as the trunk, head, neck, axilla, prevertebral soft tissues, mediastinum, or retroperitoneum [35, 44].

In a review of 25 cases, Collins et al. have reported 11 lipoblastomas and 14 cases of diffuse lipoblastoma, with 19 cases (79 %) occurring in boys; 84 % of the patients were less than 5 years old. These lesions measured 1–21 cm in greatest dimension, but 60 % measured less than 5 cm [15]. The relative number of lipoblastoma and diffuse lipoblastoma in a series of 114 cases of the Armed Forces Institute of Pathology (AFIP), was 88 well-circumscribed lesions (lipoblastomas) compared with 26 diffuse forms (diffuse lipoblastoma) [49].

Lipoblastoma usually is a painless, soft tissue mass. The symptoms, although rare, are determined by the size and the location of the tumor. Surgical excision is the treatment of choice and is usually curative in lipoblastoma. Recurrence is rare and affects patients with the diffuse rather than the circumscribed type [15, 31]. Besides recurrence, lipoblastoma may have the capacity to differentiate into mature lesions, such as a lipoma or even fibrolipoma [15, 35, 70].

On ultrasound, lipoblastoma manifests as a mass of mixed echogenicity, with highly echogenic regions interspersed with areas of diminished echogenicity.

The appearance on CT scans varies according to the amount of the adipose and other soft tissue components. Lipoblastoma usually is seen as a fatty mass with scattered foci of soft tissue density.

On MR images lipoblastoma is mostly bright on T1- and T2-weighted images, but it may be hypointense to subcutaneous fat on T1-weighted images, without the signal characteristics of a fatty tumor [35, 70]. Some hyperintense areas on T2-weighted MR images have been described, consistent with cystic or myxoid areas (Figs. 12.15, 12.16, and 12.17). Lipoblastoma does not enhance or shows poor enhancement after intravenous gadolinium administration.

The demonstration of a fatty mass on CT or MRI examination in an infant or child should raise the possibility of a lipoblastoma or diffuse lipoblastoma. Lipoma, lipoma variants, and liposarcoma are uncommon in infants and children. Radiologically and even on microscopic examination, lipoblastoma may be misdiagnosed as liposarcoma, especially myxoid liposarcoma. However, in the case of lipoblastoma, the clinical setting is quite distinct, since lipoblastoma occurs in children, while liposarcoma is very uncommon in this age group. Miller et al., in a review of 149 adipocytic tumors at a children's hospital, have reported 7 lipoblastomas and 2 liposarcomas [60]. The liposarcoma patients were aged 9 and 14 years, and the children with lipoblastoma were younger, but 29 % were more than 3 years of age. In a review of more than 2,500 cases of liposarcoma at the AFIP, only two cases of liposarcoma occurred in children below 10 years old [49].

12.2.5 Angiolipoma

This tumor is composed of mature fat cells and a network of small vessels, containing typical fibrin thrombi. These features allow differentiation from lipoma and from intramuscular hemangioma with prominent fatty elements [31]. It occurs in young adults, being rare in children and in patients older than 50 years.

Angiolipomas have been divided into noninfiltrating and infiltrating types [20]. The most common type is the noninfiltrating type, which presents as a small (median size, 2 cm), encapsulated, subcutaneous nodule located in the trunk, upper arm, and particularly the forearm, rarely

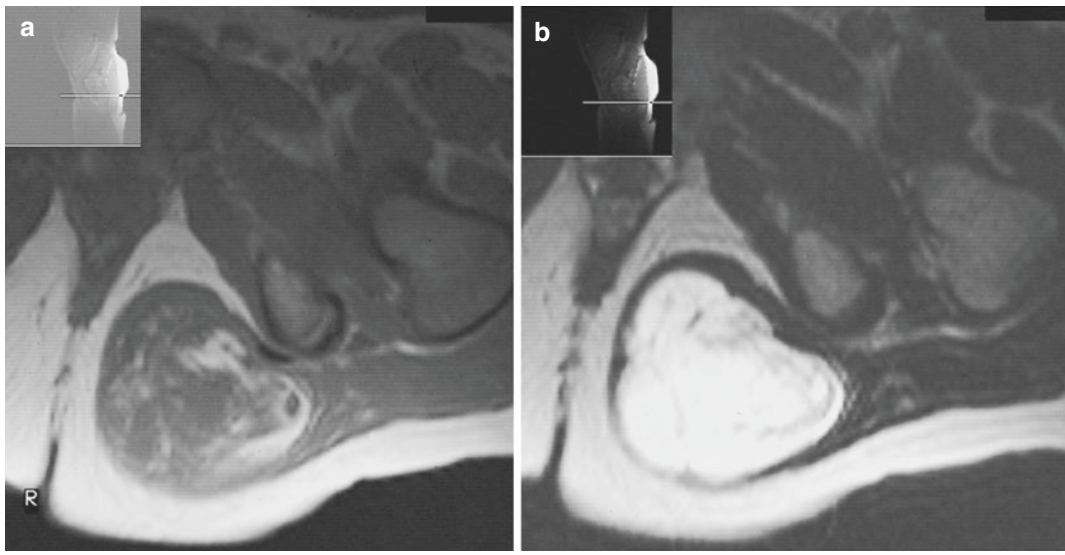

Fig. 12.15 (**a**, **b**) Lipoblastoma of the buttocks in a 5-year-old boy. (**a**) Axial SE T1-weighted MR image. (**b**) Axial TSE T2-weighted MR image. The lesion is located in the medial part of the gluteus maximus muscle protruding into the left ischiorectal fossa. On T1-WI the mass is heterogeneous and ill-defined with interspersed areas of high SI (**a**). On T2-WI the lesion is well defined and of overall high SI (**b**). The presence of fatty components is indicative for the lipomatous nature of the tumor. Although MR images do not allow differentiation from liposarcoma, the age of the patient is much in favor of a lipoblastoma

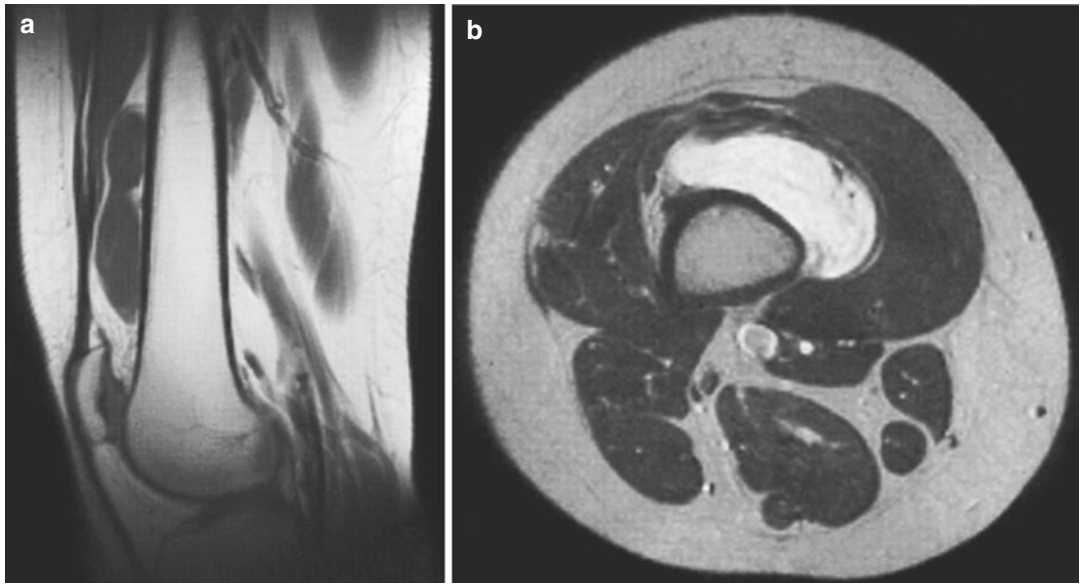

Fig. 12.16 (**a**, **b**) Lipoblastoma of the thigh in a 30-year-old woman. (**a**) Sagittal SE T1-weighted MR image. (**b**) Axial SE T2-weighted MR image. Dumbbell-shaped lesion located between the distal femoral diaphysis and the vastus intermedius muscle. The lesion is isointense to muscle on T1-weighted images (**a**) and has a very high SI on T2-weighted images (**b**). The presence of abundant immature fat cells is probably responsible for the lower SI of the lesion on T1-weighted images. As a consequence such lesions are hard to differentiate from myxoid tumors

affecting the face, hands, or feet [31, 47]. Multiplicity of these lesions is frequent. The infiltrating angiolipoma is a rare, locally aggressive, and unencapsulated variant containing foci of angiomatous proliferation [47]. Imaging is only required in the infiltrating variant of this tumor. On plain radiographs this tumor may show as a mass of fat density, with serpiginous densities and punctate calcifications. On CT scans it usually shows as a poorly delineated heterogeneous intramuscular lesion, with attenuation values ranging from those of fat to those of muscle. This variant has a hypervascular pattern on angiography that can be incorrectly diagnosed as a soft tissue sarcoma.

On ultrasound the appearance will depend on the degree of vascular proliferation and calcification. If minor appearances are usually homogenous and similar to simple lipoma but if vascular tissues predominates multiple hypoechoic areas, calcification and increased Doppler signal can be present [7]. On MR images, angiolipoma shows a mixed composition of both fatty and vascular elements. Signal intensities depend on the relative proportion of tumor components. The nonfatty areas exhibit low SI on T1-weighted images and high SI on T2-weighted images and enhance markedly after intravenous injection of gadolinium contrast (Figs. 12.18 and 12.19). The excision of this tumor is rarely radical, due to its poorly circumscribed margins and muscle invasion, and local recurrence is common.

12.2.6 Myolipoma of Soft Tissue

Myolipoma of soft tissue is a rare benign tumor exhibiting features of mature smooth muscle and mature adipose tissue [26]. It is also known as "extrauterine lipoleiomyoma." The lesion is most frequently located in the abdominal cavity, retroperitoneum, and inguinal areas and more rarely in the subcutis of the trunk and extremities [61]. The majority of the lesions (especially the deeply located abdominal lesions) are large at initial presentation, ranging from 17 to 25 cm in diameter [61].

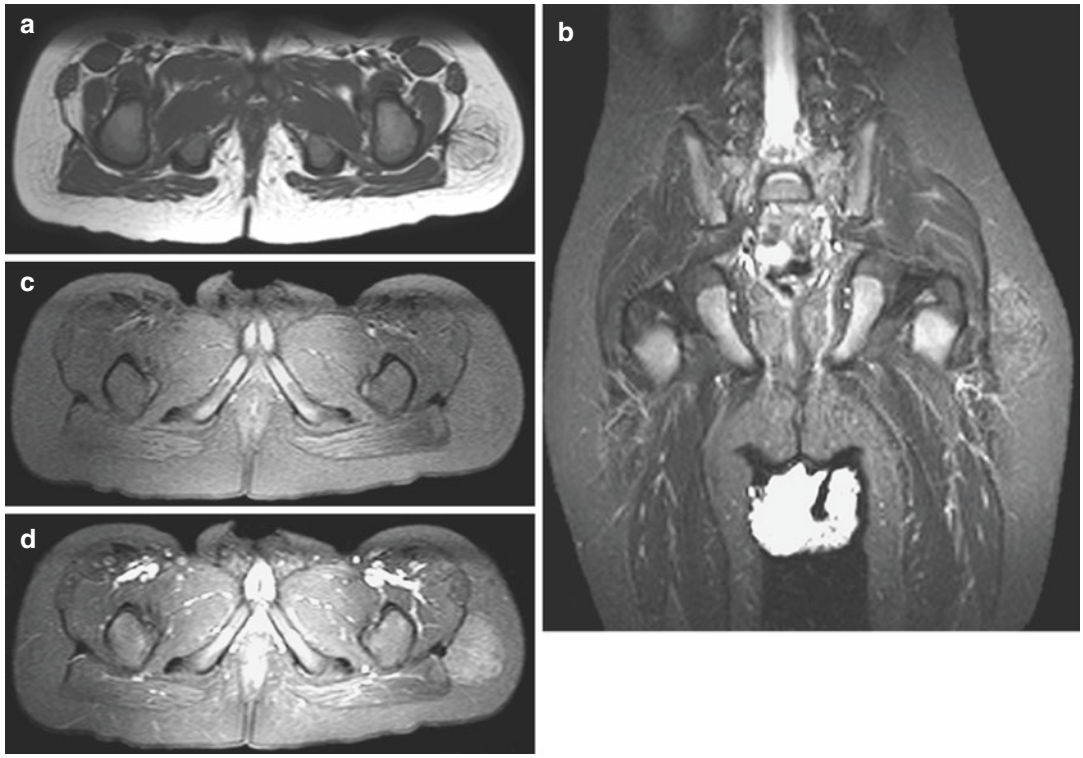

Fig. 12.17 (**a**–**d**) Lipoblastoma of the buttocks in a 5-year-old boy. (**a**) Axial SE T1-weighted MR image. (**b**) Coronal FS TSE T2-weighted MR image. (**c**) Axial FS SE T1-weighted MR image. (**d**) Axial FS SE T1-weighted MR image after gadolinium contrast administration. The lesion is located within the left buttocks. On T1-WI the mass is heterogeneous, isointense to subcutaneous tissue, and ill-defined with interspersed strands of low SI (**a**). These strands are slightly hyperintense on FS T2-WI (**b**), and only a faint contrast enhancement is seen in these nonadipocytic areas (**d**). The presence of fatty components is indicative for the lipomatous nature of the tumor. The age of the patient is an important clue in favor of a lipoblastoma

Due to the presence of nonadipocytic elements within the tumor, imaging does not allow distinction from a well-differentiated liposarcoma. Coarse calcification may be seen in large lesions. On immunohistochemical analysis, smooth muscle components are strongly positive for smooth muscle actin and desmin. Treatment consists of surgical resection. No recurrence or malignant transformation has been described.

12.2.7 Chondroid Lipoma

This is a rare adipocytic tumor, with a variable background of mature fat with cells resembling lipoblasts and brown fat cells, showing features of both lipoma and hibernoma. It contains myxoid and chondroid material and pathologically mimics myxoid liposarcoma and myxoid chondrosarcoma [31, 34]. Meis et al. have reported 20 patients, with an average age of 36 years (range 14–70 years old), with tumors measuring 1.5–11 cm in size (median, 4 cm). Cytogenetic analysis has shown it be associated with translocation between the 11 and 16 chromosomes [63].

Chondroid lipoma manifests as a well-circumscribed mass in the subcutis, superficial fascia, or muscles of the extremities and occasionally in the trunk and head and neck [11, 61] and is mostly found in women. The lesion appears as a well-defined mass with prominent fluidlike areas at sonography and CT. Areas of

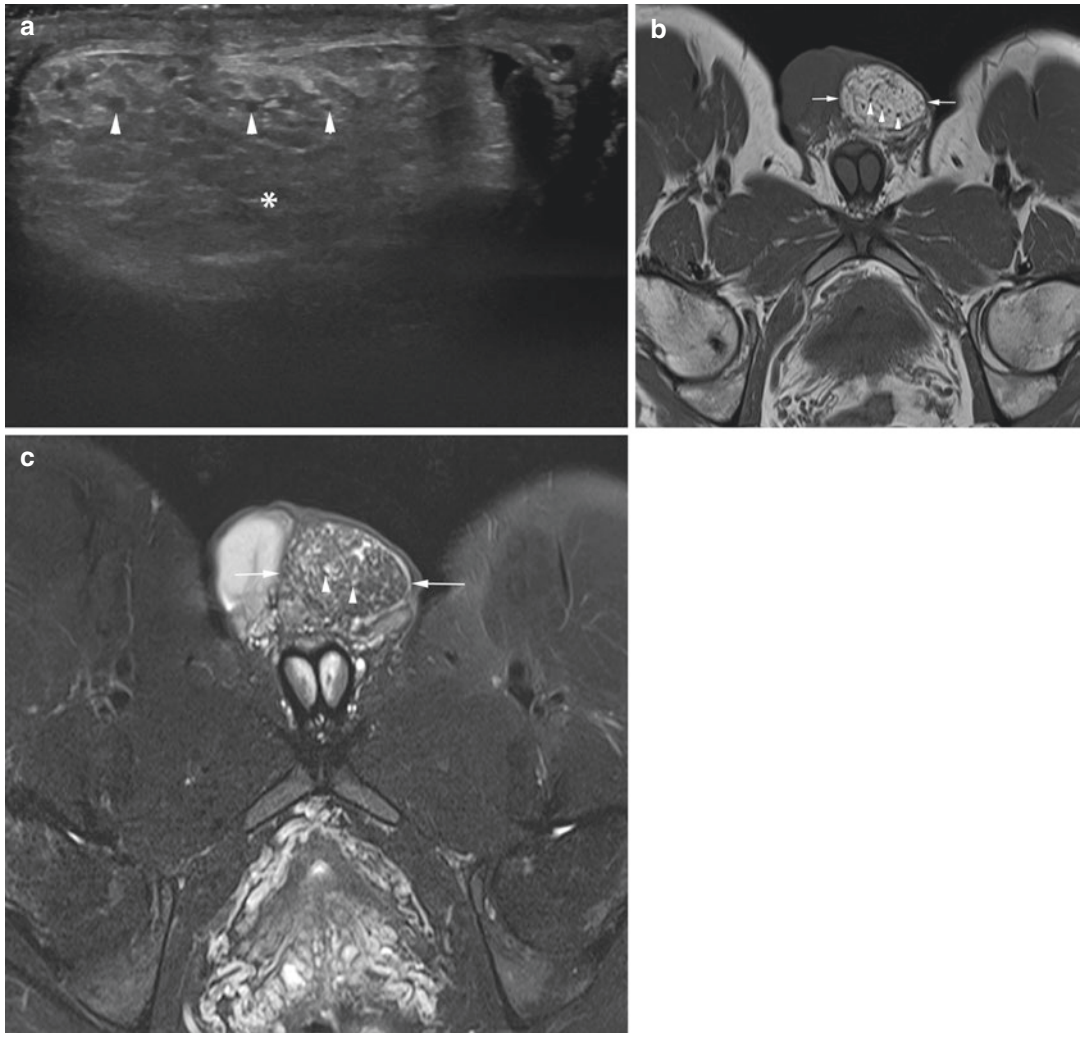

Fig. 12.18 (**a**–**c**) Angiolipoma of the left hemiscrotum. (**a**) Ultrasound. (**b**) Axial SE T1-weighted MR image. (**c**) Axial fat-suppressed SE T2-weighted MR image. The mass (*arrows*) shows predominant fat signal on ultrasound (*) and MR images. Within the lesion there are multiple vessels (*arrowheads*), hypoechoic on ultrasound, low SI on T1-weighted images, and increased SI on T2-weighted images (**a**–**c**)

bright echogenicity have been described also [34]. Calcification is usually present on CT scans and radiographs [34, 61]. The presence and nature of the calcifications – which can be irregular and curvilinear – can raise the possibility of either a malignant diagnosis (including synovial sarcoma, malignant peripheral nerve sheath tumor, epithelioid hemangioendothelioma) or a benign diagnosis (e.g., myositis ossificans) [34]. On MR images, a predominant low SI is seen on T1-weighted images, with only a few strands of high SI identical to fat, either in the periphery or the center of the lesion [61]. These lacy strands of high SI on T1-weighted images are suppressed on STIR images. On T2-weighted MR images, the mass is inhomogeneous and hyperintense, reflecting the largely myxoid consistency of the tumor (Fig. 12.20.). Other features of the mass, such as fine septations and a lobulated margin, suggest cartilage matrix [53]. However, chondroid lipoma demonstrates a whole spectrum of cellular and

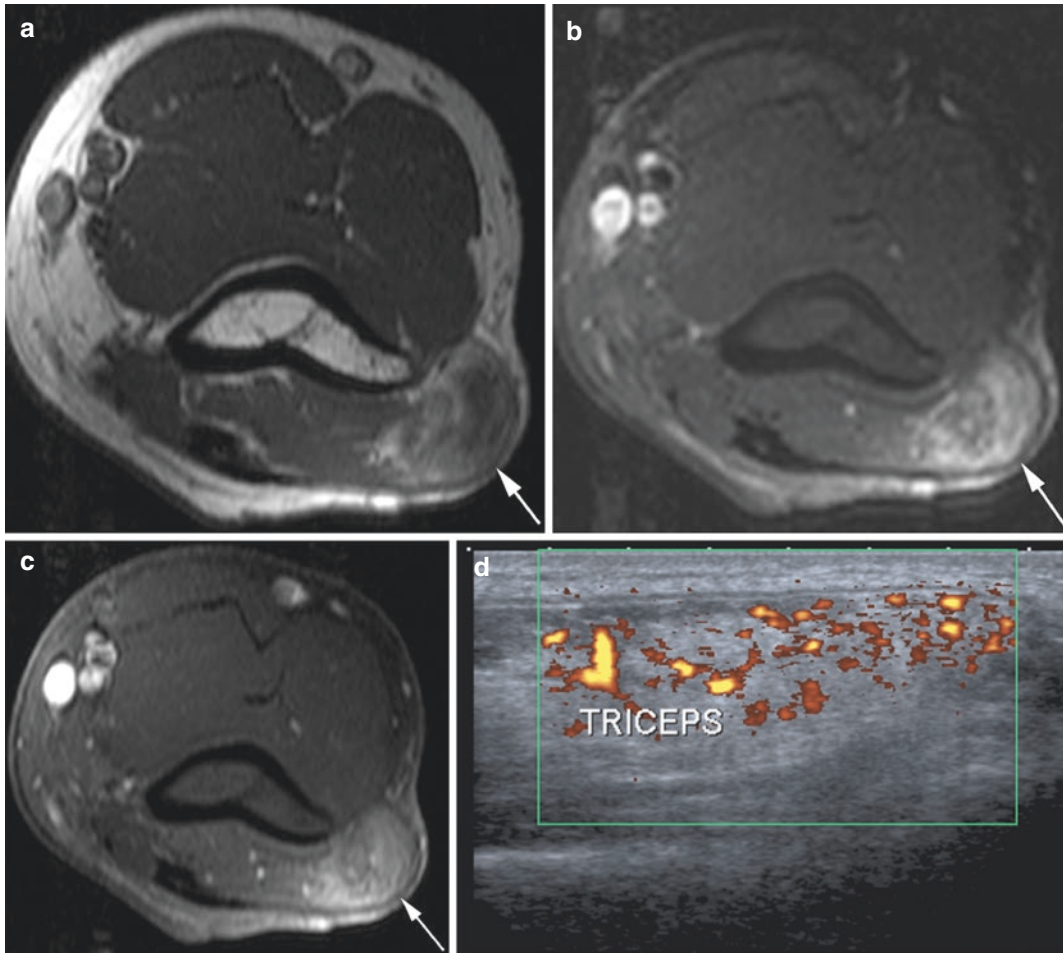

Fig. 12.19 (**a**–**d**) Angiolipoma of the left triceps. (**a**) Axial SE T1-weighted MR image. (**b**) Axial fat-suppressed SE T2-weighted MR image. (**c**) Axial fat-suppressed SE T1-weighted MR image post gadolinium. (**d**) Ultrasound. The mass (*arrow*) within the lateral head of triceps shows some fat signal on MR images with linear areas of low SI on T1-weighted images which have increased SI on T2-weighted and T1-weighted post gadolinium images (**a**–**c**). On ultrasound the lesion is hyperechoic with multiple vessels with increased Doppler signal (**d**). MRI does not allow differentiation between intramuscular angioma and angiolipoma. Tiny fatty components can be found in both lesions

matrix content, which is reflected in variable MR imaging characteristics [11]. Based on the MRI characteristics, chondroid lipoma is difficult to distinguish from myxoid liposarcoma, extraskeletal myxoid chondrosarcoma, and ancient schwannoma [11]. Because MR imaging cannot differentiate absolutely between malignant and benign lesions, biopsy is required to make a final diagnosis [34].

12.2.8 Spindle Cell Lipoma and Pleomorphic Lipoma

In these two clinically and pathologically related variants, the mature fat is replaced by collagen-forming spindle cells. Pleomorphic lipoma is considered as a pleomorphic variant of spindle cell lipoma, and it is distinguished by the presence of a marked cellular pleomorphism and

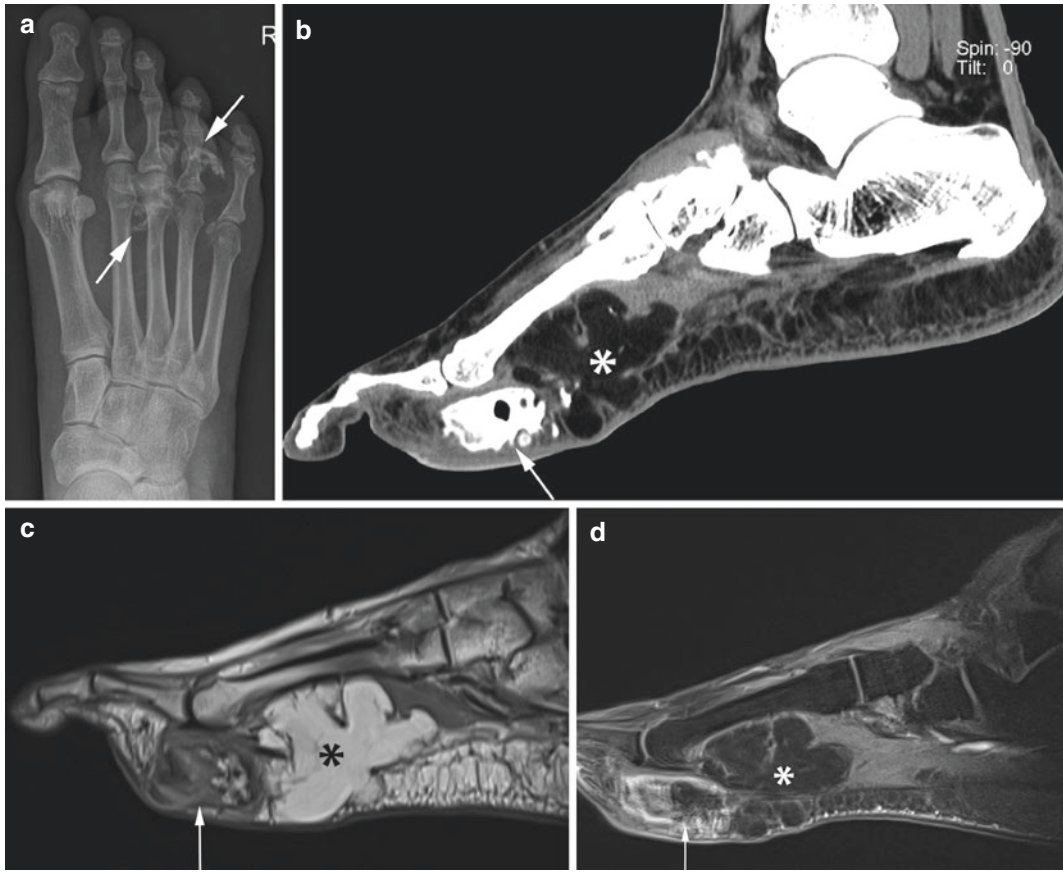

Fig. 12.20 (**a**–**d**) Chondroid lipoma within the plantar aspect of the right foot. (**a**) Plain radiograph. (**b**) CT scan. (**c**) Sagittal SE T1-weighted MR image. (**d**) Sagittal FS SE T1-weighted MR image after gadolinium contrast administration. The lesion lies separate to the metatarsals with chondroid calcification (*arrow*) and a more proximal fatty component (*). After gadolinium administration, there is a heterogeneous enhancement (**d**) of the chondroid component

scattered bizarre giant cells. Histologically the differential diagnosis from liposarcoma may be difficult [31]. Cytogenetic analysis has shown it be associated with cells showing abnormalities of chromosome 13 including deletions and monosomy, while immunohistochemistry staining is strongly positive for CD34 [63]. Spindle cell and pleomorphic lipomas typically present as a well-circumscribed nodule, confined to the subcutis of the neck or shoulder region in male patients older than 45 years. These lipomas usually manifest as a slow-growing, painless, solitary mass, with an average size between 3 and 5 cm. Although rare, multiple spindle cell lipomas have been described [25]. Fanburg-Smith et al. have reported 7 familial and 11 nonfamilial cases of multiple spindle cell lipomas, all occurring in male patients, and most of them in the sixth to eighth decades of life [25]. These patients had between 2 and more than 220 lesions, on the posterior neck or back and also involving the shoulders.

Pleomorphic and spindle cell lipomas may manifest as inhomogeneous, nonspecific fatty masses with nonadipocytic components that show increased density on CT scans and long relaxation times on both T1- and T2-weighted MR images [43] (Figs. 12.21 and 12.22). A spindle cell lipoma with marked bone erosion of the foot has been documented. On imaging, pleomorphic and spindle cell lipomas are frequently misdiagnosed as liposarcoma [47]. A spindle cell variant of well-differentiated liposarcoma has to be differentiated from a benign spindle cell lipoma [18].

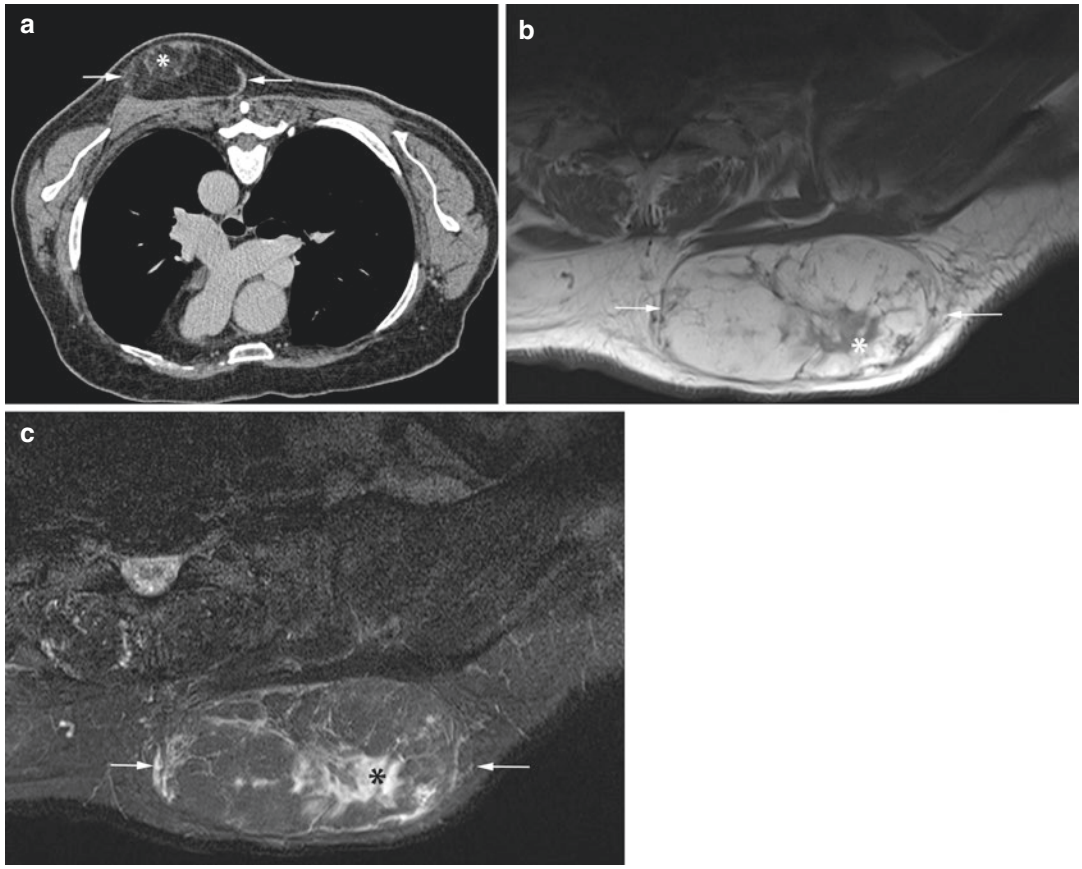

Fig. 12.21 (**a**–**c**) Spindle cell lipoma within the subcutaneous tissues of the left back. (**a**) Axial CT image. (**b**) Axial SE T1-weighted MR image. (**c**) Axial FS TSE T2-weighted MR image. The signal intensity of the lesion (*arrows*) is predominantly fat SI on all modalities. Area (*) of soft tissue density on CT and edematous SI on MRI on T2-weighted images (**a**–**c**)

12.2.9 Hibernoma

Hibernoma is a rare benign tumor composed of brown fat, first described by Merkel in 1906 and named by Gery in 1914. Its name is derived from the tumor's histological similarity to the brown glandular fat of hibernating animals. Cytogenetic analysis has shown it to be associated with cells showing abnormalities of the long arm of chromosome 11, but findings are not specific [63]. Brown fat, histologically distinct from white adipose tissue, is present in the human fetus and newborn but gradually decreases through adulthood. Brown fat plays a role in thermogenesis in hibernating animals and in the newborn, and its role is possibly to maintain a normal body weight.

Other names for hibernoma are "lipoma of immature adipose tissue," "lipoma of embryonic fat," and "fetal lipoma," due to the resemblance between brown fat and the early stages of development of white fat [31].

Hibernomas are generally well-circumscribed, encapsulated tumors, but infiltration of the surrounding tissues may occur. They show a lobular pattern, with connective tissue septa, and are composed of granular or multivacuolated cells [31]. The stroma is highly vascularized; the mixed form displaying histological features between lipoma and hibernoma is the most frequent.

The peak incidence of hibernoma is in the third or fourth decade, and although it can be seen at

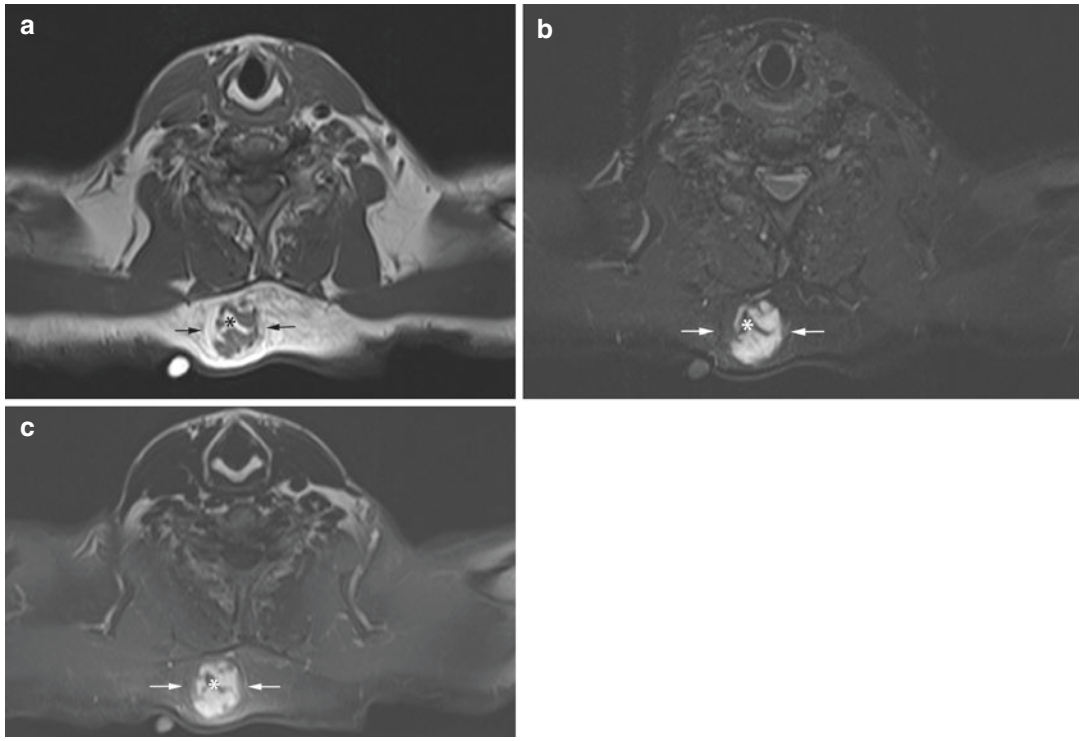

Fig. 12.22 (**a**–**c**) Spindle cell lipoma within the subcutaneous tissues of the neck. (**a**) Axial SE T1-weighted MR image. (**b**) Axial fat-suppressed SE T2-weighted MR image. (**c**) Axial fat-suppressed SE T1-weighted MR image post gadolinium. The signal intensity of the lesion (*arrows*) is predominantly nonfat SI on all modalities and enhances with gadolinium. Small area (*) of fat SI on all sequences also shows no enhancement (**a**–**c**)

any age, the patients with hibernoma are usually younger than those with lipoma. Enzinger et al. have reported a series of 32 cases, in which the median age is 26 years (range 18–52 years) [31]. Kransdorf has reported 41 cases of hibernoma, with a mean age of 32 years [44]. Several studies have reported a slight female predominance.

Usual locations are the scapular and interscapular regions, mediastinum, and upper thorax, sites corresponding to the distribution of remaining brown fat. Involvement of the neck, chest wall, retroperitoneum, arm, buttock, inguinal region, and spinal canal has also been reported, as well as some areas devoid of brown fat such as the thigh or the popliteal fossa [2, 4, 14, 31]. Mugel et al. have reported a hibernoma of the thigh extending into the pelvis, through the obturator foramen.

Hibernoma usually manifests as a superficial, soft, well-defined, painless, and slow-growing mass that, however, may suddenly increase in size. Local pain has been reported, and since hibernoma is a hypervascular mass, the overlying skin is often warm. It ranges from 5 to 10 cm in diameter, but this tumor can extend to 18 cm in the greatest dimension [31].

Radiographs often demonstrate a mass with a radiolucency consistent with a adipocytic tumor, or some increased density of the soft tissues, without osseous involvement [2]. Ultrasound displays a hyperechoic mass, and on Doppler examination, several large vascular channels may be identified within the mass.

On CT scans this condition may present as a well- or ill-defined adipocytic mass, and it may be heterogeneous, due to the presence of septations and other soft tissue components [2]. Hibernoma may show poor or strong contrast enhancement of the septa or diffusely within the mass [51]. MR images depict usually a heterogeneous or septated

mass, isointense or typically slightly hypointense to subcutaneous fat on T1-weighted MR images (Figs. 12.23 and 12.24), but frequently hyperintense to normal muscle tissue [51]. On T2-weighted MR images, the mass can be nearly isointense to subcutaneous fat, although hypointensity and areas of increased SI have been reported also [2, 10, 51]. Hibernoma demonstrates usually inhomogeneous enhancement after intravenous contrast administration, but the absence of enhancement has also been described [51].

Whereas the tumor is almost as intense as fat on T2-weighted images, fat-suppression techniques fail to suppress the fat in the tumor because of the nature and the amount of lipids (Figs. 12.23 and 12.24) [20]. Knowledge of the MR imaging characteristics, particularly hypointensity to subcutaneous fat on T1-weighted images and the absence of fat suppression on STIR or fat-suppressed T2-weighted images, may help suggest hibernoma as a potential diagnosis (Fig. 12.23). However, inasmuch as overlap exists in imaging features of hibernomas and a small number of others tumors, a specific diagnosis may not always be possible.

Today, angiography has been replaced by MRI in the diagnosis of this tumor, but, when performed, an intense vascular blush can be seen due to high vascularity of the tumor, with absence, however, of neovascularity or arteriovenous shunting [27]. The imaging features can make differentiation from liposarcoma almost impossible, and therefore surgical resection is usually performed [51]. Definitive

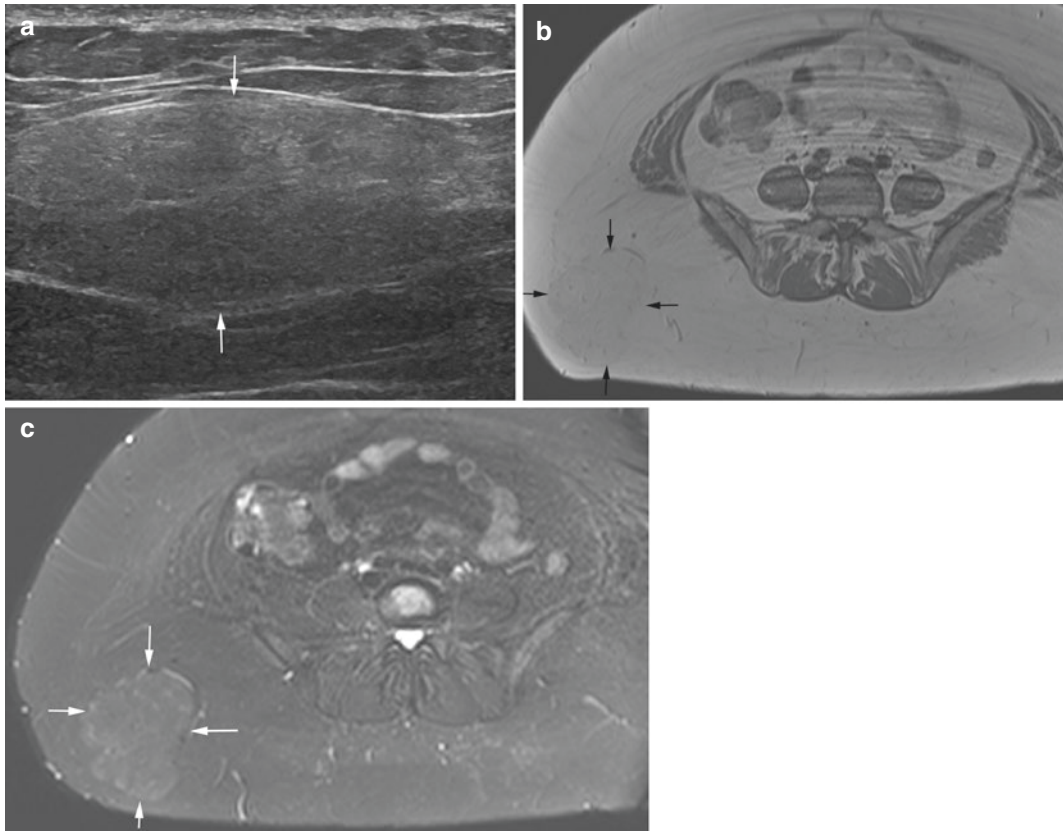

Fig. 12.23 (**a**–**c**) Hibernoma of the right buttock. (**a**) Ultrasound. (**b**) Axial SE T1-weighted MR image. (**c**) Axial fat-suppressed SE T2-weighted MR image. The mass (*arrows*) shows predominant fat signal on ultrasound and MR images but not identical to the surrounding fat. On T1-weighted images, the signal intensity is slightly lower than subcutaneous fat (**b**). On fat-suppressed SE T2-weighted images, fat suppression of yellow fat is incomplete, resulting in a relatively higher signal intensity of the mass compared to subcutaneous fat (**c**)

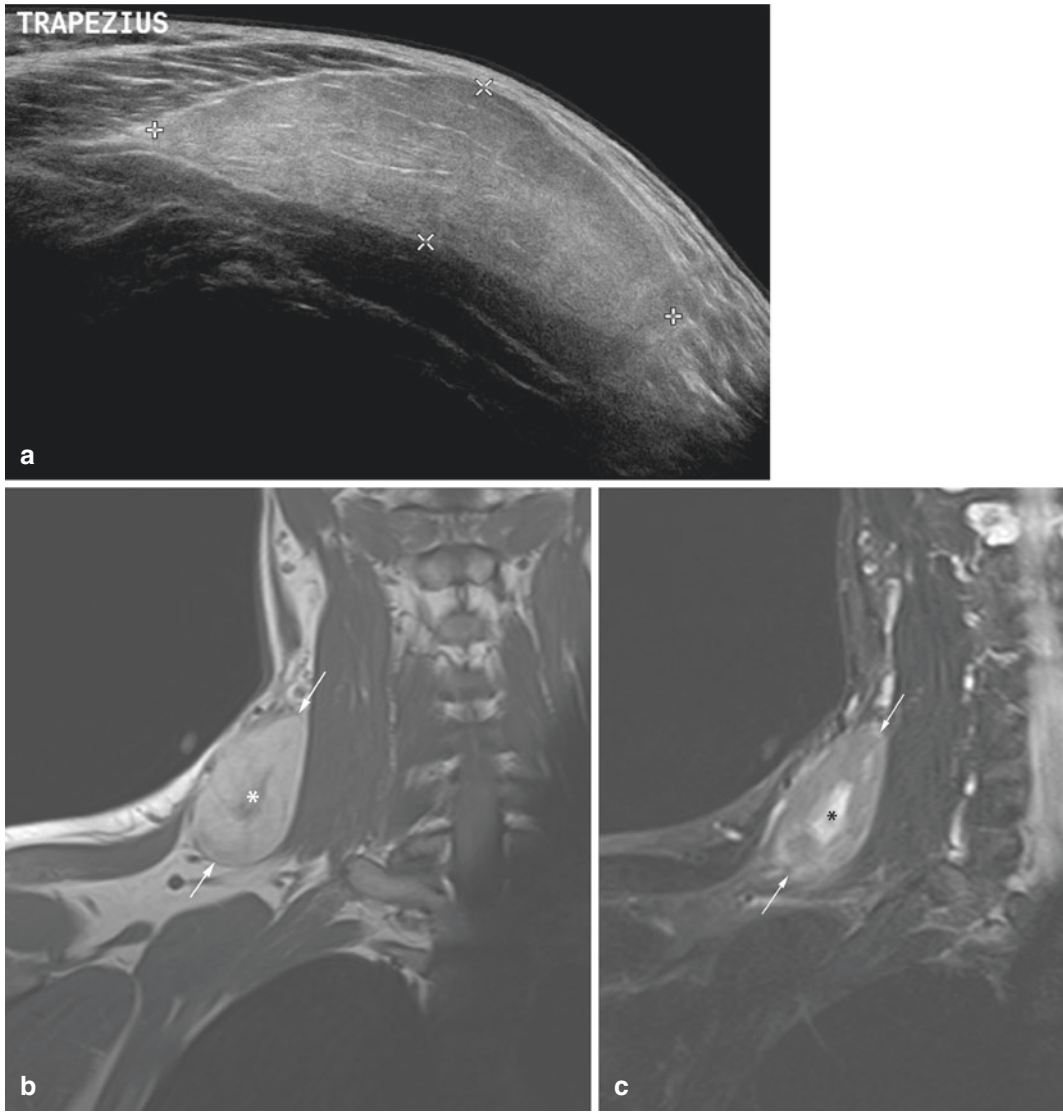

Fig. 12.24 (**a**–**c**) Hibernoma of the neck. (**a**) Ultrasound. (**b**) Coronal SE T1-weighted MR image. (**c**) Coronal fat-suppressed SE T2-weighted MR image. The mass (*arrows*) shows homogenous hyperechoic fat signal on ultrasound, but MR images show a central area (*) of non-fat SI and altered fat signal in the majority of the lesion. On T1-weighted images, the fat signal intensity is slightly lower than subcutaneous fat (**b**). On fat-suppressed SE T2-weighted images, fat suppression of yellow fat is incomplete, resulting in a relatively higher signal intensity of the mass compared to subcutaneous fat (**c**)

diagnosis is usually only made after histopathological examination of the resection specimen. Although some reports of malignancy have been described, the existence of malignant hibernoma is still debated, as some cases are considered as variants of liposarcoma [31]. There is no recurrence after complete excision.

12.2.10 Other Variants of Lipoma

Lipomas containing other mesenchymal elements are classified depending on the associated tissue: fibrous connective tissue, mucoid, cartilaginous, bony elements, smooth muscle, or small and thin-walled vessels, respectively. The

presence of nonadipocytic areas can alter the US and MRI appearance of a simple lipoma, making the differential diagnosis with well-differentiated liposarcoma sometimes complicated [29].

Occasionally, lipoma shows no evidence of fat on MR images but are still fat at histology. These lipomas are usually suggestive of malignancy on imaging and may be indistinguishable on CT or MR images from other soft tissue tumors.

In this section, some benign adipocytic variants containing nonadipocytic elements are discussed focusing on those subtypes that differ clinically and histologically from lipoma, such as fibrolipoma, ossifying lipoma, lipoma of tendon sheath, and joint and parosteal lipoma. However, these terms are not based on strict histological criteria and do not remain in the current WHO classification [26].

12.2.10.1 Fibrolipoma

Fibrous connective tissue is the most common nonadipocytic element found in benign adipocytic tumors, often with the configuration of septa [38]. When a lipoma contains connective tissue (fibrolipoma), it may demonstrate areas of low SI on T1- and T2-weighted images on MRI and hypoechoic intensity on ultrasound (Fig. 12.25).

12.2.10.2 Ossifying Lipoma and Osteolipoma

Osseous metaplasia occurring within a lipoma is referred to as osteolipoma or ossifying lipoma. If the fat component is predominant, the tumor is designated as an ossifying lipoma, whereas the term osteolipoma is used in those lesions without a predominant fat component [52].

The pathogenesis of this rare tumor is still debated. Single or repeated trauma or local ischemia has been suggested as causes of bone formation. According to others, the osseous metaplasia results from blood-borne monocytes entering the tissue and releasing an osteoinducing factor that results in transformation of fibroblasts into osteoblasts. Ossification from preexisting fibrofatty mesenchymal elements has also been suggested. Most likely, the tumor represents a benign mesenchymoma in which mesenchymal cells differentiate to bone [27, 52].

Within the soft tissues, the tumor may be located at the head and neck area and wrist, although location within the central nervous system at the tuber cinereum, hypothalamic and suprasellar region, and spinal canal has been reported also [52].

Imaging modalities such as standard radiography and CT scan are useful diagnostic tools to demonstrate the ossified components, whereas MR allows further identification of the adipose tissue component (Fig. 12.26). Definitive diagnosis requires pathological examination of the specimen after excision. The patient's prognosis after excision is favorable.

12.2.10.3 Lipoma of the Tendon Sheath and Joint

This is a very rare lesion that can be seen in two different forms. The first form is an adipocytic mass spreading along the tendon sheaths, usually in the hand or wrist and less frequently in the ankle and foot. Lipoma of tendon sheath usually occurs in young patients, affecting with equal frequency both sexes, and approximately 50% are bilateral. Pain may be referred, and rupture of a tendon has been reported [31]. The lipoma of the tendon sheath manifests as a mass in every way similar to a simple lipoma (Fig. 12.27). The second form is an intra-articular, lipoma-like lesion, consisting of hypertrophic synovial villi distended by fat that replaces the subsynovial tissue (Fig. 12.28). This lesion, called "lipoma arborescens," is more common than the tendon sheath variety. As lipoma arborescens is regarded as a nonspecific reactive lesion rather than a true adipocytic tumor, further discussion of this lesion can be found in Chap. 21 on synovial lesions.

Differential diagnosis includes synovial lipoma, pigmented villonodular synovitis, synovial chondromatosis, plexiform neuroma, and synovial hemangiomatosis due to their identical clinical picture, but the differentiation is readily made by CT and especially by MRI.

12.2.10.4 Parosteal Lipoma

When affecting the tissue adjacent to the bone, lipoma is referred to as parosteal lipoma [31, 33, 61]. Parosteal lipoma constitutes 0.3% of all

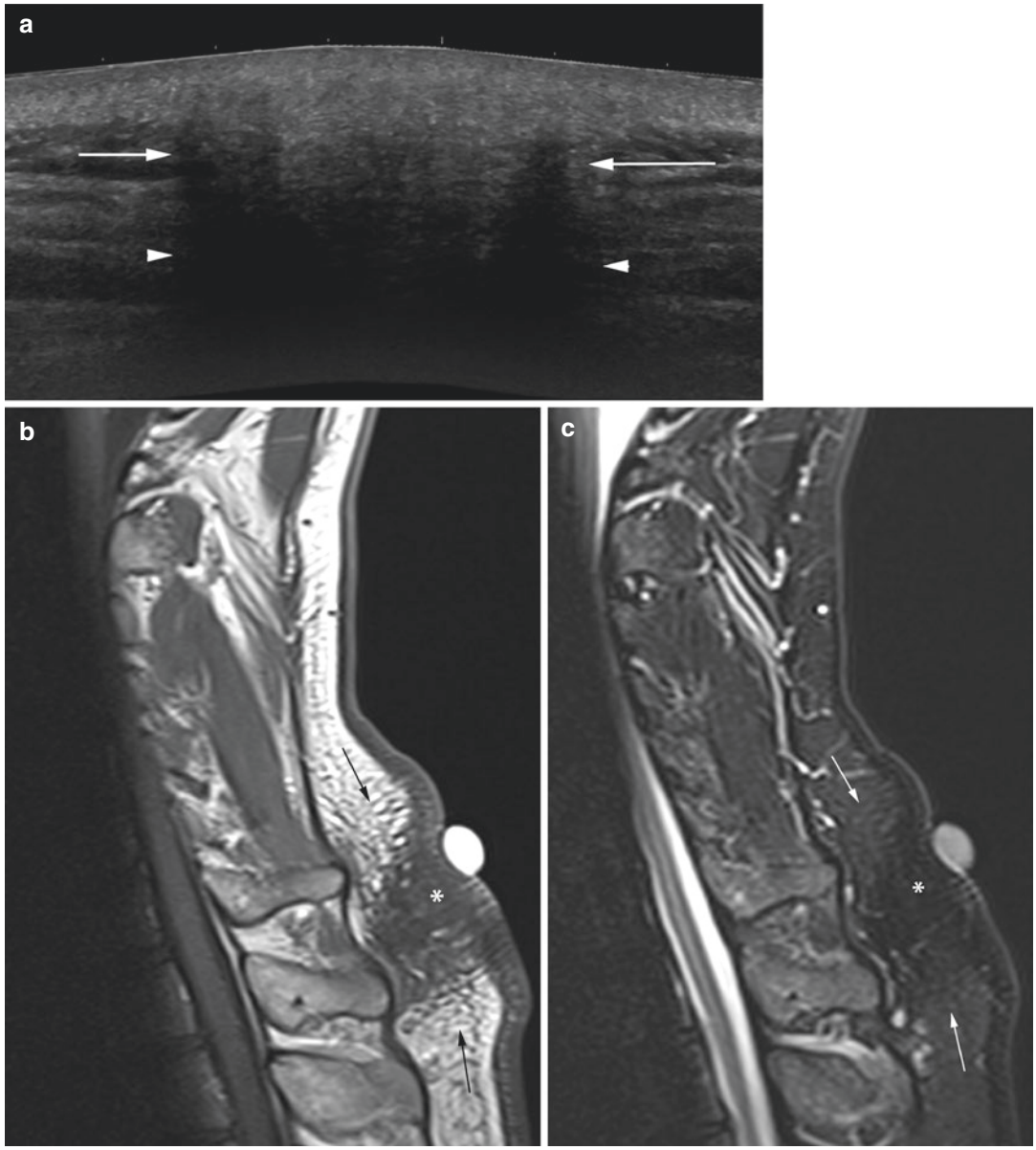

Fig. 12.25 (**a**–**c**) Fibrolipoma of the neck. (**a**) Ultrasound. (**b**) Sagittal SE T1-weighted MR image. (**c**) Sagittal fat-suppressed SE T2-weighted MR image. The mass (*arrows*) involves the dermis and subcutaneous fat. On ultrasound there is marked acoustic shadowing (*arrowheads*) due to the high fibrous component (**a**). There is a large area of low SI (*) on T1-weighted images and fat-suppressed SE T2-weighted images (**b**, **c**) while the peripheral margins of the mass show fat signal

lipomas and the imaging appearances are characteristic [33]. The gross and histological findings of parosteal lipoma are similar to those of a subcutaneous lipoma, except that the lesion has a broad-based attachment to the subjacent bone [31, 62]. The parosteal lipoma is contiguous with underlying periosteum, and some authors have referred to these lesions as "periosteal lipomas." However, "parosteal" rather than "periosteal" is the preferred terminology, since fat cells are not found in the periosteum, and it indicates contiguity with bone but avoids specifying the tissue of

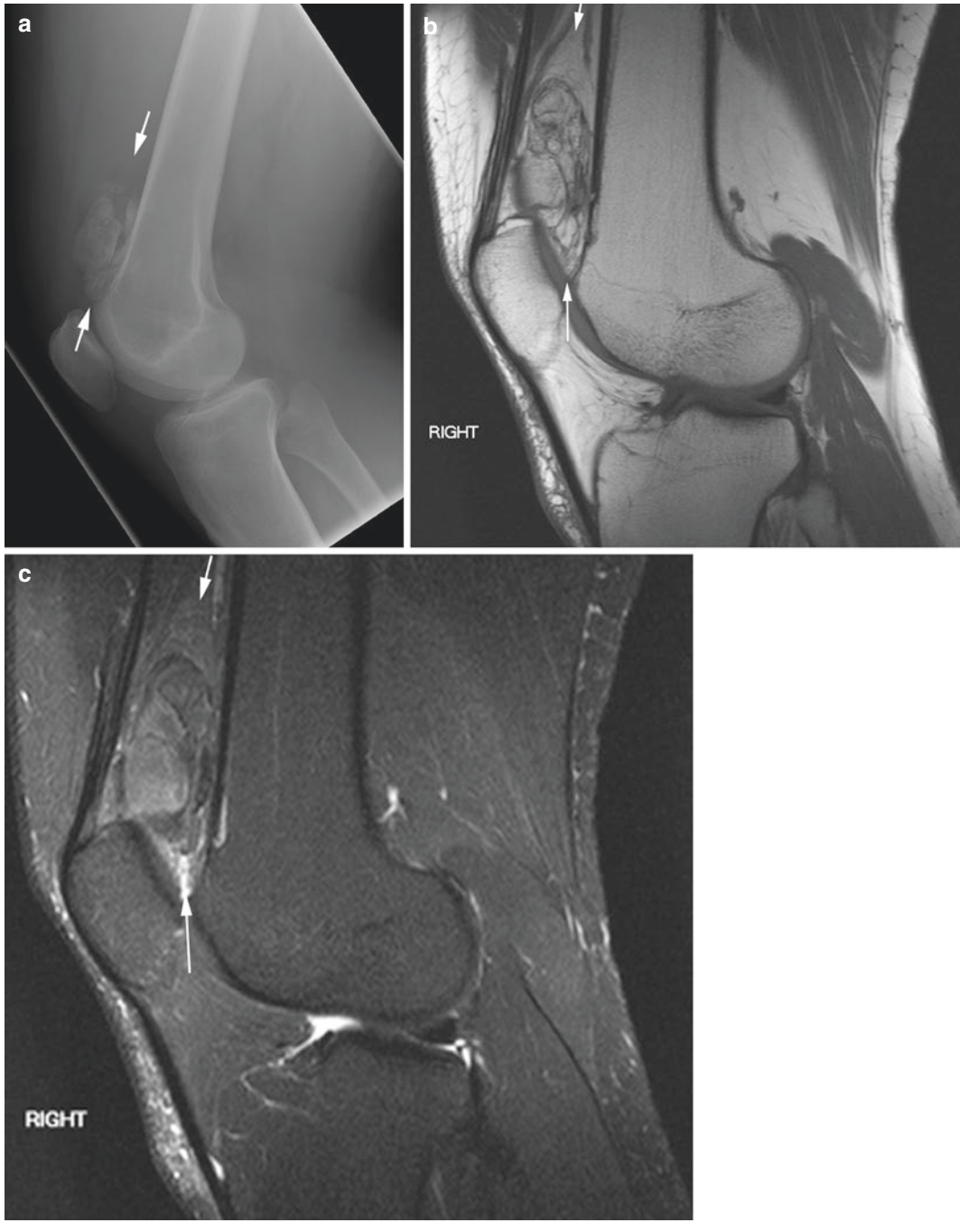

Fig. 12.26 (**a**–**c**) Ossifying lipoma of the knee. (**a**) Plain film. (**b**) Sagittal SE T1-weighted MR image. (**c**) Sagittal fat-suppressed SE T2-weighted MR image. The mass (*arrows*) involves the extra-articular fat adjacent to the anterior femur. On plain film there is marked intrinsic ossification (**a**). There are multiple linear areas of low SI on T1-weighted images and fat-suppressed SE T2-weighted images corresponding to the ossification, while the peripheral margins of the mass show fat signal (**b**, **c**)

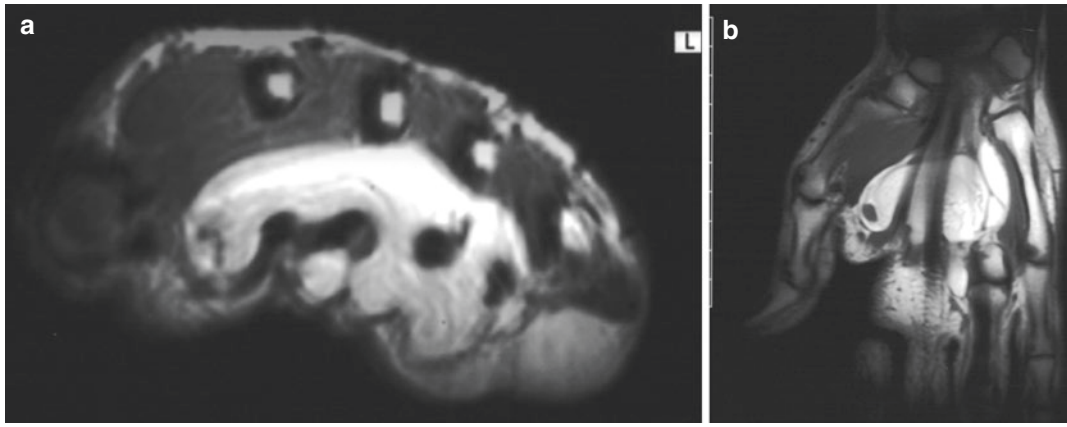

Fig. 12.27 (**a**, **b**) Lipoma of the tendon sheath of the hand in a 31-year-old man. (**a**) Axial SE T1-weighted MR image. (**b**) Coronal SE T1-weighted MR image. MR images show a fatty mass spreading along the flexor tendon sheaths of the hand (**a**, **b**). There are some thin septa and a small nodular component within the lipoma

origin [33]. The lesion is often well encapsulated except at the site where it is adherent to the bone. The behavior and morphological and imaging findings of parosteal lipoma are generally identical to those of a subcutaneous lipoma.

The usual age of patients with this lesion is similar to that of those with subcutaneous lipoma, between 40 and 60 years, with a male predominance [33]. The most frequent sites of parosteal lipomas are the arm, forearm, thigh, and calf, adjacent to the diaphysis or diametaphysis of the bone. Other locations have been reported, such as the finger, mandible, shoulder, and adjacent to the upper sacrum and iliac bone [33]. Parosteal lipoma is usually a slow-growing, generally asymptomatic, large mass, measuring up to 20 cm maximal diameter. Neurological symptoms due to nerve compression have been described in the proximal forearm, with paralysis of the posterior interosseous nerve, but involvement of the radial, sciatic, ulnar, and median nerves has also been reported, resulting in motor and/or sensory disturbances [62].

On plain radiographs this tumor may manifest as a radiolucent lesion in the soft tissues adjacent to cortical bone, with or without osseous change (Figs. 12.29 and 12.30). In parosteal lipoma, occasional osseous changes can be seen at the osseous attachment, such as bowing, bone projections, cortical erosions, periosteal reaction, and intralesional metaplastic bone formation [33]. The most common osseous manifestation is an irregular osseous excrescence into the soft tissue, with variable width at the base [33]. Mild cortical thickening is best evaluated on radiographs, with magnification views, and it may not be demonstrated on MR images. Cortical thickening is seen in the majority of cases [31]. Associated muscle atrophy may be seen and is believed to correspond to nerve impingement.

CT scans demonstrate a well-marginated mass of fat attenuation, delineating clearly the bony excrescences and the adjacent bony cortex (Figs. 12.29 and 12.30). On MR images the SI of this lipoma is identical to that of subcutaneous fat on all pulse sequences, and the mineralized portion remains of decreased signal on T1- and T2-weighted images. The fatty mass may present various septa as seen in other adipocytic tumors, which appear as low SI on T1-weighted MR images, and may become higher in intensity on long TR images. Large areas of ossification may show marrow components, and some cases have been described with hyaline cartilage or small foci of fibrocartilage and endochondral ossification extending into the soft tissue mass, with an osteochondromatous appearance. However, the lack of medullary continuity of the osseous projections, as well as the fatty content of lipoma, argues against the diagnosis of an osteochondroma [33]. Associated muscle atrophy may be seen and is believed to correspond to nerve impingement.

Fig. 12.28 (**a**–**c**) Lipoma arborescens of the knee in a 30-year-old patient with bilateral knee pain and known rheumatoid arthritis. (**a**) Plain film. (**b**) Axial SE T1-weighted MR image. (**c**) Axial fat-suppressed SE T2-weighted MR image. On plain film there is definite degenerative change (**a**). On MRI there are multiple nodular and frond-like areas (*arrows*) of fat SI on T1-weighted and fat-suppressed SE T2-weighted images arising from the joint capsule (**b**, **c**). Appearances were identical in the opposite knee

12.3 Intermediate (Locally Aggressive) Adipocytic Tumors

12.3.1 Well-Differentiated Liposarcoma

Well-differentiated liposarcoma grossly resembles lipoma and consists of variably sized fat cells but has also scattered lipoblasts, broad fibrous septa, and thick-walled blood vessels. This type of liposarcoma accounts for 50 % of all liposarcomas (including intermediate and malignant adipocytic tumors) [45]. Histologically, there are three major subtypes of well-differentiated liposarcoma: (1) "lipoma-like," (2) inflammatory, and (3) sclerosing [31]. Another variant is the spindle cell liposarcoma, arising in the subcutaneous tissue, mostly around the shoulder girdle or upper limbs. All described cases occurred in adults [18].

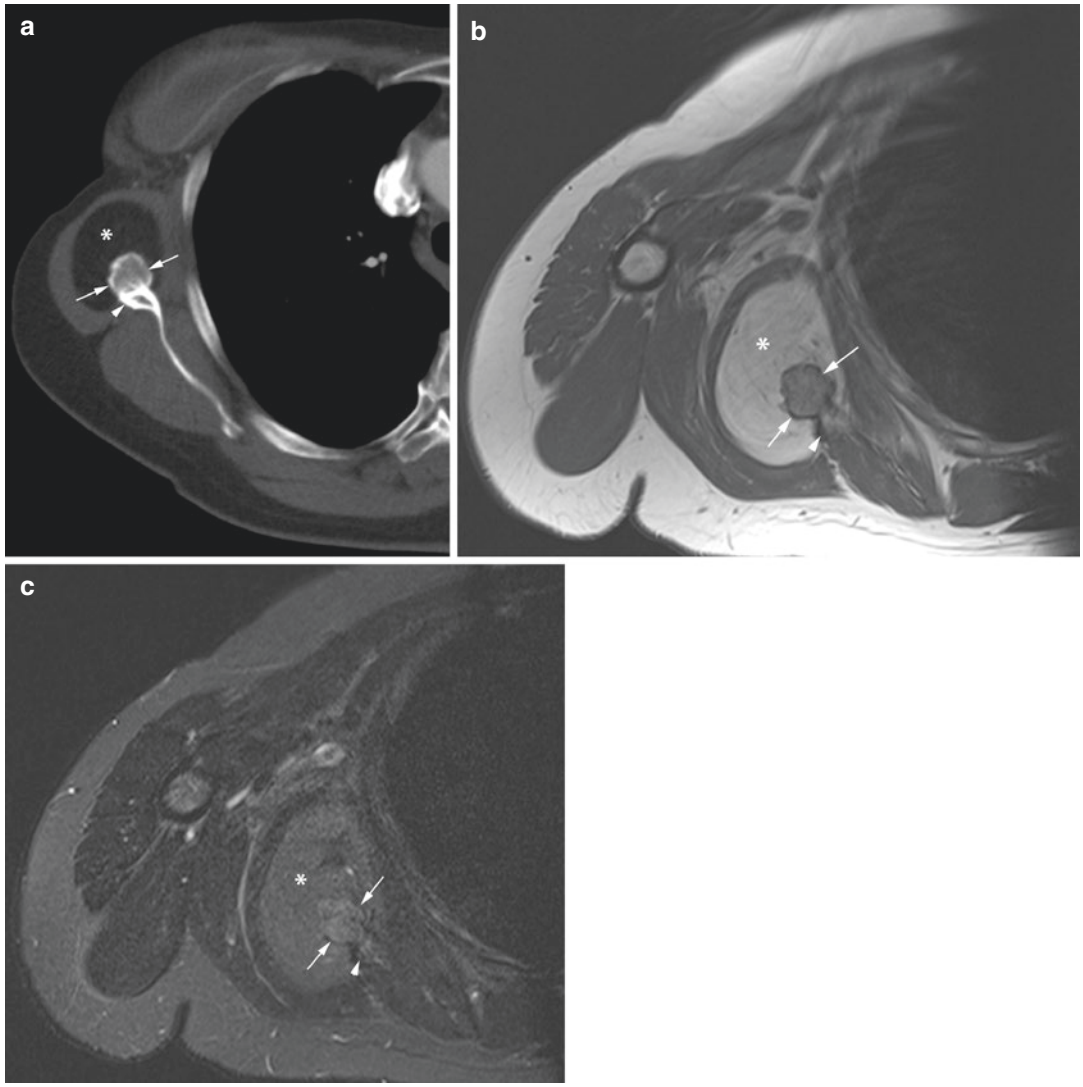

Fig. 12.29 (**a**–**c**) Parosteal lipoma of the right scapula in a 28-year-old woman. (**a**) CT of chest. (**b**) Axial SE T1-weighted MR image. (**c**) Axial fat-suppressed SE T2-weighted MR image. CT and MR images show a large fat signal soft tissue mass (*) around an exostotic-like lesion (*arrows*) at the anterior inferior border of the right glenoid (*arrowhead*) (**a**–**c**). There is no continuity between the medullary bone of the glenoid and the exostosis

The lipoma-like subtype is the most common and it simulates lipoma. The terms "well-differentiated liposarcoma" and "atypical lipoma" have been used interchangeably, but "atypical lipoma" should be reserved to designate the subcutaneous form of well-differentiated liposarcoma, especially of small size [32, 68]. Well-differentiated liposarcomas tend to be more frequent in the lower extremities, in the retroperitoneum, and in the trunk [45]. Cytogenetic analysis, namely, MDM2 presence, is now often used to distinguish lipoma from well-differentiated liposarcoma in cases where histological differentiation is difficult [63].

Liposarcomas are rare in the subcutaneous fat, occurring in deep structures, the majority of them being located in the extremities, particularly in the thigh. The retroperitoneum is the second most common site (15–20 %), where liposarcoma may attain a larger size, owing to

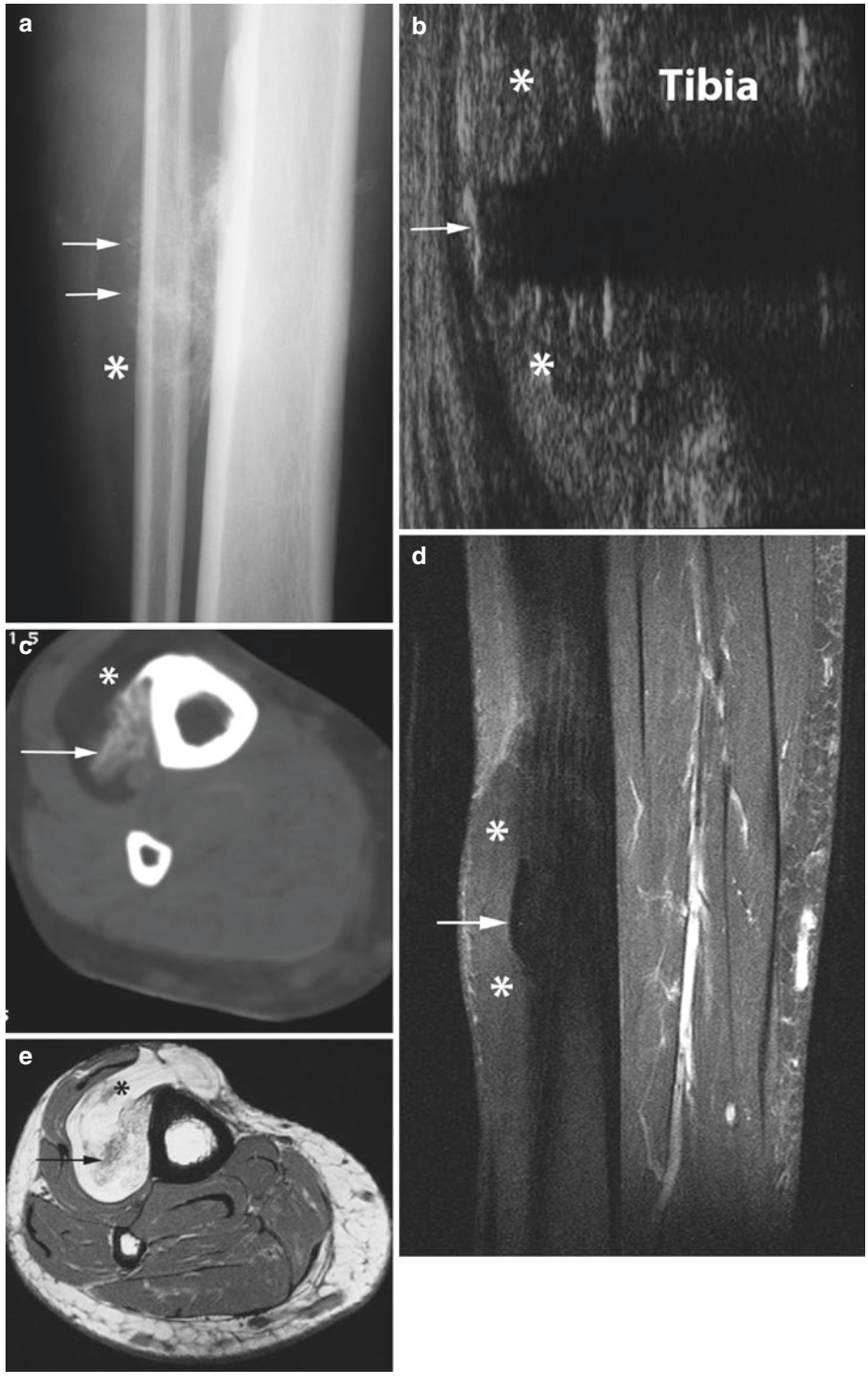

Fig. 12.30 (**a**–**e**) Parosteal lipoma of the right tibia. (**a**) Plain radiograph (**b**) Ultrasound of the leg. (**c**) CT of leg. (**d**) Sagittal fat-suppressed SE T2-weighted MR image. (**e**) Axial SE T1-weighted MR image. All images show a fat signal soft tissue mass (*) around an exostotic-like lesion (*arrows*) at the anterolateral border of the right tibia (**a**–**e**). There is no continuity between the medullary bone of the tibia and the exostosis

its later presentation and detection [32]. The well-differentiated liposarcoma, as a low-grade malignancy, is in general only locally aggressive, with recurrence if only marginally excised. There is no tendency to metastasize, but it may undergo dedifferentiation to a more aggressive liposarcoma [24, 37]. Retroperitoneal, well-differentiated liposarcomas tend to have a higher recurrence rate than those located in the extremities, probably due to their incomplete excision [32].

Well-differentiated liposarcomas have US, CT, or MRI findings that closely resemble those of subcutaneous fat or a simple lipoma. Although the amount of radiologically identifiable fat is variable, a well-differentiated liposarcoma will generally demonstrate at least 75 % adipose tissue, although very occasionally this will be as little as 25 % of the lesion volume [68]. The presence of soft tissue calcification is variable, occurring predominantly in the well-differentiated liposarcomas rather than other liposarcoma types [39].

On CT, a well-differentiated liposarcoma may appear as a well-marginated mass, with attenuation values equal to those of simple fat, mimicking a benign adipocytic tumor. However, this type usually has some thickened (more than 2 mm wide) linear or nodular soft tissue septa, which enhance after intravenous administration of contrast material [39]. On MR images there may be small nonadipocytic components of low SI on T1-weighted images or increased SI on T2-weighted images [3, 39, 48] (Figs. 12.31, 12.32, 12.33, and 12.34). The internal septa display more marked enhancement compared with those in lipoma and tend to have irregular width [38] (Fig. 12.30). Although earlier reports state that internal septa enhance only in liposarcoma, while no septal enhancement is seen in lipoma, this has been denied by Hosono, using fat-suppressed T1-weighted sequences after gadolinium administration, and reflects the authors' own experience on MRI and Doppler ultrasound [38, 50]. However, more prominent enhancement is seen in the malignant form and is probably due to the presence of malignant cellularity and inflammatory cell infiltration. Other MR imaging features suggestive of liposarcoma are non-adipose nodular areas, but there is still significant

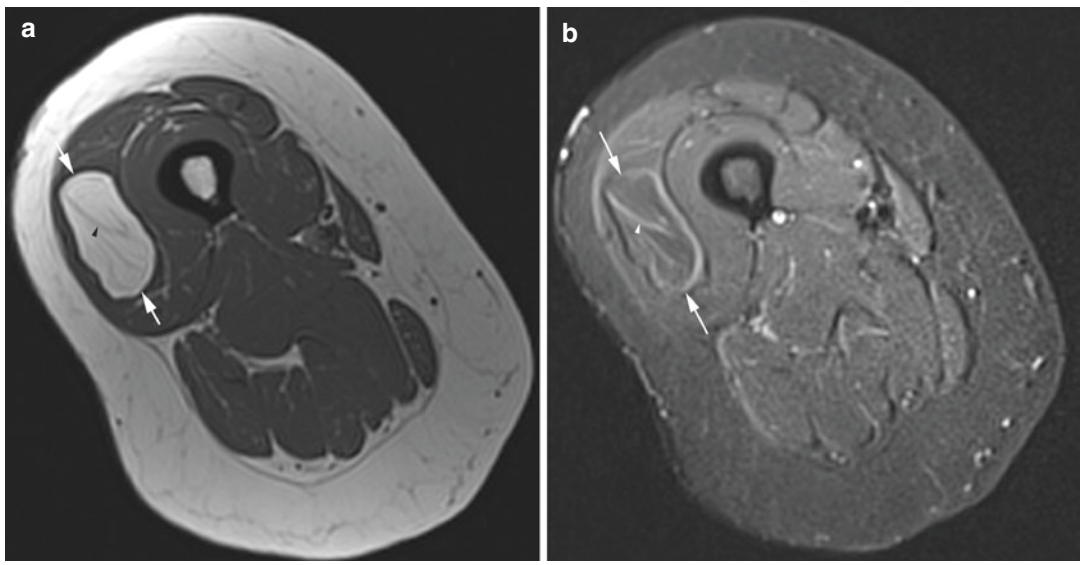

Fig. 12.31 (**a**, **b**) Well-differentiated liposarcoma of the right thigh. (**a**) Axial SE T1-weighted MR image. (**b**) Axial fat-suppressed SE T2-weighted MR image. Both images reveal a small mass (*arrows*) within the vastus lateralis muscle. The overall signal intensity equals that of subcutaneous fat, intratumoral strands (*arrowheads*) having low SI on T1- and high SI on T2-weighted images. Intratumoral strands of liposarcoma are more prominent in this case than in the lipoma shown in Fig. 12.1

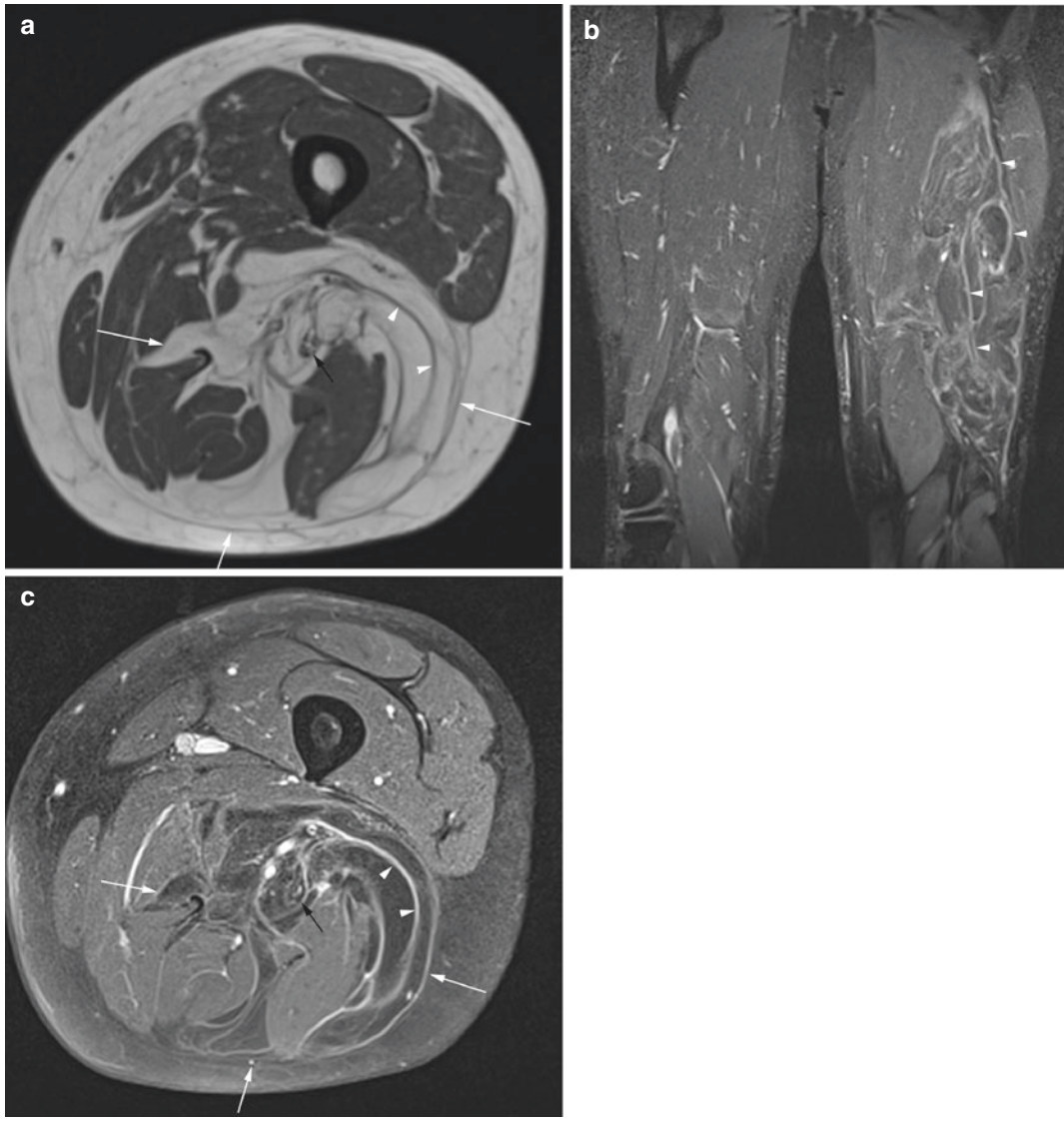

Fig. 12.32 (**a**, **b**) Well-differentiated liposarcoma of the left thigh. (**a**) Axial SE T1-weighted MR image. (**b**) Coronal fat-suppressed SE T2-weighted MR image. (**c**) Axial fat-suppressed SE T1-weighted MR image post gadolinium. Images reveal a large infiltrating mass (*white arrows*) enveloping the sciatic nerve (*black arrow*) within the posterior compartment of the thigh. The predominant signal intensity equals that of subcutaneous fat, but there are multiple thickened intratumoral strands (*arrowheads*) having low SI on T1- and high SI on T2-weighted images (**a**, **b**) with marked enhancement after contrast (**c**)

imaging overlap with some large lipomas showing these features [9, 13, 29, 68]. Other non-adipose areas within lipomas can cause overdiagnosis of liposarcoma such as fat necrosis or pressure edema in superficial lipomas [71] (see Sect. 12.4 later).

On ultrasound color Doppler examination of the internal septa shows increased vascularity [16, 50]. Of all liposarcomas, the well-differentiated type is distinguished from the other liposarcoma variants, due to its predominantly fatty composition [39].

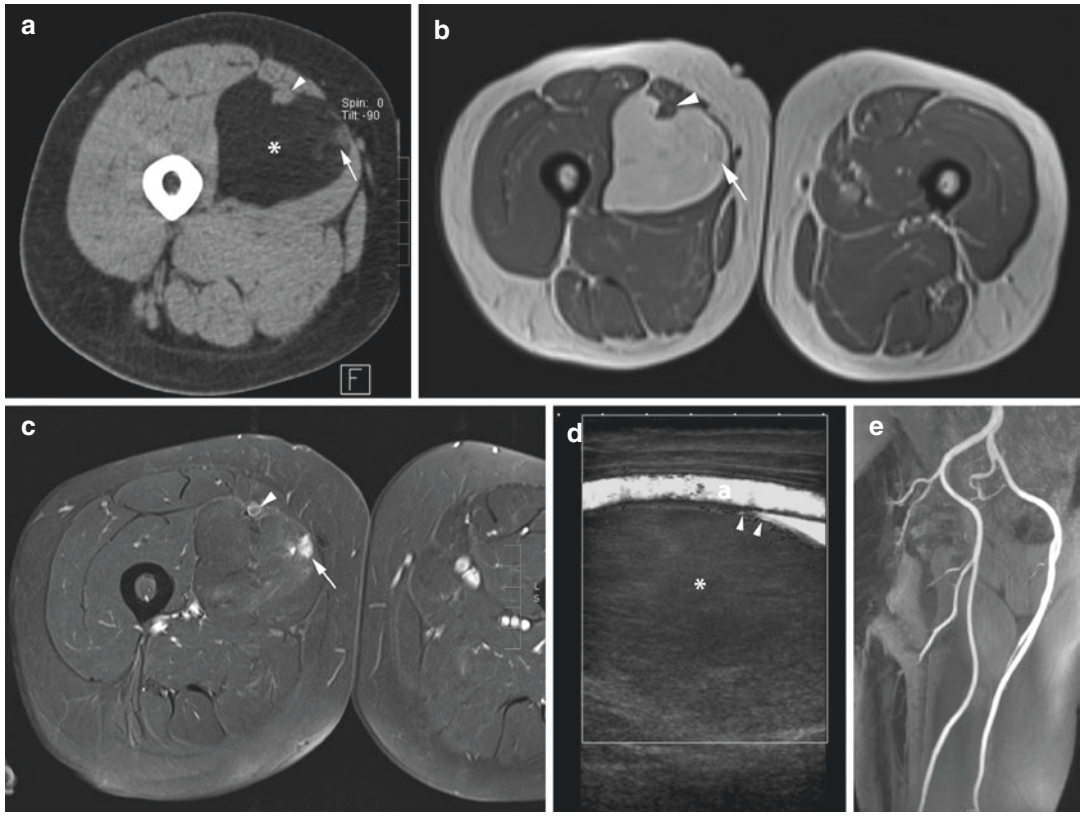

Fig. 12.33 (**a**–**e**) Well-differentiated liposarcoma, of the thigh. (**a**) CT image. (**b**) Axial SE T1-weighted MR image. (**c**) Axial fat-suppressed SE T2-weighted MR image. (**d**) Ultrasound with Doppler. (**e**) MR angiogram. CT, MR, and ultrasound images show a large fat signal soft tissue mass (*) in the anteromedial thigh with some minor loss of fat signal medially (*arrow*) compressing the femoral vein (*arrowheads*) (**a**–**d**). (**e**) MR angiography shows broad-based extrinsic compression of the superficial femoral artery, but there is no vessel stenosis

12.4 Malignant Adipocytic Tumors

Liposarcoma, excluding the well-differentiated form, is still one of the most common soft tissue sarcomas [32, 45]. The tumor originates from mesenchymal cells and differentiates to adipose tissue, the presence of mature fat cells being unnecessary for its development. Liposarcoma is currently classified into 4 histological types: dedifferentiated liposarcoma, myxoid liposarcoma, pleomorphic liposarcoma, and liposarcoma, not otherwise specified

Well-differentiated liposarcoma, sometimes termed atypical adipocytic tumor, is classified as intermediate (locally aggressive), while the other 4 malignant types are classified as malignant in the latest WHO classification [26]. Liposarcoma is preponderant in men (from 55 to 61 %), arising in the fifth and sixth decades of life and is extremely rare in infants and children, though some cases have been described [32, 49, 60]. The clinical behavior of liposarcoma varies according to the different histological types and is strongly influenced by its location. Liposarcoma usually manifests as a well-circumscribed, lobulated, and painless mass, which may be present for several months or years. The tumor may reach a very large size. Pain or functional disturbances are late complaints.

The pleomorphic and dedifferentiated types have a highly malignant behavior, with a strong tendency to recur and metastasize. Recurrence may occur after a long delay (5–10 years) following the

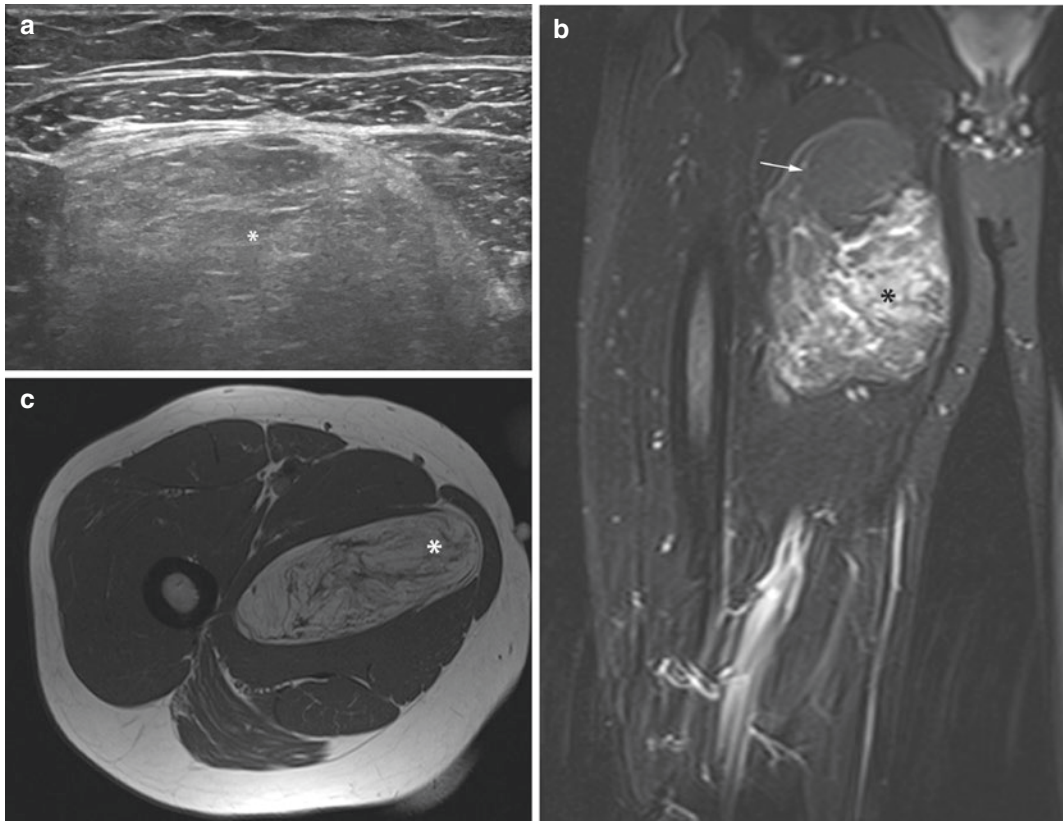

Fig. 12.34 (**a**–**c**) Well-differentiated liposarcoma of the right thigh. (**a**) Ultrasound. (**b**) Coronal fat-suppressed SE T2-weighted MR image. (**c**) Axial SE T1-weighted MR image. The mass lies in the medial compartment displacing gracilis. On ultrasound only the superficial aspect of the mass (*) deep to gracilis can be evaluated and appears homogenous (**a**). On MR images there is a large proximal area of fat SI (*arrow*) but extensive linear and more confluent areas (*) of low SI on T1-weighted images and high SI on fat-suppressed SE T2-weighted images (**b**, **c**)

initial excision [31]. Metastases are most commonly spread hematogenously, affecting predominantly the lungs and also the visceral organs and bone [32]. Myxoid liposarcoma, though of intermediate malignancy grade, may metastasize in 19–34 % of the patients, usually to extrapulmonary sites such as serosal surfaces of the pleura, pericardium, diaphragm, and soft tissues of pelvic or chest walls and retroperitoneum [32]. In a study of 95 cases of myxoid liposarcomas including some cases formerly classified as round cell liposarcomas, Kilpatrick et al. reported the development of metastases in 30 patients (35 %). Thirty-one percent of patients died from the disease [41]. They concluded that the presence of spontaneous necrosis, a percentage of more than 25 % of round cell differentiation, and age more than 45 years are significantly associated with a poor prognosis. Henricks et al., in a series of 155 dedifferentiated liposarcomas, have described a local recurrence rate of 41 %, a metastatic rate of 17 %, and a mortality of 28 % [37].

Multifocal liposarcoma, although rare, has been reported [32, 40]. A case of multicentric myxoid liposarcoma has been documented by Kemula et al. with three different sizes and location, without pulmonary, hepatic, or osseous metastases [40]. The authors agree with the hypothesis, still debated, that this represents a multicentric rather than metastatic spreading origin.

Because the histological subtype affects both prognosis and surgical planning, an accurate preoperative assessment is essential. The

radiological features of a liposarcoma depend on the histological type and tend to reflect its degree of differentiation. Although well-differentiated liposarcomas are frequently composed of more than 75 % of fat, the other types usually have less than 25 %. About 50 % of liposarcomas do not have any radiologically detectable fat [39]. This variable fat content accounts for the frequently nonspecific appearance of liposarcoma on US, CT, and MR images [21, 39, 74]. The presence of soft tissue calcification is variable, occurring predominantly in intermediate well-differentiated liposarcomas rather than the frankly malignant forms [39]. The angiographic pattern is nonspecific and cannot be used to distinguish benign from malignant tumors.

12.4.1 Dedifferentiated Liposarcoma

Dedifferentiated liposarcoma is formed by well-differentiated and poorly differentiated nonlipogenic areas. Dedifferentiation can occur into myxofibrosarcoma in more than two-thirds of cases and, occasionally, into fibrosarcoma, leiomyosarcoma, rhabdomyosarcoma, hemangiopericytoma, and even soft tissue osteosarcoma [37, 77]. Dedifferentiation occurs as a late complication (an average interval of 7.7 years) of a preexisting well-differentiated liposarcoma, most commonly of the retroperitoneum, mediastinum, or groin, but can also occur in the extremities and trunk [37, 77]. Dedifferentiation can take place either in the primary tumor as in local recurrences or even metastases, but according to Henricks et al., in a report of 155 cases, the majority of dedifferentiated liposarcoma presented as de novo lesions [37].

Dedifferentiated liposarcoma should be suspected if a nonadipocytic component appears in a previously known, well-differentiated liposarcoma. The tumor retains some of the features of the well-differentiated liposarcoma, while some mass-like areas develop a nonspecific appearance on US, CT, or MR images. These areas display tissue attenuation greater than fat on CT scans and low SI on T1-weighted images and high SI on T2-weighted images with marked enhancement after intravenous contrast administration (Figs. 12.35 and 12.36). Calcification or even ossification may be present [77].

The presence of nonfatty components within an adipocytic tumor should always suggest the possibility of a high-grade liposarcoma. However, it is not always possible to distinguish between the dedifferentiated type and other high-grade liposarcomas on the basis of imaging alone.

12.4.2 Myxoid Liposarcoma

Myxoid liposarcoma was previously considered the most common variant of liposarcoma, accounting for 39 % of all liposarcomas [32, 39, 45, 68]. Myxoid liposarcomas are well-differentiated tumors consisting of a plexiform vascular network and stellate and spindle-shaped mesenchymal cells within a basophilic myxoid matrix or ground substance [32]. Ground substance accounts for 90 % of the tumor [74]. Myxoid liposarcoma mostly presents as a painless, slowly growing mass at the lower extremities [39, 45, 68]. Other sites (in decreasing order of frequency) include the buttocks, retroperitoneum, trunk, ankle, proximal limb girdle, head and neck, and wrist. Myxoid liposarcomas occur in the intermuscular fascial planes or deep-seated areas and are rarely found in the subcutaneous tissue. Myxoid liposarcomas may be multicentric, with involvement of two or more anatomical sites. In 10 % of patients with primary liposarcoma of the thigh, a second liposarcoma occurs in the retroperitoneum 2 or more years after the removal of the primary tumor [32, 49, 76]. Most patients are aged 18–67 years, with a mean age of 42 years [32]. Of the different subtypes of liposarcoma, they have been shown to be particularly sensitive to radiotherapy [69].

Very frequently there is no radiological evidence of fat, owing to the small amount of mature fat in this subtype, which usually represents less than 10 % of its total volume [39, 74]. Therefore, it may be difficult to establish the correct diagnosis with CT and MRI due to the lack of fat density or intensity.

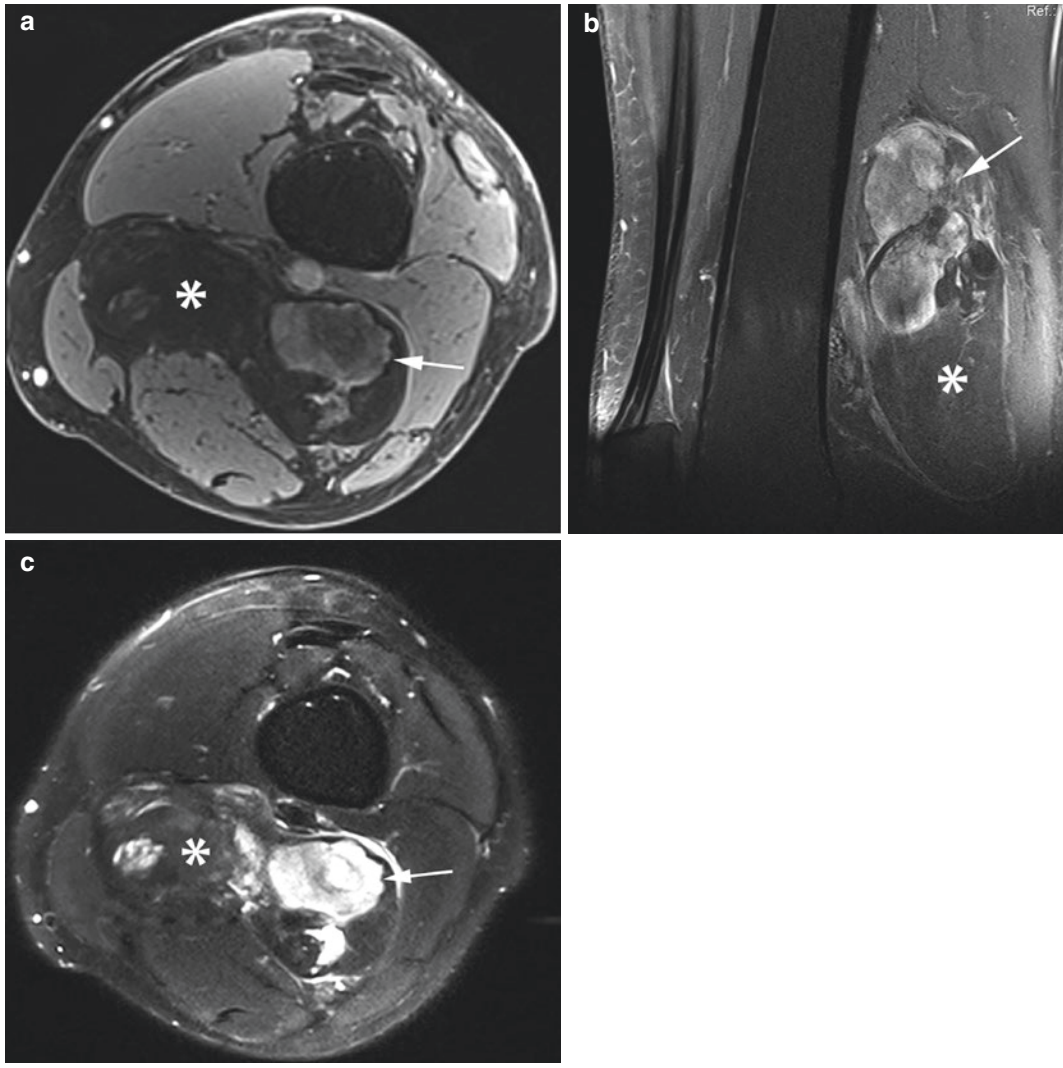

Fig. 12.35 (**a**–**c**) Dedifferentiated liposarcoma of the left thigh. (**a**) Axial. (**b**) Sagittal fat-suppressed SE T2-weighted images. (**c**) Axial fat-suppressed SE T1-weighted after Gd-contrast injection MR image. Parts of the mass show fat SI (*) (**a**–**c**), but a large irregular nodular component (*arrow*) shows high SI on T2-weighted images (**a**, **b**) and strong enhancement after contrast administration (**c**). This appearance is very suggestive of a dedifferentiated liposarcoma, with a nonfatty component within well-differentiated portion of liposarcoma

On CT scans, myxoid liposarcoma manifests as a homogeneous or slightly heterogeneous mass that is less attenuating than the surrounding muscle. On ultrasound the masses show a solid, heterogeneous nodular appearance with increased vascularity on Doppler signal. On MR images, a spectrum of MR imaging features occurs owing to several factors (Figs. 12.37 and 12.38). One factor is the fat content of the tumor. Other factors include the amount of myxoid material, the degree of cellularity and avascularity, and necrosis in the tumor. Most myxoid liposarcomas demonstrate lacy or linear, amorphous hyperintense foci within a predominantly hypointense mass on T1-weighted images. These linear foci behave like normal fat on all pulse sequences [74]. These foci are attributed to the presence of minute quantities of detectable fat within the tumor [39, 73, 74]. On T2-weighted images, a high SI is seen, with foci of intermediate SI corresponding

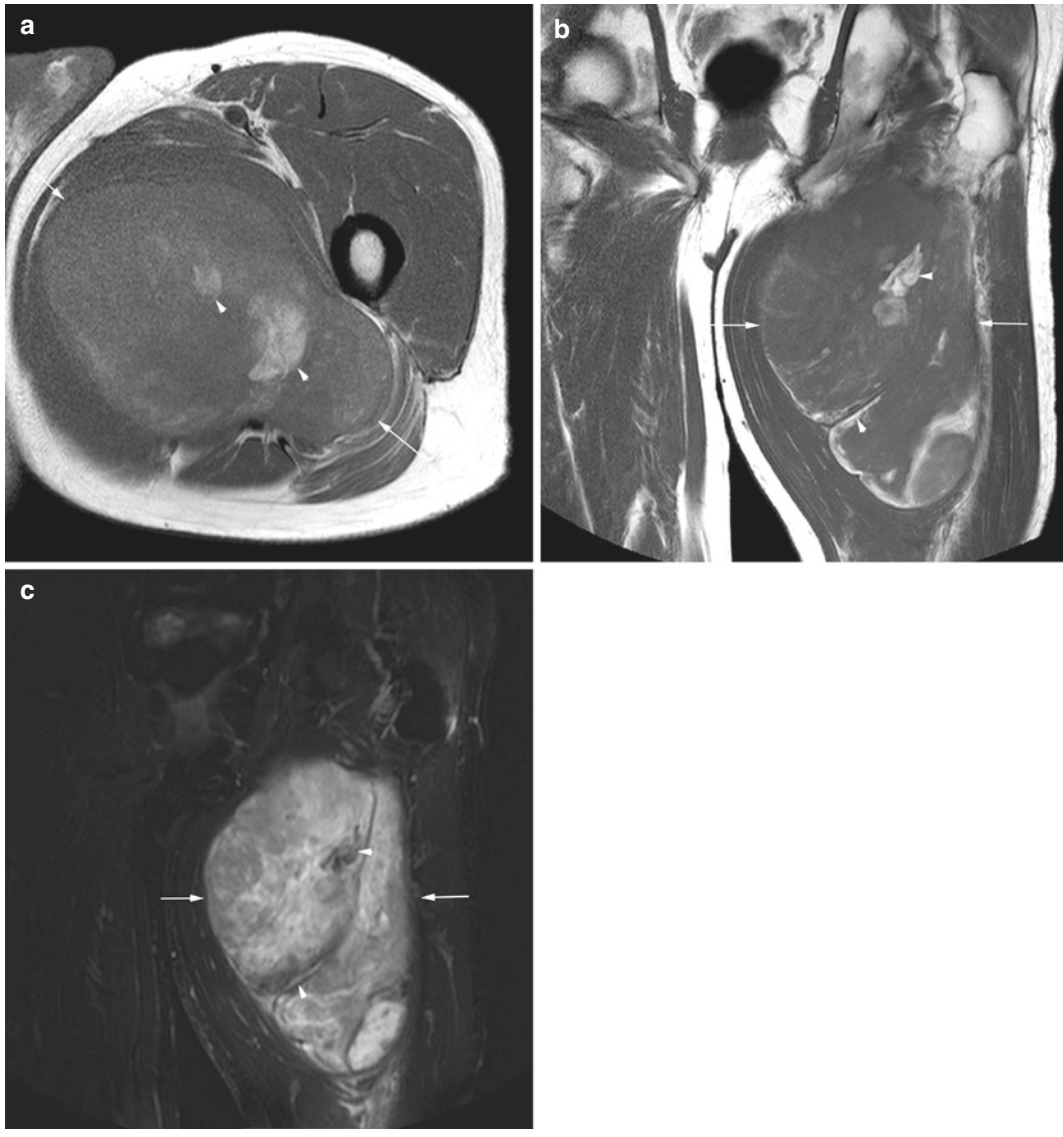

Fig. 12.36 (**a**–**c**) Dedifferentiated liposarcoma of the left thigh. (**a**) Axial. (**b**) Coronal SE T1-weighted MR images. (**c**) Coronal fat-suppressed SE T2-weighted MR image. All images show a large heterogeneous mass (*arrows*) occupying the posterior and medial compartments. Small areas of the mass show fat SI (*arrowheads*) (**a**–**c**)

to fat. Tumors with increased cellularity and vascularity tend to enhance on contrast-enhanced images, whereas tumor areas with necrosis, hypocellularity, and an accumulation of mucinous material tend not to enhance [3, 39, 74, 76]. A recent series reviewing 30 cases suggested that components that are not fat or myxoid/mucinous signal and enhance on MRI are suggestive of higher-grade sarcomatous change [54].

At morphological analysis, the mass is well defined. The lesion is frequently lobulated and may be multilobulated and septated or oval. Edema may be present in the soft tissue surrounding the tumor. There is no evidence of infiltration or invasion into adjacent structures. The lobulated pattern with internal linear septa is best visualized on T2-weighted MR images (Figs. 12.37 and 12.38).

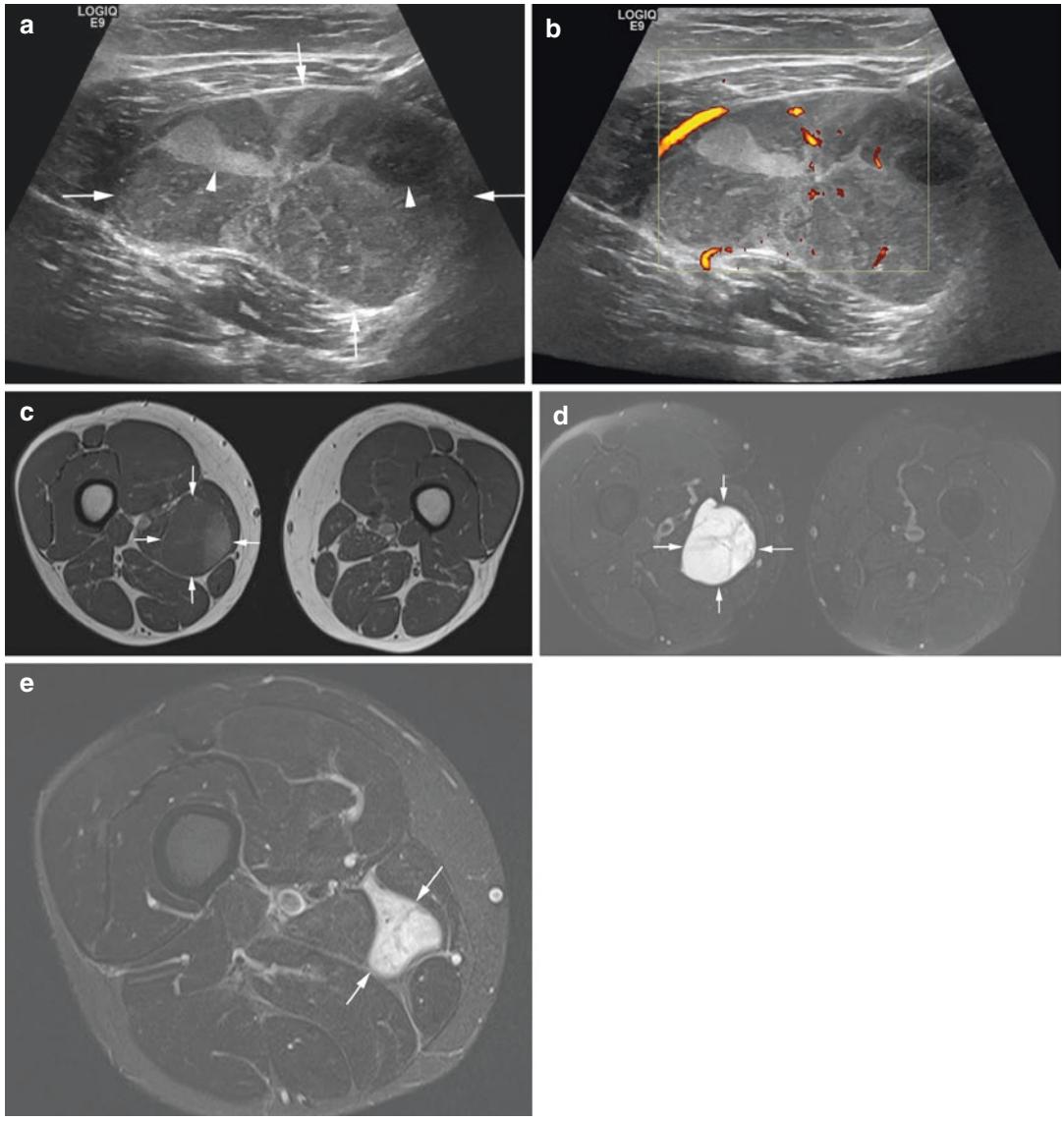

Fig. 12.37 (**a**–**e**) Myxoid liposarcoma of the right thigh. (**a**) Ultrasound. (**b**) Ultrasound with Doppler. (**c**) Coronal fat-suppressed SE T2-weighted MR image. (**c**) Axial SE T1-weighted MR image. (**d**) Axial FS TSE T2-weighted MR image. (**e**) Axial FS TSE T2-weighted MR image. The mass lies in the medial compartment displacing gracilis and the neurovascular bundle. On ultrasound the mass (*arrows*) is nodular and heterogeneous (*arrowheads*) with irregular Doppler signal (**a**, **b**). On MR images there is a lacey area of indistinct increased SI on T1-weighted images and diffuse high SI on fat-suppressed SE T2-weighted images with linear low signal (**c**, **d**). After radiotherapy the mass (*arrows*) shows a marked decrease in size (**e**)

While the mass appears solid on ultrasound, care is required as on CT and non-contrast MR images, a myxoid liposarcoma may occasionally resemble a cyst, due to the lack of fat content, with sharply demarcated margins. On CT scans, it displays attenuation values within the water range. A marked low signal on T1-weighted MR images and a high signal on T2-weighted MR images, due to the predominant myxoid matrix of this tumor, is noted [39] (Figs. 12.37 and 12.38). The homogeneous or heterogeneous enhancement seen after gadolinium contrast facilitates

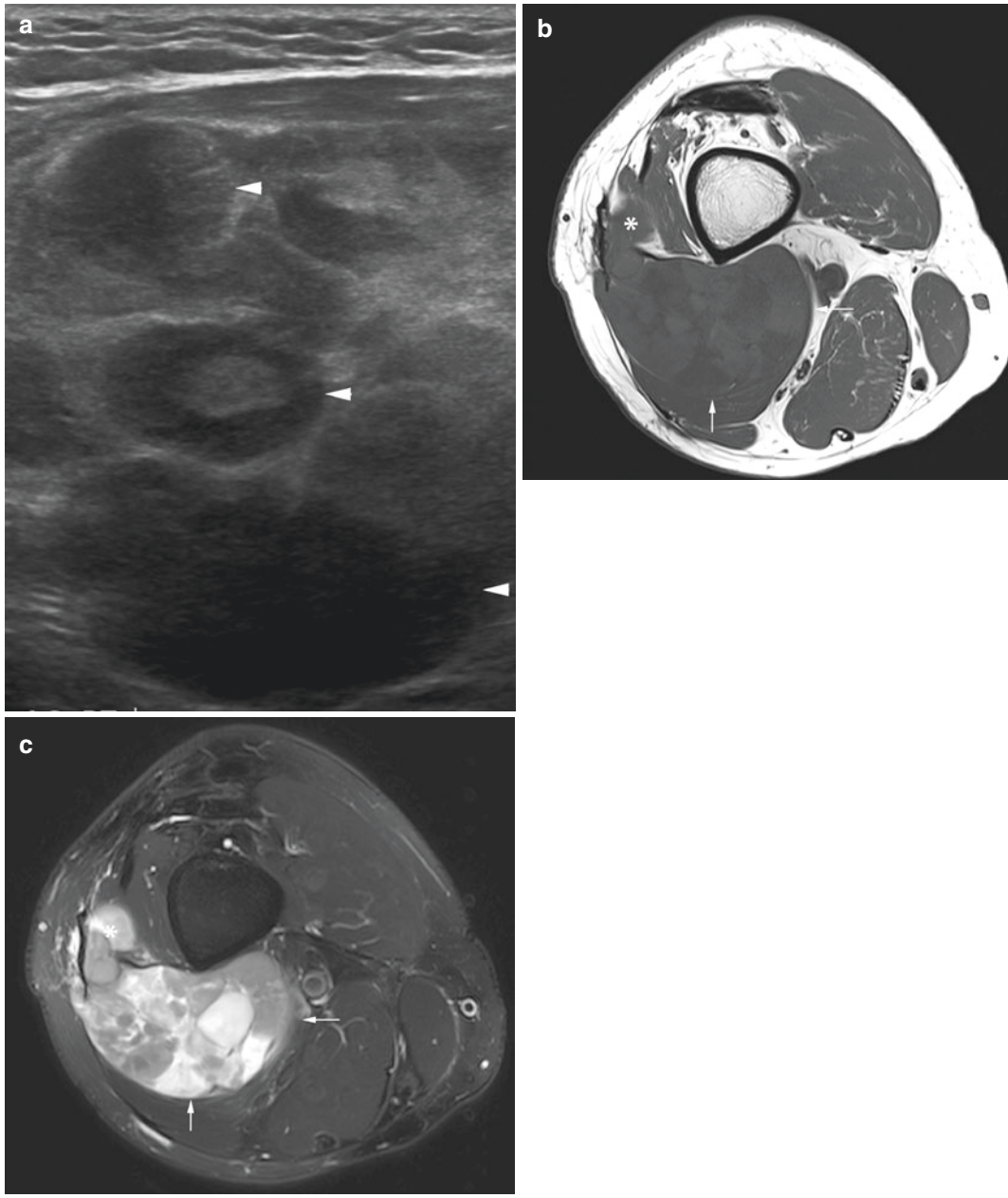

Fig. 12.38 (**a**–**c**) Myxoid liposarcoma of the right thigh. (**a**) Ultrasound. (**b**) Axial SE T1-weighted MR image. (**c**) Axial fat-suppressed SE T2-weighted MR image. The mass lies predominantly in the posterior compartment (*arrow*) but is infiltrating into the anterior compartment and fascia (*). On ultrasound the mass is nodular (*arrowheads*) with heterogeneous signal (**a**). On MR images the mass (*arrows*) is heterogeneous and low SI on T1-weighted images and diffuse high SI on fat-suppressed SE T2-weighted with no definite fat signal (**b**, **c**)

distinction between myxoid liposarcomas and nonenhancing cystic lesions [76].

Ultrasound is another useful tool in differentiating solid masses from cystic lesions. Myxoid liposarcomas appear complex, nodular, hypoechoic masses that do not meet the criteria for a simple cyst at ultrasound (Figs. 12.35 and 12.36) [50, 76]

The lesion that is perhaps the most problematic for radiologists to differentiate from the cyst-like form of myxoid liposarcoma is

intramuscular myxoma. Although there is an overlap, intramuscular myxoma is far more likely when there is a rind of perilesional fat (rather than intralesional fat); a globular, heterogeneous peripheral, and central enhancement pattern; and increased signal in the adjacent muscle on T2-weighted/fluid-sensitive sequences [32, 68].

12.4.3 Pleomorphic Liposarcomas

The pleomorphic variant shows a marked degree of cellular pleomorphism and may contain huge lipoblastic multinucleated cells [32]. However, pleomorphic liposarcomas do not consistently show MDM2 amplification suggesting that the tumor may develop from more than one tumor line with those MDM2 positive presumably related to liposarcomas and those without MDM2 developing from another tumor cell line [63]. This variant is highly aggressive and likely to metastasize [28, 63]. In one series of 155 patients with pleomorphic liposarcoma, the mean age was 57 years with 40 % occurring in the lower limb and the mean tumor size 11 cm [30].

Most pleomorphic liposarcomas present as nonspecific, heterogeneous masses with relatively well-circumscribed margins. They often do not contain a sufficient amount of fat and therefore exhibit a low SI on T1-weighted images and increased SI on T2-weighted images, as do the majority of other malignant soft tissue tumors [3, 39]. There is a marked and heterogeneous enhancement after intravenous contrast administration [3]. Radiologically, this type is not distinguishable from other aggressive sarcomas, because it contains little or no fat.

12.4.4 Liposarcoma, Not Otherwise Specified

This variant cannot be reliably differentiated clinically or radiologically from the other malignant adipocytic tumors with the diagnosis only made at histology or even molecular analysis [63, 64].

12.5 Differential Diagnosis of Lipomatous Tumors

Because of differences in treatment, prognosis, and long-term follow-up, it is important to preoperatively distinguish simple lipomas from well-differentiated liposarcomas. In the absence of radiologically identifiable fat, imaging is nonspecific. However, useful differentiating features between lipoma and well-differentiating liposarcoma are summarized in Table 12.1 [16, 29, 42, 46, 65]. Generally, an adipocytic lesion containing internal septa of more than 2 mm thickness or nonfatty nodular areas without the typical SI of muscle fibers on all pulse sequences should be considered as a liposarcoma till proven otherwise. By using these criteria, MRI is highly sensitive in the detection of well-differentiated liposarcomas and highly specific in the diagnosis of simple lipomas. However, when an extremity or body wall lesion is considered suggestive of well-differentiated liposarcoma, it is more likely (64 %) to represent one of many benign lipoma variants, containing nonfatty elements [29, 58, 68, 71].

12.5.1 Other Lesions Containing Fat or Mimicking Its Presence

There are several conditions that may mimic adipocytic tumors of the soft tissues, such as fat necrosis, hemangioma, elastofibroma, myxoid, or neural tumors [8, 48, 71]

Hemangiomas may contain a variable amount of adipose tissue interspersed between the abnormal vessels. However, its frequently typical appearance on MR images, owing to the presence of the high SI of slow-flowing blood within serpentine or tubular structures, allows the correct diagnosis to be made.

Elastofibroma dorsi, a benign fibrous tissue tumor with fatty elements, usually manifests as a periscapular mass with an intermediate SI and interlaced areas of high SI similar to fat on both T1- and T2-weighted MR images. This lesion will be further discussed in Chap. 22.

Some myxoid and neural tumors may mimic adipocytic tumors owing to their reduced tissue

attenuation on CT scans. MRI findings may be utilized as an adjunct to the cytological features to more confidently differentiate intramuscular myxoma [6], myxoid schwannoma, neurofibroma, and ganglion cyst, as well as malignant neoplasms such as myxoid liposarcoma and fibrosarcoma.

Conclusions

Because lipoma and atypical lipoma demonstrate identical tumor components and because liposarcomas are heterogeneous, incisional biopsy or incomplete resection may result in substantial sampling error, with important clinical and therapeutic consequences [39]. Imaging on the other hand is capable of evaluating the whole tumoral mass, including all its components. Consequently, imaging plays a significant role in the evaluation of adipocytic soft tissue tumors. In this regard, MRI is superior to other imaging modalities, since it easily demonstrates even minute fatty tumor components and is able to stage soft tissue tumors accurately.

One has to keep in mind that some nonadipocytic tumors may contain fatty components. Fortunately, these tumors have sufficient other characteristics, which permit a more than confident diagnosis by medical imaging. Imaging-guided biopsy should be performed in a mass lesion without MRI characteristics of a benign adipocytic soft tissue tumor always sampling the nonadipocytic component and with a separate sample sent for cytogenetic and molecular analysis if this service is available.

Key Points

1. The diagnosis of a simple lipoma is usually straightforward on MR images. The use of fat suppression is an important imaging tool in lesion characterization.
2. Lipomas containing other mesenchymal elements than fatty tissue (such as chondroid lipoma, myolipoma, and angiolipoma) are difficult to distinguish from well-differentiated liposarcomas on MR images.
3. Benign intramuscular lipomas may show infiltrative margins.
4. Demonstration of a fatty mass in patients below 3 years of age should raise the possibility of a lipoblastoma.
5. Lipomatosis of nerve is frequently associated with soft tissue and osseous hypertrophy.
6. The most important imaging parameters for differential diagnosis between a benign adipocytic tumors and a liposarcoma consist of location (superficial versus deep), size, internal composition (presence of thick nonadipocytic septa or nodules), contrast-enhancement pattern, and shape of the lesion (uni- versus multinodular). However, nonadipocytic nodules are the most specific imaging finding.

References

1. Ahuja AT, King AD, Kew J, King W, Metreweli C (1998) Head and neck lipomas: sonographic appearance. AJNR Am J Neuroradiol 19(3):505–508
2. Alvine G, Rosenthal H, Murphey M, Huntrakoon M (1996) Hibernoma. Skeletal Radiol 25(5):493–496
3. Arkun R, Memis A, Akalin T, Ustun EE, Sabah D, Kandiloglu G (1997) Liposarcoma of soft tissue: MRI findings with pathologic correlation. Skeletal Radiol 26(3):167–172
4. Atilla S, Eilenberg SS, Brown JJ (1995) Hibernoma: MRI appearance of a rare tumor. Magn Reson Imaging 13(2):335–337
5. Austin RM, Mack GR, Townsend CM, Lack EE (1980) Infiltrating (intramuscular) lipomas and angiolipomas. A clinicopathologic study of six cases. Arch Surg 115(3):281–284
6. Bancroft LW, Kransdorf MJ, Menke DM, O'Connor MI, Foster WC (2002) Intramuscular myxoma: characteristic MR imaging features. AJR Am J Roentgenol 178(5):1255–1259. doi:10.2214/ajr.178.5.1781255
7. Bang M, Kang BS, Hwang JC, Weon YC, Choi SH, Shin SH, Kwon WJ, Hwang CM, Lee SY (2012) Ultrasonographic analysis of subcutaneous angiolipoma. Skeletal Radiol 41(9):1055–1059. doi:10.1007/s00256-011-1309-x
8. Battaglia M, Vanel D, Pollastri P, Balladelli A, Alberghini M, Staals EL, Monti C, Galletti S (2009)

Imaging patterns in elastofibroma dorsi. Eur J Radiol 72(1):16–21. doi:10.1016/j.ejrad.2009.05.024
9. Bidault F, Vanel D, Terrier P, Jalaguier A, Bonvalot S, Pedeutour F, Couturier JM, Dromain C (2009) Liposarcoma or lipoma: does genetics change classic imaging criteria? Eur J Radiol 72(1):22–26. doi:10.1016/j.ejrad.2009.05.025
10. Blum A, Henrot P, Sirveaux F et al (2004) Diagnostic des lipomes des parties molles et des liposarcomes cheze l'adulte. In: Laredo J, Wybier M, Railhac J, Tomeno B, Malghem J (eds) Conduite a tenir devant une image osseuse ou des parties molles d'allure tumorale. Sauramps medical, Montpellier
11. Boets A, Van Mieghem IM, Sciot R, Van Breuseghem I (2004) Chondroid lipoma of the trunk: MRI appearance and pathologic correlation. Skeletal Radiol 33(11):666–669. doi:10.1007/s00256-004-0774-x
12. Boren WL, Henry RE Jr, Wintch K (1995) MR diagnosis of fibrolipomatous hamartoma of nerve: association with nerve territory-oriented macrodactyly (macrodystrophia lipomatosa). Skeletal Radiol 24(4):296–297
13. Brisson M, Kashima T, Delaney D, Tirabosco R, Clarke A, Cro S, Flanagan AM, O'Donnell P (2013) MRI characteristics of lipoma and atypical lipomatous tumor/well-differentiated liposarcoma: retrospective comparison with histology and MDM2 gene amplification. Skeletal Radiol 42(5):635–647. doi:10.1007/s00256-012-1517-z
14. Chitoku S, Kawai S, Watabe Y, Nishitani M, Fujimoto K, Otsuka H, Fushimi H, Kotoh K, Fuji T (1998) Intradural spinal hibernoma: case report. Surg Neurol 49(5):509–512; discussion 512–503
15. Collins MH, Chatten J (1997) Lipoblastoma/lipoblastomatosis: a clinicopathologic study of 25 tumors. Am J Surg Pathol 21(10):1131–1137
16. Cotten A (2002) Imaging of lipoma and liposarcoma. JBR BTR 85(1):14–19
17. De Maeseneer M, Jaovisidha S, Lenchik L, Witte D, Schweitzer ME, Sartoris DJ, Resnick D (1997) Fibrolipomatous hamartoma: MR imaging findings. Skeletal Radiol 26(3):155–160
18. Dei Tos AP, Mentzel T, Newman PL, Fletcher CD (1994) Spindle cell liposarcoma, a hitherto unrecognized variant of liposarcoma. Analysis of six cases. Am J Surg Pathol 18(9):913–921
19. Donati L, Candiani P, Grappolini S, Klinger M, Signorini M (1990) Congenital infiltrating lipomatosis of the face related to cytomegalovirus infection. Br J Plast Surg 43(1):124–126
20. Drevelegas A, Pilavaki M, Chourmouzi D (2004) Lipomatous tumors of soft tissue: MR appearance with histological correlation. Eur J Radiol 50(3):257–267. doi:10.1016/j.ejrad.2004.01.022
21. Einarsdottir H, Soderlund V, Larson O, Jenner G, Bauer HC (1999) MR imaging of lipoma and liposarcoma. Acta Radiol 40(1):64–68
22. Enzi G, Carraro R, Alfieri P, Busetto L, Digito M, Pavan M, Negrin P (1992) Shoulder girdle lipomatosis. Ann Intern Med 117(9):749–750
23. Evans HA, Donnelly LF, Johnson ND, Blebea JS, Stern PJ (1997) Fibrolipoma of the median nerve: MRI. Clin Radiol 52(4):304–307
24. Evans HL (1979) Liposarcoma: a study of 55 cases with a reassessment of its classification. Am J Surg Pathol 3(6):507–523
25. Fanburg-Smith JC, Devaney KO, Miettinen M, Weiss SW (1998) Multiple spindle cell lipomas: a report of 7 familial and 11 nonfamilial cases. Am J Surg Pathol 22(1):40–48
26. Fletcher CD, Bridge J, Hogendoom P, Mertens F (2013) World health organisation classification of tumours of soft tissue and bone, 4th edn. IARC Press, Lyon
27. Fuchs A, Henrot P, Walter F, Iochum S, Vignaud J, Stines J, Blum A (2002) Lipomatous tumors of soft tissues in the extremities and the waist in adults. J Radiol 83(9 Pt 1):1035–1057
28. Gardner JM, Dandekar M, Thomas D, Goldblum JR, Weiss SW, Billings SD, Lucas DR, McHugh JB, Patel RM (2012) Cutaneous and subcutaneous pleomorphic liposarcoma: a clinicopathologic study of 29 cases with evaluation of MDM2 gene amplification in 26. Am J Surg Pathol 36(7):1047–1051. doi:10.1097/PAS.0b013e3182517b96
29. Gaskin CM, Helms CA (2004) Lipomas, lipoma variants, and well-differentiated liposarcomas (atypical lipomas): results of MRI evaluations of 126 consecutive fatty masses. AJR Am J Roentgenol 182(3):733–739. doi:10.2214/ajr.182.3.1820733
30. Ghadimi MP, Liu P, Peng T, Bolshakov S, Young ED, Torres KE, Colombo C, Hoffman A, Broccoli D, Hornick JL, Lazar AJ, Pisters P, Pollock RE, Lev D (2011) Pleomorphic liposarcoma: clinical observations and molecular variables. Cancer 117(23):5359–5369. doi:10.1002/cncr.26195
31. Goldblum JR, Weiss SW, Folpe AL (2014) Benign lipomatous tumors. In: Goldblum JR, Weiss SW, Folpe AL (eds) Enzinger and Weiss's soft tissue tumors, 6th edn. Elsevier, Philadelphia
32. Goldblum JR, Weiss SW, Folpe AL (2014) Liposarcoma. In: Goldblum JR, Weiss SW, Folpe AL (eds) Enzinger and Weiss's soft tissue tumors, 6th edn. Elsevier, Philadelphia
33. Goldman AB, DiCarlo EF, Marcove RC (1993) Case report 774. Coincidental parosteal lipoma with osseous excrescence and intramuscular lipoma. Skeletal Radiol 22(2):138–145
34. Green RA, Cannon SR, Flanagan AM (2004) Chondroid lipoma: correlation of imaging findings and histopathology of an unusual benign lesion. Skeletal Radiol 33(11):670–673. doi:10.1007/s00256-004-0818-2
35. Ha TV, Kleinman PK, Fraire A, Spevak MR, Nimkin K, Cohen IT, Hirsh M, Walton R (1994) MR imaging of benign fatty tumors in children: report of four cases and review of the literature. Skeletal Radiol 23(5):361–367
36. Heaton JM (1972) The distribution of brown adipose tissue in the human. J Anat 112(Pt 1):35–39

37. Henricks WH, Chu YC, Goldblum JR, Weiss SW (1997) Dedifferentiated liposarcoma: a clinicopathological analysis of 155 cases with a proposal for an expanded definition of dedifferentiation. Am J Surg Pathol 21(3):271–281
38. Hosono M, Kobayashi H, Fujimoto R, Kotoura Y, Tsuboyama T, Matsusue Y, Nakamura T, Itoh T, Konishi J (1997) Septum-like structures in lipoma and liposarcoma: MR imaging and pathologic correlation. Skeletal Radiol 26(3):150–154
39. Jelinek JS, Kransdorf MJ, Shmookler BM, Aboulafia AJ, Malawer MM (1993) Liposarcoma of the extremities: MR and CT findings in the histologic subtypes. Radiology 186(2):455–459. doi:10.1148/radiology.186.2.8421750
40. Kemula M, Clerc D, Quillard J, Desmoulins F, Marfeuille M, Bisson M (1999) Multicentric liposarcoma. Apropos of a case. Rev Med Interne 20(1):60–63
41. Kilpatrick SE, Doyon J, Choong PF, Sim FH, Nascimento AG (1996) The clinicopathologic spectrum of myxoid and round cell liposarcoma. A study of 95 cases. Cancer 77(8):1450–1458. doi:10.1002/(SICI)1097-0142(19960415)77:8<1450::AID-CNCR5>3.0.CO;2-G
42. Kim JY, Park JM, Lim GY, Chun KA, Park YH, Yoo JY (2002) Atypical benign lipomatous tumors in the soft tissue: radiographic and pathologic correlation. J Comput Assist Tomogr 26(6):1063–1068
43. Kirwadi A, Abdul-Halim R, Fernando M, Highland A, Kotnis N (2014) MR imaging features of spindle cell lipoma. Skeletal Radiol 43(2):191–196. doi:10.1007/s00256-013-1765-6
44. Kransdorf MJ (1995) Benign soft-tissue tumors in a large referral population: distribution of specific diagnoses by age, sex, and location. AJR Am J Roentgenol 164(2):395–402. doi:10.2214/ajr.164.2.7839977
45. Kransdorf MJ (1995) Malignant soft-tissue tumors in a large referral population: distribution of diagnoses by age, sex, and location. AJR Am J Roentgenol 164(1):129–134. doi:10.2214/ajr.164.1.7998525
46. Kransdorf MJ, Bancroft LW, Peterson JJ, Murphey MD, Foster WC, Temple HT (2002) Imaging of fatty tumors: distinction of lipoma and well-differentiated liposarcoma. Radiology 224(1):99–104. doi:10.1148/radiol.2241011113
47. Kransdorf MJ, Jelinek JS, Moser RP Jr (1993) Imaging of soft tissue tumors. Radiol Clin North Am 31(2):359–372
48. Kransdorf MJ, Moser RP Jr, Meis JM, Meyer CA (1991) Fat-containing soft-tissue masses of the extremities. Radiographics 11(1):81–106. doi:10.1148/radiographics.11.1.1996399
49. Kransdorf MJ, Murphey M (2013) Lipomatous tumors. In: Kransdorf MJ, Murphey M (eds) Imaging of soft tissue tumors. 3rd edn. Lippincott Williams and Wilkins. Philadelphia, PA, USA
50. Lakkaraju A, Sinha R, Garikipati R, Edward S, Robinson P (2009) Ultrasound for initial evaluation and triage of clinically suspicious soft-tissue masses. Clin Radiol 64(6):615–621. doi:10.1016/j.crad.2009.01.012
51. Lee JC, Gupta A, Saifuddin A, Flanagan A, Skinner JA, Briggs TW, Cannon SR (2006) Hibernoma: MRI features in eight consecutive cases. Clin Radiol 61(12):1029–1034. doi:10.1016/j.crad.2006.05.018
52. Lin YC, Huang CC, Chen HJ (2001) Intraspinal osteolipoma. Case report. J Neurosurg 94(1 Suppl):126–128
53. Logan PM, Janzen DL, O'Connell JX, Munk PL, Connell DG (1996) Chondroid lipoma: MRI appearances with clinical and histologic correlation. Skeletal Radiol 25(6):592–595
54. Lowenthal D, Zeile M, Niederhagen M, Fehlberg S, Schnapauff D, Pink D, Tunn PU, Reichardt P, Hamm B, Dudeck O (2014) Differentiation of myxoid liposarcoma by magnetic resonance imaging: a histopathologic correlation. Acta Radiol 55(8):952–960. doi:10.1177/0284185113508114
55. Marom EM, Helms CA (1999) Fibrolipomatous hamartoma: pathognomonic on MR imaging. Skeletal Radiol 28(5):260–264
56. Martin DS, Sharafuddin M, Boozan J, Sundaram M, Archer C (1995) Multiple symmetric lipomatosis (Madelung's disease). Skeletal Radiol 24(1):72–73
57. Matsumoto K, Hukuda S, Ishizawa M, Chano T, Okabe H (1999) MRI findings in intramuscular lipomas. Skeletal Radiol 28(3):145–152
58. Matsumoto K, Takada M, Okabe H, Ishizawa M (2000) Foci of signal intensities different from fat in well-differentiated liposarcoma and lipoma: correlation between MR and histological findings. Clin Imaging 24(1):38–43
59. McEachern A, Janzen DL, O'Connell JX (1995) Shoulder girdle lipomatosis. Skeletal Radiol 24(6):471–473
60. Miller GG, Yanchar NL, Magee JF, Blair GK (1998) Lipoblastoma and liposarcoma in children: an analysis of 9 cases and a review of the literature. Can J Surg 41(6):455–458
61. Murphey MD, Carroll JF, Flemming DJ, Pope TL, Gannon FH, Kransdorf MJ (2004) From the archives of the AFIP: benign musculoskeletal lipomatous lesions. Radiographics 24(5):1433–1466. doi:10.1148/rg.245045120
62. Nishida J, Shimamura T, Ehara S, Shiraishi H, Sato T, Abe M (1998) Posterior interosseous nerve palsy caused by parosteal lipoma of proximal radius. Skeletal Radiol 27(7):375–379
63. Nishio J (2011) Contributions of cytogenetics and molecular cytogenetics to the diagnosis of adipocytic tumors. J Biomed Biotechnol 2011:524067. doi:10.1155/2011/524067
64. Nishio J, Aoki M, Nabeshima K, Iwasaki H, Naito M (2012) Cytogenetic and molecular cytogenetic findings in giant dedifferentiated liposarcoma of the thigh. Oncol Rep 27(3):764–768. doi:10.3892/or.2011.1584
65. Ohguri T, Aoki T, Hisaoka M, Watanabe H, Nakamura K, Hashimoto H, Nakamura T, Nakata H (2003) Differential diagnosis of benign peripheral lipoma

from well-differentiated liposarcoma on MR imaging: is comparison of margins and internal characteristics useful? AJR Am J Roentgenol 180(6):1689–1694. doi:10.2214/ajr.180.6.1801689
66. Oleaga L, Florencio MR, Ereno C, Grande J, Terrones J, Legorburu A, Grande D (1995) Fibrolipomatous hamartoma of the radial nerve: MR imaging findings. Skeletal Radiol 24(7):559–561
67. Patel RV, Gondalia JS (1991) Congenital infiltrating lipomatosis of the face. Br J Plast Surg 44(2):157–158
68. Peterson JJ, Kransdorf MJ, Bancroft LW, O'Connor MI (2003) Malignant fatty tumors: classification, clinical course, imaging appearance and treatment. Skeletal Radiol 32(9):493–503. doi:10.1007/s00256-003-0647-8
69. Pitson G, Robinson P, Wilke D, Kandel RA, White L, Griffin AM, Bell RS, Catton CN, Wunder JS, O'Sullivan B (2004) Radiation response: an additional unique signature of myxoid liposarcoma. Int J Radiat Oncol Biol Phys 60(2):522–526. doi:10.1016/j.ijrobp.2004.03.009
70. Reiseter T, Nordshus T, Borthne A, Roald B, Naess P, Schistad O (1999) Lipoblastoma: MRI appearances of a rare paediatric soft tissue tumour. Pediatr Radiol 29(7):542–545. doi:10.1007/s002470050641
71. Robinson P, Farrant JM, Bourke G, Merchant W, McKie S, Horgan KJ (2008) Ultrasound and MRI findings in appendicular and truncal fat necrosis. Skeletal Radiol 37(3):217–224. doi:10.1007/s00256-007-0417-0
72. Rubinstein A, Goor Y, Gazit E, Cabili S (1989) Non-symmetric subcutaneous lipomatosis associated with familial combined hyperlipidaemia. Br J Dermatol 120(5):689–694
73. Soulie D, Boyer B, Lescop J, Pujol A, Le Friant G, Cordoliani YS (1995) Myxoid liposarcoma. MRI imaging. J Radiol 76(1):29–36
74. Sundaram M, Baran G, Merenda G, McDonald DJ (1990) Myxoid liposarcoma: magnetic resonance imaging appearances with clinical and histological correlation. Skeletal Radiol 19(5):359–362
75. Sundaram M, McGuire MH, Herbold DR (1988) Magnetic resonance imaging of soft tissue masses: an evaluation of fifty-three histologically proven tumors. Magn Reson Imaging 6(3):237–248
76. Sung MS, Kang HS, Suh JS, Lee JH, Park JM, Kim JY, Lee HG (2000) Myxoid liposarcoma: appearance at MR imaging with histologic correlation. Radiographics 20(4):1007–1019. doi:10.1148/radiographics.20.4.g00jl021007
77. Toms AP, White LM, Kandel R, Bell RS (2003) Low-grade liposarcoma with osteosarcomatous dedifferentiation: radiological and histological features. Skeletal Radiol 32(5):286–289. doi:10.1007/s00256-002-0614-9
78. Vanhoenacker FM, De Schepper AM, Gielen JL, Parizel PM (2005) MR imaging in the diagnosis and management of inheritable musculoskeletal disorders. Clin Radiol 60(2):160–170. doi:10.1016/j.crad.2004.06.003

Fibroblastic/Myofibroblastic Tumors

13

Jan E. Vandevenne and Arthur M. De Schepper†

Contents

13.1 **Introduction** 243

13.2 **Benign Fibroblastic Proliferations** 245
13.2.1 Nodular Fasciitis 245
13.2.2 Proliferative Myositis (and Fasciitis) 248
13.2.3 Myositis Ossificans and Fibro-osseous Pseudotumor of the Digits 248
13.2.4 Ischemic Fasciitis 252
13.2.5 Elastofibroma 253
13.2.6 Fibroma of Tendon Sheath 255
13.2.7 Nuchal-Type Fibroma 258
13.2.8 Desmoplastic Fibroblastoma (Collagenous Fibroma) 262
13.2.9 Calcifying Aponeurotic Fibroma 262

13.3 **Fibromatoses** 262
13.3.1 Palmar Fibromatosis 265
13.3.2 Plantar Fibromatosis 266
13.3.3 Knuckle Pads 269
13.3.4 Extra-abdominal Desmoid Tumors 269
13.3.5 Abdominal Fibromatosis (Abdominal Desmoids) 275
13.3.6 Lipofibromatosis 276

13.4 **Fibrous Tumors of Infancy and Childhood** 276
13.4.1 Fibrous Hamartoma of Infancy 276
13.4.2 Infantile Digital Fibromatosis: Inclusion-Body Fibromatosis 278
13.4.3 Juvenile Hyaline Fibromatosis 278
13.4.4 Fibromatosis Colli 279

13.5 **Intermediate-Grade Fibrous and Fibromyoblastic Tumors** 282
13.5.1 Dermatofibrosarcoma Protuberans 282
13.5.2 Extrapleural Solitary Fibrous Tumor 285
13.5.3 Inflammatory Myofibroblastic Tumor 285
13.5.4 Low-Grade Myofibroblastic Sarcoma 285
13.5.5 Myxoinflammatory Fibroblastic Sarcoma 286
13.5.6 Infantile Fibrosarcoma 289

13.6 **Malignant Fibromyoblastic Tumors** 292
13.6.1 Adult Fibrosarcoma 292
13.6.2 Myxofibrosarcoma 293
13.6.3 Low-Grade Fibromyxoid Sarcoma 295
13.6.4 Sclerosing Epithelioid Fibrosarcoma 299

References 303

13.1 Introduction

Fibrous tissue consists of fibroblasts and an extracellular matrix containing both fibrillary structures (collagen, elastin) and nonfibrillary, gel-like ground substance. Both fibroblasts (spindle-shaped cells) and myofibroblasts, which are modified fibroblasts showing features common to fibroblasts and smooth muscle cells, produce procollagen and collagen. Collagen is the main, noncontractile component of the extracellular matrix, and elastin is the main, contractile

†Author was deceased at the time of publication

J.E. Vandevenne (✉) • A.M. De Schepper†
Department of Radiology, Ziekenhuis Oost Limburg, Campus Sint-Jan, Schiepse Bos 6, 3600 Genk, Belgium
e-mail: jan.vandevenne@zol.be

© Springer International Publishing AG 2017

F.M. Vanhoenacker et al. (eds.), *Imaging of Soft Tissue Tumors*, DOI 10.1007/978-3-319-46679-8_13

component of elastic fibers. The amorphous ground substance of fibrous tissue contains glycosaminoglycans (mucopolysaccharides), the most common types being hyaluronic acid, chondroitin 4- and 6-sulfates, and proteoglycans [100]. Fibrous tissue can be loose or dense depending on the relative amount of the three components. Dense fibrous tissue is seen in tendons, ligaments, and aponeuroses.

Fibroblastic/myofibroblastic tumors represent a very large subset of mesenchymal tumors. Many lesions in this category contain cells with both fibroblastic and myofibroblastic features, which may in fact represent functional variants of a single cell type. The relative proportions of these cell types vary not only between individual cases but also within a single lesion over time (often in proportion to cellularity). A significant subset of spindle cell and pleomorphic sarcomas are probably myofibroblastic in type, but, to date, only low-grade forms have been reproducibly characterized. Among lesions formerly known as malignant fibrous histiocytoma (MFH), at least some represent pleomorphic myxofibrosarcomas.

Principal changes and advances since the 1994 WHO classification have been the characterization of numerous previously undefined lesions, including ischemic fasciitis, desmoplastic fibroblastoma, mammary-type myofibroblastoma, angiomyofibroblastoma, cellular angiofibroma, Gardner fibroma, low-grade fibromyxoid sarcoma, acral myxoinflammatory fibroblastic sarcoma, sclerosing epithelioid fibrosarcoma, and low-grade myofibroblastic sarcoma.

Conceptual changes have included the clearer recognition of solitary fibrous tumor in soft tissue and the realization that most cases of so-called hemangiopericytoma belong in this category, as well as the reclassification of lesions formerly labeled “myxoid MFH” as “myxofibrosarcoma” and the definitive allocation of these tumors to the fibroblastic category.

The 2002 WHO classification of fibroblastic/myofibroblastic tumors [41] contained a large number of new and modified lesions. The 2013 WHO classification [40] follows this classification, except for removing myofibroma/myofibromatosis [80] and giant cell angiofibroma from the list and adding giant cell fibroblastoma and dermatofibrosarcoma protuberans.

They were categorized into four groups according to their degree of malignancy, i.e., (1) benign, (2) intermediate (locally aggressive), (3) intermediate (rarely metastasizing), and (4) malignant:

1. *Benign:*
   - Nodular fasciitis
   - Proliferative fasciitis and proliferative myositis
   - Myositis ossificans and fibro-osseous pseudotumor of digits
   - Ischemic fasciitis
   - Elastofibroma
   - Fibrous hamartoma of infancy
   - Fibromatosis colli
   - Juvenile hyaline fibromatosis
   - Inclusion-body fibromatosis
   - Fibroma of tendon sheath
   - Desmoplastic fibroblastoma
   - Mammary-type myofibroblastoma
   - Calcifying aponeurotic fibroma
   - Angiomyofibroblastoma
   - Cellular angiofibroma
   - Nuchal-type fibroma
   - Gardner fibroma
   - Calcifying fibrous tumor

2. *Intermediate (locally aggressive):*
   - Superficial fibromatoses (palmar/plantar)
   - Desmoid-type fibromatoses
   - Lipofibromatosis
   - Giant cell fibroblastoma
   - Dermatofibrosarcoma protuberans

3. *Intermediate (rarely metastasizing):*
   - Extrapleural solitary fibrous tumor
   - Inflammatory myofibroblastic tumor
   - Low-grade myofibroblastic sarcoma
   - Myxoinflammatory fibroblastic sarcoma
   - Infantile fibrosarcoma

4. *Malignant:*
   - Adult fibrosarcoma
   - Myxofibrosarcoma
   - Low-grade fibromyxoid sarcoma
   - Sclerosing epithelioid fibrosarcoma

In the case of several fibroblastic proliferations (elastofibroma, fibroma of tendon sheath, extra-abdominal desmoids, fibromatosis colli), it is unclear whether these constitute reactive fibrosing processes or true neoplasms. Fibromatoses are aggressive, infiltrating lesions, despite their histologically benign character, and aggressive fibromatoses or musculoaponeurotic desmoid tumors are by far the largest group of tumors of fibrous tissue. The terminology of childhood fibromatosis is confusing, and there are many classification systems based on different clinicopathological parameters such as age, localization, histology, and aggressiveness of the lesion [162]. Fibrous tumors of infancy and childhood and soft tissue fibrosarcomas are rare and have only sparsely been reported in the radiological literature. It is a constant finding that the majority of these tumors have a high recurrence rate after surgical resection, and recurrent lesions mostly have a more aggressive behavior than their primary counterparts. Another constant finding is the natural evolution of tumors of fibrous tissue, which are hypercellular in their initial stage and become more collagenous in later stages. Localization of the lesion and age of the patient are major diagnostic factors. Fibroma of tendon sheath, elastofibroma, all types of fibromatosis, and fibromatosis colli are characterized by typical localizations [51, 160].

13.2 Benign Fibroblastic Proliferations

Benign fibroblastic proliferations constitute a heterogeneous group of well-defined entities. Some of these, such as nodular fasciitis, grow rapidly and are richly cellular. Others, such as fibroma of the tendon sheath and elastofibroma, grow slowly, are much less cellular, and contain considerable amounts of collagen [26, 32, 130].

13.2.1 Nodular Fasciitis

Nodular fasciitis, also called pseudosarcomatous fasciitis or infiltrative fasciitis, is a benign soft tissue lesion composed of proliferating fibroblastic-myofibroblastic cells. It is characterized by rapid growth, which may arouse suspicion of sarcoma [82]. Most patients are asymptomatic or note only mild discomfort. Lesions are round to oval, in many cases sized 4 cm or less, and mostly located in the upper extremity, often at the volar aspect of the forearm [159]. The trunk and head and neck are frequently involved, and the lower extremity is inflicted less often [78, 104] (Fig. 13.1). Shimizu has reported on a series of 250 patients with a mean age of 39 years and a peak in the fourth decade, in whom 44 % of the lesions are located in the upper extremity, which is followed in frequency by the lower extremity and the trunk [137]. Lu summarized the data of 272 cases including 160 men and 112 women ranging from newborn to 77 years. The upper extremity (34 %), head and neck region (24 %), trunk (21 %), and lower extremity (14 %) were involved [96]. Multifocal lesions are rarely seen [79].

The cause is unknown and for long a trigger by local injury or a local inflammatory process was most likely. More recently, concurrent presentation of nodular fasciitis and aneurysmal bone cyst has been reported, with both tumors belonging to the biologic spectrum of USP6-induced tumors [121, 166].

There are three subtypes of nodular fasciitis according to their topography: the most common subcutaneous type, the intramuscular type, and the fascial type, which spreads along superficial fascial planes. Microscopically, nodular fasciitis can be subdivided into three types based on the predominant histological features: myxoid (type 1), cellular (type 2), and fibrous (type 3). However, since many different features may coexist in one lesion, definition of a single fixed type is not always possible. Microscopically, younger lesions consist of fibroblasts embedded in a dense reticulin meshwork and birefringent collagen. There is a rich intervening myxoid matrix. Older lesions tend to be more fibrous. Histological transformation from type 1 to type 2 and then to type 3 is indicative of the natural evolution of these lesions. Recurrence after excision is very rare and occurs in less than 2 % of the cases.

On ultrasound images, nodular fasciitis appears mostly solid, but cystic change has been

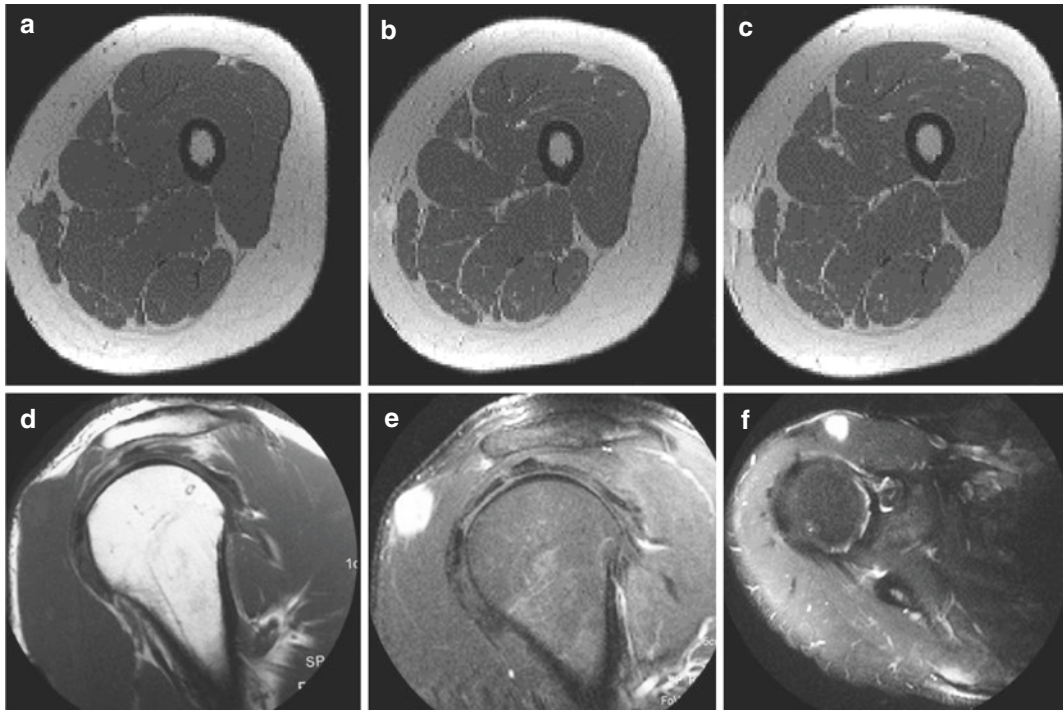

Fig. 13.1 (**a–f**) Two cases of nodular fasciitis, fascial type: a first case (**a–c**) at the fascia of the gracilis muscle and a second case (**d–f**) at the fascia of the pectoralis muscle. (**a**) Axial spin-echo T1-weighted MR image. (**b**) Axial spin-echo T1-weighted MR image after gadolinium contrast injection. (**c**) Axial spin-echo T2-weighted MR image. (**d**) Sagittal spin-echo T1-weighted MR image. (**e**) Sagittal spin-echo T1-weighted MR image after gadolinium contrast injection, with fat suppression. (**f**) Axial spin-echo T2-weighted MR image. Both lesions are in close contact with superficial fasciae. On T1-weighted images, both lesions are of slightly higher signal intensity (SI) when compared with SI of normal muscle (**a, d**). They both enhance markedly after contrast injection (**b, e**) and are of high SI on T2-weighted MR images (**c, f**)

seen. Superficial-type nodular fasciitis is reported to have a hypoechoic appearance with echogenic foci or peripheral hyperechoic nodules and quite often does not show internal vascular flow [87]. On CT scans, nodular fasciitis has low attenuation values, reflecting the myxoid character of the lesions [104]. The appearance on MR images reflects the gross morphology of the tumor. Myxoid and cellular lesions are hypointense or iso- to slightly hyperintense compared with skeletal muscle on T1-weighted images and iso- to hyperintense compared with fat on T2-weighted images. Lesions with a more fibrous histology are markedly hypointense on all spin-echo sequences [104]. Myxoid lesions show a marked and homogeneous enhancement, cellular lesions a nonhomogeneous enhancement, and fibrous lesions a moderate, nonhomogeneous enhancement [159]. Three cases in our own series had identical appearance on MR images: a central area of low signal intensity (SI) and a peripheral area of higher SI on T1-weighted images and an inverted SI pattern (high SI at the center and lower SI at the periphery) on T2-weighted images. This pattern was described in 1991 by Frei et al. [46]. On comparing these findings with the MR features of some neurogenic tumors (see Sect. 17.2.2), we named the pattern "the inverted target sign." After gadolinium (Gd) contrast injection, there was a marked enhancement of the peripheral zone, with poor enhancement of the (myxoid) center (Figs. 13.1 and 13.2). In a study

Fig. 13.2 (**a–g**) Three cases of nodular fasciitis, intramuscular type: the first case (**a–c**) at the forearm, the second case (**d, e**) at the subscapularis muscle, and the third case (**f, g**) at the pectoralis muscle. (**a**) Axial spin-echo T1-weighted MR image. (**b**) Coronal spin-echo T1-weighted MR image after gadolinium contrast injection. (**c**) Axial spin-echo T2-weighted MR image. (**d**) Axial spin-echo T2-weighted MR image. (**e**) Axial spin-echo T1-weighted MR image after gadolinium contrast injection, with fat suppression. (**f**) Coronal spin-echo T1-weighted MR image, with fat suppression. (**g**) Coronal spin-echo T1-weighted MR image after gadolinium contrast injection, with fat suppression. All three cases present with the so-called "inverted target" sign consisting of a peripheral zone of increased SI on T1-weighted MR images (**a, f**), decreased SI on T2-weighted MR images (**c, d**), and merely peripheral contrast enhancement (**b, e, g**)

on MRI appearance of 29 lesions, twelve lesions exhibited central nonenhancing areas. Transcompartmental spread was demonstrated in nine lesions. Osseous changes were seen in five cases and included extrinsic cortical saucerization, medullary edema, and transcortical osseous invasion. Two lesions demonstrated intra-articular extension [16].

The cellular type of nodular fasciitis is apt to be mistaken for a sarcoma (myxofibrosarcoma and fibrosarcoma), while the fibrous type must be differentiated from fibromatosis. Recurrent tumors have a more aggressive behavior than primary ones (Fig. 13.3).

13.2.2 Proliferative Myositis (and Fasciitis)

Proliferative myositis is a rare pseudosarcomatous process similar to proliferative fasciitis (histologically the subcutaneous counterpart). Lesions present in middle-aged and older adults, arising predominantly in the trunk, shoulder girdle, and upper arm and less often in the thigh. Typically, a painful swelling is noted with subsequent rapid growth (even over days). This tumoral lesion is benign and most often self-limiting with no tendency to recur [33]. On pathology, proliferative myositis demonstrates intense fibroblast proliferation in the stromal tissue (perimysium and epimysium), creating the characteristic "checkerboard" pattern by extending between normal muscle fibers. Microscopically, plump fibroblastic/myofibroblastic spindle cells together with larger basophilic cells resembling ganglion-like cells are seen with normal mitotic figures.

On imaging, proliferative myositis may present with characteristic features that should prompt the radiologist to include this entity in the differential diagnosis with sarcomatous lesions. The solid, ill-defined mass often presents fusiform, demonstrating thickened bands with interspersed continuous muscle fibers on longitudinal images and the "checkerboard" pattern on transverse images. On transverse ultrasound, hypoechoic linear structures are grouping bundles of muscle fibers in a "checkerboard" pattern or if grouping more randomly resembling "dry-cracked mud" (Fig. 13.4) [133]. On duplex ultrasound, vascularization may be normal or increased. CT may show an ill-defined, expansile lesion that is isointense or hypointense compared to muscle. MR imaging demonstrates a focal intramuscular expansion appearing moderately or strongly hyperintense on T2-weighted images and hypointense or isointense on T1-weighted images with marked enhancement after contrast administration. MR imaging demonstrates equally well the "checkerboard" pattern on transverse images and the preserved, continuous muscle fibers within the lesion on longitudinal images (Fig. 13.5). Moreover, MR imaging shows perilesional edema and contrast enhancement extending to the surrounding fascia, suggesting inflammatory changes [168].

The astute radiologist may suggest the diagnosis on imaging findings. If sarcoma can be excluded by biopsy and by a decrease of tumor size on imaging follow-up within weeks, (mutilating) surgery can be avoided (Fig. 13.5) [23, 67].

13.2.3 Myositis Ossificans and Fibro-osseous Pseudotumor of the Digits

- *Definition.* Myositis ossificans is a generally solitary, benign, self-limiting ossifying process occurring in the musculature of the extremities in young men and is related to trauma in about half of all cases [32, 100]. Sometimes, it occurs within other tissues, such as subcutaneous fat (panniculitis ossificans) – in one-third of the cases – tendons or fasciae (fasciitis ossificans), and periosteum of the digits (fibro-osseous pseudotumor of the digits) [32, 83, 92, 100, 109].

Most lesions in myositis ossificans measure 3–6 cm in diameter. On cross section they have a white, soft, and rather gelatinous center and firm, yellow-gray periphery with rough, granular surface [32]. Microscopically, a zonal pattern is

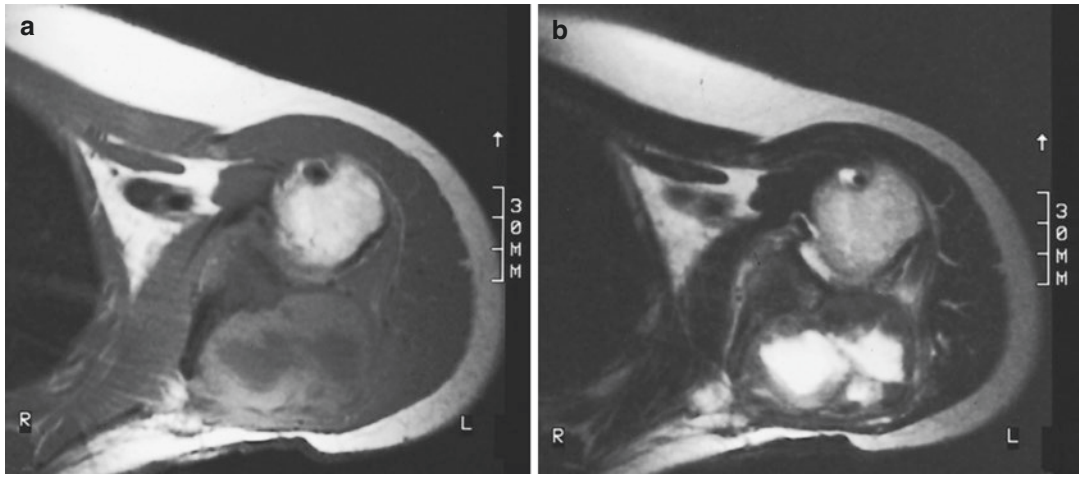

Fig. 13.3 (**a, b**) Recurrent nodular fasciitis of the fascial type in a 37-year-old woman. (**a**) Axial spin-echo T1-weighted MR image. (**b**) Axial spin-echo T2-weighted MR image. Well-delineated, oval mass within the region of the infraspinatus muscle, adjacent to the scapula. The lesion is hyperintense to muscle on the T1-weighted image, with a central, bilobate area of lower signal intensity (**a**). Central parts of the lesion show high signal intensity on the T2-weighted image (**b**), while the peripheral component remains of lower signal intensity. This case also illustrates the "inverted target sign"

observed. This refers to a progressive degree of cellular maturation from the center to the periphery, maturation being lowest in the center and highest with mature bone formation – at the periphery.

- *Incidence and Clinical Behavior.* Myositis ossificans is by far the most common bone-forming lesion of the soft tissues. The exact pathogenesis of this disorder is still unclear. A history of preceding mechanical trauma is present in about half of all cases. As causative factors in some of the other cases, infection and coagulopathy have been mentioned. Furthermore, the disease may also occur in association with burns, paraplegia, and quadriplegia or with other neuromuscular disorders such as tetanus [32, 100].

Myositis ossificans commonly affects young, active adults and adolescents, predominantly men (Figs. 13.6, 13.7, 13.8, and 13.9), but occasionally involves persons of other age groups. Pain and tenderness are the first symptoms, followed by a diffuse swelling of soft tissues. This swelling typically becomes more circumscribed and indurated after 2–3 weeks. Thereafter, it progressively changes into a firm hard mass approximately 3–6 cm in diameter, which is well outlined on palpation. Although malignant transformation into extraskeletal osteosarcoma has been suggested in the literature, it has never been proven. Hence, the prognosis of myositis ossificans is generally accepted to be excellent [32].

Principal sites of involvement are the limbs, which are affected in more than 80 % of cases. The quadriceps muscle and brachialis muscle are favored sites in the lower and upper extremity, respectively. Areas prone to trauma are more commonly afflicted.

The incidence of panniculitis ossificans differs slightly from that of myositis ossificans in that it prevails in the upper extremities of women [32, 100].

Fibro-osseous pseudotumor of the digits occurs predominantly in the fingers or toes of young adults, more often in females [83].

- *Imaging.* Acute myositis ossificans refers to early stages of disease, before ossification is radiologically visible. During these initial stages of the disease, only a slight increase in

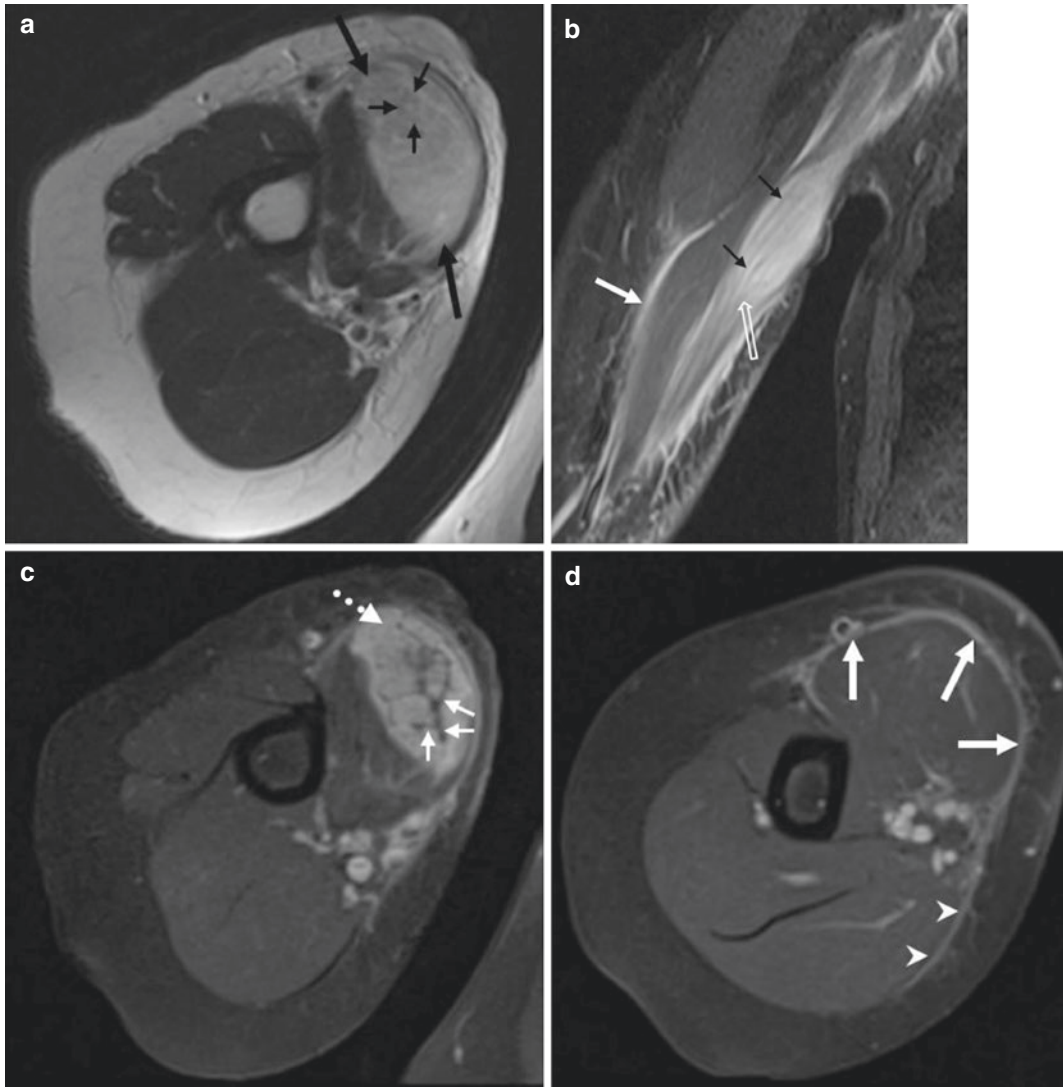

Fig. 13.4 Proliferative myositis in a 52-year-old female aerobics instructor with 3-week history of a painful swelling in the anteromedial aspect of the upper arm. (**a**) Axial T2-weighted MRI view, (**b**) coronal STIR image, and (**c, d**) axial contrast-enhanced T1-weighted MR images. (**a**, **b**) The mass appears inhomogeneously hyperintense in T2-weighted image (*large black arrows*). The hypointensities within the lesion have geometrical contours on axial images – consistent with "checkerboard-like pattern" – and are clearly continued with muscle fascicles at the upper and lower pole of the tumor in coronal image (*small black arrows*). The inferior margin of the lesion cannot be identified and seems to continue within the interfascicular space inferiorly (*empty white arrow*). (**c**) Contrast-enhanced T1-weighted MRI view showing marked inhomogeneous enhancement (*dashed white arrow*) and central branched area of decreased signal intensity tracing the interfascicular spaces (*small white arrows*), again consistent with "checkerboard-like pattern." (**d**) Inferior to the tumor, reactive fasciitis of the biceps brachialis (*plain white arrows*) and the anterior medial part of the triceps (*white arrowheads*) is noted with increased signal in STIR and contrast enhancement in T1-weighted image (Reprinted with permission from Jarraya et al. [67])

soft tissue density is observed radiologically. In general, calcification develops between 4 and 6 weeks after the initial trauma and results in a "mature" lesion. Initially, these calcifications present as irregular, floccular opacities on radiography. Over time the lamellar bone

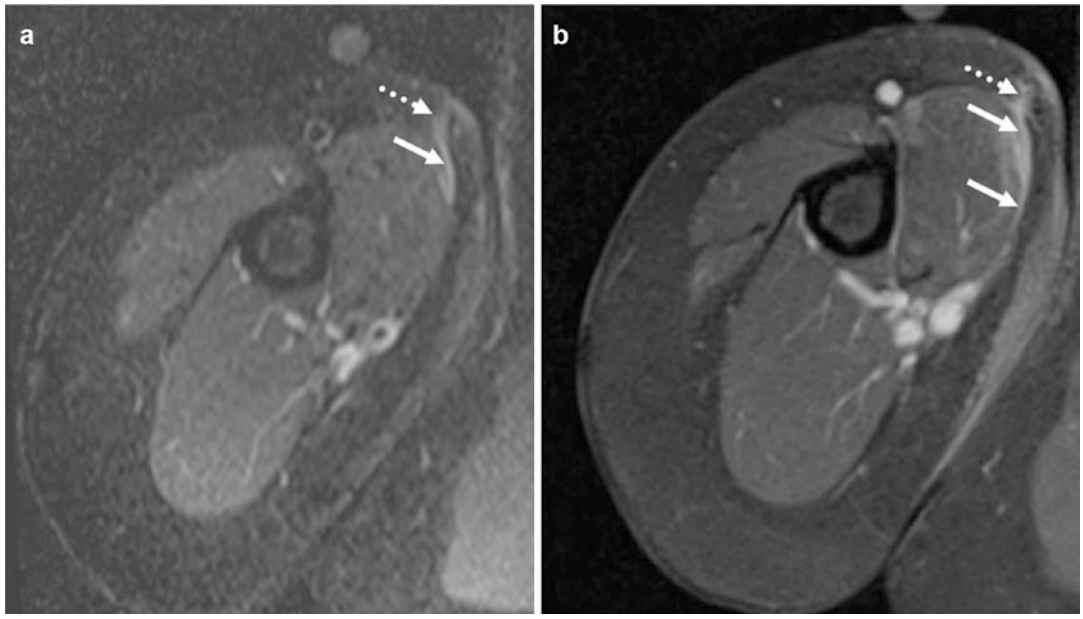

Fig. 13.5 Follow-up 7 weeks later in the same patient as in Fig. 13.4 (**a**) axial STIR and (**b**) axial contrast-enhanced T1-weighted MR image demonstrate complete resolution of the intramuscular mass with persistence of slight fascial STIR hyperintensity and contrast enhancement at the anterior medial aspect of the biceps brachialis (*plain arrows*) and along the biopsy path (*dashed arrow*) (Reprinted with permission from Jarraya et al. [67])

forms at the periphery of the lesion and proceeds toward its center [32, 100]. The centrifugal pattern of progressive maturation is well reflected by the CT appearance of the lesion during the active stage of disease: the central immature zone of the lesion appears radiolucent, whereas the outer mature zone shows calcification and ossification (Figs. 13.7 and 13.8). This appearance is referred to as the "zoning" phenomenon.

Three different appearances of myositis ossificans are noted on MRI, corresponding to the stage of maturation. Early stages of myositis ossificans, the so-called acute form, present on MRI as a mass that is isointense or even slightly hyperintense to muscle on T1-weighted images, but hyperintense on T2-weighted images (Fig. 13.6). The lesion is surrounded with variable amounts of edema, appearing hyperintense on T2-weighted image and with a hypointense rim in some cases. Following administration of gadolinium, a well-defined rim of enhancement is observed, allowing differentiation between the lesion and primary soft tissue sarcoma, which is enhanced homogeneously. The MRI appearance of the lesions during the intermediate or subacute stage is characterized by isointensity with muscle on T1-weighted images and mild increase of signal intensity on T2-weighted images [153]. These findings are explained by a central fibrous transformation as observed histologically. Occasionally, a thin rim of signal void surrounding the lesion may be observed, especially on T2-weighted images, and corresponds to a rim of calcification, although this is better observed on plain radiography and CT. Findings consistent with hemorrhage and fluid-fluid levels are rarely seen. Mature lesions (i.e., the "chronic stage") show more extensive signal voids on all sequences, corresponding to a considerable degree of peripheral calcification and ossification. In this stage lesions demonstrate increased signal intensity in an "onionskin pattern" on T2-weighted images (Fig. 13.8).

The diagnosis of myositis ossificans commonly relies on findings on plain radiography. Attention must be paid to the presence of a central

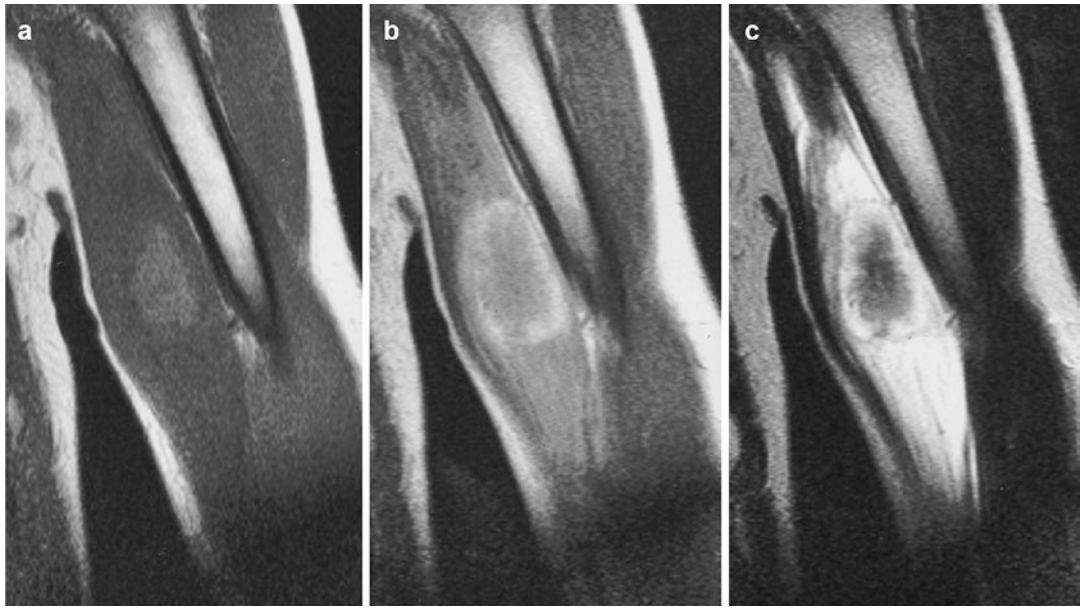

Fig. 13.6 (**a–c**) Myositis ossificans, early stage, in the left upper arm of a 7-year-old boy: (**a**) coronal T1-weighted MR image, (**b**) coronal T1-weighted MR image after gadolinium contrast injection, and (**c**) coronal T2-weighted MR image. Ill-defined mass within the biceps muscle. On the T1-weighted image, the mass is slightly hyperintense to the muscle (**a**). After contrast injection there is a marked peripheral enhancement (**b**). On the T2-weighted image, the center of the lesion remains hypointense, while the hyperintense periphery is outlined by a thin hypointense rim. Extremely high signal intensity within the whole biceps muscle (**c**). Characteristic appearance of an early-stage myositis ossificans (biopsy revealed large amounts of osteoid bone, surrounded by numerous osteoblasts)

radiolucent area, as a manifestation of the zoning phenomenon and of a lucent line separating the lesion from the underlying cortex, which are both better demonstrated on CT. As biopsies, establishing the diagnosis, may have been taken during early stages of the disease, the lesion may continue to grow for some period of time. In these cases repeated plain radiographs and CT are useful to document the maturation and to exclude a destructive growth pattern (Fig. 13.9) [84]. Plain radiography and CT are superior to MRI in demonstrating calcifications and ossification; however, in the case of early disease – "acute myositis ossificans" – MRI has proven the most accurate imaging technique, although findings are nonspecific.

The appearance of panniculitis ossificans and fibro-osseous pseudotumor of the digits is similar to that of myositis ossificans except that these conditions may lack an obvious zoning phenomenon. In the latter case, cortical erosion of the underlying bone and stippled calcification may be observed (Fig. 13.10) [83, 92, 100, 109].

13.2.4 Ischemic Fasciitis

Ischemic fasciitis, also called decubital fibroplasia or decubital fasciitis, is a pseudosarcomatous lesion presenting as a mass in areas overlying bony prominences. These lesions occur predominantly in elderly patients and can be associated with physical immobility. Usually the limb girdles, sacrum, greater trochanter, shoulders, buttocks, or posterior chest wall are involved. Histologically, a zonal appearance is noted with pseudosarcomatous proliferation of (myo-) fibroblasts and ganglion-like cells with a central area of fibrinoid degeneration that may include infarcted fat surrounded by granulation tissue (the latter distinguishing it from proliferative and nodular fasciitis).

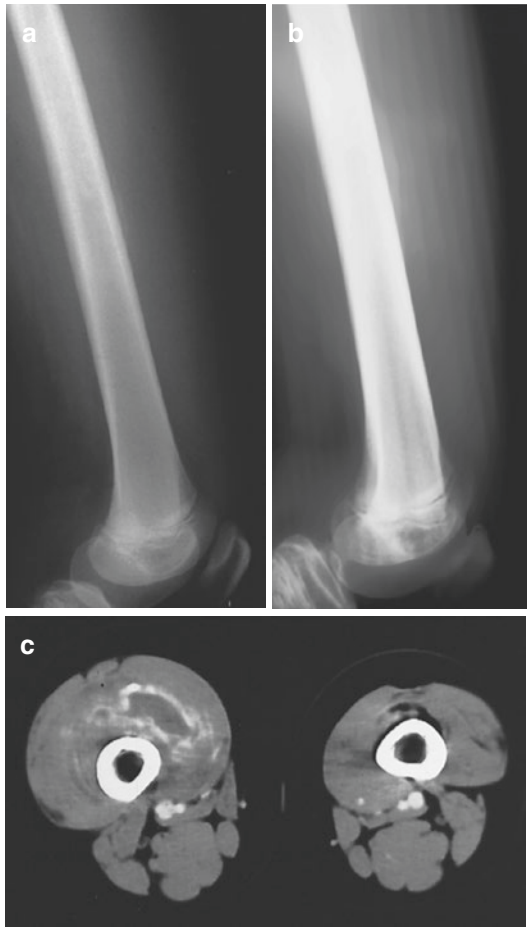

Fig. 13.7 (**a–c**) Myositis ossificans, intermediate stage of the right thigh in a 13-year-old boy: (**a**) plain radiograph a few days after trauma, (**b**) plain radiograph 5 days later, and (**c**) CT. Presence of a faint linear periosteal calcification on the ventral aspect of the right thigh (**a**). Five days later there is extensive calcification within the quadriceps muscle (**b**). On CT there is diffuse swelling of the right thigh with an eggshell calcification within the vastus intermedius muscle (**c**). The zoning phenomenon is characteristic for an intermediate stage of posttraumatic myositis ossificans

MRI signal intensities are nonspecific with low signal on T1- and high signal on T2-weighted images. After intravenous contrast administration, an irregular area of central hypointensity can be seen within the enhancing mass, possibly corresponding to the central area of fibrinoid degeneration/infarcted fat (Fig. 13.11) [64]. Perilesional edema may be seen extending beyond the fascia. Features that may help to differentiate from necrotic sarcoma and abscess include the subcutaneous location at a pressure point in an elderly, immobile patient. Surgical debridement or resection sometimes with rearrangement of local soft tissue is the treatment of choice, and recurrences are rare [134] [11].

13.2.5 Elastofibroma

Elastofibroma is generally considered to be a fibroelastic pseudotumor. It occurs almost exclusively in the subscapular region deep to the rhomboid major and latissimus dorsi muscles adjacent to the inferior angle of the scapula, in close relation with the serratus anterior muscle and ribs. It is thought to be caused by repeated mechanical friction between the chest wall and the tip of the scapula, and this hypothesis is supported by immunohistochemical data [25]. Other locations, albeit uncommon, include the infraolecranon, thoracic wall, axilla, and greater trochanter regions. Bilateral lesions are common and seen in 10–60 % of patients. Most patients are older adults, and there is a definite predominance in women. Single cases have been reported in children and in an infant [8, 24]. Half of the patients are asymptomatic, the other half presenting with pain or restricted upper limb motion [72]. Chromosomal abnormalities and familial occurrences support a genetic predisposition to elastofibroma dorsi.

On gross examination, these lesions are firm and rubbery [24, 82, 91, 99]. Histologically, lesions are composed mainly of elastin-like fibers and entrapped islands of mature adipose tissue. Microscopic examination shows hypertrophy and degeneration of elastin with a background of mature collagen and fat. CT scans show attenuation similar to that of adjacent muscle. Sometimes, there are strands of low density similar to that of subcutaneous fat [85] (Fig. 13.12a). Lesion size on CT correlates best with the size of the postoperative pathologic specimen, compared to US and MRI [107]. MRI nicely reflects the histological composition of entrapped fat within a predomi-

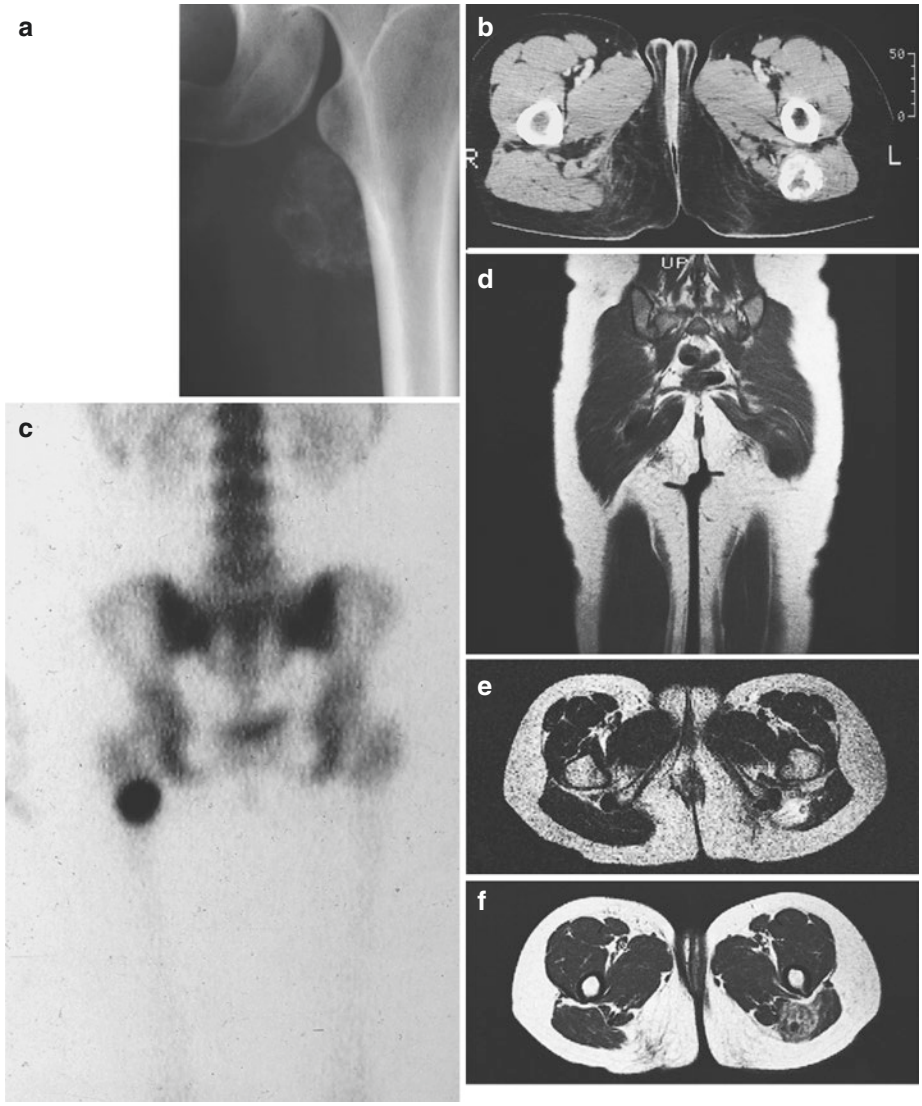

Fig. 13.8 (**a–f**) Myositis ossificans, mature stage, in the thigh of a 19-year-old professional female rower: (**a**) plain radiograph, (**b**) CT, (**c**) scintigraphy, (**d**) coronal spin-echo T1-weighted MR image, (**e**) axial spin-echo T1-weighted MR image after gadolinium contrast injection, and (**f**) axial spin-echo T2-weighted MR image. The plain radiograph reveals a rounded calcified soft tissue mass posteriorly in the thigh (**a**). CT confirms the presence of a heavily calcified lesion within a slightly hypotrophic gluteus maximus muscle. A small central zone remains uncalcified (**b**)**.** On the radionuclide scan, there is an intense tracer fixation posteriorly in the left trochanteric region (**c**). The lesion is hypointense on the T1-weighted image (**d**), is hyperintense on the T2-weighted image (**f**), and shows marked enhancement (onionskin pattern) after contrast injection (**e**). Absence of concomitant mass effect is also obvious on all MR images. History of the patient and imaging findings are in favor of a mature myositis ossificans. Despite the huge calcifications, the lesion still generates high signal intensity on the T2-weighted image

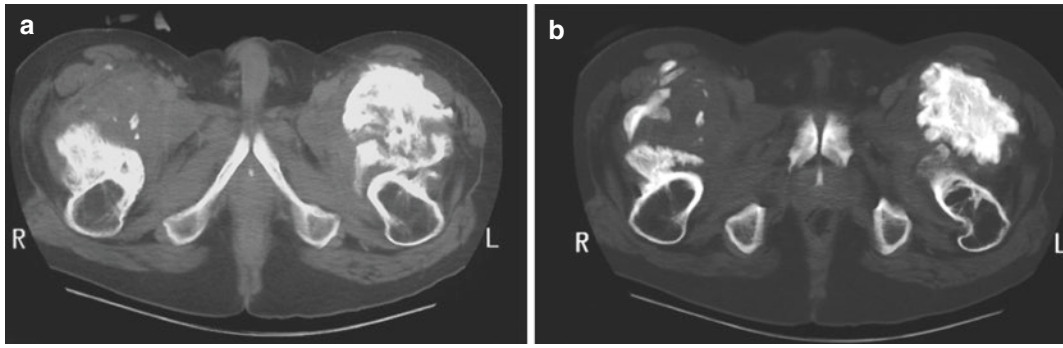

Fig. 13.9 (**a, b**) Posttraumatic myositis ossificans, mature stage, anteriorly in the proximal third of both thighs in a 33-year-old man: (**a**) CT at the level of the lesser trochanter of the femur (soft tissue window setting); (**b**) same CT section as in a (bone window setting). Huge, considerably calcified soft tissue masses within both quadriceps muscles, corresponding to the mature stage of myositis ossificans

nantly fibrous mass. On both T1- and T2-weighted images, the lesion presents as a lenticular, well-defined mass with an intermediate SI approximately equal to that of skeletal muscle. Interlaced areas have a SI similar to that of fat [81, 97]. Areas of low SI on both T1- and T2-weighted images correspond histologically to fibroelastic tissue [85] (Fig. 13.12b–d). Some lesions may present with mild to moderate uptake on 18F-FDG PET and/or diffusion restriction on MRI and should not be mistaken for metastasis [35, 60].

Surgery should not be performed for diagnostic purposes only in elderly individuals and should be reserved for symptomatic lesions [12]. Indeed, familiarity of the radiologist with this entity may make it possible to avoid some surgery [98]. Differential diagnosis is limited, but includes older desmoids, which are hypocellular, contain large amounts of collagen, and occur in younger patients.

13.2.6 Fibroma of Tendon Sheath

Fibroma of the tendon sheath consists of a benign, slow-growing, dense fibrous nodule (or multinodular mass) firmly attached to the tendon sheath and is found most frequently in the hands and feet (Fig. 13.13). The thumb, index finger, and middle finger together with lesions of the volar aspect of the wrist account for 80 % of cases. It is found most commonly in adults and is more than twice as common in men as in women. The main symptom is a small mass that rarely measures more than 2 cm and is painless but may limit motion of the involved digit [95]. Macroscopically, it resembles the lobular configuration of the much more common giant cell tumor of the tendon sheath, but it is less cellular and there are no xanthoma cells or giant cells [32]. Microscopically, this lobulated nodular lesion is composed of tightly packed spindle cells (fibroblasts), vessels, and large amounts of dense collagenous material, which is markedly hyalinized. Occasionally, there is a gradual transition from the poorly cellular hyalinized collagenous areas to more cellular areas which are thought to be characteristic of the early stages of the tumor development. More cellular forms must be differentiated from nodular fasciitis, fibrous histiocytoma, and even fibrosarcoma.

Although fibromas of the tendon sheath may resemble nodular fasciitis histologically, they involve the hands and feet almost exclusively and are slow-growing lesions, while lesions of nodular fasciitis appear suddenly, grow rapidly, and usually attain full size in 3–6 weeks. Moreover, they have a predilection for the volar aspect of the forearm [126]. Recently, intra-articular occurrence of fibroma of the tendon sheath has been reported in the joints such as the knee and the acromioclavicular and temporomandibular joint [53, 56].

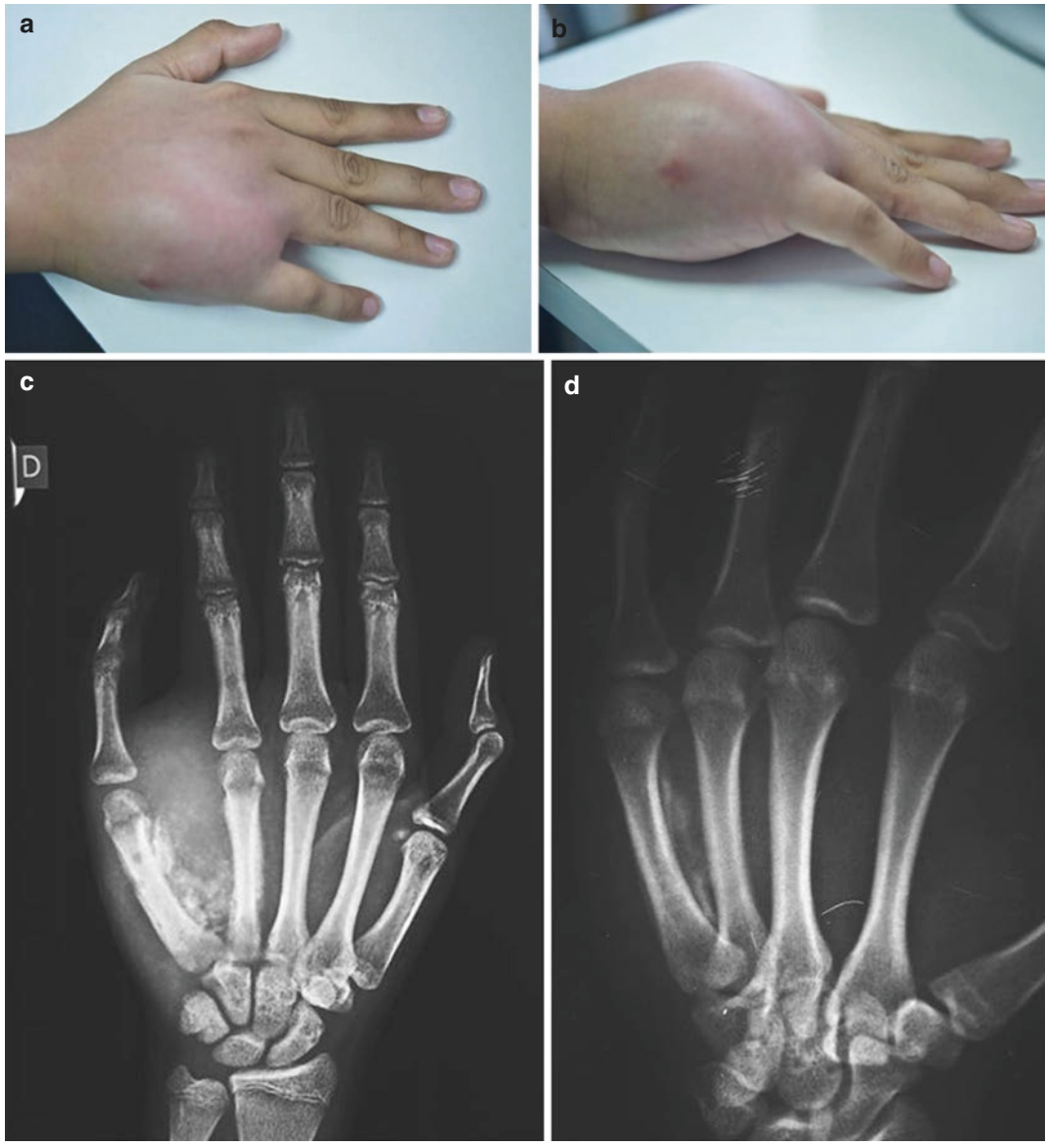

Fig. 13.10 (**a–d**) Fibro-osseous pseudotumor of the digit. (**a, b**) Hypothenar eminence swelling with a red area in the skin. Note the small punctual scar lesion due to core needle biopsy of the fifth metacarpal bone. (**c**) Anteroposterior X-ray demonstrated a calcified mass in soft tissues close to the periosteal surface. (**d**) Evolution (*shrinkage*) of the lesion 6 months later was useful to make an accurate diagnosis of fibro-osseous pseudotumor of the digit (Reprinted with permission from Liliana and Santini-Araujo [92])

Plain radiographic findings in a fibroma of the tendon sheath eroding the third metatarsal have been reported by Lourie et al. [95].

Fox et al. [44] have reported on a series of six patients with fibroma of the tendon sheath. Findings from MRI were not at all specific, i.e., low to intermediate SI on both T1- and T2-weighted images and a variable enhancement (from none to markedly enhanced) after contrast administration. MR findings depend on and reflect the relative amount of different tumor components that are cellular, myxoid, vascular, or collagenous. As a consequence, there can be an overlap in MR findings with

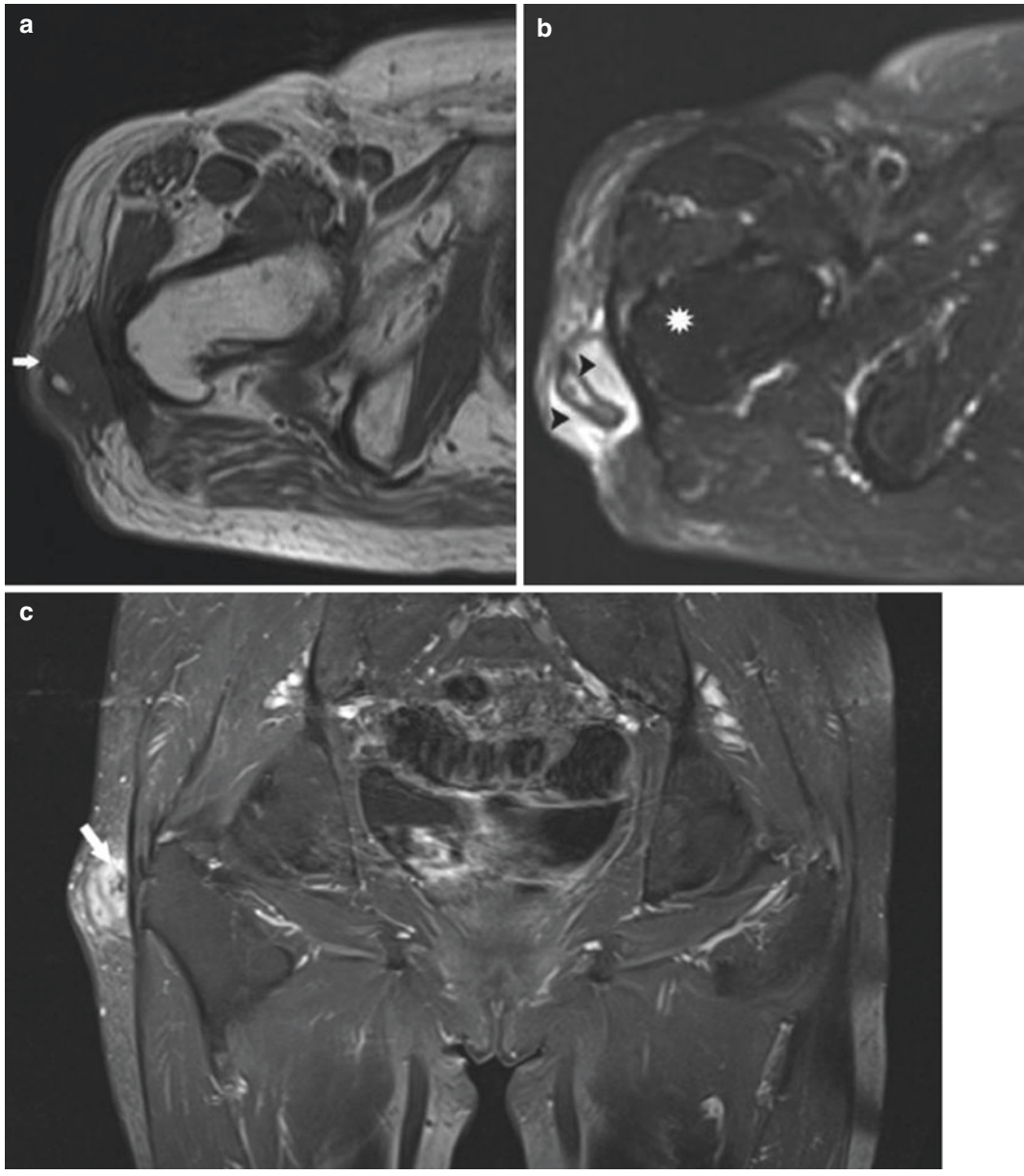

Fig. 13.11 Ischemic fasciitis, also called decubital fasciitis. A 77-year-old immobilized woman presenting with a hard, palpable, and fixed mass over the greater trochanter. MR imaging revealed a subcutaneous mass lesion abutting the iliotibial band. (**a**) On T1-weighted images (WI), the lesion was isointense to the muscle (*white arrow*), with a central focus of high signal intensity. (**b**) Fat-suppressed (FS) T2-WI showed predominantly hyperintense signal (*black arrowheads*) with intralesional foci of low SI, adjacent to the right greater trochanter (*white asterisk*). (**c**) After intravenous administration of gadolinium contrast, a marked enhancement was seen with small areas of nonenhancement, in keeping with necrotic foci (*white arrow*). Neither invasion of the gluteus muscles nor the bone marrow of the greater trochanter was seen. Histological examination revealed the diagnosis of ischemic fasciitis, with a central hypocellular area surrounded by a fibroblastic and vascular proliferating outer zone (Reproduced with permission from Ceulemans L, et al. [92])

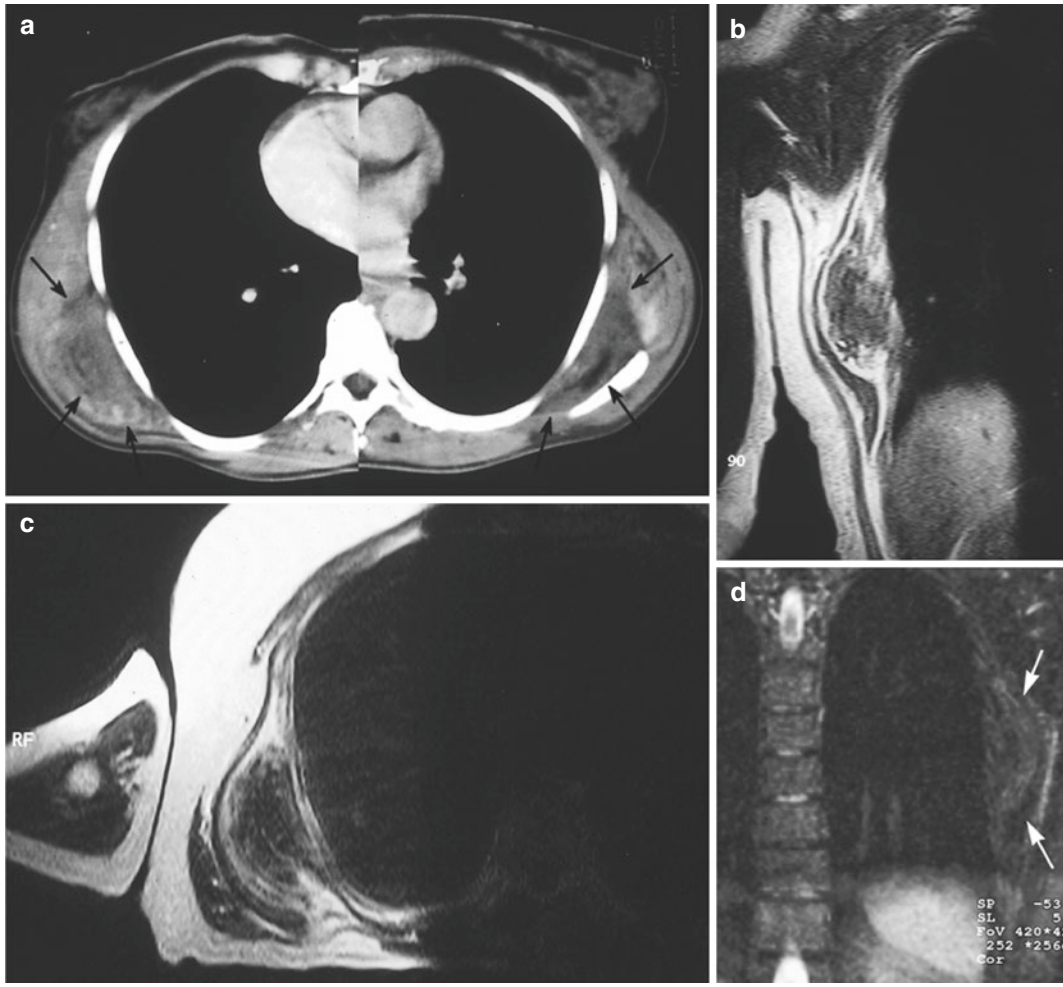

Fig. 13.12 (**a–d**) Elastofibroma dorsi in a 60-year-old woman (**a**), in a 67-year-old woman (**b, c**), and in a 56-year-old woman (**d**). A CT scan after iodinated contrast injection. (**b**) Coronal spin-echo T1-weighted MR image. (**c**) Axial turbo spin-echo T2-weighted MR image. (**d**) Coronal STIR MR image. On the CT scan, there is an oval mass between the rhomboid major and latissimus dorsi muscles on both sides (*arrows*). The lesions show mixed attenuation and enhancement after iodinated contrast injection (**a**). Oval mass within the subscapular region, showing signal intensity equal to that of fat and muscle on a T1-weighted image (**b**), and an overall low signal intensity on T2-weighted on STIR images (**c, d**). Three cases of elastofibroma showing characteristic location, attenuation on CT scan, and signal intensity on MR images, reflecting the histological composition of entrapped fat within a fibrous mass

features of giant cell tumor of the tendon sheath (Fig. 13.14). Features that may help to differentiate fibroma of the tendon sheath from the latter include the presence of band-like areas of low signal intensity representing collagenous strands, less pronounced contrast enhancement, and lack of significant decrease of signal intensity on gradient echo images (Fig. 13.13d) [20].

13.2.7 Nuchal-Type Fibroma

Nuchal-type fibroma, or collagenosis nuchae, is a benign soft tissue tumor that arises from the posterior cervical subcutaneous tissue, with a predilection for the interscapular and paraspinal regions. Nuchal fibroma is significantly more common in men, with a peak incidence during the third to the fifth decades.

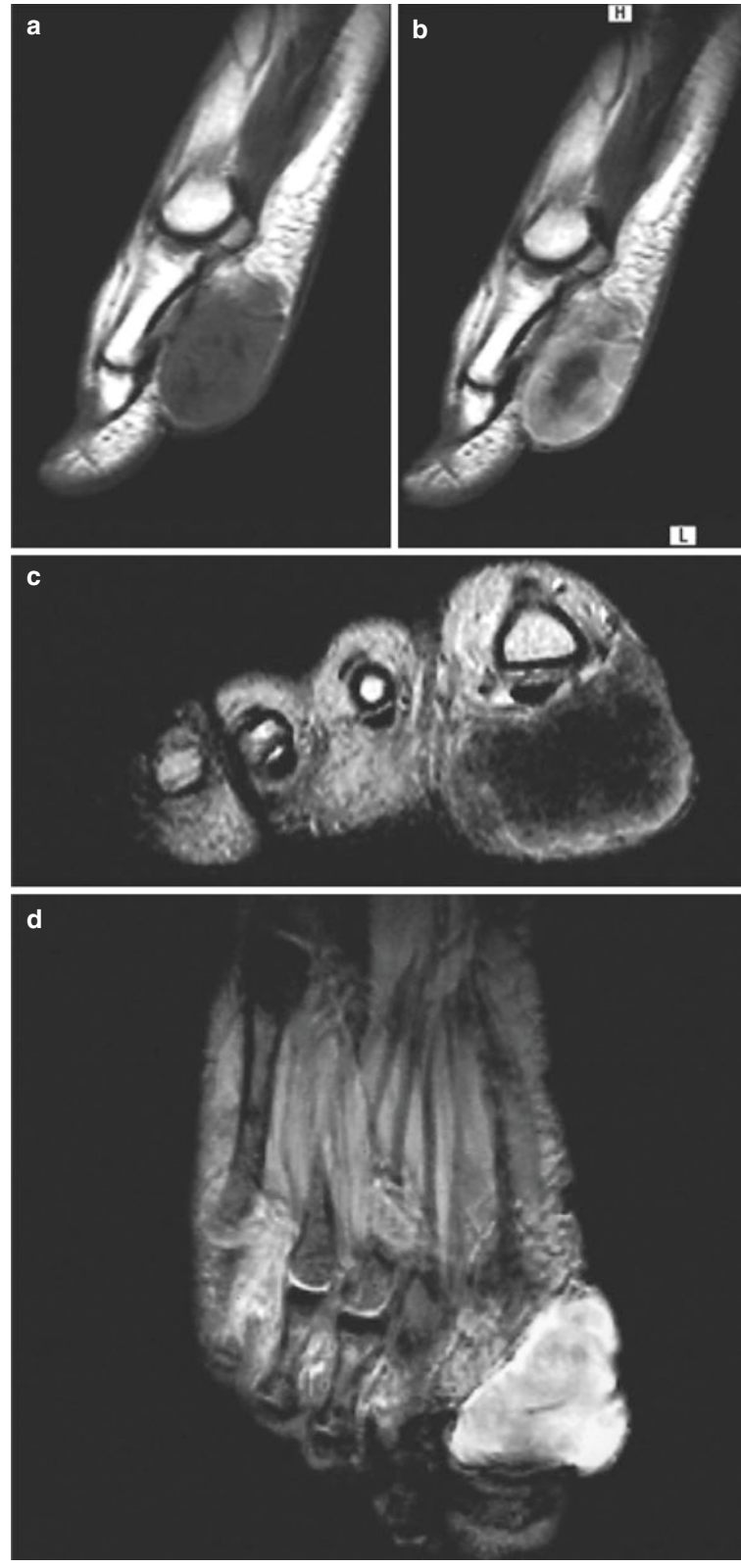

Fig. 13.13 (**a–d**) Fibroma of the tendon sheath in a 35-year-old woman. (**a**) Sagittal spin-echo T1-weighted MR image. (**b**) Sagittal spin-echo T1-weighted MR image after gadolinium contrast injection. (**c**) Axial spin-echo T2-weighted MR image. (**d**) Coronal T2*-weighted image. Large, oval mass at the plantar aspect of the left great toe. The lesion is inhomogeneous and ill-defined at the proximal pole (**a**). After contrast injection there is marked enhancement at the periphery of the lesion (**b**). On the T2-weighted image, the whole lesion is of low signal intensity (**c**). On gradient echo sequence, the periphery of the lesion is of extremely high signal intensity This gradient echo sequence may help to distinguish fibroma from giant cell tumor of the tendon sheath because in the latter an overall low signal is expected due to the T2* effect of hemosiderin (**d**)

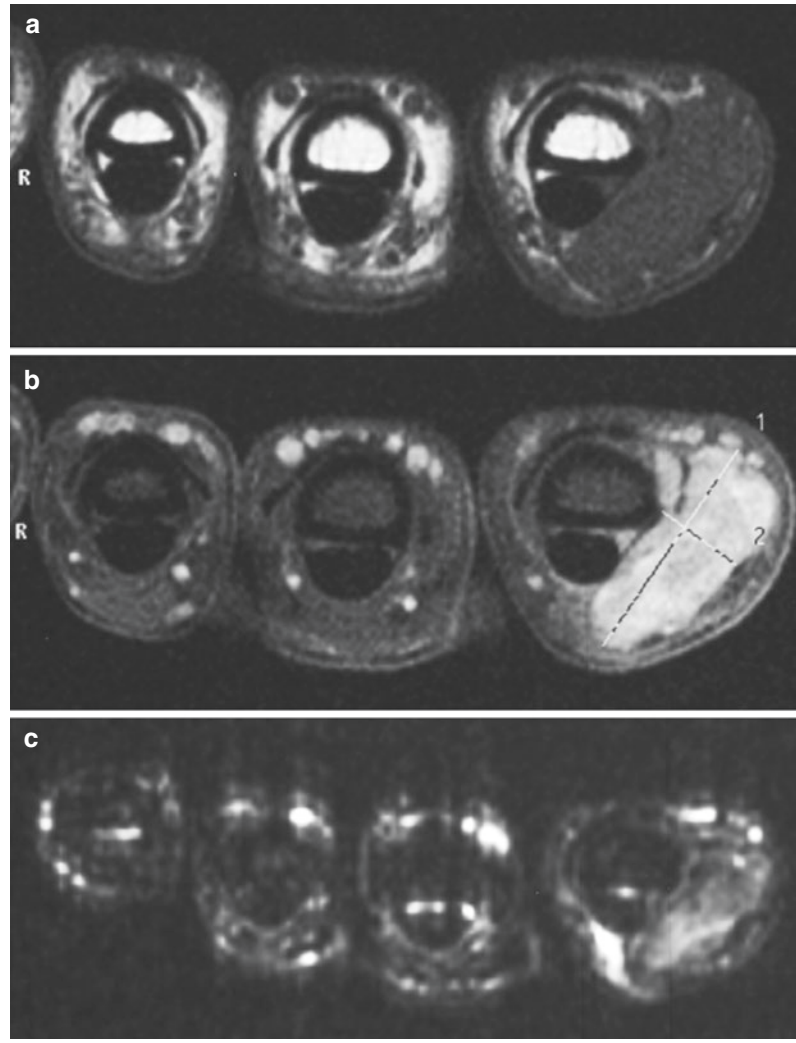

Fig. 13.14 (**a–c**) Fibroma of the tendon sheath at the volar aspect of the index finger adjacent to the flexor tendon. (**a**) Axial spin-echo T1-weighted MR image. (**b**) Axial spin-echo T1-weighted MR image after gadolinium contrast injection with fat suppression. (**c**) Axial spin-echo T2-weighted MR image with fat suppression. The lesion is of low SI on T2-weighted MR images (**c**) and enhances moderately after gadolinium contrast injection (**b**)

Microscopically, nuchal fibromas have a superficial (subcutaneous or dermal) component and consist of paucicellular, thick bundles of lobulated collagen fibers with inconspicuous fibroblasts. Entrapped adipose tissue and traumatic neuroma-like nerve proliferations are typically present. Skeletal muscle infiltration is also seen in a minority of cases. The process has a strong association with diabetes and also appears to be linked to Gardner's syndrome, fibromatosis, and dermatofibrosarcoma protuberans. Local recurrence probably reflects the persistence of local or systemic factors related to its pathogenesis [105, 131].

The MR appearance reflects the histological composition: collagen has a low SI both on T1- and T2-weighted images. Variable degree of contrast enhancement is reported. Differential diagnosis includes other soft tissue masses with low signal intensity on T2-weighted images and variable enhancement such as desmoid tumor, solitary fibrous tumor, fibroma of the tendon sheath, collagenous fibroma, neurofibroma, cicatricial fibroma, fibrosarcoma, and malignant fibrous histiocytoma [86]. Small foci of high SI on T1-weighted images are due to entrapped adipose tissue (Figs. 13.15 and 13.16). In this regard there is a strong similarity to elastofibromas.

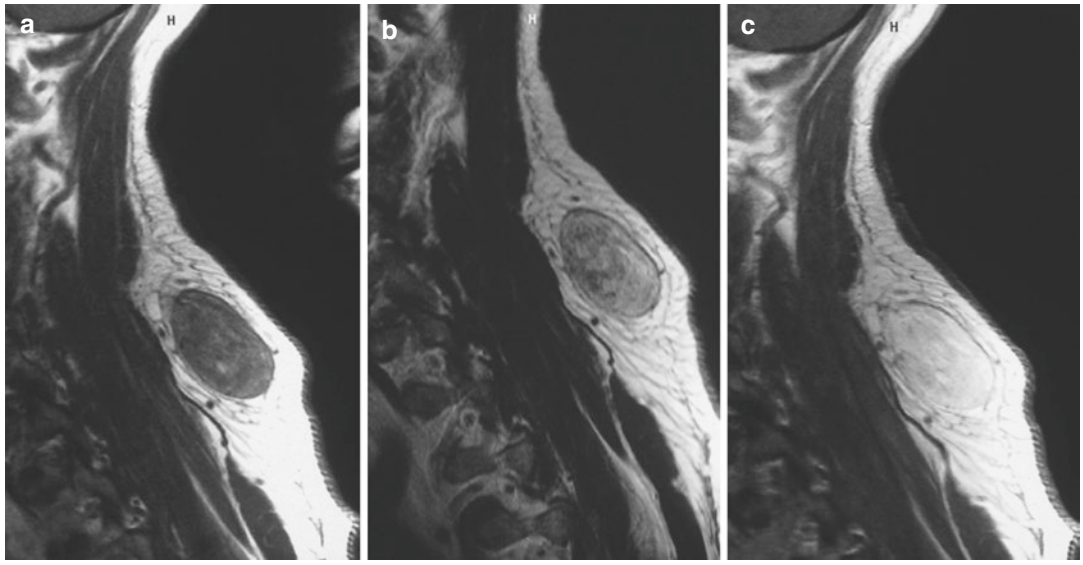

Fig. 13.15 (**a–c**) Nuchal fibroma in a 50-year-old man. (**a**) Sagittal spin-echo T1-weighted MR image. (**b**) Sagittal spin-echo T2-weighted MR image. (**c**) Sagittal spin-echo T1-weighted MR image after gadolinium contrast injection. Oval, well-delineated mass within the subcutaneous fatty tissue of the neck. There is an intermediate signal intensity on both spin-echo images owing to the mixed histological composition of entrapped fat within a collagenous mass (**a, b**). There is marked enhancement after contrast injection (**c**). Localization and MR presentation are characteristic of a nuchal fibroma

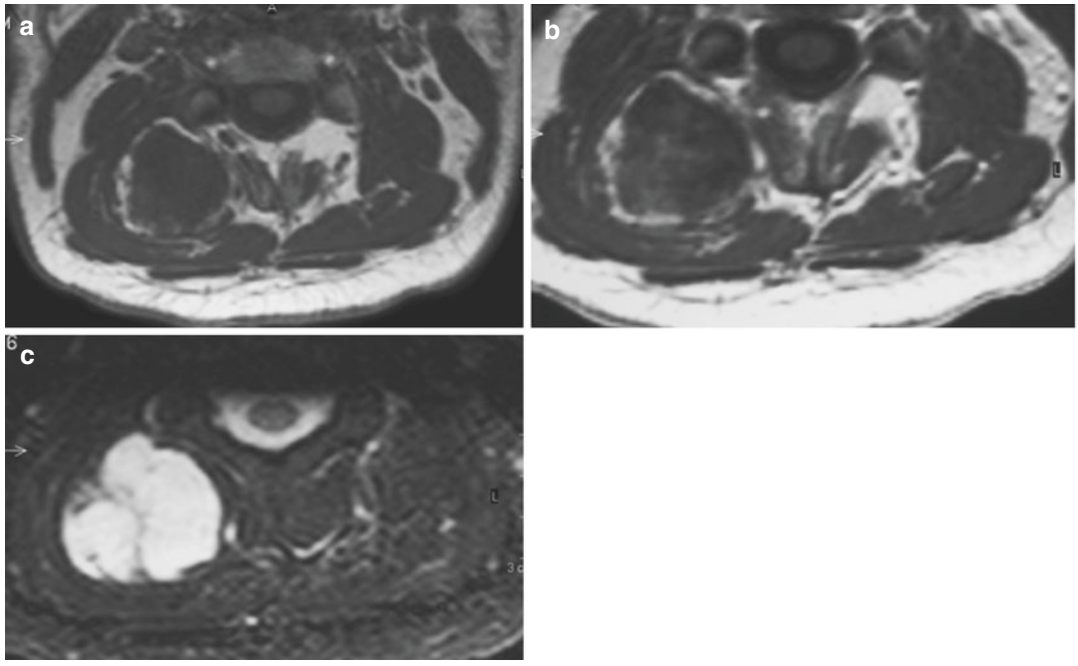

Fig. 13.16 (**a–c**) Nuchal fibroma. (**a**) Axial spin-echo T1-weighted MR image. (**b**) Axial spin-echo T1-weighted MR image after gadolinium contrast injection. (**c**) Axial short-tau inversion recovery (STIR) MR image. Atypical presentation of a nuchal fibroma with high SI on STIR sequence (**c**) and minimal, cloudy enhancement after contrast injection (**b**)

13.2.8 Desmoplastic Fibroblastoma (Collagenous Fibroma)

Desmoplastic fibroblastoma or collagenous fibroma commonly occurs in patients in the fifth and sixth decades of life, more frequent in men (75 %). The tumor often manifests as a sharply demarcated, mobile, firm, solitary mass involving the subcutaneous tissue or skeletal muscle. The common locations of the tumor are the arm, shoulder, and posterior neck or upper back. The size of reported collagenous fibromas ranges from 1 to 20 cm in the largest dimension. Histologically, the tumors appear well marginated on low-power examination. The tumor cells are relatively bland stellate- and spindle-shaped fibroblastic cells separated by densely fibrous to fibromyxoid matrix. The cellularity is low or very low, mitotic figures are very rare or absent, and tumor necrosis is not seen.

On MR images, collagenous fibroma shows areas of decreased SI on T1- and T2-weighted images and moderate to strong contrast enhancement in a heterogeneous fashion [70, 103, 165]. Because both have a high collagen content, similar MRI findings have been described in desmoid tumors (Fig. 13.17). A series of three cases has been reported with a characteristic rim enhancement thought to represent the outer capsule-like fibrous tissue of this usually noninvasive tumor [165]. Collagenous fibromas are less cellular, less vascular, and less infiltrative at their periphery and as a consequence more mobile, better circumscribed, and easier to remove than desmoids. Moreover, they occur in older (more than 40 years old) patients. Differential diagnosis is essential to prevent overtreatment in collagenous fibroma [119].

13.2.9 Calcifying Aponeurotic Fibroma

Calcifying aponeurotic fibroma is a rare, benign fibroblastic tumor usually occurring in young children and adolescents (therefore also named juvenile aponeurotic fibroma) with a male to female ratio about 2:1. It presents as a unique, hard and painless palpable mass, sized 1–3 cm, with a predilection for the volar side of the hands/fingers and feet [13]. Calcifying aponeurotic fibromas are often associated with tendons and aponeuroses and typically infiltrate the surrounding fatty, muscular, or neurovascular tissues. Histologically, a fibromatosis-like lesion with nodules of calcification is displayed on a background of hyalinized to focally chondroid stroma [37]. In the initial phase of the tumor, which is seen more often in young patients, the tumor shows infiltrative growth and often lacks calcifications, whereas in the late phase, the tumor becomes more compact and nodular, with more prominent cartilaginous differentiation and calcifications [115].

Radiography may sometimes reveal faint, stippled calcification in a focal area of soft tissue swelling, typically in the distal extremities (Fig 13.18) [111]. MR imaging is the best modality to show the extent and margin of the lesion. Signal intensity on T2-weighted images is described as a heterogeneous mixture of high and low signal and seems to be influenced by the degree of calcification and fibrous component: lower T2 signal intensities are more often seen with older age. Signal intensity on T1-weighted images is intermediate. Lesions strongly enhance after contrast medium injection allowing for delineation of the often invasive margins. Differential diagnosis includes tenosynovial giant cell tumor (showing lower signal intensities on T1- and T2-weighted images due to hemosiderin deposition), other fibromatoses, soft tissue chondroma, synovial sarcoma, and clear cell sarcoma [13]. Surgical resection is the preferred treatment. However, the propensity to invade surrounding tissues is reflected in incomplete surgical resection and (late) recurrences up to 50 %.

13.3 Fibromatoses

Fibromatoses cover a wide range of benign fibroblastic proliferations. They are classified according to Enzinger and Weiss into superficial and deep types and are further subdivided according to anatomical location:

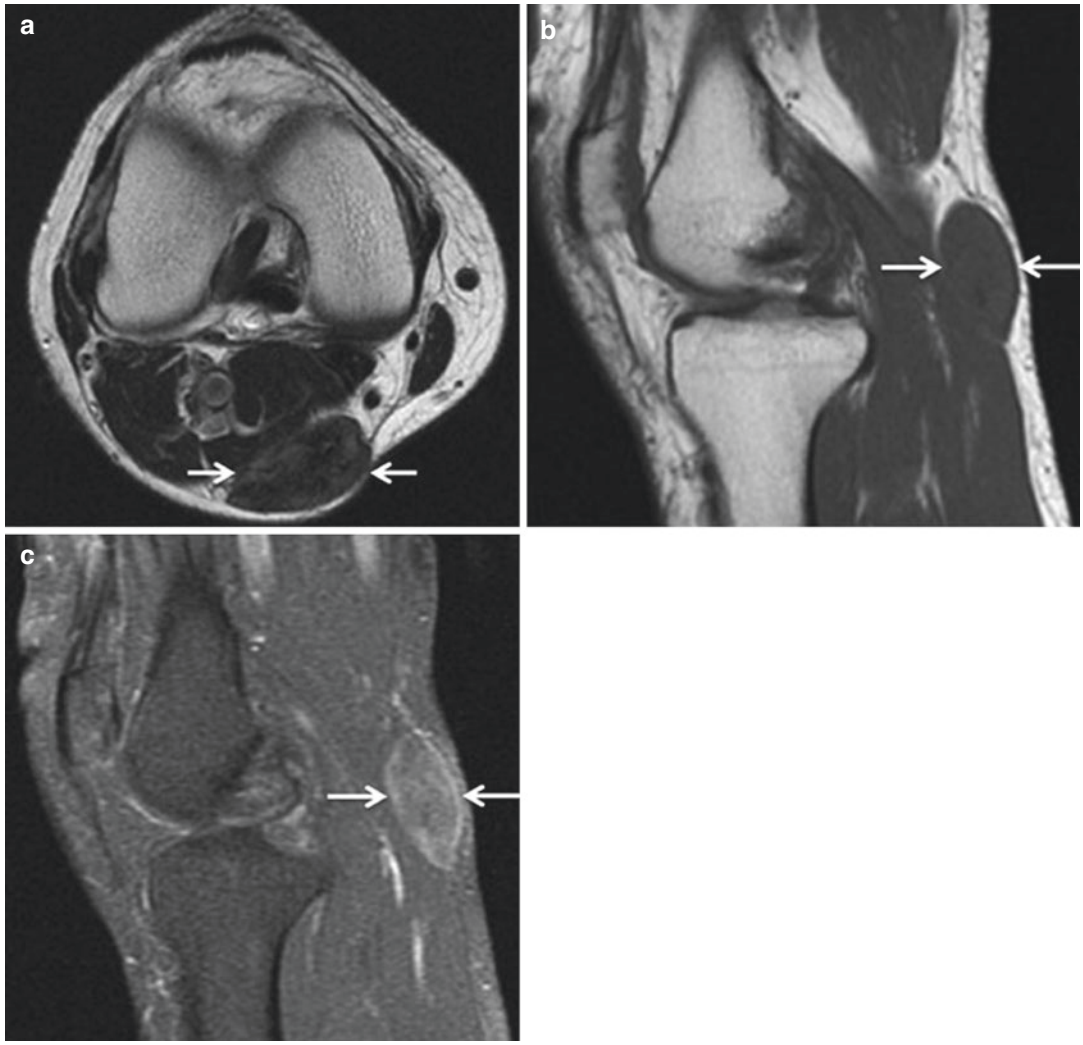

Fig. 13.17 (**a–c**) Desmoplastic fibroblastoma. A 53-year-old man with collagenous fibroma of the right knee. (**a**) Axial T2-weighted image shows low to intermediate signal intensity of a clearly margined mass (*white arrows*). (**b**) Sagittal T1-weighted image appears isointense to the muscle (*white arrows*). (**c**) Sagittal post-contrast T1-weighted image shows mild internal enhancement with rim enhancement (*white arrows*). Morphology and MR presentation do not allow differentiation between collagenous fibroma and extra-abdominal desmoids (Reprinted with permission from Yamamoto et al. [165])

1. Superficial (fascial) fibromatosis
   (a) Palmar fibromatosis (Dupuytren's contracture)
   (b) Plantar fibromatosis (Ledderhose's disease)
   (c) Penile fibromatosis (Peyronie disease)
   (d) Knuckle pads
2. Deep (musculoaponeurotic) fibromatosis
   (a) Extra-abdominal fibromatosis
   (b) Abdominal fibromatosis
   (c) Intra-abdominal fibromatosis:
   – Pelvic fibromatosis
   – Mesenteric fibromatosis
   – Gardner's syndrome

Although both superficial and deep lesions have a similar microscopic appearance, superficial lesions are slow growing, while deep ones have a more aggressive biological behavior, between that of fibrosarcomas and fibromas [15].

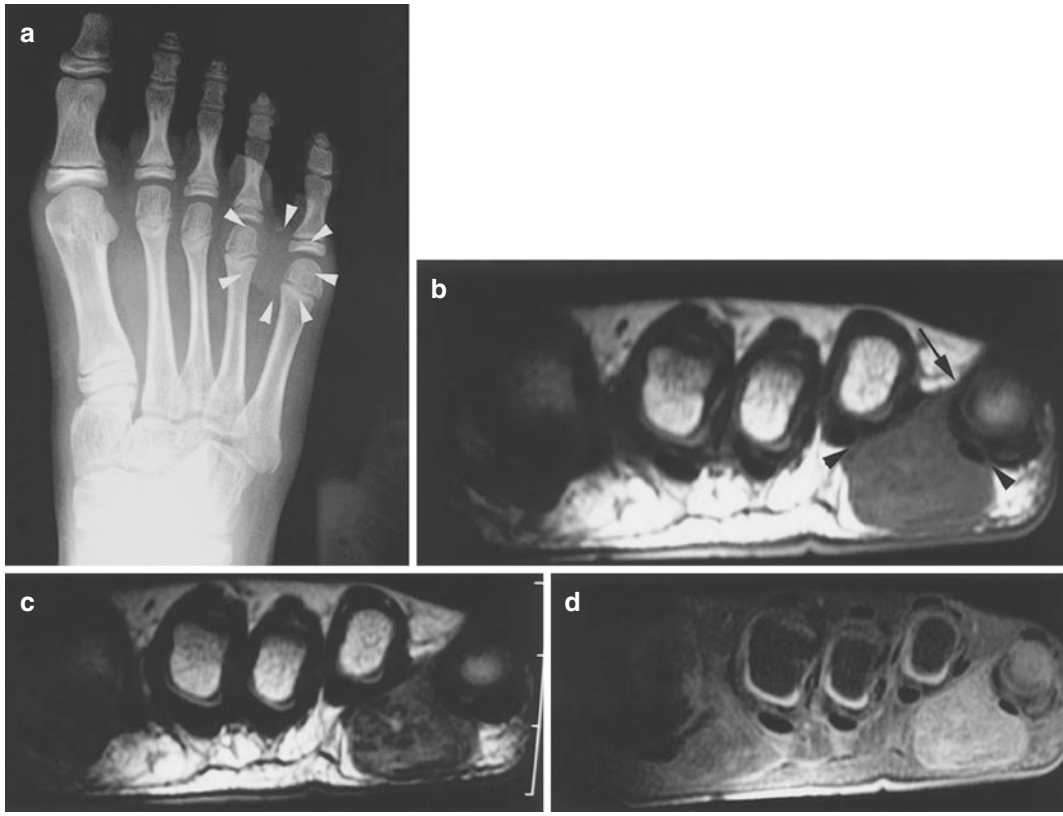

Fig. 13.18 (**a–d**) Calcifying aponeurotic fibroma. A 10-year-old girl presented with a firm, elastic, hard mass at the plantar side of the foot. (**a**) Radiographs revealed faint calcification in the mass (*arrowheads*) (**b**) T1-weighted MR image revealed an isointense lesion adherent to the flexor tendon and invading the interdigital webspace. Most of the border appeared well-defined in this case (*unusual*). (**c**) On T2-weighted images, there is a heterogeneous mixture of high- and low-signal intensity areas (**d**) Post-contrast T1-weighted images showed significant enhancement throughout the lesion (Reprinted with permission from Morii et al. [111])

Division into abdominal and extra-abdominal desmoids is arbitrary, since the lesions are histologically alike [10].

Fibromatoses are uncommon lesions, constituting 0.03 % of all neoplasms. They are found in young adults, with a peak incidence at 30 years. There is no sex predominance, and most lesions are solitary, although synchronous multicentric lesions have been reported. A familial tendency has been observed. Local recurrence after surgery is seen in as many as 50 % of patients [81].

Key criteria that establish the diagnosis are growth pattern, relationship with surrounding tissues, and cytological features. Lesions consist of uniform fibroblasts proliferating in a parallel way and intermingled with variable amounts of collagen. No atypical or hyperchromatic nuclei are found, while mitoses are infrequent. Generally, the most cellular areas are present in the center of the lesion, whereas the periphery has less numerous fibroblasts and greater amounts of dense collagen [45]. Although fibromatoses are histologically benign, their relationship to adjacent tissue is marked by interdigitating and infiltrative growth. Penile fibromatosis and intra-abdominal fibromatosis will not be discussed, since these do not belong to the locomotor system [127].

On ultrasound scans, fibromatoses appear as masses with low, medium, or high echogenicity

and smooth, sharply defined borders. On CT images, the masses are either ill-defined or well circumscribed. Before contrast administration, desmoids show variable attenuation. After contrast administration, lesions usually have a higher attenuation than that of adjacent muscle [10].

In an attempt to explain the variable CT appearance of these lesions, Francis et al. have carried out a retrospective analysis of CT findings and histopathological features in nine patients with fibromatosis. In three of four patients who had precontrast CT scans, the tumors were hyperdense relative to the muscle, while in one patient, the lesion was hypodense. The postenhancement appearance was variable. The pathological specimens have been analyzed and graded for collagen content, cellular content, tumor necrosis, and tumor vascularity. No consistent relationship can be established between the CT appearance of these lesions and their histological appearance [45].

On MR images, most lesions demonstrate slightly increased SI relative to the skeletal muscle on T1-weighted images and intermediate SI on T2-weighted images. The slight increase in SI on T1-weighted images is much less than that seen in lipomas and subacute hemorrhages. Enhancement pattern after contrast administration is variable [113, 157].

Increased SI on T2-weighted images is seen in hypercellular lesions. Lesions that are hypointense or contain hypointense foci (linear or curvilinear) on both spin-echo sequences are found to be relatively hypocellular with abundant collagen. As a consequence, most lesions are rather inhomogeneous. Although usually well demarcated on MR images, microscopically fibromatosis is seen to invade adjacent structures [127].

The conditions that deserve consideration in the differential diagnosis of intra- and extra-abdominal desmoids are malignant lesions such as fibrosarcoma, rhabdomyosarcoma, synoviosarcoma, liposarcoma, myxofibrosarcoma, lymphoma, and metastases and benign lesions such as neurofibroma, neuroma and leiomyoma, and acute hematoma of the rectus sheath and chest wall [10].

13.3.1 Palmar Fibromatosis

Palmar fibromatosis or Dupuytren's contracture primarily involves palmar aponeurosis of the hand and its extensions. Usually the disease is diagnosed clinically on the basis of characteristic history and physical examination. The earliest clinical manifestation is the appearance of a subcutaneous nodule in the palm of the hand, most frequently over the fourth and fifth ray. As the disorder progresses, the overlying skin thickens and retracts, and a cord forms, producing progressive flexion contracture of the affected ray (Fig. 13.19).

Palmar fibromatosis tends to affect adults, with a rapid increase in incidence with advancing age. It is bilateral in 40–60 % of cases. The condition is by far more frequent in men and is most common in Northern Europe. Pathogenesis in both palmar and plantar fibromatoses includes a genetic component, with family history and chromosome aberrations in 50 % of cases.

Histologically, the nodules are quite cellular, composed of whorls of proliferative myofibroblasts. Cords contain a large amount of collagen and are hypocellular. The condition is treated surgically, but the recurrence rate is high (30–40 %). The recurrence rate of lesions with mitotically active, cellular nodules is far higher (70 %) than that of hypocellular lesions.

The appearance of the nodules and cords on MR images and the correlation between the SI and the lesion's degree of cellularity have been described by Yacoe et al. [164]. On MR images, the cords had a uniformly low SI (similar to the SI of the tendon) on both T1- and T2-weighted images. Most nodules had an intermediate SI (similar to that of the muscle) on both T1- and T2-weighted images. Some nodules had a low to intermediate SI on T1-weighted images (slightly higher than that of the tendon) and a low SI on T2-weighted images. Few nodules had a low SI on both T1- and T2-weighted images and were hypocellular on histological examination.

Signal characteristics of the lesions correlate with the degree of cellularity. The preoperative assessment of cellularity may be of prognostic

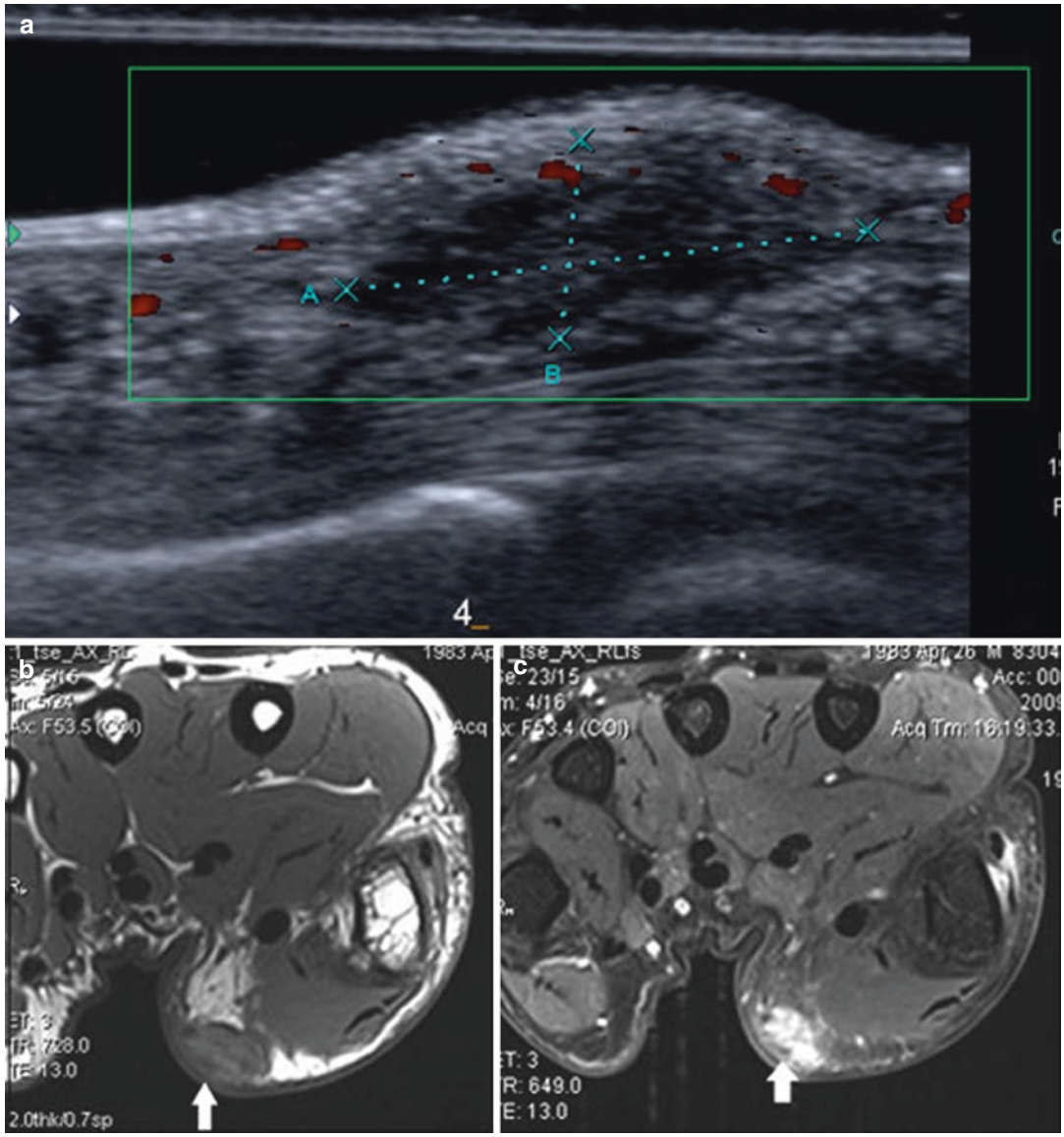

Fig. 13.19 (**a–c**) Palmar fibromatosis. (**a**) Longitudinal Doppler ultrasound. Hypoechoic nodule adjacent to the flexor tendon of the palm of the hand (*third ray*). (**b**) Axial SE T1-WI in another patient shows a hypointense lesion at the palmar aspect of the thumb (*arrow*). (**c**) Axial FS SE T1-WI after intravenous administration of gadolinium contrast medium shows diffuse enhancement (*arrow*) (Reprinted with permission from Vanhoenacker et al. [153])

significance, because highly cellular lesions tend to have a higher rate of recurrence after surgery than hypocellular lesions. As a consequence surgery may be delayed until the lesion matures and becomes more hypocellular and collagenous [44].

13.3.2 Plantar Fibromatosis

Plantar fibromatosis, also called Ledderhose's disease, is a benign, fibroblastic, proliferative, and locally invasive disorder characterized by the

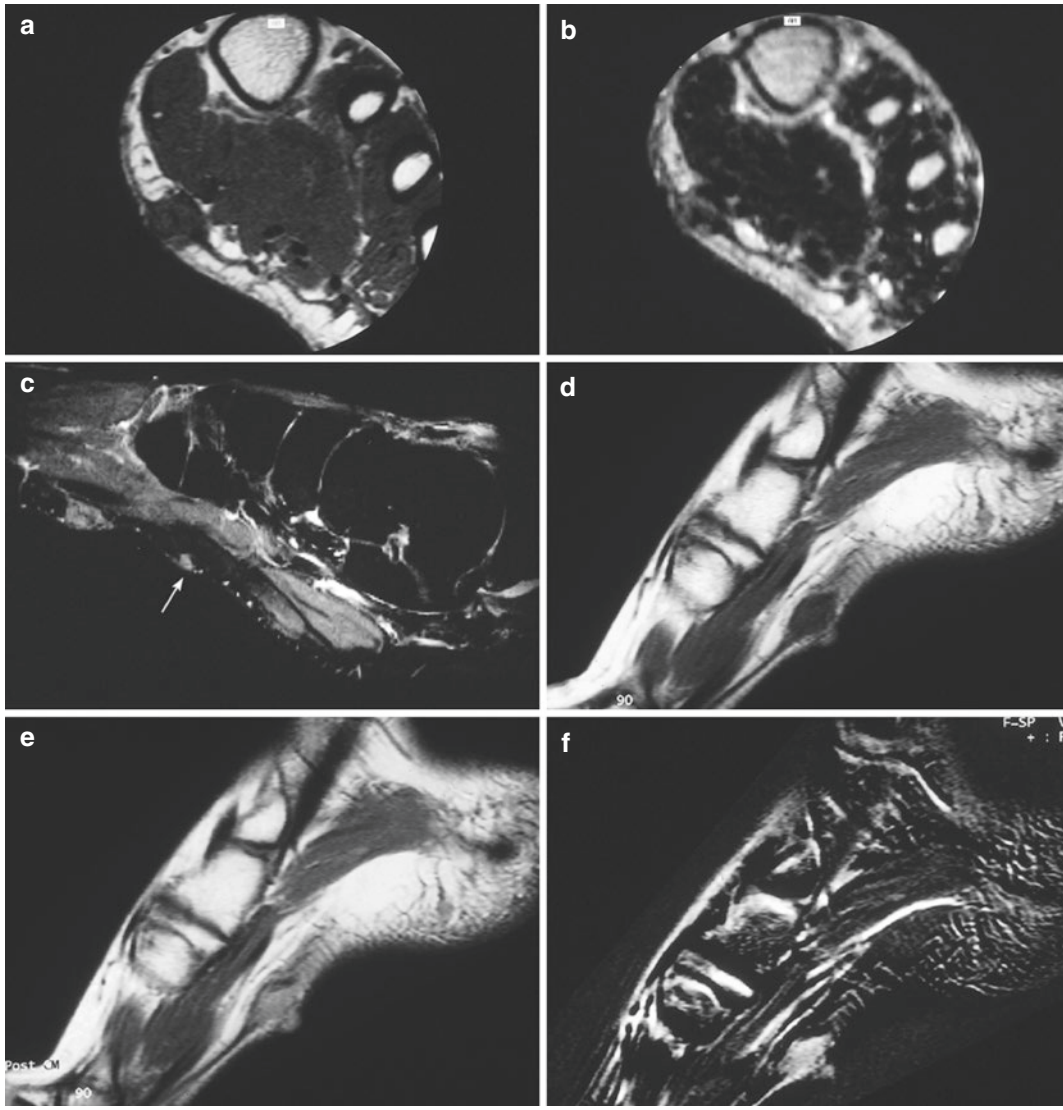

Fig. 13.20 (**a–f**) Two cases of plantar fibromatosis in a 37-year-old-man (**a–c**) and in a 13-year-old girl (**d–f**). (**a**) Axial spin-echo T1-weighted MR image. (**b**) Axial turbo spin-echo T2-weighted MR image. (**c**) Sagittal STIR MR images. (**d**) Sagittal spin-echo T1-weighted MR image. (**e**) Sagittal spin-echo T1-weighted MR image after gadolinium contrast injection. (**f**) Sagittal subtraction MR image. Subcutaneous nodular lesion of intermediate signal intensity at the sole of the foot in apposition with the plantar aponeurosis. The lesion is isointense to the muscle on the T1-weighted image (**a**) and of higher variable signal intensity on the T2-weighted (**b**) and STIR (**c**) images. On the STIR image, there is a smaller second lesion having similar signal characteristics (**c**; *arrow*). The second case reveals a lesion centered on the plantar fascia, isointense to the muscle on the T1-weighted image (**d**), with marked enhancement after gadolinium contrast injection (**e**). This is also nicely demonstrated on the subtraction image (**f**)

replacement of elements of the plantar aponeurosis by abnormal fibrous tissue, which slowly invades the skin and the deep structures (Fig. 13.20).

The plantar aponeurosis is a strong band which originates at the inner tubercle of the calcaneus and contains two layers: a superficial layer which extends to the four smaller toes and a

deeper layer which runs from lateral to medial and appears as a separate band to the great toe [89]. On ultrasound scans, the plantar aponeurosis is noted as a bright linear interface, approximately 5–8 mm from the surface of the sole [128]. On MR images the aponeurosis is seen as a thin linear strip of low SI that originates at the inferior border of the calcaneus and inserts into the distal flexor tendons near the metatarsophalangeal joints.

The etiology of plantar fibromatosis is unknown, but, as in palmar fibromatosis, trauma, neuropathy, faulty development, alcoholism, and infection have been proposed as etiologic factors. Pathogenesis in both palmar and plantar fibromatoses includes a genetic component, with family history and chromosome aberrations in 50 % of the cases. Most lesions are located at the medial aspect and just superficial to the aponeurosis. Involvement is bilateral in 19 % of patients and multiple in 32 %. There is a higher prevalence in white and middle-aged (fourth decade) male patients and in patients who have epilepsy. There is also an association with knuckle pads in 5 %, with palmar fibromatosis in 10–50 %, and with penile fibromatosis (Peyronie disease) in 5–10 % of patients. There are no reports of malignant transformation. Clinically, plantar fibromatosis presents as a nonmobile, irregular, single, or multinodular lesion located in the longitudinal medial arch of the plantar surface of the foot. The lesion frequently consists of small nodules merged with each other and with the fascial bundles [5]. Although some authors report pain as a main symptom in one-third of patients, most lesions are asymptomatic and are discovered incidentally by palpation. Unlike palmar fibromatosis, this condition rarely causes contracture of the toes.

Microscopically, the lesion consists of a proliferation of well-differentiated hyperplastic, fibroblast-like cells or myofibroblasts with an infiltrative pattern of growth and usually an abundance of proliferating cells between the heavy strands of relatively hypocellular, mature collagen. Collagen is present in the actively growing foci in every specimen: quantitatively, it usually is in an inverse ratio to the degree of cellularity [5]. Mitotic figures, necrosis, and vascular infiltration are uncommon. A cellular vascular cuffing and the presence of perivascular inflammatory cells have been described by Allen [5]. The natural history comprises a proliferative phase with increased fibroblastic activity and cellular proliferation, an involutional phase, and a residual phase in which fibroblastic activity is reduced and maturation of the collagen is noted.

If this condition is treated by simple excision, there is a recurrence rate of 50–65 %, frequently resulting in a more aggressive form. Infiltration of neighboring structures is more frequently seen in recurrent lesions [5]. Wide, radical excision, encompassing 0.5 cm of surrounding, normal-appearing fascia, is, therefore, the treatment of choice.

On ultrasound images, plantar fibromatosis is seen as a well-defined, hypoechoic nodule or mass superficial to the medial slip of the plantar aponeurosis. Plantar fibromatosis exhibits a consistent and characteristic appearance on MR images [112]. Most lesions are heterogeneous, with an overall SI equal to or slightly higher than that of the muscle on both spin-echo T1- and (spin-echo and fast spin-echo) T2-weighted images (Fig. 13.20a, b). SI on T2-weighted images reflects the stage of the disease. The proliferative phase is characterized by higher cellularity, resulting in higher SI. The low SI on T2-weighted images of the involutional and residual phases is attributed to the hypocellularity and presence of abundant collagen. Lesions are slightly hyperintense to the muscle on short-tau inversion recovery (STIR) sequences (Fig. 13.20c). After intravenous injection of Gd contrast, enhancement is inversely related to the stage of fibromatosis. "Burned-out" lesions with abundant collagen fibers enhance to a lesser degree than lesions in the proliferative phase (Fig. 13.20e, f).

Differential diagnosis has to be made between plantar fibromatosis in the residual phase, callus, and scarring. Since plantar fibromatosis in the proliferative phase may be an extremely cellular and infiltrative lesion, it has to be differentiated from aggressive fibromatosis and fibrosarcoma. If the lesion is associated

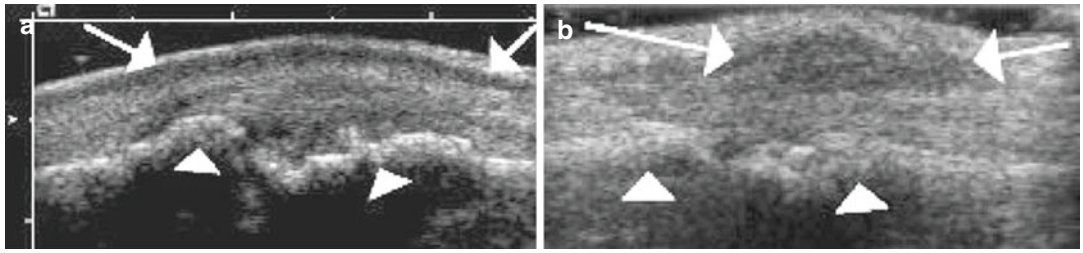

Fig. 13.21 Knuckle pads. Longitudinal ultrasound scans of finger PIP joints in two patients. Note a band-like diffuse thickening with a linear hypoechogenicity (**a**) and an ovoid, hypoechoic thickening (**b**) of the dorsal subcutaneous tissues overlying the interphalangeal joints. No distended joint capsule or increased joint fluid is seen, enabling the differentiation from synovitis (Reprinted with permission from Lopez-Ben et al. [94])

with palmar fibromatosis or Peyronie disease, or if both feet are involved, the diagnosis is almost certain [149].

13.3.3 Knuckle Pads

Knuckle pads consist of a flat or dome-shaped fibrous thickening on the dorsal aspect of the proximal interphalangeal or metacarpophalangeal joints. They are frequently associated with palmar and plantar fibromatosis. Microscopically, this condition resembles the latter fibromatosis.

On ultrasound, a platelike or ovoid thickening with a hypoechoic appearance is seen in the subcutaneous tissue superficial to the involved joints [19] (Fig. 13.21).

When confronted with periarticular soft tissue swelling at the small joints of the fingers, a clinician may confuse knuckle pads with synovitis as seen with rheumatological conditions: an ultrasound examination readily differentiates knuckle pads from synovitis [94]. MR imaging demonstrates focal thickening with intermediate signal intensity compared with muscle on T1- and T2-weighted sequences and with moderate enhancement [19].

13.3.4 Extra-abdominal Desmoid Tumors

Extra-abdominal desmoids are rare soft tissue tumors arising from the connective tissue of the muscle, overlying fascia, or aponeurosis. They have also been described as desmoid tumor, aggressive fibromatosis, or musculoaponeurotic fibromatosis. The term "desmoid" means band-like or tendon-like lesion [24].

The reported incidence of extra-abdominal desmoids is between three and four cases per million annually. The peak incidence is between ages 25 and 40 years. Although some authors report a predominance in women of childbearing age [31, 58], men and women are almost equally affected. Its cause is unknown, but surgical or accidental trauma, pregnancy, and estrogenic hormones are known associations. We have seen a recurrent desmoid tumor demonstrating an important increase in size (400 %) during pregnancy, while most desmoids regress after the menopause [136].

The localization of a large number of extra-abdominal desmoids at the lateral aspect of the shoulder and the buttocks supports the idea of a posttraumatic etiology. The notion of an inherited defect in connective tissue formation is supported by some authors, and a genetic basis for at least some desmoid tumors is suggested by Gardner's syndrome. The term Gardner's syndrome is used to describe extracolonic manifestations of familial adenomatous polyposis such as desmoid tumors, bony osteomas, dermoids and epidermoids, and/or nuchal fibromas together with abdominal wall desmoids and mesenteric desmoids [1, 148]. Some authors have hypothesized that an underlying mesenchymal defect may result in an imbalance in growth factors, resulting in multiple proliferative diseases, and may be responsible for the

coexistence of desmoids, gastrointestinal polyps/colorectal cancer, and breast cancer [125]. Others have postulated a ciliary dysfunction as the underlying pathogenetic mechanism of the extracolonic manifestations in patients with familial adenomatous polyposis [54].

Extra-abdominal desmoids arise most commonly in the lower limb or limb girdle and in the shoulder region. In cases of lower limb localization, a preference for the region of the sciatic nerve is reported [148]. Our own series consists of 30 extra-abdominal desmoid tumors in 26 patients. The localizations were as follows: head and neck region ($n=1$), upper limb ($n=4$), trunk ($n=6$), pelvis ($n=8$), and lower limb ($n=11$). Extra-abdominal desmoids never metastasize, but a multicentric, synchronous, and metachronous presentation has been reported [142, 156]. In this condition, second tumor localizations generally develop proximally to the primary lesion. In our series, 5 of 26 patients had multiple localizations.

Bone involvement is not uncommon and has been reported in up to 37 % of patients. In addition, primary intramedullary, juxtacortical, and periarticular desmoids are found, which are histologically indistinguishable from soft tissue desmoids. In the same way, bone desmoids can extend into the soft tissues just as soft tissue desmoids can involve the bone [27].

Microscopically, extra-abdominal desmoids consist of elongated spindle-shaped cells (fibroblasts) of uniform appearance, surrounded and separated from each other by varying amounts of collagen. Dense collagen is found at the periphery and fibroblasts at the center [81]. Conversely, the center of the lesions may contain dense collagen, whereas the periphery may be composed of fibroblasts [148]. In addition, myxoid change, focal hemorrhage, increased vascularity, and focal inflammation may be seen [81]. Immunohistochemistry staining was positive for actin, consistent with myofibroblastic differentiation in extra-abdominal desmoid tumors [156]. Despite their benign microscopic appearance, extra-abdominal desmoids have an aggressive behavior, which is expressed as large tumoral growth, infiltration of neighboring tissues, and a high incidence of postsurgical recurrence (between 25 and 68 %). Most recurrent tumors have a different behavior and morphology. In our series they show an increased frequency of extracompartmental spread, grow considerably faster than primary tumors, and have a tendency to invade the bone more frequently.

In a retrospective study of 138 patients with extra-abdominal desmoids, 11 died as a consequence of locally uncontrolled tumor growth [124]. Kim [77] has retrospectively analyzed the clinical records and MRI findings in 40 patients (8 juveniles, 32 adults) with proven desmoid tumor. In his series, recurrences in the juvenile patients were more often multiple (50 % versus 12 %) and appeared significantly earlier than in the adult patients.

On ultrasound scans, extra-abdominal desmoids may be well-defined or poorly defined and may show variable echogenicity because of variable degrees of cellularity, matrix water content, and collagen. In many cases, marked shadowing from the surface of the lesion, a result of the large amount of dense collagen tissue in the tumor, totally obscures the mass [43].

Because of the variability in tumor composition, the lesions have variable attenuation and enhancement on CT scans [2]. Duda has reported that extra-abdominal desmoids are iso- or hypodense relative to the muscle and enhance to 100–110 Hounsfield units (HU) after injection of iodinated contrast material [28].

On MR images, the appearance of extra-abdominal desmoids varies [24, 117]. There are remarkable differences in shape in various patients as well as in different locations in a given patient with multicentric extra-abdominal desmoids. Likewise, for a given lesion, shape may vary on follow-up examinations. The infiltrative pattern is significantly more common in juvenile patients (63 %), whereas the nodular pattern is more frequent in the adult patients (81 %) [77, 106]. In our series, the shape of the lesions was fusiform-ovoid or dumbbell and irregular or stellate when located in the subcutis (Fig. 13.22). The mean maximum diameter was 72 mm. The "sunburst" extensions of subcutaneous desmoid tumors spread along the underlying fascia (fascial

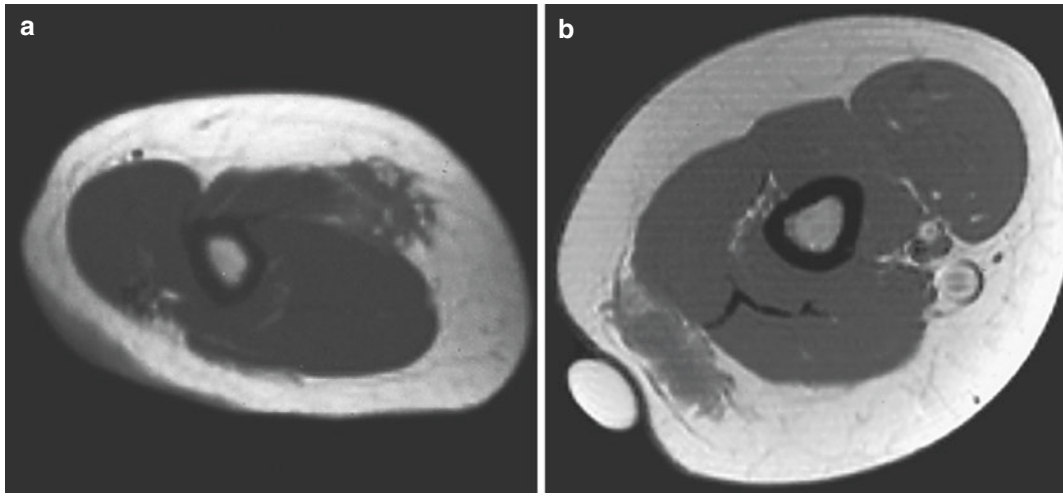

Fig. 13.22 (**a, b**) Desmoid of the upper arm (**a**) in a 23-year-old woman and (**b**) in a 44-year-old woman. (**a**) Axial spin-echo T1-weighted MR image. (**b**) Axial spin-echo T1-weighted MR image after gadolinium contrast injection. In the first patient, there is a stellar, infiltrating lesion within the subcutaneous fat of the deltoid region in close contact with the adjacent muscle fascia (**a**). In the second patient, there is a stellar, nodular infiltrating lesion within the subcutaneous fat of the deltoid region. The fat plane between the lesion and the adjacent muscle fascia is blurred (**b**). These two cases of superficial, stellar desmoid in the deltoid region with infiltration of neighboring fat and muscle fascia illustrate the characteristic shape and location of superficial aggressive fibromatosis

tail sign) and along the septa of the subcutaneous fat tissue, making complete surgical excision particularly difficult [106].

In the reported cases, extra-abdominal desmoids appear hypo- or isointense to the muscle on spin-echo T1-weighted images. SI on T2-weighted images is mostly intermediate, although very low and extremely high signal intensities have been noted occasionally. Low SI, patchy, linear, or curvilinear areas on T2-weighted images correspond to hypocellular tissue and dense collagen. On both spin-echo sequences, but predominantly on T2-weighted images, extra-abdominal desmoids are inhomogeneous, mostly with higher SI in the central part (cellular) than at the periphery (collagenous) [58, 81] (Figs. 13.23, 13.24, and 13.25).

After a retrospective study of 36 patients with histologically proven extra-abdominal desmoids, Hartman et al. have concluded that on MR images, the desmoids showed inhomogeneous SI (97 %), poor margination (89 %), neurovascular involvement (58 %), and bone involvement (37 %). Fibrosis was present in 88 % of primary desmoids and 90 % of recurrent lesions, and intermediate SI (greater than that of the muscle and lower than that of fat) was present in 75 % and 50 % of these, respectively [57].

In our personal study of 30 desmoid tumors, MR signal characteristics were variable. On T1-weighted images, lesions were usually almost homogeneous or homogeneous ($n=25$). The overall SI was rated as equal to SI of the muscle in 21 cases. The SIs on T2-weighted images mostly were heterogeneously distributed ($n=24$), with an overall SI slightly lower than ($n=15$) or equal to ($n=8$) fat. Hypointense areas were mostly curvilinear to irregular and may have a central ($n=4$) or peripheral ($n=3$) distribution within the lesion. Two cases with central low-intensity areas also show a low-SI peripheral band. The low-SI areas mostly comprise 0–20 % of the lesion ($n=14$).

There are few reports regarding the use of contrast agents in extra-abdominal desmoids. In our series, all desmoid tumors showed a moderate to strong enhancement on spin-echo Gd T1-weighted images, except for the areas of low SI on T2-weighted images, which remained unenhanced. Enhancement was more pronounced

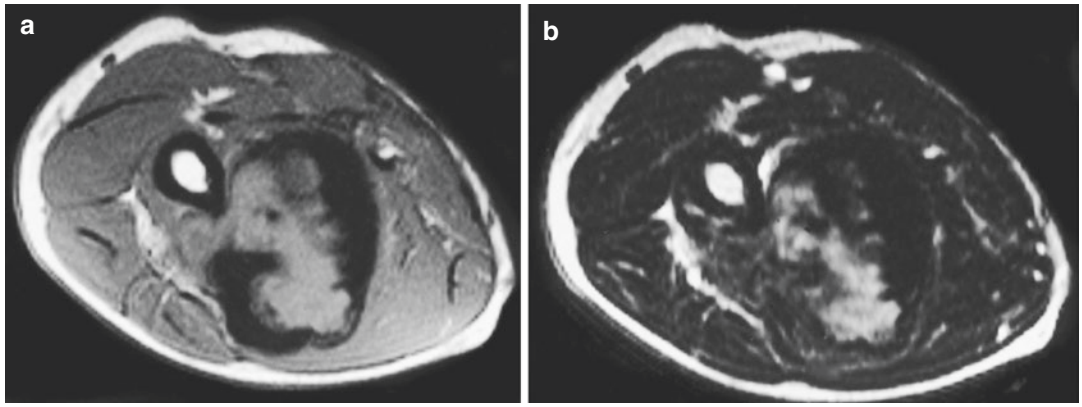

Fig. 13.23 (**a, b**) Desmoid of the forearm in a 71-year-old man. (**a**) Axial spin-echo T1-weighted MR image. (**b**) Axial spin-echo T2-weighted MR image. On the T1-weighted image, there is a large mass at the volar aspect of the forearm adjacent to the interosseous membrane, with a rim of low signal intensity at the periphery of the lesion (**a**). On the T2-weighted image, the peripheral rim remains hypointense, while the central part is of higher signal intensity (**b**). This case illustrates a pattern of natural evolution where dense collagen is responsible for low signal intensity at the periphery of the lesion on all pulse sequences

in the areas of high SI on spin-echo T2-weighted images. As a result, inhomogeneity was even better demonstrated on spin-echo Gd T1-weighted images (Figs. 13.22, 13.24, and 13.25). On follow-up examinations, the inhomogeneous pattern of contrast enhancement became more evident and paralleled the changes in SI noted on spin-echo T2-weighted images.

In cases of multicentric presentation, the distal lesion tended to be more heterogeneous and hypointense on T2-weighted images than the proximal one. Since the low SI of extra-abdominal desmoids on spin-echo T2-weighted images is thought to be a consequence of an increased amount of collagen, we presume that in these cases the distal localization is more collagenous than the proximal one.

On follow-up MR examination, the distal lesions showed a tendency to shrink, as may be concluded from their size and progressive serration of their borders. In contrast, the proximal lesions increased with time and became more convex. Moreover, during follow-up examination, the extent of the hypointense areas in the distal lesions increased, and this was associated with a further decrease in SI on spin-echo T2-weighted images.

The same phenomenon has been described by Feld in a patient with multicentric involvement in which a gluteal lesion manifested low SI on T2-weighted images, whereas a lesion in the psoas muscle showed heterogeneous, increased SI on T2-weighted images. Histological examination of the gluteal lesion revealed dense collagenous bundles, with cellular areas comprising less than 20 % of the tumor, while the lesion in the psoas muscle showed less collagenization and a more pronounced cellularity [36].

The amount of collagen in a given lesion may be reflected by SI on spin-echo T2-weighted images. This correlation between the amount of collagen and SI on spin-echo T2-weighted images suggests that older localizations of extra-abdominal desmoids (mature fibromatosis) show an increase in collagen that suggests progressive fibrosis, while, in cases of multicentric presentation, the proximal lesion seems to be less collagenous compared with the distal one (Fig. 13.26).

The relationship between cellularity and SI on T2-weighted images, as described by several authors [28, 36], could not be confirmed in our own series. Subtle changes in cellularity cannot explain substantial variance in SI on T2-weighted images, and, although there is a difference in cellularity between young and older desmoids and between primary and recurrent ones, the overall cellularity of desmoids is low. Differences in SI between different tumor components, between

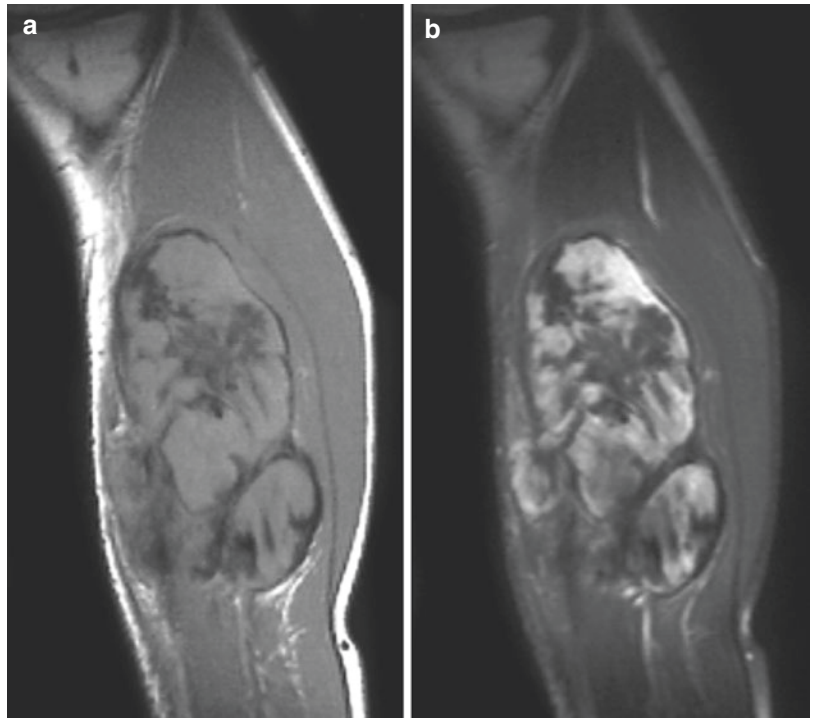

Fig. 13.24 (**a, b**) Desmoid of the calf in a 23-year-old man. (**a**) Sagittal spin-echo T2-weighted MR image. (**b**) Sagittal spin-echo T1-weighted MR image with fat suppression after gadolinium contrast injection. On the T2-weighted image, there is a polylobular mass with central areas of low signal intensity within each nodule and presence of a low-signal-intensity capsule around the lesion (**a**). After contrast injection there is marked enhancement of the peripheral zones without enhancement of the central scar-like areas (**b**). This case of deeply seated juxtacortical desmoid (adjacent to the dorsal aspect of the tibial cortex) illustrates another pattern of natural evolution where collagen is found in the center and less collagenous parts at the periphery of the lesion. Furthermore, it illustrates a frequent finding that areas of higher signal intensity on T2-weighted images enhance after gadolinium administration, whereas areas of low signal intensity on T2-weighted images do not enhance and remain hypointense on all pulse sequences

asynchronous multicentric desmoids, and between primary and recurrent desmoids will therefore be a consequence of a combination of variability in cellularity, amount of collagen, water content of the extracellular space, myxoid substance, and vascularity.

Periarticular desmoid tumors have to be differentiated from other lesions with low SI on T2-weighted images, such as pigmented villonodular synovitis, giant cell tumor of the tendon sheath, hemorrhagic synovitis, and hemophilic arthropathy [167]. Differential diagnosis of subcutaneous desmoids includes other superficial fibromatoses, such as nodular fasciitis, injection granulomas, granuloma annulare, pentazocine-induced myopathy with subcutaneous fibrosis, and postsurgical fibrosis [21, 152].

In a study comprising 13 patients, desmoid tumors usually appeared moderately hypermetabolic on FDG PET imaging even in larger masses, while smaller tumors tended to appear hypometabolic [163].

Desmoid tumors preferably are studied with MRI, diagnosed with imaged-guided biopsy, and treated according to the advice of a local multidisciplinary sarcoma unit [29]. Surgical resection with negative margins was previously considered the best treatment. However, significant functional and cosmetic consequences and a high local recurrence rate of 50 % have led to a clear preference for a "watch and wait" policy,

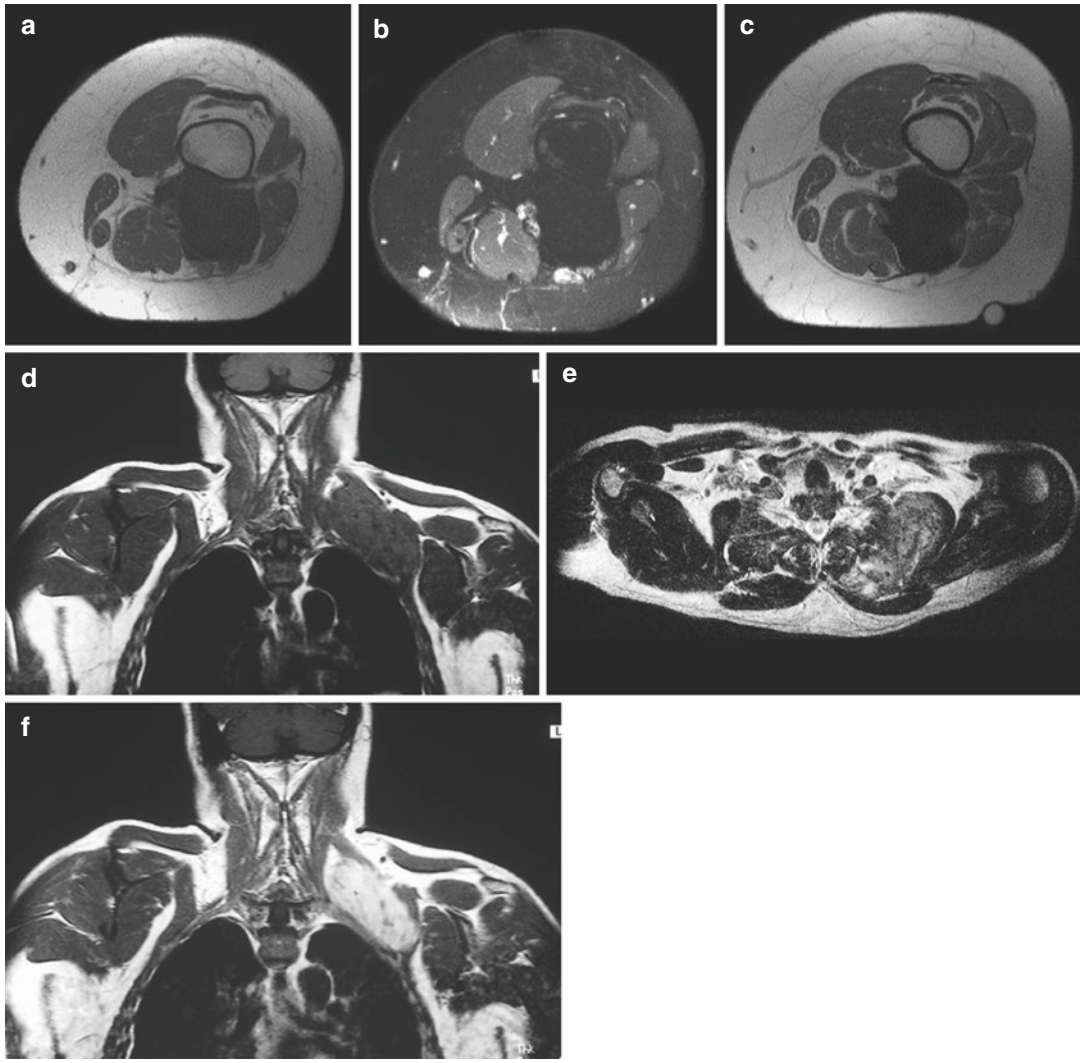

Fig. 13.25 (**a–f**) Two cases of desmoid, one located at the hamstrings (**a–c**) and the other at the left serratus muscle (**d–f**). (**a**) Axial spin-echo T1-weighted MR image. (**b**) Axial spin-echo T2-weighted MR image with fat suppression. (**c**) Axial spin-echo T1-weighted MR image, after gadolinium contrast injection. (**d**) Coronal spin-echo T1-weighted MR image. (**e**) Axial turbo spin-echo T2-weighted MR image with fat suppression. (**f**) Coronal spin-echo T1-weighted MR image after gadolinium contrast injection. The first case is an old, mature desmoid which has low SI on all pulse sequences (**a, b**) and does not enhance after contrast injection (**c**). The second case shows an ill-defined lesion, isointense to muscle on the T1-weighted image (**d**) and with a variable, mostly high SI on the T2-weighted image (**e**). In contrast with the first case, there is now a marked enhancement after gadolinium injection (**f**). These two cases demonstrate tumors of different age with different degrees of vascularity and collagen deposition having different features on MR images

using MRI to distinguish indolent from aggressive forms [123]. Natural evolution of desmoids has shown gradual regression and involution over a few years in many cases, in particular for subcutaneous (non-fascial) and intramuscular types [18, 69, 152]. Aggressive forms can sometimes be treated successfully medically (anti-inflammatory or hormonal medication); radiotherapy, chemotherapy, and radical surgery are no longer considered the primary treatment [29, 123]. European consensus on treatment approach was based on

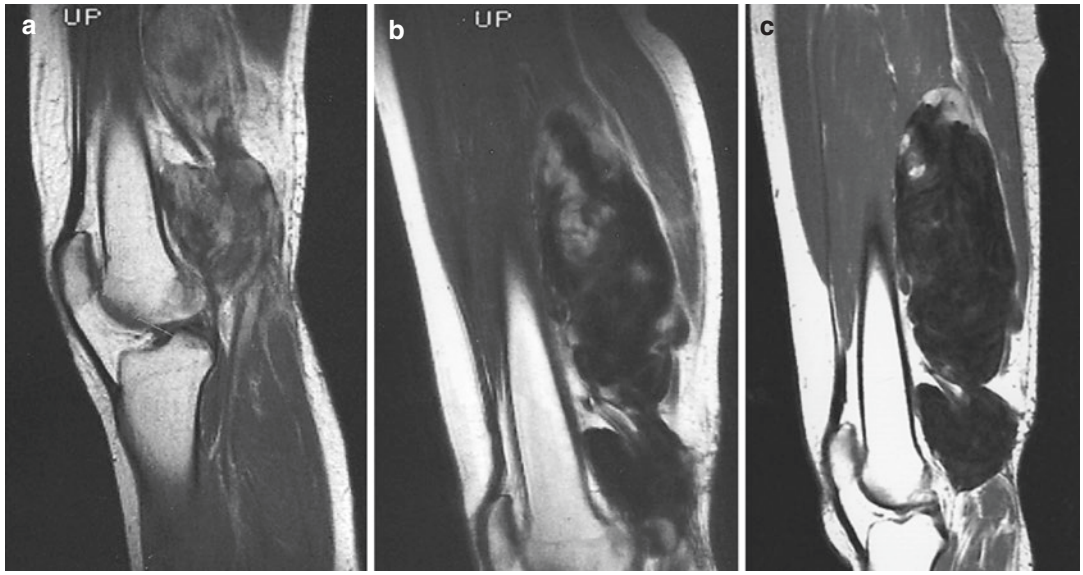

Fig. 13.26 (**a–c**) Desmoid of the popliteal fossa in a 28-year-old woman. (**a**) Sagittal spin-echo T1-weighted MR image after gadolinium contrast injection (January 1989). (**b**) Sagittal spin-echo T1-weighted MR image after gadolinium contrast injection (November 199l). (**c**) Sagittal spin-echo T1-weighted MR image after gadolinium contrast injection (April 1994). The MRI examination in 1989 shows a large, dumbbell-shaped mass in the popliteal fossa with marked, nonuniform enhancement of 80 % of the lesion (**a**). In 199l, the proximal part of the mass had increased in size, while the size of the distal part had decreased. Limited areas (20 % of the lesion) of enhancement in the proximal part and no enhancement in the distal part (**b**). On the image from MRI performed in 1994, there is no further change in tumor size. Except for two small enhancing nodules within the top of the proximal lesion (5 % of the lesion), the whole mass remains hypointense after contrast injection (**c**). This case illustrates the natural evolution of a primary desmoid tumor over a period of 6 years, showing the proximal migration of the lesion and the gradual decrease in enhancing cellular areas, together with an increase in nonenhancing collagenous components

patients' and professionals' expertise [73]. MR imaging is the preferred follow-up imaging modality, and recurrences often have a different shape, larger volume, and more indistinct borders [93].

13.3.5 Abdominal Fibromatosis (Abdominal Desmoids)

Abdominal desmoids are rare fibroblastic lesions commonly found within the musculoaponeurotic fascia of the anterior abdominal wall, especially of the rectus and oblique external muscles. Occasionally, they grow eccentrically and present as an intra-abdominal tumor. Seventy percent of cases occur in patients between the second and fourth decades, and they are common in women. There is a definite relationship with pregnancy (during or after), abdominal surgery, and trauma. It has been postulated that these tumors are estrogen sensitive. Abdominal desmoids may occur as isolated lesions or may be seen as a manifestation of Gardner's syndrome.

Abdominal desmoid tumors are well-defined lesions, 5–15 cm in diameter, and in rare cases contain calcifications, necrotic or cystic changes, or hemorrhagic components. If they originate in the rectus muscle, they do not cross the midline of the abdomen. On CT scans, most abdominal desmoids are well-defined and homogeneous and appear isodense or slightly hypodense with respect to the muscle. If lesions are hyperdense, this is due to the high density of abundant collagen and the rich capillary network [31]. The majority of lesions are either isodense or hyperdense when compared with muscle on contrast-enhanced scans.

On MR images, tumors show nonspecific high SI on T2-weighted images, while low-SI areas on T2-weighted images probably represent abundant fibrous tissue [63] (Fig. 13.27). Despite adequate resection with clear histological margins, the recurrence rate may be as high as 40 %. Sifumba has reported a tumor recurrence during pregnancy in an old scar 9 years after resection of a first abdominal desmoid [138].

13.3.6 Lipofibromatosis

Lipofibromatosis is a benign, slow-growing painless mass of congenital onset with a predilection for the hands or feet, presenting as a poorly demarcated mass involving the subcutis of deep soft tissues [38]. Median age at diagnosis is 1 year (although lesions may occur throughout childhood and in young adults) with a 2:1 male predominance. The growing tumor entraps nerves, muscles, and vasculature but rarely impedes the function of these structures [158]. Most lesions are smaller than 5 cm at detection, but sometimes lesions may involve an entire limb [145].

Histologically, mature adipose tissue admixed with a proliferative spindle cell (fibromatosis-like) component is found. Surgical resection is the treatment of choice. However, cases of incomplete resection have not shown significant progression.

MR imaging demonstrates an ill-defined fibro-fatty tumor with varying amounts of fat and fibrous components [22]. The presence of intratumoral fat on MR imaging is a distinguishing feature with other fibrous soft tissue tumors (Fig. 13.28). Differential diagnosis includes lipoblastoma, fibrous hamartoma of infancy, intramuscular lipoma, Proteus syndrome, and lipofibromatous hamartoma of the nerves [132, 155].

13.4 Fibrous Tumors of Infancy and Childhood

The following types of fibrous tumors of infancy and childhood are discussed:

1. Fibrous hamartoma of infancy
2. Infantile digital fibromatosis
3. Juvenile hyaline fibromatosis
4. Fibromatosis colli

The term “fibromatosis” is used for fibroblastic-myofibroblastic proliferations with the following characteristics: (a) a tendency to invade surrounding tissues, (b) a tendency to recur after incomplete resection, (c) absence of metastases, (d) in some fibromatoses, spontaneous regression, and (e) presentation with multifocal tumors [30].

13.4.1 Fibrous Hamartoma of Infancy

Fibrous hamartoma of infancy is a solitary, benign, painless, subcutaneous tumor usually occurring before the age of 2 years and characterized by an organoid mixture of three components: trabeculae of dense fibrocollagenous tissue, areas of immature-appearing, small, rounded, primitive mesenchymal cells, and mature fat. Sometimes a pseudoangiomatous morphologic variation is seen. The lesion occurs about twice as often in males compared to females. The most common locations are the shoulder, axilla, and upper arm, followed by the buttocks, groin, and thigh [32]. The MRI findings parallel the three components of the lesion seen histologically, with an organized arrangement of fat interspersed among heterogeneous soft tissue bands composed of mesenchymal and fibrous tissue (Fig. 13.29) [141]. Likewise, ultrasound may demonstrate a hyperechoic mass with a serpentine pattern of

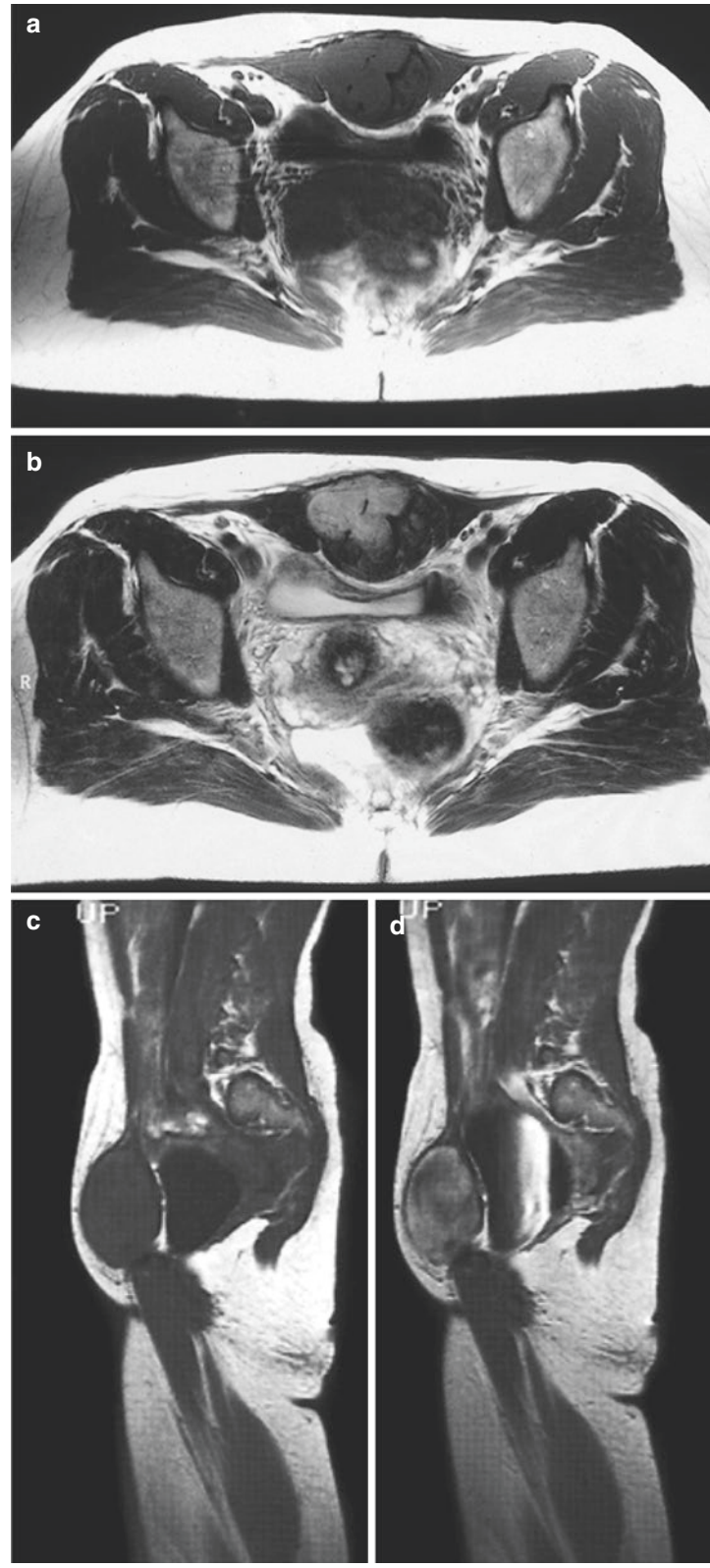

Fig. 13.27 (**a–d**) Abdominal desmoid in a 50-year-old woman (**a, b**) and in a 22-year-old woman (**c, d**). (**a**) Axial spin-echo T1-weighted MR image. (**b**) Axial turbo spin-echo T2-weighted MR image. (**c**) Sagittal spin-echo T1-weighted MR image. (**d**) Sagittal spin-echo T1-weighted MR image after gadolinium contrast injection. A polylobular mass can be seen, isointense to muscle and with low-signal-intensity septations on the T1-weighted image (**a**). On the T2-weighted image, the lesion has a mixed, overall low signal intensity (**b**). The second case involves the rectus muscle in a woman in the post-puerperal period. On the T1-weighted image, there is a well-delineated fusiform, inhomogeneous mass within the rectus muscle, with signal intensity comparable with signal intensity of muscle (c). The lesion demonstrates marked, nonuniform enhancement (**d**). These cases are illustrative of abdominal desmoids with characteristic location, patient age, and time of onset (post-puerperal)

Fig. 13.28 Lipofibromatosis. (**a**) Lateral view on the X-ray shows a bulging soft tissue shadow extending from the metatarsophalangeal crease to the midtarsal region. (**b**) Proton-density axial MR image and (**c**) T1-weighted sagittal MR image showing a peripherally well-defined fat signal intensity mass lesion with low-intensity fibrous strands passing through the intermetatarsal space, with thinning and splaying of the muscles by fat lobules (Reprinted with permission from Deepti et al. [22])

intervening hypoechoic portions [88]. Older lesions demonstrate a reduction of the mesenchymal component sometimes with capsule formation (making complete surgical resection more feasible). Fibrous hamartoma of infancy does not regress nor resolve spontaneously, and complete surgical resection is the treatment of choice.

13.4.2 Infantile Digital Fibromatosis: Inclusion-Body Fibromatosis

In infantile digital fibromatosis (Reye's disease), single or multiple fibromatous lesions arise from the fingers and toes, affecting predominantly the dorsolateral aspect of the distal parts of adjacent digits (kissing lesions). This rare entity mostly develops in patients under the age of 3 years, and histological examination typically reveals intracytoplasmic inclusion bodies [65]. The role of imaging is limited. These tumors may undergo spontaneous regression. High recurrence rates (up to 60 %) are seen after surgery [140].

13.4.3 Juvenile Hyaline Fibromatosis

Juvenile hyaline fibromatosis is a rare condition that is thought to be a mesenchymal dysplasia,

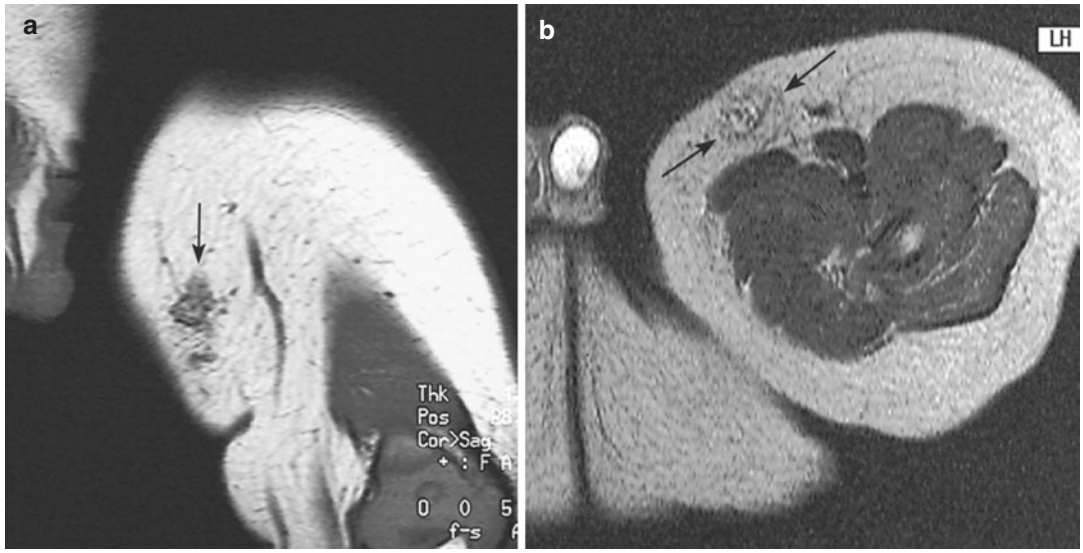

Fig. 13.29 (**a, b**) Fibrous hamartoma in a 6-month-old boy. (**a**) Coronal spin-echo T1-weighted MR image. (**b**) Axial spin-echo T2-weighted MR image. On the T1-weighted image, the lesion presents as an ill-defined, inhomogeneous mass of intermediate signal intensity within the subcutaneous tissue of the ventral aspect of the left thigh (**a**). On the T2-weighted image, the lesion is spiderlike, with low to intermediate signal intensity (**b**). MRI demonstrates the histological composition with fatty and fibrous parts

showing multiple subcutaneous tumors, hypertrophic gingiva, and flexion contractures of the extremities. Calcifications in soft tissue tumors, scoliosis, marked osteopenia, well-defined osteolytic lesions and cortical defects in tubular bones, severe acro-osteolysis, and destruction of epiphyses of the long bones are also reported. This autosomal, recessive condition is reported in children of consanguineous parents, and clinical onset occurs between 2 months and 4 years of age. Recently, the term hyaline fibromatosis syndrome is introduced as an alternative term covering both juvenile hyaline fibromatosis and infantile systemic hyalinosis because of overlapping features and mutations in the same genes [116].

Subcutaneous nodules are slow growing and may reach a large size, producing deformities. Surgical excision is often followed by tumor recurrence. The severity and the course of disease vary, but most patients survive only up to the fourth decade [139].

Histologically, the lesion is characterized by the presence of hyaline substance in the tumoral connective tissue. Diagnosis is confirmed by electron-microscopic examination [49]. Radiography will demonstrate soft tissue enlargement with focal calcifications and multiple cortical erosions (erosions often at the medial side of proximal tibia diaphysis) (Fig. 13.30). On MR images the lesions may have a lobulated appearance and are typically bright on T2-weighted images (most likely reflecting the hyaline matrix) and strongly enhance after contrast medium injection (Fig. 13.31) [150, 170]. MRI may be a significant diagnostic aid, as other fibromatosis syndromes have nodules that are of low signal on T2-weighted images [66].

13.4.4 Fibromatosis Colli

Fibromatosis colli is a peculiar growth of the sternocleidomastoid muscle that appears within the first weeks of life and is often associated with congenital muscular torticollis. It occurs in 0.4 % of newborns. There is a marked male predominance. It remains unclear whether the fibroblastic proliferation is reparative or neoplastic. Although there is a history of breech or complicated delivery in more than 4 % of the cases,

Fig. 13.30 Juvenile hyaline fibromatosis. (**a**) Anteroposterior radiograph of the hands (**a**) and forefeet (**b**) showing soft tissue enlargement, calcifications around distal phalanges, and multiple cortical erosions (Reprinted with permission from Slimani et al. [139])

microscopic appearance of the lesion differs from that of proven cases of organizing hematoma, and there is also very little demonstrable hemosiderin within it. Vascular impairment as the result of prolonged venous stasis or ischemia during labor is another possible cause. Nevertheless there is a clear association with other musculoskeletal developmental abnormalities that are associated with abnormal intrauterine positioning, including forefoot anomalies and congenital hip dislocation [41].

Clinically the lesion manifests between the second and fourth week of life as a firm mass of 2–3 cm diameter lying within the lower portion

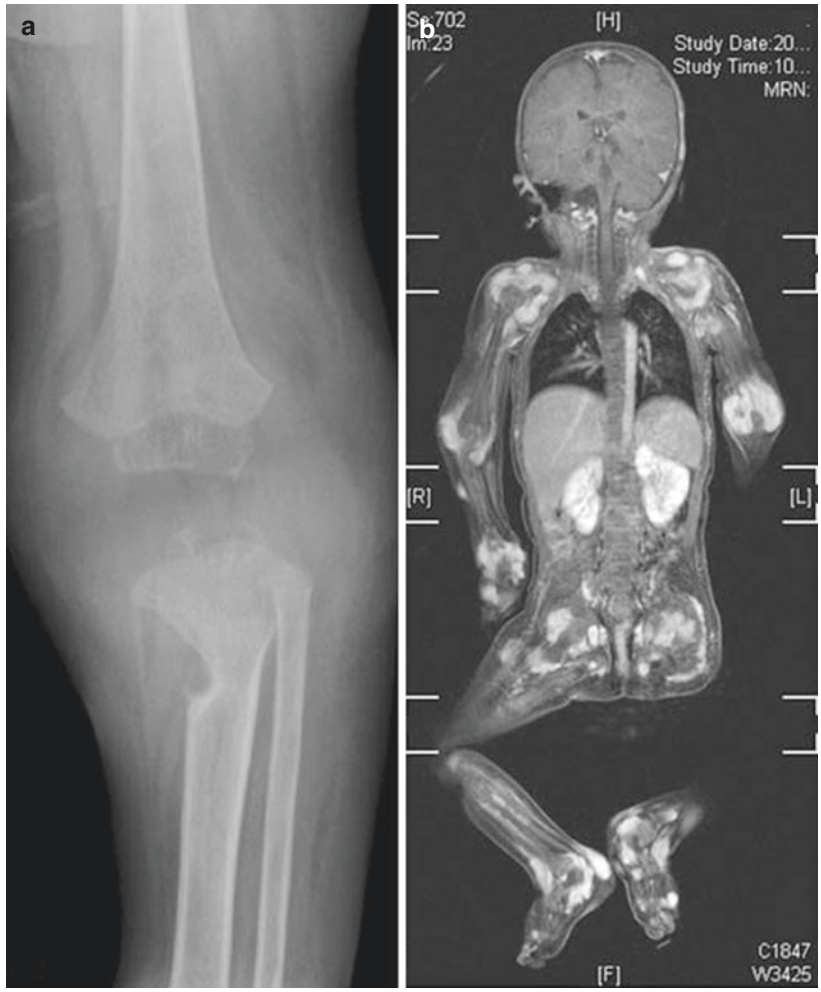

Fig. 13.31 Juvenile hyaline fibromatosis. A 15-month-old boy with stiff joints (presumed diagnosis of arthrogryposis multiplex congenita) and gingival hyperplasia. (**a**) Anteroposterior (*AP*) radiograph of the knee shows a characteristic depressed lesion at the medial side of the proximal tibial metaphysis and soft tissue swelling around the knee joint. (**b**) Coronal fat-suppressed T1-weighted whole-body MR image with contrast enhancement shows multiple enhancing homogeneous articular and periarticular soft tissue nodules throughout the whole body (Reprinted with permission from Yoo et al. [170])

of the sternocleidomastoid muscle. Initially it grows rapidly, but after a few weeks or months, growth comes to a halt. Later it begins to regress and may disappear after a period of 1 or 2 years. It never recurs and at no time does it behave aggressively. During the initial growth period, torticollis occurs in 40 % of all cases and usually is mild and transient and can be treated by physical therapy [71].

Microscopically the sternocleidomastoid muscle is partially replaced by a fibroblastic process of varying cellularity without pleomorphism or mitotic activity. Residual degenerated muscle fibers are intimately mixed with proliferating fibroblasts. Long-standing lesions may show a lower degree of cellularity and a greater amount of stromal collagen [32].

On ultrasound scans, the mass typically is found within the distal two-thirds of the sternocleidomastoid muscle (often on the ventral side) and may be hyperechoic (50 %), isoechoic, or hypoechoic relative to normal muscle. The

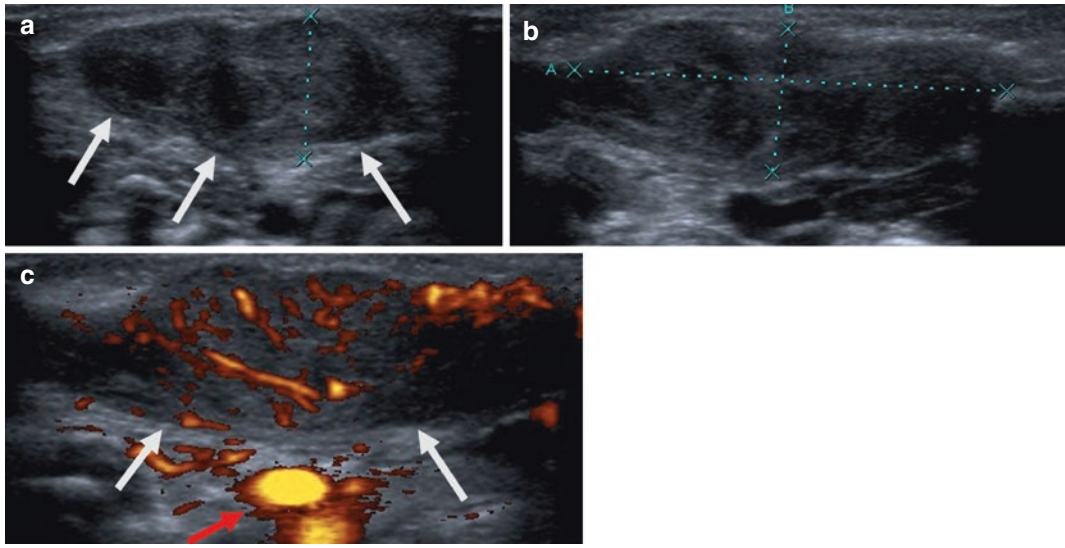

Fig. 13.32 (**a–c**) Transverse (**a**) and longitudinal (**b**) ultrasound and power Doppler ultrasound (**c**) of the middle third of the sternocleidomastoid muscle (*arrows*) in a 4-week-old girl. Normal muscle echotexture is not present within the mass that demonstrates both hypo- and hyperreflective components (**a**, **b**). Power Doppler demonstrates increased blood flow within the mass. Lower arrow points to the carotid artery (**c**). (Reprinted with permission from Peters B, Vanhoenacker F, Van Soom M, Bosmans JML (2014) *Ortho-rheumato* 12:6, p 23–25. ISSN 1379–8928)

echotexture may be homogeneous (50 %) or heterogeneous (50 %). The mass is surrounded by a hypoechoic rim in 90 % of cases [1]. Ultrasound is the method of choice for follow-up of fibromatosis colli (Fig. 13.32) [17]. On CT scans, fibromatosis colli appears as a focal or diffuse isodense enlargement of the sternocleidomastoid muscle with or without mass effect. Due to radiation constraints, CT is –however – not the preferred technique (Fig. 13.33a). Ultrasound is usually sufficient for diagnosis and MRI is rarely required. On MR images fibromatosis colli may present with a slightly increased SI on T2-weighted images compared with normal muscle or with a slightly decreased SI on T2-weighted images consistent with the presence of some fibrous tissue (Fig. 13.33) [1]. Imaging findings that are not characteristic of fibromatosis colli are mass extending beyond the margins of the sternocleidomastoid muscle, poor definition of the surrounding fascial planes, and/or mass associated with adenopathy, bone involvement, intracranial or intraspinal extension, vascular encasement, and airway compression. If essential clinical and radiological features of fibromatosis colli are present, recognition of this entity by medical imaging can prevent unnecessary diagnostic and therapeutic maneuvers [17].

13.5 Intermediate-Grade Fibrous and Fibromyoblastic Tumors

13.5.1 Dermatofibrosarcoma Protuberans

Dermatofibrosarcoma protuberans is a rare dermal tumor usually occurring in young to middle-aged adults, but also seen in children and in the elderly. It typically presents as an exophytic, nodular/multinodular slowly growing cutaneous mass. Early lesions are plaque-like with reddish discoloration which may resemble morphea or hemangioma. Rapid growth is suspicious for fibrosarcomatous change. Larger lesions may invade from the dermis to the subcutaneous fat, fascia, muscle, or bone.

On histopathology, a honeycomb appearance is seen due to neoplastic cells growing along the fibrous septa of the subcutaneous fat

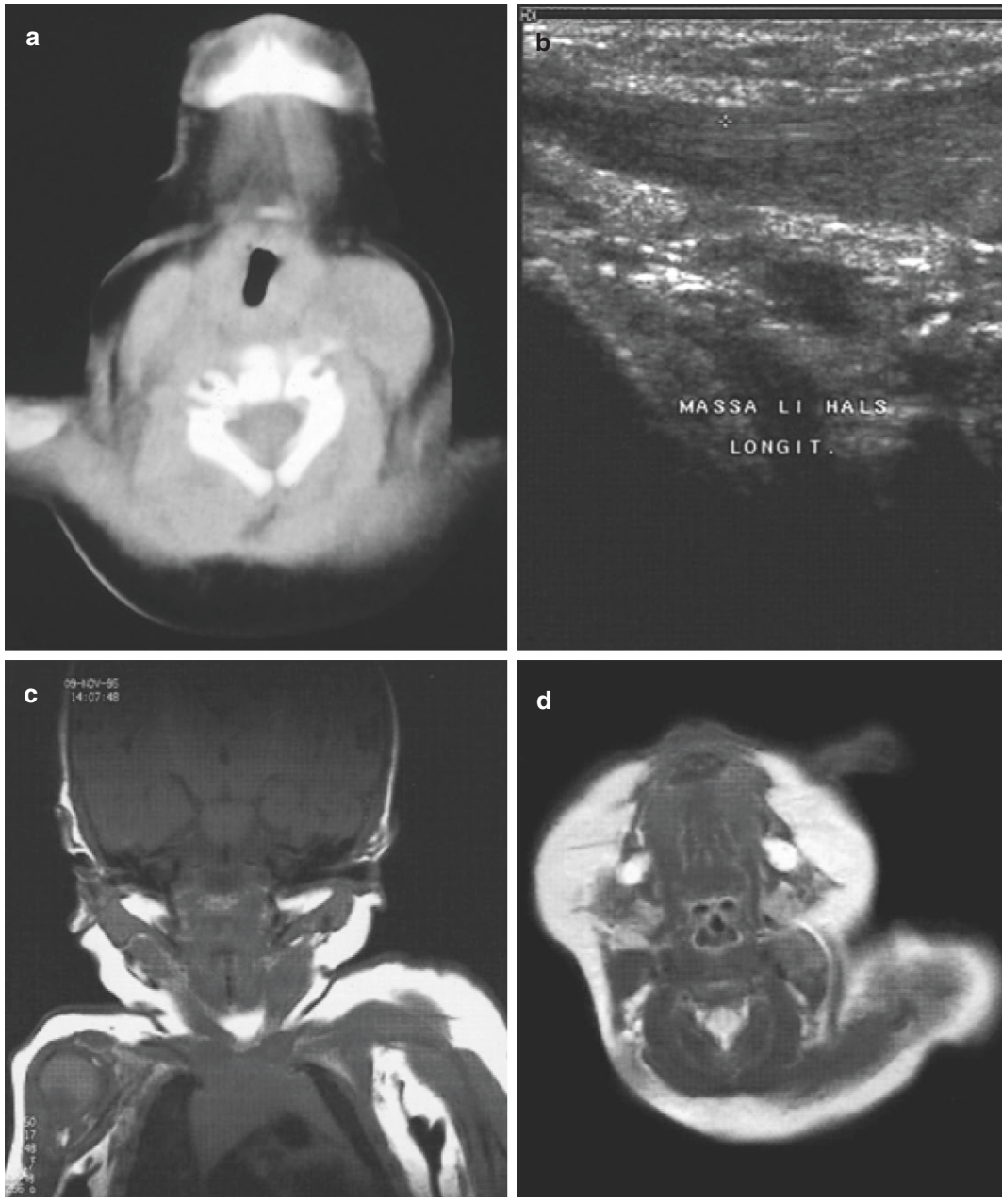

Fig. 13.33 (**a–d**) Fibromatosis colli in a l-day-old boy (**a**) and a 7-week-old girl (**b–d**) presenting clinically with torticollis. (**a**) CT scan. (**b**) Ultrasound of the left sternocleidomastoid muscle. (**c**) Coronal spin-echo T1-weighted MR image. (**d**) Axial turbo spin-echo T2-weighted MR image. CT scan showing overall enlargement of the left sternocleidomastoid muscle, without obvious change in attenuation (**a**). On ultrasound scans, there is a fusiform mass in the distal part of the muscle. The mass is hyperechoic and lacks muscle fiber structure (**b**). On the T1-weighted image, there is a fusiform enlargement of the left sternocleidomastoid muscle (**c**), while on the T2-weighted image, the lesion is less homogeneous and predominantly of high signal intensity (**d**). Characteristic age, location, and shape of a fibroma colli

interdigitating with fat lobules. It consists of collagenous stroma containing small blood vessels and spindled tumor cells. The pigmented variant contains pigmented, dendritic melanocytic cells and is known as Bednar tumor. Another variant contains a myxoid stroma.

CT demonstrates a mass without calcifications, isodense to muscle and with heterogeneous enhancement [171]. MRI is used to delineate the extent of the larger lesions, showing a well-defined mass in the subcutaneous tissue. The MRI appearance is nonspecific, showing a low signal intensity on T1- and high signal intensity on T2-weighted images and a uniform or patchy enhancement (Figs. 13.34 and 13.35) [147]. Heterogeneous intratumoral foci of hemorrhage, myxoid change, or necrosis may be present. On angiography a nonspecific, early enhancing vascular lesion is seen.

Wide local excision is the preferred treatment, if possible using Mohs micrographic surgery [146]. Local recurrences occur between 10 and 25 %, but even more often if resected with positive margins. Rarely metastases arise, usually found in the lung. Diffusion-weighted MR imag-

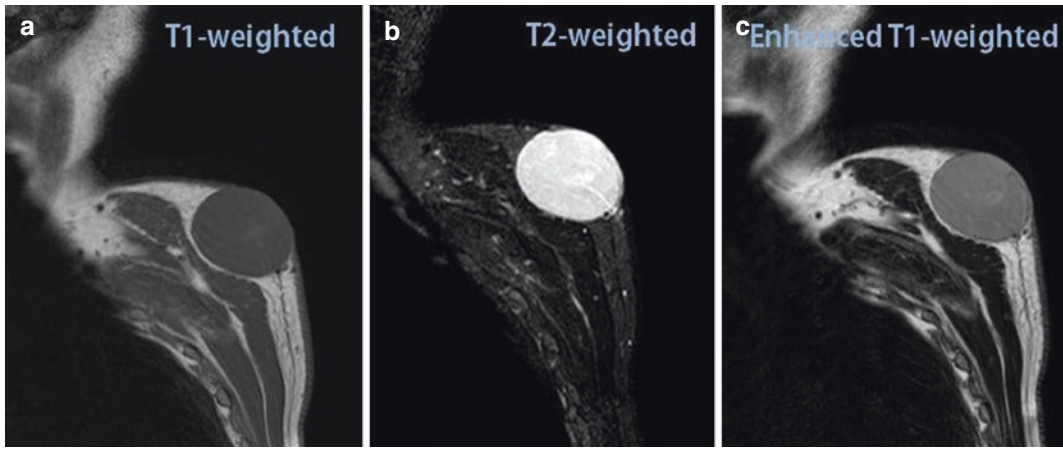

Fig. 13.34 (**a–c**) Parasagittal T1- (**a**), T2- (**b**), and post-contrast T1-weighted MR images of the upper back. Oval tumoral lesion with sharp delineation and limited to the subcutis; no signs of invasion to deeper soft tissue. The tumor was resected with wide margins. Follow-up after 24 months (not shown) revealed no recurrence (Reprinted with permission from Goto et al. [55])

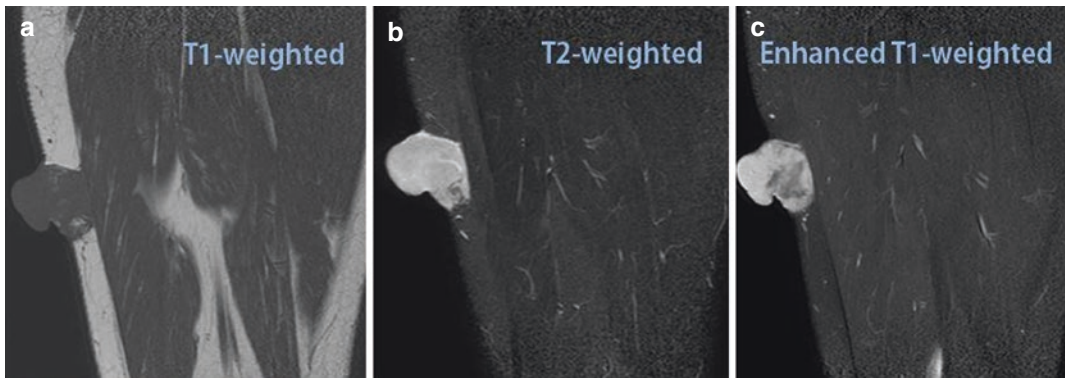

Fig. 13.35 (**a–c**) Parasagittal T1- (**a**), T2- (**b**), and post-contrast fat-saturated T1-weighted MR images of the thigh. Multinodular lesion in the subcutis with protrusion above the skin. After resection with a wide margin, no recurrence was seen over a period of 12 months (Reprinted with permission from Goto et al. [55])

ing may help to delineate the extent of recurrent lesions on a background of postoperative scar tissue [151] [55].

13.5.2 Extrapleural Solitary Fibrous Tumor

Solitary fibrous tumor is a mesenchymal tumor that arises from primitive fibroblast-like cells in connective tissue, often with a prominent, hemangiopericytoma-like branching vascular pattern. The term "hemangiopericytoma" was abandoned. It is used only to describe a morphological pattern that is shared by different entities. Currently, solitary fibrous tumor, hemangiopericytoma, lipomatous hemangiopericytoma, and giant cell angiofibroma are all lumped under the "extrapleural solitary fibrous tumor" category. Gene fusion NAB2-STAT6 has been established as the defining driver mutation of solitary fibrous tumors. This tumor can be associated with hypoglycemia secondary to production of insulin-like growth factor (Doege-Potter syndrome), osteoarthropathy, arthralgia, and clubbing [52].

This lesion is uncommon and observed in middle-aged adults without sex predilection. Solitary fibrous tumors can be found at any location of which 40 % in the subcutaneous tissue. Most solitary fibrous tumors are found at the pleura, face, and meninges. It is estimated that extrapleural solitary fibrous tumors account for about 40 % of cases. It is mostly a large, well-delineated, slowly growing, and painless mass. Histopathologically it consists of a mixture of hypocellular and hypercellular areas separated from each other by thick bands of collagen and branching, hemangiopericytoma-like vessels. Malignant solitary fibrous tumors (10–15 %) behave aggressively and show histopathological features of hypercellularity, cytological atypia, necrosis, numerous mitoses, and infiltrative growth.

Radiography and CT may sometimes demonstrate a few calcifications [114]. Color Doppler ultrasound may demonstrate increased tumoral vascularization. On MR images, solitary fibrous tumors of the extremities have nonspecific features, i.e., inhomogeneous, low to intermediate SI on T1-weighted images and inhomogeneous, intermediate to high SI on T2-weighted images [4, 161] (Figs. 13.36 and 13.37). Avid contrast enhancement is seen in a homogeneous or heterogeneous (larger lesions) pattern, and enlarged feeding or draining vessels may be noted. Dynamic contrast enhancement studies of vascular-rich areas show a rapidly ascending slope followed by a descending slope (which may resemble a malignant pattern). Digital subtraction angiography often shows marked vascularity with tumor staining and early venous filling [114].

13.5.3 Inflammatory Myofibroblastic Tumor

It is a distinctive lesion, primarily a visceral and soft tissue tumor of children and young adults, composed of myofibroblastic spindle cells accompanied by an inflammatory infiltrate of plasma cells, lymphocytes, and eosinophils. Synonyms include plasma cell granuloma, inflammatory pseudotumor, and inflammatory fibrosarcoma. All body parts can be affected and they determine the symptoms of inflammatory myofibroblastic tumor [41, 120]. The lung, mesentery/omentum, and orbits are the most common sites [68].

Findings of a mass lesion are frequently in association with fever, weight loss, and pain; these clinical symptoms resolve after resection of the tumor. Imaging studies reveal a lobulated, solid mass which can be small or large, single or multiple, and well-defined or ill demarcated, most often inhomogeneous and containing low-signal intensity areas on T1 and T2 (Fig. 13.38). Some lesions may demonstrate calcifications and lesions can be single or multiple [90].

13.5.4 Low-Grade Myofibroblastic Sarcoma

Myofibroblasts are defined as modified fibroblasts that contain contractile elements (such as in smooth muscle cells) and are capable of

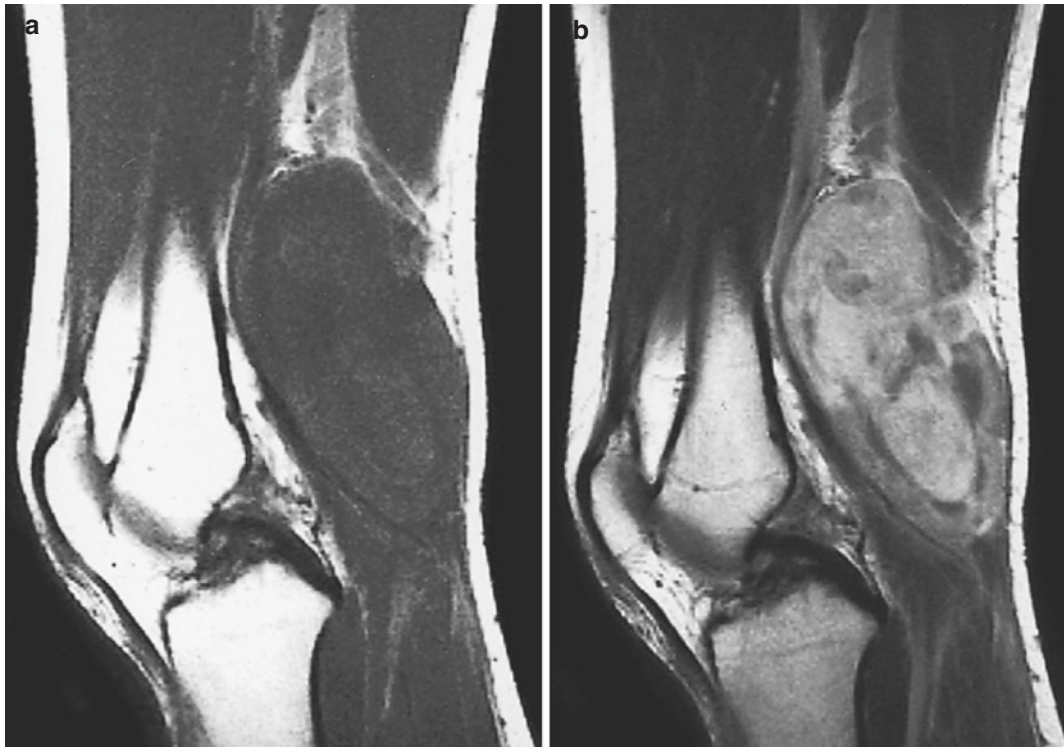

Fig. 13.36 (**a, b**) Solitary fibrous tumor of the right popliteal fossa. (**a**) Sagittal T1-weighted MR image. (**b**) Sagittal T1-weighted MR image after gadolinium contrast injection. An oval, largely homogeneous lesion is seen lying superficial to the major vessels. There is no invasion of the subcutis (**a**). After contrast administration, a strong enhancement of the mass is seen (**b**)

synthesizing stromal components (as fibroblasts do), e.g., collagen. Myofibroblast cells are present in reactive processes such as nodular fasciitis or granulation tissue. The concept of a low-grade sarcoma composed of myofibroblasts has only recently become clearly defined. Low-grade myofibroblastic sarcomas are indolent lesions and occur predominantly in the head and neck (skull base, oral cavity) and also in the extremities or trunk, involving the subcutaneous tissue, submucosa, deep soft tissue, or intraosseous areas [39]. These tumors often are unencapsulated and may infiltrate adjacent fibrous, fatty, or muscular tissue. It is difficult to distinguish inflammatory myofibroblastic tumor from low-grade myofibroblastic sarcoma; both morphological and immunohistological analyses are required. For clinical reasons, it is important to differentiate these tumors: myofibroblastic sarcomas have a tendency to recur locally (up to 75 % depending on their grade) but rarely metastasize [108].

Reports on imaging are sparse. CT may show a mass of intermediate density, enhancing after intravenous contrast medium injection. MRI may demonstrate a well-defined or ill-defined lesion with signal intensity comparable to the muscle on T1, intermediate to high signal intensity on T2, and enhancement after intravenous gadolinium (Fig. 13.39) [110].

13.5.5 Myxoinflammatory Fibroblastic Sarcoma

Myxoinflammatory fibroblastic sarcoma previously also called acral myxoinflammatory fibroblastic tumor is a rare tumor occurring in middle-aged adults (equally among men and women) and most often in the hands or feet (acral

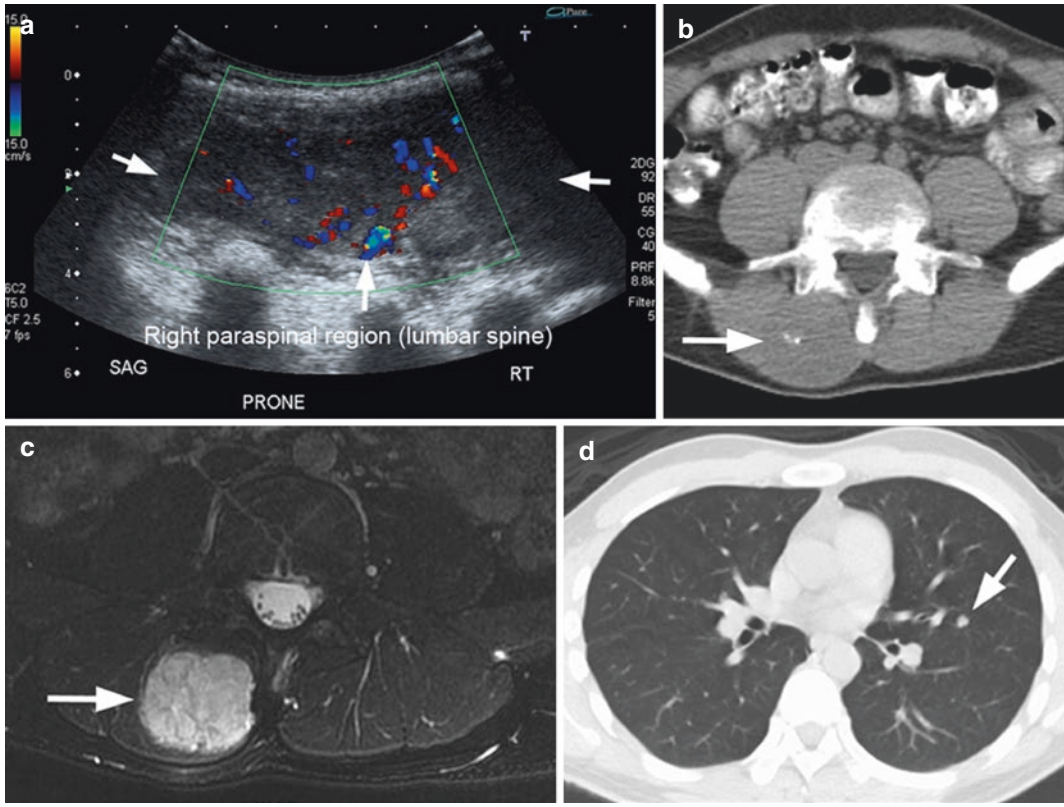

Fig. 13.37 (**a–d**) *Solitary fibrous tumor*. Intramuscular cellular tumor in the right paraspinal muscles in a 31-year-old man developing pulmonary metastasis. (**a**) Ultrasound image depicts a heterogeneous, hypoechoic mass (arrows) with prominent internal vascularity. (**b**) Non-contrast axial CT reveals a mass iso- to mildly hypodense to the muscle and a small internal calcification. (**c**) Axial T2-weighted MR image shows a predominantly hyperintense mass (*arrow*) with heterogeneous regions of low signal intensity. (**d**) Axial CT of the chest in lung windows shows a small pulmonary nodule (*arrow*) present at the time of clinical presentation, which increased in size on subsequent follow-up and was proved by biopsy to be metastasis, along with two other small lung nodules (not shown). Final histology confirmed a metastatic cellular solitary fibrous tumor without any histological signs of malignant transformation (Reprinted with permission from Musyoki et al. [114])

locations). Lesions are centered in the subcutaneous tissues and growing as single or multiple nodules along fibrous connective tissue of fat, fascia, or tendon sheaths. Bone involvement may rarely be present. Patients usually present with a slowly growing painless mass, but some may present with pain or tenderness.

On pathological examination, four elements are found: proliferative fibroblasts (spindle cells), myxoid matrix, associated inflammatory components, and Reed-Sternberg-like atypical giant cells. According to the WHO 2013 classification, this tumor can be characterized by the translocation t(1;10) [6].

On imaging, these lesions are predominantly subcutaneous, often involving adjacent tendon sheaths. Imaging characteristics are variable and depend on the relative components (myxoid, inflammatory, or fibrosclerotic), on the infiltrative degree (well-defined or poorly circumscribed), and on the shape (single or multinodular). In general, lesions are of lower signal than the muscle on T1 and of mixed signal or high signal on T2 [143]. Predominant low signal on T2 has not been described, which helps to differentiate these acral lesions from giant cell tumor of the tendon sheath. Enhancement is often heterogeneous, and enhancing areas

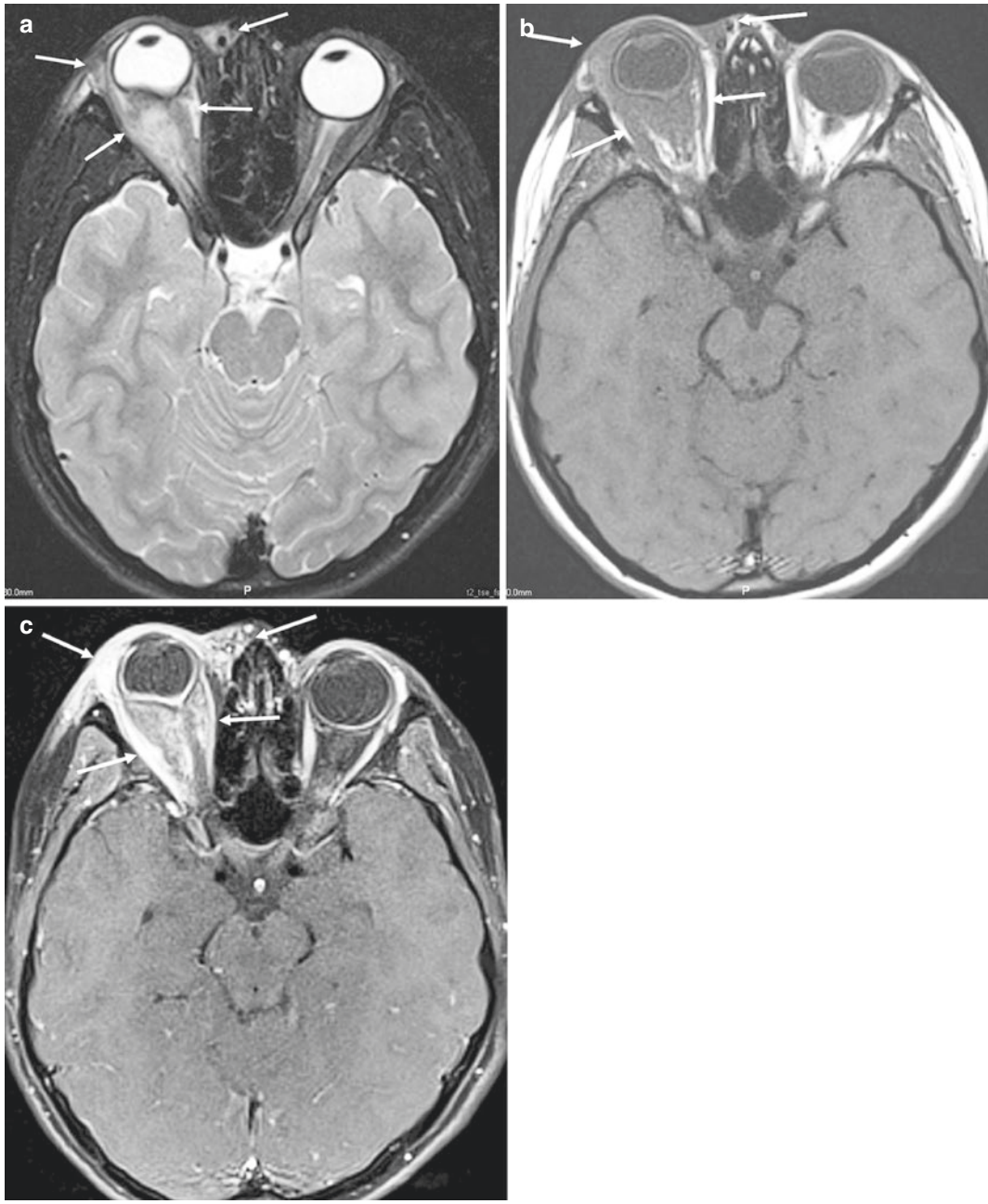

Fig. 13.38 (**a–c**) *Inflammatory myofibroblastic tumor* in a 12-year-old girl who presented with swelling of the eyelid. (**a**) Axial fat-saturated T2-weighted MR image shows hyperintense infiltrative lesion (*arrows*) involving the right orbit. (**b**) Axial precontrast T1-weighted MR image demonstrates that the lesion (*arrows*) is isointense in signal intensity relative to muscle. (**c**) Fat-saturated postcontrast T1-weighted MR image shows heterogeneous enhancement of the infiltrative lesion with retrobulbar fat infiltration, involving the optic nerve, rectus muscles, tendons, and lacrimal gland (*arrows*) (Reprinted with permission from Oguz et al. [120])

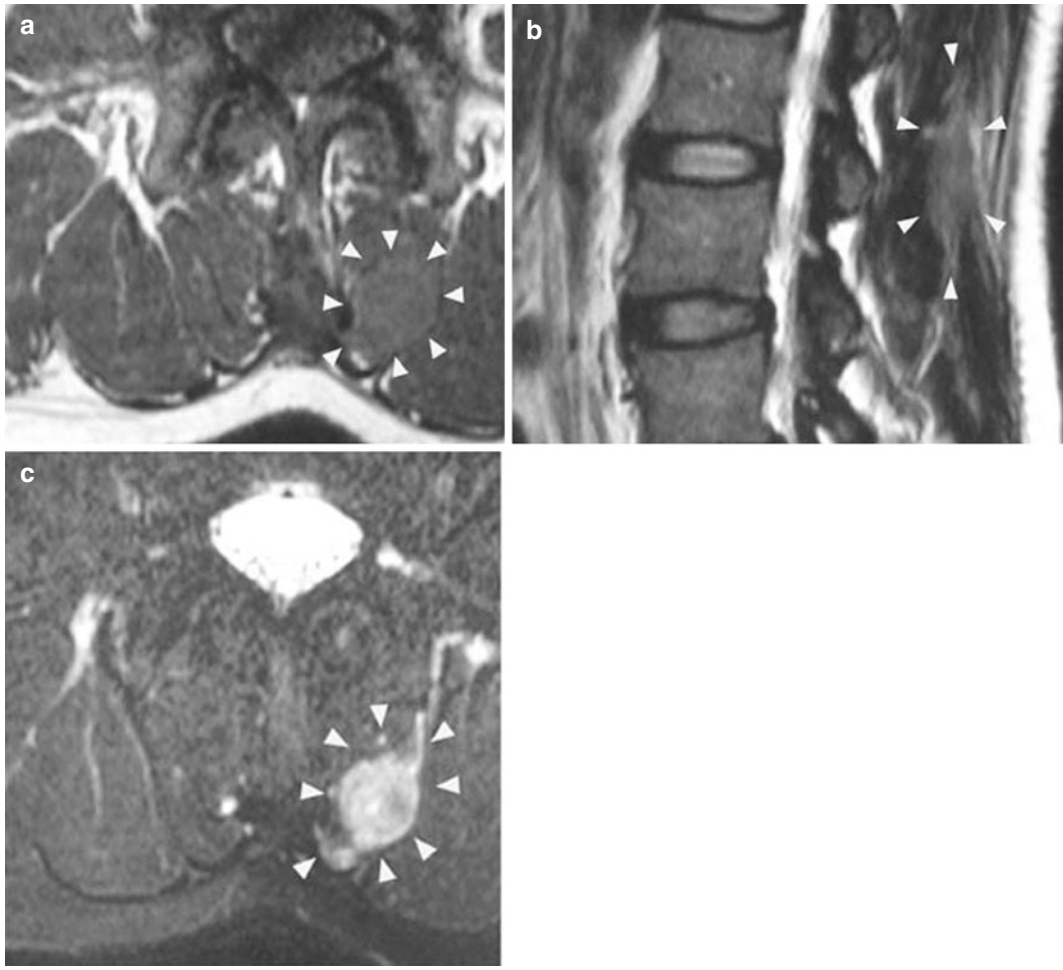

Fig. 13.39 (**a–c**) Fig. 13.37 a–c. Low-grade myofibroblastic sarcoma. MRI of the lower spine in a 46-year-old woman. T1-weighed images revealed an iso- to high-intensity mass in the multifidus muscle (**a**, *arrowheads*). T2-weighted MRI detected an ill-defined high-intensity mass (**b**, *arrowheads*). Post-contrast T1-weighted images showing significant enhancement (**c**, *arrowheads*) (Reprinted with permission from Morii et al. [110])

correspond to fibromyxoid stroma or to myxoid low-grade tumor nodules, while nonenhancing areas may be indicative for cellular, higher-grade tumor (Fig. 13.40) [48]. Acral location may lead to erroneous initial diagnosis such as glomus tumor, epidermoid inclusion cyst, or giant cell tumor of the tendon sheath.

Wide local excision combined with radiotherapy is the treatment of choice because of frequent local recurrences (more than half of the cases); metastatic disease is extremely rare [144]. Prognosis is relatively good with a long life expectancy.

13.5.6 Infantile Fibrosarcoma

Infantile, congenital, or juvenile fibrosarcoma is a rare childhood malignancy (3 % of all childhood tumors) of mesodermal origin. For some authors [32], infantile fibrosarcoma is a distinct lesion, while for others [135, 154] it cannot be differentiated from the aggressive infantile type of fibromatosis described above. It usually presents at birth or during the first year of life. Prenatal diagnosis is likely to increase due to routine antenatal ultrasound. There is no sex preponderance. The superficial and deep soft tissues of

Fig. 13.40 (**a–d**) Myxoinflammatory fibroblastic sarcoma at the middle finger of a 60-year-old man. An AP radiograph (**a**) shows a lucent lesion in the distal phalanx (*arrowhead*) with an associated pathologic fracture (*arrow*). The lateral radiograph (**b**) shows that the lesion has caused cortical destruction in the volar aspect of the phalanx (*arrowhead*). Sagittal T2 fat-suppressed MR images show a high T2 signal mass (*arrowhead*) in the volar aspect of the distal phalanx (**c**). On a T1-weighted, fat-suppressed, post-contrast image (**d**), the majority of the mass on the volar aspect (*arrowhead*) has thin peripheral enhancement, with a nodular component undergoing more diffuse enhancement dorsally (*arrow*) (Reprinted with permission from Gaetke-Udager et al. [48])

the extremities, especially distally, are the most common sites, accounting for 61 % of cases overall [41]. It tends to show a rapid increase in size and distant metastasis may occur in 8 % of cases [59]. Infantile cases are often grotesquely large in proportion to the size of the child [41]. The adjacent bone may show some deformity with cortical thickening and failure of normal tubulation. Large tumors may cause bone erosion, bowing, remodeling, or destruction. Intratumoral ossification or calcification is rare.

Histologically, infantile fibrosarcoma is an undifferentiated fibroblastic spindle cell tumor of intermediate grade of malignancy, which is densely cellular, often in a herringbone pattern with numerous mitoses and infiltrative margins. Collagen formation is not prominent. Cystic, myxoid, highly vascular, and necrotic tumor

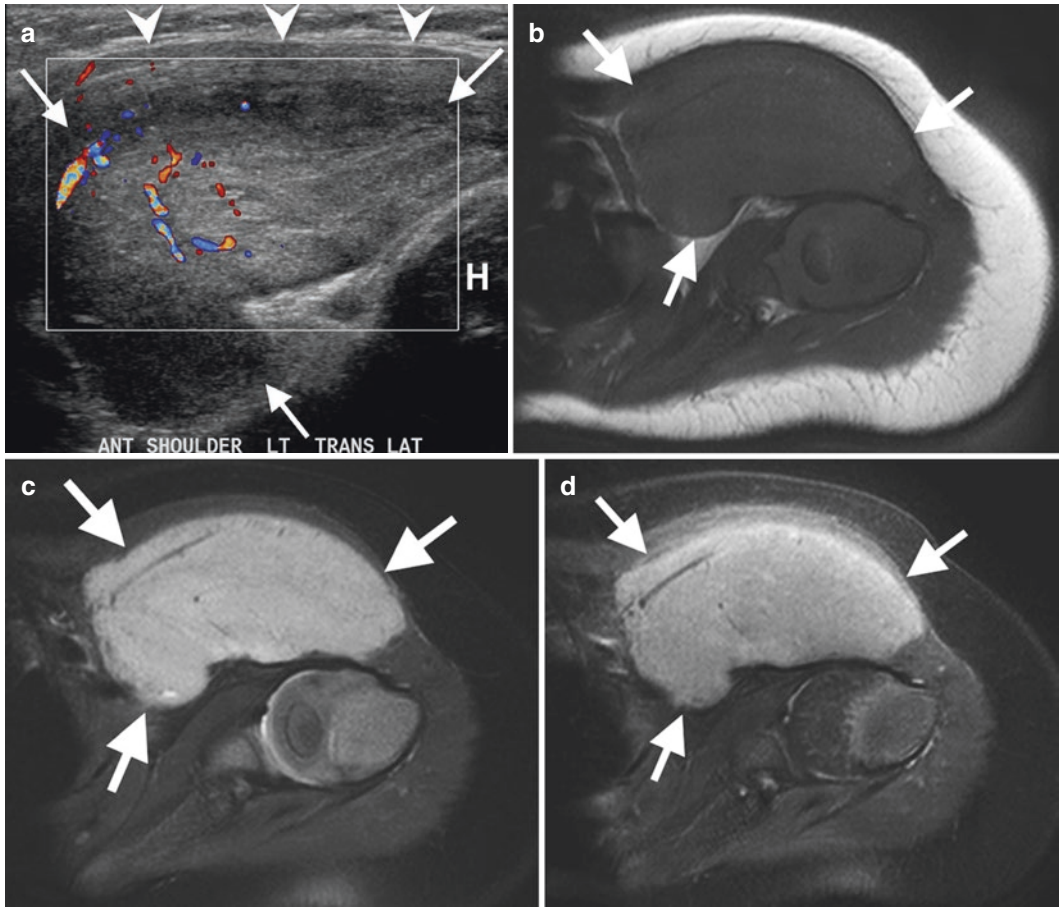

Fig. 13.41 (**a–d**) Infantile fibrosarcoma (*arrows*) located anterior to the left shoulder of a 6-month-old girl. (**a**) The mass located deep to the pectoralis muscles (*arrowheads*) and anterior to the humoral head (*H*) is echogenic and shows vascularity on ultrasound. It is iso- to slightly hyperintense on axial T1-weighted image (**b**) and hyperintense on axial T2-weighted fat-saturated image (**c**) and shows fairly homogeneous enhancement on post-contrast T1-weighted fat-saturated image (**d**) (Reprinted with permission from Ainsworth et al. [3])

components are often seen [59]. Congenital infantile fibrosarcomas have a characteristic chromosomal translocation – t(12;15) – which aids in distinguishing it from other soft tissue neoplasms.

Tumors are isoechoic on US and mildly hypodense on plain CT. CT is useful in demonstrating the extent of the tumor and the bony involvement, while disruption of soft tissue planes is better shown on MR images. Although MR imaging findings are variable and not specific, infantile fibrosarcoma should be considered in the differential diagnosis of a large mass developing in a limb at birth or during the neonatal period when MR imaging depicts a well-circumscribed mass, isointense on T1- and hyperintense on T2-weighted images, sometimes heterogeneous and septated, with strong enhancement and intratumoral hemorrhage (Fig. 13.41).

Treatment nowadays consists almost exclusively of chemotherapy. In contrast to adult fibrosarcoma, infantile fibrosarcoma (typically congenital or in children less than 10 years old) shows a more indolent clinical course with 5-year survival rates of 84–93 % [3, 9]. MRI has a role in follow-up, often demonstrating hypertrophic lipomatous tissue when the tumor regresses, and early detection of local tumor recurrence.

13.6 Malignant Fibromyoblastic Tumors

13.6.1 Adult Fibrosarcoma

Adult fibrosarcoma is a malignant tumor composed of fibroblasts with variable collagen production and herringbone architecture and is capable of recurrence and metastasis [32]. Histologic, immunohistochemical, and ultrastructural examination are important tools for diagnosing fibrosarcoma and for differentiating fibrosarcoma from nodular fasciitis, myxofibrosarcoma, musculoaponeurotic fibromatosis, and other sarcomas. Recognition of these lesions as specific tumors and entities is responsible for the decline in the incidence of fibrosarcoma and for the overdiagnosis of fibrosarcoma in earlier studies [7].

Clinically, fibrosarcoma presents as a slowly growing, solitary, palpable mass with a diameter of 3–8 cm. It may reach a large size before causing symptoms. The lesion is most common between the ages 30 and 55 years, and the incidence is slightly higher in women. The thigh and the knee region are preferential localizations, followed by the trunk, distal legs, and forearms. Less than 5 % of these tumors present in the head and neck [50]. Deep fibrosarcomas originate from the intramuscular and intermuscular fibrous tissue, fascial envelopes, aponeuroses, and tendons. They may cause periosteal and cortical thickening and rarely demonstrate intralesional calcifications or ossifications. Superficial or subcutaneous fibrosarcomas arise in tissues damaged by trauma, scarring, heat (burns), or radiation.

Macroscopically, small fibrosarcomas are well-defined, while larger fibrosarcomas tend to be poorly defined, grow in a diffusely invasive manner, and are often multiloculated. Microscopically, fibrosarcomas have a rather uniform or fasciculated growth pattern consisting of spindle-shaped cells separated by interwoven collagen fibers that are arranged in a parallel fashion. Mitotic activity is a condition for diagnosis. Grading of fibrosarcoma (well differentiated versus poorly differentiated) is based on the degree of cellularity, the cellular maturity, the amount of collagen produced by the tumor cells, and the presence of necrosis and/or intralesional hemorrhage.

Low-grade fibrosarcoma (well differentiated) is defined by sheets of uniform spindle cells with moderate cellularity arranged in a herringbone pattern, mild nuclear pleomorphism, and only rarely mitoses. A collagenous stroma is usually present. High-grade lesions (poorly differentiated) show greater nuclear pleomorphism, abundant cellularity, frequent mitotic activity, and possible tumor necrosis. Despite the fact that desmoids are characterized more by their localization and that fibrosarcomas are larger in size, differentiation between desmoids (representing more than 70 % of tumors of fibrous tissue) and fibrosarcomas (less than 5 %) is difficult even on MR images (Figs. 13.42 and 13.43). Multicentric presentation of fibrosarcoma is a rare finding which can hardly be differentiated from metastatic fibrosarcoma (Fig. 13.44). The treatment of choice is wide local excision. Simple excision of fibrosarcomas is often followed by local recurrence.

Medical imaging literature about fibrosarcoma is sparse and limited to case reports. In our series of soft tissue tumors, we had nine cases of primary fibrosarcoma and two recurrent fibrosarcomas. The age range of patients was between 16 and 77 years, with a mean age of 47 years. In contrast to results reported in the literature, nine of ten patients were men. Nine lesions were located on the lower limb, from the groin to the sole of the foot. One patient presented with multiple bone and soft tissue localizations. Diameters were between 2 and 27 cm (mean diameter, 12 cm).

All patients underwent MRI. Lesions were either homogeneous or inhomogeneous on both T1- and T2-weighted images. Most lesions showed signal intensities equal to those of muscle on T1-weighted images and low-SI areas on a background of moderate to high SI on T2-weighted images. T1-weighted images after Gd contrast were performed in nine patients. Ninety percent of the lesions showed a marked, peripheral enhancement, with a spoked-wheel appearance in three patients. Nonenhancement of

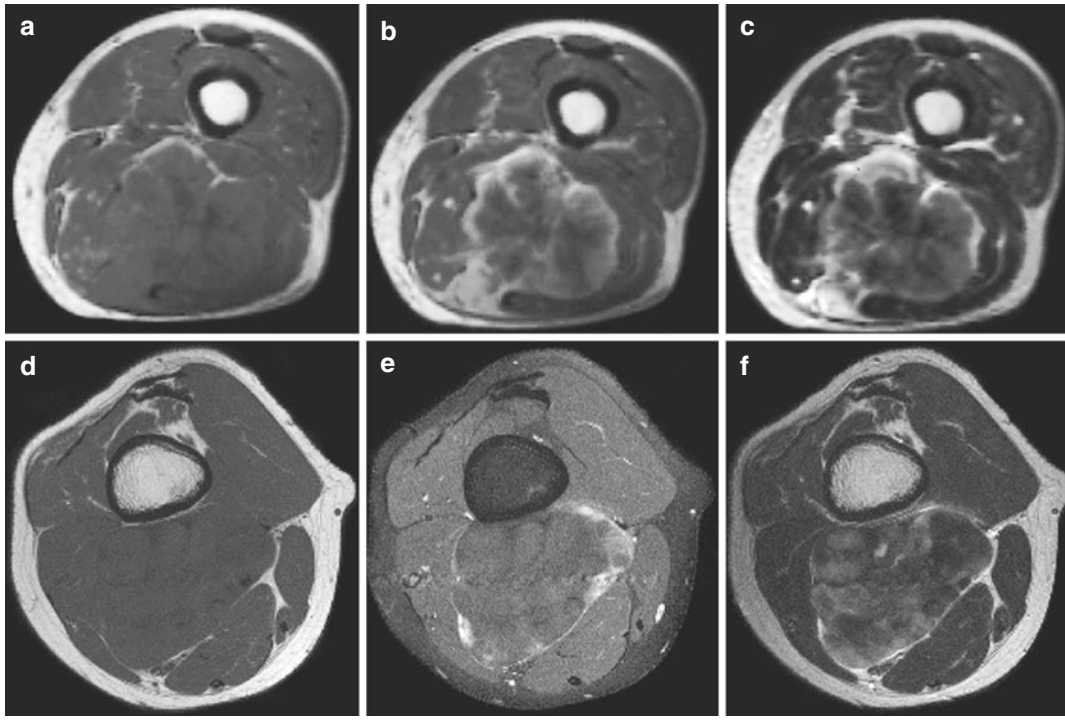

Fig. 13.42 Two cases of fibrosarcoma (**a–f**). (**a**) Axial spin-echo T1-weighted MR images. (**b**) Axial spin-echo T1-weighted MR images after gadolinium contrast injection. (**c**) Axial spin-echo T2-weighted MR images. (**d**) Axial spin-echo T1-weighted MR images. (**e**) Axial spin-echo T1-weighted MR images after gadolinium contrast injection, with fat suppression. (**f**) Turbo spin-echo T2-weighted MR images. In both cases lesions are nonhomogeneous and isointense to muscle on T1-weighted MR images (**a, d**); they are nonhomogeneous and of overall low SI on T2-weighted MR images (**b, e**) and enhance in a spoked-wheel pattern after contrast administration (**c, f**). Large size and SIs are compatible with the diagnosis of fibrosarcoma. Good delineation and speckled areas of low SI do not allow differentiation from extra-abdominal desmoids

central tumor parts was not a consequence of intratumoral necrosis. In only one case did the nonenhancing central part correspond to an area of high SI on T2-weighted images. Osseous involvement was rare, being noted only once in the group of solitary fibrosarcomas. The patient with multicentric fibrosarcoma had numerous osteolytic osseous lesions and two soft tissue nodules at the pelvic girdle (Fig. 13.44).

13.6.2 Myxofibrosarcoma

Myxofibrosarcoma, formerly known as the myxoid variant of malignant fibrous histiocytoma, is a malignant fibrous lesion that preferentially affects adults and elderly (mean age 66 years). It exhibits a slight male predominance. The majority of patients present with a slowly enlarging and painless mass. Most lesions (80 %) arise in the extremities and less frequently in the trunk, retroperitoneum, pelvis, head, and neck. Seventy percent of the masses are located in the subcutis, others in the intermuscular or intramuscular planes; they commonly have very infiltrative margins. A myxofibrosarcoma lesion is defined as low grade if 30 % or more is of myxoid component, 20 % or less is solid area and only focal, and 10 % or less is tumor necrosis [61]. Low-grade myxofibrosarcomas occur more frequently in a superficial location [118].

Histopathologically, a nodular growth pattern is seen. The myxoid matrix contains elongated, curvilinear, thin-walled capillaries and fusiform, round, or stellate cells with slightly eosinophilic cytoplasm. Low-grade lesions have a hypocellular,

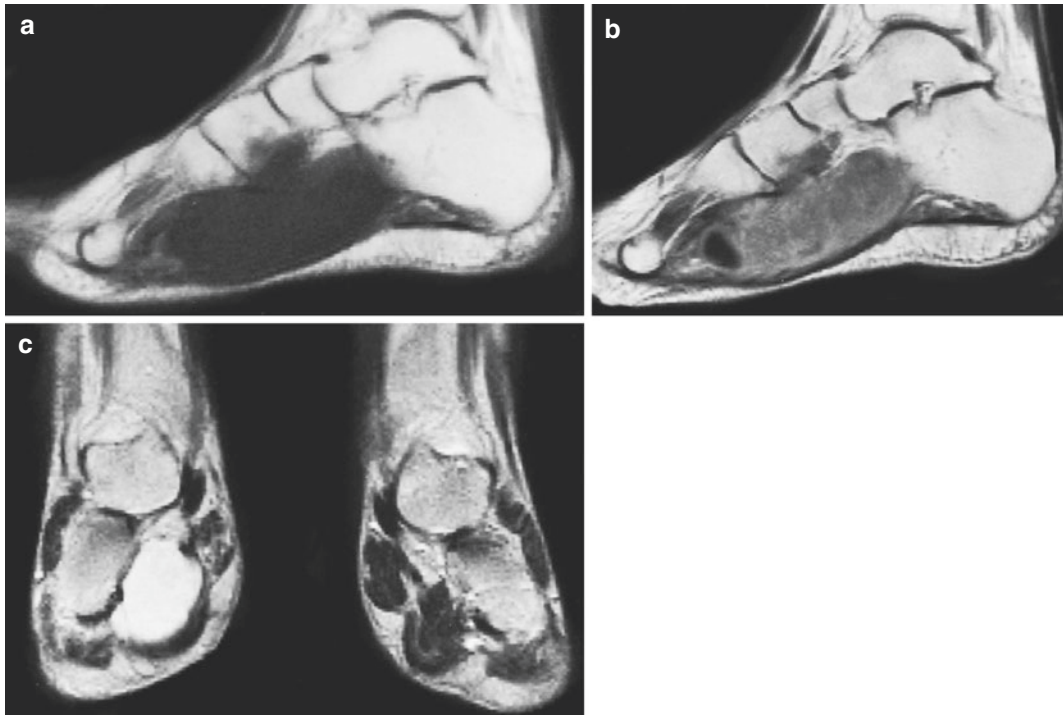

Fig. 13.43 (**a–c**) Fibrosarcoma of the foot in a 34-year-old man. (**a**) Sagittal spin-echo T1-weighted MR image. (**b**) Sagittal spin-echo T1-weighted MR image after gadolinium contrast injection. (**c**) Coronal spin-echo T2-weighted MR image. A large fusiform mass lesion is present at the foot deep to the plantar aponeurosis, with involvement of the medial cuneiform bone. Overall signal intensity on the T1-weighted image is low (**a**). The lesion shows moderate enhancement, with a nonenhancing nodule at the distal part (**b**). On the T2-weighted image, the lesion is of homogeneous high signal intensity (**c**). Age, location, and MRI characteristics suggest a malignant tumor but do not allow further histological typing

mainly myxoid aspect, whereas, in high-grade myxofibrosarcoma, high mitotic activity, pleomorphism, and intratumoral necrosis are seen.

Mentzel et al. describe local recurrences in 54 % of their cases (follow-up of 5–300 months) and metastases in 17 %. Neither the depth of the primary lesion nor the histological grade influences the incidence of local recurrence. However, because only intermediate- and high-grade neoplasms metastasize, it is important to recognize low-grade myxofibrosarcoma, because incorrect initial diagnosis and treatment may result in local recurrence, with progression to a higher-grade lesion that has the capability to metastasize [47, 104].

On ultrasound scans, a well-circumscribed hypoechoic mass is seen. On T1-weighted MR images, the lesion is homogeneous and has intermediate SI [129]. Increased perifascial T2 signal is a characteristic finding in myxofibrosarcoma [74]. T2-weighted images reflect the myxoid content of low- and intermediate-grade myxofibrosarcoma, the myxoid content being inversely proportional to the cellularity and the grade of the tumor. Gadolinium-enhanced T1-weighted images with fat suppression are key to demonstrate the fascial tail sign, with tumor extensions that may invade fascial planes around muscle compartments distant from the tumor center (Figs. 13.45, 13.46, and 13.47). The tail sign may be associated with higher local recurrences [75, 169].

High-grade myxofibrosarcoma is not easily distinguished from other adult pleomorphic sarcomas as well on histopathology as on imaging [76].

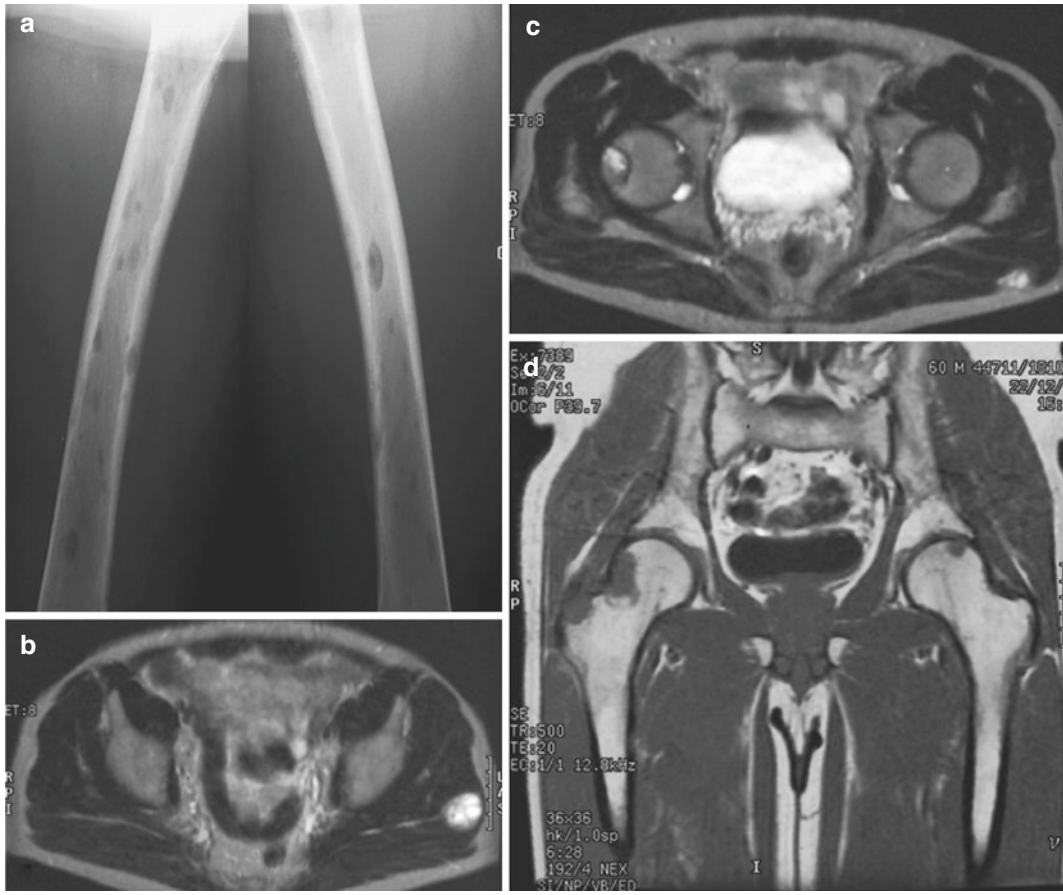

Fig. 13.44 (**a–d**) Fibrosarcoma multiforme in a 50-year-old man. (**a**) Radiographs of both femoral shafts. (**b**) Axial spin-echo T2-weighted MR image at the level of the acetabulum. (**c**) Axial spin-echo T2-weighted MR image at the level of the femoral heads. (**d**) Coronal spin-echo T1-weighted MR image. On conventional radiographs, there are multiple, oval, purely osteolytic lesions in the cortical bone of both femora (**a**). On the T2-weighted image, there is a rounded lesion within the left gluteus maximus muscle, consisting of multiple lobules of high signal intensity, separated by septa of intermediate signal intensity (**b**). On the T2-weighted image at the level of the femoral heads, there is an inhomogeneous lesion within the right femoral head, partly of high signal intensity. There is a small, high-intensity soft tissue lesion in the gluteus maximus muscle on the left side (**c**). On the coronal view, there are multiple lesions of intermediate signal intensity at both femoral heads and right greater trochanter (**d**). Coexistence of bone and soft tissue lesions is a rare finding in fibrosarcoma. Differentiation from metastatic fibrosarcoma remains difficult even histologically

Low-grade myxofibrosarcoma may not be confused with low-grade fibromyxoid sarcoma, another myxoid mesenchymal sarcoma with fibroblastic differentiation, which has – in contrast to low-grade myxofibrosarcoma – an indolent but ultimately malignant clinical course [101, 102].

13.6.3 Low-Grade Fibromyxoid Sarcoma

Low-grade fibromyxoid sarcoma previously known as Evans tumor demonstrates relatively low-grade histological features but paradoxically

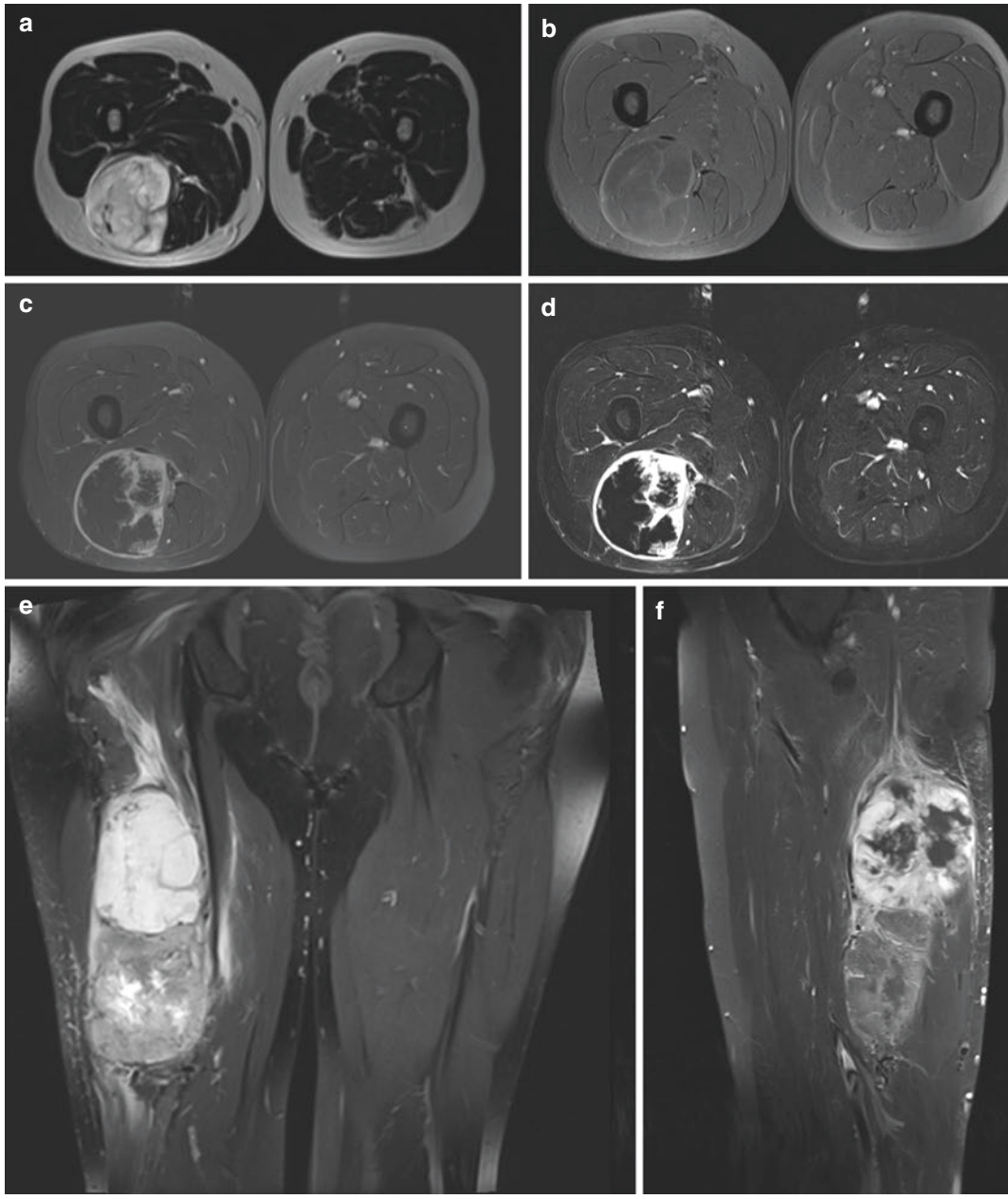

Fig. 13.45 (**a–f**) Myxofibrosarcoma in a 49-year-old man. (**a**) Axial turbo spin-echo T2-weighted MR image. (**b**) Axial fat-saturated T1-weighted MR image. (**c**) Axial fat-saturated T1-weighted MR image after gadolinium contrast injection. (**d**) Axial subtraction of the pre- and post-contrast T1 MR images. (**e**) Coronal fat-saturated T2-weighted MR image. (**f**) Sagittal fat-saturated T1-weighted MR image after gadolinium contrast injection: Large oval-shaped lesion in the hamstrings compartment showing very high T2 signal intensities (**a**), T1 signal intensities lower than the muscle (**b**), and large areas of nonenhancement centrally (**c, d**), suggesting a large myxoid component. The lesion is ill-defined with some perifascial extensions (**e**, **f**) (Courtesy of F. M. Vanhoenacker, Belgium)

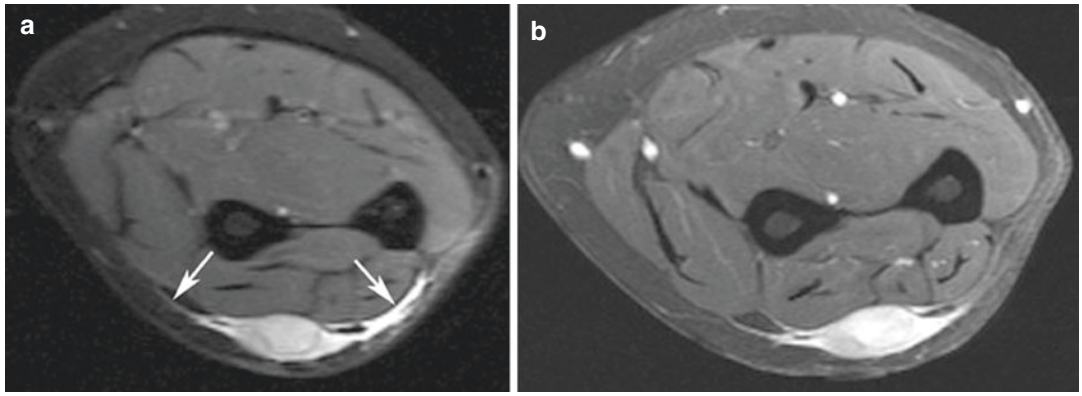

Fig. 13.46 (**a, b**) Myxofibrosarcoma in a 48-year-old woman. (**a**) Axial short-tau inversion recovery image demonstrates an intermediate-to-high signal mass in the subcutaneous tissues of the dorsal forearm. Prominent curvilinear extensions of high signal are present on both sides of the mass extending along the superficial fascial planes (*arrow*). (**b**) Axial T1-weighted post-gadolinium image with fat suppression at the same location demonstrates marked enhancement of tails, as well as of the mass, consistent with linear extension of tumor rather than edema (Reprinted with permission from Lefkowitz et al., *Skeletal Radiol* 2013, 42:809–818)

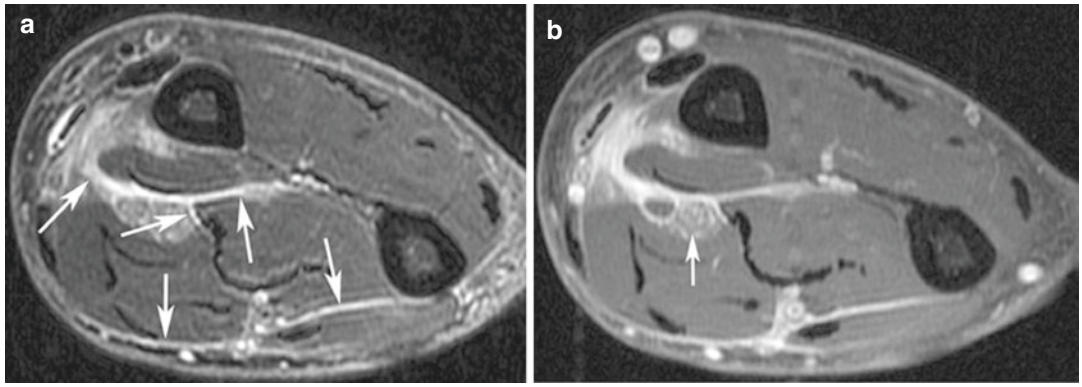

Fig. 13.47 (**a, b**) Myxofibrosarcoma of the right forearm in a 67-year-old man with high-grade myxofibrosarcoma. (**a**) Axial T2-weighted image with fat suppression demonstrates curvilinear extensions of high signal infiltrating along the deep muscular fascia between individual muscles (*arrows*). A discrete mass (not shown; average recorded size, 2.9 cm) was associated with these tails. (**b**) Axial T1-weighted post-contrast image with fat suppression demonstrates that these tails enhance avidly. Tumor also encases the median nerve (*arrow*). This appearance is characteristic of deep-seated myxofibrosarcoma, which can spread along multiple fascial planes. Being familiar with the infiltrative nature of myxofibrosarcoma, the radiologist who initially interpreted this scan reported that the tumor had spread along multiple fascial planes in the forearm. Based partially on the radiologist's recommendation, the surgeon subsequently performed an amputation despite the absence of an apparent "mass." Histopathological examination confirmed the presence of myxofibrosarcoma throughout the fascial planes of the forearm, with encasement of neurovascular structures. Amputation resulted in negative surgical margins; the patient has remained disease-free for 18 months (Reprinted with permission from Lefkowitz et al., *Skeletal Radiol* 2013, 42:809–818)

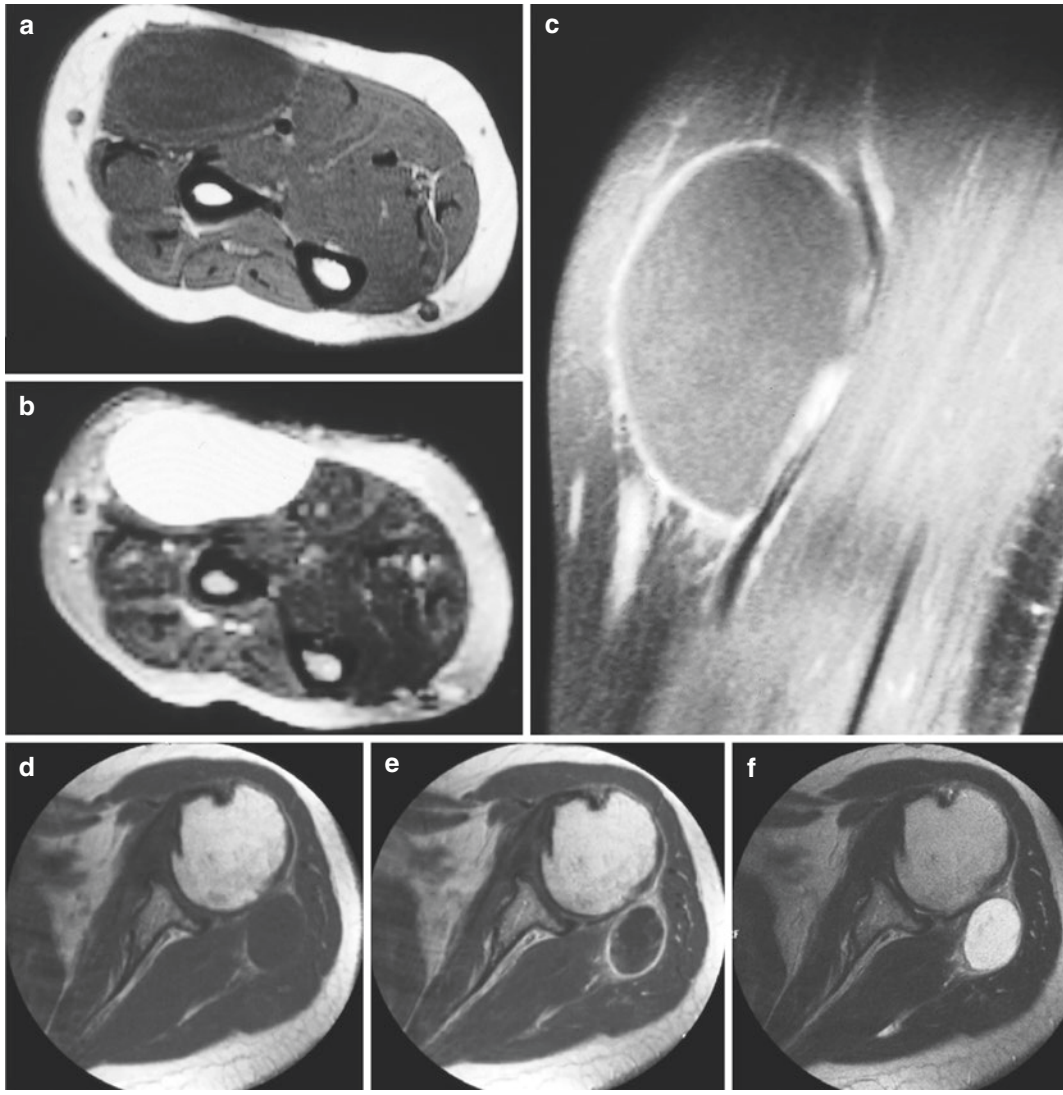

Fig. 13.48 Two cases of fibromyxoid sarcoma (**a–f**). (**a**) Axial spin-echo T1-weighted MR image. (**b**) Axial spin-echo T2-weighted MR image. (**c**) Sagittal spin-echo T1-weighted MR image after gadolinium contrast injection with fat suppression. (**d**) Axial spin-echo T1-weighted MR image. (**e**) Axial spin-echo T1-weighted MR image after gadolinium contrast injection. (**f**) Axial spin-echo T2-weighted MR image. Both have similar MRI features. Both lesions are of very low SI on T1-weighted MR image (**a, d**) and of very high SI on T2-weighted MR image (**b, c**) and show only minimal capsular enhancement after contrast administration (**c, f**). MR findings reflect the high content of myxoid tissue of both tumors

aggressive behavior characterized by high rates of local recurrence and metastasis [42]. It is a slow-growing, rare neoplasm that preferentially affects young and middle-aged adults (median age of 45 years) (Fig. 13.48). Most lesions arise from the deep soft tissues at the lower limb or thoracic wall and less frequently in the groin, buttock, axilla, and retroperitoneum [34]. The majority of cases occur in a subfascial location. They are often large at the time of diagnosis.

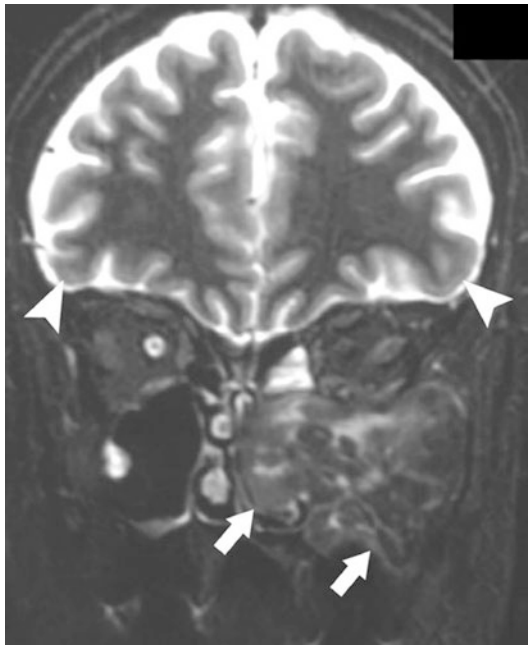

Fig. 13.49 Low-grade fibromyxoid sarcoma in the left maxillary sinus of a 48-year-old man. Coronal STIR image of maxillary sinus shows a gyriform pattern that consists of multiple folds of low signal intensity (*arrows*) in the tumor that mimic brain gyri (*arrowheads*) (Reprinted with permission from Hwang et al. [62])

Histopathologically, the lesion is characterized by intermingled fibrous and myxoid areas, a whorled growth pattern, and bland fibroblastic spindle cells. Cellularity is low and mitotic figures are uncommon. The current 2013 WHO classification considers MUC4 a highly sensitive and specific immunohistochemical marker for low-grade fibromyxoid sarcoma, and the presence of translocation t(7;16) leading to the formation of *FUS/CREB3L2* fusion gene is also a specific marker.

On ultrasound, low-grade fibromyxoid sarcoma may present as a heterogeneous ovoid mass containing nodules with target appearance. On CT, this sarcoma tends to be hypodense to muscle with focal isodensity. On MR imaging, low-grade fibromyxoid sarcoma may present as a mass with gyriform appearance (Figs. 13.49 and 13.50), displaying multiple folds of hypo- to isointense signal on T2-weighted images that enhance after intravenous contrast (probably related to highly cellular fibrous tissue). The areas of fluid-like hyperintensity between the folds in the gyriform pattern lack contrast enhancement probably representing myxoid material. The gyriform pattern is rather specific for this tumor [62].

In contrast to low-grade myxofibrosarcoma, low-grade fibromyxoid sarcoma has an aggressive clinical course characterized by a multiplicity of local recurrences and with the potential for metastasis to the lungs and occasionally to the bone. Surgical excision with wide margins is the treatment of choice. Slow tumor growth and long latency periods between diagnosis and recurrence underline the importance of a long-term clinical follow-up and imaging surveillance.

13.6.4 Sclerosing Epithelioid Fibrosarcoma

Sclerosing epithelioid fibrosarcoma is a deep-seated tumor of the limbs or limb girdles and occurs primarily in middle-aged and elderly patients without sex predilection. This malignant fibroblastic neoplasm is characterized by epithelioid fibroblasts arranged in distinct cords and nests in a densely sclerotic, hyalinized stroma. Calcifications may be present [100]. A subset seems to be related to low-grade fibromyxoid sarcoma.

Patients present with a mass of variable duration, and one-third have a history of recent enlargement and pain.

On imaging, a well-circumscribed, lobular or multinodular mass involving deep musculature with frequent periosteal attachment or bone erosion is seen. Reports on MR imaging are sparse. A large core with very low signal on T1 and T2 (probably representing the sclerotic, hyalinized stroma) may be seen, surrounded by intermediate signal in the periphery of the tumor [14, 122] (Figs. 13.51 and 13.52).

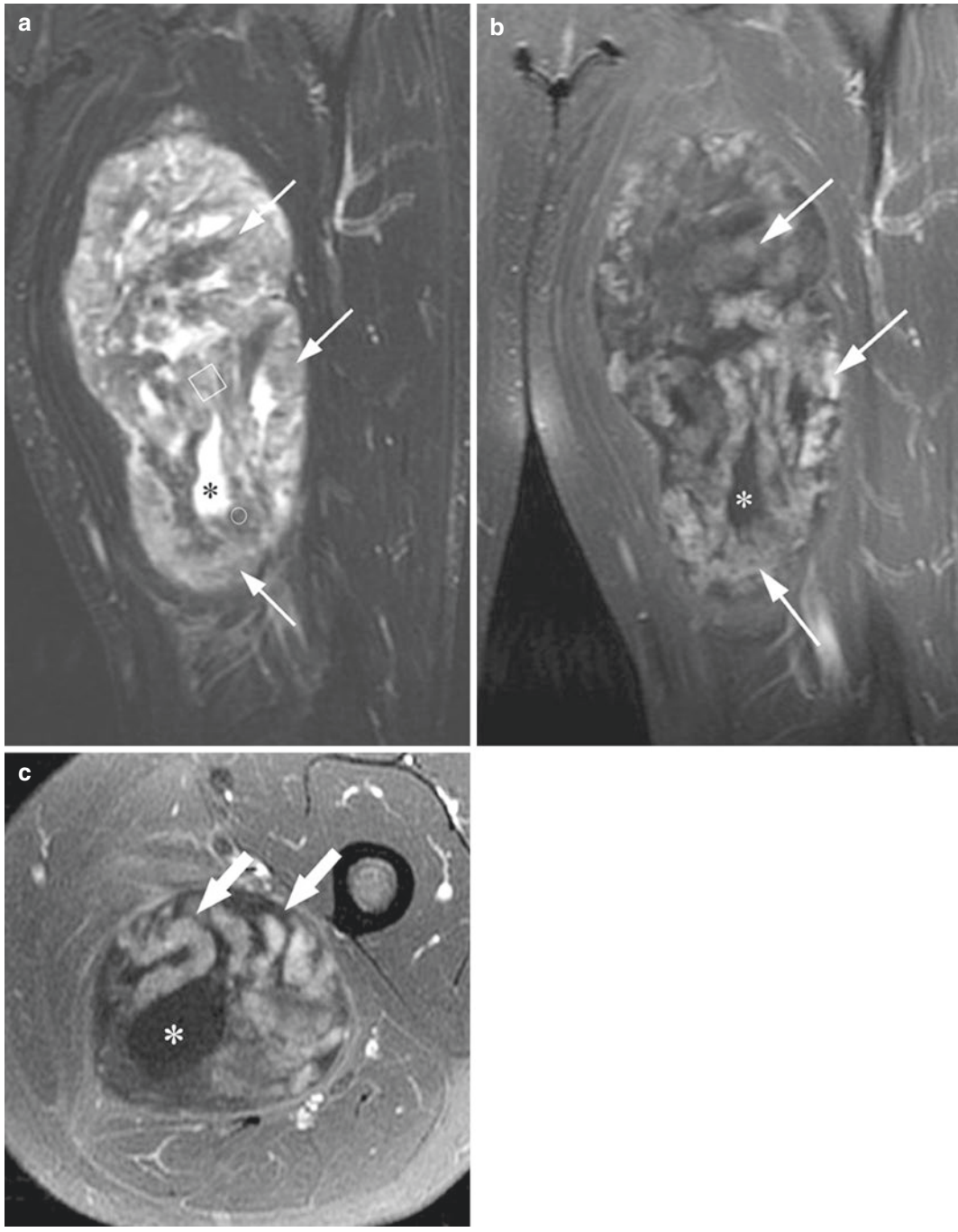

Fig. 13.50 (**a–c**) Low-grade fibromyxoid sarcoma in the thigh of a 59-year-old man. (**a**) Coronal T2-weighted fat-saturated image shows gyriform pattern (*arrows*) of heterogeneous T2 signal intensity. The gyriform pattern consists of hypo-, iso-, and hyperintense signal and probably reflects alternating areas of densely fibrotic (*circle*) and fibromyxoid (*square*) stroma of tumor. The fluid-like high-signal area (*asterisk*) probably represents predominantly myxoid area in the tumor. (**b**) Coronal and **c** axial T1-weighted fat-saturated post-contrast images show gyriform contrast enhancement (*arrows*). The myxoid component (*asterisk*) lacks contrast enhancement (Reprinted with permission from Hwang et al. [62])

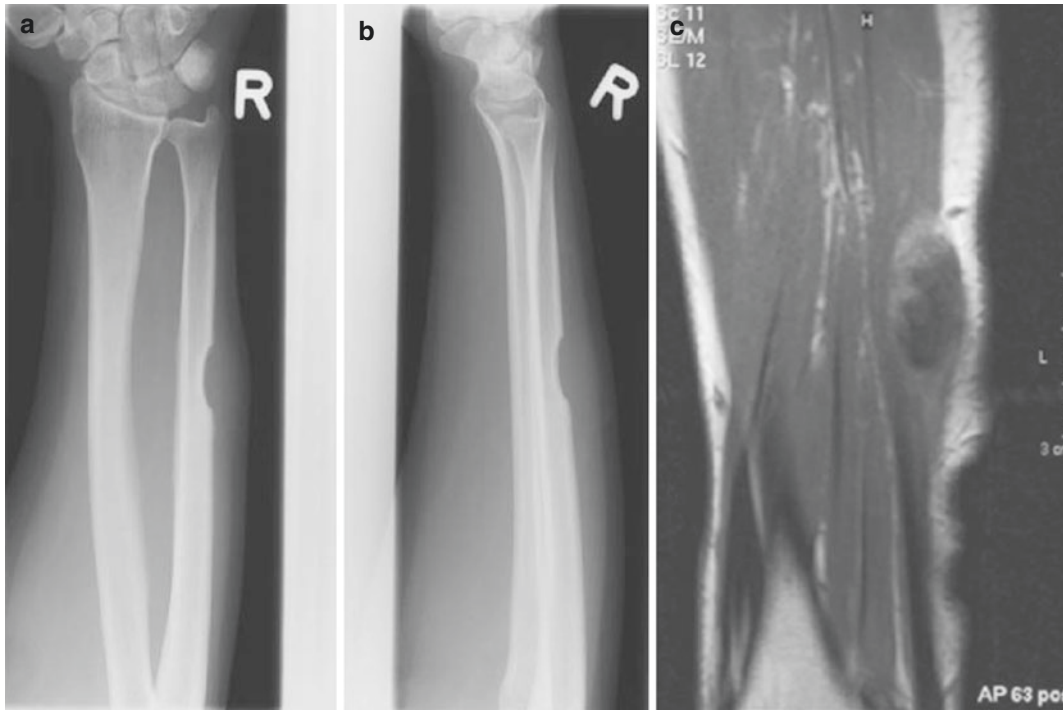

Fig. 13.51 (**a–c**) Sclerosing epithelioid fibrosarcoma in the forearm of a 32-year-old woman. (**a**) Anteroposterior and (**b**) lateral radiographs show a punched-out osteolytic lesion surrounded by a sclerotic rim at the middiaphysis of the right ulna. (**c**) An MRI scan of the right forearm shows a 5 × 1.5-cm intramuscular tumor with a large hypointense core

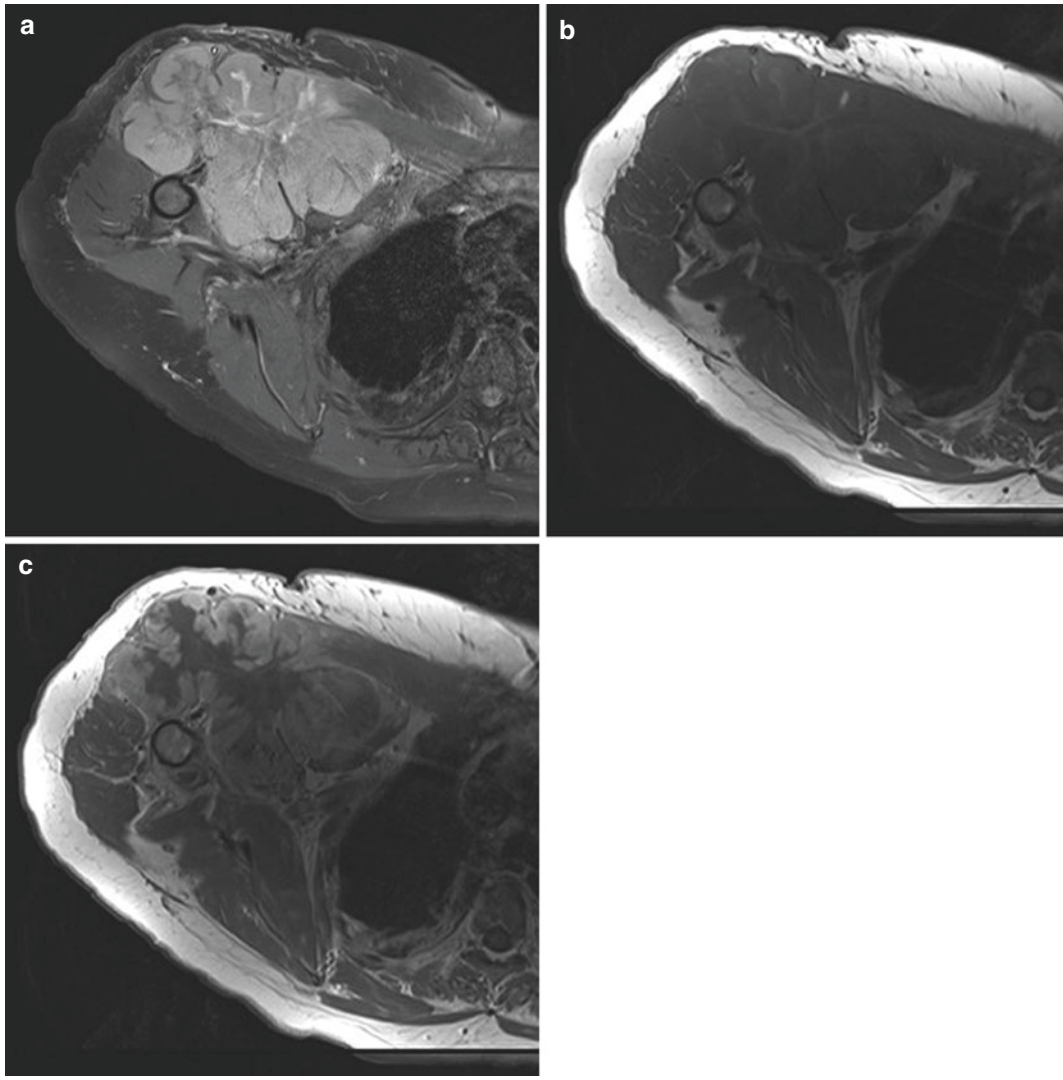

Fig. 13.52 (**a–c**) Sclerosing epithelioid fibrosarcoma in the anterior soft tissues of the right shoulder (**a**) Axial T2-weighted MR image with fat saturation (**b**) Axial T1-weighted MR image (**c**) Axial post-contrast T1-weighted MR image. A large multilobulated mass is located in the pectoralis, biceps, and brachialis muscle bellies and abutting the humeral diaphysis. Fairly homogeneous lesion with intermediate signal on T2- and low signal on T1-weighted MR images. Thick, irregular band of enhancement is seen in the periphery of the lesion

Key Points

1. Fibroblastic/myofibroblastic tumors are relatively common soft tissue tumors and often have a high rate of recurrence after local excision. The fascial tail sign should prompt the radiologist to specifically describe to the surgeon the distant tumor extensions along fascial planes.
2. Histopathological and imaging features are related to the age of the lesions. The proliferative phase of many benign and locally aggressive fibrous tumors may resemble sarcoma (pseudosarcomatous appearance). Follow-up after a few weeks (with or without biopsy at the first workup) may disclose the benign nature by demonstrating shrinkage/fibrosis of the lesion.
3. Benign tumors mostly have a characteristic location (fibromatosis colli, fibroma of the tendon sheath, elastofibroma, palmar and plantar fibromatosis, nuchal fibroma, abdominal desmoid, ischemic/decubital fasciitis, etc.).
4. Diagnosis of myositis ossificans commonly relies on plain film or CT findings demonstrating a zoning phenomenon in evolution.
5. Desmoid-type fibromatosis contains (curvilinear) components of low SI on T2 representing dense collagenous bands; using gradient echo sequences, desmoids can be differentiated from tumors having areas of low SI on T2 due to hemorrhage (such as pigmented villonodular synovitis).
6. Fibrous soft tissue lesions that contain fat (high SI on T1) include elastofibroma, lipofibromatosis, fibrous hamartoma of infancy, and some (lipomatous) solitary fibrous tumors.
7. Proliferative myositis can be characterized by the "dry-cracked mud" or "checkerboard" pattern on ultrasound, and the preserved muscle fibers within the lesion are also demonstrated on MRI.
8. Myxofibrosarcoma can be suspected when enhancing fascial tails extend around muscle bellies distant from the tumor center.
9. Low-grade fibromyxoid sarcoma is often characterized on MRI by its gyriform pattern of low SI on T2 (and enhancing) with intervening "sulci" of high SI on T2.
10. Myxoinflammatory fibroblastic sarcoma frequently occurs in acral location adjacent to tendon sheaths and is often erroneously diagnosed as giant cell tumor of the tendon sheath although myxoinflammatory fibroblastic sarcoma does not demonstrate low SI on T2 throughout the tumor.

Acknowledgment The current revision of this chapter is gratefully dedicated to the memory of Professor Arthur De Schepper (November 30, 1937–October 4, 2013).

References

1. Ablin DS, Jain K, Howell L, West DC (1998) Ultrasound and MR imaging of fibromatosis colli (sternomastoid tumor of infancy). Pediatr Radiol 28:230–233
2. Ackman JB, Whitman GJ, Chew FS (1994) Aggressive fibromatosis. AJR Am J Roentgenol 163:544
3. Ainsworth KE, Chavhan GB, Gupta AA, Hopyan S, Taylor G (2014) Congenital infantile fibrosarcoma: review of imaging features. Pediatr Radiol 44:1124–1129
4. Akisue T, Matsumoto K, Kizaki T, Fujita I, Yamamoto T, Yoshiya S, Kurosaka M (2003) Solitary fibrous tumor in the extremity: case report and review of the literature. Clin Orthop Relat Res 411:236–244
5. Allen RA, Woolner LB, Ghormley RK (1955) Soft-tissue tumors of the sole; with special reference to

plantar fibromatosis. J Bone Joint Surg Am 37-A: 14–26
6. Baheti AD, Tirumani SH, Rosenthal MH, Howard SA, Shinagare AB, Ramaiya NH, Jagannathan JP (2015) Myxoid soft-tissue neoplasms: comprehensive update of the taxonomy and MRI features. AJR Am J Roentgenol 204:374–385
7. Bahrami A, Folpe AL (2010) Adult-type fibrosarcoma: a reevaluation of 163 putative cases diagnosed at a single institution over a 48-year period. Am J Surg Pathol 34:1504–1513
8. Bulam H, Sezgin B, Findikcioglu K, Cesur N (2015) A 1-year-old boy with paraspinal elastofibroma: the youngest diagnosed elastofibroma. Ann Thorac Surg 100:302–304
9. Canale S, Vanel D, Couanet D, Patte C, Caramella C, Dromain C (2009) Infantile fibrosarcoma: magnetic resonance imaging findings in six cases. Eur J Radiol 72:30–37
10. Casillas J, Sais GJ, Greve JL, Iparraguirre MC, Morillo G (1991) Imaging of intra- and extraabdominal desmoid tumors. Radiographics 11:959–968
11. Ceulemans LJ, Jacomen G, Vanhoenacker FM (2013) Decubital ischemic fasciitis. JBR-BTR 96:52
12. Chandrasekar CR, Grimer RJ, Carter SR, Tillman RM, Abudu A, Davies AM, Sumathi VP (2008) Elastofibroma dorsi: an uncommon benign pseudotumour. Sarcoma 2008:756565
13. Cho YH, Ahn KS, Kang CH, Kim CH (2015) Calcifying aponeurotic fibroma of the dorsum of the foot: radiographic and magnetic resonance imaging findings in a four-year-old boy. Iran J Radiol 12:e23911
14. Christensen DR, Ramsamooj R, Gilbert TJ (1997) Sclerosing epithelioid fibrosarcoma: short T2 on MR imaging. Skeletal Radiol 26:619–621
15. Cintora E, del Cura JL, Ruiz JC, Grau M, Ereño C (1993) Case report 807: Infantile desmoid-type fibromatosis. Skeletal Radiol 22:533–535
16. Coyle J, White LM, Dickson B, Ferguson P, Wunder J, Naraghi A (2013) MRI characteristics of nodular fasciitis of the musculoskeletal system. Skeletal Radiol 42:975–982
17. Crawford SC, Harnsberger HR, Johnson L, Aoki JR, Giley J (1988) Fibromatosis colli of infancy: CT and sonographic findings. AJR Am J Roentgenol 151:1183–1184
18. Dalén BP, Geijer M, Kvist H, Bergh PM, Gunterberg BU (2006) Clinical and imaging observations of desmoid tumors left without treatment. Acta Orthop 77:932–937
19. De Keersmaeker A, Vanhoenacker F (2016) Imaging Features of Knuckle Pads. J Belgian Society of Radiol 100(1):67. doi: http://doi.org/10.5334/jbr-btr.1096
20. De Maeseneer M, Van Isacker T, Lenchik L, Van Caillie MA, Shahabpour M (2014) Fibroma of the tendon sheath of the long head of the biceps tendon. Skeletal Radiol 43:399–402
21. De Schepper AM, Degryse HR (1990) Imaging findings in a patient with pentazocine-induced myopathy. AJR Am J Roentgenol 154:343–344
22. Deepti AN, Madhuri V, Walter NM, Cherian RA (2008) Lipofibromatosis: report of a rare paediatric soft tissue tumour. Skeletal Radiol 37:555–558
23. Demir MK, Beser M, Akinci O (2007) Case 118: proliferative myositis. Radiology 244:613–616
24. Devaney D, Livesley P, Shaw D (1995) Elastofibroma dorsi: MRI diagnosis in a young girl. Pediatr Radiol 25:282–283
25. Di Vito A, Scali E, Ferraro G, Mignogna C, Presta I, Camastra C, Donato G, Barni T (2015) Elastofibroma dorsi: a histochemical and immunohistochemical study. Eur J Histochem 59:2459
26. Dinauer PA, Brixey CJ, Moncur JT, Fanburg-Smith JC, Murphey MD (2007) Pathologic and MR imaging features of benign fibrous soft-tissue tumors in adults. Radiographics 27:173–187
27. Dong PR, Seeger LL, Eckardt JJ, Mirra JM (1994) Case report 847. Juxtacortical aggressive fibromatosis (desmoplastic fibroma) of the forearm. Skeletal Radiol 23:560–563
28. Duda S, Bittner R, Laniado M, Lobeck H, Langer M (1989) Bildgebende Diagnostik der agressiven Fibromatosen und MRT-pathologischen Korrelation. Fortschr Röntgenstr 151:57–62
29. Eastley N, Aujla R, Silk R, Richards CJ, McCulloch TA, Esler CP, Ashford RU (2014) Extra-abdominal desmoid fibromatosis--a sarcoma unit review of practice, long term recurrence rates and survival. Eur J Surg Oncol 40:1125–1130
30. Eich GF, Hoeffel JC, Tschäppeler H, Gassner I, Willi UV (1998) Fibrous tumours in children: imaging features of a heterogeneous group of disorders. Pediatr Radiol 28:500–509
31. Einstein DM, Tagliabue JR, Desai RK (1991) Abdominal desmoids: CT findings in 25 patients. AJR Am J Roentgenol 157:275–279
32. Enzinger F, Weiss S (1995) Soft tissue tumors, 3rd edn. Mosby, St Louis
33. Enzinger FM, Dulcey F (1967) Proliferative myositis. Report of thirty-three cases. Cancer 20:2213–2223
34. Evans HL (1993) Low-grade fibromyxoid sarcoma. A report of 12 cases. Am J Surg Pathol 17:595–600
35. Fang N, Wang YL, Zeng L, Wu ZJ, Cui XJ, Wang Q, Gao S, Ding W (2016) Characteristics of elastofibroma dorsi on PET/CT imaging with (18) F-FDG. Clin Imaging 40:110–113
36. Feld R, Burk DL, McCue P, Mitchell DG, Lackman R, Rifkin MD (1990) MRI of aggressive fibromatosis: frequent appearance of high signal intensity on T2-weighted images. Magn Reson Imaging 8:583–588
37. Fetsch JF, Miettinen M (1998) Calcifying aponeurotic fibroma: a clinicopathologic study of 22 cases arising in uncommon sites. Hum Pathol 29:1504–1510
38. Fetsch JF, Miettinen M, Laskin WB, Michal M, Enzinger FM (2000) A clinicopathologic study of 45 pediatric soft tissue tumors with an admixture of adipose tissue and fibroblastic elements, and a proposal for classification as lipofibromatosis. Am J Surg Pathol 24:1491–1500

39. Fisher C (2004) Myofibrosarcoma. Virchows Arch 445:215–223
40. Fletcher DM, Julia AB, Hogendoorn PCW, Mertens F (2013) World Health Organisation classification of tumors of soft tissue and bone. IARC, Lyon, pp 45–107
41. Fletcher DM, Krishnan Unni K, Mertens F (2002) World Health Organization classification of tumours. Pathology and genetics of tumours of soft tissue and bone. IARC, Lyon, pp 47–106
42. Folpe AL, Lane KL, Paull G, Weiss SW (2000) Low-grade fibromyxoid sarcoma and hyalinizing spindle cell tumor with giant rosettes: a clinicopathologic study of 73 cases supporting their identity and assessing the impact of high-grade areas. Am J Surg Pathol 24:1353–1360
43. Fornage B (1995) Musculoskeletal ultrasound. Churchill Livingstone, New York
44. Fox MG, Kransdorf MJ, Bancroft LW, Peterson JJ, Flemming DJ (2003) MR imaging of fibroma of the tendon sheath. AJR Am J Roentgenol 180:1449–1453
45. Francis IR, Dorovini-Zis K, Glazer GM, Lloyd RV, Amendola MA, Martel W (1986) The fibromatoses: CT-pathologic correlation. AJR Am J Roentgenol 147:1063–1066
46. Frei S, de Lange EE, Fechner RE (1991) Case report 690. Nodular fasciitis of the elbow. Skeletal Radiol 20:468–471
47. Fukunaga M, Fukunaga N (1997) Low-grade myxofibrosarcoma: progression in recurrence. Pathol Int 47:161–165
48. Gaetke-Udager K, Yablon CM, Lucas DR, Morag Y (2016) Myxoinflammatory fibroblastic sarcoma: spectrum of disease and imaging presentation. Skeletal Radiol 45:347–356
49. Gallego M, Millan J, Gil-Martin R, Cespedes M, Pulpeiro R, Salamanca J (1987) Juvenile hyalin fibromatosis: radiographic and pathologic findings of a new case. J Med Imaging 1:251–257
50. Gartlan MG, Haller JR, Hoffman HT, Dolan KD (1993) Fibrosarcoma of the posterior neck. Ann Otol Rhinol Laryngol 102:820–822
51. Gielen JL, De Schepper AM, Vanhoenacker F, Parizel PM, Wang XL, Sciot R, Weyler J (2004) Accuracy of MRI in characterization of soft tissue tumors and tumor-like lesions. A prospective study in 548 patients. Eur Radiol 14:2320–2330
52. Ginat DT, Bokhari A, Bhatt S, Dogra V (2011) Imaging features of solitary fibrous tumors. AJR Am J Roentgenol 196:487–495
53. Glover M, Chebib I, Simeone FJ (2014) Intra-articular fibroma of tendon sheath arising in the acromioclavicular joint. Skeletal Radiol 43:681–686
54. Gómez García EB, Knoers NV (2009) Gardner's syndrome (familial adenomatous polyposis): a cilia-related disorder. Lancet Oncol 10:727–735
55. Goto H, Iwama Y, Kunisada M, Fujii M, Nisigori M, Sugimura K (2013) Imaging features of dermatofibrosarcoma protuberans with pathologic correlation and assessments for recurrence potential, ECR, Educational exhibit, Kobe city, Poster C2231
56. Ha DH, Choi S, Kim SJ, Lih W (2015) Intra-articular fibroma of tendon sheath in a knee joint associated with iliotibial band friction syndrome. Korean J Radiol 16:169–174
57. Hartman TE, Berquist TH, Fetsch JF (1992) MR imaging of extraabdominal desmoids: differentiation from other neoplasms. AJR Am J Roentgenol 158:581–585
58. Hawnaur JM, Jenkins JP, Isherwood I (1990) Magnetic resonance imaging of musculoaponeurotic fibromatosis. Skeletal Radiol 19:509–514
59. Hayward PG, Orgill DP, Mulliken JB, Perez-Atayde AR (1995) Congenital fibrosarcoma masquerading as lymphatic malformation: report of two cases. J Pediatr Surg 30:84–88
60. Hochhegger B, Marchiori E, Soares Souza L (2011) MR diffusion in elastofibroma dorsi. Arch Bronconeumol 47:535–536; author reply p 536
61. Huang HY, Lal P, Qin J, Brennan MF, Antonescu CR (2004) Low-grade myxofibrosarcoma: a clinicopathologic analysis of 49 cases treated at a single institution with simultaneous assessment of the efficacy of 3-tier and 4-tier grading systems. Hum Pathol 35:612–621
62. Hwang S, Kelliher E, Hameed M (2012) Imaging features of low-grade fibromyxoid sarcoma (Evans tumor). Skeletal Radiol 41:1263–1272
63. Ichikawa T, Koyama A, Fujimoto H, Honma M, Saiga T, Matsubara N, Ozeki Y, Uchiyama G, Ohtomo K (1994) Abdominal wall desmoid mimicking intra-abdominal mass: MR features. Magn Reson Imaging 12:541–544
64. Ilaslan H, Joyce M, Bauer T, Sundaram M (2006) Decubital ischemic fasciitis: clinical, pathologic, and MRI features of pseudosarcoma. AJR Am J Roentgenol 187:1338–1341
65. Ishii N, Matsui K, Ichiyama S, Takahashi Y, Nakajima H (1989) A case of infantile digital fibromatosis showing spontaneous regression. Br J Dermatol 121:129–133
66. Jabra AA, Taylor GA (1993) MRI evaluation of superficial soft tissue lesions in children. Pediatr Radiol 23:425–428
67. Jarraya M, Parva P, Stone M, Klein MJ, Guermazi A (2014) Atypical proliferative myositis: original MR description with pathologic correlation: case report. Skeletal Radiol 43:1155–1159
68. Desimpel J, Vanhoenacker FM, Pilate I, Dijck HV (2016) Inflammatory myofibroblastic tumour, {Online}. URL: http://www.eurorad.org/case.php?id=14038 doi: 10.1594/EURORAD/CASE.14038
69. Kamali F, Wang WL, Guadagnolo BA, Fox PS, Lewis VO, Lazar AJ, Conley AP, Ravi V, Toliyat M, Ladha HS, Hobbs BP, Amini B (2016) MRI may be used as a prognostic indicator in patients with extra-abdominal desmoid tumours. Br J Radiol 89:20150308
70. Kamata Y, Anazawa U, Morioka H, Morii T, Miura K, Mukai M, Yabe H, Toyama Y (2011) Natural evolution of desmoplastic fibroblastoma on magnetic resonance imaging: a case report. J Med Case Rep 5:139
71. Kaplan SL, Coulter C, Fetters L (2013) Physical therapy management of congenital muscular torti-

collis: an evidence-based clinical practice guideline: from the Section on Pediatrics of the American Physical Therapy Association. Pediatr Phys Ther 25:348–394
72. Karakurt O, Kaplan T, Gunal N, Gulbahar G, Kocer B, Han S, Dural K, Sakinci U (2014) Elastofibroma dorsi management and outcomes: review of 16 cases. Interact Cardiovasc Thorac Surg 18:197–201
73. Kasper B, Baumgarten C, Bonvalot S, Haas R, Haller F, Hohenberger P, Moreau G, van der Graaf WT, Gronchi A, Desmoid Working Group (2015) Management of sporadic desmoid-type fibromatosis: a European consensus approach based on patients' and professionals' expertise – a sarcoma patients EuroNet and European Organisation for Research and Treatment of Cancer/Soft Tissue and Bone Sarcoma Group initiative. Eur J Cancer 51:127–136
74. Kaya M, Wada T, Nagoya S, Sasaki M, Matsumura T, Yamaguchi T, Hasegawa T, Yamashita T (2008) MRI and histological evaluation of the infiltrative growth pattern of myxofibrosarcoma. Skeletal Radiol 37:1085–1090
75. Kikuta K, Kubota D, Yoshida A, Morioka H, Toyama Y, Chuuman H, Kawai A (2015) An analysis of factors related to the tail-like pattern of myxofibrosarcoma seen on MRI. Skeletal Radiol 44:55–62
76. Kilpatrick SE, Ward WG (1999) Myxofibrosarcoma of soft tissues: cytomorphologic analysis of a series. Diagn Cytopathol 20:6–9
77. Kim E, Kim C, Romero J, Chung W, Isiklar A (1995) Different biologic features of desmoid tumors demonstrated with MR imaging, RNSA, scientific exhibition, Poster 278 SK, Chicago, 25 Nov–1 Dec
78. Koenigsberg RA, Faro S, Chen X, Marlowe F (1996) Nodular fasciitis as a vascular neck mass. AJNR Am J Neuroradiol 17:567–569
79. Kotha GK, Bj V, Maryada VR, Jawalkar H (2014) Multifocal nodular fasciitis of the hand and shoulder: case report. J Hand Surg [Am] 39:2468–2471
80. Koujok K, Ruiz RE, Hernandez RJ (2005) Myofibromatosis: imaging characteristics. Pediatr Radiol 35:374–380
81. Kransdorf M, Murphey M (1997) Imaging of soft tissue tumors. Saunders, Philadelphia, pp 143–186
82. Kransdorf MJ, Meis JM, Montgomery E (1992) Elastofibroma: MR and CT appearance with radiologic-pathologic correlation. AJR Am J Roentgenol 159:575–579
83. Kwak MJ, Kim SK, Lee S, Jun S, Lee A (2015) Radiological features of a fibro-osseous pseudotumor in the digit: a case report. J Korean Soc Radiol 73:131–135
84. Lacout A, Jarraya M, Marcy PY, Thariat J, Carlier RY (2012) Myositis ossificans imaging: keys to successful diagnosis. Indian J Radiol Imaging 22:35–39
85. Lang P, Suh KJ, Grampp S, Steinbach L, Steiner E, Peterfy C, Tirman P, Schwickert H, Rosenau W, Genant HK (1995) CT and MRI in elastofibroma. A rare, benign soft tissue tumor. Radiologe 35:611–615
86. Lee GK, Suh KJ, Lee SM, Lee SJ (2010) Nuchal-type fibroma of the buttock: magnetic resonance imaging findings. Jpn J Radiol 28:538–541
87. Lee KJ, Jin W, Kim GY, Rhee SJ, Park SY, Park JS, Ryu KN (2015) Sonographic features of superficial-type nodular fasciitis in the musculoskeletal system. J Ultrasound Med 34:1465–1471
88. Lee S, Choi YH, Cheon JE, Kim MJ, Lee MJ, Koh MJ (2014) Ultrasonographic features of fibrous hamartoma of infancy. Skeletal Radiol 43:649–653
89. Lee TH, Wapner KL, Hecht PJ (1993) Current concepts review: plantar fibromatosis. J Bone Joint Surg Am 75:1080–1084
90. Li H, Wang dL, Liu XW, Geng ZJ, Xie CM (2014) MRI characterization of inflammatory myofibroblastic tumors in the maxillofacial region. Diagn Interv Radiol 20:310–315
91. Liessi G, Tregnaghi A, Barbazza R, Scapinello A, Muzzio PC (1991) Elastofibroma: CT and MR findings. J Belge Radiol 74:37–39
92. Ceulemans L, Jacomen G, Vanhoenacker FM (2013) Decubital ischemic fasciitis. J Belgian Society of Radiol 96(1):52. doi: http://doi.org/10.5334/jbr-btr.205
93. Liu D, Perera W, Schlicht S, Choong P, Slavin J, Pianta M (2015) Musculoskeletal desmoid tumours: Pre- and post-treatment radiological appearances. J Med Imaging Radiat Oncol 59:480–485
94. Lopez-Ben R, Dehghanpisheh K, Chatham WW, Lee DH, Oakes J, Alarcón GS (2006) Ultrasound appearance of knuckle pads. Skeletal Radiol 35:823–827
95. Lourie JA, Lwin KY, Woods CG (1992) Case report 734. Fibroma of tendon sheath eroding 3rd metatarsal bone. Skeletal Radiol 21:273–275
96. Lu L, Lao IW, Liu X, Yu L, Wang J (2015) Nodular fasciitis: a retrospective study of 272 cases from China with clinicopathologic and radiologic correlation. Ann Diagn Pathol 19:180–185
97. Malghem J, Baudrez V, Lecouvet F, Lebon C, Maldague B, Vande Berg B (2004) Imaging study findings in elastofibroma dorsi. Joint Bone Spine 71:536–541
98. Marin ML, Perzin KH, Markowitz AM (1989) Elastofibroma dorsi: benign chest wall tumor. J Thorac Cardiovasc Surg 98:234–238
99. Massengill AD, Sundaram M, el-Kathol MH, Khoury GY, Buckwalter JH, Wade TP (1993) Elastofibroma dorsi: a radiological diagnosis. Skeletal Radiol 22:121–123
100. Meiss-Kindblom J, Enzinger F (1996) Color atlas of soft tissue tumors. Mosby-Wolfe, St Louis
101. Mentzel T, Calonje E, Wadden C, Camplejohn RS, Beham A, Smith MA, Fletcher CD (1996) Myxofibrosarcoma. Clinicopathologic analysis of 75 cases with emphasis on the low-grade variant. Am J Surg Pathol 20:391–405
102. Mentzel T, Katenkamp D, Fletcher CD (1996) Low malignancy myxofibrosarcoma versus low malignancy fibromyxoid sarcoma. Distinct entities with

similar names but different clinical course. Pathologe 17:116–121
103. Merriman DJ, Deavers MT, Czerniak BA, Lin PP (2010) Massive desmoplastic fibroblastoma with scapular invasion. Orthopedics 33(8)
104. Meyer CA, Kransdorf MJ, Jelinek JS, Moser RP (1991) MR and CT appearance of nodular fasciitis. J Comput Assist Tomogr 15:276–279
105. Michal M, Fetsch JF, Hes O, Miettinen M (1999) Nuchal-type fibroma: a clinicopathologic study of 52 cases. Cancer 85:156–163
106. Milos RI, Moritz T, Bernathova M, Amann G, Panotopoulos J, Noebauer-Huhmann IM, Bodner G (2015) Superficial desmoid tumors: MRI and ultrasound imaging characteristics. Eur J Radiol 84:2194–2201
107. Minarro JC, Urbano-Luque MT, López-Jordan A, Roman-Torres M, Carpintero-Benítez P (2015) The comparison of measurement accuracy among three different imaging modalities in evaluating elastofibroma dorsi. An analysis of 52 cases. Int Orthop 39:1145–1149
108. Montgomery E, Goldblum JR, Fisher C (2001) Myofibrosarcoma: a clinicopathologic study. Am J Surg Pathol 25:219–228
109. Moosavi CA, Al-Nahar LA, Murphey MD, Fanburg-Smith JC (2008) Fibroosseous pseudotumor of the digit: a clinicopathologic study of 43 new cases. Ann Diagn Pathol 12:21–28
110. Morii T, Mochizuki K, Sano H, Fujino T, Harasawa A, Satomi K (2008) Occult myofibroblastic sarcoma detected on FDG-PET performed for cancer screening. Ann Nucl Med 22:811–815
111. Morii T, Yoshiyama A, Morioka H, Anazawa U, Mochizuki K, Yabe H (2008) Clinical significance of magnetic resonance imaging in the preoperative differential diagnosis of calcifying aponeurotic fibroma. J Orthop Sci 13:180–186
112. Morrison WB, Schweitzer ME, Wapner KL, Lackman RD (1994) Plantar fibromatosis: a benign aggressive neoplasm with a characteristic appearance on MR images. Radiology 193:841–845
113. Murphey MD, Ruble CM, Tyszko SM, Zbojniewicz AM, Potter BK, Miettinen M (2009) From the archives of the AFIP: musculoskeletal fibromatoses: radiologic-pathologic correlation. Radiographics 29:2143–2173
114. Musyoki FN, Nahal A, Powell TI (2012) Solitary fibrous tumor: an update on the spectrum of extrapleural manifestations. Skeletal Radiol 41:5–13
115. Nishio J, Inamitsu H, Iwasaki H, Hayashi H, Naito M (2014) Calcifying aponeurotic fibroma of the finger in an elderly patient: CT and MRI findings with pathologic correlation. Exp Ther Med 8:841–843
116. Nofal A, Sanad M, Assaf M, Nofal E, Nassar A, Almokadem S, Attwa E, Elmosalamy K (2009) Juvenile hyaline fibromatosis and infantile systemic hyalinosis: a unifying term and a proposed grading system. J Am Acad Dermatol 61:695–700
117. O'Keefe F, Kim EE, Wallace S (1990) Magnetic resonance imaging in aggressive fibromatosis. Clin Radiol 42:170–173
118. Oda Y, Takahira T, Kawaguchi K, Yamamoto H, Tamiya S, Matsuda S, Tanaka K, Iwamoto Y, Tsuneyoshi M (2004) Low-grade fibromyxoid sarcoma versus low-grade myxofibrosarcoma in the extremities and trunk. A comparison of clinicopathological and immunohistochemical features. Histopathology 45:29–38
119. Ogose A, Hotta T, Emura I, Higuchi T, Kusano N, Saito H (2000) Collagenous fibroma of the arm: a report of two cases. Skeletal Radiol 29:417–420
120. Oguz B, Ozcan HN, Omay B, Ozgen B, Haliloglu M (2015) Imaging of childhood inflammatory myofibroblastic tumor. Pediatr Radiol 45:1672–1681
121. Oliveira AM, Chou MM (2014) USP6-induced neoplasms: the biologic spectrum of aneurysmal bone cyst and nodular fasciitis. Hum Pathol 45:1–11
122. Ossendorf C, Studer GM, Bode B, Fuchs B (2008) Sclerosing epithelioid fibrosarcoma: case presentation and a systematic review. Clin Orthop Relat Res 466:1485–1491
123. Otero S, Moskovic EC, Strauss DC, Benson C, Miah AB, Thway K, Messiou C (2015) Desmoid-type fibromatosis. Clin Radiol 70:1038–1045
124. Posner MC, Shiu MH, Newsome JL, Hajdu SI, Gaynor JJ, Brennan MF (1989) The desmoid tumor. Not a benign disease. Arch Surg 124:191–196
125. Pretorius ES, Hruban RH, Fishman EK (1995) Recurrent fibromatosis in a patient with breast carcinoma. Computed tomography findings with magnetic resonance imaging and pathologic correlation. Invest Radiol 30:381–383
126. Pulitzer DR, Martin PC, Reed RJ (1989) Fibroma of tendon sheath. A clinicopathologic study of 32 cases. Am J Surg Pathol 13:472–479
127. Quinn SF, Erickson SJ, Dee PM, Walling A, Hackbarth DA, Knudson GJ, Moseley HS (1991) MR imaging in fibromatosis: results in 26 patients with pathologic correlation. AJR Am J Roentgenol 156:539–542
128. Reed M, Gooding GA, Kerley SM, Himebaugh-Reed MS, Griswold VJ (1991) Sonography of plantar fibromatosis. J Clin Ultrasound 19:578–582
129. Reuther G, Mutschler W (1988) An unusual location of a myxofibrosarcoma. ROFO 149:544–545
130. Robbin MR, Murphey MD, Temple HT, Kransdorf MJ, Choi JJ (2001) Imaging of musculoskeletal fibromatosis. Radiographics 21:585–600
131. Samadi DS, McLaughlin RB, Loevner LA, LiVolsi VA, Goldberg AN (2000) Nuchal fibroma: a clinicopathological review. Ann Otol Rhinol Laryngol 109:52–55
132. Samarakoon L, Fernanado T, Liyanage E, Wirithamulla H, Perera KS (2014) Unusual case of recurrent thigh lump in a girl: a case report. J Med Case Rep 8:245
133. Sarteschi M, Ciatti S, Sabò C, Massei P, Paoli R (1997) Proliferative myositis: rare pseudotumorous lesion. J Ultrasound Med 16:771–773

134. Sayeed SM, Tyrell R, Glickman LT (2014) Management of recurrent ischemic fasciitis, a rare soft tissue pseudosarcoma. Arch Plast Surg 41:89–90
135. Shankwiler RA, Athey PA, Lamki N (1989) Aggressive infantile fibromatosis. Pulmonary metastases documented by plain film and computed tomography. Clin Imaging 13:127–129
136. Shields CJ, Winter DC, Kirwan WO, Redmond HP (2001) Desmoid tumours. Eur J Surg Oncol 27:701–706
137. Shimizu S, Hashimoto H, Enjoji M (1984) Nodular fasciitis: an analysis of 250 patients. Pathology 16:161–166
138. Sifumba S, Thomson SR, Madaree A (1993) Desmoids don't die. S Afr Med J 83:536–537
139. Slimani S, Haddouche A, Haid S, Ladjouze-Rezig A (2011) Juvenile hyaline fibromatosis: focus on radiographic features in adulthood. Rheumatol Int 31:273–276
140. Spingardi O, Zoccolan A, Venturino E (2011) Infantile digital fibromatosis: our experience and long-term results. Chir Main 30:62–65
141. Stensby JD, Conces MR, Nacey NC (2014) Benign fibrous hamartoma of infancy: a case of MR imaging paralleling histologic findings. Skeletal Radiol 43:1639–1643
142. Sundaram M, Duffrin H, McGuire MH, Vas W (1988) Synchronous multicentric desmoid tumors (aggressive fibromatosis) of the extremities. Skeletal Radiol 17:16–19
143. Tateishi U, Hasegawa T, Onaya H, Satake M, Arai Y, Moriyama N (2005) Myxoinflammatory fibroblastic sarcoma: MR appearance and pathologic correlation. AJR Am J Roentgenol 184:1749–1753
144. Tejwani A, Kobayashi W, Chen YL, Rosenberg AE, Yoon S, Raskin KA, Rosenthal DI, Nielsen GP, Hornicek FJ, Delaney TF (2010) Management of acral myxoinflammatory fibroblastic sarcoma. Cancer 116:5733–5739
145. Teo HE, Peh WC, Chan MY, Walford N (2005) Infantile lipofibromatosis of the upper limb. Skeletal Radiol 34:799–802
146. Thornton SL, Reid J, Papay FA, Vidimos AT (2005) Childhood dermatofibrosarcoma protuberans: role of preoperative imaging. J Am Acad Dermatol 53:76–83
147. Torreggiani WC, Al-Ismail K, Munk PL, Nicolaou S, O'Connell JX, Knowling MA (2002) Dermatofibrosarcoma protuberans: MR imaging features. AJR Am J Roentgenol 178:989–993
148. Tourne Y, Saragaglia D, Butel J (1991) Les fibromes desmoïdes des parties molles à localisation extraabdominale. Ann Radiol 34:267–272
149. Van Hul E, Vanhoenacker F, Van Dyck P, De Schepper A, Parizel PM (2011) Pseudotumoural soft tissue lesions of the foot and ankle: a pictorial review. Insights Imaging 2:439–452
150. Van Raak SM, Meuffels DE, Van Leenders GJ, Oei EH (2014) Hyaline fibromatosis of Hoffa's fat pad in a patient with a mild type of hyaline fibromatosis syndrome. Skeletal Radiol 43:531–534
151. Van Steenkiste E, Van Laethem A, Biesemans G, Pans S (2016) Role of diffusion-weighted magnetic resonance imaging in the evaluation of scalp dermatofibrosarcoma protuberans. Int J Dermatol 55:226–231
152. Vandevenne JE, De Schepper AM, De Beuckeleer L, Van Marck E, Aparisi F, Bloem JL, Erkorkmaz Z, Brijs S (1997) New concepts in understanding evolution of desmoid tumors: MR imaging of 30 lesions. Eur Radiol 7:1013–1019
153. Vanhoenacker FM, Eyselbergs M, Van Hul E, Van Dyck P, De Schepper AM (2011) Pseudotumoural soft tissue lesions of the hand and wrist: a pictorial review. Insights Imaging 2:319–333
154. Vinnicombe SJ, Hall CM (1994) Infantile fibrosarcoma: radiological and clinical features. Skeletal Radiol 23:337–341
155. Vogel D, Righi A, Kreshak J, Dei Tos AP, Merlino B, Brunocilla E, Vanel D (2014) Lipofibromatosis: magnetic resonance imaging features and pathological correlation in three cases. Skeletal Radiol 43:633–639
156. Wagstaff MJ, Raurell A, Perks AG (2004) Multicentric extra-abdominal desmoid tumours. Br J Plast Surg 57:362–365
157. Walker EA, Petscavage JM, Brian PL, Logie CI, Montini KM, Murphey MD (2012) Imaging features of superficial and deep fibromatoses in the adult population. Sarcoma 2012:215810
158. Walton JR, Green BA, Donaldson MM, Mazuru DG (2010) Imaging characteristics of lipofibromatosis presenting as a shoulder mass in a 16-month-old girl. Pediatr Radiol 40(Suppl 1):S43–S46
159. Wang XL, De Schepper AM, Vanhoenacker F, De Raeve H, Gielen J, Aparisi F, Rausin L, Somville J (2002) Nodular fasciitis: correlation of MRI findings and histopathology. Skeletal Radiol 31:155–161
160. Wetzel LH, Levine E (1990) Soft-tissue tumors of the foot: value of MR imaging for specific diagnosis. AJR Am J Roentgenol 155:1025–1030
161. Wignall OJ, Moskovic EC, Thway K, Thomas JM (2010) Solitary fibrous tumors of the soft tissues: review of the imaging and clinical features with histopathologic correlation. AJR Am J Roentgenol 195:W55–W62
162. Wuisman P, Roessner A, Blasius S, Edel G, Vestring T, Winkelmann W (1994) Solitary congenital or infantile (desmoid-type) fibromatosis of the proximal end of the tibia. Skeletal Radiol 23:380–384
163. Xu H, Koo HJ, Lim S, Lee JW, Lee HN, Kim DK, Song JS, Kim MY (2015) Desmoid-Type Fibromatosis of the Thorax: CT, MRI, and FDG PET Characteristics in a Large Series From a Tertiary Referral Center. Medicine (Baltimore) 94:e1547
164. Yacoe ME, Bergman AG, Ladd AL, Hellman BH (1993) Dupuytren's contracture: MR imaging findings and correlation between MR signal intensity and cellularity of lesions. AJR Am J Roentgenol 160:813–817

165. Yamamoto A, Abe S, Imamura T, Takada K, Enomoto Y, Harasawa A, Matsushita T, Furui S (2013) Three cases of collagenous fibroma with rim enhancement on postcontrast T1-weighted images with fat suppression. Skeletal Radiol 42:141–146
166. Yamamoto M, Urakawa H, Nishida Y, Hirata H (2015) Secondary aneurysmal bone cyst in the distal humerus after resection of intra-articular nodular fasciitis of the elbow. BMC Res Notes 8:311
167. Yao L, Toranji S, Doberneck SA, Eckardt JJ (1994) Case report 818: Pericapsular desmoid tumor of the knee. Skeletal Radiol 23:217–219
168. Yiğit H, Turgut AT, Koşar P, Astarci HM, Koşar U (2009) Proliferative myositis presenting with a checkerboard-like pattern on CT. Diagn Interv Radiol 15:139–142
169. Yoo HJ, Hong SH, Kang Y, Choi JY, Moon KC, Kim HS, Han I, Yi M, Kang HS (2014) MR imaging of myxofibrosarcoma and undifferentiated sarcoma with emphasis on tail sign; diagnostic and prognostic value. Eur Radiol 24:1749–1757
170. Yoo SY, Kim JH, Kang HS, Hwang YS, Kim KJ, Kim IO, Cheon JE, Shin SM, Kim CJ, Lee JH, Lee MH, Chae JH (2010) Clinical and imaging findings of systemic hyalinosis: two cases presenting with congenital arthrogryposis. Skeletal Radiol 39: 589–593
171. Zhang L, Liu QY, Cao Y, Zhong JS, Zhang WD (2015) Dermatofibrosarcoma protuberans: computed tomography and magnetic resonance imaging findings. Medicine (Baltimore) 94:e1001

So-Called Fibrohistiocytic Tumours

14

A. Shah, R. Botchu, A.M. Davies, and S.L. James

Contents

14.1 **Benign So-Called Fibrohistiocytic Tumours** 311
14.1.1 Tenosynovial Giant Cell Tumour 311
14.1.2 Deep Benign Fibrous Histiocytoma 325

14.2 **Intermediate (Rarely Metastasising)** 328
14.2.1 Plexiform Fibrohistiocytic Tumour 328
14.2.2 Giant Cell Tumour of Soft Tissue 331

References 332

14.1 Benign So-Called Fibrohistiocytic Tumours

14.1.1 Tenosynovial Giant Cell Tumour

Tenosynovial giant cell tumour (*TSGCT*) was first described in 1852 by Chassaignac as a synovial membrane proliferation involving the flexor tendons of the finger [18]. It was later redefined as a family of benign proliferative and inflammatory lesions arising from the anatomical unit consisting of the synovium of joint, bursae and tendon sheaths [52]. Jaffe et al. [52] described the pathology of *TSGCT* as pigmented villonodular synovitis (*PVNS*), bursitis and tenosynovitis. The predominant clinical differences are determined by the anatomical location. TSGCT can be subclassified as a *localised* or *diffuse* type denoted by the prefix 'L' and 'D', respectively. Localised forms include giant cell tumour of the tendon sheath (*GCTTS*) and localised nodular synovitis (*LNS*). Diffuse forms encompass conventional *PVNS* and diffuse giant cell tumours (*D-GCT*), the extra-articular counterpart of *PVNS* [21]. Intra-articular lesions have a propensity to extend along the joint surface following the path of least resistance. In comparison, lesions of the tendon sheath tend to be nodular and grow outwards. A diffuse synovial giant cell tumour can arise in a bursa and is known as pigmented villonodular bursitis (Fig. 14.1a–c).

The aetiology for *TSGCT* remains controversial, and several theories have been postulated including a neoplastic process [95], an inflammatory or reactive process, a sequela of trauma and a localised abnormal lipid metabolism [52, 85, 91, 119, 125]. The general consensus is that the disease is either a locally aggressive neoplasm or a reactive synovitis [10]. Chromosomal abnormalities [105], autologous proliferation, high rate of local recurrence [113] and extremely rare

A. Shah • R. Botchu • A.M. Davies • S.L. James (✉)
Royal Orthopaedic Hospital NHS Foundation Trust, Birmingham, UK
e-mail: stevenjames@nhs.net

© Springer International Publishing AG 2017

F.M. Vanhoenacker et al. (eds.), *Imaging of Soft Tissue Tumors*, DOI 10.1007/978-3-319-46679-8_14

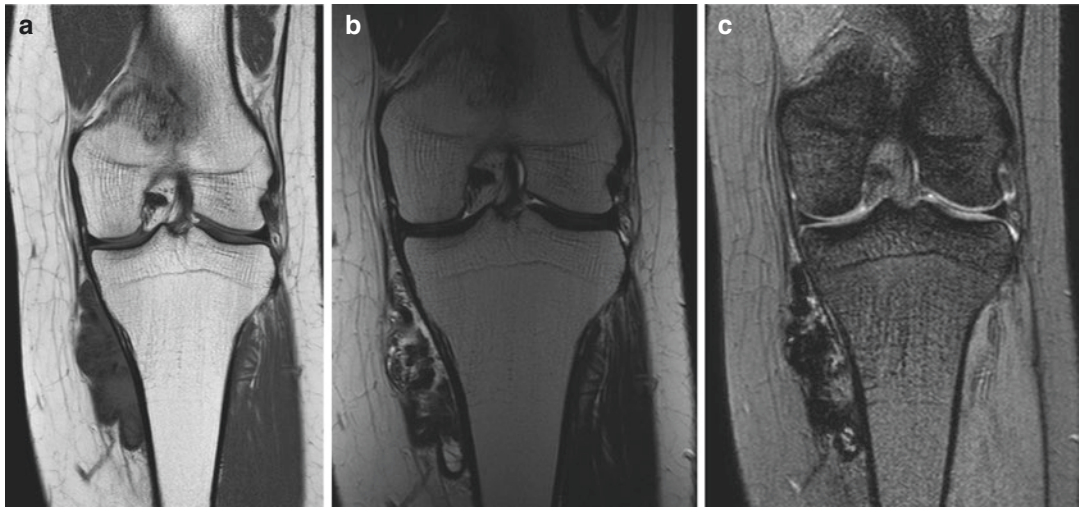

Fig. 14.1 (**a**–**c**) Pigmented villonodular bursitis within the pes anserine bursa. (**a**) Coronal T1-weighted MR image. (**b**) Coronal T2-weighted MR image. (**c**) Coronal gradient echo MR image of the left knee. A multilobulated solitary soft tissue mass is demonstrated which is of intermediate to slightly higher SI relative to skeletal muscle on T1-weighted images (**a**). It is predominantly of low SI on T2-weighted images with effusion within the bursa (**b**). The low SI is due to its haemosiderin content, which is more conspicuous on gradient echo sequences (**c**)

cases of metastases favour a neoplastic origin [3, 6, 90, 113, 117]. It has been suggested that the localised form should be considered benign with the diffuse form as aggressive and managed as per malignant lesions. Treatment options for *D-TSGCT*, therefore, include the use of chemotherapy, radiotherapy and extensive resection, or even limb amputation in some rare circumstances [6, 92]. The new WHO classification groups *GCTTS* with *LNS* and *D-GCT* with *PVNS* and describes them as one entity as either localised or diffuse-type *TSGCT*, respectively. As the clinical and imaging presentations vary, we have described these entities separately.

14.1.1.1 Localised Tenosynovial Giant Cell Tumour

Localised *TSGCT* includes extra-articular *GCTTS* (nodular tenosynovitis) and intra-articular *LNS* (synovial giant cell tumour):

- *Epidemiology*:
  GCTTS:
  GCTTS commonly occurs between 30 and 50 years of age and is rarely seen in those <10 or >60 years of age. Mild female predominance is noted with a 2:1 female-to-male ratio [116]. *GCTTS* may arise in any synovial sheath. Less commonly, they can arise from synovial lining of a joint or bursa [7]. It has a predilection for the synovium of the tendon sheaths of the hands, particularly the volar surfaces of the fingers. It is the second commonest soft tissue mass of the hand after ganglion cysts. Lesions typically occur near the interphalangeal joints and have been noted to occur more commonly in the first three fingers of the right hand [71, 79]. Less common sites include the ankle/foot, knee, elbow and hip.

  LNS:
  This reflects a rare entity and, although it shares histological features with PVNS, occurs less frequently. It is, however, important to make a distinction between the two entities as their clinical presentation and treatment differ [71]. *LNS* represents localised synovial proliferation and is more common in the fifth and sixth decade with no sex predominance [128]. It is distinguished from its diffuse counterpart by being localised to a single compartment within the joint and is almost exclusively seen in the knee [82]. The most common site within the knee is the infrapatellar (Hoffa) fat pad [71] (Fig. 14.2) and less

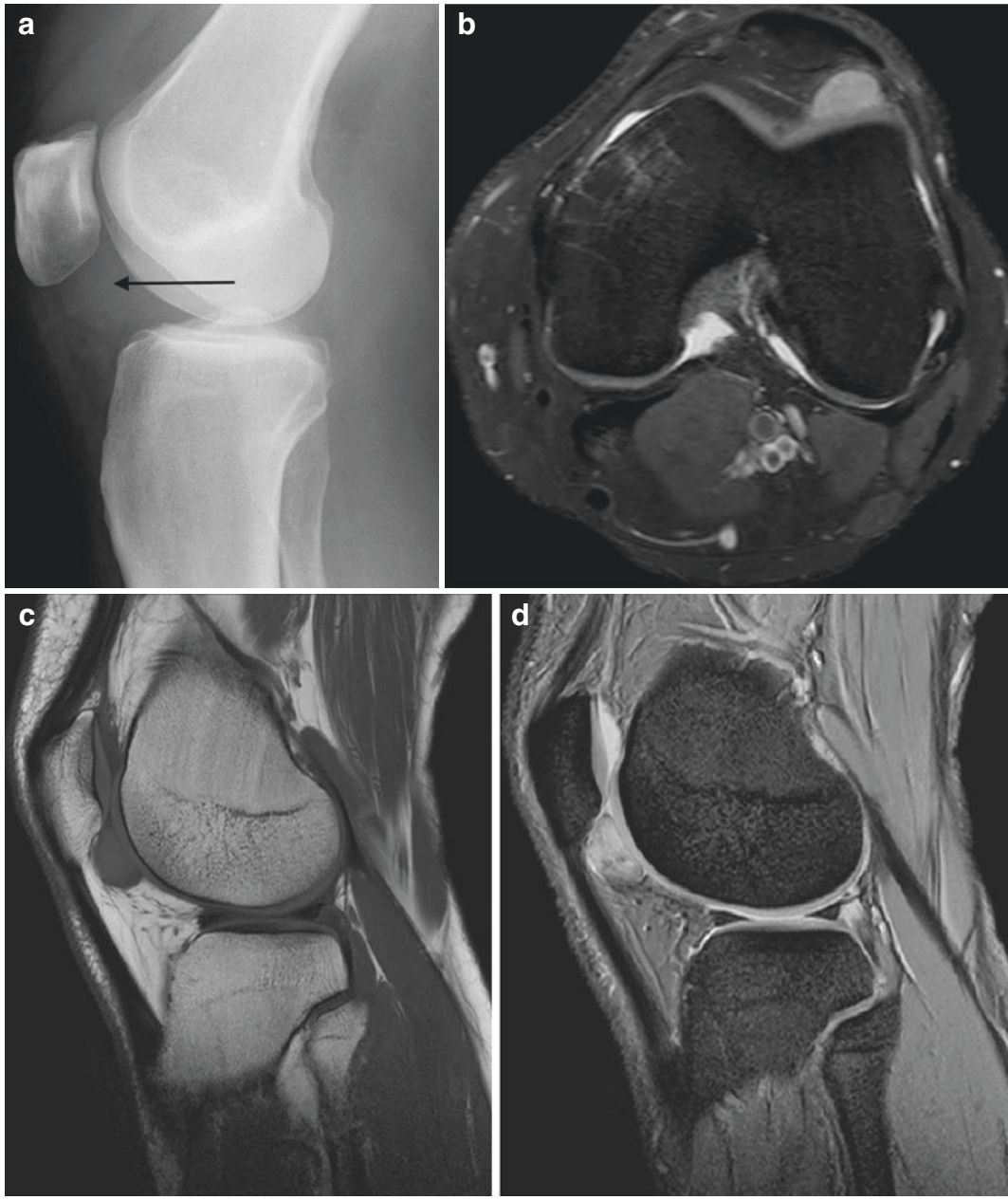

Fig. 14.2 (**a**–**d**) Localised form of pigmented villonodular synovitis (*PVNS*) of the knee within Hoffa's fat pad, which is the most common location for localised nodular synovitis (*LNS*). (**a**) Radiograph of the knee. (**b**) Axial PDFS MR image. (**c**) Sagittal T1-weighted MR image. (**d**) Sagittal gradient echo MR image. Radiograph demonstrates a dense soft tissue nodule (*arrow*) outlined by the fat within Hoffa's fat pad (**a**). *LNS* is of relatively high SI on fluid-sensitive sequences with variable internal regions of low SI, due to its haemosiderin content (**b**). It is of intermediate to slightly high SI relative to skeletal muscle on T1-weighted images (**c**). Haemosiderin is more conspicuous on gradient echo sequences (**d**). Joint effusion is atypical, unlike its diffuse counterpart, *PVNS*

Fig. 14.3 Localised nodular synovitis within the suprapatellar fat pad. Sagittal PDFS MR image demonstrates a predominantly hyperintense mass with intralesional local signal foci, which represent haemosiderin deposits

frequently in the suprapatellar recess (Fig. 14.3), intercondylar notch and adjacent to the cruciate ligaments (posterior > anterior) [48, 129]. Other reported sites include the wrist (Fig. 14.4) and ankle (Fig. 14.5).

- *Clinical behaviour and gross findings*:
  GCTTS:
  This often presents as a slow-growing painless mass. It starts as a nodular synovial lesion projecting into the tendon sheath. Exophytic growth within a restricted anatomical space and pressure effect from the adjacent tendon give rise to its multinodular appearance [71]. Lesions are typically well-circumscribed, firm and rubbery masses surrounded by a fibrous capsule. Grossly, they are often pink-grey lesions with areas of yellow or brown. Lesions are firmly attached to the deep structures and rarely involve the skin. *GCTTS* infrequently erodes or infiltrates the subjacent bone [115]. Lesions in the hand are usually small (<4 cm) and can become larger in other sites. Treatment is surgical excision, but complete excision can be difficult depending on its extent with reported recurrence rates between 4 and 45 % [54, 64]. Statistically significant risk factors for recurrence include the presence of adjacent degenerative joint disease, location at the distal interphalangeal joint of the finger or interphalangeal joint of the thumb and the radiographic presence of an osseous pressure erosion [98].
  LNS:
  This entity presents with pain, swelling and typically with locking symptoms, when present in the knee [39, 130]. It is slow growing and not infiltrative. There is no haemorrhagic effusion (Fig. 14.2), unlike *PVNS*. *LNS* is typically adherent to the synovium or may have a pedicle extending to it. Cases of torsion [47, 48] or detachment [60] have been reported. LNS is a yellow to brown well-defined mass, without diffuse frond-like projections and less haemosiderin deposition as seen in *PVNS* [48]. Curative treatment is achieved with surgical excision [48], and, in contrast to *PVNS*, synovectomy and radiotherapy are not necessary as recurrence is rare [92, 129].
- *Pathology*:
  GCTTS:
  The microscopic appearance of *GCTTS* is dependent on the proportion of mononuclear cells, multinucleate giant cells, foamy/lipid-laden macrophages, siderophages and dense hyaline stroma. Osteoclast-like giant cells with variable number of nuclei can also be seen [69]. Haemosiderin deposits are virtually always present [21]. Variable mitotic activity can be demonstrated. Although mitotic figures can occasionally be detected, they are a focal finding and do not indicate malignancy. The histological diagnosis of *GCTTS* is rarely difficult; however, it can have similarities with other soft tissue tumours, such as fibroma of the tendon sheath, synovial sarcoma and rhabdomyosarcoma [116].

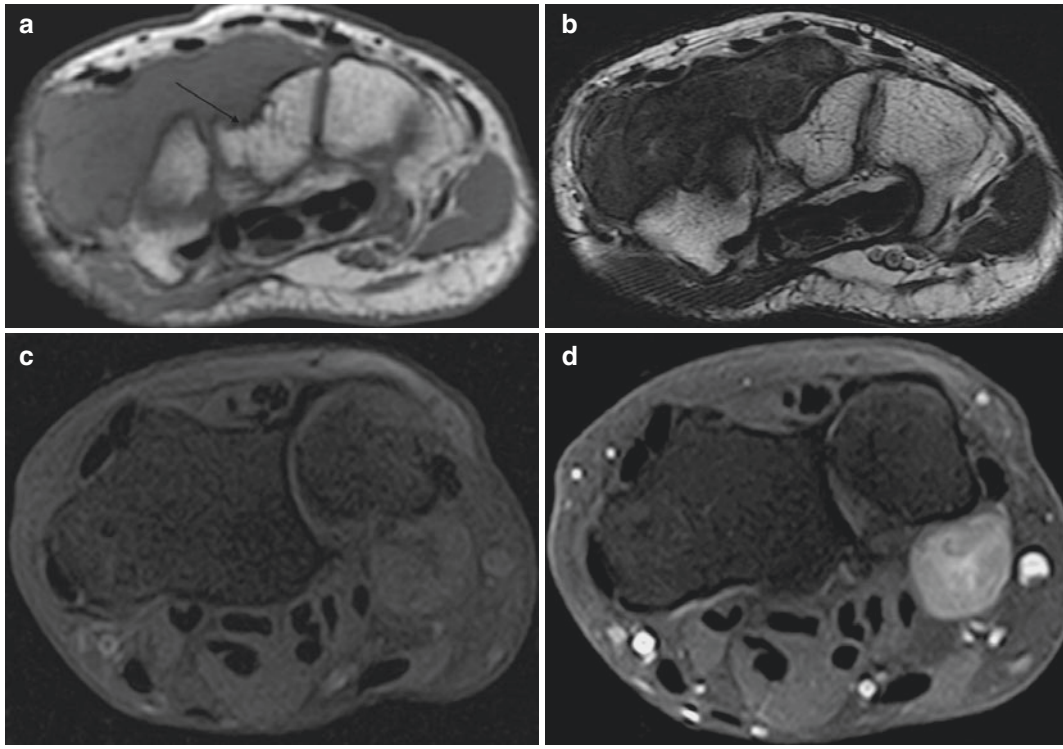

Fig. 14.4 (**a**–**d**) Localised nodular synovitis of the wrist in two patients (**a**–**d**). (**a**) Axial T1-weighted MR image. (**b**) Axial T2-weighted MR image. (**c**) Axial T1FS pre-gadolinium. (**d**) Axial T1FS post-gadolinium. A well-defined soft tissue mass that is of isointense SI to skeletal muscle on T1 demonstrates erosion of the dorsal surface of the capitate (*arrow*) (**a**). The soft tissue mass is of hypointense SI on T2 weighted, and demonstrates pressure erosion of the capitate and trapezium (**b**). There is homogeneous enhancement reflecting its vascularity (**c**, **d**)

LNS:

LNS shares histopathological similarities to *GCTTS*/*PVNS* [28]. Distinguishing features include the absence of villous fronds and haemorrhage with fewer deposits of haemosiderin, compared to PVNS [48].

- *Genetics*:

  The most frequent structural change identified in 30–60 % of *TSGCTs* is the t(1;2) translocation, which fuses the *CSF1* gene on chromosome 1, which encodes for colony-stimulating factor 1, to the collagen 6A3 (*COL6A3*) gene on chromosome 2 [21, 125]. This results in high levels of *CSF1* expression, which attracts macrophages leading to the formation of a tumour-like mass [69, 101]. Furthermore, studies have shown fusion between *CSF1* and a yet unidentified gene distinct from *COL6A3* [20, 78]. Other authors found trisomies 7 and 5 and a clonal rearrangement of chromosomes 1, 3 and 15 [105]. The *CSF1* receptor is a tyrosine kinase receptor, thus is a potential target for biological therapy. Imatinib, which is used in the treatment of renal carcinoma, chronic myeloid leukaemia and gastrointestinal stromal tumours [106], has shown to demonstrate tumour regression in patients with advanced D-GCT [15].

- *Imaging findings*:

  GCTTS:

  Radiographs are often normal but may demonstrate a well-defined dense soft tissue swelling, thought to be due to its high haemosiderin content (Fig. 14.6a). Approximately, 20 % of cases demonstrate bone erosion. Periosteal reaction, intralesional calcification or cystic degeneration is rarely seen [5, 61].

  Ultrasound (*US*) provides precise information regarding the relationship of the tumour with its underlying tendon.

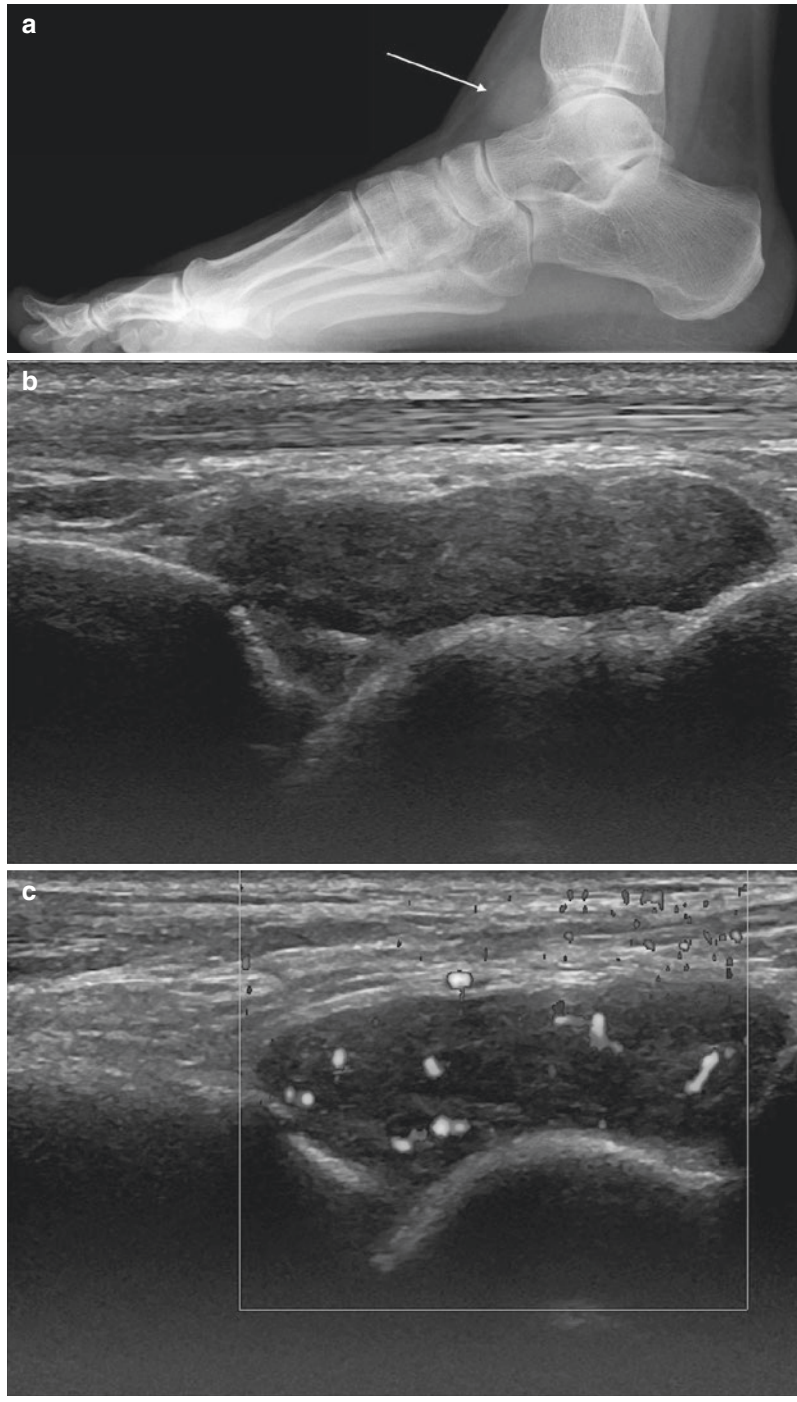

Fig. 14.5 (**a**–**e**) Localised nodular synovitis (*LNS*) of the ankle. (**a**) Radiograph. (**b**) Longitudinal ultrasound. (**c**) Longitudinal power Doppler ultrasound. (**d**) Sagittal T1-weighted MR image. (**e**) Sagittal STIR MR image. A dense well-defined soft tissue mass (*arrow*) is seen in the anterior recess of the tibiotalar joint (**a**). *LNS* on ultrasound is seen as a heterogeneous solid intra-articular mass, discrete from the overlying tendon (**b**), with increased vascularity (**c**). The mass is of isointense SI relative to skeletal muscle on T1-weighted images with low-signal foci representing its haemosiderin content (**d**). On fluid-sensitive sequences, the mass is hypointense peripherally with intralesional areas of high SI due to the presence of fat, oedema or inflammation (**e**)

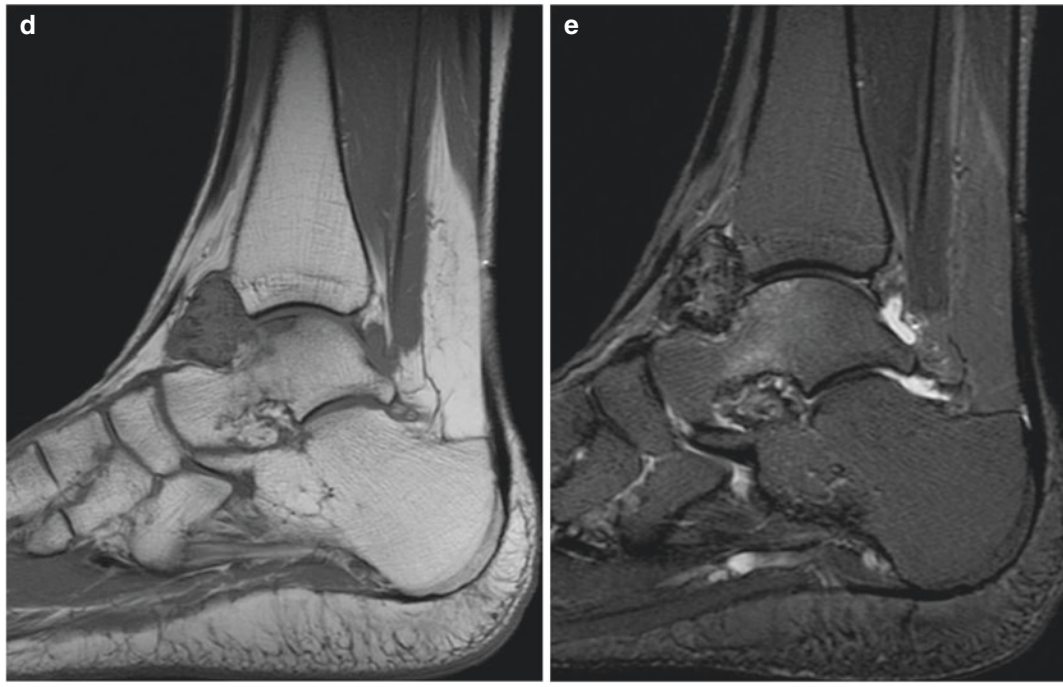

Fig. 14.5 (continued)

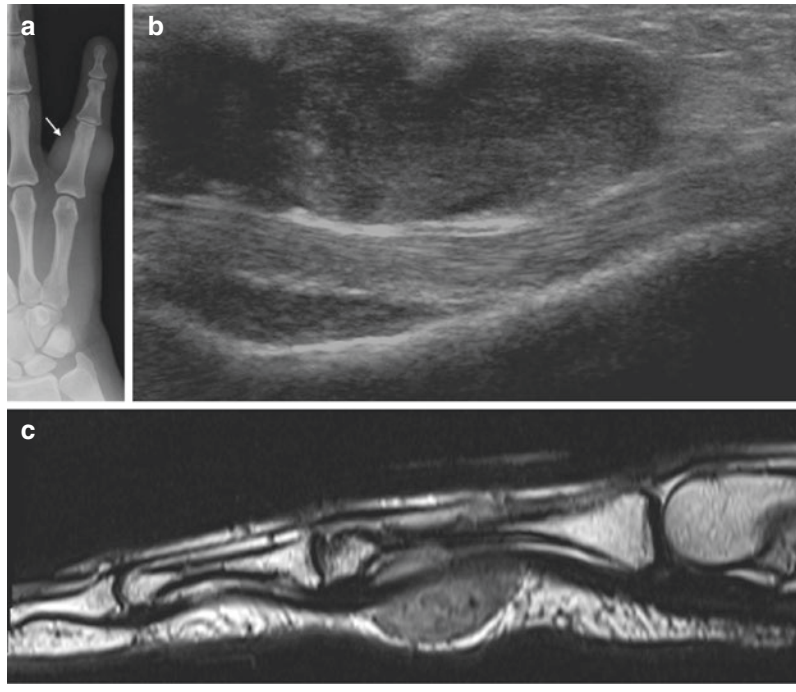

Fig. 14.6 (**a**–**c**) Giant cell tumour of the tendon sheath (*GCTTS*) of the finger. (**a**) Radiograph of the little finger demonstrates dense soft tissue swelling (*arrow*) just proximal to the PIPJ. (**b**) Longitudinal ultrasound of a *GCTTS* of the little finger demonstrates a multilobulated heterogeneous solid mass related to the flexor tendon. (**c**) Sagittal T2-weighted MR image shows the typical appearance of a *GCTTS*, which is seen as a well-circumscribed mass eccentric to or enveloping the tendon

Tumours do not move during flexion/extension as the tumour arises from the tendon sheath and not the tendon itself [77]. Lesions are solid and typically lobulated and hypoechoic (Fig. 14.6b); however, hyperechoic and heterogeneous sonographic appearances have been described [77, 120, 122]. *GCTTS* is typically hypervascular (Fig. 14.7a), and posterior acoustic shadowing can be seen in approximately 33 % of cases [77]. Bone erosions can be detected in approximately 16 % of cases [122]. The main differential for *GCTTS* in the hand is a ganglion cyst,

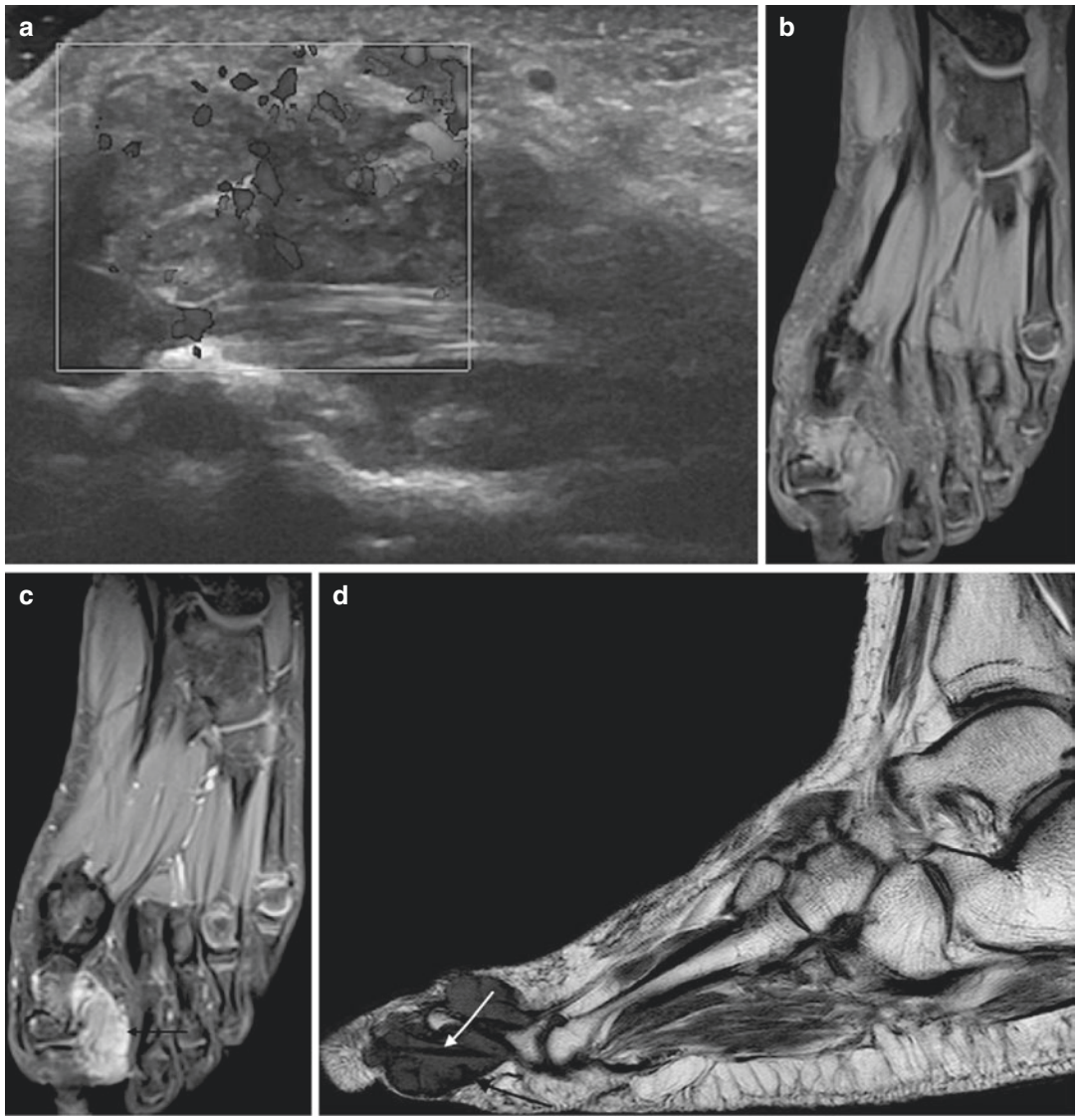

Fig. 14.7 (**a**–**d**) Giant cell tumour of the tendon sheath (*GCTTS*) of the toe. (**a**) Longitudinal power Doppler ultrasound of a *GCTTS* of the first toe. *GCTTS* are hypervascular lesions. (**b**) Long-axis T1FS pre-gadolinium and (**c**) long-axis T1FS post-gadolinium. There is homogeneous enhancement of the *GCTTS* reflecting its vascularity (*arrow*). (**d**) Sagittal T1-weighted MR images demonstrates an isointense SI mass relative to skeletal muscle encasing the flexor tendon (*white arrow*). The mass has a capsule that is typically of low signal (*black arrow*) secondary to fibrosis or haemosiderin deposits (Colour figure online)

which can be readily distinguished by its cystic structure [14]. However, ruptured ganglion cysts can appear solid and mimic a *GCTTS* [77].

Computer tomography (*CT*) identifies a dense soft tissue mass related to the tendon and is useful to detect underlying bone erosions or cysts. Contrast enhancement is typically present due to their hypervascular nature [70].

Magnetic resonance imaging (*MRI*) of *GCTTS* typically shows a well-circumscribed mass eccentric to or enveloping a tendon (Fig. 14.6c). The capsule is typically of low signal secondary to fibrosis or haemosiderin deposits (Fig. 14.7d) [55]. Tendon sheath effusion is an uncommon finding. The signal characteristics of *GCTTS* reflect its histological composition, namely, the presence of haemosiderin-laden tissue. The paramagnetic effect of haemosiderin shortens T1 and T2 relaxation times, resulting in low signal intensity (SI) on T1- and T2-weighted spin echo sequences (Fig. 14.7d) [22]. 'Blooming artefact' is seen on gradient echo (susceptibility) sequences [10]. Collagenous proliferation also contributes to the characteristically low SI [22, 55, 61]. Intralesional fat signal may be present due to the presence of foamy macrophages. As *GCTTS* is a vascular lesion, enhancement is seen post-contrast administration (Fig. 14.7c) [22]. *MRI* is useful in the detection of osseous erosions, though less sensitive than *CT*. There have been cases that have demonstrated restricted diffusion on diffusion-weighted imaging [83].

Although not generally used as initial staging investigations, *bone scintigraphy* has been used to localise primary and recurrent *GCTTS* [62]. It is thought that the hypervascularity and hypercellularity in close proximity to a joint are responsible for increased radionuclide uptake [82] of ^{99m}*Tc-MDP* [62], ^{99m}*Tc-DMSA* [11, 62], ^{67}*Ga*, ^{201}*Tl* [73] and ^{18}F-fluorodeoxyglucose positron emission tomography-computed tomography (*^{18}F-FDG PET-CT*) [26]. Furthermore, *^{18}F-FDG PET-CT* has been shown to detect recurrent disease [110]. Given its tendency to occur in the extremities, *GCTTS* should be considered in the differential diagnosis of a lesion with ^{201}Tl activity in the hands and feet [73].

LNS:

Generally, no radiographic abnormality is demonstrated on *radiographs*. Within the fat pad, *LNS* may be outlined by fat demonstrating a dense soft tissue nodule (Figs. 14.2a and 14.5a). The increased density seen is related to the iron content. Lesions do not demonstrate calcification, and its presence is suggestive of an alternative diagnosis [70].

US demonstrates a focal heterogeneous echogenic soft tissue mass with increased Doppler signal (Fig. 14.5d–e). In contrast to *PVNS*, no significant joint effusion is seen.

CT findings are similar to radiographs, demonstrating an intra-articular rounded dense soft tissue mass.

MRI is useful for pre-surgical planning. *LNS* can present as a well-defined, small ovoid lesion (Fig. 14.2) or as a large multilobulated solitary intra-articular soft tissue mass. *LNS* is of intermediate to slightly higher SI relative to skeletal muscle on T1-weighted images. It is relatively of high SI on fluid-sensitive sequences with variable circular internal regions of low SI, due to its haemosiderin content. This is more conspicuous on gradient echo sequences (Fig. 14.2a–d). Linear or cleft-like high signal internal regions may be present thought to reflect tissue necrosis [48]. Joint effusion is atypical, and there is moderate to marked inhomogeneous enhancement post-contrast (Fig. 14.4c–d). This is thought secondary to the proliferative capillaries in the collagenous stroma [22]. Osseous erosion may be seen if *LNS* occurs within confined spaces, such as the wrist (Fig. 14.4a–b).

Scintigraphy is rarely performed; however, as *GCTTS*, increased activity is often seen [74].

- *Differential diagnosis*:
  GCTTS:
  GCTTS closely resembles a fibroma of the tendon sheath (FTS) on MRI. *GCTTS* is more common by 2.7:1 [35]. Furthermore, FTS is extremely uncommon in the lower extremities; thus, a lower extremity lesion is more likely to be a *GCTTS* rather than a FTS [35]. Tophaceous gout can mimic GCTTS if localised to the tendon sheath. Generally, soft tissue tumours and tumour-like lesions affecting the extremities, such as ganglion cysts, nerve sheath tumours, foreign body granulomas and synovial sarcomas, display high SI on T2-weighted images. This is in contrast to the low/intermediate SI seen in *GCTTS*. However, extra-abdominal desmoid tumours [23] and sarcomas, such as malignant fibrous histiocytoma (now termed undifferentiated pleomorphic sarcoma), may display intermediate SI on T2 weighting due to high collagen content. The relevant clinical context can help identify haemosiderin deposition from haemophilic arthropathy, mineralised lesions and foreign bodies, which may be seen as a low-signal mass on both T1- and T2-weighted MR images.
  LNS:
  Statistically, *PVNS* is more common than *LNS* [39], but is more diffuse and demonstrates greater 'blooming artefact' due to greater haemosiderin deposits. The differential diagnoses of a mass in the infrapatellar fat pad are myriad. Hoffa's impingement is an entity characterised by ill-defined inflammation, oedema and fibrosis of the superolateral infrapatellar fat. Intra-articular chondroma of the infrapatellar fat pad has a SI pattern consistent with either cartilage matrix or bone marrow and lacks the deposition of haemosiderin. Other lesions, such as a tophus from gout, do not typically have the same imaging characteristics as *LNS* and maybe associated with erosions.

14.1.1.2 Diffuse-Type Tenosynovial Giant Cell Tumour

D-TSGCT encompasses *D-GCT* and its intra-articular analogue *PVNS*. *D-GCT*/*PVNS* is defined as a benign, locally aggressive, proliferative neoplasm.

- *Epidemiology*:
  D-GCT:
  A rare extra-articular fibrohistiocytic tumour presents as a periarticular soft tissue mass but can be intramuscular or subcutaneous [33]. It affects slightly younger adults than *GCTTS*, typically <40 years with a slight female predominance [82]. *D-GCT* has a similar location distribution and symptoms as *PVNS*.
  PVNS:
  A rare intra-articular fibrohistiocytic tumour with an incidence of two patients per million. Age and sex distribution is the same as *D-GCT*. *PVNS* occurs in large joints and is typically monoarticular. Approximately 80% occur in the knee, followed by the hip, ankle, shoulder and elbow [71]. Rare cases of involvement of the temporomandibular joint [49] and the spine [118, 121] have been reported. Malignant variants, malignant transformation, and metastases have been rarely reported [3, 6, 19].
- *Clinical behaviour and gross findings*:
  D-GCT and *PVNS* have similar clinical histopathological characteristics. Presentation includes insidious onset of pain and joint swelling which leads to limited range of motion of the affected joint. As *PVNS* becomes more advanced, the synovial mass constricts the joint, whereas *LNS* tends to grow outwards, becoming pedunculated. Erosions and subchondral cysts of the adjacent bone are common. The abnormal synovium is prone to haemorrhage and a large joint effusion is often present. The effusion is often recurrent, haemorrhagic and out of proportion to the degree of mild discomfort. *D-GCT* is a firm multinodular mass of variegated colour with alterations of

white, yellowish and brown areas. *D-GCT* contains numerous capillary fronds and nodular areas. *PVNS* is a firm red-brown or tan mass with a prominent villonodular growth pattern [81]. Despite being a benign entity, treatment with total synovectomy is recommended, although malignant transformation and metastasis have been reported [6]. External beam radiotherapy can be used as a primary treatment for unresectable cases or as adjuvant therapy for incompletely excised tumours. Intra-articular injection of yttrium-90 (90Y)-labelled colloid (radiosynovectomy) has been used as a local adjuvant after synovectomy [118]. As *D-GCT*/*PVNS* is locally aggressive, a high rate of recurrence has been reported. Recurrence can occur in 33–50% of cases, often with multiple recurrences [89, 112].

- *Pathology*:
  Microscopically, *D-GCT*/*PVNS* demonstrates histological similarities to the *GCTTS*. Synovial-like mononuclear cells with foam cells, multinucleated giant cells, inflammatory cells and siderophages are present. However, fewer giant cells are seen than in *GCTTS*. Osteogenic giant cells are common in *GCTTS*, but absent or rare in *D-GCT*. Larger mononuclear cells may have a peripheral haemosiderin rim in the cytoplasm. Cleft-like spaces and blood-filled spaces devoid of giant cells are seen in approximately 10% of cases of *D-GCT*. *PVNS* differs in that it is unencapsulated and has pronounced villonodular architecture with elongated synovial-lined spaces. The occasional predominance of the large histiocyte-like cells can make the diagnosis of *D-GCT* challenging and can be mistaken for a sarcoma. Mitotic rates up to >20 mitoses per 10 high-power fields (HPF) can be seen.
- *Genetics*:
  See section ‘genetics’ in Sect. 14.1.1.1.
- *Imaging findings*:
  Radiographs are often not diagnostic. With advanced disease, there may be evidence of soft tissue swelling, loss of joint space and periarticular erosion of the bone. The periarticular erosions are usually present on both sides of the joint and are more notable in joints with a tight capsule, such as the hips (90% of cases) and shoulder (70% of cases). The erosions tend to be circumferential and produce a classical ‘apple core’, but this can be seen with other synovial-based pathologies (e.g. synovial osteochondromatosis). Erosions are less common in capacious joints such as the knee (25% of the cases) [10, 71]. These erosive changes show well-defined sclerotic borders and are most likely due to a pressure phenomenon (Fig. 14.8). Interestingly, recent studies suggest the release of a proteolytic enzymes leading to the erosions [87]. The joint space and cartilage are preserved until late in the disease. This and the lack of new bone formation help distinguish *PVNS* from osteoarthritis. Erosions are typically multiple; however, solitary lesions may mimic a primary osteolytic bone tumour [57]. The absence of periarticular osteopenia

Fig. 14.8 *PVNS* of the right hip. Radiograph of the right hip, demonstrating well-defined osseous erosions with sclerotic borders (*arrow*). Erosions seen on both sides of a joint are typical of *PVNS*

Fig. 14.9 Radiograph of the ankle demonstrating increased juxta-articular soft tissue density (*arrow*) seen with *PVNS*

helps distinguish *D-GCT* from an inflammatory synovitis. With *PVNS*, a dense juxta-articular mass with joint effusion may be seen (Figs. 14.9 and 14.10a). Calcifications are rare in *PVNS*, and their presence is suggestive of an alternative diagnosis, such as synovial osteochondromatosis.

On *US*, *D-GCT* is a solid periarticular hypoechoic mass with well-defined margins. There is an absence of posterior acoustic enhancement and evidence of internal echoes and increased Doppler signal. Features of an intra-articular proliferative synovitis are seen with *PVNS*. Typically, there is a large joint effusion with a thickened synovium and a vascular heterogeneous mass (Fig. 14.10b). Occasionally, bone erosion may be detected.

On *CT*, *D-GCT* is a non-specific periarticular mass and *PVNS* is seen as a high-density intra-articular mass. High-attenuation tissue within the joint can also be caused by haemophilia, chronic bleeding due to another cause or calcification. Like *GCTTS*, *D-GCT*/*PVNS* is hypervascular and demonstrates enhancement post-contrast. CT is particularly useful in the assessment of cyst formation and bone erosions [10]. An associated intraosseous soft tissue mass, which extends with a narrow pedicle to the synovium, can be demonstrated [56].

MRI of *D-GCT*/*PVNS* reflects its histopathological composition. Though not specific, it is characteristically of low SI on T1- and T2-weighted sequences due to the presence of haemosiderin (Fig. 14.10c) [82], which is more conspicuous on gradient echo sequences due to the 'blooming artefact' (Fig. 14.10d). Foci of high T1 SI may be present due to lipid-laden macrophages, and fluid-sensitive sequences can vary in signal depending on the amount of blood, fibrous tissue and oedema. Marked enhancement of the synovitis component is seen post-intravenous gadolinium (Fig. 14.11). Capsular defects can result in juxta-articular ligament spread. *MRI* is the optimal modality for preoperative assessment to determine tumour size, extent and relationship with adjacent joints (Fig. 14.12). *D-GCT* is seen as a periarticular mass with the above-described MRI characteristics (Fig. 14.13).

Nuclear medicine studies are the same as those for *GCTTS* [26, 110].

- *Differential diagnosis*:

The common differentials include other *pathologies* that cause haemorrhagic synovitis such as haemophilia, synovial haemangioma, rheumatoid nodule/pannus, gout and amyloid. These pathologies will vary in the amount of effusion, location and pattern of arthropathy helping to differentiate it from *D-GCT*/*PVNS*.

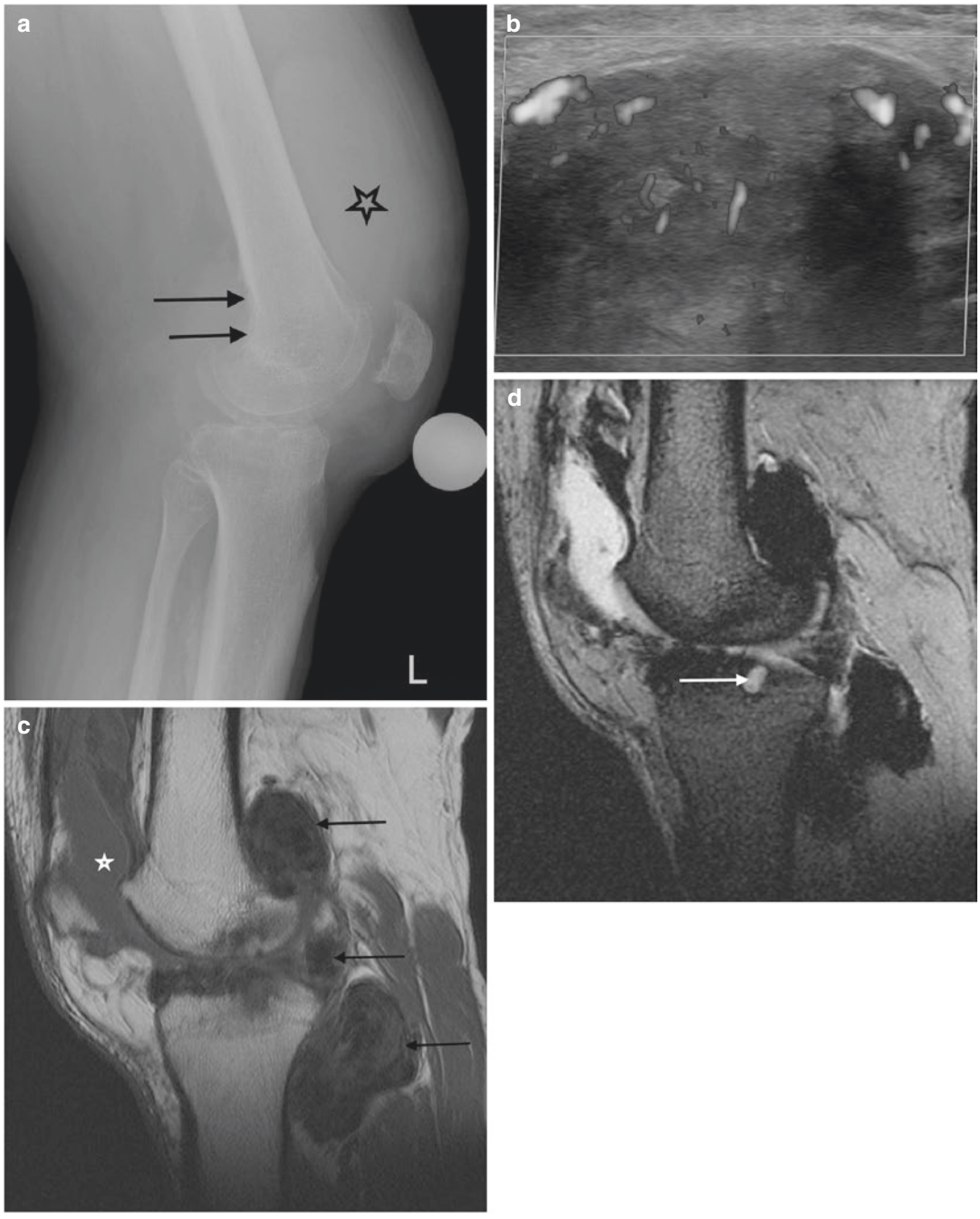

Fig. 14.10 (**a**–**d**) Pigmented villonodular synovitis (*PVNS*) of the knee. (**a**) Radiograph. (**b**) Transverse Doppler ultrasound. (**c**). Sagittal T1-weighted MR image. (**d**) Sagittal gradient echo MR image. The radiograph (**a**) demonstrates an increased density within the suprapatellar pouch with evidence of erosive changes of the posterior femoral condyles (*arrows*). Increased vascularity is typically seen with *PVNS* (**b**). In (**c**), a large joint effusion (*star*) can be seen, with multiple low T1 SI masses, predominantly in the posterior joint recess (*arrows*). The low SI is secondary to the haemosiderin content, which demonstrates susceptibility artefact on gradient echo images (**d**). Erosion and cyst formation of the tibial plateau are noted in (**d**) (*white arrow*) (Colour figure online)

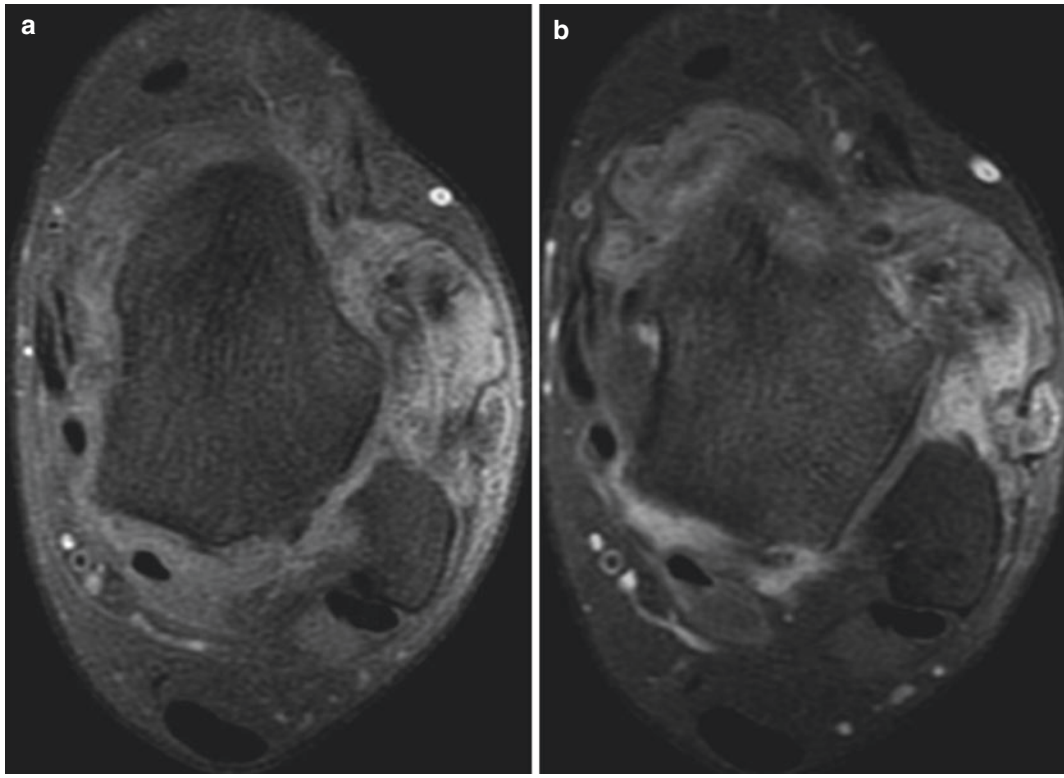

Fig. 14.11 (**a**–**b**) Pigmented villonodular synovitis (*PVNS*) of the ankle. (**a**) Axial pre-contrast T1FS MR image. (**b**) Axial post-contrast T1FS MR image. Marked contrast enhancement of *PVNS* post-gadolinium is seen

14.1.1.3 Malignant-Type Tenosynovial Giant Cell Tumour

Malignant *TSGCT* is extremely rare with less than 50 cases reported in the English literature [100]. This entity is defined by the presence of frank malignant cells coexisting with benign *TSGCT* or a malignant recurrence of a previously treated *TSGCT* [21].

- *Clinical behaviour and gross findings*:
  Differentiating between benign *TSGCT* and its malignant variant can be very difficult as there are overlapping clinicoradiological features. Most malignant *TSGCTs* are radiation-induced sarcomas, which often occur years after radiotherapy for uncontrolled *PVNS*. Malignant *TSGCT* is an aggressive sarcoma with high risk of metastases (Fig. 14.14c) and mortality [6, 69]. It occurs most commonly in the lower extremity.
- *Pathology*:
  Microscopic features of *TSGCT* are seen. Criteria for diagnosing malignant *TSGCT* were developed by the Armed Forces Institute of Pathology (AFIP) requiring five of the eight characteristics. These include an infiltrative growth pattern, diffuse pleomorphism, prominent nucleoli, mitotic ratio greater than 10 per 10 HPF, high cytoplasmic-to-nuclear ratio, necrosis, discohesion of tumour cells and a paucity of giant cells [100].
- *Genetics*:
  See section 'genetics' in Sect. 14.1.1.1.
- *Imaging findings*:
  See section 'imaging findings' in Sect. 14.1.1.2. Differentiating malignant from benign *TSGCT* is based on histological diagnosis (Fig. 14.14).

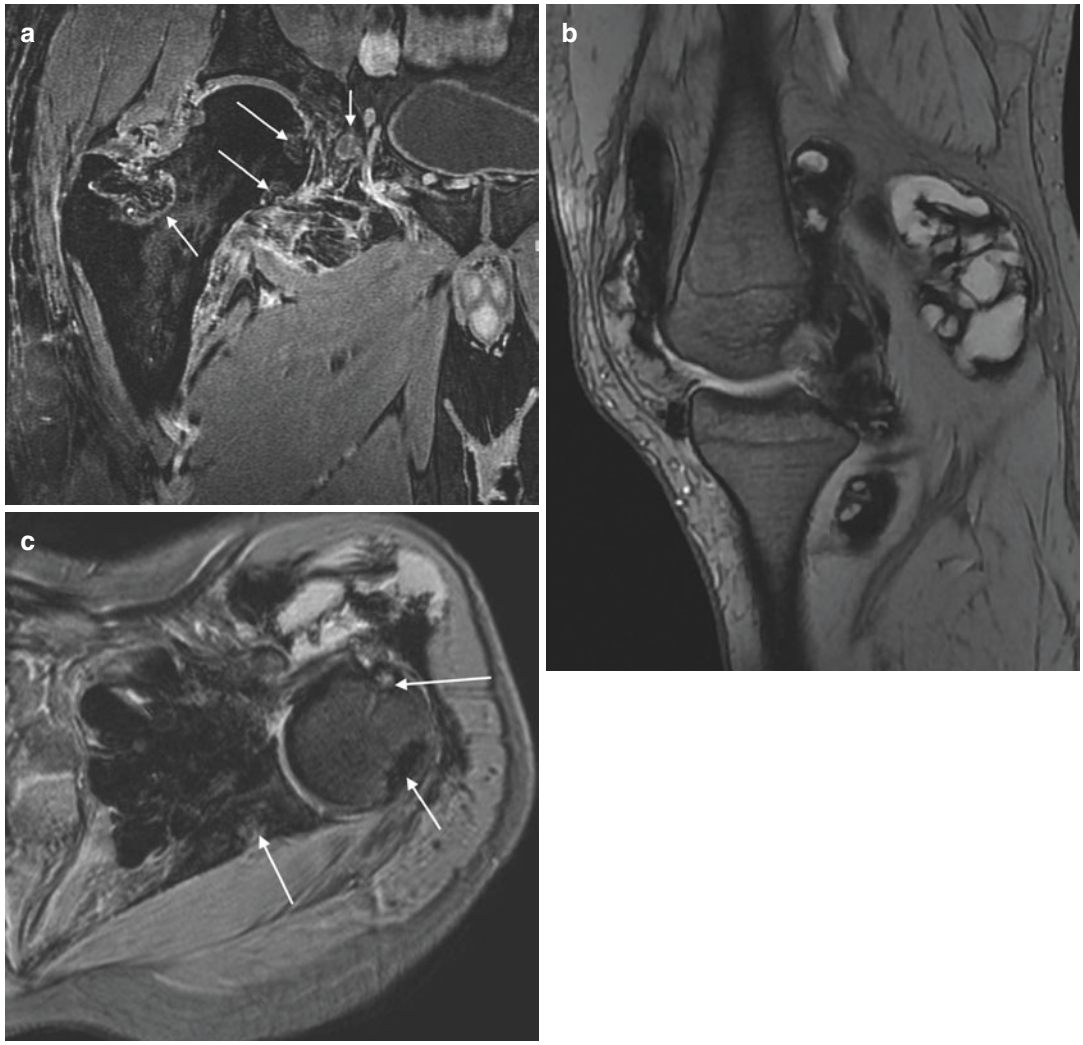

Fig. 14.12 (**a**–**c**) Three examples of the 'blooming artefact' seen with pigmented villonodular synovitis. (**a**) Coronal gradient echo MR image of the hip. (**b**) Sagittal gradient echo MR image of the knee. (**c**) Axial gradient echo MR image of the shoulder. The presence of haemosiderin causes local changes in susceptibility and therefore loss of MR signal, most conspicuous on gradient echo sequences. Erosions (*arrows*) secondary to intraosseous extension are often seen, particularly in joints with tight capsules such as the hip (**a**) and shoulder (**c**)

14.1.2 Deep Benign Fibrous Histiocytoma

A benign fibrous histiocytic tumour is of unknown aetiology and is located in the skin or deeper soft tissues. Synonyms include fibroxanthoma, dermal fibrous histiocytoma, sclerosing haemangioma, nodular subepidermal fibrosis and histiocytoma cutis. Cutaneous lesions are referred to as 'benign fibrous histiocytoma (*BFH*)' or 'dermatofibroma', and lesions in the subcutaneous and deep tissues are considered as 'deep benign fibrous histiocytoma'. A variety of subtypes have been described determined by its predominant histological composition. Rare cases of metastases have been described with certain subtypes [17, 29].

- *Clinical behaviour and gross findings*:
  Cutaneous *BFH* is a common skin mesenchymal tumour [93, 114]; in contrast, deep

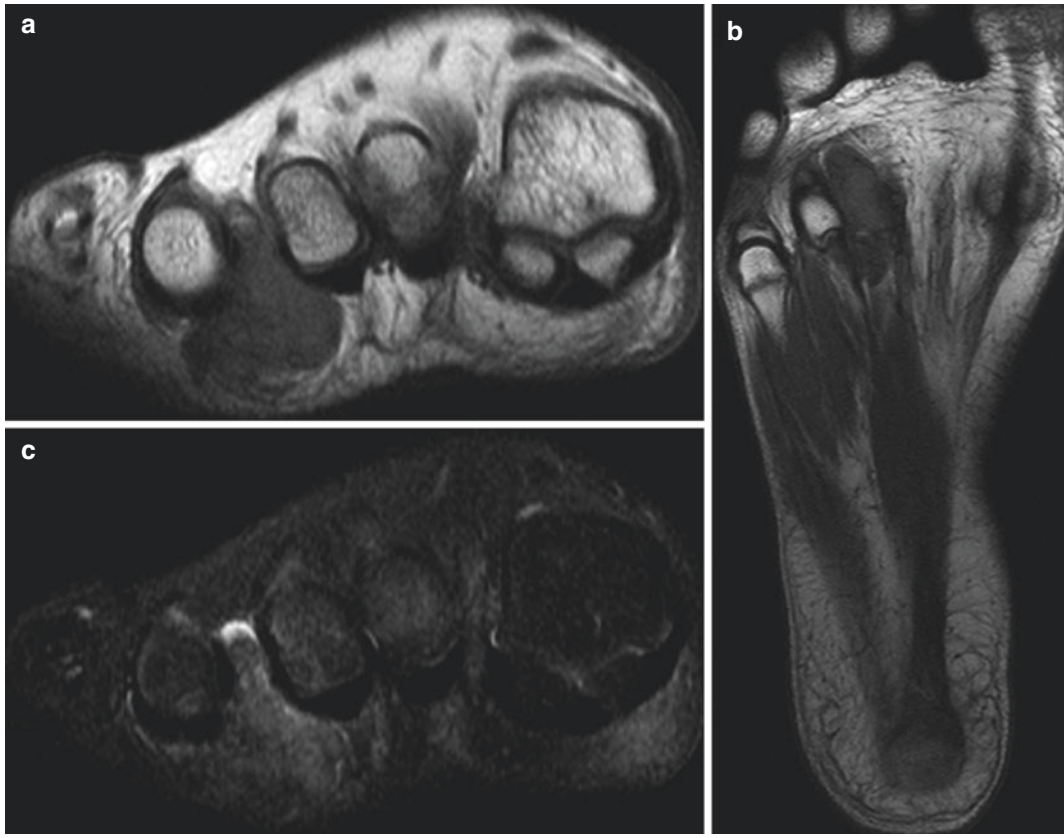

Fig. 14.13 (**a**–**c**) Diffuse giant cell tumour of the foot. (**a**) Short-axis and (**b**) long-axis T1-weighted MR images. (**c**) Short-axis STIR MR image. There is a subcutaneous, extra-articular, lobulated mass, which is of intermediate SI relative to skeletal muscle on T1-weighted images with a few foci of low signal in keeping with haemosiderin deposits (**a**, **b**). These are more conspicuous on gradient echo sequences due to 'blooming' artefacts (not shown). The mass is of high SI on fluid-sensitive sequences in keeping with oedema and inflammation (**c**). On imaging alone, this lesion could also represent a giant cell tumour of the tendon sheath (*GCTTS*); however, it is not as intimately related to the flexor tendon as would be expected for a *GCTTS*

BFH occurs rarely accounting for <1 % of fibrohistiocytic tumours [16, 32]. *BFH* most commonly occurs in young to middle-aged adults. There is a male predominance (male-to-female ratio 1.9:1). Cutaneous *BFH* is most often found in limbs (upper > lower), and deep *BFH* is most often found in the deeper subcutaneous tissues. About 10 % occur in visceral soft tissues including the paraspinal muscles, retroperitoneum or mediastinum [37]. Rarely deep *BFH* can occur in visceral organs [13]. Multiple lesions are seen in 30 % of cases [123]. Cutaneous tumours are typically small, raised papules or nodules presenting as a painless, slow-growing mass, with a clinical impression of a cyst. The overlying skin is often reddish or black, and there may be the presence of a central dimple on lateral compression [31]. Deep lesions may not be clinically apparent but are typically well-circumscribed, yellow to white masses. Cutaneous *BFH* typically are <1 cm, whereas deep *BFH* can range from 2 to 12 cm [72]. Complete surgical excision is curative. Cutaneous lesions rarely reoccur, whilst deep tumours have a higher risk of local recurrence (22–60 %). Atypical, aneurysmal and cellular fibrous histiocytoma subtypes are more

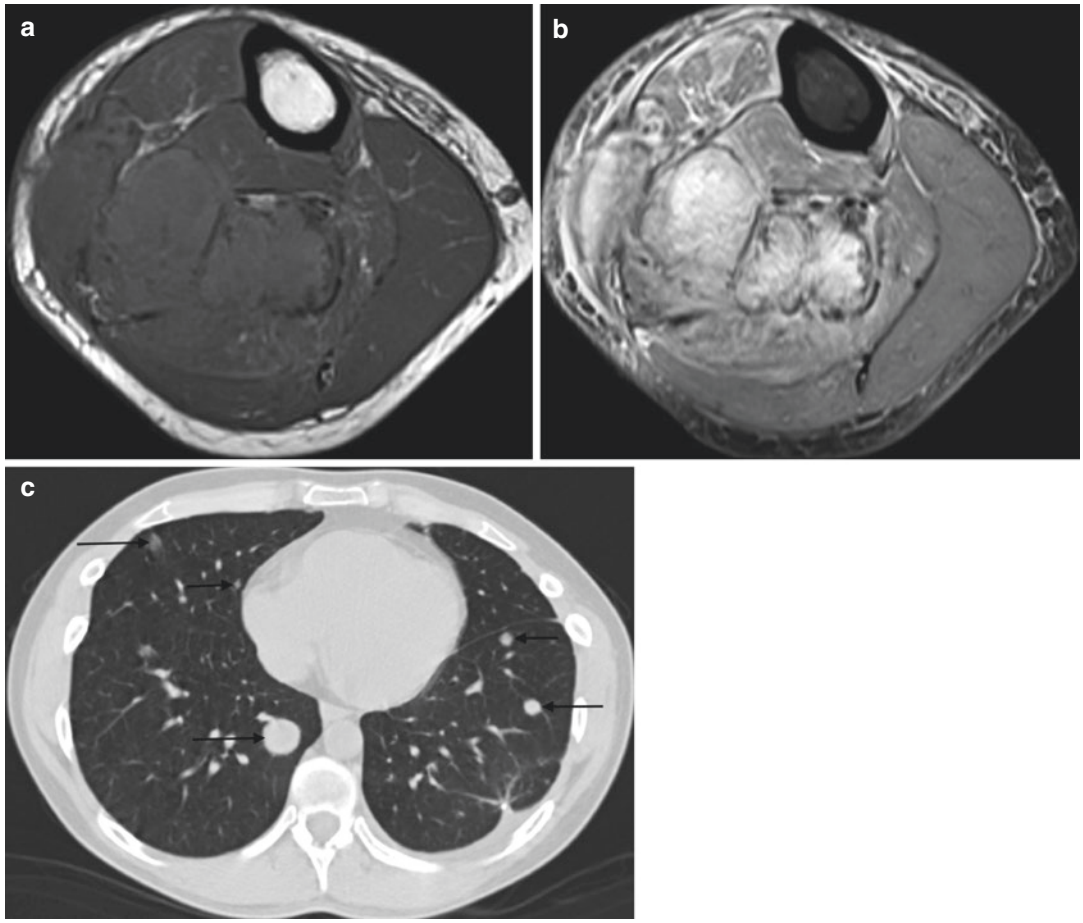

Fig. 14.14 (**a**–**c**) Malignant tenosynovial giant cell tumour (*TSGCT*) of the calf. Axial T1-weighted (**a**) and STIR (**b**) MR images. (**c**) Axial CT of the chest. There is an intermediate to slightly hyperintense SI relative to skeletal muscle on T1-weighted images within the deep compartment of the lower leg (**a**). The mass is hyperintense on fluid-sensitive sequence (**b**) with surrounding subcutaneous oedema. Foci of low signal can be seen in (**a**, **b**). This aggressive soft tissue mass is non-specific on imaging alone. Biopsy confirmed malignant *TSGCT*. Metastases are commonly found with malignant *TSGCT* as demonstrated in this case with multiple lung metastases (*arrows*) (**c**)

prone to recurrence with reported cases of metastases [41]. Risk factors for metastasis include large size, high cellularity, aneurysmal changes, marked cellular pleomorphism, high mitotic activity, tumour necrosis and repeated local recurrences [41]. These subtypes may be misinterpreted as a high-grade malignancy, as they can be painful and show rapid growth. Intralesional haemorrhage, particularly in the aneurysmal variant, can occur possibly accounting for the growth and the imaging findings [75, 109].

- *Pathology*:
  In general *BFH* consists of a storiform pattern of bland spindle cells and foamy histiocytes located in the dermis with possible extension to the subcutis [59]. *BFH* is composed of a variable mixture of multinucleated giant cells, osteoclastic giant cells and foam cells with blood vessels in a myxoid, hyalinised or collagenous stroma. Mitoses less than 5 per 10 HPF can be seen. Common subtypes include fibroblastic, histiocytic, aneurysmal and angiomatoid variants [44]. Aneurysmal variants are distinct, with

large, blood-filled pseudocystic spaces with vascular channels. These channels are surrounded by histiocytes with haemosiderin, foam cells and fibroblasts. The angiomatoid subtype has a predominance of a capillary-rich collagen stroma.

An atypical fibrous histiocytoma (*AFH*) is a variant of *BFH* that is characterised histologically by proliferation of dermal spindle cells and atypical histiocytic cells. It is also known as *pseudosarcomatous fibrous histiocytoma* or *dermatofibroma with monster cells*. There is a predominance of nuclear pleomorphism and atypia, on a background of classic *BFH* composition [58]. The presence of atypia can pose a challenge in differentiating AFH from malignant tumours such as dermatofibrosarcoma protuberans (*DFSP*) or undifferentiated pleomorphic sarcoma (*UPS*). *UPS* is composed of malignant pleomorphic sarcomatous cells, bizarre giant cells and frequent mitotic figures [8] and is described further in Chap. 21. Although *AFH* is considered to be benign, rare cases of recurrence and metastasis to the lymph nodes (Fig. 14.16c) and lungs have been reported [41, 58].

- *Genetics*:

  An array of genomic abnormalities in *BFH* and its subtypes have been reported [17], but these are inconsistent. Frau et al. have reported the presence of clonal translocation of t(16;17) (p13.3;q21.3) in *BFH* [36]. t(12;19) (p12;q13) chromosomal translocation has been reported in the aneurysmal variant of *BFH* [9]. However, these are not widely established findings.

- *Imaging findings*:

  Imaging features of this fibrous tumour are non-specific and definitive diagnosis is made histologically. The paucity of radiologic reports of *BFH* likely reflects its distribution, with the majority of tumours located superficially, and therefore usually no imaging is undertaken.

  US is useful for the assessment of superficial lesions, which demonstrates a well-defined hypoechoic nodule with peripheral vascularity [126]. Due to its fibrous nature and high cellularity, *BFH* can appear 'cystic' on *US*, that is, anechoic/hypoechoic, homogeneous and with well-defined margins [66]. However, Machiels et al. [72] reported *BFH* appearing hyperechoic on *US*, and it is likely the *US* appearance may vary according to the subtype and cellular make-up.

  On *CT*, *BFH* demonstrate a hypo- to isodense mass to skeletal muscle. Internal cystic or necrotic regions can also be seen.

  On *MRI*, the tumour is non-specific. On T1-weighted images, the lesion is iso- to hypointense to the muscle. On T2-weighted images, the mass is heterogeneous and has intermediate to high SI (Fig. 14.15) [72]. There is homogeneous enhancement post-gadolinium administration [127]. Aneurysmal *BFH* can be seen as a subcutaneous soft tissue mass with intralesional haemorrhage of differing ages causing fluid-fluid levels and large internal 'clefts' filled with blood (Fig. 14.16).

  Unusually, for a benign lesion, there has been a report of a *BFH* demonstrating uptake on ^{18}*F-FDG PET-CT* [25]; however, this is not a consistent finding [24].

- *Differential diagnosis*:

  The most important diagnostic challenge is differentiating *BFH* from aggressive forms of fibrohistiocytic neoplasms, including *DFSP* and malignant fibrous histiocytoma (known termed *UPS*). The pattern of subcutaneous extension of BFH differs from the pattern of extension seen with *DFSP* [59]. Other differentials to consider include solitary fibrous tumour (*SFT*) and nodular fasciitis.

14.2 Intermediate (Rarely Metastasising)

14.2.1 Plexiform Fibrohistiocytic Tumour

Plexiform fibrohistiocytic tumour (*PFHT*) was first described in 1988 by Enzinger and Zhang

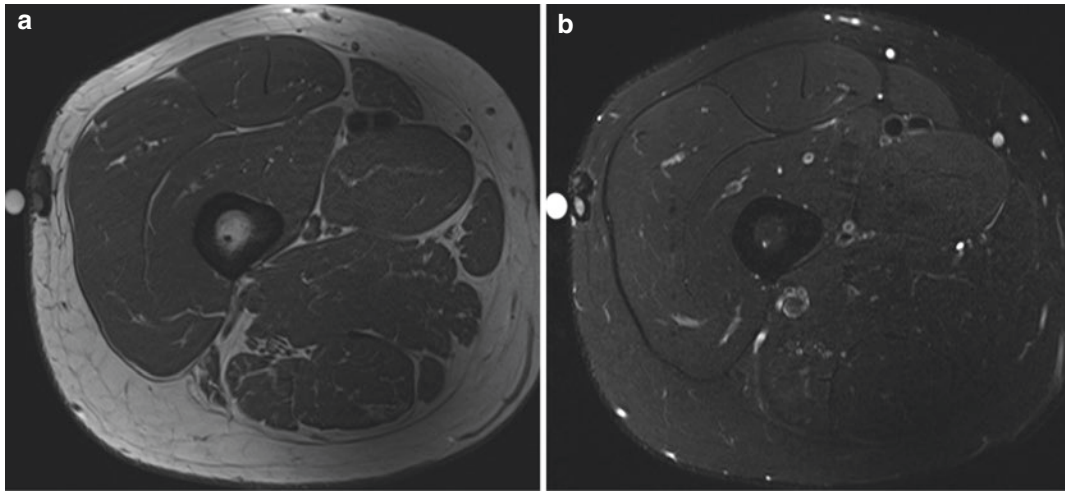

Fig. 14.15 (**a**–**b**) Benign fibrous histiocytoma (*BFH*) of the thigh. Axial T1-weighted (**a**) and T2FS (**b**) MR image. A non-specific cutaneous nodule is seen just under the skin surface. There is intralesional high T1 SI suggestive of haemorrhage. Biopsy confirmed *BFH*

[30]. It is a dermal-subcutaneous neoplasm composed of fibroblasts and histiocyte-like cells, with rare reports of lung metastasis [80, 108].

- *Clinical behaviour and gross findings*:
  PFHT is a rare, slow-growing tumour predominantly seen in children and adolescents, although a wide age range has been reported from birth to 77 years of age [30, 80]. Previously, *PFHT* was thought to have a female predominance [30, 99]; however, recent evidence suggests an equal sex distribution [46, 99]. It has a predilection for the upper extremities [30] followed by the lower extremity, trunk and head and neck. Up to 40 % recur with 6 % metastasising to regional lymph nodes [30, 46, 123]. *PFHT* may be associated with previous radiotherapy treatment [4, 43]. It clinically presents as a small, poorly defined, painless dermal mass or plaque. The overlying skin may demonstrate central depression [30]. Macroscopically, *PFHT* is a firm, multinodular, poorly circumscribed dermal mass, which can extend into skeletal muscle. It has a grey-white appearance and is fibrous or partially mucoid typically <3 cm [30, 99]. Wide surgical excision is recommended; however, clinicopathologic correlation with clinical behaviour, outcome and metastasis of PFHTs have been unsuccessful [30, 46, 51, 99]. Pulmonary metastasis and death have been reported, and therefore, staging including chest imaging is suggested. Because of a number of cases with involved margins, Mohs micrographic surgery has been used to ensure clear resection margins [94].
- *Pathology*:
  PFHT is characterised by a plexiform mass with extensive haemosiderin deposits involving the dermis and superficial subcutis. Three distinct cell types are present including mononuclear epithelioid histiocyte-like cells, spindle (myo)fibroblasts and osteoclast-type multinucleate giant cells [4]. Accordingly, three histological types are described: (i) a fibroblastic type, (ii) a nodular histiocytoid type and (iii) a mixed type [33]. Cellular and mitotic atypia with lymphovascular invasion has been rarely described [30, 80].
- *Genetics*:
  There have been three reported cases of *PFHT* with aberrant clonal chromosome abnormalities; however, a common mutation is yet to be identified [65, 97, 111].

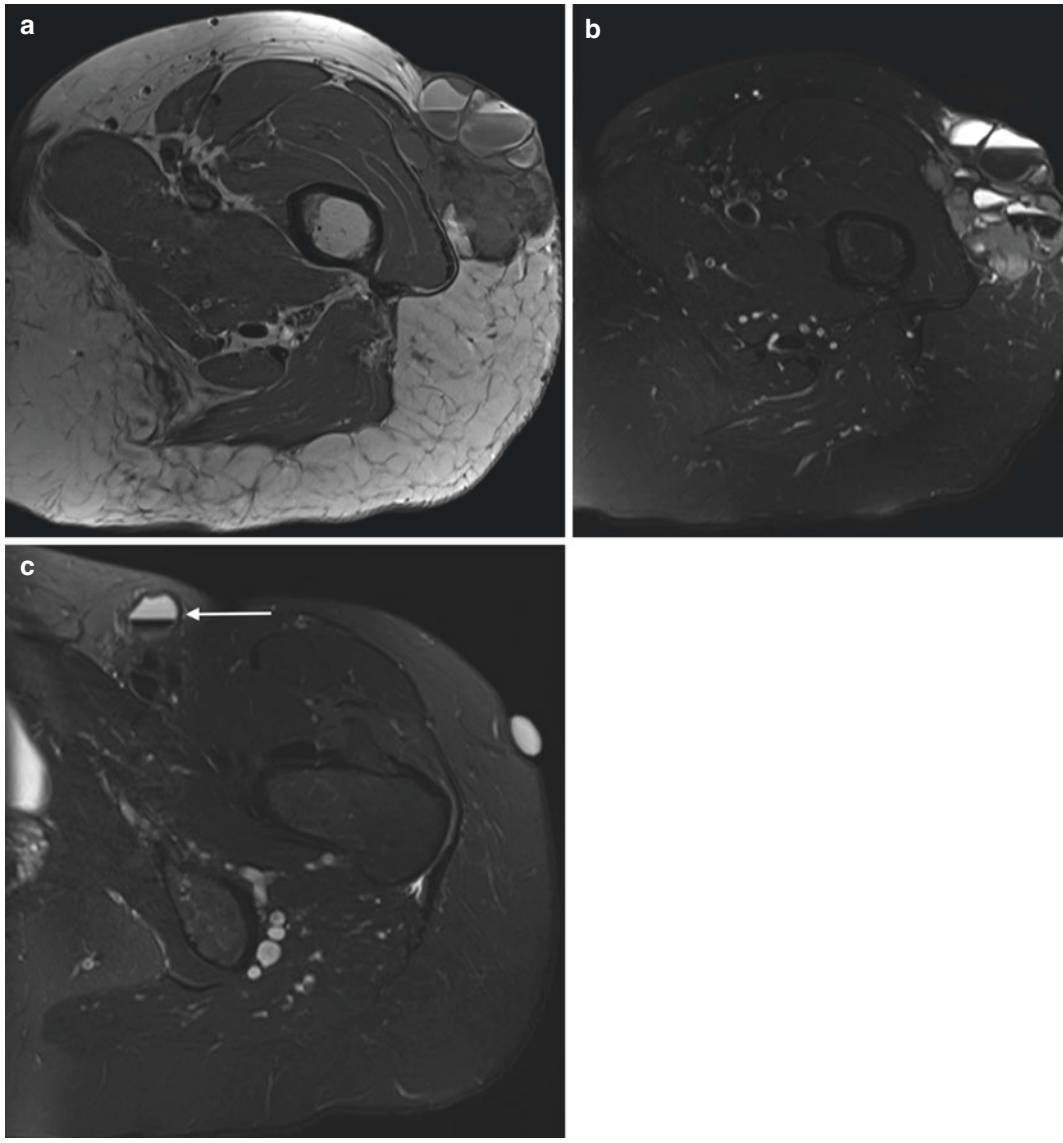

Fig. 14.16 (**a**–**c**) Aneurysmal fibrous histiocytoma of the thigh. Axial T1-weighted (**a**) and T2FS (**b**, **c**) MR image. Aneurysmal fibrous histiocytoma can be seen as a subcutaneous soft tissue mass with intralesional haemorrhage of differing ages causing fluid-fluid levels (**a**, **b**). This case demonstrates a metastasis with a fluid-fluid level (*arrow*) to an inguinal lymph node (**c**)

- *Imaging findings*:
  There is little on the imaging appearances of *PFHT* in literature. On *MRI*, *PFHT* is a poorly circumscribed subcutaneous mass, which is of low SI on both T1- and T2-weighted images, reflecting the high collagen composition. None or minimal enhancement post-gadolinium was seen [43, 84].

- *Differential diagnosis*:
  The differential diagnosis of *PFHTs* includes *BFH*, plexiform nerve sheath tumour, benign and malignant giant cell tumour of soft tissue (*GCT-ST*) and infantile myofibromatosis [30, 46, 51, 131]. Imaging findings are non-specific and therefore diagnosis is based on histology. *GCT-ST*

predominantly occurs in adults and demonstrates a solid, rather than plexiform, growth pattern. *BFH* is frequently marked by a storiform pattern. Solitary and multiple infantile myofibromatosis tends to be well demarcated and frequently displays haemangiopericytoma-like areas [63].

14.2.2 Giant Cell Tumour of Soft Tissue

GCT-ST is exceedingly rare and is histologically similar to giant cell tumour (*GCT*) of the bone [8]. There have been no reports of *GCT* of the bone and *GCT-ST* occurring simultaneously. It was first described in 1972, by Salm and Sissons [107] who noted the resemblance between the two entities. It is also known as an osteoclastoma of soft tissue and is a tumour of unpredictable behaviour [40] and low malignant potential. There have been rare reports of metastases [40]. The exact histopathogenesis of *GCT* is unknown though origin from undifferentiated mesenchymal cells has been proposed [96] or that giant cells are the result of fusion of circulating monocytes recruited into the lesion [76].

- *Clinical behaviour and gross findings*:
  GCT-ST is a painless multinodular mass, which can fungate [27]. It occurs predominantly in the fifth decade but has been reported in patients ranging from 5 to 89 years of age. No sex predominance is noted [68]. Seventy percent of tumours occur in the extremities (lower > upper), 20 % in the trunk and 7 % in the head and neck regions [34, 86, 88, 103]. A number of cases have reported *GCT-ST* localised to the mediastinum [53]. There has been reported occurrence of de novo *GCT-CT* within a surgical scar [38].
  GCT-ST is a well-circumscribed, predominantly solid, nodular mass that has a red-brown or grey surface. Peripheral mineralisation is frequently present and may be detected on radiographs [86]. Tumours range from 0.7 to 10 cm with a mean of 3 cm [34, 86, 88]. Though most lesions are superficially located, 30 % of cases are noted to extend through the superficial fascia [34, 86, 104]. There have been a few case reports of *GCT-ST* causing a paraneoplastic osteomalacia. Patients present with a clinical picture of osseous pain and muscle weakness. Biochemical profile demonstrates a normocalcaemia, hypophosphataemia, phosphaturia and increased serum alkaline phosphatase [45].
  Treatment is with surgical excision; however, the rate of local recurrence is reported at 12 % with rare cases of metastasis and even death [34, 86, 88]. Superficial *GCT-STs* have a more favourable prognosis than deep *GCT-ST*. More recently, Righi et al. [102] report the risk of recurrence to be 28 % in the skin and 45 % in deep soft tissues. The risk of recurrence is related to inadequate excision margins [50]. Adjuvant radiotherapy has also been used [12, 124]. Currently, no clinicopathological factors are predictive of the clinical course or risk of metastasis [34, 86, 88].
- *Pathology*:
  The most prominent feature of *GCT-ST* is its multinodular architecture seen in 85 % of cases [88]. Nodules are separated by fibrous septations containing haemosiderin-laden macrophages [86]. *GCT-ST* has a richly vascularised stroma containing a mixture of spindle and polygonal mononuclear stromal cells and multinucleate osteoclast-like giant cells. Approximately 1–30 mitotic figures per 10 HPF are present [34, 86, 88]. Necrosis is rare, and unlike its bony counterpart, atypia, nuclear pleomorphism and bizarre giant cells are typically absent [34, 42, 68, 86, 88]. Peripheral bone formation, seen as a peripheral shell of woven bone or as scattered bony structures, is present in approximately 50 % of cases. A third of cases demonstrate features similar to aneurysmal bone cyst (*ABC*) with the formation of blood-filled lakes with 30 % of tumours demonstrating vascular invasion [34, 42, 88].

Interestingly, the features of *GCTTS* (dense hyaline stroma, siderophages and xanthoma cells) are nearly always absent (see Sect. 14.1.1.1 above).

- *Genetics*:
  Cytogenic analysis of a single case demonstrated multiple telomeric associations involving multiple chromosomes, similar to that of *GCT* of the bone [42].
- *Imaging findings*:
  The imaging description of *GCT-ST* is not well described, initially confined to a handful of angiographic studies [2].
  In general, radiographs are normal with superficial tumours or may demonstrate increased soft tissue density. Cortical bone irregularity was noted in a case of a deep *GCT-ST* situated adjacent to the fibula [67], but this is not a common finding [27].
  Peripheral mineralisation, which is noted histologically, can be seen on *CT* [67].
  US demonstrates a non-specific heterogeneous/hypoechoic solid mass with no or minimal increased Doppler signal [12, 67].
  MRI features are non-specific but demonstrate a soft tissue mass that is of low to intermediate SI to the muscle on T1-weighted images with increased heterogeneous SI on T2-weighted images. A peripheral low-signal rim and low-signal foci were identified throughout the lesion on all imaging sequences due to the presence of haemosiderin [67]. Lee et al. demonstrated restricted diffusion on diffusion-weighted imaging in their case of *GCT-ST* [67]. There is diffuse enhancement post-contrast, which is also seen on *CT*. In tumours with *ABC*-like features, fluid-fluid levels can be demonstrated with varying SI on T1- and T2-weighted images reflecting the different stages of blood [76]. Cystic degeneration of *GCT-ST* with imaging characteristics consistent with a cystic lesion has been reported [1]. These tend to be thick walled with internal debris.
  GCT-ST has been shown to demonstrate increased uptake on ^{18}*F-FDG PET-CT* [67, 102].
  To date, four cases of paraneoplastic osteomalacia have been described [45]. Harish et al. described the MRI appearances of a *GCT-ST* as mentioned above, but furthermore, there were radiographic features of osteomalacia with Looser's zones. The *GCT-ST* was localised with an ^{111}*indium octreotide scintigram*, which demonstrated uptake in the tumour.
- *Differential diagnosis*:
  The main differential diagnoses include benign lesions such as giant cell tumour of the tendon sheath (*GCTTS*), reparative giant cell granuloma, cellular-type BFH with osteoclast-like giant cells and *PFHT*. *GCT-ST* can be misdiagnosed as an extraskeletal osteosarcoma variant, due to the common presence of osteoid formation [34, 88, 107]. Differential diagnosis of a *GCT-ST* also includes leiomyosarcoma with osteoclast-like giant cells.

Key points

1. Tenosynovial giant cell tumours have local or diffuse types, which occur in an intra- or extra-articular location, and are of low SI on both pulse sequences with marked blooming artefact on gradient echo sequences due to its haemosiderin content and avidly enhance.
2. Imaging features of other benign fibrohistiocytic tumours are non-specific and often require histological confirmation of its nature.

References

1. An SB, Choi JA, Chung JH et al (2008) Giant cell tumor of soft tissue: a case with atypical US and MRI findings. Korean J Radiol 9:462–465
2. Angervall L, Hagmar B, Kindblom LG et al (1981) Malignant giant cell tumor of soft tissues: a clinicopathologic, cytologic, ultrastructural, angiographic, and microangiographic study. Cancer 47:736–747
3. Asano N, Yoshida A, Kobayashi E et al (2014) Multiple metastases from histologically benign

intraarticular diffuse-type tenosynovial giant cell tumor: a case report. Hum Pathol 45:2355–2358
4. August C, Holzhausen HJ, Zornig C et al (1994) Plexiform fibrohistiocytic tumor. Histology, immunohistology and ultrastructure. Pathologe 15:49–53
5. Bancroft LW, Pettis C, Wasyliw C (2013) Imaging of benign soft tissue tumors. Semin Musculoskelet Radiol 17:156–167
6. Bertoni F, Unni KK, Beabout JW et al (1997) Malignant giant cell tumor of the tendon sheaths and joints (malignant pigmented villonodular synovitis). Am J Surg Pathol 21:153–163
7. Beytemur O, Albay C, Tetikkurt US et al (2014) Localized giant cell tenosynovial tumor seen in the knee joint. Case Rep Orthop 2014:840243
8. Billings SD, Folpe AL (2004) Cutaneous and subcutaneous fibrohistiocytic tumors of intermediate malignancy: an update. Am J Dermatopathol 26:141–155
9. Botrus G, Sciot R, Debiec-Rychter M (2006) Cutaneous aneurysmal fibrous histiocytoma with a t(12;19)(p12;q13) as the sole cytogenetic anomaly. Cancer Genet Cytogenet 164:155–158
10. Bravo SM, Winalski CS, Weissman BN (1996) Pigmented villonodular synovitis. Radiol Clin N Am 34:311–326, x–xi
11. Bui-Mansfield LT, Youngberg RA, Coughlin W et al (1996) MRI of giant cell tumor of the tendon sheath in the cervical spine. J Comput Assist Tomogr 20:113–115
12. Calli AO, Tunakan M, Katilmis H et al (2014) Soft tissue giant cell tumor of low malignant potential of the neck: a case report and review of the literature. Turk Patoloji Dergisi 30:73–77
13. Calonje E, Mentzel T, Fletcher CD (1994) Cellular benign fibrous histiocytoma. Clinicopathologic analysis of 74 cases of a distinctive variant of cutaneous fibrous histiocytoma with frequent recurrence. Am J Surg Pathol 18:668–676
14. Cardinal E, Buckwalter KA, Braunstein EM et al (1994) Occult dorsal carpal ganglion: comparison of US and MR imaging. Radiology 193:259–262
15. Cassier PA, Gelderblom H, Stacchiotti S et al (2012) Efficacy of imatinib mesylate for the treatment of locally advanced and/or metastatic tenosynovial giant cell tumor/pigmented villonodular synovitis. Cancer 118:1649–1655
16. Chang SE, Choi JH, Sung KJ et al (2001) Subcutaneous dermatofibroma showing a depressed surface. Int J Dermatol 40:77–78
17. Charli-Joseph Y, Saggini A, Doyle LA et al (2014) DNA copy number changes in tumors within the spectrum of cellular, atypical, and metastasizing fibrous histiocytoma. J Am Acad Dermatol 71:256–263
18. Chassaignac M (1852) Cancer de la gaine des tendons. Gas Hosp Civ Milit 47:185–190
19. Choong PF, Willen H, Nilbert M et al (1995) Pigmented villonodular synovitis. Monoclonality and metastasis - a case for neoplastic origin? Acta Orthop Scand 66:64–68
20. Cupp JS, Miller MA, Montgomery KD et al (2007) Translocation and expression of CSF1 in pigmented villonodular synovitis, tenosynovial giant cell tumor, rheumatoid arthritis and other reactive synovitides. Am J Surg Pathol 31:970–976
21. David RL (2012) Tenosynovial giant cell tumor: case report and review. Arch Pathol Lab Med 136:901–906
22. De Beuckeleer L, De Schepper A, De Belder F et al (1997) Magnetic resonance imaging of localized giant cell tumour of the tendon sheath (MRI of localized GCTTS). Eur Radiol 7:198–201
23. De Schepper AM, Degryse HR, Ramon FA et al (1992) Magnetic resonance imaging of extraabdominal desmoid tumors. J Belge Radiol 75:91–98
24. Deb P, Singh V, Dutta V et al (2014) Primary intracranial benign fibrous histiocytoma: report of an unusual case. J Cancer Res Ther 10:200–202
25. Demir MK, Ozdemir H, Genchallac H et al (2009) Dermatofibroma mimicking malignancy on integrated F-18 fluorodeoxyglucose PET-CT. Diagn Interv Radiol (Ankara, Turkey) 15:61–63
26. Dercle L, Chisin R, Ammari S et al (2015) Nonsurgical giant cell tumour of the tendon sheath or of the diffuse type: are MRI or 18F-FDG PET/CT able to provide an accurate prediction of long-term outcome? Eur J Nucl Med Mol Imaging 42:397–408
27. Dodd LG, Major N, Brigman B (2004) Malignant giant cell tumor of soft parts. Skeletal Radiol 33:295–299
28. Dorwart RH, Genant HK, Johnston WH et al (1984) Pigmented villonodular synovitis of synovial joints: clinical, pathologic, and radiologic features. AJR Am J Roentgenol 143:877–885
29. Doyle LA, Fletcher CD (2013) Metastasizing "benign" cutaneous fibrous histiocytoma: a clinicopathologic analysis of 16 cases. Am J Surg Pathol 37:484–495
30. Enzinger FM, Zhang RY (1988) Plexiform fibrohistiocytic tumor presenting in children and young adults. An analysis of 65 cases. Am J Surg Pathol 12:818–826
31. Fitzpatrick TB, Gilchrest BA (1977) Dimple sign to differentiate benign from malignant pigmented cutaneous lesions. N Engl J Med 296:1518
32. Fletcher CD (1990) Benign fibrous histiocytoma of subcutaneous and deep soft tissue: a clinicopathologic analysis of 21 cases. Am J Surg Pathol 14:801–809
33. Fletcher CDM, Bridge JA, Hogendoorn PC et al (2013) WHO classification of tumours of soft tissue and bone, 4th edn. IARC Press, Lyon
34. Folpe AL, Morris RJ, Weiss SW (1999) Soft tissue giant cell tumor of low malignant potential: a proposal for the reclassification of malignant giant cell tumor of soft parts. Modern Pathol Off J United States Can Acad Pathol Inc 12:894–902
35. Fox MG, Kransdorf MJ, Bancroft LW et al (2003) MR imaging of fibroma of the tendon sheath. AJR Am J Roentgenol 180:1449–1453

36. Frau DV, Erdas E, Caria P et al (2010) Deep fibrous histiocytoma with a clonal karyotypic alteration: molecular cytogenetic characterization of a t(16;17)(p13.3;q21.3). Cancer Genet Cytogenet 202:17–21
37. Gleason BC, Fletcher CD (2008) Deep "benign" fibrous histiocytoma: clinicopathologic analysis of 69 cases of a rare tumor indicating occasional metastatic potential. Am J Surg Pathol 32:354–362
38. Grabellus F, Sheu SY, Schmidt B et al (2009) Giant cell tumors of soft tissue arising in surgical scars. Pathologe 30:401–406
39. Granowitz SP, D'antonio J, Mankin HL (1976) The pathogenesis and long-term end results of pigmented villonodular synovitis. Clin Orthop Relat Res. 114:335–351
40. Guccion JG, Enzinger FM (1972) Malignant giant cell tumor of soft parts. An analysis of 32 cases. Cancer 29:1518–1529
41. Guillou L, Gebhard S, Salmeron M et al (2000) Metastasizing fibrous histiocytoma of the skin: a clinicopathologic and immunohistochemical analysis of three cases. Modern Pathol Off J United States Can Acad Pathol Inc 13:654–660
42. Guo H, Garcia RA, Perle MA et al (2005) Giant cell tumor of soft tissue with pulmonary metastases: pathologic and cytogenetic study. Pediatr Dev Pathol Off J Soc Pediatr Pathol Paediatr Pathol Soc 8:718–724
43. Habermann CR, Nicolas V, Steiner P (1995) Magnetic resonance tomography diagnosis of plexiform fibrohistiocytic tumor. Aktuelle Radiol 5:243–245
44. Han TY, Chang HS, Lee JH et al (2011) A clinical and histopathological study of 122 cases of dermatofibroma (benign fibrous histiocytoma). Ann Dermatol 23:185–192
45. Harish S, Jurriaans E, Jan E et al (2008) Giant cell tumour of soft tissue causing oncogenic osteomalacia: report demonstrating the use of octreotide scintigraphy in tumour localization. Clin Radiol 63:101–107
46. Hollowood K, Holley MP, Fletcher CD (1991) Plexiform fibrohistiocytic tumour: clinicopathological, immunohistochemical and ultrastructural analysis in favour of a myofibroblastic lesion. Histopathology 19:503–513
47. Howie CR, Smith GD, Christie J et al (1985) Torsion of localised pigmented villonodular synovitis of the knee. J Bone Joint Surg 67:564–566
48. Huang GS, Lee CH, Chan WP et al (2003) Localized nodular synovitis of the knee: MR imaging appearance and clinical correlates in 21 patients. AJR Am J Roentgenol 181:539–543
49. Huang YC, Chen JW, Chen YL et al (2014) Giant cell tumour of a temporomandibular joint presenting as a parotid mass: case report and analysis of the 19 cases in the literature. J Craniomaxillofac Surg Off Publ Eur Assoc Craniomaxillofac Surg 42:1778–1782
50. Icihikawa K, Tanino R (2004) Soft tissue giant cell tumor of low malignant potential. Tokai J Exp Clin Med 29:91–95
51. Jafarian F, Mccuaig C, Kokta V et al (2006) Plexiform fibrohistiocytic tumor in three children. Pediatr Dermatol 23:7–12
52. Jaffe HL, Lichtenstein L, Suro CJ (1941) Pigmented villonodular synovitis, bursitis and tenosynovitis. Arch Pathol 31:731–765
53. Jain D, Arava S, Mishra B et al (2015) Soft tissue giant cell tumor of low malignant potential of mediastinum: a rare case report. Int J Surg Pathol 23:71–74
54. Jalgaonkar A, Dhinsa B, Cottam H et al (2011) Giant cell tumours of tendon sheath of hand: causes and strategies to prevent recurrence. Hand Surg Int J Devoted Hand Up Limb Surg Relat Res J Asia Pac Fed Soc Surg Hand 16:149–154
55. Jelinek JS, Kransdorf MJ, Shmookler BM et al (1994) Giant cell tumor of the tendon sheath: MR findings in nine cases. AJR Am J Roentgenol 162:919–922
56. Jelinek JS, Kransdorf MJ, Utz JA et al (1989) Imaging of pigmented villonodular synovitis with emphasis on MR imaging. AJR Am J Roentgenol 152:337–342
57. Jergesen HE, Mankin HJ, Schiller AL (1978) Diffuse pigmented villonodular synovitis of the knee mimicking primary bone neoplasms. A report of two cases. J Bone Joint Surg Am 60:825–829
58. Kaddu S, Mcmenamin ME, Fletcher CD (2002) Atypical fibrous histiocytoma of the skin: clinicopathologic analysis of 59 cases with evidence of infrequent metastasis. Am J Surg Pathol 26: 35–46
59. Kamino H, Jacobson M (1990) Dermatofibroma extending into the subcutaneous tissue. Differential diagnosis from dermatofibrosarcoma protuberans. Am J Surg Pathol 14:1156–1164
60. Kanagawa H, Niki Y, Matsumoto H et al (2007) Localized pigmented villonodular synovitis presenting as a loose body following minor trauma in the knee: a case report. Knee 14:395–397
61. Karasick D, Karasick S (1992) Giant cell tumor of tendon sheath: spectrum of radiologic findings. Skeletal Radiol 21:219–224
62. Kobayashi H, Sakahara H, Hosono M et al (1993) Scintigraphic evaluation of tenosynovial giant-cell tumor using technetium-99m(V)-dimercaptosuccinic acid. J Nucl Med Off Publ Soc Nucl Med 34:1745–1747
63. Koujok K, Ruiz RE, Hernandez RJ (2005) Myofibromatosis: imaging characteristics. Pediatr Radiol 35:374–380
64. Lautenbach M, Kim S, Millrose M et al (2013) Nodular giant cell tumour of the tendon sheath of the hand: analysis of eighty-four cases—diagnostic decisions and outcome. Int Orthop 37:2211–2215

65. Leclerc-Mercier S, Pedeutour F, Fabas T et al (2011) Plexiform fibrohistiocytic tumor with molecular and cytogenetic analysis. Pediatr Dermatol 28: 26–29
66. Lee MH, Kim NR, Ryu JA (2010) Cyst-like solid tumors of the musculoskeletal system: an analysis of ultrasound findings. Skeletal Radiol 39:981–986
67. Lee MY, Jee WH, Jung CK et al (2015) Giant cell tumor of soft tissue: a case report with emphasis on MR imaging. Skeletal Radiol 44:1039–1043
68. Lentini M, Zuccala V, Fazzari C (2010) Polypoid giant cell tumor of the skin. Am J Dermatopathol 32:95–98
69. Li CF, Wang JW, Huang WW et al (2008) Malignant diffuse-type tenosynovial giant cell tumors: a series of 7 cases comparing with 24 benign lesions with review of the literature. Am J Surg Pathol 32:587–599
70. Lin J, Jacobson JA, Jamadar DA et al (1999) Pigmented villonodular synovitis and related lesions: the spectrum of imaging findings. AJR Am J Roentgenol 172:191–197
71. Llauger J, Palmer J, Roson N et al (1999) Pigmented villonodular synovitis and giant cell tumors of the tendon sheath: radiologic and pathologic features. AJR Am J Roentgenol 172:1087–1091
72. Machiels F, De Maeseneer M, Chaskis C et al (1998) Deep benign fibrous histiocytoma of the knee: CT and MR features with pathologic correlation. Eur Radiol 8:989–991
73. Mackie GC (2003) Pigmented villonodular synovitis and giant cell tumor of the tendon sheath: scintigraphic findings in 10 cases. Clin Nucl Med 28:881–885
74. Mahmood S, De Llano SR (2007) Localized nodular synovitis mimicking metastatic melanoma in a patient with metastatic melanoma on whole-body F-18 FDG PET/CT with MRI and pathological correlation. Clin Nucl Med 32:532–534
75. Mckenna DB, Kavanagh GM, Mclaren KM et al (1999) Aneurysmal fibrous histiocytoma: an unusual variant of cutaneous fibrous histiocytoma. J Eur Acad Dermatol Venereol JEADV 12:238–240
76. Meana Moris AR, Garcia Gonzalez P, Fuente Martin E et al (2010) Primary giant cell tumor of soft tissue: fluid-fluid levels at MRI (2010:3b). Eur Radiol 20:1539–1543
77. Middleton WD, Patel V, Teefey SA et al (2004) Giant cell tumors of the tendon sheath: analysis of sonographic findings. AJR Am J Roentgenol 183:337–339
78. Moller E, Mandahl N, Mertens F et al (2008) Molecular identification of COL6A3-CSF1 fusion transcripts in tenosynovial giant cell tumors. Genes Chromosomes Cancer 47:21–25
79. Monaghan H, Salter DM, Al-Nafussi A (2001) Giant cell tumour of tendon sheath (localised nodular tenosynovitis): clinicopathological features of 71 cases. J Clin Pathol 54:404–407
80. Moosavi C, Jha P, Fanburg-Smith JC (2007) An update on plexiform fibrohistiocytic tumor and addition of 66 new cases from the Armed Forces Institute of Pathology, in honor of Franz M. Enzinger, MD. Ann Diagn Pathol 11:313–319
81. Murphey MD, Nomikos GC, Flemming DJ et al (2001) From the archives of AFIP. Imaging of giant cell tumor and giant cell reparative granuloma of bone: radiologic-pathologic correlation. Radiographics Rev Publ Radiol Soc North Am Inc 21:1283–1309
82. Murphey MD, Rhee JH, Lewis RB et al (2008) Pigmented villonodular synovitis: radiologic-pathologic correlation. Radiographics Rev Publ Radiol Soc North Am Inc 28:1493–1518
83. Nagata S, Nishimura H, Uchida M et al (2008) Diffusion-weighted imaging of soft tissue tumors: usefulness of the apparent diffusion coefficient for differential diagnosis. Radiat Med 26:287–295
84. Ng E, Tandon AA, Ho BCS et al (2015) Characterising benign fibrous soft-tissue tumours in adults: why is it so difficult and what do we need to know? Clin Radiol 70:684–697
85. O'connell JX (2000) Pathology of the synovium. Am J Clin Pathol 114:773–784
86. O'connell JX, Wehrli BM, Nielsen GP et al (2000) Giant cell tumors of soft tissue: a clinicopathologic study of 18 benign and malignant tumors. Am J Surg Pathol 24:386–395
87. Ofluoglu O (2006) Pigmented villonodular synovitis. Orthop Clin North Am 37:23–33
88. Oliveira AM, Chou MM (2012) The TRE17/USP6 oncogene: a riddle wrapped in a mystery inside an enigma. Front Biosci (Schol Ed) 4:321–334
89. Palmerini E, Staals EL, Maki RG et al (2015) Tenosynovial giant cell tumour/pigmented villonodular synovitis: outcome of 294 patients before the era of kinase inhibitors. Eur J Cancer (Oxford England 1990) 51:210–217
90. Panagopoulos I, Brandal P, Gorunova L et al (2014) Novel CSF1-S100A10 fusion gene and CSF1 transcript identified by RNA sequencing in tenosynovial giant cell tumors. Int J Oncol 44: 1425–1432
91. Pathade SC, Kurpad R, Tauheed M (2014) Multiple Giant Cell Tumours of Tendon Sheath: A Rare Occurrence. J Clin Diagn Res JCDR 8: 170–171
92. Perka C, Labs K, Zippel H et al (2000) Localized pigmented villonodular synovitis of the knee joint: neoplasm or reactive granuloma? A review of 18 cases. Rheumatology (Oxford) 39:172–178
93. Rahbari H, Mehregan AH (1985) Adnexal displacement and regression in association with histiocytoma (dermatofibroma). J Cutan Pathol 12: 94–102
94. Rahimi AD, Shelton R, Dumas A et al (2001) Mohs micrographic surgery of a plexiform fibrohistiocytic tumor. Dermatol Surg 27:768–771

95. Rao AS, Vigorita VJ (1984) Pigmented villonodular synovitis (giant-cell tumor of the tendon sheath and synovial membrane). A review of eighty-one cases. J Bone Joint Surg Am 66:76–94
96. Raskin KA, Schwab JH, Mankin HJ et al (2013) Giant cell tumor of bone. J Am Acad Orthop Surg 21:118–126
97. Redlich GC, Montgomery KD, Allgood GA et al (1999) Plexiform fibrohistiocytic tumor with a clonal cytogenetic anomaly. Cancer Genet Cytogenet 108:141–143
98. Reilly KE, Stern PJ, Dale JA (1999) Recurrent giant cell tumors of the tendon sheath. J Hand Surg 24:1298–1302
99. Remstein ED, Arndt CA, Nascimento AG (1999) Plexiform fibrohistiocytic tumor: clinicopathologic analysis of 22 cases. Am J Surg Pathol 23:662–670
100. Richman DM, Bresler SC, Rosenthal MH et al (2015) Malignant tenosynovial giant cell tumor of the leg: a radiologic-pathologic correlation and review of the literature. J Clin imaging Sci 5:13
101. Righi A, Gambarotti M, Sbaraglia M et al (2015) Metastasizing tenosynovial giant cell tumour, diffuse type/pigmented villonodular synovitis. Clin Sarcoma Res 5:15
102. Righi S, Boffano P, Patetta R et al (2014) Soft tissue giant cell tumor of low malignant potential with 3 localizations: report of a case. Oral Surg Oral Med Oral Pathol Oral Radiol Endod 118:e135–e138
103. Rochanawutanon M, Praneetvatakul P, Laothamatas J et al (2011) Extraskeletal giant cell tumor of the larynx: case report and review of the literature. Ear Nose Throat J 90:226–230
104. Rodriguez-Peralto JL, Lopez-Barea F, Fernandez-Delgado J (2001) Primary giant cell tumor of soft tissues similar to bone giant cell tumor: a case report and literature review. Pathol Int 51:60–63
105. Rowlands CG, Roland B, Hwang WS et al (1994) Diffuse-variant tenosynovial giant cell tumor: a rare and aggressive lesion. Hum Pathol 25:423–425
106. Rubin BP (2007) Tenosynovial giant cell tumor and pigmented villonodular synovitis: a proposal for unification of these clinically distinct but histologically and genetically identical lesions. Skeletal Radiol 36:267–268
107. Salm R, Sissons HA (1972) Giant-cell tumours of soft tissues. J Pathol 107:27–39
108. Salomao DR, Nascimento AG (1997) Plexiform fibrohistiocytic tumor with systemic metastases: a case report. Am J Surg Pathol 21:469–476
109. Sheehan KM, Leader MB, Sexton S et al (2004) Recurrent aneurysmal fibrous histiocytoma. J Clin Pathol 57:312–313
110. Simon SL, Inneh IA, Lee MS et al (2011) Tenosynovial giant cell tumor of the thigh: positron emission tomography findings. Am J Orthop (Belle Mead NJ) 40:E115–E117
111. Smith S, Fletcher CD, Smith MA et al (1990) Cytogenetic analysis of a plexiform fibrohistiocytic tumor. Cancer Genet Cytogenet 48:31–34
112. Somerhausen NS, Fletcher CD (2000) Diffuse-type giant cell tumor: clinicopathologic and immunohistochemical analysis of 50 cases with extraarticular disease. Am J Surg Pathol 24:479–492
113. Somerhausen NS, Van Der Rijn M (2013) Tenosynovial giant cell tumour, diffuse type. In: Fletcher CDM, Bridge JA, Hogendoorn PCW, Mertens F (eds) World Health Organization classification of tumours. Pathology and genetics of tumours of soft tissue and bone. IARC Press, p 102–103
114. Szablewski V, Laurent-Roussel S, Rethers L et al (2014) Atypical fibrous histiocytoma of the skin with CD30 and p80/ALK1 positivity and ALK gene rearrangement. IARC Press Lyon, France. J Cutan Pathol 41:715–719
115. Uriburu IJ, Levy VD (1998) Intraosseous growth of giant cell tumors of the tendon sheath (localized nodular tenosynovitis) of the digits: report of 15 cases. J Hand Surg 23:732–736
116. Ushijima M, Hashimoto H, Tsuneyoshi M et al (1986) Giant cell tumor of the tendon sheath (nodular tenosynovitis). A study of 207 cases to compare the large joint group with the common digit group. Cancer 57:875–884
117. Ushijima M, Hashimoto H, Tsuneyoshi M et al (1985) Malignant giant cell tumor of tendon sheath. Report of a case. Acta Pathol Jpn 35:699–709
118. Van Der Heijden L, Gibbons CL, Dijkstra PD et al (2012) The management of diffuse-type giant cell tumour (pigmented villonodular synovitis) and giant cell tumour of tendon sheath (nodular tenosynovitis). J Bone Joint Surg 94:882–888
119. Vogrincic GS, O'connell JX, Gilks CB (1997) Giant cell tumor of tendon sheath is a polyclonal cellular proliferation. Hum Pathol 28:815–819
120. Wan JM, Magarelli N, Peh WC et al (2010) Imaging of giant cell tumour of the tendon sheath. Radiol Med 115:141–151
121. Wang K, Zhu B, Yang S et al (2014) Primary diffuse-type tenosynovial giant cell tumor of the spine: a report of 3 cases and systemic review of the literature. Turk Neurosurg 24:804–813
122. Wang Y, Tang J, Luo Y (2007) The value of sonography in diagnosing giant cell tumors of the tendon sheath. J Ultrasound Med Off J Am Inst Ultrasound Med 26:1333–1340
123. Weiss SW, Goldblum JR (2008) Benign fibrohistiocytic tumors. In: Enzinger and Weiss's soft tissue tumors 5e. Elsevier, Philadelphia, pp 331–342
124. Werner JA, Harms D, Beigel A (1997) Giant cell tumor of the larynx: case report and review of the literature. Head Neck 19:153–157
125. West RB, Rubin BP, Miller MA et al (2006) A landscape effect in tenosynovial giant-cell tumor from activation of CSF1 expression by a translocation in a minority of tumor cells. Proc Natl Acad Sci U S A 103:690–695
126. Wortsman X, Wortsman J (2010) Clinical usefulness of variable-frequency ultrasound in localized lesions of the skin. J Am Acad Dermatol 62:247–256

127. Yamasaki F, Takayasu T, Nosaka R et al (2016) Benign fibrous histiocytoma arising at the temporal bone of an infant-case report and review of the literature. Child's Nerv Syst. 32(1):189–93. doi: 10.1007/s00381-015-2822-3
128. Yamashita H, Endo K, Enokida M et al (2013) Multifocal localized pigmented villonodular synovitis arising separately from intra- and extra-articular knee joint: case report and literature review. Eur J Orthop Surg Traumatol Orthop Traumatol 23(Suppl 2):S273–S277
129. Yoo JH, Yang BK, Park JM (2007) Localized nodular synovitis of the knee presenting as anterior knee pain: a case report. Knee 14:398–401
130. Yotsumoto T, Iwasa J, Uchio Y (2008) Localized pigmented villonodular synovitis in the knee associated with locking symptoms. Knee 15: 68–70
131. Zelger B, Weinlich G, Steiner H et al (1997) Dermal and subcutaneous variants of plexiform fibrohistiocytic tumor. Am J Surg Pathol 21: 235–241

Tumors of Smooth and Skeletal Muscle and Pericytic Tumors

15

Miraude E.A.P.M. Adriaensen, Robert M. Kwee, and Filip M. Vanhoenacker

Contents

15.1 **Introduction** 339

15.2 **World Health Organization Classification of Muscle Tumors** 340
15.2.1 Smooth Muscle Tumors 340
15.2.2 Skeletal Muscle Tumors 343

15.3 **WHO Classification of Pericytic (Perivascular) Tumors** 348
15.3.1 Glomus Tumor 348
15.3.2 Glomangiomatosis 348
15.3.3 Malignant Glomus Tumor 349
15.3.4 Myopericytoma 352
15.3.5 Myofibroma and Myofibromatosis 354
15.3.6 Angioleiomyoma 358

Conclusion 359

References 360

M.E.A.P.M. Adriaensen (✉) • R.M. Kwee
Department of Radiology, Zuyderland Medical Center Heerlen, Henri Dunantstraat 5, 6419 PC Heerlen, The Netherlands
e-mail: miraude@gmail.com

F.M. Vanhoenacker
University Hospital Antwerp, Department of Radiology, Wilrijkstraat, 10, B-2650 Edegem, Belgium

General Hospital Sint-Maarten Duffel-Mechelen, Rooienberg 25, B-2570 Duffel, Belgium

Faculty of Medicine and Health Sciences, University of Ghent, Ghent, Belgium

15.1 Introduction

This chapter aims to discuss the relevant clinicopathological and imaging characteristics of tumors with myogenic differentiation and of pericytic tumors. Tumors with myogenic differentiation are further subdivided into smooth muscle tumors and skeletal muscle tumors. In contradistinction to other histological types of soft tissue tumors, tumors with histologically myogenic differentiation are more frequently malignant than benign. Benign muscle tumors (leiomyoma and rhabdomyoma) are relatively rare and account for less than 2% of all benign soft tissue tumors [25]. Malignant tumors with muscle differentiation (leiomyosarcoma and rhabdomyosarcoma) are more frequent and represent 2–12% and 8–9% of all soft tissue sarcomas, respectively [26].

However, many malignant soft tissue tumors that are identified on imaging to arise in muscle do not show muscle differentiation histologically. At MR imaging, these lesions are often indistinguishable from soft tissue tumors with myogenic differentiation. Therefore, histological confirmation is always required particularly if there is any suspicion for malignancy. Important general MR imaging features which may suggest malignancy, irrespective of the histological composition of the lesion, are large volume (any lesion exceeding 3 cm), ill-defined margins, inhomogeneity on all pulse sequences, intralesional hemorrhage, intralesional necrosis, extensive and peripheral enhancement pattern (with papillary projections) on static con-

© Springer International Publishing AG 2017

F.M. Vanhoenacker et al. (eds.), *Imaging of Soft Tissue Tumors*, DOI 10.1007/978-3-319-46679-8_15

trast examination, rapid enhancement with steep slope on dynamic contrast examination, extracompartmental extension, and invasion of adjacent bones and neurovascular bundles ([9] and Chap. 9). MR imaging is the primary imaging modality of choice for local staging of tumors arising in the extremities, whereas both CT and MR imaging can be used for staging tumors arising in the abdomen.

15.2 World Health Organization Classification of Muscle Tumors

Since imaging findings lack specificity, it is not possible to classify tumors by their radiological appearance. For this reason we will classify the muscular tumors on the basis of histology according to the World Health Organization (WHO) classification of soft tissue tumors ([12], Fourth revision).

Smooth Muscle Tumors

Benign

- Leiomyoma of deep soft tissue

Malignant

- Leiomyosarcoma (excluding skin)

Skeletal Muscle Tumors

Benign

- Extracardiac rhabdomyoma: adult, fetal, and genital type

Malignant

- Embryonal rhabdomyosarcoma
- Alveolar rhabdomyosarcoma
- Pleomorphic rhabdomyosarcoma
- Spindle cell/sclerosing rhabdomyosarcoma

15.2.1 Smooth Muscle Tumors

15.2.1.1 Leiomyoma of Deep Soft Tissue

Definition and Clinical Findings

Leiomyoma occurs mainly in the female reproductive tract. Further discussion of uterine smooth muscle tumors is beyond the scope of this chapter. Leiomyomata of the deep soft tissue are very rare in comparison with superficial leiomyomata. Superficial leiomyomata are further subdivided into cutaneous leiomyoma and genital leiomyoma. Cutaneous leiomyomata (leiomyoma cutis) arise from the arrector pili muscle of the skin. They present as clustered papules or less commonly as single painful nodules. The size ranges from a few millimeters up to 2 cm. Lesions arising from the deep dermis of the scrotum, nipple, areola, and vulva are designated as genital leiomyoma [27].

Leiomyomata of the deep soft tissue are further subdivided into two distinct subtypes: the deep leiomyoma of extremities (the somatic leiomyoma) and the retroperitoneal or abdominal leiomyoma [27]. The lesions are typically large at presentation (more than 5 cm) and have a rich vascularization [8, 27].

Long-term follow-up showed that deep leiomyoma may demonstrate aggressive behavior, leading to the assumption that these lesions could be potentially malignant [48]. Therefore, histological confirmation of the lesion is mandatory to make a reliable diagnosis [3].

Imaging

Superficial leiomyomata are dermatological-based lesions which are rarely referred for imaging [8]. At radiography or computed tomography (CT), leiomyomata of the deep soft tissue may occasionally show intralesional calcifications of variable morphology (either sandlike, plaquelike, or large mulberry pattern) [8, 27].

MR imaging findings are nonspecific. Because of the large size, the heterogeneous T2-signal, and high vascularity resulting in marked enhancement, the lesion may mimic a malignant STT [8, 27] (Fig. 15.1).

15.2.1.2 Leiomyosarcoma (Excluding Skin)

Definition and Clinical Findings

Leiomyosarcoma is a malignant neoplasm showing pure smooth muscle differentiation ([12], Fourth revision). Extrauterine leiomyosarcomata typically occur in adults [8].

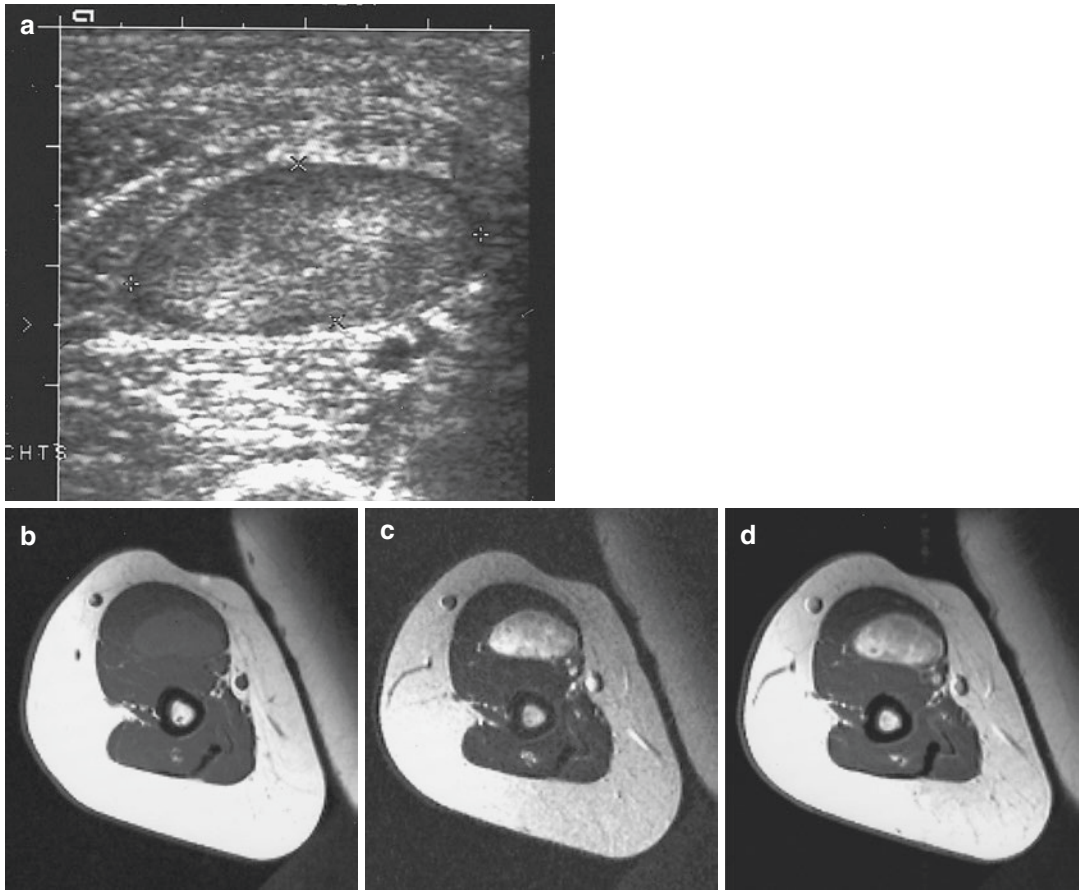

Fig. 15.1 Leiomyoma of the flexor compartment of the right arm in a 56-year-old woman. (**a**) Ultrasound, axial plane. Ultrasound shows a well-circumscribed, oval, and slightly hypoechoic mass within the biceps muscle. (**b**) Axial T1-WI. The well-defined mass is hyperintense to muscle on T1-WI. (**c**) Axial T2-WI. The well-defined mass shows an inhomogeneous, stippled high signal on T2-WI. (**d**) Axial T1-WI after IV administration of gadolinium contrast. Inhomogeneous enhancement is seen

There are four main subtypes, including cutaneous, subcutaneous, deep soft tissue, and vascular leiomyosarcoma. Cutaneous leiomyosarcoma has a far better prognosis than the subcutaneous type.

Deep soft tissue leiomyosarcomata mostly occur in the retroperitoneum (usually in the perirenal space) and only in 12–41 % in the extremities (particularly in the thigh) [7, 32, 38]. Of note, bone leiomyosarcoma is a distinct and rare entity, which is not addressed in the WHO classification of soft tissue tumors and bone ([12], Fourth revision). Deep soft tissue leiomyosarcomata in the retroperitoneum present at a more advanced stage than vascular leiomyosarcomata, which is likely because first mentioned have more space to grow before causing symptoms [7].

Vascular leiomyosarcomata arise in large vessels, most commonly in the inferior vena cava or lower extremity veins. The clinical findings depend on the involved part of the vein and the extent of the lesion. In the inferior vena cava, upper-segment involvement may manifest as Budd-Chiari syndrome, middle-segment involvement as nephrotic syndrome, and infrarenal involvement as edema in the lower extremity [34]. The lesions may cause vascular obstruction and thrombosis [4, 23].

Imaging

Cutaneous and subcutaneous leiomyosarcomata usually present as well-defined, relatively small, homogeneously enhancing tumors, often associated with fascial edema [16] (Fig. 15.2). Deep soft tissue and vascular leiomyosarcomata show similar imaging features [7, 16] and mostly present as large, heterogeneous masses with variable signal intensities, central necrosis, and marked peripheral and septal enhancement [44] (Figs. 15.3, 15.4, 15.5, and 15.6). Intralesional calcifications may be detected in a minority of leiomyosarcomata [5]. Secondary bone involvement is seen in up to 10 % [41, 44] (Fig. 15.6). Vascular leiomyosarcomata exhibit three main growth patterns: extraluminal (62 %), intraluminal (5 %), and combined extra- and intraluminal (33 %) [19]. Leiomyosarcoma of the inferior vena cava can be classified into three groups according to level affected: segment I, infrarenal; segment II, inter- and supra-renal up to but not including the main suprahepatic veins; and segment III, suprahepatic with possible intracardiac extension [22]. Intravascular leiomyosarcoma may be confused with deep vein thrombosis at US [8]. Both MR imaging and CT are useful for differentiating

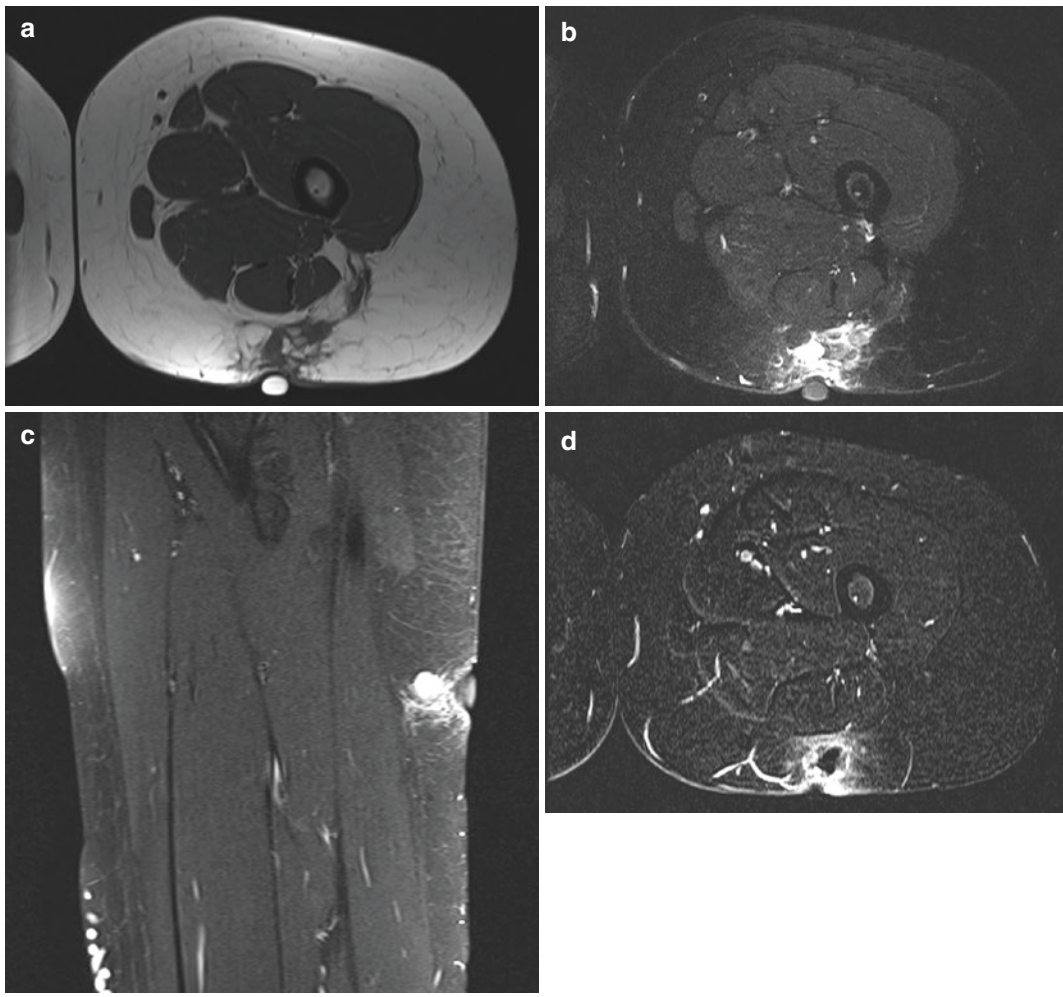

Fig. 15.2 Subcutaneous leiomyosarcoma of the thigh in a 39-year-old woman. (**a**) Axial T1-WI. (**b**) Axial FS T2-WI. (**c**) Sagittal FS T2-WI. Ill-defined, subcutaneously located mass on the dorsal side of the thigh with an intermediate signal intensity on T1-WI and hyperintense signal intensity on FS T2-WI. (**d**) Axial T1-WI after IV administration of gadolinium contrast. Inhomogeneous, mainly peripheral enhancement is seen

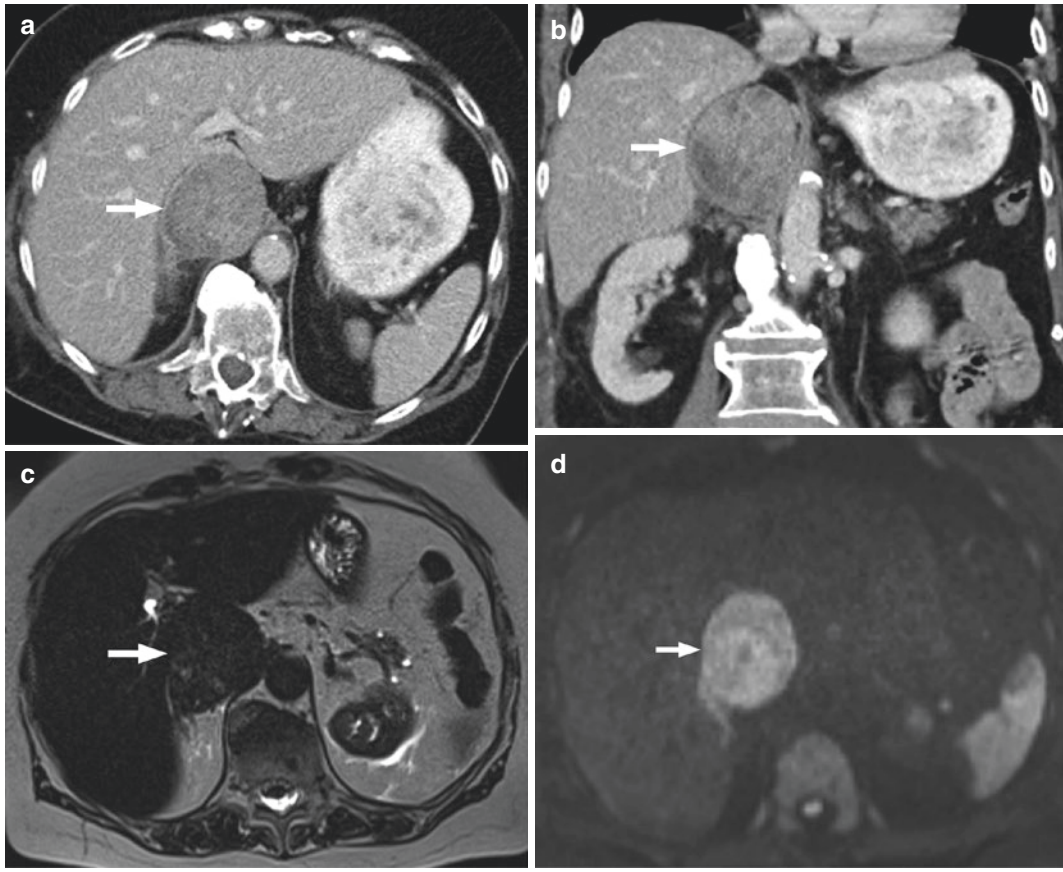

Fig. 15.3 Leiomyosarcoma of the inferior vena cava in an 84-year-old woman. (**a**) Axial contrast-enhanced CT image. (**b**) Coronal reformatted contrast-enhanced CT image. Well-delineated retroperitoneal mass with heterogeneous enhancement embedded in the inferior vena cava located between the renal veins and the confluence of the hepatic veins (i.e., middle segment). (**c**) Axial T2-WI. Heterogeneous mass slightly hyperintense signal compared to the liver parenchyma. (**d**) Axial diffusion-weighted image. Restricted diffusion in the largest part of the mass, with a small focus of absent diffusion restriction (Used with permission from Peters et al. Leiomyosarcoma of the inferior vena cava. Eurorad: radiological case database (2015), URL: http://www.eurorad.org/case.php?id=12591, DOI: 10.1594/EURORAD/CASE.12591)

intravascular leiomyosarcoma of the inferior vena cava from a simple thrombus and for staging [34].

15.2.2 Skeletal Muscle Tumors

15.2.2.1 Extracardiac Rhabdomyoma

Definition and Clinical Findings

Rhabdomyoma is a rare benign tumor composed of striated muscle cells [8]. There are two broad categories, cardiac and extracardiac rhabdomyoma. Cardiac rhabdomyoma is associated with the tuberous sclerosis complex. Extracardiac rhabdomyoma is further subdivided in adult, fetal, and genital subtypes.

Adult rhabdomyoma is a benign soft tissue neoplasm showing mature skeletal muscle differentiation ([12], Fourth revision). The adult subtype is a slowly growing painless mass most typically seen in the neck and rarely in the somatic skeletal muscle [27].

Fetal rhabdomyoma is a benign rhabdomyoblastic tumor with myotube-like differentiation ([12], Fourth revision). The less frequent fetal subtype has a predilection for the postauricular

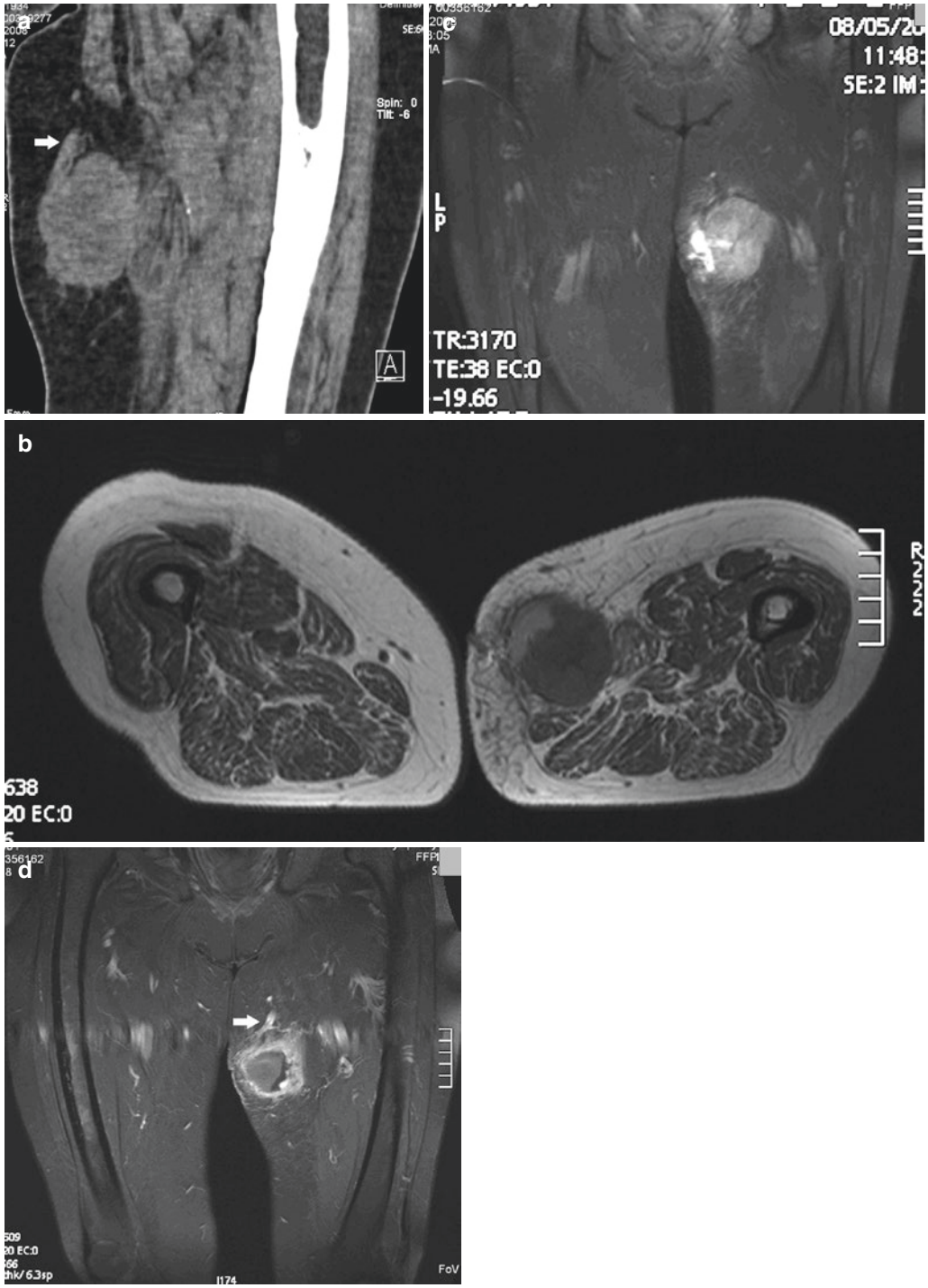

Fig. 15.4 High-grade leiomyosarcoma in the left thigh. (**a**) Coronal reformatted CT image. Large subcutaneous soft tissue mass abutting the adductor muscles. Note the intimate relationship with an adjacent subcutaneous vein (*white arrow*). (**b**) Axial T1-WI. (**c**) Coronal FS T2-WI. The mass is of inhomogeneous signal intensity on both pulse sequences. (**d**) Coronal FS T1-WI after IV administration of gadolinium contrast. There is marked inhomogeneous enhancement of the lesion. An intimate relationship with an adjacent subcutaneous vein is present (*white arrow*) (Color figure online)

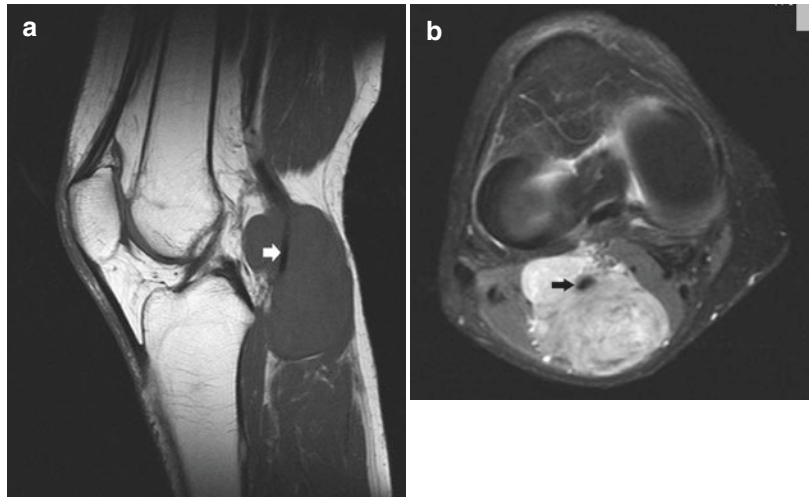

Fig. 15.5 Leiomyosarcoma of the right knee. (**a**) Sagittal T1-WI. (**b**) Axial FS T2-WI. Huge mass encasing the popliteal vessels (*arrows*)

region ([12], Fourth revision). The median age of presentation is 4 years [8, 27].

Genital rhabdomyoma are benign rhabdomyoblastic neoplasms arising in the female and male genital tract ([12], Fourth revision). The genital subtype most commonly presents as a vaginal polyp in middle-aged woman [8].

Imaging

Cardiac rhabdomyoma are usually detected on echocardiography as solitary or multiple hyperechoic mass(es) within the myocardium. Reports of both US and MR imaging features of extracardiac rhabdomyoma are scarce. Maglio et al. [28] reported a case of nonspecific oval hypoechoic mass in the neck of an adult patient. MR imaging reveals a well-delineated mass isointense or hyperintense compared to skeletal muscle on T1- and T2-weighted images (Fig. 15.7). Central necrosis and hemorrhage are rarely seen. After administration of intravenous gadolinium contrast, there is marked homogeneous or heterogeneous enhancement [8, 27] (Fig. 15.7).

15.2.2.2 Rhabdomyosarcoma

Definition and Clinical Findings

Rhabdomyosarcoma is the most common soft tissue tumor in children, accounting for 5–8 % of all childhood cancers [18, 35]. It is very rare in adults.

There are four main histological subtypes: embryonal, alveolar, pleomorphic, and spindle cell/sclerosing; each corresponding with a different prognosis. The embryonal subtype is most common in children, whereas the alveolar subtype is most common in young adults and adolescents [36].

Embryonal rhabdomyosarcoma is a primitive, malignant soft tissue tumor with phenotypical and biological features of embryonic skeletal muscle cells ([12], Fourth revision). Embryonal rhabdomyosarcomata are most frequent in the head and neck (47 %) and the genitourinary system (28 %) and only rarely involve the extremities (6 %). There is an increased incidence in Beckwith-Wiedemann syndrome [33].

Alveolar rhabdomyosarcoma is a highly cellular, malignant neoplasm containing a monomorphous population of primitive cells with round nuclei and features if arrested myogenesis ([12], Fourth revision). Alveolar rhabdomyosarcoma is more aggressive than embryonal rhabdomyosarcoma and has a poorer prognosis. The outcome is also affected by age, stage, and location. Tumors located in the extremities have a poorer prognosis ([12], Fourth revision).

Pleomorphic rhabdomyosarcoma is a high-grade sarcoma composed of bizarre polygonal, round, and spindle cells that display skeletal muscle differentiation without embryonal or alveolar components ([12], Fourth revision).

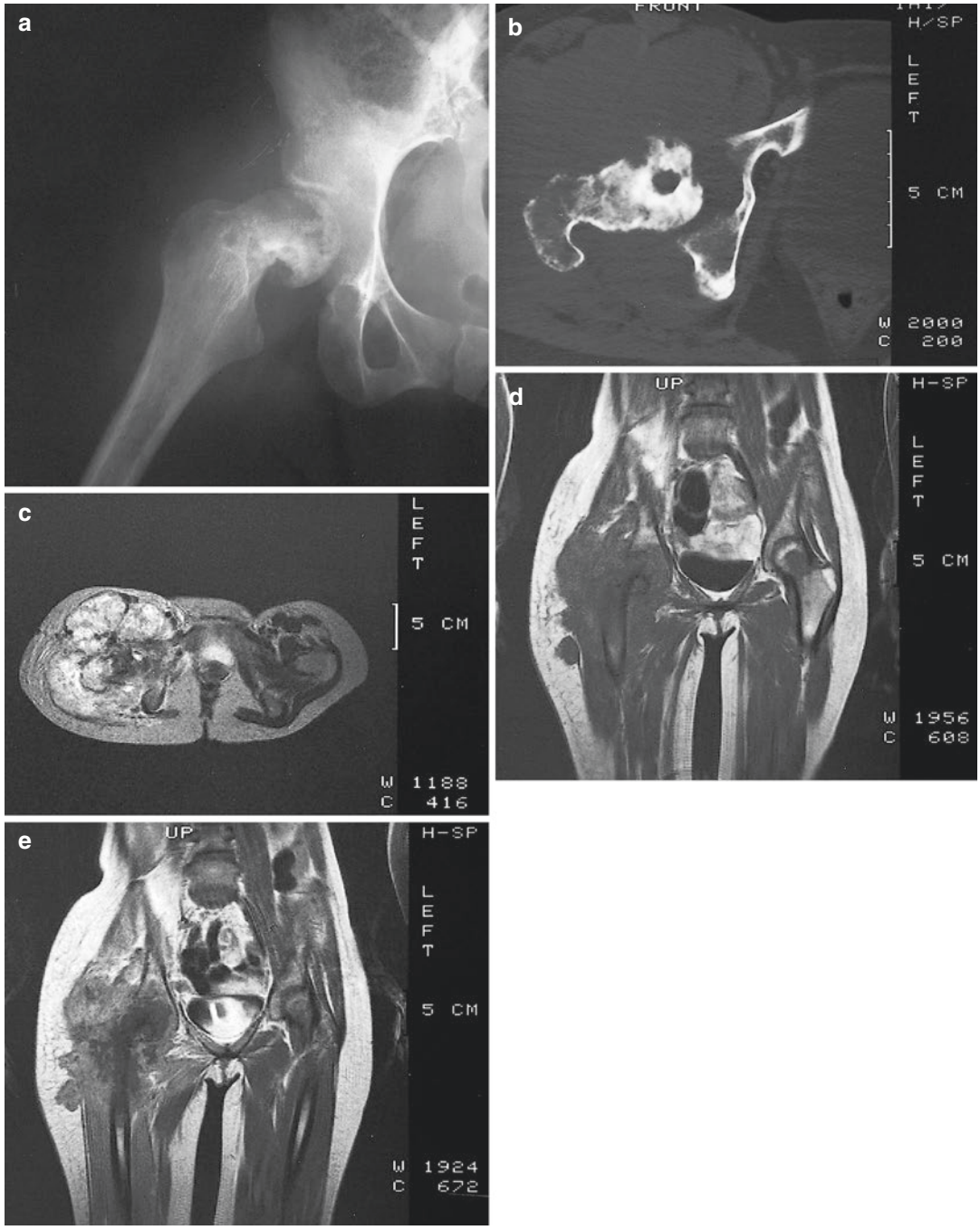

Fig. 15.6 Leiomyosarcoma of the right thigh in a 26-year-old woman with secondary bone involvement. (**a**) Plain radiograph. Plain radiograph demonstrates an indistinct soft tissue swelling with extensive mottled bone involvement and a pathological fracture of the femoral neck. (**b**) Axial CT. CT confirms areas of bone erosions and patchy sclerosis. (**c**) Axial T2-WI. (**d**) Coronal T1-WI. A soft tissue mass surrounds the hip and extends towards the midline. The infiltrating mass has a heterogeneous high signal intensity on T2-WI and an intermediate signal intensity on T1-WI (**e**) Coronal FS T1-WI after IV administration of gadolinium contrast. There is marked inhomogeneous enhancement of the lesion

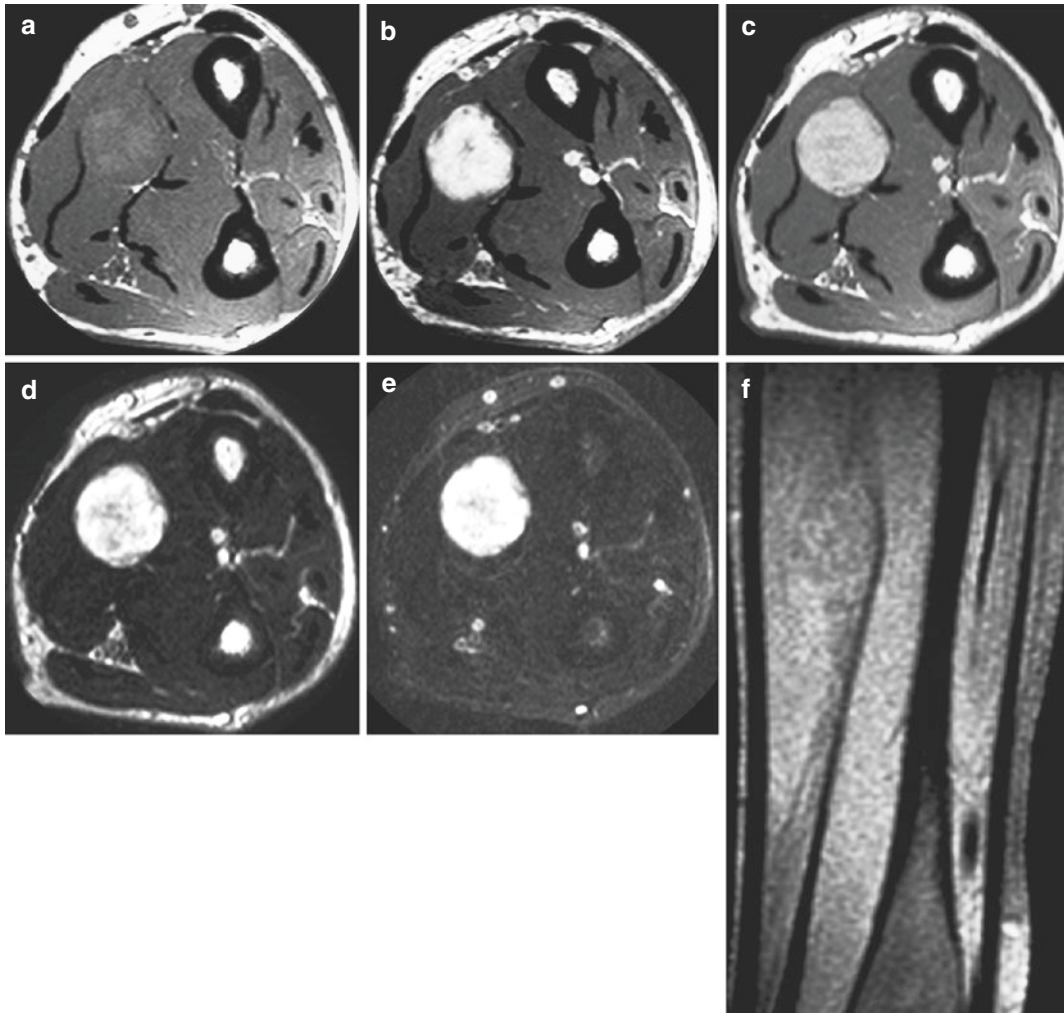

Fig. 15.7 Adult rhabdomyoma of the forearm in a 76-year-old man. (**a**) Axial T1-WI. A round mass lesion is seen between the superficial and deep flexor digitorum muscles. The lesion is inhomogeneous and has a higher signal than the adjacent normal muscle. (**b**) Axial FS T1-WI after IV administration of gadolinium contrast. There is marked inhomogeneous enhancement of the lesion. (**c**) Axial PD. (**d**) Axial T2-WI. (**e**) Axial FS T2-WI. (**f**) Sagittal T1-WI. The lesion has a high signal intensity on PD and T2-WI. The lesion remains hyperintense on T2-WI with fat suppression. On T2-WI with fat suppression and T1-WI with fat suppression, fatty components can be excluded

Pleomorphic rhabdomyosarcoma occurs almost exclusively in adults, typically in the deep soft tissues of the extremities, particularly the thigh [1]. The prognosis is poor.

Spindle cell/sclerosing rhabdomyosarcoma is an uncommon variant that has spindle cell morphology ([12], Fourth revision). Spindle cell/sclerosing rhabdomyosarcomata occur both in children and in adults with a male predilection. Tumors with spindle cell morphology occur predominantly in the paratesticular region in children and in the deep soft tissues of the head and neck in adults. Lesions with sclerosing morphology are most common in the limbs in both age groups. In children, tumors with spindle cell morphology are usually diagnosed at an early stage, with limited disease burden and a 95 % survival rate at 5 years ([12],

Fourth revision). In adults the outcome of spindle cell/sclerosing rhabdomyosarcoma is significantly worse with a recurrence rate and metastasis of approximately 40–50 % ([12], Fourth revision).

Imaging

Plain radiographs and CT may show local bone invasion, which is seen in about 25 % of cases. Bone metastases may occur and are usually lytic and more rarely mixed [8, 27].

US findings of rhabdomyosarcoma are nonspecific [49].

MR imaging features are also nonspecific; isointense to muscle on T1-weighted images and heterogeneous hyperintense on T2-weighted images, often with necrotic foci, may be seen. Marked enhancement is the rule, particularly in the alveolar subtype which has a prominent vascularity [1] (Figs. 15.8, 15.9, 15.10, 15.11, 15.12, and 15.13).

15.3 WHO Classification of Pericytic (Perivascular) Tumors

Since imaging techniques lack specificity, it is not possible to classify tumors by their radiological appearance. For this reason we will classify the pericytic (perivascular) tumors on the basis of histology according to the WHO classification of soft tissue tumors ([12], Fourth revision).

Glomus Tumors (And Variants)

Benign

- Glomus tumor
- Glomangiomatosis

Malignant

- Malignant glomus tumor

Myopericytoma, Including Myofibroma

Benign

- Myopericytoma
- Myofibroma
- Myofibromatosis

Angioleiomyoma

Benign

- Angioleiomyoma

15.3.1 Glomus Tumor

15.3.1.1 Definition and Clinical Findings

Glomus tumors are mesenchymal neoplasms composed of cells resembling the modified smooth muscle cells of the normal glomus body ([12], Fourth revision). The glomus body is an arteriovenous anastomosis that has an important role in thermoregulation [40]. The most common location of a glomus tumor is the subungual region, although glomus tumors are reported throughout the body [15, 29]. Glomus tumors are typically small (<1 cm), red-blue nodules with a long history of pain, particularly with exposure to cold or minor tactile stimulation ([12], Fourth revision). Although exquisitely tender to palpation, most lesions are not palpable as such [15].

15.3.1.2 Imaging

At US, a glomus tumor may have a flattened configuration when subungually located and in that case may present as a less conspicuous, thickened hypoechoic subungual space [15]. The normal subungual space is only 1–2 mm thick [15]. If localized lateral to the nail bed or in the palmar digital soft tissues, it assumes an ellipsoid or concentric shape [13]. Glomus tumors show a marked Doppler vascular signal, which equals the vascular signal in the normal nail bed [15] (Fig. 15.14). At MR imaging, a glomus tumor is seen as a homogeneous hyperintense lesion on T2-weighted images [40] and an intermediate- to low-signal-intensity lesion on T1-weighted images [2] (Fig. 15.14). Intense enhancement after administration of intravenous gadolinium contrast is typical [29, 46] (Fig. 15.14). Differential diagnosis of a glomus tumor includes hemangioma, vascular malformation, mucoid cyst, and epidermal inclusion cyst.

15.3.2 Glomangiomatosis

15.3.2.1 Definition and Clinical Findings

Glomangiomatosis is an extremely rare variant of glomus tumor with an overall architectural

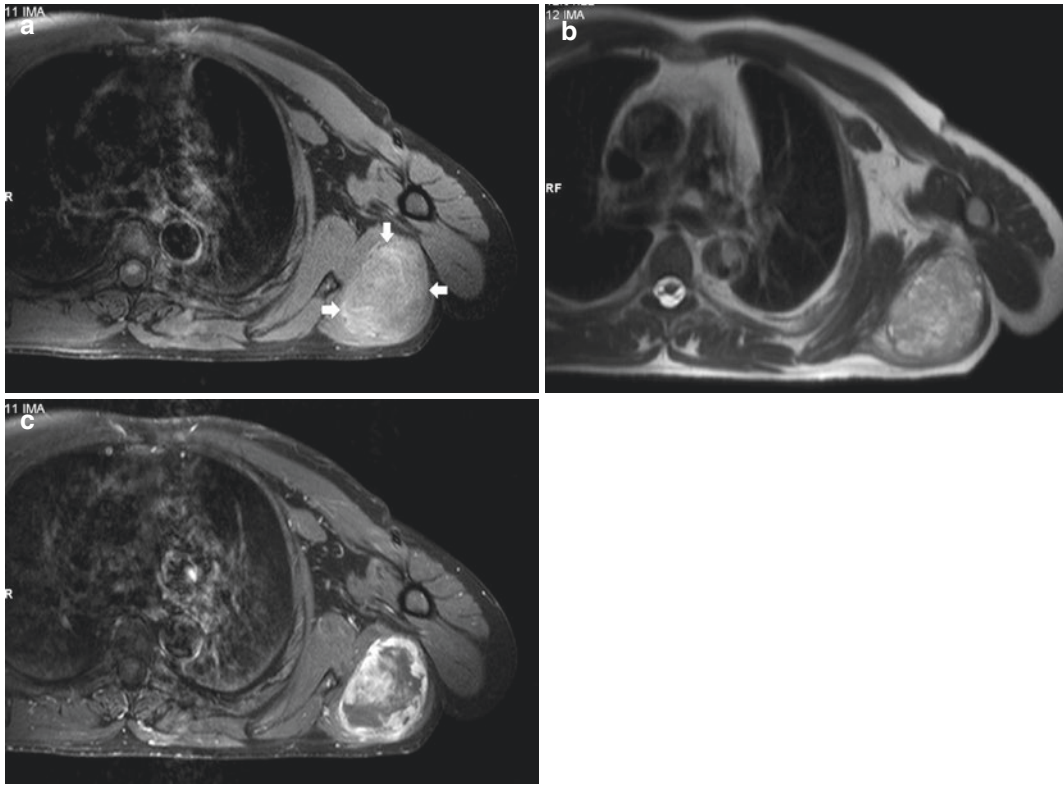

Fig. 15.8 Pleomorphic rhabdomyosarcoma in the left deltoid muscle. (**a**) Axial FS T1-WI. (**b**) Axial FS T2-HASTE. Large inhomogeneous mass on both pulse sequences. (**c**) Axial FS T1-WI after IV administration of gadolinium contrast. There is marked heterogeneous enhancement

resemblance to diffuse angiomatosis but containing nests of glomus cells investing vessel walls ([12], Fourth revision). Glomangiomatosis presents as multiple glomus tumors in one patient; they have been reported to occur in the hand and feet and exhibit sensitivity to temperature or pressure [37]. Unlike solitary glomus tumors, multiple glomus tumors are not always located in the subungual region, making diagnosis difficult: they may be clinically misdiagnosed as neuromas or painful fibromatosis [37].

15.3.2.2 Imaging

At MR imaging, glomangiomatosis presents as multiple nodules, with each nodule showing signal characteristics identical to a solitary glomus tumor: intermediate or low signal relative to muscle on T1-weighted images, and high signal intensities on T2-weighted images, with strong enhancement after intravenous administration of gadolinium-based contrast agent [37] (Fig. 15.15). This appearance is reminiscent of neurofibromatosis or multiple hemangiomas [37].

15.3.3 Malignant Glomus Tumor

15.3.3.1 Definition and Clinical Findings

Malignant glomus tumors show either marked nuclear atypia and any level of mitotic activity or atypical mitotic figures ([12], Fourth revision). There are two histological types. In one type, the malignant component resembles a leiomyosarcoma or fibrosarcoma. In the other type, the malignant component consists of sheets of highly

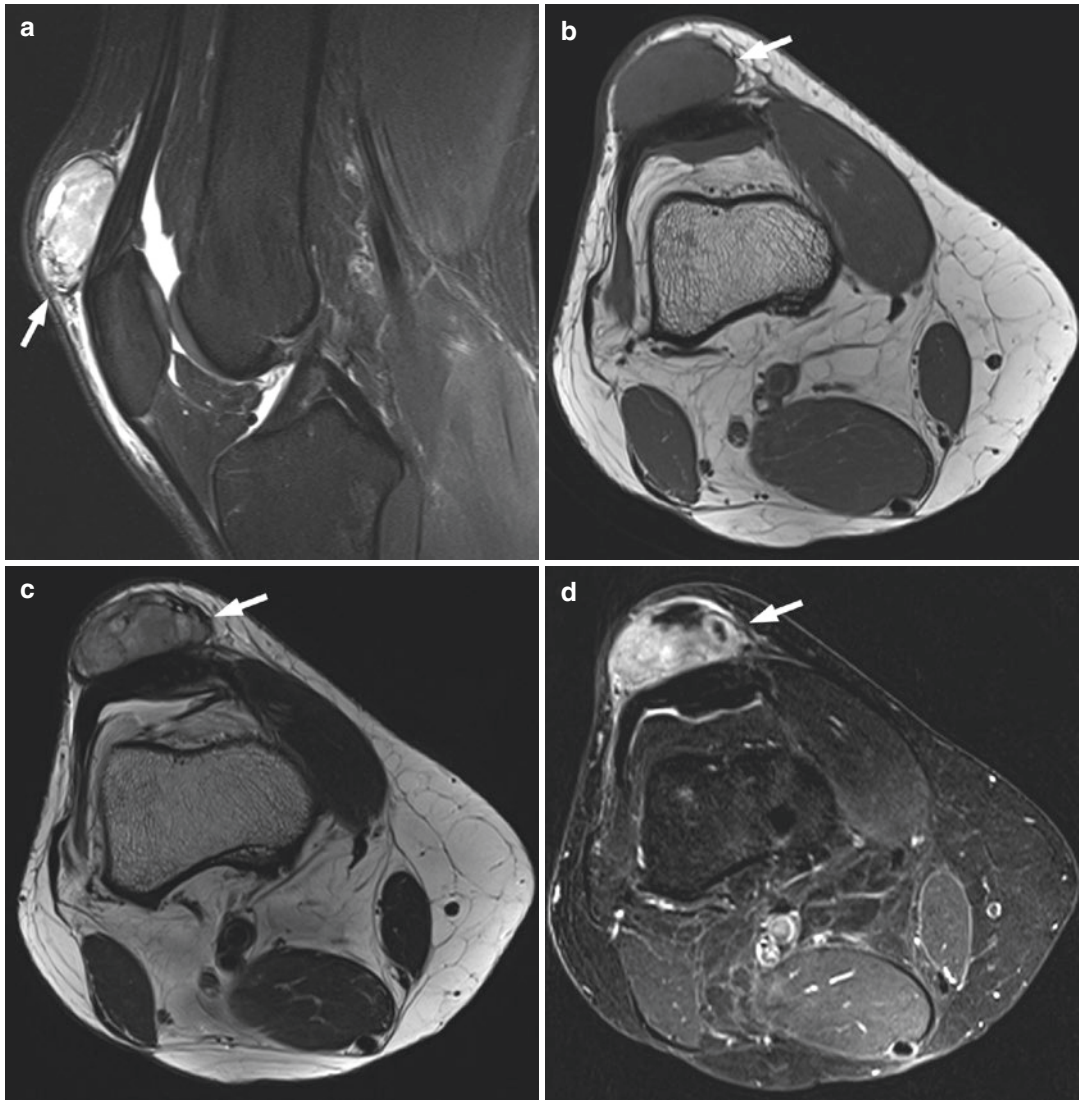

Fig. 15.9 Pleomorphic rhabdomyosarcoma of the knee. (**a**) Sagittal FS T2-WI. (**b**) Axial T1-WI. (**c**) Axial T2-WI. Ellipsoid, inhomogeneous mass on all pulse sequences located in the soft tissues ventral to the patella. (**d**) Axial FS T1-WI after IV administration of gadolinium contrast. There is marked heterogeneous enhancement

malignant-appearing round cells ([12], Fourth revision). Histologically, malignant glomus tumors are exceedingly rare and clinically malignant glomus tumors are even rarer ([12], Fourth revision). Less than 50 malignant glomus tumors have been reported in the English medical literature ([12], Fourth revision; [21]). Malignant glomus tumors are usually located deep to the fascia or in the viscera and usually measure more than 2 cm [29].

15.3.3.2 Imaging

Due to its rarity, the imaging features of malignant glomus tumors have been scarcely described. Two case studies on malignant glomus tumors

Fig. 15.10 Alveolar rhabdomyosarcoma of the left hypothenar in an 11-year-old girl, presenting with a painless swelling for 6 months. (**a**) Axial T1-WI. A large mass within the hypothenar muscles (abductor digiti minimi) with inhomogeneous, slightly hyperintense signal intensity compared to adjacent normal muscle. (**b**) Axial FS T2-WI. The lesion is ill-defined with a predominantly high signal intensity on T2-WI. Presence of inhomogeneity with a central scar-like component of low signal intensity. (**c**) Coronal FS T2-WI. The lesion has a fusiform shape. (**d**) Axial T1-WI after IV administration of gadolinium contrast. The lesion shows septal and central enhancement

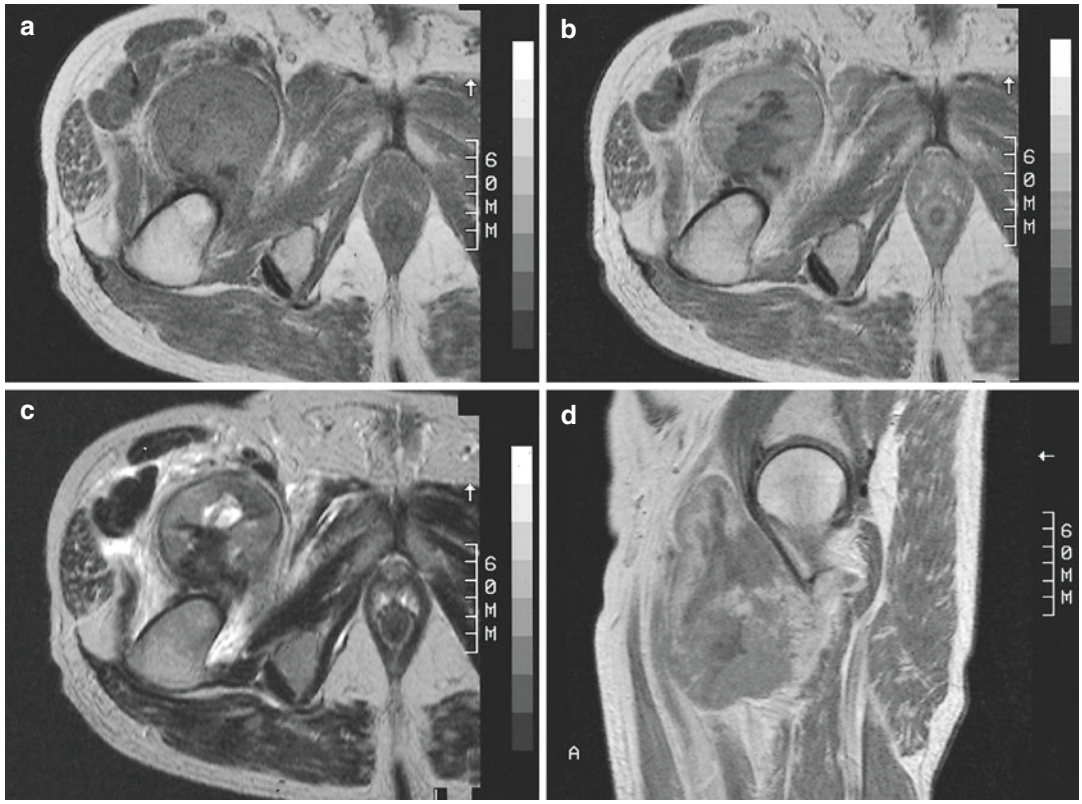

Fig. 15.11 Pleomorphic rhabdomyosarcoma of the right thigh in a 63-year-old man. (**a**) Axial T1-WI. (**b**) Axial T1-WI after IV administration of gadolinium contrast. (**c**) Axial T2-WI. (**d**) Sagittal T1-WI after IV administration of gadolinium contrast. Rounded, well-circumscribed mass with inhomogeneous intermediate signal intensity on T1-WI (**a**). The mass is even more inhomogeneous on T2-WI with the presence of a central fluid collection anterior to an area of low signal intensity (**c**). There is inhomogeneous, predominantly peripheral enhancement (**b**, **d**). A malignant tumor is suggested by the inhomogeneous appearance in all sequences, location, and volume of the lesion

reported the lesions to be well-defined and uniformly enhancing at MR imaging [21, 31], which are nonspecific findings.

15.3.4 Myopericytoma

15.3.4.1 Definition and Clinical Findings

Myopericytoma represents a benign perivascular myoid neoplasm [12]. Myopericytoma presents as a slowly growing, superficially located, painless nodule that may be present for years [12]. The majority of cases involve a solitary nodule, but cases with multiple nodules involving a single or multiple anatomic regions have been described as well [12].

15.3.4.2 Imaging

It is difficult to make an accurate, preoperative diagnosis of a myopericytoma [20, 43]. At US, a myopericytoma presents as a homogeneous hypoechoic mass with vascular Doppler signal. At MR imaging, a myopericytoma is seen as a lesion with intermediate to low signal intensity

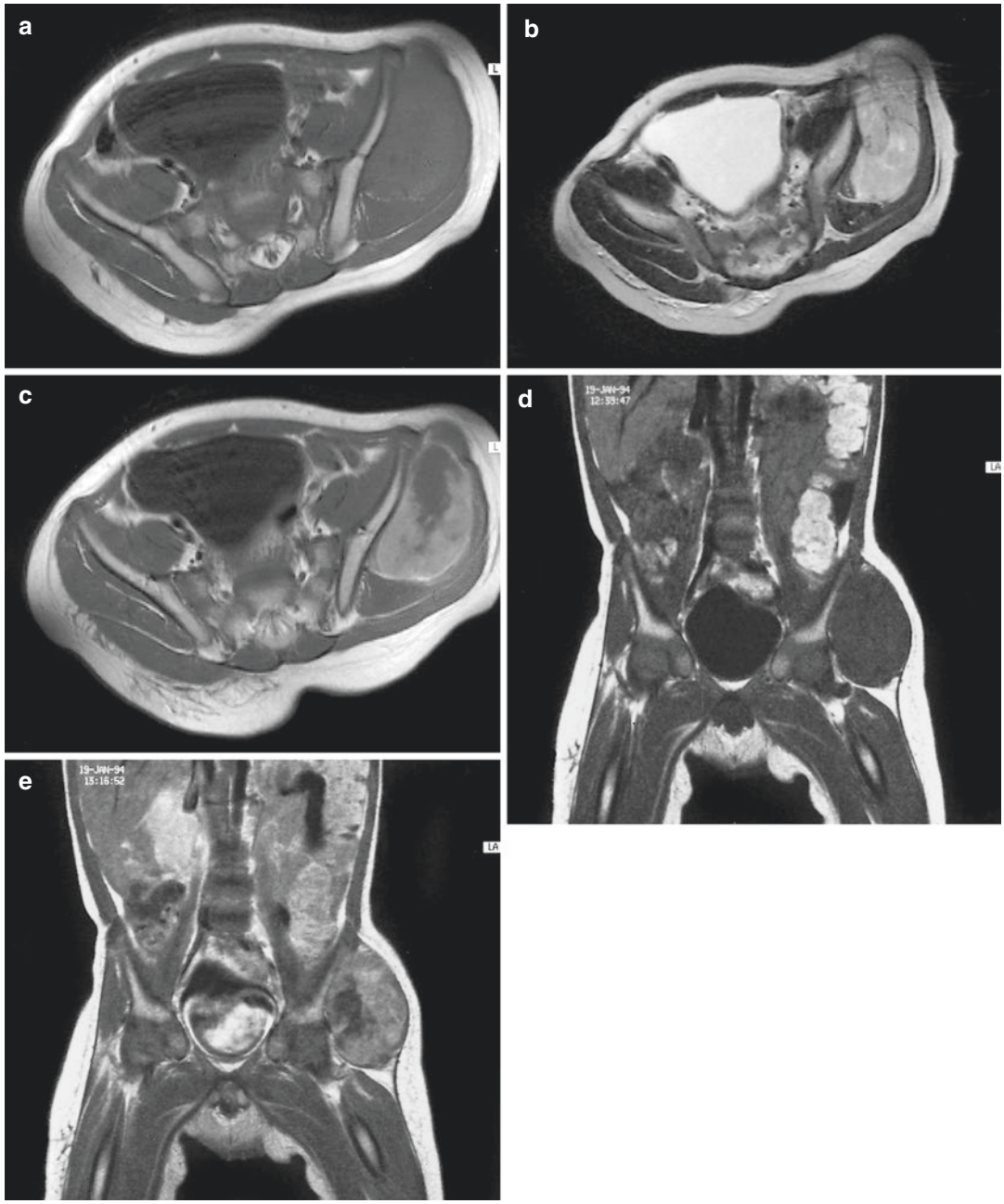

Fig. 15.12 Embryonal rhabdomyosarcoma of the left buttock in a 22-month-old boy. (**a**) Axial T1-WI. (**b**) Axial T2-WI. (**c**) Axial T1-WI after IV administration of gadolinium contrast. A large tumor arising in a gluteus muscle with a hypointense to isointense signal intensity compared to normal muscle on T1-WI and a high signal intensity with some internal strands of low signal intensity on T2-WI. There is evident enhancement of some parts of the tumor, but large areas do not enhance at all. No necrosis is seen. Comparable signal patterns are seen on a follow-up MR study 2 months later (**d**, **e**). (**d**) Coronal T1-WI 2 months later. (**e**) Coronal T1-WI after IV administration of gadolinium contrast 2 months later

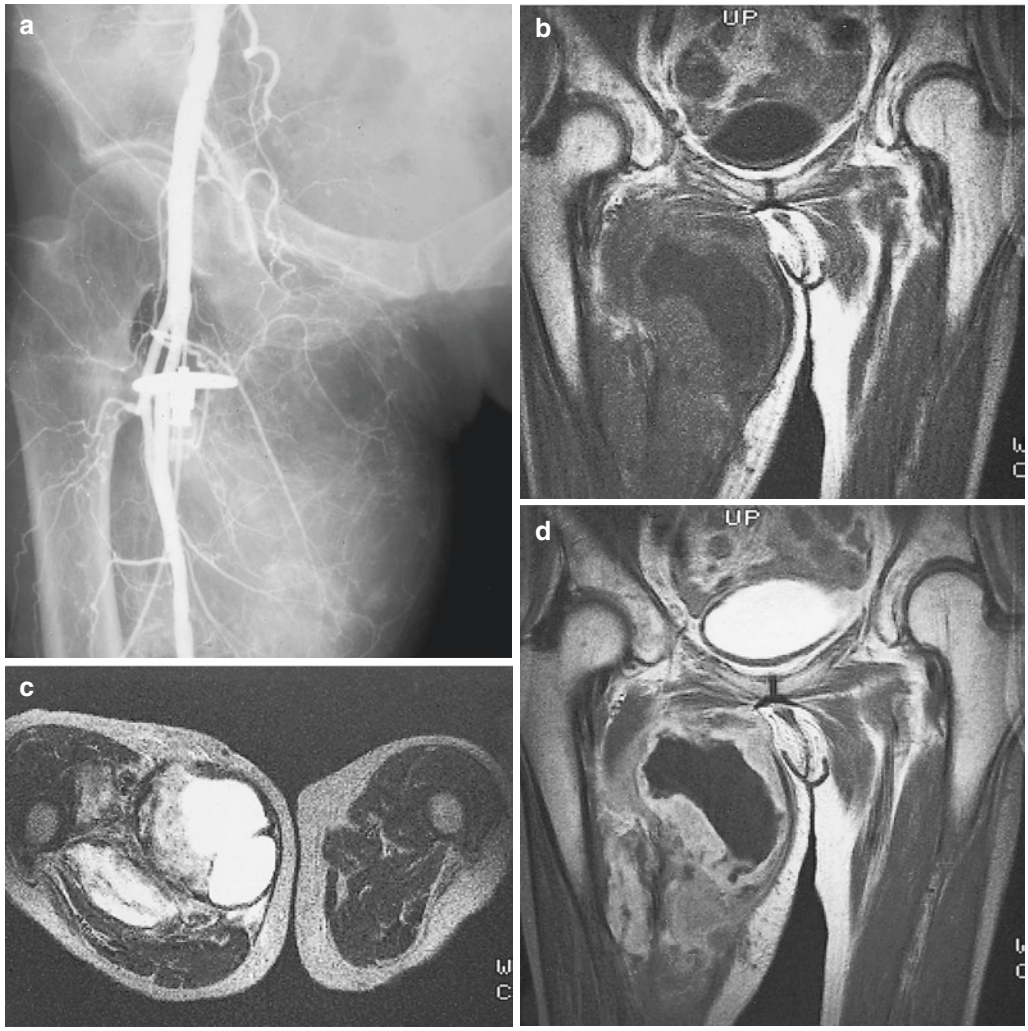

Fig. 15.13 Rhabdomyosarcoma of the adductor region of the right thigh in a 78-year-old woman. (**a**) Arteriography with direct retrograde femoral artery injection. Arteriography reveals the presence of neovascularity and of a tumoral blush. (**b**) Coronal T1-WI. (**c**) Axial T2-WI. (**d**) Coronal T1-WI after IV administration of gadolinium contrast. MR shows a large inhomogeneous, intramuscular mass with multiple central areas with a hypointense signal on T1-WI which become hyperintense on T2-WI corresponding to intralesional necrotic areas. Strong enhancement at the periphery of the lesion is seen around the necrotic areas

on T1-weighted images and a high signal intensity on water-sensitive sequences [20, 43].

15.3.5 Myofibroma and Myofibromatosis

15.3.5.1 Definition and Clinical Findings

Infantile myofibromatosis is a rare mesenchymal disorder occurring in newborns and infants, which is characterized by solitary or multiple nodular foci of myoblastic and fibroblastic tissue in the skin, musculoskeletal system, and visceral organs [10]. According to the anatomical distribution of the myofibroblastic lesions, two types of infantile myofibromatosis can be distinguished, each with a different clinical course. The solitary type is limited to the soft tissue and bone and has an excellent prognosis, since spontaneous regression with complete resolution of the lytic bone lesions may occur. It is mostly found in boys. Most

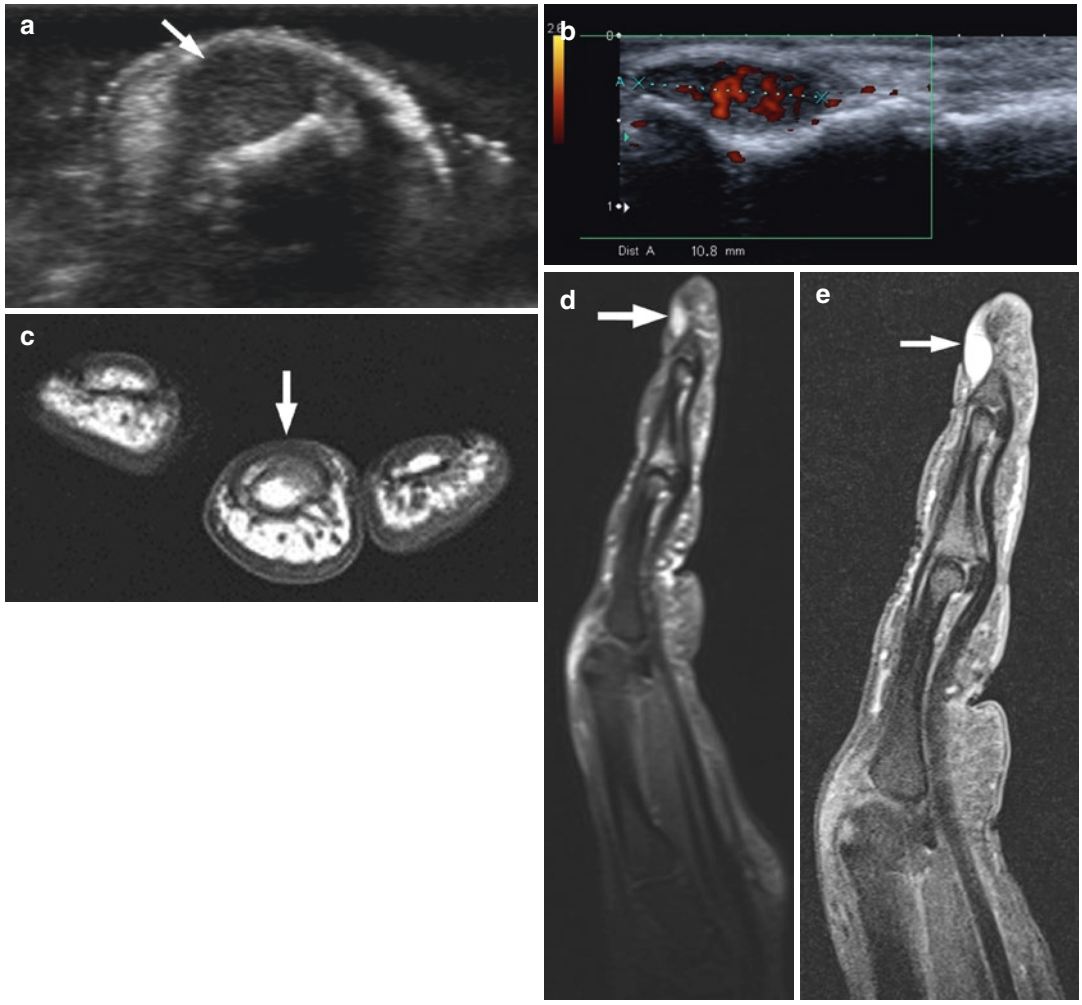

Fig. 15.14 Glomus tumor of digitus 3 of the upper extremity in a 48-year-old woman. (**a**) Transverse ultrasound image. (**b**) Longitudinal ultrasound image with Doppler. Subungually located, hypoechoic mass with Doppler vascular signal and pressure erosion of the dorsal cortex of the distal phalanx. (**c**) Axial T1-WI. (**d**) Sagittal FS T2-WI. Subungually located mass with a homogeneous intermediate to low signal intensity on T1-WI and hyperintense signal intensity on T2-WI. (**e**) Sagittal FS T1-WI after IV administration of gadolinium contrast. There is intense enhancement (Used with permission from Van Looveren et al. [50])

solitary myofibromas occur in the cutaneous/subcutaneous tissues of the head and neck region. The multicentric type shows widespread visceral involvement, mainly of lungs, myocardium, and gastrointestinal tract. The multicentric type can be lethal in early life [30]. It is mostly found in girls [47]. However, solitary and multifocal myofibromas have been described in adults as well [14].

Subcutaneous nodules are usually firm and encapsulated and frequently contain calcifications. They are the most common manifestations of infantile myofibromatosis and are easily detectable at birth. Tumors measure from less than 1 cm to a few centimeters in diameter. They contain foci of hemorrhage, cystic degeneration, necrosis, calcification, and fat [11].

15.3.5.2 Imaging

Conventional radiographs and CT show a low-density soft tissue tumor containing calcifications

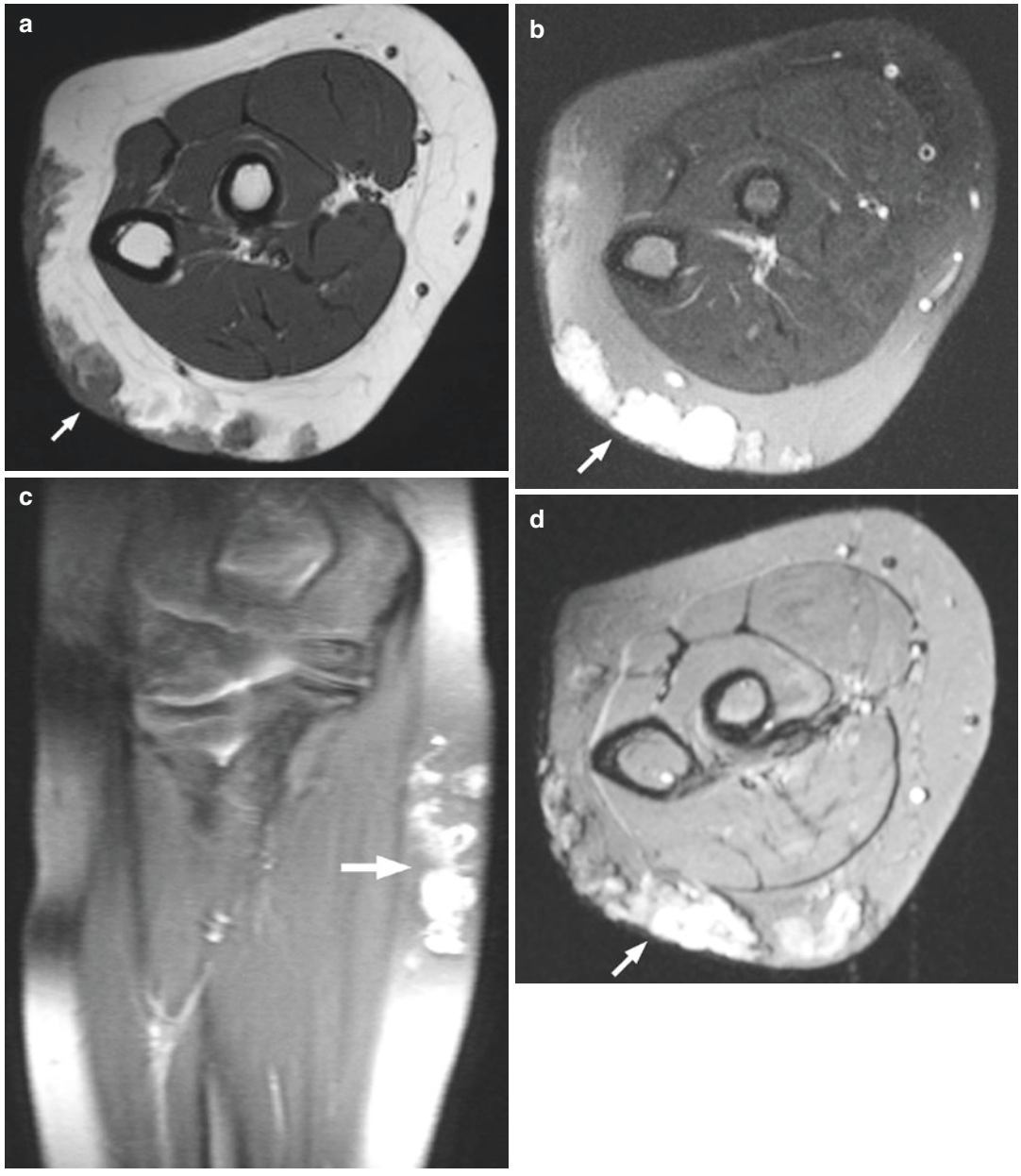

Fig. 15.15 Glomangiomatosis of the forearm. (**a**) Axial T1-WI. (**b**) Axial FS T2-WI. (**c**) Coronal FS T2-WI. Multiple nodules in the subcutaneous soft tissue with an intermediate to low signal relative to muscle on T1-WI, and high signal intensity on T2-WI. (**d**) Axial T1-WI after IV administration of gadolinium contrast. There is strong enhancement

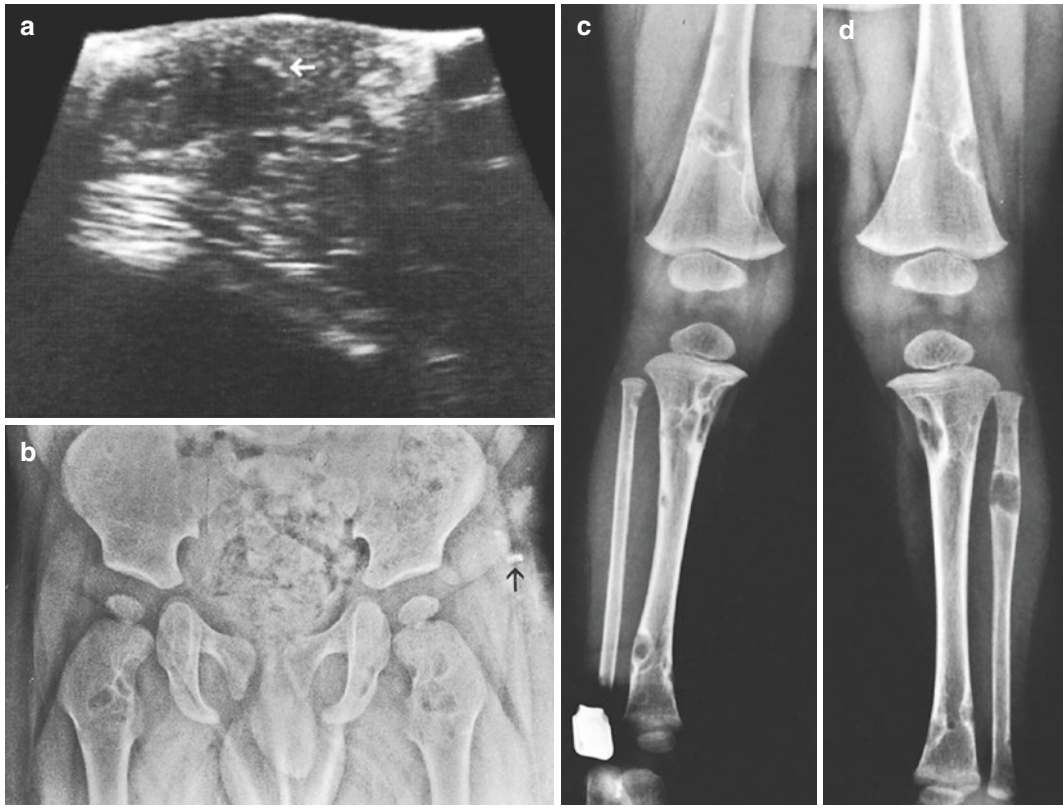

Fig. 15.16 Infantile myofibromatosis in a 10-month-old boy. (**a**) Ultrasound. Solid, echoic oval mass with a small central hyperechoic focus suggesting calcification (*arrow*). (**b**) Plain radiograph of the pelvis, anteroposterior view. Symmetrical, multiloculated osteolytic lesions in both proximal femora and ischial bones. The lesions are sharply defined and have sclerotic margins. A calcification in the soft tissue is seen lateral to the left acetabulum (*arrow*). (**c**, **d**) Plain radiographs of both legs, anteroposterior view. Multiple, rounded and ovoid, lytic metaphyseal lesions in the femur, tibia, and fibula bilaterally. They all have an intracortical localization and sclerotic margins. The lesion in the proximal left femur is slightly expansile. In this case, the age of the patient and the coexistence of bone and soft tissue lesions are indicative of infantile myofibromatosis. Follow-up demonstrated spontaneous regression and even disappearance of the lesions (Used with permission from Wassenaar [47])

within muscle or subcutaneous tissue (Fig. 15.16). The lesions enhance after administration of intravenous iodine contrast [6]. The lesions are low or isointense to muscle on T1-weighted images [11, 24] and of variable signal intensity on T2-weighted images. Lesions strongly enhance after intravenous administration of gadolinium-based contrast agent. Target sign appearances at MR imaging have also been described, consisting of either a mildly hyperintense center on T1-weighted images or a high- or low-signal-intensity center on T2-weighted images [11, 24]. Skeletal involvement is seen in the skull, spine, chest, shoulder girdle, pelvis, and extremities. Within the tubular bones, lesions are located predominantly in the metaphyseal region, centrally or eccentrically. Lesions are lytic, sharply marginated, and sometimes expansile. Although a characteristic radiological appearance of widespread lytic bone lesions associated with calcified soft tissue nodules is noted, differential diagnosis of multiple myofibromas should include fibrous dysplasia, neurofibromatosis, and lymphangiomatosis. The differential diagnosis of

solitary myofibroma should include traumatic myositis ossificans, juvenile aponeurotic fibroma, and soft tissue chondroma [42].

15.3.6 Angioleiomyoma

15.3.6.1 Definition and Clinical Findings

An angioleiomyoma is a benign dermal or subcutaneous tumor composed of well-defined smooth muscle cells arranged around vascular channels ([12], Fourth revision). There are three histopathological subtypes: solid, cavernous, and venous ([12], Fourth revision). A morphological continuum exists between angioleiomyoma and myopericytoma ([12], Fourth revision).

Angioleiomyoma is most commonly encountered in adults, with two-thirds occurring in the fourth through sixth decades of life. The tumor is typically small (less than 2 cm) and often slowly growing. It may be localized in the dermis, the subcutaneous fat, or the superficial fasciae of the extremities [45] (Fig. 15.17).

It is painful in over half of the cases [39]. Classically, tenderness and pain, which is often paroxysmal in nature and precipitated by light touch or changes in temperature, are the presenting features in 50–70 % of cases [17].

15.3.6.2 Imaging

Conventional radiographs of angioleiomyoma are mostly inconclusive. Rarely, they may show scalloping of the cortex of the adjacent bone or intralesional dystrophic calcifications [45].

At US, the tumor is homogeneously hypoechoic, with well-defined margins and without contact with the superficial fascia. Typically, the tumor is oval-shaped with the longest axis parallel to the extremity axis. Doppler US reveals hypervascularity [45] (Fig. 15.17b).

The three histopathological subtypes (solid, cavernous, and venous subtypes) all display similar MR appearance.

On T1-weighted images, the lesion appears either homogeneously or heterogeneously isointense to skeletal muscle. On T2-weighted images, it is mainly hyperintense with few low-signal-intensity foci. The smooth muscle cells and patent vessels are believed to correspond to the hyperintense areas, whereas the low-signal-intensity foci correlate with fibrous tissue or intravascular thrombi within the mass [17]. The lesion shows vivid enhancement after administration of intravenous gadolinium contrast. Hyperintense areas on T2-weighted images show strong enhancement, whereas the low-signal-intensity foci on T2-weighted images enhance less [39] (Fig. 15.18).

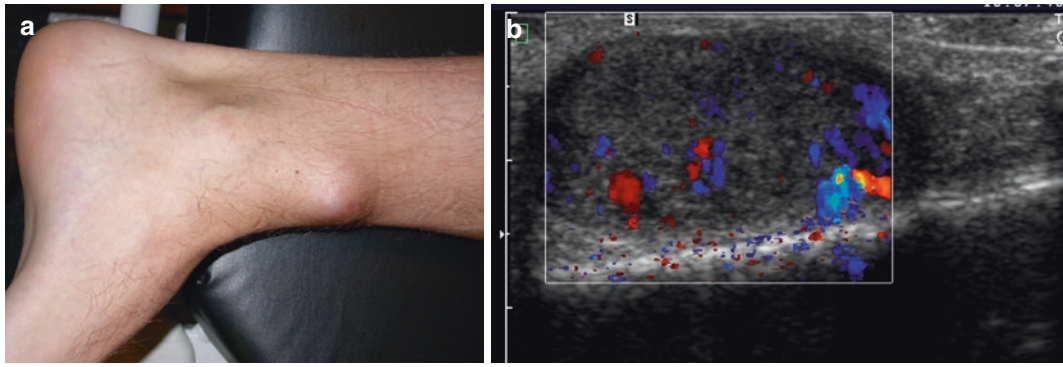

Fig. 15.17 Angioleiomyoma. (**a**) Photograph of a 34-year-old man presenting with a slowly growing mobile soft tissue mass at the left lower leg. (**b**) Longitudinal ultrasound showing a well-defined hypoechoic lesion within the subcutaneous tissue. The lesion is vascular on power Doppler

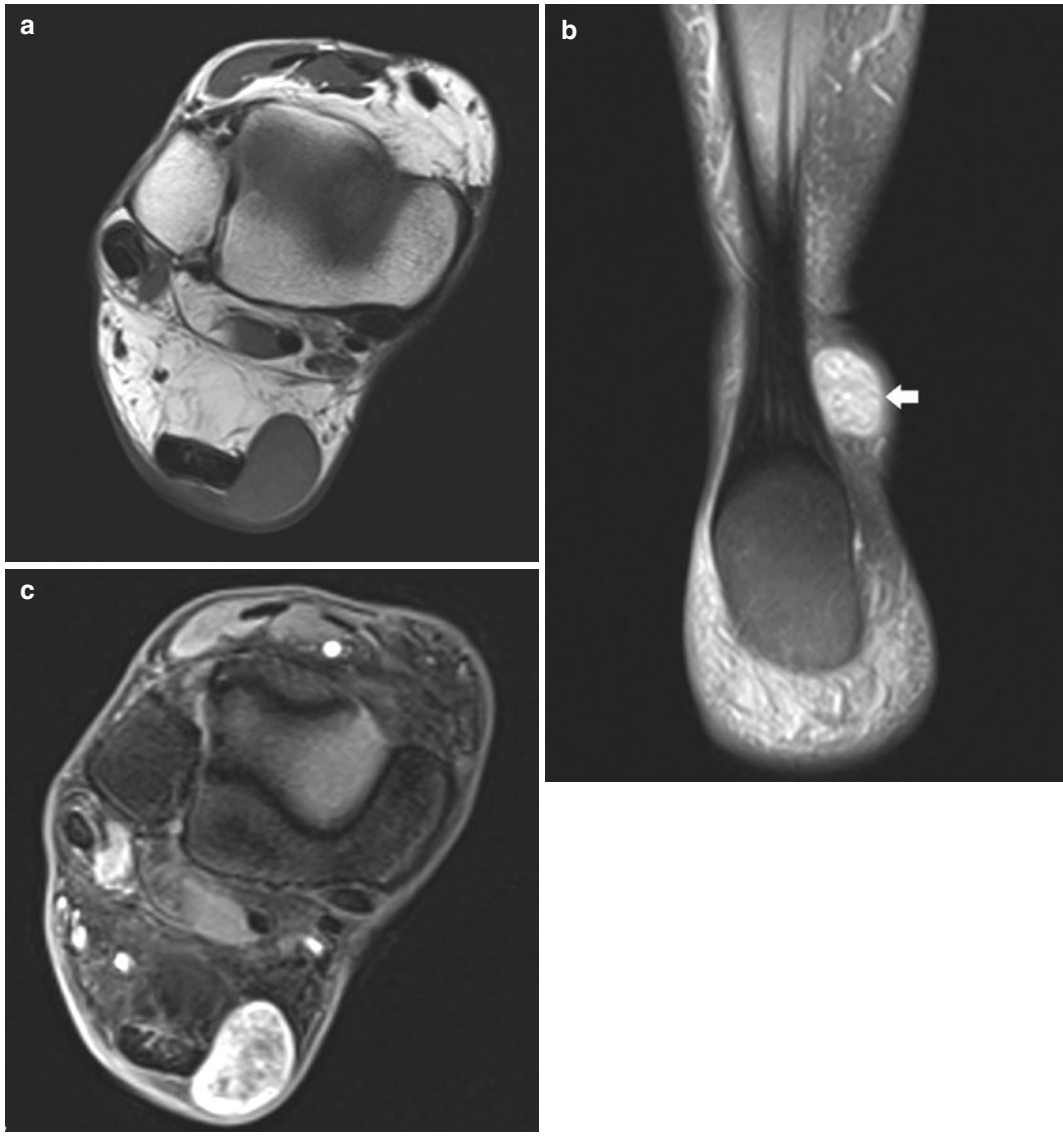

Fig. 15.18 Angioleiomyoma. (**a**) Axial T1-weighted image (WI). Well-delineated subcutaneous lesion abutting the medial aspect of the Achilles tendon. The lesion is isointense compared to muscle. (**b**) Coronal FS T2-WI. Note lesion heterogeneity with areas of high and low signal intensity (*white arrow*). (**c**) Axial FS T1-WI after intravenous (IV) administration of gadolinium contrast. There is marked but slightly inhomogeneous enhancement

Conclusion

In this chapter the relevant clinicopathological and imaging characteristics of tumors with myogenic differentiation and of pericytic tumors were discussed. In contradistinction to other histological types of soft tissue tumors, malignant tumors with histologically myogenic differentiation are more frequently malignant than benign. MR imaging of tumors with myogenic differentiation and of pericytic tumors is often nonspecific. Therefore, histological confirmation is required particularly if there is any suspicion for malignancy. MR imaging is the preferred imaging modality of choice for local staging of tumors arising in the extremities, whereas both CT and MR imaging can be used for staging tumors arising in the abdomen.

Key Points

1. Soft tissue tumors (STT) with myogenic differentiation and pericytic tumors are rare.
2. In contradistinction to other histological types of STT, tumors with histologically myogenic differentiation are more frequently malignant than benign.
3. Rhabdomyosarcoma is the most common malignant pediatric STT, the embryonal subtype being by far the most frequent.
4. Magnetic resonance imaging of muscle tumors is nonspecific, but it is the primary imaging modality of choice for local staging of tumors arising in the extremities.
5. Radiographs or computed tomography scan, although rarely diagnostic, may demonstrate intralesional calcifications.
6. Histological confirmation is mandatory in any case of suspected malignancy.

References

1. Allen SD, Moskovic EC, Fisher C, Thomas JM (2007) Adult rhabdomyosarcoma: cross- sectional imaging findings including histopathologic correlation. AJR Am J Roentgenol 189(2):371–377
2. Baek HJ, Lee SJ, Cho KH et al (2010) Subungual tumors: clinicopathologic correlation with US and MR imaging findings. Radiographics 30(6):1621–1636. doi:10.1148/rg.306105514
3. Billings SD, Folpe AL, Weiss SW (2001) Do leiomyoma of deep soft tissue exist? An analysis of highly differential smooth muscle tumors of deep supporting two distinct subtypes. Am J Surg Pathol 25(9):1134–1142
4. Blansfield JA, Chung H, Sullivan TR Jr, Pezzi CM (2003) Leiomyosarcoma of the major peripheral arteries: case report and review of the literature. Ann Vasc Surg 17(5):565–570
5. Bush CH, Reith JD, Spanier SS (2003) Mineralization in musculoskeletal leiomyosarcoma: radiologic-pathologic correlation. AJR Am J Roentgenol 180(1):109–113
6. Chateil JF, Brun M, Lebail B, Perel Y, Castell JF, Diard F (1995) Infantile myofibromatosis. Skeletal Radiol 24(8):629–632
7. Cooley CL, Jagannathan JP, Kurra V, Tirumani SH, Saboo SS, Ramaiya NH, Shinagare AB (2014) Imaging features and metastatic pattern of non-IVC retroperitoneal leiomyosarcomas: are they different from IVC leiomyosarcomas? J Comput Assist Tomogr 38:687–692. doi:10.1097/RCT.0000000000000097
8. Davies CE, Davies AM, Kindblom LG, James SL (2010) Soft tissue tumors with muscle differentiation. Semin Musculoskelet Radiol 14(2):245–256. doi:10.1055/s-0030-1253165
9. De Schepper AM, Bloem JL (2007) Soft tissue tumors: grading, staging, and tissue-specific diagnosis. Top Magn Reson Imaging 18(6):431–444. doi:10.1097/rmr.0b013e3181652220
10. De Schepper AM, Vandevenne JE (2006) Tumors of connective tissue. In: De Schepper AM, Vanhoenacker F, Parizel PM, Gielen J (eds) Imaging of soft tissue tumors, 3rd edn. Springer, Berlin Heidelberg New York, pp 188–189
11. Eich GF, Hoeffel JC, Tschäppeler H, Gassner I, Willi UV (1998) Fibrous tumours in children: imaging features of a heterogeneous group of disorders. Pediatr Radiol 28(7):500–509
12. Fletcher CDM, Bridge JA, Hogendoorn P, Mertens F (2013) World Health Organization classification of tumours of soft tissue and bone, 4th edn. IARC Press, Geneva
13. Fornage BD, Rifkin MD (1988) Ultrasound examination of the hand and foot. Radiol Clin North Am 26:114–129
14. Granter SR, Badizadegan K, Fletcher CD (1998) Myofibromatosis in adults, glomangiopericytoma, and myopericytoma: a spectrum of tumors showing perivascular myoid differentiation. Am J Surg Pathol 22(5):513–525
15. Gielen J, Ceulemans R, van Holsbeek M (2006) Ultrasound of soft tissue tumors. In: De Schepper AM, Vanhoenacker F, Parizel PM, Gielen J (eds) Imaging of soft tissue tumors, 3rd edn. Springer, Berlin Heidelberg New York, p 12
16. Gordon RW, Tirumani SH, Kurra V, Shinagare AB, Jagannathan JP, Hornick JL, Ramaiya NH (2014) MRI, MDCT features, and clinical outcome of extremity leiomyosarcomas: experience in 47 patients. Skeletal Radiol 43:615–622. doi:10.1007/s00256-014-1823-8
17. Gupte C, Butt SH, Tirabosco R, Saifuddin A (2008) Angioleiomyoma: magnetic resonance imaging features in ten cases. Skeletal Radiol 37(11):1003–1009. doi:10.1007/s00256-008-0518-4
18. Gurney JG, Davis S, Severson RK, Fang JY, Ross JA, Robison LL (1996) Trends in cancer incidence among children in the U.S. Cancer 78(3):532–541
19. Hartman DS, Hayes WS, Choyke PL, Tibbetts GP (1992) From the archives of the AFIP. Leiomyosarcoma of the retroperitoneum and inferior vena cava: radiologic-pathologic correlation. Radiographics 12:1203–1220
20. Kara A, Keskinbora M, Kayaalp ME, Seker A, Erdil M, Bülbül M (2014) An atypical presentation of myopericytoma in palmar arch and review of the literature. Case Rep Orthop 2014:759329. doi:10.1155/2014/759329
21. Khoury T, Balos L, McGrath B, Wong MK, Cheney RT, Tan D (2005) Malignant glomus tumor: a case report and review of literature, focusing on its

clinicopathologic features and immunohistochemical profile. Am J Dermatopathol 27(5):428–431
22. Kieffer E, Alaoui M, Piette JC, Cacoub P, Chiche L (2006) Leiomyosarcoma of the inferior vena cava: experience in 22 cases. Ann Surg 244:289–295
23. Killoran TP, Wells WA, Barth RJ, Goodwin DW (2003) Leiomyosarcoma of the popliteal vein. Skeletal Radiol 32(3):174–178
24. Koujok K, Ruiz RE, Hernandez RJ (2005) Myofibromatosis: imaging characteristics. Pediatr Radiol 35(4):374–380
25. Kransdorf MJ (1995) Benign soft-tissue tumors in a large referral population: distribution of specific diagnoses by age, sex, and location. AJR Am J Roentgenol 164(2):395–402
26. Kransdorf MJ (1995) Malignant soft-tissue tumors in a large referral population: distribution of specific diagnoses by age, sex, and location. AJR Am J Roentgenol 164(2):129–134
27. Kransdorf MJ, Murphey MD (2007) Imaging of soft tissue tumors, 2nd edn. Lippencott Williams & Wilkins, Philadelphia, pp 298–327
28. Maglio R, Francesco S, Paolo M, Stefano V, Francesco D, Giovanni R (2012) Voluminous extracardiac adult rhabdomyoma of the neck: a case presentation. Case Rep Surg 2012:984789. doi:10.1155/2012/984789
29. Manaster BJ et al (2010) Diagnostic imaging: Musculoskeletal non-traumatic disease. Amirsys Inc., Manitoba
30. Mashiah J, Hadj-Rabia S, Dompmartin A et al (2014) Infantile myofibromatosis: a series of 28 cases. J Am Acad Dermatol 71(2):264–270. doi:10.1016/j.jaad.2014.03.035
31. Matsumoto K, Kakizaki H, Yagihashi N, Yagihashi S (2001) Malignant glomus tumor in the branchial muscle of a 16-year-old girl. Pathol Int 51:729–734
32. McLeod AJ, Zornoza J, Shirkhoda A (1984) Leiomyosarcoma: computed tomographic findings. Radiology 152(1):133–136
33. Meyer WH, Spunt SL (2004) Soft tissue sarcomas of childhood. Cancer Treat Rev 30(3):269–280
34. Monteagudo Cortecero J, Guirau Rubio MD, Payá Romá A (2015) Leiomyosarcoma of the inferior vena cava: AIRP best cases in radiologic-pathologic correlation. Radiographics 35:616–620. doi:10.1148/rg.352130105
35. Navarro OM (2011) Soft tissue masses in children. Radiol Clin North Am 49:1235–1259. doi:10.1016/j.rcl.2011.07.008
36. Newton WA Jr, Soule EH, Hamoudi AB et al (1988) Histopathology of childhood sarcomas, Intergroup Rhabdomyosarcoma Studies I and II: clinicopathologic correlations. J Clin Oncol 6(1):67–75
37. Park EA, Hong SH, Choi JY, Lee MW, Kang HS (2005) Glomangiomatosis: magnetic resonance imaging findings in three cases. Skeletal Radiol 34(2):108–111
38. Paal E, Miettinen M (2001) Retroperitoneal leiomyoma of deep soft tissue: a clinicopathologic and immunohistochemical study of 56 cases with a comparison to retroperitoneal leiomyosarcomas. Am J Surg Pathol 25(11):1355–1363
39. Ramesh P, Annapureddy SR, Khan F, Sutaria PD (2004) Angioleiomyoma: a clinical, pathological and radiological review. Int J Clin Pract 58:587–591
40. Ramon F (2006) Tumors and tumor-like lesions of blood vessels. In: De Schepper AM, Vanhoenacker F, Parizel PM, Gielen J (eds) Imaging of soft tissue tumors, 3rd edn. Springer, Berlin Heidelberg New York, p 266
41. Seynaeve PC, De Visschere PJL, Mortelmans LL, De Schepper AM (2006) Tumors of muscular origin. In: De Schepper AM, Vanhoenacker F, Parizel PM, Gielen J (eds) Imaging of soft tissue tumors, 3rd edn. Springer, Berlin Heidelberg New York, pp 293–310
42. Tung GA, Davis LM (1993) The role of magnetic resonance imaging in the evaluation of the soft tissue mass. Crit Rev Diagn Imaging 34(5):239–308
43. Uchida Y, Kuriyama M, Yoshida Y, Yano A, Orihashi K (2012) Diagnosis and surgical management of the arterial myopericytoma. J Plast Reconstr Aesthet Surg 65(7):e200–e201. doi:10.1016/j.bjps.2012.01.015
44. van Vliet M, Kliffen M, Krestin GP, van Dijke CF (2009) Soft tissue sarcomas at a glance: clinical, histological, and MR imaging features of malignant extremity soft tissue tumors. Eur Radiol 19(6):1499–1511. doi:10.1007/s00330-008-1292-3
45. Vanhoenacker FM, Camerlinck M, Somville J (2009) Imaging findings of a subcutaneous angioleiomyoma. JBR-BTR 92(2):80–82
46. Walker EA, Fenton ME, Salesky JS, Murphey MD (2011) Magnetic resonance imaging of benign soft tissue neoplasms in adults. Radiol Clin North Am 49(6):1197–1217. doi:10.1016/j.rcl.2011.07.007, vi
47. Wassenaar (1994) Infantile myofibromatosis. Rad Doc 94–10
48. Weiss SW (2002) Smooth muscle tumors of soft tissue. Adv Anat Pathol 9(6):351–359
49. Zamorani MP, Valle M (2007) Muscles and tendon. In: Bianchi S, Martinoli C (eds) Ultrasound of the musculoskeletal system. Springer, Berlin Heidelberg New York, pp 45–96
50. Looveren K et al (2012) Subunguale glomustumor: een zeldzame benigne tumor in het nagelbed. Ortho Rheumato 10:3:56–58, ISSN 1379–8928

Vascular Tumors

16

Mariem Ben Haj Amor, Caroline Degrugillier-Chopinet, Alexandre Bridoux, François Pontana, Luc Ceugnart, and Anne Cotten

Contents

16.1 **Introduction** 363

16.2 **Classification** 364
16.2.1 WHO Classification 364
16.2.2 ISSVA Classification 364

16.3 **Vascular Tumors** 365
16.3.1 Benign Vascular 365
16.3.2 Intermediate and Malignant Vascular Tumors 368

16.4 **Vascular Malformations** 370
16.4.1 Venous Malformations (VMs) 371
16.4.2 Lymphatic Malformations (LMs) 376
16.4.3 Capillary Malformations (CMs) 381
16.4.4 Arteriovenous Malformations (AVMs) 381

16.5 **Particular Vascular Lesions** 384
16.5.1 Glomus Tumor (GT) 384
16.5.2 Synovial Hemangioma (SH) 385

16.6 **Syndromes Associated with Vascular Lesions** 385
16.6.1 PHACE Syndrome 386
16.6.2 PELVIS and SACRAL Syndromes 386
16.6.3 Kasabach-Merritt Syndrome 386
16.6.4 Klippel-Trenaunay Syndrome 387
16.6.5 Maffucci Syndrome 388
16.6.6 Parkes Weber Syndrome 388
16.6.7 Rendu-Osler-Weber Syndrome 388

References 389

M.B.H. Amor, MD • L. Ceugnart, MD
Service de Radiologie, Centre Oscar Lambret, 3, Rue Fréderic Combemale, 59000 Lille, France
e-mail: m-benhajamor@o-lambret.fr; l-ceugnart@o-lambret.fr

C. Degrugillier-Chopinet, MD
Service de Neuroradiologie, CHRU de Lille, 59037 Lille, France
e-mail: caroline.chopinet@chru-lille.fr

A. Bridoux, MD • A. Cotten, MD, PhD (✉)
Service de Radiologie et Imagerie Musculosquelettique, Centre de Consultations et d'Imagerie de l'Appareil Locomoteur, CHRU de Lille, 59037 Lille, France
e-mail: alexandre.bridoux@hotmail.fr; anne.cotten@chru-lille.fr

F. Pontana, MD, PhD
Service de Radiologie et d'Imagerie Cardiaque et Vasculaire, CHRU de Lille, 59037 Lille, France
e-mail: francois.pontana@chru-lille.fr

16.1 Introduction

Vascular soft tissue lesions represent a wide and heterogeneous spectrum of lesions. Most of the lesions are recognized on clinical history and physical examination. When imaging is requested, it should be targeted to address specific issues such as planning therapeutic management by a multidisciplinary team [1].

Ultrasound (US) coupled with color Doppler US is traditionally considered the imaging modality of choice for the initial assessment and characterization of a lesion of presumed vascular origin [2]. Magnetic resonance imaging (MRI) in combination with dynamic magnetic resonance

© Springer International Publishing AG 2017

F.M. Vanhoenacker et al. (eds.), *Imaging of Soft Tissue Tumors*, DOI 10.1007/978-3-319-46679-8_16

(MR) angiography is the most valuable modality for the classification of vascular anomalies [3]. Its role in evaluating the extent and relationship of the lesion to the adjacent structures is important, particularly for therapy planning. The aim of this chapter is to review the spectrum of vascular and lymphatic lesions of the musculoskeletal system.

16.2 Classification

The use of different terminologies in the literature for vascular lesions has led to considerable confusion [4]. For example, the term hemangioma has been applied to many vascular lesions of differing origins and clinical behaviors. Because the treatment strategy depends on the type of vascular anomaly, the correct diagnosis and classification are critical.

Several classification systems have been described but the two main classifications are:

- The classification system defined by the World Health Organization's (WHO) Committee for the Classification of Soft Tissue Tumors [5]
- The classification system defined by the International Society for the Study of Vascular Anomalies (ISSVA) [6]

These two classifications show differences in terminology for benign lesions, but they are in agreement for intermediate and malignant tumors.

16.2.1 WHO Classification

The WHO classification is based on the pathological aspects of the soft tissue tumors (Table 16.1 and Chap. 11) [5]. The term of hemangioma is defined as "a benign nonreactive lesion with an increase in the number of normal- or abnormal-appearing vessels" [7]. Subdivisions are based on the predominant type of vascular channel. No distinction is made between benign vascular tumors and vascular malformations.

Table 16.1 Histological classification of vascular tumors, WHO 2013 [5]

Benign vascular tumors
Hemangiomas of subcutaneous/deep soft tissue
Capillary
Cavernous
Arteriovenous
Venous
Intramuscular
Synovial
Epithelioid hemangioma
Angiomatosis
Lymphangioma
Vascular tumors of intermediate malignancy (locally aggressive)
Kaposiform hemangioendothelioma
Vascular tumors of intermediate malignancy (rarely metastasizing)
Retiform hemangioendothelioma
Papillary intralymphatic angioendothelioma
Composite hemangioendothelioma
Kaposi's sarcoma
Malignant vascular tumors
Epithelioid hemangioendothelioma
Angiosarcoma

16.2.2 ISSVA Classification

In 1982, Mulliken and Glowacki [8] proposed a useful classification for vascular anomalies, which was then adopted by the International Society for the Study of Vascular Anomalies (ISSVA) in 1996 and updated in 2014 [6]. This classification is based on the cellular turnover, histologic features, natural history, and physical findings of the vascular anomalies [8]. Lesions are divided into tumors (neoplastic growth of vascular endothelial cells) and vascular malformations (vascular structural anomalies with normal endothelial turnover) [6, 8, 9] (Table 16.2).

The use of this classification system has been strongly recommended in recent years because of its effectiveness and usefulness for determining the appropriate treatment in patients with vascular lesions, particularly in pediatric patients where vascular lesions represent the most common cause of soft tissue lesion [10].

Table 16.2 ISSVA classification of vascular tumors and malformations

Tumors
Benign
Infantile hemangioma
Congenital hemangioma (RICH, NICH, PICH)[a]
Others: tufted angioma, spindle cell hemangioma, epithelioid hemangioma, pyogenic granuloma
Locally aggressive or borderline
Kaposiform hemangioendothelioma, retiform hemangioendothelioma
Papillary intralymphatic angioendothelioma (PILA), Dabska tumor
Composite hemangioendothelioma, Kaposi's sarcoma, others
Malignant
Angiosarcoma
Epithelioid hemangioendothelioma
Malformations
Simple (i.e., venous, lymphatic, capillary, and arterial)
Combined: defined as two or more vascular malformations found in one lesion
Associated with other syndromes: Klippel-Trenaunay syndrome, Parkes Weber syndrome, etc.

Modified from ISSVA [6]
[a]Rapidly involuting (RICH), noninvoluting (NICH), partially involuting (PICH)

Table 16.3 Equivalence in terminology between the two main classification systems for vascular lesions

WHO classification	ISSVA
Cavernous hemangioma	Venous malformation
Venous hemangioma	Venous malformation
Intramuscular hemangioma	Venous malformation (mainly)
Lymphangioma	Lymphatic malformation (localized)
Lymphangiomatosis	Lymphatic malformation (diffuse)
Arteriovenous hemangioma	Arteriovenous malformation
Capillary hemangioma	Infantile hemangioma

Modified from Refs. [4, 11–13]

Therefore, we will use this classification in this chapter; however, Table 16.3 [4, 11–13] indicates comparison between the two classification systems.

Other entities, such as glomus tumors and synovial hemangiomas, will be discussed separately.

16.3 Vascular Tumors

16.3.1 Benign Vascular

We will only describe the most common lesions and those associated with clinical or specific nosological entities.

16.3.1.1 Infantile Hemangioma (IH)

Infantile hemangiomas are the most common vascular tumor of infancy [10]. They occur three to five times more frequently in females compared to males [14] and may be present at birth but are frequently diagnosed by 3 months of age [10]. In most cases, diagnosis is made clinically through the observation of a subcutaneous bluish red mass that looks like the surface of a strawberry (Fig. 16.1).

These tumors undergo two biologic phases:

- *The proliferative phase*, which is characterized by rapid endothelial growth in the first few months of life that stabilizes in size at approximately 9–10 months of age. Reflecting the characteristic high-flow component of this phase, the tumor manifests as a pulsatile and warm mass [15].
- *The involuting phase*, which occurs over the next several years, is a period during which the hemangioma spontaneously decreases in

Fig. 16.1 Proliferative infantile hemangioma in a 15-month-old boy. Clinical photograph shows a diffuse and lobulated mass in the arm with superficial involvement, which causes its strawberry-like appearance

size and is replaced by a residual fibrofatty mass [16]. This process is usually completed by 7–10 years of age [17].

On pathological examination, whatever the phase, IHs express a unique immunophenotype (glucose transporter protein-1 (GLUT1)), which differentiates them from other vascular lesions [18].

Infantile hemangiomas are most commonly seen on the face and neck (60 % of cases), followed by the trunk (25 %) and extremities (15 %) [19]. They are multifocal in approximately 30 % of the cases [1].

During the proliferative phase, the lesion appears as a well-defined mass with variable echogenicity. The vessels may be visible using US. Doppler demonstrates a characteristic hypervascular lesion with a high density of vessels (arteries and veins) and a low resistance on spectral analysis (Fig. 16.2) [2, 20]. Despite the high-flow nature of the lesion during this phase, there is a distinct soft tissue lesion that usually contains a single afferent artery and no direct arteriovenous shunting, unlike arteriovenous malformations [2]. During the involuting phase, IHs appear hyperechoic with a low density of vessels.

The appearance of IHs using MR imaging is indicative of their biologic phase. The proliferative phase is characterized by a well-circumscribed lobulated lesion with low or iso-signal intensity on the T1-weighted images and a high signal intensity on the T2-weighted images; the IH lesions also show an early and homogeneous enhancement after gadolinium administration (Fig. 16.2) [21]. Fast-flow vessels appearing as flow voids can be depicted within and around the lesion [2]. During the involuting phase, the increasing amount of fat within the tumor increases the signal intensity of the lesion on the T1-weighted images, which is associated with less avid contrast enhancement (Fig. 16.3).

The presence of a high resistance index on the spectral analysis or a marked perilesional edema on the T2-weighted images is suggestive of other tumoral lesions, such as sarcomas, neuroblastomas, myofibromatosis, tuft hemangiomas, metastatic neuroblastomas, or other tumors [2].

Multiple hemangiomas of the skin are usually linked with visceral hemangiomas. Segmental hemangiomas may be associated with PHACE syndrome (see Sect. 16.6.1) [22]. Most of these segmental hemangiomas are telangiectatic or reticular and do not demonstrate a high-flow pattern on Doppler US.

In the majority of the cases, no treatment is required due to spontaneous involution. However, 10–20 % of the cases require treatment, including cases with periocular location with vision compromise, high-output cardiac failure, ulceration, compression of the airway, facial hemangiomas with rapid growth and distortion, and symptomatic muscular hemangiomas. Medical treatment is usually attempted first, and propranolol is typically the first-line therapy with excellent results in most cases [23]. Other treatments include corticosteroids, vincristine, interferon, and laser therapy. Surgery is required when medical alternatives are ineffective, mostly in cases involving function-threatening, life-endangering, and disfiguring lesions [16].

Key Points

1. Infantile hemangioma.
2. The most common vascular tumor of infancy.
3. Characterized by two biologic phases (proliferative/involuting).
4. Positive for the GLUT1 marker at both stages.
5. Presence of a high-flow soft tissue mass.
6. If perilesional edema is present, other tumoral lesions must be ruled out.

16.3.1.2 Congenital Hemangioma (CH)

CHs are rare and fully developed at birth; therefore, they are potentially seen in utero. Three subtypes have been identified [6, 24, 25]:

– Rapidly involuting congenital hemangiomas (RICH), which completely regress during the first 2 years of life.
– Noninvoluting congenital hemangiomas (NICH), which demonstrate growth propor-

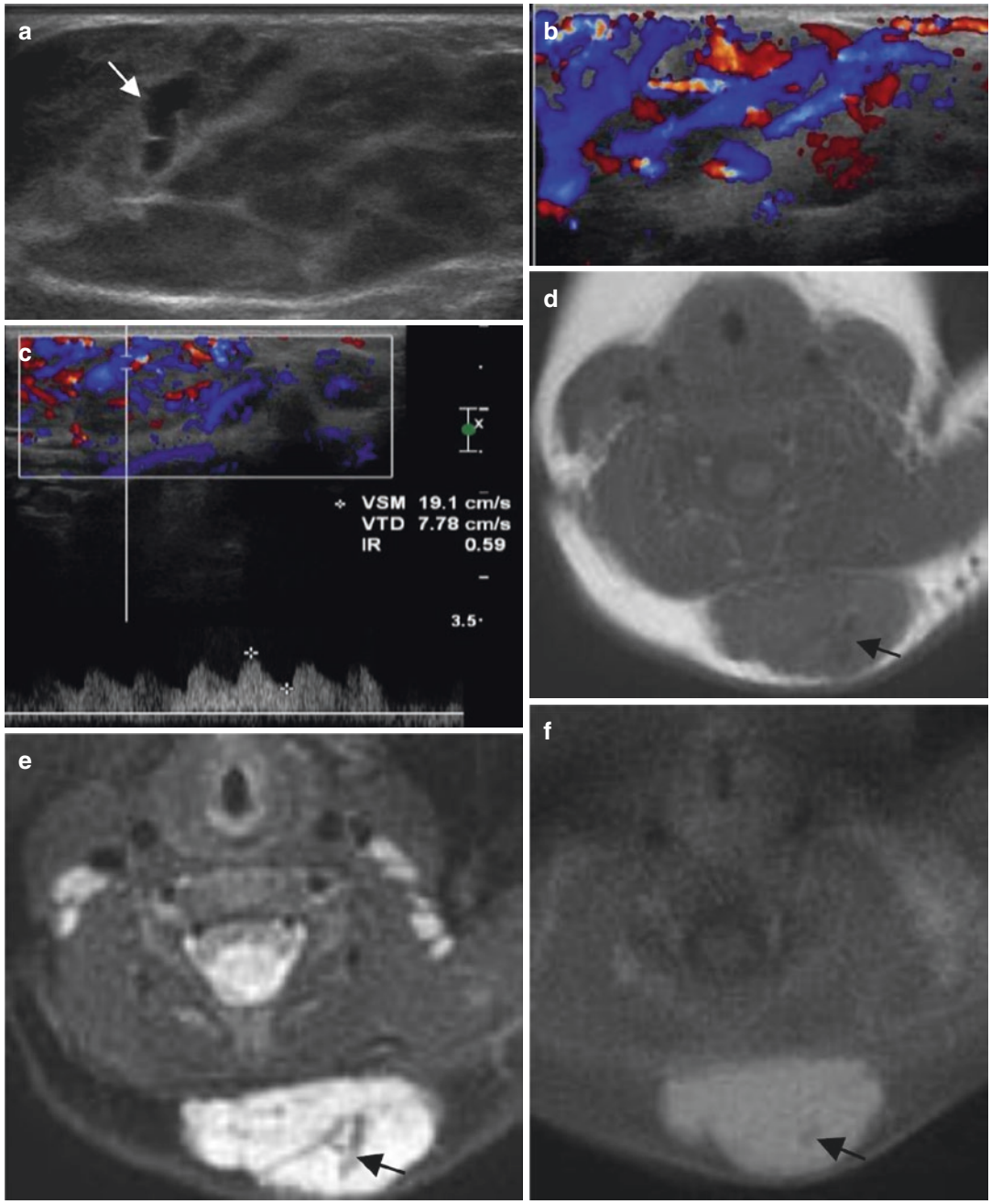

Fig. 16.2 Infantile hemangioma. Nine-month-old boy with subcutaneous mass in his posterior cervical neck. (**a**) Axial Ultrasound. (**b**) Axial color Doppler ultrasound. (**c**) Spectral analysis obtained in tumor center. (**d**) Axial T1-weighted MR image. (**e**) Axial T2-weighted MR image, with fat suppression. (**f**) Axial T1-weighted MR image after Gadolinium contrast administration with fat suppression. (**a–c**) Ultrasound shows a solid mass with well-defined margins in the subcutaneous soft tissues of the neck (**a**). The lesion is predominantly hyperechoic with scattered hypoechoic foci that correspond to vessels (*white arrow*). (**b**, **c**) Color Doppler shows hypervascular lesion with low-resistance arteries. (**d–f**) MRI shows a well-defined, lobulated soft-tissue mass confined to the subcutaneous soft tissues. The mass is isointense relative to muscle on the unenhanced T1-weighted image (**d**), hyperintense on T2-weighted image (**e**), and shows uniform enhancement (**f**). All three images demonstrate small, intralesional signal void foci (*black arrows*) due to fast flow vessels. There is no invasion of the underlying muscle and no perilesional oedema

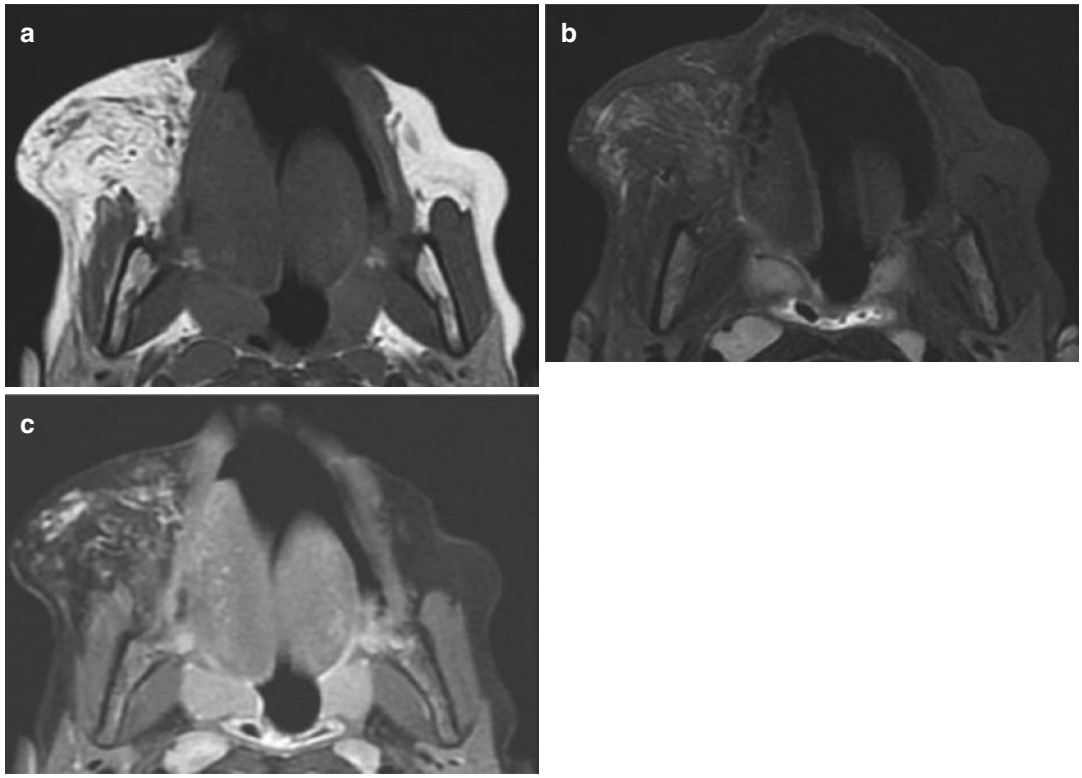

Fig. 16.3 Infantile haemangioma of the cheek in a 7-year-old girl during involution phase. (**a**) Axial T1-weighted MR image. (**b**) Axial T2-weighted MR image with fat suppression. (**c**) Axial T1-weighted MR image after Gadolinium contrast administration with fat suppression. MRI images show a subcutaneous hyperintense mass on T1-weighted image (**a**), slightly hyperintense on T2-weighted image (**b**) with minimal enhancement (**c**). No flow voids are seen

tional to that of the child without regression (Fig. 16.4).

– Partially involuting congenital hemangiomas (PICH), which have a distinct behavior, evolving from RICH to NICH-like lesions. RICH may be clinically difficult to differentiate from infantile hemangioma but the GLUT1 marker is negative.

Congenital hemangiomas share the same imaging findings on sonography. These features are similar to those of infantile hemangiomas, except for the presence of intravascular thrombi, vascular aneurysms, and arteriovenous shunting [26].

NICH are usually treated by a surgical resection [27].

16.3.1.3 Epithelioid Hemangioma

This benign vascular tumor is encountered in adult patients with a variable sex predilection [5, 28]. It is usually superficially located and is responsible for red nodules mainly on the face and fingers. Furthermore, deep locations, including in the bone, are possible [5]. Epithelioid hemangiomas are differentiated from Kimura's disease, a chronic inflammatory lesion affecting young Asian men, which shares clinical and pathological similarities to epithelioid hemangiomas [29]. The imaging is nonspecific [28].

16.3.2 Intermediate and Malignant Vascular Tumors

16.3.2.1 Kaposiform Hemangioendothelioma (KHE)

KHEs are locally aggressive, rare vascular tumors of intermediate malignancy [5, 6]. Their

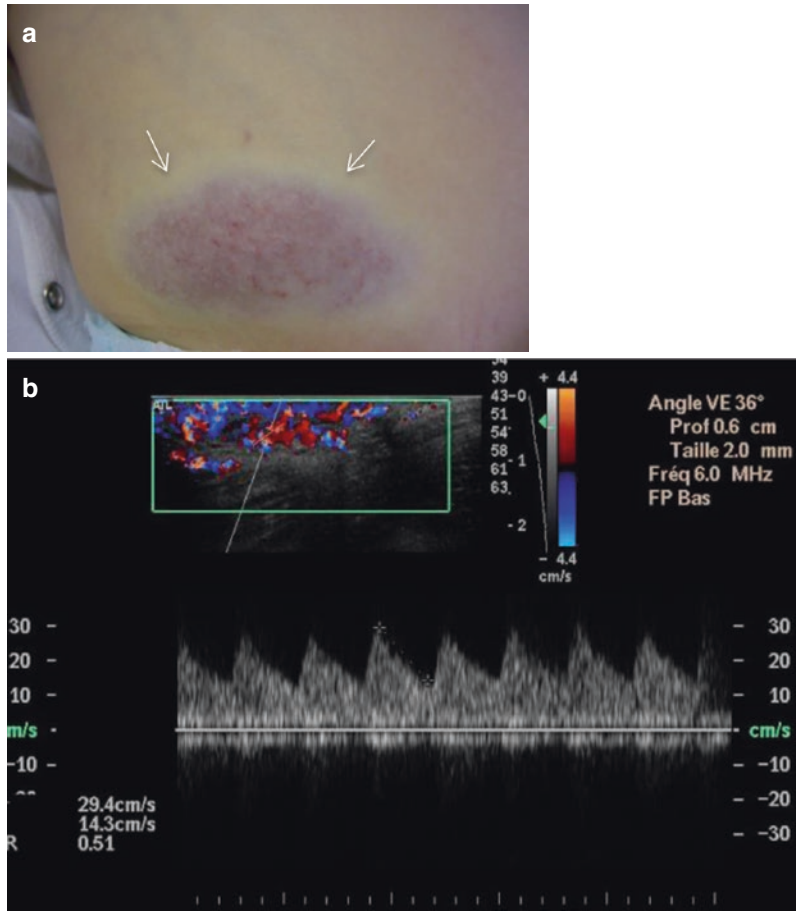

Fig. 16.4 Congential hemangioma in a 3-year-old boy. (**a**) Clinical photograph. (**b**) Axial color Doppler image with spectral display obtained in tumor center. (**a**) Non-involuting congenital hemangioma (NICH) is seen as an overlying bluish discoloration with clear peripheral halo (*arrow*). The lesion has been present since birth, growing proportionally to the patient's growth. (**b**) Color Doppler image shows the marked increased vascularity inside the lesion with low-resistance arteries. The imaging features are indistinguishable from those of infantile hemangioma

pathology is characterized by frequent lymphatic abnormalities [10]. Even if the tumor does not metastasize, intra-abdominal deep forms have a poor prognosis because they are rarely curable by surgery [30].

MR imaging helps to differentiate KHEs from infantile hemangiomas. KHE appears as an ill-defined lesion with hemosiderin deposits and smaller feeding and draining vessels. Moreover, KHEs involve multiple tissue planes and destruction of the adjacent bones is also observed [10, 15].

KHEs are often associated with Kasabach-Merritt syndrome [10] which is characterized by thrombocytopenia, microangiopathic hemolytic anemia, and localized consumption coagulopathy. In the latter case, medical treatment is recommended (propranolol, corticosteroids, vincristine) [31, 32].

16.3.2.2 Kaposi's Sarcoma

Kaposi's sarcoma (KS), also known as KS-associated herpesvirus (KSHV), is a locally aggressive vascular tumor associated with the human herpesvirus-8 (HHV-8). This tumor is probably of lymphatic origin and is characterized by neoangiogenesis and proliferation of spindle-shaped cells with inflammation and edema [33]. It is usually a multicentric disease that originates

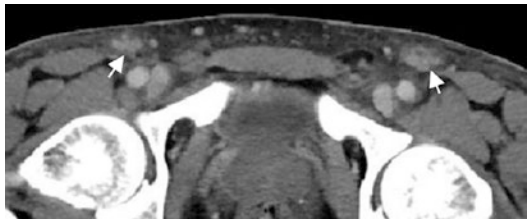

Fig. 16.5 Kaposi sarcoma in a 35-year-old man (endemic type). Computed tomography after iodinated-contrast injection shows an enhancing bilateral inguinal lymphadenopathy (*arrows*)

in the lymphoreticular system and may involve the skin, lymph nodes, lungs, gastrointestinal tract, liver, spleen, and musculoskeletal system. Four types of KSs have been described: classic KS (chronic form, patients older than 60 years old), endemic KS (middle-aged adults and children, African KS), KS in iatrogenically immunosuppressed patients (related to solid organ transplantation or immunosuppressive therapy), and AIDS-related KS [28, 33]. The topography of the lesions and their aggressivity depend on the type of KS. For example, KS AIDS is often aggressive and multifocal (face, genitals, lung, lower extremities). Imaging depends on the location of the lesion and the lymph nodes are typically hypervascular (Fig. 16.5) [28, 33].

16.3.2.3 Epithelioid Hemangioendothelioma (EH)

This rare malignant vascular tumor demonstrates a local recurrence rate of 10–15 % and a high metastatic rate (20–30 %). About half of the cases are multifocal [34, 35]. This lesion can arise in any vascular tissue and has been reported to be located on the skin, muscle, vasculature, bone, brain, and stomach. Tumor location in the liver and lungs may be confused with metastatic disease [35–37]. The adjacent vessels may be thrombosed, which may lead to symptoms. Calcifications can be observed [36, 38]. This lesion is often associated with Kasabach-Merritt syndrome.

16.3.2.4 Angiosarcoma

Angiosarcoma is a high-grade malignant tumor with a high mortality rate [39]. It may involve the skin (33 % of the cases), the deeper soft tissues (24 % of the cases), the internal organs, or the bones [38]. The presence of chronic lymphedema (Stewart-Treves syndrome) occurs in approximately 10 % of the cases and is a well-known risk factor for angiosarcoma [38]. Stewart-Treves syndrome is usually reported in the upper extremities after a mastectomy for breast cancer. Additionally, it can be seen in the lower extremities after hysterectomy for uterine cancer, trauma, or infection [40]. Angiosarcoma is rarely radiation-induced, and it exceptionally arises in vascular lesions [41]. Clinically, two types of angiosarcoma can be seen:

- A cutaneous form (purplish red plate, possibly nodular)
- A deep form (painful soft tissue mass in the lower limbs) [5, 39]

Metastasis most frequently involves the lung and lymph nodes, followed by the liver, the bones, and the soft tissues [39]. The imaging appearance depends on whether the lesion is located superficially or deep. Skin thickening or focal soft tissue nodules are observed when the lesion involves the skin and subcutaneous tissues. The imaging features are not specific and include intermediate echogenicity, variable signal intensity on T2-weighted images, and variable contrast enhancement (Fig. 16.6) [28]. When the lesion is associated with chronic lymphedema, extremity enlargement, diffuse skin thickening, and edema of the subcutaneous connective tissue can be seen (Fig. 16.7).

16.4 Vascular Malformations

Vascular malformations are defined by an abnormal vasculogenesis with a normal turnover of endothelial cells. They are subcategorized according to their hemodynamics [42]:

- Low-flow malformations (venous, lymphatic, capillary, capillary-venous, and capillary-lymphatic-venous)
- High-flow malformations (arteriovenous malformations [AVMs] corresponding to an

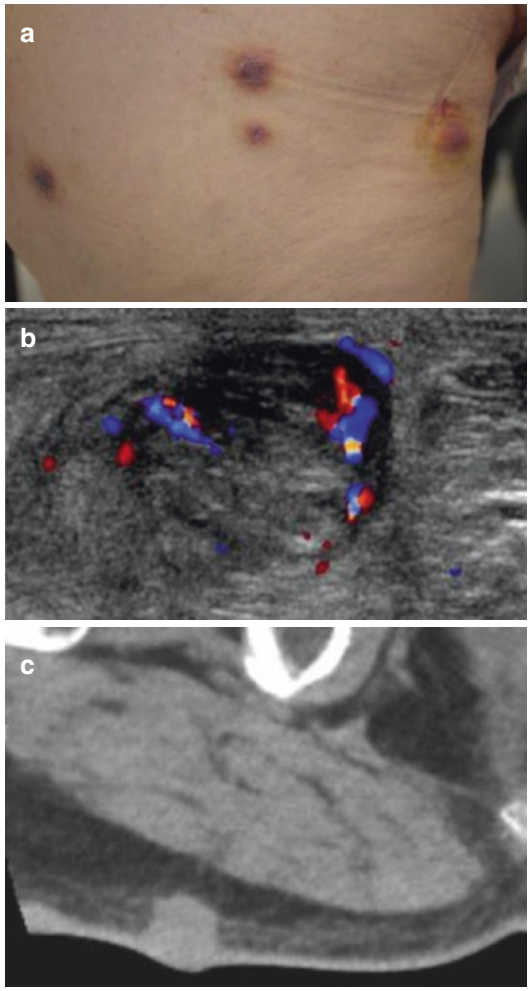

Fig. 16.6 Angiosarcoma in a 70-year-old men. (**a**) Clinical photograph. (**b**) Axial color Doppler image. (**c**) Computed tomography. (**a**) Clinical appearance of numerous skin lesions. (**b**) Ultrasound with color Doppler shows nodular superficial tissue mass, slightly hypoechogenic and predominately peripheral flow within the soft tissue mass. (**c**) Computed tomography demonstrates a non specific subcutaneous nodular lesion

anastomosis between an artery and a vein through a nidus and arteriovenous fistulas [AVFs] with a direct anastomosis between a main artery and a main vein)

This distinction is important for planning treatment. Interventional radiologists play a major role in these lesions with the increasing use of sclerotherapy and embolization therapies.

16.4.1 Venous Malformations (VMs)

VMs represent the most common peripheral vascular malformation [43, 44]. They can be simple, combined (e.g., capillary-venous and capillary-lymphaticovenous malformations), or syndromic (associated with Klippel-Trenaunay syndrome, blue rubber bleb nevus syndrome, or Maffucci syndrome). They are present at birth, but patients usually develop symptoms during late childhood or early adulthood (especially during puberty and pregnancy). They vary in size and shape and can be localized and well defined or diffuse and infiltrative. They can involve the superficial and/or deep tissues. When superficial, patients typically demonstrate bluish skin abnormalities and a soft compressible and nonpulsatile soft tissue mass [45]. They typically expand during the Valsalva maneuver and decompress with extremity elevation and local compression [17, 45]. They can also be deep, involving many anatomical structures, including the muscle, synovial membrane, bone, and liver [4, 45, 46]. They may cause pain, impaired mobility, and skeletal deformities. They are usually located on the extremities (40%), head and neck (40%), and trunk (20%) [17, 45]. Elevated D-dimer levels are a specific biomarker for VMs [47].

Pathologically, VMs are characterized by small- or large-sized venous channels connected with the normal venous system. They may contain thrombi whose dystrophic mineralization produces phleboliths [43]. Although pathologists now apply the new ISSVA nomenclature [46, 48], the historical terminology is kept in the current WHO classification (Table 16.1) [5]. Therefore, entities such as cavernous, venous, or intramuscular hemangiomas usually correspond to venous malformations and are still frequently used in pathologic reports using the WHO classification [5, 38, 46].

Phleboliths and dystrophic calcifications are easily detected on radiographs and CT and are highly suggestive of VMs (Fig. 16.8) [2]. In case of extensive malformations, the involvement of the adjacent joints or bones is possible, such as cortical erosion, periosteal reaction, regional osteopenia, and bony overgrowth [49, 50].

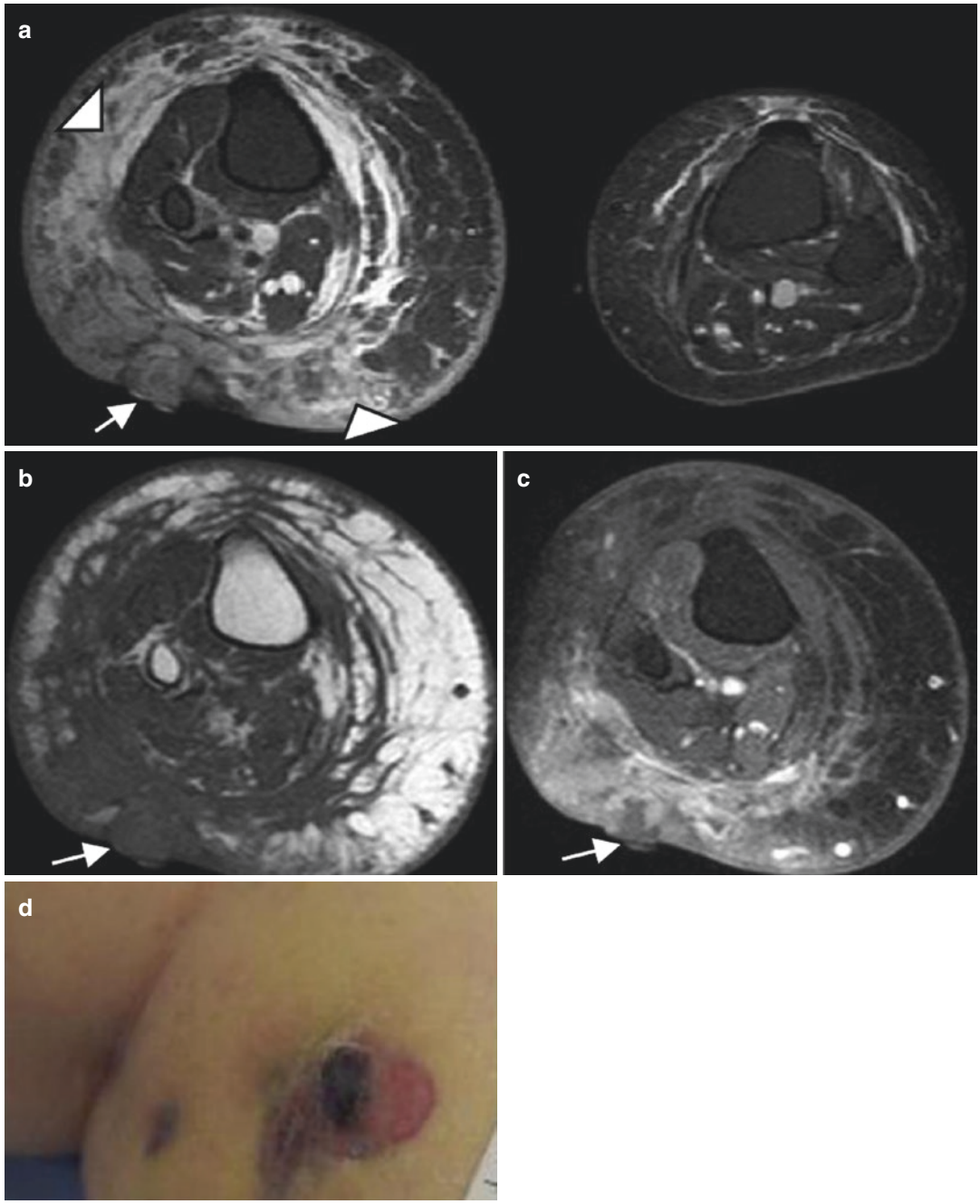

Fig. 16.7 Stewart-Treves syndrome in a 66-year-old woman who was treated 20 years ago for uterus cervical cancer. (**a**) Axial T2-weighted MR image, with fat suppression. (**b**) Axial T1-weighted MR image. (**c**) Axial T1-weighted MR image after Gadolinium contrast administration, with fat suppression. (**d**) Clinical photograph. (**a**) Axial T2-W fat-suppressed MR images reveals an enlarged right extremity with subcutaneous edema (*arrowheads*) (**a**–**c**) Nodular mass of low signal intensity on T1, with low to intermediate and heterogeneous signal intensity on T2 and a heterogeneous enhancement (*arrows*) representing the angiosarcoma. (**d**) Clinical photograph shows the purplish skin lesion

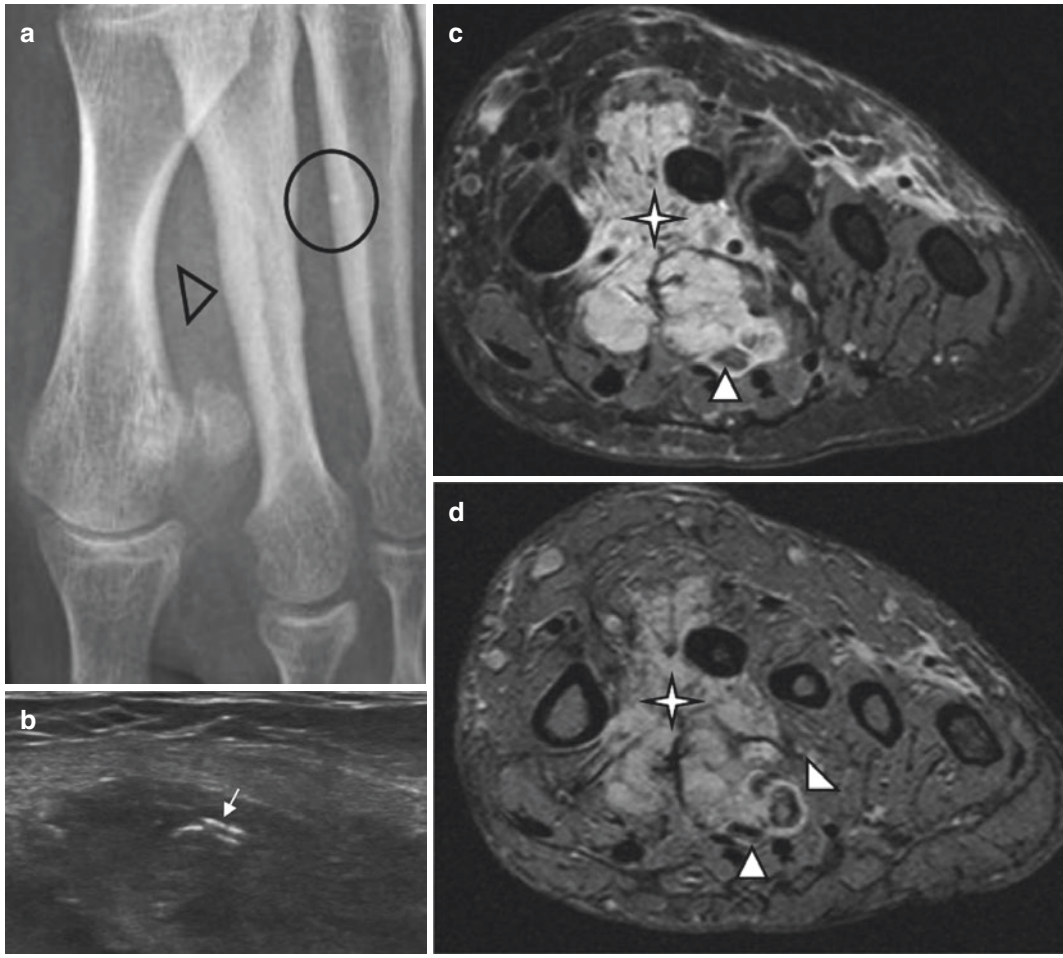

Fig. 16.8 Venous malformation of the left plantar region. (**a**) Plain radiograph. (**b**) Axial ultrasound. (**c**) Axial spin-echo T2-weighted MR image, with fat suppression. (**d**) Axial gradient-echo T2-weighted MR image. (**a**) Plain radiography demonstrates periosteal reaction, probably related to chronic vascular stasis (*black arrowhead*), and phlebolith (*circle*). This finding is characteristic of intramuscular venous malformation. (**b**) US shows hypoechogenic soft-tissue lesion with hyper echogenic foci with posterior acoustic shadowing corresponding to phleboliths (*arrow*). (**c**, **d**) Spin-echo and gradient-echo T2-weighted images show the VM as multiple slightly hyperintense serpiginous channels (*star*) with rounded hypointense phleboliths (*white arrowheads*), extending within the plantar muscles

Ultrasound shows an extremely variable appearance of the lesion, ranging from predominantly solid to multicystic lesions [1]. VMs can be well defined or infiltrative. These usually hypoechoic and heterogeneous lesions consist of tubular vascular or cavity compressible areas, reflecting the presence of vessels. The phleboliths are usually seen as hyperechoic foci. After applying compression, the movement of blood into the cavities can be identified (Fig. 16.9). Doppler US typically shows no flow or low-velocity flow. In the absence of a spontaneous vascular signal, dynamic maneuvers such as the Valsalva maneuver or manual compression by the probe followed by its decompression can cause the appearance of vascular signal although thrombosis is possible.

MRI is an excellent imaging modality to define the extent of the lesions and their relationship with the adjacent structures. VMs demonstrate well- or ill-defined limits, but they typically do not produce any significant soft tis-

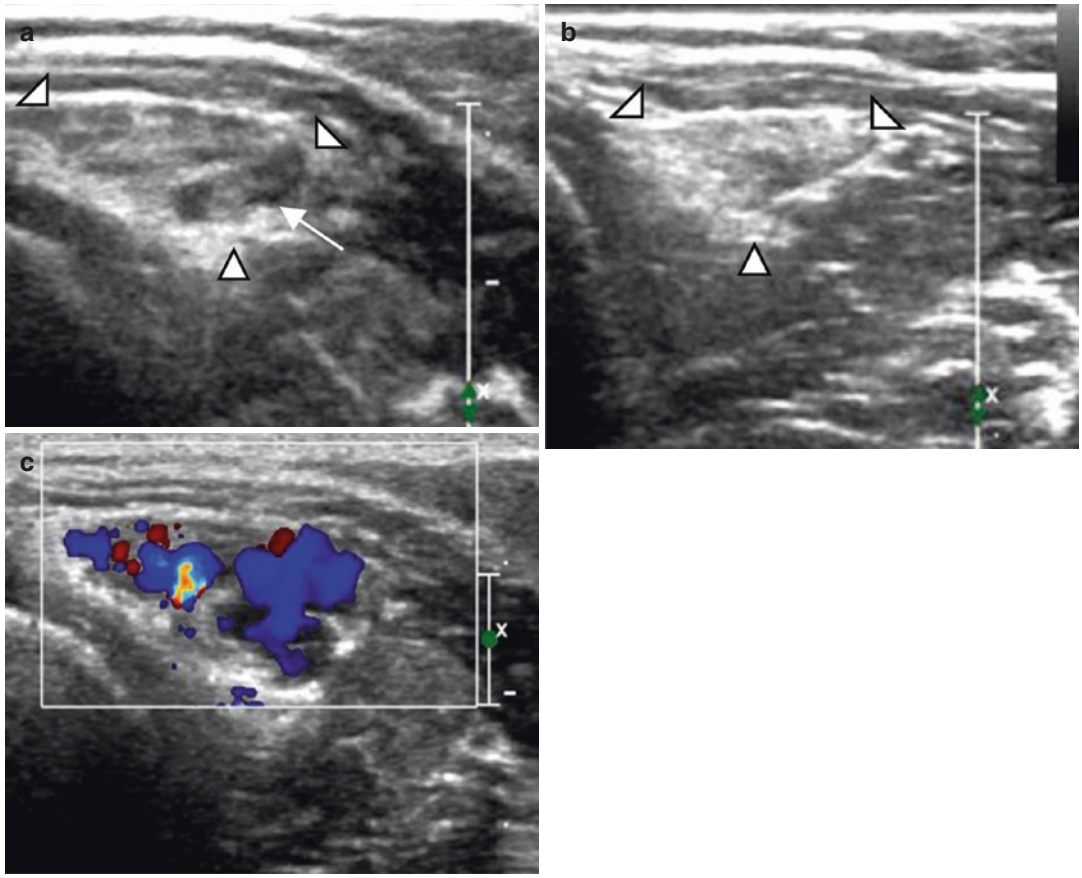

Fig. 16.9 Five-year-old girl with intramuscular venous malformation. (**a**) Ultrasound image. (**b**) Ultrasound image after local compression. (**c**) Color Doppler image. (**a**) Ultrasound image shows a heterogeneous lesion (*arrowhead*) with internal fluid component (*arrow*). (**b**) The lesion is compressible (*arrowhead*). (**c**) After decompression, filling of the cavities (vessels) can be observed on color Doppler US

sue mass syndrome, which suggests diagnosis. Vascular vessels are seen as tubular and serpiginous cavities with hypo- to iso-signal intensity on T1-weighted images and strong hyper-signal intensity on T2-weighted images, separated by hyperechoic fat (Fig. 16.10). Fat-suppressed T2-weighted images are particularly useful to evaluate the extent of the VMs. Phleboliths appear as small low-signal-intensity foci on all pulse sequences. Sometimes fluid-fluid levels due to hemorrhage or high protein content can be seen (Fig. 16.11) [1], though they are less common compared to lymphatic malformations. Contrast-enhanced 3-D acquisitions after dynamic gadolinium administration should be performed to evaluate the perfusion of the malformation and its drainage into the venous system. VMs are characterized by a lack of arterial and early venous enhancements and the absence of enlarged feeding vessels or arteriovenous shunting. They typically demonstrate a slow and progressive enhancement. Characteristic nodular enhancement of tortuous vessels can be observed on delayed venous phase images (Fig. 16.12) [3, 51]. The time between the beginning and the maximal enhancement is between 50 and 100 s [52]. Less specific appearances may be encountered when the lesion is composed of small vessels (Fig. 16.13) or in the absence of adipose tissue [53]. Intramuscular VMs often demonstrate serpiginous venous channels between the muscle

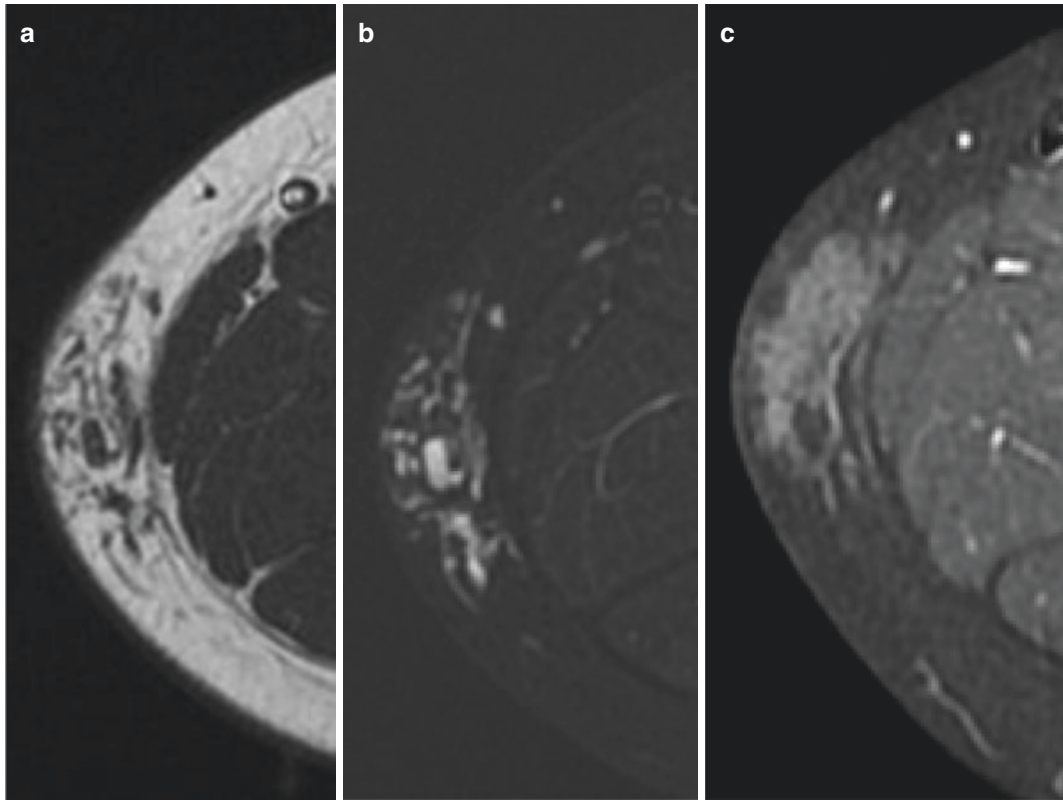

Fig. 16.10 Ten-year-old boy with subcutaneaous venous malformation. (**a**) Axial T1-weighted MR image. (**b**) Axial T2-weighted MR image with fat suppression. (**c**) Axial T1-weighted MR image after Gadolinium contrast administration with fat suppression. (**a**) MR images show multiple serpiginous areas confined to the subcutaneous soft tissues, isointense on T1-weighted image, separated by hyperintense areas corresponding to fatty components. (**b**) The lesion is hyperintense on T2-weighted image and (**c**) shows diffuse enhancement

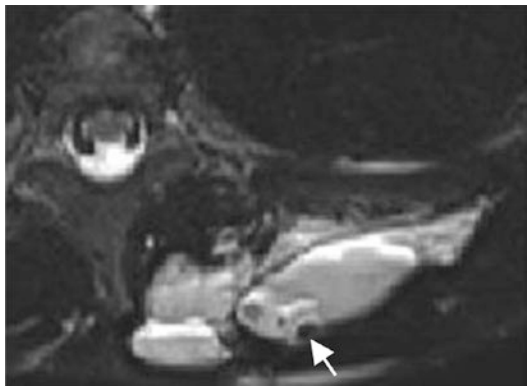

Fig. 16.11 Venous malformation with fluid-fluid level in a 5-year-old boy with recent trauma. Axial T2-weighted MR image with fat suppression reveals numerous intramuscular cavities with fluid–fluid levels. Note the presence of low signal intensity spot corresponding to phlebolith

fibers that are oriented along the long axis of the involved muscle [1]. Intra-articular involvement may lead to chronic hemarthrosis and joint destruction [54, 55] (Fig. 16.14). Localized intravascular coagulopathy is more frequent in diffuse compared to focal VMs and can be responsible for pain and thrombosis [56].

Most VMs are managed conservatively with a compression bandage of the extremity and medical antalgics for pain. In cases of major pain, joint involvement, and functional or cosmetic problems, the first-line treatment for VMs is sclerotherapy (dehydrated ethanol, sodium tetradecyl sulfate, polidocanol, and bleomycin), which can be followed by resection, laser therapy, and photodynamic therapy [57, 58].

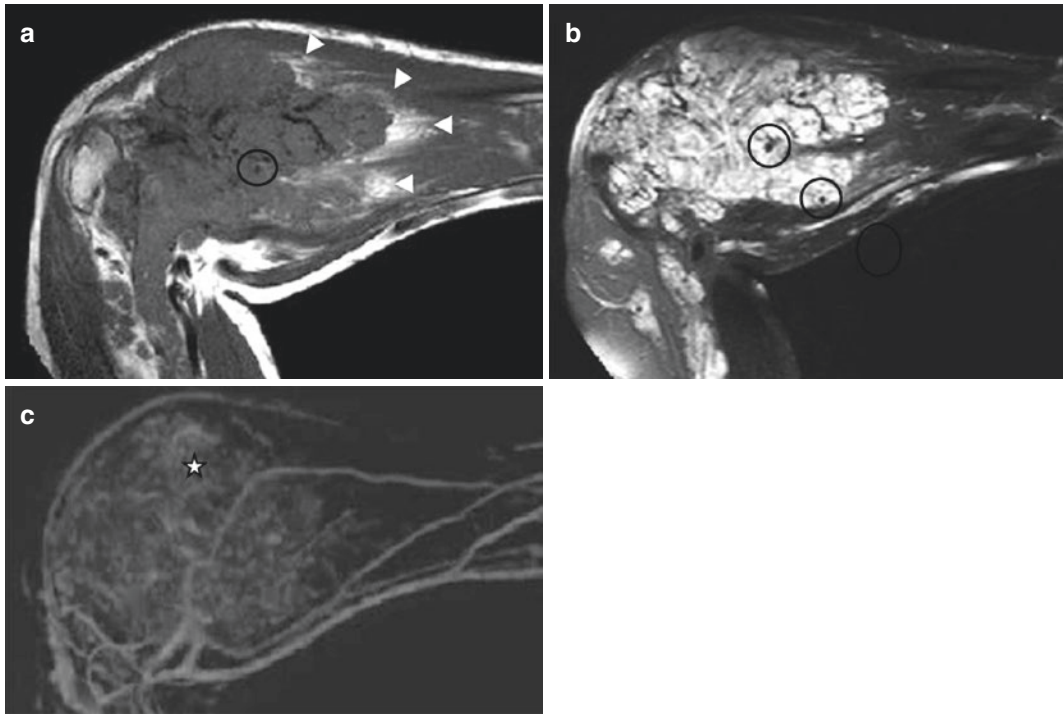

Fig. 16.12 Intramuscular venous malformation of the upper extremity. (**a**) Sagittal T1-weighted MR image. (**b**) Sagittal T2-weighted image with fat saturation. (**c**) Maximum intensity projection (MIP) after 3D contrast-enhanced MR angiography, late venous phase. (**a**) T1-weighted image shows an intramuscular and extensive lesion which involves the forearm muscles and elbow joint, surrounded by fat component (*arrowheads*). (**b**) The lesion is composed of multiple tortuous hyperintense vessels on T2-weighted image representing a slow flow vascular malformation. At least two phleboliths (*circles*) are seen as low signal foci inside the dilated veins. (**c**) Late venous phase image from gadolinium-enhanced 3D MR angiography shows characteristic filing of cavernous spaces with diffuse and nodular enhancement (*star*)

Key Points

1. Venous malformations
2. Superficial or deep (muscle, synovial membrane, bone, liver) and localized or diffuse
3. Expansion during Valsalva maneuver/decompression with extremity elevation and local compression
4. Phleboliths +++
5. Tubular and serpiginous cavities strongly hyperintense on T2-weighted images
6. Diffuse and delayed enhancement of the slow-flowing venous channels after contrast administration

16.4.2 Lymphatic Malformations (LMs)

LMs represent the second most common type of vascular malformation after venous malformations [59]. These low-flow vascular malformations are classified into three types depending on the size of the cystic cavities [1, 2, 45, 60, 61]:

- Macrocystic types (formerly cystic hygroma), with cysts >2 cm
- Microcystic types (formerly lymphangioma), with cysts between 1 and 2 cm
- Mixed types with capillary and/or venous malformations

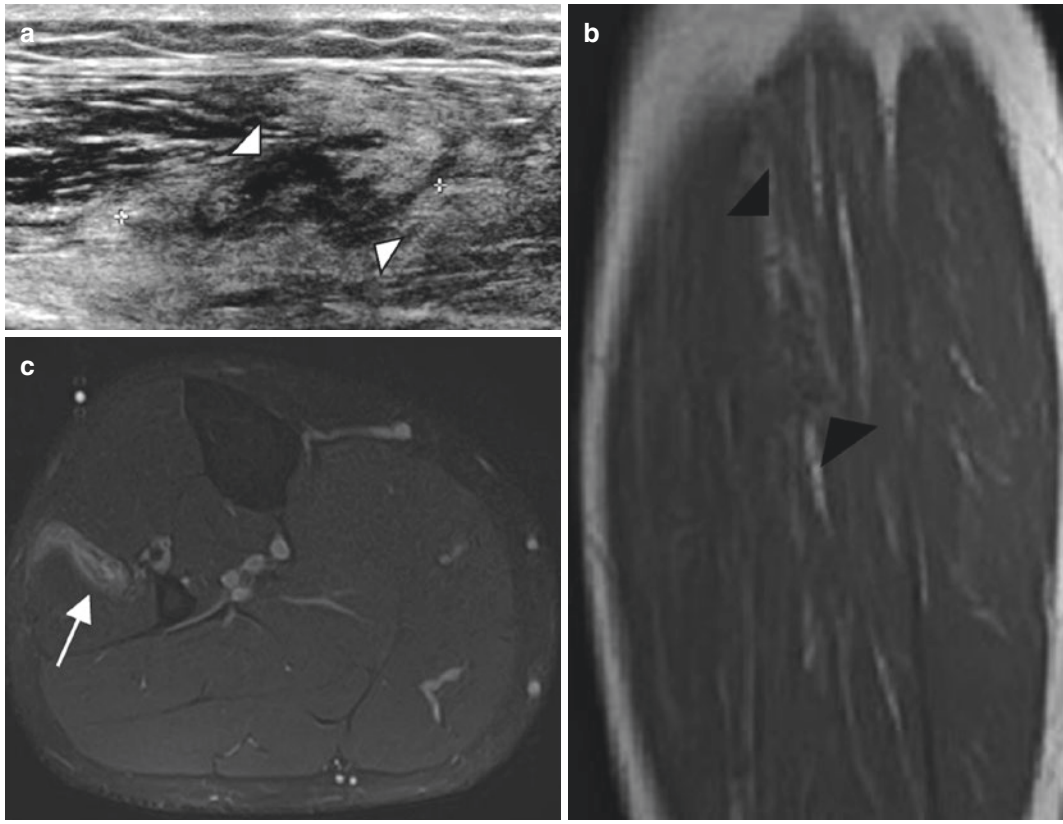

Fig. 16.13 Intramuscular venous malformation of the thigh in a 32-year-old man with pain exacerbated during exercise. (**a**) Ultrasound. (**b**) Sagittal T1-weighted MR image. (**c**) Axial T1-weighted MR image after Gadolinium contrast administration, with fat suppression (**a**) Ultrasound shows a nonspecific intramuscular soft tissue lesion (*white arrowhead*) (**b**) MR image demonstrates fat component surrounding the lesion (*black arrowheads*), (**c**) and serpiginous enhancement after gadolinium contrast administration (*arrow*)

Pathologically, they are composed of serpiginous dilated lymphatic channels that do not communicate with the normal lymphatic system [45], except in the retroperitoneum. Macrocystic and microcystic lesions are pathologically indistinguishable [61]. Diagnosis is suggested after a positive test for markers of lymph vessels, such as the vascular endothelial growth factor receptor 3 (VEGFR-3), LYVE-1, D2-40, and podoplanin [61–63]. However, it should be kept in mind that LMs can be associated with the other vascular malformations.

LMs are present at birth in half of the patients (prenatal diagnosis of macrocystic types is possible) and are diagnosed before the age of 2 years in 90% of the cases [61, 64]. They mainly involve the head and neck (55–95%) and axillary regions (20%) with a predilection for the left side of the body [64]. They can affect multiple structures (lung, intestine, liver, spleen, etc.) including the bones [38]. Macrocystic LMs are typically large and clinically manifest as a soft swelling mass with a rubbery consistency. They are well limited and mobile under a normal skin [57, 64]. Transillumination confirms the liquid nature of the lesion. The majority of the cases are asymptomatic, but complications, such as local compression, sudden increase in size secondary to bleeding (trauma), or infection from an adjacent process of the head and neck, can occur [65].

Microcystic LMs tend to infiltrate the adjacent structures. They are sometimes associated with a particular skin damage (lymphangioma

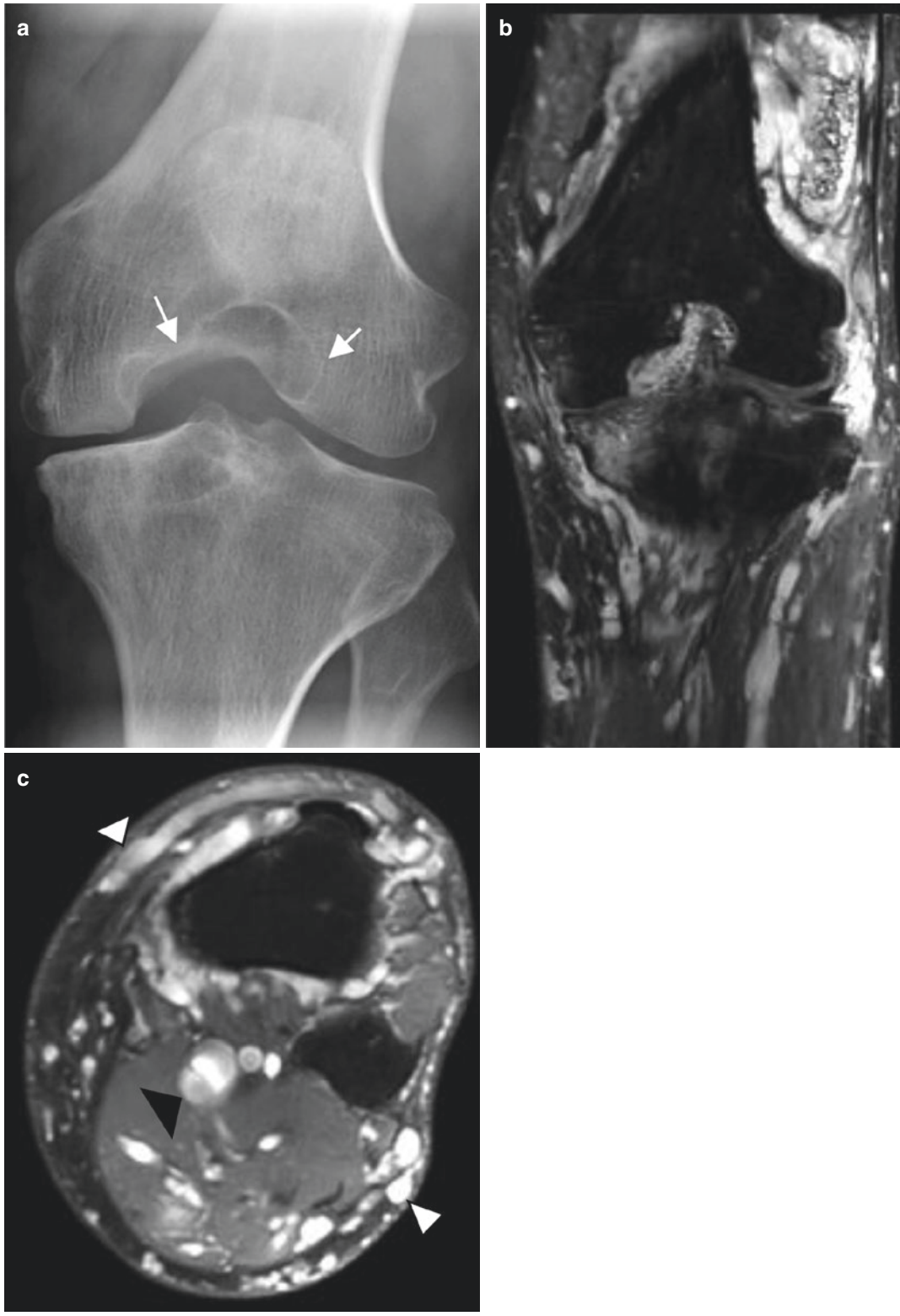
a
b
c

Fig. 16.14 Patient with diffuse and infiltrative venous malformation of the knee. (**a**) Plain radiograph. (**b**) Coronal T2-weighted image with fat saturation. (**c**) Axial T2-weighted image with fat saturation. (**a**) Plain radiograph shows a widening of intercondylar notch with erosion of the medial femoral condyle. (**b**, **c**) MRI shows infiltrative and serpentine vascular spaces with involvement of multiple compartments of the knee. Hyperintense nodular and serpentine areas of vascular vessels are seen in the subcutis (*arrowheads*), muscles and joint. Note the dilated deep veins (*black arrowhead*)

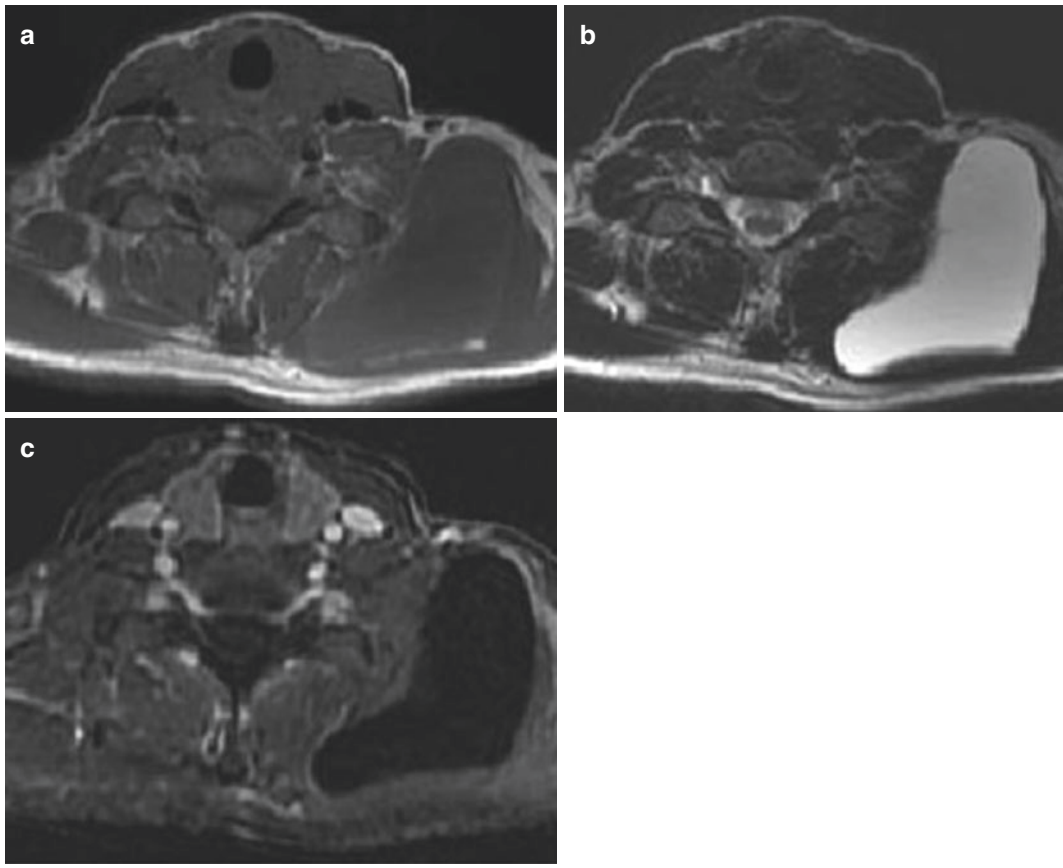

Fig. 16.15 Macrocystic lymphatic malformation in a 30-year-old woman with a swollen mass in the neck. (**a**) Axial T1-weighted MR image. (**b**) Axial T2-weighted MR image with fat suppression. (**c**) Axial T1-weighted MR image after Gadolinium contrast administration with fat suppression. (**a**) MRI demonstrates a well-defined, lobulated isointense mass on T1-weighted image, (**b**) which is highly hyperintense on T2-weighted image, (**c**) and does not enhance after gadolinium contrast administration

circumscriptum) [1, 2, 61]. More unusual locations include the mediastinum, retroperitoneum, omentum, mesentery, and bones [66].

Ultrasound demonstrates a multiloculated cystic mass and the size of the cavity determines the type of LM. The cystic spaces are mostly anechoic or hypoechoic, but levels may be observed in cases of bleeding, infection, or chylous fluid. Septa of variable thickness correspond to clusters of lymph structures. LMs do not demonstrate any associated vascularity, soft tissue components, or perilesional inflammatory changes. Calcifications are sometimes observed.

On MRI, LMs are usually seen as lobulated cystic masses with iso- to hypo-signal intensity on T1-weighted images and increased signal intensity on T2-weighted and STIR sequences (Fig. 16.15). Fluid levels can be observed in cases of superimposed hemorrhage or infection [3]. After contrast administration, macrocystic LMs

exhibit rim and septal enhancement [15, 44], whereas microcystic LMs do not show any enhancement (Fig. 16.16) [15]. However, combined lymphatic-venous malformations may show diffuse enhancement, which is related to the venous component enhancement in mixed malformations [3]. MRI is the best imaging modality to assess the exact extent of the lesion, which may

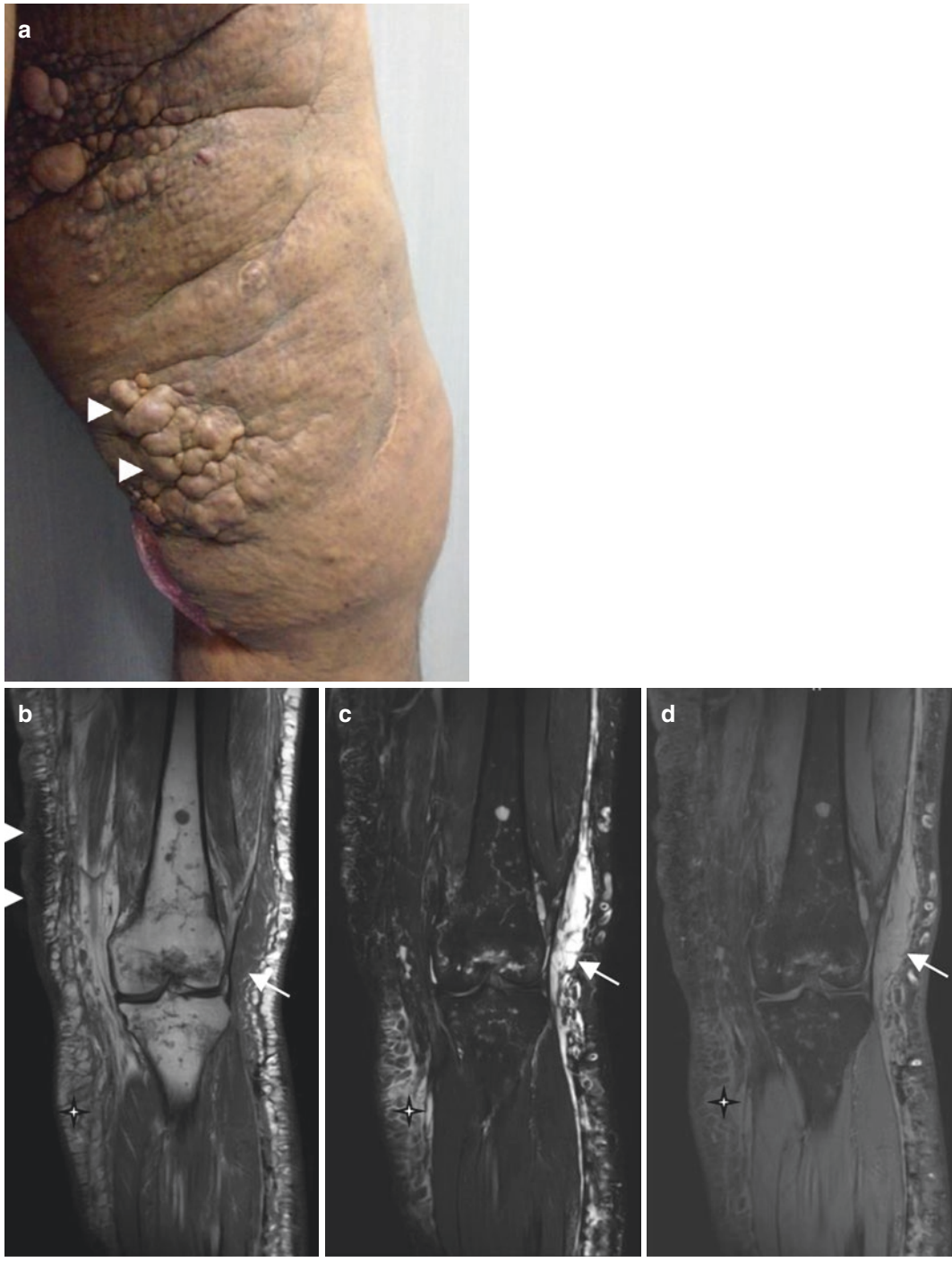

be localized or diffuse and very infiltrative [1]. Involvement of the adjacent bone may be present (Fig. 16.16). Needle aspiration confirms the diagnosis of LMs by finding lymphatic vessels.

The first-line therapy is percutaneous sclerotherapy, usually with absolute alcohol under radiological control. Several sessions are needed in extensive forms of LM. As this treatment is usually effective in macrocystic LMs, surgery is less frequently proposed [57]. Microcystic LMs are more difficult to treat and recurrence is more frequent. They should be managed conservatively as much as possible [2].

Key Points

1. Lymphatic malformations
2. Macrocystic, microcystic, or mixed
3. Most frequent in the neck and head regions and then axilla
4. Can be combined with other vascular malformations (capillary-venous)
5. Macrocystic LMs: cystic lesion/ring-septal enhancement after gadolinium contrast administration
6. Microcystic LMs: cutaneous skin damage/no significant enhancement after gadolinium contrast administration

16.4.3 Capillary Malformations (CMs)

These intradermal vascular lesions are composed of mature ectatic capillary channels and are hemodynamically inactive. The diagnosis of CMs is clinically based on the appearance of a cutaneous red discoloration [9]. CMs are present at birth in 0.3 % of children [15], and they typically regress. They usually involve the face but can develop anywhere. They can be associated with malformation syndromes, such as Sturge-Weber syndrome, Klippel-Trenaunay syndrome, and Parkes Weber syndrome. Nonspecific thickening of the skin can be observed with US or MRI [1].

16.4.4 Arteriovenous Malformations (AVMs)

AVMs are high-flow vascular malformations related to an abnormal communication between arteries and veins, with persistence of fetal capillary beds [8]. They are usually sporadic but can be seen in hereditary syndromes [26, 67]. They most often affect the head and neck region (including the brain), the extremities, and the internal organs [5]. They are present at birth in an early quiescent stage and usually do not become evident before until later childhood or adulthood. Like the other vascular malformations, they generally increase in size proportional to the growth of the child and are under hormonal influences (puberty, pregnancy). Their size can also be influenced by trauma (such as biopsy or incomplete surgery) [17, 45]. They are hemodynamically active, which can result in a red, pulsatile, warm mass with dilated superficial draining veins [68]. The presence of the shunt may induce limb hypertrophy and reflex bradycardia after compression of the lesion. Adjacent bone or joint damage is possible (marked periosteal reaction or destruction) [2, 26].

The histology of AVMs is highly variable with a combination of capillaries, venules, and arterioles in a fibrous or fibromyxoid stroma. Correlation with imaging is important for the diagnosis of AVMs. Calcifications and thrombosis are possible [5].

On US, AVMs are seen as ill-defined areas formed by multiple juxtaposed tortuous vessels, separated by hyperechoic fat. The vessels include arteries with diastolic flow and arterialized

Fig. 16.16 Microcystic lymphatic malformation. (**a**) Clinical photograph. (**b**) Coronal T1-weighted MR image. (**c**) Coronal T2-weighted MR image with fat suppression. (**d**) Coronal T1-weighted MR image after Gadolinium contrast administration with fat suppression. (**a**) Clinical photograph shows an extensive skin lesion of the thigh (*white arrowheads*). (**b**–**d**) MRI reveals the skin thickening on T1-weighted image (*white arrowhead*) (**b**) and a diffuse involvement of the subcutaneous tissue (*star*) with a lobulated and septated mass (*arrow*). There is no significant enhancement of these features (**d**), a finding characteristic of a microcystic lymphatic malformation. Note the associated involvement of the bone

draining veins with pulsatile flow (not seen in hemangiomas) [17]. The nidus is recognized by its various vascular areas and aliasing phenomena in terms of the color Doppler shunts [20].

MR imaging demonstrates tortuous structures composed of enlarged feeding arteries and draining veins without well-defined associated mass. Signal voids are observed in these vessels on both T1-W and T2-W SE sequences (Fig. 16.17), but high signal intensity is seen on gradient-echo sequences, indicating high-flow lesions [1, 45]. Gadolinium perfusion allows for the mapping of feeding arteries, draining veins, and the nidus [1]. Early venous filling is typically seen in AVMs (Fig. 16.18).

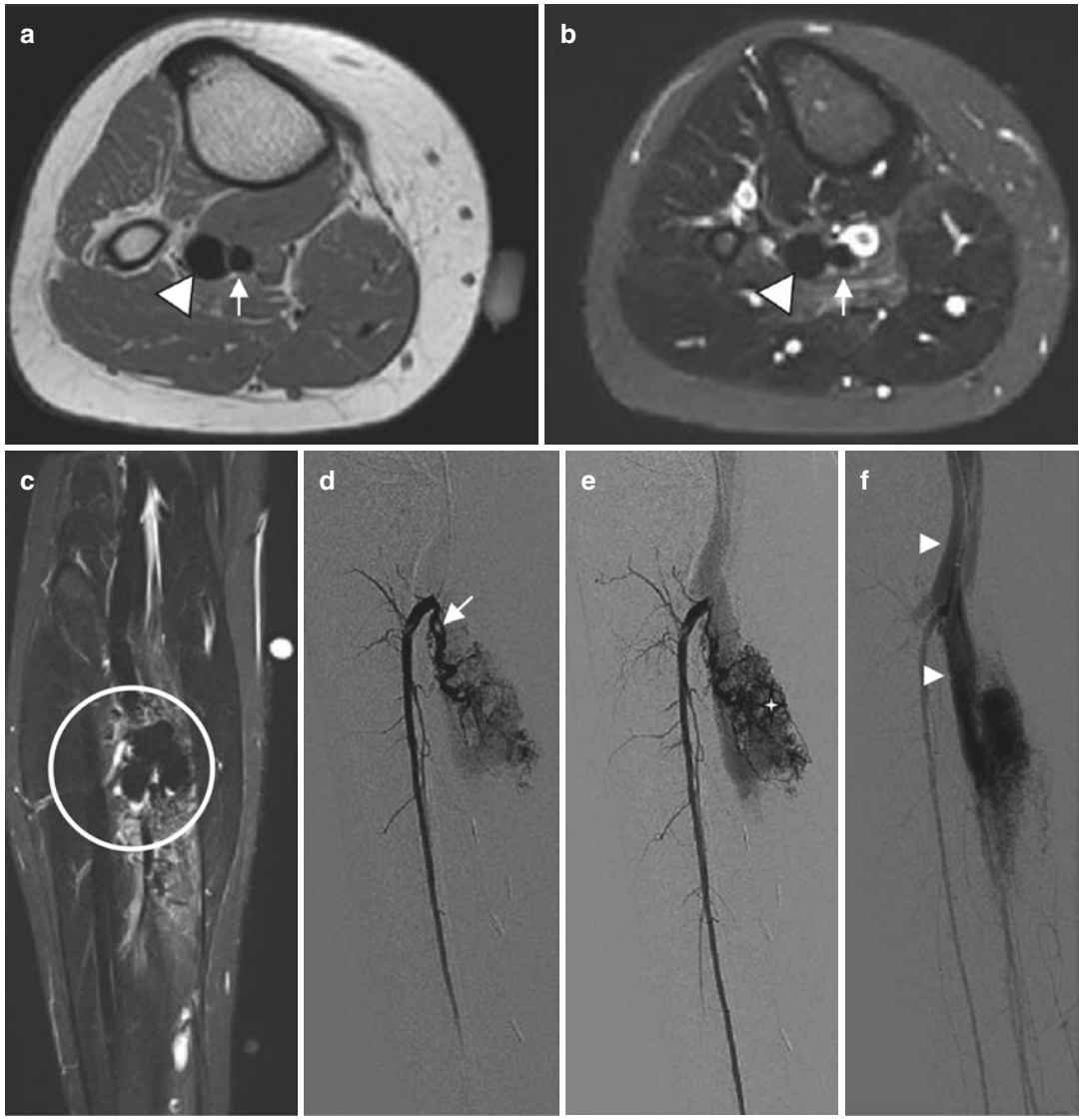

Fig. 16.17 Complex arteriovenous malformation affecting the calf in a 15-year-old woman. (**a**) Axial T1-weighted MR image. (**b**) Axial T2-weighted MR image with fat suppression. (**c**) Coronal T2-weighted MR image with fat suppression. (**d**–**f**) Conventional angiographic images acquired from early arterial phase to venous phase. (**a**, **b**) Signal voids in the high flow vessels can be depicted on both T1-weighted and T2-weighted MR images, including the feeding artery (*arrow*) and arterialized draining vein (*arrowhead*). (**c**) Coronal T2-weighted MR image reveals the nidus (*circle*). (**d**–**f**) Arteriogram acquired demonstrates a slightly enlarged tortuous artery (*arrow*) during the early arterial phase, the nidus (*star*) on late arterial phase, and then enlarged draining veins (*arrowheads*)

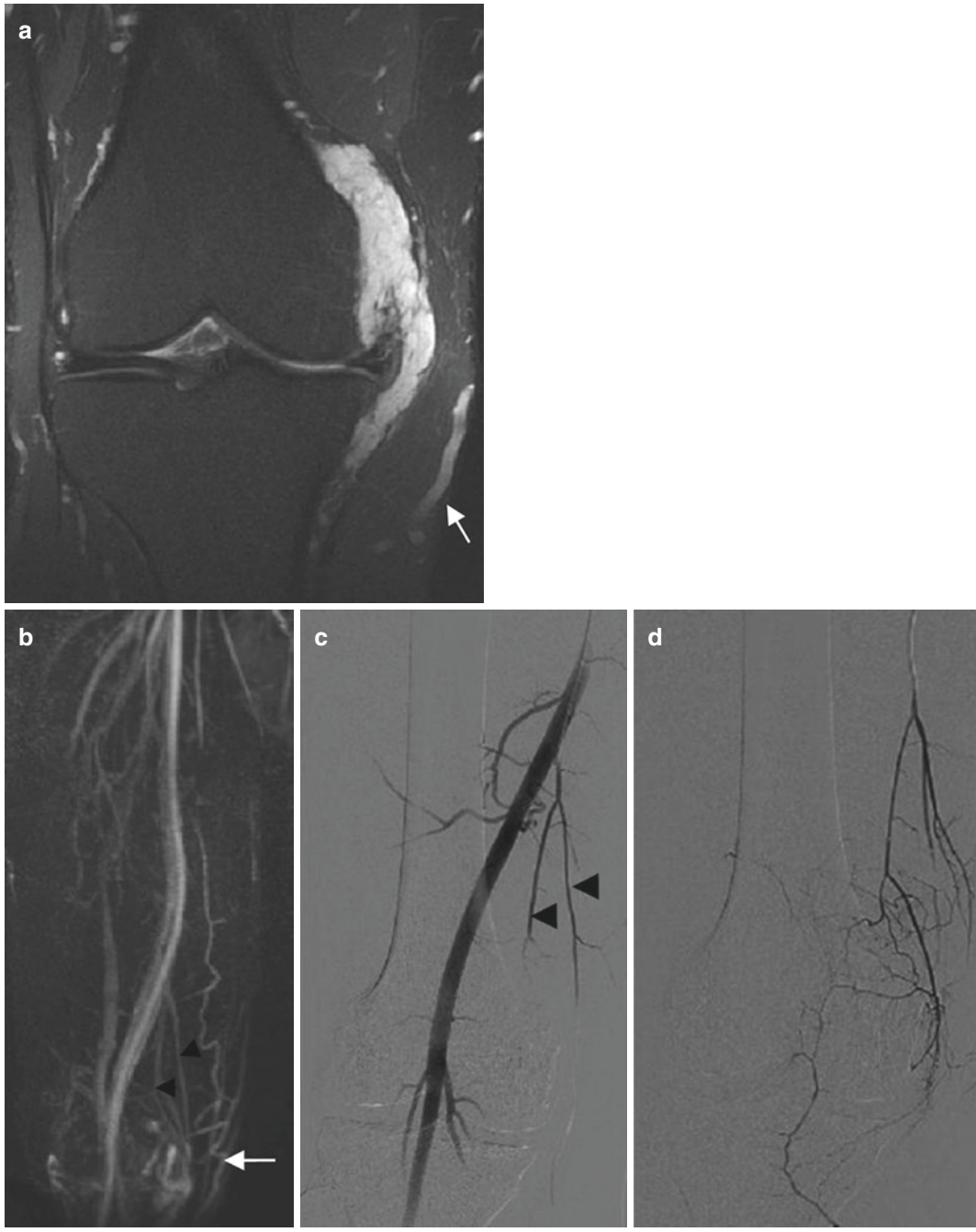

Fig. 16.18 Arteriovenous malformation of the knee in a 30-year-old man. (**a**) Coronal T2-weighted MR image with fat suppression. (**b**) Maximum intensity projection (MIP) after 3D contrast-enhanced MR angiography. (**c**, **d**) Conventional angiographic images acquired during early arterial phase before the treatment. (**a**) The lesion is composed of tortuous enlarged feeding arteries located within the medial collateral ligament with a distended vein. (**b**) Two feeding arteries (*black arrowheads*) are seen on MIP after 3D contrast-enhanced MR angiography, with the early venous feeding (*arrow*). (**c**, **d**) Conventional angiographic images confirm these findings and reveals the two feeding arteries (*arrowheads*) from the superficial femoral artery

The dynamic opacification, using time-resolved MR angiography, confirms the rapid flow when the period between the start and the maximal enhancement is 5–10 s [3, 52]. Intraosseous extension of the lesion can also be seen [68]. Arteriography is only performed when the MR features are equivocal or when embolization is considered. This technique has the advantage of selective catheterization of the feeding arteries with depiction of the nidus and early draining veins.

The goal of treatment for AVMs is the eradication of the nidus, causal factor of the shunt. Treatment includes two stages, a preoperative embolization by a biological glue and a complete surgical excision [57]. Different surgical approaches have been described, including arterial microcatheterism, direct percutaneous puncture, and retrograde venous microcatheterism [45].

Key Points

1. Arteriovenous malformations
2. Ill-defined area with multiple vessels (arteries with diastolic flow/arterialized draining veins with pulsatile flow)
3. Early venous filling

16.5 Particular Vascular Lesions

16.5.1 Glomus Tumor (GT)

According to the latest revision of the WHO classification (2013), glomus tumor is regarded as a pericystic (perivascular) tumor (see also Chaps. 11 and 15).

Glomus tumors and its rare variants, such as glomangioma (20 % of cases), glomangiomyoma (less than 10 % of cases), and the exceptional malignant glomus tumor [69], are derived from neuromyoarterial glomus bodies. These millimeter organs are involved in thermoregulation by modulation of cutaneous blood flow. They are mainly localized in the dermis, at the ends of fingers and toes, and especially under the nails [38, 70]. The most common location for GTs is the tip of the fingers, particularly the subungual area where it can lead to erosion of the adjacent phalanx [71]. They are less common in the pulp. They are mainly observed in adults and are observed as a small red-blue superficial nodule (1 mm−3 cm), with extremely intense focal pain, triggered by pressure and cold [70]. This clinical presentation results in diagnosis in 90 % of the cases when the digits are involved [72]. Subungual lesions have female predilection in contrast to the other locations [70, 73]. Other rare locations include muscles, tendons, nerves, bones, and viscera [74–76] and involve less specific symptoms [70].

On radiography, finger involvement is accompanied by bone erosion of the distal phalanx in approximately one-third of the cases [72]. GTs can be visualized using MRI or ultrasound, although they typically measures only 1.5–2 mm [77, 78]. Ultrasound shows a well-limited hypoechoic nodule which often contains small cystic internal rearrangements and a significant hyperemia on Doppler (Fig. 16.19) [79]. On MRI, dedicated coils and very thin sections with excellent spatial resolution should be used. GTs show with hypo- to iso-signal intensity on T1-weighted images and strong hypersignal intensity on T2-weighted images (Fig. 16.20) [28, 75]. MR angiography shows intense enhancement in the arterial phase with tumor blush [71, 78,

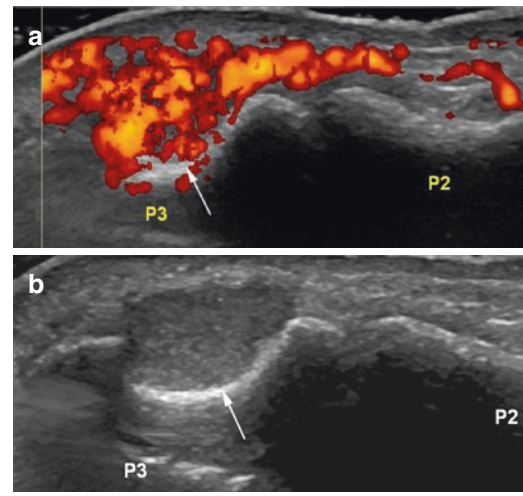

Fig. 16.19 Glomus tumor of the nail bed. (**a**) Ultrasound. (**b**) Power Doppler image. (**a**) Ultrasound images show an isoechogenic mass eroding the underlying distal phalanx (*P3*) (*arrow*). The lesion is markedly hypervascular (**b**) on power Doppler image

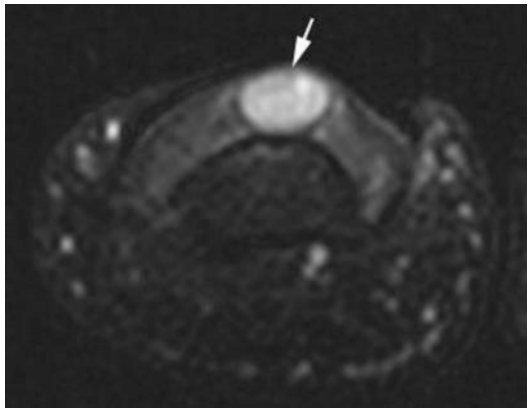

Fig. 16.20 Glomus tumor of the nail bed. Axial T2-weighted MR image with fat suppression shows a 2 mm markedly hyperintense lesion of the nail bed

80]. This is sometimes the sole sequence showing the lesion. Small lesions enhance homogeneously after gadolinium administration, while larger GTs are more heterogeneous on T2-weighted images and after contrast administration [79]. The histologic subtype of the lesion (vascular, solid, myxoid) also influences its appearance on T1-weighted images (from low to high signal intensity) [71]. Postsurgical recurrences present the typical appearance of GTs in half of the cases [78]. The main differential diagnoses include mucoid cysts, venous malformations, malignant melanomas, soft tissue chondromas, giant cell tumors, and epidermoid cysts [71, 75, 78, 80].

Surgical excision must be complete to be effective for pain and prevent recurrences (4–20 % in the subungual location) [77].

Key Points

1. Glomus tumor
2. Benign tumor of the neuromyoarterial glomus bodies
3. Tip of the fingers, mainly in the subungual area
4. Highly suggestive clinical presentation: small red-blue nodule, intense focal pain triggered by pressure and cold
5. Small highly vascular lesion of the nail bed, possible erosion of the adjacent bone

16.5.2 Synovial Hemangioma (SH)

SHs are rare vascular lesion of the synovial membrane that affect children and young adults, and 75 % of patients are symptomatic before the age of 16 years [81]. SHs mainly develop in the knee (60 %), particularly at the suprapatellar pouch. Other locations include the elbow (30 %), ankle, hip, temporomandibular joint, and tendon sheaths [81, 82]. SH may be associated with repetitive episodes of pain, swelling, and joint effusion (hemarthrosis). With time, limitation of the joint mobility and muscle atrophy can develop. Joint blocking is possible when the lesion is pedunculated. A diagnostic delay is common, and because of the repetitive bleeding into the joint, an arthropathy similar to the hemophilic arthropathy can develop. If arthrography is performed, the synovium may demonstrate irregular contours mimicking synovial chondromatosis, villonodular synovitis, or rheumatoid arthritis [82]. MRI is the best imaging modality to identify this lesion and to assess its intra- and extraarticular extent (Fig. 16.21). MRI features are usually pathognomonic: serpiginous lesion with a low or iso-signal intensity on T1-weighted images and high signal intensity on T2-weighted images due to vascular stasis, associated with fibrofatty septa and sometimes vascular structures (thrombosed or not). SH lesion enhances after gadolinium administration, sometimes heterogeneously. Joint effusion and erosive changes of the subchondral bone are often associated [83, 84].

Early surgical excision is mandatory to prevent the development of arthropathy.

16.6 Syndromes Associated with Vascular Lesions

Several well-known familial or sporadic syndromes include vascular tumors or malformations (Table 16.4) [67, 85, 86]. Most of them develop during childhood and require long-term therapeutic planning (based on the flow velocity) [67]. These patients must be followed by a multidisciplinary team.

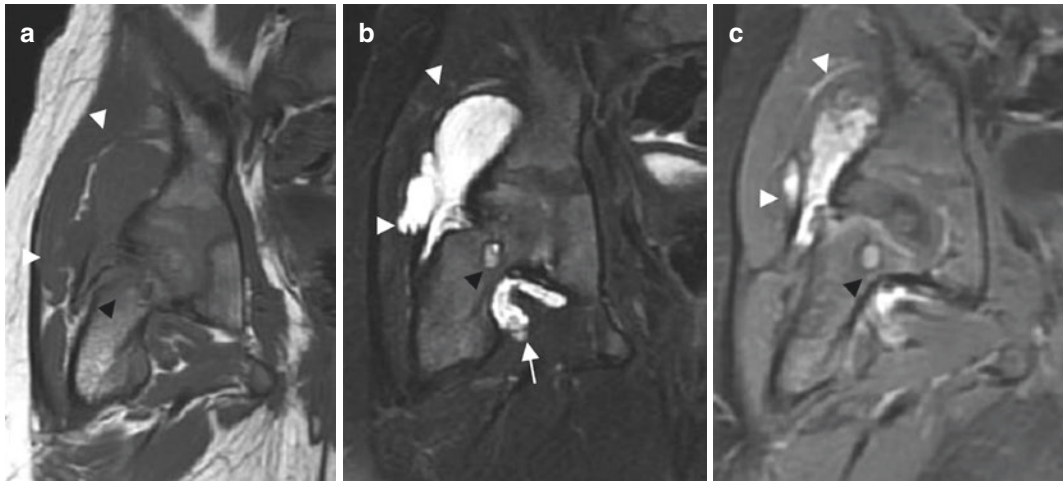

Fig. 16.21 Synovial hemangioma of the hip. (**a**) Coronal T1-weighted MR image. (**b**) Coronal T2-weighted MR image with fat suppression. (**c**) Coronal T1-weighted MR image after Gadolinium contrast administration with fat suppression. Hemangioma demonstrates a low signal intensity on T1-WI, bright signal intensity on T2-WI and enhances after gadolinium administration (*white arrowheads*). Note the hypointense area under the femoral head related to hemosiderin deposition (*arrow*) and the erosive change of the anterior aspect of the femoral neck (*black arrowhead*)

Table 16.4 Main syndromes associated with vascular tumors and malformations

Tumors		
PHACE syndrome/PELVIS and SACRAL syndrome: infantile hemangioma		
Kasabach-Merritt syndrome: kaposiform hemangioendotheliomas, tufted angiomas		
Malformations		
Syndrome	Hemodynamic	Main location
Klippel-Trenaunay	Low-flow	Extremities
Maffucci	Low-flow	Extremities
Parkes Weber	High-flow	Extremities
Sturge-Weber	Low-flow	Head
Proteus	Low-flow	Diffuse
Rendu-Osler-Weber	High-flow	Diffuse

16.6.1 PHACE Syndrome

PHACE is an acronym for the syndrome's most common clinical and imaging findings: posterior fossa malformations, segmental infantile hemangiomas of the face and neck (usually larger than 5 cm), arterial anomalies, cardiac defects or coarctation of the aorta, eye or endocrine anomalies, and sternal defects [67, 87].

16.6.2 PELVIS and SACRAL Syndromes

Infantile hemangiomas located in the lumbosacral and perineal region are at risk of underlying developmental anomalies, particularly spinal dysraphisms, anorectal and urinary tract defects. These associations have been variably named in the literature with several acronyms:

- *PELVIS* for Perineal hemangioma, External genitalia malformations, Lipomyelomeningocele, Vesicorenal abnormalities, Imperforate anus, and Skin tag
- *SACRAL* for Spinal dysraphism, Anogenital anomalies, Cutaneous malformations, Renal and urological anomalies, and Angioma of Lumbosacral localization

Evaluation with MRI is therefore recommended for such lesions in this particular location [88, 89].

16.6.3 Kasabach-Merritt Syndrome

Kasabach-Merritt syndrome is characterized by a combination of vascular lesions (kaposiform

hemangioendotheliomas, tufted angiomas), thrombocytopenia, and coagulopathy causing hemorrhage, infections, and multiple organ failure [67]. The mortality rate is close to 30 % [38], and aggressive therapy is required (steroids, vincristine, and interferons).

16.6.4 Klippel-Trenaunay Syndrome

Klippel-Trenaunay syndrome is a non-hereditary complex disorder usually affecting only one of the lower extremities, but it can spread into the pelvis and trunk. It is defined by three classic clinical findings: (1) capillary malformation (usually of affected limb), (2) bone and soft tissue limb enlargement (usually affecting one extremity), and (3) atypical varicosities or venous malformations with a characteristic abnormal lateral vein beginning at the ankle and extending to the pelvic region (Fig. 16.22) [67, 90].

Abnormal development of the deep and superficial veins explains persistent embryonic veins including lateral veins with persistent sciatic vein

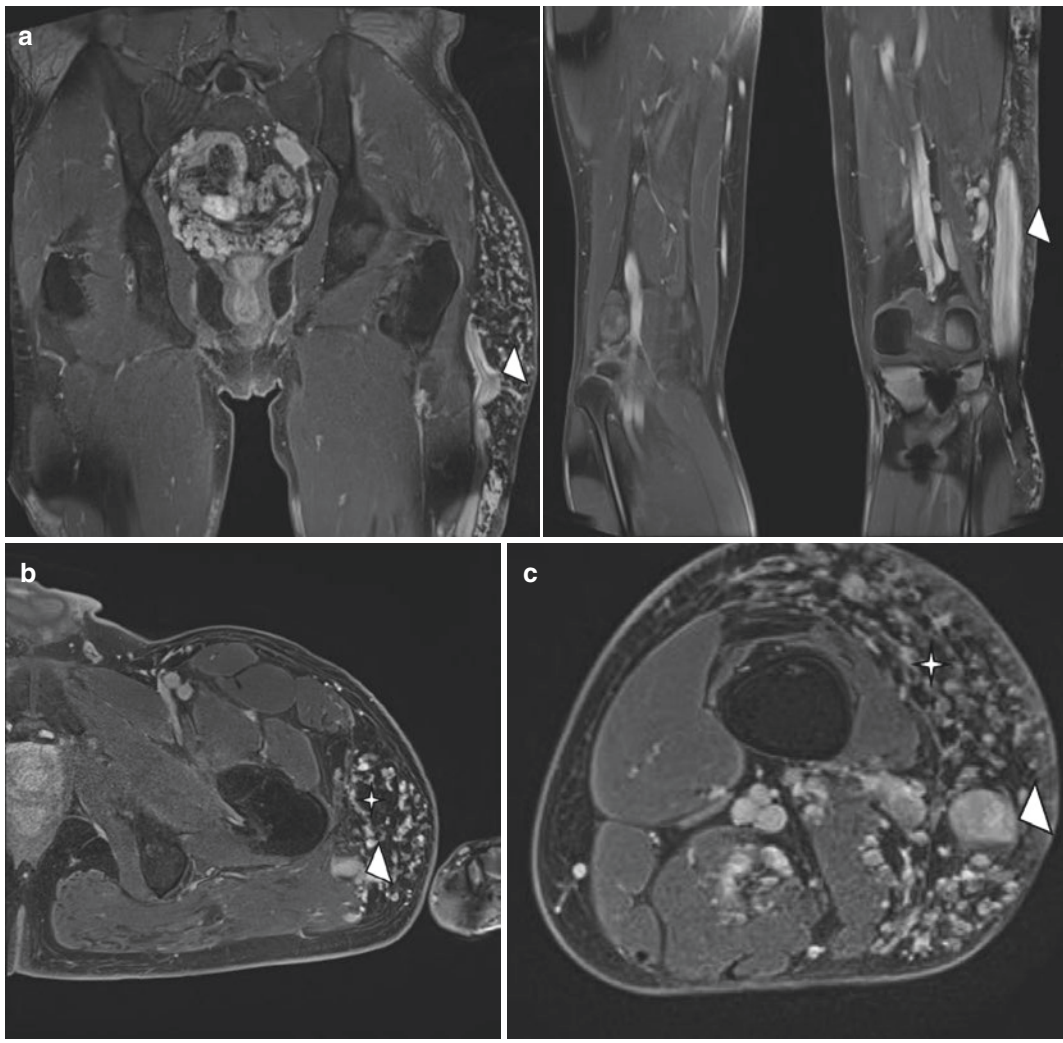

Fig. 16.22 Klippel-Trenaunay syndrome in a 30-year-old boy. (**a**) Coronal T2-weighted MR image with fat suppression. (**b**, **c**) Axial T2-weighted MR images with fat suppression of the pelvis and thigh. (**a–c**) There is hemihypertrophy of left lower extremity with extensive subcutaneous (*star*) and intramuscular venous malformations. Note the characteristic abnormal sapheneous vein (*arrowhead* in **c**)

and dilated superficial system. Hypertrophy is variable, affecting the whole leg or only the distal digits [91]. Syndactyly, polydactyly, and congenital hip dislocation can also be observed [92].

On imaging, vascular overgrowth demonstrates slow and late enhancement indicating low-flow malformations. Deep venous malformations of the femoral vein are commonly seen. Because of overgrowth of the soft tissues, the affected limb is usually larger and longer than the unaffected limb [86].

16.6.5 Maffucci Syndrome

Maffucci syndrome is a rare and non-hereditary syndrome characterized by the association of multiple enchondromas and multiple low-flow vascular malformations (mainly venous, rarely lymphatic) [93]. Clinically, it manifests before 1 year of age in 25 % of the patients and by the puberty in 80 % of all cases [67].

Enchondromas usually involve the phalanges of the hands (Fig. 16.23) and feet, and in one-half of the patients, lesions are unilateral and lead to the development of notable malformations [93]. Low-flow vascular malformations do not have the same distribution as enchondromas and usually involve the subcutaneous soft tissues of another anatomic region. Phleboliths are very suggestive [94].

The malignant transformation rate is high and involves enchondromas (chondrosarcoma) in 15–20 % of the patients [95] or vascular malformations (angiosarcoma) in 3–5 % of the cases [96]. There is also a higher incidence of other malignant tumors, such as gliomas and ovarian and pancreatic tumors. A long-term follow-up is therefore mandatory [93].

16.6.6 Parkes Weber Syndrome

Parkes Weber syndrome combines a cutaneous capillary malformation with limb hemihypertrophy, congenital varicose veins, and arteriovenous malformations (a major difference with Klippel-Trenaunay syndrome). Numerous small periarticular arteriovenous fistulas or shunts can be detected in the affected limb [97]. Cardiac failure occurs in some patients with high blood flow vascular malformations.

Fig. 16.23 Maffuci syndrome. Plain radiograph of the hand. Multiple, expansible, well-defined and predominantly lytic lesions within the phalanges and metacarpals of the hand (*stars*) correspond to multiple enchondromas. The presence of phleboliths (*arrows*) within the soft tissue are highly suggestive of a Maffuci syndrome

16.6.7 Rendu-Osler-Weber Syndrome

Hereditary hemorrhagic telangiectasia (Rendu-Osler-Weber syndrome) is a genetic, autosomal dominant disorder. It is characterized by telangiectasia and arteriovenous malformations in specific locations, leading to epistaxis and hemorrhage into the digestive tract [98]. Lesions commonly involve the mucous membranes, skin, lungs, and genitourinary and gastrointestinal systems. At imaging, Rendu-Osler-Weber syndrome is characterized by arteriovenous malformations or fistulas in the lungs, liver, central nervous system, or other sites [99].

Key Points

1. Different terminology for designating vascular tumors may cause confusion. The revised WHO classification (2013) differs from ISSVA classification for benign lesions, but there is an overall agreement for intermediate and malignant lesions.
2. Infantile hemangioma is the most common vascular tumor in infancy.
3. Venous malformation represents the most common peripheral vascular malformation, followed by lymphatic malformation.
4. A number of familial or sporadic syndromes may be associated with vascular tumors and malformations.
5. The presence of phleboliths in a soft tissue mass on plain radiographs strongly suggests a venous malformation.
6. Ultrasound coupled with color Doppler US is the imaging modality of choice for the initial assessment and characterization of a lesion of presumed vascular origin.
7. MRI has a major role in defining the lesion's extent and therapy planning. Conventional angiography has been largely replaced by dynamic magnetic resonance (MR) angiography for the classification of vascular anomalies. Arteriography is only performed when MR features are equivocal or when embolization is considered.

References

1. Restrepo R (2013) Multimodality imaging of vascular anomalies. Pediatr Radiol 43(Suppl 1):S141–S154. doi:10.1007/s00247-012-2584-y
2. Dubois J, Alison M (2010) Vascular anomalies: what a radiologist needs to know. Pediatr Radiol 40:895–905. doi:10.1007/s00247-010-1621-y
3. Flors L, Leiva-Salinas C, Maged IM, Norton PT, Matsumoto AH, Angle JF, Hugo Bonatti M, Park AW, Ahmad EA, Bozlar U, Housseini AM, Huerta TE, Hagspiel KD (2011) MR imaging of soft-tissue vascular malformations: diagnosis, classification, and therapy follow-up. Radiogr Rev Publ Radiol Soc N Am Inc 31:1321–1340. doi:10.1148/rg.315105213, -1341
4. Cohen MM (2007) Hemangiomas: their uses and abuses. Am J Med Genet A 143A:235–240. doi:10.1002/ajmg.a.31571
5. Fletcher C, Bridge J, World Health Organization (2013) Classification of tumours of soft tissue and bone. IRAC, Lyon
6. ISSVA Classification of Vascular Anomalies ©2014 International Society for the Study of Vascular Anomalies Available at "issva.org/classification"
7. Enzinger F, Weiss S (1995) Benign tumors and tumor-like lesions of blood vessels. In: Enzinger FM, Weiss SW (eds) Soft tissue tumors, 3rd edn. Mosby, St. Louis, pp 579–626
8. Mulliken JB, Glowacki J (1982) Hemangiomas and vascular malformations in infants and children: a classification based on endothelial characteristics. Plast Reconstr Surg 69:412–422
9. Enjolras O, Wassef M, Chapot R (2007) Color atlas of vascular tumors and vascular malformations. Cambridge University Press, Cambridge
10. Navarro OM, Laffan EE, Ngan B-Y (2009) Pediatric soft-tissue tumors and pseudo-tumors: MR imaging features with pathologic correlation: part 1. Imaging approach, pseudotumors, vascular lesions, and adipocytic tumors. Radiogr Rev Publ Radiol Soc N Am Inc 29:887–906. doi:10.1148/rg.293085168
11. Cohen MM (2006) Vascular update: morphogenesis, tumors, malformations, and molecular dimensions. Am J Med Genet A 140:2013–2038. doi:10.1002/ajmg.a.31333
12. Mulliken J (1993) Cutaneous vascular anomalies. Semin Vasc Surg 6(4):204–218
13. Mulliken J (2006) Mulliken and Young's vascular anomalies: hemangiomas and malformations, 1st edn. Oxford University Press, Oxford
14. Berenguer B, Mulliken JB, Enjolras O, Boon LM, Wassef M, Josset P, Burrows PE, Perez-Atayde AR, Kozakewich HPW (2003) Rapidly involuting congenital hemangioma: clinical and histopathologic features. Pediatr Dev Pathol Off J Soc Pediatr Pathol Paediatr Pathol Soc 6:495–510
15. Moukaddam H, Pollak J, Haims AH (2009) MRI characteristics and classification of peripheral vascular malformations and tumors. Skeletal Radiol 38:535–547. doi:10.1007/s00256-008-0609-2
16. Kwon E-KM, Seefeldt M, Drolet BA (2013) Infantile hemangiomas: an update. Am J Clin Dermatol 14:111–123. doi:10.1007/s40257-013-0008-x
17. Dubois J, Rypens F (2009) Vascular anomalies. Ultrasound Clin 4:471–495
18. North PE, Waner M, Mizeracki A, Mrak RE, Nicholas R, Kincannon J, Suen JY, Mihm MC (2001) A unique microvascular phenotype shared by juvenile hemangiomas and human placenta. Arch Dermatol 137:559–570

19. Finn MC, Glowacki J, Mulliken JB (1983) Congenital vascular lesions: clinical application of a new classification. J Pediatr Surg 18:894–900
20. Degrugillier-Chopinet C, Bisdorff-Bresson A, Laurian C, Breviere G-M, Staumont D, Fayoux P, Lenica D, Gautier C (2011) Role of duplex Doppler for superficial "angiomas". J Mal Vasc 36:348–354. doi:10.1016/j.jmv.2011.08.003
21. Konez O, Burrows PE (2002) Magnetic resonance of vascular anomalies. Magn Reson Imaging Clin N Am 10(363–388):vii
22. Metry DW, Dowd CF, Barkovich AJ, Frieden IJ (2001) The many faces of PHACE syndrome. J Pediatr 139:117–123. doi:10.1067/mpd.2001.114880
23. Léauté-Labrèze C, Taïeb A (2008) Efficacy of beta-blockers in infantile capillary haemangiomas: the physiopathological significance and therapeutic consequences. Ann Dermatol Venereol 135:860–862. doi:10.1016/j.annder.2008.10.006
24. Gorincour G, Kokta V, Rypens F, Garel L, Powell J, Dubois J (2005) Imaging characteristics of two subtypes of congenital hemangiomas: rapidly involuting congenital hemangiomas and non-involuting congenital hemangiomas. Pediatr Radiol 35:1178–1185. doi:10.1007/s00247-005-1557-9
25. Nasseri E, Piram M, McCuaig CC, Kokta V, Dubois J, Powell J (2014) Partially involuting congenital hemangiomas: a report of 8 cases and review of the literature. J Am Acad Dermatol 70:75–79. doi:10.1016/j.jaad.2013.09.018
26. Lowe LH, Marchant TC, Rivard DC, Scherbel AJ (2012) Vascular malformations: classification and terminology the radiologist needs to know. Semin Roentgenol 47:106–117. doi:10.1053/j.ro.2011.11.002
27. Enjolras O, Soupre V, Picard A (2004) Anomalies vasculaires superficielles (« angiomes »). EMC Pédiatrie 2004:98-745-A-10
28. Kransdorf M, Murphey M (2006) Imaging of soft tissue tumors, 2nd edn. WB Saunders Company, Philadelphia
29. Park S-W, Kim H-J, Sung KJ, Lee JH, Park IS (2012) Kimura disease: CT and MR imaging findings. AJNR Am J Neuroradiol 33:784–788. doi:10.3174/ajnr.A2854
30. Lalaji TA, Haller JO, Burgess RJ (2001) A case of head and neck kaposiform hemangioendothelioma simulating a malignancy on imaging. Pediatr Radiol 31:876–878. doi:10.1007/s002470100009
31. Hermans DJJ, van Beynum IM, van der Vijver RJ, Kool LJS, de Blaauw I, van der Vleuten CJM (2011) Kaposiform hemangioendothelioma with Kasabach-Merritt syndrome: a new indication for propranolol treatment. J Pediatr Hematol Oncol 33:e171–e173. doi:10.1097/MPH.0b013e3182152e4e
32. Fahrtash F, McCahon E, Arbuckle S (2010) Successful treatment of kaposiform hemangioendothelioma and tufted angioma with vincristine. J Pediatr Hematol Oncol 32:506–510. doi:10.1097/MPH.0b013e3181e001a9
33. Restrepo CS, Ocazionez D (2011) Kaposi's sarcoma: imaging overview. Semin Ultrasound CT MR 32:456–469. doi:10.1053/j.sult.2011.03.007
34. Weiss SW, Enzinger FM (1982) Epithelioid hemangioendothelioma: a vascular tumor often mistaken for a carcinoma. Cancer 50:970–981
35. Bruegel M, Waldt S, Weirich G, Woertler K, Rummeny EJ (2006) Multifocal epithelioid hemangioendothelioma of the phalanges of the hand. Skeletal Radiol 35:787–792. doi:10.1007/s00256-005-0943-6
36. Nuthakki S, Fessell D, Lal N, Shirkhoda A, Irwin T, Irwin R (2007) Epithelioid hemangioendothelioma mimicking a nerve sheath tumor clinically and on MR imaging. Skeletal Radiol 36(Suppl 1):S58–S62. doi:10.1007/s00256-006-0197-y
37. El Demellawy D, Nasr A, Alowami S (2009) Epithelioid hemangioendothelioma of the temporal artery presenting as temporal arteritis: case report and literature review. Rare Tumors 1:e20. doi:10.4081/rt.2009.e20
38. Weiss S, Goldblum J, Enzinger F (2008) Enzinger and Weiss's soft tissue tumors. Mosby Elsevier, Philadelphia
39. Meis-Kindblom JM, Kindblom LG (1998) Angiosarcoma of soft tissue: a study of 80 cases. Am J Surg Pathol 22:683–697
40. Nakazono T, Kudo S, Matsuo Y, Matsubayashi R, Ehara S, Narisawa H, Yonemitsu N (2000) Angiosarcoma associated with chronic lymphedema (Stewart-Treves syndrome) of the leg: MR imaging. Skeletal Radiol 29:413–416
41. Rossi S, Fletcher CDM (2002) Angiosarcoma arising in hemangioma/vascular malformation: report of four cases and review of the literature. Am J Surg Pathol 26:1319–1329
42. Jackson IT, Carreño R, Potparic Z, Hussain K (1993) Hemangiomas, vascular malformations, and lymphovenous malformations: classification and methods of treatment. Plast Reconstr Surg 91:1216–1230
43. Dubois J, Soulez G, Oliva VL, Berthiaume MJ, Lapierre C, Therasse E (2001) Soft-tissue venous malformations in adult patients: imaging and therapeutic issues. Radiogr Rev Publ Radiol Soc N Am Inc 21:1519–1531. doi:10.1148/radiographics.21.6.g01nv031519
44. Fayad LM, Fayad L, Hazirolan T, Bluemke D, Mitchell S (2006) Vascular malformations in the extremities: emphasis on MR imaging features that guide treatment options. Skeletal Radiol 35:127–137. doi:10.1007/s00256-005-0057-1
45. Cahill AM, Nijs ELF (2011) Pediatric vascular malformations: pathophysiology, diagnosis, and the role of interventional radiology. Cardiovasc Intervent Radiol 34:691–704. doi:10.1007/s00270-011-0123-0
46. Bruder E, Alaggio R, Kozakewich HPW, Jundt G, Dehner LP, Coffin CM (2012) Vascular and perivascular lesions of skin and soft tissues in children and adolescents. Pediatr Dev Pathol Off J Soc Pediatr Pathol Paediatr Pathol Soc 15:26–61. doi:10.2350/11-11-1119-PB.1

47. Dompmartin A, Ballieux F, Thibon P, Lequerrec A, Hermans C, Clapuyt P, Barrellier M-T, Hammer F, Labbé D, Vikkula M, Boon LM (2009) Elevated D-dimer level in the differential diagnosis of venous malformations. Arch Dermatol 145:1239–1244. doi:10.1001/archdermatol.2009.296
48. Wassef M (2011) Vascular tumors and pseudotumors: introduction. Ann Pathol 31:410–412. doi:10.1016/j.annpat.2011.05.013
49. Goto T, Kojima T, Iijima T, Yokokura S, Kawano H, Yamamoto A, Matsuda K (2001) Soft-tissue haemangioma and periosteal new bone formation on the neighbouring bone. Arch Orthop Trauma Surg 121:549–553
50. Sung MS, Kang HS, Lee HG (1998) Regional bone changes in deep soft tissue hemangiomas: radiographic and MR features. Skeletal Radiol 27:205–210
51. Herborn CU, Goyen M, Lauenstein TC, Debatin JF, Ruehm SG, Kröger K (2003) Comprehensive time-resolved MRI of peripheral vascular malformations. AJR Am J Roentgenol 181:729–735. doi:10.2214/ajr.181.3.1810729
52. Ohgiya Y, Hashimoto T, Gokan T, Watanabe S, Kuroda M, Hirose M, Matsui S, Nobusawa H, Kitanosono T, Munechika H (2005) Dynamic MRI for distinguishing high-flow from low-flow peripheral vascular malformations. AJR Am J Roentgenol 185:1131–1137. doi:10.2214/AJR.04.1508
53. Buetow PC, Kransdorf MJ, Moser RP, Jelinek JS, Berrey BH (1990) Radiologic appearance of intramuscular hemangioma with emphasis on MR imaging. AJR Am J Roentgenol 154:563–567. doi:10.2214/ajr.154.3.2154914
54. Redondo P, Aguado L, Martínez-Cuesta A (2011) Diagnosis and management of extensive vascular malformations of the lower limb: Part I. Clinical diagnosis. J Am Acad Dermatol 65:893–906. doi:10.1016/j.jaad.2010.12.047
55. Enjolras O, Ciabrini D, Mazoyer E, Laurian C, Herbreteau D (1997) Extensive pure venous malformations in the upper or lower limb: a review of 27 cases. J Am Acad Dermatol 36:219–225
56. Dompmartin A, Vikkula M, Boon LM (2010) Venous malformation: update on aetiopathogenesis, diagnosis and management. Phlebol Venous Forum R Soc Med 25:224–235. doi:10.1258/phleb.2009.009041
57. Brevière G, Degrugillier-Chopinet C, Bisdorff-Bresson A (2011) Anomalies vasculaires superficielle. EMC Cardiologie 6:1–21
58. Sidhu MK, Perkins JA, Shaw DWW, Bittles MA, Andrews RT (2005) Ultrasound-guided endovenous diode laser in the treatment of congenital venous malformations: preliminary experience. J Vasc Interv Radiol 16:879–884. doi:10.1097/01.RVI.0000163005.50283.62
59. Marler JJ, Mulliken JB (2005) Current management of hemangiomas and vascular malformations. Clin Plast Surg 32(99–116):ix. doi:10.1016/j.cps.2004.10.001
60. Cahill AM, Nijs E, Ballah D, Rabinowitz D, Thompson L, Rintoul N, Hedrick H, Jacobs I, Low D (2011) Percutaneous sclerotherapy in neonatal and infant head and neck lymphatic malformations: a single center experience. J Pediatr Surg 46:2083–2095. doi:10.1016/j.jpedsurg.2011.07.004
61. Chen EY, Hostikka SL, Oliaei S, Duke W, Schwartz SM, Perkins JA (2009) Similar histologic features and immunohistochemical staining in microcystic and macrocystic lymphatic malformations. Lymphat Res Biol 7:75–80. doi:10.1089/lrb.2009.0003
62. Blei F (2008) Congenital lymphatic malformations. Ann N Y Acad Sci 1131:185–194. doi:10.1196/annals.1413.016
63. Jeltsch M, Tammela T, Alitalo K, Wilting J (2003) Genesis and pathogenesis of lymphatic vessels. Cell Tissue Res 314:69–84. doi:10.1007/s00441-003-0777-2
64. Hogeling M, Adams S, Law J, Wargon O (2011) Lymphatic malformations: clinical course and management in 64 cases. Australas J Dermatol 52:186–190. doi:10.1111/j.1440-0960.2011.00777.x
65. Koeller KK, Alamo L, Adair CF, Smirniotopoulos JG (1999) Congenital cystic masses of the neck: radiologic-pathologic correlation. Radiogr Rev Publ Radiol Soc N Am Inc 19:121–146. doi:10.1148/radiographics.19.1.g99ja06121, -153
66. Zadvinskis DP, Benson MT, Kerr HH, Mancuso AA, Cacciarelli AA, Madrazo BL, Mafee MF, Dalen K (1992) Congenital malformations of the cervicothoracic lymphatic system: embryology and pathogenesis. Radiogr Rev Publ Radiol Soc N Am Inc 12:1175–1189. doi:10.1148/radiographics.12.6.1439020
67. Nozaki T, Nosaka S, Miyazaki O, Makidono A, Yamamoto A, Niwa T, Tsutsumi Y, Aida N, Masaki H, Saida Y (2013) Syndromes associated with vascular tumors and malformations: a pictorial review. Radiogr Rev Publ Radiol Soc N Am Inc 33:175–195. doi:10.1148/rg.331125052
68. Ernemann U, Kramer U, Miller S, Bisdas S, Rebmann H, Breuninger H, Zwick C, Hoffmann J (2010) Current concepts in the classification, diagnosis and treatment of vascular anomalies. Eur J Radiol 75:2–11. doi:10.1016/j.ejrad.2010.04.009
69. Kayal JD, Hampton RW, Sheehan DJ, Washington CV (2001) Malignant glomus tumor: a case report and review of the literature. Dermatol Surg Off Publ Am Soc Dermatol Surg Al 27:837–840
70. Schiefer TK, Parker WL, Anakwenze OA, Amadio PC, Inwards CY, Spinner RJ (2006) Extradigital glomus tumors: a 20-year experience. Mayo Clin Proc 81:1337–1344. doi:10.4065/81.10.1337
71. Drapé JL, Idy-Peretti I, Goettmann S, Wolfram-Gabel R, Dion E, Grossin M, Benacerraf R, Guérin-Surville H, Bittoun J (1995) Subungual glomus tumors: evaluation with MR imaging. Radiology 195:507–515. doi:10.1148/radiology.195.2.7724775
72. Van Geertruyden J, Lorea P, Goldschmidt D, de Fontaine S, Schuind F, Kinnen L, Ledoux P, Moermans JP (1996) Glomus tumours of the hand. A retrospective study of 51 cases. J Hand Surg Br Edinb Scotl 21:257–260

73. Lee D-W, Yang J-H, Chang S, Won C-H, Lee M-W, Choi J-H, Moon K-C (2011) Clinical and pathological characteristics of extradigital and digital glomus tumours: a retrospective comparative study. J Eur Acad Dermatol Venereol 25:1392–1397. doi:10.1111/j.1468-3083.2011.03979.x
74. Lee S, Le H, Munk P, Malfair D, Lee CH, Clarkson P (2010) Glomus tumour in the forearm: a case report and review of MRI findings. JBR-BTR 93:292–295
75. Baek HJ, Lee SJ, Cho KH, Choo HJ, Lee SM, Lee YH, Suh KJ, Moon TY, Cha JG, Yi JH, Kim MH, Jung S-J, Choi JH (2010) Subungual tumors: clinicopathologic correlation with US and MR imaging findings. Radiogr Rev Publ Radiol Soc N Am Inc 30:1621–1636. doi:10.1148/rg.306105514
76. González-Llanos F, López-Barea F, Isla A, Fernández-Prieto A, Zubillaga A, Alvarez F (2000) Periosteal glomus tumor of the femur: a case report. Clin Orthop 380:199–203
77. Netscher DT, Aburto J, Koepplinger M (2012) Subungual glomus tumor. J Hand Surg 37:821–823. doi:10.1016/j.jhsa.2011.10.026; quiz 824
78. Theumann NH, Goettmann S, Le Viet D, Resnick D, Chung CB, Bittoun J, Chevrot A, Drapé J-L (2002) Recurrent glomus tumors of fingertips: MR imaging evaluation. Radiology 223:143–151. doi:10.1148/radiol.2231010977
79. Glazebrook KN, Laundre BJ, Schiefer TK, Inwards CY (2011) Imaging features of glomus tumors. Skeletal Radiol 40:855–862. doi:10.1007/s00256-010-1067-1
80. Van Ruyssevelt CEA, Vranckx P (2004) Subungual glomus tumor: emphasis on MR angiography. AJR Am J Roentgenol 182:263–264. doi:10.2214/ajr.182.1.1820263
81. Devaney K, Vinh TN, Sweet DE (1993) Synovial hemangioma: a report of 20 cases with differential diagnostic considerations. Hum Pathol 24:737–745
82. Greenspan A, Azouz EM, Matthews J, Décarie JC (1995) Synovial hemangioma: imaging features in eight histologically proven cases, review of the literature, and differential diagnosis. Skeletal Radiol 24:583–590
83. Llauger J, Monill JM, Palmer J, Clotet M (1995) Synovial hemangioma of the knee: MRI findings in two cases. Skeletal Radiol 24:579–581
84. Narváez JA, Narváez J, Aguilera C, De Lama E, Portabella F (2001) MR imaging of synovial tumors and tumor-like lesions. Eur Radiol 11:2549–2560. doi:10.1007/s003300000759
85. Garzon MC, Huang JT, Enjolras O, Frieden IJ (2007) Vascular malformations. Part II: associated syndromes. J Am Acad Dermatol 56:541–564. doi:10.1016/j.jaad.2006.05.066
86. Elsayes KM, Menias CO, Dillman JR, Platt JF, Willatt JM, Heiken JP (2008) Vascular malformation and hemangiomatosis syndromes: spectrum of imaging manifestations. AJR Am J Roentgenol 190:1291–1299. doi:10.2214/AJR.07.2779
87. Oza VS, Wang E, Berenstein A, Waner M, Lefton D, Wells J, Blei F (2008) PHACES association: a neuroradiologic review of 17 patients. AJNR Am J Neuroradiol 29:807–813. doi:10.3174/ajnr.A0937
88. Drolet BA, Chamlin SL, Garzon MC, Adams D, Baselga E, Haggstrom AN, Holland KE, Horii KA, Juern A, Lucky AW, Mancini AJ, McCuaig C, Metry DW, Morel KD, Newell BD, Nopper AJ, Powell J, Frieden IJ (2010) Prospective study of spinal anomalies in children with infantile hemangiomas of the lumbosacral skin. J Pediatr 157:789–794. doi:10.1016/j.jpeds.2010.07.054
89. Stockman A, Boralevi F, Taïeb A, Léauté-Labrèze C (2007) SACRAL syndrome: spinal dysraphism, anogenital, cutaneous, renal and urologic anomalies, associated with an angioma of lumbosacral localization. Dermatol Basel Switz 214:40–45. doi:10.1159/000096911
90. Jacob AG, Driscoll DJ, Shaughnessy WJ, Stanson AW, Clay RP, Gloviczki P (1998) Klippel-Trénaunay syndrome: spectrum and management. Mayo Clin Proc 73:28–36. doi:10.1016/S0025-6196(11)63615-X
91. McGrory BJ, Amadio PC, Dobyns JH, Stickler GB, Unni KK (1991) Anomalies of the fingers and toes associated with Klippel-Trenaunay syndrome. J Bone Joint Surg Am 73:1537–1546
92. Kanterman RY, Witt PD, Hsieh PS, Picus D (1996) Klippel-Trenaunay syndrome: imaging findings and percutaneous intervention. AJR Am J Roentgenol 167:989–995. doi:10.2214/ajr.167.4.8819399
93. Zwenneke Flach H, Ginai AZ, Wolter Oosterhuis J (2001) Best cases from the AFIP. Maffucci syndrome: radiologic and pathologic findings. Armed Forces Institutes of Pathology. Radiogr Rev Publ Radiol Soc N Am Inc 21:1311–1316. doi:10.1148/radiographics.21.5.g01se301311
94. Unger EC, Kessler HB, Kowalyshyn MJ, Lackman RD, Morea GT (1988) MR imaging of Maffucci syndrome. AJR Am J Roentgenol 150:351–353. doi:10.2214/ajr.150.2.351
95. Schwartz HS, Zimmerman NB, Simon MA, Wroble RR, Millar EA, Bonfiglio M (1987) The malignant potential of enchondromatosis. J Bone Joint Surg Am 69:269–274
96. Bach AD, Walgenbach KJ, Horch RE (2000) Hemangiosarcoma of the left hand in a patient with the rare combination of Maffucci's and Stewart Treves syndrome. Vasa 29:71–73. doi:10.1024/0301-1526.29.1.71
97. Ziyeh S, Spreer J, Rössler J, Strecker R, Hochmuth A, Schumacher M, Klisch J (2004) Parkes Weber or Klippel-Trenaunay syndrome? Non-invasive diagnosis with MR projection angiography. Eur Radiol 14:2025–2029. doi:10.1007/s00330-004-2274-8
98. McDonald J, Bayrak-Toydemir P, Pyeritz RE (2011) Hereditary hemorrhagic telangiectasia: an overview of diagnosis, management, and pathogenesis. Genet Med Off J Am Coll Med Genet 13:607–616. doi:10.1097/GIM.0b013e3182136d32
99. Jaskolka J, Wu L, Chan RP, Faughnan ME (2004) Imaging of hereditary hemorrhagic telangiectasia. AJR Am J Roentgenol 183:307–314. doi:10.2214/ajr.183.2.1830307

Nerve Sheath Tumors

17

Nicolas De Vos, Filip M. Vanhoenacker,
Koenraad L. Verstraete, and Paul M. Parizel

Contents

17.1 **Introduction** 393

17.2 **Benign Nerve Sheath Tumors** 394
17.2.1 Schwannomas 394
17.2.2 Neurofibromas 405
17.2.3 Other Benign Nerve Sheath Tumors 408

17.3 **Malignant Peripheral Nerve Sheath Tumors** 412
17.3.1 Epidemiology 412
17.3.2 Topography 412
17.3.3 Histology 412
17.3.4 Clinical Presentation 413
17.3.5 Imaging Characteristics 413

17.4 **Neurofibromatoses** 417
17.4.1 Neurofibromatosis Type 1 417
17.4.2 Neurofibromatosis Type 2 418
17.4.3 Schwannomatosis 419

References 421

N. De Vos (✉) • K.L. Verstraete
Radiology Department, Ghent University, Ghent, Belgium
e-mail: nicdvos.devos@ugent.be

F.M. Vanhoenacker
Radiology Department, Ghent University, Ghent, Belgium

Radiology Department, AZ Sint-Maarten, Duffel-Mechelen, Mechelen, Belgium

Radiology Department, Antwerp University, Antwerpen, Belgium

P.M. Parizel
Radiology Department, Antwerp University, Antwerpen, Belgium

17.1 Introduction

A peripheral nerve is a rope-shaped organ with a specific concentric organization designed to guide, protect, and nourish the neuronal fibers within it. The main structure of a peripheral nerve is the axon, which is a long extension of the neuronal cell body specialized in transporting nerve impulses. Each axon is surrounded by Schwann cells, which wrap in multiple layers to form the protective myelin sheath. A layer of loose connective tissue, the endoneurium, surrounds each axon and its Schwann cells, forming a nerve fiber. Multiple nerve fibers are enclosed in robust connective tissue, the perineurium, to form a nerve fascicle. All nerve fascicles are surrounded by the epineurium, forming a peripheral nerve [25] (Fig. 17.1).

Nerve sheath tumors are neoplasms composed of cells showing nerve sheath differentiation [74]. They represent 10–12 % of all soft tissue neoplasms [47]. The fourth edition of the *WHO Classification of Tumors of Soft Tissue and Bone*, published in 2013, now incorporates a chapter specifically dedicated to nerve sheath tumors [32]. Some of these tumors were previously classified under "Tumors of the Nervous System" and "Tumors of the Skin" [31, 43]. Consequently, the updated WHO classification includes several new benign and malignant nerve sheath tumor types (Table 17.1). Morton's fibroma (neuroma) and traumatic neuroma will be discussed separately since these tumors do not belong to the group of nerve sheath tumors (Chap. 24).

© Springer International Publishing AG 2017

F.M. Vanhoenacker et al. (eds.), *Imaging of Soft Tissue Tumors*, DOI 10.1007/978-3-319-46679-8_17

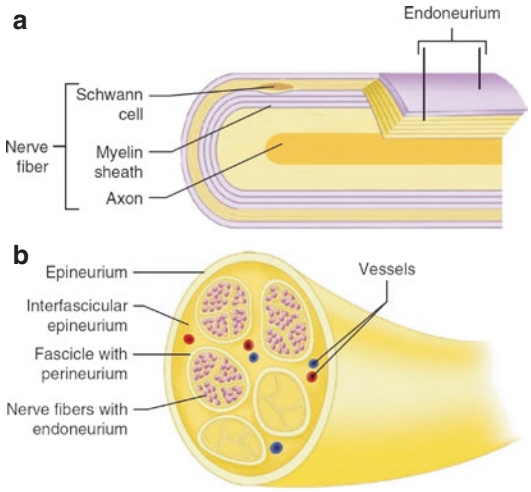

Fig. 17.1 (**a**, **b**) Nerve sheath architecture: (**a**) components of a nerve fiber surrounded by endoneurium. (**b**) Nerve trunk with five fascicles in group arrangement (Source: Penkert et al. [104])

Table 17.1 2013 WHO classification of nerve sheath tumors

Benign
Schwannoma (including variants)
Neurofibroma (including variants)
Perineurioma
Granular cell tumor
Hybrid nerve sheath tumor
Benign triton tumor
Dermal nerve sheath myxoma
Solitary circumscribed neuroma
Ectopic meningioma
Nasal glial heterotopia
Malignant
Malignant peripheral nerve sheath tumor
Epithelioid malignant nerve sheath tumor
Malignant triton tumor
Malignant granular cell tumor
Ectomesenchymoma

17.2 Benign Nerve Sheath Tumors

17.2.1 Schwannomas

17.2.1.1 Epidemiology

Schwannomas represent approximately 5 % of all benign soft tissue neoplasms [47]. They can occur at all ages, though they are uncommon in children. While most literature data indicate that schwannomas are most prevalent between the ages of 20 and 50, others have observed a bimodal age distribution with peak incidences in the third and seventh decades [62]. Men and women are equally affected. Schwannomas associated with neurocutaneous syndromes tend to occur in younger patients [24].

17.2.1.2 Topography

Schwannomas most commonly involve the major nerve trunks of the head, neck, and limbs. The flexor surfaces of the extremities are more frequently affected, especially near the elbow, wrist, and knee [24, 62, 76]. Consequently, the most common topographical locations of schwannomas include the spinal roots and cervical plexus and the vagus, peroneal, and ulnar nerves. Deeply situated schwannomas are predominantly found in the posterior mediastinum and the retroperitoneum [24, 62]. Relatively few schwannomas appear on the trunk, which contrasts with the distribution of neurofibromas in neurofibromatosis type 1 (NF1). Other sites of involvement include the scalp and the hands; the feet are usually spared. Less frequently, schwannomas have been recorded in the tongue, palate, and larynx.

17.2.1.3 Histology

General Histologic Features of Schwannomas

Schwannomas are benign, slowly growing neoplasms. They originate in a nerve and are composed exclusively of Schwann cells embedded in a collagenous matrix [38, 62]. In general, they are firm, circumscribed, and encapsulated by epineurium. Unlike neurofibromas, which incorporate axons, schwannomas grow eccentrically, displacing normal elements of the nerve to one side [22]. This implies that surgical excision can usually spare the parent nerve because schwannomas are separable from the underlying nerve fibers [48].

Macroscopically, the cut surface is relatively homogeneous, tan or gray, with irregular yellow areas and cysts, particularly in large tumors. Less often schwannomas can be (partially) hemor-

rhagic [38]. Small schwannomas tend to be spheroid, whereas larger tumors can be ovoid, sausage-shaped, or irregularly lobulated [76].

Microscopically, two types of tissue can be distinguished in schwannomas: Antoni A and B [62]. The *Antoni A* tissue is composed of compactly arranged cells which are often aligned in rows and separated by clear hyaline bands, a characteristic pattern called Verocay bodies [98]. Commonly, but not invariably, a part of, or all of, a schwannoma has a less cellular *Antoni B* pattern in which the tumor cells are separated by a finely honeycombed eosinophilic matrix [99].

Vessels in schwannomas are usually prominent [38] and are liable to spontaneous thrombosis with consequent necrosis, and sometimes hemorrhage, in the adjacent areas. The rich vascular supply of schwannomas is reflected in the often intense enhancement of these tumors on imaging studies [76].

The histologic features of schwannomas may reflect their occasional inhomogeneous appearance on computed tomography (CT) or magnetic resonance imaging (MRI) examinations and can be summarized as follows [76]:

1. Areas of decreased cellularity (Antoni B) adjacent to areas of increased cellularity (Antoni A)
2. Cystic degeneration due to vascular thrombosis and subsequent necrosis
3. Xanthomatous regions, containing aggregates of lipid-laden (foam) cells

Special Histologic Types of Schwannomas

Histologically, several variants of benign schwannoma can be distinguished.

Cellular schwannomas have a predominantly cellular growth but no Verocay bodies and are almost exclusively composed of Antoni A areas [62]. They appear circumscribed, if not encapsulated. They typically occur in middle-aged women and are more frequently found in deep structures, e.g., the retroperitoneum and posterior mediastinum [24]. Cellular schwannomas can cause erosion of bone and recur locally. Despite their increased cellularity, malignant transformation does not occur [34, 97].

Ancient schwannomas are long-standing schwannomas exhibiting degenerative changes including calcification, hyalinization, relative loss of Antoni A areas, and cystic cavitation [76]. Given the heterogeneity of these neoplasms and the fact that tumor nuclei may appear enlarged and hyperchromatic, differentiation with malignant soft tissue tumors may be difficult [41].

(Psammomatous) Melanotic schwannomas are characterized by a strong melanocytic differentiation of the Schwann cells. Schwann cells and melanocytes share a common precursor stem cell derived from the neural crest, hence this differentiation [44]. Melanotic schwannomas have a predilection for spinal nerve roots and commonly arise near the midline. It has been suggested that they display malignant behavior with local recurrence after surgery [24]. Over 50 % of patients suffering from melanotic schwannomas develop Carney's syndrome, consisting of myxomas, spotty pigmentation, and endocrine overactivity producing Cushing's syndrome [74, 75].

Plexiform (multinodular) schwannomas constitute 5 % of all schwannomas. The multinodular or plexiform pattern of growth may or may not be apparent macroscopically [24]. Only 4 % of all cases of this form reported in the literature occurred in patients with NF1; therefore, it is not to be considered associated with NF1 [33, 62, 101]. Plexiform schwannomas arise in the dermis or subcutaneous tissues and occur predominantly in young adults, without sex predilection [33, 49]. Although they can display focal nuclear pleomorphism and increased cellularity, cellular schwannomas appear to be benign lesion [76, 101].

Microcystic (reticular) schwannomas represent a new schwannoma type, recently reported in ten patients. Microcystic schwannomas are preferentially located in the gastrointestinal submucosa or subcutaneous tissue [56].

17.2.1.4 Clinical Presentation

Small schwannomas are usually asymptomatic. Pain, paresthesias, muscle atrophy, or other symptoms can occur when the tumor reaches sufficient size to compress the involved nerve or adjacent structures. On physical examination,

they can be moved from side to side, but not along the long axis of the nerve [38].

17.2.1.5 Imaging Characteristics

Plain Radiography

Schwannomas are usually not seen on plain radiography, unless they are very large [7]. Sometimes they exhibit a slightly lower attenuation of the X-ray beam than muscle (Fig. 17.2). Pressure erosions on bone can be seen as widening of the intervertebral foramina or rib notching, especially in cellular schwannomas (Figs. 17.3 and 17.4) [76]. A posterior mediastinal mass on a chest radiograph should suggest the possibility of a neurogenic tumor, for they account for 30 % of posterior mediastinal mass lesions.

Fig. 17.2 (**a**, **b**) Schwannoma of the right hand in a 73-year-old man: (**a**) plain radiograph of the right hand showing a soft tissue mass between the first and second metacarpal. (**b**) Axial T1-weighted image (T1-WI) after gadolinium contrast injection shows a well-circumscribed soft tissue tumor with subtle peripheral enhancement

Ultrasound

On ultrasound, schwannomas are usually seen as solid, ovoid, hypoechoic masses with posterior acoustic enhancement. They are often surrounded by a hyperechoic capsule. Schwannomas are oriented along the long axis of the nerve with proximal and distal taillike formations (Fig. 17.5) They are usually eccentrically located in relation to the nerve axis and do not infiltrate adjacent tissue [7, 36, 73, 83, 92]. Ancient schwannomas show marked degenerative changes, such as internal bleeding, fibrosis, calcification, and cystic necrotic alterations (Fig. 17.6) [69]. In large lesions, impressive displacement of nerve fascicles and increased internal vascularization can be seen, making it sometimes difficult to rule out malignancy.

Computed Tomography

On unenhanced CT scans, schwannomas are seen as well-circumscribed homogeneous lesions. They are hypo- to isodense relative to muscle. However, an inhomogeneous tumor appearance with low-density areas is frequently seen in larger tumors, reflecting the histologic diversity [19, 49].

On contrast-enhanced CT scans, most schwannomas become iso- or hyperdense to muscle (Fig. 17.7). Large schwannomas typically contain non-enhancing cystic or necrotic areas [19, 49].

Magnetic Resonance Imaging

Most peripheral nerve sheath tumors (PNSTs) share some common MR imaging characteristics (Table 17.2). However, none of these characteristics are pathognomonic for PNSTs [82].

On T1-weighted images (T1-WI), most PNSTs, including schwannomas, display slightly higher signal intensity than muscle, which makes them sometimes difficult to detect. On proton density-WI, they are hyperintense to muscle. On T2-WI, signal intensity is markedly increased,

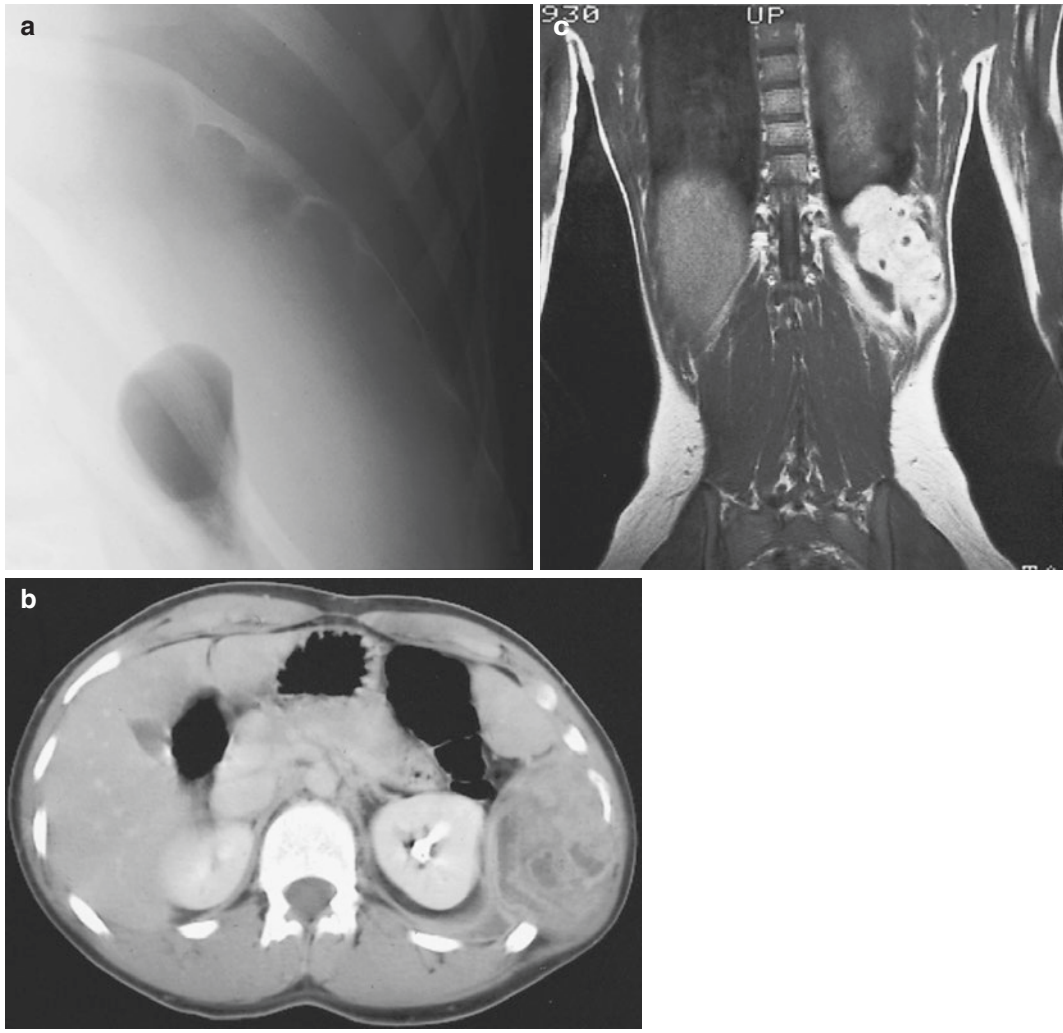

Fig. 17.3 (**a**–**c**) Schwannoma of the chest wall in a 16-year-old boy: (**a**) plain radiograph of the rib cage shows irregular scalloping (notching) of the inferior border of the left tenth rib and widening of the intercostal space. (**b**) CT scan after iodinated contrast injection shows a large, irregularly enhancing tumor with necrotic or cystic non-enhancing cavities. (**c**) Coronal T1-WI after gadolinium contrast injection shows a markedly enhancing tumor subjacent to the tenth rib

resulting in a sharp contrast between the tumor and adjacent fat and muscle (Fig. 17.8) [1, 3, 15, 42, 57, 71, 84, 100].

Most nerve sheath tumors are located in the proximity of a major nerve. Due to growth along the course of the affected nerve, nerve sheath tumors typically have a fusiform shape. Oriented along the long axis of the nerve sheath tumor, the involved nerve can be seen entering and/or exiting the neoplasm, resembling a tail coming off the tumor, hence the name of this imaging feature: the *tail sign*. This sign has proven to be the most important imaging feature that should always suggest the diagnosis of neurogenic neoplasm. The tail sign is usually easy to detect in lesions affecting large, deep nerves, but is often difficult or impossible to assess in superficial or in small lesions (Figs. 17.9, 17.10, 17.11, and 17.12) [1, 47, 57, 65, 71, 84].

Since each neurovascular bundle is normally surrounded by fat, benign masses originating in the intermuscular space around the neurovascular

bundle usually maintain a rim of fat about them as they slowly enlarge and remodel the surrounding fat plane. This rim of fat separates the tumor from the surrounding muscle tissue and appears more prominent at the tapering margins of the neoplasm. Known as the *split-fat sign*, this configuration suggests a tumoral origin in the intermuscular space about the neurovascular bundle, among which PNSTs are most frequent [54]. The split-fat sign is best appreciated on T1-WI as a hyperintense rim of fat. It is most seen in benign PNSTs and lesions of large nerves (Figs. 17.11 and 17.12). In malignant PNSTs, the rim of fat is typically incomplete, reflecting their infiltrative growth pattern [1, 54, 55, 57, 65, 67, 71, 103].

The *target sign* consists of low-to-intermediate signal intensity centrally with a ring of high signal intensity peripherally on T2-WI. Pathologically, this corresponds to fibrous tissue centrally and more myxoid tissue peripherally. Rarely, a reverse pattern of target appearance on T1-WI is seen, with central hyperintensity and peripheral

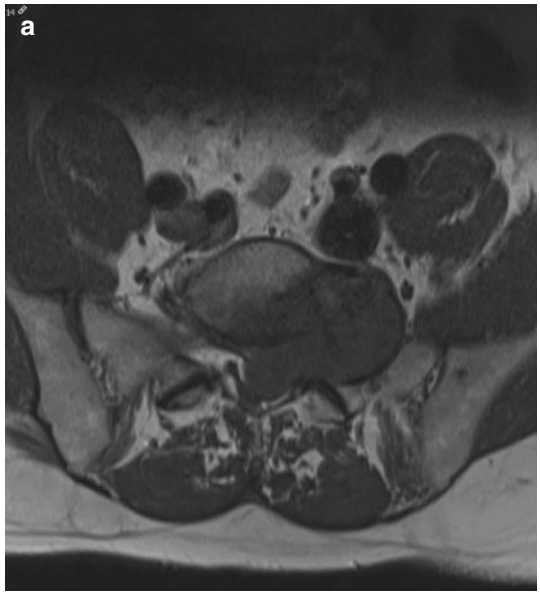

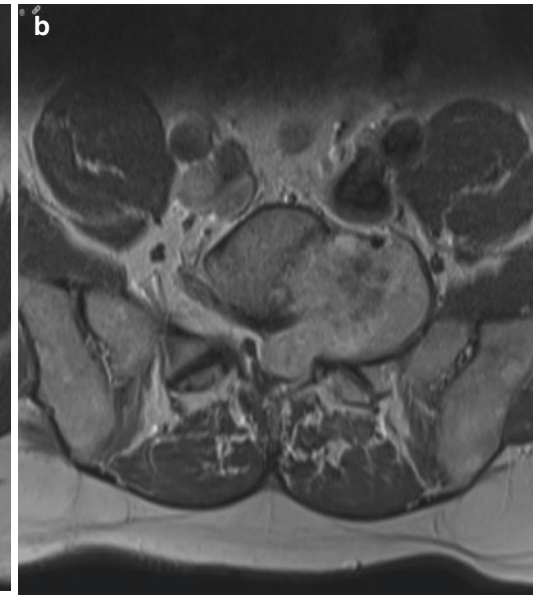

Fig. 17.4 (**a**, **b**) Schwannoma of the left intervertebral foramen L5–S1 in a 53-year-old male: (**a**) axial T1-WI shows a dumbbell-shaped lesion which causes erosion of the body of L5 and the left facet joint, resulting in widening of the left intervertebral foramen. (**b**) On the axial T1-WI after gadolinium contrast injection, the schwannoma shows diffuse enhancement

Fig. 17.5 (**a**–**e**) Cellular schwannoma of the left upper leg in a 52-year-old male: (**a**) axial T1-WI shows an isointense mass in the biceps femoris muscle which is partially surrounded by a thin fat rim (split-fat sign, *arrows*). (**b**) On coronal FS T2-WI, the lesion is hyperintense, displaying a fusiform shape with an entering and exiting nerve (tail sign, *arrows*). (**c**) Axial diffusion-weighted image (DWI) shows high signal intensity, which is indicative of restricted diffusion. (**d**) On the axial apparent diffusion coefficient (ADC) map, the lesion displays low signal intensity, confirming diffusion restriction. Although diffusion restriction may suggest a malignant peripheral nerve sheath tumors (MPNSTs), it can also be seen in benign cellular schwannomas. (**e**) Longitudinal ultrasound shows a hypoechoic well-circumscribed mass and also illustrates the tail sign (*white arrows* indicating entering and exiting nerve) and hyperechogenic rim of fat separating the tumor from the surrounding muscle

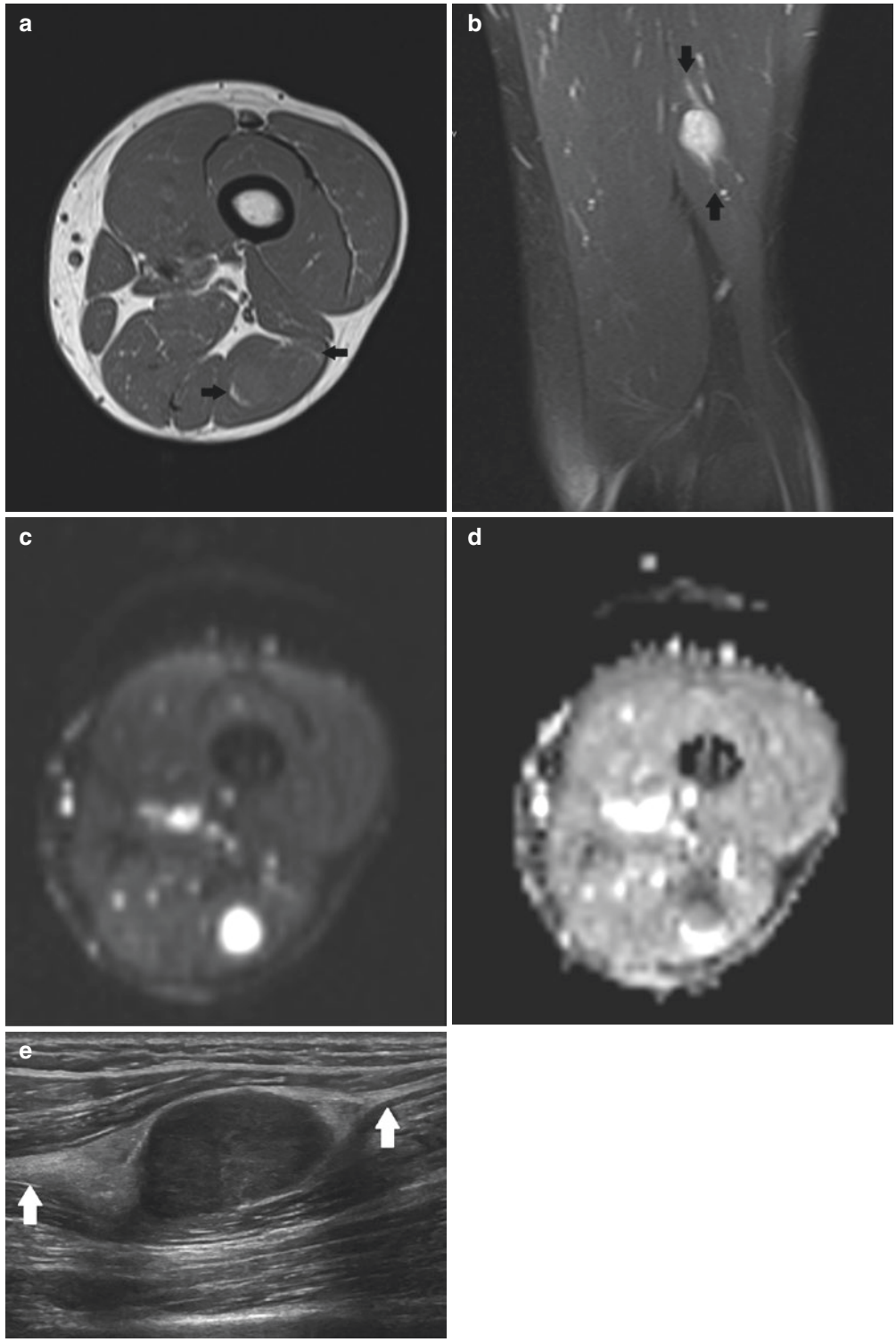
a
b
c
d
e

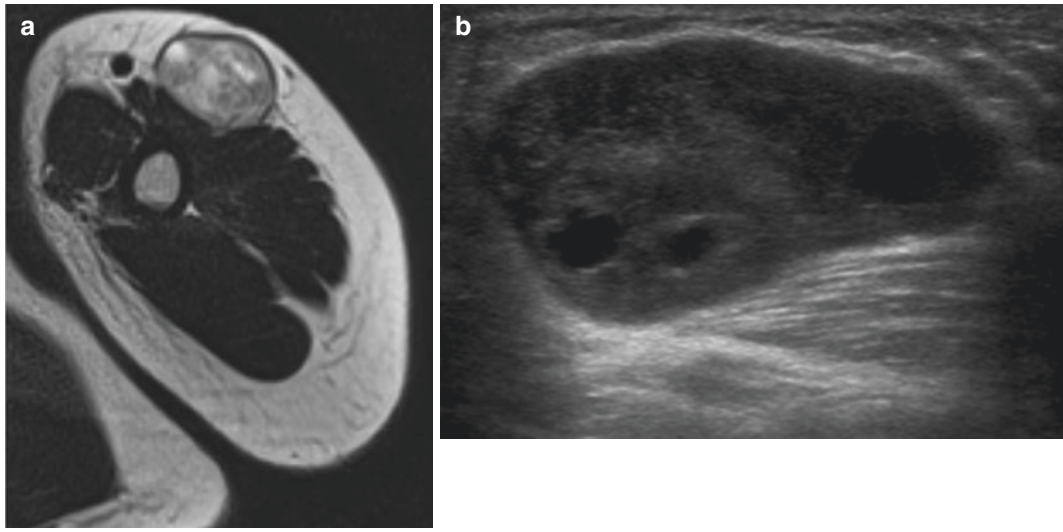

Fig. 17.6 (**a**, **b**) Ancient schwannoma of the left upper arm in a 24-year-old male: (**a**) axial T2-WI shows a heterogeneous mass of intermediate signal intensity and some well-circumscribed zones of high signal intensity. (**b**) Ultrasound shows a hypoechoic mass with intralesional nodular cystic components

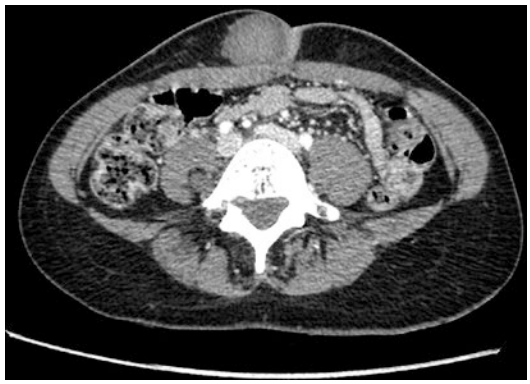

Fig. 17.7 Nerve sheath tumor in the abdominal wall in a 31-year-old female with neurofibromatosis type 2 (NF2): axial contrast-enhanced CT-image shows a well-circumscribed lesion which enhances slightly heterogeneous, displaying a density similar to muscle

Table 17.2 Imaging findings suggestive of neurogenic tumors

Location in the region of a nerve
Fusiform shape
Tail sign: entering and/or exiting nerve
Split-fat sign (T1-weighted images)
Target sign (T2-weighted images)
Fascicular sign (T2-weighted images)
Muscle atrophy/fatty replacement/edema

hypointensity. Cutaneous PNSTs are less likely than deeper lesions to demonstrate the target sign. Initially considered pathognomonic for neurofibromas, the target sign has also been observed in schwannomas, and, rarely, malignant PNSTs (Fig. 17.8) [42, 47, 55, 57, 65, 71, 92].

The *fascicular sign* represents multiple small ringlike structures with low signal intensity on T2-WI, corresponding to the fascicular bundles seen in neurogenic neoplasms. The fascicular sign is best appreciated if the tumor is surrounded by fat. It is slightly more common in schwannomas than in neurofibromas, while it is not seen in malignant PNSTs (Fig. 17.11) [3, 42, 54, 55, 57].

Nerve sheath tumors may induce muscle denervation changes, including increased fat content or decreased muscle size. These changes may be quite subtle and may require comparison with the normal contralateral side. Muscle denervation changes are best seen on T1-WI. Other abnormalities of the supplied muscles, including edematous appearance, may also be seen on T2-WI [1, 84].

The following paragraph and Table 17.4 highlight the most useful MR imaging features in the differentiation between neurofibromas and schwannomas (Table 17.4).

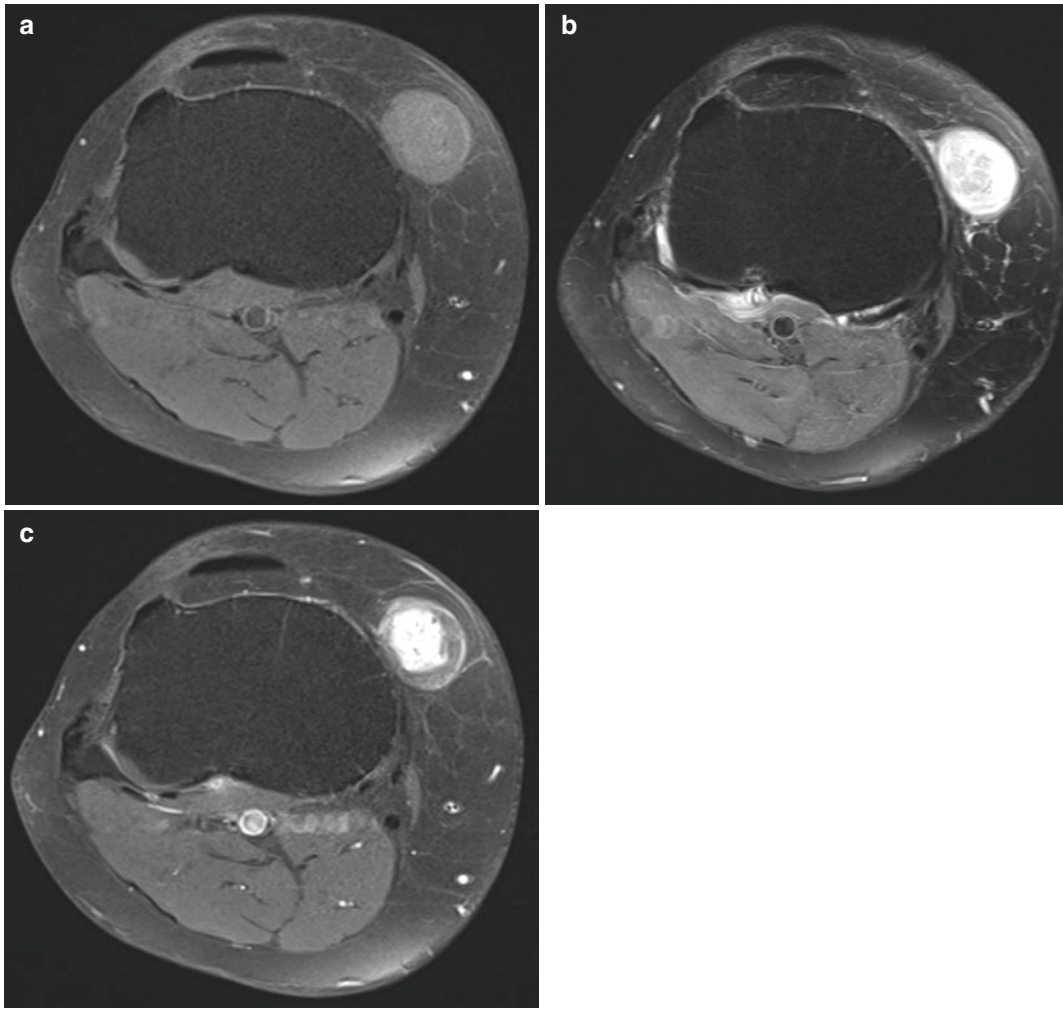

Fig. 17.8 (**a**–**c**) Schwannoma of the anteromedial side of the right knee in a 58-year-old male: (**a**) axial FS T1-WI shows that the lesion is slightly more intense than subcutaneous fat. (**b**) On axial FS T2-WI, a target appearance with central hypointensity and a peripheral high signal intensity rim can be seen (target sign). (**c**) Axial FS T1-WI after gadolinium contrast shows central enhancement. Although the target sign and central enhancement are more commonly seen in neurofibromas, there is a lot of overlap and schwannomas may have the same signal characteristics and contrast enhancement pattern

The fascicular sign is more frequently seen in schwannomas, while the target sign is more suggestive of neurofibromas. Schwannomas tend to eccentrically displace the affected nerve, while in neurofibromas, the tumor is intimately intermixed with the nerve fascicles [36, 57, 65, 92]. However, in many situations, this distinction is not possible because both lesions often have a deep location within the epineurium and similar imaging characteristics relative to the parent nerve [42]. This parameter seems to be more reliable for discrimination between lesions in larger peripheral nerves. For all practical purposes, however, visualization of a nerve eccentrically entering a mass must be considered strongly suggestive of a schwannoma [92].

Schwannomas are more frequently encapsulated by epineurium than neurofibromas and malignant PNSTs. Encapsulation is visualized on MRI as a low signal intensity rim surrounding the tumor on T1- and T2-weighed images [65, 71]. In

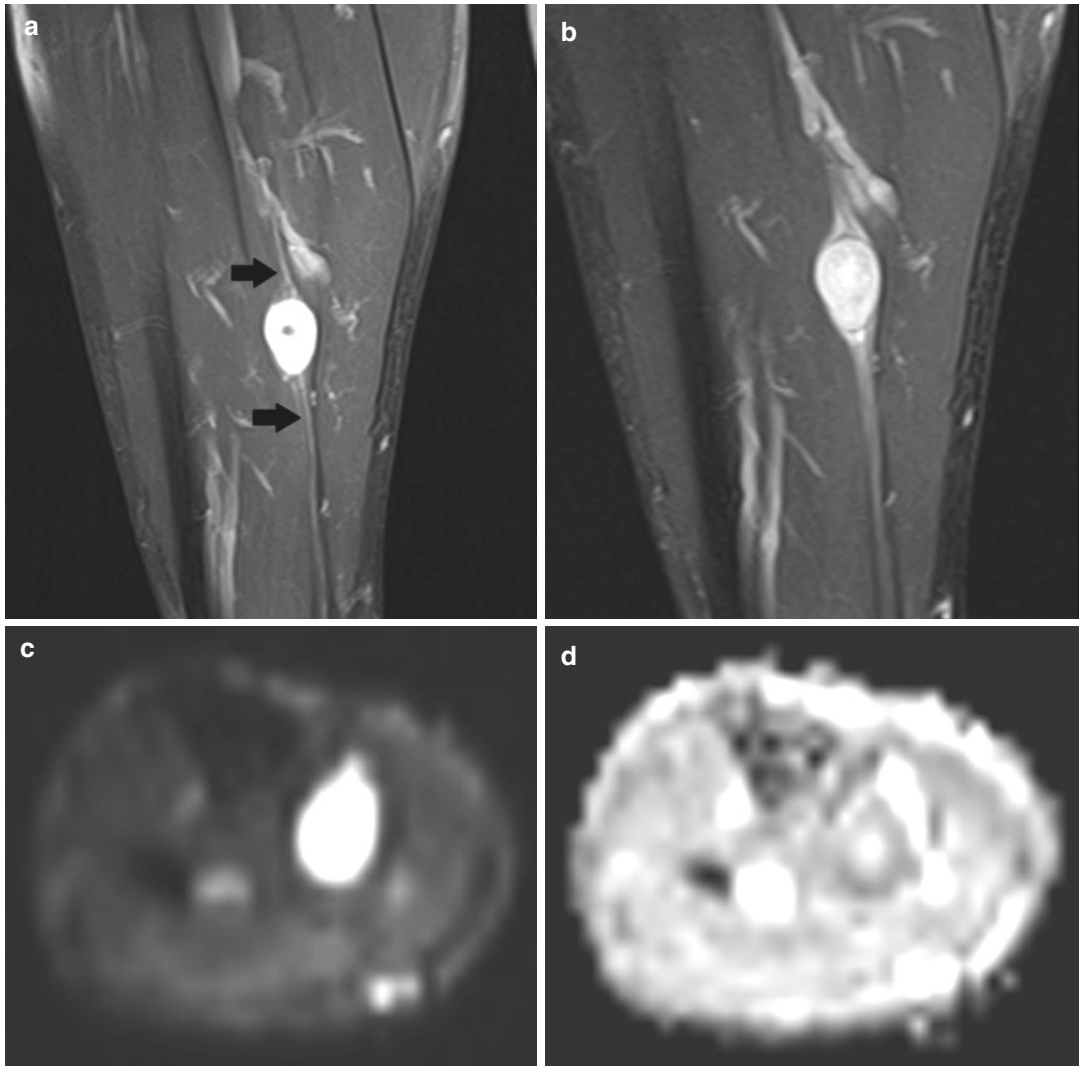

Fig. 17.9 (**a**–**d**) Ancient schwannoma of the right calf in a 60-year-old male: (**a**) coronal FS T2-WI shows the fusiform-shaped lesion to be located along the tibial nerve. An entering and exiting nerve can be seen (tail sign, *arrows*). These features are suggestive of a neural origin. (**b**) On coronal FS T1-WI, the lesion shows diffuse contrast enhancement. Only a small central zone shows no enhancement, compatible with central cyst formation or necrosis. (**c**) On the axial DWI, the schwannoma shows restricted diffusion. (**d**) On the axial ADC map, the lesion shows a low signal peripherally and a high signal centrally, in keeping with central cyst formation, which is often seen in long-standing (ancient) schwannomas

large schwannomas however, this finding may be difficult to appreciate since large tumors may make the capsule very thin [103].

Schwannomas have been reported to be more frequently associated with diffuse enhancement after gadolinium contrast administration, while neurofibromas might be more commonly associated with central enhancement after contrast (Fig. 17.4) [42]. However, this parameter must be evaluated with caution because of some inconstancy and contradictory results related by different reports [14, 24, 42, 55, 67]. Indeed, a recent

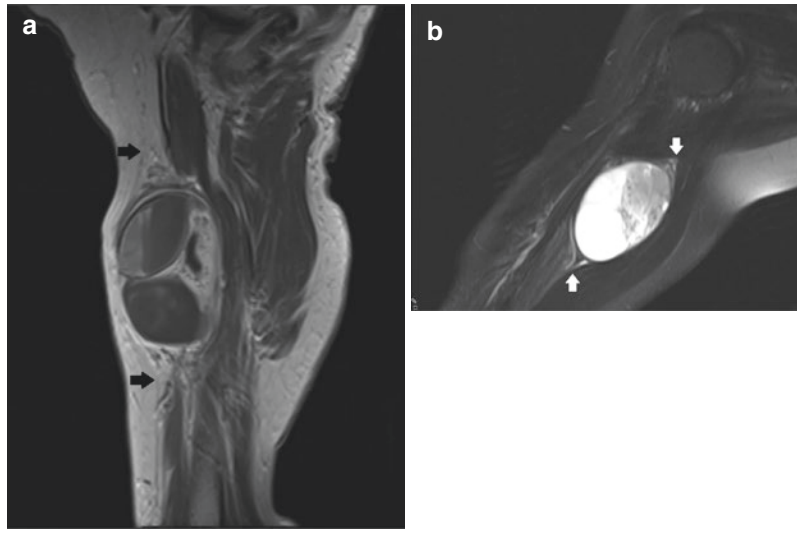

Fig. 17.10 (**a**, **b**) Ancient schwannoma of the right upper arm in a 76-year-old female: (**a**) sagittal T1-WI shows a heterogeneous, fusiform-shaped lesion. An entering and exiting nerve can be seen (tail sign, *arrows*). The lesion is separated from the triceps muscle by a layer of fat (split-fat sign). (**b**) Coronal FS T2-WI shows internal cyst formation. Again, the fusiform shape and the tail sign (*arrows*) can be seen

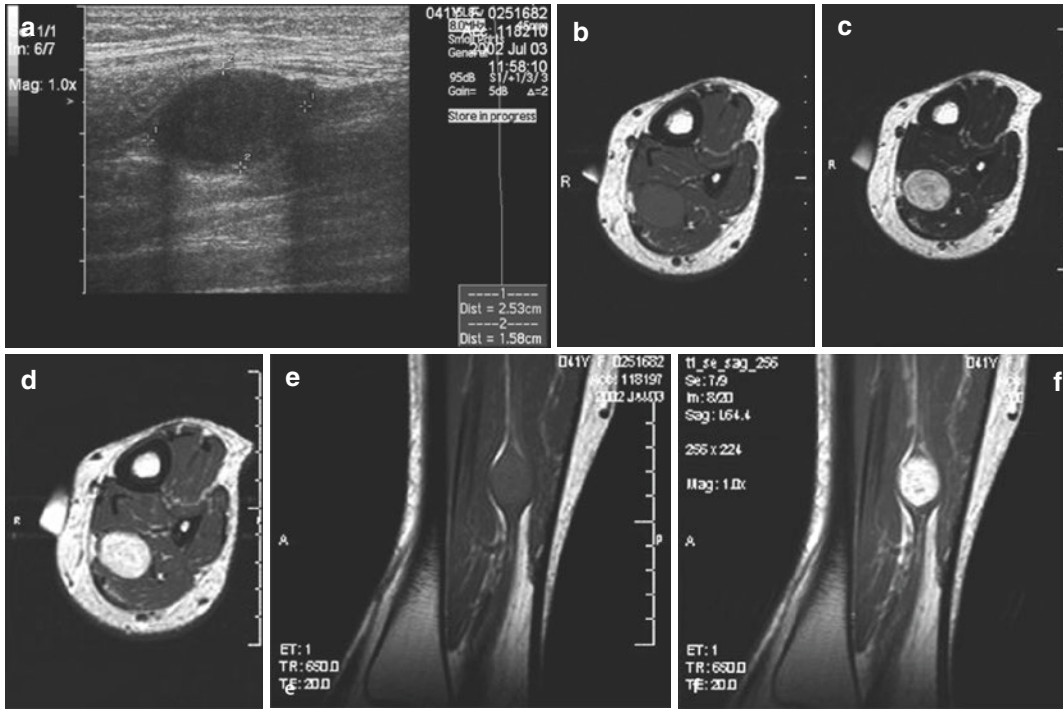

Fig. 17.11 (**a**–**e**) Schwannoma at the flexor surface of the left lower leg in a 41-year-old woman: (**a**) US shows a sharply defined, homogeneously hyporeflective tumor with a fusiform shape and an entering and exiting nerve (tail sign). (**b**) Axial T1-WI shows a well-delineated, homogeneous mass, which is isointense to the adjacent muscles. (**c**) On axial T2-WI, the tumor has a high signal intensity. Individual nerve fascicles can be seen (fascicular sign). (**d**) Axial T1-WI after gadolinium contrast injection shows homogeneous enhancement. (**e**) Coronal T1-WI shows a fusiform mass displaying the tail sign and split-fat sign (**f**) Coronal T1-WI after gadolinium contrast injection shows homogeneous enhancement

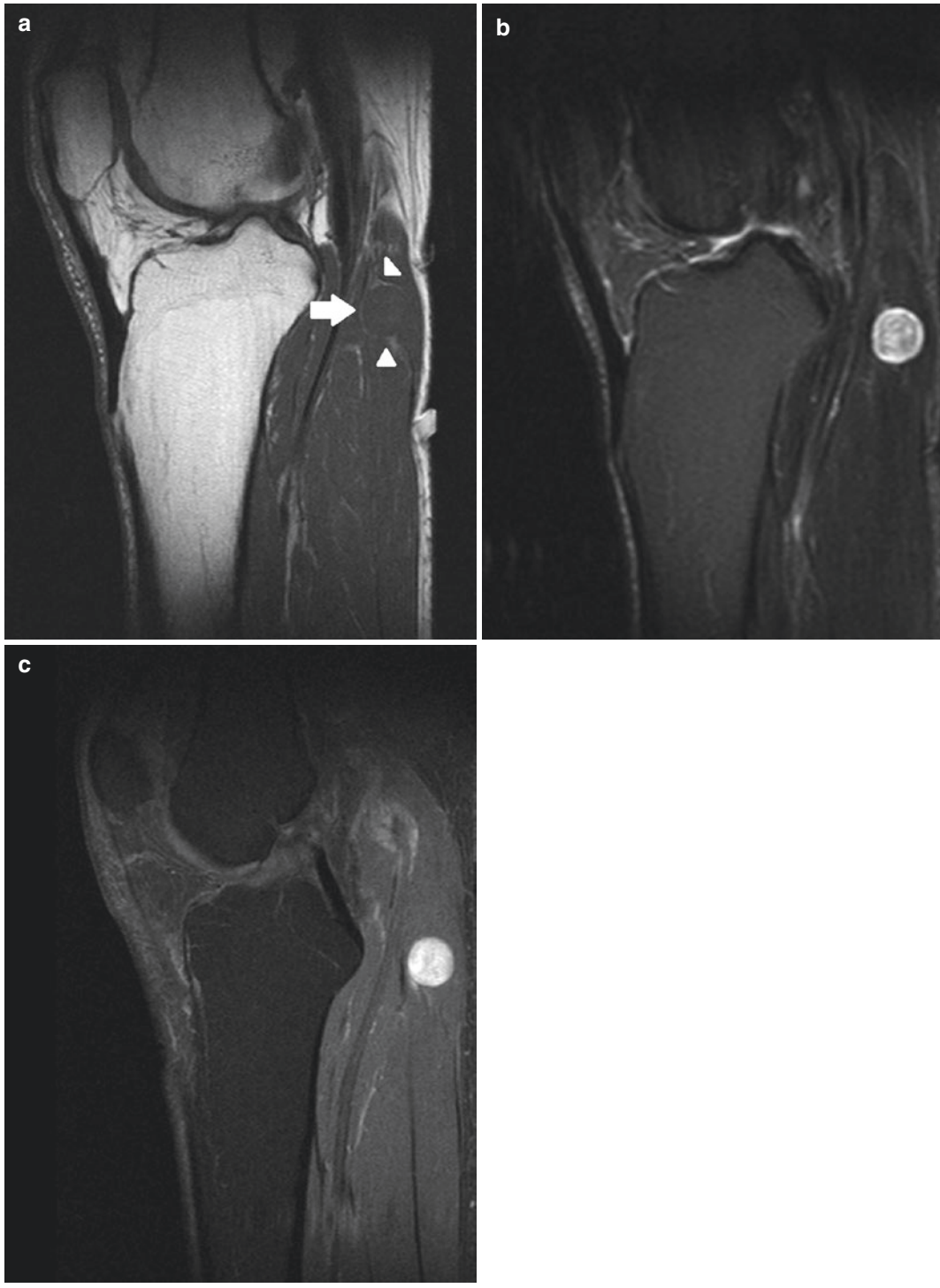

Fig. 17.12 (**a**–**c**) Neurofibroma of the left knee in a 68-year-old male: (**a**) on sagittal T1-WI, the lesion is isointense to the surrounding gastrocnemius muscle. Note that the lesion is partially surrounded by a small rim of fat, known as the split-fat sign (*arrow*). The tail sign can be seen as well (*arrowheads*). (**b**) On sagittal FS T2-WI, the lesion displays a target sign, with high signal intensity peripherally and intermediate signal intensity peripherally. (**c**) Sagittal FS T1-WI after gadolinium contrast enhancement shows diffuse intermediate enhancement with several irregular areas of marked enhancement

paper reported no significant difference with respect to vascularization pattern (Figs. 17.8 and 17.9) [92].

Ancient schwannomas exhibit degenerative changes, including internal bleeding, fibrosis, calcification, and cystic necrotic alterations, resulting in a heterogeneous appearance on MR imaging (Figs. 17.6 and 17.9). This is far less seen in neurofibromas, which most commonly display homogeneous signal intensity [1].

Special histologic schwannoma types can exhibit unique MR imaging characteristics. Cystic schwannomas display low signal intensity on T1-WI and high signal intensity on proton density- and T2-WI. Solid, highly cellular tumors have intermediate signal intensity on T1-WI. Melanotic schwannomas show high signal intensity on T1-WI, reflecting T1-shortening due to the presence of melanin [44, 54, 57, 71].

17.2.2 Neurofibromas

17.2.2.1 Epidemiology

Neurofibromas represent approximately 5% of benign soft tissue neoplasms [47]. There is no obvious predilection for any racial or ethnic group to develop neurofibromas, and these lesions have been described throughout the world [38].

Three types of neurofibromas are classically described: localized, diffuse, and plexiform. *Localized neurofibromas* are the most common type, representing approximately 90% of these lesions. The vast majority of localized neurofibromas are solitary and not associated with NF1 [24]. They develop mostly between the ages of 20 and 30. Like schwannomas, they affect both sexes equally [62]. *Diffuse neurofibromas* are an uncommon but distinctive type that primarily affects children and young adults. The majority of diffuse neurofibromas are isolated lesions not associated with NF1. *Plexiform neurofibromas* are essentially pathognomonic of NF1. Development of these lesions usually occurs in early childhood. Plexiform neurofibromas have a potential for malignant degeneration and are recognized as precursors for malignant PNSTs in NF1 patients [3].

17.2.2.2 Topography

Most localized, solitary neurofibromas are superficial lesions of cutis or subcutis (Fig. 17.7) [62]. Neurofibromas in NF1 are relatively frequent on the trunk, which contrasts with the distribution of peripheral nerve schwannomas, which are more frequent in the extremities [76].

Diffuse neurofibromas demonstrate a plaque-like elevation of the skin with thickening of the entire subcutis.

Plexiform neurofibromas may involve any or all of the following sites: the cranial and spinal nerve roots and ganglia; the major nerves of the neck, trunk, and limbs, including the sympathetic system and its ganglia; and the subcutaneous branches of the major nerves and the visceral sympathetic plexuses [76]. Below the diaphragm, plexiform neurofibromas are typically located in the retroperitoneal space and paraspinal region. Typical retroperitoneal localizations are (bilateral) parapsoatic and presacral neurofibromas. Less commonly, retroperitoneal neurofibromas are found near the celiac axis and near the origin of the superior mesenteric artery [6]. Involvement of the myenteric plexuses and mesentery of the gastrointestinal tract by plexiform neurofibromas is rare. Neurofibromas in this location cause pain, intestinal bleeding, and obstruction. The regional nerves are enlarged, and nodules of varying size are found, especially in Auerbach's plexus. The most common site is the jejunum, followed by the stomach [35].

17.2.2.3 Histology

Typically, localized neurofibromas (Table 17.3) are benign, slowly growing, and variably encapsulated neoplasms [14, 38, 62]. Neurofibromas are intimately associated with the parent nerve, growing in a longitudinal fusiform manner with the nerve entering and exiting from the lesion. Surgical resection requires sacrificing the parent nerve because the neurofibroma cannot be separated from the nerve fibers [22].

As opposed to schwannomas, most neurofibromas are solid tumors macroscopically: areas of cystic degeneration, hypocellularity, and xanthomatous material are uncommon [76]. Neural axons traversing the tumor often follow a tortuous

Table 17.3 Comparative pathology of schwannoma and neurofibroma

	Schwannoma	Neurofibroma
Cell type	Schwann cells	Schwann cells and fibroblasts
Capsule	Usually encapsulated	Usually nonencapsulated
Extension along nerve bundle	Focal	Infiltrative growth
Tumor shape	Round or fusiform	Fusiform
Tumor topography	Eccentric tumor	Central tumor
	Displacing tissue along nerve axis	Separates tissue
Intratumoral cysts	Common	Rare
Intratumoral necrosis	Common	Rare
Intratumoral hemorrhage	Common	Rare
Malignant degeneration	Very rare	More frequent
Blood supply	Thickened arteries, prominent veins	No thickened arteries, no prominent veins

course. As in schwannomas, the capacity of neurofibromas for melanogenesis, although rare, has been well documented [38].

Plexiform neurofibroma relates to a diffuse enlargement and distortion of a major nerve trunk. Disorganized growth of nerves is noticed within and occasionally also outside the nerve trunk [62]. Multiple masses are found along the course of nerve bundles or trunks, with irregular cylindrical enlargement of the affected nerves [86]. Fusiform or spherical neurofibromas along their course can produce a moniliform effect or sometimes give rise to massive growths of a similar character [76].

In many neurofibromas, the peripheral zone contains rather myxoid tissue with high water content, while the central area contains more dense collagenous tissue [86]. This concept is important to understand because it is presumed to be the histologic correlate of the so-called target appearance of neurofibromas on US and MR imaging studies.

17.2.2.4 Clinical Presentation

Solitary neurofibromas present as relatively nontender masses in the skin or subcutaneous tissue. They are somewhat mobile and moderately firm but compressible. Isolated neurofibromas in the skin usually do not exhibit an associated local change in pigmentation of the skin, although hyper- or hypopigmentation is possible. If solitary neurofibromas occur along the course of a peripheral nerve, the clinical symptoms are usually related to a space-occupying lesion but can be similar to those described for schwannoma [38]. The clinical presentation of NF-associated neurofibroma will be discussed below (see Sect. 17.4).

17.2.2.5 Imaging Characteristics

Plain Radiography

The appearance of neurofibromas on plain radiography is similar to that of schwannomas.

Ultrasound

In contrast to schwannomas, localized neurofibromas are homogeneous concentric lesions that do not displace the fascicular elements of the according nerve but rather interfere with them. On transverse images, sometimes the target sign can be seen as a hyperechoic center surrounded by a hypoechoic rim. This correlates with the ultrastructure of neurofibromas with a fibrocollagenous center surrounded by a myxomatous periphery (Fig. 17.13). Large lesions often protrude beyond the surface of the nerve, without a clear capsule [36, 65, 73].

Computed Tomography

On unenhanced CT scans, neurofibromas mostly appear as hypodense lesions due to the presence of Schwann cells, neural elements, and adipocytes [57]. Occasionally, hyperdense areas can be seen, which are believed to result from dense bands of collagen tissue produced by fibroblasts

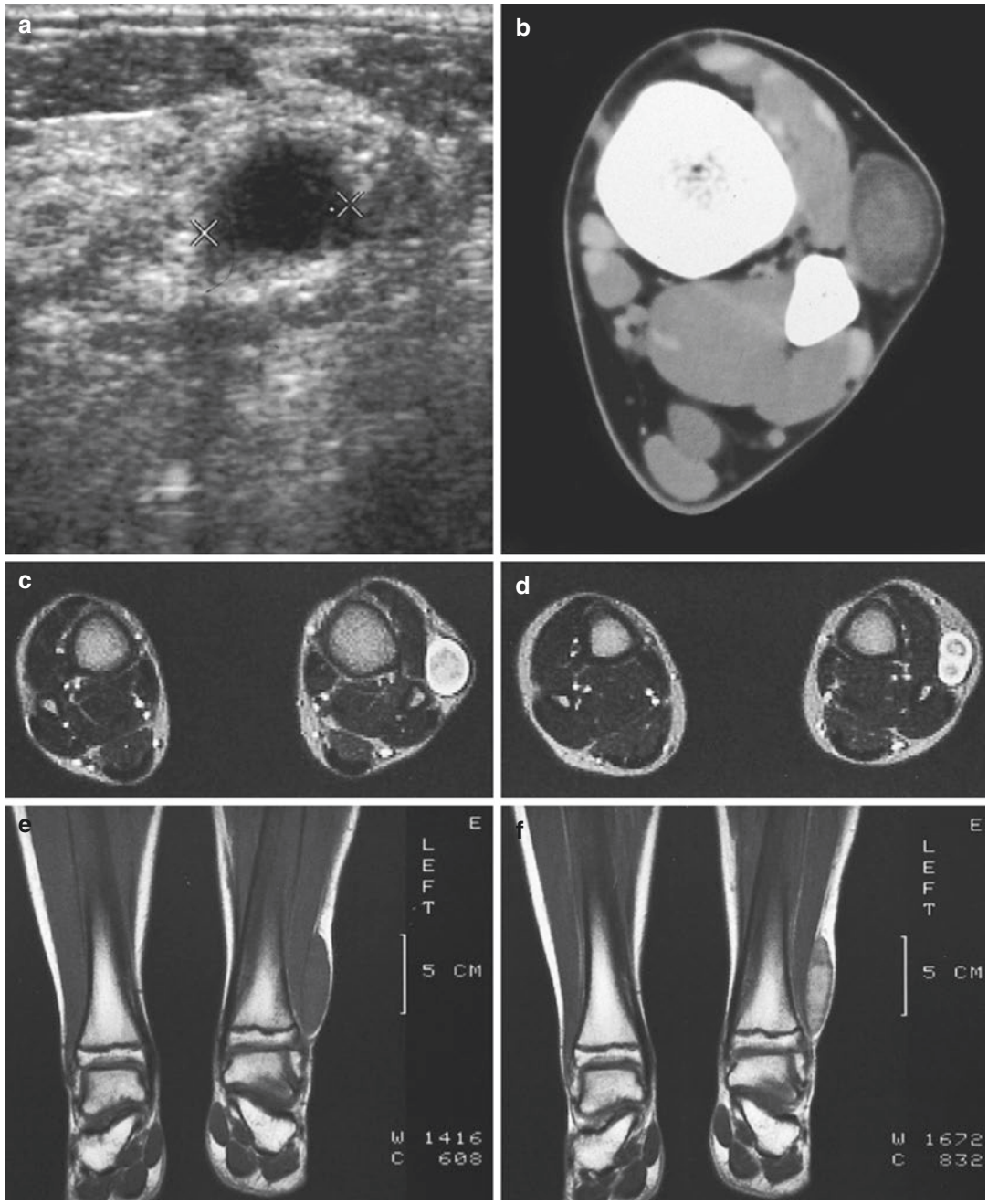

Fig. 17.13 (**a**–**f**) Neurofibroma of the cutaneous tributary of the left superficial fibular nerve in a 14-year-old boy: (**a**) axial ultrasound image 8 cm proximal to the left fibular malleolus shows a well-circumscribed anechoic mass. (**b**) CT scan after iodinated contrast injection, proximal to the left ankle joint, confirmed the mass lesion in the subcutaneous fat next to the extensor digitorum longus muscle. The central part of the lesion shows a slightly higher density than the peripheral rim (target appearance). (**c**) T2-WI 7 cm proximal to the ankle joints confirms the target appearance, with a central area of moderately high signal intensity surrounded by a rim of extremely high signal intensity. (**d**) On axial T2-WI 3 cm proximal to the ankle joints, there is bifurcation in the inferior part of the lesion. (**e**) Coronal T1-WI shows the tumor to be isointense relative to muscle. (**f**) On coronal T1-WI after gadolinium contrast injection, there is central tumor enhancement

[49]. On enhanced CT scans, neurofibromas usually show little or no contrast uptake (Fig. 17.7).

Magnetic Resonance Imaging

Most neurofibromas share several imaging features with other PNSTs (Table 20.1) [1, 3, 42, 57, 71, 84, 100].

MRI is useful for the differentiation of neurofibromas and schwannomas. However, no single MR imaging finding or combination of findings allows a definitive differentiation between schwannomas and neurofibroma (Figs. 17.12 and 17.13) (Table 17.4) [1].

Special histologic neurofibroma types exhibit unique MR imaging characteristics.

Diffuse neurofibromas demonstrate similar signal and enhancement characteristics as solitary ones, but they are often ill-defined and spread extensively along connective tissue septa and between adipose tissue. Diffuse neurofibromas typically involve the subcutaneous tissue down to the level of the fascia [15].

Plexiform neurofibromas appear as multinodular lesions and involve multiple nerve branches, creating a serpentine "bag-of-worms" configuration (Fig. 17.14) [1]. Depending on their location, plexiform neurofibromas can be deep, superficial, or a combination of both [57]. Superficial neurofibromas can mimic venous malformations on MR imaging, and MR angiography or Doppler ultrasound evaluation may be needed for further differentiation [3, 84].

17.2.3 Other Benign Nerve Sheath Tumors

17.2.3.1 Perineurioma

Perineuriomas are rare, benign, slow-growing lesions of which the prevalence may be

Table 17.4 Imaging characteristics of peripheral nerve sheath tumors (PNSTs)

	Schwannoma	Neurofibroma	MPNST
CT characteristics			
Non-enhanced	Hypodense	Hypodense	Hypodense
Contrast-enhanced	Diffuse enhancement (unless necrotic or cystic areas)	Central enhancement	Marked peripheral enhancement
MRI characteristics			
T1-WI	Hypointense	Hypointense	Nonhomogeneous, overall hypointense
T2-WI	Hyperintense	Hyperintense	Nonhomogeneous, overall hyperintense
	Target sign (uncommon)	Target sign (common)	Target sign (rare)
	Fascicular sign (common)	Fascicular sign (uncommon)	Fascicular sign (rare)
Gadolinium contrast-enhanced T1-WI	Diffuse enhancement (unless necrotic or cystic areas)	Central enhancement	Marked nonhomogeneous enhancement
Dynamic enhancement pattern	Usually delayed	Usually delayed	Usually early arterial
Diffusion-based imaging	High minimum ADC ($>1.1\times10^{-3}$ mm/s^2) Tractography: nerve tracts near-normal or partially disrupted	High minimum ADC ($>1.1\times10^{-3}$mm/s^2) Tractography: nerve tracts near-normal or partially disrupted	Low minimum ADC ($>1.1\times10^{-3}$mm/s^2) Tractography: nerve tracts partially or completely disrupted
MR spectroscopy	Trimethylamine fraction usually <50 %	Trimethylamine fraction usually <50%	Trimethylamine fraction usually >50%
18F-FDG PET/CT characteristics			
SUVmax	Low (2–3)	Low (2–3)	Increased (3–4)

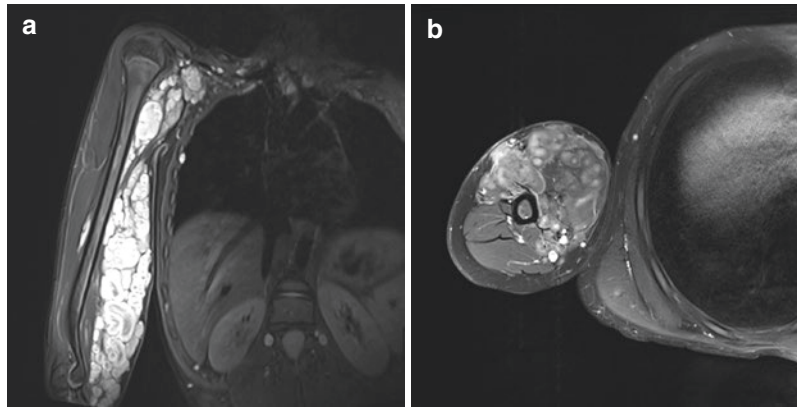

Fig. 17.14 (**a**, **b**) Plexiform neurofibroma of the right upper arm in a 3-year-old girl with neurofibromatosis type 1 (NF1): (**a**) coronal FS T2-WI shows a multinodular lesion resembling a "bag-of-worms." Multiple target signs can be seen (low signal intensity centrally and high signal intensity peripherally). (**b**) On axial FS T1-WI after gadolinium contrast, a multinodular mass with central enhancement can be seen

underestimated [66, 72]. They mainly manifest during childhood and young adulthood [9, 61]. Perineuriomas have no association with neurofibromatosis [60].

Perineuriomas are traditionally classified into intraneural and extraneural perineuriomas. The most common localization of intraneural perineuriomas is the sciatic nerve or its branches (21–47 %), followed by the ulnar, radial (12–17 %), and median nerves (6–11 %) [9, 61]. Extraneural perineuriomas most commonly present as painless nodules in the soft tissues and skin. In this chapter, we will focus on intraneural perineuriomas.

Perineuriomas are composed exclusively of neoplastic perineurial cells that demonstrate ultrastructural and immunohistochemical features similar to those of their healthy counterparts. Arranged in concentric layers around the central axon and Schwann cells, perineuriomas create an onion-bulb appearance on transverse histologic sections [9, 60].

In initial reports, most authors described perineuriomas as reactive or inflammatory processes probably related to trauma, hence the misleading historical names of this entity, including interstitial hypertrophic neuritis, localized hypertrophic neuropathy, and hypertrophic neurofibrosis [72].

Clinically, perineuriomas manifest as a slowly progressive or static mononeuropathy that includes extremity weakness, denervation signs on electromyography, and consequent muscle atrophy [9, 61, 72].

On cross-sectional ultrasound imaging, nerves affected by perineuriomas are markedly enlarged and contain large, thickened hypoechogenic fascicles [69].

On MR imaging, the affected nerve features low-to-intermediate signal intensity on T1-WI, heterogeneous high signal intensity on T2-WI, as well as avid contrast enhancement. There is gradual increase of the caliber of the nerve proximally, followed by gradual taper distally [3, 84, 93]. On axial and longitudinal MR neurography (MRN) images, the fascicular architecture is typically maintained, with the individual fascicles exhibiting uniform enlargement, resulting in a honeycomb appearance [51]. Common associated findings include denervation edema, atrophy, and fatty degeneration of dependent muscle groups [100]. The affected nerve shows increased apparent diffusion coefficient (ADC) and low fractional anisotropy (FA) values [63]. Although the imaging appearance can mimic other neurogenic benign neoplasms, a diagnosis is suggested by the combination of slowly progressive mononeuropathy, the patient's young age, and a lack of known tumor syndrome (Fig. 17.15).

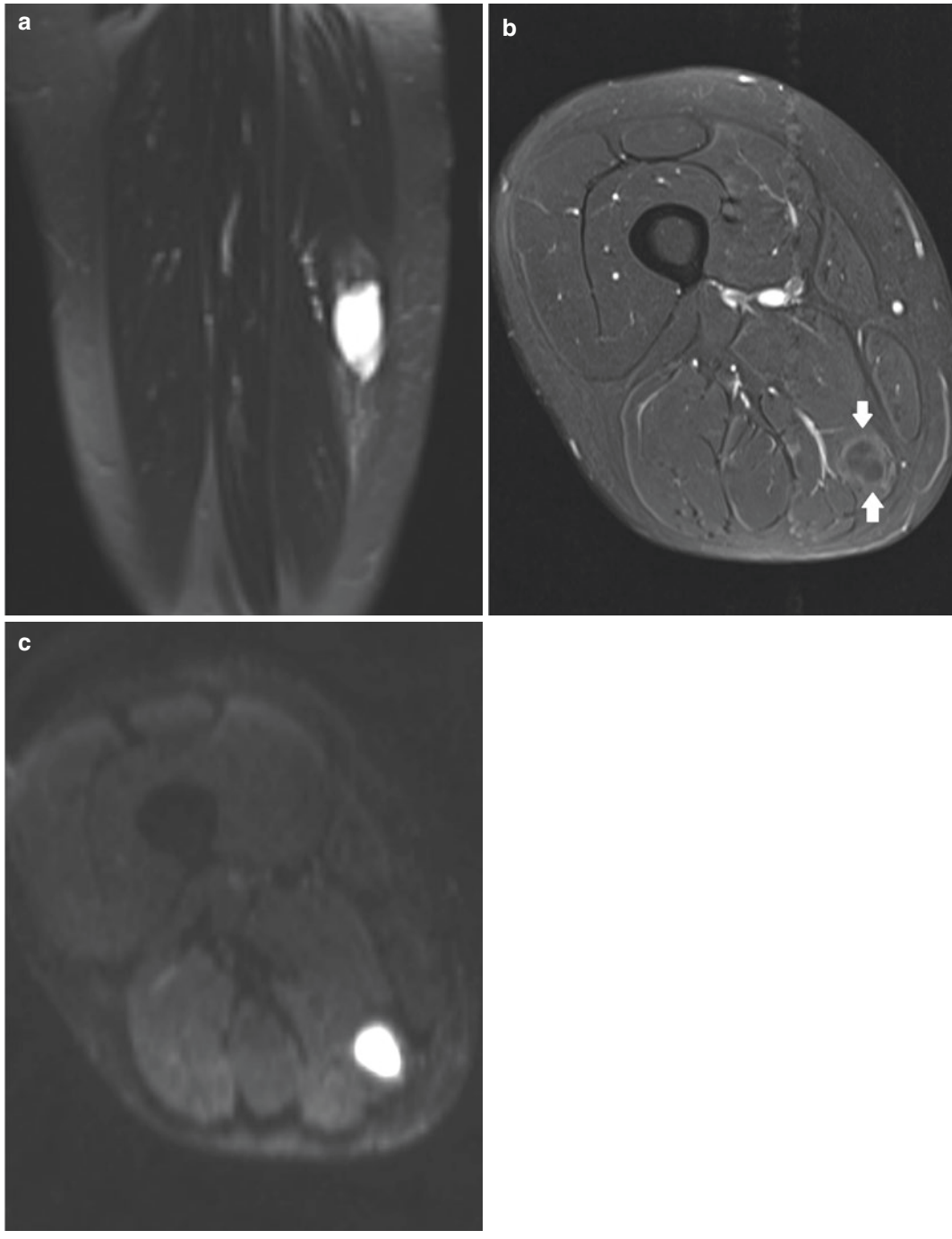

Fig. 17.15 (**a**–**c**) Myxoid perineurioma of the right upper leg in a 54-year-old female: (**a**) coronal FS T2-WI shows a fusiform hyperintense mass. (**b**) Axial FS T1-WI after gadolinium contrast injection shows minor peripheral enhancement (*arrows*). These findings are indicative of a myxoid nature. (**c**) DWI shows restricted diffusion

17.2.3.2 Granular Cell Tumors

Granular cell tumors (GCTs), also known as Abrikossoff tumors, are benign tumors with neuroectodermal differentiation. They are composed of large cells with eosinophilic, distinctively granular cytoplasm [32].

Benign GCTs most frequently occur in adults in the fourth to sixth decade of life. They are more prevalent in males than females (ratio 2–3:1) and in African-Americans [50].

Benign GCTs may arise in virtually any site. They are most commonly located in the head and neck, including the tongue. The breast, chest wall, and proximal extremities may also be involved. Benign GCTs usually affect the skin or subcutaneous tissue, but visceral involvement of the gastrointestinal and respiratory tract may occur too. A deep intramuscular location is rare and is usually closely associated to small-to-medium-sized nerves [50, 53].

While most benign GCTs are solitary, up to 10% are multifocal and may arise in association with Noonan syndrome. Multifocal benign GCTs can be regional or involve multiple organ sites [81].

MR imaging characteristics of benign GCTs are nonspecific and analogous to these of other benign PNSTs [8, 89, 93] (Table 17.2).

Malignant GCTs have been shown to have intermediate-to-low signal intensity on T1-WI and T2-WI [88, 89]. Other features suggestive of malignant GTC are invasion of adjacent structures, size larger than 4 cm, and association with major nerve trunks [8].

17.2.3.3 Hybrid Nerve Sheath Tumors

Hybrid nerve sheath tumors are uncommon benign PNSTs with combined features of more than one conventional tumor type (neurofibroma, schwannoma, perineurioma) [74].

The most common example is hybrid schwannoma/perineurioma, with around 50 cases reported so far. Hybrid schwannoma/perineuriomas have no association with neurofibromatosis and seem to rarely recur [39].

A rare type of hybrid nerve sheath tumor is the hybrid neurofibroma/schwannoma, of which only about ten cases have been reported [30]. As these tumors may occur in neurofibromatosis type 1 and type 2 and especially schwannomatosis, recognition of these tumors as a separate PNST entity could have important implications for the diagnostic criteria of these neurocutaneous syndromes [37].

17.2.3.4 Benign Triton Tumors

Benign triton tumors (also referred to as neuromuscular hamartomas, neuromuscular choristomas, or nerve rhabdomyomas) typically present in infancy or childhood. They are most frequently located around large peripheral nerve trunks such as the sciatic nerve or brachial plexus. They rarely present as intracranial lesion originating from the trigeminal or facial nerve [13, 90]. Histologically, benign triton tumors are characterized by a conglomeration of differentiated skeletal muscle, nerve fibers, and dense fibrous bands [32].

On MRI, benign triton tumors appear hypointense on T1-WI and profoundly hyperintense on T2-WI. They demonstrate mild, fairly homogeneous enhancement after administration of gadolinium. Occasionally, a cystic component can be identified [13].

17.2.3.5 Dermal Nerve Sheath Myxomas

Dermal nerve sheath myxomas (DNSMs) are benign PNSTs that typically arise in the skin or subcutis and often have a multinodular growth pattern. They most commonly arise in the extremities, especially the fingers. DNSMs are composed of small, spindled Schwann cells embedded in a myxoid matrix. Although DNSMs have often been referred to as myxoid variants of neurothekeomas, there is compelling evidence that these tumors differ clinically and biologically [32].

17.2.3.6 Solitary Circumscribed Neuromas

Solitary circumscribed neuromas (SCNs) are benign PNSTs composed of Schwann cells, axons, and perineurial fibroblasts [32]. They most commonly occur in the fourth to seventh decades of life. The skin of the head and neck and the oral mucosa are the principal sites of involvement, with less than 10% of tumors occurring on the trunk, extremities, and glans penis [46].

17.2.3.7 Ectopic Meningiomas

Ectopic meningiomas are meningothelial neoplasms occurring entirely outside the intracranial and intraspinal anatomical regions that normally contain meningothelial cells [32].

Ectopic meningiomas can occur at any age, with bimodal peaks occurring in the second and the fifth to seventh decades of life. There is a slight female predominance [52].

More than 90 % of ectopic meningiomas present in the head and neck region, especially the skull, sinonasal tract, oropharynx, middle ear, scalp, parotid gland, and neck. By definition, an intracranial or intraspinal component must be carefully excluded [32].

17.2.3.8 Nasal Glial Heterotopia

Nasal glial heterotopia (NGH) is a mass of mature heterotopic neuroglial tissue, isolated from the cranial cavity, most often presenting in and around the nose [32].

Most patients present as newborns, with >90 % of cases diagnosed by age 2 years [87]. Rare cases are reported in adults [70].

Extranasal NGH presents as a smooth noncompressible subcutaneous mass usually over the dorsum of the nose. Intranasal NGH presents with nasal obstruction or nasal deformity [70]. NGH may also occur at other sites such as the paranasal sinuses, nasopharynx, pharynx, tongue, palate, tonsil, and orbit. It is then sometimes referred to as facial glioma [4].

NGH is a nonencapsulated lesion. It is composed of variably sized islands of glial tissue separated by bands of vascularized fibrous connective tissue. The glial tissue may merge with the collagen, sometimes obscuring the diagnosis. Astrocyte enlargement or multinucleation may occasionally be seen. Neurons are rare or absent. Mitoses are absent [70].

17.3 Malignant Peripheral Nerve Sheath Tumors

17.3.1 Epidemiology

Malignant peripheral nerve sheath tumors (MPNSTs) represent about 8 % of all malignant soft tissue tumors [65]. The mean age of incidence of MPNSTs is 42 years, with 80 % of all cases occurring between the ages of 17 and 70 [47]. In sporadic cases of MPNSTs, the sex ratio is approximately equal, whereas in the setting of NF1, MPNSTs are four times more frequent in men than in women. Although up to 50 % of MPNSTs occur in association with NF1, only 10 % of patients with NF1 develop MPNSTs [38, 62].

MPNSTs can also develop as a possible delayed sequela of radiation therapy. One study showed 11 % of all MPNSTs to be postradiation sarcomas, with the mean latency period ranging from 5 to 40 years [21].

17.3.2 Topography

MPNSTs have a propensity to occur in the proximal limbs and trunk. They typically affect the large nerves of the neck and proximal extremities (including the sciatic nerve, brachial plexus, and sacral plexus), as well as the retroperitoneum, mediastinum, and viscera (Fig. 17.16) [62].

17.3.3 Histology

MPNSTs are malignant neoplasms of nerve sheath origin that locally infiltrate and also metastasize. They can develop in an unaltered nerve or in a preexisting neurofibroma. It is estimated that between 5 and 13 % of neurofibromas in NF1 eventually become malignant. Conversely, malignant transformation of schwannomas is extremely rare [38].

MPNSTs are microscopically well circumscribed to multinodular masses with fascicles resembling fibrosarcoma. The alternation of sharply demarcated hypercellular and hypocellular zones causes a marbled appearance. Areas of tumor necrosis are common. Divergent differentiation is frequently seen, leading to heterologous elements such as bone, cartilage, skeletal muscle (rhabdomyoblastic), and epithelium (glandular or squamous). MPNSTs with rhabdomyoblastic differentiation are also named malignant triton tumors [21, 24, 65, 102]. These neoplasms are not infrequently associated with NF1 [97].

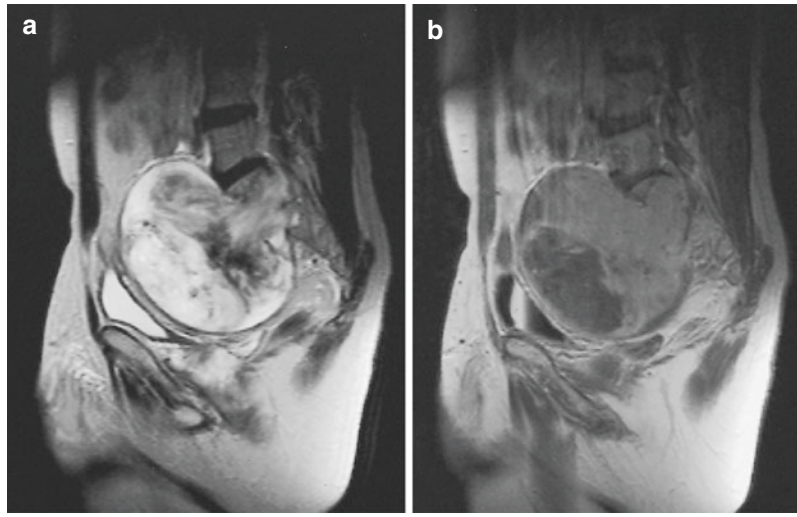

Fig. 17.16 (**a**, **b**) Presacral MPNST in a 57-year-old man: (**a**) sagittal T2-WI shows a mushroom-shaped tumor with a stalk extending from the right S1–S2 intervertebral foramen into the presacral space. Tumor architecture and signal intensity are highly heterogeneous. (**b**) Sagittal T1-WI after gadolinium contrast injection shows mild enhancement and confirms the heterogeneity. The tumor flattens the bladder, displacing the bladder anteriorly, resulting in a "layering phenomenon"

17.3.4 Clinical Presentation

Like other sarcomas, MPNSTs present as enlarging masses that are usually noted several months before the diagnosis is made. Symptoms rarely antedate the detection of a mass.

Clinical manifestations of sarcomatous degeneration of a neurofibroma are not specific. Though pain can herald malignancy, it is also a very common feature of benign neurofibromas. Therefore, the presence of pain cannot be used as an indicator of malignancy. MPNSTs originating from major nerves can also cause other symptoms of sensory or motor nerve deficit, such as paresthesias and weakness [21].

Sudden enlargement of a preexisting neurofibroma in the setting of NF1 should be regarded with great suspicion of malignant transformation and lead to immediate diagnostic imaging. When imaging findings indicate an aggressive lesion, biopsy should be performed to exclude malignant transformation [62]. As a general rule, biopsy must not be performed without the benefit of prior imaging studies. The tumor carries a higher mortality when it occurs in patients with NF1, with a poor 5-year survival rate of 15–30 %, compared to 75 % for the solitary form [24].

The aggressive nature of MPNSTs is evidenced by their tendency to local recurrence after resection. Metastasis, accounting for most of the disease-associated mortality, usually ensues within 2 years of initial diagnosis and is most common in the lungs, followed by other sites such as the liver, subcutis, and bone [62].

17.3.5 Imaging Characteristics

17.3.5.1 Plain Radiography

Radiological findings of bone erosion and destruction do not necessarily imply that the tumor is malignant, as they can also occur with benign nerve sheath tumors [76]. However, when osseous changes are seen in a patient with NF1, immediate further investigation is needed because of the known propensity of these patients to develop MPNSTs.

17.3.5.2 Ultrasound

On ultrasound, small MPNSTs often present as inhomogeneous, hypoechoic, fusiform masses connected with a peripheral nerve. While some lesions show a pseudocapsule consisting of irregularly thickened segments of the hyperechoic

outer nerve sheath, others present a poor outer margin. The growth along the course of the affected nerve is similar to benign PNSTs. With increasing size, the heterogeneity becomes more evident, and areas of heterotopic tissue – such as hypoechoic cartilage, hyperechoic bone formation, or (pseudo) glandular tissue – may be found. Duplex ultrasound usually shows a sarcoma-type anarchic hypervascularization pattern. Such neoangiogenic arteries show high-velocity duplex spectra with different flow velocities and spectral wave forms in different tumor areas. Resistance indices may be rather low, implying arteriovenous shunt vessels. Very typical for MPNSTs are corkscrew-like neovessels. These are often found entering the MPNSTs from the proximal or distal tumor-pole [36, 57, 73].

17.3.5.3 Magnetic Resonance Imaging

Conventional Anatomical MR Imaging

On conventional anatomical MR imaging, most malignant PNSTs share several imaging features with benign PNSTs (Table 17.2). On T1-WI, they are usually isointense to muscle, although in some cases areas of hyperintensity can be seen, a feature which corresponds to hemorrhage and is strongly indicative of malignancy. On T2-WI, malignant PNSTs appear heterogeneous and feature high signal intensity. Heterogeneity, however, must be regarded with caution on differentiation of benign from malignant PNSTs, because benign ancient schwannomas may frequently present with internal cystic changes and calcifications, resulting in a heterogeneous aspect [1]. MPNSTs typically lack the target sign and fascicular sign [16, 84]. They tend to display irregular shape and indistinct margins as a result of their more infiltrative growth pattern.

Additional features, which are considered highly suspicious of MPNST, include large size (>5 cm), peripheral contrast enhancement pattern, intratumoral cystic changes, lack of encapsulation, and invasion of fat planes or neighboring structures (Figs. 17.17, 17.18, and 17.19).

Heterogeneous and predominantly peripheral enhancement is more suggestive of malignant PNSTs, while central enhancement is a more specific finding of benign PNSTs [96].

In contrast to benign PNSTs, malignant PNSTs are extremely rarely encapsulated by epineurium [65, 71]. In large schwannomas, encapsulation may be difficult to appreciate since large tumors may make the capsule very thin [103]. Moreover, fast-growing malignancies may exert pressure against adjacent structures, forming a pseudocapsule consisting of compressed fibrous and connective tissue, normal tissue, vascularized tissue, and inflammatory tissue [94, 103].

The split-fat sign, which is seen in most benign PNSTs, is typically incomplete in most malignant PNSTs, reflecting their infiltrative growth pattern.

Once more, it should be emphasized that no single imaging feature or combination of features can reliably distinguish malignant from benign PNSTs [1]. Benign plexiform neurofibromas can undergo sudden enlargement and present as irregular, lobulated, infiltrating mass lesions. Any tumor of greater dimension can undergo necrosis and hemorrhage. Tumors that were seen as homogeneous and circumscribed masses on medical imaging have been found to be malignant PNSTs on histology. This problem is especially difficult when assessing neural masses in patients known to have NF1; a considerable number of these patients will develop a malignant PNST within a latency period of 10 to as many as 20 years [23].

Functional MR Imaging

The addition of functional MR imaging sequences, including diffusion-weighted imaging (DWI) and dynamic contrast-enhanced (DCE) MR imaging, to conventional MR imaging has recently been suggested as a useful approach to the assessment of PNSTs [25, 68].

Apparent diffusion coefficient (ADC) mapping allows for a semiquantitative analysis of DWI. ADC values of malignant PNSTs tend to be lower than those of benign PNSTs due to restricted diffusion secondary to increased cellularity [16, 20]. Due to the heterogeneity in cellularity present within both benign and malignant PNSTs, minimum ADC values appear to be better predictors of malignancy than average ADC

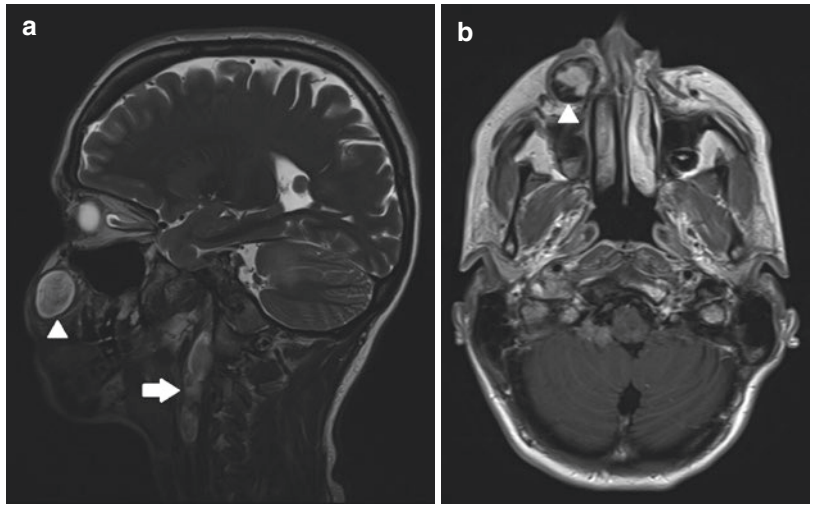

Fig. 17.17 (**a**, **b**) MPNST of the face in a 31-year-old female with NF2: (**a**) sagittal T2-WI shows a well-circumscribed mass displaying a target sign (high SI peripherally, intermediate SI centrally) (*arrowhead*). Also note a multilobulated mass in the major foramen (*arrow*). (**b**) Axial T1-WI after gadolinium contrast enhancement shows heterogeneous contrast enhancement (*arrowhead*)

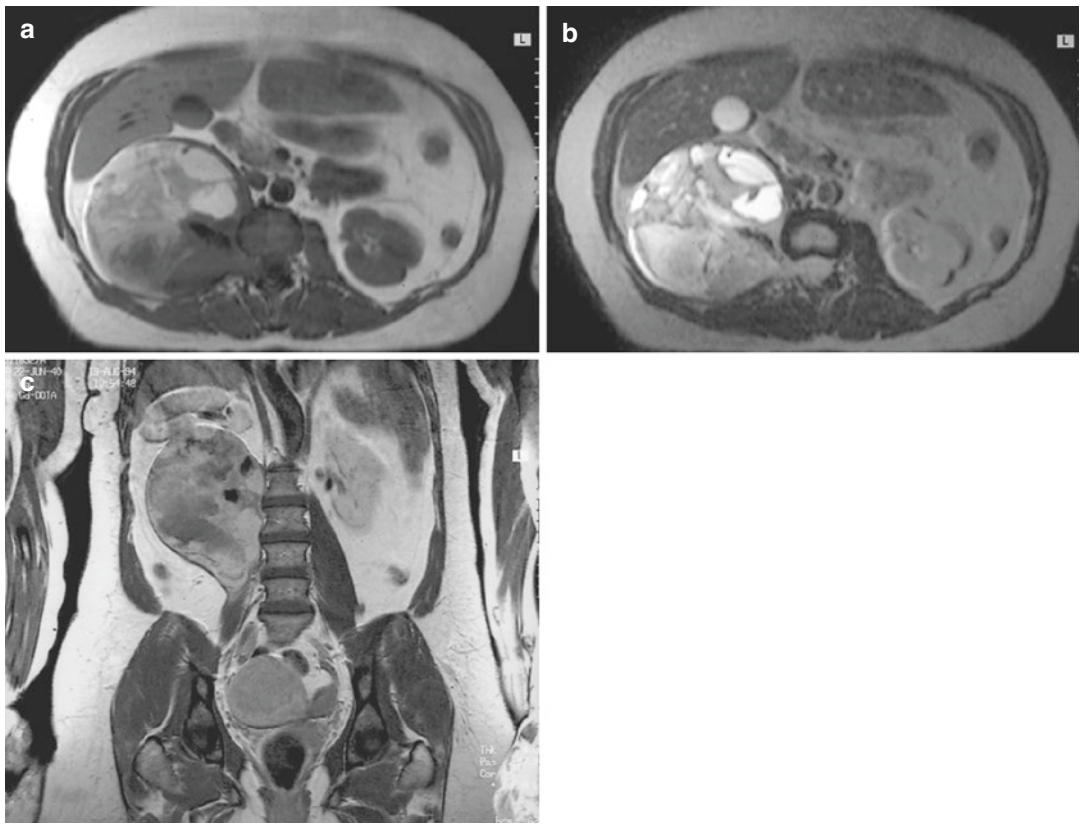

Fig. 17.18 (**a**–**c**) Parapsoas MPNST in a 54-year-old woman: (**a**) axial T1 WI shows the tumor to arise from the right intervertebral L1–L2 foramen. (**b**) On axial T2-WI, the tumor is markedly heterogeneous with different signal intensity components. (**c**) Coronal T1-WI after gadolinium contrast injection shows heterogeneous enhancement

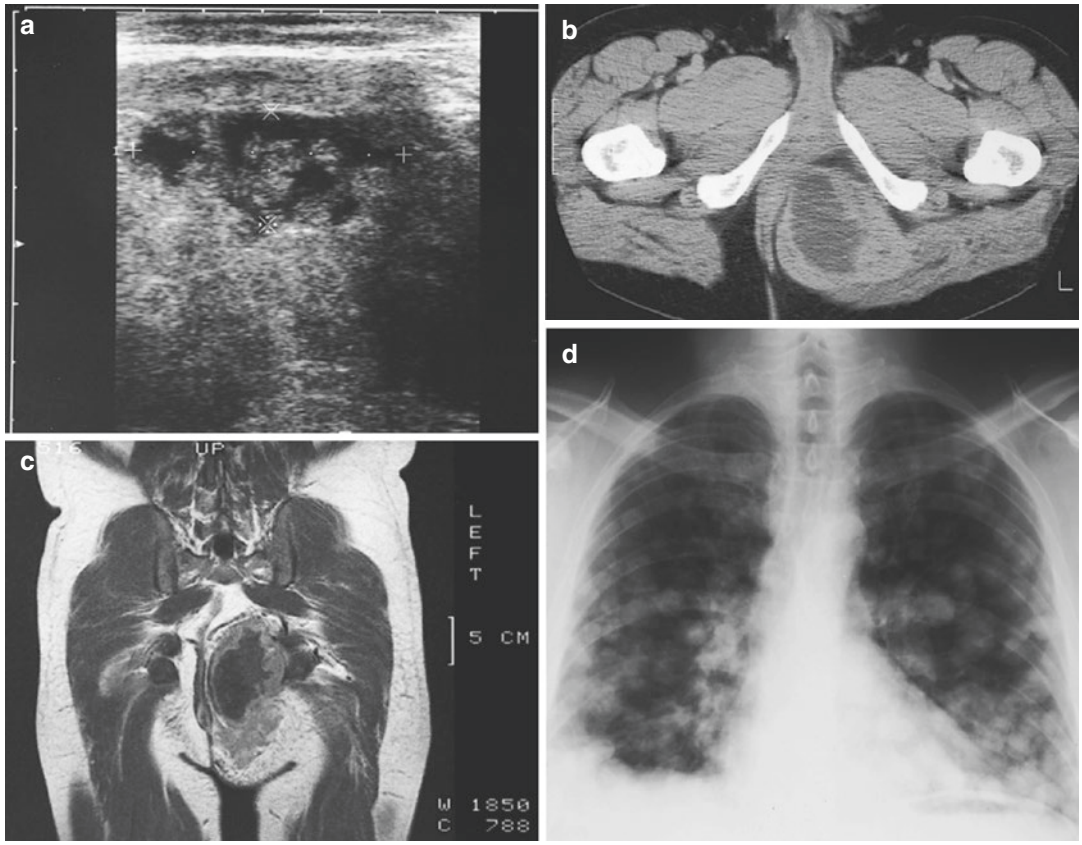

Fig. 17.19 (**a**–**d**) MPNST in the left ischiorectal fossa in a 45-year-old man: (**a**) US of the left buttock shows a heterogeneous tumor located deep to the gluteus maximus muscle. Hypoechoic foci presumably reflect necrosis. (**b**) CT scan of the pelvis after iodinated contrast injection confirms US findings. (**c**) Coronal T1-WI after gadolinium contrast injection shows peripheral enhancement, whereas the central necrotic portions do not enhance. (**d**) Chest radiograph, 10 months later, shows multiple lung metastases

values. However, benign PNSTs displaying high cellularity, including cellular schwannomas, can also generate low minimum ADC values (Fig. 17.9) [20, 84].

Most authors who study diffusion actually concentrate on diffusion tensor imaging (DTI) and tractography, an MRI technique used to produce an in vivo reconstruction of the path of neuronal fibers based on their anisotropism [68]. Benign PNSTs tend to show partial tract disruption or near-normal appearance, while malignant PNSTs can induce partial and complete disruption of tracts. However, complete tract disruption can also be seen in degenerated schwannomas and plexiform neurofibromas [17]. Preoperative MR tractography allows the surgeon to inform the patient on the predicted extent of resection and the possible compromise of nerve function and to better plan out the operative approach to safely and effectively proceed with the resection [12, 80, 83].

Fraction anisotropy (FA) allows for semiquantitative analysis of DTI and correlates with axonal and myelin sheath integrity. FA correlates with axonal and myelin sheath integrity. In peripheral nerves, FA values range between 0.3 and 0.7, with minimal side-to-side variations. Several studies have showed that FA values of nerves affected by PNSTs are significantly lower than those of unaffected contralateral nerves [17].

With DCE MR imaging, malignant PNSTs more often demonstrate early arterial contrast enhancement than benign PNSTs (50 % vs. 11 %) [20].

Metabolic MR Imaging

Metabolic MR imaging of PNSTs can be performed by means of proton magnetic resonance spectroscopy (MRS). Detection of a signal from trimethylamine (TMA) and choline-containing compounds by proton MRS has been established as a valuable indicator of malignant disease [27]. Although proton MRS has been used extensively to characterize brain tumors, far less has been done to evaluate musculoskeletal lesions and specifically PNSTs with MRS [28, 85]. Fayad and colleagues recently studied the use of 3 T proton MRS for the characterization of PNSTs. They found that qualitative interpretation of the presence or absence of a TMA signal appears to have high sensitivity (100 %) but poor specificity (50 %) for diagnosis of malignant disease. However, use of a quantitative TMA fraction threshold of 50 % increases specificity to 72.2 % [29].

17.3.5.4 Nuclear Medicine

18F-FDG PET/CT has been reported to be a good but imperfect imaging modality for the differentiation of benign neurofibromas and malignant PNSTs. Qualitative PET evaluation, consisting of visual evaluation of metabolic activity within lesions, has demonstrated good sensitivity (89–100%) and specificity (72–95%) for this purpose. Nevertheless, an explicit set of criteria for accurate visual interpretation has never been validated [18]. In quantitative PET evaluation, the metabolic activity of the tissue is measured by means of the maximal standard uptake value (SUVmax). Throughout the years, several SUVmax cutoffs, ranging from 1.5 to 6.1, have been proposed to best detect and separate malignant from benign lesions in NF1 patients [10, 11, 18, 77, 79, 91, 95]. The wide range for these quantitative uptake thresholds may be due to differences in acquisition protocols, scanner performance, and analysis methods. Consequently, quantification must be interpreted in the context of center-specific ROC analysis [18].

Several modifications to PET acquisition and post-imaging analysis have been attempted to improve test performance, particularly by adding delayed PET imaging (4 h after administration of PET) and by normalizing lesion SUVmax to normal liver activity [18, 79, 95].

17.4 Neurofibromatoses

PNSTs represent essential clinical manifestations of a group of inherited genetic disorders known as the neurofibromatoses [75]. To date, the three most widely recognized types of neurofibromatosis are neurofibromatosis type 1 (NF1), neurofibromatosis type 2 (NF2), and schwannomatosis [45] (Table 17.5).

17.4.1 Neurofibromatosis Type 1

NF1, formerly known as von Recklinghausen's disease, is the most common neurofibromatosis and has a prevalence of 1/3000. NF1 has an earlier age of onset than NF2 or schwannomatosis: by the age of 8 years, 97% of patients meet the diagnostic criteria for NF1 [58].

NF1 is inherited in an autosomal-dominant manner and 50% of cases represent new or sporadic mutations. The NF1 gene is located at 17q11.2 and codes for neurofibromin, a tumor suppressor protein [58].

Table 17.5 Comparison of neurofibromatosis type 1, neurofibromatosis type 2, and schwannomatosis

	Neurofibromatosis type 1 (NF1)	Neurofibromatosis type 2 (NF2)	Schwannomatosis
Incidence	1:3000	1:25000–40000	1:40000–1.5 million
Inheritance	Autosomal dominant 50 % new mutations	Autosomal dominant 50 % new mutations	Largely new mutations Rarely autosomal dominant
Gene	17	22	22
Hallmark imaging finding	Neurofibroma	Vestibular schwannoma	Peripheral schwannoma

The diagnosis of NF1 is essentially a clinical one. If two or more of the following criteria are fulfilled, the diagnosis of NF1 can be made [64]:

1. Six or more café au lait macules of more than 5 mm in greatest diameter in prepubertal individuals and more than 15 mm in greatest diameter in postpubertal individuals
2. Two or more neurofibromas of any type or one plexiform neurofibroma
3. Freckling in the axillary or inguinal regions
4. Optic glioma
5. Two or more iris hamartomas (Lisch nodules)
6. Distinctive bony lesions, such as sphenoid dysplasia, or thinning of the long bone cortex with or without pseudarthrosis
7. A first-degree relative (parent, sibling, or offspring) with NF1 based on the above criteria

The hallmark imaging finding of NF1 is the neurofibroma. All three types of neurofibromas (localized, diffuse, and plexiform) can be associated with NF1 (Figs. 17.14 and 17.20). Only a minority of patients with localized or diffuse neurofibromas are affected by NF1 [62]. In the setting of NF1, localized neurofibromas tend to be larger, multiple, and more commonly deeply located [65]. Conversely, plexiform neurofibromas are the hallmark lesion of NF1, although as an isolated finding, they are not pathognomonic for this condition. One-third of all patients with NF1 display plexiform neurofibromas [62].

Although considered benign tumors, neurofibromas, particularly the plexiform variety, can be locally aggressive and can undergo malignant transformation. Approximately 10% of NF1 patients will develop malignant PNSTs, necessitating vigilant surveillance [45, 58]. Due to the absence of any radiation exposure, whole-body MRI may be used for serial follow-up of individuals with plexiform neurofibromas. It also allows for assessment of local tumor extent and evaluation of whole-body tumor burden on T2-WI. 18F-FDG PET/CT allows a highly sensitive but less specific detection of MPNST and should be used in case of potential malignant transformation of a PNST [2, 78].

MPNSTs of NF1 subjects occur at an earlier age and display a higher incidence of necrosis/cystic degeneration compared with MPNSTs of non-NF1 subjects [16]. The survival rate of patients with MPNST in the setting of NF1 is significantly lower, with NF1 apparently an independent adverse prognostic factor [62].

17.4.2 Neurofibromatosis Type 2

Neurofibromatosis type 2 (NF2) has an incidence between 1/25,000 and 1/40,000. Unlike NF1, NF2 typically presents later in childhood, with a

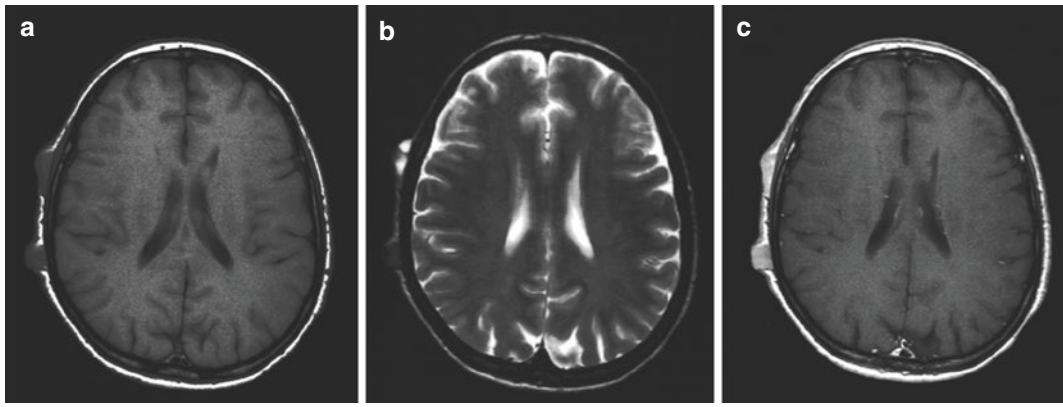

Fig. 17.20 (**a**–**c**) Subcutaneous neurofibromas in a 41-year-old woman with NF1: (**a**) axial T1-WI shows two subcutaneous nodules in the right frontal and parietal region. The lesions are sharply demarcated and relative hypointense to the subcutaneous fatty tissue. (**b**) On axial turbo spin echo T2-WI, the anterior nodule is hyperintense and appears bilobed; the posterior nodule is iso- to hypointense, presumably reflecting fibrous cellular tissue. (**c**) On axial T1-WI after gadolinium contrast enhancement, both lesions enhance, indicating vascular supply. Note that the underlying temporalis muscle enhances to a much lesser degree

formal diagnosis not made until the age of 17–24 years on average [59].

NF2 is inherited in an autosomal-dominant fashion and 50 % of cases represent new or sporadic mutations. The NF2 gene is found at 22q12 and codes for the merlin protein, which acts as a tumor suppressor protein [59].

NF2 can be diagnosed when any of the following clinical features are present [26]:

(a) Bilateral vestibular schwannomas
(b) A first-degree relative with NF2 AND
    - Unilateral vestibular schwannomas OR
    - Any two of meningioma, schwannomas, glioma, neurofibroma, and posterior subcapsular lenticular opacities
(c) Unilateral vestibular schwannomas AND
    - Any two of meningioma, schwannomas, glioma, neurofibroma, and posterior subcapsular lenticular opacities
(d) Multiple meningiomas AND
    - Unilateral vestibular schwannomas OR
    - Any two of schwannomas, glioma, neurofibroma, and cataract

The hallmark imaging finding of NF2 is the presence of bilateral vestibular schwannomas, a finding which excludes schwannomatosis. Variable involvement with meningiomas, ependymomas, neurofibromas, and spinal and peripheral nerve schwannomas is also observed (Fig. 17.21) [45].

Unlike NF1, malignant transformation in NF2 is very rare. Nevertheless, the propensity of NF2 patients to develop ependymomas and the observation that NF2 patients with intracranial meningiomas have a 2.5-fold increase in relative risk of mortality compared with NF2 patients without intracranial meningiomas underscore the importance of vigilant surveillance [59].

17.4.3 Schwannomatosis

Schwannomatosis is a rare disorder with an unknown prevalence and an incidence estimated to be between 1/40,000 and 1/1.7 million [59]. The peak incidence is between 30 and 60 years of age. No predilection for race or sex has been shown [45].

The genetics of schwannomatosis are complex and remain incompletely understood. Although schwannomatosis is largely sporadic, some cases of autosomal-dominant transmission have been observed [45]. Multiple studies have shown germline involvement of the SMARCB1

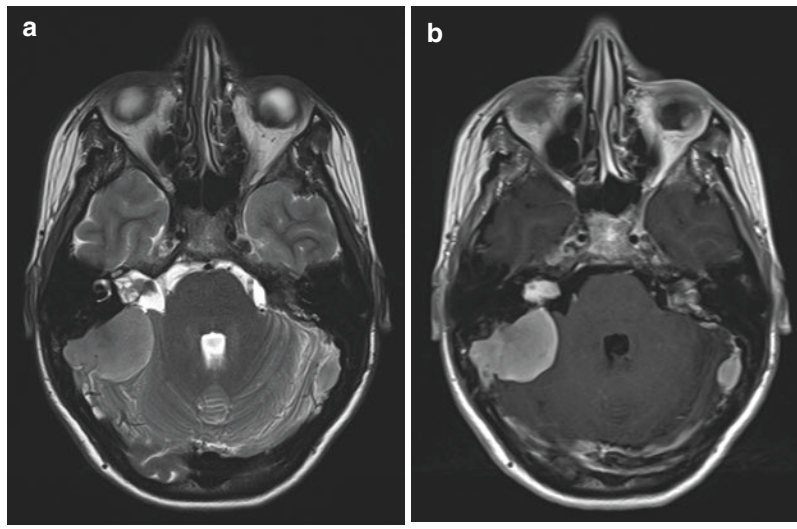

Fig. 17.21 (**a**, **b**) Bilateral vestibular schwannomas (partially resected on the left side) and meningiomas in the posterior fossa in a 31-year-old female with NF2: (**a**) on axial T2-WI, the vestibular schwannomas and meningioma display intermediate signal intensity compared to the intra-axial brain. (**b**) Axial T1-WI after gadolinium contrast injection shows marked tumor enhancement

gene in schwannomatosis. SMARCB1 is a tumor suppressor gene located on chromosome 22 [40].

The hallmark imaging finding of schwannomatosis is the presence of multiple schwannomas without concomitant involvement of cranial nerve VIII [59].

Diagnosis requires exclusion of NF2 on clinical grounds and high-quality imaging of the vestibular nerve [45].

To make the diagnosis of definite or possible schwannomatosis, the patient must not fulfill any of the existing sets of diagnostic criteria for NF2 [5]:

1. Definite schwannomatosis
   (a) Age older than 30 years *and* two or more nonintradermal schwannomas, at least one with histologic confirmation
   (b) One pathologically confirmed schwannoma plus a first-degree relative who meets the above criteria
2. Possible schwannomatosis
   (a) Age younger than 30 years *and* two or more nonintradermal schwannomas, at least one with histologic confirmation
   (b) Age older than 45 years *and* two or more nonintradermal schwannomas, at least one with histologic confirmation
   (c) Radiographic evidence of a schwannoma and a first-degree relative meeting the criteria for definite schwannomatosis
3. Segmental schwannomatosis
   (a) Meets criteria for either definite or possible schwannomatosis but limited to one limb or five or fewer contiguous segments of the spine.

Key Points

1. The updated WHO classification of nerve sheath tumors includes several new benign and malignant nerve sheath tumor types.
2. Imaging features suggestive for nerve sheath tumors include location near a nerve, fusiform shape, tail sign, split-fat sign, target sign, fascicular sign, and degenerative muscle changes.
3. On imaging studies, the differential diagnosis between a schwannoma and a neurofibroma cannot be reliably made. MRI features suggestive of a schwannoma include a fascicular appearance on T2-weighted image and diffuse enhancement. Imaging findings suggestive of neurofibroma include a target sign on T2-weighted image and central enhancement.
4. Criteria that can be of help in establishing the diagnosis of malignant peripheral nerve sheath tumors include a large mass (>5 cm) with mass effect, perilesional edema, invasion of fat planes or neighboring structures, intratumoral cystic changes, peripheral contrast enhancement on static contrast-enhanced MRI, early arterial enhancement on dynamic contrast-enhanced MRI, minimum ADC values $<1.1 \times 10^{-3}$mm/s^2 on DWI/DTI, trimethylamine fraction >50% on MRS, and SUVmax >3–4 on 18F-FDG PET.
5. Nerve sheath tumors represent essential clinical manifestations of a group of inherited genetic disorders known as the neurofibromatoses. The three most widely recognized types of neurofibromatosis are neurofibromatosis type 1 (NF1), neurofibromatosis type 2 (NF2), and schwannomatosis. Plexiform neurofibromas are the hallmark lesion of NF1 and carry a lifetime risk of 10 % for malignant degeneration, necessitating vigilant surveillance. Due to the absence of any radiation exposure, whole-body MRI may be used for serial follow-up of individuals with NF1. 18F-FDG PET/CT allows a highly sensitive but less specific detection of MPNST and should be used in case of potential malignant transformation of a PNST.

References

1. Abreu E, Aubert S, Wavreille G et al (2013) Peripheral tumor and tumor-like neurogenic lesions. Eur J Radiol 82:38–50
2. Ahlawat S, Blakeley J, Montgomery E et al (2013) Schwannoma in neurofibromatosis type 1: a pitfall for detecting malignancy by metabolic imaging. Skelet Radiol 42:1317–1322
3. Ahlawat S, Chhabra A, Blakely J (2014) Magnetic resonance neurography of peripheral nerve tumors and tumorlike conditions. Neuroimaging Clin N Am 24:171–192
4. Bajaj MS, Kashyap S, Wagh VB et al (2005) Glial heterotopia of the orbit and extranasal region: an unusual entity. Clin Exp Ophthalmol 33:513–515
5. Baser ME, Friedman JM, Evans DGR (2006) Increasing the specificity of diagnostic criteria for schwannomatosis. Neurology 66:730–732
6. Bass JC, Korobkin M, Francis IR et al (1994) Retroperitoneal plexiform neurofibromas: CT findings. AJR Am J Roentgenol 163:617–620
7. Beaman FD, Kransdorf MJ, Menke DM (2004) Schwannoma: radiologic-pathologic correlation. Radiographics 24:1477–1481
8. Blacksin MF, White LM, Hameed M et al (2005) Granular cell tumor of the extremity: magnetic resonance imaging characteristics with pathologic correlation. Skelet Radiol 34:625–631
9. Boyanton BL, Jones JK, Shenaq SM et al (2007) Intraneural perineurioma – a systematic review with illustrative cases. Arch Pathol Lab Med 131:1382–1392
10. Bredella MA, Torriani M, Hornicek F et al (2007) Value of PET in the assessment of patients with neurofibromatosis type I. Am J Roentgenol 189:928–935
11. Brenner W, Friedrich RE, Gawad KA et al (2006) Prognostic relevance of FDG PET in patients with neurofibromatosis type-1 and malignant peripheral nerve sheath tumours. Eur J Nucl Med Mol Imaging 33:428–432
12. Cage TA, Yuh EL, Hou SW et al (2015) Visualization of nerve fibers and their relationship to peripheral nerve tumors by diffusion tensor imaging. Neurosurg Focus 39:E16
13. Castro DE, Raghuram K, Phillips CD (2005) Benign triton tumor of the trigeminal nerve. AJNR Am J Neuroradiol 26:967–969
14. Cerofolini E, Landi A, Desantis G et al (1991) MR of benign peripheral nerve sheath tumors. J Comput Assist Tomogr 15:593–597
15. Chee DWY, Peh WCG, Shek TWH (2011) Pictorial essay: imaging of peripheral nerve sheath tumours. Can Assoc Radiol J 62:176–182
16. Chhabra A, Soldatos T, Durand DJ et al (2011) The role of magnetic resonance imaging in the diagnostic evaluation of malignant peripheral nerve sheath tumors. Indian J Cancer 48:328–334
17. Chhabra A, Thakkar RS, Andreisek G et al (2013) Anatomic MR imaging and functional diffusion tensor imaging of peripheral nerve tumors and tumorlike conditions. AJNR Am J Neuroradiol 34:802–807
18. Chirindel A, Chaudhry M, Blakeley JO et al (2015) F-18-FDG PET/CT qualitative and quantitative evaluation in neurofibromatosis type 1 patients for detection of malignant transformation: comparison of early to delayed imaging with and without liver activity normalization. J Nucl Med 56:379–385
19. Cohen LM, Schwartz AM, Rockoff SD (1986) Benign schwannomas: pathologic basis for CT inhomogeneities. AJR Am J Roentgenol 147:141–143
20. Demehri S, Belzberg A, Blakeley J et al (2014) Conventional and functional MR imaging of peripheral nerve sheath tumors: initial experience. Am J Neuroradiol 35:1615–1620
21. Ducatman BS, Scheithauer BW, Piepgras DG et al (1986) Malignant peripheral nerve sheath tumors – a clinicopathological study of 120 cases. Cancer 57:2006–2021
22. Ellison D, Love S, Chimelli L et al (2004) Peripheral nerve sheath neoplasms. In: Neuropathology. Mosby, Edinburgh, pp 695–702
23. Elster AD (1992) Radiologic screening in the neurocutaneous syndromes: strategies and controversies. AJNR Am J Neuroradiol 13:1078–1082
24. Enzinger FM, Weiss SW (1995) Benign tumors of peripheral nerves. In: Enzinger FM, Weiss SW (eds) Soft tissue tumors. Mosby, St. Louis, pp 821–888
25. Eppenberger P, Andreisek G, Chhabra A (2014) Magnetic resonance neurography diffusion tensor imaging and future directions. Neuroimaging Clin N Am 24:245–256
26. Evans DG, Huson SM, Donnai D et al (1992) A genetic study of type 2 neurofibromatosis in the United Kingdom. I. Prevalence, mutation rate, fitness, and confirmation of maternal transmission effect on severity. J Med Genet 29:841–846
27. Fayad LM, Jacobs MA, Wang X et al (2012) Musculoskeletal tumors: how to use anatomic, functional, and metabolic MR techniques. Radiology 265:340–356
28. Fayad LM, Salibi N, Wang X et al (2010) Quantification of muscle choline concentrations by proton MR spectroscopy at 3 T: technical feasibility. Am J Roentgenol 194:W73–W79
29. Fayad LM, Wang X, Blakeley JO et al (2014) Characterization of peripheral nerve sheath tumors with 3T proton MR spectroscopy. Am J Neuroradiol 35:1035–1041
30. Feany MB, Anthony DC, Fletcher CDM (1998) Nerve sheath tumours with hybrid features of neurofibroma and schwannoma: a conceptual challenge. Histopathology 32:405–410
31. Fletcher CDM (2014) The evolving classification of soft tissue tumours – an update based on the new 2013 WHO classification. Histopathology 64:2–11
32. Fletcher CDM (2013) WHO classification of tumours of soft tissue and bone. IARC Press, Lyon

33. Fletcher CDM, Davies SE (1986) Benign plexiform (multinodular) schwannoma – a rare tumor unassociated with neurofibromatosis. Histopathology 10:971–980
34. Fletcher CDM, Davies SE, Mckee PH (1987) Cellular schwannoma – a distinct pseudosarcomatous entity. Histopathology 11:21–35
35. Fukuya T, Lu CC, Mitros FA (1994) CT findings of plexiform neurofibromatosis involving the ileum and its mesentery. Clin Imaging 18:142–145
36. Gruber H, Glodny B, Bendix N et al (2007) High-resolution ultrasound of peripheral neurogenic tumors. Eur Radiol 17:2880–2888
37. Harder A, Wesemann M, Hagel C et al (2012) Hybrid neurofibroma/schwannoma is overrepresented among schwannomatosis and neurofibromatosis patients. Am J Surg Pathol 36:702–709
38. Harkin JC, Reed JR (1968) Tumors of the peripheral nervous system. Armed Forces Institute of Pathology, Washington, DC
39. Hornick JL, Bundock EA, Fletcher CDM (2009) Hybrid schwannoma/perineurioma clinicopathologic analysis of 42 distinctive benign nerve sheath tumors. Am J Surg Pathol 33:1554–1561
40. Hulsebos TJM, Plomp AS, Wolterman RA et al (2007) Germline mutation of INI1/SMARCB1 in familial schwannomatosis. Am J Hum Genet 80:805–810
41. Isobe K, Shimizu T, Akahane T et al (2004) Imaging of ancient schwannoma. Am J Roentgenol 183:331–336
42. Jee WH, Oh SN, Mccauley T et al (2004) Extraaxial neurofibromas versus neurilemmomas: discrimination with MRI. Am J Roentgenol 183:629–633
43. Jo VY, Fletcher CDM (2014) WHO classification of soft tissue tumours: an update based on the 2013 (4th) edition. Pathology 46:95–104
44. Khoo M, Pressney I, Hargunani R et al (2016) Melanotic schwannoma: an 11-year case series. Skeletal Radiol 45:29–34
45. Koontz NA, Wiens AL, Agarwal A et al (2013) Schwannomatosis: the overlooked neurofibromatosis? Am J Roentgenol 200:W646–W653
46. Koutlas IG, Scheithauer BW (2010) Palisaded encapsulated (“solitary circumscribed”) neuroma of the oral cavity: a review of 55 cases. Head Neck Pathol 4:15–26
47. Kransdorf MJ (1995) Benign soft-tissue tumors in a large referral population – distribution of specific diagnoses by age, sex, and location. Am J Roentgenol 164:395–402
48. Kubiena H, Entner T, Schmidt M et al (2013) Peripheral neural sheath tumors (PNST)-What a radiologist should know. Eur J Radiol 82:51–55
49. Kumar AJ, Kuhajda FP, Martinez CR et al (1983) Computed tomography of extracranial nerve sheath tumors with pathological correlation. J Comput Assist Tomogr 7:857–865
50. Lack EE, Worsham GF, Callihan MD et al (1980) Granular-cell tumor – a clinicopathologic study of 110 patients. J Surg Oncol 13:301–316
51. Lacour-Petit MC, Lozeron P, Ducreux D (2003) MRI of peripheral nerve lesions of the lower limbs. Neuroradiology 45:166–170
52. Lang FF, Macdonald OK, Fuller GN et al (2000) Primary extradural meningiomas: a report on nine cases and review of the literature from the era of computerized tomography scanning. J Neurosurg 93:940–950
53. Lazar A (2013) Granular cell tumour. In: Fletcher C, Bridge J, Hogendoorn P, Mertens F (eds) World Health Organization classification of tumours of soft tissue and bone. IARC Press, Lyon, pp 178–179
54. Lee E (2015) Useful MRI features for distinguishing benign peripheral nerve sheath tumors and myxoid tumors in the musculoskeletal system. Invest Magn Res Imaging 19:153–161
55. Li C, Huang G, Wu H et al (2008) Differentiation of soft tissue benign and malignant peripheral nerve sheath tumors with magnetic resonance imaging. Clin Imaging 32:121–127
56. Liegl B, Bennett MW, Fletcher CDM (2008) Microcystic/reticular schwannoma: a distinct variant with predilection for visceral locations. Am J Surg Pathol 32:1080–1087
57. Lin J, Martel W (2001) Cross-sectional imaging of peripheral nerve sheath tumors: characteristic signs on CT, MR imaging, and sonography. Am J Roentgenol 176:75–82
58. Lu-Emerson C, Plotkin SR (2009) The neurofibromatoses. Part 1: NF1. Rev Neurol Dis 6:E47–E53
59. Lu-Emerson C, Plotkin SR (2009) The neurofibromatoses. Part 2: NF2 and schwannomatosis. Rev Neurol Dis 6:E81–E86
60. Macarenco RS, Ellinger F, Oliveira AM (2007) Perineurioma – a distinctive and underrecognized peripheral nerve sheath neoplasm. Arch Pathol Lab Med 131:625–636
61. Mauermann ML, Amrami KK, Kuntz NL et al (2009) Longitudinal study of intraneural perineurioma a benign, focal hypertrophic neuropathy of youth. Brain 132:2265–2276
62. Meis-Kindblom JM, Enzinger FM (1996) Color atlas of soft tissue tumors. Mosby-Wolfe, St. Louis
63. Merlini L, Viallon M, De Coulon G et al (2008) MRI neurography and diffusion tensor imaging of a sciatic perineuroma in a child. Pediatr Radiol 38:1009–1012
64. Mulvihill JJ, Parry DM, Sherman JL et al (1990) NIH conference. Neurofibromatosis 1 (Recklinghausen disease) and neurofibromatosis 2 (bilateral acoustic neurofibromatosis). An update. Ann Intern Med 113:39–52
65. Murphey MD, Smith WS, Smith SE et al (1999) Imaging of musculoskeletal neurogenic tumors: radiologic-pathologic correlation. Radiographics 19:1253–1280
66. Nacey NC, Almira Suarez MI, Mandell JW et al (2014) Intraneural perineurioma of the sciatic nerve: an under-recognized nerve neoplasm with characteristic MRI findings. Skeletal Radiol 43:375–379

67. Ogose A, Hotta T, Morita T et al (2004) Diagnosis of peripheral nerve sheath tumors around the pelvis. Jpn J Clin Oncol 34:405–413
68. Ohana M, Moser T, Moussaoui A et al (2014) Current and future imaging of the peripheral nervous system. Diagn Interv Imaging 95:17–26
69. Pedro MT, Antoniadis G, Scheuerle A et al (2015) Intraoperative high-resolution ultrasound and contrast-enhanced ultrasound of peripheral nerve tumors and tumorlike lesions. Neurosurg Focus 39:E5
70. Penner CR, Thompson L (2003) Nasal glial heterotopia: a clinicopathologic and immunophenotypic analysis of 10 cases with a review of the literature. Ann Diagn Pathol 7:354–359
71. Pilavaki M, Chourmouzi D, Kiziridou A et al (2004) Imaging of peripheral nerve sheath tumors with pathologic correlation – pictorial review. Eur J Radiol 52:229–239
72. Restrepo CE, Amrami KK, Howe BM et al (2015) The almost-invisible perineurioma. Neurosurg Focus 39:E13
73. Reynolds DL, Jacobson JA, Inampudi P et al (2004) Sonographic characteristics of peripheral nerve sheath tumors. Am J Roentgenol 182:741–744
74. Rodriguez FJ, Folpe AL, Giannini C et al (2012) Pathology of peripheral nerve sheath tumors: diagnostic overview and update on selected diagnostic problems. Acta Neuropathol 123:295–319
75. Rodriguez FJ, Stratakis CA, Evans DG (2012) Genetic predisposition to peripheral nerve neoplasia: diagnostic criteria and pathogenesis of neurofibromatoses, Carney complex, and related syndromes. Acta Neuropathol 123:349–367
76. Russell DS, Rubinstein LJ (1989) Tumours of the cranial, spinal and peripheral nerve sheaths. In: Bigner DD, McLendon RE, Bruner JM (eds) Pathology of tumours of the nervous system. Edward Arnold, London, pp 533–589
77. Salamon J, Derlin T, Bannas P et al (2013) Evaluation of intratumoural heterogeneity on F-18-FDG PET/CT for characterization of peripheral nerve sheath tumours in neurofibromatosis type 1. Eur J Nucl Med Mol Imaging 40:685–692
78. Salamon J, Mautner VF, Adam G et al (2015) Multimodal imaging in neurofibromatosis type 1-associated nerve sheath tumors. Röfo 187(12): 1084–1092
79. Salamon J, Veldhoen S, Apostolova I et al (2014) F-18-FDG PET/CT for detection of malignant peripheral nerve sheath tumours in neurofibromatosis type 1: tumour-to-liver ratio is superior to an SUVmax cut-off. Eur Radiol 24:405–412
80. Schmidt M, Kasprian G, Amann G et al (2015) Diffusion tensor tractography for the surgical management of peripheral nerve sheath tumors. Neurosurg Focus 39:E17
81. Sidwell RU, Rouse P, Owen RA et al (2008) Granular cell tumor of the scrotum in a child with Noonan syndrome. Pediatr Dermatol 25:341–343
82. Simoens WA, Wuyts FL, De Beuckeleer LH et al (2001) MR features of peripheral nerve sheath tumors: can a calculated index compete with radiologist's experience? Eur Radiol 11:250–257
83. Simon NG, Cage T, Narvid J et al (2014) High-resolution ultrasonography and diffusion tensor tractography map normal nerve fascicles in relation to schwannoma tissue prior to resection report of 2 cases. J Neurosurg 120:1113–1117
84. Soldatos T, Fisher S, Karri S et al (2015) Advanced MR imaging of peripheral nerve sheath tumors including diffusion imaging. Semin Musculoskelet Radiol 19:179–190
85. Subhawong TK, Wang X, Durand DJ et al (2012) Proton MR spectroscopy in metabolic assessment of musculoskeletal lesions. Am J Roentgenol 198:162–172
86. Suh JS, Abenoza P, Galloway HR et al (1992) Peripheral (extracranial) nerve tumors – correlation of imaging and histologic-findings. Radiology 183:341–346
87. Swift AC, Singh SD (1985) The presentation and management of the nasal glioma. Int J Pediatr Otorhinolaryngol 10:253–261
88. Tan TJ, Alassiri AH, Ng TL et al (2015) Malignant granular cell tumor of the foot-multimodality imaging findings and literature review. Clin Imaging 39:543–546
89. Thacker MM, Humble SA, Mounasamy V et al (2007) Granular cell tumors of extremities – comparison of benign and malignant variants. Clin Orthop Relat Res 455:267–273
90. Thakrar R, Robson CD, Vargas SO et al (2014) Benign triton tumor: multidisciplinary approach to diagnosis and treatment. Pediatr Dev Pathol 17:400–405
91. Tsai LL, Drubach L, Fahey F et al (2012) 18F-Fluorodeoxyglucose positron emission tomography in children with neurofibromatosis type 1 and plexiform neurofibromas: correlation with malignant transformation. J Neuro-Oncol 108:469–475
92. Tsai WC, Chiou HJ, Chou YH et al (2008) Differentiation between schwannomas and neurofibromas in the extremities and superficial body the role of high-resolution and color Doppler ultrasonography. J Ultrasound Med 27:161–166
93. Wadhwa V, Thakkar RS, Maragakis N et al (2012) Sciatic nerve tumor and tumor-like lesions – uncommon pathologies. Skeletal Radiol 41:763–774
94. Walker EA, Fenton ME, Salesky JS et al (2011) Magnetic resonance imaging of benign soft tissue neoplasms in adults. Radiol Clin N Am 49:1197–1217
95. Warbey VS, Ferner RE, Dunn JT et al (2009) F-18 FDG PET/CT in the diagnosis of malignant peripheral nerve sheath tumours in neurofibromatosis type-1. Eur J Nucl Med Mol Imaging 36:751–757
96. Wasa J, Nishida Y, Tsukushi S et al (2010) MRI features in the differentiation of malignant peripheral nerve sheath tumors and neurofibromas. Am J Roentgenol 194:1568–1574

97. White W, Shiu MH, Rosenblum MK et al (1990) Cellular schwannoma – a clinicopathological study of 57 patients and 58 tumors. Cancer 66:1266–1275
98. Wippold FJ, Lammle M, Anatelli F et al (2006) Neuropathology for the neuroradiologist: palisades and pseudopalisades. Am J Neuroradiol 27: 2037–2041
99. Wippold FJ, Lubner M, Perrin RJ et al (2007) Neuropathology for the neuroradiologist: Antoni A and Antoni B tissue patterns. Am J Neuroradiol 28:1633–1638
100. Woertler K (2010) Tumors and tumor-like lesions of peripheral nerves. Semin Musculoskelet Radiol 14:547–558
101. Woodruff JM, Marshall ML, Godwin TA et al (1983) Plexiform (multinodular) schwannoma – a tumor simulating the plexiform neurofibroma. Am J Surg Pathol 7:691–697
102. Yimaz MR, Bek S, Bekmezci T et al (2004) Malignant triton tumor of the lumbar spine. Spine (Phila Pa 1976) 29:E399–E401
103. Zhang ZH, Deng L, Ding L et al (2015) MR imaging differentiation of malignant soft tissue tumors from peripheral schwannomas with large size and heterogeneous signal intensity. Eur J Radiol 84:940–946
104. Penkert G, Böhm J, Schelle T (2015) Focal peripheral neuropathies: imaging, neurological, and neurosurgical approaches. Springer, Berlin/Heidelberg

Tumors of Uncertain Differentiation

18

Simon David Sprengel, Marc-André Weber, Hendrik R. Degryse, and Filip M. Vanhoenacker

Contents

18.1 **Introduction** 426

18.2 **Classification** 426

18.3 **Benign Lesions** 426
18.3.1 Intramuscular Myxoma (Incl. Cellular Variant) 426
18.3.2 Acral Fibromyxoma 428
18.3.3 Juxta-Articular Myxoma 428
18.3.4 Myxoma of the Jaws 430
18.3.5 Deep ("Aggressive") Angiomyxoma 434
18.3.6 Pleomorphic Hyalinizing Angiectatic Tumor 435
18.3.7 Ectopic Hamartomatous Thymoma 436

18.4 **Intermediate Tumors (Locally Aggressive)** 437
18.4.1 Hemosiderotic Fibrolipomatous Tumor 437

18.5 **Intermediate Tumors (Rarely Metastasizing)** 437
18.5.1 Atypical Fibroxanthoma 437
18.5.2 Angiomatoid Fibrous Histiocytoma 439
18.5.3 Ossifying Fibromyxoid Tumor 439
18.5.4 Mixed Tumor 440
18.5.5 Phosphaturic Mesenchymal Tumor 443

18.6 **Malignant Lesions** 443
18.6.1 Synovial Sarcoma 443
18.6.2 Epithelioid Sarcoma 451
18.6.3 Alveolar Soft Part Sarcoma 454
18.6.4 Clear Cell Sarcoma of Soft Tissue 458
18.6.5 Extraskeletal Myxoid Chondrosarcoma ("Chordoid" Type) 461
18.6.6 Malignant Mesenchymoma 461
18.6.7 Desmoplastic Small Round Cell Tumor 462
18.6.8 PNET/Extraskeletal Ewing's Sarcoma 462
18.6.9 Extrarenal Rhabdoid Tumor 469
18.6.10 Neoplasms with Perivascular Epithelioid Cell Differentiation (PEComa): Clear Cell Myomelanocytic Tumor 473
18.6.11 Intimal Sarcoma 475

References 477

S.D. Sprengel (✉) • M.-A. Weber, MSc
Clinic of Diagnostic and Interventional Radiology, University Hospital Heidelberg, Im Neuenheimer Feld 110, 69120 Heidelberg, Germany
e-mail: simon.sprengel@med.uni-heidelberg.de; MarcAndre.Weber@med.uni-heidelberg.de

H.R. Degryse, MD, MSc
Department of Radiology, AZ KLINA, Augustijnslei, Brasschaat and University Hospital, Antwerp Wilrijkstraat, 10, B-2650 Edegem, Belgium
e-mail: hendrik.degryse@klina.be

F.M. Vanhoenacker, MD, PhD
Department of Radiology, AZ Sint-Maarten, Duffel-Mechelen, University Hospital Antwerp, University of Ghent, Faculty of Medicine and Health Sciences, Rooienberg, 25, B-2570 Duffel, Belgium and Wilrijkstraat, 10, B-2650 Edegem, Belgium
e-mail: filip.vanhoenacker@telenet.be

© Springer International Publishing AG 2017
F.M. Vanhoenacker et al. (eds.), *Imaging of Soft Tissue Tumors*, DOI 10.1007/978-3-319-46679-8_18

18.1 Introduction

As one may expect, the lesions of unknown differentiation constitute a very heterogeneous group of both neoplasms and tumorlike lesions. In the past, these tumors were also labeled as being "of uncertain origin." In view of the knowledge that these tumors do not arise from their normal cellular counterparts, the former classification based on "histiogenetic" concepts was no longer valuable. The current classification is based on terms of "differentiation," which depends on patterns of gene expression. For a lot of tumors, discussed in this chapter, the line of differentiation that they are recapitulating is still not clear. In contrast, for some other tumors, although the line of differentiation can be identified, the cellular counterpart cannot be identified in normal mesenchymal tissues. Nevertheless, consideration of their local growth pattern and clinical behavior allows further distinction between benign and malignant lesions, as presented below.

18.2 Classification

Tumors and tumorlike lesions of uncertain differentiation are commonly classified using the WHO classification [54], which has become the gold standard. Therefore, except for some minor changes, the latest version of this classification is used throughout this chapter.

18.3 Benign Lesions

18.3.1 Intramuscular Myxoma (Incl. Cellular Variant)

18.3.1.1 Definition

Intramuscular myxoma is a benign tumor of mesenchymal origin, histologically characterized by the presence of abundant, avascular myxoid stroma in which relatively small numbers of stellate or spindle-shaped cells and reticulum fibers are embedded. The macroscopic appearance is rather stereotypic: most tumors are ovoid or rounded and have a gelatinous consistence. Paucity of vascular structures within the lesion is obvious. On macroscopic section, the surface has a gray–white or white aspect, depending on the relative amounts of collagen. Occasionally, the lesion contains multiple small fluid-filled cavities [79, 120]. The size of the lesion mostly ranges between 5 and 10 cm in diameter, although quite large lesions with diameter surpassing 20 cm have been observed. An association exists between multiple intramuscular myxomas and fibrous dysplasia of the bone and is referred to as Mazabraud's syndrome. In the vast majority of patients with Mazabraud's syndrome, polyostotic fibrous dysplasia is present. Osseous involvement by fibrous dysplasia commonly occurs in the same anatomical region of the myxomas [79, 147, 164]. Malignant transformation of fibrous dysplasia to osteogenic sarcoma in patients with Mazabraud's syndrome has been reported in the literature [103]. Furthermore, the existence of a relationship between myxoma of the soft tissues and McCune–Albright syndrome (fibrous dysplasia, usually polyostotic in type, café au lait spots, and endocrinopathy including, but not limited to, precocious puberty, especially in women) has been mentioned [63, 88].

The exact etiology is still not clear. A traumatic factor in the genesis is unlikely, since a history of trauma is only present in less than 25 % of cases. Although familial incidence is not increased, the occasional association with fibrous dysplasia of the bone raises the possibility of a basic metabolic error or genetic mutation of both tissues [126]. Therefore, soft tissue myxoma has been considered by some authors to be "an extraskeletal manifestation of fibrous dysplasia" [147, 161].

18.3.1.2 Incidence and Clinical Behavior

Occurring almost exclusively in individuals between the fifth and seventh decades [120], the tumor is rare in young persons and virtually nonexistent in children. Female patients outnumber male patients [106, 120, 141]. In the majority of

cases, the only sign is a solitary, painless mass that is firm and often fluctuant on palpation. At the time of diagnosis, most lesions measure 5–10 cm in diameter. However, despite the large size, pain occurs in less than 25 % of cases. The rate of tumor growth is variable, and occasionally there is no apparent growth over a long period of time. There is no close relationship between the size and age of the lesion. The areas that are most frequently involved are the large muscles of the thigh, shoulder, buttocks, and upper arm. Although the majority of myxomas are solitary lesions, occasionally multiple myxomas are observed [161]. When these occur in the same region of the body, they are nearly always associated with fibrous dysplasia of the bone. The bones involved by fibrous dysplasia are usually in the vicinity of the myxoma [88, 164]. A long interval – sometimes up to 20 or 30 years – is observed between the appearance of the fibrous dysplasia, which is noted during the growth period, and the myxoma. This combination of multiple intramuscular myxomas and fibrous dysplasia (Mazabraud's syndrome) has a remarkable predilection for the right limb [161]. Following surgery, recurrence of intramuscular myxoma is rare.

18.3.1.3 Imaging

Imaging Studies Other Than MRI

As intramuscular myxomas do not contain calcifications, conventional radiographs are of little value in the diagnosis: they may be normal or reveal a nonspecific soft tissue mass. On CT, the myxoma presents as a sharply demarcated mass within the skeletal muscle. The attenuation of the lesion is intermediate between that of water and the muscle and ranges typically between 10 and 60 Hounsfield units [42, 79] (Figs. 18.1, 18.2, 18.3, 18.4 and 18.5). However, attenuation values close to those of fat have been reported and may be misleading, as they mimic a fat-containing neoplasm [91]. Owing to the paucity of vascular structures within the lesion, the myxoma presents as a poorly vascularized soft tissue mass surrounded by well-vascularized muscle on angiograms.

MRI Findings

On MRI, intramuscular myxoma presents as a well-circumscribed, homogeneous intramuscular mass. Signal intensity is low (less than or equal to that of muscle tissue) on T1-weighted images and very high (brighter than fat) on T2-weighted images, quite similar to the signal characteristics of fluid [116]. In most of the cases of myxoma, the presence of a fat rim has been demonstrated corresponding to focal atrophy of the surrounding muscle [148]. Following the administration of gadolinium chelates, inhomogeneous enhancement is observed. The degree of enhancement seems proportional to the amount of solid myxoid tissue and fibrous septa, which are both variable in degree within the myxoma [79]. The areas of low signal intensity on the contrast-enhanced images represent cystic areas on histologic examination [128] (Figs. 18.1, 18.2, 18.3, 18.4, 18.5 and 18.6).

18.3.1.4 Imaging Strategy

Conventional radiographs are of little value for the diagnosis of intramuscular myxoma. An exception is made in the case of patients with both multiple myxomas and fibrous dysplasia, but in these cases, conventional radiographs are used primarily for investigation of the bony lesions. Of note, Mazabraud's syndrome should always be taken into account when fibrous dysplasia occurs with one or more soft tissue masses. CT – like MRI – may reveal misleading findings by demonstrating fat densities within a myxoma that suggest a lipomatous tumor (lipoma or well-differentiated liposarcoma). Sarcomas, particularly with myxoid degeneration, may resemble myxomas both radiologically and histologically. Although MRI is the preferred imaging technique for staging, one has to admit that the MRI findings of intramuscular myxoma are not highly specific.

Synovial cysts, bursas, and ganglia, which can look like a myxoma, are usually juxta-articular and intermuscular and not intramuscular. Moreover, as cystic masses, they show a thin rim of enhancement after administration of intravenous contrast agent. Neurogenic tumors (e.g., neurofibroma, nerve sheath tumors) are also

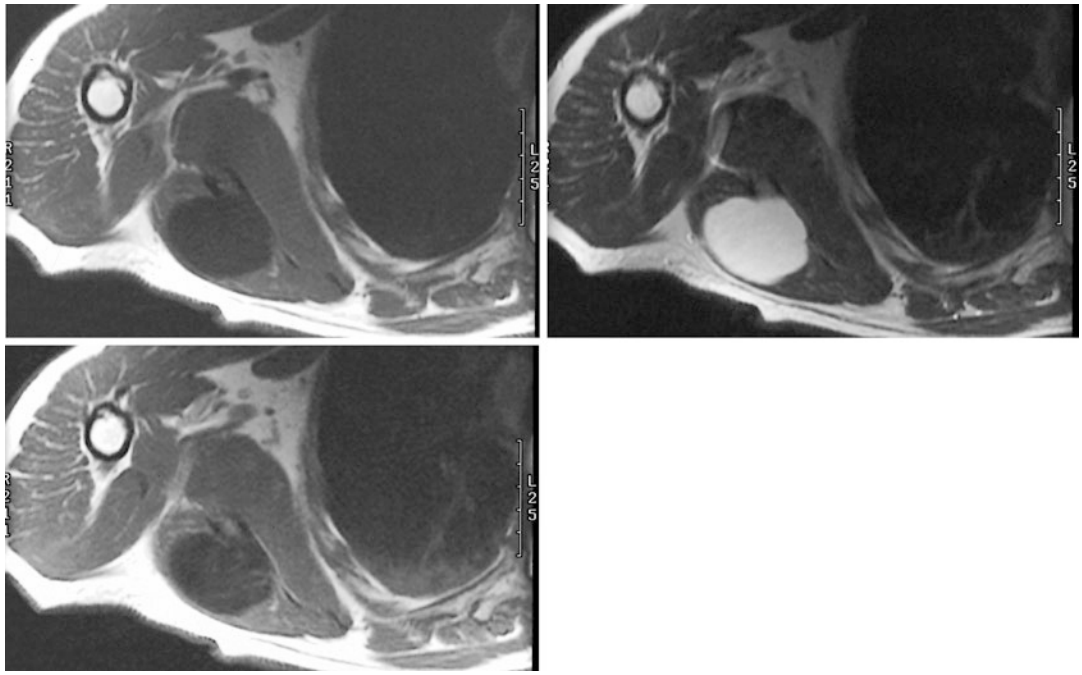

Fig. 18.1 Intramuscular myxoma at the right scapular region in a 68-year-old man. (**a**) Axial spin-echo T1-weighted MR image. (**b**) Axial spin-echo T2-weighted MR image. (**c**) Axial spin-echo T1-weighted MR image after gadolinium contrast injection. Large, rounded, intramuscular lesion at the infraspinatus fossa is visible. The mass is well circumscribed and homogeneous on both spin-echo sequences, hypointense to muscle tissue on the T1-weighted image, and hyperintense to fat on the T2-weighted image (**a**, **b**). After contrast medium injection, only a few enhancing strands are observed within the lesion. The major parts of the lesion do not enhance. This pattern of enhancement illustrates well the sparse vascularization of the lesion

rather inter- than intramuscular, and often a so-called target sign is seen on T2-weighted MR images [117].

18.3.2 Acral Fibromyxoma

(Superficial) Acral fibromyxoma (AFM) is a very rare benign tumor arising in the subungual and periungual regions in fingers and toes of adult patients usually not exceeding 2 cm in diameter. Men are more frequently affected by the slow-growing and painless lesion than women (2:1). Histologically, AFM consists of spindled fibroblast-like and stellate cells surrounded by a myxoid and/or collagenous matrix with immunoreactivity for CD34, CD99, endomysial antibody (EMA), vimentin, and CD10. After surgical excision which is the treatment of choice, recurrence is rare [9, 52].

AFM has been described as being isointense to the muscle on T1-weighted MR images, while being hyperintense on T2-weighted images. This imaging appearance distinguishes AFM from giant cell tumors of the tendon sheath, which are predominantly hypointense on T1- and T2-weighted sequences. Homogeneous enhancement is seen on post-contrast MRI. When located in deeper tissues with contact to the bone, osseous erosions or scalloping can be caused [16, 156] (Fig. 18.7).

18.3.3 Juxta-Articular Myxoma

Juxta-articular myxomas are characterized by depositions of myxoid material in the juxta-articular tissues of the knee or rarely other joints and occasionally with myxoid changes within the underlying cartilage. The term “parameniscal

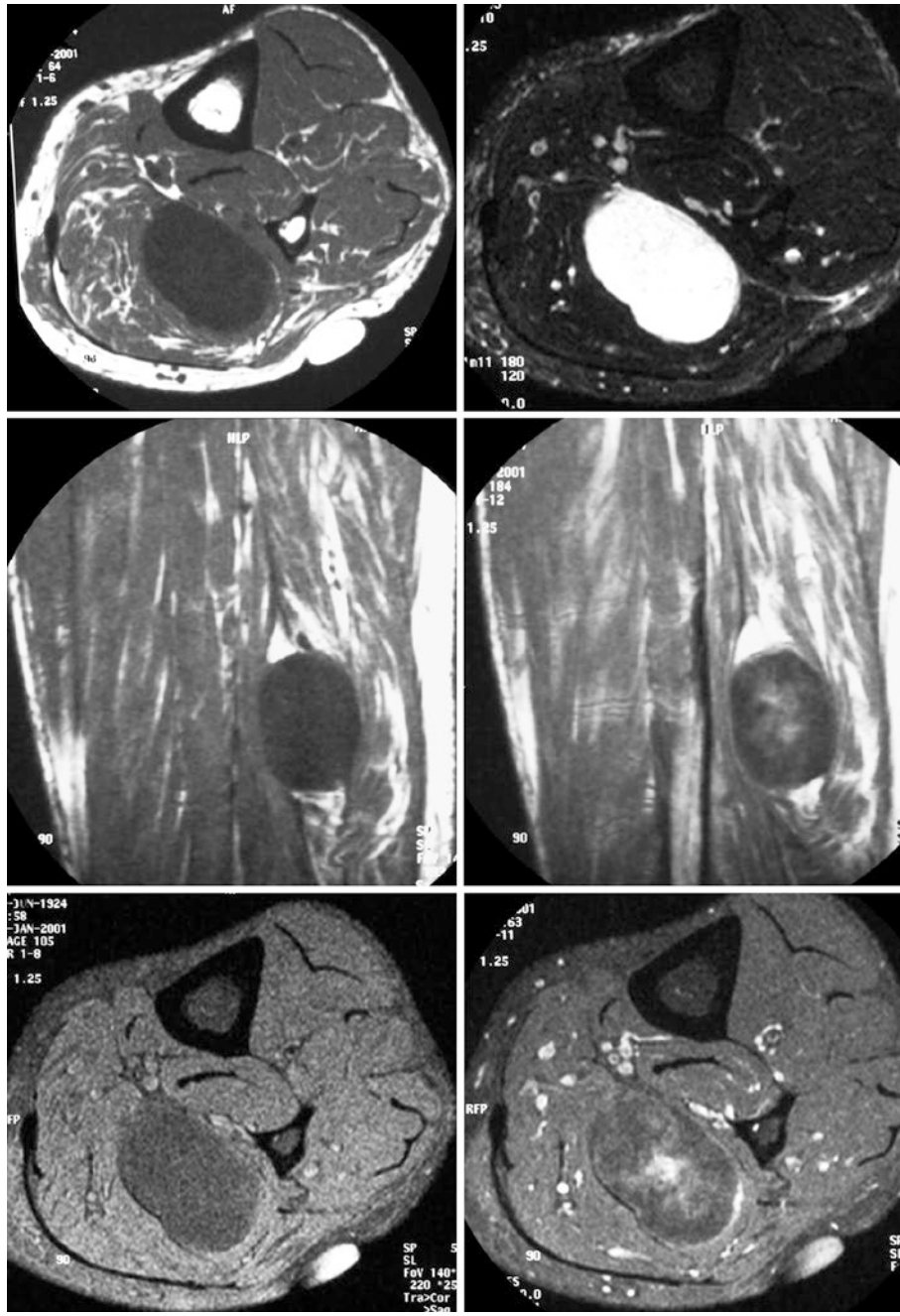

Fig. 18.2 Intramuscular myxoma of the calf. (**a**) Axial spin-echo T1-weighted MR image, (**b**) axial STIR T2-weighted MR image, (**c**) sagittal spin-echo T1-weighted MR image, (**d**) sagittal spin-echo contrast-enhanced T1-weighted MR image, (**e**) axial spin-echo T1-weighted MR image with fat suppression, and (**f**) axial spin-echo T1-weighted MR image with fat suppression after gadolinium contrast injection. Oval-shaped mass within the soleus muscle is observed. The lesion is sharply outlined. On T1-weighted images, the lesion is hypointense to muscle tissue (**a**, **c**, **e**). T2-weighted images reveal a homogeneously hyperintense aspect of the tumor, with signal intensity equivalent to fluid (**b**). Following injection of contrast medium, no enhancement is observed at the periphery of the lesion, while the central part shows a definite enhancement (**d**, **f**). The areas of enhancement correspond to regions with high amount of solid myxoid tissue

cyst" refers to small types of such lesions. Calcification of the myxoid matrix may occur in older lesions [5, 159].

Fig. 18.3 Multiple intramuscular myxomas with polyostotic fibrous dysplasia of the bones of the lumbar spine, pelvic bones, and femur in a 35-year-old man (Mazabraud's syndrome). Plain radiograph discloses multiple multilocular cyst-like lesions with a ground-glass appearance, separated from each other by thin septations within the fifth lumbar vertebra, the right pelvic bones, and the right femur, corresponding to fibrous dysplasia. These involved bones are markedly deformed. Endomedullary osteosynthetic material at the femur witnesses the previous pathologic fracture (Courtesy of Trigaux JP, Nisolle JF, Cliniques Universitaires UCL de Mont-Godinne, Belgium)

18.3.4 Myxoma of the Jaws

Although primarily a bone tumor, myxoma of the jaws (odontogenic myxoma) may manifest as a myxomatous swelling or mass in the soft tissues near the mandible or maxilla. It is characterized by higher cellularity and cellular pleomorphism than other myxomas.

Most myxomas of the jaws affect young adults. In its common presentation, the tumor overlies an osteolytic defect in the mandible and/or maxillary bone and may displace or destroy the teeth, penetrate into the maxillary sinus, or involve soft tissues of the face.

Myxoma of the jaws is seen radiologically as an expansive, well-circumscribed, most often multilocular radiolucency within the jaw bone. CT is recommended for assessing the extent of the lesion (Fig. 18.8, former Fig. 23.9). MRI is superior for demonstrating the extent of soft tissue involvement, but is inferior to CT for evaluating the underlying bony lesion [29, 83, 86, 99] (Figs. 18.8 and 18.9; former Figs. 23.9 and 23.10). The tumors are usually hyperintense in T2-weighted MR images and show contrast enhancement in the peripheral areas, while the center does not enhance [86].

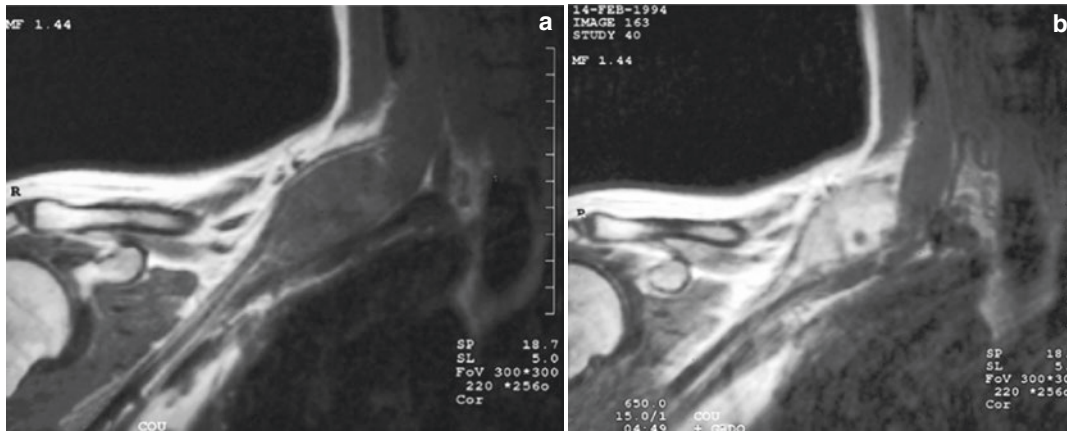

Fig. 18.4 Multiple intramuscular myxomas with polyostotic fibrous dysplasia of bone of the lumbar spine, pelvic bones, and femur in a 35-year-old man. (**a**) CT at the level of the hips. (**b**) CT at the level of right trochanteric region. CT confirms the replacement of medullary fat of the right ischium and femur by fibrous tissue. Expansion and thickening of the overlying cortex. These findings correspond to fibrous dysplasia of the bone. In addition, well-delineated, non-enhancing, homogeneously hypodense soft tissue masses are observed within the right gluteal (**a**) and adductor (**b**) muscles, corresponding to intramuscular myxomas (Courtesy of Trigaux JP, Nisolle JF, Cliniques Universitaires UCL de Mont-Godinne, Belgium)

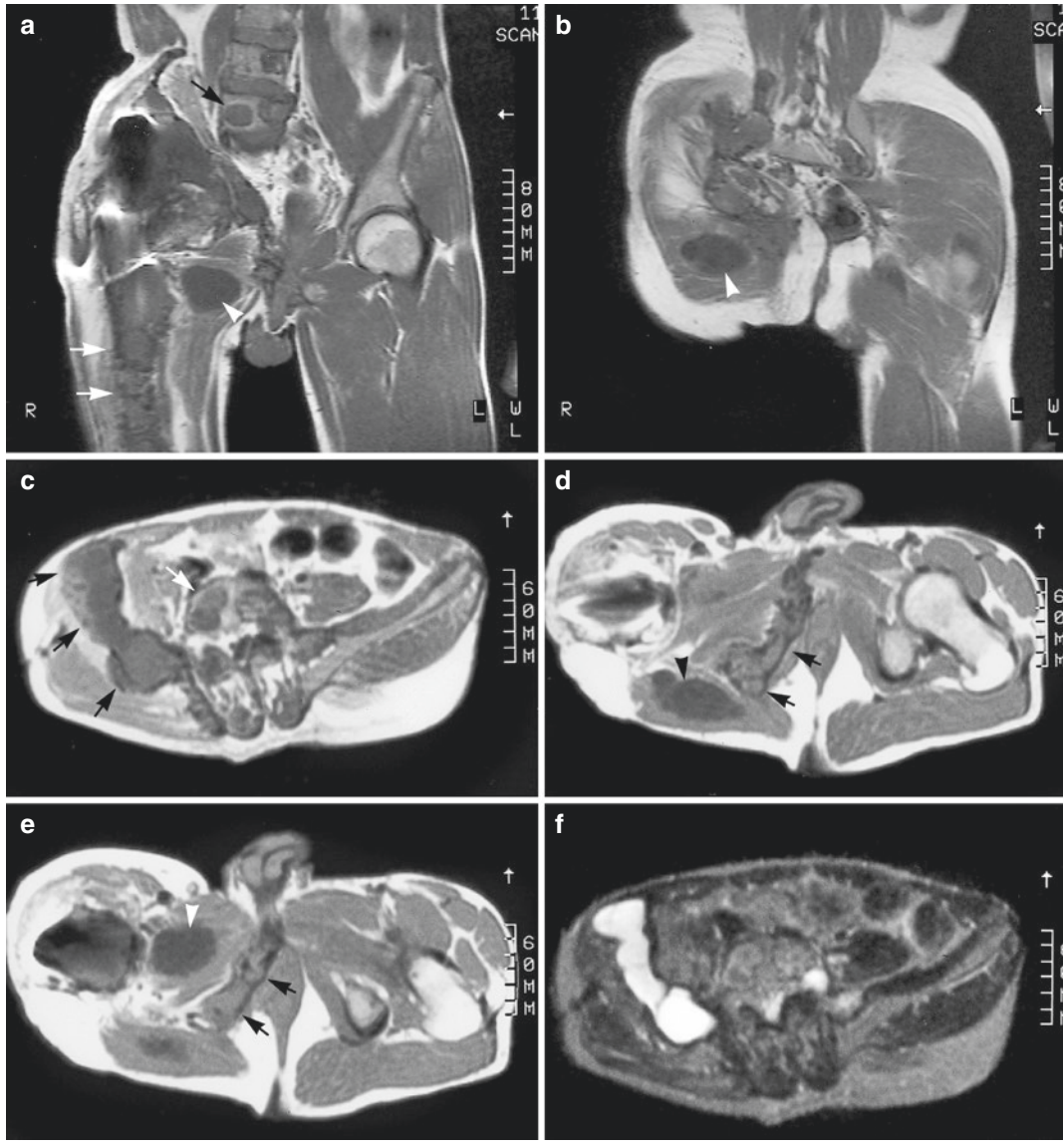

Fig. 18.5 Multiple intramuscular myxomas with polyostotic fibrous dysplasia of bone of the lumbar spine, pelvic bones, and femur in a 35-year-old man. (**a**, **b**) Coronal spin-echo T1-weighted MR images at the level of the right femoral diaphysis (**a**) and gluteal muscles (**b**). (**c**–**e**) Axial spin-echo T1-weighted MR images at the level of the iliac wings (**c**), hips (**d**), and trochanteric regions (**e**). (**f**–**h**) Axial spin-echo T2-weighted MR images at the level of the iliac wings (**f**), hips (**g**), and trochanteric regions (**h**). The intramuscular myxomas appear as homogeneous, very low-intensity soft tissue masses within the right adductor (**a**, **e**) and gluteal (**b**, **d**) muscles (*arrowheads*). The areas of the right pelvic bones, right femur, and lumbar vertebrae that are involved by fibrous dysplasia have a lobular appearance with low signal intensity (*arrows*). On T2-weighted images, both myxomas are very bright, indicating long T2 relaxation times of their myxoid matrix. The gluteal myxoma is composed of several lobules, separated from each other by low-intensity septations. The areas involved by fibrous dysplasia of the bone are best observed at the level of the right iliac wing. Due to cystic degeneration, these areas appear extremely bright on T2-weighted images. Artifacts are observed on all images in the right hip region. These are due to magnetic field inhomogeneity, which is caused by the metallic hip prosthesis (Courtesy of Trigaux JP, Nisolle JF, Cliniques Universitaires UCL de Mont-Godinne, Belgium)

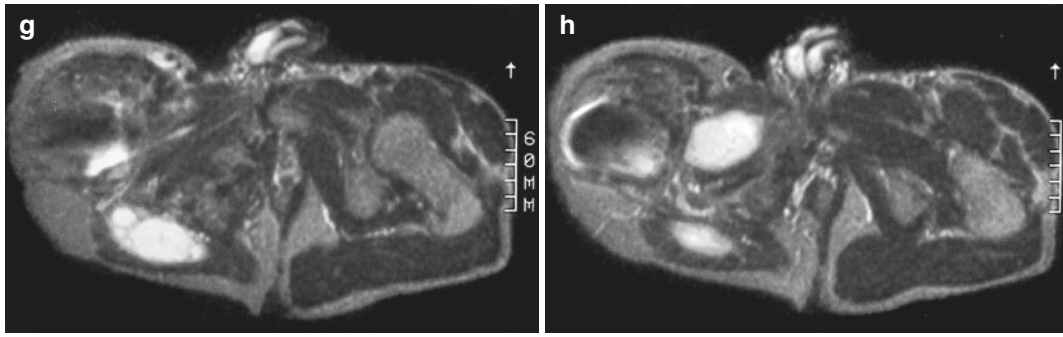

Fig. 18.5 (continued)

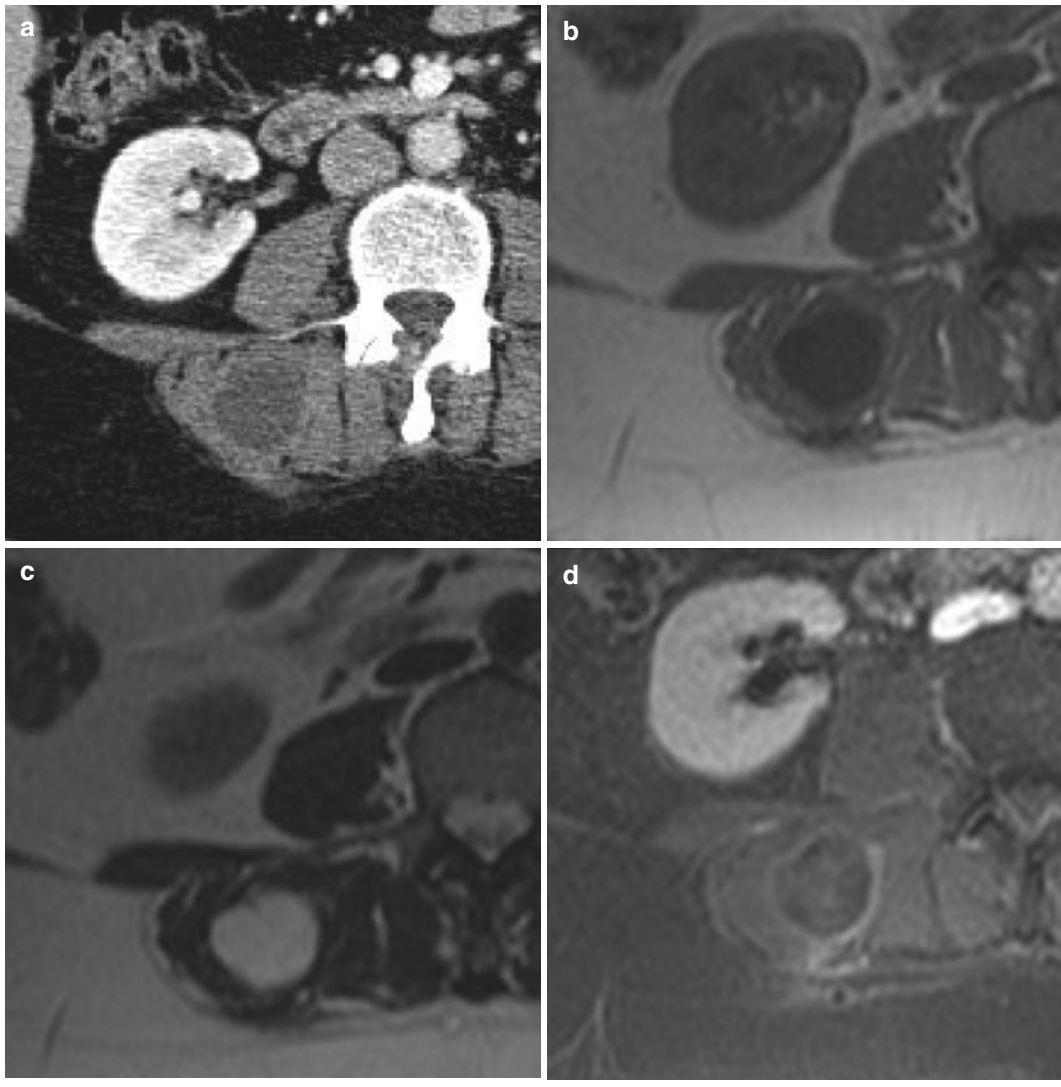

Fig. 18.6 Intramuscular myxoma in the autochthonous back muscles. (**a**) Axial CT-scan. (**b**) Axial T1-weighted MR image. (**c**) Axial T2-weighted MR image. (**d**) Axial T1-weighted MR image after gadolinium contrast injection. On CT, the myxoma presents as a well-demarcated lesion within the skeletal musculature with an intermediate attenuation (i.e., between that of water and muscle tissue) (**a**). Typically, one can see hypointensity on T1-weighted images (**b**), very high intensity on T2-weighted images (**c**), as well as inhomogeneous contrast enhancement

Fig. 18.7 Acral fibromyxoma (Used with permission from Varikatt et al. [156])

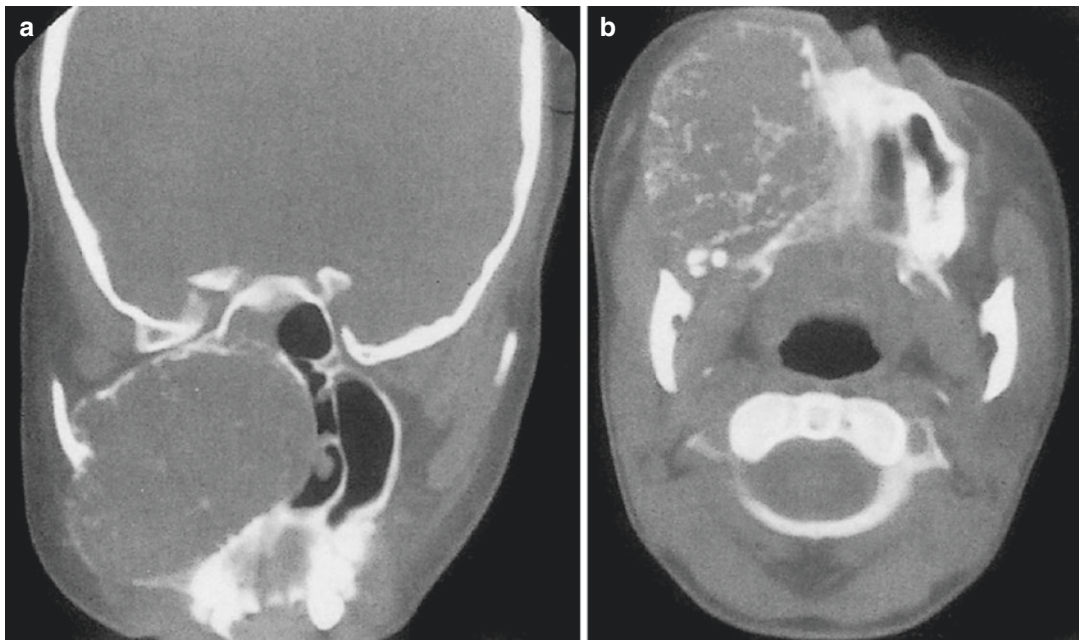

Fig. 18.8 Myxofibroma of the jaws in an 18-year-old woman. (**a**) Coronal CT. (**b**) Axial CT. The presence of an expansive myxofibroma replacing the right maxillary antrum. Expansion, thinning, and destruction of the surrounding bony margins are obvious. Bony trabeculations are well seen within the lesion (Reproduced from [29], with permission)

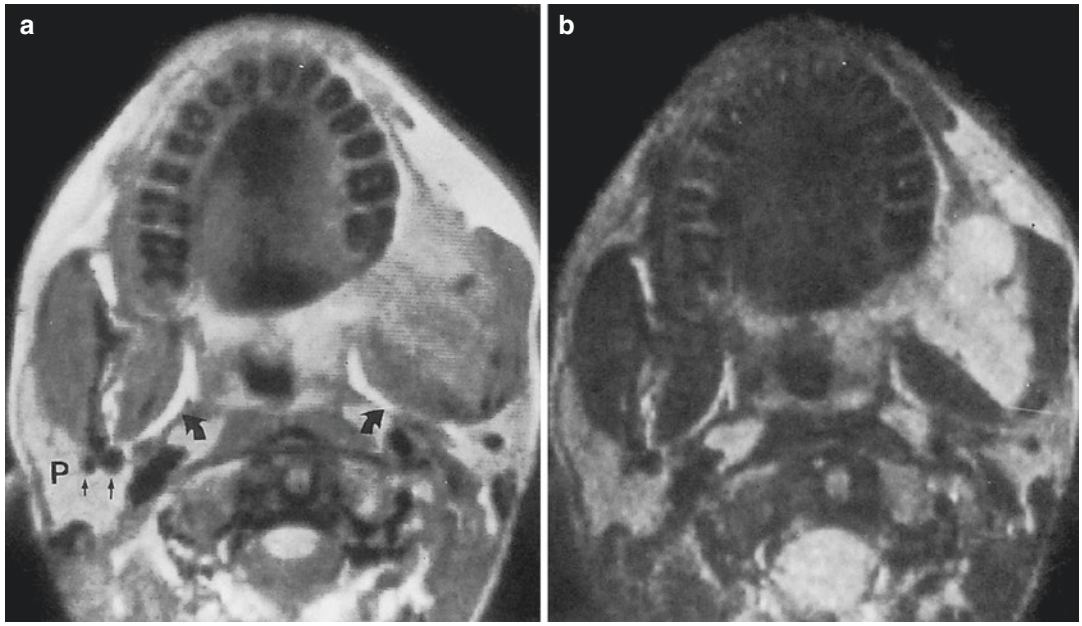

Fig. 18.9 Myxofibroma of the jaws in a 16-year-old boy. (**a**) Axial spin-echo proton density-weighted MR image. (**b**) Axial spin-echo T2-weighted MR image. Expansive lesion at the left ascending ramus of the mandible is seen. On the proton density-weighted image, the myxofibroma has increased signal intensity compared with the pterygoid and masseter muscles. The T2-weighted image reveals high signal intensity of the tumor, surpassing that of fat. Tumor margins are sharp. Note the bright signal of the parapharyngeal fat (*curved arrows*) and the presence of vascular structures (*straight arrows*) within the parotid gland (P) (Reproduced from [29], with permission)

18.3.5 Deep ("Aggressive") Angiomyxoma

18.3.5.1 Definition

Aggressive angiomyxoma is a rare, slowly growing neoplasm, which predominantly occurs in the pelvic soft tissue in women. The tumor has a gelatinous appearance, and its diameter ranges from a few centimeters to more than 20 cm [100, 113].

18.3.5.2 Incidence and Clinical Behavior

The majority of angiomyxomas occur in women between ages of 25 and 60 years. This tumor has a predilection for the gluteal, perineal, and pelvic regions. Although a slow growth pattern is seen, the tumor is focally infiltrative, often extending into the paravaginal and perirectal regions. Metastatic spread is not observed. Recurrence rate after surgical removal is high [100].

18.3.5.3 Imaging

On CT, aggressive angiomyxoma has a variable appearance. It has been described either as a predominantly cystic mass containing solid components or as a solid mass containing low-density areas [100, 163]. MRI reveals a high signal intensity mass with hypointense strands of fibrovascular tissue on T2-weigthed images. In addition, mild restriction on diffusion-weighted imaging (DWI) and high mean values in apparent diffusion coefficient (ADC) maps as well as a layered enhancement seem to be typical [113]. The lesion shows a tendency to displace pelvic organs and to grow around pelvic floor muscles, but without disrupting them (Fig. 18.10). Of note, the lack of high fat content is a key feature in differentiating aggressive angiomyxoma from myxoid liposarcoma.

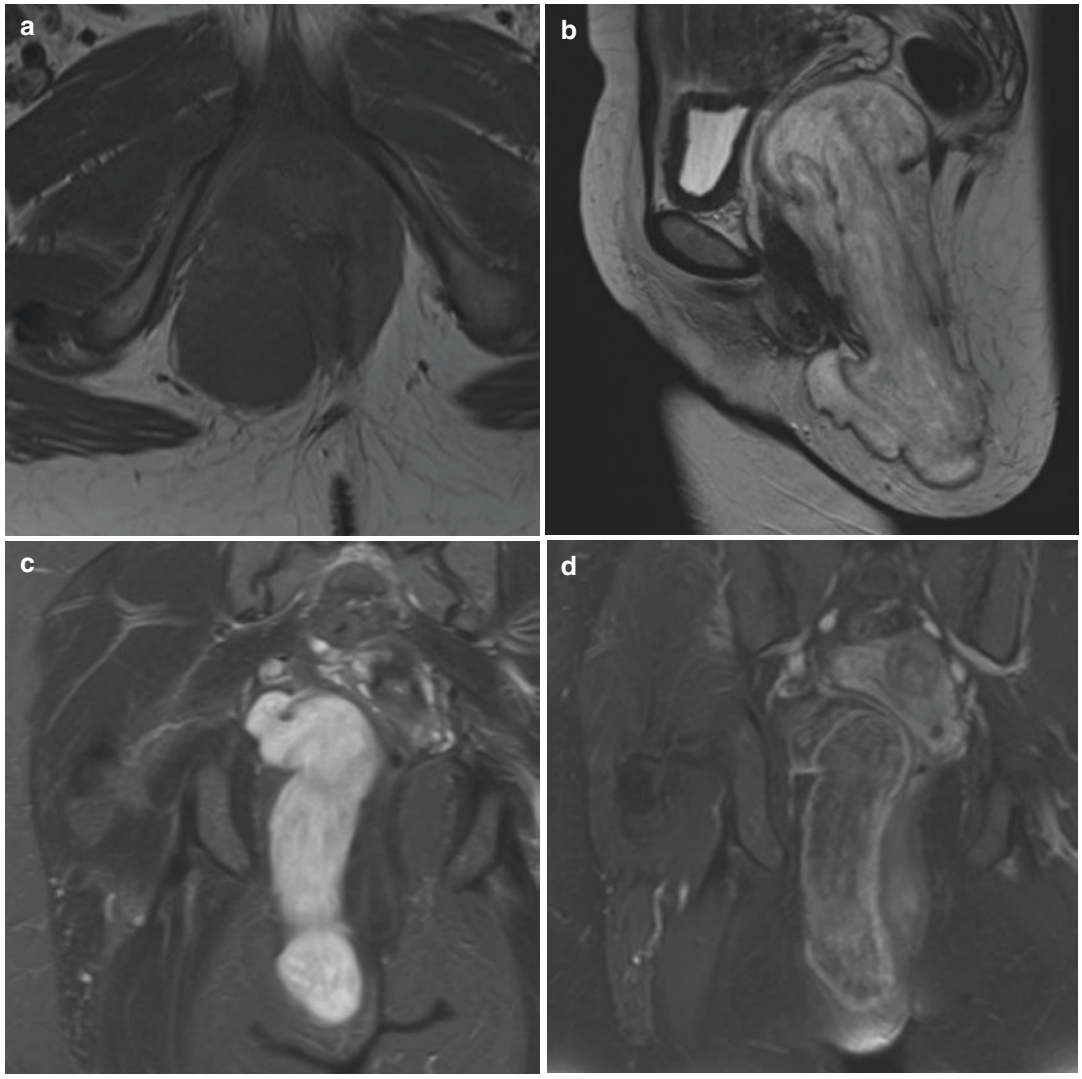

Fig. 18.10 Paravaginal aggressive angiomyxoma. (**a**) Axial T1-weighted MR image. (**b**) Sagittal T2-weighted MR image. (**c**) Coronal T2-weighted MR image with fat saturation (fs). (**d**) Coronal T1-weighted MR image after gadolinium contrast injection. The paravaginal aggressive angiomyxoma which measured more than 20 cm and displaced the uterus and bladder was initially misinterpreted as bartholinitis. On T1-weighted images, the mesenchymal tumor presents as a hypointense mass (**a**) to muscle tissue, while showing a high signal intensity on T2-weighted images (**b**, **c**) with typical hypointense strands of fibrovascular tissue, which also enhanced after gadolinium contrast injection (**d**)

18.3.6 Pleomorphic Hyalinizing Angiectatic Tumor

18.3.6.1 Definition

Pleomorphic hyalinizing angiectatic tumor (PHAT) is a very rare entity of low malignant potency which occurs in the subcutaneous tissues of the lower extremity. Grossly, the lesions have a lobulated appearance with characteristic thin-walled angiectatic vessels surrounded by fibrin and collagen [59, 142].

18.3.6.2 Incidence and Clinical Behavior

Pleomorphic hyalinizing angiectatic tumors occur mainly in the fifth decade, and men are affected

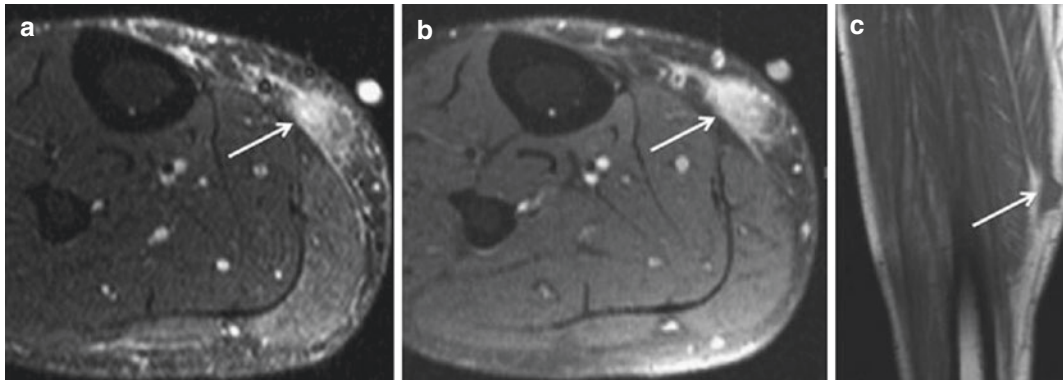

Fig. 18.11 A 46-year-old male with pleomorphic hyalinizing angiectatic tumor in the calf. The STIR image (**a**) shows a subcutaneous hyperintense lesion (*arrow*) overlying the medial soleus and medial head of the gastrocnemius muscles. Axial post-contrast image (**b**) at the same level shows relatively homogeneous enhancement of the subcutaneous mass (*arrow*), which abuts the underlying gastrocnemius muscular fascia but remains confined to the subcutaneous soft tissues. Note ill-defined margins and strands of signal abnormality extending along the fascia. Coronal T1-weighted image (**c**) demonstrates homogeneous T1 isointensity to muscle (*arrow*), with minimal infiltration of the subcutaneous fat

more frequently. Usually, these tumors are found in the superficial subcutaneous fat tissue of the trunk, as well as the upper and predominantly the lower limb. Recurrence rate after surgical removal is high; metastases have not been reported [100, 110].

18.3.6.3 Imaging

On pre-contrast CT scans, the tumor is inhomogeneously hypodense. After contrast administration, PHAT usually shows a heterogeneous enhancement with lower density around the angiectatic vessels corresponding to the hyalinized vessel walls [92]. MRI can illustrate the ill-defined margins and the infiltration of fat tissue; beyond this, MRI findings are rather unspecific, since PHAT can show solid and cystic components and variable contrast enhancement [146] (Figs. 18.11, 18.12 and 18.13).

18.3.7 Ectopic Hamartomatous Thymoma

18.3.7.1 Definition, Incidence, and Clinical Behavior

Ectopic hamartomatous thymoma (EHT) is an extremely rare benign tumor usually located in the lower neck region next to the sternocostal joint. Predominantly, men in the third and fourth decade are affected. These tumors are well defined and slow growing, not showing metastasis. Histologically, these tumors consist of spindle cells and epithelial and adipose cell elements [135]. Only seldom recurrence after resection is seen.

The histogenesis remains unclear: initially, it was thought that EHT could derive from ectopic thymus tissue along the migration path of the embryonic thymus from the pharynx to the anterior mediastinum, but since normal thymus tissue never was found in EHT, investigators now believe that it could be of branchial origin, respectively, a remnant of the submerged caudal portion of the second arch and the third and fourth branchial arch [51].

18.3.7.2 Imaging

Until the present, no specific study concerning imaging has been performed. Thus, when encountering a space-occupying lesion in the lower neck region next to the sternocostal joint in men, EHT should be incorporated into the differential diagnostic list.

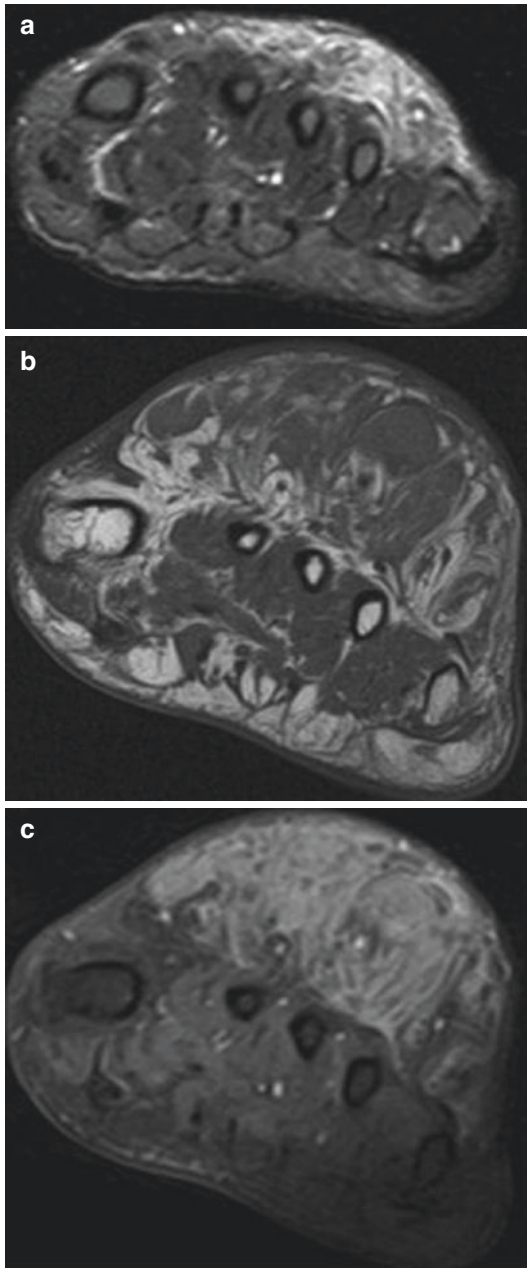

Fig. 18.12 49-year-old female with PHAT in the foot. Proton density–weighted images (**a**) with fat saturation in the coronal plane shows ill-defined hyperintense signal in the subcutaneous tissues at the dorsum of the forefoot over the metatarsal shafts. Coronal T1-weighted image (**b**) from subsequent MRI 3 years later demonstrates significant interval growth of the ill-defined soft tissue mass. Coronal post-contrast image (**c**) demonstrates diffuse enhancement within the mass on the later exam. Note interspersed fat signal throughout the lesion and ill-defined margins

18.4 Intermediate Tumors (Locally Aggressive)

18.4.1 Hemosiderotic Fibrolipomatous Tumor

18.4.1.1 Definition, Incidence, and Clinical Behavior

Hemosiderotic fibrolipomatous tumor (HFLT) is a rare soft tissue neoplasm consisting of adipocytes, hemosiderin pigments, and fibrous tissue. The tumor arises characteristically in the foot or ankle region or the dorsum of hands of middle-aged women and tends to recur in 30–50 % after excision [54]. Malignant transformation into myxoinflammatory fibroblastic sarcoma has been described [143], an entity with the same characteristic chromosome translocation t(1;10)(p22;q24) as HFLT.

18.4.1.2 Imaging

Radiography and ultrasound are usually nonspecific. MRI shows an often ill-defined tumor with fatty areas divided by reticular septations. On T1-weighted sequences, HFLT is iso- or hypointense to the muscle, while being hyperintense on T2-weigthed images, possibly due to the myxoid/fibrous content of HFLT. Contrast enhancement of the nonfatty tumor parts has been described (Fig. 18.14). Because of hemosiderin deposition in HFLT, susceptibility-weighted imaging sequences such as T2* can show characteristic blooming in foci of hemorrhage, which can be helpful to distinguish HLFT from other lipomatous lesions [121].

18.5 Intermediate Tumors (Rarely Metastasizing)

18.5.1 Atypical Fibroxanthoma

18.5.1.1 Definition, Incidence, and Clinical Behavior

Atypical fibroxanthoma (AFX) is a rare mesenchymal tumor of intermediate malignancy affecting elderly patients and arising in the sun-exposed cutis of the head and neck region. AFX

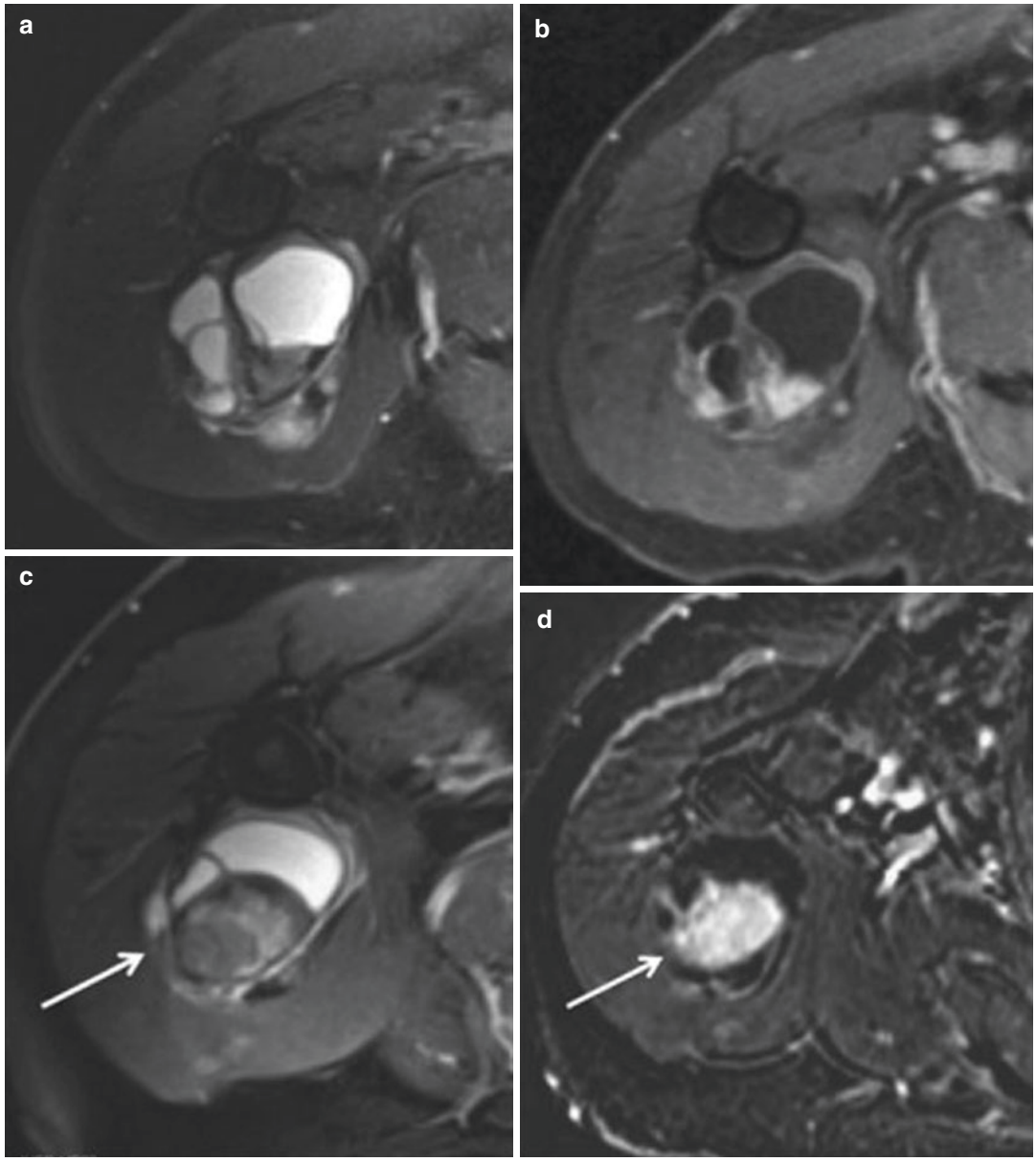

Fig. 18.13 An 87-year-old woman with PHAT of the proximal upper extremity. Axial T2-weighted with fat saturation (**a**) and post-contrast T1-weighted images (**b**) performed at presentation demonstrate a multiloculated cystic mass in the right triceps muscle, with nodular and thickened enhancing septa. Axial T2-weighted with fat saturation (**c**) and post-contrast T1-weighted images (**d**) from subsequent examinations 2.4 years later show an enlarging solid component (*arrows*) within the cystic portion of the mass. The mass was later resected, and histologic features were most suggestive of a PHAT (Used with permission from Subhawong et al. [146])

tends to show exophytic growth; ulceration and bleeding are also possible. Histologically, AFX consists of fibroblastic spindle cells as well as multinucleated epithelioid cells and giant cells. Despite the sometimes aggressive histological appearances, AFX has a benign clinical course, when diagnosed early and excised completely [89, 105].

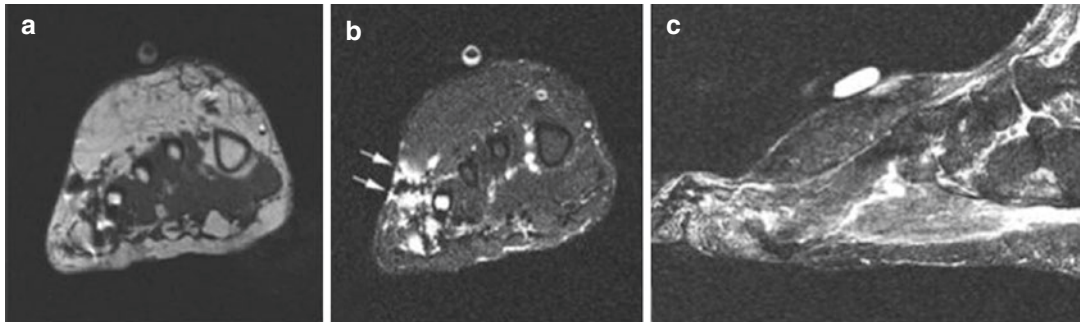

Fig. 18.14 56-year-old woman with haemosiderotic fibrolipomatous tumorsuperficial to the metatarsals. A coronal T1-weighted MR image (**a**) shows a high-signal mass superficial to the metatarsals that is predominantly fat-intense. A coronal T2-weighted fat-suppressed MR image (**b**) shows a predominantly fat-intense mass. Also present, as indicated by the arrows, are unrelated areas of high and low signal intensity that represent postsurgical changes from the patient's prior foot surgeries. A sagittal T2-weighted fat-suppressed MR image again shows a fat-intense mass superficial to the metatarsals (**c**). (Used with permission from Moretti et al. [165])

18.5.1.2 Imaging

There is only limited literature about the radiological appearance of AFX available. Ultrasonography and MRI can be used to determine the extent of the tumor or possible infiltration of subcutis. In one case study, AFX shows intermediate signal intensity on T1-weighted and T2-weighted images and diffusely heterogeneous enhancement after contrast-agent administration [96], while both malignant melanoma and squamous cell carcinoma as possible differential diagnoses tend to have a high signal intensity on T2-weighted images. Melanin within melanoma may also cause elevated T1 signal intensities.

18.5.2 Angiomatoid Fibrous Histiocytoma

18.5.2.1 Definition

Angiomatoid fibrous histiocytoma (AFH) is a rare, low-malignant soft tissue tumor. Usually, AFH presents as a well-circumscribed multilobular mass showing a fibrous pseudocapsule with typical lymphocytic infiltrates and consisting of fibroblast and histiocyte-like cells of low mitotic activity and blood-filled spaces [82].

18.5.2.2 Incidence and Clinical Behavior

AFH usually occurs in children and young adults. It predominantly affects the dermis and subcutaneous tissue in the extremities and the trunk. Metastasis is only rarely seen.

18.5.2.3 Imaging

Correspondingly, CT and MRI show a lobulated soft tissue mass sometimes with fluid–fluid levels and focal low signal intensity in T1- and T2-weighted sequences as a sign of intralesional hemorrhage [97] (Fig. 18.15).

18.5.3 Ossifying Fibromyxoid Tumor

18.5.3.1 Definition

Ossifying fibromyxoid tumor (OFMT) is a rare soft tissue tumor of still unknown origin arising in the subcutaneous tissue of the extremities usually following a benign clinical course. Yet single cases showing cellular atypia, aggressive behavior, and metastasis have been described [87]. Typically, OFMT consists of small round cells and osteoid or lamellar bone [44, 58, 87, 136].

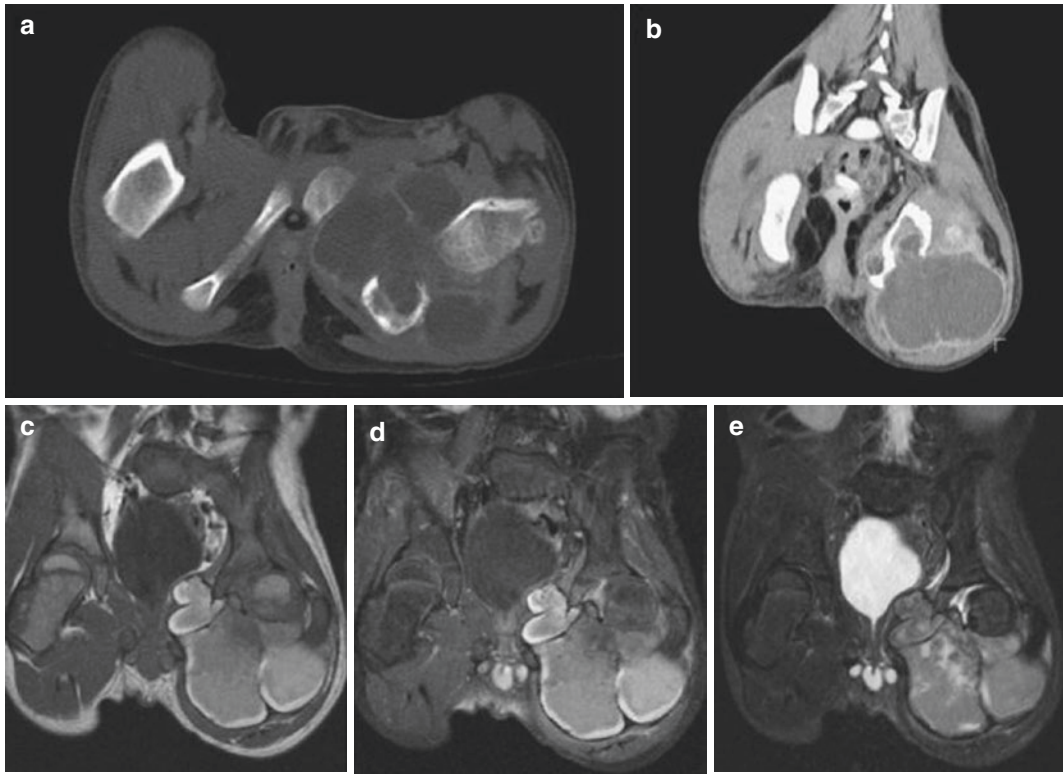

Fig. 18.15 A 5-year-old boy with AFH of the bone. Axial and coronal reformat CT scan images demonstrate an expansile lytic lesion with a large cortical break in the left posterior ischium (**a**). The mass is predominantly fluid-density with thin, enhancing septations, and an extensive extraosseous component. Coronal T1-weighted MR image demonstrates a lobulated intraosseous left ischial mass with hyperintense peripheral signal (felt to represent methemoglobin) as well as an extensive extraosseous component (**c**). A fine dark signal capsule or pseudo-capsule is also noted beyond the hyperintense rind. Coronal T1-weighted gadolinium-enhanced fat-saturated image demonstrates at most minor enhancement with much of the peripheral hyperintensity present pre-contrast. The fine dark signal rind is again noted (**d**). Coronal STIR image demonstrates heterogenous signal intensity and a dark rim (**e**). (Used with permission from Petrey et al. [166])

18.5.3.2 Incidence and Clinical Behavior

OFMT presents as a slowly growing lobulated, ossified, and encapsulated mass in the fifth to seventh decade of life with a male predominance. The tumor diameter does seldom exceed 10 cm.

18.5.3.3 Imaging

CT can demonstrate the characteristic lamellar bone formation as well as a strong contrast enhancement corresponding to the good vascularization that is typical of OFMT. In MRI, focal areas of high signal intensity on T1-weighted images of the tumor as a sign of fatty marrow spaces seem to be characteristic [67, 125] (Fig. 18.16).

18.5.4 Mixed Tumor

18.5.4.1 Myoepithelioma

Definition

Myoepithelioma is a benign tumor showing a wide range of histopathological features making the diagnosis complicated [35]. Tumors have a multinodular or lobular appearance and can be well circumscribed or infiltrative. Spindled, ovoid, or epithelioid tumor cells are seen, while atypia is absent.

Incidence and Clinical Behavior

Myoepithelioma is most frequently found in the subcutis of extremities presenting as a slow-

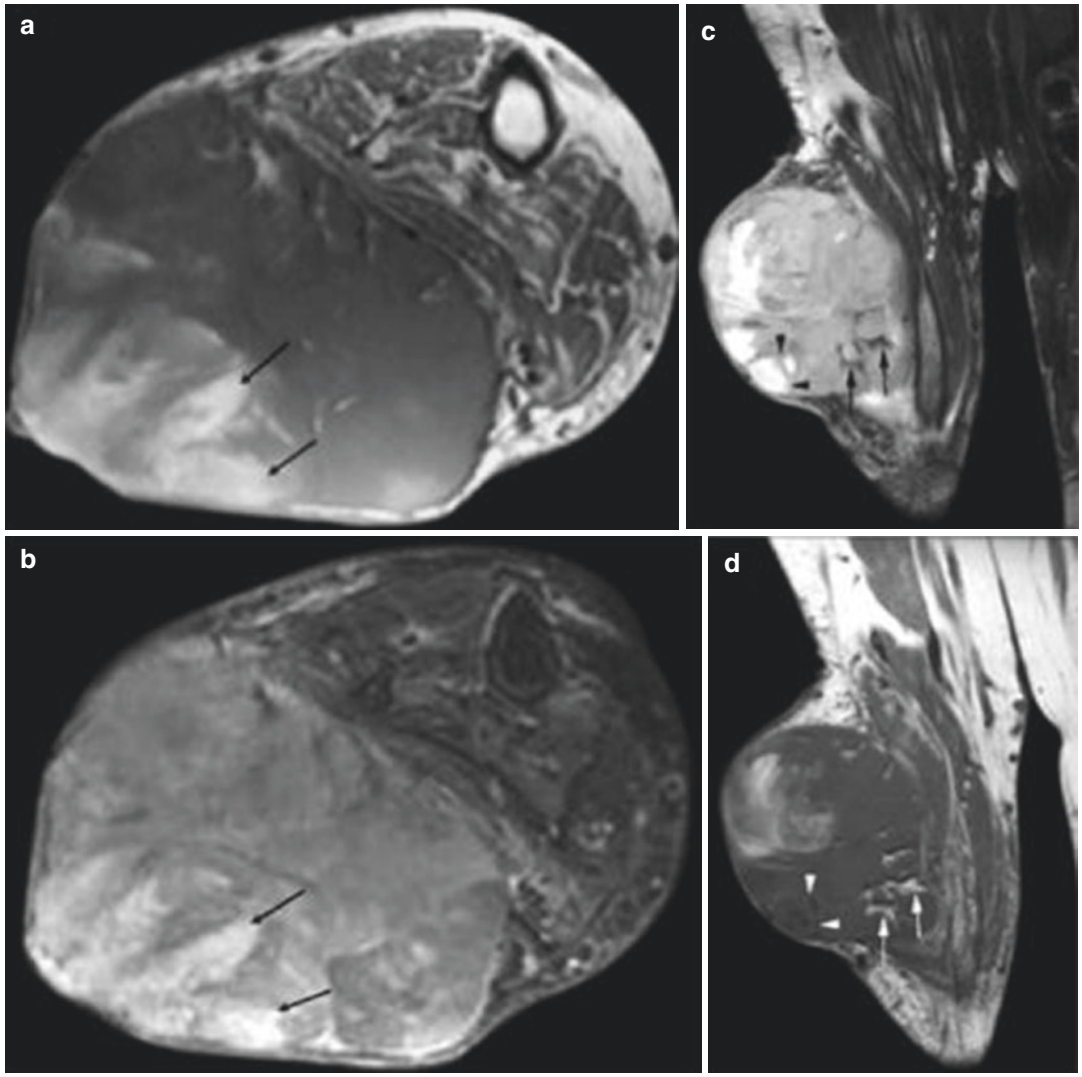

Fig. 18.16 77-year-old woman with ossifying fibromyxoid tumor of the calf. Axial T1W (**a**) and T2W FS (**b**) images through the right calf demonstrate the mass, which is subcutaneous and seen to displace, rather than infiltrate, the adjacent musculature. The mass is predominantly isointense to muscle on T1W image and of intermediate-to-high signal intensity on T2W FS image. Foci of hyperintensity are seen on the posterolateral aspect of the mass on both sequences (*arrows*), in keeping with haemorrhage. Coronal MR images show areas of low signal intensity (*black arrows*) on T2W FS (**c**) and high signal intensity (*white arrows*) on T1W (**d**) sequences, consistent with fatty marrow spaces. There are also foci consistent with necrosis, seen with areas of low signal intensity on T1W (*white arrowheads*) and high signal intensity on FSE T2W FS (*black arrowheads*) images. (Used with permission from Harish et al. [67])

growing painless (sub)cutaneous mass. There is no known predilection concerning age and sex. Recurrence after excision is rare; metastasis has not been described [74, 80, 112].

Imaging

A search of the literature reveals no specific reports on imaging findings. Thus, subcutaneous localization is the only diagnostic clue (Fig. 18.17).

18.5.4.2 Parachordoma

Definition The term "parachordoma" has been applied to a rare tumor of uncertain histogenesis but with a characteristic histologic appearance with vacuolated eosinophilic epithelioid cells.

The tumor forms a lobulated mass with diameter averaging 3.5 cm. Usually, it involves the soft tissues of the extremities adjacent to tendons, synovium, or bones [3, 33, 53].

Incidence and Clinical Behavior Parachordoma is a rare tumor, which affects both adolescents and adults. The lesion predominates in the extremities or peripheral parts of the body where it is deeply seated near tendons, synovium, and osseous structures [53]. Although recurrence has been observed following excision, parachordoma is considered a benign lesion [55].

Imaging In three case studies, parachordoma has been described as encapsulated mass which appears iso- or hypointense on T1- and hyperintense on T2-weighted MR images and presents with a diffuse contrast enhancement [28, 37, 76] (Fig. 18.18).

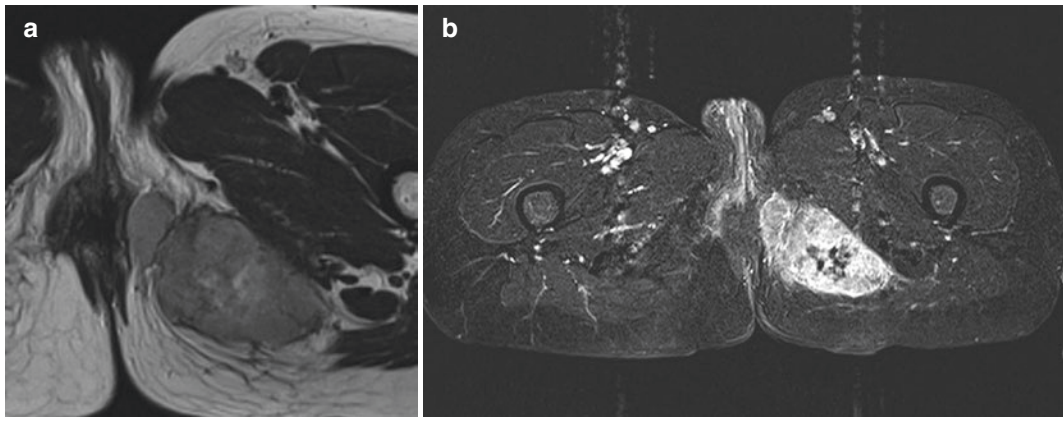

Fig. 18.17 Myoepithelioma of the left perineal/gluteal region. (**a**) Axial T1-weighted MR image with fat saturation, subtraction after gadolinium contrast injection. (**b**) Axial T1-weighted MR image with fat saturation, subtraction after gadolinium contrast injection. A 50-year-old patient with a malignant myoepithelioma of the left perineal/gluteal region. On T1-weighted images, the tumor is slightly hyperintense to the muscle, and after contrast-agent administration, a strong peripheral enhancement with a central non-enhancing necrotic area can be noted

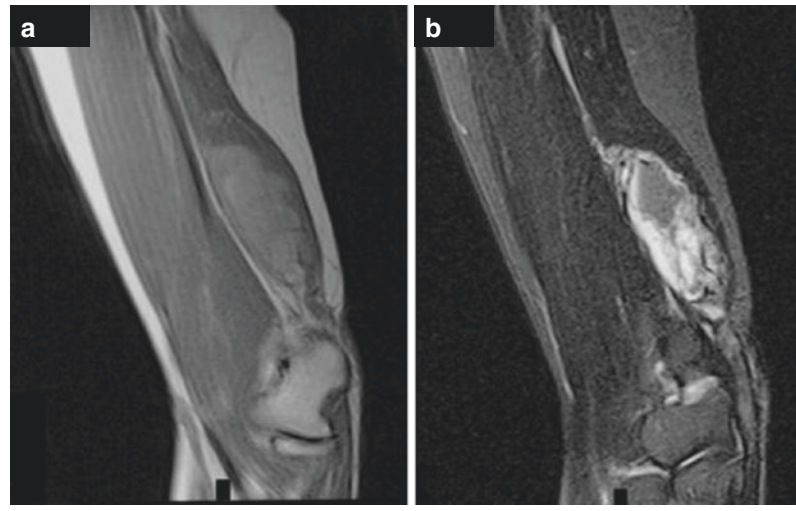

Fig. 18.18 60-year-old woman with parachordoma of the elbow. Sagittal MRI of the distal upper arm soft tissue mass shows a heterogeneous dark signal on the T1-weighted image (**a**) and a heterogeneous bright signal on the T2-weighted image (**a**). (Used with permission from Clabeaux et al. [28])

18.5.5 Phosphaturic Mesenchymal Tumor

18.5.5.1 Definition, Incidence, and Clinical Behavior

Phosphaturic mesenchymal tumor (PMT) is a rare neoplasm that causes systemic phosphate depletion and consequently an oncogenic osteomalacia by producing a phosphaturic substance, the so-called fibroblast growth factor 23 (FGF23). The tumor can occur in the soft tissue and bone; in almost half of the cases, the lower extremities are affected. There is no sex predilection and the age range of patients is wide. Clinically, muscle weakness, bone pain, and multiple fractures as well as renal phosphate wasting and elevated serum levels of FGF23 are characteristic. The tumor itself is a slow-growing ill-defined mass and can histologically be divided in three variants: osteoblastoma-like, non-ossifying fibroma-like, and the most common mixed connective tissue variant (PMTMCT). After complete excision, bone consistency and serum levels of fibroblast growth factor 23 get back to normal [48, 84].

18.5.5.2 Imaging

Since PMT usually do not exceed a diameter of 5 cm and can be located ubiquitary, diagnosis can be challenging. Radiography and CT scans often only show a general osteopenia and in case of intraosseous location lytic lesions with or without mineral deposition. Whole-body MRI is more helpful in finding the lesions, with T1 intensity depending on the vascularization and hyperintensity on T2-weighted images [48, 118]. In addition, whole-body scintigraphy with ^{111}In-octreotide and ^{68}Ga-DOTANOC PET/CT and ^{68}Ga-DOTATATE PET/CT is also excellent in detecting PMT [50] (Fig. 18.19).

18.6 Malignant Lesions

18.6.1 Synovial Sarcoma

Although synovial sarcoma is a misnomer, as it is not derived from true synovial cells, we will not go into the details of this nosological discussion.

18.6.1.1 Definition

Synovial sarcoma is a clinically and morphologically well-defined entity. It occurs primarily in the para-articular region, usually in close relationship with tendon sheaths, bursas, and joint capsules. It is, however, uncommon in joint cavities. On rare occasions, but widely reported in the radiological literature, it is also encountered in areas without any apparent relationship to synovial structures, such as in the pharynx, the larynx, the tongue, the maxillofacial region, the middle ear, precoccygeal and paravertebral regions, the mediastinum, the thoracic and abdominal wall, the heart, or even in intravascular and intraneural locations [23, 132, 140, 144]. Of note, only synovial sarcoma associated with the locomotor system is discussed in this chapter.

18.6.1.2 Incidence and Clinical Behavior

Epidemiology Synovial sarcoma accounts for approximately 5–10 % of all malignant mesenchymal neoplasms [90]. It is most prevalent in adolescents and young adults between 15 and 40 years of age (Table 18.1). Men are more susceptible than women with an average ratio of 2:1. There is no predilection for any particular race.

Clinical Behavior and Gross Findings The most typical presentation is that of a palpable deep-seated soft tissue mass. It is usually associated with pain or tenderness and may cause functional impairment of the adjacent joint. Severe functional disturbances and weight loss are infrequent. Although uncommon, involvement of nearby nerves may cause pain, numbness, or paresthesia.

It is still uncertain whether trauma contributes to the development of synovial sarcoma or not. Although in many patients there is a definite history of trauma, the majority has no such antecedents. When reported, the interval between the episode of trauma and the detection of synovial sarcoma ranges from a few weeks to as much as 40 years. However, there are also reports of patients who sustain injuries after the presence of a mass had been noted, which suggests that, at least in some cases, the relationship between both is purely coincidental.

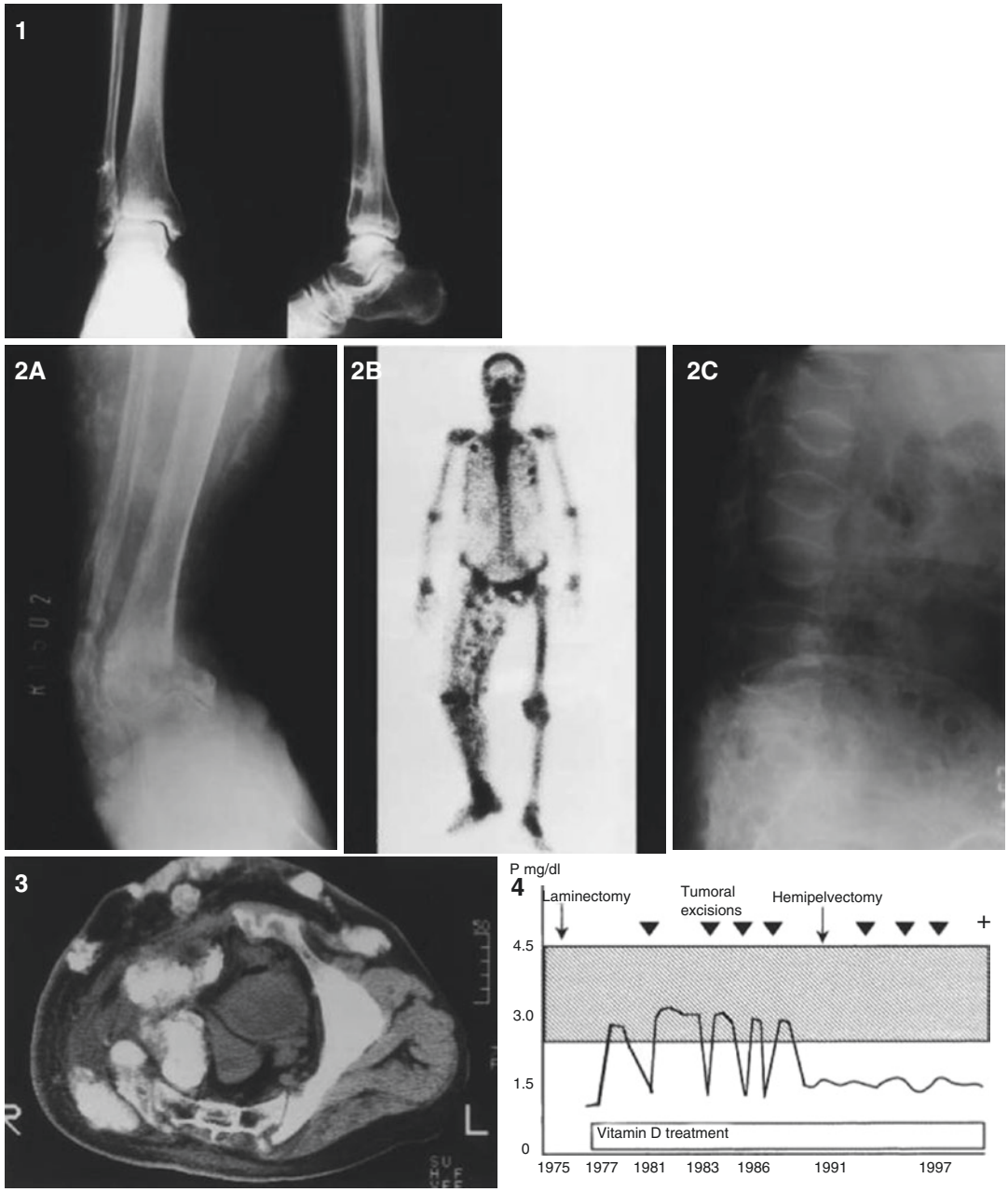

Fig. 18.19 45-year-old woman with phosphaturic mesenchymal tumor. (**1**) Radiographs showing a mineralized juxtacortical tumor adjacent to the right distal fibula. The tumor was originally diagnosed as exostosis and ignored. (**2A**) Radiograph 14 years later showing multiple mineralized soft tissue tumors in the right lower leg with pathological fractures of the tibia and fibula. (**2B**) Bone scan in 1991 showing multiple soft tissue masses in the right lower extremity and fractures of the right ankle and ribs. (**2C**) Radiograph showing multiple spinal compression fractures due to uncontrollable osteomalacia. (**3**) Computed tomography scan showing mineralized intrapelvic tumors after Hemipelvectomy. (**4**) The serum phosphate level and the clinical course (Used with permission from Ogose et al. [167])

Table 18.1 Age distribution of 345 cases of synovial sarcoma according to Enzinger et al. [45]

Age range	No. of cases	Percentage (%)
0–10 years	12	3
10–20 years	94	27
20–30 years	85	25
30–40 years	57	17
40–50 years	52	15
50–60 years	25	7
60–70 years	11	3
70–80 years	6	2
80–90 years	3	1
Total	345	100

Table 18.2 Localization of synovial sarcoma modified from Enzinger et al. [45]

Head–neck	31		9
Neck		12	3
Pharynx		7	2
Larynx		7	2
Other		5	1
Trunk	28		8
Chest		10	3
Abdominal wall		9	2.5
Other		9	2.5
Upper extremities	80		23
Shoulder		22	6
Elbow/upper arm		20	6
Forearm/wrist		24	7
Hand		14	4
Lower extremities	206		60
Hip–groin		22	6
Thigh/knee		102	30
Lower leg/ankle		33	10
Foot		45	13
Other		4	1
Total	345	345	100

As mentioned before, synovial sarcoma occurs predominantly in the extremities (80–90 %), mostly near large joints, especially the knee joint (30 %) [45] (Table 18.2). These tumors are intimately related to tendons, tendon sheaths, and bursal structures, usually beyond the confines of the joint capsule. In less than 5 % of all cases, synovial sarcoma arises in the joint space itself.

18.6.1.3 Pathology

The name of the lesion is derived from the microscopic resemblance of synovial sarcoma to normal synovium, although its origin is probably from undifferentiated mesenchymal tissue [45, 115]. Unlike most other types of sarcomas, the tumor is composed of two morphologically different types of cells that form a characteristic biphasic pattern: epithelial cells, which resemble those of carcinoma, and fibrosarcoma-like spindle cells. There are transitions between both types of cells, suggesting a close generic relationship. Depending on the relative presence of these types of cells and on their differentiation, synovial sarcomas can be classified into four different types.

The *first type* is the biphasic synovial sarcoma that is characterized by the coexistence of morphologically different but histogenetically related epithelial and spindle cells. Calcification with or without ossification is present in about 30 % of tumors. The degree of vascularity varies from a few scattered vascular structures to numerous dilated vascular spaces. In less well-differentiated tumors, hemorrhage may be prominent.

The *second type* is the monophasic fibrous synovial sarcoma with a predominant or even exclusive spindle cell pattern. This type is relatively common. Its clinical presentation is identical to the biphasic type.

The *third type* of synovial sarcoma is the monophasic epithelial form. This is a rarely recognized neoplasm with a predominant or exclusive epithelial cell pattern. It is difficult to render the diagnosis of this tumor with certainty since it closely resembles other more frequently occurring epithelial and mesenchymal tumors, such as metastatic and adnexal carcinoma, malignant melanoma, malignant epithelioid schwannoma, and epithelioid sarcoma.

The *final type* of synovial sarcoma that is histologically recognized is the poorly differentiated type. Its incidence is estimated at 20 %. It behaves more aggressively and metastasizes in a greater percentage of cases. Microscopically, this tumor is composed of small oval or spindle-shaped cells, intermediate in appearance between epithelial and spindle cells. It has a rich vascular pattern with dilated vascular spaces.

Multicystic formation is a common occurrence in synovial sarcoma. The cyst wall is thickened and composed of fibrous septa. Within the cyst, there are often several internal septa, consisting of tumor cells proliferating over the dense collagenous fibrous tissue without a lining pattern. Tumor cells may become detached from the septa in the internal lumen. Furthermore, dilated hemangiopericytomatous vasculatures can be prominent within those septa. Chromosomal rearrangements have been reported in association with synovial sarcoma, consisting of t(X;18)(p11–2;q11–2) translocation [31].

18.6.1.4 Imaging

The majority of synovial sarcomas present on *radiographs* as round or oval, lobulated masses. They are usually located close to a large joint, particularly the knee joint. In 5–30 % of cases, there is periosteal reaction, bone erosion (related to pressure from the adjacent tumor), or even bone invasion. The most characteristic finding is the presence of multiple small densities caused by focal calcifications or ossifications. This feature is seen in about 20–30 % of cases. It may range from very fine stippling to marked calcifications or even bone formation, typically in the periphery of the lesion. When present, these opacities differentiate synovial sarcoma from liposarcomas and myxoid chondrosarcomas. The irregular shape of the calcifications helps to make the differentiation from hemangioma. In some cases, extensive ossification is present, resembling osseous or cartilaginous lesions such as soft tissue chondroma, extra-articular synovial chondromatosis, ossifying myositis, tumoral calcinosis, or osteosarcoma, both parosteal and extraskeletal. Cases with extensive calcification have been reported to have a better prognosis, with higher survival rates [117, 133].

Angiography usually reveals a prominent vascularity, not only of the primary tumor but also of the metastases. This is especially true for the monophasic and poorly differentiated type of tumor [102]. There is extensive neovascularity and nonhomogeneous staining. Occasionally, the lesion is hypovascular.

Ultrasound characteristics are those of a well-defined, solid vascular tumor with prominent arterial and venous components. There may be internal cystic components due to internal hemorrhage [107]. Internal calcifications are noted in 20–30 %. Ultrasound appears useful as a detection method of local recurrence, in the guidance of fine-needle biopsy and in the examination of chil-

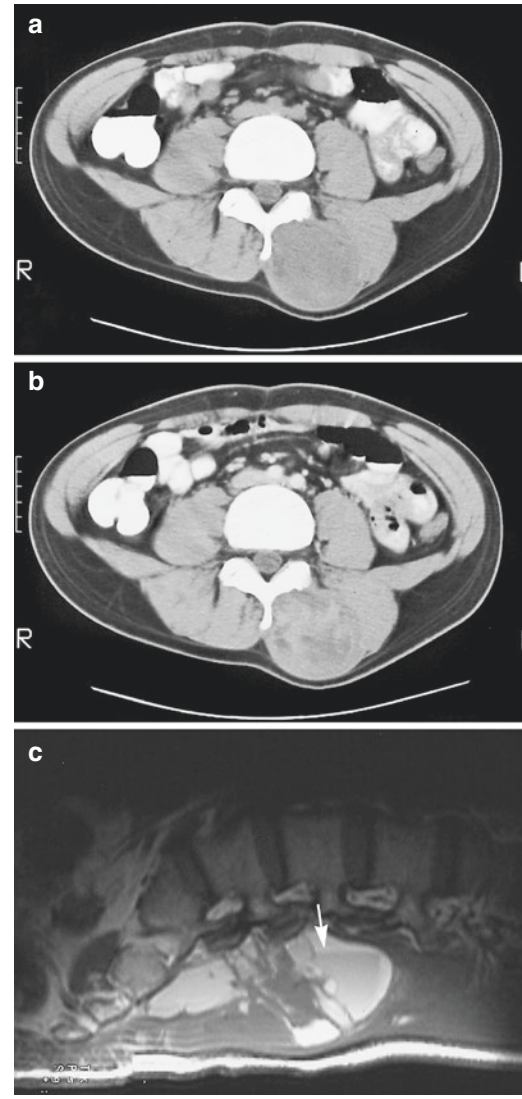

Fig. 18.20 Synovial sarcoma of the back in a 19-year-old man. (**a**) CT. (**b**) CT after iodinated contrast injection. (**c**) Sagittal spin-echo T1-weighted MR image. This is a case of a soft tissue mass in the posterior paravertebral region. There is no clear intratumoral calcification or ossification (**a**), and only mild enhancement is noted after injection of iodinate contrast medium (**b**). Fluid–fluid levels can sometimes be seen on the T1-weighted image (**c**), but are a rare and nonspecific sign (*arrow*)

dren [72]. In the early postoperative period (less than 6 months after surgery), inhomogeneous hypoechogenic lesions cannot be differentiated with certainty as recurrent tumor, hemorrhage, edema, granulation tissue, abscess formation, or any combination of these. Performed with high-frequency transducers, a lesion is considered to be a recurrent tumor when a discrete nodular hypoechogenic mass is present. Areas of diffuse abnormal echogenicity without evidence of a discrete nodule can be classified as non-tumoral.

CT shows a soft tissue mass, which may infiltrate adjacent structures, having a slightly higher density than muscle [115] (Fig. 18.20, former Fig. 23.13). Joint invasion is present when the soft tissue mass projects into the expected confines of a joint capsule or when an intra-articular ligament or tendon is involved. Although bony involvement can be identified on both MR and CT imaging, cortical bone erosion or invasion is better depicted on CT. Intratumoral calcification or ossification is also more easily seen on CT than on MR imaging. Because of its extensive vascular supply, synovial sarcoma enhances markedly after injection of contrast medium.

On *MR imaging*, most synovial sarcomas (>90%) are hypointense relative to fat and nearly isointense relative to muscle on T1-weighted MR images [117]. In rare cases, the tumor may be mostly hyperintense due to extensive intratumoral hemorrhage. Small areas of high signal on T1-weighted images are more often encountered (45%) [81, 117, 123]. They probably correspond with small foci of hemorrhage, since these areas are of high signal on T2-weighted images, too. Fluid–fluid levels, although not very frequent (15–25%) and not specific, can be a striking finding. Areas of previous hemorrhage with fluid–fluid levels or high signal intensity on all pulse sequences may be associated with a worse prognosis [117] (Figs. 23.13–23.17). On T2-weighted images, marked inhomogeneity is the rule, and various degrees of internal septation may be noted [114] (Figs. 18.21 and 18.24 former Figs. 23.14 and 23.17). This is especially true for lesions more than 5 cm in diameter which show this heterogeneous signal pattern in more than 85% of cases vs. 60% for smaller lesions [81]. A triple signal pattern on T2-weighted images is described in one third of all synovial sarcomas [12, 81, 133]. It consists of high signal similar to fluid, intermediate signal intensity equal to or slightly hyperintense relative to fat, and low signal intensity closer to that of fibrous tissue. This triple signal pattern on T2-weighted images together with the small high signal foci on T1-weighted images is suggestive for synovial sarcoma (Figs. 18.22 and 18.23, former Figs. 23.15 and 23.16). More than half of all lesions are intimately related to bone. There seems to be no notable difference between the MR imaging characteristics of the mono- and biphasic pathologic subtypes.

Heterogeneous enhancement after injection of contrast material is generally seen. Hypervascular areas are strongly enhancing, whereas necrotic and cystic areas remain hypointense. Hypervascularity may be quantified by a dynamic contrast-enhanced MR examination. Early enhancement of tumor within 7 s after arterial enhancement is a reliable sign, occurring consistently in synovial sarcoma. Other previously described so-called malignant dynamic contrast-enhanced MR imaging features, such as early plateau or washout phase and peripheral enhancement are not always found in synovial sarcoma [155].

Well-defined or reasonably well-defined margins are seen in some cases of synovial sarcoma. This finding has been described as a probable sign of benignity [132, 133]. This may be one of the reasons why synovial sarcoma is the malignant tumor most frequently misdiagnosed as benign [17, 133]. Neurovascular involvement may be suspected in cases where the tumor margin abuts and displaces the neurovascular bundle. In one study, this was confirmed at operation in two out of five cases [114]. MR often fails to demonstrate small calcifications seen on plain films or CT. Therefore, the MR images of soft tissue and bone tumors should be interpreted with corresponding CT images and plain films.

The differential diagnosis on MR imaging of an inhomogeneous septate mass with infiltrative margins and located in close proximity to a joint, a tendon, or a bursa is very limited. Without the history of trauma or signs of infection, a malignant neoplasm is the most likely consideration. Especially in combination with soft tissue calcifications, the diagnosis of a synovial sarcoma should

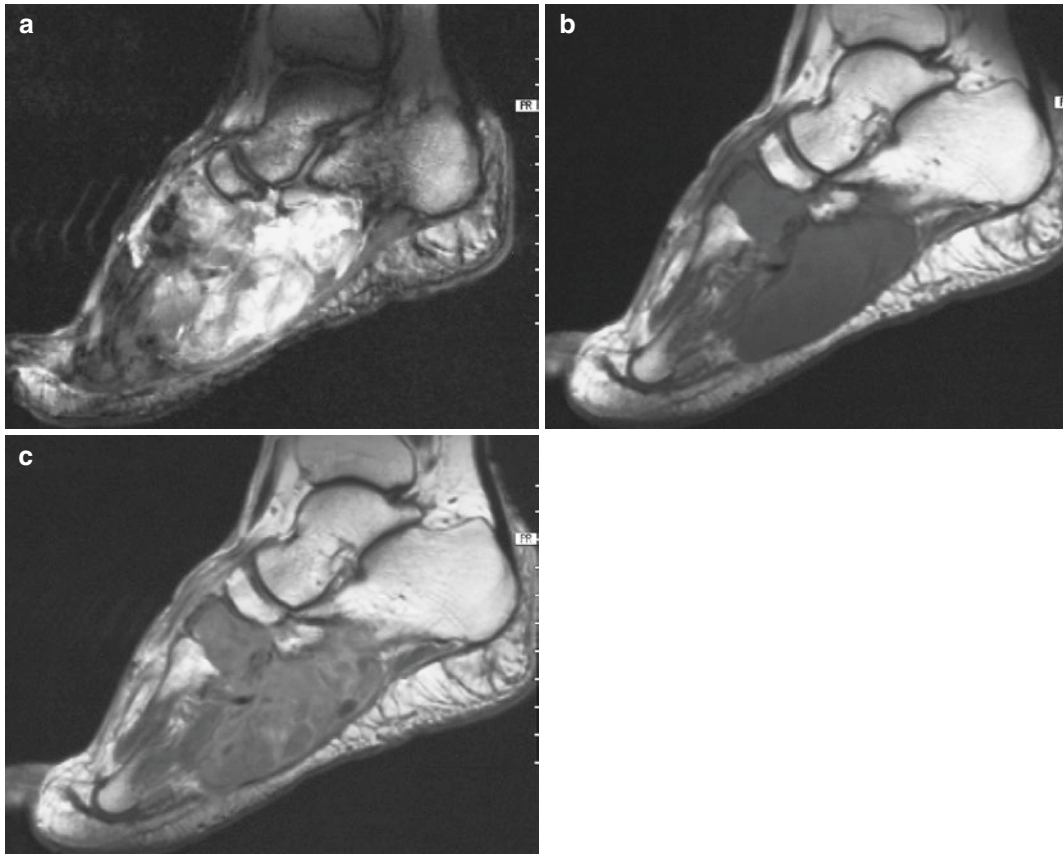

Fig. 18.21 Synovial sarcoma of the foot in a 37-year-old man. (**a**) Sagittal gradient-recalled echo T2*-weighted MR image. (**b**) Sagittal spin-echo T1-weighted MR image. (**c**) Sagittal spin-echo T1-weighted MR image after gadolinium contrast injection. Synovial sarcoma is generally hypointense on a T1-weighted image (**b**) and hyperintense on a T2-weighted image. (**a**) Large lesions such as this one are usually heterogeneous and may show internal septation. (**a**) Marked enhancement is correlated to the extensive vascular supply of these tumors. (**c**) Bone invasion is less frequent (5–30 %), but can be quite important. (**c**) The sole of the foot is a common localization of synovial sarcoma in young adults

be preferred. However, a septate configuration can also be seen in two types of benign soft tissue masses: hemangioma and synovial or ganglion cysts. Typically, these benign tumors are sharply marginated and have a homogeneous hyperintense signal that is much brighter than that of the subcutaneous fat on T2-weighted images. The pattern of contrast enhancement may be helpful as well in the differential diagnosis (Figs. 18.24 and 18.25).

18.6.1.5 Treatment, Prognosis, and Detection of Tumor Recurrence

Treatment of synovial sarcoma consists of wide local excision or limb amputation, usually in combination with chemotherapy and radiation therapy. Despite this aggressive therapy, metastatic disease or local recurrence is found in approximately 80 % of patients. Metastases most frequently affect the lung (59–94 % of distant tumor spread). Additional sites of metastatic disease include lymph nodes (4–18 %) and the bone (8–11 %). Soft tissue metastases are rare. Local recurrence occurs in 20–26 % of patients and presents usually within 2 years after initial diagnosis. The 5-year survival rate is approximately 27–55 %. Favorable prognostic factors with synovial sarcoma include extensive calcification, younger patient age, lesions less than 5 cm in diameter, and neoplasms located in the extremities [117]. According to

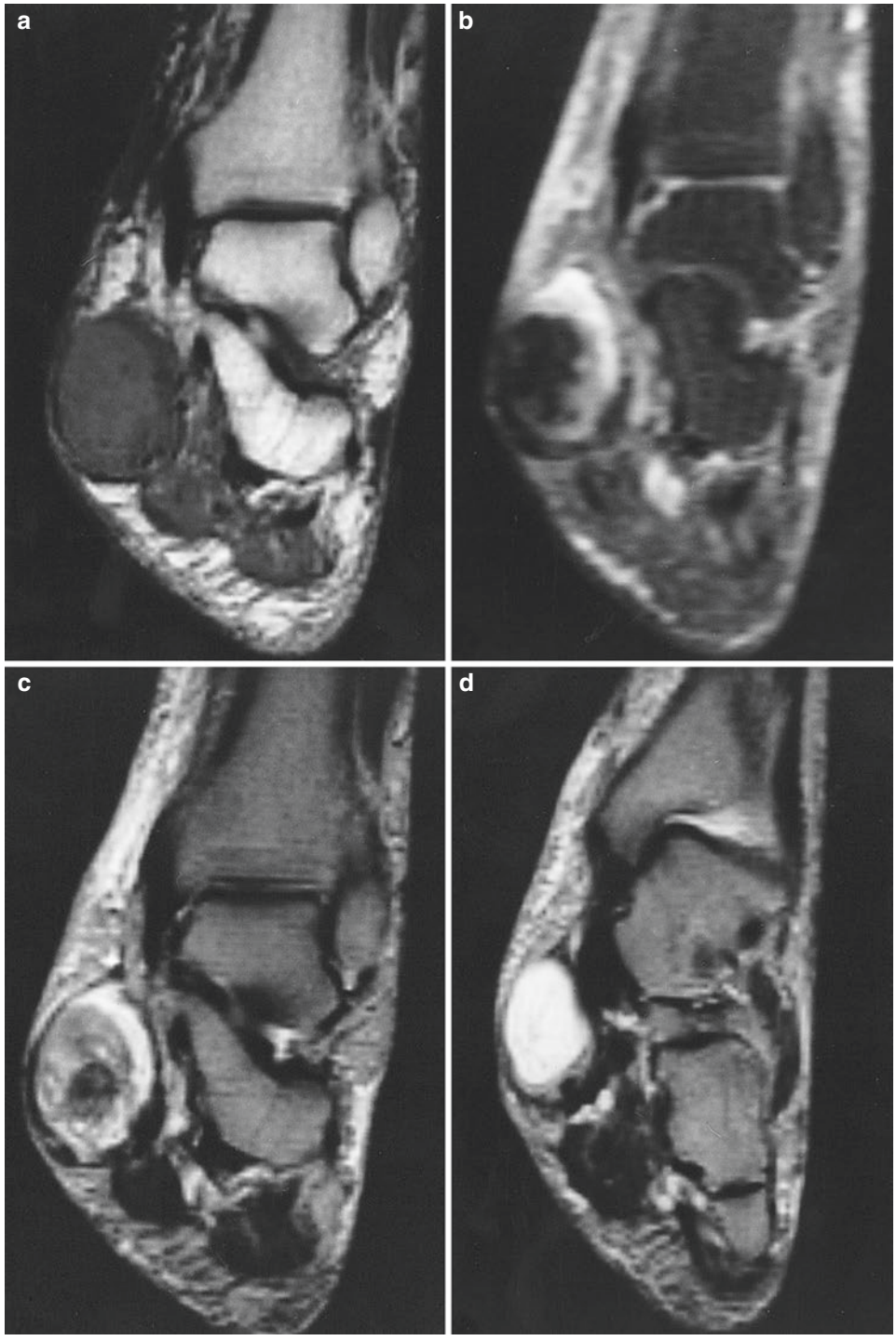

Fig. 18.22 Synovial sarcoma at the medial side of the ankle. (**a**) Coronal T1-weighted MR image. (**b**) Contrast-enhanced coronal fat-suppressed T1-weighted MR image. (**c**, **d**) Coronal fat-suppressed T2-weighted MR images. Oval mass, medially at the ankle joint, with inhomogeneous low signal intensity (**a**). Strong contrast uptake is seen at the periphery of the lesion (**b**). A triple signal pattern is seen within the lesion with signal intensities similar to fluid, intermediate, and low signal intensities (**c**, **d**)

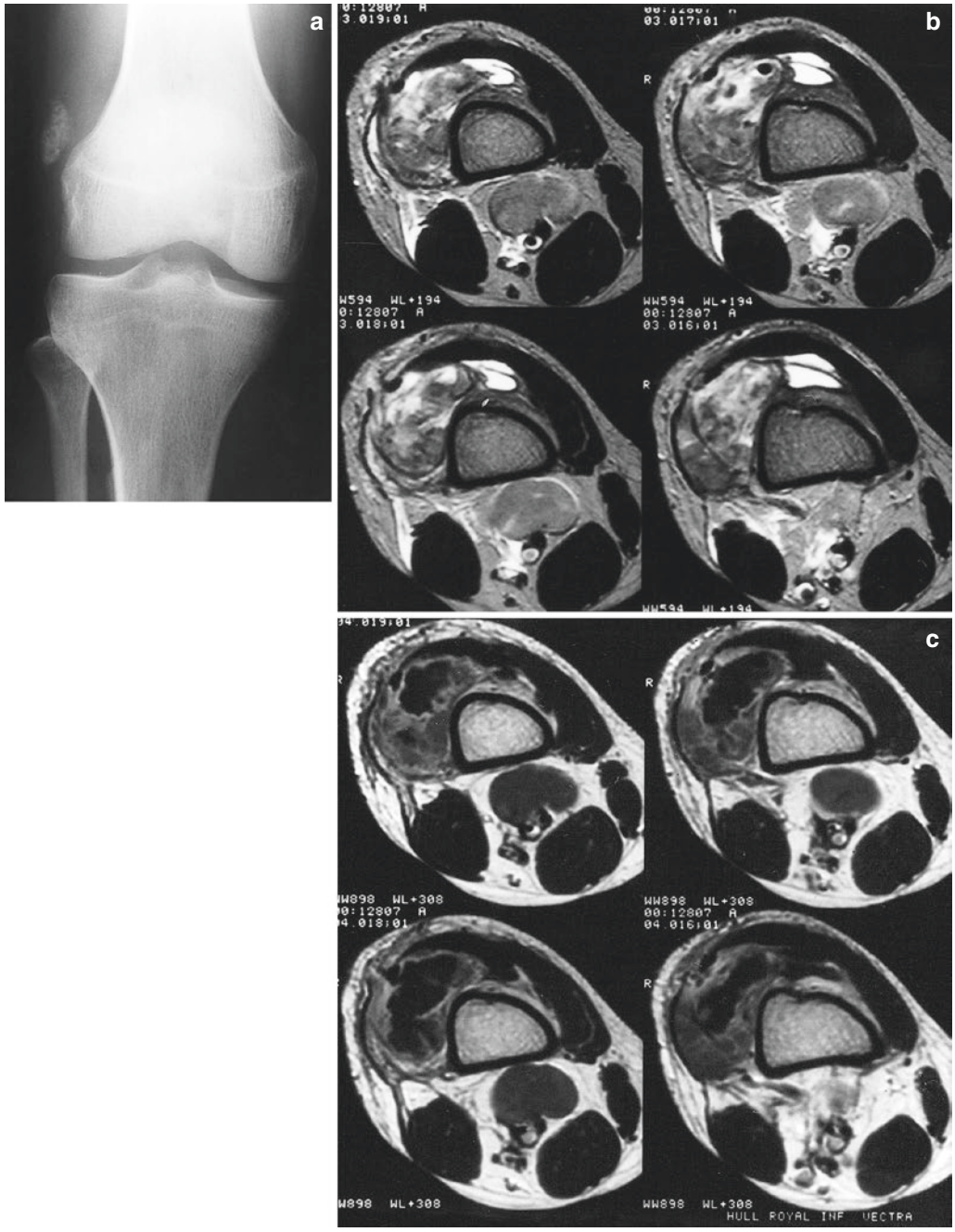

Fig. 18.23 Synovial sarcoma of the knee. (**a**) Anteroposterior radiograph of the right knee. (**b**) Axial T2-weighted MR image at the distal femur. (**c**) Axial T1-weighted MR image after intravenous gadolinium administration. A crumbly calcification is seen within a palpable soft tissue mass at the lateral side of the knee. Calcifications are seen in up to 30 % of synovial sarcomas (**a**). The tumor is of mixed signal intensity with hypointense and hyperintense areas, as well as components of intermediate signal intensity ("triple signal"); the tumor looks to be arising outside the joint, but extends down the lateral patellar retinaculum into the superolateral aspect of the knee joint (**b**). There is marked peripheral contrast enhancement within the mass, with a central irregularly delineated area of absent enhancement. There are enlarged lymph nodes around the neurovascular bundle in the popliteal fossa (**c**) (Case courtesy of Dr. A.M. Davies, Birmingham)

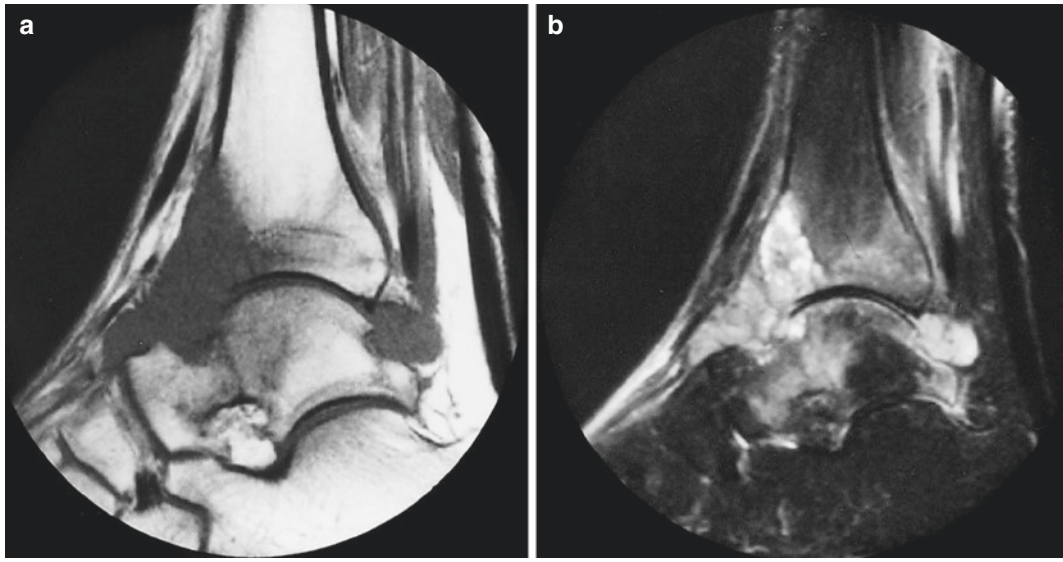

Fig. 18.24 Synovial sarcoma developing within the ankle joint. (**a**) Sagittal T1-weighted MR image. (**b**) Sagittal STIR image. A low signal intensity mass is present within the anterior and posterior recess of the ankle joint. There is associated erosion of the talar neck. The anterior cortex of the distal tibia is destroyed. Bone marrow edema is seen within the distal tibia and in the talus (**a**). The tumor is of high signal intensity on T2-weighted images, with some internal low signal intensity septa. The adjacent bone invasion and bone marrow edema are better appreciated than on the T1-weighted images (**b**) (Case courtesy of Dr. A.M. Davies, Birmingham)

Tateishi, other prognostic MRI parameters include the presence of hemorrhage and cysts or the presence of a triple signal. Together with proximal tumor distribution, large tumor size, and the absence of calcification, these parameters are associated with high tumor grade and a less favorable prognosis [151]. The value of MRI in the early detection of tumor recurrence will be discussed in detail in Chap. 26, dealing with imaging posttreatment (Fig. 18.25, former Fig. 23.18).

18.6.2 Epithelioid Sarcoma

18.6.2.1 Definition

The term "epithelioid sarcoma" was applied by Enzinger in 1970 to refer to a distinctive neoplasm that commonly involves the soft tissues of the extremities, most frequently of the hand. This tumor presents as a solitary or irregular multinodular mass located in the dermis or deep-seated and attached to tendons or fascia. The size of the lesion is variable and ranges from several millimeters to more than 15 cm in diameter. Central degeneration and necrosis are common features. Lesions located in the dermis often ulcerate through the skin. The tumor may spread along the neurovascular bundles, may invade the vessels, and, hence, may metastasize. In general, tumors located in the proximal extremity reveal a more aggressive course than those arising in the distal extremities [66]. A history of trauma is reported in up to 25 % [25, 129] histogenesis, and the nature of this neoplasm remains unknown.

18.6.2.2 Incidence and Clinical Behavior

Epithelioid sarcoma represents the most common soft tissue sarcoma of the hand. Although it may occur at any age, the tumor is found most commonly in adolescents and young adults between 10 and 35 years of age. Children and older persons are only rarely affected. This tumor is twice as common in men as in women. The principal sites of involvement are the distal upper extremity, involved in 58 % of cases, particularly the hands and forearms. This main site of involvement is followed by the distal and

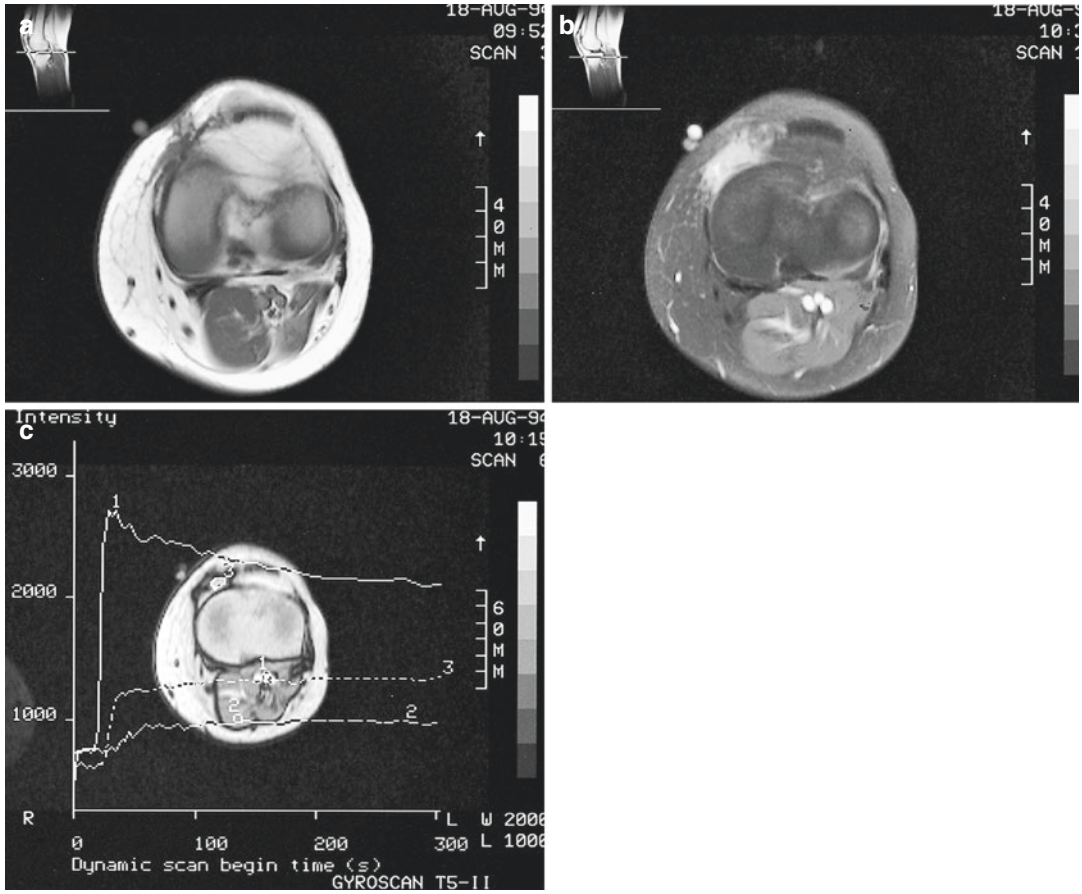

Fig. 18.25 Recurrent synovial sarcoma. (**a**) Axial spin-echo T1-weighted MR image. (**b**) Axial, fat-suppressed, spin-echo T1-weighted MR image after gadolinium contrast injection. (**c**) Signal intensity-versus-time curve calculated on a gradient-recalled echo T1-weighted MR image during gadolinium contrast injection. Synovial sarcoma quite frequently recurs after surgical excision. In this case, a small hypointense lesion located deep in the scar tissue can be noted on the T1-weighted image (**a**). After gadolinium injection, clear enhancement of this region can be noted on the fat-suppressed images (**b**). Dynamic imaging during bolus contrast injection (**c**) demonstrates the higher and more rapid uptake of contrast medium by this tissue (3) than by normal muscle (2). Repeat surgery disclosed recurrent tumor

proximal extremity, at 15 and 12 %, respectively. The trunk, head, and neck regions, with the exception of the scalp, are seldom involved [66]. Lesions may be located in the subcutis or are deep seated, usually attached to tendons, tendon sheaths, or fascial structures. Epithelioid sarcoma presents as a firm, hard nodule that may be solitary or multiple. These nodules are slowly growing and painless. Ulceration through the skin is common in intradermal lesions. Metastases, predominantly to the regional lymph nodes and lung, are observed in less than half of the cases. These develop mostly within the first year after diagnosis, but may be late and become apparent for many years after excision of the primary tumor. Recurrences, often multiple, are common and have been reported in 77 % of cases [25].

18.6.2.3 Imaging

Imaging Studies Other than MRI

Radiographs, CT, and ultrasound usually reveal a soft tissue mass. In 20–30 % of cases, ossification or a speckled pattern of calcification is observed within the nodule. In rare cases, the tumor causes cortical thinning or erosion of underlying bone [25, 66].

MRI Findings

No characteristic MRI features of epithelioid sarcoma exist [66]. Hence, MRI does not enable a specific diagnosis of this tumor. On T1-weighted images, the tumor appears mostly homogeneous and is isointense with muscle (Fig. 18.26, former Fig. 23.22). Occasionally, lesions may be heterogeneous, with either areas of increased signal, due to foci of hemorrhagic necrosis, or with relative central hypointensity, corresponding to extensive intratumoral necrosis. In contrast, on T2-weighted images, the tumor is hyperintense to the muscle, hypo-, iso-, or hyperintense to fatty tissue. A majority of lesions is homogeneous on these T2-weighted sequences. Peritumoral edema affecting the surrounding muscles is observed in nearly 70 % of cases. It typically appears as a high signal intensity area on T2-weighted or STIR images, with variable shape, or it may present as a feathery, radial pattern of increased signal intensity, extending for a maximum of 2 cm into the adjacent muscle, or as an extensive area of abnormal signal, involving completely at least one muscle [66]. Other common findings include tumor encasement of the adjacent neurovascular bundle and enlarged regional lymph nodes. The latter often shows the same increased signal intensity on T2-weighted images as the primary tumor. Inhomogeneous but strong enhancement is observed following administration of gadolinium chelates, except at the areas of central necrosis [66].

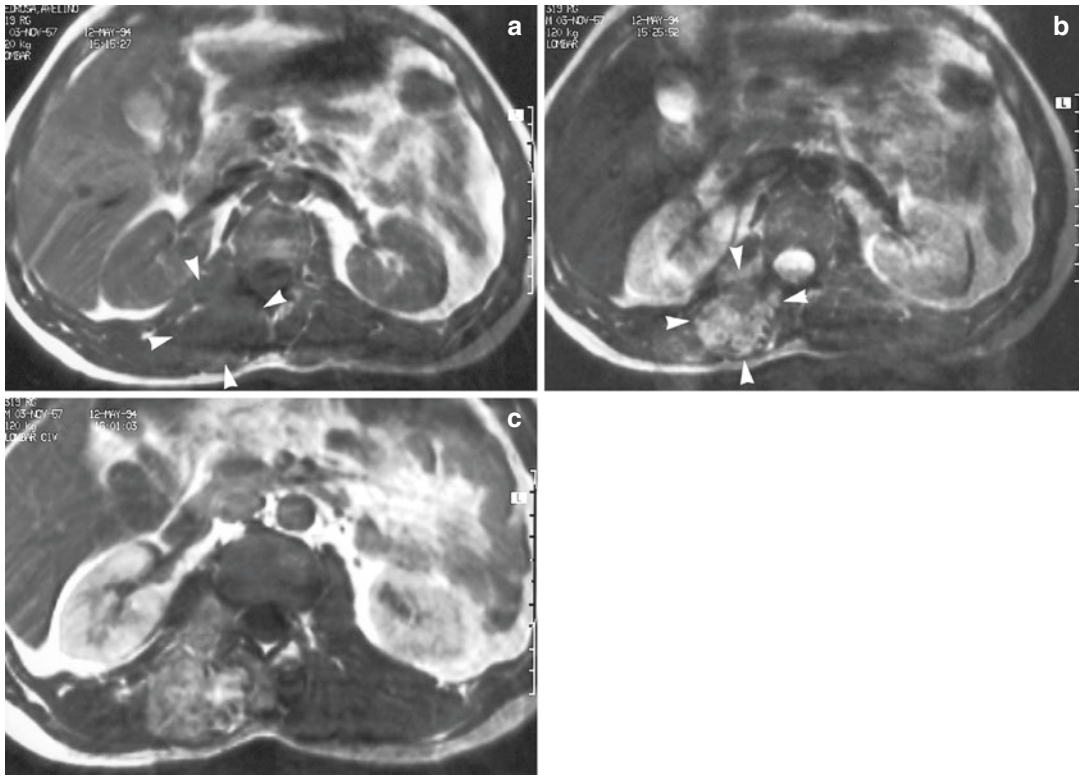

Fig. 18.26 Epithelioid sarcoma in the lumbar paraspinal region in a 37-year-old man. (**a**) Axial spin-echo T1-weighted MR image. (**b**) Axial spin-echo T2-weighted MR image. (**c**) Axial spin-echo T1-weighted MR image after gadolinium contrast injection. On the T1-weighted image, the tumor in the right paraspinal region appears nearly isointense with adjacent muscle and is only visible because of a moderate mass effect that causes asymmetry and distortion of the intermuscular fat planes (*arrowheads*) (**a**). On the T2-weighted image, the signal intensity of the nodular components within the irregularly outlined lesion is high but intermediate between that of the muscle and subcutaneous fat (*arrowheads*) (**b**). After contrast medium injection, strong but inhomogeneous enhancement is observed within the tumor

Imaging Strategy
As a result of the location of these lesions, the diagnosis is mainly based on the clinical aspect, findings on palpation, and results of biopsy. In spite of the variable appearance of the lesion, suspicion for epithelioid sarcoma should arise in all patients with multiple soft tissue nodules or persistent punched-out ulcers involving the skin and subcutaneous tissues, with enlarged draining lymph nodes, particularly when the mass is located in the distal portion of an extremity [66]. As for all soft tissue tumors, MRI seems to be superior to all other imaging techniques for assessing the extent of the tumor.

18.6.3 Alveolar Soft Part Sarcoma

18.6.3.1 Definition

Constituting less than 1 % of all soft tissue sarcomas, alveolar soft tissue sarcoma is one of the least common malignant soft tissue tumors [68]. The term refers to the pseudoalveolar pattern formed by aggregates of large granular cells surrounded by vascular channels mimicking the alveolar pattern of the respiratory alveoli. These tumors are highly hypervascular and frequently surrounded by thick, tortuous blood vessels. This is responsible for the considerable hemorrhage which often occurs during surgical removal [11]. On section, they consist of yellow–white to gray–red tissue, often with large necrotic or hemorrhagic areas [26]. Despite a relatively benign appearance – mitoses and pleomorphism are rare – alveolar soft part sarcoma is one of the most malignant soft tissue tumors. Metastatic spread develops early in the course of the disease, is common, and is observed in 40–70 % of patients [24, 34, 70, 98]. Preferential sites of metastases are the lungs, followed by the brain and skeleton. Tumor recurrence is high and is noted in 20–30 % of cases [98].

18.6.3.2 Incidence and Clinical Behavior

Alveolar soft part sarcoma can be seen at any age, but occurs predominantly in older children, adolescents, and young adults, between 11 and 35 years of age. A female predominance is observed in most series [24, 98]. At least 60 % of these tumors occur in the muscles or fascial planes of the lower limb, with the anterior portion of the thigh being most commonly affected. In decreasing order of incidence, the head and neck, upper extremity, and the trunk are the other most frequently involved areas [24, 98]. In children and infants, the head and neck region, particularly the orbit and tongue, are the most common sites of origin. Alveolar soft part sarcoma usually presents as a slowly growing, painless mass. Occasionally, pulsations may be observed on palpation. These are explained by the very rich vascularization of the tumor. At the time of diagnosis, the diameter of most tumors surpasses 5 cm.

The large majority of lesions are asymptomatic. Therefore, metastases in the lung or brain may be the first manifestation of the disease. Metastatic spread is present in more than one third of the cases at the time of initial diagnosis [11, 98].

18.6.3.3 Imaging

Imaging Studies Other than MRI On conventional radiographs, alveolar soft part sarcoma presents as a nonspecific mass which may occasionally show punctate calcifications [70, 104]. The tumor can erode the adjacent bone. Chest radiographs may reveal pulmonary metastases. Ultrasound may also disclose the tumor and shows a variable echo pattern within it. Doppler ultrasound may emphasize the marked vascularity of the lesion [34]. CT discloses the delineation of the tumor better. On non-enhanced scans, the tumor is slightly hypodense or even isodense compared with surrounding muscle. Contrast-enhanced scans show a very pronounced enhancement and may also demonstrate numerous dilated vessels within the tumor [24, 34, 70, 130] (Fig. 18.27, Fig. 23.19). Angiography shows a hypervascular mass, with arteriovenous shunting and early draining veins [34, 70] (Fig. 18.28; Fig. 23.20).

MRI Findings Alveolar soft part sarcomas appear bright both on T1- and T2-weighted images (Fig. 18.29). This is probably due to

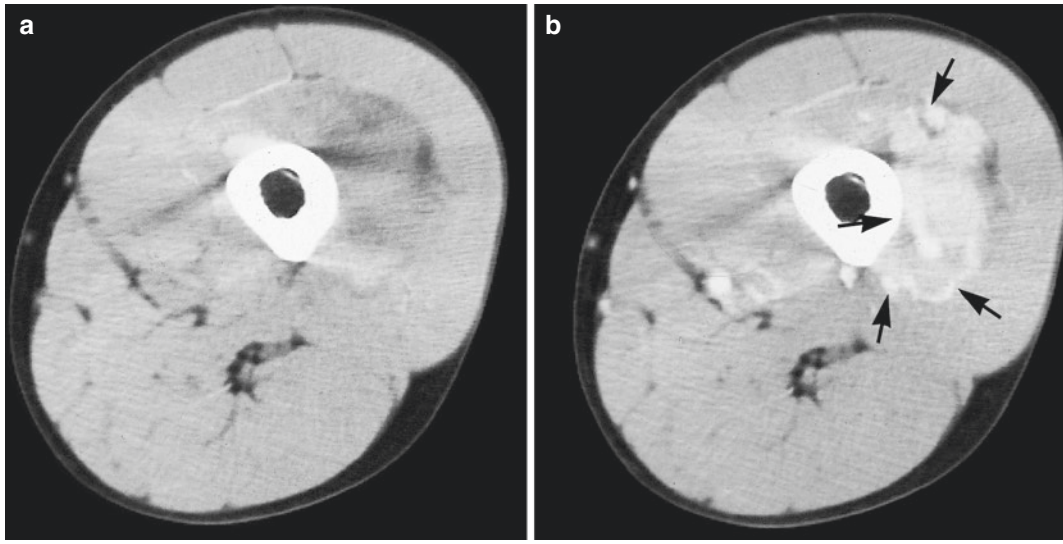

Fig. 18.27 Alveolar soft part sarcoma of the left thigh in a 26-year-old man. (**a**) Plain CT. (**b**) CT after iodinated contrast injection. The presence of a soft tissue mass at the lateral aspect of the femur with unsharp delineation from adjacent vastus intermedius and lateralis muscles. On native CT, the lesion is slightly hypodense relative to muscle. After contrast medium injection, pronounced enhancement of the lesion is seen. Thick, strongly enhancing structures are observed and correspond with enlarged vessels within the tumor (*arrows*) (**b**)

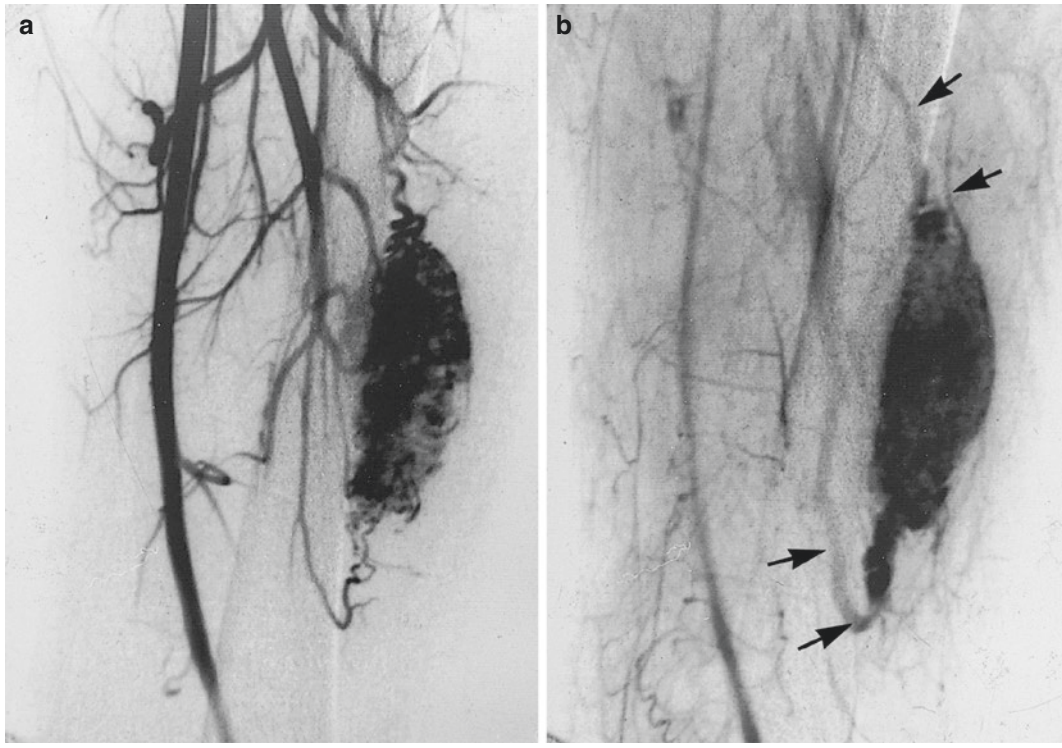

Fig. 18.28 Alveolar soft part sarcoma of the left thigh in a 26-year-old man (same patient as in Fig.23.19). (**a**) Arteriography of the left femoral artery, early phase. (**b**) Arteriography of the left femoral artery, late parenchymatous to early venous phase. During the early arteriographic phase, a highly vascularized mass lateral to the femoral shaft is observed. Thick, tortuous arteries are seen all over the lesion (**a**). A few moments later, during staining with contrast medium at the lesion, early venous drainage is observed at the upper and lower pole of the lesion (*arrows*)

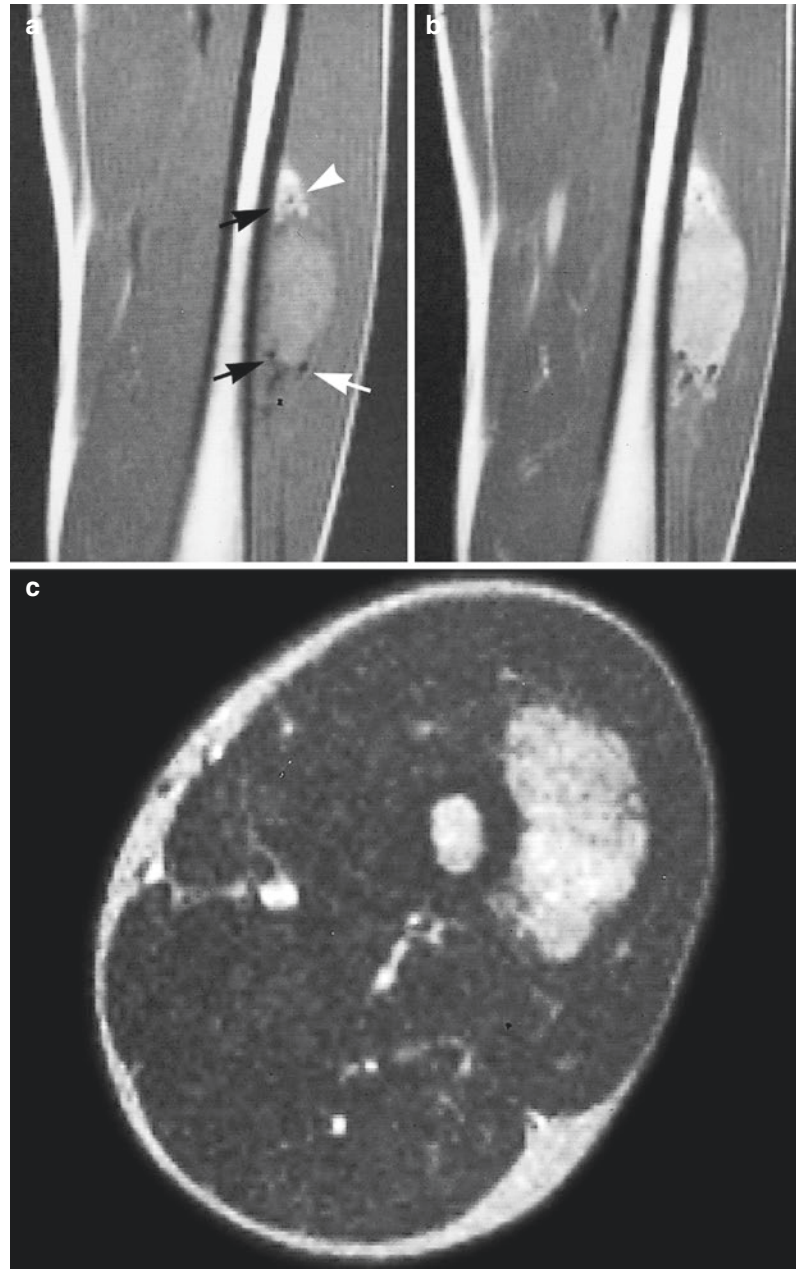

Fig. 18.29 Alveolar soft part sarcoma of the left thigh in a 26-year-old man (same patient as in Fig. 23.19). (**a**) Coronal spin-echo T1-weighted MR image. (**b**) Axial spin-echo T2-weighted MR image. (**c**) Coronal spin-echo T1-weighted MR image after gadolinium contrast injection. A well-delineated, ovoid, nearly homogeneous mass lesion lateral to the femur is seen. On T1-weighted images, signal intensity is higher than that of muscle, but lower than that of fat. Triangular region with fat signal intensity at the upper pole of the lesion (*arrowhead*). Punctate to tortuous zones with signal void both at the upper and lower poles of the lesion corresponding to rapidly flowing blood within dilated blood vessels (*arrows*). T2-weighted images disclose a mottled aspect of the lesion. Signal intensity equals that of fatty tissue. After contrast medium injection, intense enhancement is seen within the lesion. Notice the sharp peripheral demarcation of the lesion and the intact aspect of underlying bones

slowly flowing blood in some tumor vessels [34, 70, 104]. On all sequences, multiple areas of signal void are observed within the lesion, suggesting small calcifications or rapid flow within distended vessels [24, 70, 104]. On T1-weighted images, most lesions appear homogeneous, whereas on T2-weighted images, the pattern becomes inhomogeneous. This sign is important for indicating the malignant nature of the lesion, as it is observed in 72 % of malignant lesions and only in 12.5 % of benign lesions [71]. Following administration of gadolinium chelates, intense, but inhomogeneous, enhancement is noted [13, 24] (Fig. 18.30).

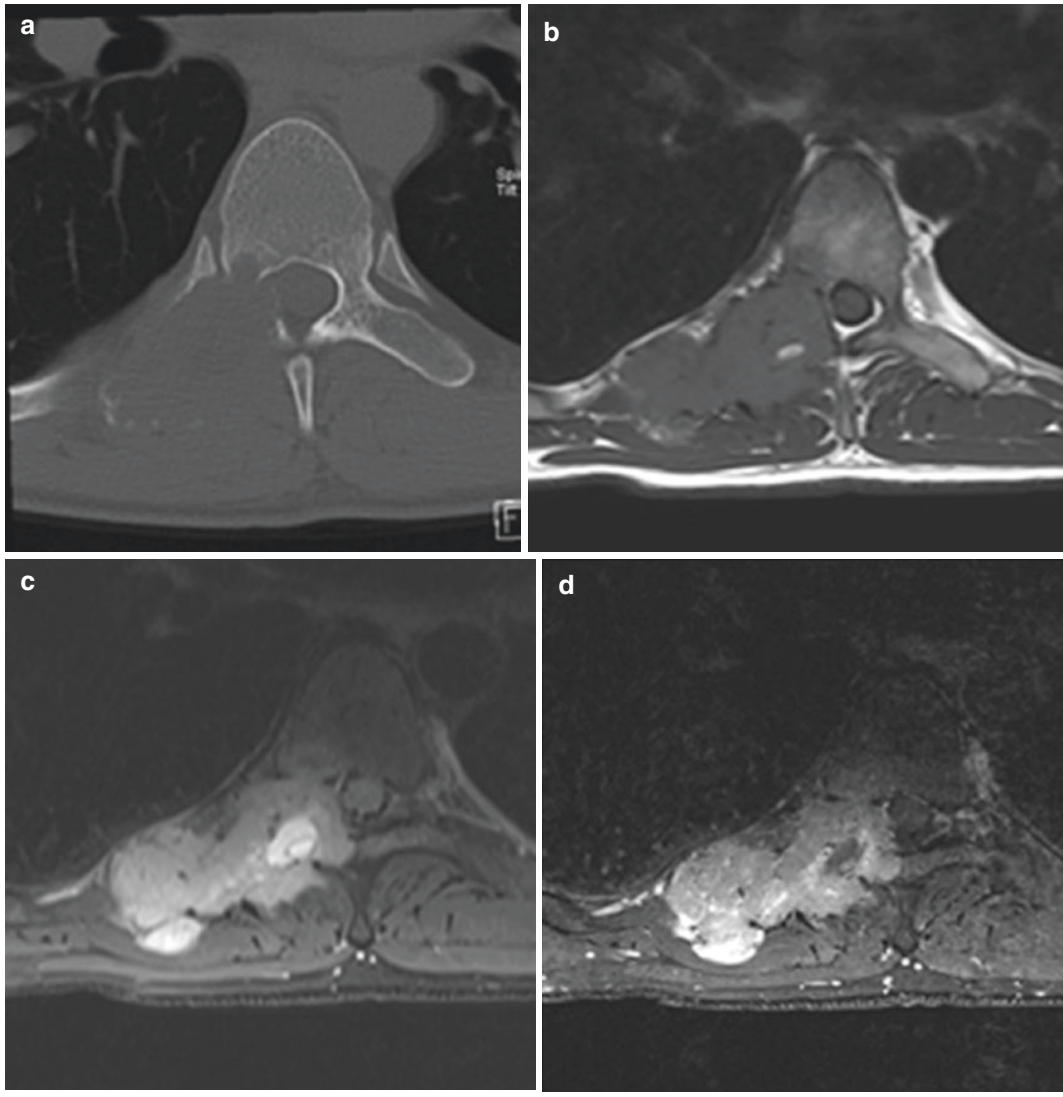

Fig. 18.30 Alveolar soft part sarcoma of the thoracic spine in a 33-year-old male. (**a**) Axial CT image. (**b**) Axial T1-weighted MR image. (**c**) Axial T2-fs-weighted MR image. (**d**) Axial T1-weighted MR image after gadolinium contrast injection. Alveolar soft part sarcoma of the thoracic spine in a 33-year-old male with endangered stability due to osteolysis of the right vertebral arch. (**a**) On T1-weighted images, the tumor is mostly homogeneous and slightly hyperintense to muscle, while hyperintense on T2-weighted images with implied hypointense septations. (**c**) After contrast-agent administration, a marked but inhomogeneous enhancement is seen

Imaging Strategy Plain radiographs are of little value in the diagnosis of alveolar soft part sarcoma as they reveal only nonspecific findings. Conventional chest radiographs are indicated for the detection of pulmonary metastases, although for this purpose, CT of the thorax is more sensitive and should be recommended during initial staging and in surveillance following therapy. Contrast-enhanced CT allows better delineation of the tumor by showing muscle infiltration. Doppler ultrasound, CT, MRI, and angiography all emphasize the hypervascular nature of this tumor. The presence of low-intensity septations on T2-weighted images only and the change from a homogeneous pattern on T1-weighted images to inhomogeneous on

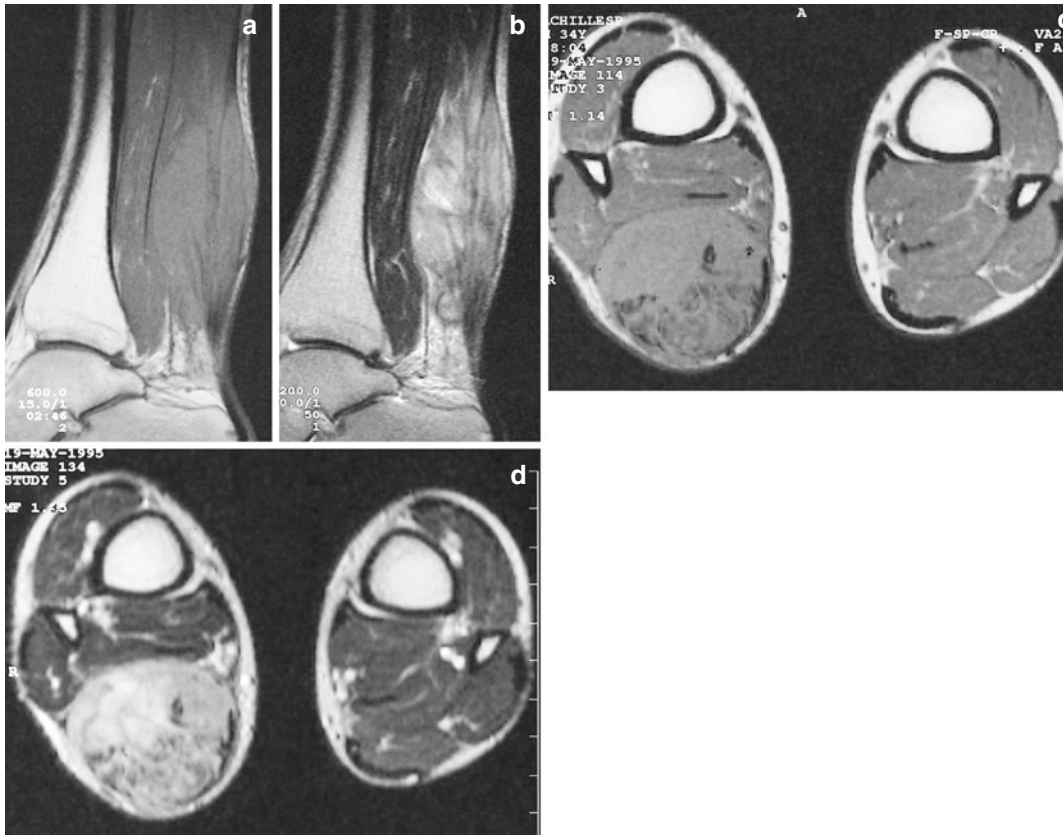

Fig. 18.31 Clear cell sarcoma of the left calf in a 34-year-old man. (**a**, **b**) Sagittal and axial spin-echo T1-weighted MR images. (**c**, **d**) Sagittal and axial turbo spin-echo T2-weighted images. The presence of a large, fusiform mass extending along the Achilles tendon. On the sagittal T1-weighted MR image, the lesion appears homogeneous. On the axial view, numerous hypointense, curvilinear dashes are observed within the posterior portion of the mass. The bulk of the mass is nearly homogeneous and is slightly hyperintense to muscle on the T1-weighted MR images. Fat planes between tumor and adjacent muscles are partially obliterated (**a**, **b**). On the T2-weighted MR images, fine, low-intensity septations are observed between the markedly hyperintense components of the lesion (**c**, **d**). The curvilinear dashes of signal voids, as described on T1-weighted images, persist on these T2-weighted images. In view of their posterior location, they may represent dense fibrous tissue in remnants of the invaded Achilles tendon (**d**)

T2-weighted images are useful criteria for indicating the malignancy of the mass [71]. Together with the bright appearance of these tumors on both T1- and T2-weighted images, the radiologic findings may be helpful in characterizing these lesions [11, 34, 70, 71, 104, 158].

18.6.4 Clear Cell Sarcoma of Soft Tissue

18.6.4.1 Definition

Clear cell sarcoma (malignant melanoma of the soft parts) is an extremely rare, slow-growing malignant tumor, the cells of which are capable of producing melanin. In contrast to malignant melanoma of the skin, clear cell sarcomas are more deeply located and mostly arise in the soft tissues of the limbs, in the vicinity of tendons, aponeuroses, and fascial structures. Tumor size ranges from 1 cm to more than 10 cm. Since the lesion is mostly well delineated, and lacks perilesional edema, bone invasion, satellite nodules, or intratumoral necrosis, it may be misinterpreted as a nonaggressive mass. Besides its histological appearance, current diagnosis relies to a large degree on the immunohistochemical analysis,

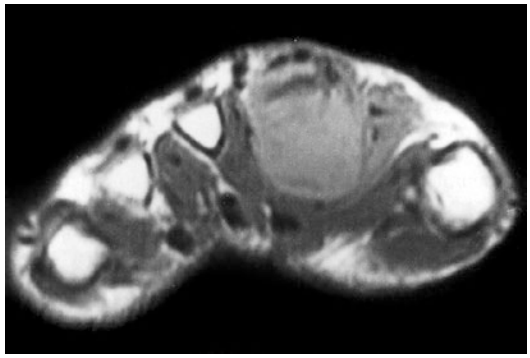

Fig. 18.32 Clear cell sarcoma of the left hand in a 41-year-old man. Axial spin-echo T1-weighted MR image. Demonstration of a rounded mass in the second digit. The mass appears hyperintense and homogeneous on this image. Destruction of the metacarpal bone is noted and confirms the aggressive behavior of the tumor (Reprinted from [36])

since the presence of the melanocytic marker S-100 protein and the melanoma-specific HMB-45 monoclonal antibody is considered very sensitive for the diagnosis of clear cell sarcoma [65, 138].

18.6.4.2 Incidence and Clinical Behavior

Clear cell sarcomas are rare, accounting for only 0.8–1 % of all malignancies of the musculoskeletal system [43, 46]. Young adults between the ages of 20 and 40 years are most frequently affected. However, clear cell sarcoma has also been reported in both very young and very old persons. The tumor predominates in females. The extremities are the most commonly involved areas. Lesions located in the lower limb (foot and ankle, knee, thigh) outnumber those in the upper limb. The head and neck region and the trunk are seldom affected. The tumor presents as a slowly growing mass, which causes pain or tenderness in nearly half of the cases. The skin overlying the lesion remains uninvolved, except in bulky lesions ulcerating to the epidermis. Despite the tumor's slow growth and prolonged clinical course, the prognosis is poor as the recurrence rate is high and the development of metastases is common [46].

18.6.4.3 Imaging

Imaging Studies Other Than MRI Radiographs do not contribute substantially to the diagnosis and may only show the presence of a nonspecific, noncalcified soft tissue mass. Involvement of the underlying bone is uncommon, but if present an important finding [36]. Angiography reveals variable vascularization of the sarcoma and may show either hypervascular or poorly vascularized lesions [46].

MRI Findings On MRI, clear cell sarcomas present as elliptical, smoothly outlined masses (Fig. 18.31, former Fig. 23.23). A large majority of lesions are homogeneous both on T1- and T2-weighted images. Bone destruction and intratumoral necrosis are rare and were observed in 10 and 5 %, respectively, in a series of 21 cases (Fig. 18.32, former Fig. 23.24) [36]. On T1-weighted images, most clear cell sarcomas have slightly increased signal intensity, compared with muscle (Figs. 18.31, 18.32 and 18.33, former Figs. 23.23–23.25). This results from shortening of the T1 relaxation time, which is due to the paramagnetic effect of intralesional melanin. Since hyperintensity on T1-weighted images is rarely seen in soft tissue tumors, this observation is a quite characteristic sign, which allows narrowing the list of differential diagnoses [36]. Nearly 85 % of clear sarcomas are hyperintense to muscle tissue on T2-weighted images (Figs. 18.31, 18.32, and 18.33, former Figs. 23.23 and 23.25). At first sight, this may be surprising, as shortening of the T2 time and hence hypointensity on T2-weighted images might be expected because of the paramagnetic effect of melanin. However, since signal intensity on T2-weighted images also depends on intra- and extracellular water content, it has been suggested that hyperintensity of clear cell sarcomas on T2-weighted images could be caused by a low nucleocytoplasmic index, by abundance of loose connective tissue between the cellular nests, or by high amount of myxoid stroma, found in these hyperintense lesions. Following administration of gadolinium, strong enhancement is observed in the majority of cases [36].

Imaging Strategy MRI is the imaging technique of choice for demonstrating the extent of the tumor, yet it also lacks specificity. Of interest, however, is the fact that high signal intensity on

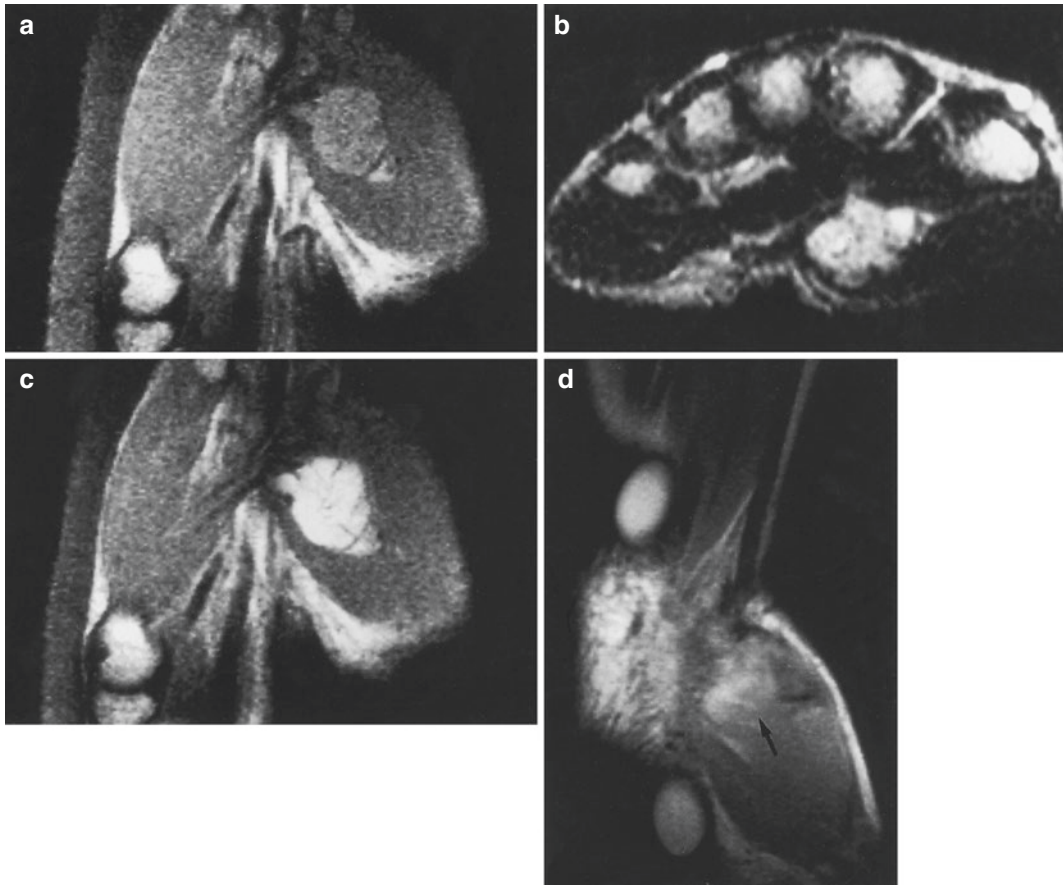

Fig. 18.33 Clear cell sarcoma of the right hand in a 25-year-old woman. (**a**) Coronal spin-echo T1-weighted MR image. (**b**) Axial fast spin-echo T2-weighted MR image. (**c**) Coronal spin-echo T1-weighted MR image after gadolinium contrast injection. (**d**) Coronal spin-echo T1-weighted MR image after gadolinium contrast injection, performed 6 weeks after initial surgery. The presence of a well-circumscribed mass within the thenar muscle. The mass is slightly hyperintense relative to muscle on native T1-weighted images (**a**). On T2-weighted images, signal intensity is high. There is no peritumoral edema (**b**). Following gadolinium contrast injection, strong homogeneous enhancement is seen (**c**). Since the images did not display aggressive characteristics, the surgeon decided to perform an excisional biopsy. Pathological examination, however, revealed clear cell sarcoma. Section margins were borderline. On the MR examination, performed 6 weeks after initial surgery, an indeterminate enhancing area was observed on the T1-weighted images after gadolinium contrast injection (**d**). Subsequently, the thenar muscle was widely excised. Pathological examination disclosed small nests of malignant cells. Since then, a transradial–ulnar amputation has been performed. At 19 months after initial therapy, no metastatic disease has been demonstrated (Reprinted with permission from [36])

T1-weighted images, which most commonly reflects the presence of fat or methemoglobin within a tumor, may also be caused by the presence of melanin and may hence point to the nature of the lesion. Furthermore, it should be stressed that clear cell sarcoma often has a benign appearance on MRI studies, but nevertheless behaves as a relentless, highly malignant soft tissue sarcoma. Therefore, when a well-defined, homogeneous, strongly enhancing mass with slightly higher signal intensity than that of muscle on native T1-weighted images is encountered, the differential diagnosis should include clear cell sarcoma.

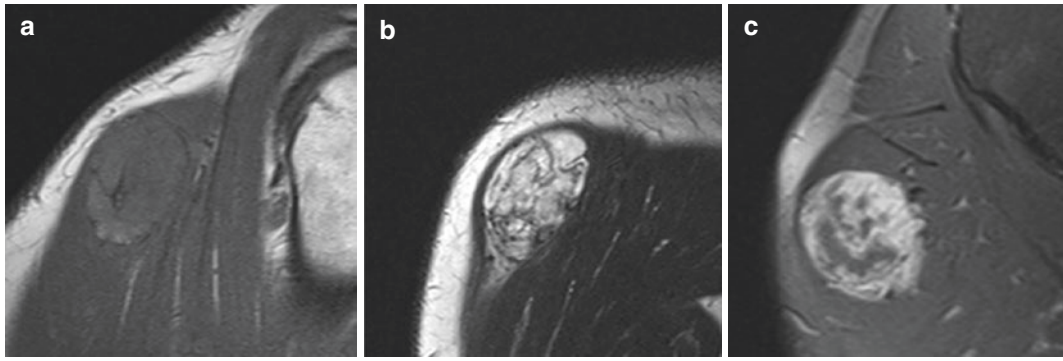

Fig. 18.34 Extraskeletal myxoid chondrosarcoma in a 51-year-old man in the dorsal deltoid muscle. (**a**) Coronal T1-weighted MR image. (**b**) Coronal T2-weighted MR image. (**c**) Coronal T1-weighted MR image after gadolinium contrast injection. On T1-weighted images, isointensity of the encapsulated tumor is present (**a**), while the T2-weighted images disclose a typical hyperintensity with a lobulated enhancement after contrast-agent administration, the latter being suggestive of chondroid tissue

18.6.5 Extraskeletal Myxoid Chondrosarcoma ("Chordoid" Type)

18.6.5.1 Definition, Incidence, and Clinical Behavior

Extraskeletal myxoid chondrosarcoma (EMC) is a very rare tumor characterized by abundant myxoid matrix and malignant chondroblastic cells. The tumor is well demarcated often showing a pseudocapsule with a multinodular and septated architecture and intratumoral hemorrhage and cysts. EMC predominantly affects women in the sixth decade and arises mostly in the deep soft tissues of proximal extremities and limb girdle presenting as a sometimes tender and movement-restricting mass. Tumor sizes up to 25 cm have been described [44, 111]. Long-term follow-up after resection/chemotherapy is needed, since one-fourth of the patients suffer from local recurrences and pulmonary metastases have been described; a 10-year survival rate is around 70 % [41, 101, 111].

18.6.5.2 Imaging

MRI imaging is not specific but often shows the well-circumscribed encapsulated and lobulated mass which, corresponding to the proportion of myxoid tissue, is typically hyperintense on T2-weighted images with hypointense septa. On T1-weighted sequences, ECM has been described as iso- to hypointense, where upon T1-hyperintense areas can be found in case of intratumoural hemorrhage. Fluid–fluid levels are not typical. Heterogeneous enhancement has been reported [85, 153, 158] (Fig. 18.34).

18.6.6 Malignant Mesenchymoma

18.6.6.1 Definition

The term "malignant mesenchymoma" refers to a group of malignant soft tissue tumors that are characterized by the presence of two or more different tissue components in the same neoplasm [119]. This group is further subdivided into two subcategories. The first category is the smallest one and comprises those tumors that are characterized by coexisting rhabdomyosarcomatous and liposarcomatous elements in the same neoplasm. The second category is much larger and consists of neoplasms containing a specific type of sarcoma together with more or less prominent foci of malignant cartilaginous or osseous tissue [19, 46]. The origin of these tumors remains unclear, and many authors now assume that these tumors arise from primitive mesenchymal cells that have differentiated along multiple cell lines. Though, it has to be discussed if the tumors showing the lines of differentiation as described above could also meet criteria for other entities.

18.6.6.2 Incidence and Clinical Behavior

As may be expected from the heterogeneity of this group of tumors, clinical presentation is widely variable. However, most of these tumors affect older persons, nearly always older than 55 years [19]. Occurrence in children and young adults is only rarely seen. The retroperitoneum and thigh are frequently involved. The prognosis is depending from the prevalent mesenchymal component.

18.6.6.3 Imaging

Imaging findings are related to the prevalent tissue component, with some tumors showing calcifications which can lead to misdiagnosis of, for example, myositis ossificans [108]. The MRI findings in the case presented in Fig. 18.35 (former Fig. 23.26) include a nearly homogeneous mass on T1-weighted images. On T2-weighted images, the tumor seemed to be composed of multiple hyperintense nodules with a hypointense center. Gadolinium contrast-enhanced T1-weighted images disclosed strong enhancement of the tumor parts that were very bright on unenhanced T2-weighted images.

18.6.7 Desmoplastic Small Round Cell Tumor

18.6.7.1 Definition

Desmoplastic small round cell tumor (DSRCT) is a rare tumor consisting of small round tumor cells of uncertain histiogenesis, occurring predominantly in the abdominal cavity. The tumor is characterized by a unique chromosomal translocation t(11;22) (p13;q12) resulting in a fusion of Ewing's sarcoma (ESW) gene and the Wilms' tumor gene [15].

18.6.7.2 Incidence and Clinical Behavior

DSRCT affects young adults or children with a marked male predominance. Usually, the tumor arises in the abdominal cavity [62], while primary extra-abdominal DSRCT is a rarity. Patients present, dependent on the primary site, with symptoms as pain, acute and distended abdomen, organ obstruction, or ascites. Metastasis is frequently seen, especially in subcutaneous and muscle tissue. Prognosis is poor, with an estimated 5-year survival rate of 20 % [8].

18.6.7.3 Imaging

As described above, the most common findings are multiple omental or serosal soft tissue masses, which have a low attenuation and only moderate homogeneous enhancement [152]. Lesions larger than 10 cm are likely to show signs of central necrosis or hemorrhage. Calcification is relatively commonly seen on CT scans, especially after radiotherapy. Bone metastases have been described as blastic or mixed blastic and lytic [8]. On T1-weighted MR images, DSRCT has an inhomogeneous low or isointense signal intensity relative to skeletal muscle. On T2-weighted images, inhomogeneous high signal intensity is typical. Sometimes small cysts or fluid–fluid levels as well as signs of hemorrhage or necrosis can be identified [152] (Fig. 18.36).

18.6.8 PNET/Extraskeletal Ewing's Sarcoma

18.6.8.1 PNET

Introduction

Primitive neuroectodermal tumors (PNET) form part of the heterogeneous group of small round (blue) cell tumors of childhood and adolescence. This group also contains conventional neuroblastoma, rhabdomyosarcoma, lymphoma, and Ewing's sarcoma.

Purely for practical reasons, Dehner introduced the distinction between central PNET (cPNET) and peripheral PNET (pPNET), as he was well aware that little knowledge was available concerning the actual biology of these neoplasms and of their interrelationships [38]. This classification applies knowledge of neuroectodermal derivatives to the PNET. The

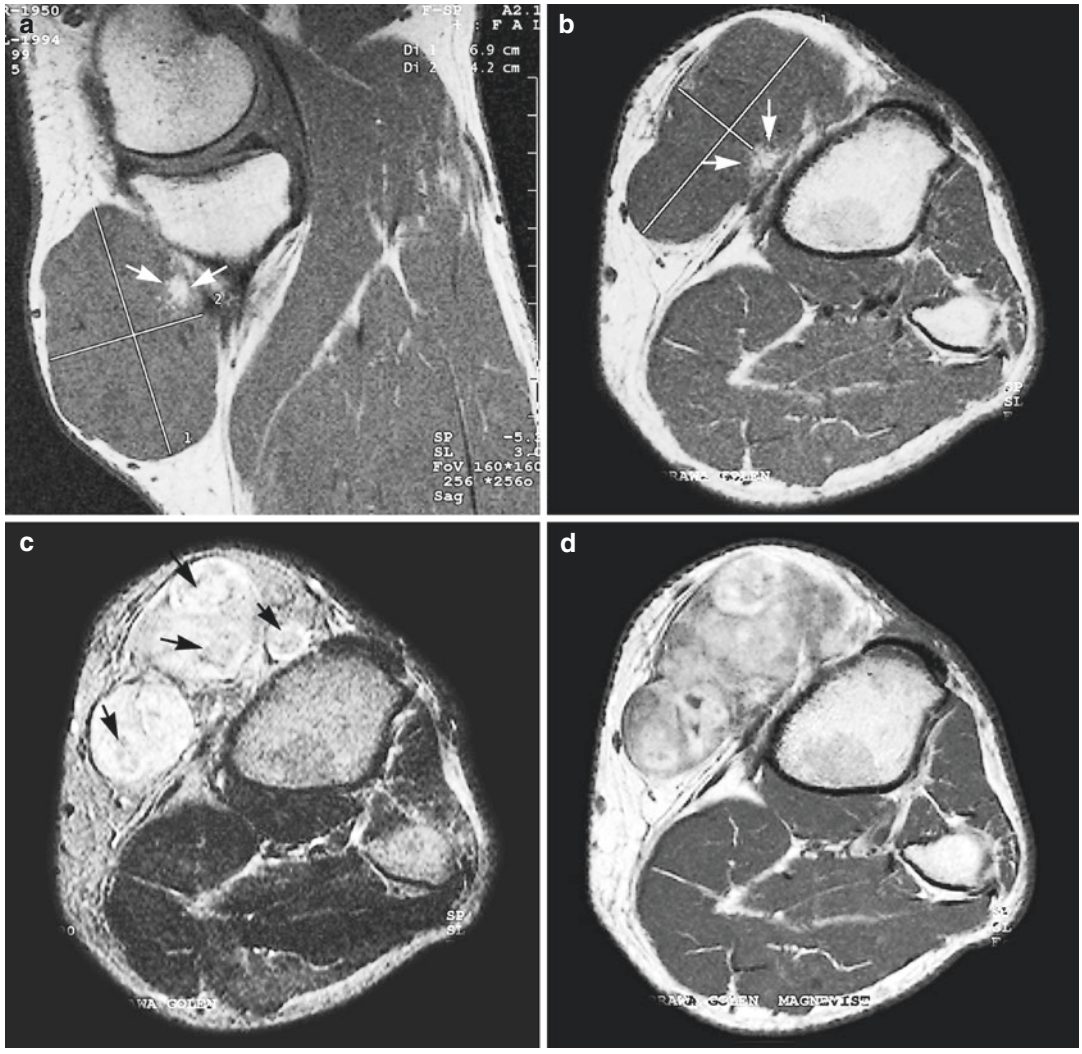

Fig. 18.35 Mesenchymoma of the proximal third of the left leg in a 44-year-old woman. (**a**, **b**) Sagittal and axial spin-echo T1-weighted MR images. (**c**) Axial spin-echo T2-weighted MR image. (**d**) Axial spin-echo T1-weighted MR image after gadolinium contrast injection. The presence of an ovoid soft tissue mass within the subcutaneous fat layer, just anterior to the tibia. The mass is sharply outlined. On the T1-weighted images, a nearly homogeneous appearance with low signal intensity in the major portions of the tumor is seen. A high signal intensity nodule is observed in the posterior aspect of the tumor, indicating the presence of fat within the tumor (*arrows*) (**a**, **b**). On the T2-weighted image, multiple rounded to ovoid, very hyperintense nodules are shown. Irregular low-intensity areas are seen within these nodules (*arrows*). Likewise, the tissue between the nodules presents with low signal intensity (**c**). The gross appearance of the tumor is much more inhomogeneous on T2- than on T1-weighted images. Likewise, the pattern of enhancement is inhomogeneous. The strongest enhancement is observed at the periphery of the nodular components of the tumor in the same areas that are very bright on T2-weighted images (**c**, **d**)

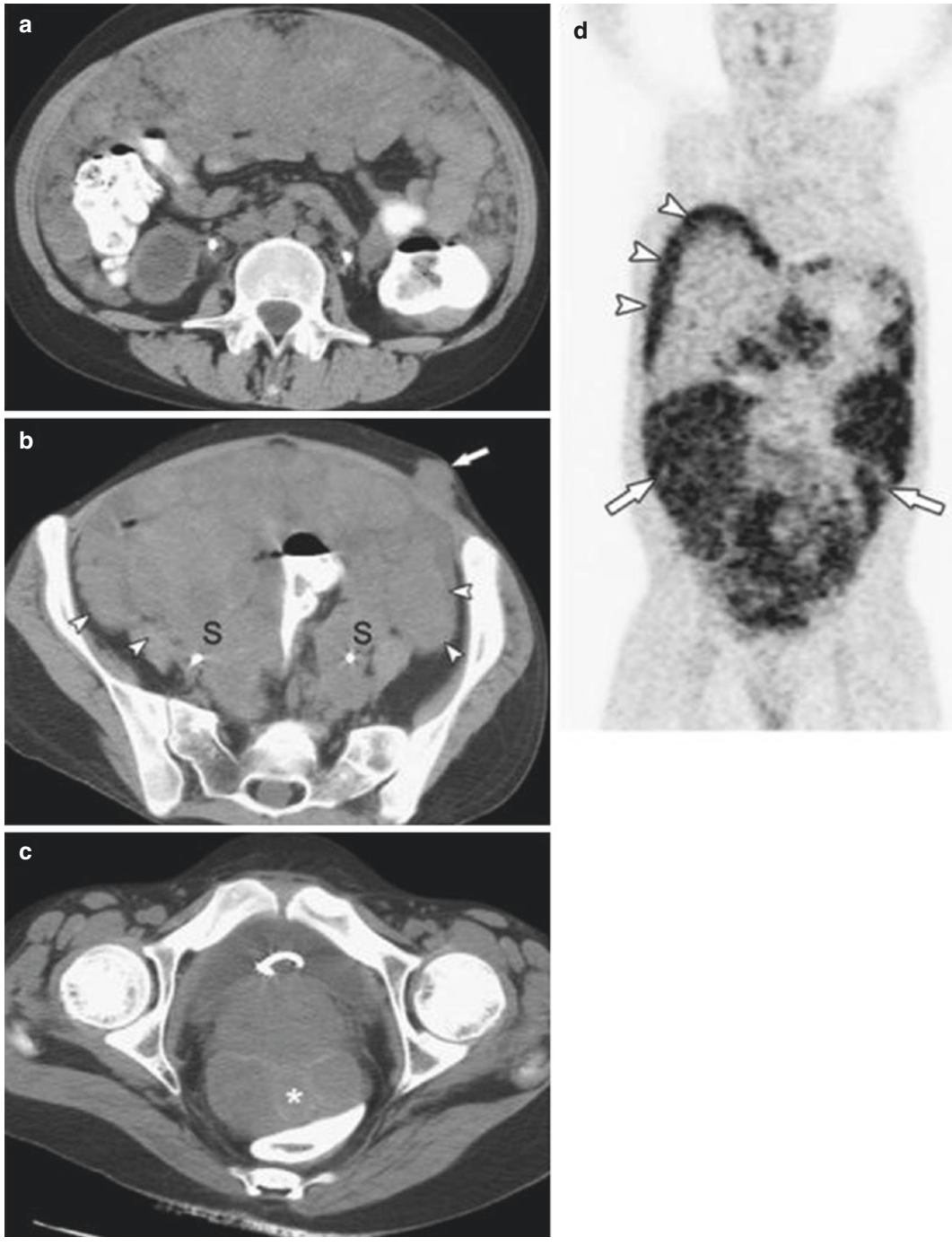

Fig. 18.36 Desmoplastic round cell tumor in a 14-year-old boy. Axial (unenhanced) CT image (**a**) shows diffuse studding of the omentum and peritoneal surfaces by innumerable soft tissue masses. Axial image through the pelvis shows lobulated low attenuation masses (*arrowheads*) and a large retrovesical mass (*) displacing the rectum posteriorly (**b, c**). Note subcutaneous metastatic nodules in the lower left abdominal wall (*arrow*). Bilateral nephroureteral stents (s) were inserted to relieve obstructive hydronephrosis. Maximum intensity projection FDG PET (**d**) shows hypermetabolic peritoneal (*arrows*) and serosal disease (*arrowheads*) (SUV max 8.0) (Used with permission from: Arora et al. [8])

neuroectoderm generates the brain and spinal cord, on the one hand, and the entire autonomic nervous system, dorsal root ganglia, adrenal medulla, and part of the neuroendocrine system, on the other, among many other derivatives. It must be stressed that this division of the PNET does not have any clinical, pathologic, or prognostic implications. In this chapter, only pPNET will be discussed. Peripheral primitive neuroectodermal tumors constitute a group of uncommon tumors with similar histology, and are aggressive and poorly differentiated neoplasms, occurring mainly in children and young adults. These tumors originate in the soft tissues or bone, outside the central or sympathetic nervous system, and are composed of undifferentiated, small, round, hyperchromatic tumor cells.

pPNET and Ewing's sarcoma form a special group within the small round (blue) cell tumors. Several common characteristics have been discovered that distinguish them from other small round (blue) cell tumors, namely, a unique chromosomal translocation, t(11;22) (q24;12), and the expression of a membrane glycoprotein, known as the MIC2 gene product (see Chap. 6: Genetics and Molecular Biology of Soft Tissue Tumors) [7]. In addition to pPNET of soft tissue and Ewing's sarcoma of the bone, there are also osseous pPNET and extraskeletal Ewing's sarcoma. It was also noted that extraskeletal Ewing's sarcoma and some atypical forms of Ewing's sarcoma of the bone display neuroectodermal features. Because of these shared phenotypical and genotypical characteristics, very typical for Ewing's sarcoma and pPNET, it is now generally accepted that these two neoplasms are related to each other. They are thought to correspond to distinct neural crest lineages or tumors arrested at different stages of development. pPNET is the most differentiated and can be considered the neural variant of Ewing's sarcoma [10, 39, 122]. According to Ewing's sarcoma/pPNET classification proposed by Schmidt [137], diagnosis of pPNET is reserved to those cases that express at least two different neural markers and/or Homer Wright rosettes, the others being termed Ewing's sarcoma. This classification has proven to be useful [20]. Due to the identification of the common nonrandom chromosome rearrangements in Ewing's sarcoma, peripheral primitive neuroectodermal tumor, Askin's tumor, which affects the thoracic wall, and neuroepithelioma, these tumors are now considered entities of the Ewing's sarcoma family of tumors (ESFT).

Incidence and Clinical Behavior

Most pPNETs are diagnosed between the ages of 14.6 and 20.8 years. Seventy-five percent occur before the age of 30 years [90, 137]. Peripheral PNET presenting at birth is uncommon, but reported [69]. Peripheral PNET occurs predominantly in Whites and Hispanics and rarely occurs in individuals of African or Asian descent [127]. Men are affected more frequently than women [77, 90, 137]. These tumors represent about 1 % of all sarcomas. By definition, pPNET never arise from the sympathetic nervous system. Therefore, cases usually occur outside the vertebral axis of the body [15]. They are found most frequently in the thoracopulmonary region, abdomen, pelvis, and lower extremities [77, 137, 150]. They are also reported in the orbit, kidney, stomach [32], retroperitoneum [73], vulva, colon, hand [69], uterus [127], middle ear, diploe, and maxilla [6, 77]. The pPNET can give rise to symptoms and signs of neurologic failure [69]. According to Schmidt's classification, prognosis is worse for pPNET than for Ewing's sarcoma [137].

A special entity of pPNET is Askin's tumor. This was first described as a "malignant small cell tumor of the thoracopulmonary region of childhood" [10], but it is now classified as a pPNET of the chest wall [145]. It is found principally in young adults and adolescents [20] but can occur at all ages (Fig. 18.37; former Fig. 22.6). In contrast to the pPNET in general, Askin's tumors seem to have a preference for girls [10, 64]. Usually, the mass has already achieved a considerable size by the time of diagnosis [21] and is painful in just over half of the cases [134]. Pleural effusion may also occur [10, 21, 93, 145].

pPNET can provoke constitutional symptoms. Fever, anorexia, weight loss, cough, and

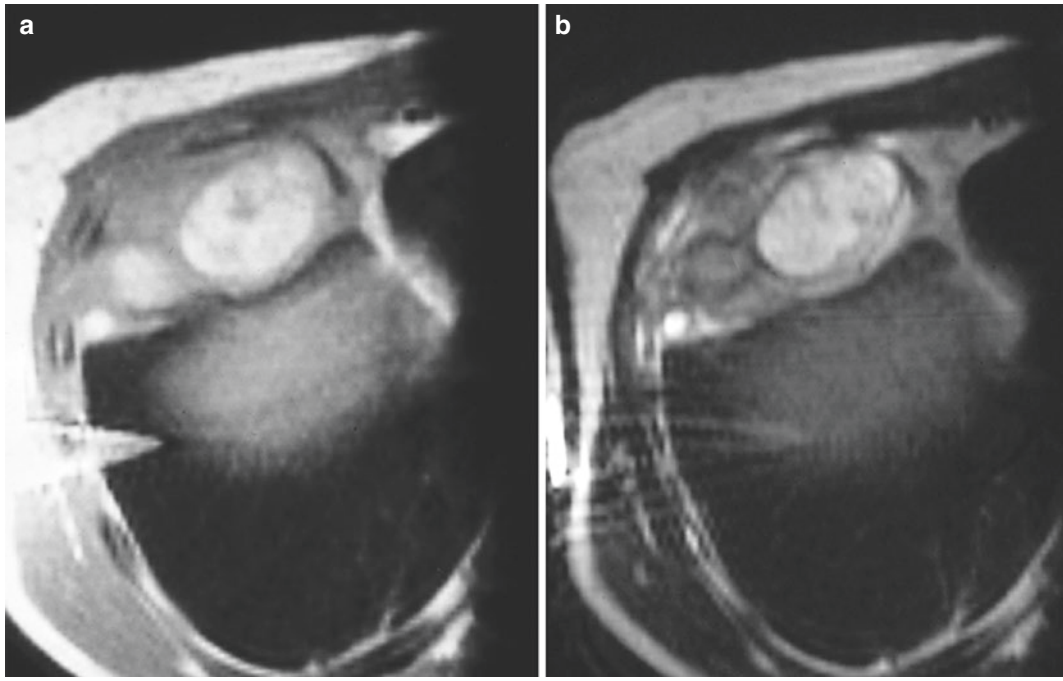

Fig. 18.37 Askin's tumor (pPNET) in a 19-year-old man presenting with a mass lesion at the anterior thoracic wall. (**a**) Axial spin-echo, contrast-enhanced T1-weighted MR image. (**b**) Axial spin-echo T2-weighted MR image. The presence of a multinodular, enhancing mass lesion at the anterior aspect of the thoracic wall (**a**). On T2-weighted images, the nodules present with different signal intensities (**b**). Age, localization, morphology, and signal intensity characteristics are in favor of a pPNET of the chest wall, also called Askin's tumor

dyspnea are frequent. In cases of Askin's tumor, shoulder pain, Horner's syndrome, and cervical lymphadenopathy can also occur [10, 21, 77, 93, 145]. Askin's tumors, as with PNET in general, are highly aggressive. One study of 30 cases showed a 2-year survival rate of 38 % and a 6-year survival rate of 14 % [30]. Relapse is most common at the thorax, where it presents as local chest wall recurrence or disseminated pulmonary metastasis. Metastasis to mediastinal lymph nodes may also occur. The next most common manifestation of relapse is distant skeletal metastasis. Infrequently, the disease recurs in the liver, adrenals, brain, retroperitoneum, and sympathetic chain. These sites must be considered in follow-up CT examinations [10, 21, 93, 145].

Esthesioneuroblastoma, also known as olfactory neuroblastoma, has long been considered a member of the pPNET/Ewing's sarcoma family. Although a primitive neural tumor, recent studies raise doubts about the legitimacy of its membership because of the failure to identify the MIC2 gene product [73].

Imaging Characteristics

Plain Radiography

Little is known concerning the radiographic presentation of pPNET. On plain radiographs, Askin's tumor commonly presents as a mass of the chest wall with soft tissue density. Rib erosion occurs very often [10, 21, 93, 145]. In about 10 % of cases, the tumor is seen as a paraspinal or mediastinal mass. In 15 % of cases, a usually small, pleural effusion is observed. Rarely, calcifications are present [10, 21, 64, 93, 145].

Ultrasound

As in the plain radiograph, ultrasound of Askin's tumor reveals only nonspecific features. A complex, solid mass may be revealed, with mixed echogenicity and sometimes with cystic compo-

nents. When present, a pleural effusion can be seen [134].

CT and MRI

On CT, pPNET presents as a large, ill-defined mass with a heterogeneous appearance due to extensive cystic degeneration. As a rule, there is no calcification [77], although our series contains a pPNET with extensive calcification (Fig. 18.38; former Fig. 22.1). After the injection of iodinated contrast, the tumor has a heterogeneous appearance [77, 134, 160]. On T1-weighted MR images, pPNET generally has a signal intensity equal to or greater than that of muscle; on T2-weighted sequences, a heterogeneous high signal has been reported [158, 160, 162]. Frequently, evidence of hemorrhage or necrosis is found (Fig. 18.39). Larger tumors show up as heterogeneous masses, while smaller ones tend to be more homogeneous [49, 77, 160].

18.6.8.2 Extraskeletal Ewing's Sarcoma

Definition

Extraskeletal Ewing's sarcoma is a rare soft tissue tumor, histologically indistinguishable from the osseous form. The major differences are in the age group of prevalence and the site of predilection. These tumors are commonly deeply located and have diameters ranging from 5 to 10 cm. On

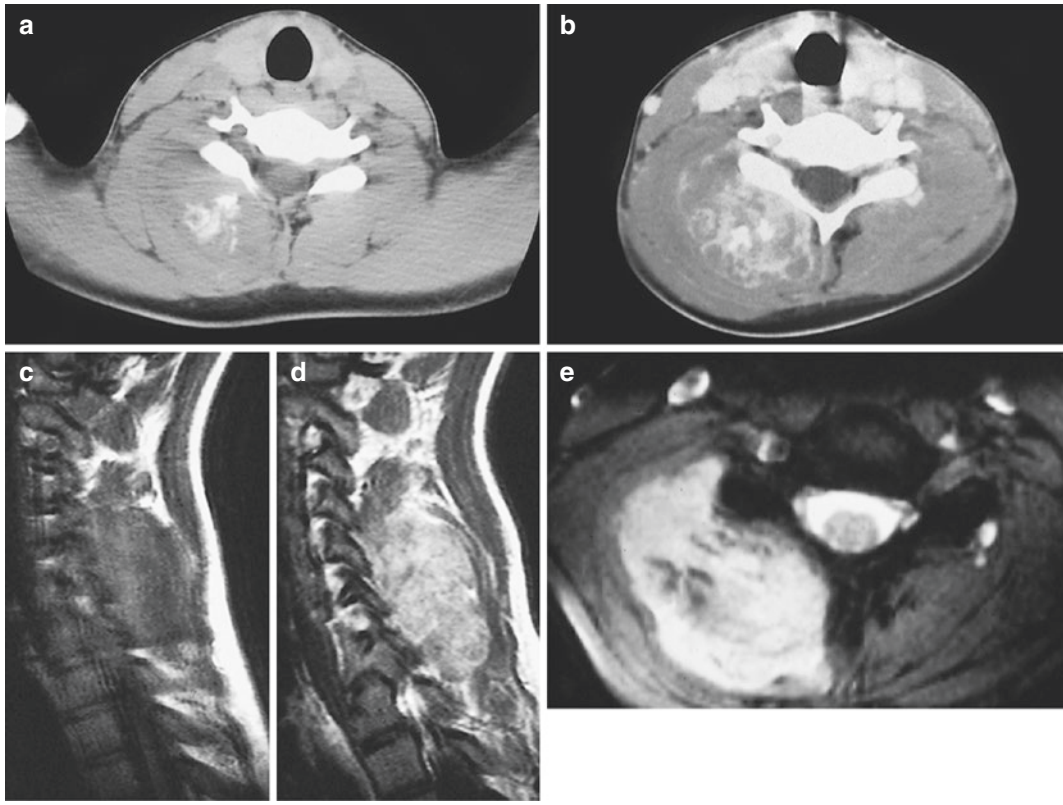

Fig. 18.38 pPNET of the lower neck in a 12-year-old girl. (**a**) CT. (**b**) CT after iodinated contrast injection. (**c**) Sagittal spin-echo T1-weighted MR image. (**d**) Sagittal spin-echo, contrast-enhanced T1-weighted MR image. (**e**) Axial gradient-echo T2-weighted MR image. Large mass within the deep cervical muscles on the right side of the neck. The tumor contains irregular calcifications (**a**). There is marked enhancement after contrast injection (**b**). On the T1-weighted images, the lesion is of low signal intensity and shows considerable enhancement after intravenous administration of gadolinium contrast (**c**, **d**). On the T2-weighted image, the lesion has high signal intensity with central signal voids, due to intralesional calcifications. The lesion neighbors the cervical vertebrae, without manifesting osseous involvement (**e**)

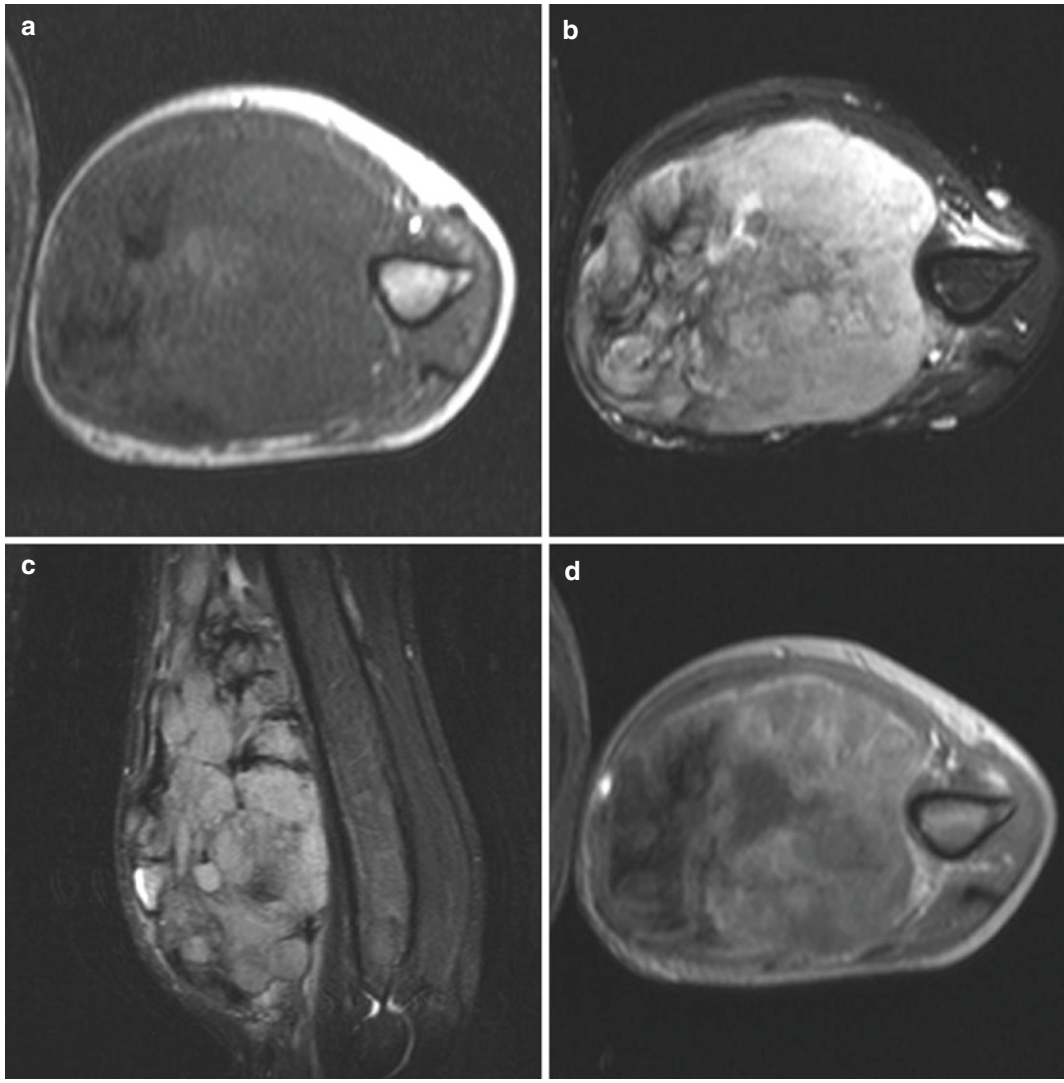

Fig. 18.39 Primitive neuroectodermal tumor of the medial upper extremity of a 20-year-old patient with neurofibromatosis type I. (**a**) Axial T1-weighted MR image. (**b**) Axial T2-weighted MR image. (**c**) Coronal T2-weighted MR image with fat saturation. (**d**) Axial T1-weighted MR image after gadolinium contrast injection. MRI revealed a T1-hypo- and T2-hyperintense tumor with spots of hemorrhage (**a**, **b**) and a lobulated appearance seen on the STIR images as well as necrotic, non-enhancing areas medially (**d**)

pathology, the tumor is multilobulated, is richly vascular, and often contains large areas of necrosis, cyst formation, or hemorrhage [47].

Incidence and Clinical Behavior

In contrast to the osseous form, extraskeletal Ewing's sarcoma occurs in somewhat older persons, with a median age of about 20 years (more than 75 % of the patients are between 10 and 30 years of age). This tumor is slightly more common in men and occurs chiefly in the paravertebral and intercostal regions. Soft tissues of the lower extremities and very rarely of the pelvic and hip regions, retroperitoneum, and upper extremities also may be involved [4]. Patients usually present with a rapidly growing mass, which is painful in about one-third of cases. Sensory or motor disturbances are

observed if the tumor involves the spinal cord or peripheral nerves. Metastatic spread – most commonly to lungs or skeleton – and recurrence are common and observed in nearly 65 % of cases [47, 122].

Imaging Characteristics

Imaging Studies Other than MRI

Plain radiographs reveal only a nonspecific soft tissue mass of widely variable size. Small areas of amorphous calcifications are not observed in untreated tumors but may develop during chemotherapy [122]. On ultrasound, these tumors are mostly well circumscribed. Ultrasound features are mostly those of a hypoechoic or partly anechoic mass, although a mixed echo pattern may also be recognized [122]. Unenhanced CT scans show either low attenuation throughout the tumor or only focal areas of hypodensity. Enhancement on post-contrast sequences is moderate but variable and reflects the different vascularization pattern (Figs. 18.40 and 18.43a, Fig. 22.3) [122].

MRI

On MRI, extraskeletal Ewing's sarcoma presents as a well-circumscribed mass within the involved muscle (Figs. 18.41 and 18.42, Figs. 22.4 and 22.5). Intermediate signal intensity is observed on T1-weighted images. T2-weighted images demonstrate a heterogeneous, mottled appearance of the mass containing areas of high signal intensity. Heterogeneous enhancement is observed after administration of gadolinium chelates [4].

Imaging Strategy

None of the findings of the various imaging modalities are characteristic for extraskeletal Ewing's sarcoma. The role of imaging consists mainly of establishing local tumor extent. Despite the nonspecific findings, extraskeletal Ewing's sarcoma should be included in the differential diagnosis when a noncalcified soft tissue mass is observed in the paravertebral region of the chest or in an extremity, especially in the appropriate age group.

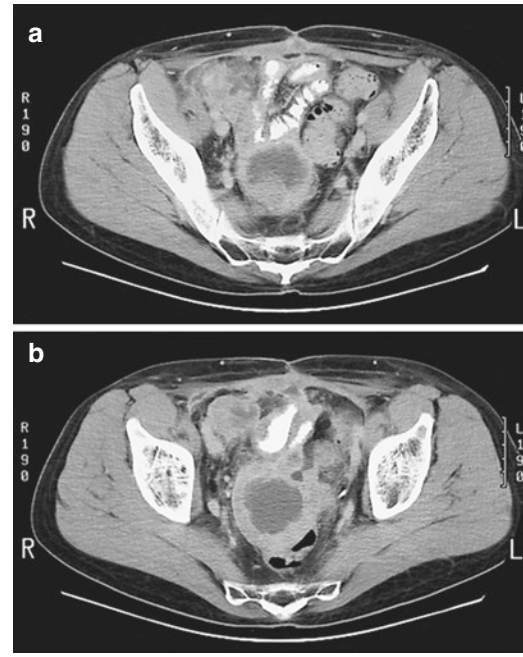

Fig. 18.40 Extraskeletal Ewing's sarcoma of the pelvis in a 36-year-old man. (**a**) CT after iodinated contrast injection. (**b**) Section at a lower level than in (**a**). Hourglass-shaped soft tissue tumor in the pelvis, with major tumor component in a right anterolateral position to the rectum and smaller component anteriorly in the right iliac fossa. Ill-defined, hypodense area without enhancement within the major tumor component, suggesting a necrotic center of the tumor (**a**). Necrotic areas within both tumor components are more clearly seen at the caudal section (**b**). Sequel from previous laparotomy and thickening of bowel walls following radiotherapy are observed at both levels

18.6.9 Extrarenal Rhabdoid Tumor

18.6.9.1 Definition

Extrarenal rhabdoid tumors (ERRTs) are aggressive malignancies which arise in the central nervous system and rarely in soft tissues and are characterized by typical neoplastic cells with large nuclei and eccentric cytoplasm with prominent eosinophilic, cytoplasmic inclusions [124]. Grossly, ERRTs are unencapsulated masses, usually less than 5 cm in diameter with a soft and gray cut surface with foci of coagulative and hemorrhagic necrosis. Genetically, an inactivation/deletion of tumor suppressor gene *SNF/INI1/SMARCB1* has been described being involved in renal and extrarenal rhabdoid tumor pathogenesis [157].

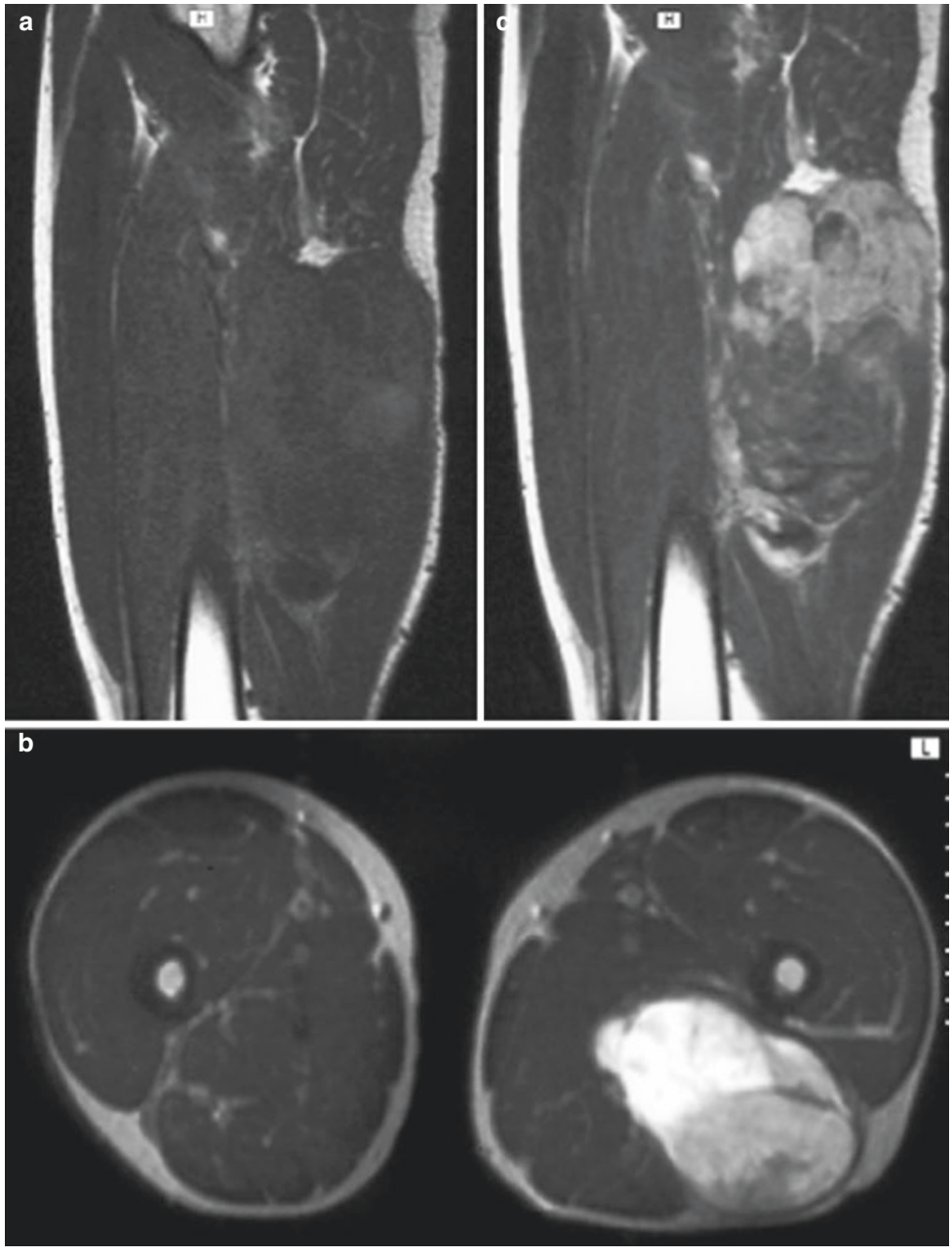

Fig. 18.41 Extraskeletal Ewing's sarcoma of the left thigh in a 29-year-old man. (**a**) Sagittal spin-echo T1-weighted MR image. (**b**) Axial spin-echo T2-weighted MR image. (**c**) Sagittal spin-echo T1-weighted MR image after gadolinium contrast injection. A large polylobular mass at the posterior aspect of the femur is seen. On the T1-weighted image, the lesion appears inhomogeneous, and signal intensity is nearly equal to that of surrounding muscle. Ill-defined, slightly hyperintense area posteriorly in the lesion suggests intratumoral hemorrhage. On the T2-weighted image, the polylobular shape of the lesion is confirmed by the presence of several lobules with different appearances. Some lobules are very bright and contain low-intensity septations, while others have intermediate signal intensity, equal to that of fat. Demarcation from surrounding muscle and subcutaneous fat is sharp (**b**). Highly variable degree of enhancement is observed at the various tumor constituents. Pronounced, but inhomogeneous, enhancement is observed at the cranial parts of the tumor. A mottled, only slightly enhancing pattern is observed at the lower pole of the tumor (**c**)

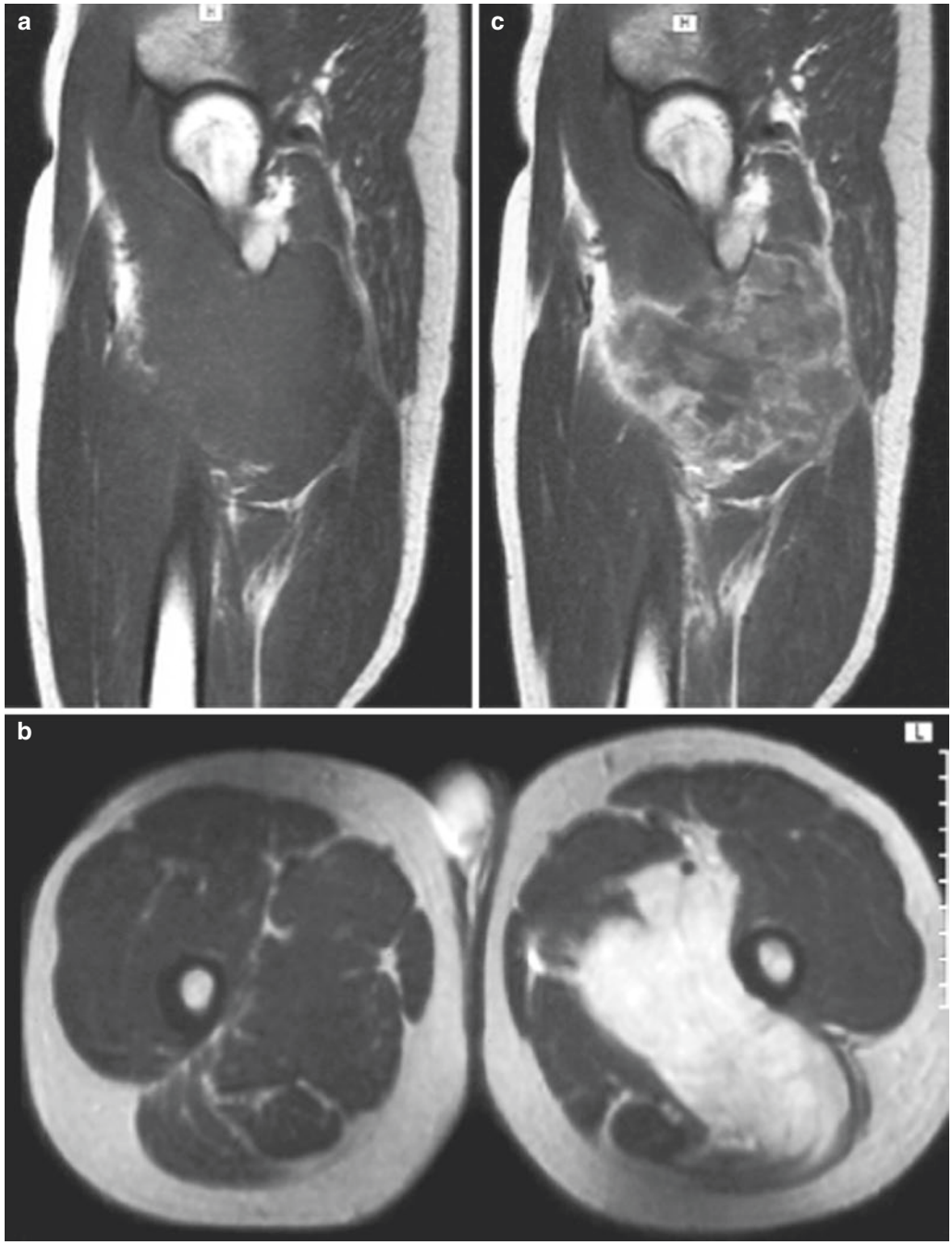

Fig. 18.42 Extraskeletal Ewing's sarcoma at the infratrochanteric region of the left thigh in a 32-year-old man. (**a**) Sagittal spin-echo T1-weighted MR image. (**b**) Axial spin-echo T2-weighted MR image. (**c**) Sagittal spin-echo T1-weighted MR image after gadolinium contrast injection. The presence of a polylobular low-intensity mass medial to the proximal third of the left femur. The mass is homogeneous and slightly hyperintense to muscle on the T1-weighted image (**a**). On the T2-weighted image, the lesion has an inhomogeneous appearance. Signal intensity surpasses that of subcutaneous fat (**b**). After contrast medium injection, inhomogeneous pattern of enhancement is observed at the tumor. Central non-enhancing areas are likely to represent intratumoral necrosis (**c**). Notice the absence of bony erosion and cortical involvement despite the intimate contact over a long distance

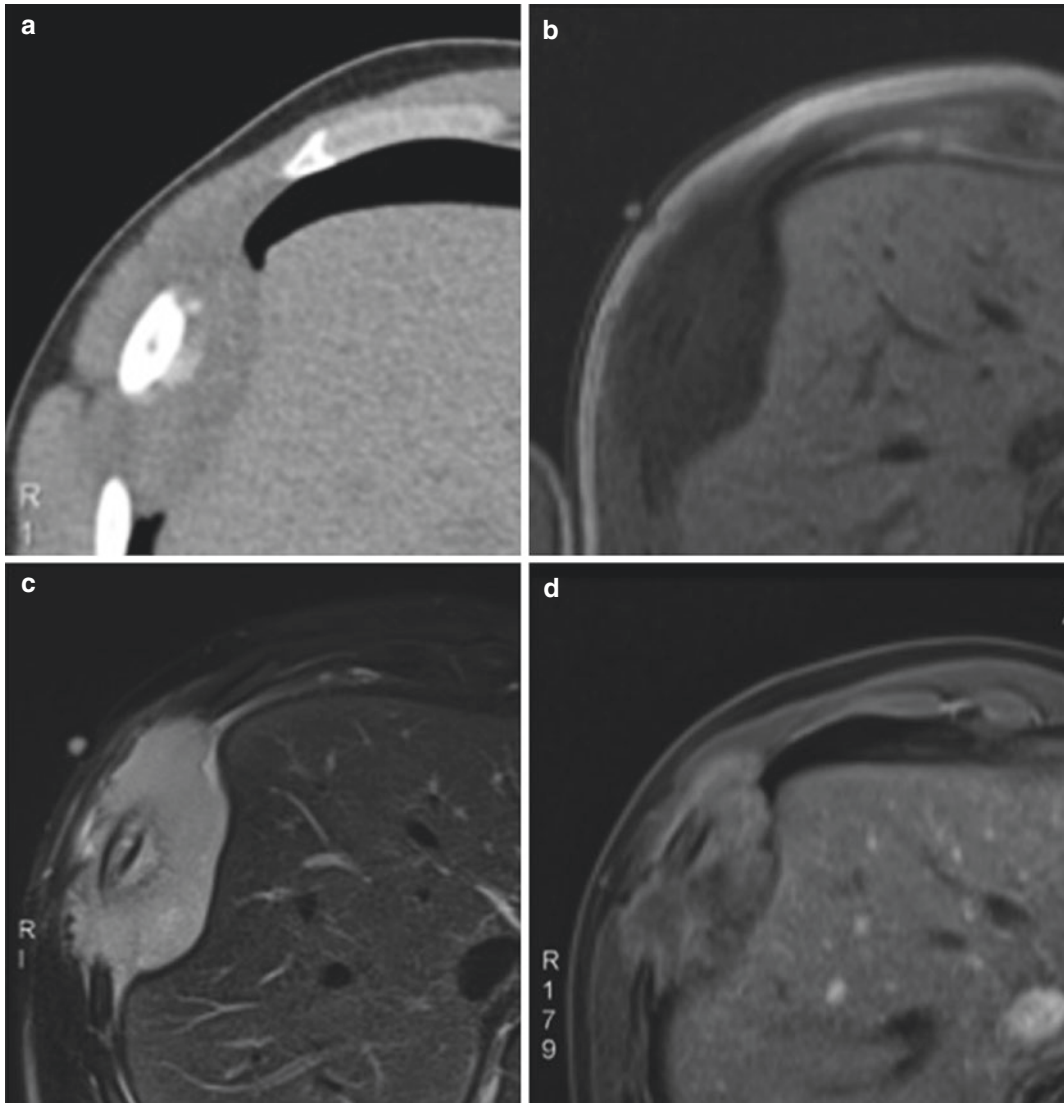

Fig. 18.43 Extraskeletal Ewing's sarcoma in a 23-year-old patient. (**a**) Axial CT scan. (**b**) Axial T1-weighted MR image. (**c**) Axial T2-fs-weighted MR image. (**d**) Axial T1-fs-weighted MR image after gadolinium contrast injection. A 23-year-old patient presented with pain at the right chest wall for more than a month without known trauma. The CT scan showed a sharply lineated soft tissue mass encasing the seventh right rib with additional periosteal reaction. (**a**) The lesion was isointense to muscle on T1-weighted images (**b**) and homogeneously hyperintense on T2-weighted images with fat suppression (**c**), showing an infiltration of the muscles of the thorax wall as well as leading to an impression of the liver. After intravenous administration of gadolinium contrast heterogeneous enhancement, predominantly at the periphery of the lesion could be seen (**d**)

18.6.9.2 Incidence and Clinical Behavior

ERRT almost exclusively affects children or infants. To date, family history is only rarely described [14]. Soft tissue lesions arise most frequently in deep, axial locations. Sometimes, the liver or mediastinum can also be affected [2]. A fatal clinical course with a 5-year survival not exceeding 20 % is typical [124].

18.6.9.3 Imaging

There are no specific studies describing imaging findings of ERRT, making biopsy crucial for diagnosis. ERRT, which can be locally invasive, demonstrates hypodensity on CT scans, and on MRI they present with hypointensity on T1-weighted images and heterogeneous hyperintensity on T2-weighted images. Usually, ERRT is enhancing after contrast-agent administration [2, 61] (Figs. 18.44 and 18.45).

18.6.10 Neoplasms with Perivascular Epithelioid Cell Differentiation (PEComa): Clear Cell Myomelanocytic Tumor

18.6.10.1 Definition

Neoplasms with perivascular epithelioid cell differentiation (PEComa) include angiomyolipoma (AML) as the most common PEComa, lymphangioleiomyomatosis (LAM), clear cell "sugar" tumor (CCST) of the lung, clear cell myomelanocytic tumor (CCMMT) of the falciform ligament/ligamentum teres, and unusual clear cell tumors of the viscera. Typically, PEComas are mesenchymal tumors composed of epithelioid cells which are in perivascular location sometimes showing intramural involvement and demonstrate immunoreactivity to melanocytic and muscle markers such as HMB-45, smooth muscle actin, and melan-A [95].

18.6.10.2 Incidence and Clinical Behavior

PEComa usually affects women in a wide variety of locations; however, bones are only rarely involved [40]. CCMMT is painful but benign and occur predominantly in young children [56]. PEComas located in the uterus can cause vaginal bleeding. In other locations, PEComas tend not to evoke symptoms. They can behave as benign lesions, but there have been reports of malignant, mostly epithelioid, AML [27, 94] and CCST [60].

18.6.10.3 Imaging

Since extrarenal AML of the soft tissues is extremely rare [78], little is known about the

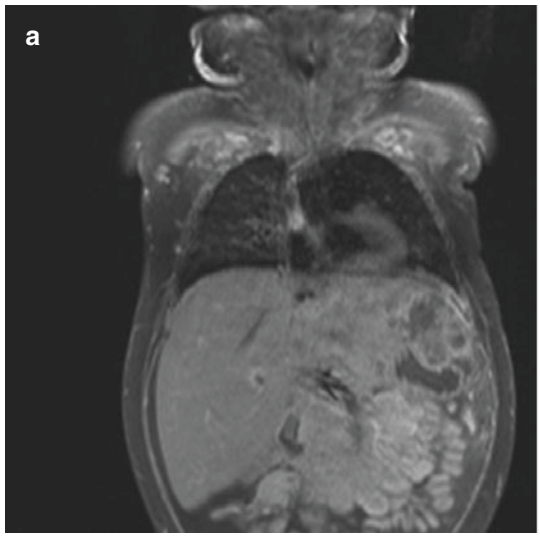

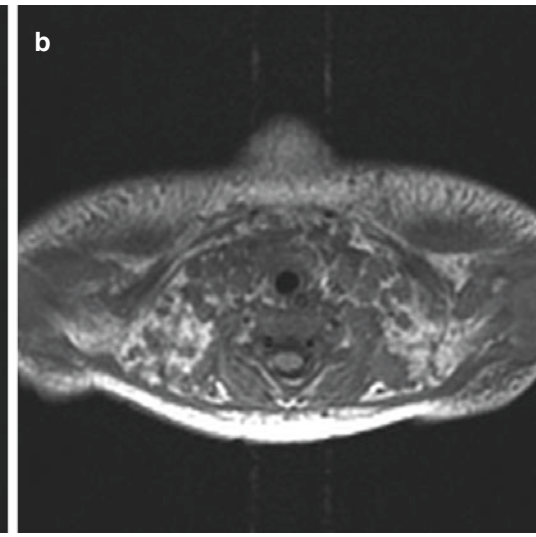

Fig. 18.44 Extrarenal rhabdoid tumor. (**a**) Coronal T1-weighted MR image after gadolinium contrast injection. (**b**) Axial T2-weighted MR image. One-year old patient with a metastasized hepatic rhabdoid tumor and a diffuse infiltration of the omentum (**b**), as well as lymphangiosis carcinomatosa of the right lung and innumerous T2-isointense tumor nodules cervically (**b**)

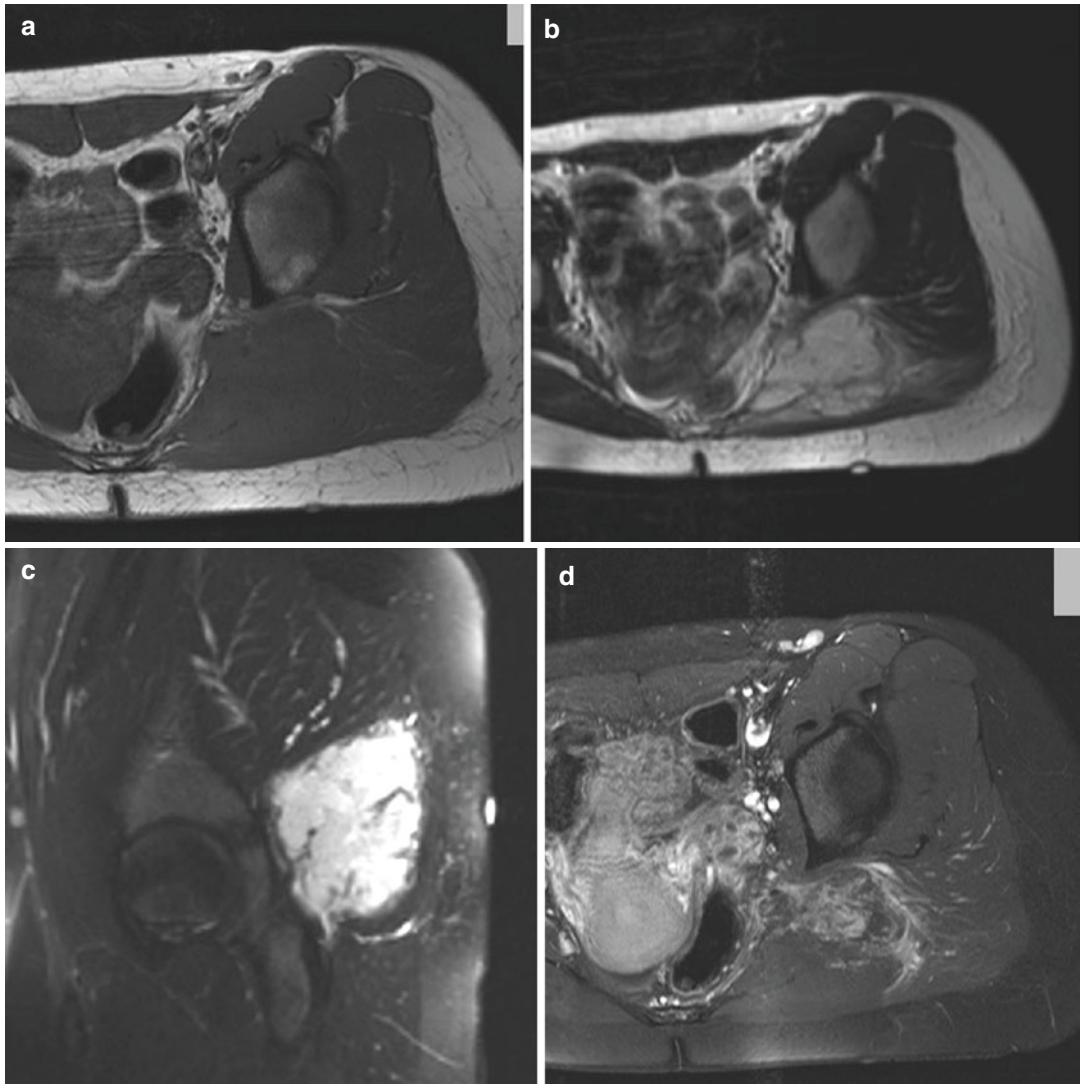

Fig. 18.45 Extrarenal rhabdoid tumor in the left gluteal region of an 18-year-old patient. (**a**) Axial T1-weighted MR image. (**b**) Axial T2-weighted MR image. (**c**) Sagittal T2-weighted MR image with fat suppression. (**d**) Axial T1-fs-weighted MR image after gadolinium contrast injection. As described in literature, the lesion is isointense on T1-weighted images (**a**) and hyperintense on T2-weighted images (**b**) with inhomogeneous central enhancement (**c**)

imaging characteristics. Retroperitoneal extrarenal angiomyolipoma has been described as hyperechoic in ultrasound and fat isodense on CT scans as well as T1-hyperintense with a marked hypervascularization and contrast enhancement [149, 154] (Fig. 18.46).

LAM normally manifests in the lung leading to interstitial reticular opacities. CT scans demonstrate bilateral diffuse thin-walled cysts surrounded by normal lung parenchyma [1]. Moreover, unilateral or bilateral pleural effusions can frequently be seen. Extrapulmonal manifes-

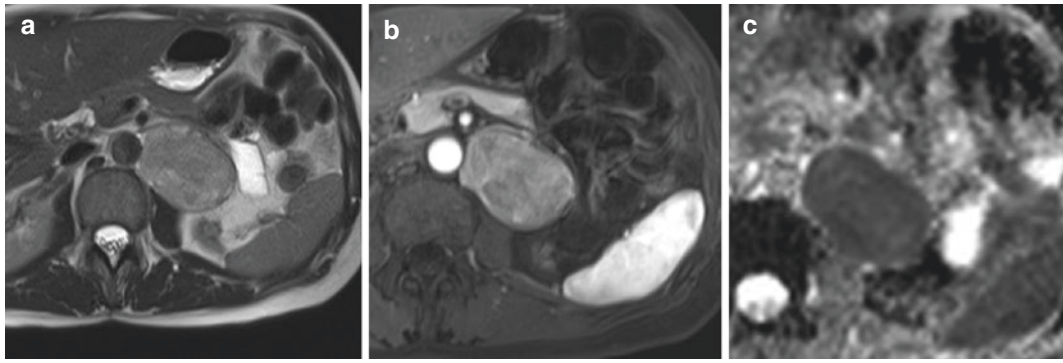

Fig. 18.46 Retroperitoneal angiomyolipoma in a 45-year-old patient. (**a**) Axial T2-weighted MR image. (**b**) Axial T1-weighted MR image after gadolinium contrast injection. (**c**) ADC map. The well-demarcated lesion was iso- to hyperintense on T2-weighted images (**a**), while showing a strong enhancement (**b**) and a marked diffusion restriction (**c**)

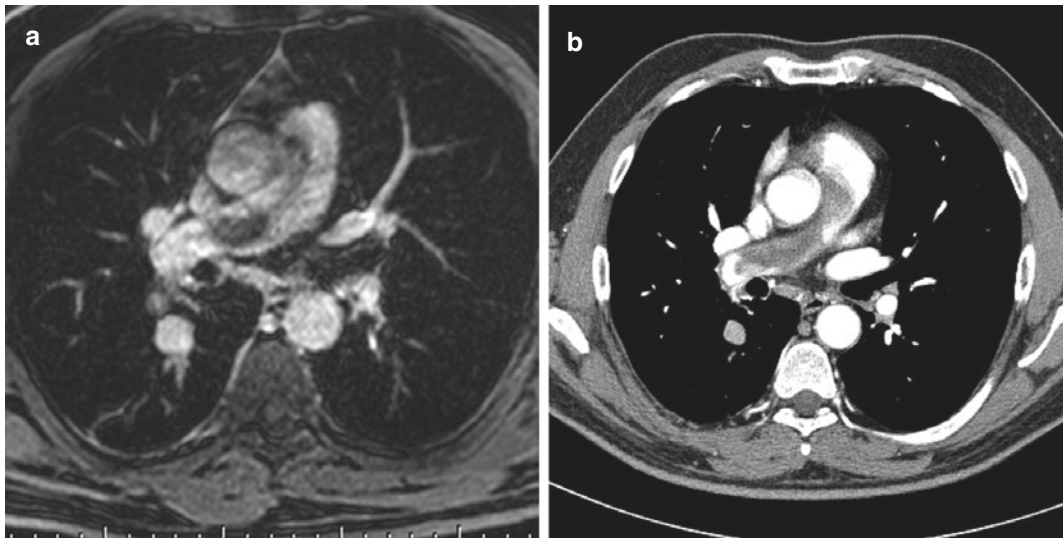

Fig. 18.47 Thoracic intimal sarcoma. (**a**) Axial T2-weighted MR image after gadolinium contrast injection and (**b**) axial CT image after contrast-agent injection. Intimal sarcomas typically present as enhancing filling defects in MRI or CT (**a**, **b**), which can mimic thromboembolic disease especially when the wall-adherent material does not show enhancement or extraluminal growth (Courtesy of Prof. Dr. med. Claus Peter Heußel, Heidelberg)

tations are well demarcated and encapsulated and tend to show cystic changes [109].

CCMMT has only once been reported in the soft tissues of the thigh, showing a benign appearance corresponding to their clinical behavior. Detailed MRI characteristics have not been described until the present [57].

To sum up, imaging of soft tissue PEComa is not specific, while lesions tend to show a high fat fraction, hypervascularization, and strong enhancement.

18.6.11 Intimal Sarcoma

18.6.11.1 Definition

Intimal sarcomas are rare malignant tumors of mesenchymal origin and arise mainly in large

arteries of the pulmonary or systemic circulation leading to vessel obstruction and embolic tumor dissemination. Histologically, they consist of cells of fibroblastic and myofibroblastic differentiation, spindle cells, and myxoid areas [75]. An amplification of the 12q13–14 region as possible genetic marker has been described [18].

18.6.11.2 Incidence and Clinical Behavior

Intimal sarcomas mostly affect adults in their fifth decade. Pulmonary intimal sarcomas which are slightly more frequent in females are predominantly located in the pulmonary trunk causing pulmonary embolic disease [22].

Aortic intimal sarcomas are mostly found between the celiac artery and the iliac bifurcation causing abdominal angina and intermittent claudication of the lower extremities, as well as malignant hypertension or aneurysm forming.

Intimal sarcomas have a very poor prognosis with a mean survival times around 1 year depending on treatment and location/metastatic spread [139].

18.6.11.3 Imaging

While radiographs are usually not diagnostic, CT may show polypoid intraluminal soft tissue masses typical for intimal sarcomas (Fig. 18.47). If not polypoid and no other signs of malignancy are present, the non-enhancing defect may be not distinguishable from thrombus or embolus material. Contrast-enhanced MRI can be more specific by detecting the tumoral vascularization which is not seen in thrombus formations [131].

Key Points

1. When multiple intramuscular myxomas are encountered, one should look for associated fibrous dysplasia to exclude Mazabraud's syndrome.
2. An amyloid tumor has a low signal intensity on all pulse sequences.
3. The lack of high fat content is a key feature in differentiating aggressive angiomyxoma, a slowly growing neoplasm occurring in the pelvic soft tissue in women, from myxoid liposarcoma.
4. Hemosiderotic fibrolipomatous tumor consists of adipocytes, fibrous tissue, and hemosiderin pigments and can therefore show a characteristic blooming in susceptibility-weighted imaging.
5. Phosphaturic mesenchymal tumor causes systemic phosphate depletion and consequently an oncogenic osteomalacia. Whole-body MRI and scintigraphy are the diagnostic tools of choice for finding the sometimes very small lesions.
6. Synovial sarcoma is a misnomer, as it is not derived from true synovial cells.
7. The presence of a triple signal on T2-weighted images together with high signal intensity areas on T1-weighted images and calcifications on CT scan or radiographs are suggestive for a synovial sarcoma.
8. A clear cell sarcoma should be considered in the differential diagnosis, when a well-defined extremity lesion with a relatively high signal intensity on T1-weighted images and strong enhancement pattern is seen in a young patient.
9. Peripheral primitive neuroectodermal tumors and extraskeletal Ewing's sarcoma are small blue cell tumors, sharing phenotypical and genotypical characteristics.

   They are aggressive and poorly differentiated neoplasms, occurring mainly in children and young adults.
10. Askin's tumor is a pPNET with preferential location at the thoracopulmonary region.
11. Imaging features of both pPNET and Ewing's sarcoma are hard to differentiate from other malignant soft tissue tumors; they frequently contain areas of cystic degeneration, necrosis, and hemorrhage.
12. Contrast-enhanced MRI can help to distinguish thromboembolic disease from intimal sarcoma by detecting the tumoral vascularization.

References

1. Abbott GF, Rosado-de-Christenson ML, Frazier AA, Franks TJ, Pugatch RD, Galvin JR (2005) From the archives of the AFIP: lymphangioleiomyomatosis: radiologic-pathologic correlation. Radiographics 25:803–828. doi:10.1148/rg.253055006
2. Abdullah A, Patel Y, Lewis TJ, Elsamaloty H, Strobel S (2009) Extrarenal malignant rhabdoid tumors: radiologic findings with histopathologic correlation. Cancer Imaging 10:97–101. doi:10.1102/1470-7330.2010.0010
3. Ali S, Leng B, Reinus WR, Khilko N, Khurana JS (2013) Parachordoma/myoepithelioma. Skeletal Radiol 42:431–457–8. doi:10.1007/s00256-012-1413-6
4. Allam K, Sze G (1994) MR of primary extraosseous Ewing sarcoma. AJNR Am J Neuroradiol 15:305–307
5. Allen PW (2000) Myxoma is not a single entity: a review of the concept of myxoma. Ann Diagn Pathol 4:99–123. doi:10.1053/adpa.2000.0099
6. Alobid I, Bernal-Sprekelsen M, Alos L, Benitez P, Traserra J, Mullol J (2003) Peripheral primitive neuroectodermal tumour of the left maxillary sinus. Acta Otolaryngol 123:776–778. doi:10.1080/00016480310001213
7. Ambros IM, Ambros PF, Strehl S, Kovar H, Gadner H (1991) MIC2 is a specific marker for Ewing's sarcoma and peripheral primitive neuroectodermal tumors. Evidence for a common histogenesis of Ewing's sarcoma and peripheral primitive neuroectodermal tumors from MIC2 expression and specific chromosome aberration. Cancer 67:1886–1893
8. Arora VC, Price AP, Fleming S, Sohn MJ, Magnan H, LaQuaglia MP, Abramson S (2013) Characteristic imaging features of desmoplastic small round cell tumour. Pediatr Radiol 43:93–102. doi:10.1007/s00247-012-2485-0
9. Ashby-Richardson H, Rogers GS, Stadecker MJ (2011) Superficial acral fibromyxoma: an overview. Arch Pathol Lab Med 135:1064–1066. doi:10.5858/2009-0684-RSR1
10. Askin FB, Rosai J, Sibley RK, Dehner LP, McAlister WH (1979) Malignant small cell tumor of the thoracopulmonary region in childhood: a distinctive clinicopathologic entity of uncertain histogenesis. Cancer 43:2438–2451
11. Asvall JE, Hoeg K, Kleppe K, Prydz PE (1969) Alveolar soft part sarcoma. Clin Radiol 20:426–432
12. Bakri A, Shinagare AB, Krajewski KM, Howard SA, Jagannathan JP, Hornick JL, Ramaiya NH (2012) Synovial sarcoma: imaging features of common and uncommon primary sites, metastatic patterns, and treatment response. Am J Roentgenol 199:208–215. doi:10.2214/AJR.11.8039
13. Benedikt RA, Jelinek JS, Kransdorf MJ, Moser RP, Berrey BH (1994) MR imaging of soft-tissue masses: role of gadopentetate dimeglumine. J Magn Reson Imaging 4:485–490
14. Biegel JA (2006) Molecular genetics of atypical teratoid/rhabdoid tumors. Neurosurg Focus 20:2–7
15. Biegel JA, Conard K, Brooks JJ (1993) Translocation (11;22)(p13;q12): primary change in intra-abdominal desmoplastic small round cell tumor. Genes Chromosom Cancer 7:119–121. doi:10.1002/gcc.2870070210
16. Bindra J, Doherty M, Hunter JC (2012) Superficial acral fibromyxoma. Radiology Case Reports 7:751. doi:10.2484/rcr.v7i3.751
17. Blacksin MF, Siegel JR, Benevenia J, Aisner SC (1997) Synovial sarcoma: frequency of nonaggressive MR characteristics. J Comput Assist Tomogr 21:785–789
18. Bode-Lesniewska B, Zhao J, Speel EJM, Biraima AM, Turina M, Komminoth P, Heitz PU (2001) Gains of 12q13-14 and overexpression of mdm2 are frequent findings in intimal sarcomas of the pulmonary artery. Virchows Arch 438:57–65. doi:10.1007/s004280000313
19. Brady MS, Perino G, Tallini G, Russo P, Woodruff JM (1996) Malignant mesenchymoma. Cancer 77:467–473. doi:10.1002/(SICI)1097-0142(19960201)77:3<467::AID-CNCR7>3.0.CO;2-H
20. Brinkhuis M, Wijnaendts LCD, van der Linden JC, Baak JPA, Meijer CJLM, van Unnik AJM, Voûte PA (1995) Peripheral primitive neuroectodermal tumour and extra-osseous Ewing's sarcoma; a histological, immunohistochemical and DNA flow cytometric study. Virchows Arch 425:611–616. doi:10.1007/BF00199351
21. Burge HJ, Novotny DB, Schiebler ML, Delany DJ, McCartney WH (1990) MRI of Askin's tumor. Case report at 1.5 T. Chest 97:1252–1254. doi:10.1378/chest.97.5.1252
22. Burke AP, Virmani R (1993) Sarcomas of the great vessels. A clinicopathologic study. Cancer 71:1761–1773. doi:10.1002/1097-0142(19930301)71:5<1761::AID-CNCR2820710510>3.0.CO;2-7
23. Carrillo R, El-Naggar AK, Rodriguez-Peralto JL, Batsakis JG (1992) Synovial sarcoma of the tongue: case report and review of the literature. J Oral Maxillofac Surg 50:904–906. doi:10.1016/0278-2391(92)90288-B
24. Castillo M, Lee YY, Yamasaki S (1992) Infratemporal alveolar soft part sarcoma: CT, MRI and angiographic findings. Neuroradiology 34:367–369
25. Chase DR, Enzinger FM (1985) Epithelioid sarcoma. Diagnosis, prognostic indicators, and treatment. Am J Surg Pathol 9:241–263
26. Christopherson WM, Foote FW, Stewart FW (1952) Alveolar soft-part sarcomas; structurally characteristic tumors of uncertain histogenesis. Cancer 5:100–111
27. Cibas ES, Goss GA, Kulke MH, Demetri GD, Fletcher CDM (2001) Malignant epithelioid angiomyolipoma ("Sarcoma Ex Angiomyolipoma") of the kidney: a case report and review of the literature. Am J Surg Pathol 25:121
28. Clabeaux J, Hojnowski L, Valente A, Damron TA (2008) Case report. Clin Orthop Relat Res 466:1251–1256. doi:10.1007/s11999-008-0125-7

29. Cohen MA, Mendelsohn DB (1990) CT and MR imaging of myxofibroma of the jaws. J Comput Assist Tomogr 14:281
30. Contesso G, Llombart-Bosch A, Terrier P, Peydro-Olaya A, Henry-Amar M, Oberlin O, Habrand JL, Dubousset J, Tursz T, Spielmann M (1992) Does malignant small round cell tumor of the thoracopulmonary region (Askin tumor) constitute a clinicopathologic entity? An analysis of 30 cases with immunohistochemical and electron-microscopic support treated at the Institute Gustave Roussy. Cancer 69:1012–1020
31. Crew AJ, Clark J, Fisher C, Gill S, Grimer R, Chand A, Shipley J, Gusterson BA, Cooper CS (1995) Fusion of SYT to two genes, SSX1 and SSX2, encoding proteins with homology to the Kruppel-associated box in human synovial sarcoma. EMBO J 14:2333–2340
32. Czekalla R, Fuchs M, Stölzle A, Nerlich A, Poremba C, Schaefer K-L, Weirich G, Höfler H, Schneller F, Peschel C, Siewert JR, Schepp W (2004) Peripheral primitive neuroectodermal tumor of the stomach in a 14-year-old boy: a case report. Eur J Gastroenterol Hepatol 16:1391–1400
33. Dabska M (1977) Parachordoma: a new clinicopathologic entity. Cancer 40:1586–1592
34. Daly BD, Cheung H, Gaines PA, Bradley MJ, Metreweli C (1992) Imaging of alveolar soft part sarcoma. Clin Radiol 46:253–256. doi:10.1016/S0009-9260(05)80165-5
35. Dardick I (1995) Myoepithelioma: definitions and diagnostic criteria. Ultrastruct Pathol 19:335–345. doi:10.3109/01913129509021906
36. De Beuckeleer LH, De Schepper AM, Vandevenne JE (2000) MR imaging of clear cell sarcoma (malignant melanoma of the soft parts): a multicenter correlative MRI-pathology study of 21 cases and literature review. Skeletal Radiol 29:187–195
37. De Comas AM, Deavers MT, Raymond AK, Madewell JE, Lewis VO (2011) Intraneural parachordoma of the arm with regional metastases. Skeletal Radiol 40:943–946. doi:10.1007/s00256-011-1151-1
38. Dehner LP (1986) Peripheral and central primitive neuroectodermal tumors. A nosologic concept seeking a consensus. Arch Pathol Lab Med 110: 997–1005
39. Dehner LP (1993) Primitive neuroectodermal tumor and Ewing's sarcoma. Am J Surg Pathol 17:1
40. Desy NM, Bernstein M, Nahal A, Aziz M, Kenan S (2012) Primary perivascular epithelioid cell neoplasm (PEComa) of bone: report of two cases and review of the literature. Skeletal Radiol 41:1469–1474
41. Drilon AD, Popat S, Bhuchar G, D'Adamo DR, Keohan ML, Fisher C, Antonescu CR, Singer S, Brennan MF, Judson I, Maki RG (2008) Extraskeletal myxoid chondrosarcoma: a retrospective review from 2 referral centers emphasizing long-term outcomes with surgery and chemotherapy. Cancer 113:3364–3371. doi:10.1002/cncr.23978
42. Ekelund L, Herrlin K, Rydholm A (1982) Computed tomography of intramuscular myxoma. Skeletal Radiol 9:14–16
43. Enzinger FM (1965) Clear-cell sarcoma of tendons and aponeuroses – an analysis of 21 cases. Cancer 18:1163–1174
44. Enzinger FM, Shiraki M (1972) Extraskeletal myxoid chondrosarcoma. An analysis of 34 cases. Hum Pathol 3:421–435
45. Enzinger FM, Weiss SW (1995) Synovial sarcoma. In: Enzinger FM, Weiss SW (eds) Soft tissue tumors, 3rd edn. Mosby, St. Louis, pp 735–786
46. Enzinger FM, Weiss SW (1995) Malignant soft tissue tumors of uncertain type. In: Enzinger FM, Weiss SW (eds) Soft tissue tumors, 3rd edn. Mosby, St Louis, pp 1067–1093
47. Enzinger FM, Weiss SW (1995) Primitive neuroectodermal tumors and related lesions. In: Enzinger FM, Weiss SW (eds) Soft tissue tumors, 3rd edn. Mosby, St Louis, pp 929–964
48. Farmakis SG, Siegel MJ (2015) Phosphaturic mesenchymal tumor of the tibia with oncogenic osteomalacia in a teenager. Pediatr Radiol 45:1423–1426. doi:10.1007/s00247-015-3301-4
49. Faubert C, Inniger R (1991) MRI and pathological findings in two cases of Askin tumors. Neuroradiology 33:277–281. doi:10.1007/BF00588237
50. Ferraz MP, Watanabe T, Sado HN, Ono CR, Buchpiguel CA, Correa PHS, Martin RM (2013) Concordance between whole body scintigraphy 111In-Octreotide and 99mTc-Sestamibi uptake in the detection of four tumor-induced osteomalacia cases. J Clin Endocrinol Metab jc. 2013–3563. doi:10.1210/jc.2013-3563
51. Fetsch JF, Laskin WB, Michal M, Remotti F, Heffner D, Ellis G, Furlong M, Miettinen M (2004) Ectopic hamartomatous thymoma: a clinicopathologic and immunohistochemical analysis of 21 cases with data supporting reclassification as a branchial anlage mixed tumor. Am J Surg Pathol 28:1360
52. Fetsch JF, Laskin WB, Miettinen M (2001) Superficial acral fibromyxoma: a clinicopathologic and immunohistochemical analysis of 37 cases of a distinctive soft tissue tumor with a predilection for the fingers and toes. Hum Pathol 32:704–714. doi:10.1053/hupa.2001.25903
53. Fisher C, Miettinen M (1997) Parachordoma: a clinicopathologic and immunohistochemical study of four cases of an unusual soft tissue neoplasm. Ann Diagn Pathol 1:3–10
54. Fletcher CDM, Unni KK, Mertens F (2012) WHO classification of tumours of soft tissue and bone. IARC Press, Lyon
55. Folpe AL, Agoff SN, Willis J (1999) Parachordoma is immunohistochemically and cytogenetically distinct from axial chordoma and extraskeletal myxoid chondrosarcoma. Am J Surg Pathol 23:1059
56. Folpe AL, Goodman ZD, Ishak KG, Paulino AF, Taboada EM, Meehan SA, Weiss SW (2000) Clear

cell myomelanocytic tumor of the falciform ligament/ligamentum teres: a novel member of the perivascular epithelioid clear cell family of tumors with a predilection for children and young adults. Am J Surg Pathol 24:1239–1246
57. Folpe AL, McKenney JK, Li Z, Smith SJ, Weiss SW (2002) Clear cell myomelanocytic tumor of the thigh: report of a unique case. Am J Surg Pathol 26:809–812
58. Folpe AL, Weiss SW (2003) Ossifying fibromyxoid tumor of soft parts: a clinicopathologic study of 70 cases With emphasis on atypical and malignant variants. Am J Surg Pathol 27:421
59. Fujiwara M, Yuba Y, Wada A, Ozawa T, Tanaka T (2014) Pleomorphic hyalinizing angiectatic tumor of soft parts: report of a case and review of the literature. J Dermatol 31:419–423. doi:10.1111/j.1346-8138.2004.tb00696.x
60. Gaffey MJ, Mills SE, Askin FB, Ross GW, Sale GE, Kulander BG, Visscher DW, Yousem SA, Colby TV (1990) Clear cell tumor of the lung. A clinicopathologic, immunohistochemical, and ultrastructural study of eight cases. Am J Surg Pathol 14:248–259
61. Garcés-Iñigo EF, Leung R, Sebire NJ, McHugh K (2009) Extrarenal rhabdoid tumours outside the central nervous system in infancy. Pediatr Radiol 39:817–822. doi:10.1007/s00247-009-1288-4
62. Gerald WL, Miller HK, Battifora H, Miettinen M, Silva EG, Rosai J (1991) Intra-abdominal desmoplastic small round-cell tumor: report of 19 cases of a distinctive type of high-grade polyphenotypic malignancy affecting young individuals. Am J Surg Pathol 15:499
63. Glass-Royal MC, Nelson MC, Albert F, Lack EE, Bogumill GP (1989) Case report 557. Skeletal Radiol 18:392–398. doi:10.1007/BF00361433
64. Gonzalez-Crussi F, Wolfson SL, Misugi K, Nakajima T (1984) Peripheral neuroectodermal tumors of the chest wall in childhood. Cancer 54:2519–2527
65. Granter SR, Weilbaecher KN, Quigley C, Fletcher CD, Fisher DE (2001) Clear cell sarcoma shows immunoreactivity for microphthalmia transcription factor: further evidence for melanocytic differentiation. Mod Pathol 14:6–9. doi:10.1038/modpathol.3880249
66. Hanna S, Kaste S, Jenkins J, Hewan-Lowe K (2002) Epithelioid sarcoma: clinical, MR imaging and pathologic findings. Skeletal Radiol 31:400–412
67. Harish S, Polson A, Morris P, Malata C, Griffiths M, Bearcroft PWP (2006) Giant atypical ossifying fibromyxoid tumour of the calf. Skeletal Radiol 35:248–253. doi:10.1007/s00256-005-0014-z
68. Hashimoto H (1995) Incidence of soft tissue sarcomas in adults. In: Schmidt D, Harms D (eds) Soft tissue tumors. Springer, Berlin, pp 1–16
69. El Hayek M, Trad O, Islam S (2004) Congenital peripheral primitive neuroectodermal tumor refractory to treatment. J Pediatr Hematol Oncol 26:770–772
70. Hermann G, Abdelwahab IF, Klein MJ, Kenan S, Lewis MM (1993) Case report 796. Alveolar soft part sarcoma. Skeletal Radiol 22:386–389
71. Hermann G, Abdelwahab IF, Miller TT, Klein MJ, Lewis MM (1992) Tumour and tumour-like conditions of the soft tissue: magnetic resonance imaging features differentiating benign from malignant masses. BJR 65:14–20. doi:10.1259/0007-1285-65-769-14
72. Hodler J, YU SJ, Steinert HC, Resnick D (1995) MR imaging versus alternative imaging techniques. Magn Reson Imaging Clin N Am 3:591–608
73. Horiguchi Y, Nakashima J, Ishii T, Hata J, Tazaki H (1994) Primitive neuroectodermal tumor of the retroperitoneal cavity. Urology 44:127–129
74. Hornick JL, Fletcher C (2003) Myoepithelial tumors of soft tissue – a clinicopathologic and immunohistochemical study of 101 cases with evaluation of prognostic parameters. Am J Surg Pathol 27:1183–1196
75. Hottenrott G, Mentzel T, Peters A, Schröder A, Katenkamp D (1999) Intravascular ("intimal") epithelioid angiosarcoma: clinicopathological and immunohistochemical analysis of three cases. Virchows Arch 435:473–478
76. Huang C-C, Cheng S-M (2012) Clinical and radiological presentations of pelvic parachordoma. Rare Tumors 4:13–15. doi:10.4081/rt.2012.e5
77. Ibarburen C, Haberman JJ, Zerhouni EA (1996) Peripheral primitive neuroectodermal tumors. CT and MRI evaluation. Eur J Radiol 21:225–232. doi:10.1016/0720-048X(95)00731-5
78. Ieremia E, Robson A (2014) Cutaneous PEComa: a rare entity to consider in an unusual site. Am J Dermatopathol 36:e198–e201. doi:10.1097/DAD.0000000000000041
79. Iwasko N, Steinbach L, Disler D, Pathria M, Hottya G (2002) Imaging findings in Mazabraud's syndrome: seven new cases. Skeletal Radiol 31:81–87
80. Jo VY (2015) Myoepithelial tumors: an update. Surg Pathol Clin 8:445–466. doi:10.1016/j.path.2015.05.005
81. Jones BC, Sundaram M, Kransdorf MJ (1993) Synovial sarcoma: MR imaging findings in 34 patients. AJR Am J Roentgenol 161:827–830. doi:10.2214/ajr.161.4.8396848
82. Justin Wong SB, Wee A, Puhaindran ME, Pang B, Lee VKM (2015) Angiomatoid fibrous histiocytoma with prominent myxoid stroma: a case report and review of the literature. Am J Dermatopathol 37:623–631. doi:10.1097/DAD.0000000000000263
83. Kaffe I, Naor H, Buchner A (1997) Clinical and radiological features of odontogenic myxoma of the jaws. Dentomaxillofacial Radiol 26:299–303. doi:10.1038/sj.dmfr.4600261
84. Kalil RK (2015) Phosphaturic mesenchymal tumor. In: Tumors and tumor-like lesions of bone. Springer London, London, pp 589–597
85. Kapoor N, Shinagare AB, Jagannathan JP, Shah SH, Krajewski KM, Hornick JL, Ramaiya NH (2014) Clinical and radiologic features of extraskeletal myx-

oid chondrosarcoma including initial presentation, local recurrence, and metastases. Radiol Oncol 48:235–242. doi:10.2478/raon-2014-0005
86. Kheir E, Stephen L, Nortje C, van Rensburg LJ, Titinchi F (2013) The imaging characteristics of odontogenic myxoma and a comparison of three different imaging modalities. Oral Surg Oral Med Oral Pathol Oral Radiol 116:492–502. doi:10.1016/j.oooo.2013.05.018
87. Kilpatrick SE, Ward WG, Mozes M, Miettinen M, Fukunaga M, Fletcher C (1995) Atypical and malignant variants of ossifying fibromyxoid tumor – clinicopathological analysis of 6 cases. Am J Surg Pathol 19:1039–1046
88. Kitagawa Y, Ishihara Y, Hayashi M, Kim Y, Fujii N, Ito H (2011) Mazabraud syndrome associated with McCune–Albright syndrome. J Orthop Sci 16:129–132. doi:10.1007/s00776-010-0004-4
89. Koch M, Freundl AJ, Agaimy A, Kiesewetter F, Künzel J, Cicha I, Alexiou C (2015) Atypical fibroxanthoma – histological diagnosis, immunohistochemical markers and concepts of therapy. Anticancer Res 35:5717–5735
90. Kransdorf MJ (1995) Malignant soft-tissue tumors in a large referral population – distribution of diagnoses by age, sex, and location. AJR Am J Roentgenol 164:129–134. doi:10.2214/ajr.164.1.7998525
91. Kransdorf MJ, Moser RPJ, Jelinek JS, Weiss SW, Buetow PC, Berrey BH (1989) Intramuscular Myxoma: MR features. J Comput Assist Tomogr 13:836
92. Kuang P (2013) CT findings of pleomorphic hyalinizing angiectatic tumor (PHAT) of soft parts of the neck. Jpn J Radiol 31:204–207. doi:10.1007/s11604-012-0157-5
93. Kurashima K, Muramoto S, Ohta Y, Fujimura M, Matsuda T (1994) Peripheral neuroectodermal tumor presenting pleural effusion. Intern Med 33:783–785
94. L'Hostis H, Deminiere C, Ferriere J-M, Coindre J-M (1999) Renal angiomyolipoma: a clinicopathologic, immunohistochemical, and follow-up study of 46 cases. Am J Surg Pathol 23:1011
95. Lao IW, Yu L, Wang J (2015) Malignant perivascular epithelioid cell tumor (PEComa) of the femur: a case report and literature review. Diagn Pathol 10:54. doi:10.1186/s13000-015-0292-2
96. Lee S, Joo KB, Park C-K, Kim T-S, Bae J (2013) A case of atypical fibroxanthoma of subungual type: ultrasound and magnetic resonance imaging findings. Clin Imaging 37:155–158. doi:10.1016/j.clinimag.2012.01.035
97. Li C-S, Chan WP, Chen W-T, Chang C-P, Shih L-S, Chen R-C, Tu H-Y (2004) MRI of angiomatoid fibrous histiocytoma. Skeletal Radiol 33:604–608. doi:10.1007/s00256-004-0769-7
98. Lieberman PH, Brennan MF, Kimmel M, Erlandson RA, Garin-Chesa P, Flehinger BY (1989) Alveolar soft-part sarcoma. A clinico-pathologic study of half a century. Cancer 63:1–13
99. Limdiwala P, Shah J (2015) Odontogenic myxoma of maxilla: a review discussion with two case reports. Contemp Clin Dent 6:131–136. doi:10.4103/0976-237X.149310
100. Llauger J, Perez C, Coscojuela P, Palmer J, Puig J (1990) Aggressive angiomyxoma of pelvic soft tissue: CT appearance. Urol Radiol 12:25–26
101. Lockyer MG, Rosen DG (2015) Extraskeletal myxoid chondrosarcoma presenting as a plantar fibroma: case report and review of the literature. Anticancer Res 35:6171–6174
102. Lois JF, Fischer HJ, Mirra JM, Gomes AS (1986) Angiography of histopathologic variants of synovial sarcoma. Acta Radiol Diagn (Stockh) 27:449–454
103. Lopez-Ben R, Siegal GP, Pitt MJ, Jaffe KA (1999) Osteosarcoma in a patient with McCune-Albright syndrome and Mazabraud's syndrome. Skeletal Radiol 28:522–526. doi:10.1007/s002560050556
104. Lorigan JG, O'Keeffe FN, Evans HL, Wallace S (1989) The radiologic manifestations of alveolar soft-part sarcoma. AJR Am J Roentgenol 153:335–339. doi:10.2214/ajr.153.2.335
105. López L, Vélez R (2016) Atypical fibroxanthoma. Arch Pathol Lab Med 140:376–379. doi:10.5858/arpa.2014-0495-RS
106. Luna A, Martinez S, Bossen E (2005) Magnetic resonance imaging of intramuscular myxoma with histological comparison and a review of the literature. Skeletal Radiol 34:19–28
107. Marzano L, Failoni S, Gallazzi M, Garbagna P (2004) The role of diagnostic imaging in synovial sarcoma. Our experience. Radiol Med 107:533–540
108. Massengill A, Seeger L, Yao L, Mirra J, Eckardt J (1995) Malignant mesenchymoma of the thigh. Skeletal Radiol 24:301–304. doi:10.1007/BF00198421
109. Matsui K, Tatsuguchi A, Valencia J, Yu ZX, Bechtle J, Beasley MB, Avila N, Travis WD, Moss J, Ferrans VJ (2000) Extrapulmonary lymphangioleiomyomatosis (LAM): clinicopathologic features in 22 cases. Hum Pathol 31:1242–1248
110. Matsumoto K, Yamamoto T (2002) Pleomorphic hyalinizing angiectatic tumor of soft parts: a case report and literature review. Pathol Int 52:664–668
111. Meis-Kindblom JM, Bergh P, Gunterberg B, Kindblom LG (1999) Extraskeletal myxoid chondrosarcoma: a reappraisal of its morphologic spectrum and prognostic factors based on 117 cases. Am J Surg Pathol 23:636
112. Michal M, Miettinen M (1999) Myoepitheliomas of the skin and soft tissues. Virchows Arch 434:393–400. doi:10.1007/s004280050358
113. Miguez Gonzalez J, Dominguez Oronoz R, Lozano Arranz P, Calaf Forn F, Barrios Sanchez P, Garcia Jimenez A (2015) Aggressive angiomyxoma: imaging findings in 3 cases with clinicopathological correlation and review of the literature. J Comput Assist Tomogr 39:914–921. doi:10.1097/RCT.0000000000000305
114. Morton MJ, Berquist TH, McLeod RA, Unni KK, Sim FH (1991) MR imaging of synovial sarcoma. AJR Am J Roentgenol 156:337–340. doi:10.2214/ajr.156.2.1846054

115. Murphey M, Kransdorf M, Smith S (1999) Imaging of soft tissue neoplasms in the adult: malignant tumors. Semin Musculoskelet Radiol 3:39–58. doi:10.1055/s-2008-1080050
116. Murphey MD, McRae GA, Fanburg-Smith JC, Temple HT, Levine AM, Aboulafia AJ (2002) Imaging of soft-tissue myxoma with emphasis on CT and MR and comparison of radiologic and pathologic findings. Radiology 225:215–224. doi:10.1148/radiol.2251011627
117. Murphey MD, Smith WS, Smith SE, Kransdorf MJ, Temple HT (1999) From the archives of the AFIP. Radiographics 19:1253–1280. doi:10.1148/radiographics.19.5.g99se101253
118. Nakanishi K, Sakai M, Tanaka H, Tsuboi H, Hashimoto J, Hashimoto N, Tomiyama N (2013) Whole-body MR imaging in detecting phosphaturic mesenchymal tumor (PMT) in tumor-induced hypophosphatemic osteomalacia. Magn Reson Med Sci 12:47–52
119. Nash A, Stout AP (1961) Malignant mesenchymomas in children. Cancer 14:524
120. Nielsen GP, O'Connell JX, Rosenberg AE (1998) Intramuscular myxoma: a clinicopathologic study of 51 cases with emphasis on hypercellular and hypervascular variants. Am J Surg Pathol 22:1222–1227
121. O'Driscoll D, Athanasian E, Hameed M, Hwang S (2015) Radiological imaging features and clinicopathological correlation of hemosiderotic fibrolipomatous tumor: experience in a single tertiary cancer center. Skeletal Radiol 44(5):641–648
122. O'Keeffe F, Lorigan JG, Wallace S (1990) Radiological features of extraskeletal Ewing sarcoma. BJR 63:456–460. doi:10.1259/0007-1285-63-750-456
123. O'SULLIVAN PJ, HARRIS AC, Munk PL (2008) Radiological features of synovial cell sarcoma. BJR 81:346–356. doi:10.1259/bjr/28335824
124. Oda Y, Tsuneyoshi M (2006) Extrarenal rhabdoid tumors of soft tissue: clinicopathological and molecular genetic review and distinction from other soft-tissue sarcomas with rhabdoid features. Pathol Int 56:287–295
125. Ogose A, Otsuka H, Morita T, Kobayashi H, Hirata Y (1998) Ossifying fibromyxoid tumor resembling parosteal osteosarcoma. Skeletal Radiol 27:578–580
126. Okamoto S, Hisaoka M, Meis-Kindblom JM (2002) Juxta-articular myxoma and intramuscular myxoma are two distinct entities. Virchows Arch 440:12–15
127. Peres E, Mattoo TK, Poulik J, Warrier I (2005) Primitive neuroectodermal tumor (PNET) of the uterus in a renal allograft patient: a case report. Pediatr Blood Cancer 44:283–285. doi:10.1002/pbc.20237
128. Peterson KK, Renfrew DL, Feddersen RM, Buckwalter JA, el-Khoury GY (1991) Magnetic resonance imaging of myxoid containing tumors. Skeletal Radiol 20:245–250
129. Prat J, Woodruff JM, Marcove RC (1978) Epithelioid sarcoma: an analysis of 22 cases indicating the prognostic significance of vascular invasion and regional lymph node metastasis. Cancer 41:1472–1487
130. Radin DR, Ralls PW, Boswell WD, Lundell C, Halls JM (1984) Alveolar soft part sarcoma: CT findings. J Comput Assist Tomogr 8:344–345
131. Rafal RB, Nichols JN, Markisz JA (1995) Pulmonary-artery sarcoma – diagnosis and postoperative follow-up with gadolinium-diethylenetriamine pentaacetic acid-enhanced magnetic-resonance-imaging. Mayo Clin Proc 70:173–176. doi:10.1016/S0025-6196(11)64285-7
132. Rangheard AS, Vanel D, Viala J, Schwaab G, Casiraghi O, Sigal R (2001) Synovial sarcomas of the head and neck: CT and MR imaging findings of eight patients. AJNR Am J Neuroradiol 22:851–857
133. Reyes J, Mexia MA, Tapia DQ, Aramburu JA (1997) Extensively calcified synovial sarcoma. Skeletal Radiol 26:671–673
134. Saifuddin A, Robertson RJH, Smith SEW (1991) The radiology of Askin tumours. Clin Radiol 43:19–23. doi:10.1016/S0009-9260(05)80348-4
135. Sakurai H, Kaji M, Mukai K, Suemasu K (2010) Ectopic hamartomatous thymoma—a truly rare neoplasm: report of a case. Surg Today 40:146–149
136. Schaffler G, Raith J, Ranner G, Weybora W, Jeserschek R (1997) Radiographic appearance of an ossifying fibromyxoid tumor of soft parts. Skeletal Radiol 26:615–618. doi:10.1007/s002560050296
137. Schmidt D, Herrmann C, Jürgens H, Harms D (1991) Malignant peripheral neuroectodermal tumor and its necessary distinction from Ewing's Sarcoma. A report from the kiel pediatric tumor registry. Cancer 68:2251–2259. doi:10.1002/1097-0142(19911115)68:10<2251::AID-CNCR2820681025>3.0.CO;2-X
138. Schnarkowski P, Peterfy CG, Johnston JO, Weidner N (1996) Clear cell sarcoma mimicking peripheral nerve sheath tumor. Skeletal Radiol 25:197–200
139. Seelig MH, Klingler PJ, Oldenburg WA, Blackshear JL (1998) Angiosarcoma of the aorta: report of a case and review of the literature. J Vasc Surg 28:732–737
140. Shaw GR, Lais CJ (1993) Fatal intravascular synovial sarcoma in a 31-year-old woman. Hum Pathol 24:809–810
141. Silver WP, Harrelson JM, Scully SP (2002) Intramuscular Myxoma: a clinicopathologic study of 17 patients. Clin Orthop Relat Res 403:191
142. Smith MEF, Fisher C, Weiss SW (1996) Pleomorphic hyalinizing angiectatic tumor of soft parts: a low-grade neoplasm resembling neurilemoma. Am J Surg Pathol 20:21
143. Solomon DA, Antonescu CR, Link TM, O'Donnell RJ, Folpe AL, Horvai AE (2013) Hemosiderotic fibrolipomatous tumor, not an entirely benign entity. Am J Surg Pathol 37:1627–1630. doi:10.1097/PAS.0b013e31829ff078
144. Spielmann A, Janzen DL, O'Connell JX, Munk PL (1997) Intraneural synovial sarcoma. Skeletal Radiol 26:677–681

145. Stefanko J, Turnbull AD, Helson L, Lieberman P, Martini N (1988) Primitive neuroectodermal tumors of the chest wall. J Surg Oncol 37:33–37. doi:10.1002/jso.2930370110
146. Subhawong TK, Subhawong AP, Montgomery EA, Fayad LM (2012) Pleomorphic hyalinizing angiectatic tumor: imaging findings. Skeletal Radiol 41:1621–1626. doi:10.1007/s00256-012-1443-0
147. Sundaram M, McDonald DJ, MERENDA G (1989) Intramuscular Myxoma – a rare but important association with fibrous dysplasia of bone. AJR Am J Roentgenol 153:107–108. doi:10.2214/ajr.153.1.107
148. Surov A, Weber M-A (2014) Malignant and benign lesions of the skeletal musculature. Semin Ultrasound CT MR 35:290–307. doi:10.1053/j.sult.2013.12.004
149. Tan Y, Zhang H, Xiao E-H (2013) Perivascular epithelioid cell tumour: dynamic CT, MRI and clinicopathological characteristics – analysis of 32 cases and review of the literature. Clin Radiol 68:555–561. doi:10.1016/j.crad.2012.10.021
150. Tanida S, Tanioka F, Inukai M, Yoshioka N, Saida Y, Imai K, Nakamura T, Kitamura H, Sugimura H (2000) Ewing's sarcoma/peripheral primitive neuroectodermal tumor (pPNET) arising in the omentum as a multilocular cyst with intracystic hemorrhage. J Gastroenterol 35:933–940. doi:10.1007/s005350070009
151. Tateishi U, Hasegawa T, Beppu Y, Satake M, Moriyama N (2004) Synovial sarcoma of the soft tissues: prognostic significance of imaging features. J Comput Assist Tomogr 28:140–148
152. Tateishi U, Hasegawa T, Kusumoto M, Oyama T, Ishikawa H, Moriyama N (2002) Desmoplastic small round cell tumor: imaging findings associated with clinicopathologic features. J Comput Assist Tomogr 26:579–583
153. Tateishi U, Hasegawa T, Nojima T, Takegami T, Arai Y (2005) MRI features of extraskeletal myxoid chondrosarcoma. Skeletal Radiol 35:27–33. doi:10.1007/s00256-005-0021-0
154. Tseng CA, Pan YS, Su YC, Wu DC, Jan CM (2004) Extrarenal retroperitoneal angiomyolipoma: case report and review of the literature. Abdom Imaging 29:721–723
155. van Rijswijk CS, Hogendoorn PC, Taminiau AH, Bloem JL (2001) Synovial sarcoma: dynamic contrast-enhanced MR imaging features. Skeletal Radiol 30:25–30
156. Varikatt W, Soper J, Simmons G, Dave C, Munk J, Bonar F (2008) Superficial acral fibromyxoma: a report of two cases with radiological findings. Skeletal Radiol 37:499–503. doi:10.1007/s00256-008-0454-3
157. Versteege I, Sévenet N, Lange J, Rousseau-Merck MF, Ambros P, Handgretinger R, Aurias A, Delattre O (1998) Truncating mutations of hSNF5/INI1 in aggressive paediatric cancer. Nature 94:203–206. doi:10.1038/28212
158. Vilanova JC, Woertler K, Narváez JA, Barceló J, Martínez SJ, Villalón M, Miró J (2006) Soft-tissue tumors update: MR imaging features according to the WHO classification. Eur Radiol 17:125–138. doi:10.1007/s00330-005-0130-0
159. Wakely PE Jr, Bos GD, Mayerson J (2005) The cytopathology of soft tissue mxyomas: ganglia, juxtaarticular myxoid lesions, and intramuscular myxoma. Am J Clin Pathol 123:858–865. doi:10.1309/39YX-94KX-T0T2-CNUX
160. Winer-Muram HT, Kauffman WM, Gronemeyer SA, Jennings SG (1993) Primitive neuroectodermal tumors of the chest wall (Askin tumors): CT and MR findings. AJR Am J Roentgenol 161:265–268. doi:10.2214/ajr.161.2.8392786
161. Wirth WA, Leavitt D, Enzinger FM (1971) Multiple intramuscular myxomas. Another extraskeletal manifestation of fibrous dysplasia. Cancer 27:1167–1173
162. Xu Q, Xu K, Yang C, Zhang X, Meng Y, Quan Q (2011) Askin tumor: four case reports and a review of the literature. Cancer Imaging 11:184–188. doi:10.1102/1470-7330.2011.0025
163. Yaghoobian J, Zinn D, Ramanathan K, Pinck RL, Hilfer J (1987) Ultrasound and computed tomographic findings in aggressive angiomyxoma of the uterine cervix. J Ultrasound Med 6:209–212
164. Zoccali C, Teori G, Prencipe U, Erba F (2009) Mazabraud's syndrome: a new case and review of the literature. Int Orthop 33:605–610. doi:10.1007/s00264-007-0483-x
165. Moretti VM, Brooks J, Ogilvie CM (2010) Case report: hemosiderotic fibrohistiocytic lipomatous lesion: a clinicopathologic characterization – springer. Clin Orthop Relat Res 468(10):2808–13. doi:10.1007/s11999-010-1242-7. Epub 2010 Feb 2
166. Petrey WB, LeGallo RD, Fox MG, Gaskin CM (2011) Imaging characteristics of angiomatoid fibrous histiocytoma of bone. Skeletal Radiol 40:233–237
167. Ogose A et al (2001) Recurrent malignant variant of phosphaturic mesenchymal tumor with oncogenic osteomalacia. Skeletal Radiol 30:99–103

Undifferentiated/Unclassified Sarcoma

19

A. Shah, R. Botchu, A.M. Davies, and S.L. James

Contents

19.1 **Undifferentiated/Unclassified Sarcoma** 483
19.1.1 Epidemiology 484
19.1.2 Clinical Behaviour and Gross Findings 485
19.1.3 Pathology 485
19.1.4 Genetics 485
19.1.5 Imaging Findings 486
19.1.6 Differential Diagnosis 490

References 490

19.1 Undifferentiated/ Unclassified Sarcoma

USTS is defined as an *STS* with no identifiable line of differentiation when analysed by available histological, cytological and genetic tests. It must be emphasised that *USTS* is a diagnosis of exclusion following thorough attempt to subclassify an *STS*.

USTSs do not have distinct clinical or morphological characteristics that would otherwise classify them under a specific type of sarcoma. There are a number of factors, which may significantly influence the pathologist to label a sarcoma as *USTS*. These include: (1) clinical context/patient age, (2) the extent of tissue sampling, (3) the availability of immunohistochemistry, (4) the availability of electron microscopy, (5) the availability of cytogenetic and molecular genetic testing and (6) the experience of the pathologist [15].

Broad groups of *USTS* have been described, which is based on cell morphology: (1) spindle cell morphology (undifferentiated spindle cell sarcoma, 'USCS'), (2) pleomorphic morphology (undifferentiated pleomorphic sarcoma, 'UPS'), (3) round cell morphology (undifferentiated round cell sarcoma, 'URCS'), (4) epithelioid morphology (undifferentiated epithelioid sarcoma, 'UES') and (5) undifferentiated sarcoma (not otherwise specified, 'USNOS'). As further genetic advances are made, new subgroups are being found. Multiple factors are involved in the ability to subclassify *STSs*. Whether or not a detailed attempt to subclassify *USTS* depends not only on the range of therapeutic options available but also on the tumour stage and the patient's general clinical condition [15]. It is vital to ensure the tumour is a sarcoma and not a lymphoma, carcinoma or melanoma. An assessment also needs to be made of the likelihood that subclassification may have a therapeutic impact. This would be more relevant, for example, in a round cell sarcoma rather than a pleomorphic sarcoma. Despite the reclassification of *MFH* to *UPS*, studies have not demonstrated any differences in overall survival,

A. Shah • R. Botchu • A.M. Davies • S.L. James (✉)
Royal Orthopaedic Hospital NHS Foundation Trust, Birmingham, UK
e-mail: stevenjames@nhs.net

© Springer International Publishing AG 2017

F.M. Vanhoenacker et al. (eds.), *Imaging of Soft Tissue Tumors*, DOI 10.1007/978-3-319-46679-8_19

local recurrence or distant metastasis [10]. This further indicates that histological subclassification is only useful if it predicts clinical behaviour and prognosis and impacts treatment options [11, 23].

Attempts to subclassify round cell sarcomas (*RCS*) should be made for a number of reasons as it has the greatest clinical impact. Not only are they predominantly seen in young patients, they are among the most aggressive *STSs*, yet the most chemosensitive (Fig. 19.1). Thus, one should avoid the non-discriminatory label of *URCS*.

To optimise treatment, *USCS* should be differentiated from two other spindle-celled sarcomas (monophasic synovial sarcoma and fibrosarcomatous variant of dermatofibrosarcoma protuberans (*DFSP*)).

Epithelioid sarcomas can be readily subclassified, and the differential diagnosis of *UES* is metastatic carcinoma or metastatic melanoma [15]. Once epithelial or melanocytic differentiation has been excluded, diagnosis of an *UES* can be made.

19.1.1 Epidemiology

USTS accounts for 20 % of all *STSs* and is the third most common *STS* subtype [36]. *USTSs* occur in all ages; however, *URCS* is more commonly seen in young patients, whereas *UPS* predominantly occurs in the elderly. *USTSs* may occur in any location; however, it most commonly occurs in the extremity (lower > upper) [34], followed by the retroperitoneum and trunk. Around 1–5 % of cases have been reported to arise in bone [27]. Male sex predominance (male/female ratio 1.2:1) is reported in literature [25, 27].

The aetiology of *USTS* is unknown; however, approximately 25 % of *USTSs* are radiation induced [17, 22]. Two theories have been postulated. The more common is that *USTSs* represent a common 'morphologic pattern', irrespective of its differentiation, rather than a specific type of malignancy. It is suggested that there is a final common pathway of cancer progression, in which tumours become progressively more undifferentiated, resulting in a high-grade *USTS* [26]. The second theory

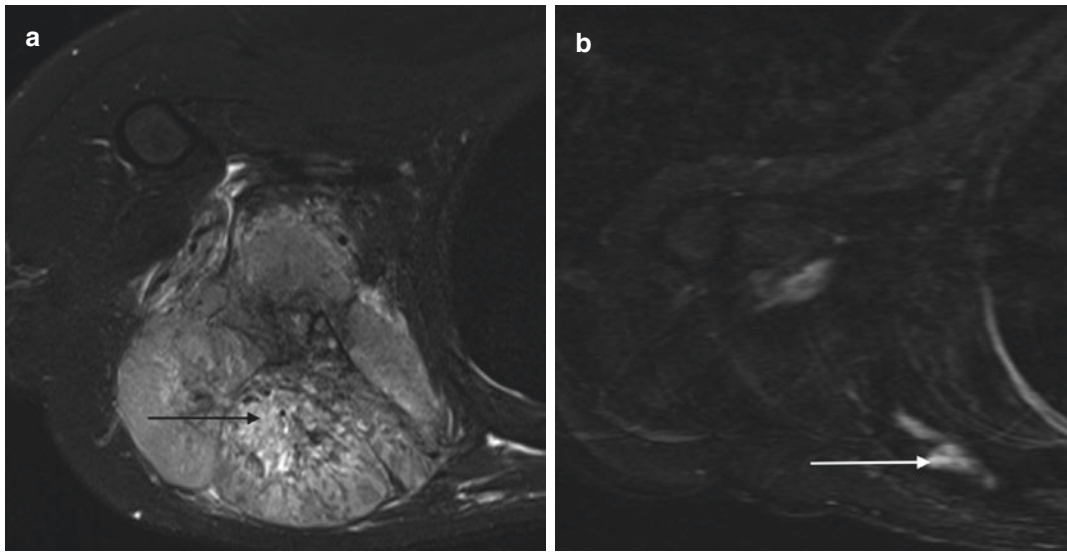

Fig. 19.1 (**a**, **b**) Round cell sarcoma (Ewing sarcoma). (**a**) Pre-chemotherapy axial T2FS MR image. (**b**) Post-chemotherapy axial T2FS MRI image. These pre- and post-chemotherapy images demonstrate that round cell sarcomas are very chemosensitive. The tumour in (**a**, *black arrow*) has significantly reduced as demonstrated in (**b**, *white arrow*), after appropriate chemotherapy was given to the patient. This case demonstrates the necessity to subclassify round cell sarcomas if possible

proposes that undifferentiated sarcomas are the result of transformation of mesenchymal stem cells, rather than the result of the loss of differentiation markers from previously differentiated sarcomas [9, 13, 26].

19.1.2 Clinical Behaviour and Gross Findings

USTS has an aggressive clinical behaviour [18], presenting as a deep-seated, often intramuscular, painless solid mass [30]. Up to 5 % of cases demonstrate extensive haemorrhage, presenting as a fluctuant mass and may be misinterpreted as a haematoma. Tumours can be between 5–15 cm and >20 cm when in the retroperitoneum. Therefore, an underlying malignancy should be excluded in those thought to have spontaneous musculoskeletal haemorrhage or a haematoma out of proportion to the degree of trauma [30]. Macroscopically, *USTS* has a pseudocapsule and is a pale fleshy mass with internal areas of haemorrhage or necrosis. USTS has a high propensity for local recurrence, with reported rates exceeding 31 % [34] with 30–50 % of patients having metastases at the time of diagnosis [4]. About 90 % of metastases are in the lung [32]. The overall 5-year survival is reported to be between 36 and 50 % [4, 30].

The mainstay of treatment is surgical resection [8] with pre- or post-operative radiotherapy [29]. Chemotherapy, including doxorubicin and ifosfamide, has also been used [8, 11].

19.1.3 Pathology

USTS can be subdivided according to the cellular morphology into spindle cell morphology, pleomorphic morphology, round cell morphology, epithelioid morphology and not otherwise specified. There is no specific characteristic feature between the subsets apart from their lack of an identifiable line of differentiation [16].

UPS can appear similar to other pleomorphic sarcomas with bizarre multinucleate giant cells [16]. *USCS* demonstrates a fascicular architecture with pale eosinophilic cytoplasm and tapering nuclei [16]. *URCS* has a round/oval cellular morphology with high nuclear to cytoplasmic ratio. As mentioned previously, it is important to ensure that a *URCS* is not in fact an Ewing sarcoma. Little knowledge of *UES* exists [37], but it closely resembles metastatic carcinoma or melanoma.

In the future, further genomic profiling and identifying chromosomal translocations will enable some of the seemingly undifferentiated sarcomas to be subtyped [3, 5, 6, 28]. Although by definition, a *USTS* has no reproducible immunophenotype, pattern of protein expression and no line of differentiation.

19.1.4 Genetics

Two different entities have been reported for *URCS* and *USCS*, both arising in children and young adults. There are those sarcomas with fusions of *EWSR1* to non-ETS transcription factor genes such as *SP3*, *PATZ1*, *POU5F1*, *SMARCA5* or *NFATC2*. These are often classified as *URCS* rather than an Ewing sarcoma [16]. However, there remains uncertainty whether these tumours represent a distinct entity or a variant of Ewing sarcoma.

There is another group of undifferentiated tumours with reported distinct genetic events. One involving *CIC-DUX4* gene fusion resulting from a chromosomal translocation of t(4;19)(q35;q13) or t(10;19)(q26.3;q13). The second genetic abnormality involves a *BCOR-CCNB3* gene fusion, as the result of an inversion of the X-chromosome. Studies suggest this may represent a distinct entity [35]. These tumours are clinically treated as an Ewing sarcoma. There have been a number of irreproducible chromosomal aberrations detected in *URCS* and *USCS* [1, 2, 21, 38, 39].

UPS, including many tumours formerly called *MFH*, generally have complex and non-specific karyotype. To date, a number of cytogenetic abnormalities have been reported [14, 16]. These studies further consolidate the evidence that *UPS* is characterised by various complex chromosomal gains and losses.

19.1.5 Imaging Findings

USTS is a histological diagnosis of exclusion and imaging appearances are non-specific [12].

Radiographs may be normal or reveal a non-specific soft tissue density, which is often greater than 5 cm in diameter (Fig. 19.2). *Radiographs* can detect periosteal reaction, cortical erosion and pathologic fracture [30]. Calcification or ossification can be detected in 5–20 % of patients [24, 27]. Calcifications within the tumour may be punctate or curvilinear. Peripheral heterotopic bone formation may be present and can mimic myositis ossificans.

USTS on *ultrasound* is non-specific, but typically is a well-defined heterogeneous mass. Hyperechoic areas represent a cellular composition, and hypoechoic regions represent necrotic or haemorrhagic tissue (Fig. 19.3). *USTS* demonstrates increased Doppler signal (Fig. 19.4). *Ultrasound* is the modality of choice for image-guided biopsy and can be used to target suitable areas for biopsy, avoiding necrotic components and the feeding vessels.

On unenhanced *CT*, *USTS* is often a large, lobulated, soft tissue mass, hypo- to isodense to muscle. There are intralesional areas of low attenuation (myxoid, haemorrhage or necrosis). Solid portions of the *USTS* can demonstrate a diffuse heterogenous pattern or a nodular and peripheral pattern of enhancement post-contrast [7, 19] (Fig. 19.5). Fat attenuation is not observed in these tumours, and its presence is suggestive of a liposarcoma. *CT* may be used to evaluate the internal matrix and assess underlying bony structures for cortical erosion or periosteal reaction. Approximately 10 % of retroperitoneal lesions demonstrate calcification.

MRI provides the best assessment of the size and extent of the lesion and its relation to the adjacent bones, soft tissues and the neurovascular bundle. As with other modalities, the *MRI* features are non-specific. *USTS* is commonly intermediate to low intensity on T1-weighted images (WI) and intermediate to high on T2-WI [31] (Fig. 19.6).

Fig. 19.2 Radiograph of biopsy confirmed *USCS*. The radiograph demonstrates a bulging dense solid mass at the wrist

The signal intensity heterogeneity is related to the tumour components: fibrous tissue with high collagen content (low signal intensity on all pulse sequences), myxoid tissue (low signal intensity on T1 weighting and high signal intensity on T2 weighting) and haemorrhage (variable signal intensity with or without fluid-fluid levels) [20, 31] (Fig. 19.7). Tumours with extensive necrosis appear cystic. Calcification may present as foci of low signal on both T1-WI and T2-WI. Tumour margins are relatively well defined, often with a low signal intensity margin, representing a pseudocapsule. Aggressive tumours such as *USTSs* emphasises that the presence of a well-defined

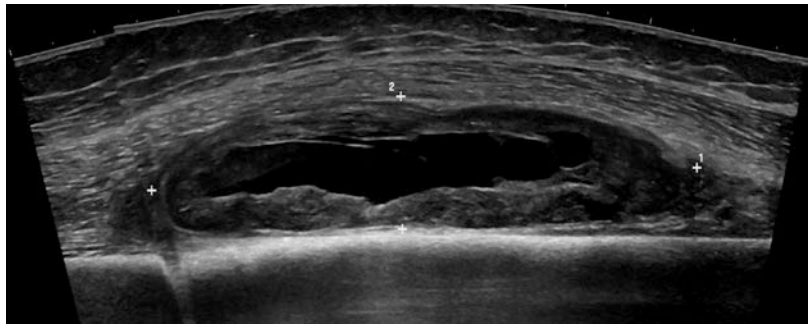

Fig. 19.3 *UPS* of the thigh. Longitudinal panoramic ultrasound of a deep soft tissue mass in thigh demonstrates a heterogeneous solid mass with a hypoechoic centre. This represents haemorrhage/necrosis, which is frequently seen in *USTSs*. Ultrasound is the modality of choice for image-guided biopsy and can be used to target suitable areas for biopsy, avoiding haemorrhagic/necrotic components

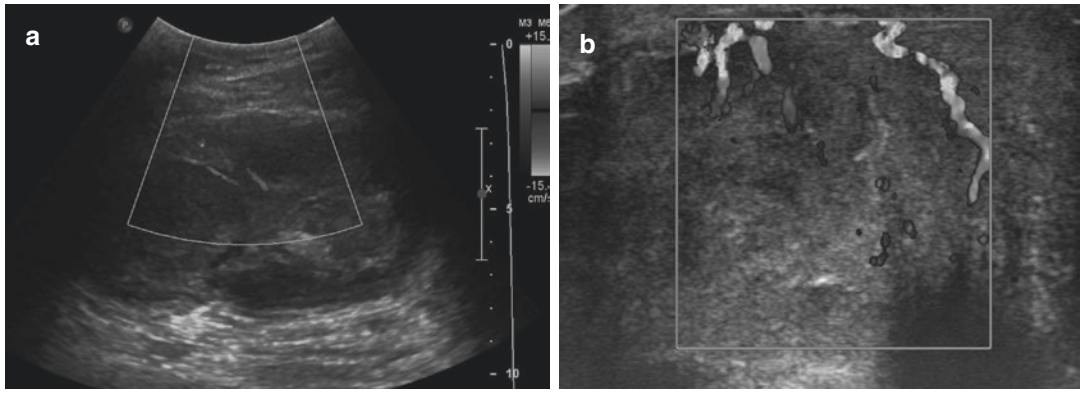

Fig. 19.4 (**a**) and (**b**) transverse Doppler ultrasound of a solid thigh mass. The tumour in (**a**) and (**b**) demonstrates increased Doppler signal. Biopsy of the tumour in (**a**) confirmed a *UPS* and in (**b**) a *USCS*

Fig. 19.5 Contrast-enhanced axial CT demonstrates a peripheral enhancing (*black arrow*) soft tissue mass with a non-enhancing necrotic centre (*white arrow*). Biopsy confirmed a *UPS* (Color figure online)

margin is a poor radiological indicator of malignancy. As with *CT*, solid components of *USTS* typically reveal nodular and peripheral enhancement (Fig. 19.6d, e).

USTS demonstrates avid uptake on ^{18}F-fluorodeoxyglucose positron emission tomography-computed tomography (*^{18}F-FDG PET-CT*) (Fig. 19.8) and is useful in defining not only the extent of the tumour, but the presence of metastatic spread [32]. Increased uptake can be seen on ^{99m}Tc bone scintigraphy and is useful for detecting osseous metastases. As the tumours are hypervascular, increased radionuclide uptake on both dynamic and blood pool images can be seen.

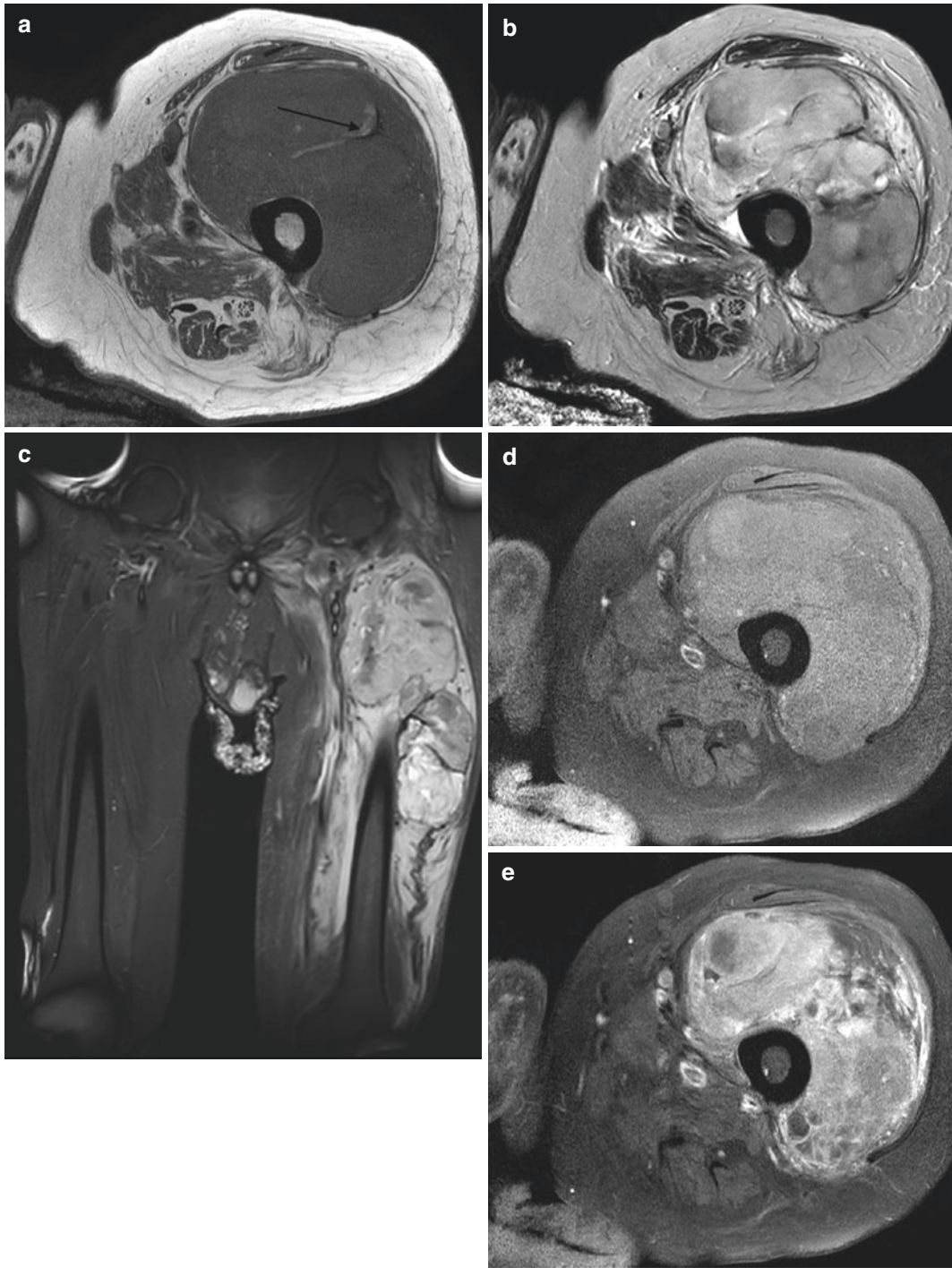

Fig. 19.6 (**a**–**e**) *USTS* of the thigh. (**a**) Axial T1-weighted MR image. (**b**) Axial T2-weighted MR image. (**c**) Coronal STIR MR image. (**d**) Axial pre-contrast T1FS. (**e**). Axial post-contrast T1FS. The *MRI* features of an *USTS* are non-specific. *USTSs* are commonly intermediate to low intensity compared to skeletal muscle on T1-weighted images (**a**). Intralesional areas of high T1 SI represent blood (**a**, *arrow*) and can be confirmed on fat suppression images. The tumour is intermediate to high on T2-weighted and fluid-sensitive images (**b**, **c**). Solid components of a *USTS* typically demonstrate contrast enhancement (**d**, **e**). Biopsy of this mass confirmed an *UPS*

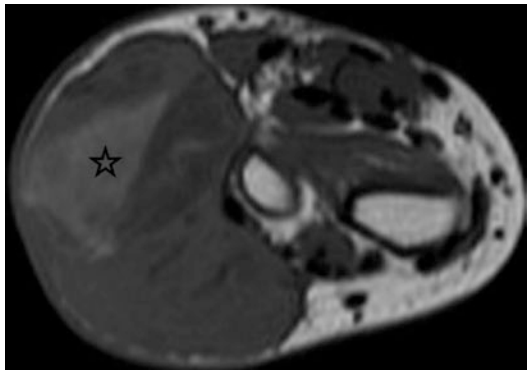

Fig. 19.7 Axial T1-weigthed MR image of a *USCS* of the wrist. Intralesional haemorrhage is often seen with *USTS*. The peripheral low T1 SI of the mass corresponds to solid components, and the intralesional high T1 SI (*star*) represents blood

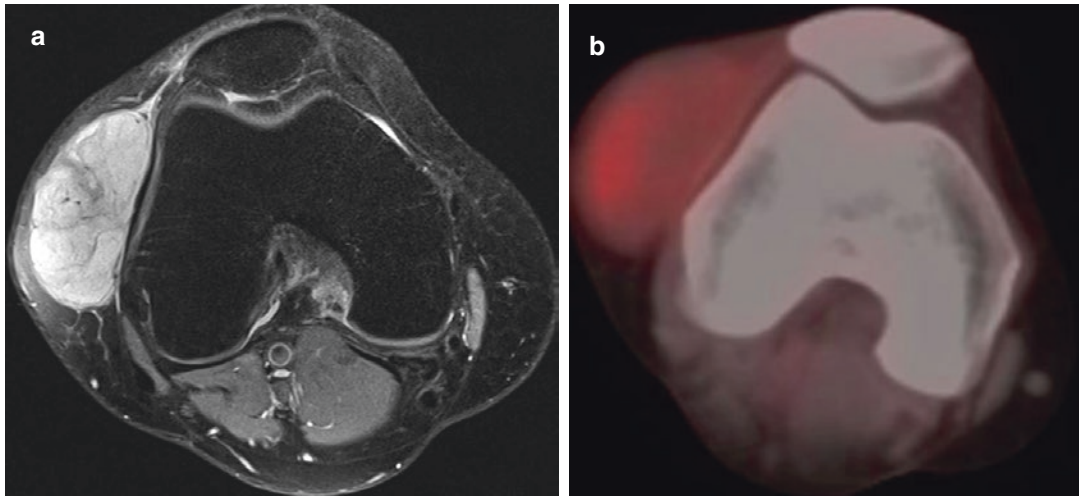

Fig. 19.8 (**a**, **b**) *UPS* of the knee. (**a**) Axial STIR MR image. (**b**) Axial ^{18}F-FDG PET-CT. The hyperintense subcutaneous soft tissue mass seen adjacent to the lateral femoral condyle (**a**) demonstrates areas of avid uptake on the PET-CT (**b**)

19.1.6 Differential Diagnosis

The imaging appearances of *USTS* have considerable overlap between different types of sarcomas, and no significant differences in the intrinsic characteristics of these lesions have been described [40]. Differential diagnosis includes liposarcoma, leiomyosarcoma, rhabdomyosarcoma, Ewing sarcoma, synovial sarcoma, myositis ossificans and haematoma.

Key Points

1. Undifferentiated/unclassified is a new category added to the 2013 WHO classification of soft tissue tumours.
2. Previously, there was a heterogeneous group of sarcomas that were classified as *malignant fibrous histiocytoma*; however with modern analytical techniques, a number of these tumours can now be subclassified. The term for the remaining tumours, without a line of differentiation, is *undifferentiated pleomorphic sarcoma*.
3. The subgroups of undifferentiated soft tissue sarcoma are based on morphological features, which includes spindle cell morphology, pleomorphic morphology, round cell morphology and epithelioid morphology.
4. Undifferentiated soft tissue sarcoma is a diagnosis of exclusion. Where possible, attempts to subclassify a sarcoma should be made, particularly if this will impact clinical management.
5. Imaging features of undifferentiated sarcomas are non-specific and diagnosis is made on histology.
6. These tumours tend to be large with areas of haemorrhage and necrosis.

References

1. Alaggio R, Bisogno G, Rosato A et al (2009) Undifferentiated sarcoma: does it exist? A clinicopathologic study of 7 pediatric cases and review of literature. Hum Pathol 40:1600–1610
2. Alaggio R, Ninfo V, Rosolen A et al (2006) Primitive myxoid mesenchymal tumor of infancy: a clinicopathologic report of 6 cases. Am J Surg Pathol 30:388–394
3. Carneiro A, Francis P, Bendahl PO et al (2009) Indistinguishable genomic profiles and shared prognostic markers in undifferentiated pleomorphic sarcoma and leiomyosarcoma: different sides of a single coin? Lab Invest J Tech Methods Pathol 89:668–675
4. Chan CY, Janarthan N, Vivek AS et al (2008) The outcome of pleomorphic sarcoma at University Malaya Medical Center – a fifteen-year review. Med J Malaysia 63:311–314
5. Coindre JM, Hostein I, Maire G et al (2004) Inflammatory malignant fibrous histiocytomas and dedifferentiated liposarcomas: histological review, genomic profile, and MDM2 and CDK4 status favour a single entity. J Pathol 203:822–830
6. Coindre JM, Mariani O, Chibon F et al (2003) Most malignant fibrous histiocytomas developed in the retroperitoneum are dedifferentiated liposarcomas: a review of 25 cases initially diagnosed as malignant fibrous histiocytoma. Modern Pathol Off J US Can Acad Pathol, Inc 16:256–262
7. Cong Z, Gong J (2011) Primary malignant fibrous histiocytoma of the liver: CT findings in five histopathological proven patients. Abdom Imaging 36:552–556
8. Constantinidou A, Pollack S, Loggers E et al (2013) The evolution of systemic therapy in sarcoma. Expert Rev Anticancer Ther 13:211–223
9. Dei Tos AP (2006) Classification of pleomorphic sarcomas: where are we now? Histopathology 48:51–62
10. Delisca GO, Mesko NW, Alamanda VK et al (2015) MFH and high-grade undifferentiated pleomorphic sarcoma-what's in a name? J Surg Oncol 111: 173–177
11. Eriksson M (2010) Histology-driven chemotherapy of soft-tissue sarcoma. Ann Oncol Off J Eur Soc Med Oncol/ESMO 21(Suppl 7):vii270–vii276
12. Faizi NA, Thulkar S, Sharma R et al (2012) Magnetic resonance imaging and positron emission tomography-computed tomography evaluation of soft tissue sarcoma with surgical and histopathological correlation. Indian J Nucl Med IJNM Off J Soc Nucl Med, India 27:213–220
13. Fletcher CD (2006) The evolving classification of soft tissue tumours: an update based on the new WHO classification. Histopathology 48:3–12
14. Fletcher CD, Dal Cin P, De Wever I et al (1999) Correlation between clinicopathological features and karyotype in spindle cell sarcomas. A report of 130 cases from the CHAMP study group. Am J Pathol 154:1841–1847
15. Fletcher CDM (2008) Undifferentiated sarcomas: what to do? and does it matter? A surgical pathology Perspective. Ultrastruct Pathol 32:31–36
16. Fletcher CDM, Bridge JA, Hogendoorn PC et al (2013) WHO classification of tumours of soft tissue and bone, 4th edn. IARC Press, Lyon
17. Gladdy RA, Qin LX, Moraco N et al (2010) Do radiation-associated soft tissue sarcomas have the same prognosis as sporadic soft tissue sarcomas?

J Clin Oncol Off J Am Soc Clin Oncol 28:2064–2069
18. Henderson MT, Hollmig ST (2012) Malignant fibrous histiocytoma: changing perceptions and management challenges. J Am Acad Dermatol 67:1335–1341
19. Karki B, Xu YK, Wu YK et al (2012) Primary malignant fibrous histiocytoma of the abdominal cavity: CT findings and pathological correlation. World J Radiol 4:151–158
20. Kransdorf MJ, Murphey MD (2006) Malignant fibrous and fibrohistiocytic tumors. In: Imaging of soft tissue tumors, 2nd edn. Lippincott Williams & Wilkins, Philadelphia
21. Kreiger PA, Judkins AR, Russo PA et al (2009) Loss of INI1 expression defines a unique subset of pediatric undifferentiated soft tissue sarcomas. Modern Pathol Off J US Can Acad Pathol, Inc 22:142–150
22. Laskin WB, Silverman TA, Enzinger FM (1988) Postradiation soft tissue sarcomas. An analysis of 53 cases. Cancer 62:2330–2340
23. Lehnhardt M, Daigeler A, Hauser J et al (2008) The value of expert second opinion in diagnosis of soft tissue sarcomas. J Surg Oncol 97:40–43
24. Manaster BJ, May DA, Disler DG (2013) Musculoskeletal imaging: the requisites, 4th edn. Saunders, Philadelphia
25. Mankin HJ, Hornicek FJ, Delaney TF et al (2012) Pleomorphic spindle cell sarcoma (PSCS) formerly known as malignant fibrous histiocytoma (MFH): a complex malignant soft-tissue tumor. Musculoskelet Surg 96:171–177
26. Matushansky I, Charytonowicz E, Mills J et al (2009) MFH classification: differentiating undifferentiated pleomorphic sarcoma in the 21st century. Expert Rev Anticancer Ther 9:1135–1144
27. Meyers SP (2007) MRI of bone and soft tissue tumors and tumorlike lesions: differential diagnosis and Atlas. Thieme, Stuttgart/New York
28. Mills AM, Beck AH, Montgomery KD et al (2011) Expression of subtype-specific group 1 leiomyosarcoma markers in a wide variety of sarcomas by gene expression analysis and immunohistochemistry. Am J Surg Pathol 35:583–589
29. Mullen JT, Kobayashi W, Wang JJ et al (2012) Long-term follow-up of patients treated with neoadjuvant chemotherapy and radiotherapy for large, extremity soft tissue sarcomas. Cancer 118:3758–3765
30. Murphey MD (2007) World Health Organization classification of bone and soft tissue tumors: modifications and implications for radiologists. Semin Musculoskelet Radiol 11:201–214
31. Murphey MD, Gross TM, Rosenthal HG (1994) From the archives of the AFIP. Musculoskeletal malignant fibrous histiocytoma: radiologic-pathologic correlation. Radiogra Rev Publ Radiol Soc N Am, Inc 14:807–826; quiz 827–808
32. Nascimento AF, Raut CP (2008) Diagnosis and management of pleomorphic sarcomas (so-called "MFH") in adults. J Surg Oncol 97:330–339
33. Oda Y, Tamiya S, Oshiro Y et al (2002) Reassessment and clinicopathological prognostic factors of malignant fibrous histiocytoma of soft parts. Pathol Int 52:595–606
34. Peiper M, Zurakowski D, Knoefel WT et al (2004) Malignant fibrous histiocytoma of the extremities and trunk: an institutional review. Surgery 135:59–66
35. Pierron G, Tirode F, Lucchesi C et al (2012) A new subtype of bone sarcoma defined by BCOR-CCNB3 gene fusion. Nat Genet 44:461–466
36. Reichardt P (2014) Soft tissue sarcomas, a look into the future: different treatments for different subtypes. Future Oncol 10:s19–s27
37. Sakharpe A, Lahat G, Gulamhusein T et al (2011) Epithelioid sarcoma and unclassified sarcoma with epithelioid features: clinicopathological variables, molecular markers, and a new experimental model. Oncologist 16:512–522
38. Selvarajah S, Yoshimoto M, Prasad M et al (2007) Characterization of trisomy 8 in pediatric undifferentiated sarcomas using advanced molecular cytogenetic techniques. Cancer Genet Cytogenet 174:35–41
39. Surace C, Storlazzi CT, Engellau J et al (2005) Molecular cytogenetic characterization of an ins(4;X) occurring as the sole abnormality in an aggressive, poorly differentiated soft tissue sarcoma. Virchows Archiv Int J Pathol 447:869–874
40. Tateishi U, Hasegawa T, Onaya H et al (2005) Myxoinflammatory fibroblastic sarcoma: MR appearance and pathologic correlation. AJR Am J Roentgenol 184:1749–1753

Part IV

Imaging of Other Soft Tissue Masses

Synovial Lesions

20

V. Vasilevska Nikodinovska and
Filip M. Vanhoenacker

Contents

20.1 **Introduction** 495

20.2 **Benign Synovial Lesions** 496
20.2.1 Benign Cystic Lesions 496
20.2.2 Giant Cell Tumors and PVNS 516
20.2.3 Other Synovial Tumors and Tumorlike Lesions 516

20.3 **Malignant Tumors Around the Joints** 518
20.3.1 Synovial Sarcoma 518
20.3.2 Metastatic Spread of Cancer 518

References 518

V. Vasilevska Nikodinovska (✉)
University Surgical Clinic "St. Naum Ohridski", Department of Radiology, University "Ss. Cyril and Methodius", ul.11 Oktomvri bb, 1000 Skopje, Macedonia
e-mail: v_vasilevska@yahoo.com

F.M. Vanhoenacker
University Hospital Antwerp, Department of Radiology, Wilrijkstraat, 10, B-2650 Edegem, Belgium

General Hospital Sint-Maarten Duffel-Mechelen, Rooienberg 25, B-2570 Duffel, Belgium

Medicine and Health Sciences, University of Ghent, Ghent, Belgium

20.1 Introduction

The synovial membrane is derived from embryonic mesenchyme and lines nonarticular areas in synovial joints (inner surface of the capsule), bursae, and tendon sheaths. The synovium is a special collagenous tissue that elaborates synovial fluid which lubricates the articular surface movement. Cells of the synovial membrane regulate the exchange of substances between blood and synovial fluid, and they synthesize hyaluronate, which is a major component of the synovial fluid [5]. There are considerable differences in the appearance of the synovial membrane, depending on local mechanical factors and the nature of the underlying tissue. For instance, in high-pressure joints the synovium is flat and acellular, whereas in low-pressure joints it resembles cuboidal or columnar epithelium [46].

In most radiological textbooks, discussion of synovial tumors includes benign cystic synovial tumors, giant cell tumors, pigmented villonodular synovitis (PVNS), and synovial sarcoma.

However, according to the World Health Organization Classification of Tumors (2013), PVNS and giant cell tumors are classified as so-called fibrohistiocytic tumors [24]. Therefore, these tumors are discussed more appropriately in Chap. 14.

Synovial sarcoma has been known for longer time as a misnomer, as it is not derived from true synovial cells. Currently, synovial sarcoma

© Springer International Publishing AG 2017

F.M. Vanhoenacker et al. (eds.), *Imaging of Soft Tissue Tumors*, DOI 10.1007/978-3-319-46679-8_20

is regarded as a malignant tumor of uncertain differentiation [24]. It will be discussed in Chap. 18.

20.2 Benign Synovial Lesions

20.2.1 Benign Cystic Lesions

There are several types of cystic para-articular soft tissue lesions, like synovial cysts, ganglion (cysts), and bursae. As there is much controversy in the radiological literature about the nomenclature and classification of these benign para-articular cystic lesions, we will first propose a logical classification, related to their possible pathogenesis, before discussing their appearance on imaging.

Cyst mimickers such as infectious processes, traumatic lesions, vascular lesions, and neoplasms [97] will be discussed in other chapters of this book.

20.2.1.1 Classification and Pathogenesis

Cystic lesions can be divided into four categories, mainly based upon the combination of two criteria (Table 20.1) [56, 103]:

1. The anatomical location and *relationship with the adjacent joint*, e.g., a communicating stalk with the joint. This communication can be visualized by imaging [109] or can be surgically proven.
2. The *histological composition* of the cyst wall and the contents.

(Arthro)synovial Cyst The term synovial cyst describes a continuation or herniation of the synovial membrane through the joint capsule. In the French literature, the term "arthrosynovial" cyst is preferred, which refers to their intimate relationship with the adjacent joint. Indeed, there is always a communication with the adjacent joint, and the histological composition is identical to that of the joint cavity; the wall consists of fibrous tissue lined with synovium continuous with the synovial membrane of the joint. It represents a collection of synovial fluid, lined by a continuous layer of "true" synovial cells, and is considered to be true cyst. The histological composition of a synovial cyst may change in time and as accumulated fluid becomes more viscous. This may result in increased pressure within the cyst and communication with the joint may become interrupted. Due to increased intracystic pressure, the layer of lining cells disappears and the cyst is transformed into a ganglion cyst (see infra) [81]. The presence of synovial cysts is always associated with increased joint effusion, which leads to increased intra-articular pressure, regardless of the underlying joint abnormality [66] that causes herniation of joint fluid and synovium through a "locus minoris resistentiae" of the joint capsule.

Baker's cyst or popliteal cyst is the most characteristic example of a synovial cyst. It is a fluid-filled mass which represents a distention of a preexisting bursa in popliteal fossa, the medial gastrocnemius–semimembranosus bursa, which results from an extrusion of synovial fluid through a breach between the medial gastrocnemius

Table 20.1 Classification of para-articular cystic lesions

	Communication with joint	Wall composition	Cell lining	Contents
(Arthro)synovial cyst	Present	Continuous mesothelial lining	"True" synovial cells	Mucinous fluid
Ganglion (cyst)	May be present	Discontinuous mesothelial lining	Flattened pseudosynovial cells	Mucinous fluid
Bursitis de novo	Absent	Fibrous wall	No mesothelial lining	Fibrinoid necrosis
Bursa (permanent)	Absent	Continuous mesothelial lining	"True" synovial cells	Mucoid fluid

muscle and semimembranosus tendon [30, 36] (Fig. 20.1). There is a joint connection as "ball-valve"-like mechanism, which is opened during knee flexion and closed during extension [2, 59, 79]. Other examples can be seen near other joints (spine, shoulder [98], elbow, hip [54, 85], hand [60], foot, and ankle [80]), but are less frequent. They are usually associated with joint diseases [8], such as labral tears [54, 85, 98], osteoarthrosis, and inflammatory and posttraumatic joint diseases [11, 25, 26, 34, 36, 63, 100, 108].

Ganglion (Cyst) Ganglia are benign cystic lesions that arise from the joint capsule or tendon sheath, most commonly from the limb joints, with rare occurrence at the spine. They contain mucinous fluid, which is highly viscous, proteinaceous material, rich in hyaluronic acid, glycosamine, albumin, and globulin [68], but their wall consists of a (discontinuous) layer of flattened pseudosynovial cells, surrounded by dense fibrous connective tissue (pseudocapsule) [41, 56, 61, 72, 102–104]. They are not true cysts because they lack a cellular lining and are made of a gelatinous, viscous material [13]. A communication with the adjacent joint is not always present (40–100 % of the cases) [88, 89, 112].

The pathogenesis of ganglion cysts is controversial. Several theories have been proposed, including displacement of the synovial tissue during embryogenesis, proliferation of pluripotential mesenchymal cells, mucoid degeneration of collagen, degeneration of connective tissues after trauma and repetitive microtraumas (degenerative theory), and migration of synovial fluid into the cyst (synovial herniation theory) [15, 29, 57, 101]. Pathogenesis is usually multifactorial.

Based upon the similar appearance on imaging and surgery and on the similar wall composition of synovial cysts and ganglion cysts, we believe that the synovial herniation hypothesis is the most satisfactory. According to this theory, both synovial cysts and ganglion cysts are formed by a herniation of synovium through a breach in the adjacent articulation. Ganglion cyst could represent an advanced stage of a synovial cyst which underwent histological changes due to increased intracystic pressure [81] which proved that both types of para-articular cysts are variants of the same disease spectrum. At one end of the spectrum, we have the pure (arthro)synovial cysts, which represent an extension of the joint cavity outside the joint, caused by herniation through a "locus minoris resistentiae" within the joint capsule. This explains why the histological composition of those cysts is exactly a copy of that of the adjacent joint and why the cellular lining consists of a continuous layer of "true" synovial cells. As those cysts grow and may extend further away from the joint into the soft tissues, they may undergo degenerative changes. First, the cellular lining may become discontinuous and individual cells may flatten, as they may be subject to fluctuations in intracystic pressure. This results in para-articular cysts, in which the wall composition consists of a discontinuous layer of pseudosynovial cells. Ultimately, the original communication with the joint may be obliterated. Therefore, at the other end of the disease spectrum, a ganglion cyst may represent an advanced degenerative stage of a synovial cyst, in which the continuous synovial lining and the communication with the joint may be lost during the process of degeneration (Fig. 20.2). Meniscal and ganglion cysts are commonly associated with degeneration of underlying anatomic structures [101].

The following arguments support the "synovial" theory in their pathogenesis:

1. The *similar histological composition* of synovial and ganglion cysts: both the contents (mucinous fluid) and the cellular lining are very similar (continuous layer of true synovial cells in arthrosynovial cysts versus a discontinuous lining of flattened pseudosynovial cells in ganglion cysts).
2. The *morphology* of some ganglion cysts, e.g., their course along capsular arteries or capsular nerve branches, may explain a peculiar form. This is especially true for adventitial cystic disease and perineural cysts, which can be considered as variants of ganglion cysts [60, 79, 81] (Fig. 20.3).

a
b
c
d
e
f
SUPERFICIAL
SEMIMEMB
MED GAST
DEEP
g
h

Fig. 20.1 (**a**–**h**) Synovial cyst – Baker's cyst in different patients: (**a**) axial fat-suppressed turbo spin echo T2-weighted MR image; (**b**) sagittal fat-suppressed proton density MR image. (**c**) lateral radiography of the right knee; (**d**) computed tomography; (**f**) axial fat-suppressed proton density MR image; (**e**) sagittal fat-suppressed proton density MR image. (**g**) axial ultrasound of the popliteal fossa; (**h**) longitudinal ultrasound of the popliteal fossa in another patient. Soft tissue mass in the popliteal fossa with typical extension toward the joint which is well appreciated on the axial and sagittal MR images. Due to its fluid content, the lesion is of high signal intensity on T2-WI (**a**, **b**). Another patient with soft tissue mass in the popliteal fossa, with internal secondary osteochondromatosis, due to long-standing degenerative joint disease presented with calcifications at radiography (**c**) which is well depicted on computed tomography (**d**). Baker's cyst on CT is shown as hypodense lesion with sharp delineated hyperdense borders (**d**). On axial and sagittal MR images, intralesional calcifications are of low signal intensity (**e**, **f**). In a third case, ultrasound shows an uncomplicated Baker's cyst as an anechoic, well-demarcated lesion. The lesion has a deep and a superficial component and typically extends between the medial gastrocnemius muscle and semimembranosus tendon (**g**). In case of cyst rupture, ultrasound reveals volume decrease of the cyst compared to previous images and presence of fluid around the cyst extending to the calf (**h**). A Baker's cyst represents a distended gastrocnemius–semimembranosus bursa and is lined by a normal synovial membrane. It may be the result of increased intra-articular pressure in cases of joint effusion. In the knee joint, these effusions are often associated with meniscal tears, rheumatoid disease, osteochondral lesions, or degenerative disease

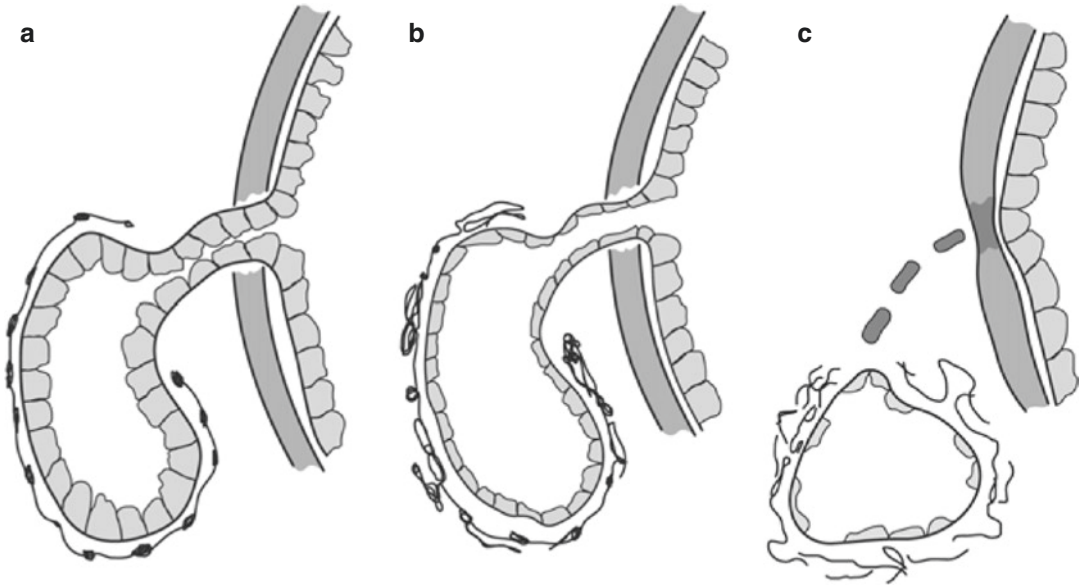

Fig. 20.2 (**a**–**c**) Pathogenesis according to the "synovial herniation hypothesis" of (**a**) (arthro)synovial cyst: this lesion originates from a herniation of the synovial membrane through the joint capsule. The histological composition is identical to the joint cavity, and the cellular lining consists of true synovial cells; (**b**, **c**) ganglion cyst: during the process of degeneration, and increased intracystic pressure, the cellular lining may change, partially disappear, and become discontinuous. Ultimately, the original communication with the joint may be obliterated

3. *Functional arguments*
   - When the para-articular cyst is directly injected or after arthrography of the adjacent joint, there is often a delayed opacification of the joint or cyst, respectively [56, 57].

The fluctuating volume of some cysts, sometimes complicated by rupture (Figs. 20.4 and 20.5), argues for a communication with the adjacent joint, which acts as a reservoir of synovial fluid [56, 69, 84, 103].

Kumarasamy et al. reported a theory for explaining of the ganglion within the tendons; either mucinous degeneration of fibrous tissue or herniation of hypersecreting synovium of adjacent

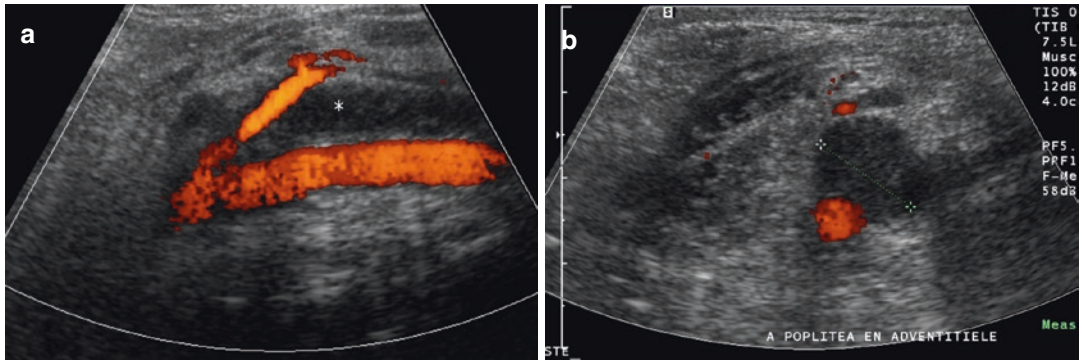

Fig. 20.3 (**a**, **b**) Adventitial cystic disease of the popliteal artery. (**a**) Longitudinal and (**b**) axial Doppler ultrasound. Note anechoic lesion within the wall of the popliteal artery (asterisks on (**a**) and calipers on (**b**)). The lumen of the artery is patent and shows colored Doppler signal. Note also the presence of a small arterial branch communicating with the main artery on the longitudinal image (**a**). Adventitial cyst may result from dissection of fluid around articular branches of arteries, veins, or nerves. On ultrasound, it presents as an anechoic cystic lesion near by the colored arterial flow (**a**, **b**)

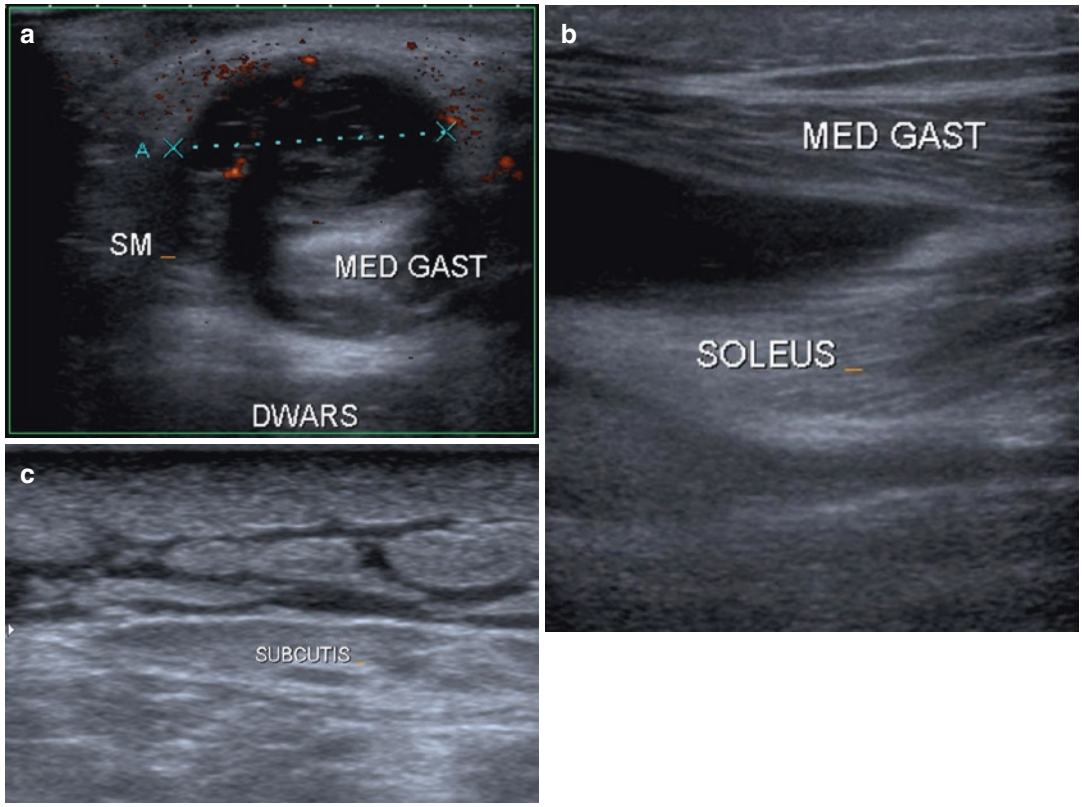

Fig. 20.4 (**a**–**c**) Ultrasound of a ruptured Baker's cyst in a 68-year-old female with rheumatoid arthritis: (**a**) axial image shows a typical Baker's cyst extending between the medial gastrocnemius muscle and semimembranosus tendon. The wall is thickened due to inflammation. Note also some intralesional septations and subtle vascularity due to inflammation; (**b**) longitudinal image shows pointing of the inferior border of Baker's cyst in keeping with cyst rupture. (**c**) Longitudinal image of the calf shows diffuse edema within the subcutis

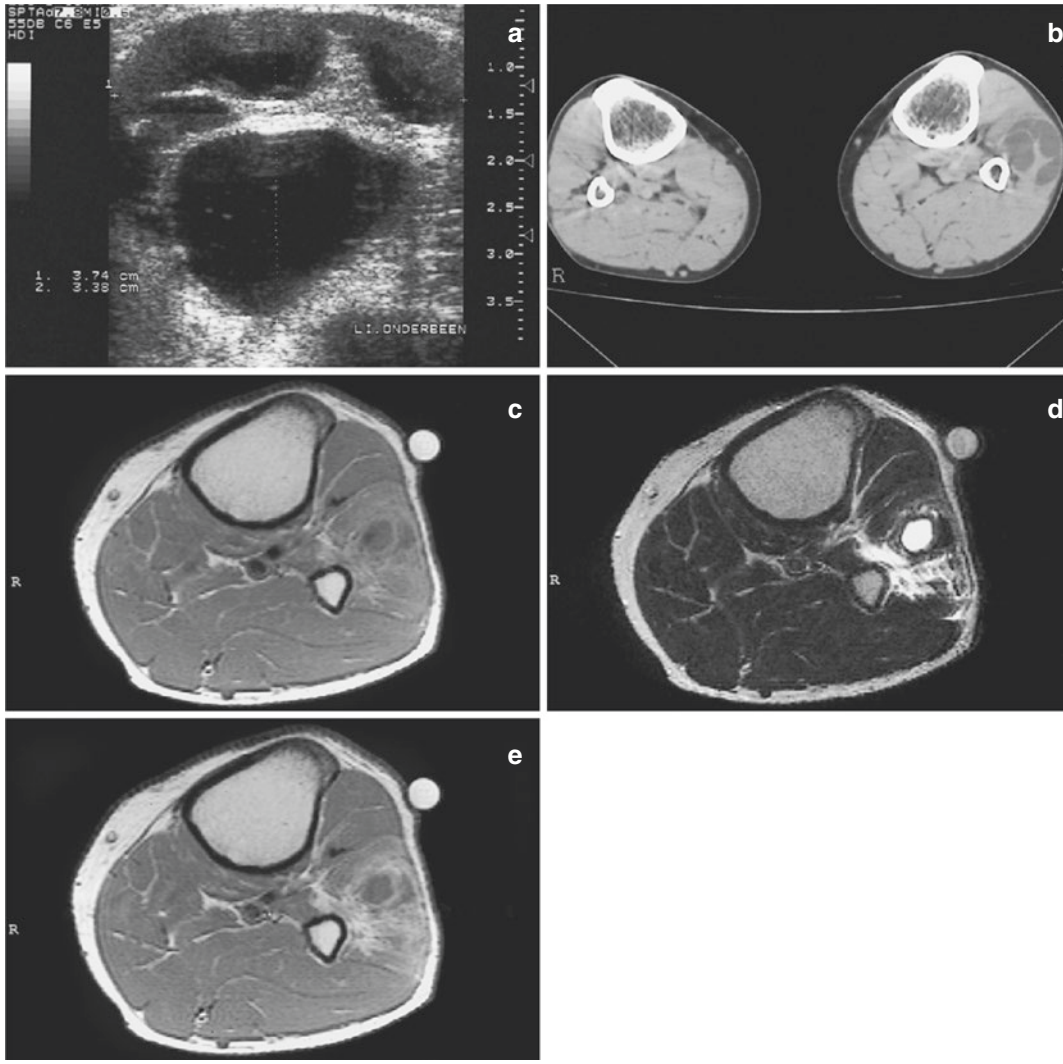

Fig. 20.5 (**a**–**e**) Ruptured ganglion cyst in the lower leg of a 54-year-old man: (**a**) ultrasound; (**b**) CT without contrast injection; (**c**) axial spin echo T1-weighted MR image; (**d**) axial turbo spin echo T2-weighted MR image; (**e**) axial spin echo T1-weighted MR image after gadolinium contrast injection. Ultrasound clearly shows a multiloculated cystic lesion in the lower leg (**a**). The image corresponds perfectly with the findings on nonenhanced CT (**b**). The lesion is clearly delineated with sharp borders. The adjacent fibular bone is not eroded. The MRI examination (**c**–**e**) was performed 2 weeks later. The cyst is ruptured, and there is fluid in the inter- and intramuscular fat planes (**d**). There is no evidence of hemorrhage (**c**). After gadolinium injection (**e**) enhancement is seen in the periphery of the lesion as a result of local inflammatory changes. This may lead to confusion in the differential diagnosis against other inflammatory soft tissue changes

joints through a one-way valve type of mechanism may cause intratendinous cysts [2].

Ganglion cysts may be located anywhere around the joints. A para-articular location in fat layers (Figs. 20.6, 20.7, 20.8) or muscle (Fig. 20.9) is most frequently seen. Dissection of fluid around arteries or veins or nerves results in adventitial cystic disease [105] or peri- or intraneural cysts [52, 73, 106] where anatomic explanation is vicinity to neurovascular bundle. Adventitial cyst disease is found within a vessel wall (arteries or veins), and vascular branch would be the conduit from the joint, leading to dissection to the main parent vessel with accumulation of a mucinous

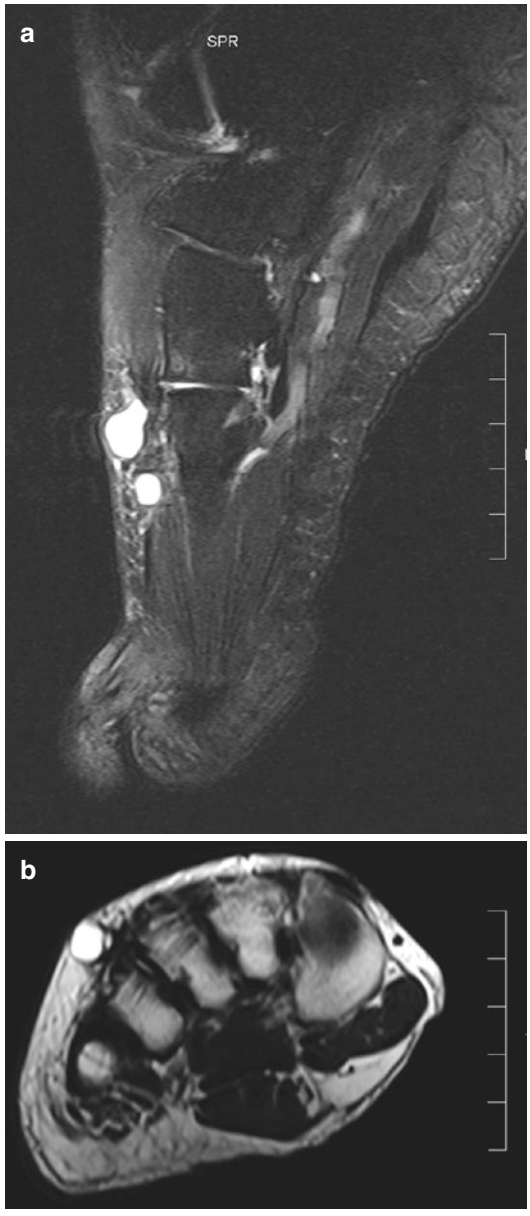

Fig. 20.6 (**a**, **b**) Ganglion cysts in the subcutaneous fat of the dorsum of the foot: (**a**) sagittal fat-suppressed T2-weighted MR image; (**b**) short-axis T2-weighted MR image. Within subcutaneous tissue of the dorsum of the foot, there are multiple ganglion cysts which present ovoid, well-demarcated high signal intensity lesions (**a**, **b**). There is no obvious communication with the adjacent joints

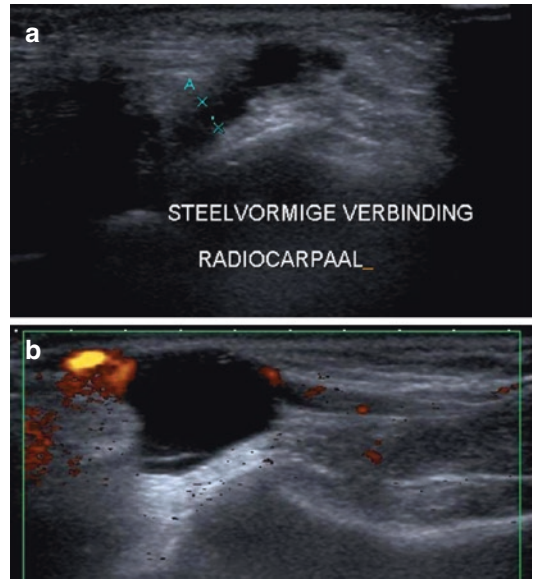

Fig. 20.7 (**a**, **b**) Ganglion cyst on the wrist in tennis player: (**a**) longitudinal ultrasound; (**b**) longitudinal Doppler ultrasound. On ultrasound, note a polylobulated anechoic, relatively well-demarcated lesion (**a**). On Doppler ultrasound, there is distension of the ganglion cyst with displacement of an adjacent blood vessel (**b**)

substance within the adventitia (Fig. 20.3) [65, 74, 90]. Articular (synovial) theory explains intraneural ganglion cysts with joint fluid dissection within an articular branch and extending to the parent nerve [90, 94, 112], where joint connection was found in 40 % [88, 89] to 100 % of the cases, which was an explanation for the cyst recurrences [112]. High is the percentage (53 %) of the extraneural rupture of intraneural cysts [84]. The most common location of an intraneural ganglion cyst is in the peroneal nerve at the level of the fibular head [88–90], followed by the tibial nerve at the superior tibiofibular joint and ankle, the ulnar nerve at the elbow, the median nerve at the wrist, and the suprascapular nerve at the glenohumeral joint [93]. The presence of a combination of intraneural ganglia and vascular adventitial cysts in the same patient suggests that their content can dis-

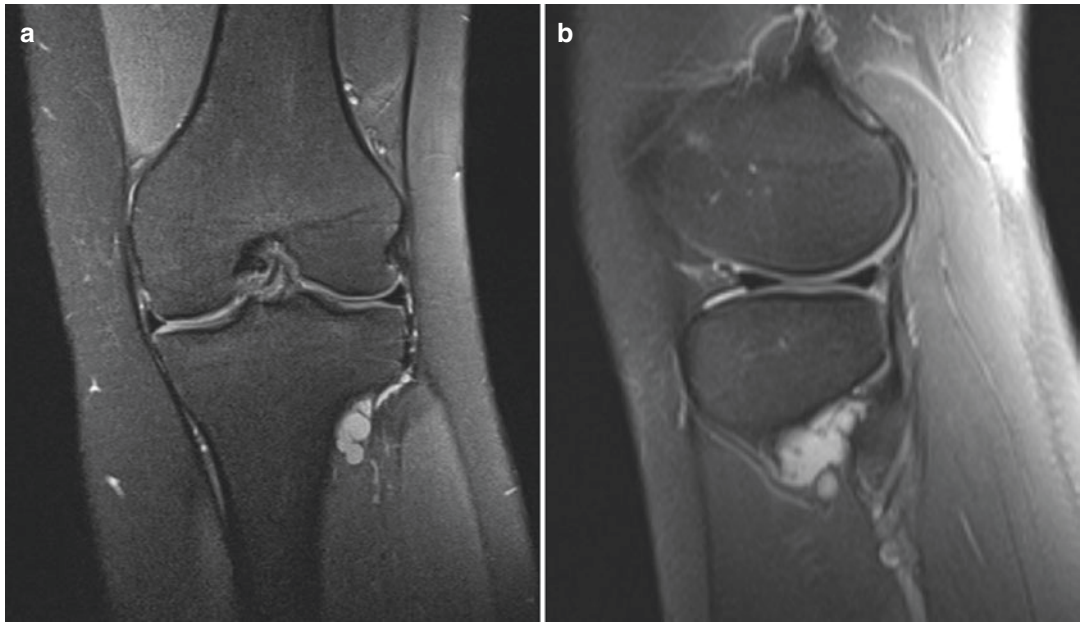

Fig. 20.8 (**a**, **b**) Ganglion cysts of the proximal tibiofibular joint. (**a**) Coronal fat-suppressed proton density MR image; (**b**) sagittal fat-suppressed proton density MR image. Anterior to the proximal tibiofibular joint, there is polylobulated cystic lesion containing intralesional septa. The lesion is clearly demarcated from the surrounding tissue (**a**, **b**)

Fig. 20.9 Intramuscular ganglion cyst. CT scan of the left lower leg shows a sharply demarcated low-density lesion within the medial gastrocnemius muscle

sect from a joint along neurovascular bundles [93].

A meniscal cyst (parameniscal ganglion cysts) is formed adjacent or within the menisci (Fig. 20.10) and is considered as a particular form of a ganglion cyst, in which synovial fluid is extruded through a horizontal meniscal tear (Fig. 20.10a), due to translocation of synovial cells or extravasation of synovial fluid into the meniscus [95], and accumulates at the menisco-capsular margin, resulting in an encapsulated mass around the meniscus [11, 31, 38]. Meniscal cysts are lined by flat spindle-shaped cells, have no synovial lining, and are characterized by myxoid contents [40], and the wall is formed of dense fibrous connective tissue (not synovium) as a distinguishing feature [36].

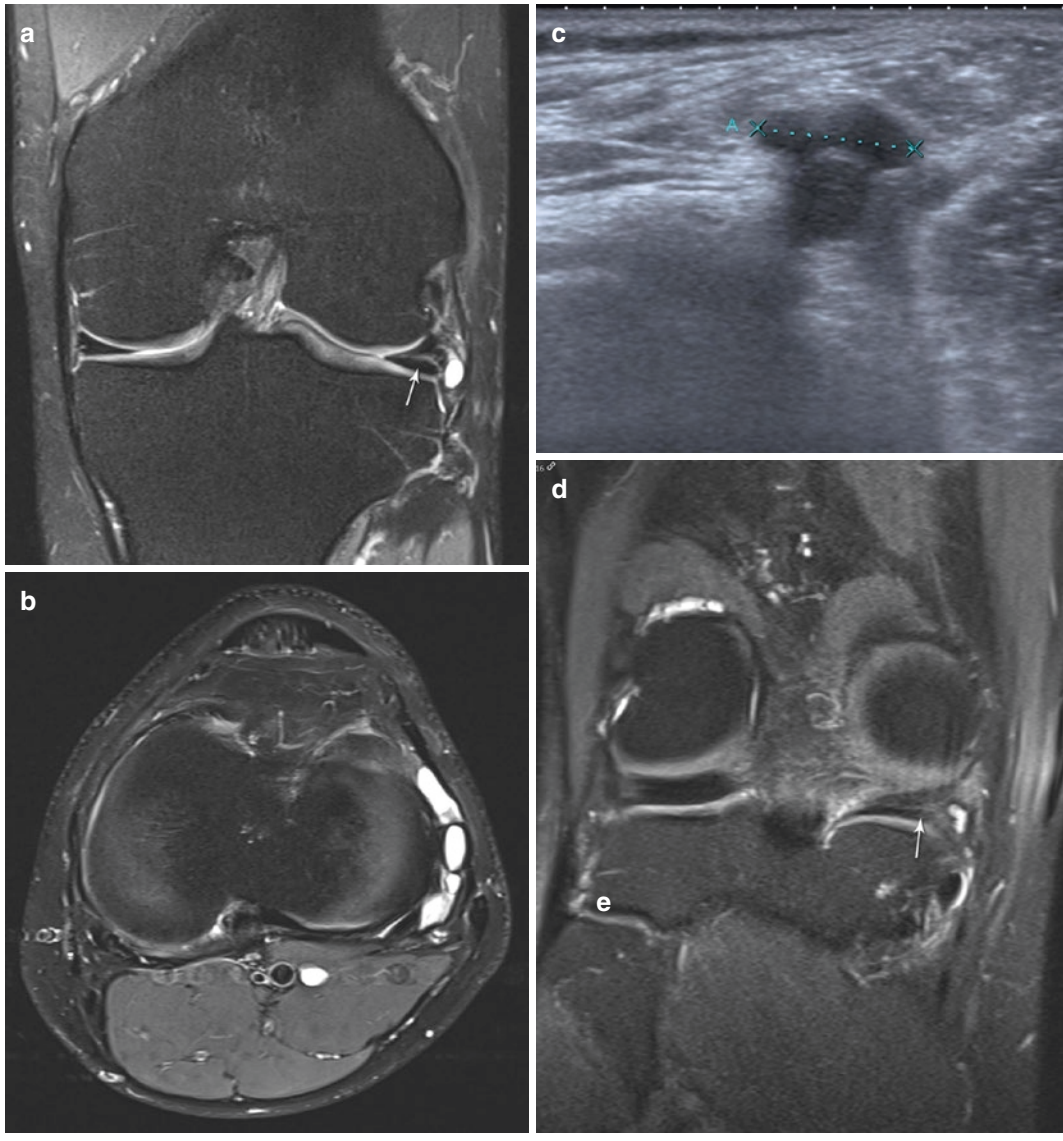

Fig. 20.10 (**a**–**d**) Meniscal cyst in different patients: (**a**) coronal T2-weighted fat-suppressed MR image; (**b**) axial T2-weighted fat-suppressed MR image; (**c**) longitudinal ultrasound; (**d**) coronal fat-suppressed proton density MR image. On coronal and axial MR image, multicystic lesion extruded from the peripheral border of the lateral meniscus, which is associated with horizontal meniscal tear (*arrow*) (**a**, **b**). In a second patient, meniscal cyst is well depicted on ultrasound as anechoic lesion adjacent to the posterior horn of medial meniscus (**c**). The transverse meniscal tear is seen on the MR image. (*arrow*) (**d**)

Other examples of intra-articular locations are paralabral (Figs. 20.11 and 20.12) (shoulder and hip) and cruciate ligament cysts (Fig. 20.13) [31, 115]. The full-thickness tears at the transitional zone of the labrum of the hip, which is with relative hypovascularity ("watershed zone"), as a weak point, may be a key factor in the development of paralabral cysts [55, 62]. On MR arthrography in 94 % of the cases, paralabral cysts of the hip are filled with intra-articular contrast material [55]. Arthrosynovial cyst of the hip joint can be developed after total hip arthroplasty as a sign of a deteriorating prosthesis surface [51]. A similar case was reported after primary

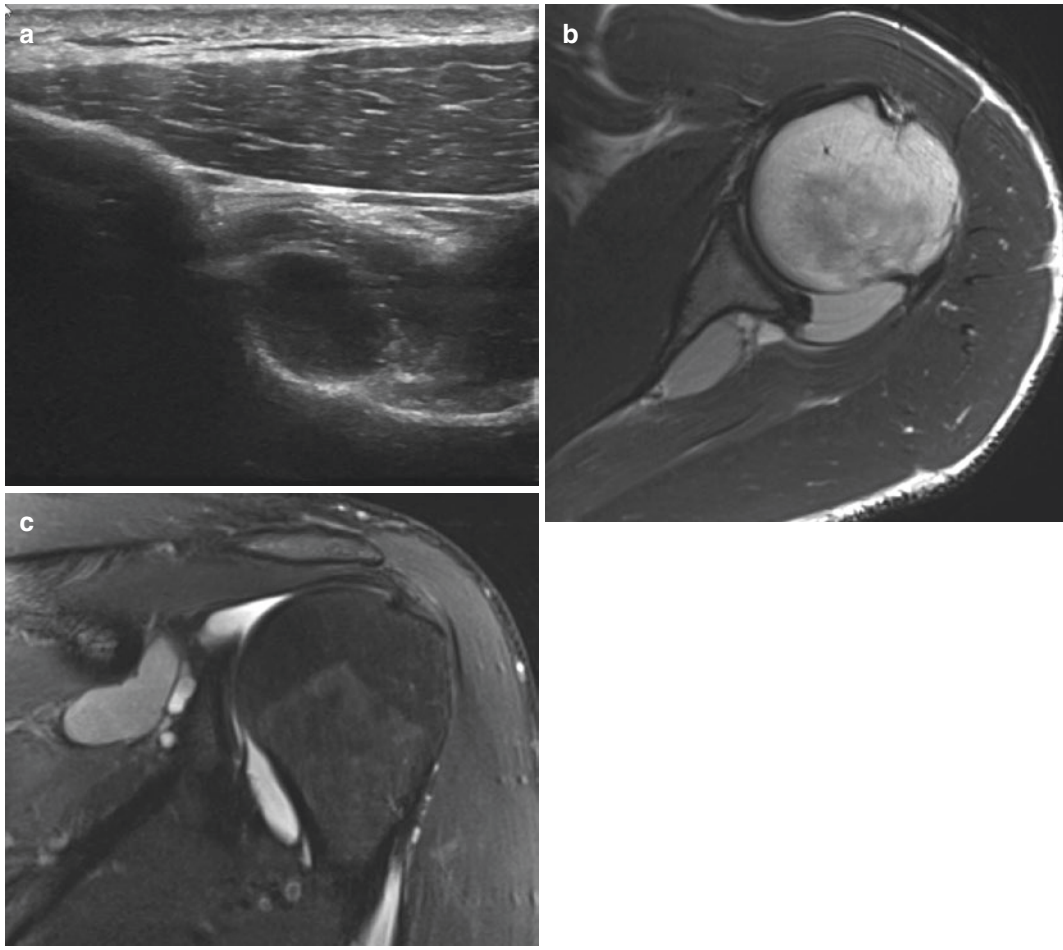

Fig. 20.11 (**a**–**c**) Ganglion cyst in the spinoglenoid notch of the shoulder (paralabral cyst): (**a**) ultrasound axial section; (**b**) axial T2-weighted MR image; (**c**) coronal fat-suppressed T2-weighted MR image. On ultrasound, there is a well-demarcated anechoic lesion (**a**) which is of high signal intensity on T2-weighted MR image and is located at the spinoglenoid notch of the scapula (**b**, **c**)

total knee arthroplasty where popliteal cyst contains polyethylene debris, confirming joint communication [67].

A possible cause of intra-articular ganglion cyst is repetitive minor trauma [6, 53, 68] and most commonly is associated with the anterior cruciate ligament (Fig. 20.13), but can also occur at the posterior cruciate ligament, posterior joint capsule, and infrapatellar fat pad, from chondral fractures or with subchondral bone cysts [3, 6, 19, 31, 42, 47, 53, 68, 86, 111].

Recent reports indicate that all juxtafacet cysts (either synovial, ganglion, and flavum ligament cysts) arise from degenerated facet joints [27, 48, 71, 92] with increased segmental motion as a trigger for herniation of the facet joint synovium [4, 16].

Rare localizations include temporomandibular joint [35], ganglia arising from the transverse acetabular ligament [10], and a ganglion cyst arising from the anterior horn of the medial meniscus impinged between the medial meniscus and the anterior cruciate ligament [31].

Extracapsular ganglia may arise from the medial or from the lateral head of the gastrocnemius muscle with “bunch of grapes” appearance

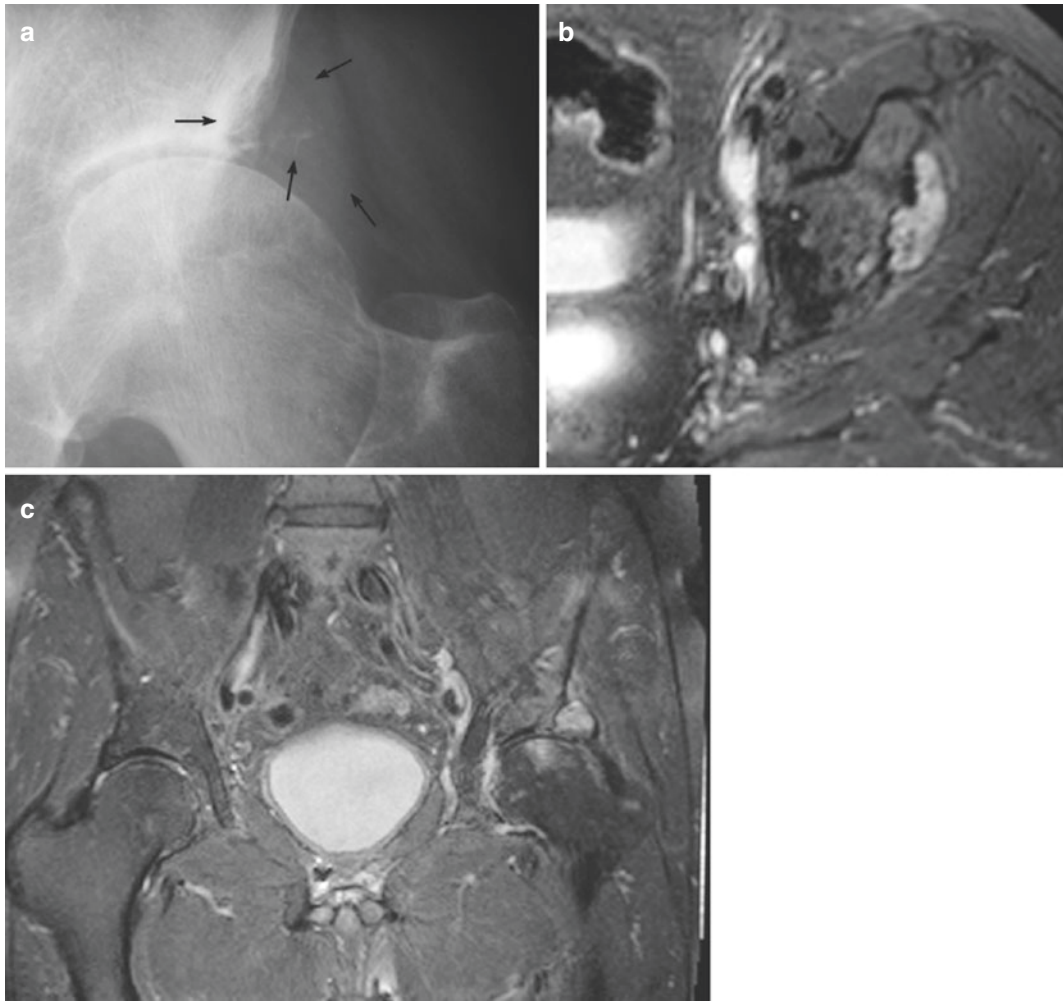

Fig. 20.12 (**a**–**c**) Paralabral cyst of the left hip. (**a**) Standard radiograph; (**b**) axial fat-suppressed T2-weighted MR image; (**c**) coronal fat-suppressed TSE T2-weighted MR image. Plain radiography (**a**) reveals the presence of a sclerotic defined erosion at the superolateral aspect of the left acetabulum (*arrows*). On axial and coronal FS TSE T2-weighted MR images, there is a multicystic structure within the acetabular labrum, extending at the lateral aspect of the left acetabulum, causing pressure erosion (**b**, **c**). Note also the presence of internal bone debris on the standard radiographs (**a**), which appears as *hypointense dot-like structures* within the labral cyst on the FS TSE T2-weighted MR images. There is bone marrow edema at the lateral aspect of the left femoral head, as well as in the acetabulum, due to preexisting osteoarthrosis of the hip

[23, 39] or intramuscular ganglia within the peroneus longus muscle [58] or within the tendon of semimembranosus muscle, few centimeters above the insertion of the muscle without communication with the knee joint or any adjacent bursae [2, 44]. The bicipital intertubercular groove very rarely serves as the origin of an intra-articular ganglion cyst of the long head of the biceps tendon, which on MRI can be presented as cyst of the biceps tendon in the intertubercular groove with extension to the shoulder joint [83].

Other para-articular locations such as the subperiosteal area of the diaphyses of the long bones

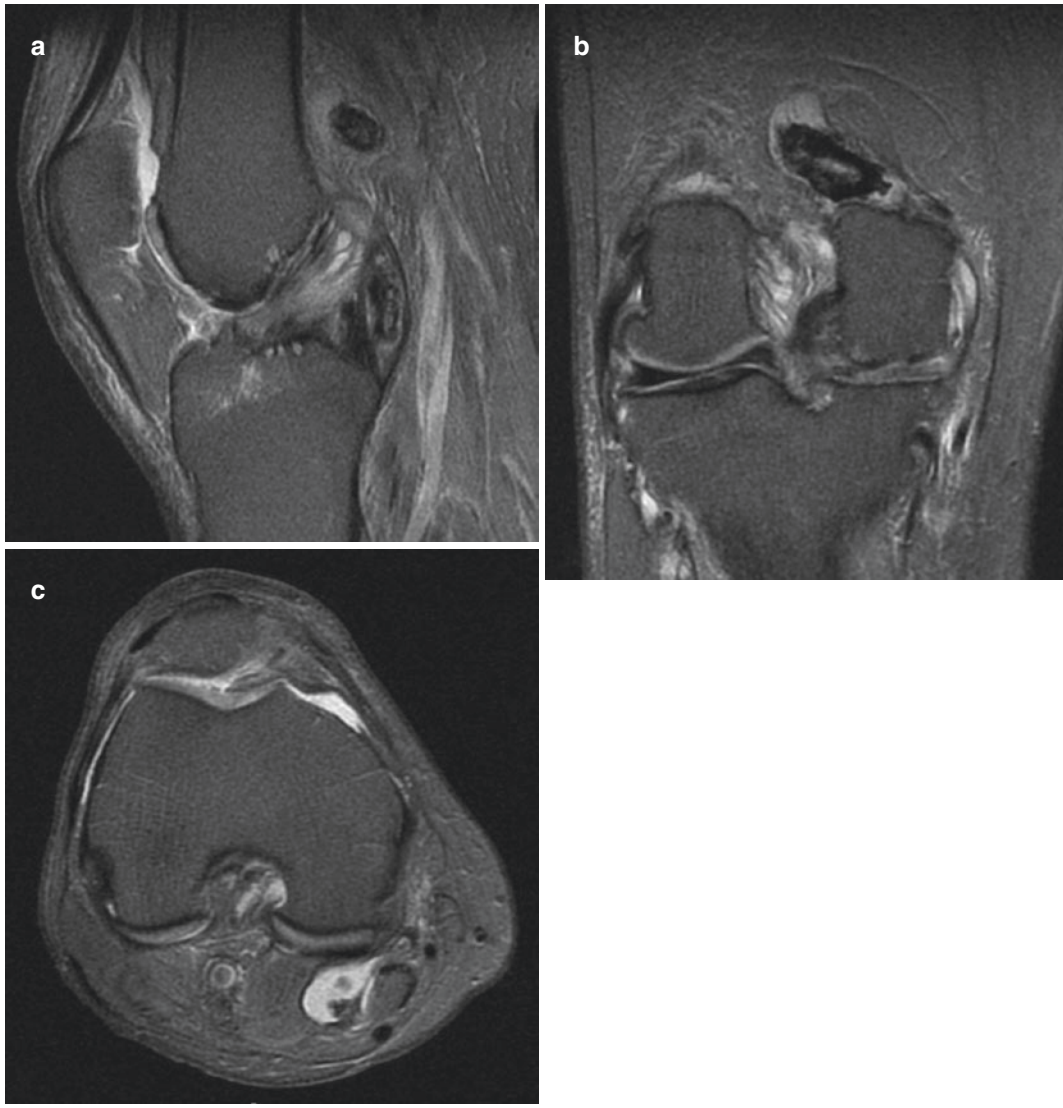

Fig. 20.13 (**a**–**c**) Ganglion small cysts of anterior cruciate ligament. (**a**) Sagittal fat-suppressed proton density MR image; (**b**) coronal fat-suppressed proton density MR image; (**c**) axial fat-suppressed proton density MR image. The fibers of the anterior cruciate ligament are interspersed by elongated elliptic small areas of high signal intensity which are clearly delineated on sagittal image (**a**). On coronal and axial image may be difficult to distinguish anterior cruciate ligament cysts from partial tears of the ACL (**b**, **c**)

(periosteal ganglion) are rare [46, 57] (Fig. 20.14), while intraosseous ganglia are frequent.

Bursa De Novo (Adventitious Bursa) Inflammation of connective tissue in areas subject to chronic frictional irritation may result in fibrinoid necrosis, with formation of a bursa de novo or an adventitious bursa. This consists of a cystic structure filled with cellular debris, extracellular fluid, altered ground substance, and inflammatory exudate [107]. The first metatarsophalangeal joint is the most typical location, although other areas of chronic friction may provoke formation of an adventitious bursa (e.g., bursitis de novo at the

medial side of medial malleolus in skaters due to chronic friction) (Fig. 20.15) [18].

Bursa Bursae are enclosed flattened sacs, synovium-lined structures, which are normally interposed between ligaments or tendons and adjacent bony surfaces. Its main function is to reduce friction between adjacent moving structures. They have an anatomically predisposed topography, with or without connection to joint spaces. Containing a small amount of lubricating, mucinous fluid normally is quiescent and is

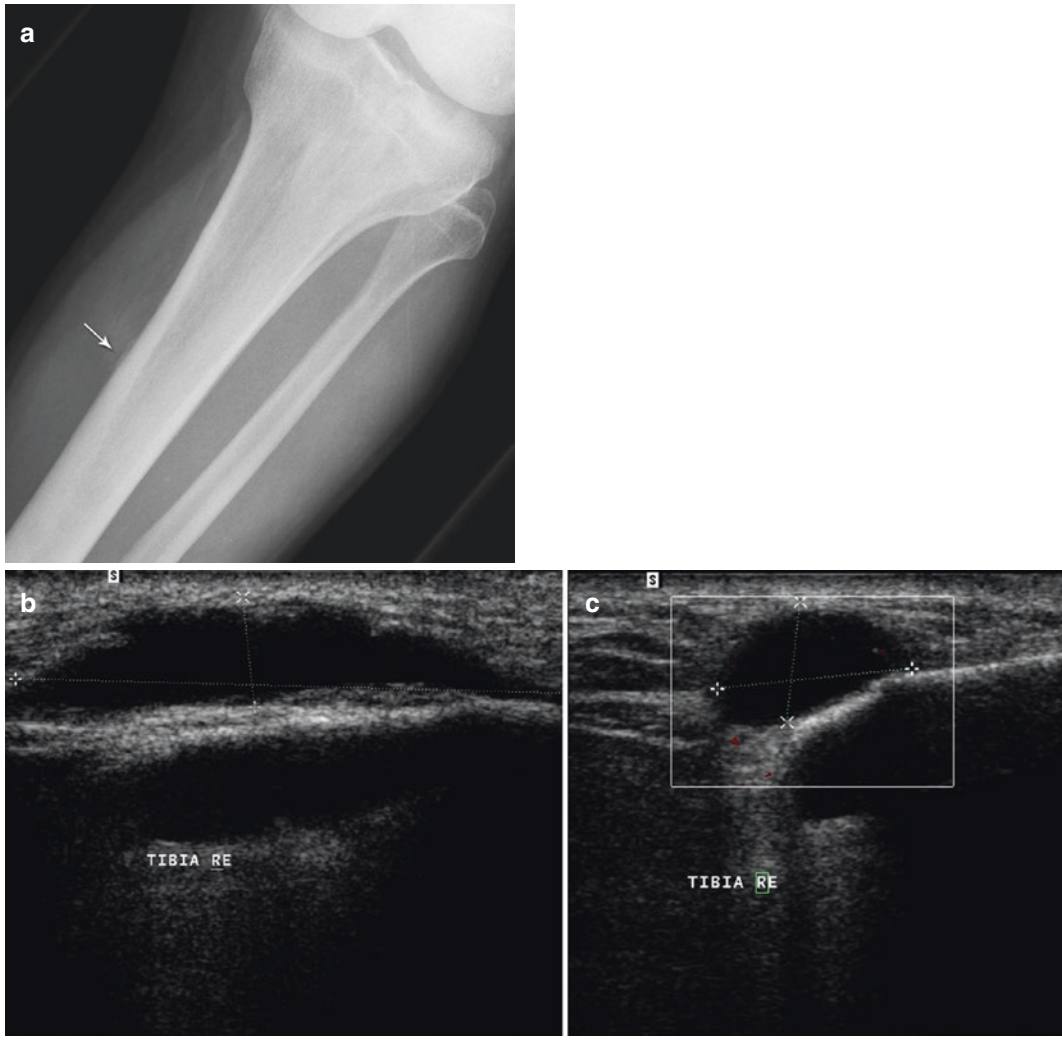

Fig. 20.14 (**a**–**f**) Subperiosteal ganglion cyst of different patients: (**a**) radiography; (**b**) ultrasound, longitudinal section; (**c**) ultrasound, axial section; (**d**) axial T1-weighted MR image; (**e**) axial T1-weighted fat-suppressed gadolinium-enhanced MR image; (**f**) axial T2-weighted fat-suppressed MR image. At radiography a discrete elevation of the periosteum can be seen at the medial aspect of tibia (*arrow*) (**a**). On ultrasound, ganglion cyst is presented as well-demarcated anechoic lesion (measurements) adjacent to outer hyperechoic cortex of the tibia (**b**, **c**). On T1-weighted image, the lesion is with intermediate signal intensity with broad base at the outer aspect of the tibial cortex elevating the periosteum (*arrow*) and extruding to the subcutaneous tissue (*near skin marker*) (**d**). The lesion is with low signal intensity on fat-suppressed T1-weighted image after gadolinium contrast enhancement (**e**) and with very high signal intensity on fat-suppressed T2-weighted image, presented in another patient, where elevated periosteum can be seen (*arrows*) (**f**)

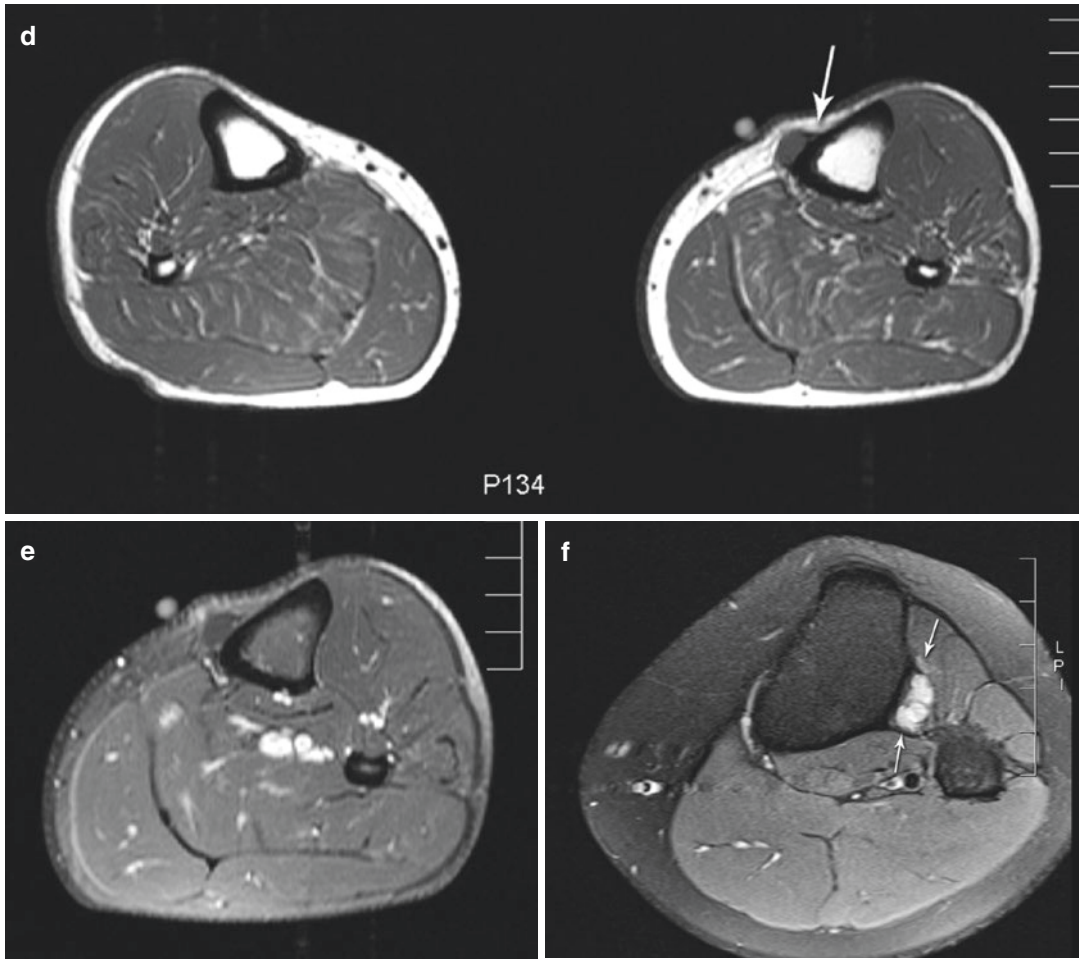

Fig. 20.14 (continued)

normal not to be visualized on MR images [6, 14, 61]. Bursitis is an inflammation of a bursa, and/or filled with abnormal accumulation of fluid [7, 14], usually due to chronic mechanical friction, but may be also caused by an infectious or rheumatoid disease, overuse, trauma, and hemorrhage [37]. The presence of internal joint derangement, and collagen vascular diseases, may cause thickening of the synovial lining with increasing of fluid content within bursa [7] (Figs. 20.16, 20.17, and 20.18), and the presence of internal loose bodies, synovial debris, or bleeding may give heterogeneous appearance to bursa (Fig. 20.15c).

In extra-articular cysts (e.g., prepatellar bursitis), there is associated intra-articular derangement [30] (Fig. 20.19).

20.2.1.2 Clinical Manifestations

Clinically, these cysts present as palpable soft tissue masses. There may be associated symptoms related to underlying intra-articular pathology [43]. Symptoms are nonspecific including local pain or limitation of joint mobility and are usually due to mass effect on the surrounding tissues [17, 33, 37, 41, 60, 78, 112, 115]. Tenderness may be caused by expanding cyst, which is enlarged into the calf with compression of the adjacent structures, causing symptoms from the popliteal vein compressions [33] or direct compression of the artery with resultant ischemia [115]. Depending on cyst size and location, they may cause peripheral nerve compression [41, 50, 60, 112] leading to entrapment symptoms [115],

compressive median nerve neuropathy (carpal tunnel syndrome) [45, 75], or very rare ulnar nerve compression in Guyon's canal with sudden decrease of strength or sensory loss [49]. Intraneural ganglion cysts may cause progressive paralysis [78]. Small cysts are usually asymptomatic. Symptoms of intra-articular ganglion cyst include clicking or popping sensations and decreased range of motion [3, 19, 68]. Ruptured popliteal cysts and leakage of synovial fluid result in tenderness, erythema, and warmth of the calf. Pseudo-thrombophlebitis is a well-known complication, due to rupture of a Baker's cyst [21].

However, cystic lesions often are asymptomatic [37, 76] and may be discovered during routine MR imaging of the joint for suspected internal derangement [89].

20.2.1.3 Imaging

The role of imaging is to define the cystic nature of those lesions and to demonstrate a possible communication with the joint. This is important for the surgeon because the resection of the communicating stalk with the joint is essential to avoid postsurgical recurrence of the cyst.

Conventional Radiography Standard radiography is nonspecific and may reveal an ill-defined or rounded, noncalcified soft tissue mass

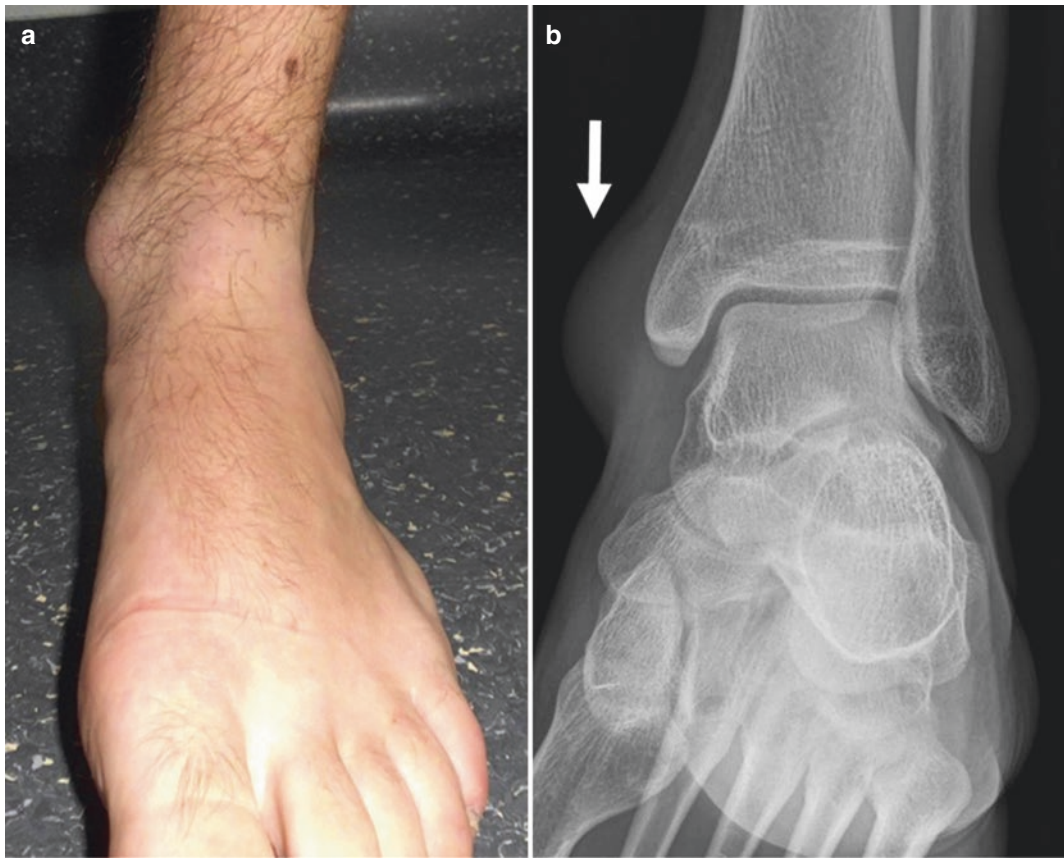

Fig. 20.15 (**a**–**e**) Adventitious bursa due to chronic friction at the medial malleolus in a skater: (**a**) clinical picture; (**b**) radiography Figure part a and are lacking. Please add, will send it by e-mail. (**c**) ultrasound; (**d**) axial fat-suppressed proton density MR image; (**e**) coronal fat-suppressed proton density MR image. On clinical examination a soft tissue swelling at the medial aspect of the ankle can be seen (**a**) which is seen also at radiography (*arrow*) (**b**). On ultrasound, a well-demarcated heterogeneously hypoechoic structure is seen in the subcutaneous tissue near the medial malleolus with intralesional hyperechoic debris (**c**). MR reveals a clearly demarcated cystic lesion (*arrow*), with intralesional strands (**d**, **e**) (Image used with permission from De Keersmaeker et al. [18, 83])

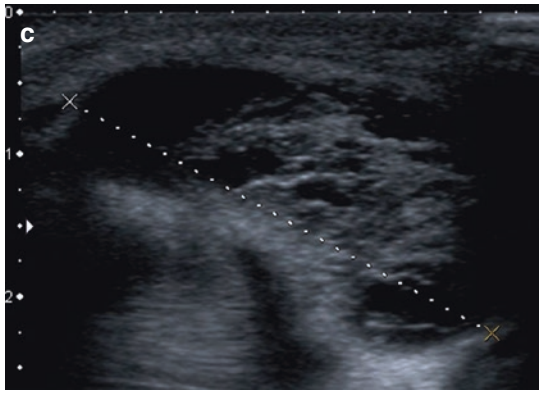

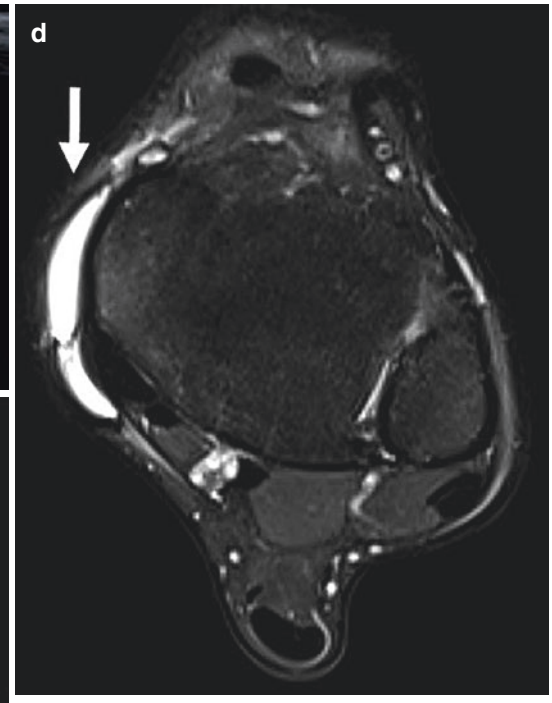

Fig. 20.15 (continued)

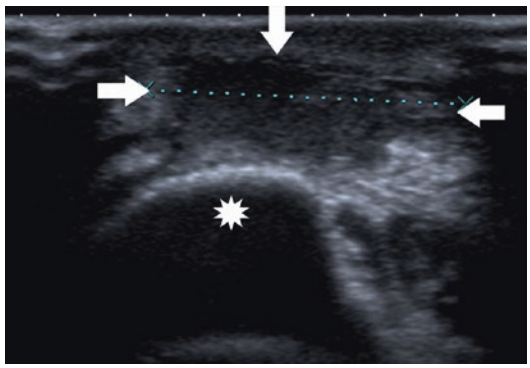

Fig. 20.16 Chronic frictional tennis bursitis olecrani. Axial ultrasound at the dorsal aspect of the olecranon process (*) of the elbow reveals a hypoechoic structure (*arrows*) containing echoic debris filling larger part of the bursal lumen

(Figs. 20.15b). Radiographs may also demonstrate signs of associated degenerative joint disease, osteoarthritis, rheumatoid arthritis, acetabular dysplasia, bone erosion, calcification, gas, or calcified loose bodies in a communicating cyst (Fig. 20.1c) [2].

Ultrasound Ultrasound is the imaging technique of choice to confirm the presence of a cyst and to allow for precise localization and extent of the cyst [76, 113]. Synovial cysts and ganglion cysts, although similar in many ways, display different histopathological characteristics justifying their descriptions as separate entities [28]. On US, it appears as anechoic masses (Figs. 20.1,

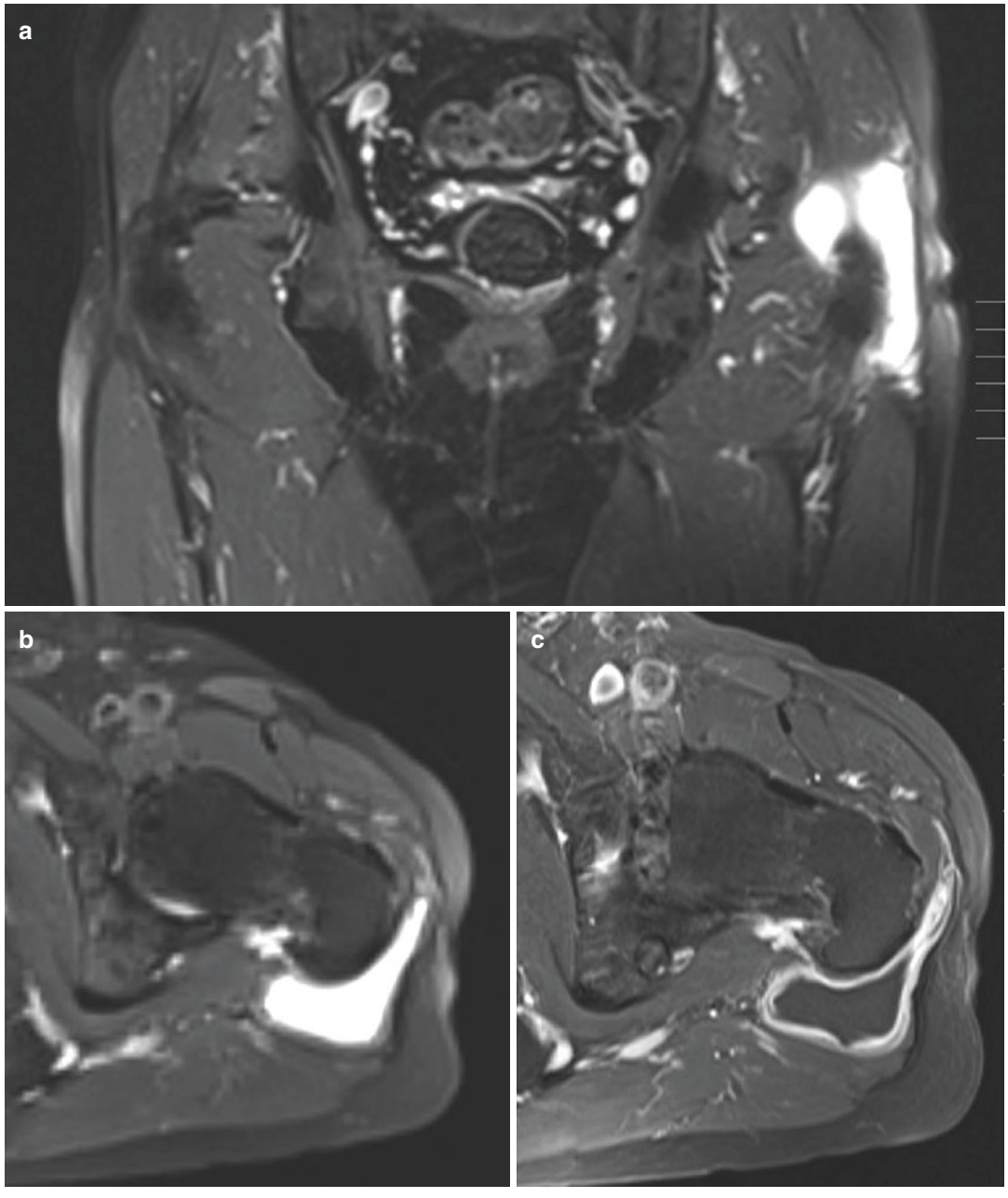

Fig. 20.17 (**a**–**c**) Chronic bursitis at the greater trochanter. (**a**) Coronal fat-suppressed proton density MR image; (**b**) axial fat-suppressed proton density MR image; (**c**) axial fat-suppressed T1-weighted MR image after intravenous administration of gadolinium contrast. On fat-suppressed proton density images, the lesion is of high signal intensity with clear demarcation from surrounding structures (**a**, **b**). There is peripheral enhancement of the wall of the lesion after contrast administration (**c**)

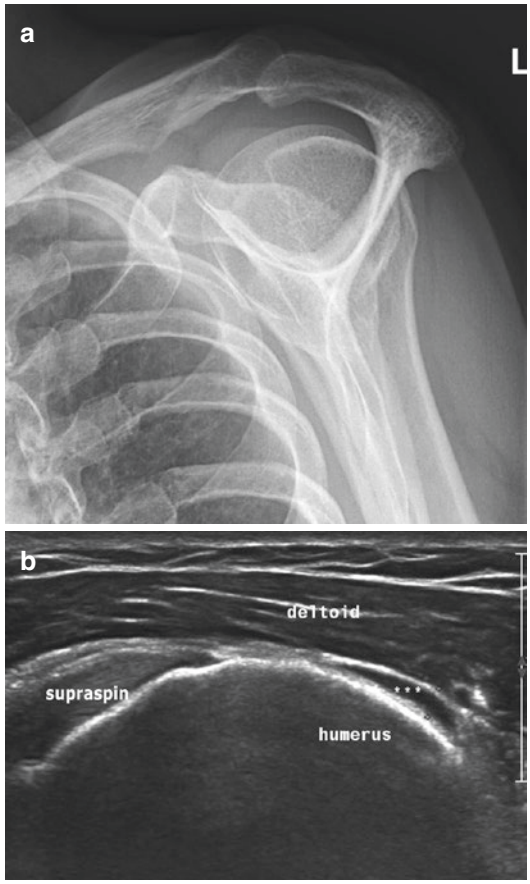

Fig. 20.18 (**a**, **b**) Subacromion–subdeltoid bursitis above the supraspinatus tendon in a 50-year-old female. (**a**) Radiography; (**b**) ultrasound. Radiography shows an acromion type III, predisposing for impingement (**a**). Ultrasound reveals well-delineated anechoic structure with thin wall (++) (**b**)

20.3, 20.7, 20.11 and 20.18) and may have a visible communication with a joint in 25 % of the cases [96] or tendon sheath [114]. The lesion may be multiloculated and may contain some fine internal septations. US is an accurate technique to define the cystic nature in superficial cysts around the wrist and the hand (Figs. 20.7 and 20.20), but it has limited ability to visualize deeper lying structures and their relationship with the adjacent joint [96]. Furthermore, cysts containing debris or hyperplastic synovium may simulate solid mass lesions on ultrasound examinations (Fig. 20.15c).

A normal bursa is not visualized on ultrasound or is seen only as a thin hypoechoic space or sac in a typical anatomical location. When a bursa is distended, it appears as a hypoechoic structure with well-defined margins and contents of variable echogenicity. The internal appearance varies according to the pathology. In a simple bursitis, there may be just anechoic fluid, with or without septa. In chronic bursitis due to impingement or overuse, more frequently there is bursal wall thickening (Fig. 20.16), with internal debris of variable echogenicity. The echogenic contents may even mimic a solid mass [96, 114] which is especially true for a bursitis de novo (Fig. 20.16).

CT Scan Due to its low soft tissue contrast, CT is of limited value in assessing soft tissue lesions. Para-articular cysts are of lower attenuation than muscle (Figs. 20.1 and 20.9) and of higher attenuation than fat. Rim enhancement is seen after intravenous contrast administration. A possible communication with the joint is sometimes difficult to define on axial images.

Arthrography/Direct Cyst Puncture Arthrography can be useful to demonstrate the communication of the cyst with the joint cavity [55]. However, cysts may fail to fill when the communication is very narrow or when the cyst is filled with highly viscous fluid. Joint communication can sometimes be demonstrated on delayed images (2 hours after the injection) [57].

MRI The technique of choice to confirm the cystic nature of the lesions is MR imaging. MR imaging can depict compartmental anatomy, exact location and extension of the cystic lesions, and its relationship to the joint and surrounding structures (Figs. 20.1, 20.5, 20.6, 20.8, 20.10, 20.11, 20.12, 20.13, 20.14, 20.15, 20.17, and 20.20). It is

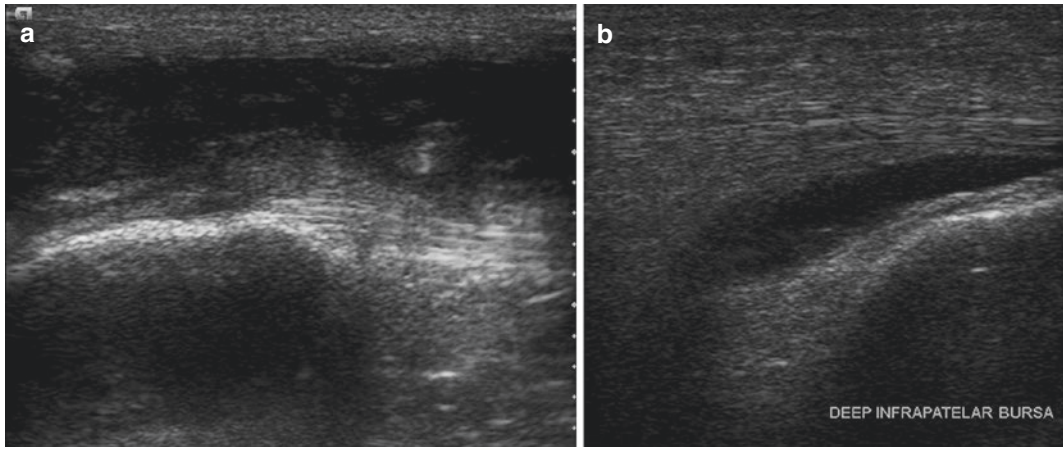

Fig. 20.19 (**a**, **b**) Chronic frictional prepatellar and infrapatellar bursitis in two different patients: (**a**) ultrasound longitudinal section of prepatellar bursa; (**b**) ultrasound longitudinal image of the deep infrapatellar bursa. In the first patient, a hypoechoic structure with thick irregular wall and internal hyperechoic debris is seen within subcutaneous tissue anterior to patella (hyperechoic cortex) and to the patellar tendon (typical lamellar striated appearance) (**a**). The irregular delineation may result from repetitive friction. In the second patient, a well-defined anechoic elliptical structure is seen between patellar tendon and tibia (**b**)

very accurate in depicting associated joint disorders, such as meniscal tears [39] (associated with meniscal cysts) (Fig. 20.10), labral tears (in case of a paralabral cyst [54, 62, 85, 98, 115]) (Figs. 20.11 and 20.12), ligamentous abnormalities, or inflammatory changes. Paralabral cysts of the hip, when labral tear is absent, should raise suspicion for other differential diagnoses such as atypical ganglion or synovial cyst, atypical presentation of synovitis, or possibly tumor [85].

The narrow neck connecting a popliteal cyst to the knee joint is usually identified on axial MRI images [8, 9], which is commonly found just below the proximal attachment of the medial head of the gastrocnemius [34]. Maximum intensity projections (MIP) of 3D acquisitions with fat saturation may be helpful to demonstrate the stalk communicating with the adjacent joint and allow visualization of "occult" connections not readily appreciated with standard MR imaging [91]. It was reported that using the vastly undersampled isotropic projection reconstruction (VIPR) pulse sequence more effectively can determine joint connections with typical and atypical ganglion cysts (around the knee) [1]. Using positional spine MRI, synovial juxtafacet cysts are depicted differently, with variation of the size according to patient position (slightly bigger in the extension (standing) position compared to the supine position) [70, 71].

The diagnosis of a cystic mass is usually straightforward by analysis of the signal intensities of the lesion. They are typically hypo- or isointense to muscle on T1-weighted images, especially if they contain protein-rich gelatinous substances, and homogeneously hyperintense on T2-weighted images. The cysts usually show subtle rim enhancement (Fig. 20.17) due to peripheral fibrovascular tissue in the cyst wall. However, there are some pitfalls. Atypical imaging presentations of popliteal cysts have been described as a cause of diagnostic difficulty [68], with atypical cyst content due to debris or hemorrhage. Chronic inflammation may cause marked thickening of the synovial membrane and, therefore, mimic a solid soft tissue mass. In case of a complex content due to intracystic debris or hemorrhage may simulate a neoplastic lesion. In those cases, typical location of the cyst and communication with the joint suggest the diagnosis [70]. Central enhancement should be regarded with caution, as this may indicate the presence of another well-delineated soft tissue lesion of high T2-weighted image signal,

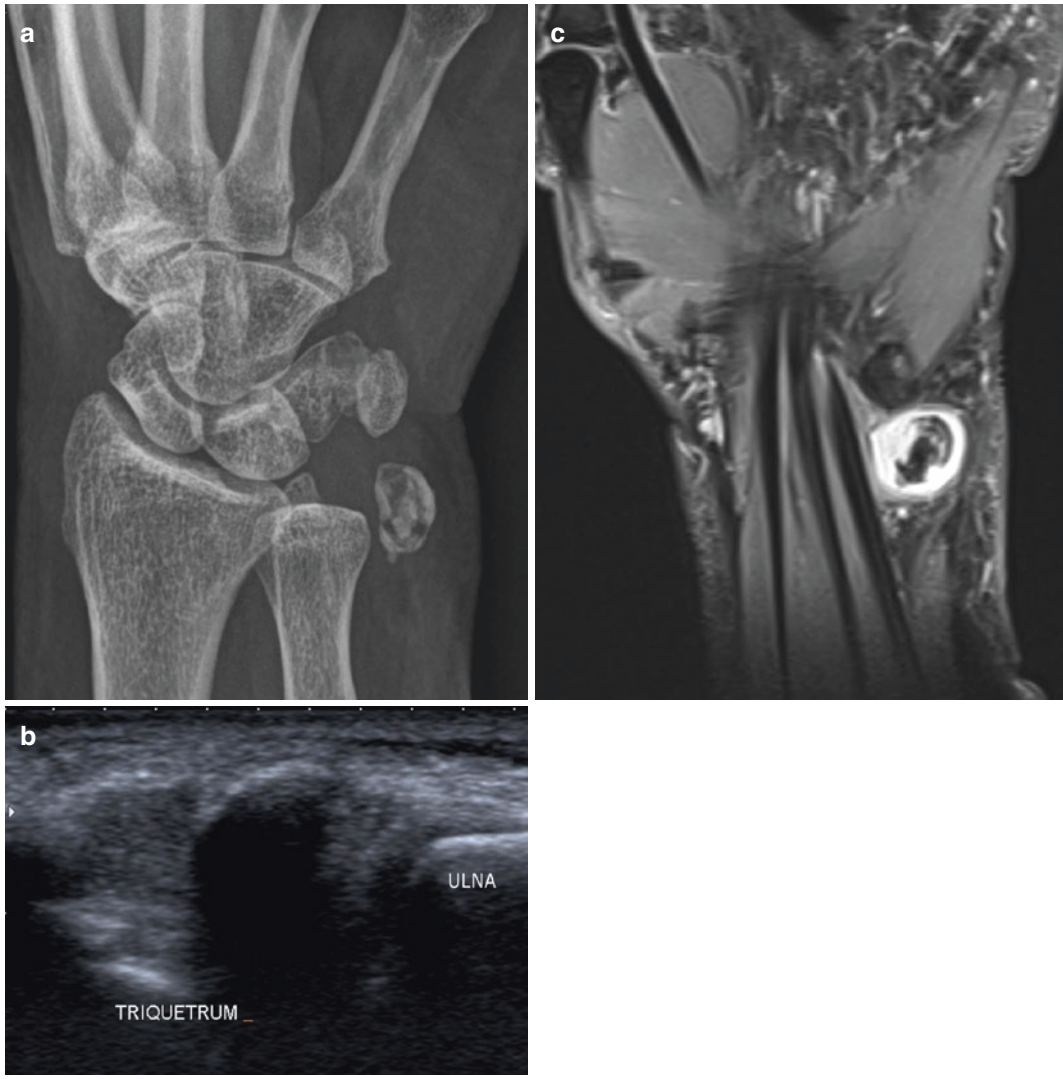

Fig. 20.20 (**a**–**c**) Secondary osteochondromatosis in a distended pisotriquetral recess in a 65-year-old female: (**a**) radiography; (**b**) longitudinal ultrasound; (**c**) coronal fat-suppressed T2-weighted MR image. Radiography shows a layered calcification within the soft tissue adjacent to the distal ulna and proximal to the pisiform bone (**a**). On longitudinal ultrasound, note a hyperreflective line with retro-acoustic shadowing suggesting a calcification, surrounded by a small amount of fluid (**b**). On fat-suppressed T2-weighted image, a low signal intensity calcification is seen within the pisotriquetral recess proximal to the pisiform bone (**c**)

such as myxoma, myxoid liposarcoma, hemangioma, and synovial sarcoma [24, 104].

A cruciate ligament ganglion may demonstrate the same signal intensity as a cruciate ligament tear and may simulate a false-positive diagnosis of cruciate ligament tear (Fig. 20.13).

Cystic lesions are well circumscribed, but may be lobulated, or multicystic with internal septa, or may have the "bunch of grapes" appearance [39] (Figs. 20.8 and 20.10). They may also contain intralesional debris or calcified loose bodies [66, 99] (Figs. 20.1 and 20.20) that may arise in the joint due to trauma, arthropathy, or synovial osteochondromatosis. Through the posterior joint–bursal communication, calcified loose body may pass into a popliteal cyst or may develop primarily in the cyst due to chondrometaplasia [20, 22]. Elevated pressure may cause cyst rupture

with leakage of synovial fluid. This is seen as high signal intensity edema in the adjacent soft tissues and fascial planes on fat-suppressed T2-weighted sequences. Ruptured cysts are irregularly delineated (Fig. 20.5) and must be differentiated from other soft tissue tumors and hemorrhagic or inflammatory lesions [63, 84].

20.2.2 Giant Cell Tumors and PVNS

According to the current WHO classification, these tumors will be discussed in Chap. 14.

20.2.3 Other Synovial Tumors and Tumor like Lesions

20.2.3.1 Synovial Chondromatosis and Synovial Chondrosarcoma

Synovial chondromatosis is characterized by metaplasia of the subsynovial connective tissue with subsequent cartilage formation. In rare cases, there is malignant degeneration into synovial chondrosarcoma. These entities are discussed in Chap. 24.

20.2.3.2 Synovial Hemangioma

Synovial hemangioma is a separate localization of a hemangiomatous tumor. Because it represents a vascular lesion and not a synovial tumor, this entity is discussed in Chap. 16.

20.2.3.3 Para-articular Chondroma

Para-articular chondroma is a very rare cartilaginous tumor arising from the capsule or the para-articular connective tissue of a joint. It is discussed in detail in Chap. 24.

20.2.3.4 Lipoma Arborescens

Lipoma arborescens consists of a lipoma-like lesion, consisting of hypertrophic synovial villi distended by fat that replaces the subsynovial tissue.

Lipoma arborescens is of unknown etiology, but it is frequently associated with degenerative joint disease, diabetes mellitus, chronic synovitis, or rheumatoid arthritis and joint trauma. Therefore, lipoma arborescens is usually regarded as a nonspecific reactive and secondary process to traumatic or inflammatory stimuli, involving the synovial membrane [82, 87]. Hallelet al. have suggested renaming this process as "villous lipomatous proliferation of synovial membrane," since "lipoma arborescens" implies a neoplastic connotation [32]. However, according to Vilanova [110], a minority of lipoma arborescens may appear in joints with no other associated changes, and these lesions could be categorized rather as primary lipoma arborescens [32].

The knee is the usual site of involvement, with a predilection for the suprapatellar pouch, although it may also affect the wrist, hip, shoulder, elbow, and ankle as well as in periarticular bursae and tendon sheaths [82, 106]. Although usually affecting one joint, polyarticular involvement or bilateral presentation may occur [87].

Lipoma arborescens has been observed in patients aged between 9 and 68 years, with equal predominance in men and women [82]. The clinical presentation consists of painless joint swelling over many years, following by progressive pain and intermittent episodes of joint effusion [82]. Plain radiographs are rarely diagnostic but may reveal radiolucent areas in an articular or periarticular soft tissue swelling [82]. Lipoma arborescens is displayed as a nonspecific synovially based lesion on ultrasound (Fig. 20.21a). Due to its soft consistency, dynamic compression

Fig. 20.21 (**a**–**f**) Lipoma arborescens in different patients, located at the elbow (**a**–**d**) and knee (**e**, **f**). (**a**) Longitudinal ultrasound; (**b**) axial T1-weighted MR image; (**c**–**d**) axial and sagittal fat-suppressed T2-weighted MR image; (**e**) sagittal fat-suppressed T2-weighted MR image; (**f**) sagittal T1-weighted MR image. On ultrasound of the elbow in patient 1, an echoic frond-like synovial proliferation is present surrounded by large joint effusion (**a**) On MRI, a frond-like synovial proliferation with similar signal intensity to that of the subcutaneous fat is seen on all pulse sequences (**b**–**d**). A similar morphology and signal intensity on MRI is seen in another patient with a lipoma arborescens of the knee. The lesion is located at the suprapatellar pouch, associated with large effusion (**e**, **f**)

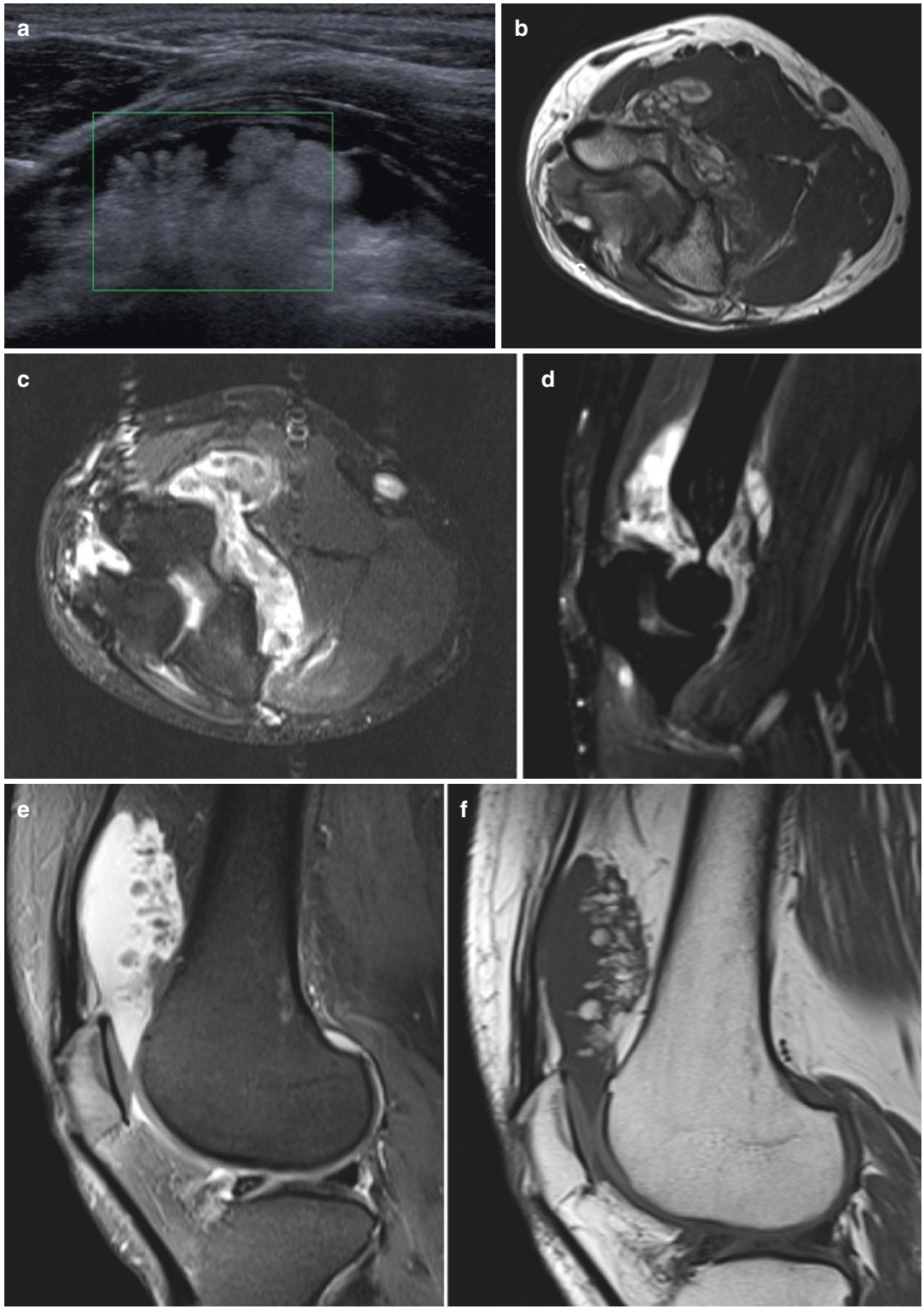
a
b
c
d
e
f

during ultrasound results in bending and deformation of the villous projections [82]. CT arthrography and MRI demonstrate a frond-like fatty mass within the joint associated with joint effusion (Fig. 20.21c–f). On MR, the villous proliferations display a signal intensity of fat on all pulse sequences contrasting with the increased fluid within the joint. The mass-like subsynovial fat deposits may be separated by low signal intensity septa on T1- and T2-weighted images. On contrast administration, although the hypertrophied subsynovial fatty tissue does not enhance, the overlying thickened synovium may display diffuse enhancement [82]. The differential diagnosis includes the synovial lipoma [77], PVNS (see Chap. 14), synovial chondromatosis (see Chap. 24), plexiform neurofibroma (see Chap. 17), and synovial hemangiomatosis (see Chap. 16) due to their identical clinical picture, but the differentiation is readily made by CT and especially by MRI. The absence of susceptibility artifact related to hemorrhagic products on gradient imaging differentiates this condition from PVNS [82] (see Chap. 14). The recommended treatment for lipoma arborescens is surgical or arthroscopic synovectomy.

20.3 Malignant Tumors Around the Joints

20.3.1 Synovial Sarcoma

As discussed earlier in the introduction of this chapter, synovial sarcoma is a misnomer. According to the most recent WHO classification (2013), this tumor will be discussed in Chap. 18 (Tumors of Uncertain Differentiation).

20.3.2 Metastatic Spread of Cancer

The metastatic spread of cancer to the joint and synovium is one of the rarest manifestations of malignant diseases, and involvement of more than one joint is exceptional. It is more commonly seen in patients with leukemia and other hematologic malignancies and is rarely reported in those with solid tumors [64]. MRI shows a combination of bone and joint involvement, with nonspecific signal behavior. The diagnosis can be confirmed by joint cytology and/or synovial biopsy.

Synovial involvement of a lymphoma will be discussed in the chapter of soft tissue lymphoma (Chap. 22).

Key Points

1. Cystic soft tissue lesions can be divided into four groups (synovial cyst, ganglion cyst, bursa de novo, and permanent bursa), based upon the combination of their anatomical location and histological composition.
2. The diagnosis of a cystic lesion is usually straightforward on ultrasound and/or MR imaging. If there is any doubt, however, on the true cystic nature of the lesion, gadolinium contrast administration should be performed to exclude a pseudocystic benign or malignant tumor.

References

1. Amrami KK, Desy NM, Stanley DW, Skinner JA, Felmlee JP, Barger AV, Block WF, Spinner RJ (2007) Evaluation of ganglion cysts using vastly undersampled isotropic projection reconstruction (VIPR). J Magn Reson Imaging 26(3):768–772
2. Ananthi Kumarasamy S, Kannadath BS, Soundamourthy S, Subramanian A, Sinhasan SP, Bhat RV (2014) Semimembranosus ganglion cyst. Anat Cell Biol 47:207–209
3. Andrikoula S, Vasiliadis H, Tokis A, Kosta P, Batistatou A, Georgoulis A (2007) Intra-articular ganglia of the knee joint associated with the anterior cruciate ligament: a report of 4 cases in 3 patients. Arthroscopy 23:800.e1–800.e6
4. Apostolaki E, Davies AM, Evans N, Cassar-Pullicino VN (2000) MR imaging of lumbar facet joint synovial cysts. Eur Radiol 10:615–623
5. Barland P, NovokoffAB HD (1962) Electron microscopy of the human synovial membrane. J Cell Biol 14:207
6. Beaman F, Peterson J (2007) MR imaging of cysts, ganglia, and bursae about the knee. Radiol Clin N Am 45:969–982

7. Beaman FD, Peterson JJ (2007) MR imaging of cysts, ganglia, and bursae about the knee. Magn Reson Imaging Clin N Am 15:39–52
8. Billières J, Lascombes P, Peter R (2014) Popliteal cysts: etiologic and therapeutic approach. Rev Med Suisse 10(432):1211–1215
9. Blankenbaker DG, De SAA, Keene JS (2006) Sonography of the iliopsoas tendon and injection of the iliopsoas bursa for diagnosis and management of the painful snapping hip. Skeletal Radiol 35:565–571
10. Botchu R, Esler CN, Lloyd DM, Rennie WJ (2013) Ganglia arising from the transverse acetabular ligament: a report of two cases. J Orthop Surg 21(3):380–382
11. Campbell SE, Sanders TG, Morrison WB (2001) MR imaging of meniscal cysts: incidence, location, and clinical significance. AJR Am J Roentgenol 177:409–413
12. Cao Y, Jones G, Han W, Antony B, Wang X, Cicuttini F, Ding C (2014) Popliteal cysts and subgastrocnemius bursitis are associated with knee symptoms and structural abnormalities in older adults: a cross-sectional study. Arthritis Res Ther 16:R59
13. Chang YM, Chan CP, Kung Wu SF, Hao SP, Chang LC (1997) Ganglion cyst and synovial cyst of the temporomandibular joint. Two case reports. Int J Oral Maxillofac Surg 26:179–181
14. Chatra PS (2012) Bursae around the knee joints. Indian J Radiol Imaging 22(1):27–30
15. Chen AC, Lee WC, Hsu KY, Chan YS, Yuan LJ, Chang CH (2010) Arthroscopic ganglionectomy through an intrafocal cystic portal for wrist ganglia. Arthroscopy 26:617–622
16. Christophis P, Asamoto S, Kuchelmeister K, Schachenmayr W (2007) "Juxtafacet cysts", a misleading name for cystic formations of mobile spine (CYFMOS). Eur Spine J 16:1499–1505
17. de Bruijn KMJ, Franssen G, van Ginhoven TM (2013) A stepwise approach to 'groin pain': a common symptom, an uncommon cause. BMJ Case Rep 16:2013
18. De Keersmaeker A, Peters B, Pilate I, Bosmans JL,Vanhoenacker FM (2016). Ongewone zwelling aan de binnenenkel bij een 17-jarige skater. Ortho-Rhumato 14(1):14–16
19. Deng DY, Yee K, Burkhalter W, Okimoto KC, Kon K, Kurahara DK (2014) An intra-articular ganglion cyst in a patient with juvenile idiopathic arthritis. Pediatric Rheumatol 12:14. doi:10.1186/1546-0096-12-14. eCollection 2014
20. Dhillon M, Prasad P, Goel A, Kar A (2009) Giant osteochondral body in a popliteal cyst. Indian J Orthop 43(1):93–96
21. Dressler F, Wermes C, Schirg E, Thon A (2008) Popliteal venous thrombosis in juvenile arthritis with Baker cysts: report of 3 cases. Pediatr Rheumatol Online J 6:12
22. El Andaloussi Y, Fnini S, Hachimi K, Ouarab M, Trafeh M (2006) Osteochondromatosis of a popliteal bursa. Joint Bone Spine 73:219–220
23. Fang CSJ, McCarthy CL, McNally EG (2004) Intramuscular dissection of Baker's cysts: report on three cases. Skeletal Radiol 33:367–371
24. Fletcher CDM, Bridge JA, Hogendoorn PCW, Mertens F (eds) (2013) WHO classification of tumours of soft tissue and bone. IARC Press, Lyon
25. Fritschy D, Fasel J, Imbert JC, Bianchi S, Verdonk R, Wirth CJ (2006) The popliteal cyst. Knee Surg Sports Traumatol Arthrosc 14:623–628
26. Frush TJ, Noyes FR (2015) Baker's cyst: diagnostic and surgical considerations. Sports Health 7(4):359–365
27. Ganau M, Ennas F, Bellisano G, Ganau L, Ambu R, Faa G, Maleci A (2013) Synovial cysts of the lumbar spine – pathological considerations and surgical strategy. Neurol Med Chir 53(2):95–102
28. Giard MC, Pineda C (2015) Ganglion cyst versus synovial cyst? Ultrasound characteristics through a review of the literature. Rheumatol Int 35(4): 597–605
29. Goldberg RP, Genant HK (1978) Calcified bodies in popliteal cysts: a characteristic radiographic appearance. AJR Am J Roentgenol 131:857–859
30. Guermazi A, Hayashi D, Roemer FW, Niu J, Yang M, Lynch JA, Torner JC, Lewis CE, Sack B, Felson DT, Nevitt MC (2010) Cyst-like lesions of the knee joint and their relation to incident knee pain and development of radiographic osteoarthritis: the MOST study. Osteoarthritis Cartilage 18(11):1386–1392
31. Guolong M, Zhi G, Yong H (2013) An intratendinous ganglion cyst causing impingement between the anterior cruciate ligament and anterior root of the medial meniscus: a case report. BMC Sport Sci Med Rehabil 5:22
32. Hallel T, Lew S, Bansal M (1988) Villous lipomatous proliferation of the synovial membrane (lipoma arborescens). J Bone Joint Surg 70A:264–270
33. Handy JR (2001) Popliteal cysts in adults: a review. Semin Arthritis Rheum 31:108–118
34. Hayashi D, Roemer FW, Dhina Z, Kwoh CK, Hannon MJ, Moore C, Guermazi A (2010) Longitudinal assessment of cyst-like lesions of the knee and their relation to radiographic osteoarthritis and MRI-detected effusion and synovitis in patients with knee pain. Arthritis Res Ther 12:R172
35. Heng-Kun W, Yan-Ling G, Wen-Feng Z, Zhe S, Ren-Xin W, Xiao-Tao Z (2014) Ganglion cyst of the temporomandibular joint. Rev Stomatol Chir Maxillofac Chir Orale 115:62–64
36. Herman AM, Marzo JM (2014) Popliteal cysts: a current review. Orthopedics 37(8):e678–e684
37. Hill CL, Gale DR, Chaisson CE, Skinner K, Kazis L, Gale ME, Felson DT (2003) Periarticular lesions detected on magnetic resonance imaging: prevalence in knees with and without symptoms. Arthritis Rheum 48(10):2836–2844
38. Hulet C, Souquet D, Alexandre P, Locker B, Beguin J, Vielpeau C (2004) Arthroscopic treatment of 105 lateral meniscal cysts with 5-year average follow-up. Arthroscopy 20(8):831–836
39. James SL, Connell DA, Bell J, Saifuddin A (2007) Ganglion cysts at the gastrocnemius origin: a series of ten cases. Skeletal Radiol 36:139–143

40. Janzen DL, Peterfy CG, Forbes JR, Tirman PFJ, Genant HK (1994) Cystic lesions around the knee joint: MR imaging findings. AJR Am J Roentgenol 163:155–161
41. Ji JH, Shafi M, Kim WY, Park SH, Cheon JO (2007) Compressive neuropathy of the tibial nerve and peroneal nerve by a Baker's cyst: case report. Knee 14(3):249–252
42. Kang CN, Kim DW, Kim DJ, Kim SJ (1999) Intra-articular ganglion cysts of the knee. Arthroscopy 15(4):373–378
43. Kang JH, Koh IH, Kim JS, Choi JR (2013) Coexisting intraarticular disorders are unrelated to outcomes after arthroscopic resection of dorsal wrist ganglions. Clin Orthop Relat Res 471:2212–2218
44. Kim SK, Park JM, Choi JE, Rhee SK, Shim SI (2010) Intratendinous ganglion cyst of the semimembranosus tendon. Br J Radiol 83:e79–e82
45. Klauser AS, Faschingbauer R, Bauer T, Wick MC, Gabl M, Arora R, Cotten A, Martinoli C, Jaschke WR (2010) Entrapment neuropathies II: carpal tunnel syndrome. Semin Musculoskelet Radiol 14(5):487–500
46. Kobayashi H, KotouraY HM, TsuboyamaT SH, Konishi J (1996) Periosteal ganglion of the tibia. Skelet Radiol 25:381–383
47. Krudwig WK, Schulte KK, Heinemann C (2004) Intra-articular ganglion cysts of the knee joint: a report of 85 cases and review of the literature. Knee Surg Sports Traumatol Arthrosc 12:123–129
48. Kusakabe T, Kasama F, Aizawa T, Sato T, Kokubun S (2006) Facet cyst in the lumbar spine: radiological and histopathological findings and possible pathogenesis. J Neurosurg Spine 5:398–403
49. Kwak KW, Kim MS, Chang CH, Kim SH (2011) Ulnar nerve compression in Guyon's canal by ganglion cyst. J Korean Neurosurg Soc 49:139–141
50. Ladak A, Spinner RJ, Amrami KK, Howe BM (2013) MRI findings in patients with tibial nerve compression near the knee. Skeletal Radiol 42(4):553–559
51. Legaye J, Lenfant P, Delos M (2004) Arthrosynovial cyst of the hip after total hip arthroplasty with a ceramic-on-ceramic interface. Rev Chir Orthop Reparatrice Appar Mot 90(5):475–478
52. Levien LJ, Benn CA (1998) Adventitial cystic disease: a unifying hypothesis. J Vasc Surg 28:193–205
53. Lunhao B, Yu S, Jiashi W (2011) Diagnosis and treatment of ganglion cysts of the cruciate ligaments. Arch Orthop Trauma Surg 131:1053–1057
54. Magee T, Hinson G (2000) Association of paralabral cysts with acetabular disorders. AJR Am J Roentgenol 174(5):1381–1384
55. Magerkurth O, Jacobson JA, Girish G, Brigido MK, Bedi A, Fessell D (2012) Paralabral cysts in the hip joint: findings at MR arthrography. Skeletal Radiol 41:1279–1285
56. Malghem J, Lebon C, Vandeberg B, Maldague B, Lecouvet F (2004) Les kystes mucoides atypiques. In: Laredo JD, Tomeni B, Malghem J et al (eds) Conduite a tenir devant une image osseuse ou des parties molles d'allure tumorale. Sauramps Medical, Montpellier, pp 363–376
57. Malghem J, Vande berg BC, Lebon C, Lecouvet FE, Maldague BE (1998) Ganglion cysts of the knee: articular communication revealed by delayed radiography and CT after arthrography. Am J Roentgenol 170:1579–1583
58. Marano AA, Therattil PJ, Ajibade DV, Datiashvili RO (2015) Ganglion cyst of the peroneus longus. Eplasty 15:ic20, eCollection
59. Marra MD, Crema MD, Chung M, Roemer FW, Hunter DJ, Zaim S, Diaz L, Guermazi A (2008) MRI features of cystic lesions around the knee. Knee 15:423–438
60. Maynou C, Mestdagh H, Butruille Y, Lecomte-Houcke M (1997) Compression of the ulnar nerve at the wrist due to an arthro-synovial cyst. Apropos of 2 cases. Ann Chir Main Memb Super 16(2):146–151
61. McCarthy CL, McNally EG (2004) The MRI appearance of cystic lesions around the knee. Skeletal Radiol 33:187–209
62. McCarthy JC, Noble PC, Schuck MR, Wright J, Lee J (2001) The watershed labral lesion: its relationship to early arthritis of the hip. J Arthroplasty 16(8 Suppl 1):81–87
63. Meredith DS, Losina E, Neumann G, Yoshioka H, Lang PK, Katz JN (2009) Empirical evaluation of the inter-relationship of articular elements involved in the pathoanatomy of knee osteoarthritis using magnetic resonance imaging. BMC Musculoskelet Disord 10:133
64. Metyas SK, LumCA RAS, Vaysburd M, Forrestier DM, Quismorio FP (2003) Inflammatory arthritis secondary to metastatic gastric cancer. J Rheumatol 30:2713–2715
65. Michaelides M, Papas S, Pantziara M, Ioannidis K (2014) High spatial resolution MRI of cystic adventitial disease of the iliofemoral vein communicating with the hip joint. Cardiovasc Intervent Radiol 37:271–274
66. Miller TT, Staron RB, Koenigsberg T, Levin TL, Feldman F (1996) MR imaging of Baker cysts: association with internal derangement, effusion and degenerative arthropathy. Radiology 201:247–250
67. Moretti B, Patella V, Mouhsine E, Pesce V, Spinarelli A, Garofalo R (2007) Multilobulated popliteal cyst after a failed total knee arthroplasty. Knee Surg Sports Traumatol Arthrosc 15(2):212–216
68. Nahra ME, Bucchieri JS (2011) Open and arthroscopic excision of ganglion cyst and related tumors. In: Wiesel SW (ed) Operative techniques in orthopaedic surgery, vol 3. Lippincott Williams & Wilkins p, Philadelphia, pp 3010–3021
69. Nahra ME, Bucchieri JS (2004) Ganglion cysts and other tumor related conditions of the hand and wrist. Hand Clin 20:249–260
70. Niggemann P, Grosskurth D, Beyer HK (2009) Pathomechanisms of spinal canal stenosis – upright MRI image gallery. Z Orthop Unfall 147:205–209
71. Niggemann P, Kuchta J, Hoeffer J, Grosskurth D, Beyer HK, Delank KS (2012) Juxtafacet cysts of the lumbar spine: a positional MRI study. Skeletal Radiol 41:313–320

72. Nikolopoulos I, Krinas G, Kipriadis D, Ilias A, Giannakopoulos A, Kalos S (2011) Large infrapatellar ganglionic cyst of the knee fat pad: a case report and review of the literature. J Med Case Reports 5:351
73. Nucci F, Artico M, Santoro A, Bardella L, Delfini R, Bosco S, Palma L (1990) Intraneural synovial cyst of the peroneal nerve: report of two cases and review of the literature. Neurosurgery 26:339–344
74. Oi K, Yoshida T, Shinohara N (2011) Rapid recurrence of cystic adventitial disease in femoral artery and an etiologic consideration for the cyst. J Vasc Surg 53:1702–1706
75. Okada K, Miyake J, Kataoka T, Moritomo H, Murase T, Yoshikawa H (2012) Median nerve neuropathy in the forearm due to recurrence of anterior wrist ganglion that originates from the scaphotrapezial joint: case report. J Brachial Plex Peripher Nerve Inj 7(1):1
76. Park HJ, Jeon YH, Rho MH, Lee EJ, Park NH, Park SI, Jo JH (2011) Incidental findings of the lumbar spine at MRI during herniated intervertebral disk disease evaluation. AJR Am J Roentgenol 196(5):1151–1155
77. Poorteman L, Declercq H, Natens P, Wetzels K, Vanhoenacker F (2015) Intra-articular synovial lipoma of the knee joint. BJR Case Rep. doi:http://dx.doi.org/10.1259/bjrcr.20150061
78. Rendon D, Pescador D, Cano C, Blanco J (2014) Intraneural ganglion cyst on the external popliteal nerve. BMJ Case Rep 2
79. Resnick D (1999) Ganglion. In: Petterson H, Allison D, Resnick D, Boutin RD, Andersson I (eds), The Encyclopaedia of medical imaging. Vol 3: Musculoskeletal and soft tissue imaging, NICER Institute, Oslo, p 176
80. Roth J, Scheer I, Kraft S, Keitzer R, Riebel T (2006) Uncommon synovial cysts in children. Eur J Pediatr 165(3):178–181
81. Sameshima T, Shibahashi K, Nozaki T, Akabane A, Kihara A, Horiuchi H, Morita A (2013) Atlantoaxial intraspinal juxtafacet cyst. Neurol Med Chir 53(2):125–128
82. Sanamandra SK, Ong KO (2014) Lipoma arborescens. Singapore Med J 55(1):5–11
83. Saremi H, Yavarikia A, Karbalaeikhani A (2014) Intra-articular ganglion cyst of the long head of the biceps tendon originating from the intertubercular groove. Arch Bone J Surg 2(3):232–233
84. Shahid KR, Hébert-Blouin MN, Amrami KK, Spinner RJ (2011) Extraneural rupture of intraneural ganglion cysts. J Surg Orthop Adv 20(2):136–141
85. Sherman PM, Matchette MW, Sanders TG, Parsons TW (2003) Acetabular paralabral cyst: an uncommon cause of sciatica. Skeletal Radiol 32(2):90–94
86. Shetty GM, Nha KW, Wang KH, Choi JY, Kim DH, Chae DJ (2009) Central popliteal mass due to communicating posterior cruciate ligament cyst: an indication for a combined approach. Arthroscopy 25(9):1051–1053
87. Soler T, Rodriguez E, Bargiela A, Da Riba M (1998) Lipoma arborescens of the knee: MR characteristics in 13 joints. J Comput Assist Tomogr 22:605–609
88. Spinner RJ, Atkinson JL, Scheithauer BW, Rock MG, Birch R, Kim TA, Kliot M, Kline DG, Tiel RL (2003) Peroneal intraneural ganglia: the importance of the articular branch. Clin Ser J Neurosurg 99:319–329
89. Spinner RJ, Atkinson JL, Tiel RL (2003) Peroneal intraneural ganglia: the importance of the articular branch. A unifying theory. J Neurosurg 99:330–343
90. Spinner RJ, Desy NM, Agarwal G et al (2013) Evidence to support that adventitial cysts, analogous to intraneural ganglion cysts, are also joint-connected. Clin Anat 26:267–281
91. Spinner RJ, Edwards PK, Amrami KK (2006) Application of three-dimensional rendering in joint-related ganglion cysts. Clin Anat 19(4):312–322
92. Spinner RJ, Hebert-Blouin MN, Maus TP, Atkinson JL, Desy NM, Amrami KK (2010) Evidence that atypical juxtafacet cysts are joint derived. J Neurosurg Spine 12:96–102
93. Spinner RJ, Scheithauer BW, Desy NM, Rock MG, Holdt FC, Amrami KK (2006) Coexisting secondary intraneural and vascular adventitial ganglion cysts of joint origin: a causal rather than a coincidental relationship supporting an articular theory. Skeletal Radiol 35(10):734–744
94. Spinner RJ, Wang H, Howe BM, Colbert SH, Amrami KK (2012) Deep ulnar intraneural ganglia in the palm. Acta Neurochir 154:1755–1763
95. Stein D, Cantlon M, Mackay B, Hoelscher C (2013) Cysts about the knee: evaluation and management. J Am Acad Orthop Surg 21(8):469–479
96. Teefey SA, Dahiya N, Middleton WD, Gelberman RH, Boyer MI (2008) Ganglia of the hand and wrist: a sonographic analysis. AJR Am J Roentgenol 191(3):716–720
97. Telischak NA, Wu JS, Eisenberg RL (2014) Cysts and cystic-appearing lesions of the knee: a pictorial essay. Indian J Radiol Imaging 24(2):182–191
98. Tirman PF, Feller JF, Janzen DL, Peterfy CG, Bergman AG (1994) Association of glenoid labral cysts with labral tears and glenohumeral instability: radiologic findings and clinical significance. Radiology 190(3):653–658
99. Torreggiani WC, Al-Ismail K, Munk PL, Roche C, Keogh C, Nicolaou S, Marchinkow LP (2002) The imaging spectrum of Baker's (popliteal) cysts. Clin Radiol 57:681–691
100. Traistaru R, Popecku R, Gruia C, Rogoveanu O (2013) A complex assessment of patients with knee osteoarthritis and Baker's cyst: observational study. Rom J Morphol Embryol 54(3):593–601
101. Tschirch FTC, Schmid MR, Pfirrmann CWA, Romero J, Hodler J, Zanetti M (2003) Prevalence and size of meniscal cysts, ganglionic cyst, synovial cysts of the popliteal space, fluid-filled bursae, and other fluid collections in asymptomatic knees on MR imaging. AJR Am J Roentgenol 180:1431–1436
102. Underwood JCE, Hunter J (2004) Underwood JCE general and systemic aethology. Churchill Livingstone, Edinburgh

103. Vandevenne JE, Vanhoenacker F, Hauben E, De Schepper AM (1997) Nosologie des kystes para-articulaires. In: Bard H, Drapé JL, Goutallier D, Laredo JD (eds) Le genou traumatiqueet dégéneratif. Sauramps Médical, Montpellier, pp 293–303
104. Vanhoenacker FM, Van de Perre S, De Vuyst D, De SAM (2003) Proceeding of the meeting of the KBVR-SRBR Osteo-articular section Brussels, June 21, 2003. Cystic lesions around the knee. JBR-BTR 86:302–304
105. Vanhoenacker FM, Vandevenne JE, De Schepper AM, De Leersnijder J (2000) Letter to the editor. Regarding "adventitial cystic disease: a unifying hypothesis". J Vasc Surg 31:621–622
106. Vanhoenacker FM, Verstraete KL (2015) Soft tissue tumors about the shoulder. Semin Musculoskelet Radiol 9(3):284–299
107. Van Holsbeeck M, Introcaso JH (2001) Sonography of bursae. In: Van Holsbeeck M, Introcaso JH (eds) Musculoskeletal ultrasound, 2nd edn. Mosby, St Louis, pp 131–169
108. Vasilevska V, Szeimies U, Staebler A (2008) MRI diagnosis of Baker cyst and significance of associated medial compartment knee osteoarthritis. Radiol Oncol 42(2):51–58
109. Vasilevska Violeta (2009) Assessment of radiological staging and histopathological correlation in management of musculoskeletal soft tissue tumors. Doctoral thesis Medical Faculty, University Ss.Cyril and Methodius, Skopje, Macedonia. pp 90–91
110. Vilanova JC, Barcelo J, Villalon M, Aldoma J, Delgado E, Zapater I (2003) MR imaging of lipoma arborescens and the associated lesions. Skeletal Radiol 32:504–509
111. Vilchez F, Erquicia J, Pelfort X, Monllau JC (2009) Symptomatic ganglions in the knee joint. Report of three cases and literature review. Acta Ortop Mex 23(4):223–227
112. Weyns F, Bringmans T, Vandevenne J, Daenekindt T, Van Goethem A, Wuyts J, Vanormelingen L, Vandersteen M (2012) Peripheral neuropathy caused by joint-related cysts: a review of 17 cases. Acta Neurochir 154(10):1741–1753
113. Ward EE, Jacobson JA, Fessel DP, Hayes CW, Van Holsbeeck M (2001) Sonographic detection of Baker's cysts: comparison with MR imaging. AJR Am J Roentgenol 176:373–380
114. Wang SC, Chhem RK, Cardinal E, Cho KH (1999) Joint sonography. Radiol Clin North Am 37:653–668
115. Yukata K, Nakai S, Goto T, Ikeda Y, Shimaoka Y, Yamanaka I, Sairyo K, Hamawaki J (2015) Cystic lesion around the hip joint. World J Orthop 6(9):688–704

Pseudotumoral Lesions

21

Filip M. Vanhoenacker, Meriem Mechri Rekik, and Rodrigo Salgado

Contents

21.1 **Introduction** 523

21.2 **Clinical Behavior and Imaging** 524
21.2.1 Normal Anatomy Variations and Muscular Anomalies 524
21.2.2 Inflammatory and Infectious Lesions 527
21.2.3 Traumatic Nerve Lesions Presenting as a Soft Tissue Mass 541
21.2.4 Other Posttraumatic Lesions 545
21.2.5 Skin Lesions 554
21.2.6 Metabolic Lesions 556
21.2.7 Vascular Lesions 562
21.2.8 Miscellaneous 563

21.3 **Conclusion and Diagnostic Strategy** 568

References 568

F.M. Vanhoenacker (✉) • R. Salgado
University Hospital Antwerp,
Department of Radiology, Wilrijkstraat, 10,
B-2650 Edegem, Belgium

General Hospital Sint-Maarten Duffel-Mechelen,
Rooienberg 25, B-2570 Duffel, Belgium

Faculty of Medicine and Health Sciences,
University of Ghent, Ghent, Belgium
e-mail: filip.vanhoenacker@telenet.be

M.M. Rekik
Institut d'orthopédie Mohamed Kassab,
Ksar Said, Tunisie

21.1 Introduction

Tumorlike soft tissue lesions are a common clinical problem. Their etiology is very broad ranging from pure anatomic variants over posttraumatic events to metabolic conditions and many other origins. A common feature of many of these lesions is the fact that they are mostly reactive in nature. Several of these conditions are self-limiting, or do not require significant intervention.

Although it is possible to estimate the incidence of true soft tissue tumors, it is more difficult to estimate the incidence of pseudotumors and this for several reasons. First, many patients often do not seek medical advice for benign lesions or for normal anatomic variants. Moreover, many radiologists are not familiar with the spectrum of non-tumoral masses, as such adding to the confusion between these pseudotumoral processes and a "true" tumoral process. As a consequence, in a significant number of instances, these pseudotumoral masses require a biopsy for a definite diagnosis.

In this chapter, we will discuss infectious and inflammatory pseudotumoral lesions, hematomas, and gout, as well as normal variants and vascular lesions which may simulate tumoral disease. Other pseudotumoral pathology such as ganglion and synovial cysts (see Chap. 20) and lipoma arborescens (see Chaps. 12 and 20) will be discussed in other chapters of this book.

© Springer International Publishing AG 2017

F.M. Vanhoenacker et al. (eds.), *Imaging of Soft Tissue Tumors*, DOI 10.1007/978-3-319-46679-8_21

21.2 Clinical Behavior and Imaging

21.2.1 Normal Anatomy Variations and Muscular Anomalies

Variations in muscular anatomy can simulate a soft tissue tumor, causing unnecessary surgery [175]. Muscular anomalies or variants reported in the upper limbs include accessory palmaris longus muscle (Fig. 21.1), duplication of the hypothenar muscle, anomalous extensor indicis and extensor digitorum brevis muscles, and Langer's axillary arch [175].

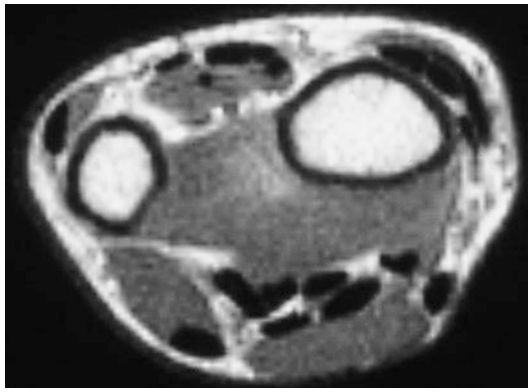

Fig. 21.1 Accessory palmaris longus muscle in a 15-year-old boy. Axial T1-weighted MR image after gadolinium contrast injection. The MR image reveals an additional mass, located superficially of the flexor digitorum tendons, with similar MR characteristics as normal skeletal muscle

In the lower extremities, anatomic variants occur almost exclusively in the soleus muscle [52]. Though present from birth, an accessory soleus muscle usually manifests in the late adolescent age because of muscle hypertrophy secondary to increased physical activity, especially in athletes [139]. It arises either from the anterior surface of the soleus muscle or from the soleal line of the tibia and fibula and appears as a soft tissue mass between the medial malleolus and the Achilles tendon [52, 139]. Up to 25 % of patients may present with an asymptomatic soft tissue swelling medial to the os calcaneus [139] (Fig. 21.2). Symptoms, when present, have been attributed to closed compartment ischemia and are accentuated by exercise [52].

Herniation of muscle through fascial planes can also mimic a tumor. It can be found in athletes, soldiers, or other professions requiring great strains on the legs. Most of the herniations have a constitutional origin, where muscle strain or hypertrophy leads to rupture of fascia on specific constitutional weaker locations [118]. The anterior tibial compartment is a common location for muscle herniations, where the herniation is palpable as a soft tissue mass [85]. Herniation of

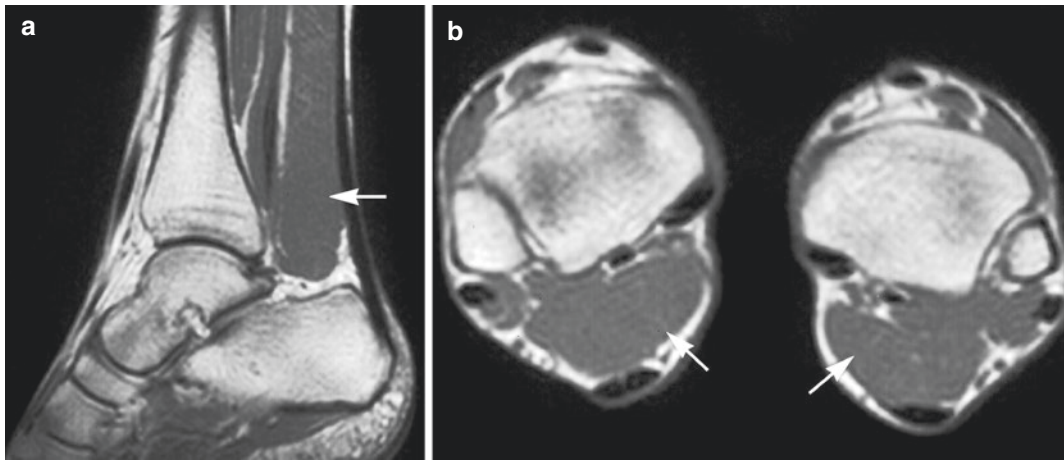

Fig. 21.2 Accessory soleus muscle in an adult man: (**a**) sagittal spin echo T1-weighted MR image; (**b**) axial spin echo T1-weighted MR image. There is a muscle belly within Kager's fat triangle, anterior to the Achilles tendon (*arrows*). Signal intensity and bilateral presentation of abnormality are in favor of accessory soleus muscle

the m. extensor digitorum longus, m. peroneus longus and brevis, and m. gastrocnemius is also possible [118]. This can be asymptomatic, but also more prominent after exercise [81, 118]. Herniations can be multiple and bilateral [27] (Fig. 21.3).

The diagnosis of a muscular anomaly is mainly based on knowledge of the most common locations and the aspect of the lesion on imaging. Both anatomy variations and muscle herniations can be depicted with ultrasound, where the suspicious mass is identified as having the same ultrasound appearance as normal muscular tissue. The ability of dynamic evaluation further increases the diagnostic accuracy. As expected, the signal characteristics on MR imaging of these lesions

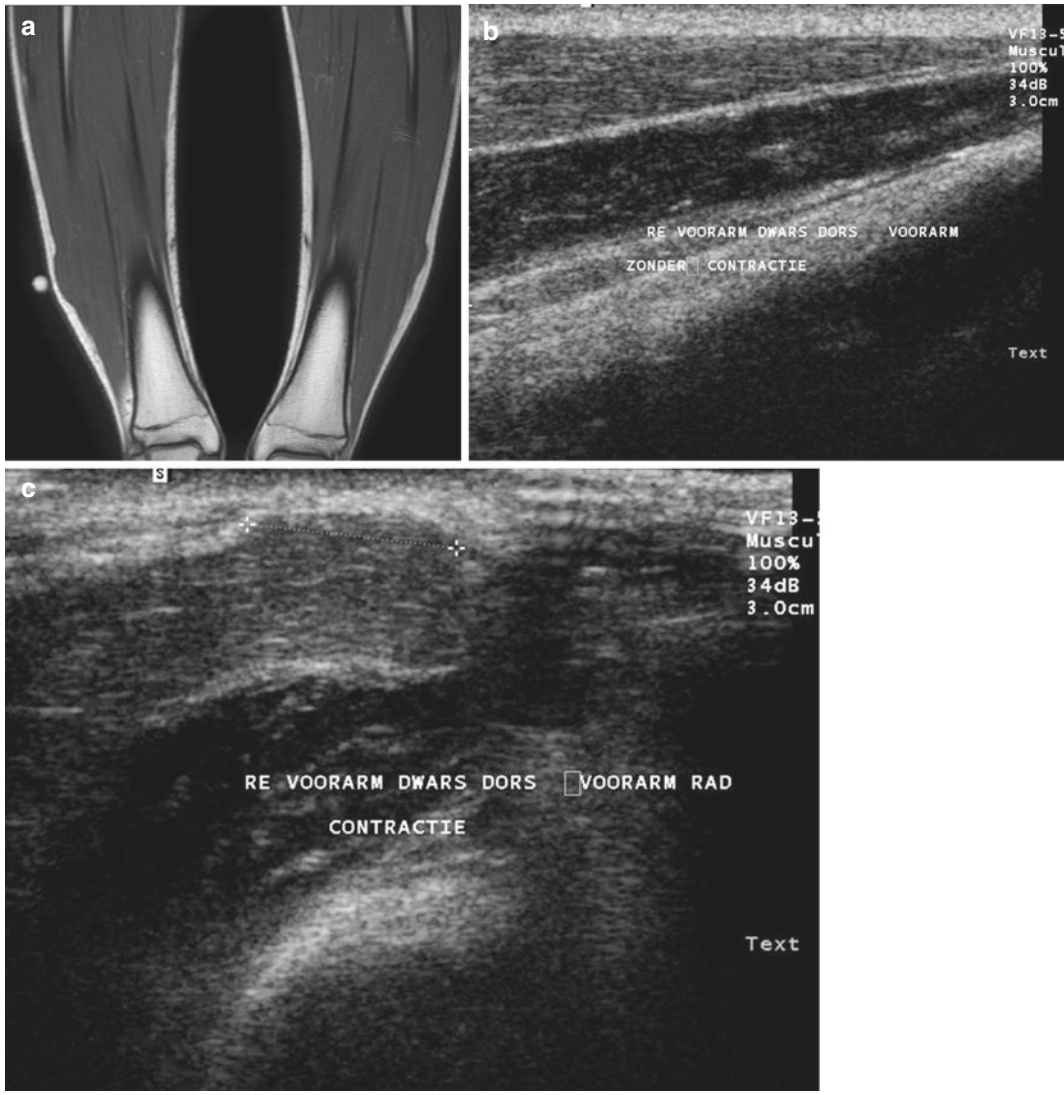

Fig. 21.3 Muscle herniation in two different patients. (**a**) Long-standing bilateral muscle herniation in a 15-year-old male: a coronal spin echo T1-weighted MR image. A focal bulging of the peroneus muscle compartment is seen, more pronounced on the right side. As expected, this protruding mass has the same signal characteristics of normal muscle tissue (**b**, **c**). Ultrasound of the forearm without (**b**) and with muscle contraction (**c**) in another patient. Note the presence of a mushroom-shaped lesion bulging through a focal defect in the superficial fascia. The lesion is only visible with muscle contraction (**c**)

are identical to skeletal muscle on all pulse sequences, as long as there is no adjacent edema or contusion. When in doubt, a dynamic MR examination with forced dorsiflexion and plantar flexion of the ankle allows a better evaluation of the changes in shape and size of a muscle herniation [27, 118]. MR imaging of the fascial defect is possible but difficult.

Other anomalies such as an accessory breast or nipple may mimic a soft tissue tumor (Fig. 21.4).

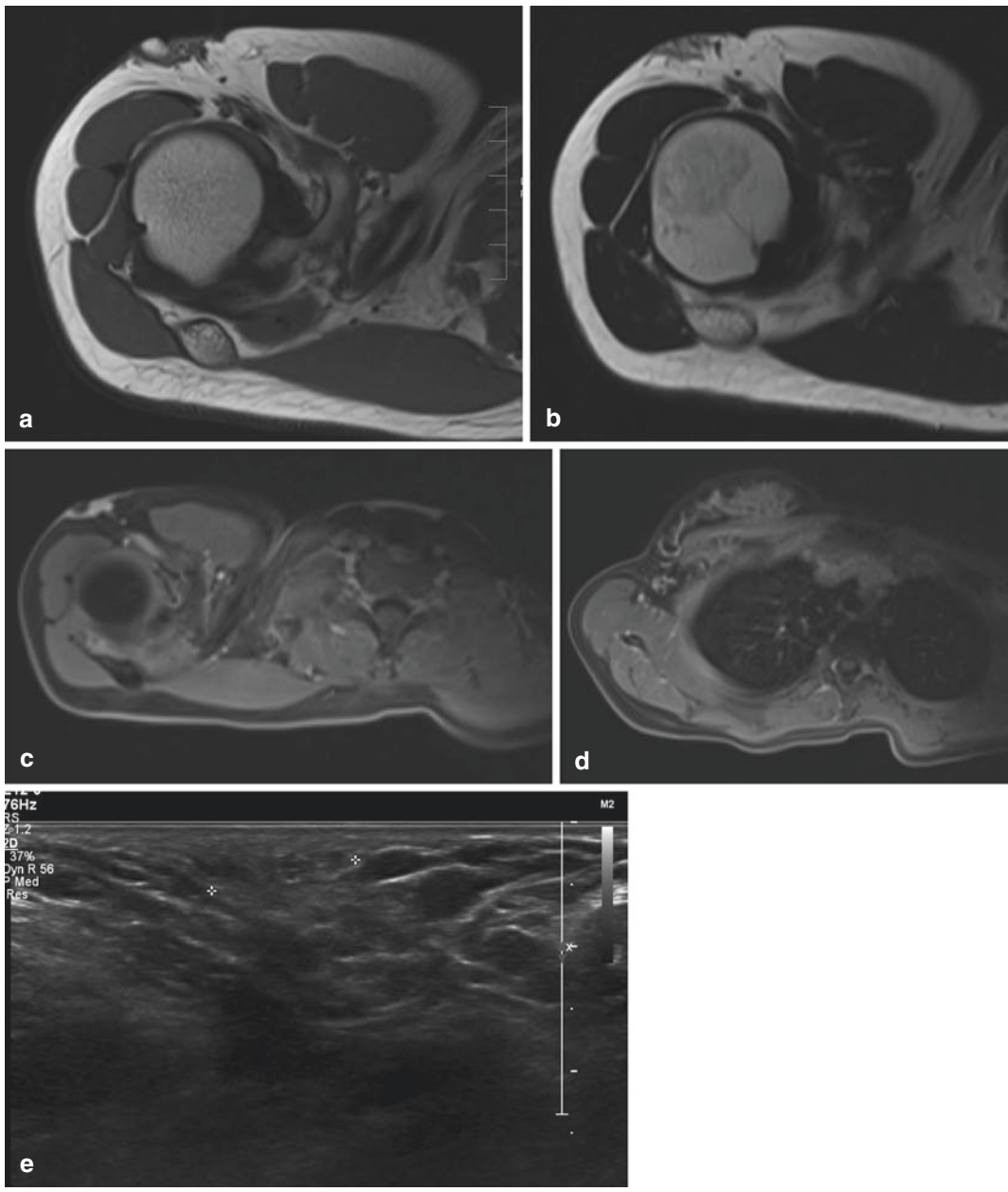

Fig. 21.4 Accessory breast in a 21-year-old female with a palpable swelling in the right axilla. The lesions enlarge and are slightly painful in the second half of the menstrual cycle: (**a**) axial T1-weighted MR image; (**b**) axial T2-weighted MR image. (**c**, **d**) Axial FS T1-WI MR image before (**c**) and after intravenous injection of gadolinium contrast (**d**). Presence of a small soft tissue "mass" ventrolateral in the right axilla on both pulse sequences, with signal intensities comparable to the signal intensity of normal adjacent breast. The lesion enhances similarly as breast tissue (**d**) Ultrasound (**e**) shows an echotexture similar as breast tissue

It is usually present along the primitive milk line above or below the normal breast location and is the most frequently encountered congenital anomaly of the breast [103]. Other more rare locations include the axilla, scapula, thigh, and vulva [102], since the primitive milk line extends from the axilla to the groin. Patients with accessory breast tissue may be asymptomatic or may present with swelling and pain. As accessory breast tissue is subject to the same spectrum of physiological changes and pathological processes as proper breast tissue it may therefore come to attention during menarche, pregnancy, lactation, or in case of benign and malignant breast disease [46, 67].

21.2.2 Inflammatory and Infectious Lesions

21.2.2.1 Cellulitis

Acute infectious cellulitis is an infection of the subcutaneous fat not extending beyond the superficial fascial planes (Fig. 21.5). It is usually associated with a hemolytic group A *Streptococcus* infection. Cellulitis will only on rare occasions present as a soft tissue mass [174]. An association with abscesses, ascending lymphangitis, regional lymphadenitis, osteomyelitis, and pyoarthrosis is possible [79]. Lymphedema may mimic infectious cellulitis; but the latter is more localized than lymphedema, which tends to affect the entire extremity.

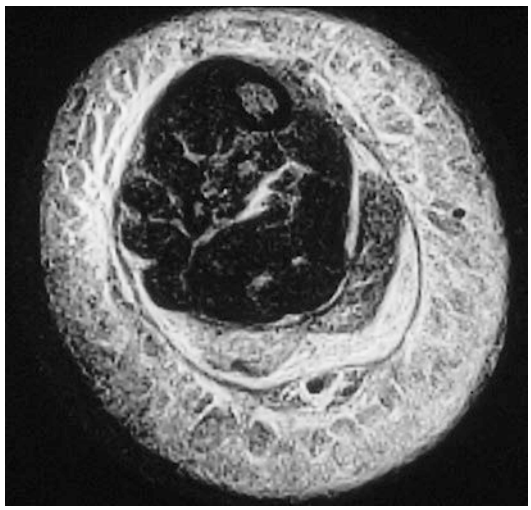

Fig. 21.5 A 24-year-old woman with an infection of the lower leg. Axial turbo spin echo T2-weighted MR image. Thickening of the skin and subcutaneous fat, with multiple septations of high signal intensity, corresponding to edema/cellulitis. The gastrocnemius muscle also has an abnormal signal intensity and appears atrophic

CT shows diffuse infiltration of the subcutaneous fat and thickening of the skin. On MRI, cellulitis appears as an ill-defined area, hypointense on T1-weighted sequences and hyperintense on T2-weighted sequences [150]. Cellulitis may be diagnosed when T2-weighted images reveal subcutaneous thickening with fluid collections and when subcutaneous tissue, superficial fascia, or both show contrast enhancement [165]. The depth of soft tissue involvement of the infection can be best evaluated on T2-weighted images [150]. However, as the sensitivity of magnetic resonance imaging exceeds the specificity, the extent of the deep fascial involvement can be overestimated [165], leading to the wrong diagnosis of necrotizing fasciitis.

21.2.2.2 Necrotizing Fasciitis

Necrotizing fasciitis is a rare soft tissue infection, involving deep fascial planes. It has a predilection for older patients, especially for those with malignancy, poor nutrition, and alcohol or drug abuse. It can also be found after trauma, or around foreign bodies in surgical wounds. However, it is important to remember that it can also appear in otherwise healthy subjects with no known risk factors. Early recognition is critical, since this entity is a surgical emergency. The clinical course can be fulminant and the mortality rate can be as high as 73 % [150]. The causative organisms are mostly group A hemolytic *Streptococcus* and *Staphylococcus aureus*, on occasion acting in synergy. Other both aerobic and anaerobic pathogens may also be involved [34].

Necrotizing fasciitis has similar signal behavior on MR as cellulitis, except for a deeper extension. A hyperintense signal on T2-weighted images in deep fasciae with fluid collections, thickening, and peripheral enhancement after intravenous contrast medium injection suggests necrotizing fasciitis [165]. However, this is not typical for necrotizing soft tissue infection, as other non-necrotizing conditions can have similar MR signal characteristics [112]. Therefore, clinical correlation is of utmost importance [34].

21.2.2.3 Lymphedema and Lymphangitis

Lymphedema is classified as primary or secondary lymphedema. The primary form is more common in children and is associated with a variety of hereditary or genetic syndromes [194]. Secondary lymphedema has no age preference. Local causes include trauma, surgery, infection, chronic inflammation, and radiotherapy (Fig. 21.6). It can also be associated with systemic disease, with a more generalized edema. Secondary lymphedema is usually a clinical diagnosis.

MRI of chronic lymphedema reveals deformity of lymphatics at different tissue levels [107]. In the subcutaneous tissue, it shows a diffuse edema or a honeycomb pattern consistent with reticular lymphangiectasia and "lakes" with increased signal intensity on T2-weighted images [107].

(MR) lymphography and lymphoscintigraphy can give additional information on lymphatic morphology and function [123, 194].

21.2.2.4 Abscess

A soft tissue abscess is a well-delineated fluid collection surrounded by a well-vascularized fibrous pseudocapsule. It can present as a soft tissue mass without a suggestive history or symptoms [85], and the radiologist must therefore always consider a possible infectious origin of a mass with undetermined characteristics. In one-third of cases, abscesses are multiple [85]. Associated inflammation is possible, distorting normal muscle anatomy and fascial planes [16]. Depending on the causal organism and degree of inflammation, the margins of an abscess can be well-defined or infiltrating.

Conventional radiography has little value, unless there is gas development within the abscess (Fig. 21.7). Ultrasound shows an elongated or lobulated fluid collection, which may show peripheral vascularity on color Doppler (Fig. 21.8). In case of intralesional gas, dirty shadowing may be present (Fig. 21.9). It is also useful in guiding an aspiration biopsy or percutaneous catheter drainage.

On MR imaging, an abscess is hypointense to isointense relative to muscle tissue on T1-weighted images. On T2-weighted images, the central portion of the abscess is usually hyperintense, but the capsule may display an isointense or hypointense signal intensity relative to subcutaneous fat [85]. On T1-weighted images, the pseudocapsule can have a variable signal intensity compared to skeletal muscle. After

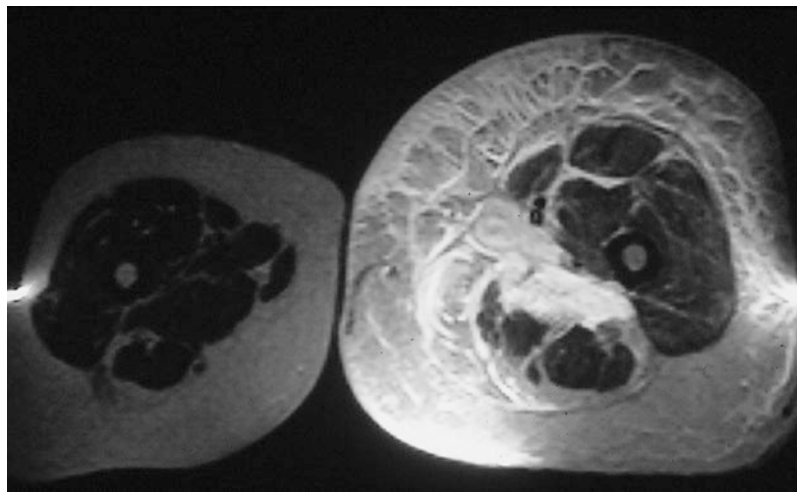

Fig. 21.6 Lymphedema of the left upper leg in a 48-year-old woman, with a history of vulval carcinoma treated with surgery and radio- and chemotherapy. Axial turbo spin echo T2-weighted MR image. There is an important thickening of the subcutaneous fat secondary to lymphedema, probably as a consequence of the intrapelvic surgery. Note the important increase in volume of the left thigh compared with the contralateral leg. An inflammation of the left adductor muscles can also be seen

Fig. 21.7 Gas gangrene of the upper arm in a young man. Plain radiograph. Presence of a soft tissue swelling with intralesional air collection and an air-fluid level, indicating soft tissue abscess

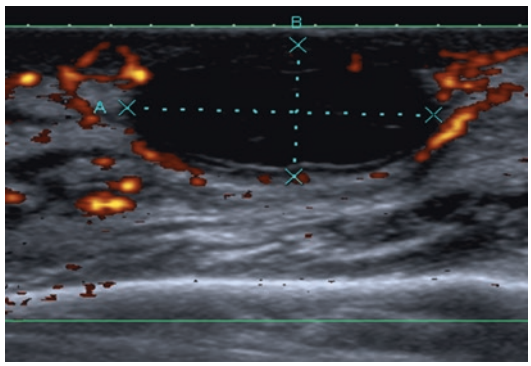

Fig. 21.8 Soft tissue abscess. Ultrasound shows a hypoechogenic collection with peripheral color Doppler signal

intravenous contrast medium injection, a peripheral rim of enhancement is seen, corresponding to the inflammatory and cellular component of the abscess (Fig. 21.10). Enhancement after intravenous contrast medium injection can also be absent [85].

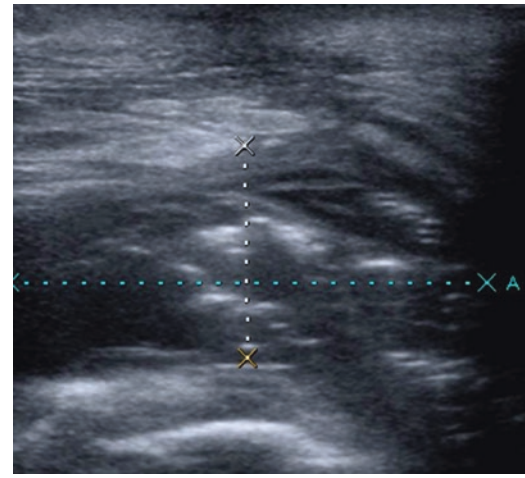

Fig. 21.9 Intramuscular abscess. Ultrasound shows a hypoechogenic collection intralesional dirty shadowing in keeping with gas bubbles

A variable degree of peripheral edema in muscle and subcutaneous tissue can be seen, displaying a hyperintense signal intensity on T2-weighted images. Inhomogeneity on T2-weighted sequences may be a consequence of intralesional gas bubbles and/or necrotic material [190].

The described signal characteristics can be different in an immunocompromised host [85]. The peripheral edema usually seen on T2-weighted images is sometimes absent. Similarly, T1-weighted images will not always show the pseudocapsule. The infected fluid in the center of the abscess can have an inhomogeneous signal intensity [9]. If the content is sufficiently viscous, it can even show mild increased signal intensity on T1-weighted images [21]. In the proximity of bone, a soft tissue abscess is often associated with osteomyelitis or a periosteal reaction (Fig. 21.11).

21.2.2.5 Pyomyositis

Pyomyositis, also called bacterial myositis, is a rare cause of single or multiple abscesses of skeletal muscle of unknown etiology. It was initially mainly found in tropical regions where lack of footwear, insect bites, and minor trauma, if

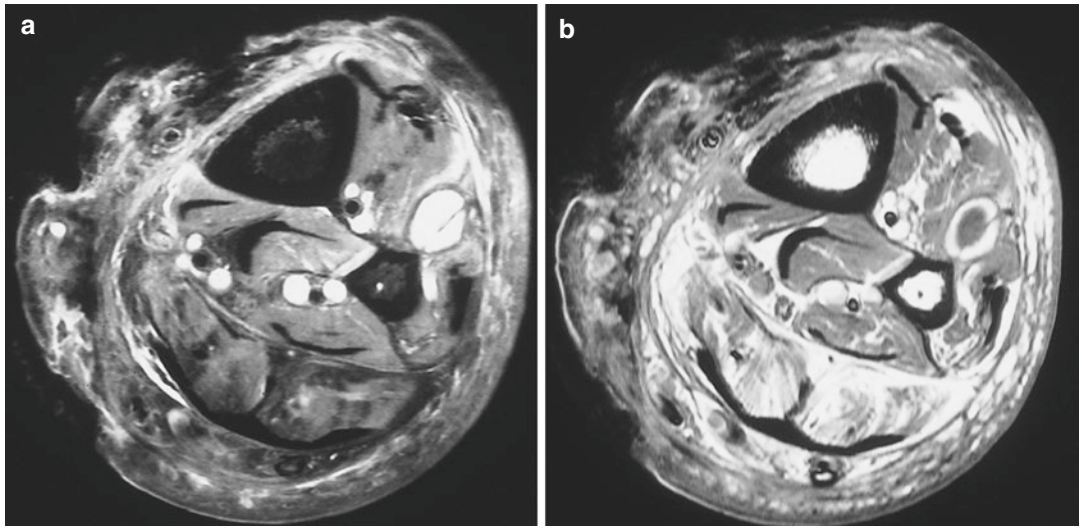

Fig. 21.10 A 65-year-old man with untreated diabetes mellitus: (**a**) axial proton density-weighted MR image with fat suppression; (**b**) axial spin echo T1-weighted MR image after gadolinium contrast administration. Besides a diffuse cellulitis and lymphedema, the images also reveal a fluid collection, located in the lower leg between the extensor digitorum and tibialis anterior muscles, with spontaneous high signal intensity on the proton density images (**a**). After contrast administration a peripheral enhancement can be seen, corresponding to granulation tissue at the periphery of a soft tissue abscess (**b**)

untreated, may lead to pyomyositis. Diabetes, HIV infection, and malignancy can, as immune-compromising conditions, however, also predispose to pyomyositis [35, 90, 144, 147], as such contributing to an increased incidence of this disease in industrialized regions with a more temperate climate. It is considered one of the most common musculoskeletal complications of AIDS [144, 154]. In 70–90 % of cases, the infection is caused by *Staphylococcus aureus* [35, 90, 144, 147]. Other pathogens such as *Streptococcus pyogenes*, *Mycobacterium tuberculosis*, *Mycobacterium avium-intracellulare*, *Nocardia asteroides*, *Cryptococcus neoformans*, and *Toxoplasma*, *Salmonella*, and *Microsporidia* species have also been reported [195].

In general, normal skeletal muscle has a high intrinsic resistance to bacterial infection and abscess formation. Therefore, some authors suggest that underlying muscle damage may facilitate the onset of pyomyositis. This is supported by the presence of previous trauma to the affected muscles in 20–50 % of cases [35, 72].

The clinical course of disease can be divided into three stages [39]. The first stage or invasive phase occurs during the first 2 or 3 weeks after infection, with subacute presentation such as local swelling, mild pain, variable fever, and anorexia. Diagnosis in this stage is difficult due to multiple differential diagnoses. During the second or suppurative phase, definitive abscess and pus are clearly evident. High fever, chills, local tenderness, swelling, and myalgia are frequent findings. It should be noted that local erythema and regional adenitis are usually absent in pyomyositis [45]. Aspiration of the lesion at this time reveals pus. The third stage of the disease is so severe that even toxic shock syndrome has been reported [83].

However, symptoms may be absent when the lesion is deep-seated or due to a superimposed transient bacteremia [144].

Laboratory data are not specific for pyomyositis. Leukocytosis and an increase in the erythrocyte sedimentation rate are often seen, but may be absent in patients with neutropenia or end-stage acquired immunodeficiency syndrome. Eosinophilia is reported only in tropical cases and may be due to a parasitic cause of infection [44, 45]. Interestingly, creatine phosphokinase

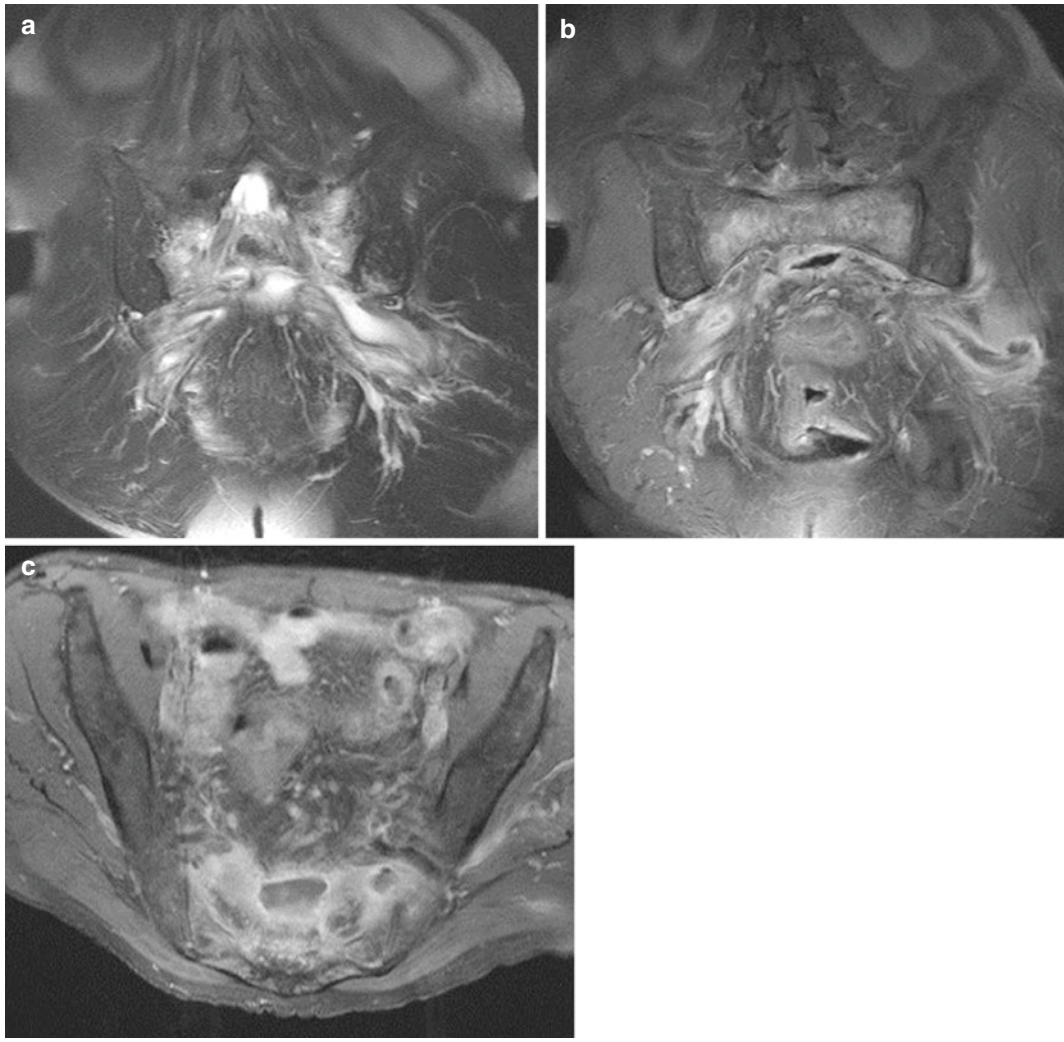

Fig. 21.11 (**a**, **b**) Sacral osteomyelitis and multiple pelvic abscesses. (**a**) Oblique FS coronal T2-weighted MR image; (**b**) oblique coronal FS T1-WI MR image. (**b**) Oblique coronal contrast-enhanced FS T1-WI MR image. (**c**) Axial contrast-enhanced FS T1-WI MR image. Bilateral T2-hyperintense presacral collections (**a**) with peripheral rim enhancement (**b**, **c**). Note increased T2-signal and contrast enhancement of the sacrum in keeping with sacral osteomyelitis

and aldolase levels remain normal. Blood cultures are positive in only 5–30 % of patients and in 1.8 % the outcome is fatal due to sepsis and shock [110, 195]. Culture of aspirated pus has been reported as negative in 15–30 % of cases [35, 44].

The muscles of the thigh and gluteus region are most often affected. Pyomyositis has also been described in the obturator, serratus anterior, deltoideus, triceps, biceps, iliopsoas, gastrocnemius, abdominal, and paraspinal muscles (Fig. 21.12) [35, 79, 90, 147]. In AIDS patients, pyomyositis may be multifocal 43 % of cases in the study of Fleckenstein et al. [58]. Multiplicity of lesions in AIDS patients is not specific for pyomyositis and may be found in other pathologic conditions such as polymyositis, Kaposi sarcoma, and lymphoma [58].

Magnetic resonance imaging is the most precise technique to use in determining the exact location and defining the extent of the disease [51], and it plays a pivotal role in early diagnosis. On T1-weighed images the abscess collection

Fig. 21.12 Pyomyositis in 2-year-old child. Coronal T2-weighted MR image shows diffuse increased signal within the right upper arm muscles

has a low signal intensity compared with surrounding muscle tissue. On occasion, a high-intensity peripheral rim is noted, probably representing blood breakdown products [72, 110]. Pus in the abscess can have an intermediate to high signal on T1-weighed images depending on the protein content. T2-weighed images reveal a hyperintense collection in the affected muscle, with increased signal in the surrounding muscle tissue representing edema, organized phlegmonous collections, or hyperemia [154]. Intravenous administration of contrast material can further discriminate between viable and necrotic muscle tissue, the latter lacking enhancement.

On occasion the imaging presentation of pyomyositis can be confused with a sarcomatous lesion, especially when further clinical and biochemical information is inconclusive. Key elements in the differential diagnosis favoring an infectious origin are the extension of the perilesional inflammatory reaction and the possible association of cellulitis. However, previous surgery or local radiotherapy at the site of a sarcoma may be accompanied by locoregional stranding, which may cause difficulties in the differential diagnosis [72].

Scintigraphy is rarely used for detection [202], but may detect additional abscesses on a distance of the primary lesion [147].

Pyomyositis can be effectively treated by antibiotic therapy in the first stage of disease, but during the later stages, drainage should be initiated early and serve as the main component of therapy, either by percutaneous computed tomography (CT) or ultrasound-guided drainage or by open surgery [72].

21.2.2.6 Muscular Cystic Echinococcosis

Human hydatid disease is a parasitic infection due to the development in the organism of *Echinococcus granulosus* larvae, a parasitic tapeworm, with dogs being the definitive hosts, sheep the intermediate hosts, and humans the incidental intermediate hosts. Ingestion of contaminated water or food and contact with dogs are known causes of infection. The disease is still endemic in several regions and has the highest incidence in the Mediterranean Basin, Middle East, South America, New Zealand, Australia, Central Asia, and China [138]. According to various authors, the incidence of musculoskeletal echinococcosis including involvement of subcutaneous tissue is around 1–5.4 % among all the cases of hydatid disease [10]. Alveolar echinococcosis due to infection by *Echinococcus multilocularis* is more rare, but has a more invasive nature sometimes mimicking a malignant lesion. Muscular echinococcosis may be primary, but may also occur secondarily resulting from the spread cysts from other areas either spontaneously or after operations for cystic echinococcosis in other regions of the body [87, 88]. The growth of cysts within a muscle is difficult because of muscle contractility and the presence of lactic acid. The affinity for muscles of the neck, trunk, and limb roots could be explained by the volume of the muscle mass, the increased vascularity, and the decreased activity of these muscle groups [15].

Primary muscular cystic echinococcosis disease is rare, with only isolated cases being

described in the literature [15, 201]. Only few cases of primary subcutaneous cystic echinococcosis of the inferior limbs have been reported. Cystic echinococcosis of superficial muscles presents as a painless soft tissue mass with fluctuating consistency and evolves slowly. This mass may be accompanied with neurovascular compression signs, inflammation in case of fissuring, infection of the cyst [69], or skin fistula. Deep muscular cystic echinococcosis especially of the psoas muscle which is relatively more frequent [158] may be discovered by chance. Hydatid serology is often negative [122]. It is particularly useful in postoperative monitoring when looking for a local or more remote recurrence [62].

Muscular cystic echinococcosis may have different appearances on imaging techniques.

MR has proven superior over ultrasound in detecting this multivesicular structure. More solid appearances are also possible, making it sometimes difficult to differentiate it with other soft tissue tumors [107]. Even in these cases, MR can often reveal the vesicular nature of the lesion, which if frequently still focally preserved.

Ultrasonography and magnetic resonance imaging are the imaging tools of choice to confirm the diagnosis before surgery [62]. The imaging characteristics of soft tissue involvement resemble those of hydatid cysts found in the liver. Ultrasonographic appearance of cystic echinococcosis may vary. The cyst wall usually manifests as an echogenic line. Simple cysts (type I) do not demonstrate internal structures. Detachment of the endocyst from the pericyst (type II) appears as well-defined fluid collection with a localized split in the wall and "floating membranes" inside the cavity [17]. Multivesicular cysts (type III) manifest as well-defined fluid collections in a honeycomb pattern with multiple septa representing the wall of the daughter cysts (Fig. 21.13). Multivesicular or inhomogeneous muscle hydatids may have a nonspecific appearance that may simulate hematoma, abscess, or necrotic soft tissue tumor [62, 68]. Calcified cysts may be seen. Computed tomography is useful in doubtful cases, in deep muscular localizations, and in appraising the exact localization of the cyst and its relationship with the neural and vascular elements as well as the state of the adjacent bone. MRI imaging characteristics may differ depending on the life cycle stage of the parasite [162]. Typically, the lesion consists of a mother cyst, containing multiple daughter vesicles. On T1-weighted images these daughter vesicles are seen as hypointense cysts within the intermediate signal of the mother cyst. The signal intensity of the daughter cysts on T2-weighted images can be high or low, with some authors suggesting a relation with the presence and absence, respectively, of viable scolices [15]. A rim of low [15] signal intensity on T2-weighted images surrounds the lesion. This rim is composed of three layers: an endocyst, ectocyst, and adventitia. The adventitia develops as a reaction following compression and inflammation of surrounding tissue. It is well vascularized, enhancing after intravenous contrast injection [111, 120] (Figs. 21.14 and 21.15). Edema or acute inflammation caused by compression in soft tissue adjacent to the cyst is uncommon but may be seen.

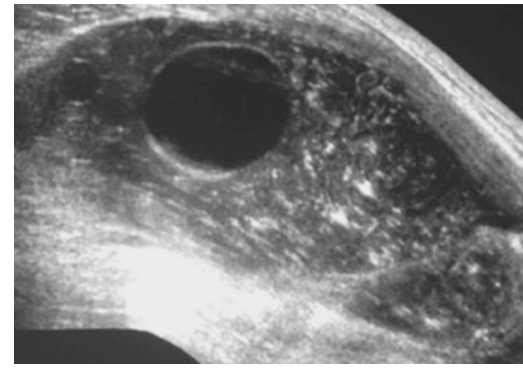

Fig. 21.13 Soft tissue echinococcosis of the calf. Ultrasonography shows a well-defined multicystic fluid collection with vesicles, calcifications, and small echoes corresponding to hydatid sand

21.2.2.7 Other Inflammatory Myopathies

Inflammatory myopathies include focal myositis, nodular myositis, proliferative myositis, and diabetic muscle infarction. Clinically, inflammatory myopathies often present as a diffuse swelling of the thigh or calf, with or without tenderness. Only on rare occasions, they present as a solitary soft tissue mass. These different

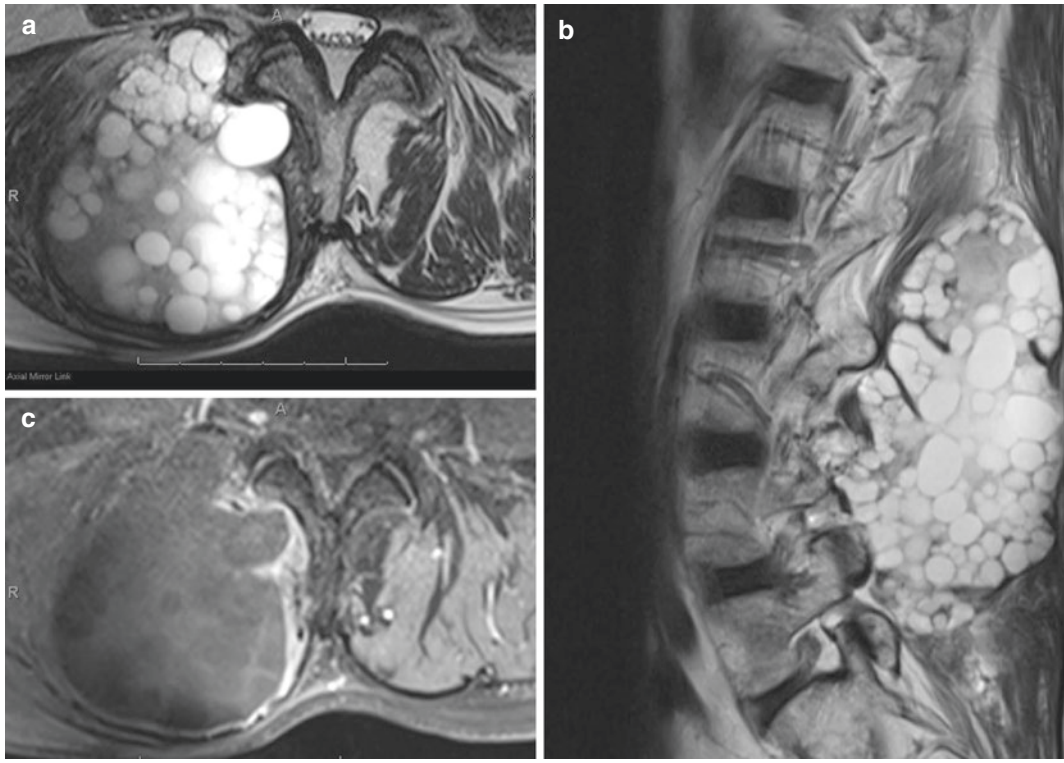

Fig. 21.14 Multicystic echinococcus cyst in the right paravertebral muscles: (**a**) axial FS T2-weighted MR image; (**b**) sagittal FS T2-weighted MR image; (**c**) axial T1-weighted MR image after gadolinium contrast injection. Large multicystic lesion is seen on T2-WI. (**a**, **b**) Because of vascularization of the pericyst, peripheral enhancement can be seen after gadolinium contrast injection (**c**) (Images courtesy of S. Dekeyzer, Aachen)

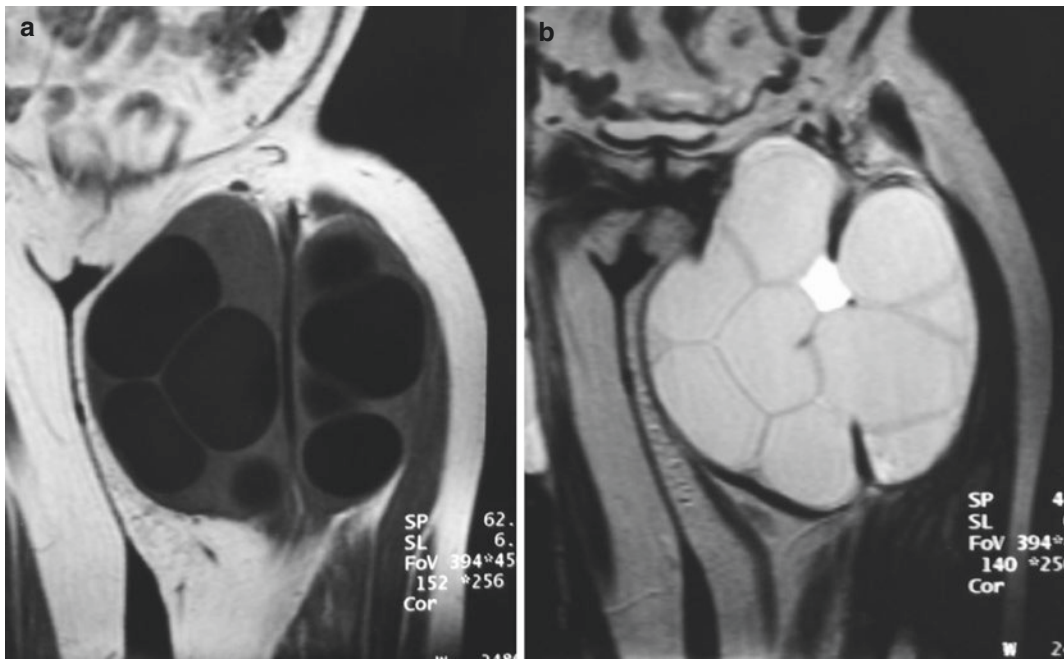

Fig. 21.15 Multicystic echinococcosis of the left thigh. Coronal T1-WI (**a**) and T2-WI (**b**) MRI shows multivesicular hydatidosis of adductor space

entities are only distinguishable by their histologic appearances [85], often requiring a biopsy for correct diagnosis.

On MR imaging studies, myopathies are characterized by non-focal hypointense areas on T1-weighted images and hyperintense signal on T2-weighted images [86]. These diffuse signal changes are even better seen when a T2-weighted fat suppression sequence is used [74]. Differential diagnosis includes infectious myositis, trauma, muscular denervation, muscular dystrophy (such as Duchenne's [106] or Becker's muscular dystrophy), rhabdomyolysis, polymyositis, dermatomyositis [74], and soft tissue malignancy. In most of these cases, clinical and laboratory tests will permit to make the correct diagnosis.

Focal Myositis. Focal myositis is a relative rare usually self-limiting soft tissue pseudotumor. It is usually found in the lower extremities, 50 % of the cases being located in the thigh and 25 % in the lower leg. Other more rare locations include the neck, tongue, perioral region, forearm, hand, abdomen, eyelids, and paraspinal muscles [94]. There is no sex or age predilection [94].

Typically, focal myositis presents as a local intramuscular soft tissue swelling, which can rapidly grow in a few weeks (Fig. 24.16). In more than 50 % of the cases, pain is the main symptom. Usually the process is limited to one muscle, but involvement of multiple muscles has been reported. One-third of the patients with focal myositis evolve to polymyositis or a polymyositis-like syndrome, suggesting that focal myositis is a localized form of polymyositis [14].

On MRI, focal myositis is of increased signal intensity on T2-weighted images, in one or more muscle groups. In contradistinction to most soft tissue sarcomas, the internal muscle bundle is spared (Fig. 21.16) [184].

Diabetic Muscle Infarction. Diabetic muscle infarction is a rare complication of diabetes mellitus. Patients with poorly controlled type 1 insulin-dependent diabetes mellitus and severe end-organ damage are most frequently affected, although it may occur in a well-controlled patient without known diabetic complications [89]. Although the pathogenesis is still to be completely clarified, the most likely hypothesis is that the muscle infarction is secondary to vascular disease such as arteriosclerosis and diabetic microangiopathy [178], while some authors suggest an alteration in the coagulation-fibrinolysis system [140].

Diabetic muscle infarction typically presents as a sudden onset of severe pain in the thigh (especially in the quadriceps muscle) or calf, with diffuse enlargement of the involved muscle or muscle groups. After subsequent partial resolution, a painful palpable mass can be found in up to one-third of the cases [178]. Bilateral involvement has been described, with a reported

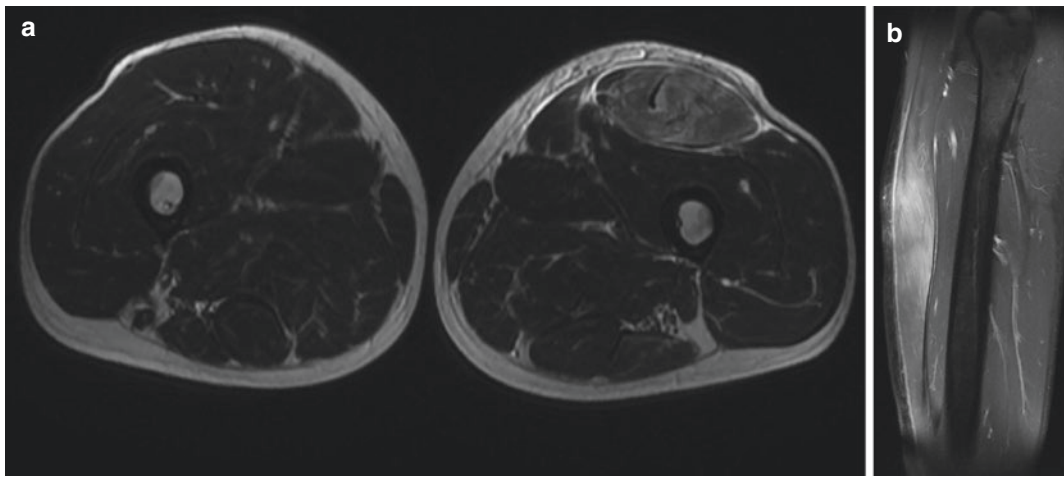

Fig. 21.16 Focal myositis of the left rectus femoris muscle. (**a**) Axial FS T2-weighted MR image; (**b**) sagittal FS T2-weighted MR image. There is diffuse increased signal within the rectus femoris muscle with sparing of the individual muscle bundles

frequency varying from 8 % to more than one-third of the cases [11, 89, 172, 178].

Clinically, it is frequently misdiagnosed as an abscess, neoplasm, or myositis, often requiring a biopsy for further evaluation [33, 47, 89]. Commonly there is elevated erythrocyte sedimentation rate, but no leucocytosis. This can be helpful in the differentiation from pyomyositis [89].

The diagnosis may be suspected on ultrasound if a well-marginated, hypoechoic intramuscular lesion with intralesional linear echogenic structures is present. There is typically absence of intralesional motion or swirling of fluid when pressure is applied with the transducer. This differentiates diabetic infarction from an abscess or a necrotic mass [47, 105].

MR images display enlargement of the involved muscles, with uniform increased signal intensity on T2-weighted and inversion recovery images demonstrating the edematous and inflammatory changes [11, 33, 86, 89]. T1-weighted images show normal or decreased signal intensity in the involved muscles, the swelling being sometimes less appreciated on this sequence [89].

Perifascial and subcutaneous edema are best evaluated on inversion recovery and fat-suppressed T2-weighted images [84]. Additionally, MRI can detect subclinical muscle infarction months before the onset of clinical symptoms [89].

Atypical presentations have been reported as a high signal of the affected muscle on T1-weighted images, presumably reflecting intramuscular hemorrhage [169].

21.2.2.8 Bursitis

Bursae are spaces near joints containing small amounts of fluid, reducing friction between different structures. The clinical most important are the trochanteric, subdeltoideal, ischiogluteal, pes anserina, iliopsoas, retrocalcaneal, and olecranon bursae, because they are the most commonly affected ones.

The amount of fluid may increase due to inflammation following overuse, direct trauma (rheumatoid), arthritis, or infection, resulting in a soft tissue mass. Imaging of bursitis is further discussed in Chap. 20.

21.2.2.9 Granulomatous Disorders

Tuberculous Infection of Soft Tissue

Tuberculous infection of soft tissue often accompanies involvement of lymph nodes, bones, or joints (Fig. 21.17) [174]. Without proper treatment, it can evolve to a cold abscess. A periosteal reaction in adjacent bone can sometimes be found [174].

Sarcoidosis

Sarcoidosis is a systemic granulomatous disorder which can affect multiple organs. Muscle involvement is rare and occurs in 1.4–6 % of patients with sarcoidosis [73, 136]. Three main clinical presentations of muscular sarcoidosis can be distinguished: an acute myositis, a diffuse atrophic form, and a nodular form [12, 134, 177]. Clinical symptoms are often absent.

The acute myositis type occurs exclusively in the early stage of sarcoidosis, presenting as myalgia secondary to inflammation. MR imaging is usually negative, presumably because of the sparse distribution and small size of epithelioid cell granulomas [135].

In the diffuse atrophic myopathic form, patients can present with myalgia, muscle weakness, and atrophy [134]. The muscles of de proximal portions of the extremities are frequently involved [117]. MR imaging findings are nonspecific revealing proximal muscle atrophy with fatty replacement [125]. Differentiation from a corticoid myopathy is mainly based on clinical and laboratory findings.

The least common form is the nodular presentation, presenting as a single or multiple sarcoid nodules (Fig. 21.18). They may or may not be clinically palpable. These nodules appear elongated and extend along muscle fibers [134]. On ultrasound examination, sarcoid nodules present with a hyperechoic center and a hypoechoic peripheral zone [134]. They may also present with well-defined borders and an overall hypoechogenic aspect [177].

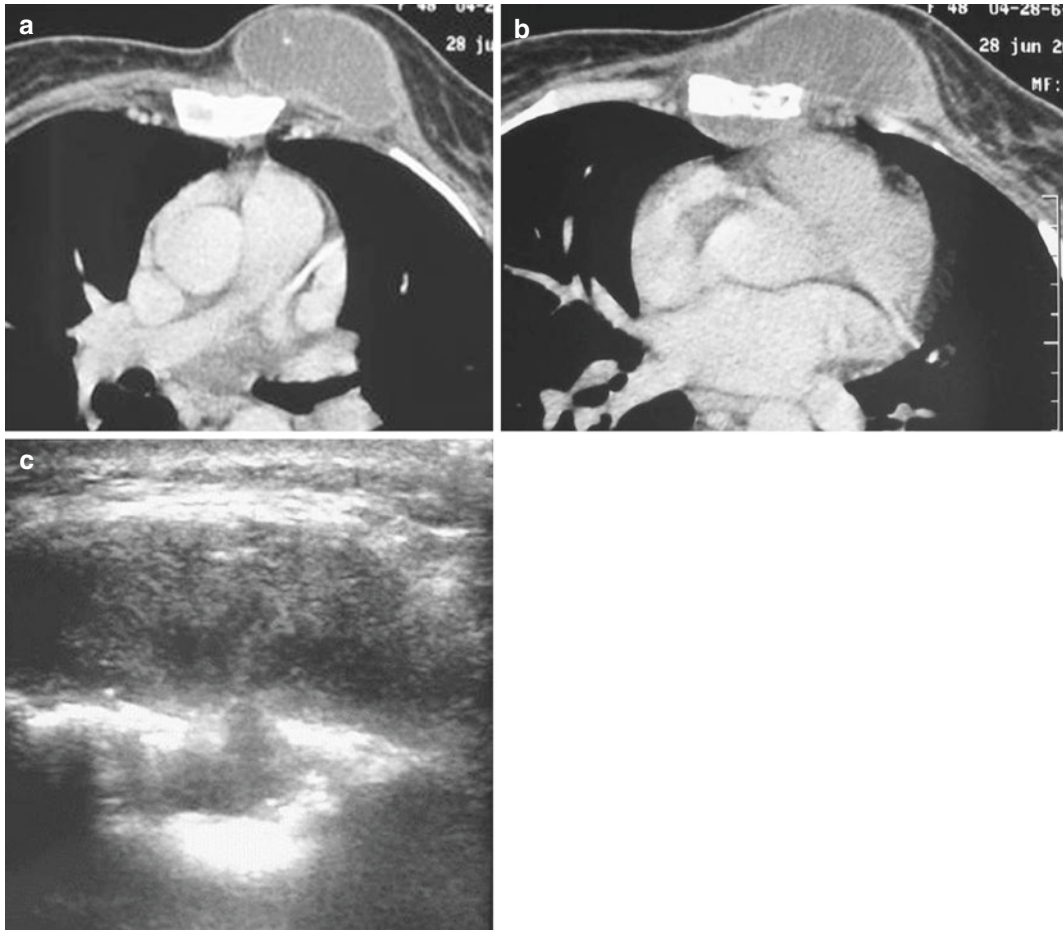

Fig. 21.17 Tuberculous osteomyelitis involving the sternum and adjacent abscess: axial CT images (**a**, **b**) shows sternal osteolysis associated to pre- and retrosternal fluid collection with peripheral enhancement after intravenous contrast administration. Ultrasonography (**c**) shows sternal osteolysis with pre- and retrosternal fluid collection

On MR imaging, the nodules may have a star-shaped hypointense center on all axial pulse sequences ("dark star" sign), which is believed to correspond with fibrous tissue and does not enhance after intravenous contrast administration [135, 136, 186, 199]. However, this central structure is not present in the acute stage of the disease. It can also be absent in small nodules (<10 mm), presumably because of the short time of granulomatous inflammation in these small structures.

The peripheral area of the nodules is slightly hyperintense compared to muscle on T1-weighted images, with homogeneous high signal intensity on T2-weighted images. There is homogeneous enhancement after intravenous contrast administration, secondary to the high cellularity of granulomas and edema [177].

Coronal and sagittal images may show the "three stripes" sign, consisting of a hypointense inner stripe and hyperintense outer stripes [134, 199]. However, after steroid therapy the sarcoid nodules may disappear [177], or only the inner stripe may be visualized [136].

Diffusion weighted imaging (DWI) may be useful to differentiate the two components of sarcoidosis, active inflammation and fibrosis. Areas of active inflammation are of high signal on DWI [166].

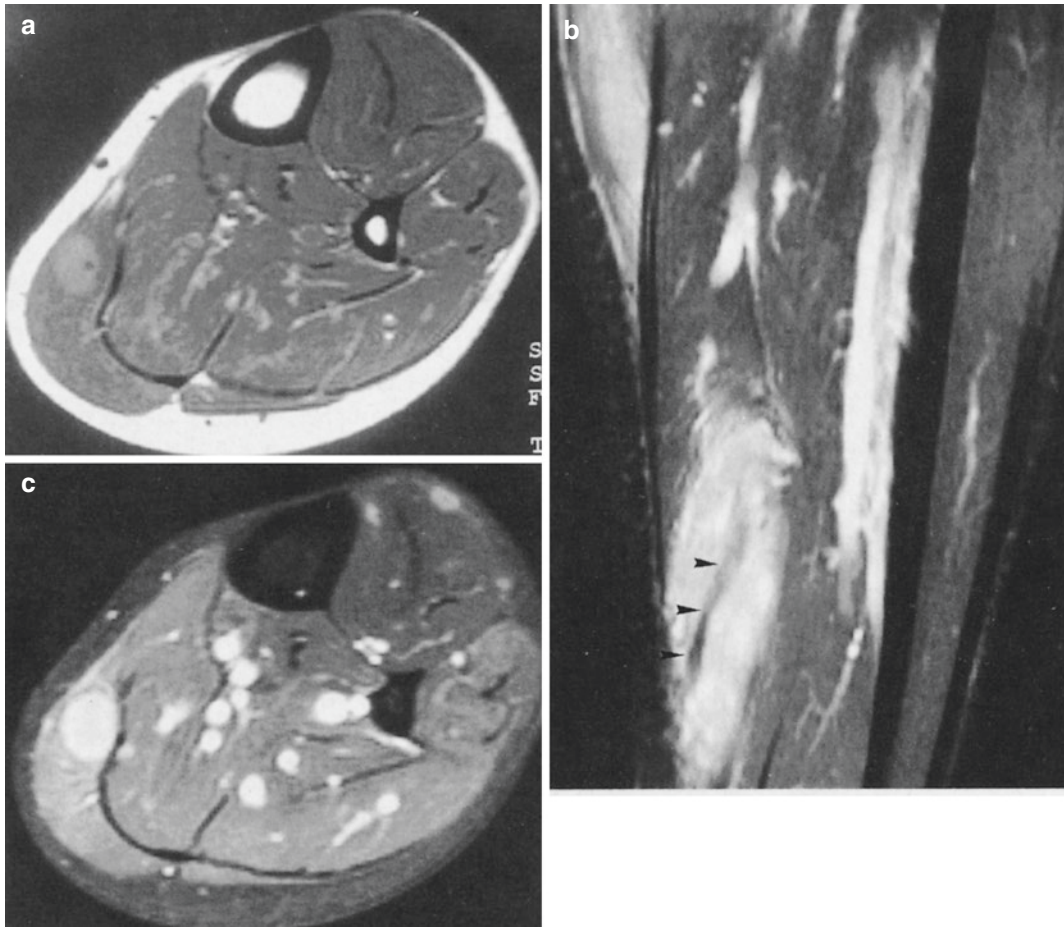

Fig. 21.18 A 56-year-old woman with a tender palpable mass in the left calf: (**a**) axial spin echo T1-weighted MR image; (**b**) sagittal spin echo T1-weighted MR image with fat suppression; (**c**) axial spin echo T1-weighted MR image with fat suppression after intravenous contrast administration. A nodular lesion, slightly hyperintense compared to muscle, is shown on the axial T1-weighted image (**a**), with a central hypointense center presumably corresponding to fibrous tissue. After intravenous contrast administration, a homogeneous enhancement of these large and other smaller nodules is seen (**c**). The sagittal image further demonstrates the three layer composition, with a linear low-intensity stripe interposed between two high-intensity areas (**b**), longitudinally extending between normal muscle tissue. This case illustrates a rare soft tissue presentation of sarcoidosis

Very rarely periosteal reaction is seen in case of muscular sarcoidosis [176].

Positron emission tomography with fluorine-18-fluorodeoxyglucose ((18)F-FDG) is promising in detecting occult disease and assessing disease activity during treatment [12, 71, 91, 113, 148].

Cat Scratch Disease

Cat scratch disease is a benign, self-limiting cause of regional lymphadenitis affecting mostly children and young adults. In more than 90% of the cases, there is a history of recent contact with cats, cat scratch, or both. In contrast, the site of inoculation is not always found. The Gram-negative bacillus *Rochalimae henselae*, also called *Bartonella henselae*, is the microorganism most often incriminated. In an otherwise healthy host, the adenitis resolves spontaneously within 3 weeks to several months, even without antibiotic therapy [49].

Cat scratch disease has a wide spectrum of clinical manifestations, ranging from regional lymphadenitis to disseminated infection. Regional lymph node enlargement occurs most commonly at the medial epitrochlear region of the elbow [119]. Other locations include the axilla, groin, and popliteal fossa [65, 164]. A typical case includes skin lesions and an associ-

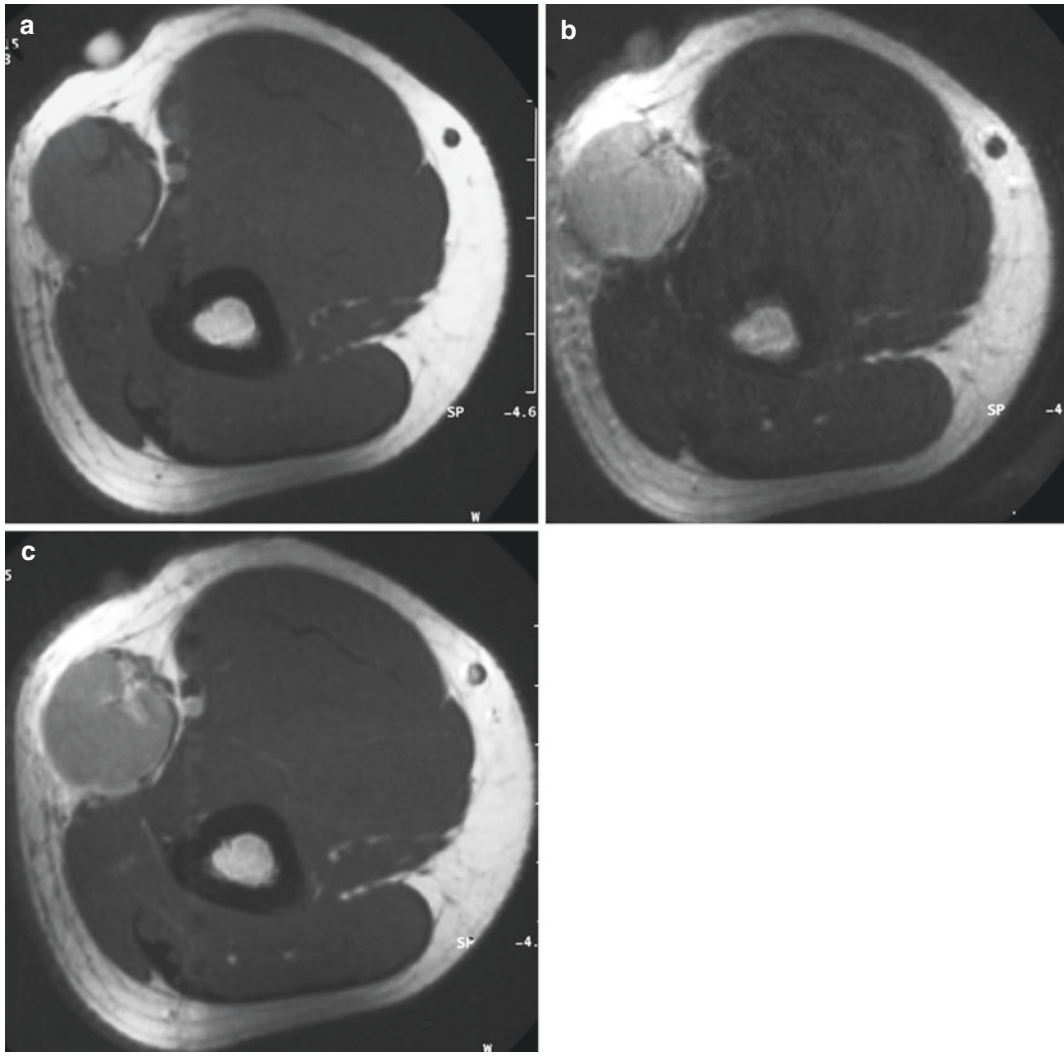

Fig. 21.19 Cat scratch disease in a 15-year-old boy: (**a**) axial spin echo T1-weighted MR image; (**b**) axial turbo spin echo T2-weighted MR image; (**c**) axial spin echo T1-weighted MR image after intravenous contrast administration. A round, well-defined lesion is located adjacent to the neurovascular bundle at the left elbow. On T1-weighted images (**a**) the lesion has slightly higher and relative homogeneous signal intensity compared to muscle, with a more intermediate signal intensity on T2-weighted images (**b**). After contrast administration there is moderate, mostly homogeneous enhancement of this mass

ated enlarged painful reactive adenopathy commonly presenting along a single lymph node chain. Involved glands can have diameters up to 5 cm [112]. Multiple nodes at a single site may be involved as well. Disseminated infection is unusual (5–10 %) [112], most frequently seen in immune-compromised patients. Neurological involvement is uncommon [112].

The sonographic finding of an epitrochlear mass due to cat scratch disease most commonly consists of a hypoechoic lobular or oval mass with central hyperemia on power Doppler and a possible adjacent fluid collection. The adjacent or intranodal fluid collection is believed to correspond to nodal suppuration or necrosis. Asymmetrical shape and a hyperechoic hilum seem to differentiate cat scratch disease from other epitrochlear masses (including sarcoma, metastatic disease, or lymphoma) [119].

CT shows a soft tissue mass corresponding to involved lymph nodes. Central necrosis can be seen as a low attenuation [49, 191]. MR

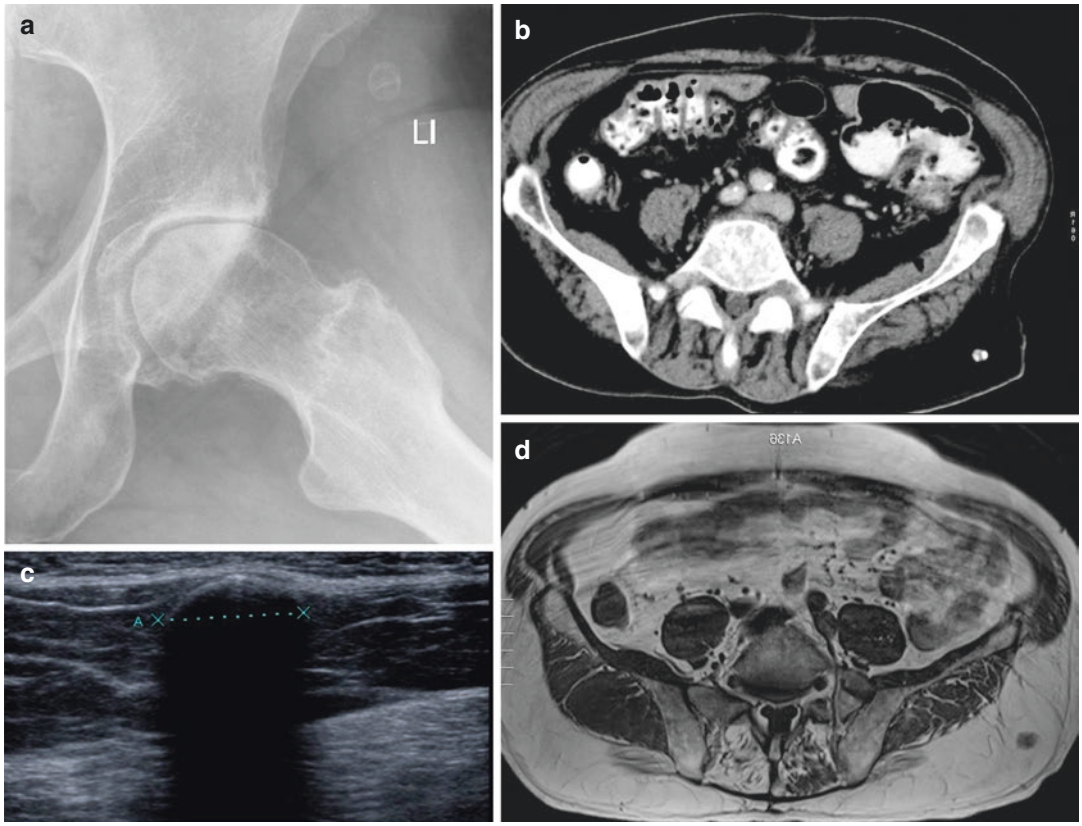

Fig. 21.20 Typical subcutaneous injection granuloma in the left gluteal area: (**a**) plain radiograph of the left hip, (**b**) CT, (**c**) ultrasound, and (**d**) axial turbo spin echo T2-weighted MR image. A round, well-defined ringlike calcification lesion is seen within the subcutaneous tissue of the left gluteus region on plain films (**a**) and CT (**b**). On ultrasound, there is a linear reflection with the subcutis with retroacoustic shadow. (**c**) The lesion is of low signal intensity on T2-weighted images (**d**)

images reveal the regional lymphadenopathy as homogeneous or heterogenic masses surrounded by edema [49, 65]. T1-weighted images show a homogeneous isointense signal intensity compared to muscle (Fig. 21.19). On T2-weighted images the area of the mass and surrounding edema becomes hyperintense. After intravenous contrast injection, there may be homogeneous or slight peripheral enhancement of the involved lymph nodes and adjacent soft tissue edema [49, 65].

Bone involvement is rare, usually presenting as lytic lesions. A periosteal reaction and associated sclerosis can be found [80]. A single osteolytic lesion can simulate Langerhans cell histiocytosis [20].

The final diagnosis is based on polymerase chain reaction for DNA analysis or serologic testing. Culture of *Bartonella* species is difficult and usually unsuccessful. Histology reveals nonspecific granulomas with central necrosis at later stages [119].

Injection Granulomas

Injection granulomas are most often encountered in the upper outer quadrant of the buttocks and in the deltoid muscle [153]. They may be located either within the subcutaneous fat or gluteus muscles. The typical location and the absence of muscle distortion are the clues to the diagnosis. On plain films and CT subcutaneous injection, granulomas appear as small well-defined nodules, most often containing ringlike calcifica-

tions. These lesions are hypointense on T1-weighted MR images. On T2-weighted images, injection granulomas can be hyperintense or hypointense, depending on whether the major pattern of the lesion is inflammatory or fibrous. This pattern depends on the time elapsed after injection (Fig. 21.20). Intramuscular granulomas may have a linear pattern of calcification along the course of the muscle fibers.

Mycetoma

Mycetoma is an implantation mycosis characterized by large tumorlike swellings and caused by actinomycetes (actinomycetoma) and fungi (eumycetoma) [161]. It is mostly located in the foot, responsible for 70 % of infections [60], but it has also been reported in hands, arms, legs, and back [3]. This disease is mainly found in tropical and subtropical regions of the world and the majority of patients are reported from Mexico, Senegal, Sudan, and India. The true prevalence and incidence are not well defined [160]. It usually affects young adults with male predominance. The causative agents are organisms living in the soil, and infection is generally acquired by an accidental painless inoculation through the skin by a thorn or splinter in barefoot individuals [55]. Incubation period varies from several weeks to months. Initially, the patient presents with a painless bump, which develops into a classic triad of chronic induration, draining sinuses, and fungal grain discharge. Early diagnosis is important because infection can invade deep tissues, muscle, bone, and even visceral organs, causing damage, deformity, or even death secondary to systemic spread [168, 192].

The radiologic findings include soft tissue swelling, periosteal reaction, cortical erosions, rounded lucencies (Fig. 21.21a), reactive sclerosis commonly affecting calcaneus and metatarsals, initially surrounding lucencies and then extend largely, joint destruction, osteopenia due to long-term immobilization, and bone lysis occurring in the late course of the disease [192]. If treatment is successful, the periosteal reaction coalesces, forming "melting snow" appearance on the cortex of small bones [151]. Ultrasonography (US) typically shows hypoechoic masses containing hyperechoic spots corresponding to fungal grains. This characteristic appearance on US is seen when fungal granules are of large size and previous to sinus formation. Computed tomography (Fig. 21.21b) is the preferred imaging tool to assess cortical erosions. The masses have similar density to muscles and fungal granules have a high density.

MRI (Figs. 21.21c and 21.22) can characterize the soft tissue masses of mycetoma, provide an early diagnosis, and assess the local extension of the infection. Mycetoma is characterized by the formation of microabscesses consisting of aggregates of the fungal granules ("sulfur granules") and surrounded by granulation tissue. On MRI mycetoma appears as small, round hyperintense lesions (representing granulation tissue) measuring 2–5 mm, surrounded by a low signal intensity rim (representing fibrous septa). The central low signal intensity dot is the result of susceptibility artifact caused by the presence of a conglomeration of fungal grains. This finding was first reported by Sarris et al., as the "dot-in-circle" sign. This sign can also be demonstrated on T1-weighted images following intravenous gadolinium administration [163].

Before sinus formation and discharge of fungal grains, early diagnostic may be difficult and mycetoma may be mistaken for a neoplasm (Kaposi sarcoma), neuropathic foot, or other chronic bacterial or tuberculosis infection [96, 208]. Biopsy and culture are required for the final diagnosis and identify causal agents to ensure correct antimicrobial therapy.

21.2.3 Traumatic Nerve Lesions Presenting as a Soft Tissue Mass

21.2.3.1 Morton's Fibroma

The term Morton's neuroma is a misnomer as it does not represent a true neuroma but rather perineural fibrosis and nerve degeneration, most likely due to repetitive compression and irritation of the interdigital nerve. Therefore, the term Morton's fibroma is preferred [81].

Morton's fibromas are most commonly found in the second and third intermetatarsal spaces and

Fig. 21.21 Mycetoma (Madura foot) (**a**) lateral radiograph of the hindfoot showing soft tissue shadow (*arrow*) in the region of Kager fat without bone erosion. (**b**) Axial CT scan of the foot showing several rounded lesions (*arrow*) involving medial soft tissues of the foot with extrinsic bone erosions of the calcaneus (**c**) axial T1-weighted MR image of the ankle showing multiple inflammatory granulomata, appearing as conglomerates of small (2–5 mm) round hypointense lesions, several with "dot-in-circle sign" (*arrows*)

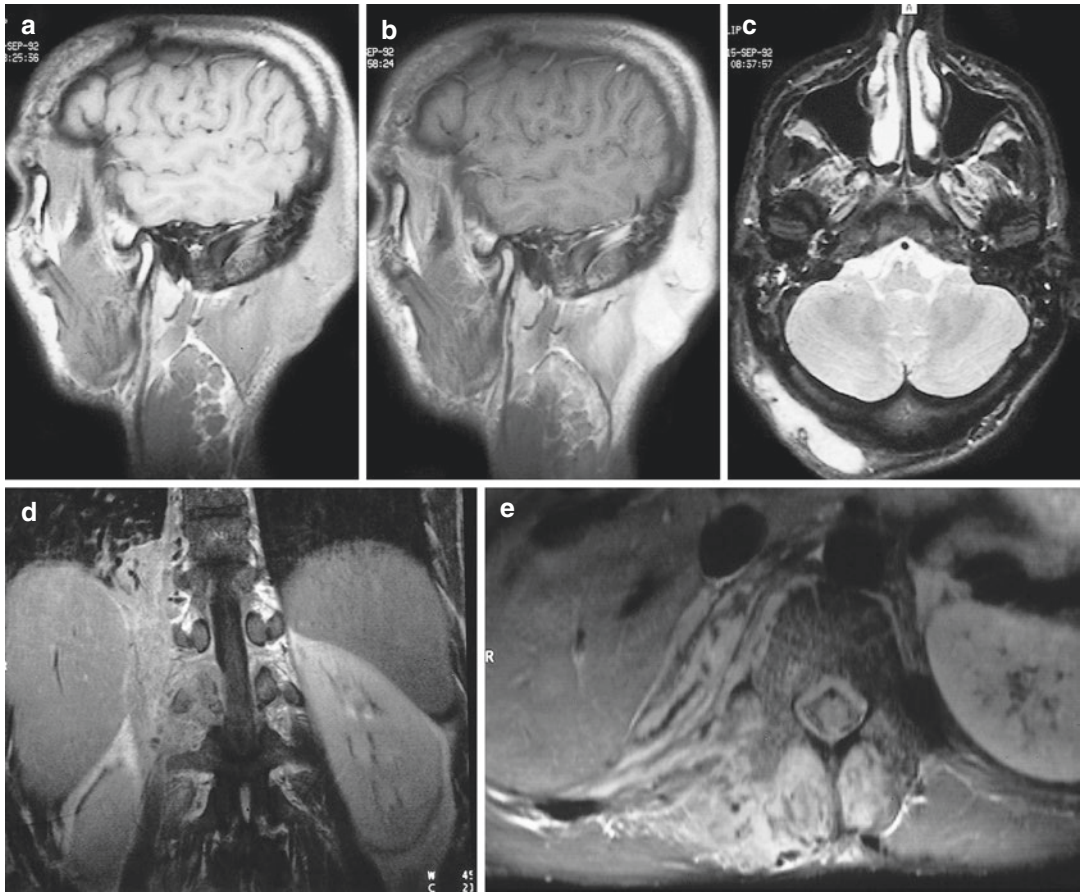

Fig. 21.22 Actinomycotic abscess in a 21-year-old man (**a**–**c**) and a 23-year-old man (**d**, **e**): (**a**) sagittal spin echo T1-weighted MR image; (**b**) sagittal T1-weighted MR image after gadolinium contrast injection; (**c**) axial T2-weighted MR image; (**d**) coronal spin echo T1-weighted MR image; (**e**) axial turbo spin echo T2-weighted MR image with fat suppression. In the first patient, there is a collar-button-like mass involving the right splenius and semispinalis muscles which is isointense to muscle on T1-weighted images (**a**) and hyperintense on T2-weighted images (**c**). After contrast injection there is moderate enhancement of the lesion without evidence of necrosis (**b**). After resection of the slowly growing mass, the lesion proved to be an actinomycotic abscess. In the second patient, the images show an ill-defined structure of homogeneous intermediate signal intensity on T1-weighted images (**d**) at the level of the paraspinal muscles on a low thoracic level. The lesion extends both cranially and caudally, invading the right psoas muscles and the spine (**d**, **e**)

less frequently in the first and fourth. More than one intermetatarsal space may be affected as well. Morton's fibroma is most commonly diagnosed in middle age, with a female predominance, and is believed to be related to the use of high-heeled shoes with increased weight bearing on the forefoot [196]. Although Morton's fibroma is a common cause of intermetatarsalgia, in many cases it is not associated with clinical symptoms. Lesions with a transverse diameter smaller than 5 mm are often asymptomatic, as studies on healthy volunteers have shown, with a prevalence of small (<5 mm) Morton's fibromas of approximately 30 % in asymptomatic individuals [19]. Lesions with a transverse diameter of 5 mm or more are most likely symptomatic.

Ultrasound examination is reliable and the most cost-effective imaging technique in detecting Morton's fibroma [24]. A well-defined hypoechoic mass in the plantar soft tissues is seen at the level of the metatarsal heads (Fig. 22.23a). Dynamic ultrasound examination

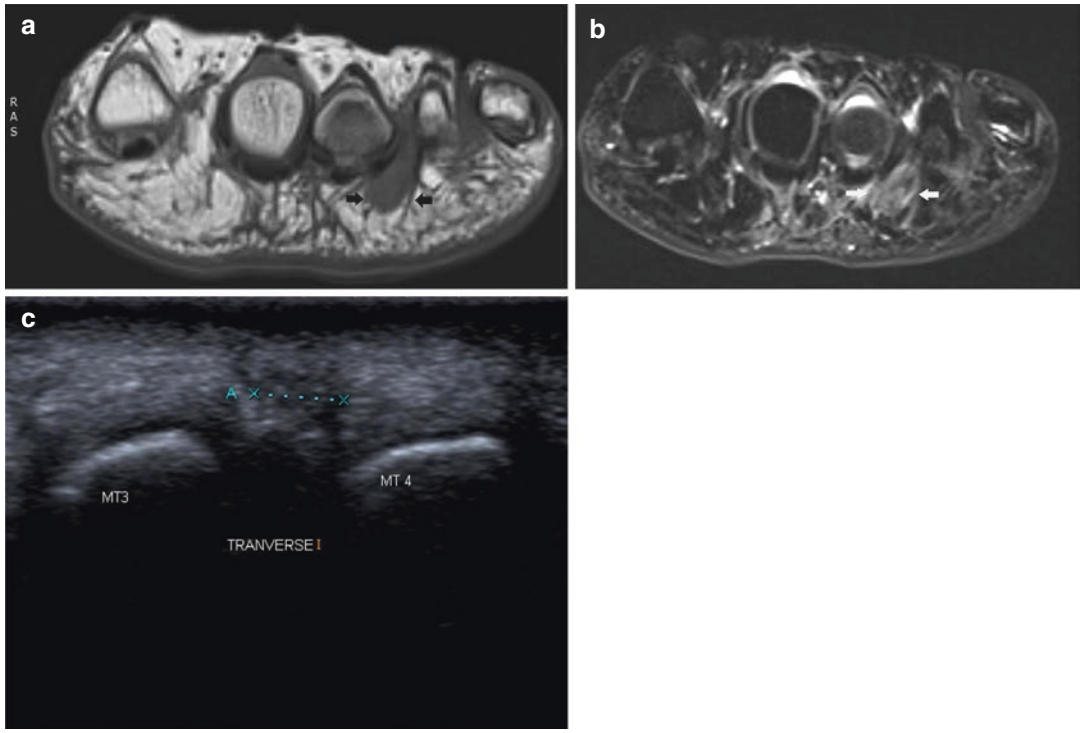

Fig. 21.23 Morton's fibroma: (**a**) coronal T1-weighted MR image; (**b**) coronal FS T2-weighted MR image. (**c**) Corresponding coronal ultrasound at the forefoot. On T1-WI, a well-defined hypointense (isointense to muscle) lesion is seen at the intermetatarsal space between the third and fourth metatarsal head (*black arrows*) (**a**). The lesion is slightly heterogeneously hyperintense on FS T2-WI (*white arrows*) (**b**). On ultrasound the lesion is hypoechoic (**c**). The location and morphology of the tumor are characteristic of Morton's neuroma

using Mulder's test can increase conspicuity and diagnostic confidence. For this test, the patient's forefoot is held in the sonographer's non-imaging hand while performing lateral compression of the metatarsals and applying the transducer to the plantar aspect of the intermetatarsal regions. When this maneuver is performed on patients with a Morton's fibroma, the mass is compressed between the metatarsal heads eliciting characteristic pain before it is plantarily displaced, often coinciding with a palpable click (Mulder's sign) [9]. Elastography may be useful to detect smaller and less-defined lesions [133]. Although ultrasound has been proposed as a useful technique for guidance to inject corticosteroid, local anesthetic, or alcohol [9, 197], according to other authors, this technique seems not to improve the efficacy and safety of therapeutic injections if the clinician is well trained and is familiar with forefoot anatomy [109, 143].

Although in experienced hands, clinical examination and ultrasound may suffice for the diagnosis of Morton's fibroma [24], MR imaging has been proven to be highly sensitive and specific in diagnosing Morton's fibroma and may be used for difficult cases, differential diagnosis, and precise preoperative assessment [42, 203, 205]. On MRI, Morton's fibroma appears typically as a tear-shaped, spindle-shaped, or dumbbell-shaped lesion in the region of the neurovascular bundle on the plantar side of the deep intermetatarsal ligament (Fig. 21.23). Morton's fibromas display typical signal intensities on MR imaging sequences: isointense to muscle on T1-WI and hypointense relative to fat tissue on T2-WI [205]. There is no typical enhancement pattern, varying from low to moderate to marked enhancement. In the appropriate clinical setting, administration of gadolinium contrast medium is not required for a reliable diagnosis of a Morton's fibroma. MR plays an impor-

tant role in excluding other pathologies that can mimic Morton's fibroma such as intermetatarsal or subcapitometatarsal bursitis (which occurs dorsal to the transverse metatarsal ligament), osteonecrosis of the metatarsal heads, metatarsophalangeal joint synovitis or dislocation, tendon sheath ganglion, pigmented villonodular synovitis, stress fractures, and other disorders associated with metatarsalgia [204, 205].

In most cases, therapy is conservative mainly comprising of footwear modifications, radiofrequency ablation, physical therapy, and local (corticosteroid and anesthetic) injections into the affected webspace. Surgical excision is only performed when necessary [9].

21.2.3.2 Traumatic Neuroma

Traumatic neuroma is a nonneoplastic reactive hyperplasia of nerve tissue and usually occurs at the proximal end of a nerve trunk that has been severed, partially transected, or injured as a result of trauma. Traumatic neuromas are classified into neuroma-in-continuity (NIC) after partial nerve transection or end-bulb neuromas (EBN) after complete disruption. EBNs lack distal continuity with the parent nerve, while NICs are contiguous both proximally and distally [2].

The most common location for traumatic neuromas is the lower extremity after amputation, followed by the head and neck, where they have been reported to occur after the extraction of teeth.

After limb amputation, neuromas may be asymptomatic when not compressed, but can cause unexplained pain and discomfort particularly when a prosthesis is worn. Physical examination may reveal a painful nodule at the site of the transected nerve, local tenderness over the injured nerve with distally radiating tingling (Tinel sign), denervation atrophy of the muscles, and sensory or trophic changes [38].

On imaging, traumatic neuroma may mimic a peripheral nerve sheath tumor (PNST). The history of a previous trauma is the key finding to the correct diagnosis.

Ultrasound reveals a hypoechoic mass at the distal end of site of the amputated nerve in case of an EBN [76]. In a transected nerve, ultrasound may reveal a focal gap due to nerve discontinuity and scar tissue at the level of transection and EBN formation at the proximal and distal stump margin [206]. An NIC is seen as a spindle-shaped mass on the course of the involved nerve and may mimic a PNST. Ultrasound-guided steroid or alcohol injection in painful stump neuroma has been reported as a successful method for pain relief [37, 104].

On MRI (Fig. 21.24), an EBN is seen as a T2 hyperintense nerve terminating in a baseball-shaped mass resembling a balloon on a string or a green onion appearance [2, 38]. To differentiate an NIC from a PNST, administration of gadolinium contrast is not useful as both lesions may demonstrate contrast enhancement. The lack of a target sign on T2-WI in a traumatic neuroma in conjunction with the clinical history of a previous trauma is the most useful clue to the correct diagnosis of a traumatic neuroma [2].

Distal denervation muscle atrophy serves as a useful secondary sign of nerve injury on MR imaging [38].

21.2.4 Other Posttraumatic Lesions

21.2.4.1 Hematoma and Contusion

A contusion is caused by a capillary rupture that provokes bleeding between the tissue muscle fibers, resulting in edema and inflammatory reaction. Contusions are not always painful, may present as a mass, and thereby cause clinical confusion. A soft tissue contusion appears on MR images as a diffuse interstitial infiltration due to edema. It is hyperintense on T2-weighted images but without architectural muscle distortion. However, the muscle may increase in volume, owing to inflammation. The history of a previous trauma is required to differentiate muscle contusion from focal myositis, which may have a similar imaging appearance.

The ultrasound appearance of hematomas is variable in time. Acute hematomas are hyperechoic and they become more hypoechoic with aging. They may have well-defined or irregular margins (Fig. 21.25a). Dynamic evaluation with muscle contraction is valuable for assessing dis-

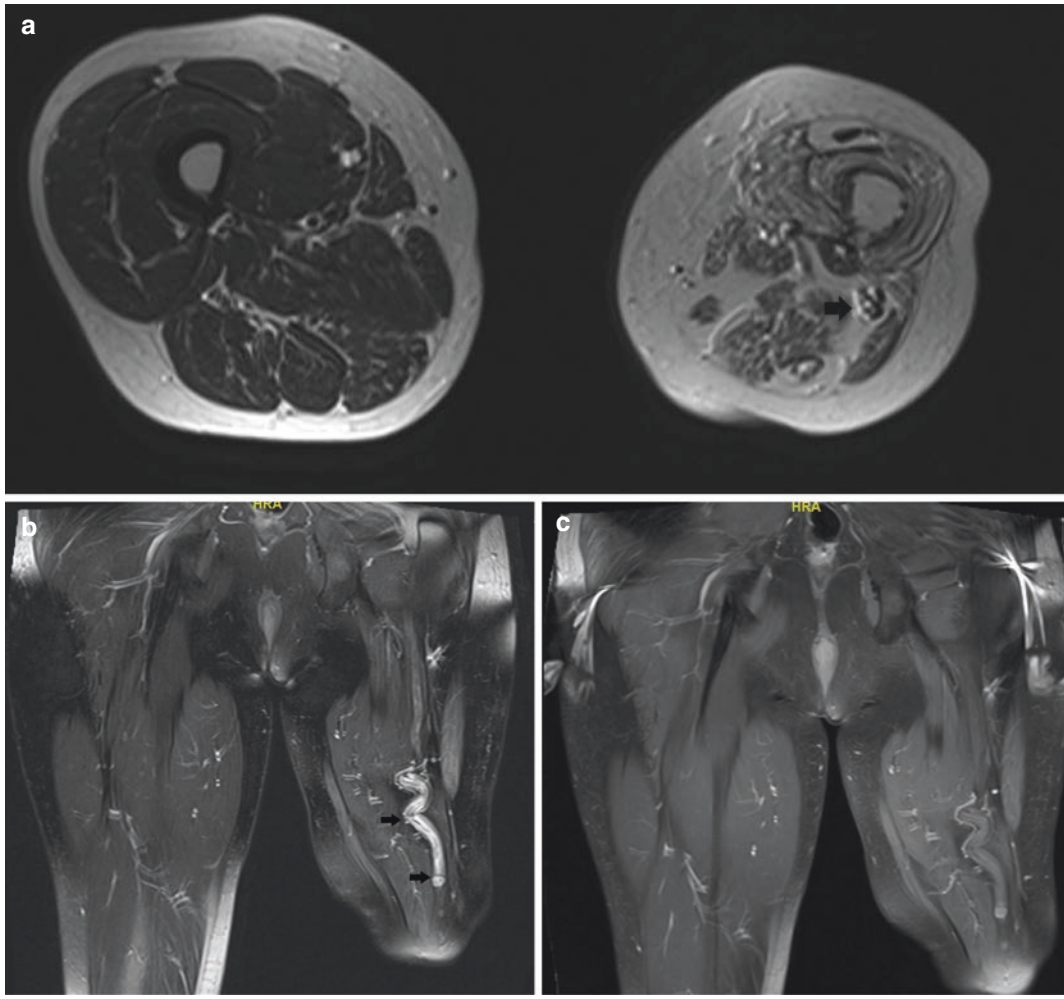

Fig. 21.24 Amputation neuroma of the left sciatic nerve in 46-year-old male: (**a**) axial T2-weighted MR image; (**b**) coronal FS T2-weighted MR image. (**c**) Coronal FS T1-WI following administration of gadolinium contrast. T2-WI. There is enlargement of the left sciatic nerve proximal to the site of amputation (*arrows* in **a**, **b**). Absence of significant enhancement of the sciatic nerve (**c**). Note muscle atrophy and fatty infiltration at the amputation stump

ruption of muscle architecture. On CT, acute hematoma appears as a hyperdense area; MR imaging has replaced CT in the imaging of hematomas.

The MR imaging appearance of muscular hematomas (Figs. 21.25 and 21.26) reflects the pathophysiology of forming hemoglobin breakdown products, which are the main constituents of a hemorrhagic collection. Further discussion of the pathophysiology of hemoglobin degradation is beyond the scope of this chapter.

In an acute hematoma, the signal characteristics are dominated by intracellular deoxyhemoglobin. The lesion is iso- or slightly hypointense on T1-weighted images compared with muscle. Susceptibility effects also lead to low signal on T2-weighted images [28].

A hematoma in the early subacute stage is characterized by the presence of intracellular methemoglobin. This produces a high signal intensity on T1-weighted images, often visualized as a high-intensity peripheral rim. This high-intensity rim is a useful sign, as it may be the only clue that the mass is a hematoma. Susceptibility effects persist on T2-weighted images.

When loss of cell compartmentalization occurs in late subacute hematomas, extracellular methe-

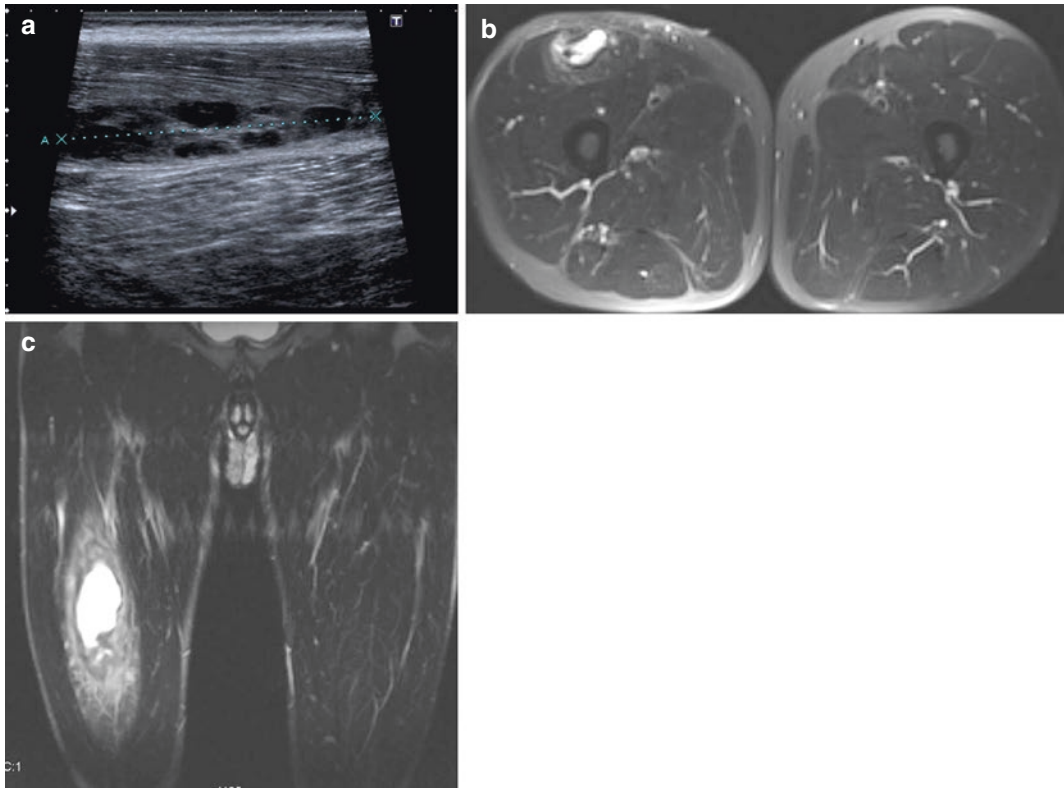

Fig. 21.25 Muscle hematoma in the right rectus femoris muscle. (**a**) Sagittal ultrasound shows focal disruption of the muscle fibers (hematoma); (**b**) axial FS T2-WI; (**c**) coronal FS T2-WI FS T2-WI. MRI confirms discontinuity of the right rectus femoris and the presence of a hyperintense hematoma with surrounding muscle edema

moglobin results in Tl shortening. On T2-weighted images, the hematoma may be outlined by an area of high signal intensity (Fig. 21.25b-c). Diffuse edema is also present within the muscle in acute and subacute hematomas.

Finally, hemosiderin in a chronic hematoma also produces susceptibility effects on T2-weighted images. This results in low signal intensity on T1-weighted images and particularly on T2-weighted images. Blooming artifact is seen when using gradient echo imaging. Furthermore, this phenomenon is accelerated at the periphery of the collection, resulting in a peripheral hypointense rim, whereas the central portion of the hematoma may remain hyperintense [28].

It is important to differentiate hematoma from hemorrhagic tumor, because hemorrhage may obscure tumor tissue. T1-weighted images with fat suppression can aid in the differentiation, further discrimination methemoglobin from fatty tissue [39]. The best features suggesting hematoma are the progressive decrease in size of the lesion, the presence of fluid-fluid levels, and the time-dependent signal intensity changes. Conversely, the presence of enhancing nodules after contrast medium administration may suggest the presence of tumor [85]. Nevertheless, organized hematomas can show some enhancement.

When in doubt a biopsy should be performed to establish a confident diagnosis, especially if there is an increase in size of the hemorrhagic mass.

A chronic expanding hematoma is an entity characterized by its persistence and increasing size for more than 1 month after the initial hemorrhage [108]. MR reveals a heterogeneous signal intensity on both T1- and T2-weighted images, with a peripheral rim of low signal intensity [6]. Although the absence or presence of contrast enhancement is often used to distinguish a hematoma or a hemorrhagic neoplasm, intrale-

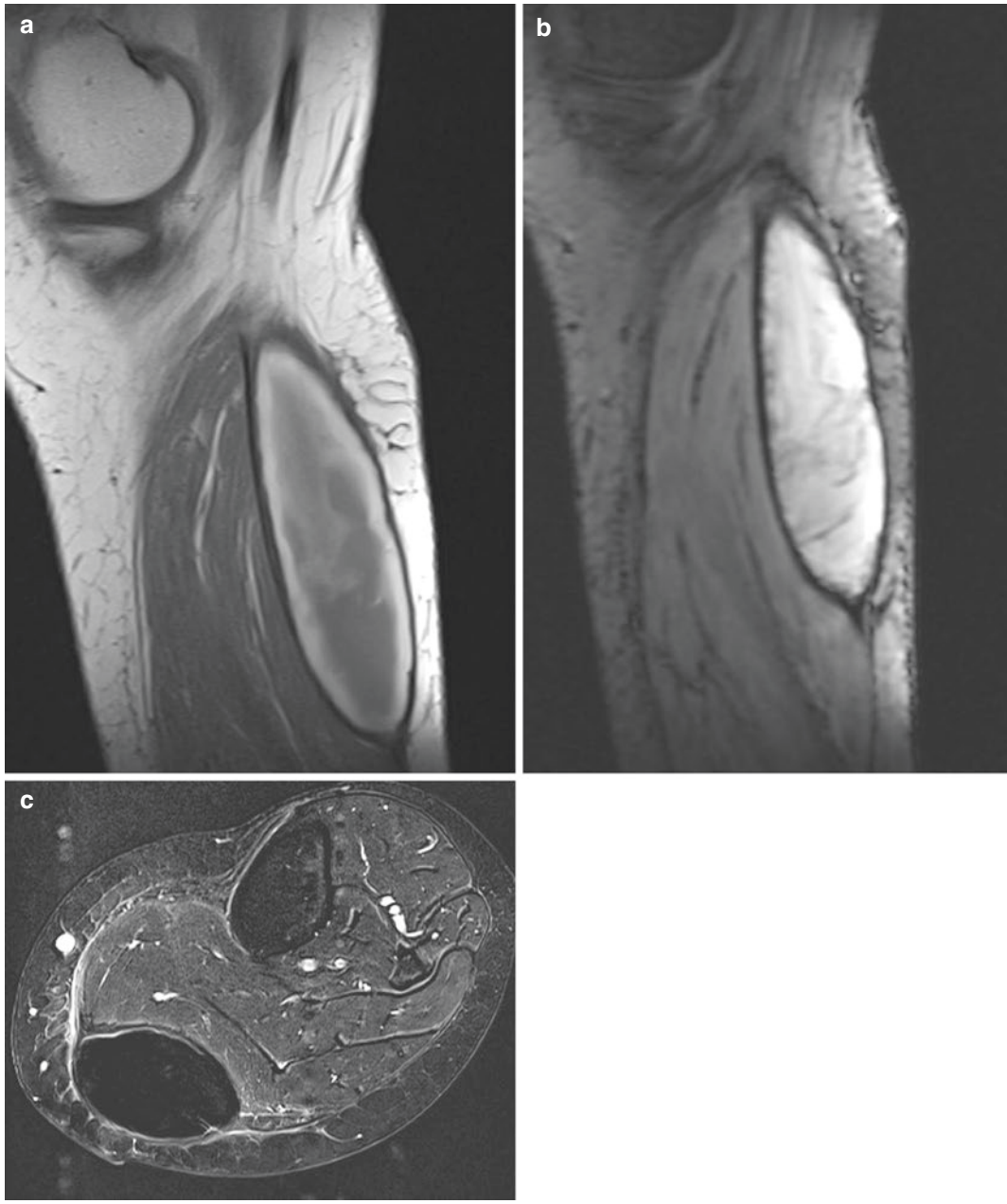

Fig. 21.26 Subacute hematoma of the calf: (**a**) sagittal spin echo T1-weighted MR image, (**b**) sagittal gradient MR image. There is a fusiform mass of intermediate signal intensity of the center, high signal intensity of the periphery, and adjacent subtle dark peripheral rim on T1-weighted images. The different layers are due to the presence of, respectively, intra- and extracellular methemoglobin and hemosiderin (**a**). On gradient images, overall signal intensity is very high, exception made for a low signal intensity peripheral rim caused by hemosiderin (**b**). Signal intensities are characteristic for a subacute hematoma. (**c**) Axial substraction image after injection of intravenous gadolinium contrast shows the absence of nodular enhancement which argues against the presence of underlying tumoral mass lesion

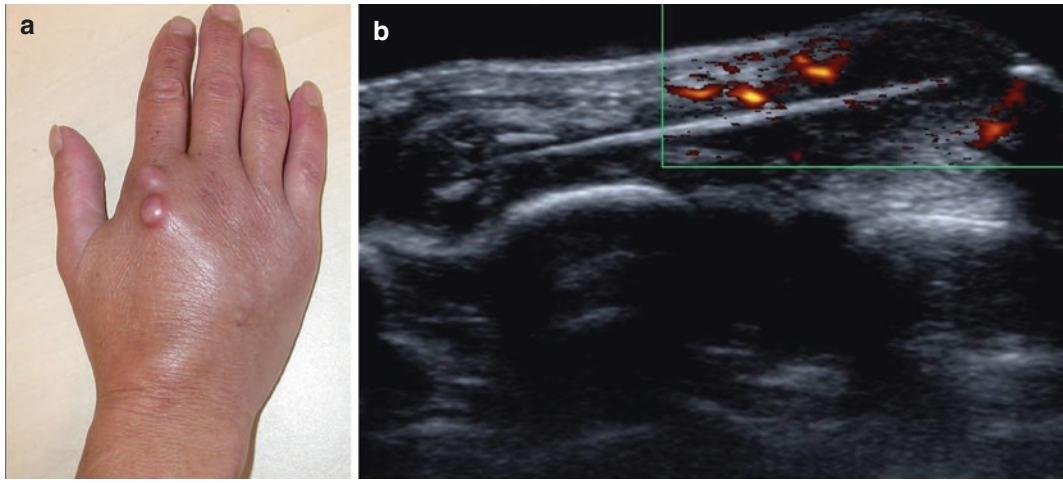

Fig. 21.27 Inflammatory reaction surrounding a wooden splinter at the dorsal aspect of the hand. (**a**) Clinical picture of the right hand showing swelling of the dorsum of the hand. There are two more pronounced red noduli at the second metacarpal corresponding to focal abscesses. (**b**) Ultrasound showing the wooden splinter as a linear reflection with surrounding power Doppler signal in keeping with increased vascularity

sional nodular enhancement pattern may be seen in chronic expanding hematoma [108].

21.2.4.2 Foreign Body Reactions

Foreign bodies such as plastic, wood, glass, and silica may penetrate the soft tissues and produce an inflammatory reaction. Clinically, a foreign body reaction first appears as a painful soft tissue swelling, and after a quiescent period of weeks or months, the symptoms may reappear [175]. If not removed immediately, a foreign body can become encapsulated with fibrous tissue and form a granuloma. The presence of histiocytes and giant cells with a surrounding inflammatory reaction is useful in establishing the diagnosis.

Different imaging methods have each their advantages and limitations in the evaluation of foreign bodies. Radio-opaque bodies can be demonstrated on conventional radiographs. When the lesion is in or near the bone, radiographs can show osteolytic and/or osteoblastic bone lesions [99, 159]. Since a positive history of penetrating trauma is not always obvious, and some lesions can be radiolucent, a foreign body reaction can be mistaken for a neoplasm [99, 159].

Ultrasound is a primary imaging tool when conventional radiographs fail in detecting the foreign object. Its use in the detection and guided retrieval of a suspected foreign body has been well established [29]. Ultrasound shows large differences in acoustic impedance between hyperechoic foreign bodies and hypoechoic surrounding inflammatory tissue (Fig. 21.27).

On MR imaging studies, the foreign body itself is usually low, due to the presence of few mobile protons in the commonly found foreign materials (glass, wood, metal, etc.) [85, 99, 124, 182]. However, dispersed oil droplets can induce a granulomatous reaction and present as subcutaneous or intramuscular soft tissue masses with high signal on T1-weighted images [101]. An intralesional fat-fluid level may be seen at the interface of fatty and necrotic components in case of injection granulomas in bodybuilders. The combination of the clinical history and the typical location at usual locations for injection (such as the shoulder and gluteus muscles) are the clues to the correct diagnosis of these pseudotumoral soft tissue masses [8, 185].

The foreign body reaction appears isointense to muscle on T1-weighted images and hyperintense compared to subcutaneous fat on T2-weighted images. It is usually seen as an elongated lesion without well-defined margins and surrounded by edema, best seen on T2-weighted images. The foreign body itself

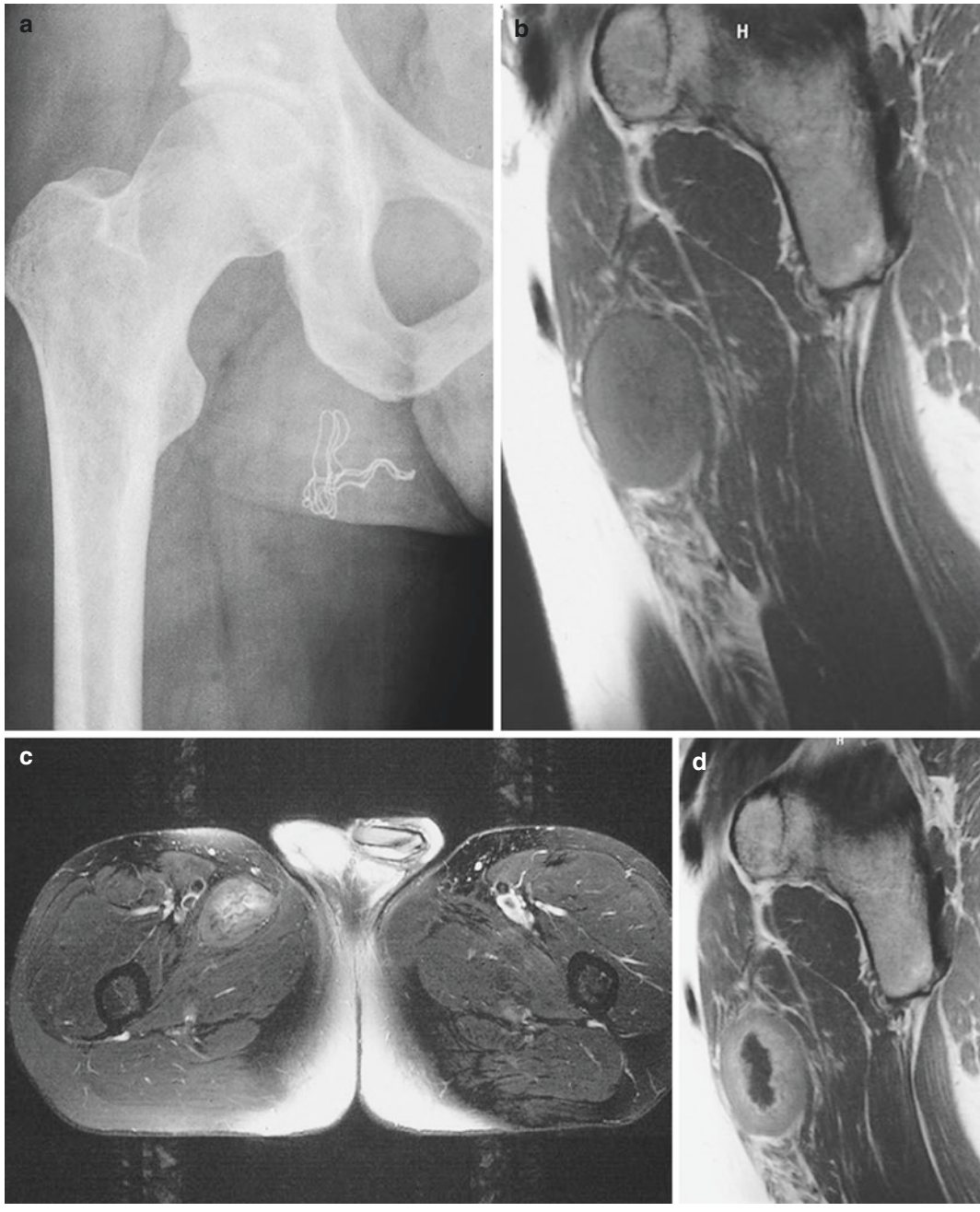

Fig. 21.28 Foreign body in a 31-year-old man with a textiloma (gossypiboma) three years after orthopedic surgery: (**a**) plain radiograph of the right proximal thigh; (**b**) sagittal spin echo T1-weighted MR image; (**c**) axial fat saturated turbo spin echo T2-weighted MR image; (**d**) sagittal spin echo T1-weighted MR image after gadolinium contrast administration. Presence of a foreign body, corresponding with a retained surgical sponge (**a**). A well-circumscribed nodular lesion is seen at the anteromedial aspect of the right thigh, with a slight hypointense center on T1-weighted MR images (**b**). On T2-weighted MR images, the lesion is inhomogeneous and has a predominantly intermediate signal intensity (**c**). No sign of necrosis is observed. After gadolinium contrast administration, there is strong enhancement of the periphery of the lesion (**d**)

is hypointense both on T1-weighted images and T2-weighted images [85, 99, 182] (Fig. 21.28).

21.2.4.3 Calcific Myonecrosis

Calcific myonecrosis is an uncommon and late sequela of trauma, occurring with a reported delay ranging from 10 to 64 years after an initial traumatic event [54, 78, 145, 179]. The average age at the time of diagnosis is 56 years [78]. A fusiform soft tissue mass develops in the traumatized compartment, often mimicking a neoplastic process [100, 131, 207]. It is almost exclusively found in the lower extremities, especially in the anterior and lateral compartments of the leg [54, 145]. Other reported more unusual locations include the foot [78, 141] and upper extremities [100].

The exact pathogenesis is still unknown. It usually occurs after trauma of the femur or tibia, with subsequent development of compartment syndrome, although it also can take place after neurovascular injury without compartment syndrome [66]. One hypothesis states that the occurrence of compartment syndrome leads to decreased regional circulation with necrosis and fibrosis [131]. The end result is cystic degeneration of the involved muscle, with platelike calcification of a rind of fibrous tissue around the central liquefaction zone or hematoma. The expansive character of the lesion is believed to be secondary to intralesional hemorrhage [131]. Some investigators believe that pathologic processes like posttraumatic cysts of soft tissue, chronic expanding hematoma, and calcific myonecrosis share a common pathophysiological mechanism [78]. Mentzel proposes the unifying term of "ancient hematoma" to describe these entities [121].

Plain radiographs show a fusiform mass along with the long axis of the muscles with peripheral calcifications, often with a linear plate- or plaquelike configuration, which may precipitate in the cystic area of the lesion. Ultrasound demonstrates scattered but predominantly peripherally located calcifications visible as echogenic foci with retroacoustic shadowing. Central areas of liquefaction or mobile calcium debris may also be seen [145]. Computed tomography (CT) clearly depicts the compartmental distribution with peripheral calcifications and sometimes fluid-calcium levels. Concomitant pressure erosions in adjacent bone may be present, usually with no or minimal periosteal reaction. However, erosions can be extensive thereby mimicking a soft tissue sarcoma. On MRI the periphery of the lesion shows a low-intensity rim on T1-WI because of abundant calcification. T1- and T2-WI demonstrate the heterogeneity of the lesion explained by repeated intralesional hemorrhage with accumulation of blood (breakdown) products, liquefaction necrosis, and calcified areas. Hyperintensity on T1-WI is the result of subacute hemorrhage with subsequent hemoglobin degradation to methemoglobin or the presence of a proteinaceous content of cystic parts in the lesion. The lesion may also show hyperintense areas on T2-WI corresponding with cystic parts or liquefaction necrosis. Other parts of the lesion demonstrate intermediate to low signal intensity according to the degree of calcification. There is typically no enhancement after intravenous contrast administration, unless there is superimposed inflammation often due to mobilization of plaque and penetration through the muscle fascia [54, 66] (Fig. 21.29).

Infection of the mass without recent surgical interventions is very rare but has been reported [78].

21.2.4.4 Hypothenar Hammer Syndrome

The hypothenar hammer syndrome is a rare clinical entity, with a typical presentation of unilateral digital ischemia due to embolic digital artery occlusion from a thrombosed palmar ulnar artery. It is commonly found in adult males who usually in an occupational context repeatedly strike an object with the heel of the palm of the dominant hand. This causes damage to the superficial division of the distal ulnar artery as it passes over the hamate bone in the hypothenar region (Fig. 21.30).

While most cases are unilateral, Ferris found in a large series a striking incidence of similar changes in the asymptomatic and less traumatized hand [57]. Based on the findings in this series, he hypothesized that preexisting fibrodysplasia of the palmar ulnar artery may predispose

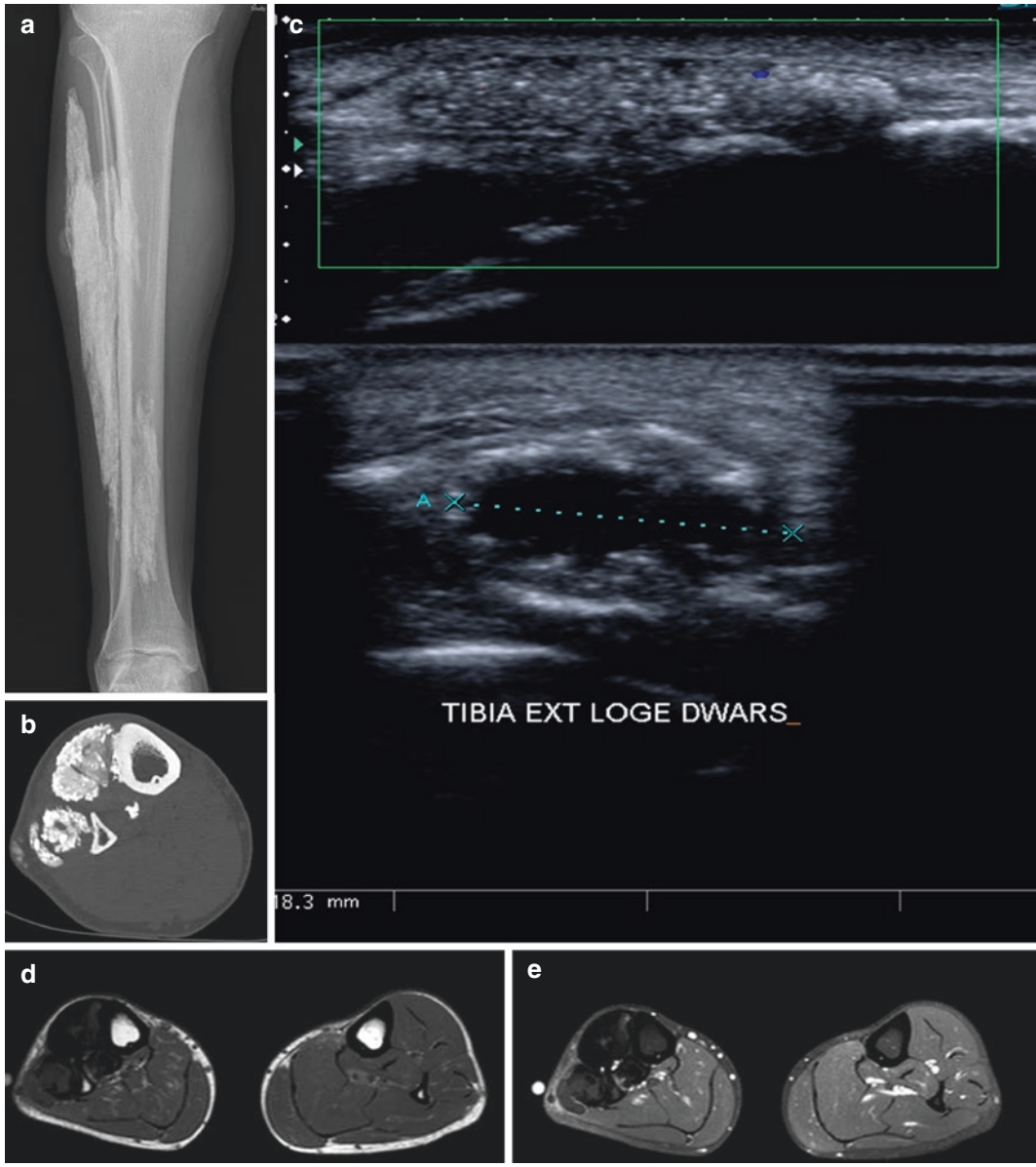

Fig. 21.29 A 52-year-old male with a fusiform mass in the right lower leg and a previous history of motor vehicle accident 34 years previously: (**a**) plain radiograph, (**b**) axial CT of the right lower leg, (**c**) longitudinal (*upper image*) and axial (*lower image*) ultrasound, (**d**) axial T1-weighted MR image, and (**e**) axial FS T1-weighted MR image after administration of gadolinium contrast. Plain radiograph (**a**) reveals peripherally plaque-like calcifications anterolaterally in the right lower leg. On CT, the lesion is located within the anterior and peroneal compartment. The calcifications are denser in the periphery than in the center. There is subtle pressure erosion on the fibula (**b**). US shows mobile calcium debris on the upper image, whereas peripherally located platelike calcifications with retroacoustic shadowing are seen in other areas (*low* image) (**c**). Due to the presence of calcifications, the lesion is of low signal on T1- and T2-weighted images (not shown), (**d**) and there is only subtle subcutaneous enhancement at the peroneal compartment, due to superposed inflammatory reaction around the plate of calcification that penetrated the fascia (**e**) (Case courtesy of H. Declercq, Dendermonde)

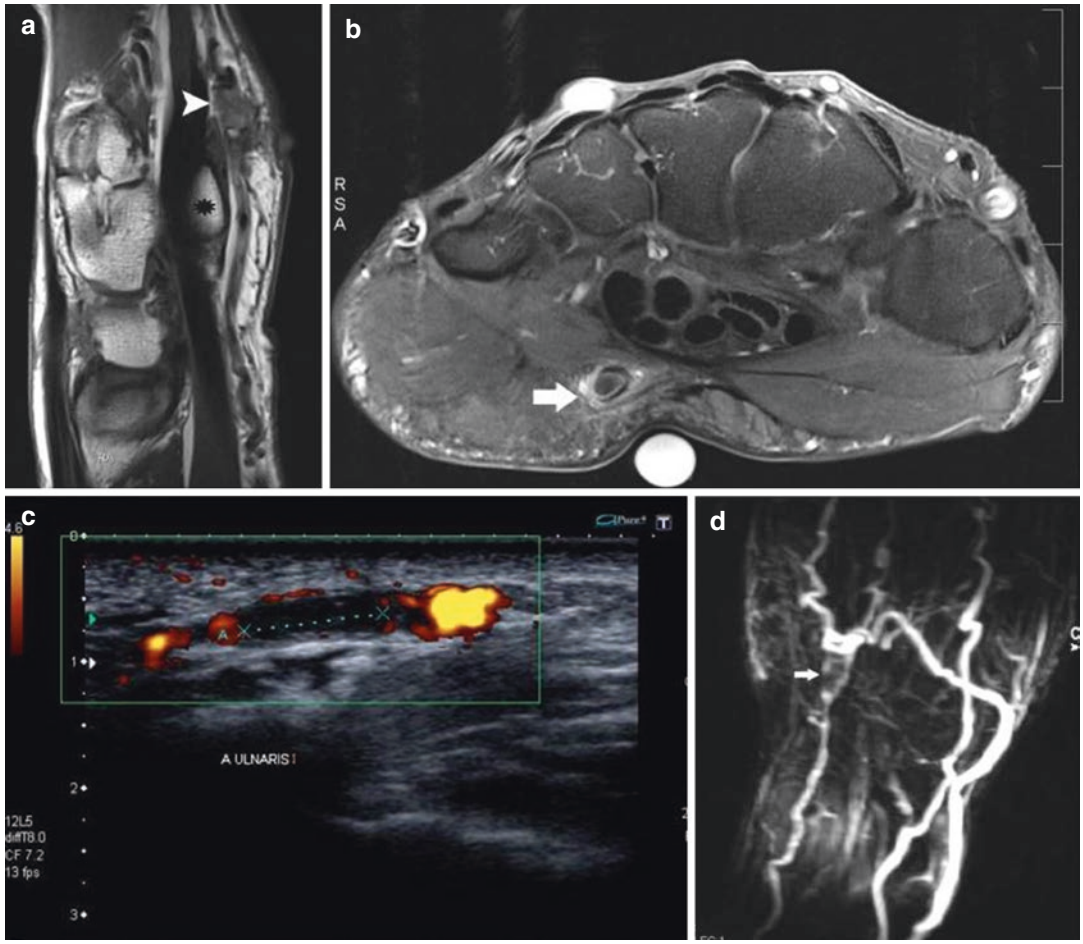

Fig. 21.30 Hypothenar hammer syndrome. (**a**) Sagittal SE T1-WI shows a hypointense lesion superficial to the flexor tendons (*arrowhead*) and immediately distal to the hamulus of the hamate (*asterisk*). (**b**) Axial FS SE T1-WI after intravenous administration of gadolinium contrast medium shows focal aneurysmal dilatation of the ulnar artery with central thrombosis (*arrow*). Note only faint peripheral enhancement. (**c**) Doppler ultrasound shows intraluminal thrombosis of the aneurysm of the ulnar artery. (**d**) MR angiography shows multiple stenoses at the distal ulnar artery with aneurysmal dilatation with internal clot formation (*arrow*) (Reproduced with permission from: Vanhoenacker et al. [182])

to artery damage when subjected to repetitive local trauma.

The typical location of the lesion on the distal part of the ulnar artery distal to the hamulus of the hamate bone, the history of repeated trauma and digital ischemia, the signal intensity of the lesion (indicative of thrombosis), and direct demonstration of occlusion of the ulnar artery with different imaging techniques (Doppler ultrasound, MR and CT angiography) may allow a correct diagnosis (Fig. 21.30) [26, 50, 64, 182, 193]. Catheter angiography [57] is currently rarely required for diagnosis. It may show segmental ulnar artery occlusion in the affected palm or "corkscrew" elongation with alternating stenoses and ectasia (Fig. 21.30). Multiple digital artery occlusions may be demonstrated as well.

Treatment is mostly conservative, with surgery only used in rare instances.

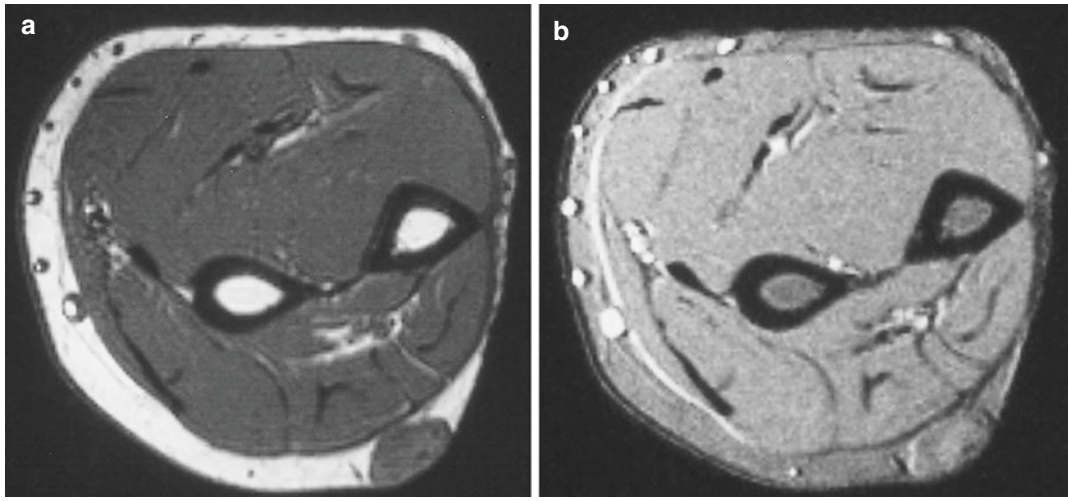

Fig. 21.31 A 60-year-old man with a subcutaneous lesion in the left lower arm: (**a**) axial spin echo T1-weighted MR image; (**b**) axial gradient echo T2-weighted MR image. The images reveal a well-defined nodular mass in the subcutaneous fat, with no specific signal characteristics (**a**, **b**). A biopsy confirmed the diagnosis of a pilomatricoma

21.2.5 Skin Lesions

21.2.5.1 Pilomatricoma

Pilomatricoma, formerly known as calcifying epithelioma of Malherbe, is a benign slow-growing superficial tumor of the hair follicle, most commonly seen in children and young adults [97]. The term "pilomatrixoma" was also previously used, better indicating its histological origin from hair matrix cells. The lesion is typically found (in decreasing order of prevalence) in the head, neck, upper extremities, trunk, and lower extremities, presenting as a solitary subcutaneous calcified mass. Non-calcified pilomatricomas are also possible [116]. Most lesions are small, usually less than 3 cm, but larger masses have been reported [82]. A rare association of multiple pilomatricomas with myotonic dystrophy, Steinert disease, Turner syndrome, sarcoidosis, and Gardner syndrome has been described [97, 149].

On ultrasound, the lesion is oval-shaped or rounded and usually relatively hyperechogenic and well-defined. The majority of the lesions are slightly heterogeneous with often some small intralesional calcifications. Areas of increased power Doppler may be seen, particularly at the periphery. Irregular delineation is rare [111].

MR images reveal a well-defined subcutaneous tumor, with intermediate signal intensity on T1-weighted images and low-to-intermediate signal intensity on gradient echo and T2-weighted images (Fig. 21.31) [23]. T2-weighted fat-suppressed images may show bands of hyperintense signal radiating away from a lower signal intensity center toward the periphery [23, 77]. On gadolinium-enhanced T1-weighted images, enhancement is possible but not necessary [23, 77, 82, 116]. A possible inhomogeneous appearance is due to the amorphous calcification of the tumor.

A pilomatrix carcinoma is an uncommon aggressive form, representing up to 9 % of benign pilomatricomas at any age [114]. Local invasion is possible, but distant metastasis is rare.

21.2.5.2 Granuloma Annulare

Granuloma annulare is a benign inflammatory dermatosis of unknown cause, characterized by formation of discolored dermal papules that tend to be ring-shaped or annular. It typically presents as a rapidly growing, solitary, painless, subcutaneous nodule without calcification in children less than 5 years old [93].

Clinically four forms can be distinguished: three cutaneous forms (erythematous, perforating, and

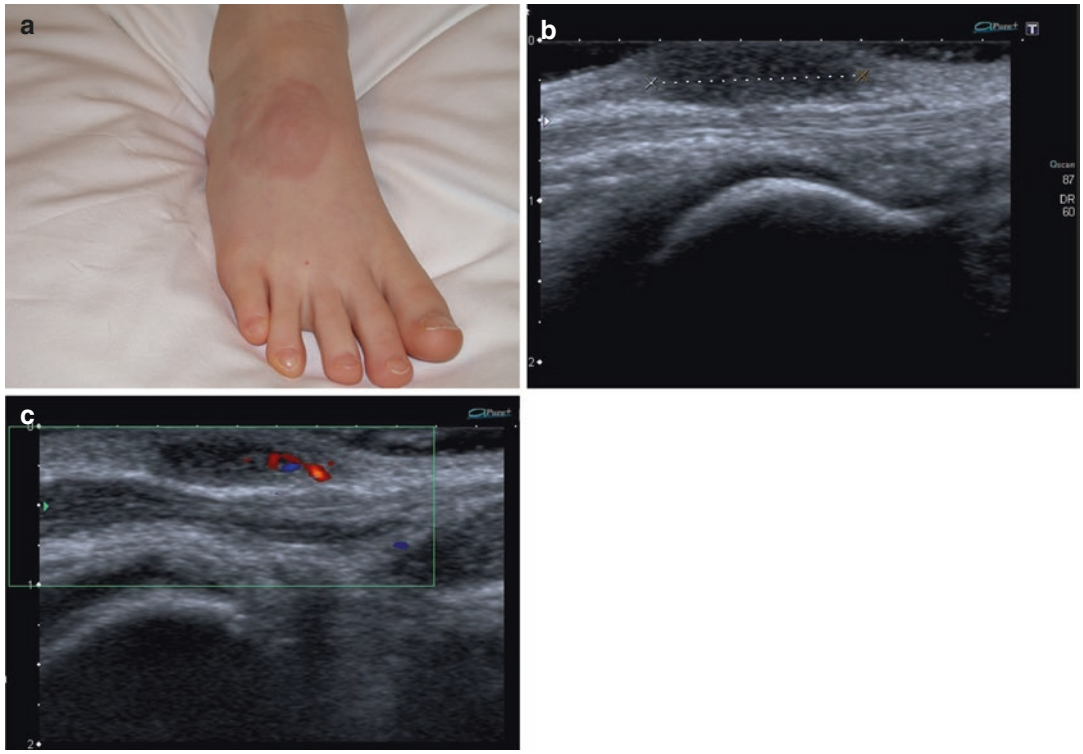

Fig. 21.32 Granuloma annulare in a young child: (**a**) clinical image. Note a reddish discolored annular plaque over dorsal aspect of foot; (**b**) longitudinal ultrasound; (**c**) color Doppler. There is a hypoechogenic nodular mass in the subcutaneous fat (**b**), with slightly increased Doppler signal (**c**)

generalized) and the subcutaneous form. It is this latter form that can present as a soft tissue mass and requires local staging by imaging modalities.

Radiographs generally display a soft tissue mass of increased density in the subcutaneous compartment, without evidence of bone involvement or mineralization [94, 181]. Ultrasound reveals an ill-defined solid mass that is hypoechoic to surrounding fat [127, 155, 181]. There may be some faint increased Doppler signal (Fig. 21.32).

The MR characteristics of subcutaneous granuloma annulare have been described by several authors [41, 94, 181]. T1-weighted images show an ill-defined subcutaneous mass, isointense to muscle, with a slightly hypointense signal intensity compared to fat on T2-weighted images (Fig. 21.33) [181]. Nevertheless, T2-weighted images may show a heterogeneous hyperintense lesion [41].

After intravenous contrast injection, a diffuse enhancement can be seen [170].

21.2.5.3 Epidermal Inclusion Cyst

Epidermal inclusion cysts (or infundibular cyst) are benign subcutaneous cysts formed by the cystic enclosure of the epithelium within the dermis. They are filled with a mixture of keratin and lipid-rich debris [174]. Commonly they are iatrogenic [152], resulting from mechanical obstruction, scarring, or inflammation [209]. Lesions can occur anywhere, but are mostly found in the head, neck, and trunk. Less than 10 % occur in the extremities [174].

On ultrasound, the lesion appears as a circumscribed rounded or oval hypoechoic mass with retroacoustic sound enhancement (Fig. 21.34), sometimes in association with a hair follicle. There may be slight heterogeneity. An onion peel appearance, which is frequent in testicular epidermoid cyst, is rare in cutaneous lesions. There is no increased Doppler, unless there may be rupture of the cysts. In the latter scenario, the lesion is irregularly delineated and there may be increased Doppler signal [111].

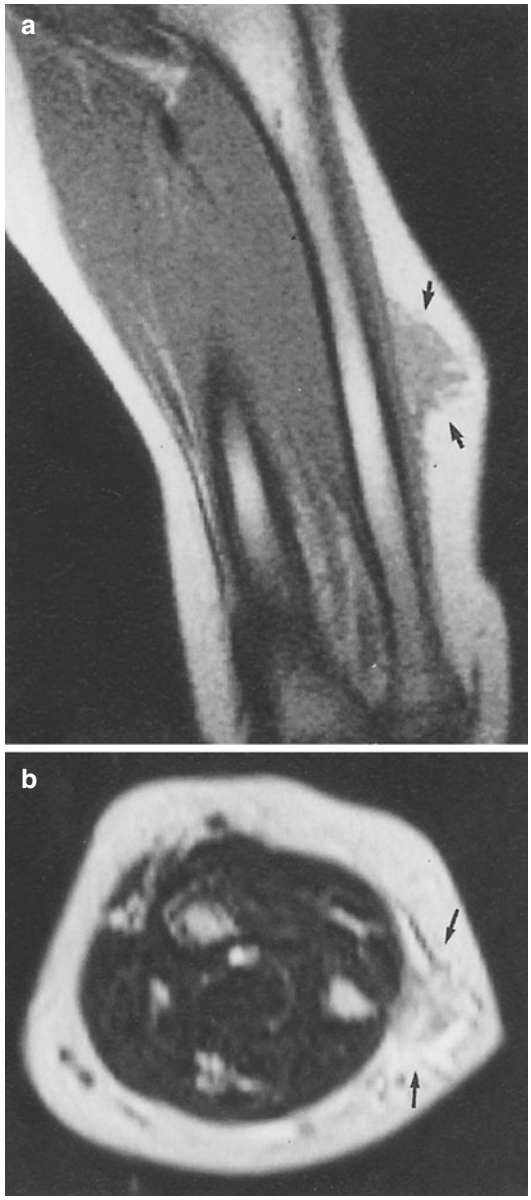

Fig. 21.33 A 4-year-old girl with a small but rapidly growing nodule on the extensor aspect of the left forearm: (**a**) sagittal spin echo T1-weighted MR image; (**b**) axial spin echo T2-weighted MR image. The lesion appears isointense to muscle on T1-weighted images (**a**), with a small hyperintense peripheral rim on T2-weighted images (**b**). The peripheral high signal rim on T2-weighted images is suggestive for a small zone of perilesional edema. These findings are compatible with a subcutaneous granuloma annulare in a child

The MR findings resemble that of a simple cyst, with signal characteristics varying with the cholesterol and keratin debris of the cyst. High cholesterol and keratin debris content can appear hyperintense to muscle on T1-weighted images, particularly if fat suppression is used (Fig. 21.34). Uncomplicated cysts show no contrast enhancement [111]. Cysts may rupture, provoking a foreign body reaction, granulomatous reaction, or abscess formation [209]. On occasion, they may be multiloculated.

21.2.6 Metabolic Lesions

21.2.6.1 Gout and Pseudogout

Gout is a metabolic disorder characterized by hyperuricemia and deposits of monosodium urate monohydrate crystals in periarticular soft tissues. In pseudogout, depositions consist of calcium pyrophosphate dihydrate crystals (CPPD). The disorders most frequently affect the first metatarsophalangeal joint, followed by the ankle, knee, wrist, fingers, and elbow. Clinical and radiographic findings are usually diagnostic (Figs. 21.35 and 21.36). On occasion, these conditions may present as a soft tissue mass [31, 157, 187]. Calcification of the mass is seen in pseudogout (Fig. 21.35) (reproduced with permission from Vanhoenacker et al. (2011) Pseudotumoural soft tissue lesions of the hand and wrist: a pictorial review. *Insights Imaging*. 2011 Jun; 2(3): 319–333).

The MR imaging features of gouty arthritis include synovial thickening and joint effusion [171]. Both conditions display a low-to-intermediate signal intensity on T1-weighted images [171]. T2-weighted image characteristics vary from a heterogeneously hypointense to hyperintense mass on T2-weighted images [31], depending on the degree of inflammation. Enhancement after intravenous contrast injection may be seen [36] (Fig. 21.36).

21.2.6.2 Calcific Tendinosis

Calcific tendinosis, also known as calcific tendonitis or calcium hydroxyapatite disease, is a self-limiting inflammatory disorder, characterized by the deposition of hydroxyapatite crystals

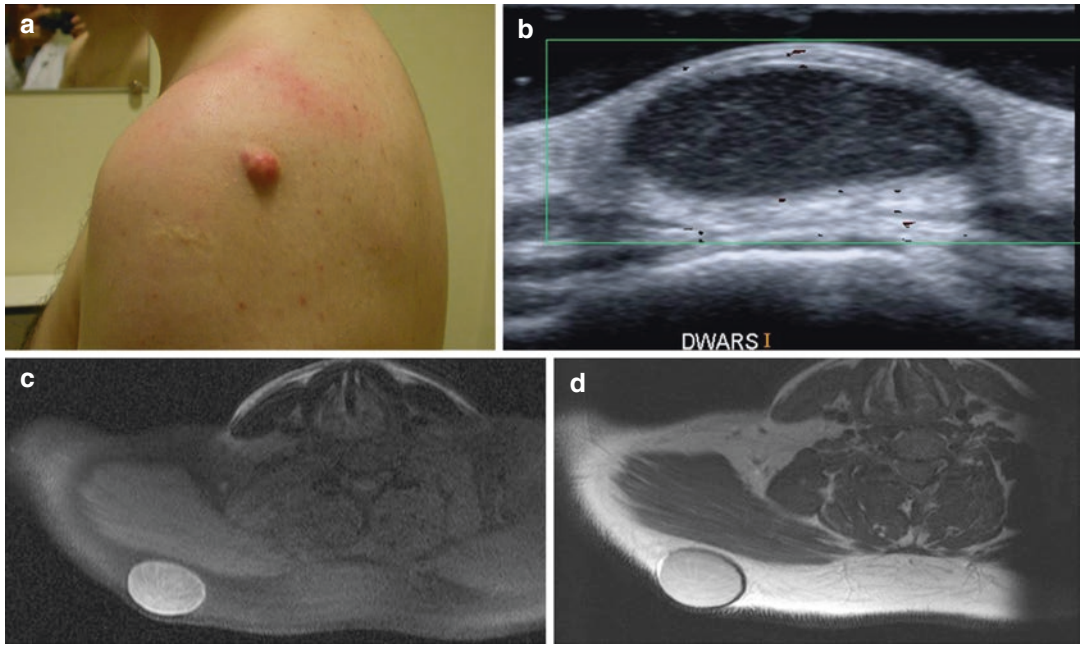

Fig. 21.34 Epidermal inclusion cyst at back of the trunk: (**a**) clinical image of an epidermoid inclusion cyst on a typical location. (**b**) ultrasound shows a well-defined hypoechoic ovoid lesion with retroacoustic sound enhancement; (**c**) axial FS T1-weighted MR image. The lesion is of high signal due to the presence of cholesterol and keratin debris; (**d**) axial T2-weighted MR image. Note the presence of a chemical shift artifact at the ventral interface of the lesion and the adjacent subcutaneous fat

in tendons and periarticular soft tissue (Fig. 21.35). It is mostly seen in the shoulder, but other locations as the hip, hand, and wrist are also possible.

Radiography has an important role, revealing amorphous calcification or a radio-opaque dense mass at the suspected site. Bone erosion of the adjacent cortical bone is not common but has been reported [40, 53, 59], presumably secondary to inflammation at the tendon insertion or mass effect. This can lead to the wrong diagnosis of an aggressive neoplasm, especially when previous imaging studies are not available. While periarticular calcifications are typically encountered at the tendon attachment sites, they can occur in and around ligamentous structures with concomitant inflammation [5].

Both T1- and T2-weighted images demonstrate a signal void in the area of calcification (Fig. 21.37). A high signal intensity in surrounding muscles related to edema can be seen on T2-weighted images [174]. Bone marrow edema can also incidentally be found [40], on occasion mimicking an osseous metastasis [92, 200].

21.2.6.3 Tumoral Calcinosis

Idiopathic tumoral calcinosis is characterized by the presence of progressively enlarging juxta-articular calcified soft tissue masses. Chemical analysis of these deposits shows a mixture of amorphous calcium carbonate, calcium phosphate, and hydroxyapatite crystals [128, 146]. An inborn error of phosphorus and vitamin D metabolism is the most probable hypothesis in the pathogenesis of idiopathic tumoral calcinosis; however, the exact pathogenesis remains unclear. Familial occurrence and hyperphosphatemia are observed in only one-third of the reported cases [1, 61, 63, 198]. In its idiopathic form, tumoral calcinosis usually occurs in the first three decades of life. There is apparently no sex predominance [146]. Predilection for black people and people from tropical climates has been reported [13, 63].

Macroscopically, tumoral calcinosis is well circumscribed and has a multinodular growth

Fig. 21.35 Examples of pseudomasses of the fingers due to metabolic diseases. (**a**) clinical picture of tophaceous gout. Periarticular soft tissue swelling best seen at the proximal interphalangeal joint of the third finger. (**b**) corresponding plain radiograph showing soft tissue swelling and adjacent periosteal new bone formation (*arrow*). (**c**) ultrasound of another patient with tophaceous gout at the metacarpophalangeal joint of the thumb, showing a hypoechoic mass with intralesional reflections with retroacoustic shadowing due to monosodium urate crystal deposition (*arrows*). (**d**) pseudogout (hydroxyapatite deposition disease) in another patient. Plain radiograph showing linear and amorphous calcifications at the joint capsule of the distal interphalangeal joint of the index (*arrows*)

Fig. 21.36 Tophaceous gout of the patella and quadriceps tendon in a 51-year-old man: (**a**) sagittal T1-weighted MR image, (**b**) sagittal FS T2-weighted MR image, (**c**) sagittal FS T1-weighted MR image after administration of gadolinium contrast, and (**d**) sagittal reformatted cone beam CT image. There is a soft tissue mass within the distal quadriceps extending into the superior aspect of the patella. The mass was hypointense on T1-weighted images (WI) (**a**, *arrows*) and slightly heterogeneous hyperintense on fat saturated intermediate-WI (**b**, *arrows*). A bone infarct is seen in the distal femur (*arrowhead* in **a**, **b**). After administration of gadolinium contrast, heterogeneous enhancement was seen (**c**) cone beam CT shows the soft tissue mass as being slightly hyperdense to the surrounding soft tissue (**d**, *arrow*). Partially sclerotic delineated osteolysis is seen at the patella (**c**, *arrowhead*) (Reproduced by permission from Vansevenant et al. [187])

pattern with yellow-gray pasty cut surface. A milky heterogeneous material can be washed out revealing cystic spaces delineated by fibrous walls.

Two histological types are distinguished on microscopic level, corresponding to the so-called active and inactive stages. The former is more frequent. It is characterized by the presence of a

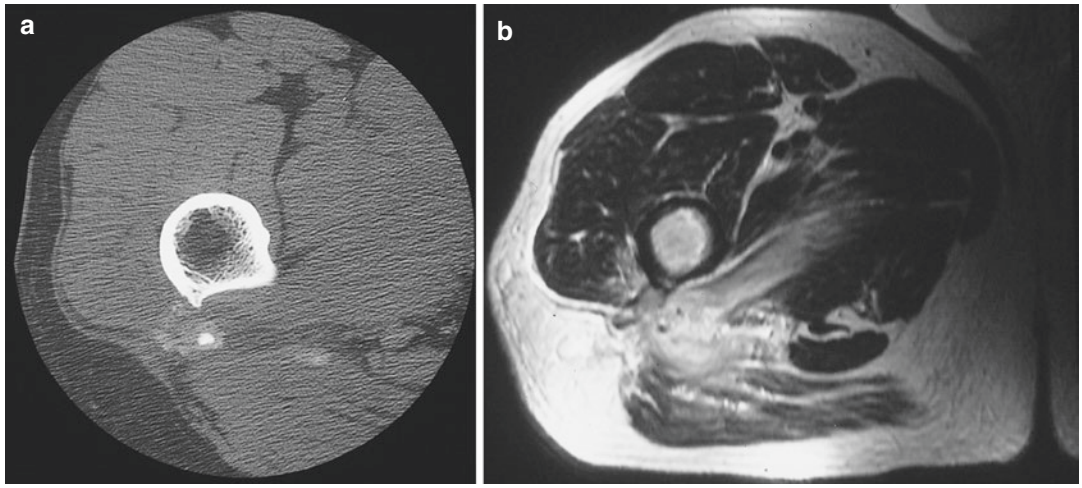

Fig. 21.37 A 47-year-old man with a painful right thigh, but no history of trauma: (**a**) CT scan; (**b**) axial turbo spin echo T2-weighted MR image. Multiple calcifications located posteriorly of the femur are present on CT scan (**a**). MR imaging reveals an ill-defined process of increased signal intensity at the gluteus muscles, with edema extending in the gluteus maximus, adductor magnus, and vastus lateralis muscles. Multiple small soft tissue calcifications posterior form the linea aspera can be seen. These imaging findings are characteristic of calcific tendonitis of multiple muscles, mainly the right gluteus maximus muscle

large central calcified granular area bordered by an inflammatory infiltrate with predominant epithelioid histiocytes mixed with several lymphocytes and scattered giant multinuclear macrophages. The cellular infiltrate is limited by thick fibrous septa. In the inactive stage, the inflammatory infiltrate is absent.

Clinically, it presents as a slow-growing soft tissue mass in the vicinity of large joints, with the hip joint being the most common site [126, 130]. The other sites are the elbow, shoulder, knee, wrist, hand, and foot [61, 63, 129, 130]. The size of the lesion varies considerably depending on the location. Lesions at the buttock tend to be larger than those at the elbow [30, 130].

The disease is more often multiple than solitary [61]. The lesion is usually painless, but growing lesions may interfere with joint motion or cause pain by nerve compression [7, 25, 115]. The overlying skin is usually intact, although ulcerations or sinuses occasionally appear, draining chalky white or yellow milklike fluid. However, the mass can become a site of secondary infection [115].

Laboratory analysis usually indicates normal calcemia, parathyroid hormone level, renal function, alkaline phosphatase, and uremia. Phosphatemia and vitamin D levels are normal or slightly elevated [156].

On radiographs (Fig. 21.38a), the characteristic appearance of tumoral calcinosis is a well-demarcated lobulated calcified mass located in the periarticular soft tissue, commonly at the extensor side. The lobules are separated by radiolucent lines, histologically corresponding to fibrous septa. This may cause a "chicken wire" appearance of plain radiographs. Fluid-calcium levels may be seen on upright radiographs [25, 130, 173].

Generally, the mass is unattached to bones and there are no osseous anomalies, although periosteal reaction or pressure erosion of the adjacent bone rarely occurs [95]. Associated diaphysitis and periostitis of tubular bones has been described as well [43].

Radionuclide bone scans show increased uptake of Tc-99 m-labeled phosphate compound in the mass and help to detect and quantify all lesions especially asymptomatic ones [1, 7].

Tumoral calcinosis can be examined by ultrasound (Fig. 21.38c), especially when the lesion is not very calcified. Typically, the lesion appears as a multiloculated mass with multiple cavities limited by echoic thin septa. Some of these septa may be vascularized on color

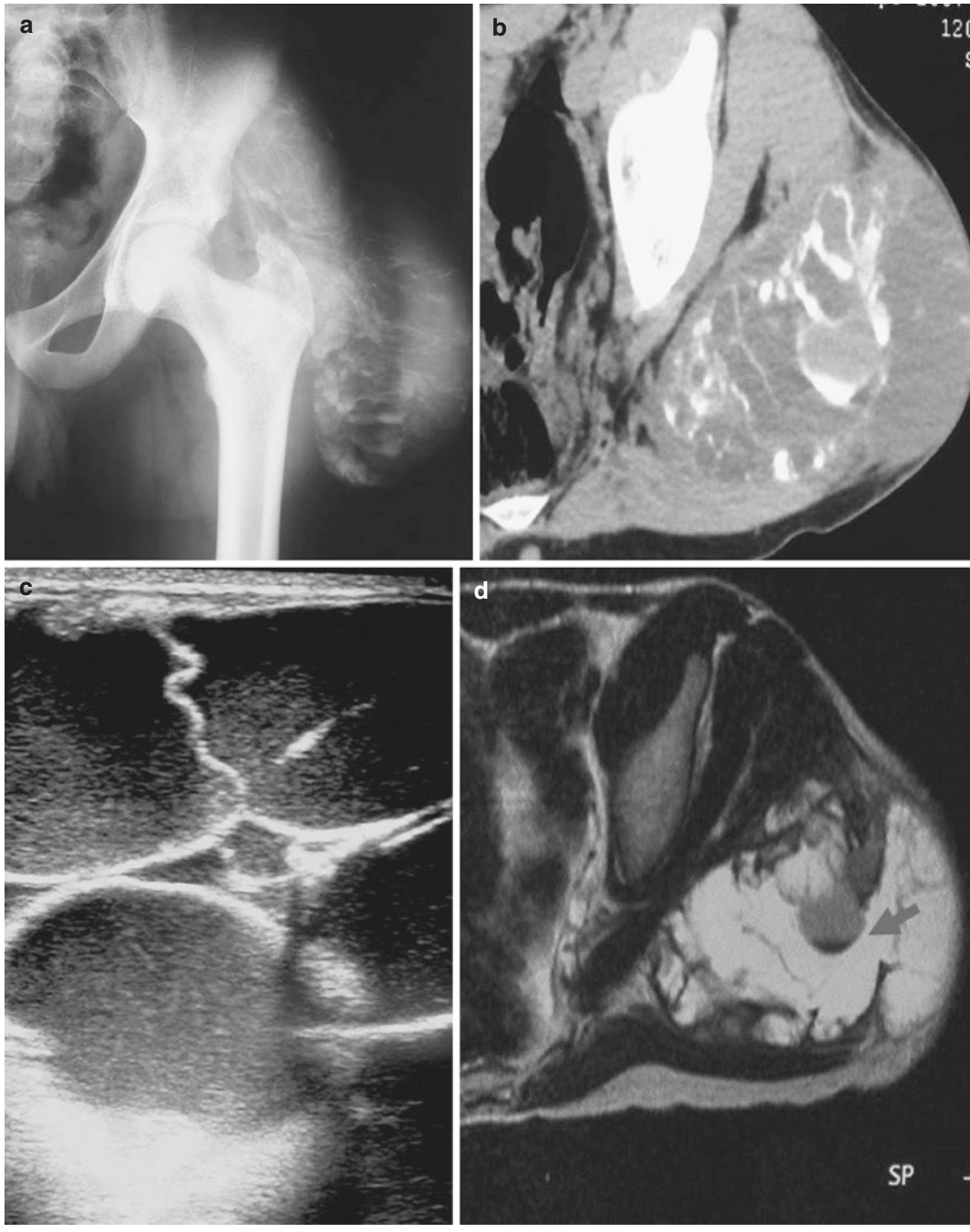

Fig. 21.38 Tumoral calcinosis in a 12-year-old boy. (**a**) Anteroposterior radiograph of the left hip shows a well-demarcated lobulated calcified mass with fluid-calcium levels also known as the "sedimentation sign." (**b**) CT image of the left hip: the mass shows a mainly cystic component with low-attenuation centers and thin calcified walls. Fluid-calcium levels are noted. (**c**) Ultrasound study shows multicystic mass. Cysts contain hypoechoic liquid and are separated by hyperechoic thin septa. (**d**) Axial T2-weighted MR image shows a well-circumscribed multicystic mass with heterogeneous and high signal intensity (*arrow*)

Doppler. Cavities are filled with anechoic or echoic fluid. In some cases fluid-fluid levels can be seen. When the lesions are entirely calcified, they appear as a hyperechogenic mass with an acoustic shadow [13].

Computed tomography (Fig. 21.38b) appearances vary. The lesion may consist mainly of large cystic components with low-attenuation centers and thin layers of calcium outlining the walls. More commonly, there is a more nodular calcified component separated by low-attenuation septa. Fluid-calcium levels may be seen. Some of the septa may enhance after contrast injection [13].

On MRI (Fig. 21.38d), tumoral calcinosis is seen as a well-circumscribed multicystic mass. On T1-weighted images, the mass appears inhomogeneous and is of intermediate to low signal. Interestingly, the lesion displays heterogeneous and relatively high signal intensity on T2-weighted images, despite the large calcium component. This hyperintense T2 signal may be attributed to the granulomatous foreign body reaction [115] or to the hypervascularity of the lesion [128] or to the semifluid nature of the calcium material ("milk of calcium") [30].

Multiple intraocular fluid-fluid or fluid-calcium levels may be seen [173]. On MRI, the calcium deposit has low intensity on T1- and T2-weighted images; the supernatant fluid floating above the calcium has high signal intensity on T2 images and low signal intensity on T1-weighted images [137].

A low signal intensity of the entire lesion in all sequences has been described probably due to the lesion's high calcium concentration [132].

The septa separating the cysts are of low signal on T1-weighted images and variable signal on T2-weighted images and enhance after gadolinium contrast injection. The inner layers of the septa can hold calcified incrustations, which explain the low signal on both T1- and T2-weighted images. The outer layers are composed of connective tissue associated to a variable degree of vascularization and inflammatory reaction, accounting for the high intensity present on T2-weighted and on post-contrast T1-weighted images [30].

MRI is superior to CT to detect septal enhancement and provides accurate information about the location, extent, and relation with adjacent structures. Although MR imaging provides only additional information, it does not affect treatment or prognosis.

The diagnosis of idiopathic tumoral calcinosis is one of exclusion. The differential diagnosis includes chronic renal failure, primary hyperparathyroidism, calcinosis universalis, calcinosis circumscripta, chronic vitamin D intoxication, milkalkali syndrome, collagen vascular diseases, and calcium pyrophosphate dihydrate crystal deposition disease [4, 167].

The treatment is symptomatic since the cause of the disease is unknown. Medical treatment using calcitonin, diphosphonates, steroids, phenylbutazone, and radiation therapy has proved unsuccessful [7, 25, 130]. Complete surgical excision of tumoral calcinosis is the treatment of choice. Inadequate excision leads to a high level of recurrence in patients with and without metabolic disturbances, and growth of recurrent masses is frequently more rapid than that of the initial lesions [7, 25, 61, 129, 130]. It is thought that recurrences are quite common in cases with hyperphosphatemia [146] or with predisposing genetic abnormality [70].

21.2.7 Vascular Lesions

Adventitial cystic disease is an unusual condition of uncertain etiology in which a mucin-containing cyst forms within the adventitia of the artery, narrowing the arterial lumen and causing symptoms of intermittent claudication. It usually involves the popliteal artery. Less common sites of involvement include the external iliac, common femoral, ulnar, and radial arteries [18]. On ultrasound, adventitial cysts appear hypo- or anechoic masses adjacent to the affected vessel. Color Doppler may show arterial stenosis or occlusion [188]. CT or MR angiography shows a focal, smoothly tapered stenosis of the popliteal artery at the level of the femoral condyles, due to a non-enhancing cyst-like mass causing extrinsic compression of an enhancing arterial lumen [32, 174, 188]. MR

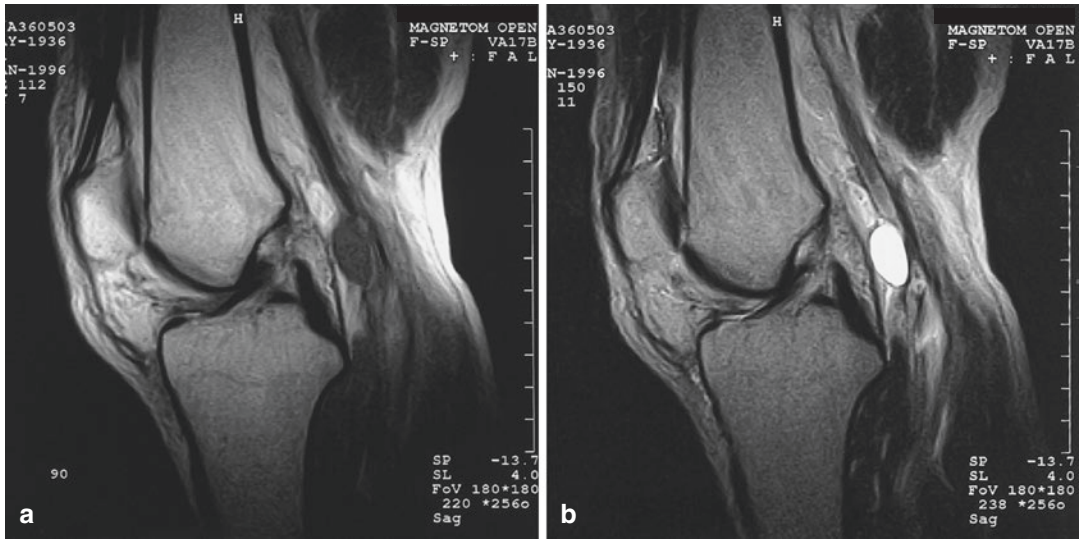

Fig. 21.39 A 46-year-old man with claudicatio intermittens: (**a**) sagittal spin echo T1-weighted MR image; (**b**) sagittal turbo spin echo T2-weighted MR image. MR imaging reveals a well-defined cystic process around the popliteal artery, hypointense on T1-weighted images (**a**) and hyperintense on T2-weighted images (**b**). These findings are suggestive for an adventitial cyst around the popliteal artery

imaging may reveal cyst-like structures closely to the compressed artery [189] (Fig. 21.39).

The presence of a pulsatile mass with bruit in close proximity to an artery in a patient with a history of trauma suggests the diagnosis of aneurysm. Likewise, when a soft tissue tumor entirely surrounds and obliterates a major artery, an aneurysm or a pseudoaneurysm should be considered. Peripheral arterial aneurysms are most commonly found in the popliteal artery, often in association with widespread atherosclerotic disease.

An aneurysm or pseudoaneurysm is recognized on MR by the following features: signal void in regions of flowing blood, hyperintensity on T1- and T2-weighted images due to subacute hemorrhage, and hypointense areas caused by hemosiderin deposits. Moreover, MR imaging demonstrates a characteristic flow-related artifact in the direction of the phase encoding gradient [175]. A major vein engulfed by or adjacent to a mass should evoke a lesion of venous origin [175].

Congenital or posttraumatic acquired arteriovenous malformations are characterized by dilated, tortuous blood vessels, infiltrating muscles (see Chap. 16).

Varicositas of the round ligament in pregnant women is a condition which may mimic a soft tissue mass in the groin or an inguinal herniation. It typically occurs in the second trimester of the pregnancy. Demonstration of venous flow on color Doppler with flow reversal during Valsalva maneuver is the clue to the correct diagnosis [75] (Fig. 21.40).

21.2.8 Miscellaneous

21.2.8.1 Pseudohypertrophy of Calf Muscles

Enlargement of the ipsilateral muscle compartment may rarely occur in patients with long-standing radiculopathy, peripheral nerve injury, anterior horn cell diseases, or acquired peripheral neuropathy.

Long-standing denervation is a well-known cause of muscle atrophy and fatty degeneration. When the patients continue to exercise the affected muscle, hypertrophy of the partially denervated muscle fibers may occur which results macroscopically in a pseudohypertrophy.

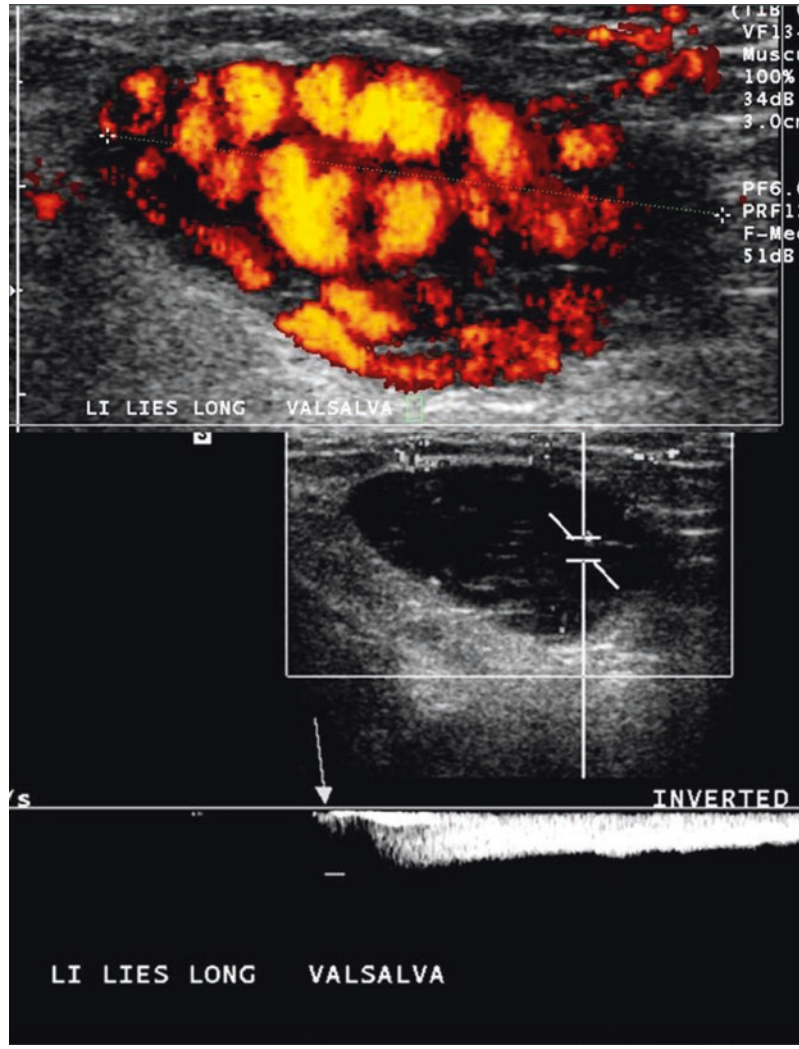

Fig. 21.40 Varicositas of the round ligament in pregnant women presenting with a mass lesion in the left groin. Color Doppler shows venous flow with flow reversal during Valsalva maneuver

On imaging, a combination of fatty infiltration and muscle hypertrophy is seen within the muscles innervated by the affected nerves. Most often the calf muscles are involved due to an underlying disc herniation at the S1 level (Fig. 21.41) [22].

21.2.8.2 Geyser Phenomenon

Cystic lesions adjacent to the acromioclavicular (AC) joint are often secondary to a long-standing rotator cuff tear, in which there is communication of joint fluid of the glenohumeral joint with the AC joint through a large rotator cuff tear (Fig. 21.42). On a shoulder arthrogram, the leakage of dye from the glenohumeral joint to the upper surface of the AC resembles a geyser, hence its name "geyser phenomenon" [183, 184].

21.2.8.3 Elastofibroma Dorsi

Elastofibroma is a fibroelastic pseudotumor. It occurs almost exclusively in the subscapular region beneath the rhomboideus major and latissimus dorsi muscles adjacent to the inferior angle of the scapula. It is thought to be caused by repeated mechanical friction between the chest wall and the tip of the scapula, which was the site of the lesion in 99 % of the reported cases. Other less common locations include the olecranon, axilla, and greater trochanter regions. Bilateral lesions are common and seen in

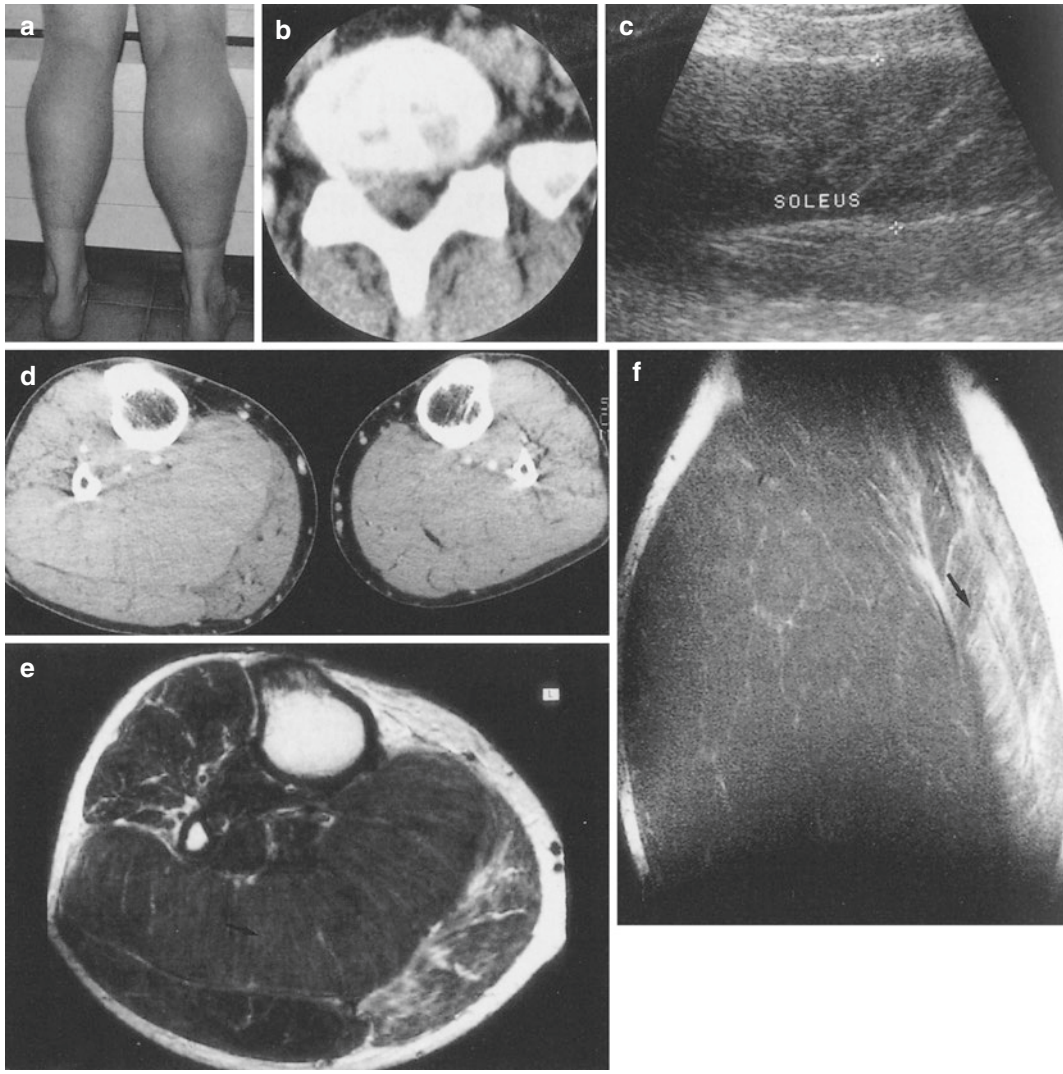

Fig. 21.41 A 41-year-old man with unilateral right-sided calf enlargement, following chronic ipsilateral S1 radiculopathy: (**a**) clinical photograph; (**b**) axial CT scan of the lumbar spine; (**c**) ultrasonography of the right lower limb; (**d**) axial CT scan of the lower limbs; (**e**) axial spin echo T1-weighted MR image; (**f**) coronal spin echo T1-weighted MR image. The clinical photograph (**a**) demonstrates a clinically painless and progressive enlargement of the right calf. CT images at the level of the lumbar spine reveal a since 3-year known right-sided disc herniation compressing the S1 nerve root (**b**). In the right lower limb, ultrasound shows reflective linear strands within the muscle belly of the soleus muscle (**c**), while on CT an enlarged circumference of the right lower leg is shown compared with the left leg (**d**). Note the hypertrophy of the soleus muscle and decreased density of the medial head of the gastrocnemius muscle. MR images (**e**, **f**) confirm the true muscular hypertrophy of the soleus and gastrocnemius muscles. The muscle fibers are intermingled with fine linear streaks of high signal intensity, corresponding to tiny fatty bands (*arrow*) in pseudohypertrophy

10–60 % of patients. Most patients are middle-aged to older adults, and there is a definite predominance in women. Single cases have been reported in children [48]. Half of the patients are asymptomatic, and 50 % have pain on arm motion.

On gross examination, these lesions have an oval or lenticular shape and are firm and rubbery. Histologically, lesions are composed mainly of elastin-like fibers and entrapped islands of mature adipose tissue. Microscopic examination shows hypertrophy and degeneration of elastin

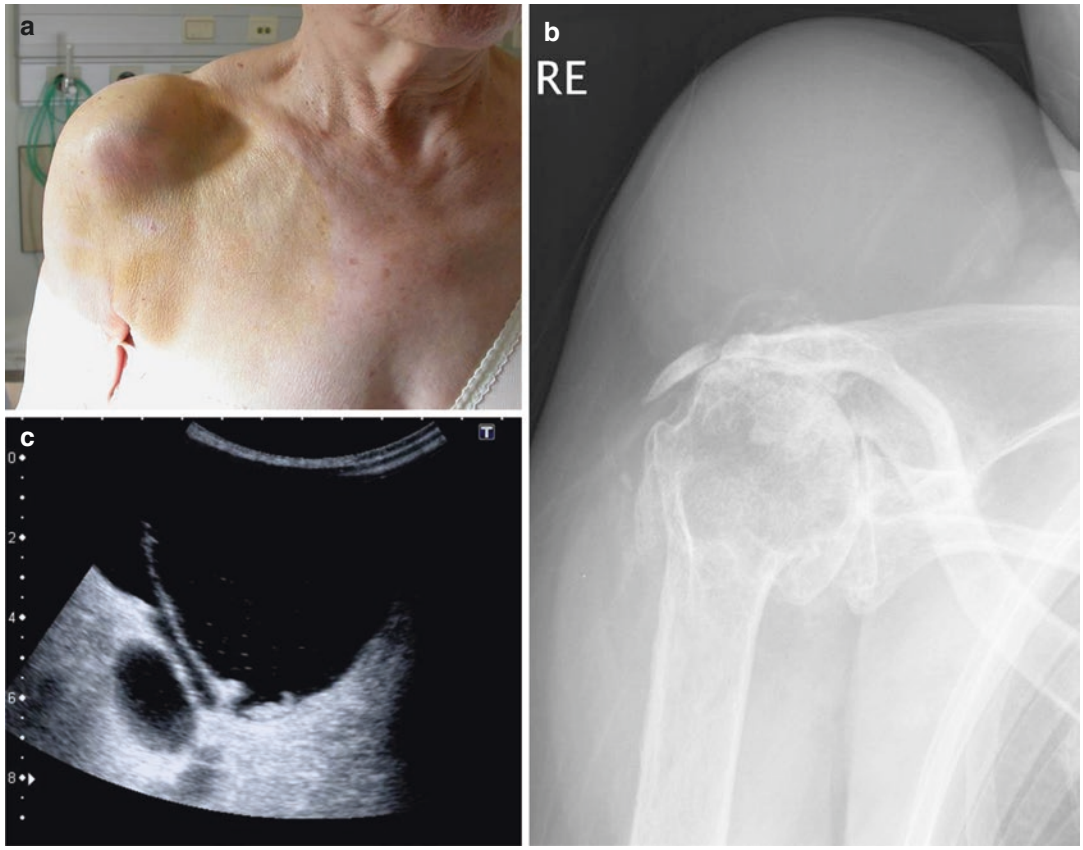

Fig. 21.42 Geyser phenomenon in a long-standing rotator cuff tear: (**a**) clinical image showing a patient presenting with a soft mass on top of the AC joint, (**b**) plain radiograph of the right shoulder showing marked narrowing of the acromiohumeral space, in keeping with a large rotator cuff tear. Note also swelling at the AC joint. (**c**) Ultrasound showing a cystic lesion communicating with the AC joint. A full-thickness rotator cuff tear was present on ultrasound (not shown)

with a background of mature collagen and fat. It consists of entrapped fat within a fibrous matrix. On imaging, the lesion has a multilayered appearance, resembling lasagna (Fig. 21.43). Ultrasound shows alternating hyperechogenic and hypoechogenic bands [180]. There is usually no increased vascularity on color Doppler examination. On MRI, the alternating bands of low signal intensity correspond to fibrous components, whereas intermingled fatty components are similar to fat on all pulse sequences (Fig. 21.43) [180, 184].

CT scans show attenuation similar to that of adjacent muscle. Sometimes there are strands of low density similar to that of subcutaneous fat [98]. Mild and moderate uptake of 18 F-FDG is frequently seen, which should be known to avoid making wrong diagnosis [56].

Invasive procedures should not be performed for diagnostic purposes in elderly individuals. Familiarity of the radiologist with this entity may make it possible to avoid unnecessary surgery [142]. Differential diagnosis is limited, but includes older desmoids, which are hypocellular,

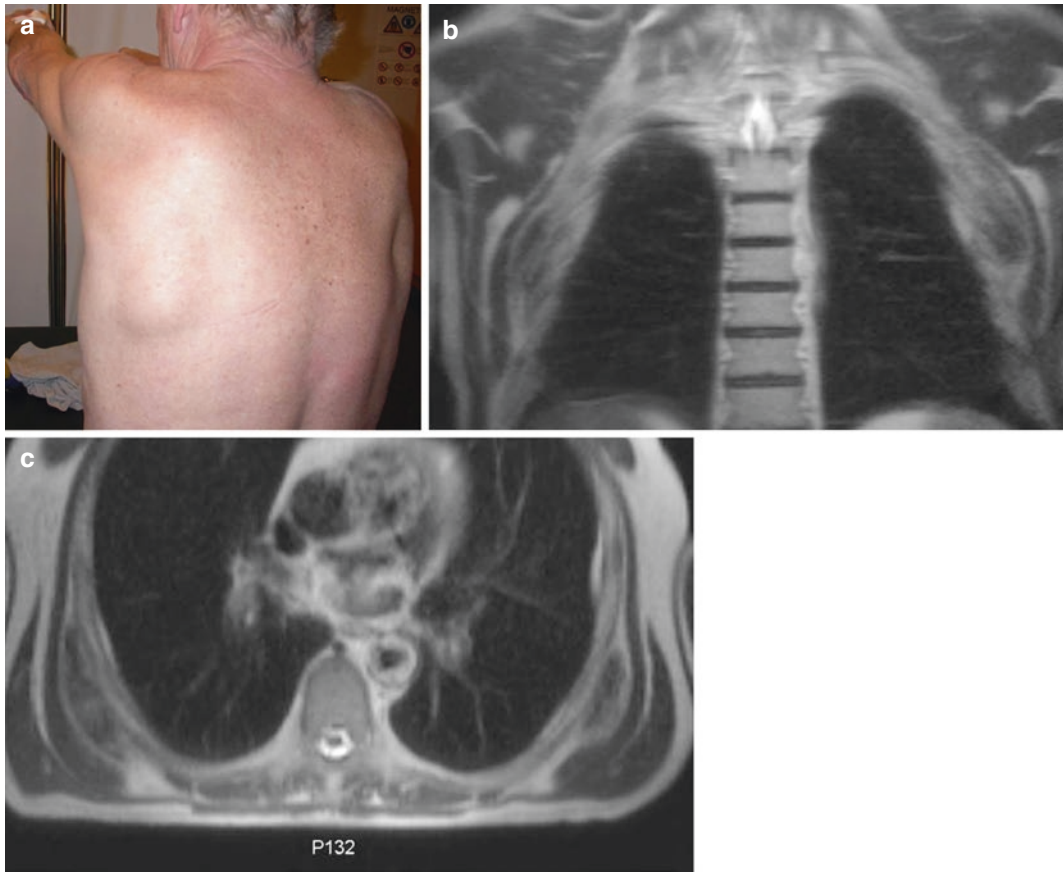

Fig. 21.43 Elastofibroma dorsi. (**a**) Clinical image of the patient showing a left periscapular soft tissue mass when the patient elevated his shoulder. (**b**) Coronal HASTE demonstrates a bilateral fusiform soft tissue mass between the serratus anterior muscle and the thoracic wall. The lesion has a multilayered appearance, consisting of alternating bands of low signal with intermingled fatty components, resembling lasagna. (**c**) Axial T2-WI showing the intimate relationship of the lesion with the apex of the scapula, the serratus anterior muscle and the thoracic wall

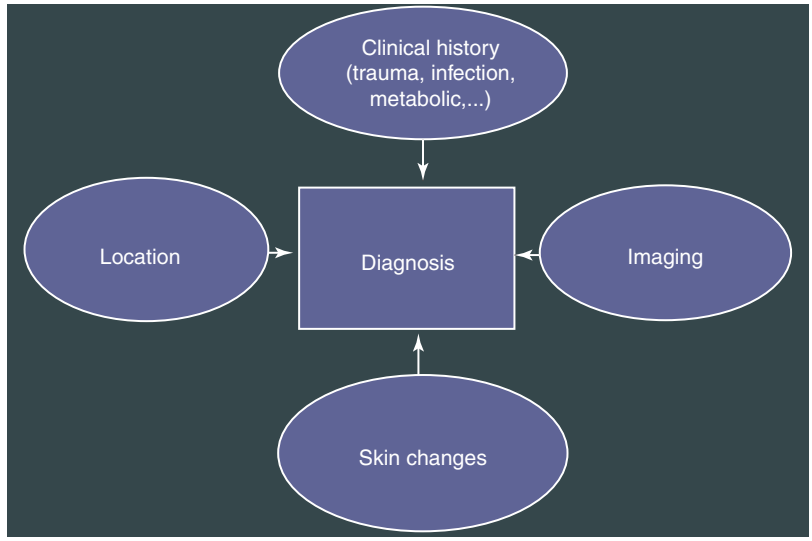

Fig. 21.44 Summarizes the diagnostic strategy of pseudotumoral lesion of soft tissue. The correct diagnosis of a pseudotumor is based on the combination of imaging findings, relevant clinical findings, and location of the lesion. The knowledge of associated skin lesions (e.g., in epidermoid cyst) or discoloration (e.g., in cellulitis) may be helpful as well

Key Points

1. Soft tissue pseudotumors encompass a vast range of pathologies varying from normal anatomic variants, inflammatory and infectious lesions, posttraumatic masses, and others. Knowledge of the common presentation of these entities in combination with relevant clinical findings can direct the clinician to the correct diagnosis, thereby limiting the need for invasive procedures in these often reactive benign lesions. The radiological approach of soft tissue pseudotumors thereby is no different than for their "true" tumoral counterparts.
2. When a mass with undetermined imaging characteristics is encountered, an infectious or inflammatory origin has always to be included in the differential diagnosis.
3. Morton's fibroma and traumatic "neuroma" are reactive nonneoplastic lesions that may mimic nerve sheath tumors. The typical location at the intermetatarsal spaces of the foot is the clue to the diagnosis of a Morton's fibroma, whereas the history of a previous trauma and the absence of a target sign suggest the presence of a traumatic "neuroma."

contain large amounts of collagen, and occur in younger patients.

21.3 Conclusion and Diagnostic Strategy

The imaging approach of pseudotumoral lesions of soft tissues is generally very similar to the approach of "true" soft tissue tumoral counterparts.

Knowledge of the normal anatomy and existence and common presentation of these diseases, in combination with the relevant clinical findings (clinical history, location, skin changes), enables correct diagnosis in most cases, thereby limiting the need for invasive procedures. Biopsy should be performed in indeterminate cases (Fig. 21.44).

References

1. Adams WM, Laitt RD, Davies M, O'Donovan DG (1999) Familial tumoral calcinosis: association with cerebral and peripheral aneurysm formation. Neuroradiology 41:351–355
2. Ahlawat S, Belzberg AJ, Montgomery EA, Fayad LM (2016) MRI features of peripheral traumatic neuromas. Eur Radiol 26:1204–1212. doi:10.1007/s00330-015-3907-9
3. Ameen M (2009) Managing mycetomas. Trop Doct 39:66–68. doi:10.1258/td.2008.080151
4. Ammar A, Ben Romdhane K, Khattech R, Ben Othman M, Ben Ghachem M (1994) Tumoral calci-

nosis: a clinical and pathological study of 8 cases reported in Tunisia. Rev Chir orthopédique réparatrice l'appareil Mot 80:261–266
5. Anderson SE, Bosshard C, Steinbach LS, Ballmer FT (2003) MR imaging of calcification of the lateral collateral ligament of the knee: a rare abnormality and a cause of lateral knee pain. AJR Am J Roentgenol 181:199–202. doi:10.2214/ajr.181.1.1810199
6. Aoki T, Nakata H, Watanabe H, Maeda H, Toyonaga T, Hashimoto H, Nakamura T (1999) The radiological findings in chronic expanding hematoma. Skeletal Radiol 28:396–401
7. Aprin H, Sinha A (1984) Tumoral calcinosis. Report of a case in a one-year-old child. Clin Orthop Relat Res (185):83–86
8. Ardies L, De Beule T, Degroote T, Vanhoenacker FM, Vanhoenacker PK (2012) Bilateral intramuscular pseudotumor in a bodybuilder. JBR-BTR 95:108
9. Ata AM, Onat SS, Ozcakar L (2016) Ultrasound-Guided diagnosis and treatment of Morton's neuroma. Pain Physician 19:E355–E358
10. Ben Ayed M, Kamoun N, Makni K, Ben Romdhane K (1986) Hydatid cyst: 281 cases, of which 86 cases had an unusual localization, seen during a 10-year period (1972–1981). Tunis Med 64:389–395
11. Bajaj G, Nicholas R, Pandey T, Montgomery C, Jambhekar K, Ram R (2014) MR imaging findings in diabetic muscle infarction. J Ark Med Soc 111:91–93
12. Balageas A, Sanguinet F, Lequen L, Delbrel X (2013) [Muscular sarcoidosis: a case report of muscle and fascia involvement and literature]. La Rev médecine interne/fondée. par la Société Natl Fr médecine interne 34:706–712.
13. Barnacle AM, Gower PE, Mitchell AWM (2002) Ultrasonography of acute and chronic tumoral calcinosis. Clin Radiol 57:146–149. doi:10.1053/crad.2001.0726
14. Bashir WA, O'Donnell P (2010) The myositides: the role of imaging in diagnosis and treatment. Semin Musculoskelet Radiol 14:217–226. doi:10.1055/s-0030-1253163
15. Bayram M, Sirikci A (2000) Hydatic cyst located intermuscular area of the forearm: MR imaging findings. Eur J Radiol 36:130–132
16. Beauchamp NJ, Scott WW, Gottlieb LM, Fishman EK (1995) CT evaluation of soft tissue and muscle infection and inflammation: a systematic compartmental approach. Skeletal Radiol 24:317–324
17. Beggs I (1985) The radiology of hydatid disease. AJR Am J Roentgenol 145:639–648. doi:10.2214/ajr.145.3.639
18. Beltran LS, Bencardino JT, Desai P, Paksima N (2012) Adventitial cystic disease of the radial artery–two case reports and a review. Bull NYU Hosp Jt Dis 70:262–267
19. Bencardino J, Rosenberg ZS, Beltran J, Liu X, Marty-Delfaut E (2000) Morton's neuroma: is it always symptomatic? AJR Am J Roentgenol 175:649–653. doi:10.2214/ajr.175.3.1750649
20. Berg LC, Norelle A, Morgan WA, Washa DM (1998) Cat-scratch disease simulating Histiocytosis X. Hum Pathol 29:649–651
21. Berquist TH, Ehman RL, King BF, Hodgman CG, Ilstrup DM (1990) Value of MR imaging in differentiating benign from malignant soft-tissue masses: study of 95 lesions. AJR Am J Roentgenol 155:1251–1255. doi:10.2214/ajr.155.6.2122675
22. De Beuckeleer L, Vanhoenacker F, De Schepper A, Seynaeve P (1999) Hypertrophy and pseudohypertrophy of the lower leg following chronic radiculopathy and neuropathy: imaging findings in two patients. Skeletal Radiol 28:229–232
23. De Beuckeleer LH, De Schepper AM, Neetens I (1996) Magnetic resonance imaging of pilomatricoma. Eur Radiol 6:72–75
24. Bignotti B, Signori A, Sormani MP, Molfetta L, Martinoli C, Tagliafico A (2015) Ultrasound versus magnetic resonance imaging for Morton neuroma: systematic review and meta-analysis. Eur Radiol 25:2254–2262. doi:10.1007/s00330-015-3633-3
25. Bittmann S, Günther MW, Ulus H (2003) Tumoral calcinosis of the gluteal region in a child: case report with overview of different soft-tissue calcifications. J Pediatr Surg 38:E4–E7
26. Blum AG, Zabel J-P, Kohlmann R, Batch T, Barbara K, Zhu X, Dautel G, Dap F (2015) Pathologic conditions of the hypothenar eminence: evaluation with multidetector CT and MR imaging. Radiographics 26:1021–1044. doi:10.1148/rg.264055114
27. Braunstein JT, Crues JV (1995) Magnetic resonance imaging of hereditary hernias of the peroneus longus muscle. Skeletal Radiol 24:601–604
28. Bush CH (2000) The magnetic resonance imaging of musculoskeletal hemorrhage. Skeletal Radiol 29:1–9
29. Cardinal E, Chhem RK, Beauregard CG (1998) Ultrasound-guided interventional procedures in the musculoskeletal system. Radiol Clin North Am 36:597–604
30. Chaabane S, Chelli-Bouaziz M, Jelassi H, Mrad K, Smida M, Ladeb MF (2008) Idiopathic tumoral calcinosis. Acta Orthop Belg 74:837–845
31. Chaoui A, Garcia J, Kurt AM (1997) Gouty tophus simulating soft tissue tumor in a heart transplant recipient. Skeletal Radiol 26:626–628
32. Chappel P, Gielen J, Salgado R, Van Dyck P, Vanhoenacker FM (2007) Cystic adventitial disease with secondary occlusion of the popliteal artery. JBR-BTR organe la Société R belge Radiol orgaan van K Belgische Ver voor Radiol 90:180–181.
33. Chason DP, Fleckenstein JL, Burns DK, Rojas G (1996) Diabetic muscle infarction: radiologic evaluation. Skeletal Radiol 25:127–132
34. Chaudhry AA, Baker KS, Gould ES, Gupta R (2015) Necrotizing fasciitis and its mimics: what radiologists need to know. AJR Am J Roentgenol 204:128–139. doi:10.2214/AJR.14.12676
35. Chauhan S, Jain S, Varma S, Chauhan SS (2004) Tropical pyomyositis (myositis tropicans): current perspective. Postgrad Med J 80:267–270
36. Chen CK, Yeh LR, Pan HB, Yang CF, Lu YC, Wang JS, Resnick D (1999) Intra-articular gouty tophi of the knee: CT and MR imaging in 12 patients. Skeletal Radiol 28:75–80

37. Chen P-J, Liang H-W, Chang K-V, Wang T-G (2013) Ultrasound-guided injection of steroid in multiple postamputation neuromas. J Clin Ultrasound 41: 122–124. doi:10.1002/jcu.21885
38. Chhabra A, Williams EH, Wang KC, Dellon AL, Carrino JA (2010) MR neurography of neuromas related to nerve injury and entrapment with surgical correlation. AJNR Am J Neuroradiol 31:1363–1368. doi:10.3174/ajnr.A2002
39. Chiedozi LC (1979) Pyomyositis. Review of 205 cases in 112 patients. Am J Surg 137:255–259
40. Chung CB, Gentili A, Chew FS (2004) Calcific tendinosis and periarthritis: classic magnetic resonance imaging appearance and associated findings. J Comput Assist Tomogr 28:390–396
41. Chung S, Frush DP, Prose NS, Shea CR, Laor T, Bisset GS (1999) Subcutaneous granuloma annulare: MR imaging features in six children and literature review. Radiology 210:845–849. doi:10.1148/radiology.210.3.r99mr11845
42. Claassen L, Bock K, Ettinger M, Waizy H, Stukenborg-Colsman C, Plaass C (2014) Role of MRI in detection of Morton's neuroma. Foot Ankle Int 35:1002–1005. doi:10.1177/1071100714540888
43. Clarke E, Swischuk LE, Hayden CK (1984) Tumoral calcinosis, diaphysitis, and hyperphosphatemia. Radiology 151:643–646. doi:10.1148/radiology.151.3.6718723
44. Crum-Cianflone NF (2006) Infection and musculoskeletal conditions: Infectious myositis. Best Pract Res Clin Rheumatol 20:1083–1097. doi:10.1016/j.berh.2006.08.005
45. Crum-Cianflone NF (2008) Bacterial, fungal, parasitic, and viral myositis. Clin Microbiol Rev 21:473–494. doi:10.1128/CMR.00001-08
46. DeFilippis EM, Arleo EK (2014) The ABCs of accessory breast tissue: basic information every radiologist should know. AJR Am J Roentgenol 202:1157–1162. doi:10.2214/AJR.13.10930
47. Delaney-Sathy LO, Fessell DP, Jacobson JA, Hayes CW (2000) Sonography of diabetic muscle infarction with MR imaging, CT, and pathologic correlation. AJR Am J Roentgenol 174:165–169. doi:10.2214/ajr.174.1.1740165
48. Devaney D, Livesley P, Shaw D (1995) Elastofibroma dorsi: MRI diagnosis in a young girl. Pediatr Radiol 25:282–283
49. Dong PR, Seeger LL, Yao L, Panosian CB, Johnson BL, Eckardt JJ (1995) Uncomplicated cat-scratch disease: findings at CT, MR imaging, and radiography. Radiology 195:837–839. doi:10.1148/radiology.195.3.7754017
50. Drapé J-L, Feydy A, Guerini H, Desmarais E, Godefroy D, Le Viet D, Chevrot A (2005) Vascular lesions of the hand. Eur J Radiol 56:331–343. doi:10.1016/j.ejrad.2005.03.013
51. Drosos G (2005) Pyomyositis. A literature review. Acta Orthop Belg 71:9–16
52. Ekstrom JE, Shuman WP, Mack LA (1990) MR imaging of accessory soleus muscle. J Comput Assist Tomogr 14:239–242
53. El-Essawy MT, Vanhoenacker FM (2012) Calcific tendinopathy of the pectoralis major insertion with intracortical protrusion of calcification. JBR-BTR organe la Société R belge Radiol orgaan van K Belgische Ver voor Radiol 95:374.
54. Eyselbergs M, Catry F, Scharpé P, Vanhoenacker FM (2011) Case 9086 Calcific myonecrosis Eurorad. http://www.eurorad.org/case.php?id=9086. doi:10.1594/EURORAD/CASE.9086
55. Fahal AH, Shaheen S, Jones DHA (2014) The orthopaedic aspects of mycetoma. Bone Joint J 96-B:420–425. doi:10.1302/0301-620X.96B3.31421
56. Fang N, Wang Y-L, Zeng L, Wu Z-J, Cui X-J, Wang Q, Gao S, Ding W (2016) Characteristics of elastofibroma dorsi on PET/CT imaging with (18) F-FDG. Clin Imaging 40:110–113. doi:10.1016/j.clinimag.2015.08.009
57. Ferris BL, Taylor LM, Oyama K, McLafferty RB, Edwards JM, Moneta GL, Porter JM (2000) Hypothenar hammer syndrome: proposed etiology. J Vasc Surg 31:104–113
58. Fleckenstein JL, Burns DK, Murphy FK, Jayson HT, Bonte FJ (1991) Differential diagnosis of bacterial myositis in AIDS: evaluation with MR imaging. Radiology 179:653–658. doi:10.1148/radiology.179.3.2027969
59. Flemming DJ, Murphey MD, Shekitka KM, Temple HT, Jelinek JJ, Kransdorf MJ (2003) Osseous involvement in calcific tendinitis: a retrospective review of 50 cases. AJR Am J Roentgenol 181:965–972. doi:10.2214/ajr.181.4.1810965
60. Foltz KD, Fallat LM (2004) Madura foot: atypical finding and case presentation. J Foot Ankle Surg 43:327–331. doi:10.1053/j.jfas.2004.07.002
61. Fujii T, Matsui N, Yamamoto T, Yoshiya S, Kurosaka M (2003) Solitary intra-articular tumoral calcinosis of the knee. Arthroscopy 19:E1. doi:10.1053/jars.2003.50018
62. García-Alvarez F, Torcal J, Salinas JC, Navarro A, García-Alvarez I, Navarro-Zorraquino M, Sousa R, Tejero E, Lozano R (2002) Musculoskeletal hydatid disease: a report of 13 cases. Acta Orthop Scand 73:227–231. doi:10.1080/000164702753671858
63. Geirnaerdt MJ, Kroon HM, van der Heul RO, Herfkens HF (1995) Tumoral calcinosis. Skeletal Radiol 24:148–151
64. Genchellac H, Demir MK, Unlu E, Temizöz O, Ozdemir H (2008) Hypothenar hammer syndrome: gray-scale and color Doppler sonographic appearances. J Clin Ultrasound 36:98–100. doi:10.1002/jcu.20364
65. Gielen J, Wang XL, Vanhoenacker F, De Schepper H, De Beuckeleer L, Vandevenne J, De Schepper A (2003) Lymphadenopathy at the medial epitrochlear region in cat-scratch disease. Eur Radiol 13: 1363–1369
66. Gielen JL, Blom RM, Vanhoenacker FM, De Schepper AMA, Van de Vijver K (2008) An elderly man with a slowly growing painless mass in the soft tissues of the lower leg: presentation. Skeletal Radiol 37(335):337–338. doi:10.1007/s00256-007-0436-x

67. Giron GL, Friedman I, Feldman S (2004) Lobular carcinoma in ectopic axillary breast tissue. Am Surg 70:312–315
68. Gossios KJ, Kontoyiannis DS, Dascalogiannaki M, Gourtsoyiannis NC (1997) Uncommon locations of hydatid disease: CT appearances. Eur Radiol 7:1303–1308. doi:10.1007/s003300050293
69. Hammami T, Noomane F, Ketata M, Ganneme Y, Nasr M, Zouari K, Hamdi A (2002) Hydatid cyst of the thigh: three cases. Rev Chir orthopédique réparatrice l'appareil Mot 88:193–196
70. Hammoud S, McCarthy EF, Weber K (2005) Tumoral calcinosis in infants: a report of three cases and review of the literature. Clin Orthop Relat Res (436):261–264
71. Han EJ, Jang YS, Lee IS, Lee JM, Kang S, Kim HS (2013) Muscular sarcoidosis detected by F-18 FDG PET/CT in a hypercalcemic patient. J Korean Med Sci 28:1399–1402. doi:10.3346/jkms.2013.28.9.1399
72. Hashemi SA, Vosoughi AR, Pourmokhtari M (2012) Hip abductors pyomyositis: a case report and review of the literature. J Infect Dev Ctries 6:184–187
73. Heckmann JG, Stefan H, Heuss D, Hopp P, Neundörfer B (2001) Isolated muscular sarcoidosis. Eur J Neurol 8:365–366
74. Hernandez RJ, Keim DR, Chenevert TL, Sullivan DB, Aisen AM (1992) Fat-suppressed MR imaging of myositis. Radiology 182:217–219. doi:10.1148/radiology.182.1.1727285
75. Heymans J, Vanhoenacker FM, Vankelecom F (2011) Round ligament varicocele. JBR-BTR organe la Société R belge Radiol orgaan van K Belgische Ver voor Radiol 94:92.
76. Hobson-Webb LD, Walker FO (2004) Traumatic neuroma diagnosed by ultrasonography. Arch Neurol 61:1322–1323. doi:10.1001/archneur.61.8.1322
77. Hoffmann V, Roeren T, Möller P, Heuschen G (1998) MR imaging of a pilomatrixoma. Pediatr Radiol 28:272. doi:10.1007/s002470050350
78. Holobinko JN, Damron TA, Scerpella PR, Hojnowski L (2003) Calcific myonecrosis: keys to early recognition. Skeletal Radiol 32:35–40. doi:10.1007/s00256-002-0549-1
79. Hopkins KL, Li KC, Bergman G (1995) Gadolinium-DTPA-enhanced magnetic resonance imaging of musculoskeletal infectious processes. Skeletal Radiol 24:325–330
80. Hopkins KL, Simoneaux SF, Patrick LE, Wyly JB, Dalton MJ, Snitzer JA (1996) Imaging manifestations of cat-scratch disease. AJR Am J Roentgenol 166:435–438. doi:10.2214/ajr.166.2.8553962
81. Van Hul E, Vanhoenacker F, Van Dyck P, De Schepper A, Parizel PM (2011) Pseudotumoural soft tissue lesions of the foot and ankle: a pictorial review. Insights Imaging 2:439–452. doi:10.1007/s13244-011-0087-2
82. Ichikawa T, Nakajima Y, Fujimoto H, Koyama A, Honma M, Yatsuzuka M, Ohtomo K, Uchiyama G, Ushigome S, Ohba S (1997) Giant calcifying epithelioma of Malherbe (pilomatrixoma): imaging features. Skeletal Radiol 26:602–605
83. Immerman RP, Greenman RL (1987) Toxic shock syndrome associated with pyomyositis caused by a strain of Staphylococcus aureus that does not produce toxic-shock-syndrome toxin-1. J Infect Dis 156:505–507
84. Jawahar A, Balaji R (2014) Magnetic resonance imaging of diabetic muscle infarction: report of two cases. Iowa Orthop J 34:74–77
85. Jelinek J, Kransdorf MJ (1995) MR imaging of soft-tissue masses. Mass-like lesions that simulate neoplasms. Magn Reson Imaging Clin N Am 3:727–741
86. Jelinek JS, Murphey MD, Aboulafia AJ, Dussault RG, Kaplan PA, Snearly WN (1999) Muscle infarction in patients with diabetes mellitus: MR imaging findings. Radiology 211:241–247. doi:10.1148/radiology.211.1.r99ap44241
87. Junghanss T, da Silva AM, Horton J, Chiodini PL, Brunetti E (2008) Clinical management of cystic echinococcosis: state of the art, problems, and perspectives. Am J Trop Med Hyg 79:301–311
88. Kazakos CJ, Galanis VG, Verettas DAJ, Polychronidis A, Simopoulos C (2005) Primary hydatid disease in femoral muscles. J Int Med Res 33:703–706
89. Khoury NJ, El-Khoury GY, Kathol MH (1997) MRI diagnosis of diabetic muscle infarction: report of two cases. Skeletal Radiol 26:122–127
90. King RJ, Laugharne D, Kerslake RW, Holdsworth BJ (2003) Primary obturator pyomyositis: a diagnostic challenge. J Bone Joint Surg Br 85:895–898
91. Kolilekas L, Triantafillidou C, Manali E, Rontogianni D, Chatziioannou S, Papiris S (2009) The many faces of sarcoidosis: asymptomatic muscle mass mimicking giant-cell tumor. Rheumatol Int 29:1389–1390. doi:10.1007/s00296-009-0989-1
92. Kraemer EJ, El-Khoury GY (2000) Atypical calcific tendinitis with cortical erosions. Skeletal Radiol 29:690–696
93. Kransdorf MJ (1995) Benign soft-tissue tumors in a large referral population: distribution of specific diagnoses by age, sex, and location. AJR Am J Roentgenol 164:395–402. doi:10.2214/ajr.164.2.7839977
94. Kransdorf MJ, Murphey MD, Temple HT (1998) Subcutaneous granuloma annulare: radiologic appearance. Skeletal Radiol 27:266–270
95. Kuhlmann JN, Mimoun M, Baux S (2004) Tumeral calcinosis: case report of an erosive form affecting the long finger. Chir Main 23:305–307
96. Kumar A, Detrisac DA, Krecke CF, Jimenez MC (1991) Actinomycosis of the thigh presenting as a soft-tissue neoplasm. J Infect 23:187–190
97. Lan M-Y, Lan M-C, Ho C-Y, Li W-Y, Lin C-Z (2003) Pilomatricoma of the head and neck: a retrospective review of 179 cases. Arch Otolaryngol Head Neck Surg 129:1327–1330. doi:10.1001/archotol.129.12.1327
98. Lang P, Suh KJ, Grampp S, Steinbach L, Steiner E, Peterfy C, Tirman P, Schwickert H, Rosenau W, Genant HK (1995) CT and MRI in elastofibroma. A rare, benign soft tissue tumor. Radiologe 35:611–615

99. Laor T, Barnewolt CE (1999) Nonradiopaque penetrating foreign body: “a sticky situation”. Pediatr Radiol 29:702–704. doi:10.1007/s002470050678
100. Larson RC, Sierra RJ, Sundaram M, Inwards C, Scully SP (2004) Calcific myonecrosis: a unique presentation in the upper extremity. Skeletal Radiol 33:306–309. doi:10.1007/s00256-003-0740-z
101. Lee SY, Lee NH, Chung MJ, Chung GH (2004) Foreign-body granuloma caused by dispersed oil droplets simulating subcutaneous fat tissue on MR images. AJR Am J Roentgenol 182:1090–1091. doi:10.2214/ajr.182.4.1821090
102. Lesavoy MA, Gomez-Garcia A, Nejdl R, Yospur G, Syiau TJ, Chang P (1995) Axillary breast tissue: clinical presentation and surgical treatment. Ann Plast Surg 35:356–360
103. Lewis EJ, Crutchfield CE, Ebertz MJ, Prawer SE (1998) Report of a nipple nevus and an overview of accessory mammary tissue. Cutis 62:243–246
104. Lim K-B, Kim Y-S, Kim J-A (2012) Sonographically guided alcohol injection in painful stump neuroma. Ann Rehabil Med 36:404–408. doi:10.5535/arm.2012.36.3.404
105. Lim YW, Thamboo TP (2005) Diabetic muscle infarction of the peroneus brevis: a case report. J Orthop Surg (Hong Kong) 13:314–316
106. Liu GC, Jong YJ, Chiang CH, Jaw TS (1993) Duchenne muscular dystrophy: MR grading system with functional correlation. Radiology 186:475–480. doi:10.1148/radiology.186.2.8421754
107. Liu NF, Wang CG (1998) The role of magnetic resonance imaging in diagnosis of peripheral lymphatic disorders. Lymphology 31:119–127
108. Liu PT, Leslie KO, Beauchamp CP, Cherian SF (2006) Chronic expanding hematoma of the thigh simulating neoplasm on gadolinium-enhanced MRI. Skeletal Radiol 35:254–257. doi:10.1007/s00256-005-0042-8
109. Mahadevan D, Attwal M, Bhatt R, Bhatia M (2016) Corticosteroid injection for Morton’s neuroma with or without ultrasound guidance: a randomised controlled trial. Bone Joint J 98-B:498–503. doi:10.1302/0301-620X.98B4.36880
110. Major NM, Tehranzadeh J (1997) Musculoskeletal manifestations of AIDS. Radiol Clin North Am 35:1167–1189
111. Malghem J, Lecouvet F, Marot L, Perlepe V, Clapuyt P, Larbi A V berg B (2015) Tiercé de petites tumeurs et pseudotumeurs sous-cutanées. In : Cotten A, Vande Berg B (eds) 15émes Mises au point en imagerie ostéo-articulaire. Bruxelles, Lille, pp 219–243 In: Cotten A, Vande berg B (ed) Tiercé petites tumeurs pseudotumeurs sous-cutanées. Cotten A, Vande Berg B (eds) 15émes Mises au point en Imag. ostéo-articulaire. Bruxelles, Lille, pp 219–243
112. Margileth AM (1993) Cat scratch disease. Adv Pediatr Infect Dis 8:1–21
113. Marie I, Lahaxe L, Vera P, Edet-Samson A (2010) Follow-up of muscular sarcoidosis using fluorodeoxyglucose positron emission tomography. QJM 103:1000–1002. doi:10.1093/qjmed/hcq055
114. Marrogi AJ, Wick MR, Dehner LP (1992) Pilomatrical neoplasms in children and young adults. Am J Dermatopathol 14:87–94
115. Martinez S, Vogler JB, Harrelson JM, Lyles KW (1990) Imaging of tumoral calcinosis: new observations. Radiology 174:215–222. doi:10.1148/radiology.174.1.2294551
116. Masih S, Sorenson SM, Gentili A, Seeger LL (2000) Atypical adult non-calcified pilomatricoma. Skeletal Radiol 29:54–56
117. Matsuo M, Ehara S, Tamakawa Y, Chida E, Nishida J, Sugai T (1995) Muscular sarcoidosis. Skeletal Radiol 24:535–537
118. Mellado JM, Pérez del Palomar L (1999) Muscle hernias of the lower leg: MRI findings. Skeletal Radiol 28:465–469
119. Melville DM, Jacobson JA, Downie B, Biermann JS, Kim SM, Yablon CM (2015) Sonography of cat scratch disease. J Ultrasound Med 34:387–394. doi:10.7863/ultra.34.3.387
120. Memis A, Arkun R, Bilgen I, Ustun EE (1999) Primary soft tissue hydatid disease: report of two cases with MRI characteristics. Eur Radiol 9:1101–1103. doi:10.1007/s003300050798
121. Mentzel T, Goodlad JR, Smith MA, Fletcher CD (1997) Ancient hematoma: a unifying concept for a post-traumatic lesion mimicking an aggressive soft tissue neoplasm. Mod Pathol 10:334–340
122. Ben Miled-M’rad K, Bouricha A, Hantous S, Zidi A, Mestiri I, El Hammami S, Djilani-Horchani H, Ghedira H, Belhabib D, Megdiche L, Hamzaoui A, Kilani T (2003) Ultrasonographic, CT, and MRI findings of chest wall hydatidosis. J Radiol 84:143–146
123. Mitsumori LM, McDonald ES, Wilson GJ, Neligan PC, Minoshima S, Maki JH (2015) Mr lymphangiography: how i do it. J Magn Reson Imaging 42:1465–1477. doi:10.1002/jmri.24887
124. Monu JU, McManus CM, Ward WG, Haygood TM, Pope TL, Bohrer SP (1995) Soft-tissue masses caused by long-standing foreign bodies in the extremities: MR imaging findings. AJR Am J Roentgenol 165:395–397. doi:10.2214/ajr.165.2.7618565
125. Moore SL, Teirstein AE (2003) Musculoskeletal sarcoidosis: spectrum of appearances at MR imaging. Radiographics 23:1389–1399. doi:10.1148/rg.236025172
126. Van Muylder L, Declercq H, Vanhoenacker FM (2013) Secondary tumoral calcinosis with intraosseous extension. JBR-BTR organe la Société R belge Radiol orgaan van K Belgische Ver voor Radiol 96:50
127. Navarro OM (2011) Soft tissue masses in children. Radiol Clin North Am 49(1235–59):vi–vii. doi:10.1016/j.rcl.2011.07.008
128. Neeman Z, Wood BJ (2003) Angiographic findings in tumoral calcinosis. Clin Imaging 27:184–186
129. Niall DM, Fogarty EE, Dowling FE, Moore DP (1998) Spontaneous regression of tumoral calcinosis in an infant: a case report. J Pediatr Surg 33:1429–1431

130. Noyez JF, Murphree SM, Chen K (1993) Tumoral calcinosis, a clinical report of eleven cases. Acta Orthop Belg 59:249–254
131. O'Keefe RJ, O'Connell JX, Temple HT, Scully SP, Kattapuram SV, Springfield DS, Rosenberg AE, Mankin HJ (1995) Calcific myonecrosis. A late sequela to compartment syndrome of the leg. Clin Orthop Relat Res (318):205–213
132. Ohashi K, Yamada T, Ishikawa T, Yamaguchi S, Nakajima H, Takagi M (1996) Idiopathic tumoral calcinosis involving the cervical spine. Skeletal Radiol 25:388–390
133. Ormeci T, Güler O, Malkoc M, Keskinbora M, Güngören FZ, Mahirogulları M (2016) Diagnostic value of elastography in the diagnosis of intermetatarsal neuroma. J Foot Ankle Surg. doi:10.1053/j.jfas.2016.01.025
134. Otake S (1994) Sarcoidosis involving skeletal muscle: imaging findings and relative value of imaging procedures. AJR Am J Roentgenol 162:369–375. doi:10.2214/ajr.162.2.8310929
135. Otake S, Banno T, Ohba S, Noda M, Yamamoto M (1990) Muscular sarcoidosis: findings at MR imaging. Radiology 176:145–148. doi:10.1148/radiology.176.1.2353084
136. Otake S, Imagumbai N, Suzuki M, Ohba S (1998) MR imaging of muscular sarcoidosis after steroid therapy. Eur Radiol 8:1651–1653. doi:10.1007/s003300050604
137. Ovali GY, Tarhan S, Serter S, Bayindir P, Okcu G, Demireli P, Pabuscu Y (2007) A rare disorder: idiopathic tumoral calcinosis. Clin Rheumatol 26:1142–1144. doi:10.1007/s10067-006-0269-3
138. Ozsoy M, Keles C, Kahya M, Keles G (2011) Primary echinococcal cyst in the axillary region. J Infect Dev Ctries 5:825–827
139. Palaniappan M, Rajesh A, Rickett A, Kershaw CJ (1999) Accessory soleus muscle: a case report and review of the literature. Pediatr Radiol 29:610–612. doi:10.1007/s002470050660
140. Palmer GW, Greco TP (2001) Diabetic thigh muscle infarction in association with antiphospholipid antibodies. Semin Arthritis Rheum 30:272–280. doi:10.1053/sarh.2001.19961
141. Papanna MC, Monga P, Wilkes RA (2010) Post-traumatic calcific myonecrosis of flexor hallucis longus. A case report and literature review. Acta Orthop Belg 76:137–141
142. Parratt MTR, Donaldson JR, Flanagan AM, Saifuddin A, Pollock RC, Skinner JA, Cannon SR, Briggs TWR (2010) Elastofibroma dorsi: management, outcome and review of the literature. J Bone Joint Surg Br 92:262–266. doi:10.1302/0301-620X.92B2.22927
143. Pasquali C, Vulcano E, Novario R, Varotto D, Montoli C, Volpe A (2015) Ultrasound-guided alcohol injection for Morton's neuroma. Foot Ankle Int 36:55–59. doi:10.1177/1071100714551386
144. Patel SR, Olenginski TP, Perruquet JL, Harrington TM (1997) Pyomyositis: clinical features and predisposing conditions. J Rheumatol 24:1734–1738
145. Peeters J, Vanhoenacker FM, Camerlinck M, Parizel PM (2010) Calcific myonecrosis. JBR-BTR organe la Société R belge Radiol orgaan van K Belgische Ver voor Radiol 93:111.
146. Polykandriotis EP, Beutel FK, Horch RE, Grünert J (2004) A case of familial tumoral calcinosis in a neonate and review of the literature. Arch Orthop Trauma Surg 124:563–567. doi:10.1007/s00402-004-0715-0
147. Pretorius ES, Hruban RH, Fishman EK (1996) Tropical pyomyositis: imaging findings and a review of the literature. Skeletal Radiol 25:576–579
148. Promteangtrong C, Salavati A, Cheng G, Torigian DA, Alavi A (2014) The role of positron emission tomography-computed tomography/magnetic resonance imaging in the management of sarcoidosis patients. Hell J Nucl Med 17:123–135
149. Pujol RM, Casanova JM, Egido R, Pujol J, de Moragas JM (1995) Multiple familial pilomatricomas: a cutaneous marker for Gardner syndrome? Pediatr Dermatol 12:331–335
150. Rahmouni A, Chosidow O, Mathieu D, Gueorguieva E, Jazaerli N, Radier C, Faivre JM, Roujeau JC, Vasile N (1994) MR imaging in acute infectious cellulitis. Radiology 192:493–496. doi:10.1148/radiology.192.2.8029421
151. Reeder MM (1973) Tropical diseases of the soft tissues. Semin Roentgenol 8:47–71
152. Reinherz RP (1993) Epidermal inclusion cysts. J Foot Ankle Surg 32:247
153. Resendes M, Helms CA, Fritz RC, Genant H (1992) MR appearance of intramuscular injections. AJR Am J Roentgenol 158:1293–1294. doi:10.2214/ajr.158.6.1590126
154. Restrepo CS, Lemos DF, Gordillo H, Odero R, Varghese T, Tiemann W, Rivas FF, Moncada R, Gimenez CR (2004) Imaging findings in musculoskeletal complications of AIDS. Radiographics 24:1029–1049. doi:10.1148/rg.244035151
155. Riebel T, Scheer I (2011) Subcutaneous annular granuloma: a differential diagnosis not to be forgotten in expansive lower leg (soft-tissue) lesions of young children. Ultraschall Med 32:604–607. doi:10.1055/s-0029-1245498
156. Rodriguez-Peralto JL, Lopez-Barea F, Torres A, Rodriguez-Gonzalez JI, Diaz-Faes J (1989) Tumoral calcinosis in two infants. Clin Orthop Relat Res (242):272–276.
157. Ryckaert T, Crevits I, Brijs S, Debakker G, Rosseel F, Tieleman A, De Man R (2015) Pseudotumoral tophaceous involvement of the achilles paratenon. JBR-BTR organe la Société R belge Radiol orgaan van K Belgische Ver voor Radiol 98:34–6.
158. Saad H, Hamdi A, Gargouri R, Zouari K, Sghaier MS, Balti MH, Tabka H, Achour H (1990) Hydatic cyst of the psoas muscle. Apropos of 3 cases. Ann Chir 44:299–301
159. Sakayama K, Fujibuchi T, Sugawara Y, Kidani T, Miyawaki J, Yamamoto H (2005) A 40-year-old gossypiboma (foreign body granuloma) mimicking a

malignant femoral surface tumor. Skeletal Radiol 34:221–224. doi:10.1007/s00256-004-0821-7
160. van de Sande WWJ, Fahal AH, Goodfellow M, Mahgoub ES, Welsh O, Zijlstra EE (2014) Merits and pitfalls of currently used diagnostic tools in mycetoma. PLoS Negl Trop Dis 8:e2918. doi:10.1371/journal.pntd.0002918
161. van de Sande WWJ, Maghoub ES, Fahal AH, Goodfellow M, Welsh O, Zijlstra E (2014) The mycetoma knowledge gap: identification of research priorities. PLoS Negl Trop Dis 8:e2667. doi:10.1371/journal.pntd.0002667
162. Sarisoy HT, Memisoglu K, Tamer GS, Sarlak AY (2008) Primary hydatid disease in adductor muscles. Clin Investig Med Médecine Clin Exp 31: E296–E299
163. Sarris I, Berendt AR, Athanasous N, Ostlere SJ (2003) MRI of mycetoma of the foot: two cases demonstrating the dot-in-circle sign. Skeletal Radiol 32:179–183. doi:10.1007/s00256-002-0600-2
164. Schiettecatte A, Shahabpour M, Vanhoenacker FM, Goossens A, Pouliart N, Machiels F, de Mey J (2007) An unusual case of cat-scratch disease of the knee: case report and differential diagnosis. JBR-BTR organe la Société R belge Radiol orgaan van K Belgische Ver voor Radiol 90:391–394
165. Schmid MR, Kossmann T, Duewell S (1998) Differentiation of necrotizing fasciitis and cellulitis using MR imaging. AJR Am J Roentgenol 170:615–620. doi:10.2214/ajr.170.3.9490940
166. Sekine T, Amano Y, Hidaka F, Takagi R, Machida T, Naito Z, Kumita S (2012) Hepatosplenic and muscular sarcoidosis: characterization with MR imaging. Magn Reson Med Sci 11:83–89
167. Senol U, Karaal K, Cevikol C, Dincer A (2000) MR imaging findings of recurrent tumoral calcinosis. Clin Imaging 24:154–156
168. Sharif HS, Clark DC, Aabed MY, Aideyan OA, Mattsson TA, Haddad MC, Ohman SO, Joshi RK, Hasan HA, Haleem A (1991) Mycetoma: comparison of MR imaging with CT. Radiology 178:865–870. doi:10.1148/radiology.178.3.1994434
169. Sharma P, Mangwana S, Kapoor RK (2000) Diabetic muscle infarction: atypical MR appearance. Skeletal Radiol 29:477–480
170. Shehan JM, El-Azhary RA (2005) Magnetic resonance imaging features of subcutaneous granuloma annulare. Pediatr Dermatol 22:377–378. doi:10.1111/j.1525-1470.2005.22427.x
171. Van Slyke MA, Moser RP, Madewell JE (1995) MR imaging of periarticular soft-tissue lesions. Magn Reson Imaging Clin N Am 3:651–667
172. Spengos K, Wöhrle JC, Binder J, Schwartz A, Hennerici M (2000) Bilateral diabetic infarction of the anterior tibial muscle. Diabetes Care 23:699–701
173. Steinbach LS, Johnston JO, Tepper EF, Honda GD, Martel W (1995) Tumoral calcinosis: radiologic-pathologic correlation. Skeletal Radiol 24:573–578
174. Stoker DJ, Saifuddin A (1999) The radiologic features of non-neoplastic tumors of soft tissue. Semin Musculoskelet Radiol 3:81–96. doi:10.1055/s-2008-1080052
175. Sundaram M, Sharafuddin MJ (1995) MR imaging of benign soft-tissue masses. Magn Reson Imaging Clin N Am 3:609–627
176. Suresh S, Tirabosco R, Saifuddin A, O'Donnell P (2007) An unusual presentation of muscular sarcoidosis. Skeletal Radiol 36:995–998. doi:10.1007/s00256-007-0321-7
177. Tohme-Noun C, Le Breton C, Sobotka A, Boumenir ZE, Milleron B, Carette MF, Khalil A (2004) Imaging findings in three cases of the nodular type of muscular sarcoidosis. AJR Am J Roentgenol 183:995–999. doi:10.2214/ajr.183.4.1830995
178. Trujillo-Santos AJ (2003) Diabetic muscle infarction: an underdiagnosed complication of long-standing diabetes. Diabetes Care 26:211–215
179. Tuncay IC, Demirörs H, Isiklar ZU, Agildere M, Demirhan B, Tandogan RN (1999) Calcific myonecrosis. Int Orthop 23:68–70
180. Van Camp E, Vanhoenacker F, Bernard Ph, Bosmans JL, Verstraete KL (2013) Tuméfaction sous-scapulaire avec charactéristiques spécifiques à l'imagerie. Orthorhumatology 11:16–18
181. Vandevenne JE, Colpaert CG, De Schepper AM (1998) Subcutaneous granuloma annulare: MR imaging and literature review. Eur Radiol 8:1363–1365. doi:10.1007/s003300050553
182. Vanhoenacker FM, Eyselbergs M, Van Hul E, Van Dyck P, De Schepper AM (2011) Pseudotumoural soft tissue lesions of the hand and wrist: a pictorial review. Insights Imaging 2:319–333. doi:10.1007/s13244-011-0076-5
183. Vanhoenacker FM, Mespreuve MF, De Schepper AM, Cornelis S (2001) The geyser phenomenon in a long-standing rotator cuff tear. J Belge Radiol 84:167
184. Vanhoenacker FM, Verstraete KL (2015) Soft tissue tumors about the shoulder. Semin Musculoskelet Radiol 19:284–299. doi:10.1055/s-0035-1549322
185. Al-Ismail K, Torreggiani WC, Munk PL, Nicolaou S (2002) Gluteal mass in a bodybuilder: radiological depiction of a complication of anabolic steroid use. Eur Radiol. 12:1366–69
186. Vanhoenacker P, Brijs S, Geusens E, De Man R, Dujardin P, Tanghe W (1994) MR imaging of primary muscular sarcoidosis. Case report. RöFo Fortschritte auf dem Gebiete der Röntgenstrahlen und der Nukl 161:570–571. doi:10.1055/s-2008-1032589
187. Vansevenant M, Vanhoenacker FM, Catry F (2015) Tophaceous gout of the extensor mechanism of the knee. JBSR 99:93–94. doi:http://doi.org/10.5334/jbr-btr.861
188. Veraldi GF, Scudo G, Scorsone L, Mezzetto L, Castellani RL (2014) Cystic adventitial disease of the popliteal artery: report of two cases and review of the literature. G Chir 35:229–234
189. Verbeek PA, Shahabpour M, Peeters EY, Machiels F, Van den Brande RM, Vanhoenacker FM (2005) Proceedings of the SRBR-KBVR osteoarticular section meeting of June 29, 2004 in Antwerp. Cystic

adventitial disease. JBR-BTR organe la Société R belge Radiol orgaan van K Belgische Ver voor Radiol 88:200–204
190. Wall SD, Fisher MR, Amparo EG, Hricak H, Higgins CB (1985) Magnetic resonance imaging in the evaluation of abscesses. AJR Am J Roentgenol 144:1217–1221. doi:10.2214/ajr.144.6.1217
191. Wang C-W, Chang W-C, Chao T-K, Liu C-C, Huang G-S (2009) Computed tomography and magnetic resonance imaging of cat-scratch disease: a report of two cases. Clin Imaging 33:318–321. doi:10.1016/j.clinimag.2009.01.006
192. White EA, Patel DB, Forrester DM, Gottsegen CJ, O'Rourke E, Holtom P, Charlton T, Matcuk GR (2014) Madura foot: two case reports, review of the literature, and new developments with clinical correlation. Skeletal Radiol 43:547–553. doi:10.1007/s00256-013-1751-z
193. Winterer JT, Ghanem N, Roth M, Schaefer O, Lehnhardt S, Thürl C, Horch RE, Laubenberger J (2002) Diagnosis of the hypothenar hammer syndrome by high-resolution contrast-enhanced MR angiography. Eur Radiol 12:2457–2462. doi:10.1007/s00330-002-1324-3
194. Wright NB, Carty HM (1994) The swollen leg and primary lymphoedema. Arch Dis Child 71:44–49
195. Wu CM, Davis F, Fishman EK (1998) Musculoskeletal complications of the patient with acquired immunodeficiency syndrome (AIDS): CT evaluation. Semin Ultrasound CT MR 19:200–208
196. Wu KK (1996) Morton's interdigital neuroma: a clinical review of its etiology, treatment, and results. J Foot Ankle Surg 35:112–129; discussion 187–188.
197. Yablon CM (2013) Ultrasound-guided interventions of the foot and ankle. Semin Musculoskelet Radiol 17:60–68. doi:10.1055/s-0033-1333916
198. Yamaguchi T, Sugimoto T, Imai Y, Fukase M, Fujita T, Chihara K (1995) Successful treatment of hyperphosphatemic tumoral calcinosis with long-term acetazolamide. Bone 16:247S–250S
199. Yanagisawa N, Okamura T (2016) Muscular sarcoidosis mimicking soft tissue tumor. Intern Med 55:95–96. doi:10.2169/internalmedicine.55.5661
200. Yang I, Hayes CW, Biermann JS (2002) Calcific tendinitis of the gluteus medius tendon with bone marrow edema mimicking metastatic disease. SkeletalRadiol31:359–361.doi:10.1007/s00256-002-0516-x
201. Yörükoğlu Y, Zengin M, Dolgun A, Nazliel K, Salman E, Paşaoğlu E, Yucel E (1993) Primary muscular hydatid cyst causing arterial insufficiency: case report and literature review. Angiology 44:399–401
202. Yousefzadeh DK, Schumann EM, Mulligan GM, Bosworth DE, Young CS, Pringle KC (1982) The role of imaging modalities in diagnosis and management of pyomyositis. Skeletal Radiol 8:285–289
203. Zanetti M, Strehle JK, Kundert HP, Zollinger H, Hodler J (1999) Morton neuroma: effect of MR imaging findings on diagnostic thinking and therapeutic decisions. Radiology 213:583–588. doi:10.1148/radiology.213.2.r99nv06583
204. Zanetti M, Strehle JK, Zollinger H, Hodler J (1997) Morton neuroma and fluid in the intermetatarsal bursae on MR images of 70 asymptomatic volunteers. Radiology 203:516–520. doi:10.1148/radiology.203.2.9114115
205. Zanetti M, Weishaupt D (2005) MR imaging of the forefoot: Morton neuroma and differential diagnoses. Semin Musculoskelet Radiol 9:175–186. doi:10.1055/s-2005-921938
206. Zeidenberg J, Burks SS, Jose J, Subhawong TK, Levi AD (2015) The utility of ultrasound in the assessment of traumatic peripheral nerve lesions: report of 4 cases. Neurosurg Focus 39:E3. doi:10.3171/2015.6.FOCUS15214
207. Zohman GL, Pierce J, Chapman MW, Greenspan A, Gandour-Edwards R (1998) Calcific myonecrosis mimicking an invasive soft-tissue neoplasm. A case report and review of the literature. J Bone Joint Surg Am 80:1193–1197
208. Goldsmith LA et al (2012) Fitzpatrick's dermatology in general medicine, 8th edn. McGraw-Hill, New York
209. Kransdorf MJ, Murphey MD (2014) Imaging of soft tissue tumors, 3rd edn. Edited by Kransdorf MJ, Murphey MD. Wolters Kluwer Health/Lippincott Williams & Wilkins, Philadelphia

Soft Tissue Lymphoma

22

Jan L. Gielen, Filip M. Vanhoenacker,
and Peter Bracke

Contents

22.1 **Introduction** 577
22.2 **Epidemiology** 578
22.3 **Pathogenesis** 578
22.4 **Clinical Manifestations** 579
22.5 **Imaging** 579
22.5.1 Radiological Imaging 579
22.5.2 Nuclear Medicine and Hybrid Imaging 585
22.6 **Staging** 587
22.7 **Differential Diagnosis** 590
Conclusion 590
References 591

J.L. Gielen, MD, PhD (✉)
University hospital of Antwerp,
Department of Radiology and Sports,
University of Antwerp, Faculty of Medicine,
Wilrijkstraat 10, 2650 Edegem/Antwerp, Belgium
e-mail: Jan.gielen@uza.be

F.M. Vanhoenacker, MD, PhD
University hospital of Antwerp and Ghent,
Department of Radiology, Edegem, Belgium

St.-Maarten ziekenhuis, Duffel-Mechelen, Belgium

P. Bracke, MD
Klina, Department of Radiology,
Brasschaat, Belgium

22.1 Introduction

Lymphoma can involve any part of the musculoskeletal system. Primary soft tissue lymphoma involves in decreasing order of frequency the muscles, subcutaneous tissues (mycosis fungoides), the skin, synovium, nerve roots, and bone. Secondary lymphomatous involvement of the musculoskeletal system is more common, while primary malignant extranodal soft tissue lymphoma is very rare and accounts for only 0.01–2 % of soft tissue tumors [22, 32, 34]. Secondary involvement of soft tissue by lymphoma can occur as part of disseminated disease or as extension from adjacent bone or lymph nodes. An increased incidence has been noted in recent years, possibly related to an increase in the number of immunocompromised patients [25]. Classification of malignant lymphoma continues to evolve from increased understanding of normal lymphoid cell differentiation as well as from observations on behavior and response to therapy within lymphoma subtypes. Therefore comparing studies and data should be made with precaution, respecting the fact that lymphoma has been classified by several systems over the past 30 years.

The purpose of further classifying non-Hodgkin's lymphomas into specific categories is to describe the individual behavior and to develop appropriate treatment strategies for each type of lymphoma.

© Springer International Publishing AG 2017

F.M. Vanhoenacker et al. (eds.), *Imaging of Soft Tissue Tumors*, DOI 10.1007/978-3-319-46679-8_22

The most common classification system used in the 1980s–1990s was the International Working Formulation (IWF). The IWF divided non-Hodgkin's lymphomas into three grades based on the microscopical appearance. This type of histological grading into low-grade, intermediate-grade, and high-grade lymphoma is found throughout case reports and in the literature [28, 32].

Since the utilization of the IWF, additional work is done that further classifies non-Hodgkin's lymphomas into individual cancers, each with specific features and behavior. This newer system is called the Revised European American Lymphoma (REAL) classification (1994). This REAL classification was so far updated in 1999 and revised in 2008 in line with the WHO modification [13, 16] which recognizes three major categories of lymphoid malignancies based on morphology and cell lineage: B-cell neoplasms, T-cell/natural killer (NK)-cell neoplasms, and Hodgkin's lymphoma.

Almost all cases described in the literature and reflected in our series are non-Hodgkin's lymphomas, the majority of the B-cell type.

Histological and immunophenotypic studies show a range of small lymphocytic, follicular, mixed, small noncleaved, and large cell (diffuse large B-cell lymphoma (DLBCL) (anaplastic, immunoblastic, and centroblastic) lymphoma. Only a minority of T-cell lymphoma of the soft tissues are reported in the literature [1, 8, 18, 20, 28].

A distinctive subtype of soft tissue lymphomas has been reported by Isaacson and Wright [15] in 1983 and named MALT lymphomas, which stands for *mucosa-associated lymphoid tissue*. These are the extranodal equivalent of monocytoid (marginal zone) B-cell lymphomas occurring in lymphoid organs such as the lymph node. Although MALT lymphomas occur most frequently in the stomach, they have also been described in various nongastrointestinal sites, such as the salivary gland, conjunctiva, thyroid, orbit, lung, breast, kidney, skin, liver, and prostate, as well as the central nervous system. Most of these organ systems lack native lymphoid tissue but acquire MALT in close association with chronic inflammation or autoimmune processes. MALT lymphomas appear to have similar clinical, pathological, and molecular features regardless of the organ of origin.

In the revised REAL-WHO classification, the MALT lymphomas were definitively classified among the marginal zone B-cell lymphomas.

22.2 Epidemiology

The disease mainly affects patients in their sixth to seventh decades. There is no sex predilection. As far as race is described in literature, there have been no black patients with primary soft tissue lymphoma. Ninety-five percent of lymphomas occur in the extremities, with 75 % in the lower extremities [21]. Earlier studies also report a minor predilection for the gluteus and psoas muscles [3]. Primary soft tissue lymphoma is rather rare, the reported frequency depending on the strictness of definition. Lymphomas originating at soft tissue account for 0.011–2 % of primary lymphomas [35].

Although extranodal lymphomas are common in HIV-1-positive disease in general, there are only few reports of primary soft tissue non-Hodgkin's lymphoma in literature [30].

MALT lymphoma represents about 8 % of all non-Hodgkin's lymphomas [15]. Nongastrointestinal locations represent about 30–40 % of all low-grade mucosa-associated lymphoid tissue (MALT) lymphomas.

22.3 Pathogenesis

Little is known about the etiology and pathogenesis of soft tissue lymphoma. An association has been described between B-cell lymphoma and rheumatoid arthritis [11]. Chronic local immune stimulation may have a significant role in the pathogenesis of these lymphomas, unlike the frequently reversible and EBV-positive lymphomas that occur in rheumatoid patients undergoing immunosuppressive therapy.

An increased incidence of soft tissue lymphomas has been described in patients who have previously undergone orthopedic surgery using

metallic implants and after joint replacement, in acquired immune deficiency syndrome, and after organ transplantation with immunosuppressive treatment [6, 18, 27]. Some studies also suggest a possible correlation between dioxin pollution, the use of chlorinated drinking water, the exposure to chlorophenols or phenoxy herbicides, and the presence of soft tissue sarcoma and non-Hodgkin's lymphoma.

22.4 Clinical Manifestations

The clinical presentation is nonspecific. Lymphomas are relatively large tumors at presentation, varying from 2 cm to more than 15 cm. The soft tissue mass is often the only clinical finding. Pain and tenderness may be present and are more often found in case of lymphoma than in soft tissue sarcoma. In some cases increased serum levels of lactate dehydrogenase are found [7]. The general signs associated with the nodal type of lymphoma are only found in less than 2 % of reported cases.

In rare cases, a nephrotic syndrome can be the initial presentation of soft tissue lymphoma [10, 20]. Locations such as the stomach, intestine, skin, endocrine, and salivary glands, as well as the central nervous system, can present with atypical, nonspecific signs and symptoms related to the site of origin [33]. Neurological and skin involvements usually dominate the clinical presentation of intravascular lymphomatosis (IL) and mycosis fungoides. IL is a rare entity, only recently included in the lymphoma classification, whose main characteristics result from tumoral infiltration of the blood vessels, presenting with skin rash or neurological symptoms due to necrotic or demyelinating disorders.

22.5 Imaging

22.5.1 Radiological Imaging

Plain radiographs are usually of little help in the assessment of soft tissue lymphoma, as they rarely show associated bone abnormalities.

On ultrasound, lesions are relatively heterogeneous, hyporeflective, or isoreflective in comparison with adjacent muscles (Fig. 22.4). The infiltrative pattern of the lesions can be appreciated by their rather irregular borders toward the adjacent muscle groups. Ultrasound can easily depict the infiltration of the subcutaneous fat by the tumor. In some cases, apparent coarsening of fibroadipose septa and swelling of muscle bundles may occur [2]. As with other soft tissue tumors, ultrasound has a very low specificity but can be used for monitoring therapy and biopsy guidance. Ultrasound can especially be used in the follow-up of skin involvement.

Computed tomography shows lesions with an attenuation similar to that of muscle [19, 26]. As a consequence the lesion often cannot be distinguished from adjacent muscle fibers and presents as a diffuse soft tissue swelling. In the same way, a clinically apparent mass lesion in non-Hodgkin's lymphoma should not be neglected on the basis of an apparently unremarkable CT scan. After intravenous administration of iodinated contrast material, enhancement of soft tissue lymphomas is mostly poor, though diffuse [10].

Angiography is of little or no value; lymphomas mostly present as hypovascular mass lesions [3].

On magnetic resonance imaging, lymphomas might present as large masses (Fig. 22.1). In our own series of non-Hodgkin's soft tissue lymphoma, we found areas of mild hyperintensity on Tl-weighted images (WI) in ten out of fourteen cases (Figs. 22.2b and 22.3a). The hyperintensity on T1-WI of the majority of soft tissue lymphoma (Hodgkin and non-Hodgkin) was confirmed by Suresh et al. [31]. Signal intensities isointense to or slightly lower than adjacent muscles on T1-WI are half as frequent (Figs. 22.1a and 22.2b). On T1-weighted SE images, the lesions are homogeneous [34]. Tl-WI with fat suppression demonstrate a hyperintense aspect of the infiltrating lesion in comparison to the surrounding muscle tissue (Fig. 22.1b and 22.6c). The vast majority of the lesions are of intermediate SI on T2-WI with only a minority of hyperintense lesions [35]. A homogeneous, intermediate SI of the soft tissue

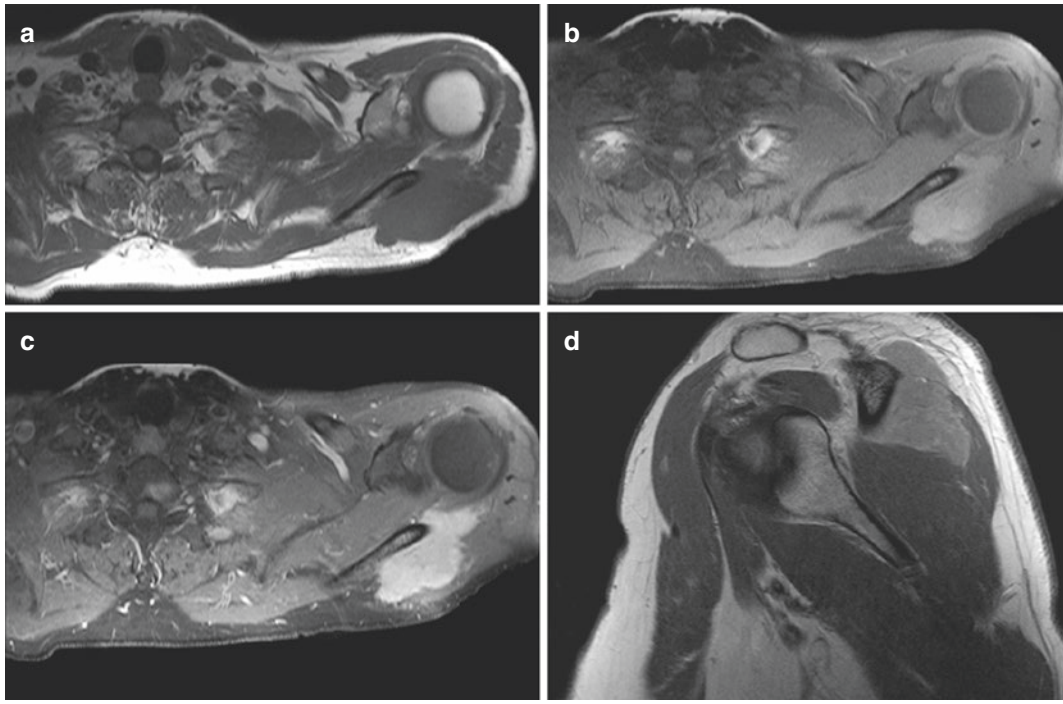

Fig. 22.1 (**a–d**) B-cell non-Hodgkin's lymphoma in a 55-year-old man: (**a**) axial spin-echo T1-weighted MR image; (**b**) axial spin-echo T1-weighted MR image with fat suppression; (**c**) axial spin-echo T1-weighted MR image after gadolinium contrast injection with fat suppression; (**d**) sagittal spin-echo T2-weighted image. The T1-weighted image shows a diffuse infiltrating mass with a slightly higher signal intensity than adjacent muscle (**a**). With fat suppression the lesion becomes more hyperintense, and the extent of the lesion in the infraspinatus, trapezoid, and deltoid muscle becomes apparent (**b**). After intravenous contrast administration, there is a diffuse moderately heterogeneous contrast enhancement providing a good differentiation between muscle fibers and tumor on the T1-weighted image (**c**). On the T2-weighted image, the lesion is better depicted owing to the hyperintense appearance relative to the low signal intensity of muscle, illustrating the extent of tumoral involvement with a sharp transition zone to the surrounding trapezoid muscle (**d**). The T2-weighted image and the T1-FS-weighted image after gadolinium confirm an intact aspect of the cortical bone of the scapula with a sharp demarcation between the relative hyperintense aspect of the tumor and the cortical bone of the scapula (**c**, **d**)

Fig. 22.2 (**a–e**) Giant B-cell lymphoma in a 68-year-old woman: (**a**) axial CT image after IV contrast injection; (**b**) axial spin-echo T1-weighted MR image; (**c**) axial spin-echo T1-weighted MR image after gadolinium contrast injection with fat suppression; (**d**) coronal spin-echo T1-weighted MR image after gadolinium contrast injection with fat suppression; (**e**) axial spin-echo STIR-weighted image. CT image after contrast shows a butterfly-shaped lesion consisting of a soft tissue mass enveloping the cortical bone of the iliac crest. The lesion shows a homogeneous contrast enhancement making the lesion mildly hyperdense in comparison to the gluteal and iliac muscles (**a**). The T1-weighted image shows no apparent destruction of the iliac wing. The lesion is rather homogeneous presenting with a signal intensity similar to the surrounding muscle structures (**b**). Both T1- and T2-weighted images with fat suppression illustrate focal areas of abnormal bone marrow due to permeative bone infiltration characteristic of lymphoma without apparent bone destruction. The presentation is typical for the "wraparound" sign seen in bone and soft tissue lymphoma (**c–e**). The hyperintensity of the lesion after fat suppression allows better evaluation of the tumor extent and better delineates the transition of tumoral tissue to normal gluteal and iliac muscle fibers. The tumor enhances homogeneously showing minor internal septation (**c**, **d**)

mass on T2-WI FSE images is most common [35]. Only one report describes a relative low to isointense signal relative to muscle of lymphoma on T2-WI with a hyperintense signal on STIR images [23]. In our studies we have two similar patients presenting with a low SI on T2-weighted images (Fig. 22.4d). After intravenous administration of gadolinium-DTPA, there is a mild to moderate, diffuse enhancement (Figs. 22.1c, d, 22.3e, 22.5e and 22.6d, e) with homogeneous or heterogeneous enhancement pattern being equally frequent [35]. There

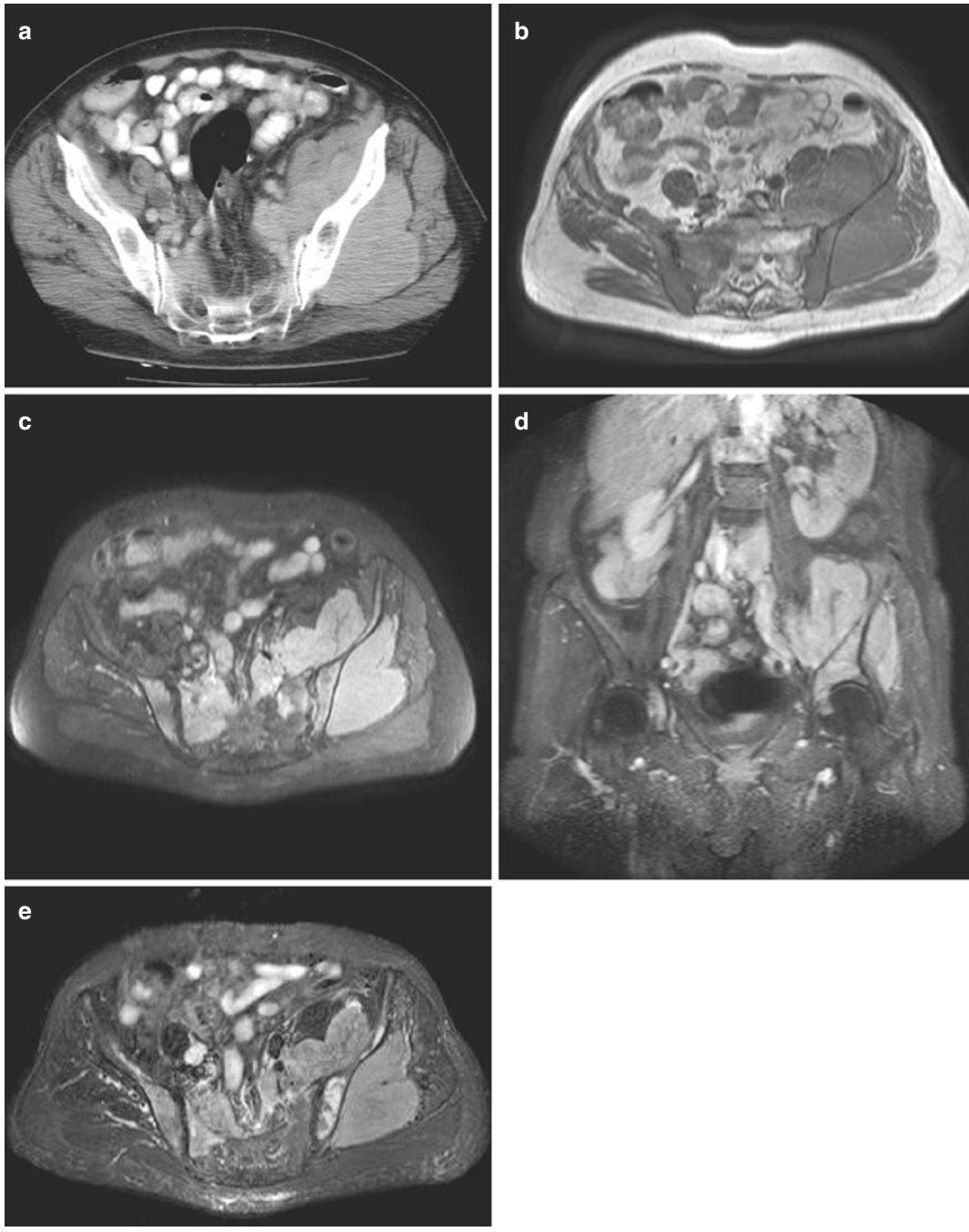

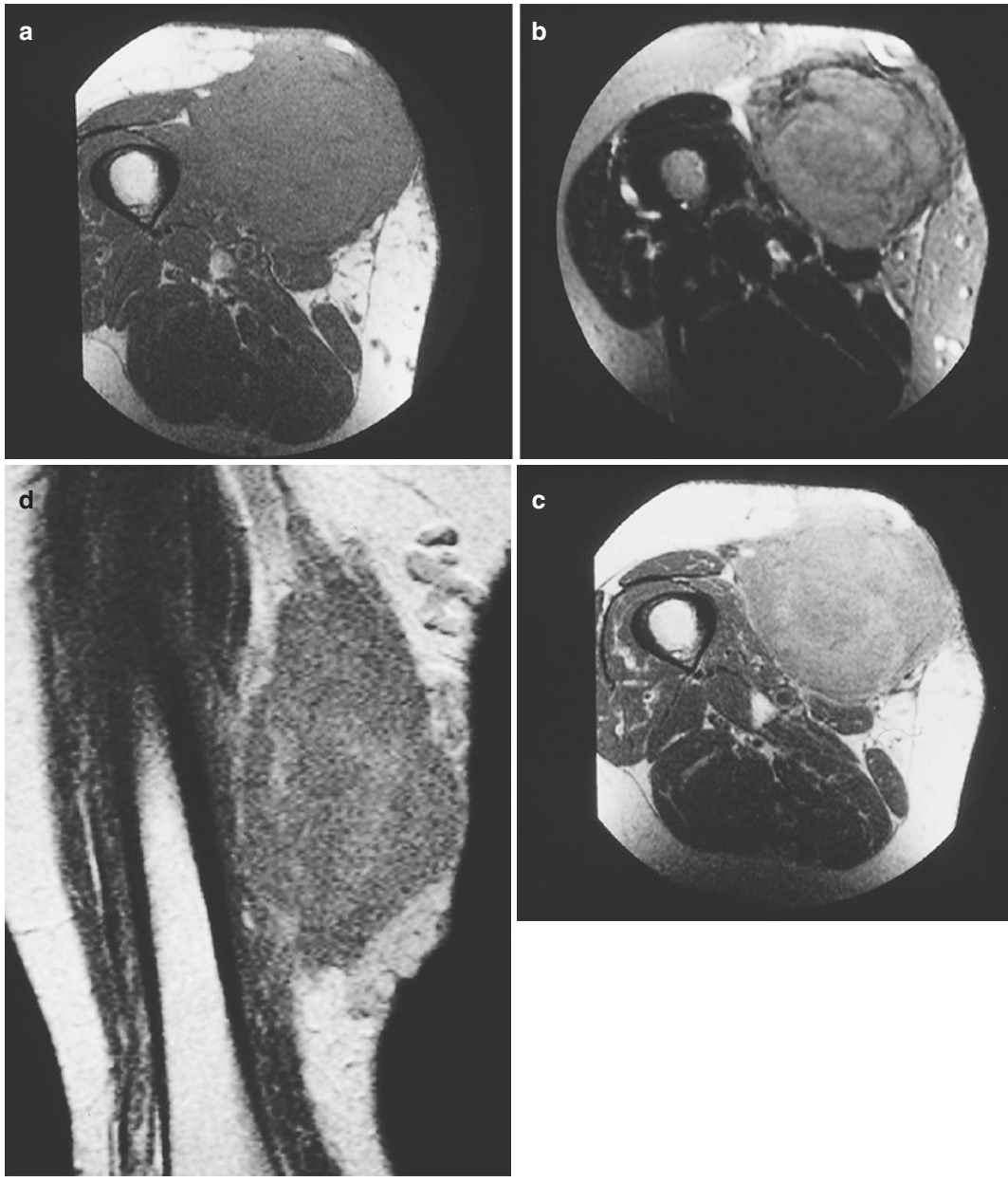

Fig. 22.3 (**a–d**) Biopsy-proven non-Hodgkin's lymphoma of the quadriceps muscle in a 64-year-old woman: (**a**) axial spin-echo Tl-weighted MR image; (**b**) axial spin-echo T2-weighted MR image; (**c**) coronal; (**d**) axial spin-echo Tl-weighted MR images after gadolinium contrast injection. On a Tl-weighted image, the lesion presents as a nodular mass, infiltrating the fascia and superficial fibers of the rectus femoris, vastus intermedius, and adductor longus muscles. The lesion has a slightly higher signal intensity than adjacent muscle. There is an extensive tumoral spread into the subcutis and cutis resulting in venous obstruction and superficial varices (**a**). After contrast injection there is a diffuse, moderately heterogeneous contrast enhancement providing a good differentiation between muscle fibers and tumor on Tl-weighted images (**c**, **d**). On a T2-weighted image, the extent of the lesion can be depicted better owing to the hyperintense appearance relative to the low signal intensity of muscle (**b**). The T2-weighted or fat-suppressed images also allow better appreciation of venous involvement

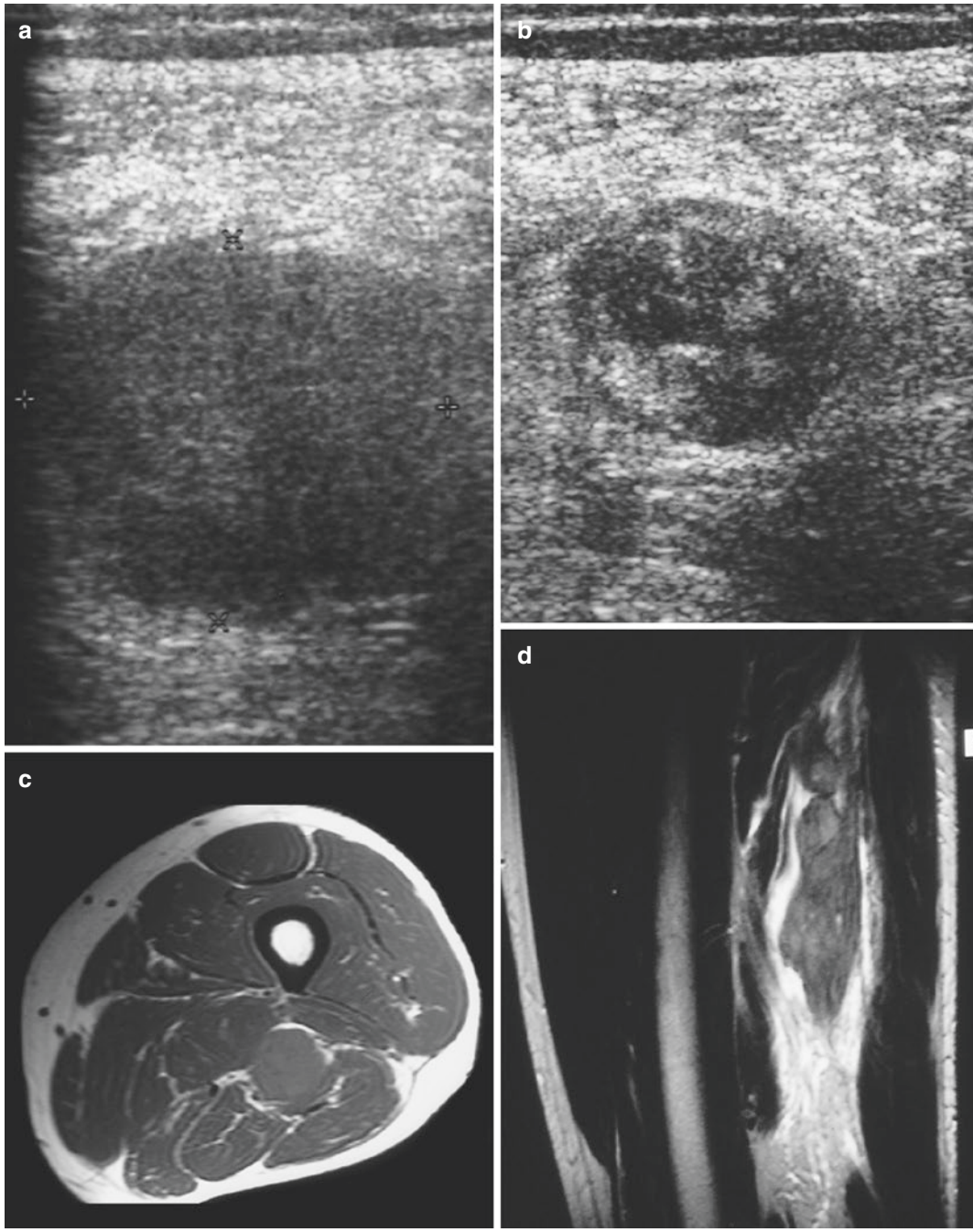

Fig. 22.4 (**a–d**) A 66-year-old man with left sciatica presenting with a type B non-Hodgkin's lymphoma in and around the sciatic nerve: (**a**, **b**) ultrasound; (**c**) axial spin-echo Tl-weighted MR image; (**d**) sagittal spin-echo T2-weighted MR image. A nodular type of lesion is found on ultrasound between the hamstring muscles. The lesion is sharply demarcated and presents with similar but more heterogeneous echogenicity to that of the hamstring muscles (**a**). In the caudal border of the lesion, hyper-echogenicity is due to infiltration of the tumor in the surrounding fat (**b**). On T1-weighted images, there is a nodular lesion in the center of the hamstrings along the neurovascular bundle. The lesion has a mildly hyperintense to isointense appearance, making differentiation with adjacent muscle groups relatively difficult (**c**). On T2-weighted images, a mildly hyperintense, bead-like lesion extending along the nerve root with irregular fat planes toward the biceps femoris (caput longum) muscle is seen

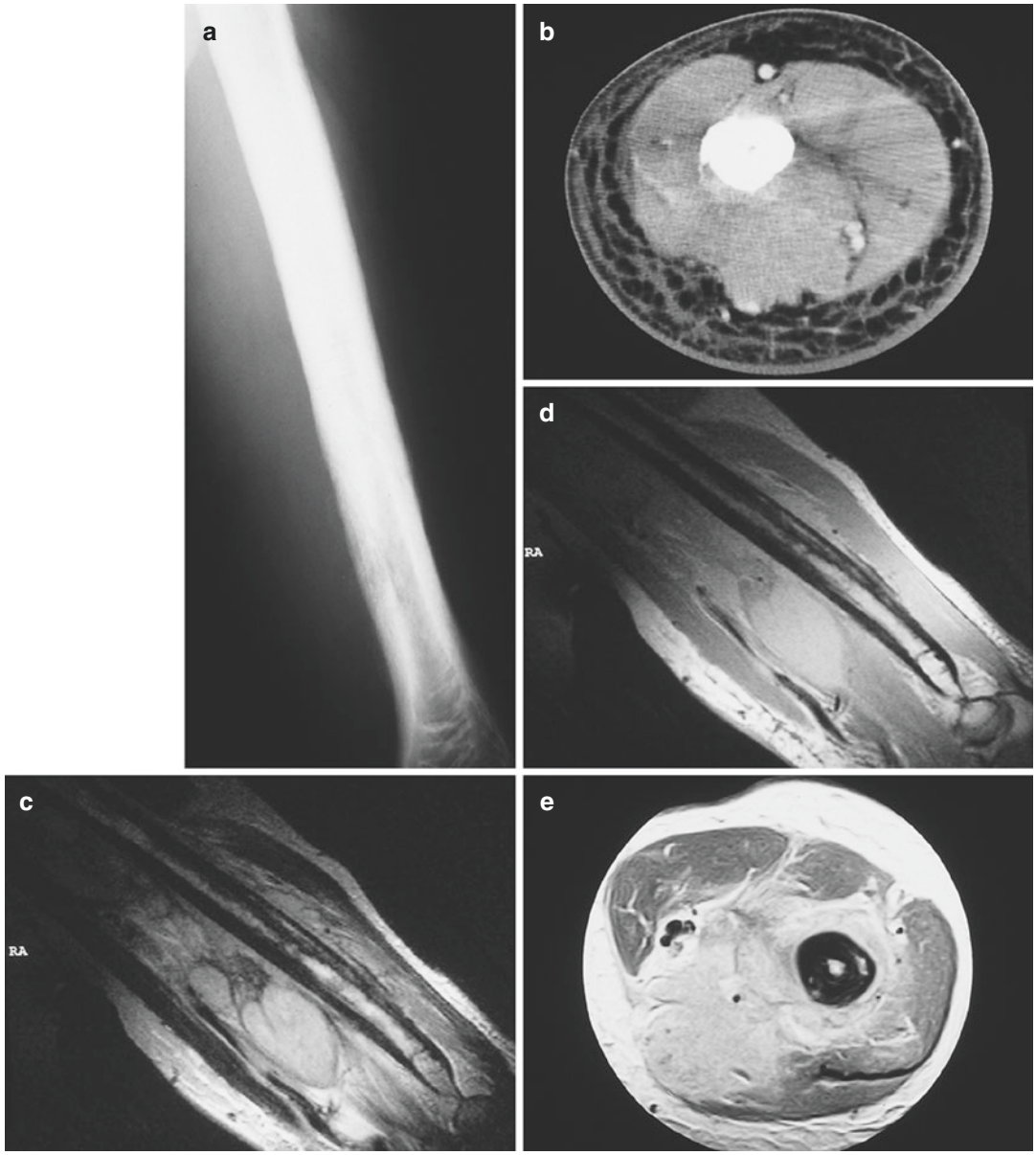

Fig. 22.5 (**a–e**) A 64-year-old man with a palpable soft tissue mass at the left upper arm (non-Hodgkin's lymphoma): (**a**) radiography of the left humerus; (**b**) CT scan after iodinated contrast injection; (**c**, **d**) sagittal spin-echo T1- and T2-weighted MR images; (**e**) axial spin-echo T1-weighted MR image after gadolinium contrast administration. The initial radiographic examination reveals a permeated aspect of the cortex of the left humerus of a lengthy area with linear and irregular periosteal abnormalities (**a**). Contrast-enhanced CT scan shows a diffuse iso-attenuating infiltrating mass, whereas the borders of the lesion cannot be distinguished from the adjacent muscle fibers. The density of the bone marrow is abnormal (**b**). The higher signal intensity of the tumor on corresponding T1- and T2-weighted images (**c**, **d**) is indicative of a diffuse infiltrating mass extending along the humeral shaft and infiltrating the brachioradial and triceps compartments. The bony "wraparound" sign of the tumor resulting in periosteal reaction at the humeral diaphysis and in bone marrow involvement is considered highly suggestive of soft tissue lymphoma. T1-weighted images after gadolinium contrast administration allow evaluation of tumor extension into different compartments and exclusion of invasion of the neurovascular bundle (**e**)

are in general no signs of necrosis or hemorrhage before treatment.

Two different morphological patterns are encountered: a more lobular, which is usually more superficial, and a deeper, diffuse infiltrative pattern. In both cases lesions behaved aggressively, often infiltrating multiple muscle groups or compartments, with no respect for compartment boundaries. Multicompartmental involvement is noted in 50 % of cases often extending into the subcutaneous tissues in about 40 % of cases [2, 35] (Fig. 22.6a–e). The transition of the tumor is irregular without cleavage planes toward adjacent muscle fibers (Figs. 22.3 and 22.4). Infiltration along the neurovascular bundle (Fig. 22.2) and extension through subcutaneous strands are often present (five out of eleven cases in our series). These strands are hypointense on TI-WI and mildly hyperintense on T2-WI. There is little or no gadolinium-DTPA enhancement in these strands corresponding to perilesional edema. Often there is an encasement of major vascular structures. MRI is the imaging technique of choice for demonstrating neurovascular encasement and defining the extent of cortical bone and marrow involvement, found in 7 out of 24 cases in the series of Suresh et al. [31]. Lymphoma can infiltrate and/or surround the cortical bone with changes in the signal intensity of the adjacent marrow. In these cases, differentiation between secondary soft tissue lymphoma by extracortical spread of primary bone lymphoma and primary soft tissue lymphoma with secondary bone involvement is often not possible (Fig. 22.5). The first possibility is supported by findings of Hicks and the second by findings of Moulopoulos [14, 24].

Moulopoulos [24] reviewed a series of 13 stage 4 lymphomas with bone involvement. If tumor was present on either side of the bony cortex but the contour of the affected bone was preserved, it was described as “wrapped around” (Fig. 22.3). This wraparound sign is indicative of a primary soft tissue lymphoma and is not found in patients with myeloma or metastatic disease.

Hicks et al. [14] showed that the absence of cortical destruction in the case of a soft tissue mass adjacent to a bone lymphoma does not exclude the possibility of an extension of the primary bone disease into adjacent soft tissues. In their study of primary bone lymphoma, they showed the presence of intracortical channels which are filled with tumor.

In those studies, however, the intraosseous component preceded the development of a soft tissue mass or was very extensive in proportion to the soft tissue mass itself. In our series the soft tissue component of the tumors was accompanied by only a mild endomedullary component in four cases (Fig. 22.3). The soft tissue component was obviously more extensive than the bone marrow abnormalities. Intracortical channels were not shown either before or after intravenous gadolinium-DTPA administration. Consequently these lesions are considered primary soft tissue lymphoma with secondary bony involvement.

22.5.2 Nuclear Medicine and Hybrid Imaging

Similar to systemic lymphoma [^{18}F]fluorodeoxyglucose positron emission tomography (FDG-PET) shows a marked accumulation of radionuclide, and therefore FDG-PET or FDG-PET-CT is strongly recommended before treatment for patients with routinely FDG-avid, potentially curable lymphomas to better delineate the extent of disease; however, currently it is not routinely indicated because of limitations imposed by cost and restriction in availability [5] (Fig. 22.6f).

A diffuse, widespread accumulation of radioisotope in the affected muscle can also be seen in rhabdomyolysis [20]. Rhabdomyolysis can be a sequela of lymphoma, as a result of the tendency of malignant lymphoma to increase the amount of muscle damage. Muscle damage may be caused by diffuse infiltration into muscles, by involvement of multiple neighboring muscle compartments and metastasizing into other soft tissues, as well as a sequela of cytotoxic actions. This cytotoxic action with acute tubular necrosis can account for the number of patients reported with renal dysfunction associated with muscle lymphomas.

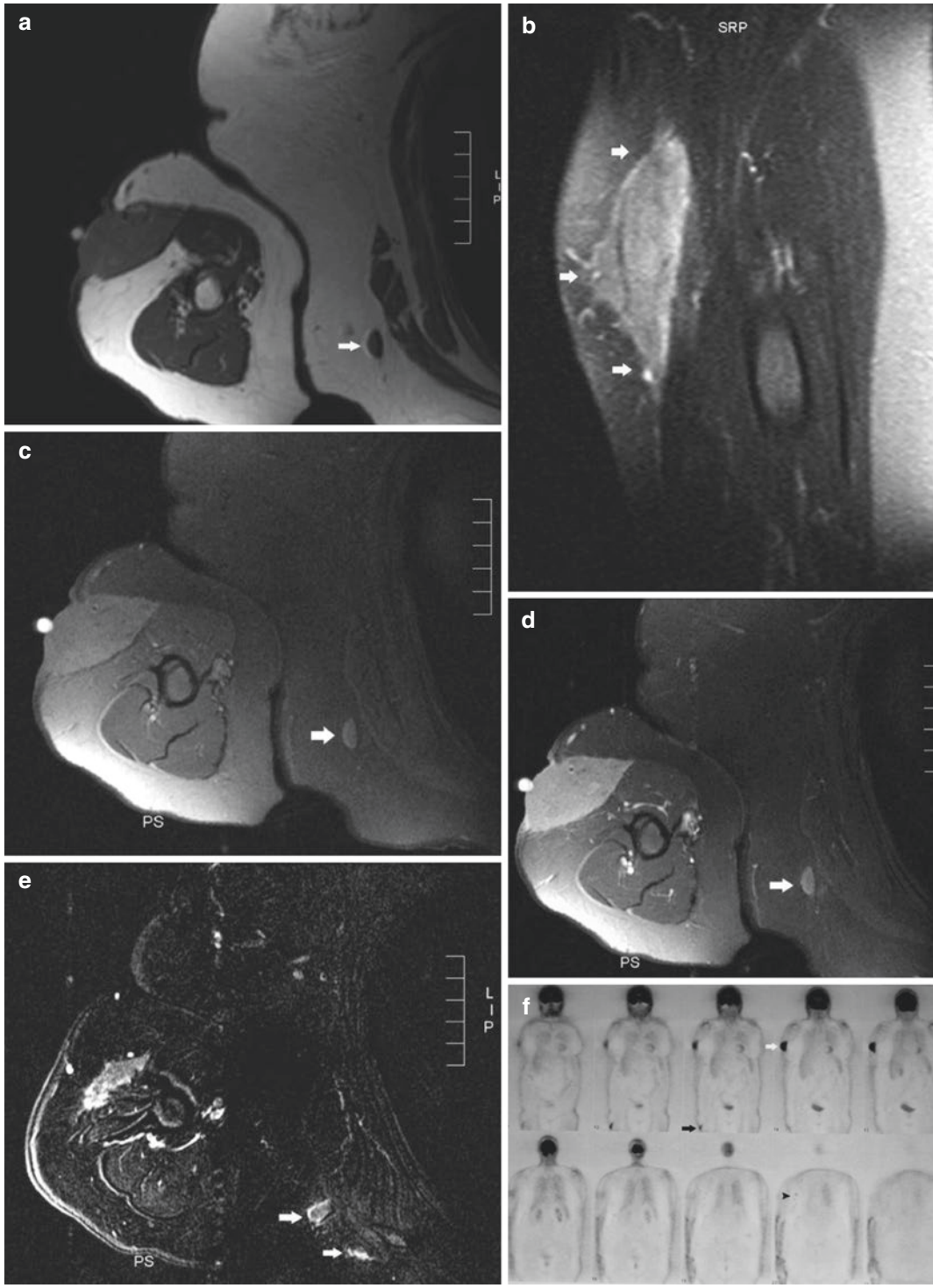

The different imaging modalities are complementary rather than competitive in the initial evaluation of malignant lymphoma. The imaging characteristics are not specific for lymphoma subtypes.

PET is essential for the follow-up and posttreatment assessment of soft tissue lymphoma (diffuse large B-cell lymphoma (DLBCL) and Hodgkin's lymphoma). PET is recommended in the other,

incurable histologic types of tumors solely if they were PET positive before treatment [5]. Change in size and FDG avidity are the main imaging parameters assessed under the revised International Working Group response criteria [5, 35].

Post-therapy inflammatory changes may persist for up to 2 weeks (after chemotherapy alone) and for up to 2–3 months or longer (after radiation therapy or combined chemotherapy and radiation therapy). To minimize the amount of these potentially confounding interpretation finding, PET scans should not be performed for at least 3 weeks, and preferably 6–8 weeks, after completion of therapy [17].

Current data are inadequate to recommend routine surveillance PET scans after the restaging study [5].

Table 22.1 Staging of lymphoma

Stage I
Involvement of a single lymph node region or lymphoid organ (thymus) (I) or of a single extralymphatic organ or site (IE)
Stage II
Involvement of two or more lymph node regions on the same side of the diaphragm (II) or localized involvement of extralymphatic organ or site and of one or more lymph node regions on the same side of the diaphragm (IIE)
Stage III
Involvement of lymph node regions on both sides of the diaphragm (III) which may also be accompanied by localized involvement of extralymphatic organ or site (IIIE) or by involvement of the spleen (IIIS) or both (IIISE)
Stage IV
Diffuse or disseminated involvement of one or more extralymphatic organs or tissues with or without associated lymph node enlargement

22.6 Staging

In addition to characterization, imaging techniques are mandatory to determine the stage or local and distant cancer spread. All new treatment information is categorized and evaluated by the stage of the disease. AJCC Manual for Staging Cancer is used to stage lymphoma (Table 22.1). It was originally developed for Hodgkin's disease and later expanded to include non-Hodgkin's lymphoma.

Determining the local extent of the cancer requires MRI, and distant spread may be studied by CT of the abdomen and thorax, MRI of the brain and skeletal scintigraphy and/or PET-CT scan, and blood tests. Although an extranodal presentation of lymphoma means stage IV disease (involves one or more organs outside the lymph system or a single organ and a distant lymph node site), imaging will be used to exclude involvement of other nodal or organ involvement (Figs. 22.7 and 22.8).

For primary nodal and primary extranodal involvement, PET-CT is preferred for staging of FDG-avid lymphomas, and CT scan is preferred in all other scenarios. A chest x-ray is no longer required in lymphoma staging because it is less accurate than CT. Moreover, CT identifies more hilar nodes and may better discriminate between a single large nodal mass and an aggregate of individual nodes [4].

Fig. 22.6 Subcutaneous B-cell lymphoma at the right upper arm, MRI (**a**–**e**) and PET (**f**) (Reprinted with permission from reference Vanhoenacker FM, Baten A, Vandeputte V (2009) Imaging findings of a cutaneous B-Cell Lymphoma. JBR-BTR 92:285–288). (**a**) Axial T1-WI demonstrating a well-demarcated slight hyperintense mass involving the subcutaneous fat and the skin at the anterior-lateral aspect of the upper arm. The lesion has an intimate relationship with the fascia of the biceps muscle. There is a small additional subcutaneous lesion within the subcutaneous tissue of the chest wall with similar SI characteristics (*arrow*). (**b**) Coronal fat-suppressed T2-WI of the right upper arm shows a large fusiform mass (*white arrows*), which is of intermediate signal intensity. (**c**) Axial fat-suppressed T1-WI. The lesion has a slightly higher signal intensity than the muscle. The small additional subcutaneous lesion within the subcutaneous tissue of the chest wall is seen as well (*arrow*). (**d**) Axial fat-suppressed T1-WI after intravenous injection of gadolinium contrast. Marked and homogeneous enhancement of the lesion as well of a subcutaneous nodule at the back of the trunk is demonstrated (*arrow*). (**e**) Axial subtraction image of the enhanced and nonenhanced MR images at a slightly different level. The homogeneous enhancement pattern is more obvious. Notice also the presence of two enhancing satellite nodules at the subcutaneous tissue of the chest wall (*arrows*). (**f**) [^{18}F]fluorodeoxyglucose (FDG) positron emission tomography. Notice a focal area of intense FDG uptake at the right upper arm (*white arrow*), as well as two additional foci of increased uptake at the right chest wall (*black arrowhead*) and a fourth small subcutaneous lesion at the right thigh (*black arrow*)

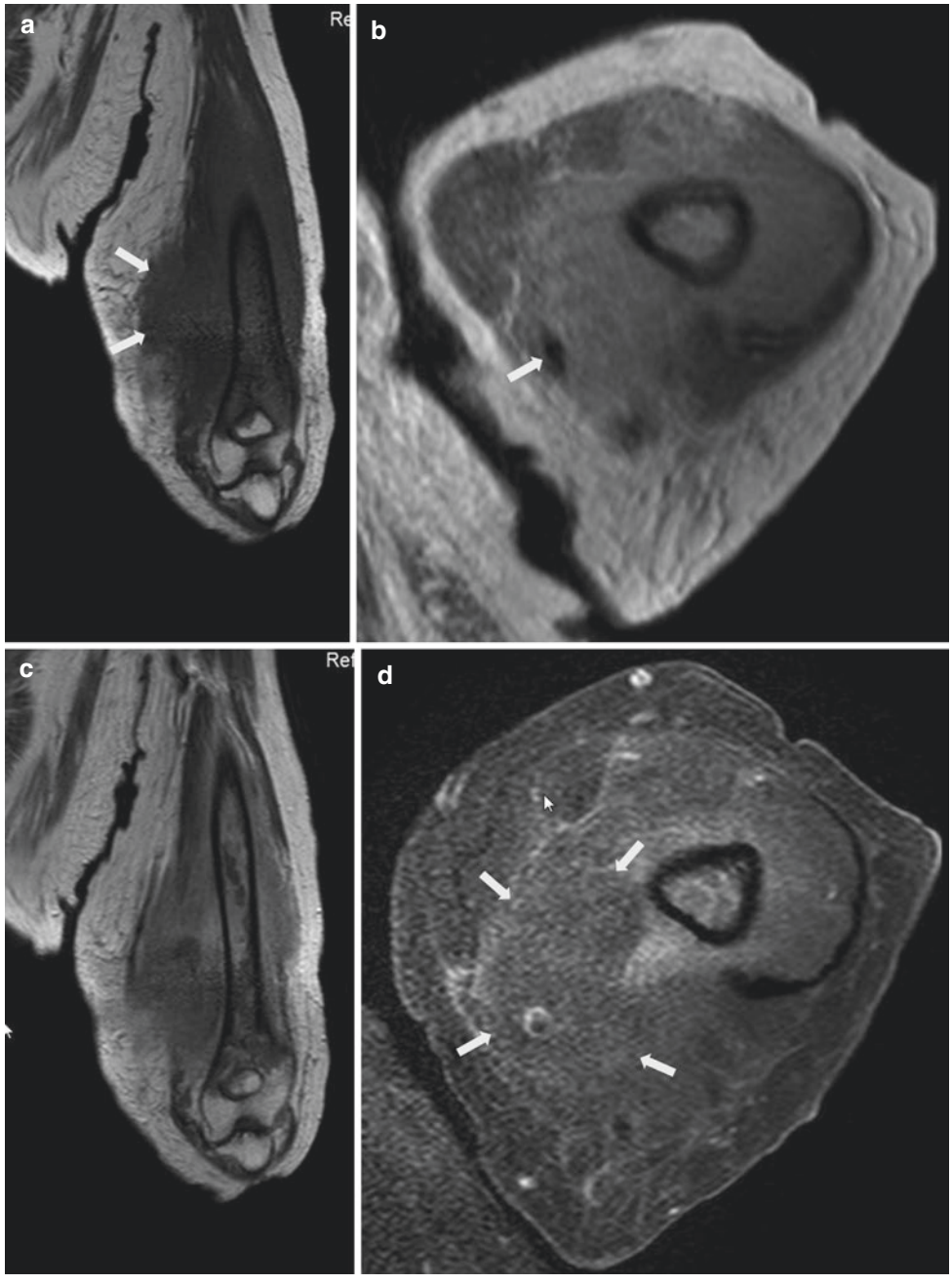

Fig. 22.7 B-cell lymphoma at the left humerus in 76-year-old female mimicking osteomyelitis (Courtesy of Dr. Hugo Declercq, Dendermonde). (**a**) Coronal T1-WI demonstrating low SI at the endomedullary cavity of the humeral diaphysis and distal metaphysis. Extension of the lesion at the posteromedial subcutaneous tissue (*arrows*). Infiltration of the muscle compartment is not identified due to isointensity of the lesion and muscle. The cortical bone of the humerus is not destructed. (**b**) Axial T2-WI, homogeneous hyperintense tumor mass at the endomedullary cavity of the humerus with invasion of the extra-osseous tissue, wrapped around the humerus, invasion at the posteromedial subcutaneous tissue, and encasement of the neurovascular bundle (*arrow*). (**c**) Coronal T1-WI after intravenous gadolinium administration demonstrating nonhomogeneous enhancement with central areas with absence of enhancement at the endomedullary bone and the medial soft tissues similar to abscess formation. (**d**) Axial T1-WI FS after intravenous gadolinium administration marked nonhomogeneous enhancement with absence of enhancement at the medial soft tissue (*arrows*)

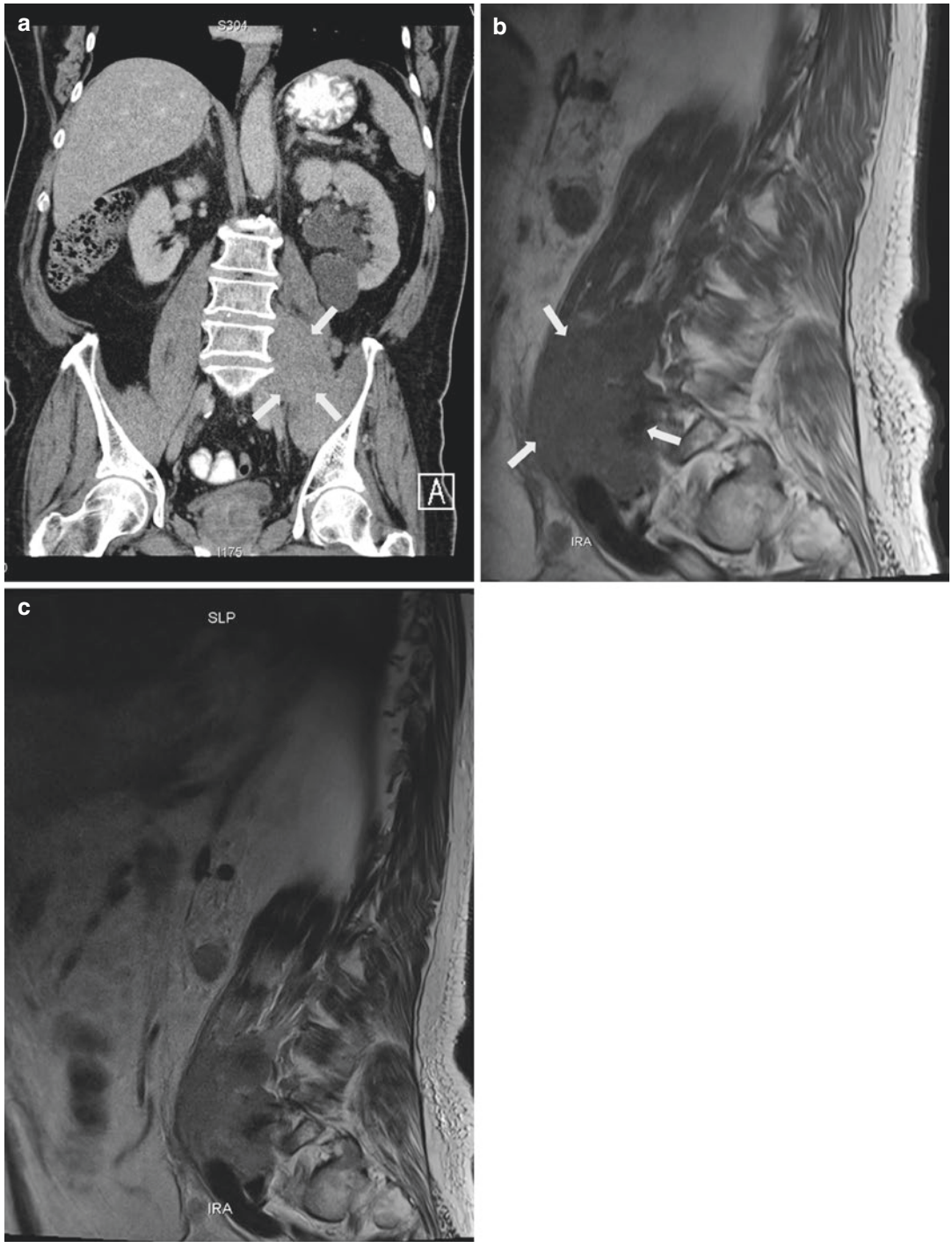

Fig. 22.8 Retroperitoneal lymphoma in 81-year-old male. (**a**) Coronal CT of the abdomen after intravenous administration of jodium contrast. Mass at the left psoas region, isointense with muscle (*arrows*). No destruction or major disk space narrowing at the lumbar segments is present. (**b**) Sagittal T1-WI of the lumbar spine demonstrating an isointense mass compared to muscle involving multiple lower lumbar segments (*arrows*). (**c**) Sagittal T2-WI of the lumbar spine demonstrating nonhomogeneous slight hyperintense mass compared to muscle tissue

Contrast-enhanced CT is preferred for radiation therapy planning. Variably FDG-avid histologies should be staged with a CT scan [4].

22.7 Differential Diagnosis

Lymphoma in an extranodal site can be confused with a wide variety of both inflammatory and neoplastic conditions.

Fine-needle aspiration biopsy (FNAB), core biopsy, or open biopsy is mandatory for a definite diagnosis. In the majority of cases, it is possible to obtain a specific diagnosis and subtype of soft tissue lymphoma using FNAB [34]. Reliable differentiation of lymphoma from other small-round-cell tumors, such as rhabdomyosarcoma or Ewing's sarcoma, and from metastatic carcinoma is necessary for therapeutic purposes. Light microscopy is usually sufficient for diagnosis. However, myxofibrosarcoma may be difficult to distinguish from Hodgkin's disease. This resemblance occurs more often in the presence of tumors in which histiocyte-like cells are intermingled with chronic inflammatory cells [9]. In these cases immunohistochemical examination is mandatory. Leu-M1 is a marker for Reed-Sternberg cells, which are not found in myxofibrosarcoma. Anaplastic, sarcomatoid lymphoma appearing primarily in the soft tissues without peripheral lymphadenopathy can create considerable diagnostic difficulties even for the pathologist, as it may be mistaken for sarcoma [1]. An accurate histological diagnosis is essential, because treatment of a muscle mass based on histological diagnosis of an undifferentiated neoplasm may lead to unnecessary radical surgery [29].

Diagnosing non-Hodgkin's lymphoma requires a great deal of skill and an expert pathologist. The use of fluorescence in situ hybridization (FISH) and DNA microarray technology and the use of CD markers are just some of the tests and technologies that may be used to achieve a correct diagnosis.

Moreover, a correct diagnosis of primary lymphoma is essential because the long-term prognosis is usually good if the tumor is properly managed. Collaboration between the radiologist and pathologist is a prerequisite for a correct diagnosis. If lymphoma is suspected or in the imaging differential diagnosis, appropriate immunohistochemical characterization of tumors will drastically reduce the incidence of "undifferentiated" histopathological diagnoses and will optimize patient management. Correct diagnosis is essential to guide appropriate management with chemotherapy and avoid unnecessary surgery. In this regard, the presence of adenopathies and the infiltrative pattern of lymphomas in contrast to sarcomas can help pathologists in orienting the tissue diagnosis. Tumor size is not a prognostic tool in predicting survival [12].

Conclusion

Whenever a soft tissue mass is encountered, which is iso- to slightly hyperintense on Tl-WI and intermediate to hyperintense on T2-WI with a diffuse infiltrative pattern extending into different muscle groups, lymphoma should be included in the differential diagnosis. There are in general no signs of necrosis or hemorrhage before treatment.

A soft tissue mass wrapped around the bone is especially suspected for extranodal primary soft tissue lymphoma.

Determining the local extent requires MRI, and distant spread may be studied by CT of the abdomen and thorax, MRI of the brain and skeletal scintigraphy and/or PET-CT scan, and blood tests.

For primary nodal and primary extranodal involvement, PET-CT is preferred for staging of FDG-avid lymphomas, and CT scan is preferred in all other scenarios.

Contrast-enhanced CT is preferred for radiation therapy planning. Variably FDG-avid histologies should be staged with a CT scan.

Key Points

1. Whenever a soft tissue mass is encountered, which is iso- to slightly hyperintense on Tl-WI and intermediate to hyperintense on T2-WI extending into different muscle groups, lymphoma should be included in the differential diagnosis.
2. A soft tissue mass wrapped around the bone is especially suspicious for extranodal primary soft tissue lymphoma.
3. After intravenous administration of gadolinium-DTPA, there is a mild to moderate, diffuse enhancement in cases of lymphoma.
4. There are in general no signs of necrosis or hemorrhage before treatment.

References

1. Axiotis CA, Fuks J, Jennings TA, Kadish AS (1988) Peripheral T-cell lymphoma presenting as a soft tissue mass of the extremity. Arch Pathol Lab Med 112: 850–851
2. Beggs I (1997) Primary muscle lymphoma. Clin Radiol 52:203–212
3. Bruneton JN, Drouillard J, Balu-Maestro C et al (1990) Imaging of malignant lymphoma of muscular sites. J Radiol 71:185–189
4. Cheson BD, Fisher RI, Barrington SF, Cavalli F, Schwartz LH, Zucca E, Lister TA (2014) Recommendations for initial evaluation, staging, and response assessment of Hodgkin and non-Hodgkin lymphoma: the Lugano classification. J Clin Oncol 32(27):3059–3068
5. Cheson BD, Pfistner B, Juweid ME, Gascoyne RD, Specht L, Horning SJ, Coiffier B, Fisher RI, Hagenbeek A, Zucca E, Rosen ST, Stroobants S, Lister TA, Hoppe RT, Dreyling M, Tobinai K, Vose JM, Connors JM, Federico M, Diehl V (2007) Revised response criteria for malignant lymphoma. J Clin Oncol 25:579–586
6. Chevalier X, Amoura Z, Viard JP, Souissi B, Sobel A, Gherardi R (1993) Skeletal muscle lymphoma in patients with the acquired immunodeficiency syndrome: a diagnostic challenge. Arthritis Rheum 36: 426–427
7. Damron TA, Le MH, Rooney MT, Vermont A, Poiesz BJ (1999) Lymphoma presenting as a soft tissue mass: a soft tissue sarcoma simulator. Clin Orthop 360:221–230
8. Ellstein J, Xeller C, Fromowitz F, Elias JM, Saletan S, Hurst LC (1984) Soft tissue T- cell lymphoma of the forearm : a case report. J Hand Surg [Am] 9:346–350
9. Enzinger F, Weiss SW (1995) In: Enzinger FM, Weiss SW (eds) Soft tissue tumors, 3rd edn. Mosby, St Louis, p 367
10. Girad T, Nochy D, Montravers F (2004) Intravascular large B-cell lymphoma revealed by a nephritic syndrome: a one year remission induced by a high frequency CHOP and rituximab. Leuk Lymphoma 45(8):1703–1705
11. Goodlad JR, Hollowood K, Smith MA, Chan JK, Fletcher CD (1999) Primary juxtaarticular soft tissue lymphoma arising in the vicinity of inflamed joints in patients with rheumatoid arthritis. Histopathology 34:199–204
12. Grunshaw ND, Chalmers AG (1992) Skeletal muscle lymphoma. Clin Radiol 45:399–400
13. Harris NL, Jaffe ES, Kiebold J, Flandrin G, Muller-Hermelink HK, Vardiman J (2000) Lymphoma classification-from controversy to consensus: the REAL and WHO Classification of lymphoid neoplasms. Ann Oncol 11(suppl 1):3–10
14. Hicks DG, Gokan T, O'Keefe RJ et al (1995) Primary lymphoma of bone: correlation of MR imaging features with cytokine production by tumor cells. Cancer 75:973–980
15. Isaacson P, Wright DH (1983) Malignant lymphoma of mucosa associated lymphoid tissue: a distinctive type of B-cell lymphoma. Cancer 52:1410–1416
16. Jaffe ES (2009) The 2008 WHO classification of lymphomas: implications for clinical practice and translational research. Hematology Am Soc Hematol Educ Program 1:523–531
17. Juweid ME, Stroobants S, Hoekstra OS, Mottaghy FM, Dietlein M, Guermazi A, Wiseman GA, Kostakoglu L, Scheidhauer K, Buck A, Naumann R, Spaepen K, Hicks RJ, Weber WA, Reske SN, Schwaiger M, Schwartz LH, Zijlstra JM, Siegel BA, Cheson BD (2007) Use of positron emission tomography for response assessment of lymphoma: Consensus recommendations of the Imaging Subcommittee of the International Harmonization Project in Lymphoma. J Clin Oncol 25:571–578
18. Lum GH, Cosgriff TM, Byrne R, Reddy V (1993) Primary T-cell lymphoma of muscle in a patient infected with human immunodeficiency virus. Am J Med 95:545–546
19. Malloy PC, Fishman EK, Magid D (1992) Lymphoma of bone, muscle and skin: CT findings. AJR Am J Roentgenol 159:805–809
20. Masaoka S, Fu T (2002) Malignant lymphoma in skeletal muscle with rhabdomyolysis: a report of two cases. J Orthop Sci 7(6):688–693

21. Maurer R, Tanner A, Honegger HP, Schmid U, Schmid L (1988) Primary non-Hodgkin lymphoma of the muscles. Schweiz Med Wochenschr 118: 354–357
22. Meister HP (1992) Malignant lymphomas of soft tissues. Verh Dtsch Ges Pathol 76:140–145
23. Metzler JP, Fleckenstein JL, Vuitch F, Frenkel EP (1992) Skeletal muscle lymphoma: MRI evaluation. Magn Reson Imaging 10:491–494
24. Moulopoulos LA, Dimopoulos MA, Vourtsi A, Gouliamos A, Vlahos L (1999) Bone lesions with soft tissue mass: magnetic resonance imaging diagnosis of lymphomatous involvement of the bone marrow versus multiple myeloma and bone metastases. Leuk Lymphoma 34:179–184
25. Murphey MD, Kransdorf MJ, Smith SE (1999) Imaging of soft tissue neoplasms in the adult: malignant tumors. Semin Musculoskelet Radiol 3:39–58
26. Panicek DM, Lautin JL, Schwartz LH, Castellino RA (1997) Non-Hodgkin lymphoma in skeletal muscle manifesting as homogeneous masses with CT attenuation similar to muscle. Skeletal Radiol 26:633–635
27. Radhi JM, Ibrahiem K, Al-Tweigeri T (1998) Soft tissue malignant lymphoma at sites of previous surgery. J Clin Pathol 51:629–632
28. Salamao DR, Nascimento AG, Lloyd RV, Chen MG, Habermann TM, Strickler JG (1996) Lymphoma in soft tissue: a clinicopathologic study of 19 cases. Hum Pathol 27:253–257
29. Schwalke MA, Rodil JV, Vezeridis MP (1990) Primary lymphoma arising in skeletal muscle. Eur J Surg Oncol 16:70–73
30. Sipsas NV, Kontos A, Panayiotakopoulos GD (2002) Extranodal non-Hodgkin lymphoma presenting as a soft tissue mass in the proximal femur in a HIV+ patient. Leuk Lymphoma 43(12):2405–2407
31. Suresh S, Saifuddin A, O'Donnel P (2008) Lymphoma presenting as a musculoskeletal soft tissue mass: MRI findings in 24 cases. Eur Radiol 18(11):2628–2634
32. Travis WD, Banks PM, Reiman HM (1987) Primary soft tissue lymphoma of the extremities. Am J Surg Pathol 11:359–366
33. Vanhoenacker FM, Baten A, Vandeputte V (2009) Imaging findings of a cutaneous B-Cell Lymphoma. JBR-BTR 92:285–288
34. Wakely P, Frable WJ, Kneisl JS (2001) Soft tissue aspiration cryopathology of malignant lymphoma and leukemia. Cancer 93(1):35–39
35. Lim CY, Ong KO (2013) Imaging of musculoskeletal lymphoma. Cancer Imaging 13(4):448–457

Soft Tissue Metastases

23

Hend Riahi, Mohamed Fethi Ladeb,
Mouna Chelli Bouaziz, and Meriem Mechri

Contents

23.1 **Introduction** 593

23.2 **Epidemiology** 593
23.2.1 Prevalence 593
23.2.2 Primary Tumors 594
23.2.3 Site of Involvement 594
23.2.4 Time Interval 594

23.3 **Pathophysiological Mechanisms** 594
23.3.1 Factors Causing Muscle Resistance to Metastases 594

23.4 **Clinical Features** 594

23.5 **Imaging Diagnosis** 595
23.5.1 Radiographs 595
23.5.2 Ultrasound 595
23.5.3 CT 595
23.5.4 MRI 596
23.5.5 Radionuclide Imaging 597

23.6 **Biopsy** 597

23.7 **Differential Diagnosis** 598

23.8 **Prognosis** 598

23.9 **Treatment** 599

Conclusion 599

References 599

H. Riahi (✉) • M.F. Ladeb • M.C. Bouaziz
M. Mechri
Department of Radiology, Institut d'Orthopédie
Mohamed Kassab, Ksar Said, Tunisie
e-mail: hend.riahi@gmail.com; fethiladeb@hotmail.fr

23.1 Introduction

Soft tissue metastases are uncommon and can easily be clinically and histopathologically confused with primary soft tissue sarcomas. The differential diagnosis between soft tissue metastasis and a primary soft tissue sarcoma is however relevant, because their treatment is markedly different.

Although soft tissue metastasis can represent the first manifestation of a primary malignancy, it is usually seen as late evidence of recurrence in advanced cancer [6, 14, 48].

There are several case reports on the subject, but only few large case series. Therefore, no definite guidelines about the management of patients with soft tissue metastases (STM) are currently available [24].

23.2 Epidemiology

23.2.1 Prevalence

The first description of a soft tissue metastasis was provided by Wittich in 1854 [30]. The prevalence of STM varies in autopsy series from 6 to 17.5 % [7, 23, 42, 45] and in radiological series from 1.2 to 1.8 % [8, 45]. This inconsistency between autopsy and clinical studies may be due to the fact that soft tissue metastases are usually asymptomatic and therefore undetected clinically and radiologically [45].

© Springer International Publishing AG 2017

F.M. Vanhoenacker et al. (eds.), *Imaging of Soft Tissue Tumors*, DOI 10.1007/978-3-319-46679-8_23

23.2.2 Primary Tumors

The lung, skin, kidney, and colon are the most common sites of primary carcinomas resulting in clinically recognized soft tissue metastases [6, 13, 32]. Other primary tumors known to metastasize to bone, such as the prostate, breast, and thyroid, are very unusual sources of reported soft tissue metastases [11, 34, 37, 50]. The most common histological diagnosis overall is that of adenocarcinoma, most frequently from the lung or gastrointestinal tract. Squamous cell carcinomas and renal clear-cell carcinomas are also relatively common, but many histological types have been reported. In addition to squamous-cell carcinomas of the lung, other squamous-cell carcinomas from the hypopharynx, esophagus, and cervix may metastasize to the soft tissues. Rarely, myeloma, lymphoma, melanoma, astrocytoma, chondroblastoma, and primary sarcoma have been reported to metastasize to the soft tissue [6].

23.2.3 Site of Involvement

The thigh muscles, iliopsoas, and paraspinous muscles are the most frequently affected sites [26]. Skeletal muscle metastases are nearly four times more frequent than subcutaneous ones. One plausible explanation is that subcutaneous metastases are less likely to cause pain and therefore to come to clinical attention than skeletal metastases [6].

23.2.4 Time Interval

Four articles mentioned [9, 13, 26, 48] the time interval between primary tumor detection and metastasis which was extremely variable (3 to 60 months, 5 months to 9 years, 1 month to 38 years, and 8 months to 15 years). In 27 to 47 % of cases, soft tissue metastasis was the first clinical manifestation of malignancy [9, 26, 29, 48].

23.3 Pathophysiological Mechanisms

Several pathophysiological mechanisms of soft tissue metastatic spread have been highlighted in the literature. The hematogeneous route is the most favored pathway. The presence of tumoral arterial emboli confirms this hypothesis [23]. Malignant tumors can metastasize into soft tissue via venous route, especially through the paravertebral venous plexus, which have multiple connections with the inferior vena cava and the mesenterial venous system [2]. Some reports suggest that muscle metastases can originate in intramuscular aberrant lymph nodes, especially for psoas muscle metastases, which may arise in the psoas lymph nodes located between the musculature and the spine [47, 53]. Furthermore, soft tissue metastasis may result from perineural spread. According to the literature, this pathway is typical of tumor extension in lymphoma [43]. However, it has also been described in several solid malignancies, especially in head and neck tumors [3, 4].

23.3.1 Factors Causing Muscle Resistance to Metastases

Although muscles represent 50 % of the body mass, hematogenous metastases are rare [6, 9, 29]. Several factors have been implicated in the rarity of this phenomenon such as mechanical destruction of tumor cells by muscle movements, turbulence and variations in blood flow (common metastatic sites such as the liver, lung, and bone have relatively constant blood flow), changes in pH and local temperature [9, 41], and inhibition of enzyme-dependent processes of invasion or tumor growth by lactic acid, diffusible protease, and different oxygen tension in the muscles [39, 46]

23.4 Clinical Features

The most frequent symptoms are pain and palpable mass [28]. Other symptoms consist of swelling and cutaneous erythema, painless soft tissue lump, and solitary metastasis incidentally found during staging CT [24, 45]. Clinical features of soft tissue metastasis may mimic a primary soft tissue sarcoma. However, a painful mass is more commonly observed in patients with soft tissue metastasis than in primary sarcomas. The lesion size usually ranges between 1 and 20 cm (6 cm) [27].

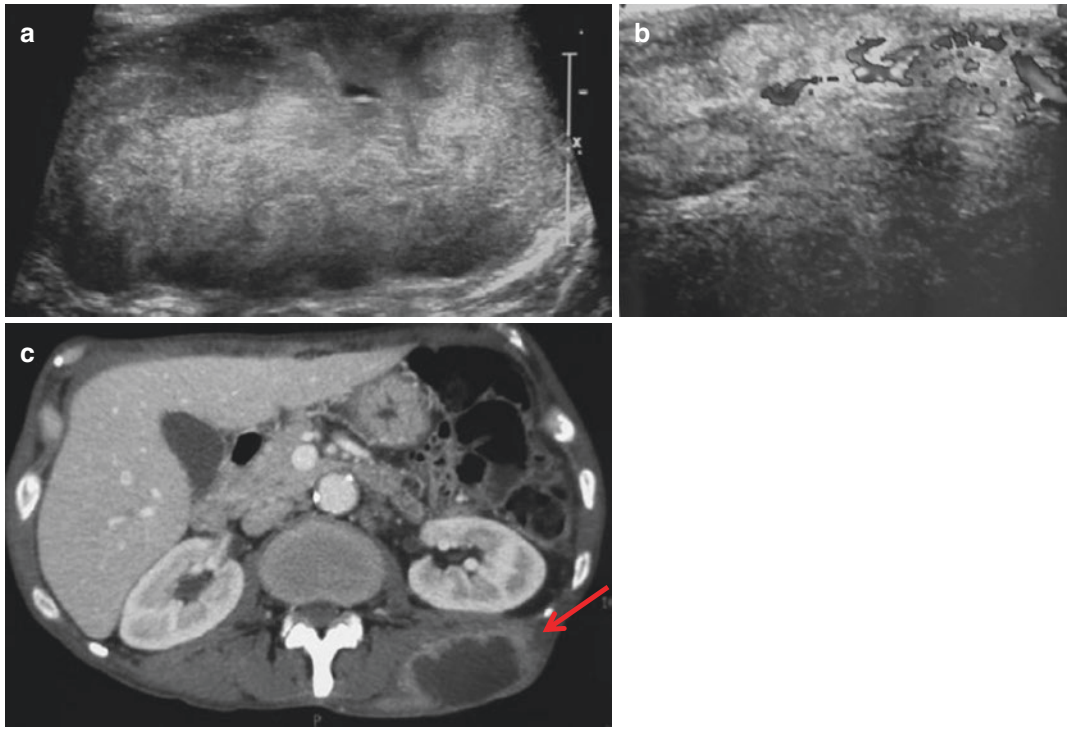

Fig. 24.1 Intramuscular metastases. (**a**) Gray-scale and (**b**) color Doppler 12–5 MHz US images in patient with previously diagnosed malignancy (lung adenocarcinoma): well-defined lobulated shape hypoechoic nodules located within the muscle. Color Doppler imaging shows a hypervascular pattern. (**c**) Contrast-enhanced CT demonstrates an intramuscular (M. left erector spinae) lesion with central low attenuation and rim enhancement (*arrow*)

23.5 Imaging Diagnosis

Diagnostic studies of soft tissue metastases are not specific.

23.5.1 Radiographs

Radiographs may show soft tissue opacity [6]. In some cases, calcifications within the soft tissue masses can be recognized especially in pancreatic and gastric carcinoma metastases [19, 33, 42]. Ossifications have been reported in abdominal wall and psoas muscle metastases of colonic carcinomas, especially mucinous carcinomas [40].

23.5.2 Ultrasound

Superficial soft tissue masses are particularly amenable to high-resolution ultrasound examination. The merits of US include its ability to distinguish between a solid and cystic mass and to determine the size and location of the mass [12].

In most cases, metastases appear as well-circumscribed hypoechoic and hypervascularized masses (Figs. 24.1, 24.2, and 24.5) [21].

Sonographic guidance provides a safe, rapid, and accurate method for localizing superficial soft tissue masses suggestive of metastatic disease and then guiding needle biopsies to acquire cytologic material for a definitive diagnosis [1].

23.5.3 CT

CT is not an ideal method for characterization of soft tissue metastases. Furthermore, soft tissue metastases cannot be reliably distinguished from the primary soft tissue sarcoma [51].

CT appearance of soft tissue metastases is widely variable: “abscess-like” lesion with rim enhancement and central hypo-attenuation, focal

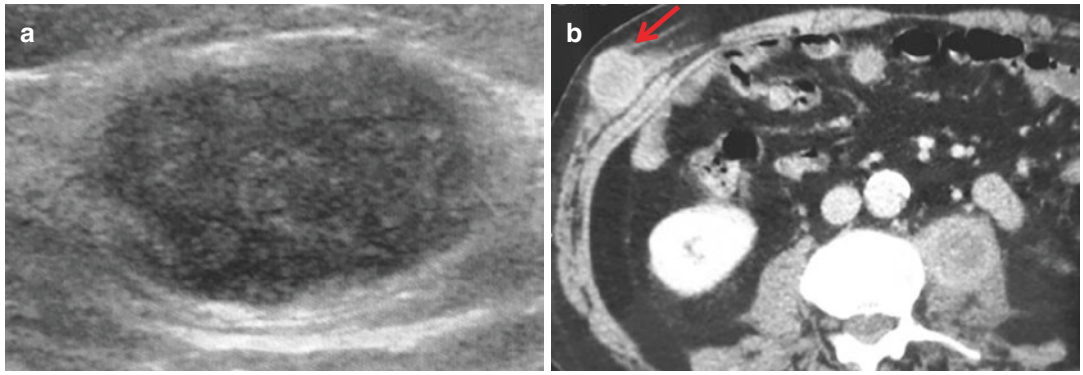

Fig. 24.2 Intramuscular metastasis from choroid melanoma. (**a**) Gray-scale US reveal a small solid homogeneously hypoechoic nodule with spiculated margins in the subcutaneous tissue of the abdominal wall. (**b**) Axial contrast-enhanced helical CT image shows enhancing lesion in right external and internal oblique muscles (*arrow*) and a left psoas extension of a vertebral metastasis

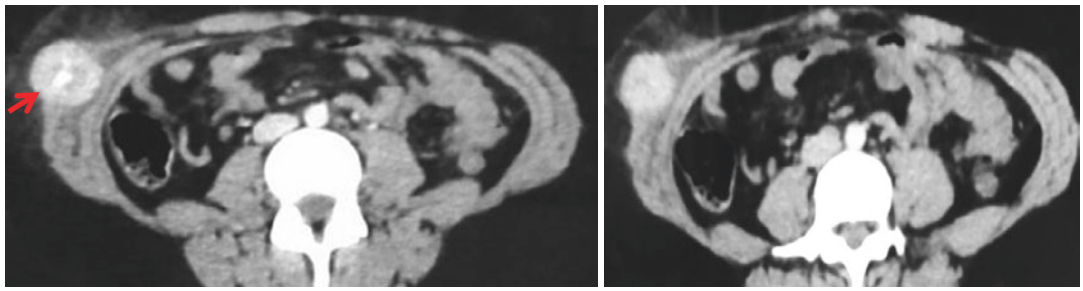

Fig. 24.3 17-year-old woman with osteosarcoma. Contrast-enhanced abdominal CT scan shows enhancing lesion in right external and internal oblique muscles with multifocal calcifications (*arrows*)

masses with homogeneous contrast enhancement, diffuse metastatic infiltration manifested as soft tissue swelling and diffuse heterogeneous contrast enhancement, multifocal calcification, and intramuscular bleeding with muscle enlargement and area of high attenuation [45]. The most common appearance of soft tissue metastases on contrast-enhanced CT is that of a rim-enhancing mass with central hypo-attenuation (Figs. 24.1, 24.2, 24.3, 24.4, and 24.5) [29].

CT may guide lesion biopsy and direct appropriate local radiation.

23.5.4 MRI

MR imaging is the preferred technique for muscle and soft tissue assessment, even though MRI appearances of soft tissue metastasis are not specific [13, 52].

On MRI, soft tissue metastases are of low or intermediate signal intensity compared to normal muscle on T1-weighted sequences and high signal intensity on T2-weighted sequences [17, 22, 42].

However, high signal intensity of metastases on T1-weighted images has been also described, particularly in malignant melanoma metastases because they contain melanin and may often bleed [54]. High signal intensity has also been reported in metastases of renal cell carcinoma, but its cause is still unknown [20, 35].

After administration of contrast medium, most muscle metastases show marked heterogeneous enhancement related to tumor necrosis (Fig. 24.4). In addition, extensive peritumoral enhancement has been reported as one of the characteristic features of IM [13, 48].

Edema of surrounding soft tissue is common [6]. Erosion of the adjacent bone might rarely be observed on MRI [17].

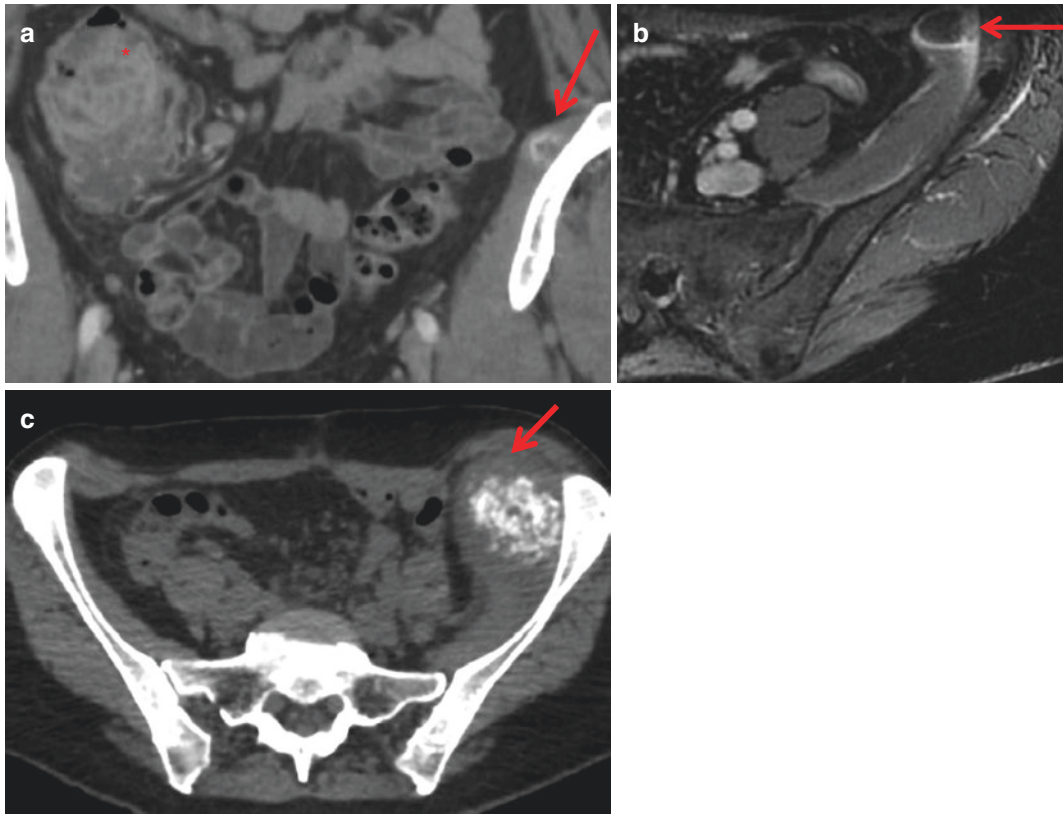

Fig. 24.4 Skeletal muscle metastasis in patient with caecal mucinous adenocarcinoma (*asterisk*). (**a**) Contrast-enhanced CT demonstrates intramuscular lesion with central low attenuation and rim enhancement (*arrow*). (**b**) Axial fat-suppressed (FS) T1-weighted gadolinium-enhanced image shows well enhancing mass in left psoas including central necrosis. (**c**) Two months later, nonenhanced CT shows enlargement of the left psoas muscle with multifocal calcifications

Diffusion-weighted imaging (DWI) is considered as a useful method in the assessment of tumor cellularity in soft tissue sarcomas and can be used as a noninvasive tool to monitor treatment responses [36, 49]. In soft tissue metastases, Surov described low or moderate ADC values and moderate to high signal intensity on diffusion images [44].

23.5.5 Radionuclide Imaging

Technetium-99 m-labeled nuclear scan can show increased uptake within the soft tissue mass [48]. ^{18}F-FDG PET/CT was demonstrated to have a higher sensitivity compared with MRI in detecting soft tissue metastases [10 31]. However, there were false positives in few cases, which should be taken into consideration. PET/CT, which performs anatomical and metabolic assessment, is very sensitive in the detection of soft tissue metastases and provides more information for clinical tumor staging. Compared to CT, PET is more sensitive because it detects soft tissue lesions before the density and morphology of the soft tissues are altered, providing a clear view of highly metabolic nodules within the soft tissue. ^{18}F-FDG PET/CT imaging may reveal the primary tumors of the soft tissue metastases, which is helpful for differential diagnosis.

23.6 Biopsy

After appropriate imaging, early percutaneous biopsy is recommended. It is advocated to biopsy in case of solitary or late metastases and in case

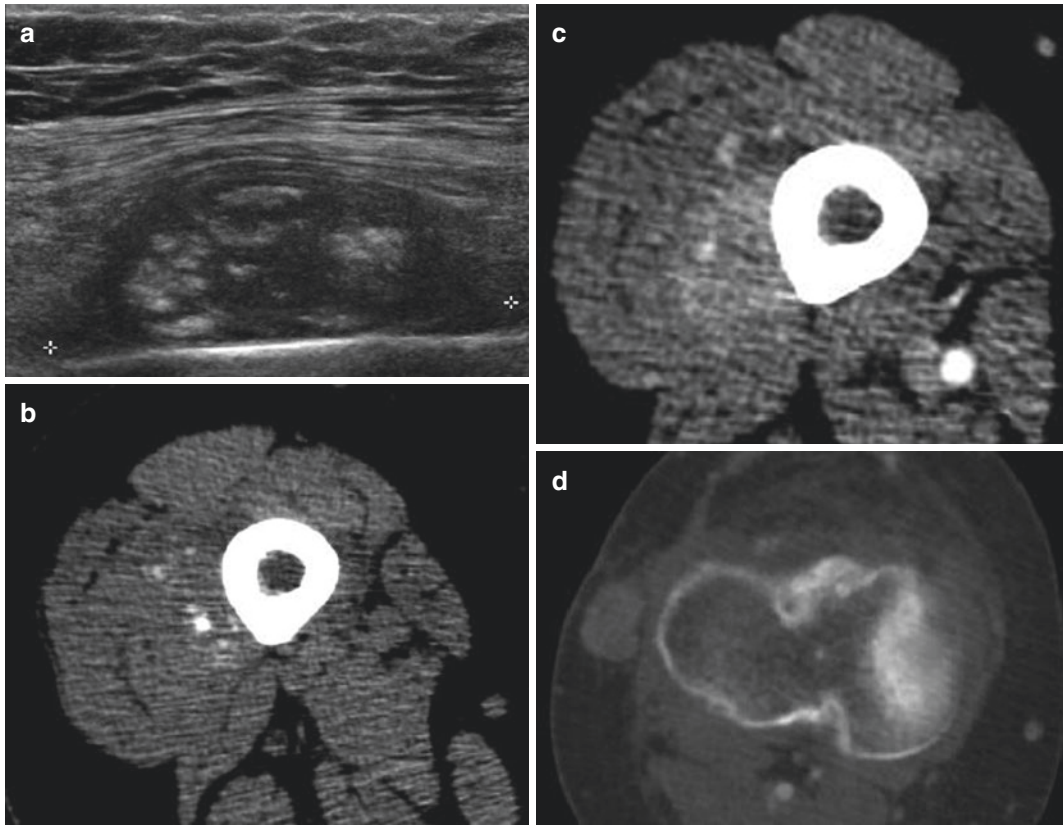

Fig. 24.5 Intramuscular metastases. (**a**) US image in patient with previously diagnosed osteosarcoma: well-defined hypoechoic mass with multifocal hyperechoic areas located within the vastus intermedius. (**b**) Nonenhanced and (**c**) contrast-enhanced CT demonstrates an intramuscular (vastus intermedius) lesion with multifocal calcifications and homogeneous contrast enhancement. (**d**) Contrast-enhanced CT at a lower level shows a subcutaneous round mass with homogeneous contrast enhancement

of unknown primary tumor. Biopsy is not recommended in case of a disseminated disease.

23.7 Differential Diagnosis

Several benign tumors and soft tissue sarcoma cannot be differentiated radiologically from metastases [5, 16, 28]. Psoas involvement by metastatic disease is frequently confused with psoas abscess or hematoma, both clinically and radiographically. Therefore, confirmation of soft tissue metastases can only be established by histopathology.

Calcification within soft tissue metastases has been confused with myositis ossificans [6]. In addition, ischiogluteal bursitis, which occurs frequently in patients with cancer, can also mimic muscle metastasis [18].

23.8 Prognosis

The presence of soft tissue metastasis influences the primary tumor treatment. Reported studies show that the survival of patients with soft tissue metastases ranges from less than 9 months to not more than 3 years after soft tissue metastases diagnosis, although survival up to 5 years has been reported in some cases [24]. The presence of a skin metastasis in a lung cancer patient indicates a poor prognosis, with a median survival of 2–4 months [10, 25, 38].

23.9 Treatment

The treatment of soft tissue metastases depends on their localization and clinical presentation as well as on the prognosis related to the primary tumor. Therapeutic options include observation, radiotherapy, chemotherapy, and surgery. For painful masses in the context of a widespread metastatic disease, radiotherapy, chemotherapy, or both may be indicated based on the primary tumor, the organ involved, the extent of involvement, symptoms attributable to the various sites, the patient's age, and health status [6].

Conclusion

Radiologists should know various imaging and clinical findings of soft tissue metastases and suspect it in cases of painful and multiple masses. The diagnosis is based on imaging techniques, especially MRI, CT, and ^{18}F-FDG PET/CT. However, the confirmation of diagnosis is based on the histological examination if necessary.

Key Points

1. Soft tissue metastases are uncommon and their prevalence varies in autopsy series from 6 to 17.5 %.
2. The thigh muscles, iliopsoas, and paraspinous muscles are the most frequent affected sites.
3. The most frequent symptoms are pain, palpable mass, swelling, and cutaneous erythema.
4. Radiographs and CT are not ideal methods for characterization of soft tissue metastasis.
5. On US, soft tissue metastases appear as well-circumscribed hypoechoic and hypervascularized masses.
6. On MRI, soft tissue metastases are of low or intermediate signal intensity compared to normal muscle tissue on T1-weighted sequences and high signal intensity on T2-weighted sequences.
7. It is advocated to biopsy solitary or late metastases and in case of unknown primary tumor.

References

1. Alexander AA, Nazarian LN, Feld RI (1997) Superficial soft-tissue masses suggestive of recurrent malignancy: sonographic localization and biopsy. AJR Am J Roentgenol 169(5):1449–1451
2. Batson OV (1940) The function of the vertebral veins and their role in the spread of metastases. Ann Surg 112:138–149
3. Blandino A, Gaeta M, Minutoli F, Pandolfo I (2000) CT and MR findings in neoplastic perineural spread along the vidian nerve. Eur Radiol 10:521–526
4. Chong VF, Fan YF (2002) Hypoglossal nerve palsy in nasopharyngeal carci- noma. Eur Radiol 8:939–945
5. Crundwell N, O'Donnell P, Saifuddin A (2007) Non-neoplastic conditions presenting as soft-tissue tumours. Clin Radiol 62:18–27
6. Damron TA, Heiner J (2000) Distant soft tissue metastases: a series of 30 new patients and 91 cases from the literature. Ann Surg Oncol 7(7):526–534
7. Garcia OA, Fernandez FA, Satue EG, Buelta L, Val-Bernal JF (1984) Metastasis of malignant neoplasms to skeletal muscle. Rev Esp Oncol 31:57–67
8. Glockner DM, White LM, Sundaram M, McDonald DJ (2000) Unsus- pected metastases presenting as solitary soft tissue lesions: a fourteen-year review. Skeletal Radiol 29:270–274
9. Herring CL Jr, Harrelson JM, Scully SP (1998) Metastatic carcinoma to skeletal muscle. A report of 15 patients. Clin Orthop Relat Res 355:272–281
10. Hidaka T, Ischii Y, Kitamura S (1996) Clinical features of skin metastasis from lung cancer. Intern Med 35:459–462
11. Hoshi S, Orikasa S, Suzuki K et al (1995) High-energy underwater shock wave treatment for internal iliac muscle metastasis of prostatic cancer: a first clinical trial. Jpn J Cancer Res 86:424–428
12. Hung EH et al (2014) Ultrasound of musculoskeletal soft-tissue tumors superficial to the investing fascia. AJR Am J Roentgenol 202(6):W532–W540
13. Lee BY, Choi JE, Park JM, Jee WH, Kim JY, Lee KH, Kim HS, Song KS (2008) Various image findings of skeletal muscle metastases with clinical correlation. Skeletal Radiol 37(10):923–928
14. Leinung S, Möbius C, Udelnow A, Hauss J, Würl P (2007) Histopathological outcome of 597 isolated soft tissue tumors suspected of soft tissue sarcoma: a

single-center 12-year experience. Eur J Surg Oncol 33:508–511
15. Magee T, Rosenthal H (2002) Skeletal muscle metastases at sites of documented trauma. AJR Am J Roentgenol 178:985–988
16. Martin S, Rapariz JM, Osés MJ, Martinez C (2007) A possible cause of multiple intramuscular masses: Mazabraud's syndrome. Eur Radiol 18:417–421
17. Mignani G, McDonald D, Boriani S, Avella M, Gaiani L, Campanacci M (1989) Soft tissue metastasis from carcinoma. A case report. Tumori 75:630–633
18. Mills GM, Baethge BA (1993) Ischio-gluteal bursitis in cancer patients: an infrequently recognized cause of pain. Am J Clin Oncol 16:229–231
19. Mulsow FW (1943) Metastatic carcinoma of skeletal muscles. Arch Pathol 35:112
20. Nabeyama R, Tanaka K, Matsuda S, Iwamoto Y (2001) Multiple intramuscular metastases 15 years after radical nephrectomy in a patient with stage IV renal cell carcinoma. J Orthop Sci 6:189–192
21. Nazarian LN, Alexander AA, Kurtz AB et al (1998) Superficial melanoma metastases: appearances on gray-scale and color Doppler sonography. AJR Am J Roentgenol 170:459–463
22. O'Brien JM, Brennan DD, Taylor DH et al (2004) Skeletal muscle metastasis from uterine leiomyosarcoma. Skeletal Radiol 33:655–659
23. Pearson CM (1959) Incidence and type of pathologic alterations observed in muscle in a routine autopsy study. Neurology 9:757–766
24. Perisano C, Spinelli MS, Graci C, Scaramuzzo L, Marzetti E, Barone C, Fabbriciani C, Maccauro G (2012) Soft tissue metastases in lung cancer: a review of the literature. Eur Rev Med Pharmacol Sci 16(14): 1908–1914
25. Perng DW, Chen CH, Lee YC, Perng RP (1996) Cutaneous metastasis of lung cancer: an ominous prognostic sign. Zhonghua Yi Xue Za Zhi (Taipei) 57:343–347
26. Plaza JA, Perez-Montiel D, Mayerson J, Morrison C, Suster S (2008) Metastases to soft tissue: a review of 118 cases over a 30-year period. Cancer 112(1):193–203
27. Pop D, Nadeemy AS, Venissac N, Guiraudet P, Otto J, Poudenx M, Mouroux J (2009) Skeletal muscle metastasis from non-small cell lung cancer. J Thorac Oncol 4:1236–1241
28. Prado MA, Miró RL, Leal IM, Vargas J, Dorrego EJ (2002) Intramuscular myxoma: differential diagnosis and review of the literature. Orthopedics 25:1297–1299
29. Pretorius ES, Fishman EK (2000) Helical CT of skeletal muscle metastases from primary carcinomas. AJR Am J Roentgenol 174:401–404
30. Prior C (1953) Metastatic tumors in striated muscle; re- view and case report. Riv Anat Patol Oncol 6:543–560
31. Qiu DS, Xu LY, Shames S (2014) The value of 18F-fluorodeoxyglucose positron emission tomography combined with computed tomography in the detection and characterization of soft tissue metastasis. Mol Clin Oncol 2(5):761–766
32. Abed R, Grimer RJ, Carter SR, Tillman RM, Abudu A, Jeys L (2009) Soft-tissue metastases. J Bone Joint Surg Br 91-B:1083–1085
33. Rosenbaum LH, Nicholas JJ, Slasky BS, Obley DL, Ellis LD (1984) Malignant myositis ossificans: malignant myositis ossificans: occult gastric carcinoma presenting as an acute rheumatic disorder. Ann Rheum Dis 43:95–97
34. Sahai S, Leigh D (1995) Metastasis of adenocarcinoma of breast to gluteus medius. Iowa Med 85:369–370
35. Sakamoto A, Yoshida T, Matsuura S et al (2007) Metastasis to the gluteus maximus muscle from renal cell carcinoma with special emphasis on MR features. World J Surg Oncol 5:88–92
36. Schnapauff D, Zeile M, Niederhagen MB et al (2009) Diffusion- weighted echo-planar magnetic resonance imaging for the assessment of tumor cellularity in patients with soft-tissue sarcomas. J Magn Reson Imaging 29:1355–1359
37. Schultz SR, Bree RL, Schwab RE, Raiss G (1986) CT detection of skeletal muscle metastases. J Comput Assist Tomogr 10:81–83
38. Schwartz RA (1995) Cutaneous metastatic disease. J Am Acad Dermatol 33:161–182
39. Sridhar KS, Rao RK, Kunhardt B (1987) Skeletal muscle metastases from lung cancer. Cancer 59:1530–1534
40. Stabler J (1995) Case report: ossifying metastases from carcinoma of the large bowel demonstrated by bone scintigraphy. Clin Radiol 50:730–731
41. Stulc JP, Petrelli NJ, Herrera L, Lopez CL, Mittelman A (1985) Isolated metachronous metastases to soft tissues of the but- tock from a colonic adenocarcinoma. Dis Colon Rectum 28:117–121
42. Sudo A, Ogihara Y, Shiokawa Y, Fujinami S, Sekiguchi S (1993) Intramuscular metastasis of carcinoma. Clin Orthop Relat Res 296:213–217
43. Suresh S, Saifuddin A, O'Donnell P (2008) Lymphoma presenting as a musculoskeletal soft tissue mass: MRI findings in 24 cases. Eur Radiol 18:1628–1634
44. Surov A, Fiedler E, Voigt W, Wienke A, Holzhausen HJ, Spielmann RP, Behrmann C (2011) Magnetic resonance imaging of intramuscular metastases. Skeletal Radiol 40(4):439–446
45. Surov A, Hainz M, Holzhausen HJ, Arnold D, Katzer M, Sshmidt J, Spielmann RP, Behrmann C (2010) Skeletal muscle metastases: primary tumours, prevalence, and radiological features. Eur Radiol 20: 649–658
46. Suto Y, Yamaguchi Y, Sugihara S (1997) Skeletal muscle metastases from lung carcinoma: MR findings. J Comput Tomogr 21:304–305
47. Travis WD, Banks PM, Reiman HM (1987) Primary extranodal soft tissue lymphoma of the extremities. Am J Surg Pathol 11:359–366
48. Tuoheti Y, Okada K, Osanai T et al (2004) Skeletal muscle metastases of carcinoma: a clinicopathological study of 12 cases. Jpn J Clin Oncol 34:210–214

49. Van Rijswijk CS, Kunz P, Hogendoorn PC, Taminiau AH, Doornbos J, Bloem JL (2002) Diffusion-weighted MRI in the characterization of soft- tissue tumors. J Magn Reson Imaging 15:302–307
50. Warde P, Gospodarowicz M (1993) Carcinoma of the prostate: case report. Can J Surg 36:89–90
51. Weekes RG, McLeod RA, Reiman HM, Pritchard DJ (1985) V CT of soft-tissue neoplasms. AJR Am J Roentgenol 144(2):355–360
52. Williams JB, Youngberg RA, Bui-Mansfield LT, Pitcher JD (1997) MR imaging of skeletal muscle metastases. AJR Am J Roentgenol 168:555–557
53. Yang WT, Yeo W, Metreweli C (1999) Imaging of iliopsoas metastasis. Clin Radiol 54:85–89
54. Yoshioka H, Itai Y, Niitsu M et al (1999) Intramuscular metastasis from malignant melanoma: MR findings. Skeletal Radiol 28:714–716

Miscellaneous

24

Filip M. Vanhoenacker, Astrid Van Hoyweghen, Hendrik R. Degryse, and Annemiek Snoeckx

Contents

24.1 **Introduction** 603

24.2 **Chondro-osseous Soft Tissue Tumors** 604

24.2.1 Benign Chondro-osseous Soft Tissue Tumors 604

24.2.2 Malignant Chondro-osseous Soft Tissue Tumors 608

24.2.3 Gastrointestinal Stromal Tumors 611

References 618

F.M. Vanhoenacker (✉)
University Hospital Antwerp, Department of Radiology, Wilrijkstraat, 10, B-2650 Edegem, Belgium

General Hospital Sint-Maarten Duffel-Mechelen, Rooienberg 25, B-2570 Duffel, Belgium

Faculty of Medicine and Health Sciences, University of Ghent, Ghent, Belgium
e-mail: filip.vanhoenacker@telenet.be

A. Van Hoyweghen • A. Snoeckx
University Hospital Antwerp, Department of Radiology, Wilrijkstraat, 10, B-2650 Edegem, Belgium

H.R. Degryse
KLINA, Department of Radiology, Augustijnenlei, 100, B-2930 Brasschaat, Belgium

24.1 Introduction

Although chondrogenic tumors are usually located within the bone, chondro-osseous soft tissue lesions may occur and are included as a separate chapter in the current WHO classification (2013) (see also Chap. 11). Myositis ossificans is regarded as a (myo)fibroblastic lesion (Chap. 13), and extraskeletal myxoid chondrosarcoma (EMC) is a misnomer as it represents a tumor of uncertain differentiation, since it shows little histological evidence of cartilaginous differentiation (see also Chap. 18).

Extraskeletal osteosarcoma, soft tissue osteosarcoma, shows the similar histologic features of bone osteosarcoma without systematic genetic differences [8].

Gastrointestinal stromal tumor (GIST) is the most common primary mesenchymal tumor of the gastrointestinal tract. As GISTs present most often with abdominal symptoms and detected by ultrasound or CT scans of the abdomen, these lesions are usually not considered as musculoskeletal tumors as such. However, they have been included in the WHO revision of 2013 [8], and therefore GIST will be discussed shortly in this chapter on miscellaneous soft tissue lesions.

© Springer International Publishing AG 2017

F.M. Vanhoenacker et al. (eds.), *Imaging of Soft Tissue Tumors*, DOI 10.1007/978-3-319-46679-8_24

24.2 Chondro-osseous Soft Tissue Tumors

24.2.1 Benign Chondro-osseous Soft Tissue Tumors

24.2.1.1 Soft Tissue Chondroma

Definition The term extraskeletal chondroma refers to small, well-defined nodules that are composed of at least focal areas of cartilage and do not have any connection with bone, periosteum nor intra-articular synovium. Two-thirds of the lesions contain mature, viable cartilage, whereas immature chondroblasts are observed in the other one-third of cases [17]. The greatest diameter of the lesion seldom exceeds 3 cm [6]. Most chondromas are ovoid or have a lobular appearance and are sharply delineated. Some of these lesions undergo focal fibrous changes, ossification, or myxoid changes, possibly combined with focal hemorrhage or granuloma formation. Calcifications occur in 33–70 % of cases.

Incidence and Clinical Behavior Extraskeletal chondromas are rare, representing approximately 1.5 % of all benign soft tissue tumors [16]. The majority afflict the distal extremities [16]. Preferential sites of involvement are the digits, hands, and feet (Fig. 24.1) [4, 16]. The trunk, head and neck region, and skin are less commonly involved [4, 13, 27]. Location in the bladder is exceptional [3]. Repeated microtrauma has been incriminated in the pathogenesis, which may explain the relative high incidence of soft tissue chondroma in the hands and fingers [16]. They are most commonly encountered between 30 and 60 years of age [4]. They usually present as painless solitary slowly enlarging soft tissue masses. On palpation the chondroma is usually firm and mobile. Simple excision is the treatment of choice. Local recurrence is seen in 15–20 % [4, 17], but there is no malignant transformation [4]. Para-articular (osteo)chondromas consist of a special type of extraskeletal cartilaginous chondroma that is most frequently seen in Hoffa's fat pad of the knee (Fig. 24.2), but cases in the elbows, hips, and ankles have also been reported [9, 14, 19, 32]. The tumors arise from the capsule or the para-articular connective tissue of a large joint (mainly the knee) and are due to cartilaginous metaplasia [9]. The terminology to designate this para-articular lesion is confusing, and similar lesions have previously been reported as capsular osteochondroma, extraskeletal osteochondroma, ossifying chondroma, para-articular chondroma, giant extrasynovial intra-articular osteochondroma, and Hoffa's disease [19, 32].

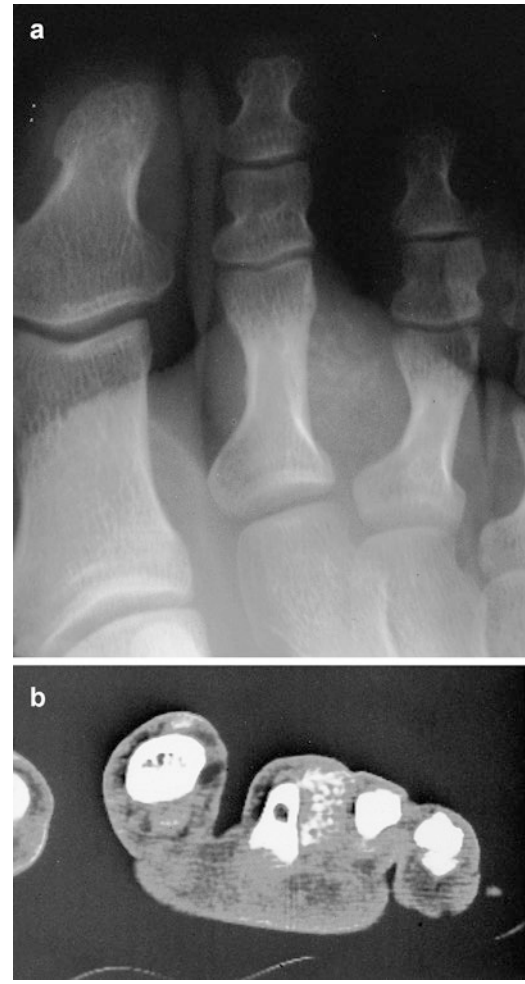

Fig. 24.1 (**a**, **b**) Extraskeletal chondroma of the foot in a 37-year-old man: (**a**) plain radiograph; (**b**) CT. Soft tissue mass with multiple punctate and ringlike calcifications between the second and third toes (**a**). Calcifications are better demonstrated on CT (**b**). Localization in the forefoot and presence of characteristic calcifications are suggestive of extraskeletal chondroma

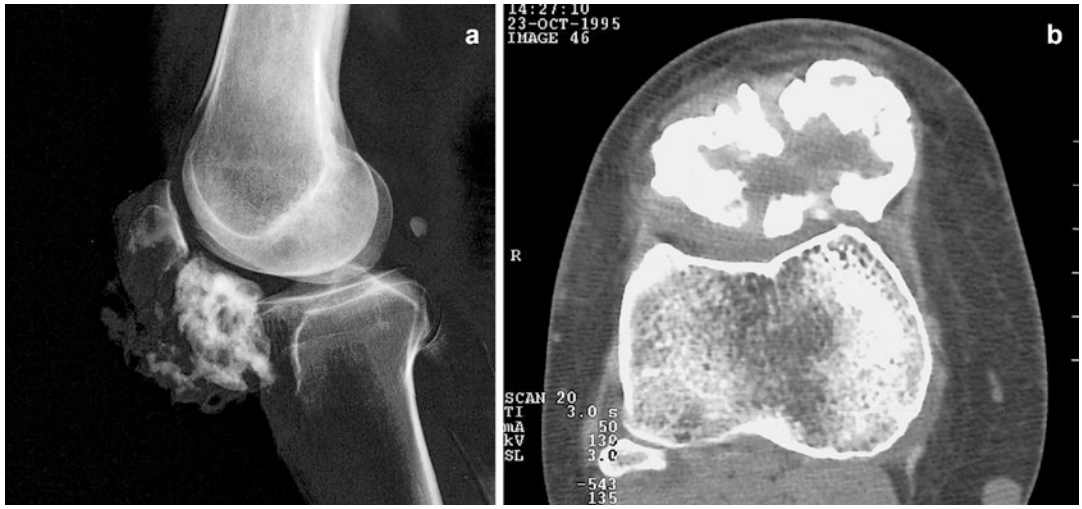

Fig. 24.2 (**a**, **b**) Extraskeletal chondroma below the right patella in a 54-year-old woman: (**a**) plain radiograph; (**b**) CT at the level of the proximal tibia; plain radiograph and CT show a pronounced, dense calcification at the periphery of the mass (**a, b**)

Imaging On plain radiography and CT, an extraskeletal chondroma presents as a well-demarcated soft tissue mass. Calcifications are observed in 33–77 % of cases [6, 16, 33]. The pattern of calcification is most typically that of curvilinear, ringlike densities, outlining the soft tissue lobules. Less commonly, these calcifications may also be punctate or mixed punctate and curvilinear or rim-like [16, 33] (Figs. 24.1 and 24.2). Ossification is less common [16]. In long-standing cases, the tumor can cause cortical pressure erosion and reactive cortical sclerosis on an adjacent bone [6, 16, 33].

On MRI, soft tissue chondromas appear on T1-weighted images as well-circumscribed masses that are isointense relative to skeletal muscle. On T2-weighted images the hyaline cartilage typically presents with very high signal intensity (Fig. 24.3). Mineralized areas cause foci of signal void on all sequences [16]. Diagnosis of chondromas without foci of calcification is more difficult, and these lesions have to be differentiated from other soft tissue masses, especially those of synovial origin. After intravenous injection of gadolinium the majority of chondromas exhibit marked and mostly peripheral contrast enhancement (Figs. 24.3 and 24.4).

24.2.1.2 Synovial Osteochondromatosis

Definition Synovial osteochondromatosis (SC) is characterized by the formation of numerous metaplastic cartilaginous or osteocartilaginous nodules of small size, within the joint (Figs. 24.5, 24.6 and 24.7), tendon sheath (Fig. 24.8) [6, 20, 28], or bursa [18]. Although the lesion has an intimate relationship with the synovium, it is currently classified as a neoplastic lesion of bone rather than soft tissue according to the WHO Classification of Tumours of Soft Tissue and Bone [8].

Two forms of SC are described in the literature. Primary SC is defined by subsynovial cartilage metaplasia, synovial hyperplasia, and production of similar-sized round cartilaginous nodules. The secondary form occurs as part of a preexisting joint disease, such as degenerative joint disease, arthritis, or trauma. In the secondary form, formation of nodules in the joint space is caused by the dislodgement of bony or cartilaginous tissue. These loose bodies undergo concentric layering of synovial cells, by which nourishment is provided. These nodules are more irregular and are often larger and of heterogeneous size compared to nodules of primary form [20]. Milgram proposed the following staging

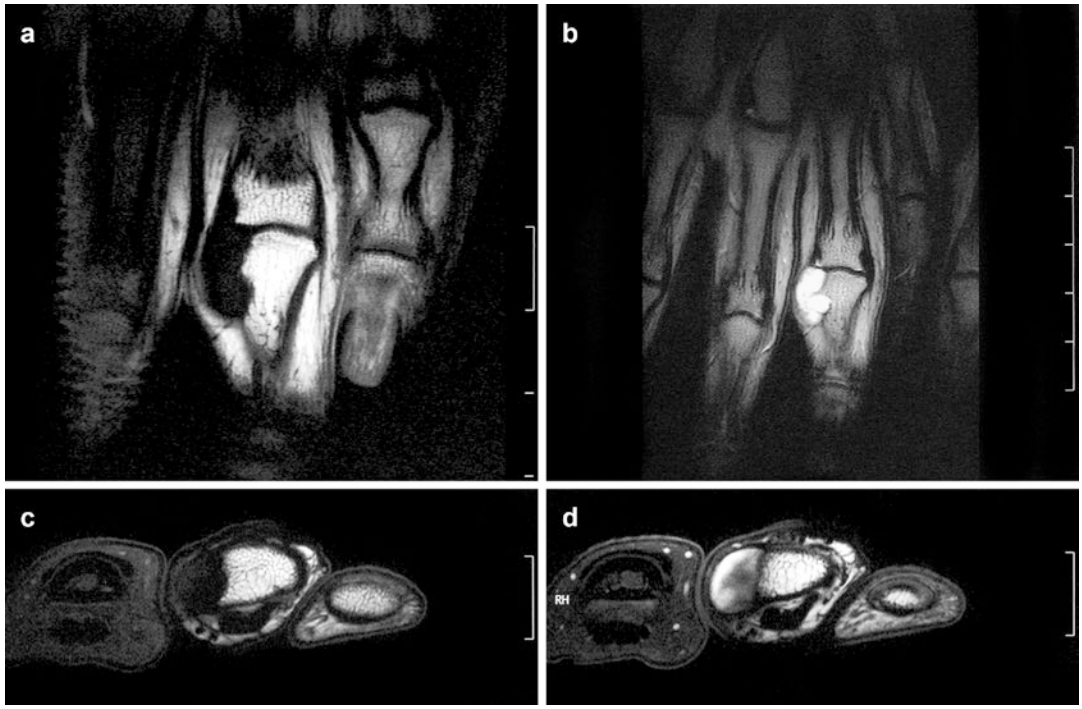

Fig. 24.3 (**a–d**) Soft tissue chondroma of the finger in a young woman: (**a**) coronal spin-echo T1-weighted MR image; (**b**) coronal spin-echo T2-weighted MR image; (**c**) transverse spin-echo T1-weighted MR image; (**d**) transverse spin-echo T1-weighted MR image after gadolinium contrast injection (same level as in **c**). Lobulated soft tissue mass near the radial aspect of the proximal third of the basic phalanx of the fourth finger. On T1-weighted image the mass presents with homogeneous low intensity (**a, c**). T2-weighted image reveals very high signal intensity of the matrix of the lesion, with internal low-intensity linear structures, corresponding to septations separating the cartilaginous lobules (**b**). Gadolinium-enhanced T1-weighted images show pronounced ringlike enhancement at the periphery of the lesion (**d**)

system [18]. In the initial stage, there is active synovial disease without loose bodies. The transitional stage is characterized by persistent synovial disease and formation of loose bodies, whereas in the third stage, detached intra-articular nodules varying from 1 mm to 10 mm are present, with burned-out intrasynovial disease. The nodules often detach and form loose bodies in the joint space. Approximately two-thirds of them calcify or ossify.

Rarely, the nodules are extra-articular. Chondrosarcoma arising in synovial chondromatosis has been reported but is uncommon [15].

Incidence and Clinical Behavior Synovial osteochondromatosis commonly occurs in large joints, such as the hip (Figs. 24.5 and 24.6), knee, shoulder, ankle, or elbow (Fig. 24.7) [20], but small joints such as the metacarpophalangeal, interphalangeal, distal radioulnar, acromioclavicular, proximal tibiofibular joint, apophyseal joints, and temporomandibular joint may be involved as well [10, 20]. The clinical history is often characterized by joint pain of several years' duration.

Imaging Plain radiography and CT easily demonstrate the calcified or ossified nodules of chondromatosis (Figs. 24.5 and 24.7). Nonmineralized nodules are seen on (CT or MR) arthrograms as filling defects outlined by contrast material. Bone scintigraphy shows an uptake of tracer within the nodules [20].

Ultrasound may show a heterogeneous mass containing foci of hyperechogenicity, in keeping

Fig. 24.4 (**a–c**) Extraskeletal osteochondroma at the popliteal fossa: (**a**) sagittal spin-echo T1-weighted MR image with fat suppression; (**b**) sagittal spin-echo T1-weighted MR image with fat suppression after gadolinium contrast injection; (**c**) axial spin-echo T2-weighted MR image with fat suppression. Rounded soft tissue mass at the popliteal fossa. The central region of signal void corresponds to extensive calcification, as observed in extraskeletal osteochondroma. The periphery of the lesion is slightly hyperintense to muscle and fat on fat-suppressed T1-weighted images (**a**), markedly hyperintense on fat-suppressed T2-weighted images (**c**), and shows pronounced enhancement following gadolinium contrast injection (**b**)

with chondral fragments or fronds of the synovium with underlying cartilage nodule formation. Posterior acoustic shadowing is seen in case of sufficient mineralization or enchondral bone formation (Fig. 24.7). Depending on the site involved, fragments may change in position during dynamic US examination [20]. Power Doppler sonography has been reported to reveal an avascular process [23].

MRI findings are an increased amount of joint fluid and intra-articular nodules (Fig. 24.6). In the early stage, nonspecific synovitis may be seen. Uncalcified osteochondromas are isointense relative to muscle on T1-weighted images and hypointense relative to synovial fluid. Calcified lesions, occurring in up to 77 % of cases, are seen as small, round signal voids. Ossified nodules may demonstrate signal intensities of fatty bone marrow. In joints that have a very tense capsule, such as the hip joint, synovial chondromatosis can cause erosions of the bone [20] (Fig. 24.6).

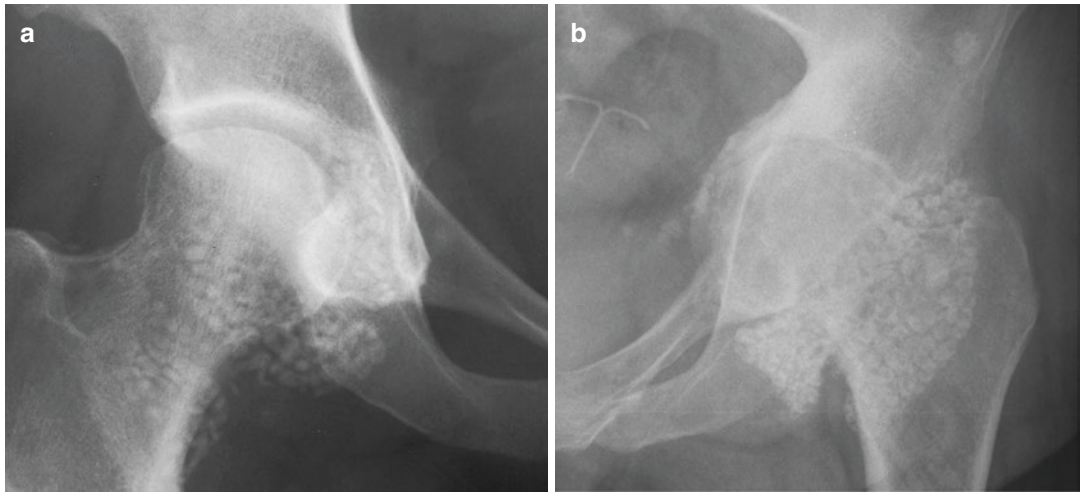

Fig. 24.5 (**a–b**) Primary (**a**) and secondary (**b**) synovial chondromatosis of the hip in two different patients: (**a**) plain radiograph of the right hip in a 36-year-old woman. Notice the presence of rice grain-like ossified nodules in the right hip joint. In primary synovial chondromatosis, the joint space is normal or can be even enlarged. Furthermore, the nodules are typically small and of uniform size in the primary form, whereas they are often larger and of heterogeneous size in the secondary form. (**b**) Plain radiograph of the left hip in a 41-year-old woman with a previous history of an acetabular fracture due to a motor vehicle accident. There are multiple ossified nodules in the left hip joint. Note marked protrusion of the acetabulum and central cartilage loss, in keeping with secondary posttraumatic synovial chondromatosis

24.2.2 Malignant Chondro-osseous Soft Tissue Tumors

24.2.2.1 Mesenchymal Chondrosarcoma

Definition Mesenchymal chondrosarcoma (MCS) is a biphasic, high-grade malignant neoplasm [4, 11] that presents on macroscopy as a multilobulated mass of variable size. On cross section, the tumor shows a mixture of gray-white tissue and foci of the cartilage and bone. On microscopy the tumor exhibits a proliferation of primitive round cells and interspersed small islands of well-differentiated hyaline cartilage [30].

Incidence and Clinical Behavior Extraskeletal mesenchymal chondrosarcoma occurs less frequently than the myxoid variant. However, 30–50 % or half of all mesenchymal chondrosarcomas are extraskeletal in location, whereas the others are intraosseous [30]. There is a slight female predominance. A bimodal age distribution is noted and related to anatomic location. When occurring in the third decade of life, tumors are located mainly in the head or neck, often in the brain, meninges, and periorbital regions. Tumors arising in the fifth decade of life afflict preferentially the soft tissues (thigh) [30]. The mesenchymal chondrosarcoma has an aggressive behavior and frequently metastasizes to lungs, lymph nodes, and bones. The prognoses are variable, with a 10-year survival rate of nearly 27.3 % [4, 30].

Imaging Calcifications within the tumor are common and well demonstrated by plain radiography and CT (Figs. 24.9 and 24.10). The degree and type of calcification are variable and range from ring and arcs, flocculent or stippled calcification, to dense mineralization [4]. In rare cases, the tumor involves underlying bone [11].

On MRI, extraskeletal mesenchymal chondrosarcoma presents as a lobulated soft tissue mass, but further imaging appearance may be nonspecific. Signal intensity of the tumor equals that of muscle on T1-weighted images and is intermediate to high on T2-weighted images [11]. Following administration of gadolinium

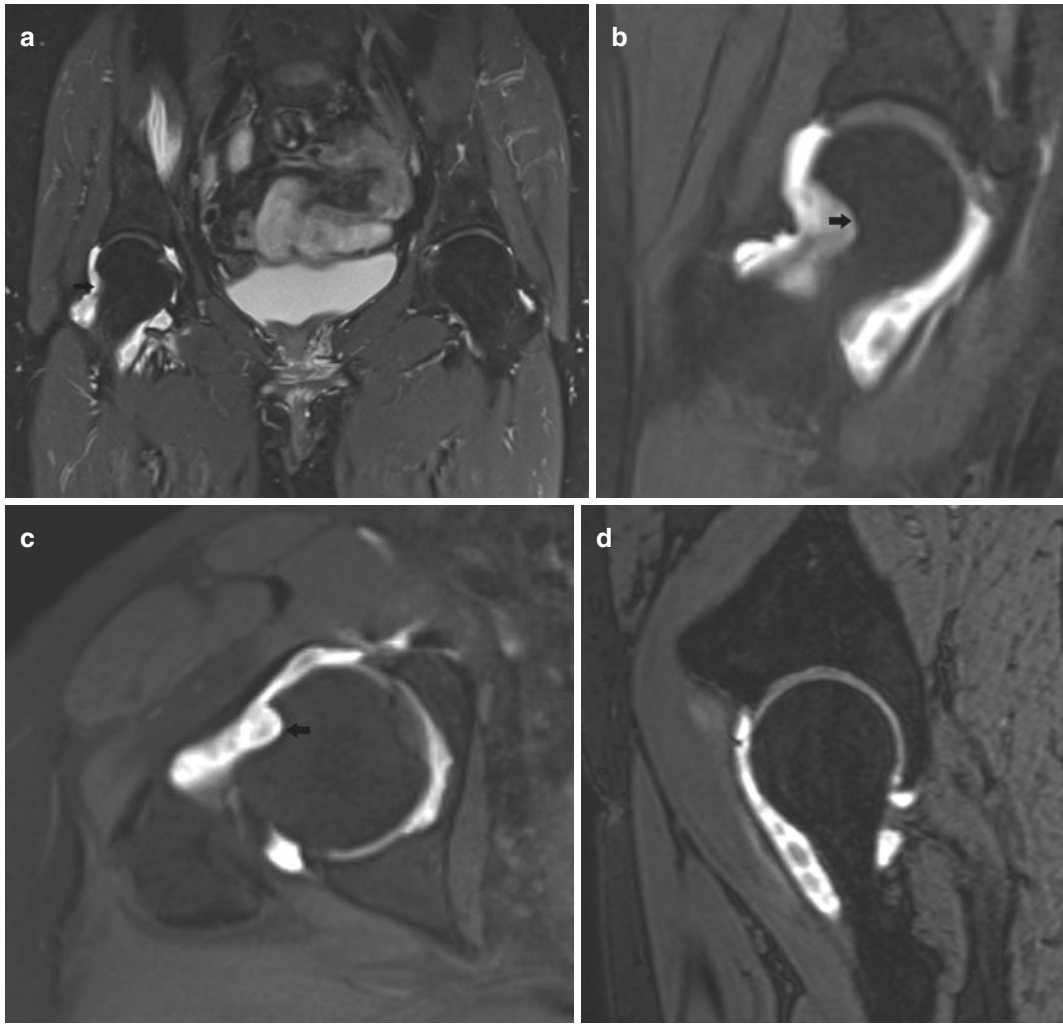

Fig. 24.6 (**a–d**) Intra-articular synovial chondromatosis of the right hip joint in a 55-year-old woman: (**a**) coronal FS T2-WI of the pelvis shows joint effusion within the right hip and multiple hypointense intra-articular nodules. Note erosion at the lateral aspect of the right femoral neck (*black arrow*), (**b–d**) oblique coronal, axial, and sagittal MR arthrograms of the right hip confirming multiple intra-articular nodules, and an erosion at the lateral aspect of the right femoral neck (*arrows* in **b** and **c**)

contrast, inhomogeneous enhancement is observed, especially at the periphery (Fig. 24.11). Areas of calcifications may be of low signal intensity [11].

24.2.2.2 Extraskeletal Osteosarcoma

Definition Extraskeletal osteosarcoma is a malignant mesenchymal neoplasm that secrete bone matrix, which may mineralize. Chondroblastic and fibroblastic components may occur as well [8]. The neoplasm is located in the deep soft tissues with less than 10 % originating in the dermis or subcutis. A distinction is made between various subtypes, depending on the relative amounts of tissue constituents including osteoblastic, chondroblastic, fibroblastic, telangiectatic types, small cell variant, and well-differentiated types [8].

Incidence and Clinical Behavior Soft tissue osteosarcoma is rare and accounts for approximately 1 % of all soft tissue sarcomas and nearly

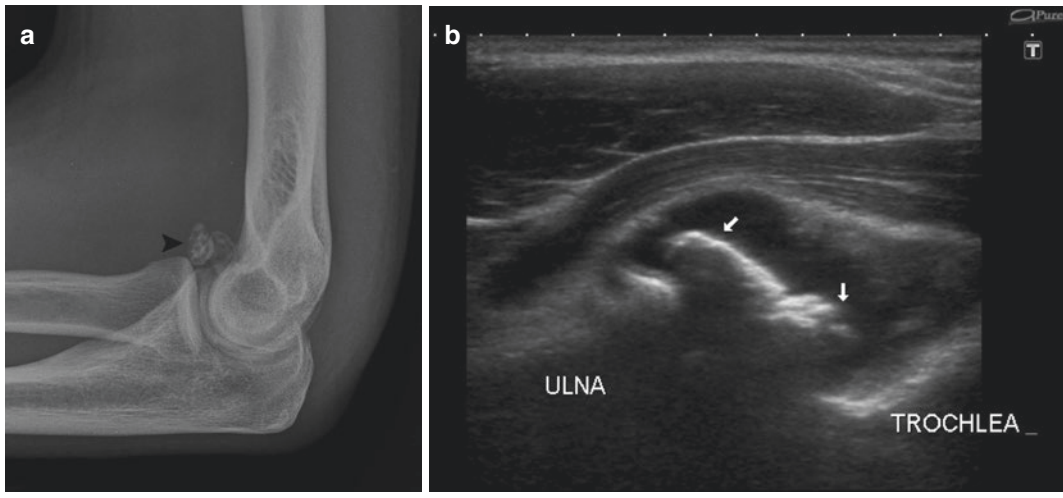

Fig. 24.7 (**a, b**) Synovial chondromatosis of the elbow in a 21-year-old male: (**a**) plain radiograph (lateral view) showing two ossified nodules at the ventral aspect of the elbow joint (*arrowheads*). (**b**) Longitudinal ultrasound shows joint effusion and intra-articular loose bodies with retro-acoustic shadowing (*arrows*)

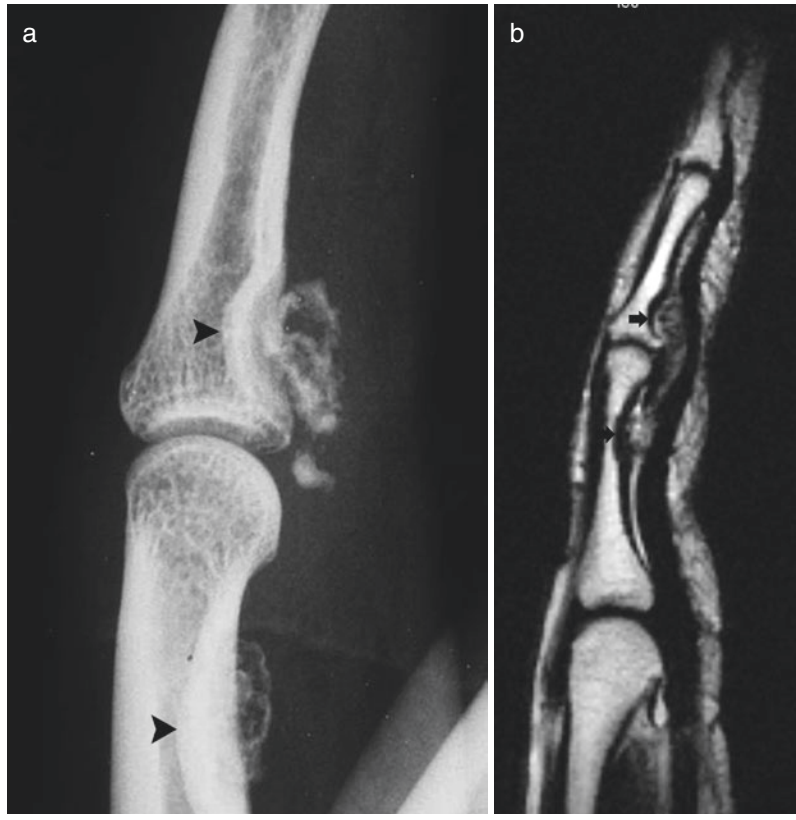

Fig. 24.8 (**a, b**) Tenosynovial chondromatosis of the finger in a 45-year-old male: (**a**) Plain radiograph (lateral view) showing calcified nodules at the flexor side of the proximal and middle phalanx of the finger. Note scalloping due to pressure erosion of the palmar cortex of the proximal and middle phalanx (*black arrowhead*). (**b**) On sagittal T2-WI, the lesions are of mixed signal. Area of low signal corresponds to calcifications, whereas high signal areas are due to hyaline cartilage. Note also scalloping of the palmar cortex of the proximal and middle phalanx (*black arrowheads*)

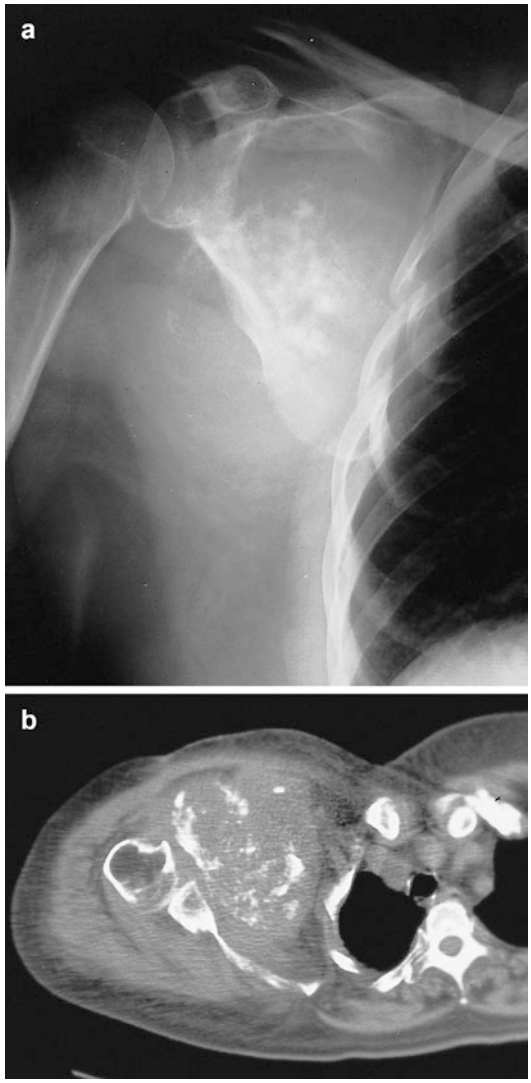

Fig. 24.9 (**a, b**) Extraskeletal mesenchymal chondrosarcoma of the right axilla in a 50-year-old man: (**a**) plain radiograph; (**b**) CT. Ill-defined mass with coarse intralesional calcifications located in the subscapular region (**a**, **b**). Calcifications are commonly seen in the mesenchymal type of extraskeletal chondrosarcoma

4 % of all osteosarcomas [24]. The tumor afflicts adults, with mean age of 50 years at presentation, which is in contrast to its intraosseous counterpart, which is most common in the first two decades of life [16]. More than half of the tumors occur in the lower extremity, in approximately 50 % of cases in the thigh. Other common locations are the upper extremity, trunk, and retroperitoneum [8]. A history of irradiation is found in 4–13 % [2]. Some patients have a history of trauma, but the causal relationship with trauma is unclear [8]. The tumor typically presents as a slowly growing soft tissue mass, causing pain and tenderness in 25–50 % of cases. Development of local recurrences following surgery and metastatic spread to lungs and lymph nodes are common. Nearly 75 % of patients die of the tumor within 5 years. Tumors less than 5 cm in diameter and negative margins at resection have a relatively better prognosis [5, 8].

Imaging Calcifications within the tumor are observed on plain radiography and CT in about half of all cases [26]. Their appearance depends on the amount of mineralization. Most commonly the calcifications appear as a cloudlike density and predominantly located in the center of the lesion, in contrast to myositis ossificans [12, 22, 29]. Adjacent bone may be secondarily involved [8].

On T1-weighted MR images, the extraskeletal osteosarcoma presents as a well-defined mass with mixed low signal intensity [31] (Fig. 24.12). Tumors in which calcification or osteoid material is not discernible on plain radiography may be hyperintense to muscle on T1-weighted images [31]. Mixed but predominantly high signal intensity is observed on T2-weighted images (Fig. 24.12). Areas of high signal intensity on both T1- and T2-weighted images are consistent with hemorrhage within the tumor. In some tumors large cystic or necrotic components have been demonstrated [12, 31]. Calcifications present as signal voids on all sequences.

24.2.3 Gastrointestinal Stromal Tumors

Definition
Gastrointestinal stromal tumors (GISTs) are submucosal tumors thought to be derived from pluripotent mesenchymal cells in the gastrointestinal tract surrounding the myenteric plexus or the interstitial cells of Cajal (ICC). There are two distinct types of interstitial cells of Cajal: the myenteric type and the intramuscular type. The myenteric

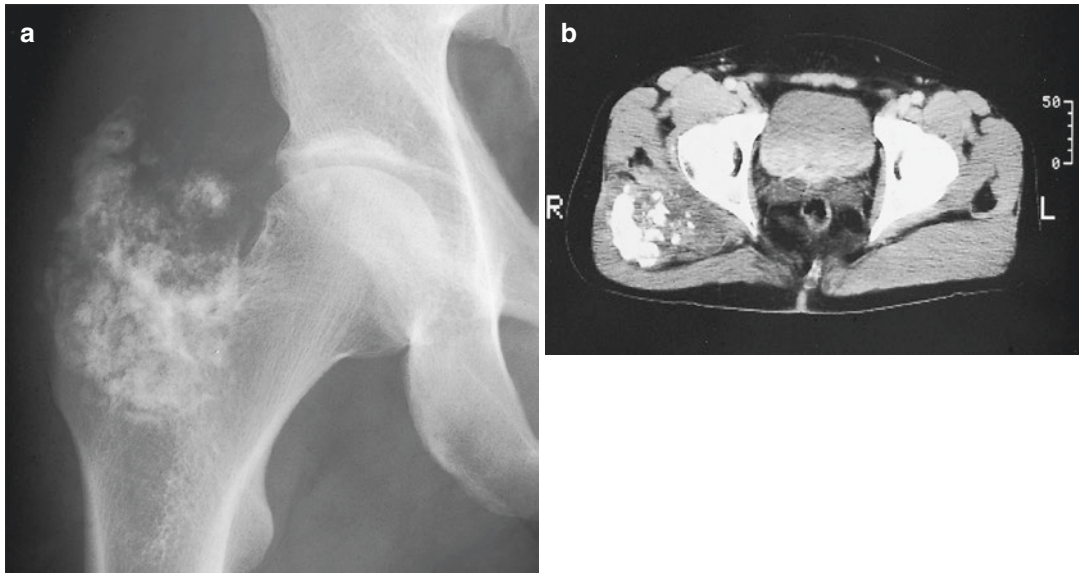

Fig. 24.10 (**a, b**) Extraskeletal mesenchymal chondrosarcoma of the buttock in a 32-year-old man: (**a**) plain radiograph; (**b**) CT; large calcified mass superior to the trochanter major (**a**). CT reveals a soft tissue component medially and the calcified component laterally within the mass (**b**). Findings on plain radiography and CT are indicative of a lesion of cartilaginous origin

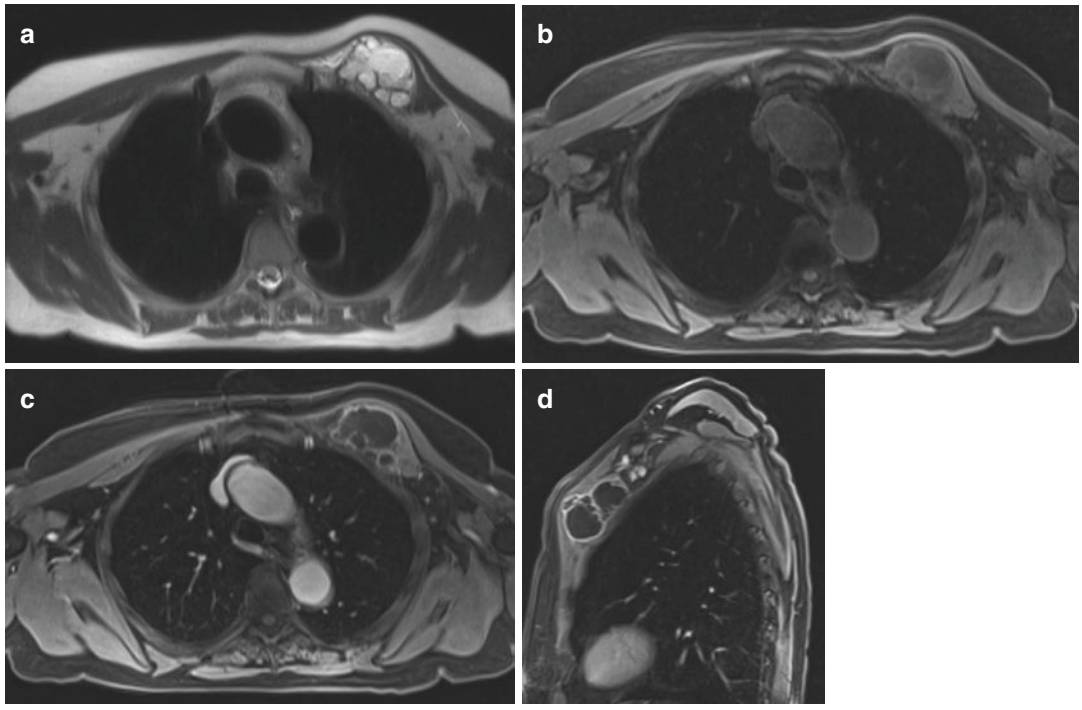

Fig. 24.11 (**a–d**) Extraskeletal chondrosarcoma of the left pectoralis minor in 63-year-old female: (**a**) axial T2-weighted HASTE MR image; (**b**) axial FS T1-WI**.** (**c**) Axial and (**d**) sagittal FS T1-WI following administration of gadolinium contrast. T2-WI reveal the lobulated shape of the lesion with the cartilaginous lobules being markedly hyperintense contrasting with intralesional low-intensity septa. The lesion is isointense with muscle on T1-WI (**b**). Following administration of gadolinium, pronounced peripheral enhancement is observed (**c**, **d**)

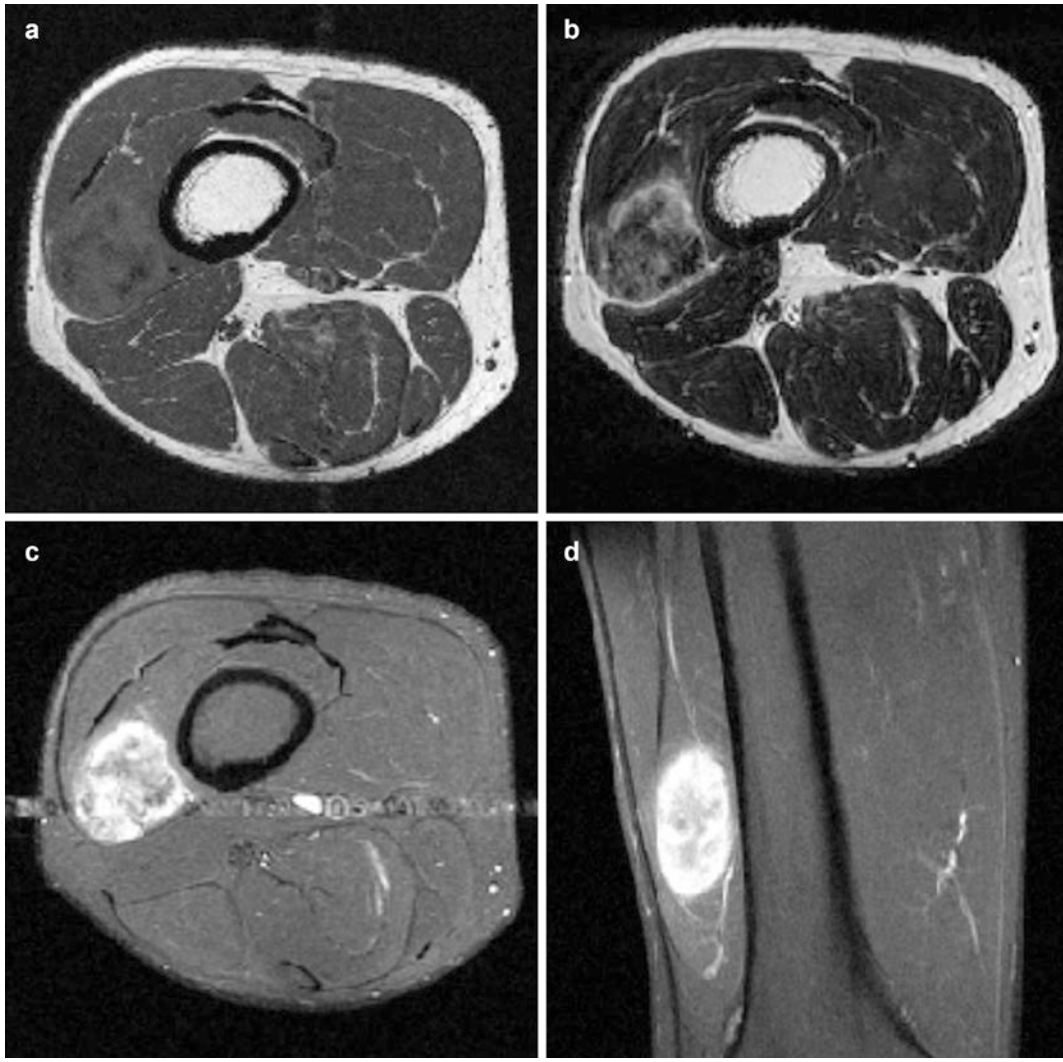

Fig. 24.12 (**a–d**) Extraskeletal osteosarcoma of the thigh in a 48-year-old male (reproduced from Vanhoenacker et al. [26], with permission): an axial spin-echo T1-weighted MR image; (**b**) axial fast spin-echo T2-weighted MR image; (**c**, **d**) axial (**c**) and coronal (**d**) spin-echo T1-weighted MR images with fat suppression after gadolinium contrast injection. Ovoid soft tissue mass, deeply located within the muscle compartment adjacent to the bony structures. The mass remains unattached to the underlying bone. Patchy areas of signal void within the center of the lesion on all sequences, consistent with osteoid tissue. The tumor itself appears discretely hyperintense to muscle on T1-weighted images (**a**), hyperintense on T2-weighted images (**b**). Following contrast injection marked enhancement is observed throughout the lesion (**c**, **d**)

type serves as a pacemaker for the contraction of smooth muscle cells, generating spontaneous electrical slow waves that will ultimately induce peristalsis. The intramuscular type plays a role in the stimulation of smooth muscle cells. They form a network, necessary for the propagation of the slow waves. The interstitial cells of Cajal are derived from mesoderm. They are named after a Spanish pathologist and Nobel Prize laureate Santiago Ramón y Cajal.

Incidence and Clinical Behavior

GISTs are the most common mesenchymal tumors in the gastrointestinal tract and can occur anywhere, from the esophagus to the anus. 40–60 % occur in the stomach; the second most common

site is the small bowel. The annual incidence is reported to be around 11–14 per million per year, although subclinical GISTs are thought to be more common.

In adults, there is no gender predilection. GISTs are most commonly seen in middle-aged persons and are very rare under the age of 40. However, with certain syndromes, such as the Carney triad (combination of GIST, pulmonary chondroma, and extra-adrenal paraganglioma) and Carney-Stratakis syndrome (consisting of hereditary GIST and paraganglioma), they can be seen in pediatric cases. In children, 85 % of GISTs are c-KIT negative and there is a female predilection. There is also an association between GISTs and neurofibromatosis type 1.

GISTs tend to present with specific symptoms such as early satiety and bloating, unless they ulcerate or bleed or become large enough to cause obstruction or pain. While small, they can be asymptomatic and discovered incidentally on imaging. In children, the most common presentation is chronic GI bleeding.

GISTs show a tendency toward metastasis to the liver and peritoneal cavity, rather than locoregional lymph nodes. They hardly ever metastasize to the lungs, as opposed to most soft tissue sarcomas [1, 25].

Histopathology

A clear distinction between GIST and leiomyoma or sarcoma cannot be made with light microscopy alone, and additional immunohistochemical or molecular analysis is required. About 95 % of GIST show overactivation of KIT (CD117), a growth receptor with tyrosine kinase activity, which is not expressed by the other spindle cell-derived tumors of the GI tract such as leiomyoma or sarcoma. Some KIT-negative GISTs exhibit activating mutations in another receptor gene with tyrosine kinase activity, the PD-GFRalfa. This is important to know for therapeutic reasons. GISTs are divided into three categories: 70 % are of the spindle cell type, 20 % are of the epitheloid type and 10 % are of mixed type.

Imaging Features

Although no longer the examination of choice, an upper GI barium swallow may show a mass protruding from the GI wall, with or without ulceration. Sensitivity and specificity however are (very) low.

Ultrasound can show a hypoechoic mass, but lacks sensitivity and specificity, as it is hampered by intraluminal air reflections in most of the gastrointestinal tract. Endoscopic ultrasound is better at delineating a submucosal tumor accessible by endoscopy, but is not as performant to evaluate extension in surrounding tissues.

Computed tomography (CT) is the imaging modality of choice for the evaluation of gastric and small bowel GISTs. In certain regions, such as the rectum or liver, MRI may be advantageous, but in general the spatial and temporal resolution of CT is more appropriate for the evaluation of small bowel. Intravenous contrast administration is necessary, with scanning in arterial and venous phases to document the hypervascular character (Fig. 24.13a–c), and additional oral contrast administration is preferred for its ability to better delineate the luminal side of the tumor. In general, GISTs are solid, smoothly contoured submucosal masses that show exophytic growth and enhance brightly after intravenous contrast administration, except in larger masses where there might be areas of necrosis that cause a more heterogeneous appearance and can lead to ulceration (Fig. 24.14). CT is also the preferred modality to detect metastases in the liver or peritoneal cavity.

On magnetic resonance imaging (MRI), GISTs are usually isointense to muscle on T1-weighted images (WI) (Fig. 24.13e) and hypo- to isointense on T2-WI, except in areas of necrosis, where they also demonstrate a high signal on T2 (Fig 24.13d). The solid areas enhance after gadolinium administration; the necrotic areas do not enhance (Fig. 24.13f). MRI has the advantage over CT of better tissue contrast, allowing better delineation of small intramural masses.

PET-CT is highly sensitive for the detection of GIST, but not specific (Fig. 24.13h, i). However, PET is better at predicting early response to tyro-

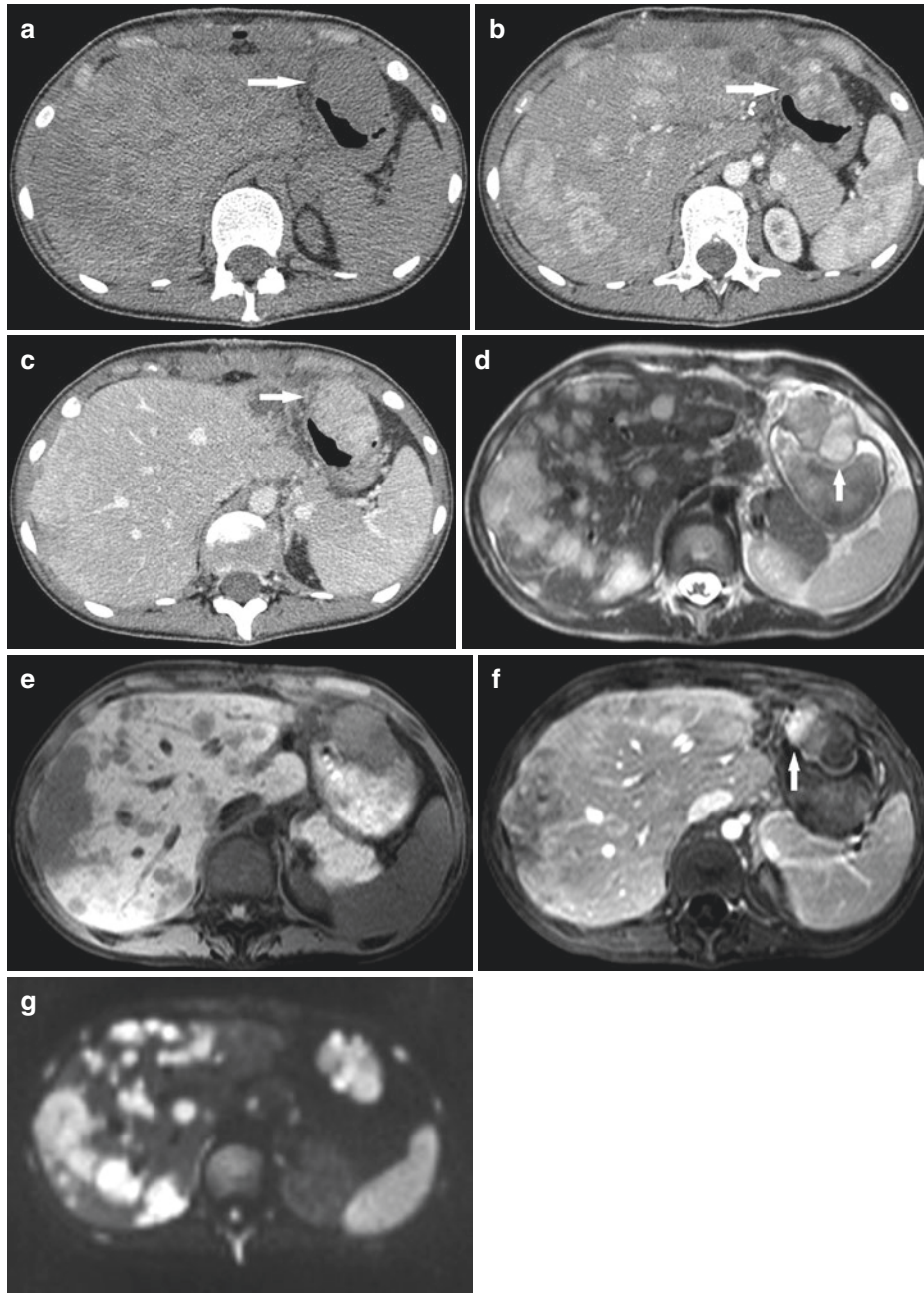

Fig. 24.13 (**a**–**i**) Immunohistochemically proven GIST of the stomach in a 21-year-old female presenting with right upper quadrant abdominal discomfort and early satiety. (**a**) Nonenhanced CT shows an isodense mass centered on the stomach wall (*arrow*) and suspicion of multiple masses in the liver. (**b**) In the arterial phase, the mass enhances heterogeneously (*arrow*), and the presence of multiple enhancing masses in the liver is confirmed. (**c**) In the venous phase, the mass becomes more homogeneous and appears to be sharply demarcated (*arrow*). The liver metastases are barely visible, stressing the need for arterial phase images in the workup and follow-up of GISTs. (**d**) On fat-saturated T2-weighted MRI, the mass is slightly hyperintense to muscle and shows an area with higher signal intensity in keeping with a more or less necrotic area (*arrow*). (**e**) The mass is isointense to muscle on fat-saturated T1-WI. (**f**) After administration of gadolinium contrast, the mass progressively enhances (*arrow*), with exception of the area with high signal intensity on T2-WI. (**g**) Diffusion-weighted imaging shows diffusion restriction in all lesions. (**h**) PET-CT shows the primary tumor as well as the liver metastases to be avidly PET-positive. (**i**) Although rare, this patient has metastases to the lung, discovered on PET-CT

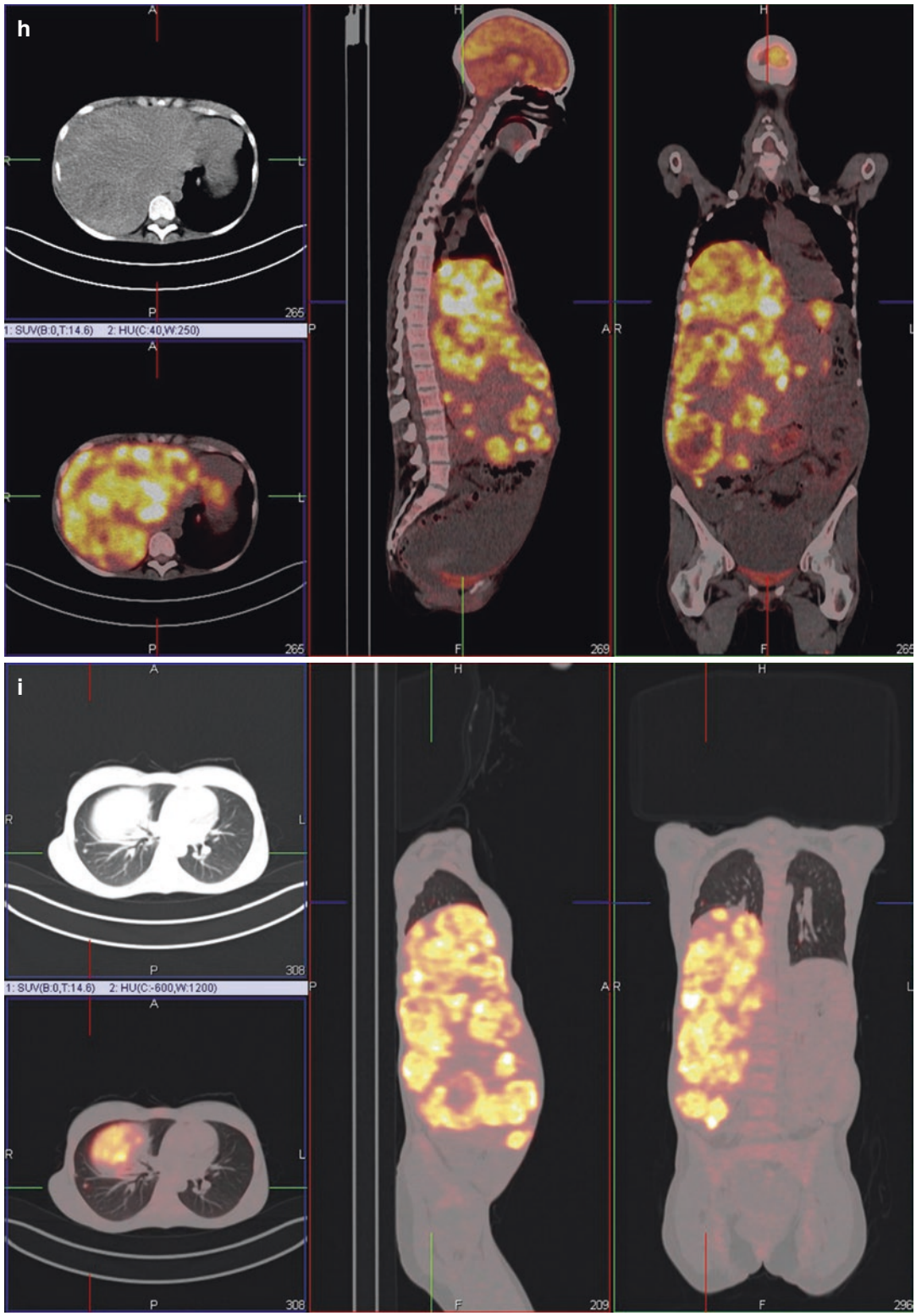

Fig. 24.13 (continued)

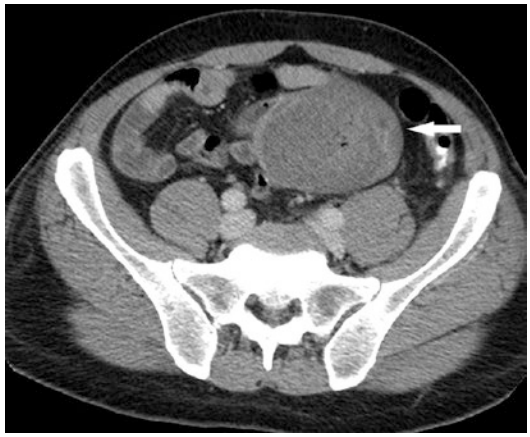

Fig. 24.14 GIST of the small bowel in a 55-year-old male presenting with gastrointestinal bleeding and negative endoscopic survey of stomach and colon. Venous phase CT shows a large, sharply demarcated heterogeneously enhancing and partly necrotic tumor centered on the small bowel wall (*arrow*). Despite the large size of the primary tumor (>10 cm), no metastases were detected on further workup

sine kinase inhibitors (imatinib) than CT alone, with hypermetabolic foci indicating viable tumor, at primary site and in metastases. On CT, tumor response will usually be evident as tumor shrinkage, but in certain cases, only a decline of the density of the lesion will be noticeable. Even in the presence of lesion growth, this lower density is still considered tumor response (necrosis). Special care should also be taken in diagnosing new lesions and thus declaring disease progression: some lesions will simply become more conspicuous after treatment and therefore detectable, instead of actually being new [7].

Treatment

There is no consensus on whether small GISTs (<2 cm) should be monitored or resected. Surveillance can be an option in gastric GIST with repeated endoscopic ultrasound assessment, but this is not an option in lesions that are not accessible with endoscopy.

For tumors ≥2 cm, surgery is the treatment of choice. Regional lymph node dissection is usually not necessary as node involvement is rare. Adjuvant therapy with imatinib is recommended for patients with a considerable risk of recurrence. Neoadjuvant treatment with imatinib can be given to reduce tumor size in borderline resectable tumors, facilitating surgical resection and organ preservation.

In metastatic disease, imatinib will be given after confirmation of the diagnosis by biopsy and determination of the tumor genotype. Second-line treatment with sunitinib can be considered when tumor progression occurs, after increasing the initial dose of imatinib [21, 34].

Prognosis

In general, the risk of recurrence depends on several tumor characteristics, such as tumor size, mitotic rate, and site (with gastric GISTs usually yielding a lower recurrence risk than small bowel GISTs). Small GISTs (<2 cm) with low mitotic rates have virtually no risk of recurrence after complete resection. Another important factor influencing recurrence risk is the presence of tumor rupture during surgery. Finally, the genotype of the tumor also influences the tumor response to imatinib. Before the advent of imatinib, survival rates were poor, with only 35 % 5-year survival for the total patient population at presentation and almost half the patients presenting with metastatic disease. Survival has definitely improved with the availability of targeted therapy.

Key Points

1. The presence of central calcifications or ossifications within a soft tissue mass should suggest the possibility of an extraskeletal cartilaginous or osseous tumor. Plain radiography and/or CT remain very powerful tools in the preoperative characterization of these tumors.
2. MRI is useful for the evaluation of early-stage osteochondromatosis, which is not yet calcified.
3. GISTs are submucosal mesenchymal tumors involving the gastrointestinal tract from the esophagus to the anus.

References

1. Beham AW, Schaefer I-M, Schüler P, Cameron S, Ghadimi BM (2012) Gastrointestinal stromal tumors. Int J Colorectal Dis 27:689–700. doi:10.1007/s00384-011-1353-y
2. Berner K, Bjerkehagen B, Bruland ØS, Berner A (2015) Extraskeletal osteosarcoma in Norway, between 1975 and 2009, and a brief review of the literature. Anticancer Res 35:2129–2140
3. Carter MD, Rendon RA, Merrimen J (2015) A rare case of bladder chondroma. Can Urol Assoc J 9:E136–E138. doi:10.5489/cuaj.2552
4. Cho S-J, Horvai A (2015) Chondro-osseous lesions of soft tissue. Surg Pathol Clin 8:419–444. doi:10.1016/j.path.2015.05.004
5. Choi LE, Healey JH, Kuk D, Brennan MF (2014) 25.1.2.1. J Bone Joint Surg Am 96:e2. doi:10.2106/JBJS.M.00339
6. Christoforou D, Strauss EJ, Abramovici L, Posner MA (2012) Benign extraosseous cartilage tumours of the hand and wrist. J Hand Surg Eur 37:8–13. doi:10.1177/1753193411421419
7. Darnell A, Dalmau E, Pericay C, Musulén E, Martín J, Puig J, Malet A, Saigí E, Rey M (2006) Gastrointestinal stromal tumors. Abdom Imaging 31:387–399. doi:10.1007/s00261-004-0092-8
8. Fletcher CDM, Bridge JA, Hogendoorn PCW, Mertens F (eds) (2013) WHO classification of tumours of soft tissue and bone. IARC Press, Lyon
9. González-Lois C, García-de-la-Torre P, SantosBriz-Terrón A, Vilá J, Manrique-Chico J, Martínez-Tello J (2001) Intracapsular and para-articular chondroma adjacent to large joints: report of three cases and review of the literature. Skeletal Radiol 30:672–676. doi:10.1007/s002560100398
10. Guffens F, Dom M, Vanhoenacker F (2015) Case report: primary osteochondromatosis of the right TMJ. Eurorad. doi:10.1594/EURORAD/CASE.13176
11. Gupta SR, Saran RK, Sharma P, Urs AB (2015) A rare case of extraskeletal mesenchymal chondrosarcoma with dedifferentiation arising from the buccal space in a young male. J Maxillofac Oral Surg 14:293–299. doi:10.1007/s12663-013-0500-0
12. Hoch M, Ali S, Agrawal S, Wang C, Khurana JS (2013) Extraskeletal osteosarcoma: a case report and review of the literature. J Radiol Case Rep 7:15–23. doi:10.3941/jrcr.v7i7.1245
13. Hwang SM, Kim JH, Kim MW, Jung YH, Kim HD, Kim HI, Hwang MK (2015) Soft tissue chondroma presenting as a dermal mass in the toe. Arch Plast Surg 42:383–385. doi:10.5999/aps.2015.42.3.383
14. Ingabire MI, Deprez FC, Bodart A, Puttemans T (2012) Soft tissue chondroma of Hoffa's fat pad. JBR-BTR 95:15–17
15. Jonckheere J, Shahabpour M, Willekens I, Pouliart N, Dezillie M, Vanhoenacker F, De Mey J (2014) Rapid malignant transformation of primary synovial chondromatosis into chondrosarcoma. JBR-BTR 97:303–307
16. Kransdorf MJ, Meis JM (1993) From the archives of the AFIP. Extraskeletal osseous and cartilaginous tumors of the extremities. Radiographics 13:853–884. doi:10.1148/radiographics.13.4.8356273
17. Lichtenstein L, Goldman RL (1964) Cartilage tumors in soft tissues, particularly in the hand and foot. Cancer 17:1203–1208
18. Milgram JW, Hadesman WM (1988) Synovial osteochondromatosis in the subacromial bursa. Clin Orthop Relat Res 236:154–159
19. Mozella Ade P, da Silveira Moller JV, de Araújo Barros Cobra HA (2015) Tumor formation in Hoffa's infrapatellar fat: case report. Rev Bras Ortop 50:117–121. doi:10.1016/j.rboe.2015.01.006
20. Murphey MD, Vidal JA, Fanburg-Smith JC, Gajewski DA (2007) Imaging of synovial chondromatosis with radiologic-pathologic correlation. Radiographics 27:1465–1488. doi:10.1148/rg.275075116
21. Nunobe S, Sano T, Shimada K, Sakamoto Y, Kosuge T (2005) Surgery including liver resection for metastatic gastrointestinal stromal tumors or gastrointestinal leiomyosarcomas. Jpn J Clin Oncol 35:338–341. doi:10.1093/jjco/hyi091
22. Okada K, Ito H, Miyakoshi N, Sageshima M, Nishida J, Itoi E (2003) A low-grade extraskeletal osteosarcoma. Skeletal Radiol 32:165–169. doi:10.1007/s00256-002-0589-6
23. Roberts D, Miller TT, Erlanger SM (2004) Sonographic appearance of primary synovial chondromatosis of the knee. J Ultrasound Med 23:707–709
24. Sabloff B, Munden RF, Melhem AI, El-Naggar AK, Putnam JB (2003) Radiologic-pathologic conferences of the University of Texas M. D. Anderson Cancer Center: Extraskeletal osteosarcoma of the pleura. AJR Am J Roentgenol 180:972. doi:10.2214/ajr.180.4.1800972
25. Scarpa M, Bertin M, Ruffolo C, Polese L, D'Amico DF, Angriman I (2008) A systematic review on the clinical diagnosis of gastrointestinal stromal tumors. J Surg Oncol 98:384–392. doi:10.1002/jso.21120
26. Vanhoenacker FM, Van de Perre S, Van Marck E, Somville J, Gielen JL, De Schepper AM (2004) Extraskeletal osteosarcoma: report of a case with unusual imaging features and histopathological correlation. Eur J Radiol Extra 49:97–102. doi:10.1016/S1571-4675(03)00132-9
27. Vescovi P, Meleti M, Merigo E, Manfredi M, Corradi D, Giovannacci I, Poli T, Nammour S (2014) Soft tissue chondroma of the oral cavity: an extremely rare tumour localized on the hard palate. Case Rep Med 2014:414861. doi:10.1155/2014/414861
28. Walker EA, Murphey MD, Fetsch JF (2011) Imaging characteristics of tenosynovial and bursal chondromatosis. Skeletal Radiol 40:317–325. doi:10.1007/s00256-010-1012-3
29. Wang XL, Malghem J, Parizel PM, Gielen JL, Vanhoenacker F, De Schepper AMA (2003) Pictorial essay. Myositis ossificans circumscripta. JBR-BTR 86:278–285

30. Xu J, Li D, Xie L, Tang S, Guo W (2015) Mesenchymal chondrosarcoma of bone and soft tissue: a systematic review of 107 patients in the past 20 years. PLoS One 10, e0122216. doi:10.1371/journal.pone.0122216
31. Yu JS, Ashman CJ, Dardani M (2000) Case 1. Extraskeletal osteosarcoma. AJR Am J Roentgenol 175:886–887. doi:10.2214/ajr.175.3.1750886
32. Zhang BX, Chew D, Critchley I (2012) Review of para-articular soft tissue osteochondromas of the knee. ANZ J Surg 82:878–884. doi:10.1111/j.1445-2197.2012.06206.x
33. Zlatkin MB, Lander PH, Begin LR, Hadjipavlou A (1985) Soft-tissue chondromas. AJR Am J Roentgenol 144:1263–1267. doi:10.2214/ajr.144.6.1263
34. Gastrointestinal stromal tumours: ESMO Clinical Practice Guidelines for diagnosis, treatment and follow-up (2014) Ann Oncol 25:iii21–iii26. doi: 10.1093/annonc/mdu255

Part V

Soft Tissue Tumors in Pediatric Patients

Imaging of Soft Tissue Tumors in the Pediatric Patient

25

Lennart Jans and Koenraad L. Verstraete

Contents

25.1 **Introduction** 623

25.2 **The Role of Imaging** 624

25.3 **Imaging Modalities** 625
25.3.1 Ultrasound 625
25.3.2 Plain Film/CT 630
25.3.3 MR Imaging 630

25.4 **Role of Imaging Tissue Characterization** 630

References 631

25.1 Introduction

Pediatric soft tissue tumors are rare. About 5 % of soft tissue tumors arise in utero and in young children (0–5 years) and only 7 % in children between 6 and 15 years old [1, 2].

About 79 % of soft tissue tumors in children between 0 and 5 years old are benign, as are 70 % in those from 6 to 15 years [3].

Some tumors are more frequently encountered in the pediatric age group [4–25]. Most common malignant tumors in children between 0 and 5 years are fibrosarcoma (36 % of malignant soft tissue tumors in this age group), rhabdomyosarcoma (21 %), giant cell fibroblastoma (7 %), dermatofibrosarcoma protuberans (6 %), angiomatoid malignant fibrous histiocytoma (5 %), and malignant peripheral nerve sheath tumor (5 %). In children between 6 and 15 years, the most common malignant tumors are angiomatoid fibrous histiocytoma (16 %), synovial sarcoma (13 %), rhabdomyosarcoma (11 %), fibrosarcoma (8 %), and malignant fibrous histiocytoma (7 %) [1, 2].

The Kiel Pediatric Tumor Registry ($n=4272$ soft tissue malignancies) found rhabdomyosarcoma to be the most frequent sarcoma (44.6 %), followed by Ewing tumors (22.3 %), malignant peripheral nerve sheath tumors (8.1 %), synovial sarcomas (5.0 %), leiomyosarcomas (3.2 %), fibrosarcomas (2.4 %), extrarenal malignant rhabdoid tumors (2 %), and alveolar soft tissue sarcomas

L. Jans (✉) • K.L. Verstraete
Department of Radiology and Nuclear Medicine and Faculty of Medicine and Health Sciences, Ghent University, De Pintelaan, 185, 9000 Gent, Belgium
e-mail: LENNART.JANS@UGent.be

© Springer International Publishing AG 2017

F.M. Vanhoenacker et al. (eds.), *Imaging of Soft Tissue Tumors*, DOI 10.1007/978-3-319-46679-8_25

Table 25.1 Preferential location of soft tissue tumors

Location	Tumor
Neck	Cystic hygroma – lymphangioma
Sternocleidomastoid muscle	Capillary hemangioma
	Fibromatosis colli
Trunk	Askin (PNET) tumor
Axilla	Cystic hygroma-lymphangioma
Upper limb	
Wrist	Ganglion cyst
Wrist, volar aspect	Fibrolipohamartoma of median nerve
Hand, volar aspect	Fibrolipohamartoma of median nerve
Finger, dorsal aspect	Digital fibroma
Lower limb	
Thigh	Fibrohamartoma of infancy
Knee	Synovial hemangioma
Knee, tibiofibular joint	Ganglion cyst
Ankle	Ganglion cyst
Foot, extensor aspect	Ganglion cyst
Upper and lower limbs	Myositis ossificans
Hand and feet	Calcifying aponeurotic fibroma
Joints, *periarticular*	Synovial hemangioma
Cutis, *subcutis*	Dermatofibrosarcoma protuberans

(1.1 %). A further group (11.3 %) includes rare tumors, intermediate fibrohistiocytic tumors, and unclassified sarcomas [15]. Embryonal rhabdomyosarcomas are 2.5 times more frequent than alveolar rhabdomyosarcomas, which are prognostically unfavorable and located predominantly in the extremities and the trunk. With regard to clinical findings, histology, molecular biology, and prognosis, embryonal and alveolar rhabdomyosarcomas have to be considered as two different tumor types. The family of Ewing tumors includes extraosseous Ewing sarcoma and primitive neuroectodermal tumors, the former tumors without and the latter with neural differentiation. Many cases of infantile malignant peripheral nerve sheath tumors and infantile fibrosarcomas are low-grade malignancies and are prognostically more favorable than in adults [26].

The most common benign masses in young children between birth and 5 years are hemangioma (15 % of all benign tumors in this age group), fibromatosis (11 %), granuloma annulare (10 %), infantile myofibromatosis (8 %), and lipoblastoma (8 %). The most frequent benign tumors in older children (6–15 years) are fibrous histiocytoma (17 %), nodular fasciitis (16 %), hemangioma (13 %), and fibromatosis (5 %) [1, 2] (Table 25.1). Imaging findings of common pediatric soft tissue tumors are illustrated in Fig. 25.1, 25.2, 25.3, 25.4, 25.5, 25.6, and 25.7.

Location In children younger than 6 years of age, 60 % of benign and malignant lesions occur in the head and neck region, the lower extremity, or the trunk. In children of 6–15 years old, benign tumors often occur in the hand or wrist, the head and neck region, and the lower extremities [1, 2], whereas malignant soft tissue tumors are more common in the extremities or the trunk. Many of the primary sites of childhood rhabdomyosarcoma, such as the orbit, bladder, prostate, and paratesticular region, are rarely primary sites of the non-rhabdomyosarcoma tumors in children and of other soft tissue sarcomas in adults [1, 2].

25.2 The Role of Imaging

Benign masses with characteristic clinical presentation may be recognized by experienced clinicians and may not require imaging. Most cutaneous or subcutaneous masses are small and often excised without imaging.

Children frequently have nonspecific symptoms and complaints are often initially neglected or diagnosis may be delayed. As children often have injuries related to play, pain and soft tissue masses may be attributed to trauma. Therapeutic options and long-term survival of soft tissue tumors is strongly related to the disease stage at the time of diagnosis. This stresses the importance of performing timely and dedicated imaging studies.

Current methods of diagnosis such as dynamic contrast-enhanced MR imaging, PET scan, molecular biology, immunology, and cytogenetics give additional insight into the biology of tumors and may help us in tailoring therapeutic strategies according to these biologic and imaging characteristics.

Fig. 25.1 Fibromatosis colli in 6-week-old boy. (**a**) Ultrasound shows a heteroechoic thickening of the central part of the sternocleidomastoid muscle. (**b–d**) Axial and sagittal T2-weighted MR images show a hypointense focal thickening (*long arrows*) of the right sternocleidomastoid muscle. The left sternocleidomastoid muscle (*short arrow*) is normal

Tables present the most common locations for tumors (Table 25.1), multiplicity (Table 25.2), different shapes associated with specific soft tissue tumors (Table 25.3), and specific MR features, including the presence of signal voids (Table 25.4) and fluid-fluid levels (Table 25.5) [4–25].

25.3 Imaging Modalities

25.3.1 Ultrasound

The value of ultrasound is limited. In a study by Brouns et al. [27] about the delay in diagnosis of soft tissue sarcoma, wrong diagnosis on ultrasound was the most frequent reason for this delay.

Ultrasound demonstrates the shape, volume, borders and compressibility of small masses, and the relationships to adjacent structures and allows to differentiate solid from cystic lesions.

Dynamic US examination of a soft tissue mass (e.g., flexion or extension maneuvers) allows to evaluate the relationship of the lesion to the underlying fascia, muscles, or tendons. Deeper-seated tumors or larger tumors are more difficult to examine adequately because anatomic landmarks are lacking and depth penetration is limited. To achieve deeper penetration and a wider field of view, transducers with lower frequency

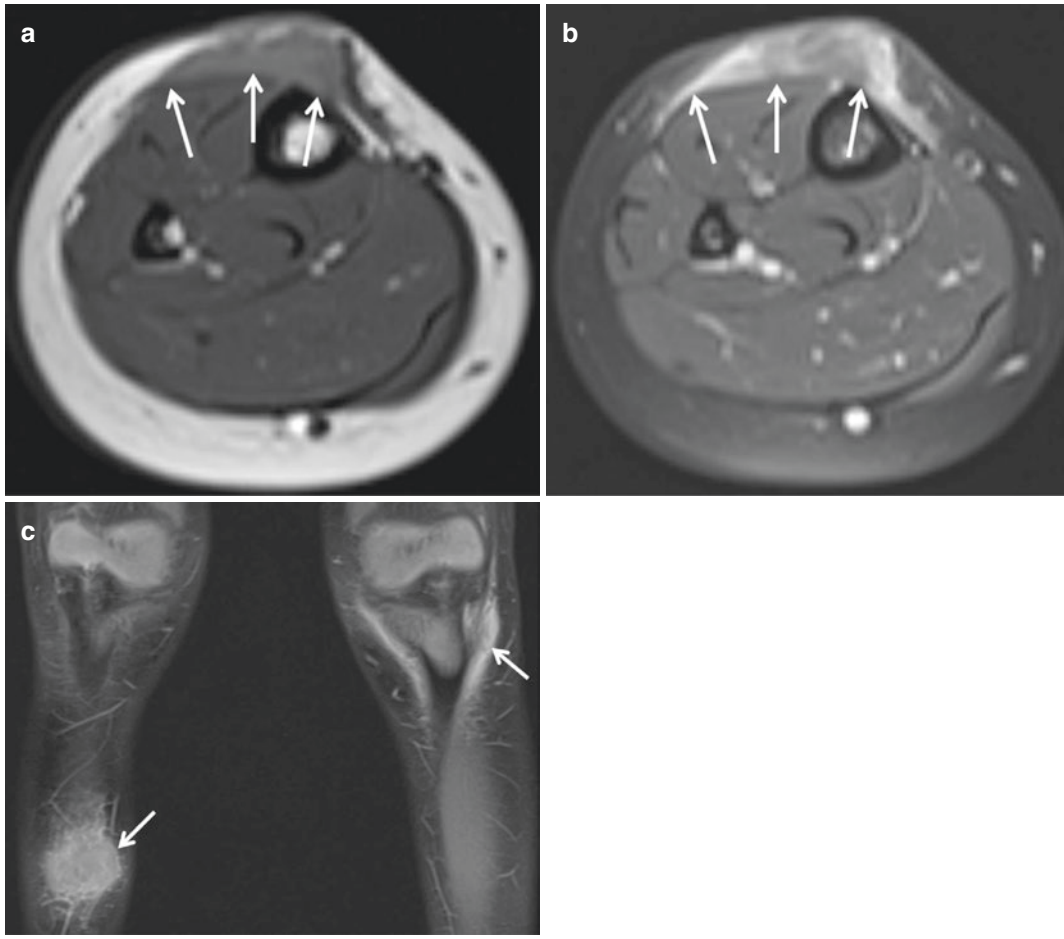

Fig. 25.2 Granuloma annulare in a 3-year-old girl. (**a**, **b**) Axial T1-weighted images show a subcutaneous soft tissue lesion (*arrows*) enhancing after contrast administration. (**c**) Coronal fat-saturated (FS) T2-weighted MR image shows multiple ill-defined hyperintense lesions (*arrows*)

(5 MHz) are useful but result in a lower spatial resolution.

However, since there are no pathognomonic ultrasound criteria for grading soft tissue tumors, ultrasound often does not allow to differentiate between benign and malignant soft tissue masses. The specificity of ultrasound is low, resulting in the inability to give an accurate tissue-related diagnosis.

Some soft tissue masses with a characteristic shape and/or echogenicity include neurogenic tumors (oval, hyporeflective masses often with posterior acoustic enhancement), lipomas (oval, mostly well-circumscribed, homogeneous masses), ganglion cysts (anechoic and rounded), hemangiomas (irregular, slightly hyperreflective lesions, often with echogenic phleboliths with posterior acoustic shadowing), and lymphangiomas (polylobular, poorly defined with cystic and solid components and septa) [28, 29].

Color Doppler helps quantify the degree of vascularization and analysis of flow patterns and is useful in diagnosing tumor vascularity (as what occurs in hemangiomas), evaluates response to chemotherapy, and guides biopsy [28].

Ultrasound may also be useful in detecting retained foreign bodies in patients with a pseudotumoral inflammatory mass and in diagnosing a ganglion cyst, bursitis, or abscess.

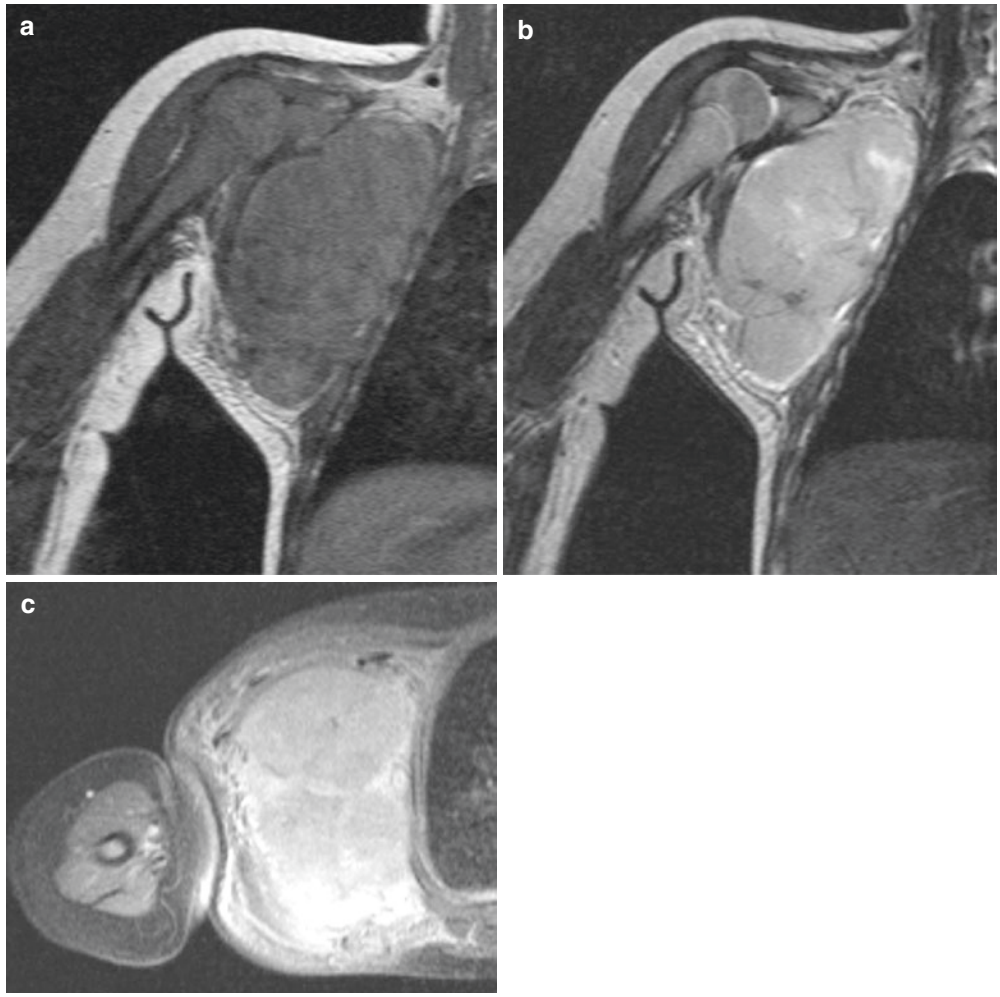

Fig. 25.3 Fibrosarcoma in a 1-year-old girl. (**a**–**b**) Coronal T1- and T2-weighted MR images show a large soft tissue mass in the right axilla. (**c**) Axial CE FS T1-weighted image depicts intense homogeneous enhancement of the lesion

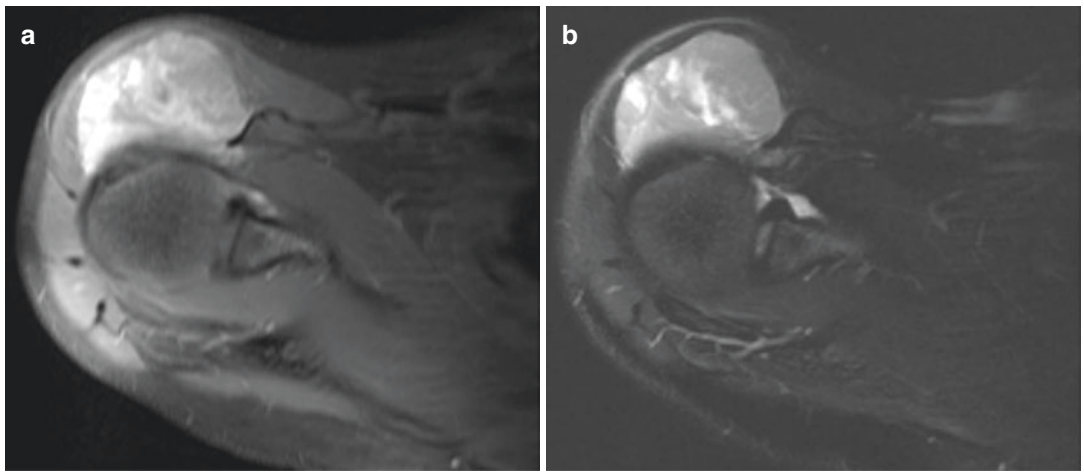

Fig. 25.4 Synovial sarcoma in a 16-year-old-girl. Axial (**a**) FS T2-weighted and (**b**) CE FS T1-weighted MR images show a heterogeneous, partially enhancing mass in the soft tissues anterior of the shoulder

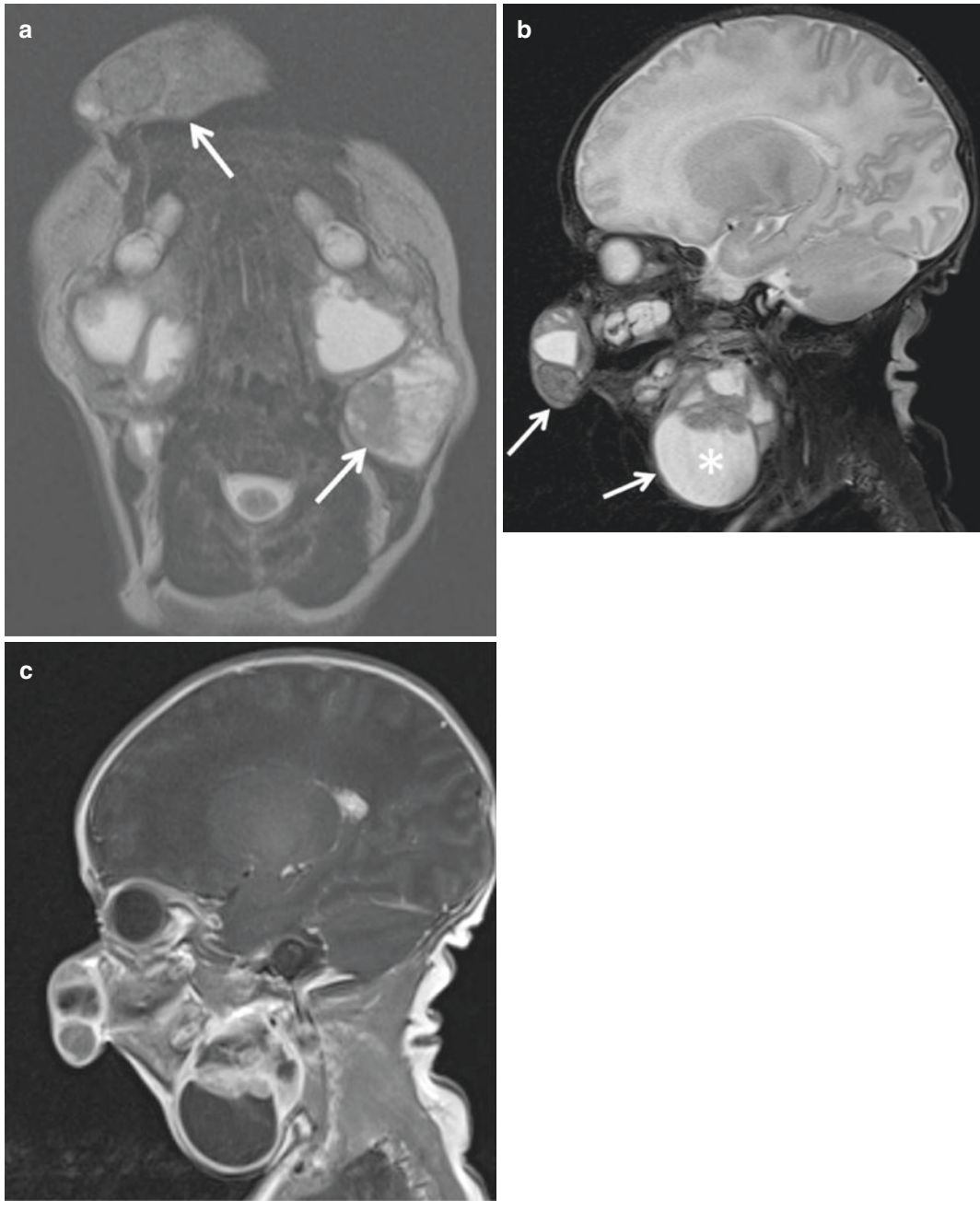

Fig. 25.5 Infantile rhabdomyosarcoma in a 1-day-old girl. (**a**, **b**) Axial and sagittal FS T2-weighted images show multiple soft tissue lesions (*arrows*) with cystic and solid components anterior to the nose and in the submandibular space. (**c**) Sagittal CE FS T1-weighted image shows enhancement of the solid components of the mass

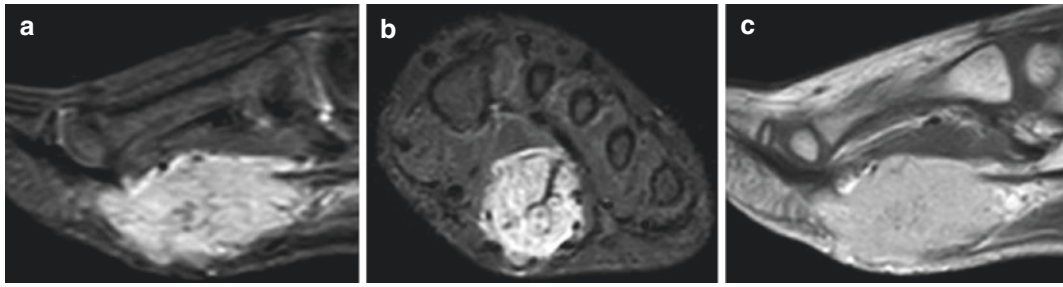

Fig. 25.6 Infantile hemangioma in a 4-year-old boy. (**a**, **b**) Sagittal and coronal FS T2-weighted images show a soft tissue mass with flow voids (*arrows*) due to the presence of vessels with high flow. (**c**) Sagittal CE T1-weighted image shows intense homogeneous enhancement of the mass

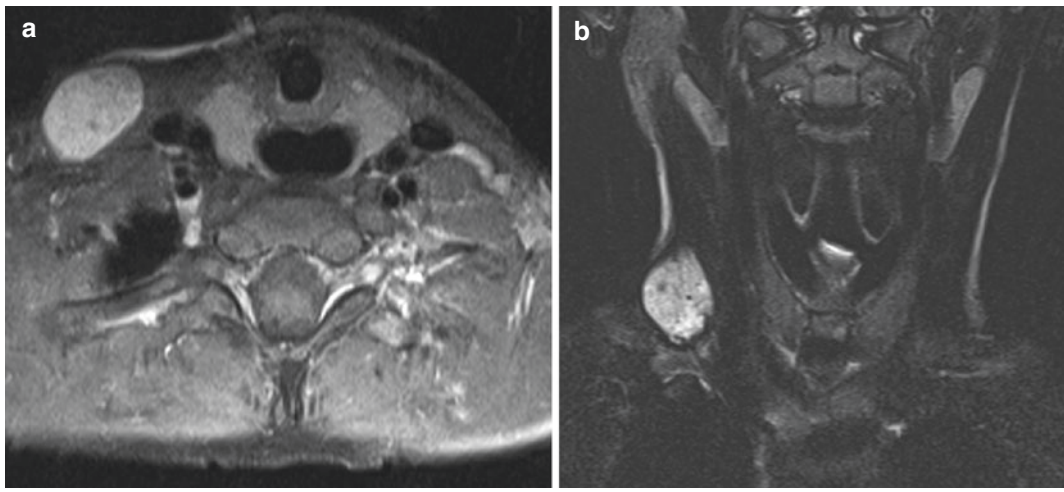

Fig. 25.7 Infantile hemangioma in a 4-year-old boy. (**a**) Coronal FS T2-weighted image shows a soft tissue mass on the right side of the neck. (**b**) Axial CE T1-weighted image shows marked homogeneous enhancement of the mass

Table 25.2 Multiplicity

Venous malformation
Lipoma (5–8 %)
Neurofibroma
Dermatofibrosarcoma protuberans
Desmoid

Table 25.3 Shape

Fusiform (ovoid)	Neurofibroma
	Lipoma
Dumbbell	Neurofibroma
Moniliform	Neurofibroma
Round	Cyst
	Schwannoma
Serpiginous	Hemangioma
	Lymphangioma

Table 25.4 Intratumoral signal void

Flow	Hemangioma (capillary)
	Arteriovenous malformation
Calcification	Hemangioma (phlebolith)
	Lipoma (well differentiated and dedifferentiated)
	Myositis ossificans (marginal)
	Myofibromatosis

Table 25.5 Fluid-fluid levels

Hemangioma
Cystic lymphangioma
Synoviosarcoma
Hematoma

25.3.2 Plain Film/CT

Plain films are of limited value in workup of a pediatric soft tissue mass. Involvement of adjacent osseous structures may be detected (e.g., in myofibromatosis, juvenile hyaline fibromatosis, infantile fibrosarcoma, and angiomatosis). Associated bone alterations may be visible (e.g., macrodactyly in fibrolipohamartoma), and the presence and morphology of intralesional calcifications (e.g., hemangiomas, myofibromatosis) or ossifications may be evaluated and lead to a correct diagnosis. Plain films may also identify pseudotumoral lesions (e.g., myositis ossificans).

CT examination shows involvement of the adjacent bony structures more accurately than on plain films, and intralesional calcifications, fat, fluid, vessels, blood, and gas may be adequately recognized on CT. However, MR imaging is the first choice cross-sectional imaging technique for evaluation of soft tissue tumors.

25.3.3 MR Imaging

MR imaging is the key modality for imaging soft tissue tumors in children.

Fat-saturated (FS) T1- and T2-weighted sequences are typically obtained. Gadolinium-enhanced T1-weighted images help to define the local tumor extent, demonstrate intratumoral necrosis, and play a role in follow-up [30, 31]. Dynamic contrast-enhanced MR imaging is useful for assessment of tumor vascularization and therapy follow-up [31].

25.4 Role of Imaging Tissue Characterization

Characterization of a tumor consists of both grading and the tissue-specific diagnosis [32].

Although histology is the gold standard, prediction of a histological diagnosis remains one of the goals of imaging. If imaging studies could provide a specific diagnosis or a limited differential diagnosis, decisions on biopsy and treatment could be simplified.

MR tissue characterization is limited for two reasons. First of all, MR images provide indirect information about tumor histology by showing signal intensities related to some physicochemical properties of tumor components (e.g., fat, blood, water, collagen) and, consequently, reflect gross morphology of the lesion rather than underlying histology. Soft tissue tumors belonging to the same histologic group may have a different composition or different proportions of tumor components resulting in different MR signals; this feature is well exemplified by the group of lipomatous tumors. Only lipomas and well-differentiated liposarcomas are predominantly fatty, while lipoblastomas have less than 25 % fat.

The second difficulty in obtaining a tissue-specific diagnosis on soft tissue tumors on MR imaging is related to the time-dependent changes that occur during natural evolution or as a consequence of therapy. Young fibrous tumors are highly cellular, with a high water content that results in high SI on T2-WI. As they become more collagenous and less cellular, a decrease in SI is seen which is more characteristic of fibrous tissue. Another example of time-related changes is the signal intensity of malignant tumors that undergo changes as a consequence of intratumoral necrosis or hemorrhage.

The highest confidence in characterization is seen in benign masses such as lipomas, hemangiomas, benign neurogenic tumors, periarticular cysts, hematomas, and abscesses. Laor and Burrows reported on the ability of MR imaging to differentiate between different subtypes of hemangiomas [17]. A mass lesion with MR signal in keeping with high flow most often corresponds to an infantile capillary hemangioma, whereas a high flow pattern without obvious mass represents an arteriovenous hemangioma. A mass lesion with slow flow MR signal corresponds to a venous hemangioma or a lymphangioma. Slow flow diffusely enhancing lesions correspond to venous hemangiomas, whereas septal enhancement is seen in lymphangiomas [17].

The imaging parameters for predicting the malignancy of soft tissue tumors in adults and children have been discussed by several groups [33–35] and include size, shape, margin, homogeneity of signal intensity on different sequences,

contrast enhancement on both static and dynamic studies, peritumoral edema, hemorrhage/necrosis, growth rate, and extent (intra- or extra-compartmental, bone involvement, and neurovascular displacement/encasement) (see Chap. 10). Few studies have been published on differentiation between benign and malignant soft tissue tumors in children. One must always approach an apparently benign, small, well-circumscribed tumor carefully, and masses should be considered to be indeterminate unless the tissue-specific diagnosis can be given with reference to the child's age, signal features, and location.

Key Messages

1. Soft tissue tumors are rare in childhood and adolescence. They are mostly benign. Hemangiomas are the most common benign, and rhabdomyosarcomas the most common malignant soft tissue tumors.
2. Despite its limitations, ultrasound remains a valuable diagnostic modality in children suspected of having a soft tissue tumor.
3. Plain film and CT demonstrate calcified lesions or intralesional calcifications.
4. MR imaging is the first choice modality of grading, staging, and characterizing pediatric soft tissue tumors.
5. As long-term survival of children with malignant soft tissue tumors is strongly related to disease stage at the time of diagnosis, early detection is mandatory.
6. Tissue-specific diagnosis by imaging is achievable in the majority of benign tumors but is notoriously difficult in malignant tumors.
7. Children with a soft tissue tumor should be referred to specialized centers for diagnosis, treatment, and follow-up.

References

1. Kransdorf M (1995) Malignant soft tissue tumors in a large referral population: distribution of specific diagnoses by age, sex and location. Am J Roentgenol 164:129–134
2. Kransdorf M (1995) Benign soft tissue tumors in a large referral population: distribution of specific diagnoses by age, sex and location. AJR Am J Roentgenol 164:395–402
3. Murphey MD, Fairbairn KJ, Parman LM et al (1995) From the archives of the AFIP. Musculoskeletal angiomatous lesions: radiologic-pathologic correlation. Radiographics 15:893–917
4. Sangkhathat S (2015) Current management of pediatric soft tissue sarcomas. World J Clin Pediatr 4: 94–105
5. Billings SD, Giblen G, Fanburg-Smith JC (2005) Superficial low-grade fibromyxoid sarcoma (Evans tumor): a clinicopathologic analysis of 19 cases with a unique observation in the pediatric population. Am J Surg Pathol 29(2):204–210
6. Bisogno G, Sotti G, Nowicki Y et al (2004) Soft tissue sarcoma as a second malignant neoplasm in the pediatric age group. Cancer 100(8):1758–1765
7. Bleyer WA (1993) What can be learned about childhood cancer from "Cancer statistics review 1973–1988"? Cancer 15:3229–3236
8. Colon F, Upton J (1995) Pediatric hand tumors. Hand Clin 11:223–243. Conrad EU, Bradford L, Chansky HA (1996) Pediatric soft-tissue sarcomas. Orthop Clin North Am 27:655–664
9. De Maeseneer M, Vande Walle H, Lenchik L et al (1998) Subcutaneous granuloma annulare: MR imaging findings. Skeletal Radiol 27:215–217
10. Fleming ID (1992) Staging of pediatric cancers. Semin Surg Oncol 8:94–97
11. Fletcher BD, Hanna SL (1996) Pediatric musculoskeletal lesions simulating neoplasms. Magn Reson Imaging Clin N Am 4:721–747
12. Gallego MS, Millan JM, Gil-Martin R et al (1987) Juvenile hyalin fibromatosis: radiographic and pathologic findings of a new case. J Med Imaging 1:251–257
13. Garcia-Pena P, Mariscal A, Abellan C et al (1999) Juvenile xanthogranuloma with extracutaneous lesions. Pediatr Radiol 22:377–378
14. Ha TV, Kleinman PK, Fraire A et al (1994) MR imaging of benign fatty tumors in children: report of four cases and review of the literature. Skeletal Radiol 23:361–367
15. Harms D (2004) Soft tissue malignancies in childhood and adolescence. Pathological and clinical relevance based on data from the kiel pediatric tumor registry. Handchir Mikrochir Plast Chir 36(5):268–274
16. Johnson GL, Baisden BL, Fishman EK (1997) Infantile myofibromatosis. Skeletal Radiol 26: 611–614
17. Laor T, Burrows PE (1998) Congenital anomalies and vascular birthmarks of the lower extremities. Magn Reson Imaging Clin N Am 6:497–519
18. Merton DA, Needleman L, Alexander AA et al (1992) Lipoblastoma: diagnosis with computed tomography, ultrasonography, and color Doppler imaging. J Ultrasound Med 11:549–552
19. Meyer William H, Spunt Sheri L (2003) Soft tissue sarcomas of childhood. Cancer Treat Rev 30(3):269–280
20. Upton J, Coombs C (1995) Vascular tumors in children. Hand Clin 11:307–337

21. Vazquez E, Enriquez G, Castellote A et al (1995) US, CT, and MR imaging of neck lesions in children. Radiographics 15:105–122
22. Navarro OM, Laffan EE, Ngan B (2009) Pediatric soft-tissue tumors and pseudotumors: MR imaging features with pathologic correlation. Part 1. Imaging Approach, pseudotumors, vascular lesions, and adipocytic tumors. Radiographics 29:887–906
23. Laffan EE, Ngan B, Navarro OM (2009) Pediatric soft-tissue tumors and pseudotumors: MR imaging features with pathologic correlation. Part 2. Tumors of fibroblastic/myofibroblastic, so-called fibrohistiocytic, muscular, lymphomatous, neurogenic, hair matrix, and uncertain origin. Radiographics 29(4):e36
24. Ahn JM, Yoon HK, Suh YL et al (2000) Infantile fibromatosis in childhood: findings on MR imaging and pathologic correlation. Clin Radiol 55(1):19–24
25. Navarro OM (2011) Soft tissue masses in children. Radiol Clin North Am 49:1235–1259
26. Lawrence W Jr (1994) Soft tissue sarcomas in adults and children: a comparison. CA Cancer J Clin 44:197–199
27. Brouns F, Stas M, De Wever I (2003) Delay in diagnosis of soft tissue sarcomas. Eur J Surg Oncol 29(5):440–445
28. Ozbek SS, Arkun R, Killi R et al (1995) Image-directed color Doppler ultrasonography in the evaluation of superficial solid tumors. J Clin Ultrasound 23:233–238
29. Yang WT, Ahuja A, Metreweli C (1997) Sonographic features of head and neck hemangiomas and vascular malformations: review of 23 patients. J Ultrasound Med 16:39–44
30. Shapeero LG, Vanel D, Verstraete K, Bloem JL (1999) Dynamic contrast-enhanced MR imaging for soft tissue sarcomas. Semin Musculoskeletal Radiol 3:101–114
31. Van der Woude HJ, Verstraete KL, Hogendoorn PC et al (1998) Musculoskeletal tumors: does fast dynamic contrast-enhanced subtraction MR imaging contribute to the characterization? Radiology 208:821–828
32. De Schepper A, Ramon F, Degryse H (1992) Statistical analysis of MRI parameters predicting malignancy in 141 soft tissue masses. Rofo Fortschr Geb Rontgenstr Neuen Bildgeb Verfahr 156:587–591
33. Berquist T, Ehman R, King B et al (1990) Value of MR imaging in differentiating benign from malignant soft tissue masses: study of 95 lesions. AJR Am J Roentgenol 155:1251–1255
34. Crim J, Seeger L, Yao L et al (1992) Diagnosis of soft tissue masses with MR imaging: can benign masses be differentiated from malignant ones? Radiology 185:581–586
35. Moulton J, Blebea J, Dunco D et al (1995) MR imaging of soft tissue masses: diagnostic efficacy and value of distinguishing between benign and malignant lesions. AJR Am J Roentgenol 164:1191–1199

Part VI

Imaging After Treatment

Follow-Up Imaging of Soft Tissue Tumors

26

Johan L. Bloem and Carla S.P. Van Rijswijk

Contents

26.1 **Introduction** 635
26.2 **Therapy-Induced Changes in Normal Tissue** 636
26.3 **Monitoring Response to Therapy** 636
26.4 **Locoregional Recurrence** 643
26.5 **Metastases** 646
References 649

J.L. Bloem (✉) • C.S.P. Van Rijswijk
Department of Radiology,
Leiden University Medical Center (LUMC),
Gebouw 1., Postbus 9600, 2300 RC,
Leiden, The Netherlands
e-mail: j.l.bloem@lumc.nl

26.1 Introduction

The aim of therapy in patients with soft tissue sarcoma is to irradicate (curative) or modify biologic behavior (palliative) of sarcoma while minimizing damage of normal tissues. This is done by local (surgery, isolated limb perfusion, and radiation) or systemic (neoadjuvant and adjuvant chemotherapy) therapy. Prognosis of patients with soft tissue sarcoma is mainly influenced by local recurrence and development of distant metastasis and thus also by response to treatment [1]. Approximately one-third of all patients with soft tissue sarcomas will develop local recurrence or distant metastatic disease, with the highest risk in the first few years after treatment; however, late recurrences after 5 years do occur [2–4]. The overall survival mainly depends on the development of metastatic disease.

The patterns of recurrence vary with the anatomic site of the primary tumor [5]. Patients with extremity and superficial trunk primaries have a higher predilection for metastases and a lower probability of locoregional recurrences. In contrast, patients with retroperitoneal or head and neck tumors have a higher tendency toward locoregional recurrences compared to metastases. In this chapter we'll address several topics related to therapy. After a brief discussion on therapy-induced changes in normal tissue, which is important in diagnosing recurrence, we'll

© Springer International Publishing AG 2017

F.M. Vanhoenacker et al. (eds.), *Imaging of Soft Tissue Tumors*, DOI 10.1007/978-3-319-46679-8_26

address monitoring the response to treatment, imaging locoregional recurrence, and finally diagnosis of metastases.

26.2 Therapy-Induced Changes in Normal Tissue

Surgery, radiation therapy, isolated limb perfusion, systemic chemotherapy, angiogenesis-inhibiting drugs, therapy- and cancer-induced cachexia, and supportive therapy such as blood transfusions, erythropoietin (Epo), corticosteroids, growth colony stimulating factor (G-CSF), and peripheral stem cell transplantation may all cause acute and/or chronic reversible or irreversible changes in normal tissue. These changes are often seen on imaging during and/or following therapy and need to be differentiated from residual or recurrent tumor and metastatic disease. These changes include edema, avascular necrosis, mucoid degeneration, serous atrophy, osteopenia, regeneration or reconversion of hematopoietic marrow, extramedullary hematopoieses, hematoma, seroma, denervation of muscle, and therapy-induced cancers. Most diagnostic problems related to these therapy effects occur in the bone marrow of patients with osseous tumors. Bone marrow changes do occur in patients with soft tissue tumors but then pose less of a diagnostic problem. In this chapter we'll limit the discussion to changes that may cause diagnostic problems in patients with soft tissue tumors.

Various soft tissue tumors such as neurofibromatosis and giant cell tumors are treated with biologicals such as imatinib (Gleevec). In these patients extensive bone marrow changes displaying low signal intensity on T1-weighted MR images and high signal intensity on fluid-sensitive MR sequences may be seen. These may progress during treatment and may completely disappear following cessation of treatment. Although avascular necrosis has been supposed as the cause for these changes, the transient nature is more likely to reflect edema [6, 7].

In the soft tissues, commonly seen changes are early (edema and inflammation) and late (fibrosis) effects of radiation therapy. Especially the early effects are easily identified because of the linear margins reflecting the radiation portals. The signal intensities of hematoma (high signal intensity of methemoglobin on T1- and fluid-sensitive sequences) and hygroma (low signal intensity on T1 and high signal on fluid-sensitive sequences) allow an easy diagnosis. Follow-up imaging (also with US) and Gd-chelate-enhanced imaging are useful in excluding tumor nodules within or surrounding these postsurgical changes. Denervated muscle is easily recognized as a high signal muscle on fluid-sensitive sequences (early edema) or high signal intensity muscle on T1-weighted sequences (late atrophy).

26.3 Monitoring Response to Therapy

With some exceptions, most soft tissue tumors, and especially sarcomas, are treated with resection. Resection is often supplemented by neoadjuvant (presurgical) chemotherapy, radiation therapy before or following resection, and adjuvant chemotherapy (postsurgical). In addition trials with chemoradiation have shown promising results [8]. In contrast to chemotherapy protocols, there is still debate about the optimal use of radiation therapy as an adjunct to surgery. There are advantages and disadvantages for both pre- and postoperative scheduling of radiation. For imaging it is important to realize that the effect of radiation therapy takes at least 4 weeks to happen. Many histological changes including necrosis, liquefaction, hemorrhage, hyalinization, angiogenesis, and fibrosis occur secondary to radiation and complicate image interpretation.

Volume measurements have been proven to be insufficient (with the exception of myxoid liposarcoma) in monitoring response to radiation therapy [9–12]. Likewise tumor volume measurements are inaccurate in monitoring response to (neo)adjuvant chemotherapy and chemoradiation. Tumor biology in sarcomas is normally heterogeneous and in addition changes over time, even without therapy. Volume measurements do not capture the complicated spontaneous and therapy-induced changes within the sarcomas.

The revised RECIST 1.1 criteria originate from the era of cytotoxic chemotherapy [13]. Nowadays and even more so in the future, targeted therapies will use tumor-specific pathways to modify tumor progression, vasculature, and growth. This requires matching imaging techniques to monitor response. The EORTC soft tissue and bone sarcoma group proposed a histological grading system based on the amount of viable (also called stainable) tumor relative to necrosis. Grades are from A (no stainable tumor cells) to E (>50 % stainable tumor cells). Relationships between this new grading system and prognosis or outcome have yet to be determined. In this chapter we therefore still use the value of <10 % viable tumor to indicate good response. Compared to the older system of less than 10 % of viable tumor as a cutoff value for good response, this new system has, apart from grade A, also grade B (single or clusters of stainable tumor cells <1 % of whole specimen) and grade C 1–10 % stainable tumor cells [10].

The PERCIST criteria are a step forward for imaging evaluation because they include metabolic information visualized by FDG-PET imaging [13]. Especially with the advent of various mechanisms of chemotherapy that change tumor biology, we need to make use of an integrated approach using functional parameters obtained with multiple imaging techniques including MR (angiogenesis, membrane integrity, hypoxia, etc.) and PET [14–17]. This approach of tumor profiling has been described as radiomics [17]. For this chapter a survey of this futuristic approach is beyond our scope. In this chapter we'll briefly describe currently available clinical approaches.

Changes in tumor volume assessed with MR are also not very accurate in defining response. Only an increase in tumor volume not caused by massive hemorrhage within the tumor correlates with a poor histologic response. An unchanged or decreasing tumor volume is not predictive of a good response.

Gd-chelate-enhanced MR imaging improves identification of viable components within the tumor [14, 18]. However, static contrast-enhanced MR images are not sufficiently specific to differentiate viable tumor from early immature granulation tissue, neovascularity in necrotic areas, and reactive hyperemia. Also, static Gd-chelate-enhanced imaging results in an overestimation of the volume of residual viable tumor because the small molecular agent Gd-chelate passes from the intravascular space to the interstitium outside the tumor [18, 19]. Fast or dynamic contrast-enhanced (DCE) MRI reflects angiogenesis, in particular flow, permeability, and interstitial pressure and is thus more accurate in identifying and localizing residual viable tumor after chemotherapy thereby improving differentiation between good and poor respondents (Figs. 26.1 and 26.2). Details of this technique are presented in Chap. 5.

Therapy-induced changes in capillary permeability (time-intensity curve analysis, quantification of Ktrans) and vascular density (maximal enhancement) are often observed before changes in tumor volume. Direct visual inspection of the (subtraction) images before and after chemotherapy allows easy detection of highly vascular and/or highly perfused viable tumor tissue. Alternatively parametric analysis (see Chap. 5) using dedicated software can be used [19, 20]. When more than 10 % of the total tumor volume enhances early (defined as enhancement within 6 s after arterial enhancement), a poor response with more than 10 % of tumor tissue remaining viable should be suspected. Several pitfalls have to be avoided. Young granulation tissue at the margins of necrotic tumor may enhance early. Arterioles or small physeal vessels enhance early as well. Spatial resolution is a limitation. Tumor nests smaller than 3–5 mm^2 cannot be depicted.

Diffusion-weighted MR imaging with high b-values has potential in assessing the chemotherapeutic response of soft tissue sarcoma [12, 15, 21–23].

An increase in diffusion reflected by increasing apparent diffusion coefficient (ADC) values of sarcoma after chemotherapy corresponds to cell death (disintegration of cell membranes) and reduction in tumor cell density. Early response to chemotherapy may, however, result in a decrease of diffusion caused by dehydration, congestion, and decreased capillary permeability. It is still unclear which method of determining changes of ADC values over time is appropriate for soft tis-

sue sarcoma. Increase of the minimum ADC value seems to correlate better with good response than increase of the average ADC ratios [21].

The value of color Doppler ultrasonography with spectral analysis has been demonstrated in patients with bone and soft tissue sarcomas as long as there is a soft tissue mass. Blood flow parameters that can be measured by spectral analysis include peak velocity, mean velocity, volume flow rate, pulsatility index, and resistive index ([peak systolic velocity/end-diastolic velocity]/peak systolic velocity) [18, 24, 25]. Response to neoadjuvant chemotherapy can be reliably predicted after two cycles, but not sooner. In a good respondent, a vascular tumor with low vascular resistive index in feeding arteries changes into a system with an increased or even normalized resistive index and decreased flow and shunting in the tumor. In good respondents, the resistive indices calculated in the tumor-

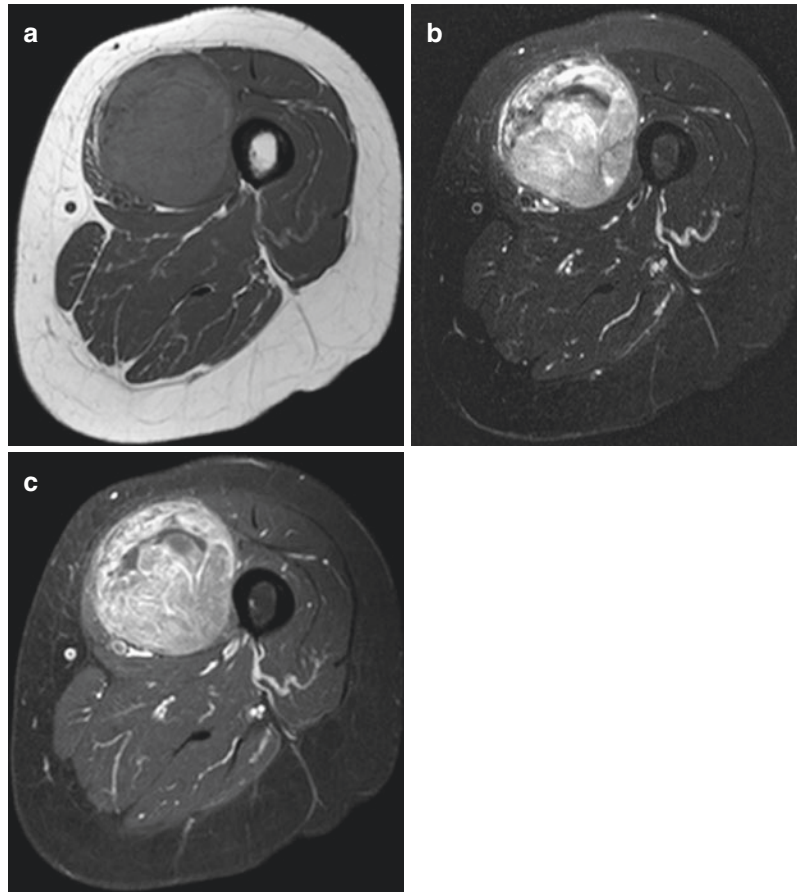

Fig. 26.1 Adult patient with synovial sarcoma medial to the femur with central necrosis diagnosed on the resected specimen. T1- (**a**) and T2-weighted frequency-selected fat-suppressed (**b**) and T1 fat-suppressed Gd-enhanced static (**c**) axial images show the tumor with centrally less enhancement. On this panel parametric images (**d**) obtained during dynamic Gd-enhanced data acquisition with a temporal resolution of 3 s and processed with ISP software package (Philips) are displayed. *Upper left* is one of the enhanced images, *upper middle* the electronically subtracted image, *upper right* time to peak, and *lower right* the wash-in rate. Below the images, a time-intensity curve is exhibited (horizontal axis time, vertical axis relative signal intensity). Artery, viable, and necrotic tumors are labeled. Following neoadjuvant chemotherapy, the same parameters are displayed (**e**). Note that the necrotic central area has increased (subtraction images), the time to peak has become longer, and the wash-in rate has decreased. Following resection the patient had a recurrent mass which has high signal intensity and fluid-fluid levels on the T2 fat-suppressed image (**f**), and on the static Gd-enhanced images (**g**), no central enhancement is observed. On the parametric images (**h**), no enhancement is observed on all parametric images nor on the time-intensity curve. A large hematoma without viable tumor was evacuated

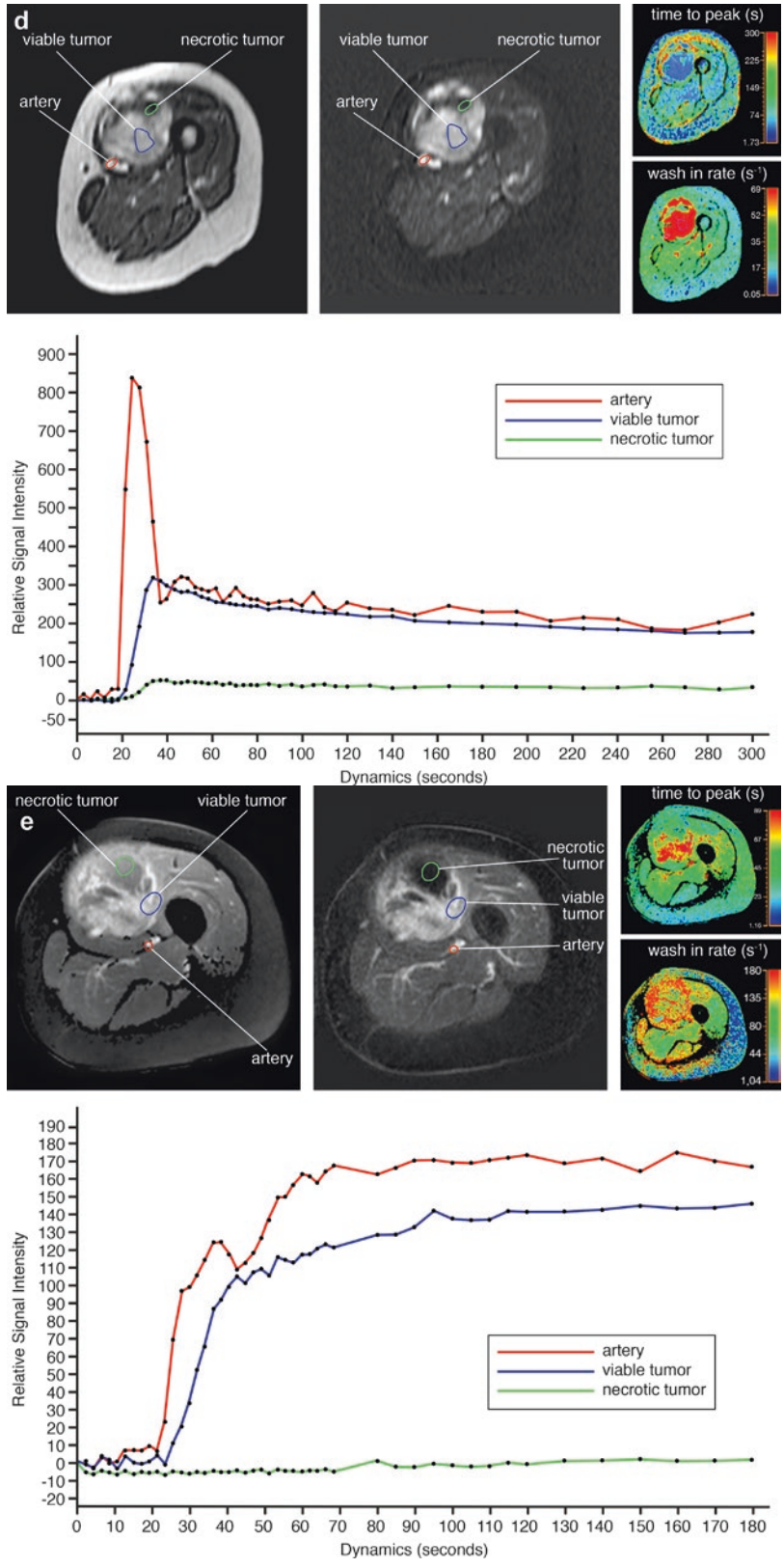

Fig. 26.1 (continued)

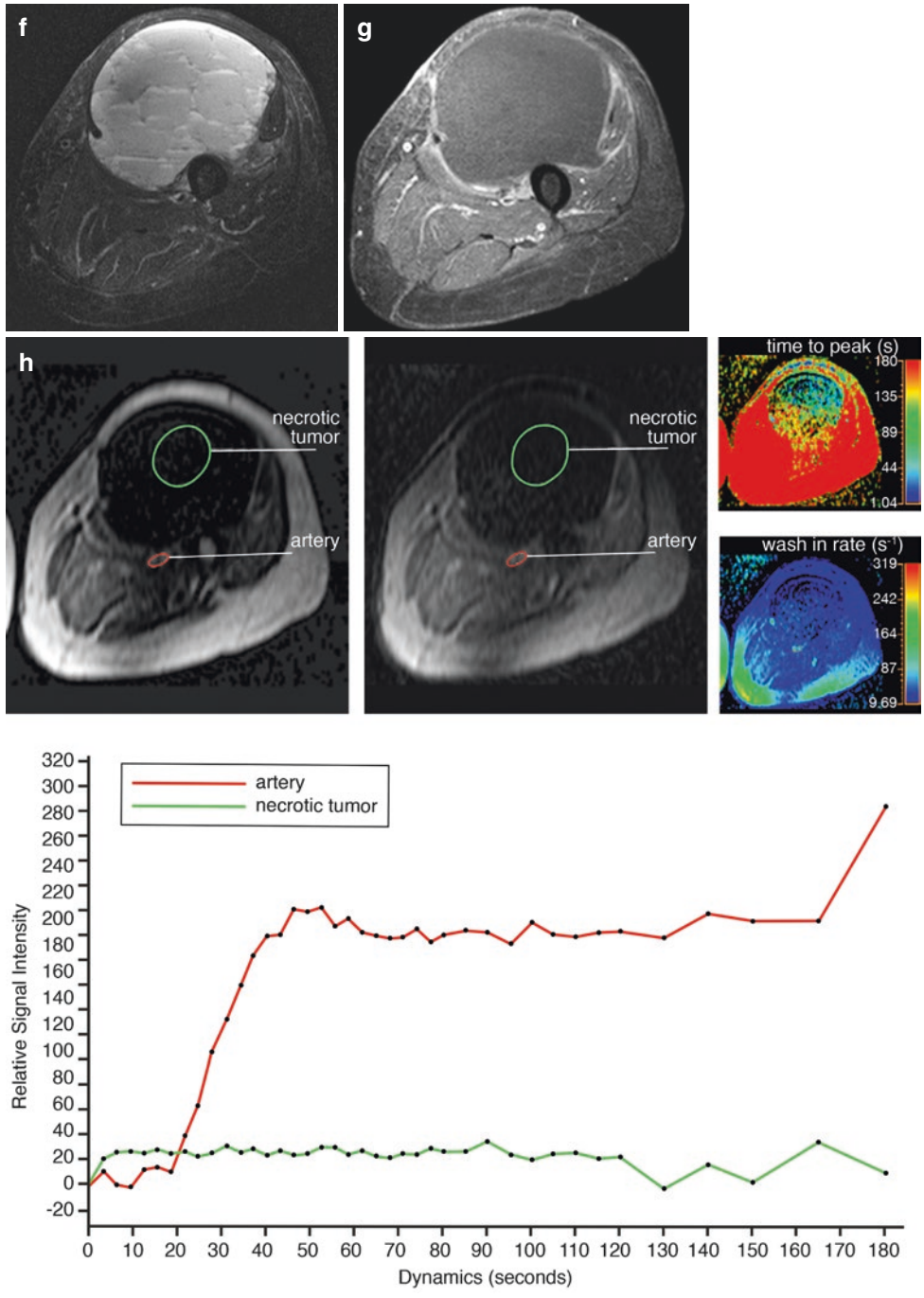

Fig. 26.1 (continued)

feeding artery are almost equal to the resistive indices in the contralateral reference artery. Apparently, increase of peripheral resistance corresponds to the reduction or disappearance of intratumoral high-velocity Doppler shifts, which indicates the reduced need for attracting blood from the host's circulation in chemotherapy-sensitive tumors [26].

Early studies demonstrate the potential of Doppler ultrasonography with microbubble-

based contrast agents in evaluating tumor response to chemotherapy. A decrease of contrast uptake the day after isolated limb perfusion with high-dose chemotherapy and tumor necrosis factor has been reported to correlate with a favorable histologic response. No ultrasound parameters have been reported that can predict the response to therapy before the start of treatment.

There have been conflicting reports on the usefulness of glucose metabolism imaged by 18F-deoxyglucose positron emission tomography (18F-FDG-PET) as a parameter to assess response to chemotherapy in sarcoma [27]. Following chemotherapy, the standardized uptake value (SUV) decreases. Most studies report a larger decrease of SUVmax in responders as opposed to nonresponders [28–33]. Most studies are in heterogeneous populations of bone and soft tissue sarcoma. It seems that metabolic tumor volumes are a better target than SUVmax values. Differences in metabolic volume, defined as the number of voxels within the volume of interest that have an uptake greater than that of the chosen background threshold, have been reported to correlate better with response [29]. This tumor component correlates with the viable tumor as defined by early enhancement on DCE MRI and seems a promising venue of further research.

With the advent of insights in analyzing metabolic tumor volume or residual viable tumor using various SUV parameters and the rise of reliable commercial software packages to quantify DCE MRI, it is too early to define the clinical role of these techniques [27]. For the time being, we still rely on DCE MRI in combination with high-resolution MR to monitor response and, at the same time, to identify viable tumor nests before surgery. It is likely that with the advent of targeted

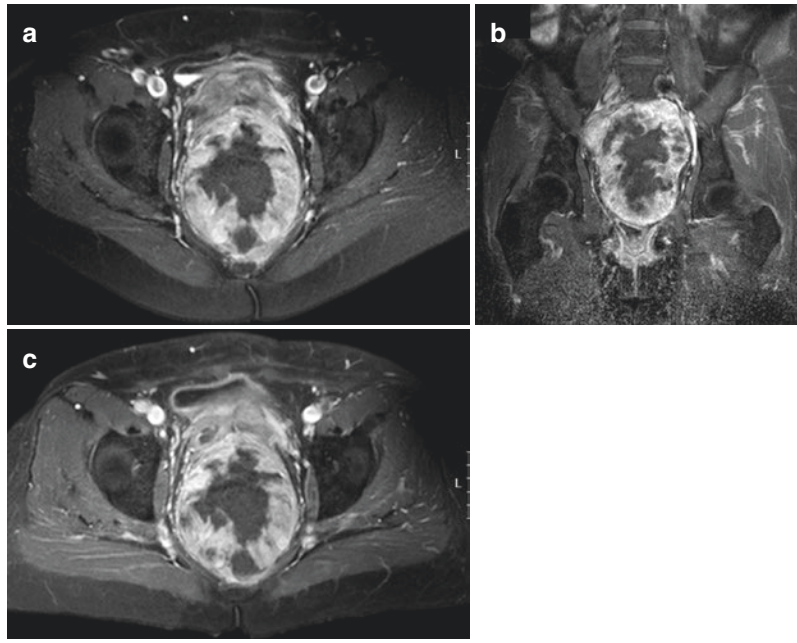

Fig. 26.2 A 64-year-old patient with solitary fibrous tumor; following presurgical radiation therapy, 50 % of the tumor was necrotic. Axial (**a**) and coronal (**b**) Gd-chelate-enhanced fat-suppressed T1-weighted images show the tumor in the pelvis. Enhancement is mainly seen in the periphery. Following radiation therapy (**c**), little change is seen on the axial fat-suppressed Gd-enhanced static image. On this panel parametric images (**d**) obtained during dynamic Gd-enhanced data acquisition with a temporal resolution of 3 s and processed with ISP software package (Philips) are displayed. *Upper left* is one of the enhanced images, upper middle the electronically subtracted image, *upper right* time to peak, and *lower right* the wash-in rate. Below the images is a time-intensity curve (horizontal axis time, vertical axis relative signal intensity). Artery, viable, and necrotic tumors are labeled. Following radiation therapy, the same parameters are displayed (**e**). Note that the time-intensity curve of the peripheral enhancing part has decreased relative to the arterial curve. Time to peak has increased, while only minor change is seen for the wash-in rate

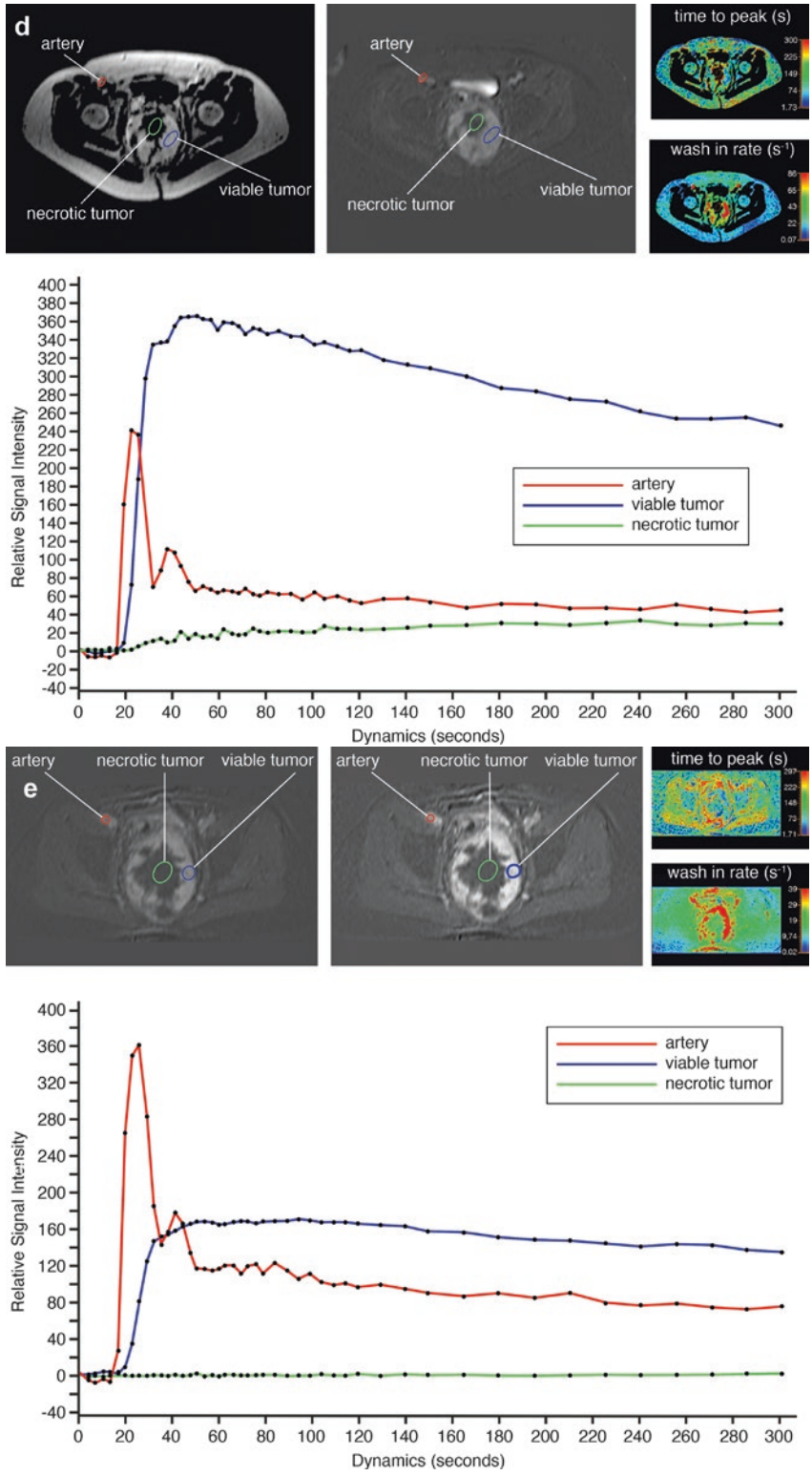

Fig. 26.2 (continued)

predominantly cytostatic, metabolic, and angiogenesis-inhibiting cancer treatments, 18F-FDG-PET will take a prominent place together with other PET tracers requiring cyclotron, DCE MRI, and ultrasonography in monitoring and guiding treatment. The combination of several techniques, displaying various characteristics of tumor phenotype in 4D, is likely to be the future. This requires advanced automated analysis of large data sets.

26.4 Locoregional Recurrence

The benefit of early detection of local recurrence depends on the availability of therapeutic options that can prolong survival. Radical compartmental resection with or without adjuvant radiotherapy and/or chemotherapy may provide long-term salvage in patients with a local recurrence of soft tissue sarcoma [34]. The risk for local recurrence depends on tumor site, size, grade, and adequacy of surgical margins. Although about 2–20 % of all resections will have positive margins and thus increased risk for local recurrence, its impact on overall survival remains controversial [1, 4, 35].

Several guidelines have been recommended for the follow-up of soft tissue sarcoma consisting of a combination of clinical history, physical examination, blood tests, chest radiographs, CT, and MR imaging [36–42]. The ACR advises MR follow-up at least twice a year during the first 5 years after treatment of the primary tumor and once a year 5–10 years after treatment. The ESSR and ESMO advocate 3–4 MRs during the first 2–3 years in intermediate- or high-grade sarcomas and 2–3 MRs during the first 3 years in low-grade sarcomas. An MR once a year 5–10 years after primary treatment is also advocated by ESSR [34, 43–47]. Most institutions rely on consensus-based guidelines due to the absence of evidence-based guidelines. Surveillance strategies that, through early detection and treatment, improve survival and quality of life while minimizing costs have yet to be identified in randomized clinical trials. Only few studies have been reported on the efficacy of surveillance strategies for the follow-up of soft tissue sarcoma [37, 38, 48]. According to Whooley et al., clinical assessment and physical examination are the most useful tools for evaluating locoregional recurrence, whereas routine MR imaging of the primary tumor site and laboratory blood tests appear ineffective strategies. In a retrospective review of 141 patients, they detected by routine annual imaging only one asymptomatic local recurrence; all others were found on physical examination of the primary site [37, 48]. However, MR imaging has shown to be useful in patients in whom physical examination is hampered due to radiotherapy changes.

When indicated, MR imaging is the most useful technique for identifying suspected local recurrence or residual disease after incomplete resection [34, 49]. An MR using a T2-weighted sequence with frequency-selective fat saturation or short tau inversion recovery (STIR) or Dixon sequence with water reconstruction is considered to be the most useful first step for detecting recurrent tumor (Fig. 26.3). The morphology of the lesion and the signal intensity contribute to the definition of its character. Low signal intensity on T2-weighted images or diffuse high signal intensity on T2-weighted images excludes tumor recurrence in 99 % of patients. Mature scar tissue usually exhibits low signal intensity (Fig. 26.4) because of its fibrous tissue content, as described in previous studies. Diffuse high signal intensity with a feather-like appearance, without mass effect, generally represents post-therapy change or inflammation. High signal intensity mass-like

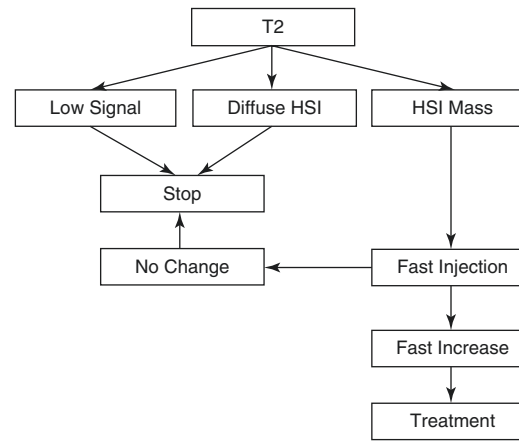

Fig. 26.3 Flowchart of MR imaging in the follow-up of aggressive soft tissue tumors

lesions on T2-weighted images require further examination with intravenous Gd-chelates [50].

Fat-suppressed T1-weighted fast spin echo sequences after Gd-chelate injection can be used to distinguish non-enhancing post-therapy hygroma, seroma, or hematoma from enhancing tumor recurrence, post-therapy fibrosis, granulation tissue, or inflammatory masses (Fig. 26.5). The T1 fat-suppressed images obtained after administration of the contrast agent should be compared to subtraction images (for instance, obtained in the dynamic sequence, see below) or to pre-contrast T1 fat-suppressed images to correct for pseudo-enhancement caused by scaling effects. Absence of contrast enhancement excludes recurrent tumor. On these standard contrast-enhanced images, the differentiation between recurrent viable tumor and post-therapy fibrosis or inflammatory pseudomasses may remain difficult. However, in these cases dynamic contrast-enhanced MR imaging may prove helpful

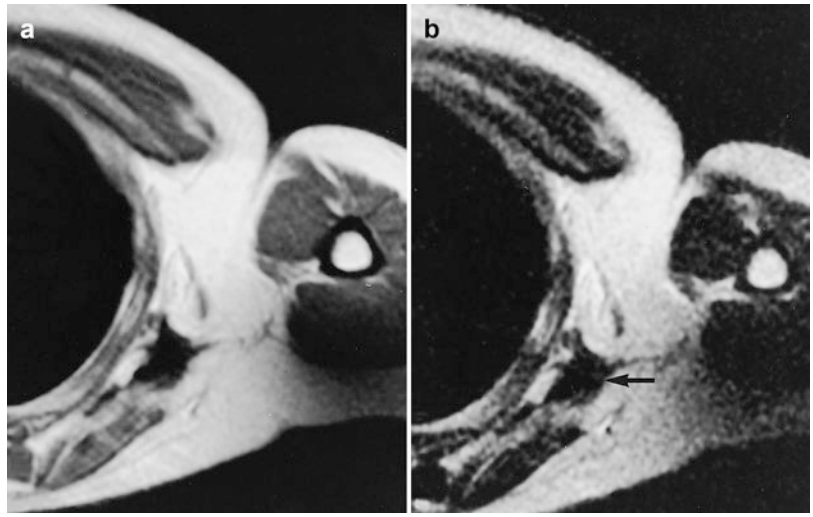

Fig. 26.4 (**a**, **b**) Malignant soft tissue tumor studied after surgery and radiotherapy in a 30-year-old male: (**a**) axial T2-weighted MR image shows low signal intensity (*arrow*) indicative of no recurrence; (**b**) the scar also has low signal on T1-weighted MR image

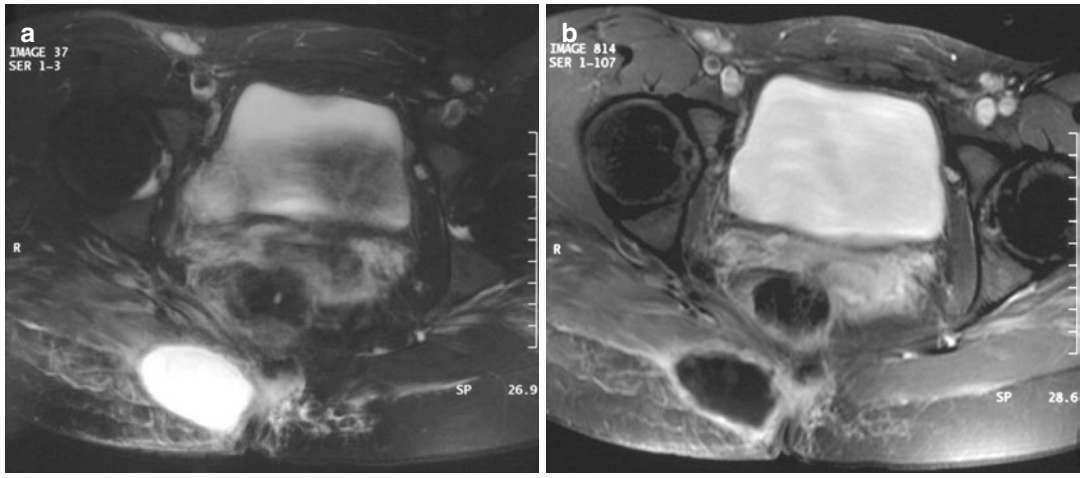

Fig. 26.5 (**a**, **b**) Three months after resection of desmoid-type fibromatosis of the pelvis in a 26-year-old female: (**a**) axial T2-weighted MR image shows a well-defined mass with homogeneous high signal intensity; (**b**) on axial fat-suppressed T1-weighted MR image after intravenous administration of gadolinium, chelate is only a small rim of enhancement seen consistent with a postoperative seroma that resolved spontaneously

[34, 51]. Dynamic contrast-enhanced MR imaging allows differentiation between inflammation and recurrent or residual tumor. After a rapid bolus injection of contrast, viable tumor exhibits rapid progressive increase of signal intensity followed by washout or plateau phase, whereas the signal from inflammatory changes will also increase but later [52] (Fig. 26.6). The exception is young granula-

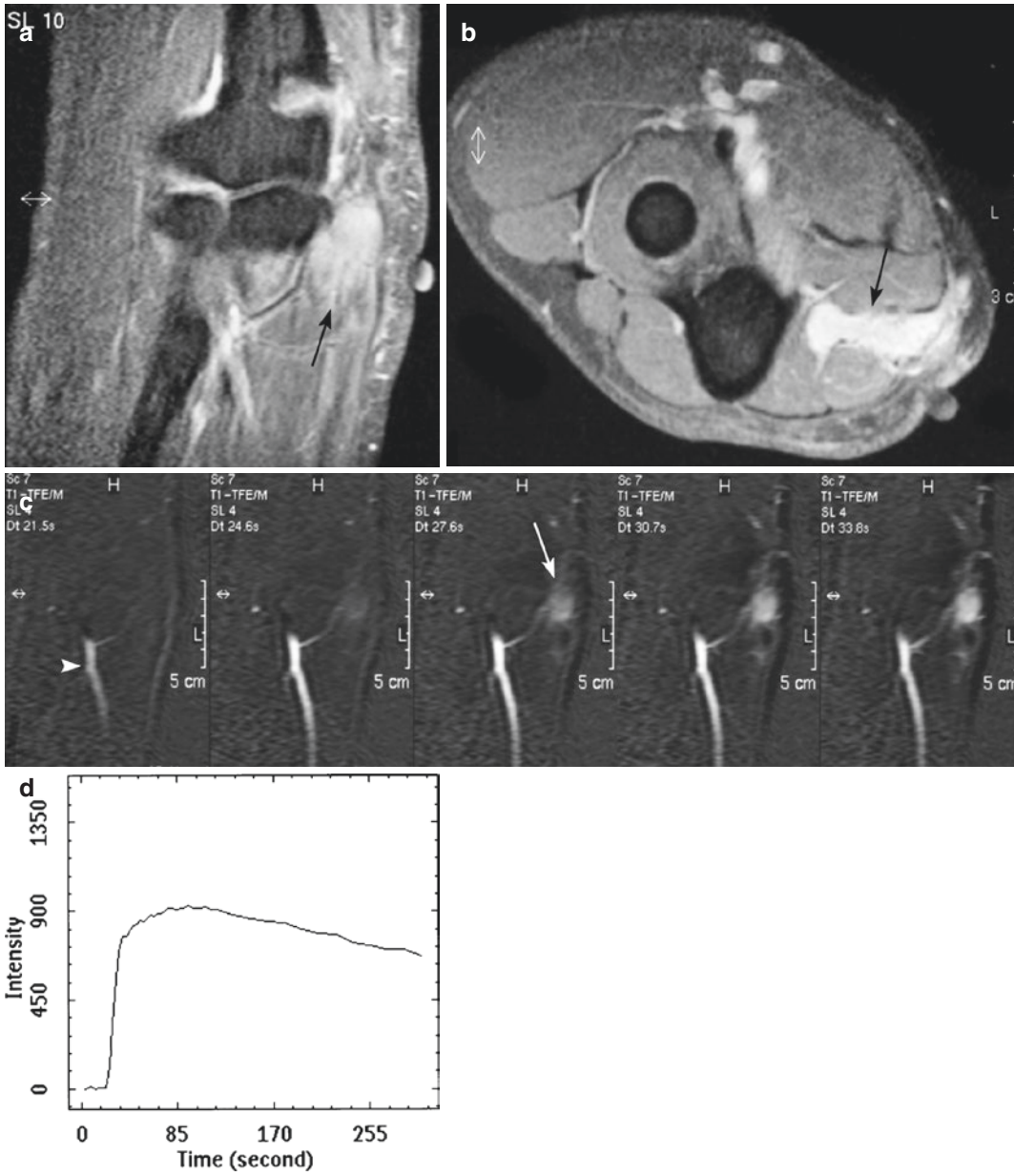

Fig. 26.6 (**a–d**) Fifteen months after resection and radiotherapy of a liposarcoma of the elbow in a 25-year-old male: (**a**, **b**) coronal and axial fat-suppressed T1-weighted MR image after gadolinium chelate shows an ill-defined homogeneous enhancing soft tissue mass (*arrow*). Markers on the skin demonstrate the surgical scar; (**c**) coronal consecutive dynamic contrast-enhanced subtraction images of the same level obtained with a temporal resolution of 3 s. Tumor enhancement (*arrow*) is seen 3 s after arrival of the bolus contrast in the artery (*arrowhead*) suggestive of tumor recurrence; (**d**) time-intensity curve of a region of interest in the soft tissue mass demonstrating rapid progressive enhancement followed by a washout phase. Histologic examination after Tru-Cut biopsy showed recurrence of liposarcoma

tion issue and reactive changes secondary to surgery or radiation within the last 6 months.

Diffusion-weighted imaging has potential in adding specificity in the diagnosis of recurrent tumor. Preliminary studies have shown a statistical difference between recurrent tumor and nonneoplastic masses secondary to earlier treatment [34, 51].

Each case of a suspicious (recurrent) mass should be treated as if it is a new sarcoma. Confirmation should be obtained by cytological sampling or core-needle (Tru-Cut or Jamshidi) biopsy after locoregional restaging by MR imaging. Histological biopsy should always be performed after MR imaging because reactive changes, hemorrhage, and edema secondary to biopsy may hamper interpretation of MR images and therefore interfere with staging.

Preliminary studies of positron emission tomography (PET) demonstrate the potential of PET with FDG as an additional tool for detecting local recurrence of soft tissue sarcoma. Moreover, PET seems particularly useful in patients with extensive histories of surgery and radiation therapy, in the setting in which MR imaging interpretation can be difficult [53, 54]. The caveat here is that a negative PET-CT can only be used to exclude recurrence, if the initial tumor accumulates sufficient FDG.

Desmoid-type fibromatoses are benign fibroblastic proliferations that arise in the deep soft tissues and are characterized by infiltrative growth in the surrounding soft tissue structures and the absence of a pseudocapsule. Because of this growth pattern, local recurrence after surgery is virtually unavoidable. Routine follow-up MR imaging of patients with desmoid-type fibromatosis seems justified not only to detect (often asymptomatic) local recurrence but also to evaluate the natural behavior of these lesions as they change from cellular active lesions toward mature, collagenous inert lesions [55] (Fig. 26.7).

26.5 Metastases

Early detection of pulmonary metastases is an important component of surveillance because the overall survival of sarcoma patients mainly depends on the development of distant metastases (Fig. 26.8). Metastatic spread is found predominantly in the lungs, and about 70 % of all patients who develop metastases will have distant disease confined to the lungs [56]. CT is superior to PET-CT in the detection of pulmonary metastases [57].

Pulmonary metastasectomy is considered a standard practice since there is indeed a small population that can be cured. Whooley et al. studied the cost-effectiveness of chest radiograph surveillance in primary soft tissue sarcomas in a retrospective analysis. They proved the utility of chest radiograph surveillance on the basis of a review of 74 patients with first recurrence confined to the lungs (79 % of all first recurrences). Although chest CT is recommended as part of the staging evaluation for all patients with high-grade soft tissue sarcomas due to higher sensitivity than chest radiographs, the role of CT in the surveillance of metastatic disease has not been determined yet. However, extrapolations of results of chest CT at time of initial staging didn't demonstrate cost-effectiveness of routine use of surveillance chest CT over chest radiographs when the risk of pulmonary metastatic disease was low (thus in low-grade tumors) [38, 58]. However, in our practice we routinely use chest CT rather than plain films to rule out pulmonary metastases.

Fig. 26.7 (**a–g**) Desmoid-type fibromatosis in the thigh in a 47-year-old male: (**a**) axial fat-suppressed T1-weighted MR image after gadolinium chelate. The relatively well-defined soft tissue mass shows inhomogeneous enhancement. The non-enhancing area demonstrated low signal intensity on all pulse sequences; (**b**) 3 months after resection, axial fat-suppressed T1-weighted MR image after gadolinium chelate reveals a postoperative seroma; (**c**, **d**) 12 months after resection, axial and coronal fat-suppressed T1-weighted MR image after gadolinium chelate. Spontaneous regression of the postoperative seroma but appearance of new small intramuscular enhancing nodules suggestive of multifocal recurrence (*arrow*); (**e**, **f**) the nodules were identified on ultrasound as hypoechoic soft tissue masses; (**g**) ultrasound-guided histological Tru-Cut biopsy was performed and recurrence of desmoid-type fibromatosis was confirmed

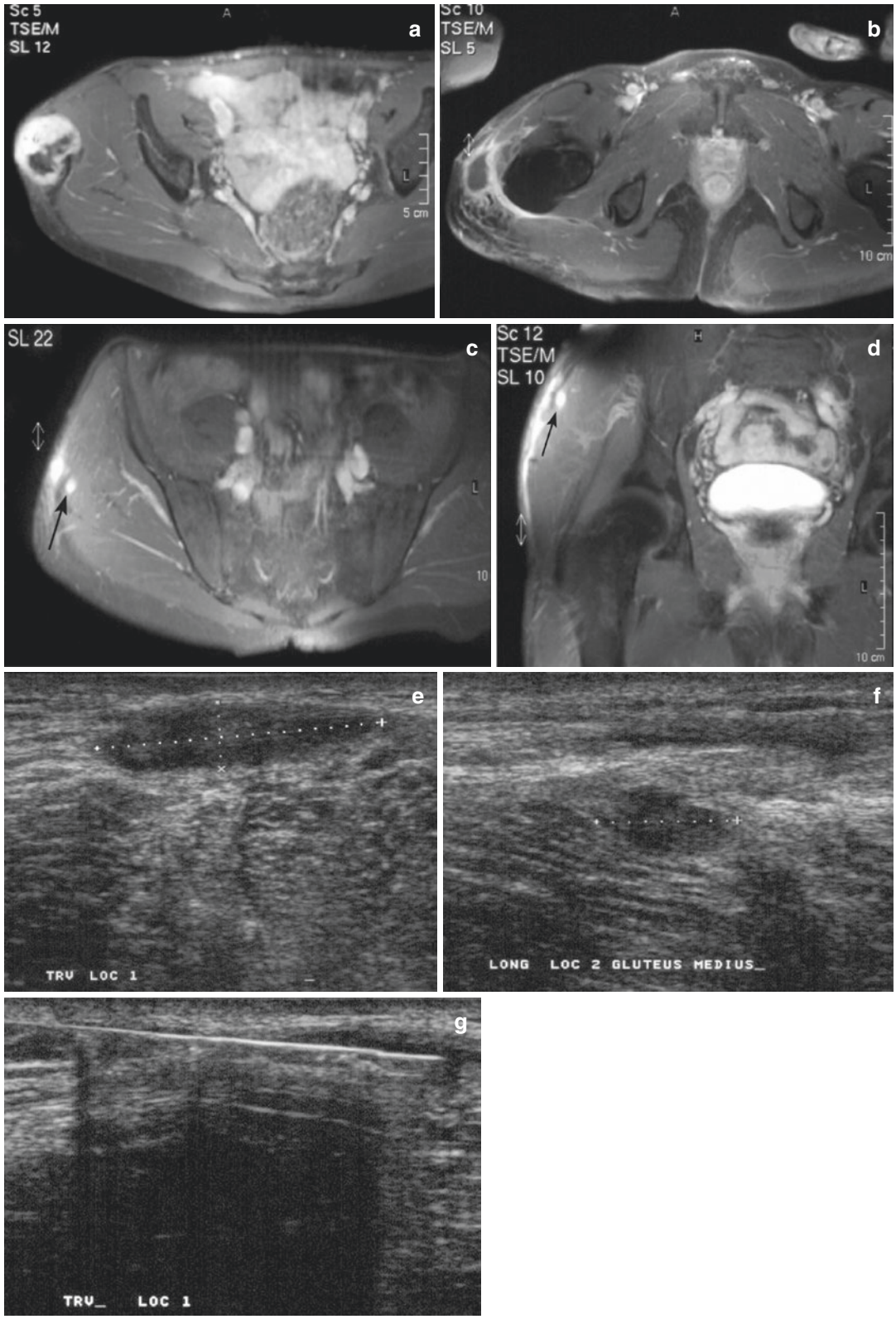
Sc 5
TSE/M
SL 12
a
5 cm
Sc 10
TSE/M
SL 5
b
10 cm
SL 22
c
10
Sc 12
TSE/M
SL 10
d
10 cm
e
TRU LOC 1
f
LONG LOC 2 GLUTEUS MEDIUS
g
TRU LOC 1

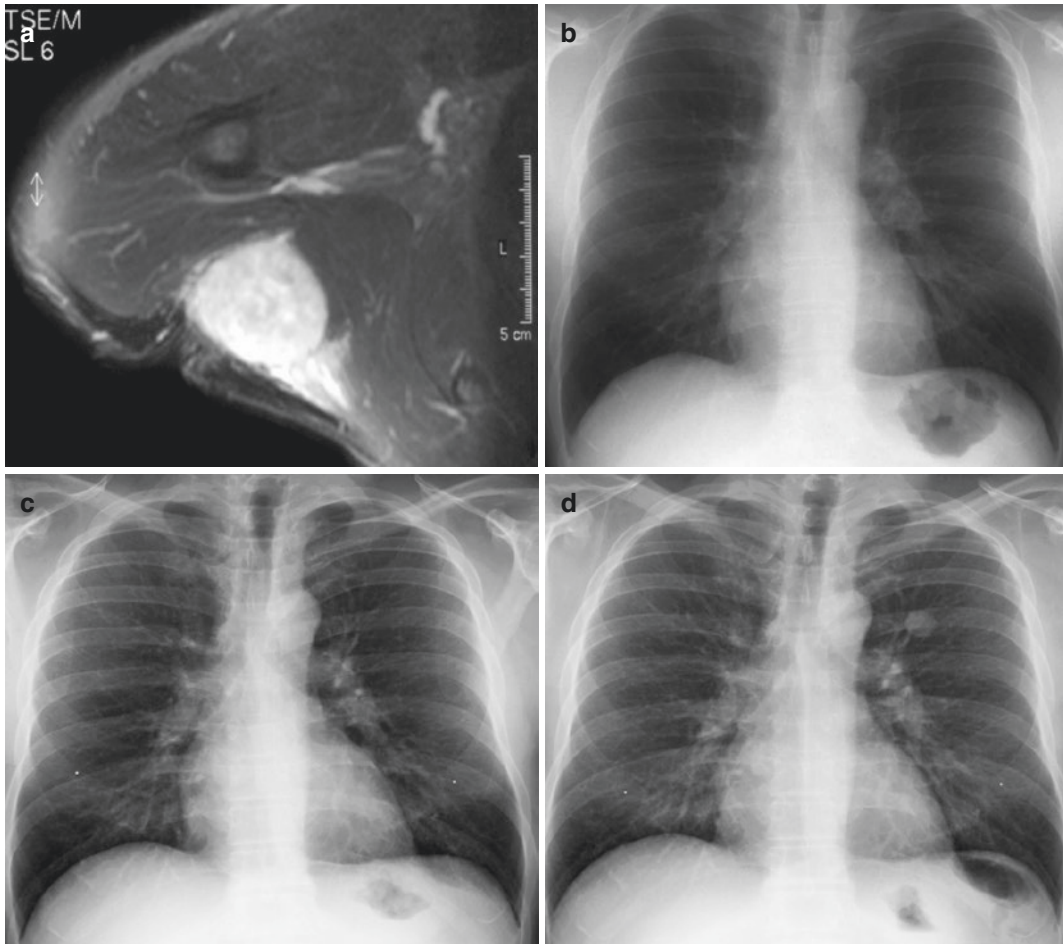

Fig. 26.8 (**a–d**) Myxofibrosarcoma of the axilla in a 42-year-old man: (**a**) fat-suppressed axial T2-weighted MR image of the axilla. Staging chest CT at time of diagnosis demonstrated no lung metastases; (**b**) 3 weeks after resection, normal chest radiograph; (**c**) 3 months after resection, normal chest radiograph; (**d**) 6 months after resection, a new solitary lung nodule in the left upper lobe is demonstrated. Metastasectomy was performed

Key Points

1. Therapy-induced changes in normal tissue can be quite extensive but can be diagnosed by combining imaging findings (morphology, location, MR signal intensities) with information on tumor therapy and supportive therapy including timing of therapeutic interventions.
2. Monitoring response of sarcomas to therapy is complicated because of spontaneous and therapy-induced change of biologic behavior of sarcomas. Functional imaging, including dynamic Gd-chelate-enhanced MR, diffusion MR, MRS, and PET-CT, is in the process of replacing volume-based assessments such as RECIST 1.1.
3. Clinical evaluation based on attention to the clinical history (pain, swelling) and physical examination seems to be a reliable initial method in local surveillance strategies. A rational and practical surveillance algorithm should include routine office visits every 4 months for 2

years, every 6 months for 3 years, and then annually. When the initial tumor site is difficult to palpate (retroperitoneum, ENT area), when the tumor is not bulky in presentation (no pseudocapsule such as desmoid-type fibromatosis), or when there is clinical suspicion, MR imaging or PET-CT (when the initial tumor was FDG active) is indicated. In other situations the role of MR imaging is based on consensus and not on proof of added value. Most organizations advise MR imaging annually or biannually, depending on grade and margins, for the first 2–3 years. For metastases, chest radiographs or low-dose pulmonary CT is indicated. In case of local recurrence, PET-CT probably is an effective method to diagnose locoregional extent of disease.

4. MR obtained 3–6 months following local therapy may be useful in defining posttreatment situation in order to facilitate interpretation of later MR examinations.
5. CT is superior to PET-CT in detecting or excluding pulmonary metastases.

Acknowledgment The input of Dr. Yvonne van Schrage (surgery), Dr. Stijn Krol (radiotherapy), and Prof. Judith Bovee (pathology) is greatly appreciated.

References

1. Zagars GK, Ballo MT, Pisters PW et al (2003) Prognostic factors for patients with localized soft-tissue sarcoma treated with conservation surgery and radiation therapy: an analysis of 225 patients. Cancer 97(10):2530–2543
2. Huth JF, Eilber FR (1988) Patterns of metastatic spread following resection of extremity soft-tissue sarcomas and strategies for treatment. Semin Surg Oncol 4(1):20–26
3. Gibbs JF, Lee RJ, Driscoll DL, McGrath BE, Mindell ER, Kraybill WG (2000) Clinical importance of late recurrence in soft-tissue sarcomas. J Surg Oncol 73(2):81–86
4. Lewis JJ, Leung D, Casper ES, Woodruff J, Hajdu SI, Brennan MF (1999) Multifactorial analysis of long-term follow-up (more than 5 years) of primary extremity sarcoma. Arch Surg 134(2):190–194
5. Gerrand CH, Bell RS, Wunder JS et al (2003) The influence of anatomic location on outcome in patients with soft tissue sarcoma of the extremity. Cancer 97(2):485–492
6. Karmazyn B, Cohen MD, Jennings SG, Robertson KA (2012) Marrow signal changes observed in follow-up whole-body MRI studies in children and young adults with neurofibromatosis type 1 treated with imatinib mesylate (Gleevec) for plexiform neurofibromas. Pediatr Radiol 42:1218–1222
7. Campiotti L, Codari R, Appio L, Ultori C, Solbiati F, Maria GA, Venco A (2007) Bone marrow necrosis related to imatinib mesylate therapy for cml bilineal blast crisis. Leuk Res 31:1768–1770
8. Meyer JM, Perlewitz KS, Hayden JB et al (2013) Phase I trial of preoperative chemoradiation plus sorafenib for high-risk extremity soft tissue sarcomas with dynamic contrast-enhanced MRI correlates. Clin Cancer Res 19:6902–6911
9. Roberge D, Skamene T, Nahal A et al (2010) Radiological and pathological response following pre-operative radiotherapy for soft-tissue sarcoma. Radiother Oncol 97:404–407
10. Wardelmann E, Haas RL, Bovée JV, Terrier P, Lazar A, Messiou C, LePechoux C, Hartmann W, Collin F, Fisher C, Mechtersheimer G, DeiTos AP, Stacchiotti S, Jones RL, Gronchi A, Bonvalot S (2016) Evaluation of response after neoadjuvant treatment in soft tissue sarcomas; the European Organization for Research and Treatment of Cancer-Soft Tissue and Bone Sarcoma Group (EORTC-STBSG) recommendations for pathological examination and reporting. Eur J Cancer 53:84–95. doi:10.1016/j.ejca.2015.09.021, Epub 2015 Dec 14
11. Miki Y, Ngan S, Clark JCM et al (2010) The significance of size change of soft tissue sarcoma during preoperative radiotherapy. Eur J Surg Oncol 36: 678–683
12. Messiou C, Bonvalot S, Gronchi A, Vanel D, Meyer M, Robinson P, Morosi C, Bloem JL, Terrier PH, Lazar A, Le Péchoux C, Wardelman E, Winfield JM, Boulet B, Bovée J, Haas RL (2016) Evaluation of response after pre-operative radiotherapy in soft tissue sarcomas; the European Organisation for Research and Treatment of Cancer - Soft Tissue and Bone Sarcoma Group (EORTC - STBSG) and Imaging Group recommendations for radiological examination and reporting with an emphasis on magnetic resonance imaging. Eur J Cancer 56:37–44. doi:10.1016/j.ejca.2015.12.008, Epub 2016 Jan 20
13. Costelloe CM, Chuang HH, Madewell JE et al (2010) Cancer response criteria and bone metastases: RECIST 1.1, MDA and PERCIST. J Cancer 1:80–92
14. Bloem JL, Reiser MF, Vanel D (1990) Magnetic resonance contrast agents in the evaluation of the musculoskeletal system. Magn Reson Q 6:136–163

15. Li SP, Padhani AR (2012) Tumor response assessments with diffusion and perfusion MRI. J Magn Reson Imaging 35:745–763
16. Sheikhbahaei S, Marcus C, Hafezi-Nejad N, Taghipour M, Subramaniam RM (2015) Value of FDG PET/CT in patient management and outcome of skeletal and soft tissue sarcomas. PET Clin 10(3):375–393. doi:10.1016/j.cpet.2015.03.003, Epub 2015 Apr 16
17. Vallières M, Freeman CR, Skamene SR, El Naqa I (2015) A radiomics model from joint FDG-PET and MRI texture features for the prediction of lung metastases in soft-tissue sarcomas of the extremities. PET Clin 10(3):375–393. doi:10.1016/j.cpet.2015.03.003, Epub 2015 Apr 16
18. van der Woude HJ, Bloem JL, Schipper J et al (1994) Changes in tumor perfusion induced by chemotherapy in bone sarcomas: color Doppler flow imaging compared with contrast-enhanced MR imaging and three-phase bone scintigraphy. Radiology 191:421–431
19. Verstraete KL, De Deene Y, Roels H et al (1994) Benign and malignant musculoskeletal lesions: dynamic contrast-enhanced MR imaging—parametric "first-pass" images depict tissue vascularization and perfusion. Radiology 192:835–843
20. Egmont-Petersen M, Hogendoorn PC, van der Geest RJ et al (2000) Detection of areas with viable remnant tumor in postchemotherapy patients with Ewing's sarcoma by dynamic contrast-enhanced MRI using pharmacokinetic modeling. Magn Reson Imaging 18: 525–535
21. Oka K, Yakushiji T, Sato H et al (2010) The value of diffusion-weighted imaging for monitoring the chemotherapeutic response of osteosarcoma: a comparison between average apparent diffusion coefficient and minimum apparent diffusion coefficient. Skeletal Radiol 39:141–146
22. Schnapauff D, Zeile M, Niederhagen MB et al (2009) Diffusion-weighted echo-planar magnetic resonance imaging for the assessment of tumor cellularity in patients with soft-tissue sarcomas. J Magn Reson Imaging 29:1355–1359
23. Padhani AR, Liu G, Koh D-M et al (2009) Diffusion-weighted magnetic resonance imaging as a cancer biomarker: consensus and recommendations. Neoplasia 11:102–125
24. Taylor GA, Perlman EJ, Scherer LR et al (1991) Vascularity of tumors in children: evaluation with color Doppler imaging. AJR Am J Roentgenol 157: 1267–1271
25. Kiessling F, Krix M, Heilmann M et al (2003) Comparing dynamic parameters of tumor vascularization in nude mice revealed by magnetic resonance imaging and Doppler sonography. Invest Radiol 38:516–524
26. van der Woude HJ, Bloem JL, van Oostayen JA et al (1995) Treatment of high-grade bone sarcomas with neoadjuvant chemotherapy: the utility of sequential color Doppler sonography in predicting histopathologic response. AJR Am J Roentgenol 165:125–133
27. Becher S, Oskouei S (2015) Pet imaging in sarcoma. Orthop Clin North Am. 46(3):409–415, xi. doi:10.1016/j.ocl.2015.03.001. Epub 2015 Apr 11
28. Benz MR, Tchekmedyian N, Eilber FC et al (2009) Utilization of positron emission tomography in the management of patients with sarcoma. Curr Opin Oncol 21:345–351
29. Gaston LL, Di Bella C, Slavin J et al (2011) 18F-FDG PET response to neoadjuvant chemotherapy for Ewing sarcoma and osteosarcoma are different. Skeletal Radiol 40:1007–1015. Nucl Med Rev Cent East Eur. 2016;19(1):22–27. doi:10.5603/NMR.2016.0005
30. Dancheva Z, Bochev P, Chaushev B, Yordanova T, Klisarova A (2015) Dual-time point 18FDG-PET/CT imaging may be useful in assessing local recurrent disease in high grade bone and soft tissue sarcoma. Phys Med Biol 60(14):5471–5496. doi:10.1088/0031-9155/60/14/5471, Epub 2015 Jun 29
31. Vallières M, Freeman CR, Skamene SR, El Naqa I (2015) A radiomics model from joint FDG-PET and MRI texture features for the prediction of lung metastases in soft-tissue sarcomas of the extremities. Clin Imaging 39(5):866–870. doi:10.1016/j.clinimag.2015.05.014, Epub 2015 Jun 3
32. Schuler MK, Platzek I, Beuthien-Baumann B, Fenchel M, Ehninger G, van den Hoff J (2015) (18)F-FDG PET/MRI for therapy response assessment in sarcoma: comparison of PET and MR imaging results. Clin Imaging 39(5):866–870
33. Hongtao L, Hui Z, Bingshun W et al (2012) 18F-FDG positron emission tomography for the assessment of histological response to neoadjuvant chemotherapy in osteosarcomas: a meta-analysis. Surg Oncol 21: e165–e170
34. Noebauer-Huhmann IM, Weber MA, Lalam RK, Trattnig S, Bohndorf K, Vanhoenacker F, Tagliafico A, van Rijswijk C, Vilanova JC, Afonso PD, Breitenseher M, Beggs I, Robinson P, de Jonge MC, Krestan C, Bloem JL (2015) Soft tissue tumors in adults: ESSR-approved guidelines for diagnostic imaging. Semin Musculoskelet Radiol 19(5), e1. doi:10.1055/s-0036-1572350.Epub2016Feb
35. Singer S, Antman K, Corson JM, Eberlein TJ (1992) Long-term salvageability for patients with locally recurrent soft-tissue sarcomas. Arch Surg 127(5): 548–553
36. Trovik CS, Bauer HC, Alvegard TA et al (2000) Surgical margins, local recurrence and metastasis in soft tissue sarcomas: 559 surgically-treated patients from the Scandinavian Sarcoma Group Register. Eur J Cancer 36(6):710–716
37. Whooley BP, Gibbs JF, Mooney MM, McGrath BE, Kraybill WG (2000) Primary extremity sarcoma: what is the appropriate follow-up? Ann Surg Oncol 7(1):9–14
38. Kane JM III (2004) Surveillance strategies for patients following surgical resection of soft tissue sarcomas. Curr Opin Oncol 16(4):328–332

39. Patel SR, Zagars GK, Pisters PW (2003) The follow-up of adult soft-tissue sarcomas. Semin Oncol 30(3):413–416
40. Beitler AL, Virgo KS, Johnson FE, Gibbs JF, Kraybill WG (2000) Current follow-up strategies after potentially curative resection of extremity sarcomas: results of a survey of the members of the society of surgical oncology. Cancer 88(4):777–785
41. Davies AM, Vanel D (1998) Follow-up of musculoskeletal tumors. I Local recurrence. Eur Radiol 8(5):791–799
42. Goel A, Christy ME, Virgo KS, Kraybill WG, Johnson FE (2004) Costs of follow-up after potentially curative treatment for extremity soft-tissue sarcoma. Int J Oncol 25(2):429–435
43. National Guideline Clearinghouse. ACR Appropriateness Criteria® follow-up of malignant or aggressive musculoskeletal tumors. Available from: http://www.guideline.gov/content.aspx?id=32617
44. Grobmyer SR, Brennan MF (2003) Predictive variables detailing the recurrence rate of soft tissue sarcomas. Curr Opin Oncol 15(4):319–326
45. Cancer Research UK. Follow up for soft tissue sarcoma. Available from: http://www.cancerresearchuk.org/about-cancer/type/sarcoma/treatment/follow-up-for-soft-tissue-sarcoma
46. AMSOS (2015) Austrian Musculoskeletal Oncology Society. http://www.amsos.at
47. ESMO/European Sarcoma Network Working Group (2014) Soft tissue and visceral sarcomas: ESMO Clinical Practice Guidelines for diagnosis, treatment and follow-up. Ann Oncol 25(Suppl 3):iii102–iii112
48. Whooley BP, Mooney MM, Gibbs JF, Kraybill WG (1999) Effective follow-up strategies in soft tissue sarcoma. Semin Surg Oncol 17(1):83–87
49. Vanel D, Lacombe MJ, Couanet D, Kalifa C, Spielmann M, Genin J (1987) Musculoskeletal tumors: follow-up with MR imaging after treatment with surgery and radiation therapy. Radiology 164(1):243–245
50. Panicek DM, Schwartz LH, Heelan RT, Caravelli JF (1995) Non-neoplastic causes of high signal intensity at T2-weighted MR imaging after treatment for musculoskeletal neoplasm. Skeletal Radiol 24(3):185–190
51. Del Grande F, Subhawong T, Weber K, Aro M, Mugera C, Fayad LM (2014) Detection of soft-tissue sarcoma recurrence: added value of functional MR imaging techniques at 3.0 T. Radiology 271(2):499–511
52. Vanel D, Shapeero LG, Tardivon A, Western A, Guinebretiere JM (1998) Dynamic contrast-enhanced MRI with subtraction of aggressive soft tissue tumors after resection. Skeletal Radiol 27(9):505–510
53. Kole AC, Nieweg OE, van Ginkel RJ et al (1997) Detection of local recurrence of soft-tissue sarcoma with positron emission tomography using [18F]fluorodeoxyglucose. Ann Surg Oncol 4(1):57–63
54. Johnson GR, Zhuang H, Khan J, Chiang SB, Alavi A (2003) Role of positron emission tomography with fluorine-18-deoxyglucose in the detection of local recurrent and distant metastatic sarcoma. Clin Nucl Med 28(10):815–820
55. Vandevenne JE, De Schepper AM, De Beuckeleer L et al (1997) New concepts in understanding evolution of desmoid tumors: MR imaging of 30 lesions. Eur Radiol 7(7):1013–1019
56. Billingsley KG, Lewis JJ, Leung DH, Casper ES, Woodruff JM, Brennan MF (1999) Multifactorial analysis of the survival of patients with distant metastasis arising from primary extremity sarcoma. Cancer 85(2):389–395
57. Dancheva Z, Bochev P, Chaushev B, Yordanova T, Klisarova A (2016) Dual-time point 18FDG-PET/CT imaging may be useful in assessing local recurrent disease in high grade bone and soft tissue sarcoma. Nucl Med Rev Cent East Eur 19(1):22–27. doi:10.5603/NMR.2016.0005
58. Fleming JB, Cantor SB, Varma DG et al (2001) Utility of chest computed tomography for staging in patients with T1 extremity soft tissue sarcomas. Cancer 92(4):863–868

Index

A
Abdominal fibromatosis (abdominal desmoids), 275–276
Abrikossoff tumors. *See* Granular cell tumors (GCTs)
Abscess
  diffusion MRI, 108
  inflammatory and infectious lesions, 528–529
  intramuscular, 529
Accessory breast, 526
Accessory palmaris longus muscle, 524
Accessory soleus muscle, 524
Acral fibromyxoma (AFM), 428, 433
Acromioclavicular (AC) joint, 564, 566
Adenocarcinoma, 138, 594
Adipocytic tumors
  benign
    angiolipoma, 211–212
    chondroid lipoma, 213–215
    fibrolipoma, 221
    hibernoma, 217–220
    lipoblastoma, 210–211
    lipoma, 198–203
    lipomatosis, 203–208
    myolipoma of soft tissue, 212–213
    nerve, lipomatosis of, 208–210
    ossifying lipoma, 221
    osteolipoma, 221
    parosteal lipoma, 221–225
    pleomorphic lipoma, 215–217
    spindle cell lipoma, 215–217
    tendon sheath and joint lipoma, 221
  differential diagnosis, 237–238
  intermediate (locally aggressive), 225–230
  malignant, 230–232
    dedifferentiated liposarcoma, 232
    liposarcoma, not otherwise specified, 237
    myxoid liposarcoma, 232–237
    pleomorphic liposarcomas, 237
  MRI role, 198
  WHO classification, 188
Adiposis dolorosa, 207–208
Adult fibrosarcoma, 292–293
Adventitial cystic disease, 562
AJCC manual for staging cancer, 145–146, 587
Alveolar rhabdomyosarcoma, 347–348, 351
Alveolar soft part sarcoma
  definition, 454
  imaging, 454–458
  incidence and clinical behavior, 454
  left thigh, 454–456
  of thoracic spine, 456, 457
American Joint Committee on Cancer (AJCC), 145, 188
Amputation neuroma, 545, 546
Amyloidosis, 12–14
Angioleiomyoma
  clinical findings, 358
  definition, 358
  imaging, 358–359
  vascular leiomyoma /angiomyoma, 21–24
Angiolipoma, 211–212
Angiomatoid fibrous histiocytoma (AFH)
  definition, 439
  imaging, 439, 440
  incidence and clinical behavior, 439
Angiomyolipoma (AML), 473
Angiomyxoma, aggressive
  definition, 434
  imaging, 434–435
  incidence and clinical behavior, 434
  paravaginal, 434–435
Angiosarcoma, 370, 371
Apparent diffusion coefficient (ADC), 409, 414, 434, 637, 638
Armed Forces Institute of Pathology (AFIP), 324
Arteriovenous malformations (AVMs)
  calf, 382
  definition, 381
  dynamic opacification, 384
  histology of, 381
  of knee, 382, 383
  magnetic resonance imaging, 382
  treatment for, 384
  ultra sound, 381–382
Arthrography, 513
Arthrosynovial cyst, 496–497
Articular and synovial sheath masses
  amyloidosis, 12–14
  synovial osteochondromatosis/synovial chondromatosis, 11
  tenosynovial giant cell tumor, 11–12

© Springer International Publishing AG 2017

F.M. Vanhoenacker et al. (eds.), *Imaging of Soft Tissue Tumors*, DOI 10.1007/978-3-319-46679-8

Askin's tumor, 465, 466. *See also* Primitive neuroectodermal tumors (PNET)
Atypical fibrous histiocytoma (AFH), 328
Atypical fibroxanthoma (AFX)
  definition, 437–438
  imaging, 439
  incidence and clinical behavior, 437–438

B
Baker's cyst, 497, 499
B-cell lymphoma, 588
  subcutaneous, 587
Benign adipocytic tumors
  angiolipoma, 211–212
  chondroid lipoma, 213–215
  fibrolipoma, 221
  hibernoma, 217–220
  lipoblastoma, 210–211
  lipoma, 198–203
  lipomatosis, 203–208
  myolipoma of soft tissue, 212–213
  nerve, lipomatosis of, 208–210
  ossifying lipoma, 221
  osteolipoma, 221
  parosteal lipoma, 221–225
  pleomorphic lipoma, 215–217
  spindle cell lipoma, 215–217
  tendon sheath and joint lipoma, 221
Benign cystic lesions
  arthrosynovial cyst, 496–497
  Baker's cyst, 496
  bursa de novo (adventitious bursa), 507–510
  clinical manifestations, 509–510
  ganglion (cyst), 497–507
  imaging
    arthrography/direct cyst puncture, 513
    conventional radiography, 510–511
    CT scan, 513
    MRI, 513–516
    ultrasound, 511–513
Benign fibroblastic/myofibroblastic tumors
  calcifying aponeurotic fibroma, 262
  desmoplastic fibroblastoma (collagenous fibroma), 262
  elastofibroma, 253–255
  fibroma of tendon sheath, 255–258
  ischemic fasciitis, 252–253
  myositis ossificans and fibroosseous pseudotumor of digits, 247–252
  nodular fasciitis, 245–247
  nuchal-type fibroma, 258–261
  proliferative myositis (and fasciitis), 247
Benign fibrous histiocytoma (BFH)
  clinical behaviour and gross findings, 325–327
  differential diagnosis, 328
  genetics, 328
  imaging findings, 328–330
  pathology, 327–328
Benign lesions
  acral fibromyxoma, 428
  deep ("aggressive") angiomyxoma, 434–435
  ectopic hamartomatous thymoma, 436–437
  intramuscular myxoma (incl. cellular variant), 426–428
  juxta-articular myxoma, 428–430
  myxoma, of Jaws, 430–434
  pleomorphic hyalinizing angiectatic tumor, 435–436
Benign triton tumors, 411
Benign vascular tumors
  congenital hemangioma, 366–369
  epithelioid hemangioma, 368
  infantile hemangioma, 365–368
Bilateral vestibular schwannomas, 419
Biopsy
  diagnostic accuracy, 133–138
  immunohistochemistry, 138
  intra-*versus* extra-compartmental spread, 131–133
  needle, technique and choice of, 138–139
  open surgical biopsy, 135
  safety rules, 133
Biphasic synovial sarcoma, 445
Budd–Chiari syndrome, 342
Bursa, 508
Bursa de novo (adventitious bursa), 507–510
Bursitis, 536

C
Calcific myonecrosis, 551, 552
Calcific tendinosis, 556–558, 560
Calcifying aponeurotic fibroma, 262
Calcium pyrophosphate dihydrate crystals (CPPD), 556
Capillary malformations (CMs), 381
Cardiac rhabdomyoma, 345
Carney's syndrome, 395
Carney–Stratakis syndrome, 614
Carney triad syndrome, 614
Catheter angiography, 553
Cat scratch disease
  central necrosis, 539
  computed tomography (CT), 539
  definition, 538
  epitrochlear mass, 539
  location, 538
  polymerase chain reaction, 540
  Rochalimae henselae, 538
Cellulitis, 527
Chondroid lipoma, 213–215
Chondro-osseous soft tissue tumors
  extraskeletal osteosarcoma, 609–611
  soft tissue chondroma, 604–605
  synovial osteochondromatosis, 605–610
  WHO classification, 192–193
Choroid melanoma, 596
Chronic bursitis, 512, 513
Classification of Tumors of Soft Tissue and Bone, 393
Claudicatio intermittens, 562, 563

Clear cell myomelanocytic tumor (CCMMT)
definition, 473
imaging, 473–475
incidence and clinical behavior, 473
Clear cell sarcoma
clinical behavior, 459
definition, 458–459
imaging, 459–460
incidence, 459
Collagen 6A3 (COL6A3) gene, 315
Color Doppler ultrasound (CDUS)
characteristics, 5–11
principles, 4
superficial soft tissue tumors, 11
tumorlike lesions, 11
Computed tomography (CT), 60
features, 49–51
vs. MRI, 51–55
Computed tomography pulmonary angiography (CTPA), 53
Congenital hemangioma (CH)
noninvoluting, 366–369
partially involuting, 368
rapidly involuting, 366
Contrast-enhanced MRI
fat-suppressed contrast-enhanced T1-weighted imaging, 79–81
static *vs.* dynamic enhanced MRI, 81
subtraction images, 81
T1-weighted imaging, 79
Conventional anatomical MR imaging, 414
Conventional imaging modalities (CIMs), 63
Conventional radiography, 60
Core needle biopsy (CNB), 133
CSF1 gene, 315
Cyst. *See* Ganglion (cyst)
Cytogenetics, 124

D
DCE. *See* Dynamic contrast-enhanced (DCE) MR imaging
Dercum disease, 207–208
Dermal nerve sheath myxomas (DNSMs), 411
Dermatofibrosarcoma protuberans, 282–285
Desmoid tumors, extra-abdominal, 269–275
Desmoid-type fibromatoses
of pelvis, 644
in thigh, 646
Desmoplastic fibroblastoma (collagenous fibroma), 262
Desmoplastic small round cell tumor (DSRCT), 462, 464
Diabetes mellitus, 530
Diabetic muscle infarction, 535–536
Diagnostic algorithm, 181–182
Diffuse giant cell tumours (D-GCT)
clinical behaviour and gross findings, 320–321
differential diagnosis, 322
epidemiology, 320
imaging findings, 321–322
pathology, 321
Diffuse neurofibromas, 405
Diffuse-type tenosynovial giant cell tumour (D-TSGCT)
clinical behaviour and gross findings, 320–321
differential diagnosis, 322–323
epidemiology
diffuse giant cell tumours, 320
pigmented villonodular synovitis, 320
genetics, 321
imaging findings, 321–322
pathology, 321
Diffusion MRI
clinical applications, 108–109
imaging technique, 106
qualitative, 106
quantitative, 106–107
Diffusion tensor imaging (DTI), 416
Diffusion weighted imaging (DWI), 414, 434
sarcoidosis, 537
soft tissue metastases, 597
Distal denervation muscle atrophy, 546
DWI. *See* Diffusion weighted imaging (DWI)
Dynamic contrast-enhanced MRI
clinical applications, 101–105
evaluation and postprocessing techniques, 88–101
imaging techniques, 87–88
principles, 85–87
Dynamic contrast-enhanced (DCE) MR imaging, 414, 637, 641
Dystrophic calcification
soft tissue mineralization disorders, 35

E
Ectopic hamartomatous thymoma (EHT)
definition, 436
imaging, 436
incidence and clinical behavior, 436
Ectopic meningiomas, 412
Elastofibroma, 253–255
Elastofibroma dorsi
computed tomography, 566
definition, 564
differential diagnosis, 566–568
left periscapular soft tissue mass, 567
locations, 564
magnetic resonance imaging, 566
ultrasound, 566
Embryonal rhabdomyosarcoma, 347, 353, 624
Enchondromas, 388
End-bulb neuromas (EBN). *See* Traumatic neuroma
Epidermal inclusion cysts, 555–557
Epithelioid hemangioendothelioma (EH), 370
Epithelioid hemangioma, 368
Epithelioid sarcoma
definition, 451
imaging, 452–454
incidence and clinical behavior, 451–452
in lumbar paraspinal region, 453
European Society for Medical Oncology (ESMO), 154

European Society of Musculoskeletal Radiology (ESSR), 155
External beam radiotherapy, 321
Extra-abdominal desmoid tumors, 269–275
Extracardiac rhabdomyoma
  clinical findings, 345
  definition, 345
  imaging, 345, 347
Extrapleural solitary fibrous tumor, 285
Extrarenal rhabdoid tumors (ERRTs)
  definition, 469
  imaging, 473, 474
  incidence and clinical behavior, 472
Extraskeletal chondroma
  of foot, 604
  at popliteal fossa, 607
  right patella, 604, 605
Extraskeletal Ewing's sarcoma
  definition, 467–468
  imaging characteristics, 469–472
  incidence and clinical behavior, 468–469
  of left thigh, 470, 471
  of pelvis, 469
Extraskeletal myxoid chondrosarcoma (EMC), 461, 603
Extraskeletal osteochondroma, 604, 607
Extraskeletal osteosarcoma
  definition, 609
  imaging, 611
  incidence and clinical behavior, 609–611
  of thigh, 611, 613

F

Fascicular sign, 400
Fat necrosis, US findings, 33–34
Fat-suppressed T1-weighted imaging (FS T1-WI)
  contrast-enhanced, 79–81
  unenhanced MRI, 76–77
Fetal rhabdomyoma, 345
^{18}F-Fluorodeoxyglucose positron emission tomography (^{18}F-FDG PET), 60
^{18}F-Fluorodeoxyglucose positron emission tomography-computed tomography (^{18}F-FDG PET-CT), 487, 489, 597
Fibroblastic/myofibroblastic tumors
  abdominal fibromatosis (abdominal desmoids), 275–276
  benign proliferations
    calcifying aponeurotic fibroma, 262
    desmoplastic fibroblastoma (collagenous fibroma), 262
    elastofibroma, 253–255
    fibroma of tendon sheath, 255–258
    ischemic fasciitis, 252–253
    myositis ossificans and fibroosseous pseudotumor of digits, 247–252
    nodular fasciitis, 245–247
    nuchal-type fibroma, 258–261
    proliferative myositis (and fasciitis), 247
  extra-abdominal desmoid tumors, 269–275
  fibromatoses, 262–265
  infancy and childhood, fibrous tumors
    fibromatosis colli, 279–282
    fibrous hamartoma, 276–278
    infantile digital fibromatosis, 278
    juvenile hyaline fibromatosis, 278–279
  intermediate-grade
    dermatofibrosarcoma protuberans, 282–285
    extrapleural solitary fibrous tumor, 285
    infantile fibrosarcoma, 289–291
    inflammatory myofibroblastic tumor, 285
    low-grade myofibroblastic sarcoma, 285–286
    myxoinflammatory fibroblastic sarcoma, 286–289
  knuckle pads, 269
  lipofibromatosis, 276
  malignant
    adult fibrosarcoma, 292–293
    low-grade fibromyxoid sarcoma, 295–299
    myxofibrosarcoma, 293–295
    sclerosing epithelioid fibrosarcoma, 299–302
  palmar fibromatosis, 265–266
  plantar fibromatosis, 266–269
  US findings, 29–32
  WHO classification, 188–189
Fibrohistiocytic tumours (so-called)
  fibrous histiocytoma, deep benign, 325–328
  intermediate (rarely metastasising)
    giant cell tumour of soft tissue, 331–332
    plexiform fibrohistiocytic tumour, 328–331
  tenosynovial giant cell tumour
    diffuse-type, 320–324
    localised type, 312–320
    malignant-type, 324–325
  WHO classification, 189–190
Fibrolipoma, 221
Fibroma
  nuchal-type, 258–261
  of tendon sheath, 255–258
Fibroma of the tendon sheath (FTS), 320
Fibromatosis, 262–265
  palmar, 265–266
  plantar, 266–269
Fibromatosis colli, 625
fibroosseous pseudotumor, digits, 247–252
Fibrosarcoma, 627
Fibrous tumors, infancy and childhood
  fibromatosis colli, 279–282
  fibrous hamartoma, 276–278
  infantile digital fibromatosis, 278
  juvenile hyaline fibromatosis, 278–279
Fine-needle aspiration biopsy (FNAB), 133, 590
Fluid-sensitive sequences, 77–78
Fluorescence in situ hybridization (FISH), 124, 591
Focal myositis, 535
Follow-up imaging
  locoregional recurrence, 643–646
  metastases, 646–648
  monitoring response, to therapy, 636–643
  therapy-induced changes, in normal tissue, 636
  volume measurements, 636

Foreign body reactions, 549–551
Fraction anisotropy (FA), 416
Frozen section role, 118
Functional MR imaging, 414–416

G
Ganglion (cyst)
adventitial cystic disease, 497, 500
of anterior cruciate ligament, 505, 507
benign cystic lesions, 497
dorsum, of foot, 501, 502
intramuscular, 503
of left hip, 504, 506
in lower leg, 499, 501
meniscal cyst, 503, 504
para-articular cyst, 497, 498
pathogenesis of, 497
of proximal tibiofibular joint, 501, 503
in spinoglenoid notch of shoulder, 504, 505
US finding, 27–28
on wrist, 501, 502
Gas gangrene, 529
Gastrointestinal stromal tumors (GISTs), 603
definition, 611, 613
histopathology, 614
imaging features, 614–617
incidence and clinical behavior, 613–614
prognosis, 617
of small bowel, 614, 617
of stomach, 614, 615
treatment, 617, 618
WHO classification, 193
Gd-chelate-enhanced imaging, 637
Genetics role, 122, 126
Genital rhabdomyoma, 345
Geyser phenomenon, 564, 566
Giant B-cell lymphoma, 579, 580
Giant cell tumor. *See* Pigmented villonodular synovitis (PVNS)
Giant cell tumour of soft tissue (GCT-ST), 330
Giant cell tumour of the tendon sheath (GCTTS)
clinical behaviour and gross findings, 314
differential diagnosis, 320
epidemiology, 312
imaging findings
computer tomography, 319
magnetic resonance imaging, 319
radiographs, 315
scintigraphy, 319
ultrasound, 315–319
pathology, 314
Glomangiomatosis
clinical findings, 349–350
definition, 349
of forearm, 356
imaging, 350–351
Glomus tumor (GT), 384, 385
clinical findings, 348–349
definition, 348
imaging, 349
of upper extremity, 355
US finding, 20–21
Glucose transporter protein-1 (GLUT1), 366
Gout, 556, 559
Grading
combined parameters, 164–165
individual parameters, 162–164
World Health Organization (WHO), 162
Granular cell tumors (GCTs), 411
Granuloma annulare, 554–555, 626
Granulomatous disorders
cat scratch disease, 538–541
injection granulomas, 540–541
mycetoma, 541–543
sarcoidosis, 536–538
tuberculous osteomyelitis, 536, 537

H
Haemosiderin, 313, 314, 322
Hematoma
acute, 545–547
biopsy, 547
of calf, 546, 548
computed tomography, 546
contusion, 545
diffusion MRI, 108
hemosiderin, 547
magnetic resonance imaging, 546
muscle contraction, dynamic evaluation, 545–546
Hemosiderotic fibrolipomatous tumor (HFLT)
definition, 437
imaging, 437, 439
incidence and clinical behavior, 437
Hereditary hemorrhagic telangiectasia. *See* Rendu–Osler–Weber syndrome
Hibernoma, 217–220
Human herpesvirus-8 (HHV-8), 369
Hybrid nerve sheath tumors, 411
Hypothenar hammer syndrome, 551–553

I
Infancy and childhood, fibrous tumors
fibromatosis colli, 279–282
fibrous hamartoma, 276–278
infantile digital fibromatosis, 278
juvenile hyaline fibromatosis, 278–279
Infantile fibrosarcoma, 289–291
Infantile hemangioma (IH), 629
of cheek, 366, 368
glucose transporter protein-1, 366
involuting phase, 365–366
magnetic resonance imaging, 366
in posterior cervical neck, 366, 367
proliferative phase, 365, 366
treatment, 366
Infantile myofibromatosis, 355, 357. *See also* Myofibromatosis

Infantile rhabdomyosarcoma, 628
Inflammatory and infectious lesions
  abscess, 528–529
  bursitis, 536
  cellulitis, 527
  diabetic muscle infarction, 535–536
  focal myositis, 535
  granulomatous disorders, 536–541
  lymphedema and lymphangitis, 528
  muscular cystic echinococcosis, 532–534
  necrotizing fasciitis, 527
  pyomyositis, 529–532
Inflammatory myofibroblastic tumor, 285
Infrapatellar (Hoffa) fat pad, 312, 313
Injection granulomas, 540–541
Intermediate (locally aggressive) adipocytic tumors, 225–230
Intermediate and malignant vascular tumors
  angiosarcoma, 370, 371
  epithelioid hemangioendothelioma, 370
  kaposiform hemangioendothelioma, 368–369
  Kaposi's sarcoma, 369–370
Intermediate-grade fibroblastic/myofibroblastic tumors
  dermatofibrosarcoma protuberans, 282–285
  extrapleural solitary fibrous tumor, 285
  infantile fibrosarcoma, 289–291
  inflammatory myofibroblastic tumor, 285
  low-grade myofibroblastic sarcoma, 285–286
  myxoinflammatory fibroblastic sarcoma, 286–289
Intermediate tumors (rarely metastasising)
  angiomatoid fibrous histiocytoma, 439, 440
  atypical fibroxanthoma, 437–439
  giant cell tumour of soft tissue
    clinical behaviour and gross findings, 331
    differential diagnosis, 332
    genetics, 332
    imaging findings, 332
    pathology, 331–332
  mixed tumor, 440, 441
  ossifying fibromyxoid tumor, 439–441
  phosphaturic mesenchymal tumor, 443, 444
  plexiform fibrohistiocytic tumour
    clinical behaviour and gross findings, 329
    differential diagnosis, 330–331
    genetics, 329
    imaging findings, 330
    pathology, 329
International Society for the Study of Vascular Anomalies (ISSVA), 364–365
International Working Formulation (IWF), 578
Interstitial cells of Cajal (ICC), 611, 613
Intimal sarcoma
  definition, 475–476
  imaging, 476
  incidence and clinical behavior, 476
Intramuscular abscess, 529
Intramuscular myxoma (incl. cellular variant)
  in autochthonous back muscles, 427, 432
  of calf, 427, 429
  definition, 426
  imaging
    computed tomography, 427
    magnetic resonance imaging, 427
  incidence and clinical behavior, 426–427
  with polyostotic fibrous dysplasia, 427, 430, 431
  right scapular region, 427, 428
Intratumoral signal void, 625, 629
Intravascular lymphomatosis (IL), 579
Ischemic fasciitis, 252–253

J
Juxta-articular myxoma, 428–430

K
Kaposiform hemangioendothelioma (KHE), 368–369
Kaposi's sarcoma (KS), 369–370
Kasabach–Merritt syndrome, 369, 370, 386–387
Kiel Pediatric Tumor Registry, 623
Klippel–Trenaunay syndrome, 387–388
Knuckle pads, 269

L
Leiomyoma, of deep soft tissue
  clinical findings, 340
  definition, 340
  imaging, 341
Leiomyosarcoma
  clinical findings, 341–343
  cutaneous, 343
  deep soft tissue, 342
  definition, 341
  imaging, 343–345
  of inferior vena cava, 343
  in left thigh, 344
  of right knee, 345
  of right thigh, 346
  subcutaneous, 342, 343
  vascular, 342, 343
Light microscopy role
  histology, 119–120
  immunohistochemistry, 120–122
Lipoblastoma, 210–211
Lipofibromatosis, 276
Lipoma, 198–200
  chondroid, 213–215
  intermuscular, 200–203
  intramuscular, 200–203
  multiple, 203
  ossifying, 221
  parosteal, 221–225
  pleomorphic, 215–217
  spindle cell, 215–217
  tendon sheath and joint, 221
  US finding, 24–27

Lipoma arborescens, 516–518
Lipomatosis
  adiposis dolorosa, 207–208
  diffuse, 203
  multiple symmetrical, 204–207
  of nerve, 208–210
  shoulder girdle, 208
Liposarcoma
  after resection and radiotherapy of, 645
  dedifferentiated, 232
  myxoid, 232–237
  pleomorphic, 237
  well-differentiated, 225–230
Liposarcoma, not otherwise specified, 237
Localised nodular synovitis (LNS)
  clinical behaviour and gross findings, 314
  differential diagnosis, 320
  epidemiology, 312–316
  imaging findings
    computer tomography, 319
    magnetic resonance imaging, 313, 315, 319
    radiographs, 313, 316
    ultrasound, 316–317, 319
  pathology, 315
Localised tenosynovial giant cell tumour (Localised TSGCT)
  giant cell tumour of the tendon sheath
    clinical behaviour and gross findings, 314
    differential diagnosis, 320
    epidemiology, 312
    imaging findings, 315–319
    pathology, 314
  localised nodular synovitis
    clinical behaviour and gross findings, 314
    differential diagnosis, 320
    epidemiology, 312–316
    imaging findings, 313, 315–317, 319
    pathology, 315
Localized intravascular coagulopathy, 375
Localized neurofibromas, 405, 406
Locoregional recurrence, 643–646
Locus minoris resistentiae, 497
Long-standing denervation, 563
Low-grade fibromyxoid sarcoma, 295–299
Low-grade myofibroblastic sarcoma, 285–286
Lymphangioleiomyomatosis (LAM), 473–474
Lymphatic malformations (LMs)
  diagnosis, 377
  macrocystic, 376, 377, 379
  magnetic resonance imaging, 379–380
  microcystic, 376–379, 381
  pathology, 377
  ultrasound, 379
Lymphedema, 528

M

Macrocystic lymphatic malformations, 376, 377, 379
Maffucci syndrome, 388
Magnetic resonance imaging (MRI)
  adipocytic tumors, 198
  contrast-enhanced MRI
    fat-suppressed contrast-enhanced T1-weighted imaging, 79–81
    static *vs.* dynamic enhanced MRI, 81
    subtraction images, 81
    T1-weighted imaging, 79
  diffusion MRI
    clinical applications, 108–109
    imaging technique, 106
    qualitative, 106
    quantitative, 106–107
  dynamic contrast-enhanced MRI
    clinical applications, 101–105
    evaluation and postprocessing techniques, 88–101
    imaging techniques, 87–88
    principles, 85–87
  imaging planes, 72
  local staging, 71
  tissue characteristics, 72
  unenhanced MRI
    fat-suppressed T1-weighted imaging (FS T1-WI), 76–77
    fluid-sensitive sequences, 77–78
    T2* gradient echo imaging, 78–79
    T1-weighted imaging (T1-WI), 73–75
Malignant adipocytic tumors, 230–232
  dedifferentiated liposarcoma, 232
  liposarcoma, not otherwise specified, 237
  myxoid liposarcoma, 232–237
  pleomorphic liposarcomas, 237
Malignant fibroblastic/myofibroblastic tumors
  adult fibrosarcoma, 292–293
  low-grade fibromyxoid sarcoma, 295–299
  myxofibrosarcoma, 293–295
  sclerosing epithelioid fibrosarcoma, 299–302
Malignant fibrous histiocytoma (MFH), 189
Malignant glomus tumor
  clinical findings, 352
  definition, 352
  imaging, 352
Malignant lesions
  alveolar soft part sarcoma, 454–458
  clear cell myomelanocytic tumor, 473–475
  clear cell sarcoma of soft tissue, 458–460
  desmoplastic small round cell tumor, 462, 464
  epithelioid sarcoma, 451–454
  extrarenal rhabdoid tumor, 469–473
  extraskeletal myxoid chondrosarcoma, 461
  intimal sarcoma, 475–476
  malignant mesenchymoma, 461–462
  PNET/extraskeletal Ewing's sarcoma, 462–471
  synovial sarcoma, 443–451
Malignant mesenchymoma
  definition, 461
  imaging, 463
  incidence and clinical behavior, 462

Malignant peripheral nerve sheath tumors (MPNSTs)
clinical presentation, 413
epidemiology, 412
of face, 414, 415
histology, 412
imaging characteristics
magnetic resonance imaging, 414–417
nuclear medicine, 417
plain radiography, 413
ultrasound, 413–414
in left ischiorectal fossa, 414, 416
parapsoas, 414, 415
presacral, 413
topography, 412
Malignant-type tenosynovial giant cell tumour (Malignant TSGCT)
clinical behaviour and gross findings, 324
genetics, 324
imaging findings, 324, 327
pathology, 324
Maximum intensity projections (MIP), 514
Mazabraud's syndrome, 426, 427
McCune–Albright syndrome, 426
Mesenchymal chondrosarcoma (MCS)
of buttock, 612
definition, 608
imaging, 608–610
incidence and clinical behavior, 608
of left pectoralis minor, 612
of right axilla, 611
Metabolic lesions
calcific tendinosis, 556–557, 560
gout and pseudogout, 556, 558, 559
tumoral calcinosis, 557–562
Metabolic MR imaging, 417
Metastases, 646
Metastatic spread, of cancer, 518
Microcystic lymphatic malformations, 376–379, 381
Molecular studies role
diagnosis, 124–125
genetic alterations, 122–124
prognosis, 125
techniques, 124
treatment, 125–126
Monophasic epithelial synovial sarcoma, 445
Monophasic fibrous synovial sarcoma, 445
Morton's fibroma
definition, 542
elastography, 544
intermetatarsalgia, 543
magnetic resonance imaging, 544
Mulder's test, 544
treatment, 545
ultrasound, 543
Mucosa-associated lymphoid tissue (MALT) lymphomas, 578
Muscle herniations, 524, 525
Muscle tumors
pericytic (perivascular) tumors
angioleiomyoma, 358–359
glomangiomatosis, 349–352, 356
glomus tumor, 348–349, 355
malignant glomus tumor, 352
myofibroma and myofibromatosis, 355–358
myopericytoma, 354–355
skeletal
extracardiac rhabdomyoma, 345, 347
rhabdomyosarcoma, 345–354
smooth
leiomyoma of deep soft tissue, 340–341
leiomyosarcoma (excluding skin), 341–346
Muscular anomalies, 524
diagnosis of, 525
Muscular cystic echinococcosis
alveolar, 532
of calf, 533
computed tomography, 533
definition, 532
diabetic muscle infarction, 535–536
differential diagnosis, 535
focal myositis, 535
of left thigh, 533, 534
magnetic resonance imaging, 533
in right paravertebral muscles, 533, 534
ultrasonography, 533
Musculoskeletal Tumor Society (MSTS), 146
Mycetoma, 541–543
Mycosis fungoides, 579
Myoepithelioma
definition, 440
imaging, 441, 442
incidence and clinical behavior, 440–441
of left perineal/gluteal region, 442
Myofibromatosis
clinical findings, 355–357
definition, 355
imaging, 357–358
infantile, 355, 357
Myolipoma of soft tissue, 212–213
Myopericytoma
clinical findings, 354
definition, 354
imaging, 354–355
Myositis ossificans, 603
digits, 247–252
Myxofibrosarcoma, 293–295, 648
Myxoid liposarcoma, 232–237
Myxoid perineurioma, 409, 410
Myxoid tumors, 108–109
Myxoinflammatory fibroblastic sarcoma, 286–289
Myxoma, of jaws, 430–434

N

Nasal glial heterotopia (NGH), 412
Necrosis, 331
Necrotic tumors, 108
Necrotizing fasciitis, 527
Nephrotic syndrome, 579
Nerve, lipomatosis of, 208–210
Nerve-related tumorlike lesions, 16–19
Nerve sheath tumors
benign triton tumors, 411

dermal nerve sheath myxomas, 411
ectopic meningiomas, 412
granular cell tumors, 411
hybrid nerve sheath tumors, 411
malignant peripheral
clinical presentation, 413
epidemiology, 412
histology, 412
imaging characteristics, 413–417
topography, 412
nasal glial heterotopia, 412
neurofibromas
clinical presentation, 406
epidemiology, 405
histology, 405–406
imaging characteristics, 406–408
topography, 405
neurofibromatoses
type 1, 417–418
type 2, 418–419
perineurioma, 408–410
schwannomas
clinical presentation, 395–396
epidemiology, 394
histology, 394–395
imaging characteristics, 396–405
schwannomas, 394
topography, 394
schwannomatosis, 419–420
solitary circumscribed neuromas, 411
Neurofibromas
clinical presentation, 406
epidemiology, 405
histology, 405–406
imaging characteristics
computed tomography, 406–408
magnetic resonance imaging, 408
plain radiography, 406
ultrasound, 406, 407
topography, 405
Neurofibromatoses
type 1, 417–418
type 2, 418–419
Neuroma-in-continuity (NIC). *See* Traumatic neuroma
Nodular fasciitis, 245–247
Non-Hodgkin's lymphomas, 578
B-cell, 579, 580
diagnosis, 590
at left upper arm, 581, 584
of quadriceps muscle, 582
sciatic nerve, 584
Noninvoluting congenital hemangioma (NICH), 366–369
Nuchal-type fibroma, 258–261
Nuclear medicine, 417

O

Ossifying fibromyxoid tumor (OFMT), 194
definition, 439
imaging, 440, 441
incidence and clinical behavior, 440
Ossifying lipoma, 221
Osteochondromatosis, secondary, 515
Osteoclastoma. *See* Giant cell tumour of soft tissue (GCT-ST)
Osteolipoma, 221
Osteosarcoma, 596

P

Palmar fibromatosis, 265–266
Para-articular chondroma, 516
Parachordoma
definition, 441–442
imaging, 442
incidence and clinical behavior, 442
Parameniscal cyst, 428–430
Paravaginal aggressive angiomyxoma, 434, 435
Parkes Weber syndrome, 388
Parosteal lipoma, 221–225
Partially involuting congenital hemangioma (PICH), 368
Particular vascular lesions
glomus tumor, 384, 385
synovial hemangioma, 385, 386
Pathology grading and staging
common used grading classifications, 127
staging, 127–128
Pediatric soft tissue tumors
fibromatosis colli, 625
fibrosarcoma, 627
fluid-fluid levels, 625, 629
granuloma annulare, 626
imaging
MR, 630
plain film/CT, 630
roles, 624–625
ultrasound, 625–626
imaging tissue characterization, 630–631
infantile hemangioma, 629
infantile rhabdomyosarcoma, 628
intratumoral signal void, 625, 629
multiplicity, 625, 629
preferential location of, 624
shape, 625, 629
synovial sarcoma, 627
Pelvis syndrome, 386
Percutaneous musculoskeletal biopsy (PMSB), 133
Pericytic (perivascular) tumors
angioleiomyoma, 358–359
glomangiomatosis, 349–352, 356
glomus tumor, 348–349, 355
malignant glomus tumor, 352
myofibroma and myofibromatosis, 355–358
myopericytoma, 354–355
US finding
angioleiomyoma (vascular leiomyoma/angiomyoma), 21
glomus tumor, 20–21
WHO classification, 191
Perineurioma, 408–410
Peripheral arterial aneurysms, 564
Peripheral mineralisation, 331, 332

Peripheral nerve sheath tumors (PNSTs), 393, 396
US finding, 16
WHO classification, 193
Peripheral neurogenic tumors
nerve-related tumorlike lesions, 16–19
peripheral nerve sheath tumors, 16
US finding, 14–16
Phosphaturic mesenchymal tumor (PMT), 443, 444
Pigmented villonodular synovitis (PVNS), 11–12, 311, 312
clinical behaviour and gross findings, 320–321
differential diagnosis, 322
epidemiology, 320
imaging findings, 321–322
pathology, 321
Pilomatricoma, 554
US findings, 29
Plain films, 630
Plain radiography
angiography, 47–48
bone involvement, 45–47
location, 42
radiodensity, 43–45
rate of growth, 42
shape and margins, 43
size, 42
Plantar fibromatosis, 266–269
Pleomorphic hyalinizing angiectatic tumor (PHAT)
in calf, 436
definition, 435
in foot, 437
imaging, 436–438
incidence and clinical behavior, 435–436
of proximal upper extremity, 438
Pleomorphic lipoma, 215–217
Pleomorphic liposarcomas, 237
Pleomorphic rhabdomyosarcoma, 348, 350, 352
Plexiform fibrohistiocytic tumour (PFHT)
clinical behaviour and gross findings, 329
differential diagnosis, 330–331
genetics, 329
imaging findings, 330
pathology, 329
Plexiform neurofibromas, 405, 406, 409
Positron emission tomography (PET), 646
characterization and grading, 60–62
evaluation of disease extent, 62–64
recurrence, detection of, 66
response evaluation, 64–65
Posterior fossa malformations, 386
Post-therapy fibrosis, 644
Primitive neuroectodermal tumors (PNET)
central, 462
definition, 462
Ewing's sarcoma, 465
imaging characteristics
CT, 467
MRI, 467
plain radiography, 466
ultrasound, 466–467
incidence and clinical behavior, 465–466
peripheral, 462, 465
Schmidt's classification, 465
Proliferative myositis (and fasciitis), 247
Proton nuclear MR spectroscopy, 109
Pseudocapsule, 147
Pseudogout, 556, 558
Pseudohypertrophy, of calf muscles, 563–564
Pseudotumoral lesions
anatomy variations and muscular anomalies, 524–527
inflammatory and infectious lesions
abscess, 528–529
bursitis, 536
cellulitis, 527
diabetic muscle infarction, 535–536
focal myositis, 535
granulomatous disorders, 536–541
lymphedema and lymphangitis, 528
muscular cystic echinococcosis, 532–534
necrotizing fasciitis, 527
pyomyositis, 529–532
metabolic lesions
calcific tendinosis, 556–557, 560
gout and pseudogout, 556, 558, 559
tumoral calcinosis, 557–562
miscellaneous
calf muscles, pseudohypertrophy of, 563–565
elastofibroma dorsi, 564–568
Geyser phenomenon, 565, 566
skin lesions
epidermal inclusion cysts, 555–557
granuloma annulare, 554–555
pilomatricoma, 554
traumatic nerve lesions
calcific myonecrosis, 551, 552
foreign body reactions, 549–551
hematoma and contusion, 545–549
hypothenar hammer syndrome, 551–553
Morton's fibroma, 542–545
traumatic neuroma, 545
vascular lesions, 562–563
Pulmonary metastasectomy, 646
PVNS. *See* Pigmented villonodular synovitis (PVNS)
Pyomyositis
in AIDS patients, 531
definition, 529
magnetic resonance imaging, 531
within right upper arm muscles, 532
scintigraphy, 532
stages, 530
Staphylococcus aureus, 530
treatment, 532

R

Radiography. *See* Plain radiography
Rapidly involuting congenital hemangioma (RICH), 366
Rare sweat gland and duct tumors, nonspecific US appearance, 32–33
Rendu–Osler–Weber syndrome, 388
Retroperitoneal extrarenal angiomyolipoma, 474, 475

Retroperitoneal lymphoma, 587, 589
Reverse transcription polymerase chain reaction (RT-PCR), 124
Revised European American Lymphoma (REAL), 578
Rhabdomyolysis, 585
Rhabdomyoma, adult, 345
  of forearm, 347
Rhabdomyosarcoma, 623
  of adductor region, 354
  alveolar, 347–348, 351
  clinical findings, 345–348
  definition, 345
  embryonal, 347, 353
  imaging, 348
  pleomorphic, 348, 350, 352
  spindle cell/sclerosing, 348
Rheumatoid nodule, 33
Round cell sarcomas (RCS), 484

S
Sacral osteomyelitis, 529, 531
Sarcoidosis, 536–538
Schwann cells, 393
Schwannomas
  ancient, 395, 400, 403
  anteromedial side, of right knee, 400, 401
  cellular, 395, 398
  of chest, 396, 397
  clinical presentation, 395–396
  epidemiology, 394
  flexor surface, of left lower leg, 403
  histology, 394–395
  imaging characteristics
    computed tomography, 396
    magnetic resonance imaging, 396–405
    plain radiography, 396
    ultrasound, 396
  of left intervertebral foramen, 396, 398
  melanotic, 395
  microcystic, 395
  plexiform, 395
  of right hand, 396
  schwannomas, 394
  topography, 394
Schwannomatosis
  definite, 420
  genetics of, 419
  imaging findings, 420
  possible, 420
  segmental, 420
Sclerosing epithelioid fibrosarcoma, 299–302
SH. *See* Synovial hemangioma (SH)
Short tau inversion recovery (STIR), 643
Shoulder girdle lipomatosis, 208
Skeletal muscle tumors
  extracardiac rhabdomyoma
    clinical findings, 345
    definition, 345
    imaging, 345, 347
  rhabdomyosarcoma
    clinical findings, 345–348
    definition, 345
    imaging, 348
  WHO classification, 191
Skin lesions
  epidermal inclusion cysts, 555–557
  granuloma annulare, 554–555
  pilomatricoma, 554
Smooth muscle tumors
  leiomyoma of deep soft tissue
    clinical findings, 340
    definition, 340
    imaging, 341
  leiomyosarcoma (excluding skin)
    clinical findings, 341–343
    definition, 341
    imaging, 343–345
  WHO classification, 190–191
Soft tissue chondroma
  definition, 604
  of finger, 605, 606
  imaging, 605
  incidence and clinical behavior, 604
Soft tissue lymphoma
  classification, 578
  clinical manifestations, 579
  differential diagnosis, 590
  epidemiology, 578
  imaging
    nuclear medicine and hybrid, 585–587
    radiological, 579–585
  mucosa-associated lymphoid tissue, 578
  non-Hodgkin's lymphomas, 578
  pathogenesis, 578–579
  primary, 577
  secondary, 577
  staging, 587–590
Soft tissue metastases (STM)
  biopsy, 597–598
  choroid melanoma, 596
  clinical features, 594
  differential diagnosis, 598
  epidemiology, 593–594
  imaging diagnosis, 595–597
  intramuscular metastases, 595
  osteosarcoma, 596
  pathophysiological mechanisms, 594
  prognosis, 598
  treatment, 599
Soft tissue mineralization disorders
  dystrophic calcification, 35
  ectopic calcifications, 34
  ectopic ossification, 34
  physiological biomineralization, 34
  tumoral calcinosis, 35
  US findings, 34–35
Solitary circumscribed neuromas (SCNs), 411
Solitary fibrous tumor, 641, 642
Spinal dysraphism, 386

Spindle cell lipoma, 215–217
Split-fat sign, 398
Squamous-cell carcinomas, 594
Staging
  AJCC/UICC staging system, 145–146
  distant metastasis, 149–150
  intra-/extracompartmental tumor growth, 149
  local staging, 150
    after inadequate resection, 154
    bone involvement, 151–152
    joint invasion, 152–154
    neurovascular encasement, 151
  lymph node metastasis, 149
  MSTS/Enneking staging system, 146
  rationale, 145
  surveillance and repeat staging, 154–157
  tumor depth
    deep tumors, 148
    superficial tumors, 147
  tumor size, 147
Staphylococcus aureus, 527
Static *vs.* dynamic enhanced MRI, 81
Stewart-Treves syndrome, 370, 372. *See also* Angiosarcoma
Subacromion–subdeltoid bursitis, 513
Superficial leiomyomata, 340. *See also* Leiomyoma, of deep soft tissue
  cutaneous, 340
  genital, 340
Superficial soft tissue tumors
  and tumorlike lesions
    basal cell carcinoma, 29
    epidermoid cyst, 28–29
    fat necrosis, 33–34
    fibroblastic/myofibroblastic tumors, 29–32
    pilomatricoma, 29
    rare sweat gland and duct tumors, nonspecific US appearance, 32–33
    rheumatoid nodule, 33
    soft tissue mineralization disorders, 34–35
    synovial sarcoma, 35–36
  US finding, 11
Suprapatellar recess, 314
Syndromes associated with vascular lesions
  Kasabach–Merritt syndrome, 386–387
  Klippel–Trenaunay syndrome, 387–388
  Maffucci syndrome, 388
  Parkes Weber syndrome, 388
  perineal hemangioma, 386
  posterior fossa malformations, 386
  Rendu–Osler–Weber syndrome, 388
  spinal dysraphism, 386
Synovial chondromatosis, 516
Synovial hemangioma (SH), 385, 386, 516
Synovial lesions
  benign cystic lesions
    arthrosynovial cyst, 496–497
    Baker's cyst, 496
    bursa de novo (adventitious bursa), 507–509
    clinical manifestations, 509–510
    ganglion (cyst), 497–507
    imaging, 510–516
  lipoma arborescens, 516–518
  malignant tumors around the joints
    metastatic spread, of cancer, 518
    synovial sarcoma, 518
  para-articular chondroma, 516
  synovial chondromatosis and synovial chondrosarcoma, 516
  synovial hemangioma, 516
  synovial membrane, 495
Synovial osteochondromatosis (SC)
  definition, 605–606
  of elbow, 606, 610
  of hip, 606, 608
  imaging, 606–608
  incidence and clinical behavior, 606
  intra-articular, 606, 609
  primary, 605, 608
  secondary, 605, 608
  ultrasound, 606–608
  US findings, 11
Synovial sarcoma, 518, 627
  age distribution, 443, 445
  within ankle joint, 448, 451
  of back, 446, 447
  biphasic, 445
  definition, 443
  detection of tumor recurrence, 448–451
  of foot, 447, 448
  imaging, 446–448
  incidence and clinical behavior, 443–445
  of knee, 447, 450
  localization of, 445
  medial side of ankle, 449
  medial to femur with central necrosis, 638–640
  monophasic epithelial, 445
  monophasic fibrous, 445
  pathology, 445–446
  prognosis, 448–451
  recurrent, 452
  treatment, 448–451
  US findings, 35–36

T
Tail sign, 397
Target sign, 398
Technetium-99 m-labeled nuclear scan, 597
Tendon sheath and joint lipoma, 221
Tenosynovial giant cell tumour (TSGCT), 11–12
  diffuse-type
    clinical behaviour and gross findings, 320–321
    differential diagnosis, 322–323
    epidemiology, 320
    genetics, 321
    imaging findings, 321–322
    pathology, 321
  localised type
    clinical behaviour and gross findings, 314

differential diagnosis, 320
epidemiology, 312–314
imaging findings, 315–319, 323–326
pathology, 314–315
malignant-type
clinical behaviour and gross findings, 324
genetics, 324
imaging findings, 324, 327
pathology, 324
T2* gradient echo imaging, 78–79
Thoracic intimal sarcoma, 475
Tissue sampling
adequate, 116
fixation, 118
treatment, fresh material, 116–117
Tissue-specific diagnosis
imaging parameters
computed tomography, 166
diagnostic groups of STT, 174, 175
fluid-fluid levels, 174
intratumoral signal void, 177
lesion, 172
magnetic resonance imaging, 170
morphology, 172, 173
plain films, 166
ultrasound, 166
nonimaging parameters
concomitant diseases, 166, 173
location, 165, 169–170
multiplicity/bilateral lesions, 166
patient's age, 165
relative prevalence, 165
Traumatic nerve lesions
calcific myonecrosis, 551, 552
foreign body reactions, 549–551
hematoma and contusion, 545–549
hypothenar hammer syndrome, 551–553
Morton's fibroma, 542–545
traumatic neuroma, 545, 546
Traumatic neuroma, 545–546
Tuberculous osteomyelitis, 536, 537
Tumoral calcinosis
computed tomography, 562
definition, 557
diagnosis, 562
laboratory analysis, 560
magnetic resonance imaging, 562
pathogenesis, 557
radiography, 560
radionuclide bone scans, 560
sites, 560
soft tissue mineralization disorders, 35
treatment, 562
ultrasound, 560–562
Tumor bank, 118–119
Tumor necrosis, 596
Tumors of uncertain differentiation
benign lesions
acral fibromyxoma, 428
deep ("aggressive") angiomyxoma, 434–435
ectopic hamartomatous thymoma, 436–437
intramuscular myxoma (incl. cellular variant), 426–428
juxta-articular myxoma, 428–430
myxoma, of Jaws, 430–434
pleomorphic hyalinizing angiectatic tumor, 435–436
classification, 426
intermediate tumors (locally aggressive)
hemosiderotic fibrolipomatous tumor, 437
intermediate tumors (rarely metastasizing)
angiomatoid fibrous histiocytoma, 439, 440
atypical fibroxanthoma, 437–439
mixed tumor, 440, 441
ossifying fibromyxoid tumor, 439–441
phosphaturic mesenchymal tumor, 443, 444
malignant lesions
alveolar soft part sarcoma, 454–458
clear cell myomelanocytic tumor, 473–475
clear cell sarcoma of soft tissue, 458–460
desmoplastic small round cell tumor, 462, 464
epithelioid sarcoma, 451–454
extrarenal rhabdoid tumor, 469–473
extraskeletal myxoid chondrosarcoma, 461
intimal sarcoma, 475–476
malignant mesenchymoma, 461–462
PNET/extraskeletal Ewing's sarcoma, 462–471
synovial sarcoma, 443–451
WHO classification, 193–194
T1-weighted imaging (T1-WI)
contrast-enhanced MRI, 79
unenhanced MRI, 73–75

U

Ultrasound (US)
articular and synovial sheath masses
amyloidosis, 12–14
synovial osteochondromatosis/synovial chondromatosis, 11
tenosynovial giant cell tumor, 11–12
characteristics, 5–11
ganglion cyst, 27–28
lipoma, 24–27
pericytic (perivascular) tumors
angioleiomyoma (vascular leiomyoma/angiomyoma), 21
glomus tumor, 20–21
peripheral neurogenic tumors, 14–16
nerve-related tumorlike lesions, 16–19
peripheral nerve sheath tumors, 16
principles, 4
superficial soft tissue tumors, 11
superficial soft tissue tumors and tumorlike lesions
basal cell carcinoma, 29
epidermoid cyst, 28–29
fat necrosis, 33–34
fibroblastic/myofibroblastic tumors, 29–32
pilomatricoma, 29

Ultrasound (US) (*cont.*)
rare sweat gland and duct tumors, nonspecific US appearance, 32–33
rheumatoid nodule, 33
soft tissue mineralization disorders, 34–35
synovial sarcoma, 35–36
tumorlike lesions, 11
vascular tumors, 21–24
Undifferentiated pleomorphic sarcoma (UPS), 328, 483
of knee, 488, 489
of thigh, 486, 487
Undifferentiated/unclassified sarcoma
clinical behaviour and gross findings, 485
differential diagnosis, 490
epidemiology, 484–485
epithelioid sarcoma, 483, 484
genetics, 485
imaging findings, 486–489
intralesional haemorrhage, 486, 489
pathology, 485
pleomorphic sarcoma, 483
round cell morphology, 483
spindle cell sarcoma, 483
of thigh, 486, 488
WHO classification, 194–195
Unenhanced MRI
fat-suppressed T1-weighted imaging (FS T1-WI), 76–77
fluid-sensitive sequences, 77–78
T2* gradient echo imaging, 78–79
T1-weighted imaging (T1-WI), 73–75
Union Internationale Contre le Cancer (UICC), 146

V
Varicositas, in pregnant women, 563, 564
Vascular lesions, 562–563
Vascular malformations
arteriovenous, 381–384
capillary, 381
lymphatic, 376–381
venous, 371–379
Vascular tumors
angioleiomyoma (vascular leiomyoma / angiomyoma), 21–24
benign
congenital hemangioma, 366–369
epithelioid hemangioma, 368
infantile hemangioma, 365–368
intermediate and malignant vascular tumors
angiosarcoma, 370, 371
epithelioid hemangioendothelioma, 370
kaposiform hemangioendothelioma, 368–369
Kaposi's sarcoma, 369–370
ISSVA classification, 364–365
malformations
arteriovenous, 381–384
capillary, 381
lymphatic, 376–381
venous, 371–379
particular vascular lesions
glomus tumor, 384, 385
synovial hemangioma, 385, 386
syndromes associated with vascular lesions
Kasabach–Merritt syndrome, 386–387
Klippel–Trenaunay syndrome, 387–388
Maffucci syndrome, 388
Parkes Weber syndrome, 388
perineal hemangioma, 386
posterior fossa malformations, 386
Rendu–Osler–Weber syndrome, 388
spinal dysraphism, 386
WHO classification, 191–192, 364
Vastly undersampled isotropic projection reconstruction (VIPR), 514
Venous malformations (VMs)
definition, 371
diffuse and infiltrative, 375, 379
with fluid-fluid level, 374, 375
intramuscular, 373, 374, 376
of left plantar region, 371, 373
magnetic resonance imaging, 373
pathology, 371
subcutaneaous, 374, 375
symptoms, 371
ultrasound, 373

W
World Health Organization (WHO) classification, 340, 364
adipocytic tumors, 188
chondro-osseous tumors, 192–193
fibroblastic/myofibroblastic tumors, 188–189
fibrohistiocytic tumors, 189–190
gastrointestinal stromal tumors, 193
pericytic (perivascular) tumors, 191
peripheral nerve sheath tumors, 193
skeletal muscle tumors, 191
smooth muscle tumors, 190–191
of tumors 2013, 126
tumors of uncertain differentiation, 193–194
undifferentiated/unclassified sarcoma, 194–195
vascular tumors, 191–192